INGENIERIA DE RESERVORIOS GEOTERMICOS

I.	FUNDAMENTOS DE HIDROLOGIA	Dr. Gerardo Hiriart L.
II.	FUNDAMENTOS DE TERMODINAMICA	Dr. Jesús Rivera
III.	CLASIFICACION DE LOS RESERVORIOS GEOTERMICOS	Dr. Jesús Rivera
IV.	FLUJO DE FLUIDOS Y CALOR EN MEDIO POROSO	Dr. Héber Cinco Ley
V.	FLUJO DE FLUIDOS Y CALOR EN POZOS GEOTERMICOS	Dr. Francisco Córdoba
VI.	PRUEBAS DE PRESION	Dr. Fernando Samaniego
VII.	MODELOS MATEMATICOS DE SIMULACION	Dr. Ismael Herrera
VIII.	ASPECTOS PRACTICOS DE PRODUCCION	Ing. Alfonso Aragón

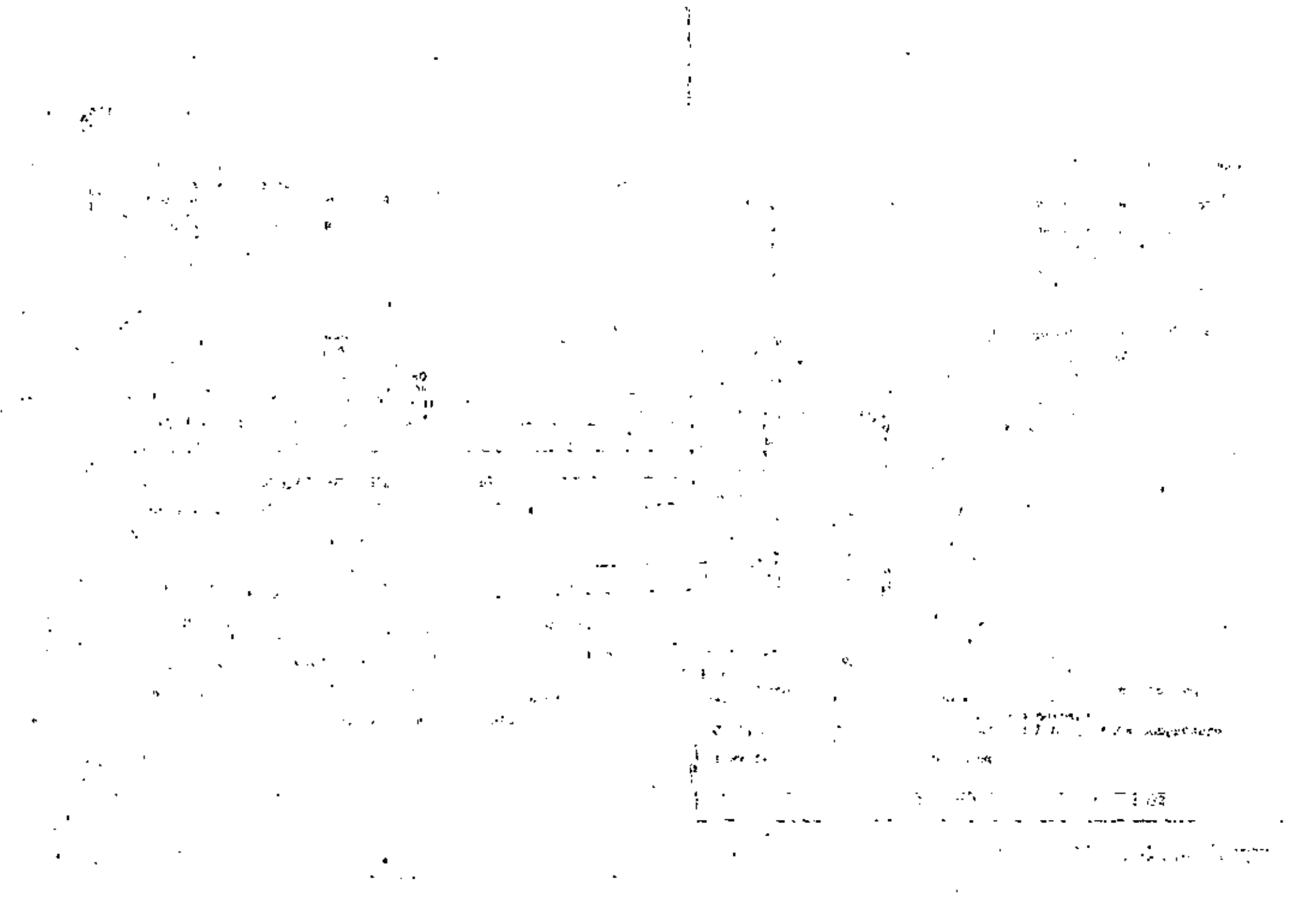

PROGRAMA DE LA ASIGNATURA: INGENIERIA DE RESERVORIOS GEOTERMICOS

Clave: _____ Núm. de créditos: _____ Carrera: .....

Duración del curso — semanas: 9 — Teoría: 150 hrs.
horas: 225 — Prácticas: 75 hrs.

OBJETIVO DEL CURSO: Comprensión de los fundamentos teóricos y prácticos de la ingeniería de reservorios geotérmicos. El propósito del enfoque teórico es el de introducir los principios de flujo de fluidos y calor en medio poroso. El enfoque práctico está dirigido a transmitir las experiencias de campo y resultados prácticos obtenidos en estas teorías.

TEMAS

Núm.	Título	Horas:
I	FUNDAMENTOS DE HIDROLOGIA	12.5
II	FUNDAMENTOS DE TERMODINAMICA	12.5
III	CLASIFICACION DE LOS RESERVORIOS GEOTERMICOS	12.5
IV	FLUJO DE FLUIDOS Y CALOR EN MEDIO POROSO	25.0
V	FLUJO DE FLUIDOS Y CALOR EN POZOS GEOTERMICOS	25.0
VI	PRUEBAS DE PRESION	25.0
VII	MODELOS MATEMATICOS DE SIMULACION	12.5
VIII	ASPECTOS PRACTICOS DE PRODUCCION	25.0

OBJETIVO Y CONTENIDO DE LOS TEMAS

TEMA I: FUNDAMENTOS DE HIDROLOGIA

OBJETIVO: Introducir los conceptos y parámetros comúnmente usados en flujo en medio poroso..

CONTENIDO:

- I.1 Porosidad
- I.2 Compresibilidad
- I.3 Permeabilidad
- I.4 Permeabilidad relativa
- I.5 Ecuación de Darcy

TEMA II: FUNDAMENTOS DE TERMODINAMICA

OBJETIVO: Introducción de los conceptos termodinámicos necesarios para analizar el comportamiento de reservorios geotérmicos.

CONTENIDO:

- II.1 Energía interna
- II.2 Entalpía
- II.3 Entropía
- II.4 Curva de presión de vapor
- II.5 Equilibrio de fases

TEMA III: CLASIFICACION DE LOS RESERVORIOS GEOTERMICOS

OBJETIVO: Comprensión del sistema de clasificación generalmente usado para reservorios geotérmicos.

CONTENIDO:

- III.1 Clasificación de acuerdo a la curva de presión de vapor
- III.2 Reservorios geotérmicos semi-termales
- III.3 Reservorios geotérmicos hiper-termales
- III.4 Reservorios geotérmicos geopresurizados
- III.5 Hipótesis acerca del origen y naturaleza de los reservorios geotérmicos.
- III.6 Modelo geológico típico de un reservorio geotérmico

CURSO: "INGENIERIA DE RESERVORIOS GEOTERMICOS"

THERMODYNAMIC AND HYDRODYNAMIC PROPERTIES OF HYDROTHERMAL SYSTEMS

by

Henry J. Ramey, Jr.
William E. Brigham
H. K. Chen
Paul G. Atkinson
Norio Arihara

Stanford University
Stanford, California, U.S.A.

April 20, 1974

From the Proceedings of an NSF conference on "The Utilization of Volcano Energy," Hilo, Hawaii, February 4-8, 1974.

THERMODYNAMIC AND HYDRODYNAMIC PROPERTIES OF HYDROTHERMAL SYSTEMS

by

Henry J. Ramey, Jr., William E. Brigham, H. K. Chen,
Paul G. Atkinson, and Norio Arihara

Stanford University
Stanford, California

INTRODUCTION

Geothermal energy has received much attention in recent years as one of the sources that can help relieve the energy crisis in the next decade. There is considerable literature on the possible methods of geothermal energy extraction, and practical usage of geothermal energy is growing worldwide.

The goal of any geothermal production system is to extract heat from the earth, and to extract it at a high enough temperature and rate that it can be used commercially to generate power or process heat. Most present geothermal systems are geared toward power generation. To evaluate these systems we must predict the amount of heat present and the rate at which it can be extracted. These are the prime factors affecting the economics of any recovery process.

These two factors--amount of heat and recovery rate--in turn depend on basic physical properties of the reservoir rocks and the fluids contained within them. The amount of heat present depends on the heat capacity and density of the rock and the fluids within it. The rate of heat extraction depends on the thermal conductivity and the fluid flow characteristics, i.e., permeability and relative permeability, of the water and steam in the rocks. All these important basic characteristics of the rock and fluids are functions of both the temperature and pressure of the reservoir system.

Portunately there is an extensive body of literature available to help one estimate many of these fluid and rock properties. Much of this information can be found in the petroleum literature, for the petroleum industry has had an interest in the use of underground heat for oil recovery since the early 1900's. In the paper we summarize some of the data that is useful for geothermal systems. A large fraction of these data are extracted from the petroleum literature.

STORAGE AND TRANSPORT OF HEAT IN ROCKS

Neglecting heat of phase change and heat of reaction, there are three important thermal properties in any process involving heat transfer: thermal conductivity, heat capacity, and thermal diffusivity. Thermal conductivity is generally shown by the symbol, k, and units in the c-g-s system are cal/sec-cm-°C. Many of the references, however, are given in British thermal units, Btu/hr-ft-°F. The conversion factor is:

$$1 \frac{\text{Btu}}{\text{hr-ft-°F}} = \frac{4{,}134 \times 10^{-3} \text{ cal}}{\text{sec-cm-°C}} \qquad (1)$$

The specific heat generally used is the specific heat at constant pressure, or $(\partial H/\partial T)_p$, and the symbol is C_p. The c-g-s unit, cal/gm-°C, is numerically the same as the British unit, Btu/lb-°F. Thermal diffusivity is a collection of terms, $k/\rho C_p$, where ρ is the density. It is often indicated by the symbol α. This grouping is the ratio of the ability to transfer heat, k, to the ability to store heat, ρC_p. In the c-g-s system the dimensions are cm^2/sec, and in the British system ft^2/hr. Many references use British units. The conversion factor is:

$$1 \frac{ft^2}{hr} = \frac{0.258\ cm^2}{sec} \qquad (2)$$

Thermal Conductivity

An early evaluation of rock thermal conductivity was made by Birch and Clark.[1,2] They studied a broad range of rock materials including some eighteen igneous rocks, seven sedimentary and metamorphic rocks, and certain single crystals and glasses. With the exception of the anorthosites and the glasses (both man-made and natural) all the materials showed a reduction of thermal conductivity with temperature increase. This behavior is as should be expected. See Figures 1 and 2, from Birch and Clark.[1]

Probably the most important finding by Birch and Clark was that the thermal conductivity of a mixture could be estimated by assuming that the various components of the system were in series. The total thermal resistivity of the system is equal to the volumetric weighted average of resistivity of each component. The total conductivity is thus the harmonic average:

$$\frac{1}{k_{ave}} = \frac{x_1}{k_1} + \frac{x_2}{k_2} + \ldots + \frac{x_n}{k_n} \qquad (3)$$

where x = volumetric fraction of each component.

Birch and Clark's data were mostly for rocks of low porosity. Somerton[3] was an early investigator of the thermal conductivity of fluid-containing rocks. He studied unconsolidated sands, sandstones, silty sandstones, siltstone, shale and limestone. He developed an empirical equation to predict the effect of fluid saturation on the thermal conductivity of porous rocks. It was:

$$\frac{k}{k_1} = \left(\frac{k_2}{k_1}\right)^{c\phi} \qquad (4)$$

where k = thermal conductivity of fluid-saturated rock

k_1 = thermal conductivity of rock solids

k_2 = thermal conductivity of saturating fluid

ϕ = porosity - fraction

c = empirical constant approximately equal to 1.

The empirical constant, c, was actually found to range from 0.9 to 2.3 with the larger values found at lower porosities. The product, $c\phi$, ranged from 0.325 to 0.460.

In 1961 Kunii and Smith[4] measured thermal conductivities of porous rocks saturated with various fluids. They proposed an equation (their Eqn. 3) to relate the fluid saturated conductivity to the conductivity of dry rock. Some of their results are reproduced here as Figures 3 and 4 to show the correspondence of their data to their model. Water may increase conductivity more than two-fold depending on the nature of the porous medium. Their data were run on Boise, Bartlesville, Berea and Rangely sandstones.

Smith and his coworkers[5,6] also studied the effect of fluid flow on the thermal conductivity of porous systems. In general they found that thermal conductivity in the direction of flow was increased as the flow velocity increased.[5] Figure 5 shows this effect with water and brine. They made a correlation of this effect through use of the product of the Reynolds' Number and the Prandtl Number (Fig. 6). Thermal conductivity perpendicular to the direction of flow, however, remained nearly constant--unaffected by flow rate.[6]

Anand, Somerton and Gomaa[7] recently have shown empirical methods of predicting thermal conductivities of fluid saturated rocks when there is little thermal data available. These methods are based on regression analysis equations. The thermal conductivity of dry rock (containing air) was correlated as follows:

$$\lambda_d = 0.3386\ \rho^{1.034} - 3.194\ \phi + 0.5304\ k^{0.100} + 0.0131\ F - 0.0311 \qquad (5)$$

where λ_d = thermal conductivity of dry rock, Btu/hr-ft-°F

ρ = bulk density, gm/cc

ϕ = fractional porosity

k = permeability, millidarcies

F = formation electrical resistivity factor

The formation resistivity factor is a common formation evaluation term which can be extracted from electric logs. It is the ratio of the actual resistivity to that if the rock pores were totally filled with formation water. In the absence of data on this parameter, the following empirical relationship can be used:

$$F = 1/\phi^m \qquad (6)$$

where m = cementation factor, often near 2.0 for sandstones.

Where the rock is fluid saturated the thermal conductivity is higher, and Anand, et al., found the following empirical equation was useful:

$$\frac{k}{k_1} = \left(\frac{k_2}{k_1}\right)^{c\phi} \qquad (4)$$

where k = thermal conductivity of fluid-saturated rock

k_1 = thermal conductivity of rock solids

k_2 = thermal conductivity of saturating fluid

ϕ = porosity - fraction

c = empirical constant approximately equal to 1.

The empirical constant, c, was actually found to range from 0.9 to 2.3 with the larger values found at lower porosities. The product, $c\phi$, ranged from 0.325 to 0.460.

In 1961 Kunii and Smith[4] measured thermal conductivities of porous rocks saturated with various fluids. They proposed an equation (their Eqn. 3) to relate the fluid saturated conductivity to the conductivity of dry rock. Some of their results are reproduced here as Figures 3 and 4 to show the correspondence of their data to their model. Water may increase conductivity more than two-fold depending on the nature of the porous medium. Their data were run on Boise, Bartlesville, Berea and Rangely sandstones.

Smith and his coworkers[5,6] also studied the effect of fluid flow on the thermal conductivity of porous systems. In general they found that thermal conductivity in the direction of flow was increased as the flow velocity increased.[5] Figure 5 shows this effect with water and brine. They made a correlation of this effect through use of the product of the Reynolds' Number and the Prandtl Number (Fig. 6). Thermal conductivity perpendicular to the direction of flow, however, remained nearly constant--unaffected by flow rate.[6]

$$\frac{\lambda_s}{\lambda_d} = 1 + 0.299 \left[\left(\frac{\lambda_f}{\lambda_a} \right)^{0.330} - 1 \right]$$

$$+ 4.57 \left[\frac{\phi}{(1-\phi)} \frac{\lambda_f}{\lambda_d} \right]^{0.482m} \left(\frac{\rho_s}{\rho_d} \right)^{-4.30} \qquad (7)$$

where λ_s = thermal conductivity of fluid-saturated rock, Btu/hr-ft-°F

λ_f = thermal conductivity of the saturating fluid

λ_a = thermal conductivity of air

ρ_s = bulk density of saturated rock

ρ_d = bulk density of dry rock

Lastly, the effects of temperature were included. Anand, et al., used a modification of Tikhomirov's[8] correlation to show this effect. Their results were as follows:

$$\lambda_T = \lambda_{68°} - 0.709 \times 10^{-3} (T - 528) (\lambda_{68°} - 0.800) \cdot \left[\lambda_{68°} \left\{ T \times 10^{-3} \right]^{0.545\lambda_{68°} + 0.738} \right] \qquad (8)$$

where λ_T = thermal conductivity at temperature, T, Btu/hr-ft-°F

$\lambda_{68°}$ = thermal conductivity at 68°F

T = temperature, °R = °F + 460

A graph of their data compared to this equation is shown in Figure 7. The match appears to be satisfactory. The equation properly predicts that high conductivity materials have lower thermal conductivity at higher temperatures, while low conductivity materials exhibit increasing conductivities with temperature.

Often rocks contain two fluids rather than one. Gomaa and Somerton[9,10] discuss this effect in two recent papers. If both fluids are liquid, or if neither fluid is boiling or condensing, the thermal conductivity of the system is a simple square root relationship between the thermal conductivity and the fluid content, as follows:

$$\lambda - \lambda_1 = (\lambda_2 - \lambda_1)\ (S_2)^{1/2} \qquad (9)$$

where λ = thermal conductivity of rock containing two fluids

λ_1 = thermal conductivity of rock saturated with fluid 1

λ_2 = thermal conductivity of rock saturated with fluid 2

S_2 = the fraction of pore space filled with fluid 2

If the fluids are a liquid and vapor in equilibrium with each other, for example water and steam, the thermal conductivity may be far higher than predicted by Eqns. 8 and 9. The combination of heat transfer by boiling and mass flow by capillary pressure effects can cause the effective thermal conductivity to increase 2 to 5 fold. This is called the "heat pipe" effect. The amount of increase depends on the permeability of the rock, the latent heat of vaporization, the vapor saturation and the direction of heat flow with respect to gravity. The empirical equation they found to predict this additional term is as follows:

$$\lambda_{HP} = 0.003\ \phi^{0.357}\ k^{0.424}\ \frac{LY}{\sqrt{\nu_\ell\ \nu_v}}\ (1 + 0.107 \sin \phi)\ F(S) \qquad (10)$$

$$F(S) = \sin\left[\frac{\pi\left(1-S_{\ell}\right)}{1-S_{\ell c}}\right]\sin\left[\frac{\pi\left(1-S_{v}\right)}{1-S_{vc}}\right] \cdot \left[0.74 + 0.61S_{v} + 1.56S_{v}^{2} + 2.85S_{v}^{3}\right] \quad (11)$$

$$S_{\ell c} = 0.098\ k^{-0.236} \quad (12)$$

$$S_{vc} = 0.060\ k^{-0.236} \quad (13)$$

where S_{ℓ} and S_{v} = the fraction of pore space filled with liquid and vapor, respectively

ϕ = porosity, fraction

k = permeability, darcies

L = latent heat of vaporization, Btu/lb

γ = vapor pressure-temperature derivative, lb/in^2-°F

ν_{ℓ} and ν_{g} = viscosity of liquid and vapor, ft^2/day

ψ = angle of heat flow direction, positive upward

λ_{HP} = additional thermal conductivity due to heat pipe effect, Btu/hr-ft-°F

By this stage, it should be clear that there is a problem in this study with respect to symbols and units. The symbol k has been used widely to represent both the thermal conductivity and permeability. Even the Greek symbol λ has been used often in various literatures to represent both heat and fluid conductivities of porous solids. Rather than totally recast equations in a single set of symbols and units, we have elected to preserve the symbols of the original study, where possible, and to define symbols and units where presented. This is done because the purpose of

of studies such as this is usually to guide a reader to further information, rather than to replace it. The pertinent literature is far too voluminous for a single paper to serve a true summary purpose.

We turn now to a review of pertinent information on heat capacity and density.

Heat Capacity and Density

Somerton's[3] data on heat capacity of rocks shows that most reservoir materials behave similarly. Figure 8 shows some of the results of his work. Martin and Dew[11] point out that these data can be approximated roughly by a linear equation for heat capacity as a function of temperature:

$$c_p = \frac{T + 2000}{10{,}000} \qquad (14)$$

where c_p = heat capacity of rock, Btu/lb-°F

T = temperature, °F

Somerton also found that where rock is made up of minerals with many differing materials, the average heat capacity follows Kopp's Law, which states that the heat capacity is the mass weighted average of the constituents.

In general, rock volume changes only slightly with temperature. Further, many rocks containing large percentages of quartz behave much alike. Figure 9 shows the data of Somerton and Selim[12] for three sandstones and quartz. There is little difference in the results for the four materials.

Thermal Diffusivity

Because the thermal conductivity of many materials behaves similarly as a function of temperature, and because many materials have similar heat capacity-temperature behavior, it seems logical to expect that thermal diffusivity-temperature relationships will agree for many materials. The data of Somerton and Boozer[13] show that, indeed, many porous materials do exhibit similar trends in thermal diffusivity as a function of temperature. A notable exception was found with a tuffaceous sandstone, as seen in Figure 10; however, a fairly good approximating line could be drawn through the rest of the data in Figure 10. Thus use of this figure for quick estimation appears reasonable.

Heats of Phase Change and Reaction

In gas and oil reservoirs, very low heats of phase change and low heats of solution, plus the high heat capacity of the solid phase (rock) due to high mass of rock leads to nearly isothermal behavior for most fluid production thermodynamic paths. Exceptions are: (1) the process of oil recovery by underground combustion[57] and (2) oil recovery by steam injection.[58] The first involves release of large amounts of heat due to oxidation of a part of the oil, and the second releases heat by condensation of the injected steam. Actually several types of spontaneous oil oxidation reactions may occur leading even to ignition.[59] There appears little purpose to cite existing studies of oil oxidation reaction kinetics, other than to warn such information is available should pore space reactions become important in geothermal energy extraction. We turn now to a consideration of the effects of elevated temperatures on the flow characteristics of porous rocks.

TEMPERATURE AND PRESSURE EFFECT ON PERMEABILITY OF POROUS MEDIA

It is well known that the viscous flow of fluids through porous media follows Darcy's Law, which is expressed as:

$$v = -\frac{k}{\mu}\left[\frac{dp}{ds} - \rho g \frac{dz}{ds}\right] \tag{15}$$

where v is volume rate of flow across a unit area of the porous medium, k is permeability of the medium to a fluid at constant temperature, μ is viscosity of the fluid, p is pressure, ρ is the density of the fluid, g is the acceleration due to gravity, z is the vertical coordinate, and s is the coordinate along the direction of flow.

The permeability of a porous medium to a gas phase usually exceeds the permeability of the same medium to a liquid phase. The difference in these permeabilities is due to the phenomenon known as slip[14], reactions between liquids and the solid, and relative permeabilities. Slip is related to the mean free path of the gas molecules. Consequently, the permeability of a porous medium to gas should be a function of the temperature, pressure, and the nature of the gas. Klinkenberg[14] developed the relation between the permeability of a porous medium to gas and to a non-reactive liquid, viz:

$$k_g = k_\ell \left(1 + \frac{4c\bar{\lambda}}{r}\right) \tag{16}$$

This equation was derived assuming that all the capillaries in the porous medium are of the same diameter, and are oriented at random through the

solid material. In Eqn. 16, k_g and k_ℓ are permeabilities respectively to gas and to a single liquid phase completely filling the pores of the medium at constant temperature, $\bar{\lambda}$ is the mean free path of the gas molecules, r is the radius of capillaries, and c is a proportionality constant. Then, the mean free path can be expressed as:

$$\bar{\lambda} = \frac{1}{\sqrt{2\pi}\, d^2 n} = \frac{RT}{\sqrt{2\pi}\, p_m N d^2} \tag{17}$$

where d is collision diameter, n is concentration of molecules per unit volume, N is Avogadro's Number, p_m is mean pressure, T is temperature, and R is universal gas constant. Therefore, by combining Eqns. 16 and 17, we obtain:

$$k_g = k_\ell \left(1 + \frac{4CRT}{\sqrt{2\pi}\, rNd^2 p_m}\right) = k_\ell \left(1 + \frac{b}{p_m}\right) \tag{18}$$

where b is called the Klinkenberg factor, which is constant for a given gas and a given porous medium at a constant temperature. As easily seen from Eqn. 18, a graph of k_g vs. $1/p_m$ should result in a straight line with an intercept of k_ℓ and a slope of bk_ℓ as shown in Figure 11. Slope must become steeper as the temperature increases. Thus, the permeability to a gas is greater at low pressures, and is at a minimum at a maximum pressure of flow.

The permeability defined in Eqn. 15 requires that the porous medium is saturated completely with one homogeneous, single-phase fluid. The permeability thus defined is called the absolute permeability. When the

medium contains more than one fluid, the conductance of the medium to one fluid phase is commonly called the effective permeability. It depends on the volume fraction of each phase present in the pore space (called the saturation), the wetting characteristics of the fluids, and even the saturation history of the fluids. This will be discussed more thoroughly below. Another term, the relative permeability, is also commonly used. It is defined as the ratio of the effective permeability to some base absolute permeability value.

Wettability and Capillary Pressure

When more than one fluid exists in a porous medium, the static and flow properties of the medium depend upon the microscopic distribution of these phases within the pores. This distribution is controlled by the wettability of the porous medium. The wettability is the degree of preference of the porous medium surface for the various fluid phases. In petroleum engineering, water and oil are often considered wetting and non-wetting phase respectively. In geothermal systems that have water and steam coexisting in the same pore spaces, water will be the wetting phase and steam will be the non-wetting phase. Thus the discussion that follows concerning oil and water can in many respects be directly related to steam-water systems.

Wettability of an oil-water-solid system is schematically shown in Figure 12.[15] The terms γ_{os} and γ_{ws} are surface tension between oil and solid, and between water and solid, respectively. γ_{ow} is interfacial tension between oil and water. θ is called contact angle. Then, for the equilibrium state:

Contact angles of less than 90°, measured through the water phase, indicate preferentially water-wet conditions, whereas contact angles greater than 90° indicate preferentially oil-wet conditions. The distribution of either the wetting or non-wetting phase within the pore spaces does not depend solely upon the saturation of that phase, but depends also upon the direction of the saturation change. The terms "drainage" and "imbibition" refer to flow resulting in a decrease and increase, respectively, in the wetting phase saturation.

Since the wettability and direction of saturation change influence the fluid distribution, these factors would be expected to affect similarly both the capillary pressure and relative permeability characteristics. The capillary pressure, p_c, in porous media is defined as the pressure difference existing across the interface separating two immiscible fluids at rest, one of which wets the surfaces of the rock in preference to the other. The water-oil capillary pressure is defined as the pressure in the oil phase minus the pressure in the water phase, or:

$$p_c = p_o - p_w \tag{20}$$

For the gas-liquid case (or steam-water):

$$p_c = p_g - p_\ell \tag{21}$$

Figure 13 shows the capillary pressure characteristics of a strongly water-wet rock. It is seen in Figure 13 that the pressure in the oil phase (non-wetting) must exceed that in the water phase (wetting) before oil will enter the initially water-saturated rock. This would also be seen in a steam-water system. This entrance pressure is referred to as the threshold pressure

or displacement pressure. The minimum saturation point in Figure 13 gives the irreducible water saturation.

It has long been recognized that the vapor pressure above the curved surface of a liquid is a function of the curvature of the liquid surface. The capillary pressure is also a function of the curvature of the liquid surface. Considering that the liquid and vapor respectively are the wetting and non-wetting phases, the capillary pressure, pertaining to static equilibrium at curved surfaces of vapor-liquid phase separation, may be written as[16]:

$$p_c = p_g - p_{g'} + \frac{RT}{Mv_\ell} \ln \frac{p_{g'}}{p_g} \qquad (22)$$

where p_g is the pressure in the vapor phase, $p_{g'}$ is the equilibrium vapor pressure of the liquid above a flat surface, M is the molecular weight, and v_ℓ is the specific volume of liquid. Then, the pressure in the liquid phase is:

$$p_\ell = p_{g'} - \frac{RT}{Mv_\ell} \ln \frac{p_{g'}}{p_g} \qquad (23)$$

As the liquid is the wetting phase, p_g, is greater than p_g. Then p_ℓ is smaller than $p_{g'}$. Therefore, if liquid pressures and temperatures are measured in the two-phase portion of the porous medium, liquid pressures must be lower than the normal (plane-surface) saturation pressures corresponding to the measured temperatures. Since capillary pressure values are a function of the liquid saturation, the vapor pressure lowering must be a function of the liquid saturation of the porous medium.

Relative Permeability

Figure 14 shows typical water-oil relative permeability characteristics for a water-wet core.[17] In this figure the permeability to oil at reservoir connate water saturation was used as the base value for relative permeabilities. These data were taken for the case where the water saturation increased while the oil saturation decreased. If the data had been taken for decreasing water saturation, there would be a marked difference. The water (wetting phase) permeability data would be unchanged, but the oil (non-wetting phase) permeabilities would have been higher, especially at the right hand side of the graph. Further, the end points of the curves--the irreducible water saturation and the residual oil saturation--likely would have changed.

Muskat, et al.,[18] presented relative permeability curves for gases and liquids in unconsolidated sands, as given in Figure 15, which shows that for practical purposes the curves for the relative permeabilities k_{rg} and k_{rl} are independent of the nature of the unconsolidated sand. This is in marked contrast with most consolidated media, where the relative permeabilities must nearly always be measured, for they vary widely depending on the nature of the fluids and the porous system.

Temperature Effect on Relative Permeability

The relative permeability is affected by the test environment. The important factors are temperature, pressure, fluids and core condition. Several investigators have reported experimental results of the effect of temperature on relative permeability.

Poston, et al.,[19] using unconsolidated sand, found that the irreducible water saturation increased and the residual oil saturation decreased

with increasing temperature, as shown in Figures 16 and 17. This observation can be seen another way by considering Figure 14. In effect the higher temperature caused both relative permeability curves to shift to the left on the saturation axis. Poston, et al., speculated that if the relative permeability has changed, the capillary pressure should also be temperature sensitive.

Sinnokrot, et al.,[20] studied capillary pressure behavior of three consolidated sandstones and one limestone sample over a temperature range of 75° to 325°F by the restored state method. Their work confirmed the observation of Poston, et al., that the irreducible water saturation increased and apparent residual oil saturation decreased with increase in temperature. They concluded that capillary pressure curves for sandstones were displaced toward higher wetting phase saturations with an increase in temperature level, indicating an increase in water wetness with temperature level increase. Figure 18 shows part of their work.

Weinbrandt, et al.,[21] found results similar to Poston's when increasing from room temperature to 175°F in Boise sandstone. Representative data are shown in Figure 19. They also obtained data on absolute permeability in an increasing temperature level sequence from 75 to 315°F, as shown in Figure 20. The absolute permeability decreased drastically as temperature increased. Afinogenov[22] found similar results up to temperatures of 212°F.

Lo and Mungan[23] also studied relative permeabilities as a function of temperature and found results similar to Weinbrandt, et al. and Poston. They also studied systems of differing wetness characteristics and the results were found to be similar in both oil-wet and water-wet systems.

Poston, et al., pointed out that the changes in rock-fluid characteristics as functions of temperature level were all in a direction suggestive of an increase in water wetness with temperature increase. Contrary to this, Weinbrandt, et al., considered that temperature induced changes were too large to be explained by obvious factors such as change in contact angle interfacial tension, etc. They speculated that most of the above observations concerning temperature sensitivity may have been a result of thermally-induced mechanical stress. Work is continuing to attempt to clarify these results and the reasons for them.

Pressure Effect on Pore Volume

Von Conten and Choudhary[24] investigated experimentally the temperature effect on pore volume compressibility, which is defined as:

$$c_f = -\frac{1}{V_p}\left[\frac{\partial V_p}{\partial p}\right]_T \qquad (24)$$

where V_p is pore volume and p is compacting pressure which is equal to overburden pressure minus pore pressure. Figure 21 is a plot of cumulative fractional pore volume change versus compacting pressure for sandstone at 75°F and 400°F. The pore volume compressibility, which is the slope of these curves, becomes smaller at higher pressure.

Somerton and Selim[12] showed the effect of temperature on sandstone volume, as indicated earlier in the paper in Figure 9.

Pressure Effect on Permeability

Afinogenov[22] presented data on the absolute permeability decrease as affected by external pressure. From his data he introduced an empirical formula to predict this effect:

$$\frac{k_p}{k_o} = \left(1 + \frac{127 \times 10^{-5}}{p}\right)^{-1} \qquad (25)$$

where effective pressure, p, is defined as:

$$p = p_{con} - 0.85\, p_{pore}$$

p_{con} and p_{pore} are confining pressure and pore pressure respectively in atmospheres. He deduced that this permeability decrease was due to a decrease in the cross-sectional area of the pores and to a more torturous pore space configuration under the effect of pressure.

Zoback and Byerlee[25] measured the permeability of Berea sandstone as a function of both confining pressure and pore pressure. They reported that the permeability decreased with increased confining pressure, and increased as pore pressure was increased. Qualitatively, this agrees with Afinogenov's results. They found also that pore pressure had a significantly larger effect upon permeability than did confining pressure. This does not agree with the results of Afinogenov. They speculated that the matrix through which the fluid flows has a higher compressibility than does the granular framework through which the confining pressure stresses are transmitted.

Many other investigators, such as Fatt and Davis[26], Wyble[27], Dobrynin[28], Gray, et al.[29], and Wilhelmi and Somerton[30], have reported the effect of overburden pressure on the permeability of sandstone. Figure 22 is the

experimental results provided by Fatt and Davis. The permeability of sandstone decreased with increase in overburden pressure. Most of the decrease took place over the range of zero to 3000 psi overburden pressure.

PHYSICAL STATES OF WATER

The physical states of water of interest in geothermal reservoirs are: compressed liquid, saturated liquid, superheated (also called dry or unsaturated) steam, saturated (or wet) steam, and the dense fluid state.

The term "saturation" may thus have several meanings in geothermal reservoir engineering. "Saturation" can refer to: (1) the volume fraction of pore space occupied by a fluid phase, (2) the thermodynamic state of the fluid phases with reference to some appropriate vapor pressure curve, and (3) the usual sense of solids and gases being dissolved in a liquid phase. Care must be used that the term "saturation" is not misunderstood.

Figure 23 is a graph of the vapor pressure curve of water, showing the position of the critical point at 221.07 bar and 374.1°C (3206.2 psia and 705.4°F). Point A on this figure is in the superheated steam region, point B is at saturation conditions where both liquid and vapor may coexist, and point C is in the compressed liquid region. Points D and E are in the dense fluid region. Figure 24 is an expanded form of Figure 23 showing the initial thermodynamic state of various geothermal fields around the world. Note that the geopressured aquifers found in the Gulf Coast area of the United States, with temperatures of 260°C (500°F) and pres-

sures in excess of 700 bar (10,000 psia), are off the scales of both Figures 23 and 24, and might be considered as dense fluids.

Gibb's Phase Rule teaches that in order to specify the thermodynamic state of a single phase of water, two independent thermodynamic properties (e.g., pressure and temperature) must be specified. But if two phases are present (e.g., saturated steam and water) specification of only one intensive property defines the system. A geothermal aquifer at saturated conditions must follow some appropriate vapor pressure curve as fluid is produced.

It can be shown from thermodynamic analysis that a geothermal system initially containing a single-phase fluid (either compressed liquid or superheated steam) will tend to deplete isothermally. But once two phases form, a system should deplete along some sort of vapor pressure curve appropriate for the fluids in the pore space.

Properties of Interest

A thermodynamic equation of state for water expresses the pressure-volume-temperature (PVT) relationships. These describe the specific volume, v, (or density, $\rho = 1/v$) as a function of pressure and temperature for the various phases. In addition we require the energy related properties, specific enthalpy, h, and specific entropy, s, and specific heats, c_p and c_v.

The transport properties that are important are viscosity and thermal conductivity. Viscosity is basically an internal resistance of the fluid to flow, due to molecular interaction. Thermal conductivity affects the rate of heat transfer of the rock-fluid system.

Data describing the forementioned properties for impure water is meager, although a fair amount is known about the solubility of numerous substances found in geothermal waters. Ionic equilibrium calculations can be used to estimate which chemicals will remain dissolved, and which ones will precipitate under changing pressure, temperature, and composition conditions. The reader is referred to textbooks on geochemistry (Krauskopf[31]) and ionic equilibrium calculations (Butler[32]) and also to work on the chemistry of geothermal systems by White[33], Fournier and Truesdell[34], and Helgeson.[62]

Equations of State

Since the early part of this century there has been an international effort to standardize the various thermodynamic and transport properties of pure water. The well-known Keenan and Keyes[35] steam tables were a result of these efforts. The ASME Steam Tables[36] are one of the more recent products of these efforts, and are used as a basis for much of the data in this report. These tables present the results of a series of accurate matching of analytic functions (the 1967 IFC Formulation for Industrial Use) to accepted and standardized experimental data (the 1963 International Skeleton Tables). The results are presented in tabular and graphical form. The analytic functions are also given, and can be programmed for use on a computer. Another recent source of water properties is the Steam Tables by Keenan, et al.[37]

The rest of this review will be devoted to describing the properties mentioned above, both for pure and impure water. Data will be presented in tabular or graphical form, and several simplified analytic forms will be discussed.

Pure Saturated Steam and Water

For conditions below the critical state (221.07 bar, 374.1°C; 3206.2 psia, 705.4°F) the liquid and vapor phases can coexist in equilibrium. When liquid and vapor are in equilibrium they are described as being saturated, and such states lie along the vapor pressure curve (see Figures 23 and 24). This curve is of great interest, and a number of simplified analytic approximations have been presented. A few will be given here. Whiting and Ramey[38] used an integrated form of the Clausius-Clapeyron equation to develop the following approximation by a least mean square curve match over the temperature range 150-315°C (300-600°F):

$$\ln p = \frac{-4667.0754}{(T + 273)} + 12.59833 \; ; \quad \text{where } p = \text{bar}, \; T = °C. \qquad (26\text{-a})$$

Or:

$$\ln p = \frac{-8400.7358}{(T + 460)} + 15.272703 \; ; \quad \text{where } p = \text{psia}, \; T = °F. \qquad (26\text{-b})$$

This match is claimed to have an average difference from the actual data of only 0.048%.

In oil and gas technology, the Cox Chart is a useful empirical technique for representing the vapor pressure curves of hydrocarbon fluids. This is a graph of ln p vs. 1/(T-77.4), T in °R, and it is useful because both hydrocarbon and water vapor pressure curves tend to graph as straight lines. Thus, by choosing two points for water at opposite ends of the vapor pressure curve we can determine that the equation of this straight line is of the form:[61]

$$\ln p = \frac{-7001.4928}{(T + 382.2)} + 14.46928 \text{ ; where } p = \text{psia}, T = {}^\circ\text{F}. \qquad (27)$$

This function is a match over the whole vapor pressure curve, whereas the Whiting and Ramey approximation is for the range 150–315°C. Finally, Farouq Ali[39] observed that a graph of pressure vs. temperature on log-log paper yields a straight line. Hence:

$$T = 115.1\ p^{0.225} \quad (T = {}^\circ\text{F},\ p = \text{psia}) \qquad (28\text{-a})$$

or

$$T = 116.7\ p^{0.225} - 17.778 \quad (T = {}^\circ\text{C},\ p = \text{bar}) \qquad (28\text{-b})$$

Equation 28 is reported to have a maximum of 1% error over the pressure range 1–200 bar (10–3,000 psia).

The specific volume of saturated steam, v_g, and water, v_f, are shown as a function of pressure on Figure 25. The overall specific volume of mixtures of steam and water can be determined at a particular pressure (or temperature) if the quality, x, of the mixture is known. Quality is defined:

$$x \triangleq \frac{\text{Mass of mixture as steam}}{\text{Total mass of mixture}} \qquad (29)$$

The effect of quality on specific volume can be seen on Figure 25, and can be calculated from tables using the relation:

$$v_{mix} = x\ v_g + (1 - x)\ v_f$$

$$= v_f + x\ v_{fg} \ , \qquad (30)$$

where v_{mix} = mixture specific volume

v_g = saturated gas specific volume

v_f = saturated liquid specific volume

$v_{fg} = v_g - v_f$

The second expression results in more accurate numerical results in hand calculations if steam quality is low.

The enthalpy of saturated steam and water is shown as a function of pressure in Figure 26. Points B and C on this diagram correspond with those on Figure 23. There is a maximum enthalpy of 2.8×10^6 Joules/kg (1204.8 Btu/lb_m) that saturated steam may have under any conditions. This occurs between 31.16 and 31.85 bar (452 and 462 psia).

The overall enthalpy of saturated mixtures can be calculated from the relation:

$$h_{mix} = x\, h_g + (1 - x)\, h_f$$
$$= h_f + x\, h_{fg} \qquad (31)$$

where h_{mix} = mixture specific enthalpy

h_f = saturated liquid specific enthalpy

h_g = saturated gas specific enthalpy

h_{fg} = latent heat of vaporization per unit mass

The specific enthalpy of such mixtures is shown in Figure 26.

The latent heat of vaporization per unit mass, h_{fg}, is the increase in enthalpy as a fluid vaporizes from saturated liquid to saturated steam at constant pressure or temperature. At atmospheric pressure h_{fg} is approximately 2.3×10^6 Joules/kg (1000 Btu/lb_m). Farouq Ali[39] (p. 5) has presented the approximation:

$$h_{fg} = 1318\ p^{-0.08774} \qquad (32)$$

for use in hand calculations. The maximum error is reported to be 1.9%. The units used in Eqn. 32 are p, psia; h_{fg}, Btu/lb_m.

There appears to be some uncertainty about the viscosity of saturated steam and water. Accepted values are presented in the ASME Steam Tables. Figure 27 shows the viscosity of saturated steam and water vs. temperature. The viscosities of the two phases tend to approach one another as they approach the critical temperature.

Farouq Ali[39] recommends use of the following equation for the viscosity of steam:

$$\mu/100 = 88.02 + 0.32827\ T + 0.0002135\ T^3 - \rho\ (1858 - 5.90\ T) \qquad (33)$$

where μ = viscosity of steam, centipoise

T = temperature, °C

ρ = density of steam, gm/cc

The density of steam can be determined from steam tables. For pressures up to 1000 psia, the density of steam can also be determined from the following relation developed by Farouq Ali (p. 22):

$$\rho = 0.0000440189\ p^{0.9588} \qquad (34)$$

where ρ = density of steam, gm/cc

p = pressure, psia

The thermal conductivity of water first increases as the temperature increases and reaches a maximum at about 150°C. Thereafter it decreases. This is shown in Figure 28.

Impure Saturated Water

Chemical content will tend to have the same effect on the properties of saturated water and steam as they will on the unsaturated phases. Hence, with the exception of the vapor pressure curve, discussion of the effect of impurities will be postponed until later sections.

The vapor pressure of water in a geothermal system will not necessarily be that presented in the steam tables. For a fixed pressure, the boiling temperature of water will be elevated by the presence of impurities. This is equivalent to a lowering of vapor pressure. However, the effect is usually rather small. For example, at 4.621 bar (67.013 psia) pure water would boil at 148.89°C (300°F), whereas a 100,000 ppm (parts per million) sodium chloride brine would boil at 150.62°C (303.113°F). This difference would probably not be measurable in a geothermal system. However, significant vapor pressure lowering has been observed with production of 350,000 ppm brines in the Imperial Valley, California.

The vapor pressure data presented in steam tables were measured for flat surface interfaces. If the steam-water interface is a strongly curved surface, as might occur in small pores in porous media, then there could be significant vapor pressure lowering effects (Calhoun, et al.[40]; Edlefsen and Anderson[41]). Cady, Bilhartz, and Ramey[42] have investigated this phenomenon with regard to geothermal aquifers. They did not observe vapor pressure lowering in unconsolidated sandstone cores. However, a recent study by Strobel[56] indicates a potential vapor pressure lowering at very low liquid contents in experiments with a single, consolidated core. Continued experimentation is in progress.

Pure Compressed Liquid Water

The compressed liquid region lies above the vapor pressure curves in the pressure-temperature planes of Figure 23 and Figure 24. Enthalpy and PVT behavior for compressed water is given in various tables[35,37] and in the ASME Steam Tables[36] for pressures up to 1070 bar (15,500 psia).

A technique commonly used in oil reservoir engineering for relating compressed water at some given reservoir condition to its state at surface conditions is via the formation volume factor, B_w. This is defined as the volume of liquid at reservoir conditions divided by the volume of liquid that would remain if it were brought to some standard surface conditions, commonly 20°C and 1 bar (70°F and 14.67 psia).

$$B_w \triangleq \frac{\text{initial volume of liquid at reservoir conditions}}{\text{volume of liquid remaining at standard conditions}} \qquad (35)$$

Figure 29 is a graph of the Formation Volume Factor, B_w, for pure liquid water as function of pressure and temperature. Note that for constant temperature, as pressure decreases, B_w increases slowly up to saturation conditions, below which it falls rapidly.

The specific volume-pressure behavior of a compressed liquid under an isothermal expansion or contraction process is often of interest (particularly in unsteady liquid flow through an aquifer). This P-V behavior is usually expressed in terms of the isothermal coefficient of compressibility, c_ℓ, which is defined:

$$c_\ell \triangleq -\frac{1}{v}\left(\frac{\partial v}{\partial p}\right)_T \qquad (36)$$

c_i can be viewed as the fractional decrease in specific volume caused by an isothermal unit increase in pressure. Although the isothermal compressibility of liquid water is often used in ground water hydrology and oil reservoir engineering, it appears to have been seldom reported for high values of temperature (greater than 120°C; 240°F). Table 1 summarizes high temperature results reported by Whiting and Ramey.[38] As can be seen, the isothermal compressibility for water is reasonably constant with pressure, but varies with temperature.

Table 2 presents the enthalpy of compressed pure water over a range of pressures and temperatures. It can be seen that the liquid enthalpy is only weakly dependent on pressure, but strongly dependent on temperature.

The viscosity of pure compressed water is presented in various Steam Tables.[35-37] The viscosity of high pressure liquid is almost constant with pressure, and generally only about 10-15% higher than the corresponding value for saturated liquid at the same temperature. Hence Figure 27, which shows the viscosity of saturated liquid as a function of temperature, can be used as a good estimate of compressed liquid viscosity.

The specific heat, c_p, of compressed water is also presented in the Steam Tables[35-37] for pressures up to 1035 bar (15000 psia). Values of c_p range from 4100 to 5000 Joules/Kg. °C (1.00 to 1.20 Btu/lb_m °F), except at temperatures greater than 260°C (500°F). Near the critical point values become very high.

Impure Compressed Water

The waters produced from geothermal systems often contain a dissolved chemical content high in chlorides and sulfates. Brines from some areas,

such as the Imperial Valley Salton Sea Geothermal Resource Area, have up to ten times the dissolved solids content of seawater. In addition, geothermal liquids often contain dissolved noncondensable gases.

Amyx, Bass and Whiting[43] (p. 450) state "Literature relative to the effect of composition on the properties (of water) is meager, and is limited to gas solubility data over the temperature range 32-250°F (0-121°C) at pressures ranging from 0-6000 psia (0-415 bar)." These authors summarize the work of numerous workers (Dodson and Standing[44], Rowe[45], Beal[46], Bridgman[47]) on the effect of natural gas solubility on the PVT behavior of water.

Long and Chierici[48] have presented experimental data on the PVT behavior of aqueous solutions of sodium chloride. Their results were measured for temperatures over the range 20-100°C, pressures from 2-500 kg/cm^2, and salinities from 0-300g/L. They also presented analytic curve matches giving density, ρ, as a function of salinity, pressure, and temperature over the range of experimental conditions. It is unfortunate that data for higher temperatures were not measured. But results do give a quantitative indication of the effect of chemical composition on the PVT behavior of water.

Amyx, Bass and Whiting[43] (p. 466) present data from Van Wingen[49] on the viscosity of oil field brines at pressures to 7100 psia, and temperatures to 300°F. This data suggests that dissolved solids have only a small effect on the viscosity of saline brines. Stanley and Batten[50] have presented data on the viscosity of sea water compared to pure water from 0-30°C. They observed that for practical purposes, the increase is not significant.

Although important information is available there is a need for PVT data for geothermal waters at conditions characteristic of geothermal reservoirs, showing the effect of chemical composition. In addition, more information is needed about the solubility and PVT characteristics of noncondensable gases dissolved in geothermal waters.

Pure Superheated Steam

Superheated steam occurs on the pressure-temperature plane at temperatures above the vapor pressure line, e.g., point A on Figure 23. This state is also called "dry" steam. The ASME Steam Tables[15] (1967, Table 3) present data for the enthalpy and PVT behavior of superheated steam for temperatures up to 815°C (1500°F). Figure 30 is a diagram showing the specific volume of dry steam as a function of pressure and temperature. One convenient means of calculating specific volumes of dry steam is via the real gas law equation of state:

$$Pv_g = \frac{zRT}{M} \qquad (37)$$

$$= z\bar{R}T$$

where P = pressure, bar

v_g = specific volume of steam, m^3/kg

z = gas law deviation (also compressibility) factor

$R = 0.08288 \ \frac{bar\ m^3}{kg_{mole}\ ^oK}$

M = molecular weight of water, 18 kg/kg_{mole}

$\bar{R} = R/M = 0.004605 \ \frac{bar\ m^3}{kg\ ^oK}$

T = absolute temperature, ^oK

OR, for English units

p = psia

v_g = ft /lb$_m$

$R = 10.72 \frac{\text{ft psia}}{16 \text{ mole}^\circ\text{R}}$

$M = 18 \text{ lb}_m/\text{lb}_{\text{mole}}$

$\bar{R} = 0.5956 \frac{\text{ft psia}}{\text{lb}_m {}^\circ\text{R}}$

$T = {}^\circ\text{R}$

The gas law deviation factor, z, for steam is presented in Figure 31.

Figure 32 presents a pressure-enthalpy diagram for superheated steam. Point A on this diagram corresponds to point A in Figure 23. If a dry steam reservoir were to produce at constant temperature, its state would follow the isotherms on Figure 32. As indicated by the arrow below point A, the produced steam would tend to increase in enthalpy. Whiting and Ramey[38] have suggested that this tendency is a potential means of identifying the initial state of a geothermal fluid reservoir as dry steam.

Values for the viscosity of superheated steam are presented in the ASME Steam Tables[34] (1967, Table 10 and Fig. 7). Table 3 presents values of dry steam viscosity over a range of conditions. Except near the vapor pressure curve, the viscosity of dry steam is essentially independent of pressure, and is also only slightly higher than that of saturated steam at the same temperature.

The specific heat at constant pressure, c_p, of dry (and saturated) steam is presented in Table 9 of the ASME Steam Tables. Except near the vapor pressure curve and at higher pressures and temperatures, it is approximately 2100 J/kg-$^\circ$C (0.5 Btu/lb$_m$-$^\circ$F).

Mixtures of Dry Steam and Other Noncondensable Gases

Two of the recognized dry steam geothermal reservoirs in the world (the Geysers Field in California, and Larderello in Italy) are known to produce quantities of noncondensable gases along with their steam. Typically such gases contain carbon dioxide, hydrogen sulfide, ammonia, methane, and ethane. The quantity and proportions produced vary as a function of time, flow rate, and from well to well over the fields.

It is clear that the noncondensable gas content of a dry steam reservoir will effect the thermodynamic and transport properties of the produced fluid. Unfortunately, almost no experimental work seems to have been done on the properties of dry steam and noncondensable gas mixtures. However, generalized correlations have been extensively developed for natural gas mixtures of hydrocarbons. These correlations are based on reduced pressures and temperatures:

$$\text{Reduced Pressure, } p_r \triangleq \frac{\text{actual pressure}}{\text{pseudo critical pressure}} \tag{38}$$

$$\text{Reduced Temperature, } T_r \triangleq \frac{\text{actual temperature}}{\text{pseudo critical temperature}} \tag{39}$$

where the pseudo critical pressure and temperature are the molar average of the component critical values.

Amyx, Bass and Whiting[61] (pp. 260-268) have discussed and summarized correlations available for determining the PVT behavior of mixtures of natural gases with impurities such as nitrogen and carbon dioxide. On the basis of their discussion, the best method for estimating the effect of a noncondensable gas on steam compressibility appears to be through the use of an additive compressibility factor as first defined by Eilerts et al.[51]

$$Z_a = Z_{st} Y_{st} + Z_{ncg} Y_{ncg} \quad (40)$$

where Z_a = additive compressibility factor

Z_{st} = steam compressibility factor

Y_{ncg} = noncondensable gas compressibility factor

Z_{st} = Mole fraction steam in mixture

Y_{ncg} = mole fraction noncompressible gas in mixture

Amyx, Bass and Whiting[43] (pp. 260-268) present graphs of the compressibility factor, z, for nitrogen (from Eilerts et al.[51]), carbon dioxide (from Olds et al.[52]), and hydrogen sulfide (from Reamer et al.[53]). For purposes of reservoir calculations, it is expected that the noncondensable gas content of many geothermal steams will have a minimal effect on PVT behavior.

The effect of noncondensable gases on geothermal steam viscosity is also of interest. Again, there appears to be almost no experimental data available, and we must resort to correlations. Amyx, Bass and Whiting[43] (pp. 278-286) present the results of numerous correlations for natural gases. On the basis of their discussion, a rule proposed by Herning and Zipperer[54] for calculating the viscosity of mixtures of gases appears to be the most promising correlating method. In this rule the viscosity of the mixture, μ_m, is given by

$$\mu_m = \frac{\sum_{i=1}^{n} \mu_i Y_i M_i}{\sum_{i=1}^{n} Y_i M_i} \quad (41)$$

where μ_m = viscosity of mixture

μ_i = viscosity of i^{th} component

M_i = molecular weight of i^{th} component

Y_i = mole fraction of the i^{th} component in mixture

n = total number of components in the mixture

Basically this is an averaging calculation weighted by the mass of each component present. The viscosity of various gases over a range of temperatures can be found in standard physical properties reference books (e.g., see Weast[55], pp. F41-F44). For practical purposes, the noncondensable gas content will not significantly affect the viscosity of most geothermal steams.

A Note on Units

In general, equations and numerical values have been expressed in metric units (bar, °C, m, kg), with values for engineering units given in parenthesis (psia, °F, ft, lb_m). Viscosity is given in centipoise. For convenience of writing this is not true in every case. Units are always specified where equations are presented throughout the paper.

Note the following conversions:

Pressure:	1 psia	= 0.06895 bar
	1 bar	= 1.0197 kg/cm^2
	1 bar	= 0.9869 atm.
Specific Volume:	1 ft^3/lb_m	= 0.062428 m^3/kg
	1 ft^3/lb_m	= 62.43 cc/gm
Enthalpy:	1 Btu/lb_m	= 2324.4 Joules/kg
Viscosity	1 c.p.	= 6.72×10^{-4} lb_m ft sec
	1 c.p.	= 2.089×10^{-5} lb_f sec/ft^2

Acknowledgment

Preparation of this report was funded by the National Science Foundation as a portion of the study "Stimulation of Geothermal Aquifers," Grant No. GI-34925, principal investigators Drs. Paul Kruger and Henry J. Ramey, Jr., Stanford University.

TABLE 1

Isothermal Compressibility of Liquid Water, $psia^{-1}$

p,psia	300°F	400°F	500°F
700	3.793×10^{-6}	5.811×10^{-6}	7.146×10^{-6}
800	3.795×10^{-6}	5.815×10^{-6}	7.152×10^{-6}
1000	3.913×10^{-6}	5.821×10^{-6}	10.703×10^{-6}

TABLE 2

Enthalpy of Compressed Water in Btu/lb

and Joules/kg $\left[\text{(Btu/lb)}/\text{(J/kg)}\right]$ at Various Pressures and Temperatures

(Data from Ref. 36)

Temperature		Pressure, psia/bar				
°F	°C	$100/6.9$	$500/34.5$	$1000/69.0$	$2000/138.$	$5000/345$
70	21	$38.33/8.91\times10^{4}$	$39.44/9.17\times10^{4}$	$40.82/9.49\times10^{4}$	$43.58/1.013\times10^{5}$	$51.7/1.202\times10^{5}$
200	93	$168.3/3.91\times10^{5}$	$169.2/3.93\times10^{5}$	$170.3/3.96\times10^{5}$	$172.6/4.01\times10^{5}$	$179.5/4.17\times10^{5}$
400	204	X	$375.4/8.73\times10^{5}$	$376.0/8.74\times10^{5}$	$377.2/8.77\times10^{5}$	$381.2/8.86\times10^{5}$
600	316	X	X	X	$614.5/1.43\times10^{6}$	$604.6/1.40\times10^{6}$

TABLE 3

Viscosity in Centipoise of Superheated Steam at Various Conditions

(Data from Ref. 36)

Temperature		Saturation Conditions			Pressure psia bar						
°F	°C	P, psia	P, bar	.c.p.	1/.06895	5/.345	10/.690	50/3.45	100/6.9	500/34.5	1000/69
200	93	11.5	.79	.01	.012	.012	.012	X	X	X	X
300	149	67	4.62	.014	.014	.014	.014	.014			
400	204	247.3	17.1	.0155	.016	.016	.016	.016			
500	260	681	47.0	.0177	.0186	.0186	.0186	.0186	.0186	.0180	
600	316	1543	106.4	.02	.02	.02	.02	.02	.02	.02	.02

FIGURE 1

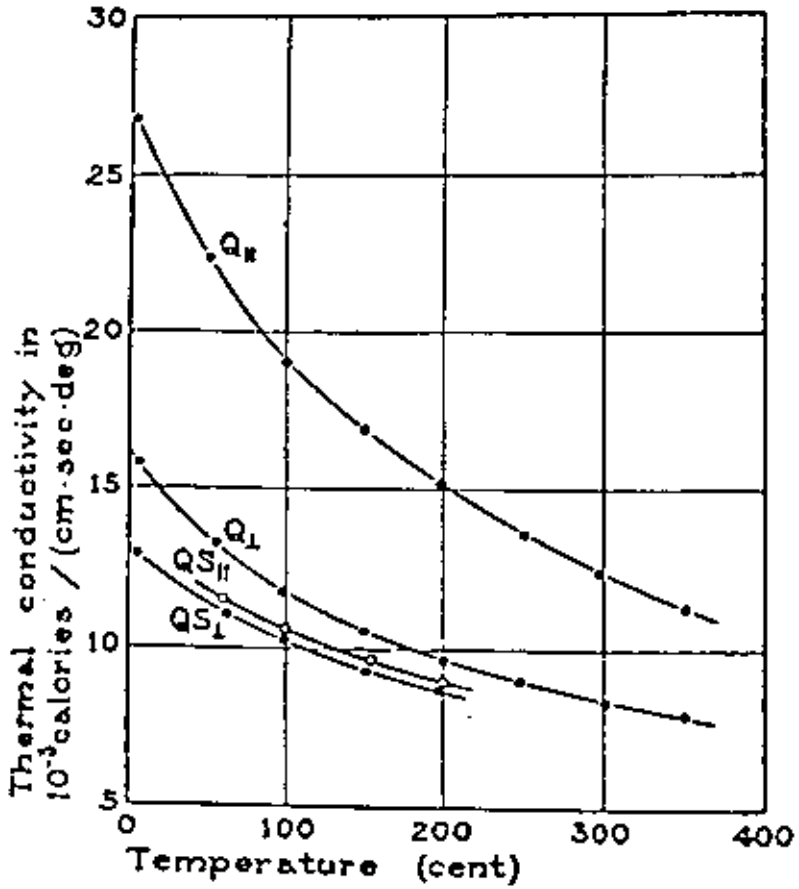

Thermal conductivity of quartz and of a quartzitic sandstone.

$QS_{\perp}$	Quartzitic sandstone, Penn., $\perp$ bed-plane.
$QS_{\parallel}$	Quartzitic sandstone, Penn., $\parallel$ bed-plane.
$Q_{\perp}$	Quartz single crystal $\perp$ optic axis.
$Q_{\parallel}$	Quartz single crystal $\parallel$ optic axis.

(Ref. 1)

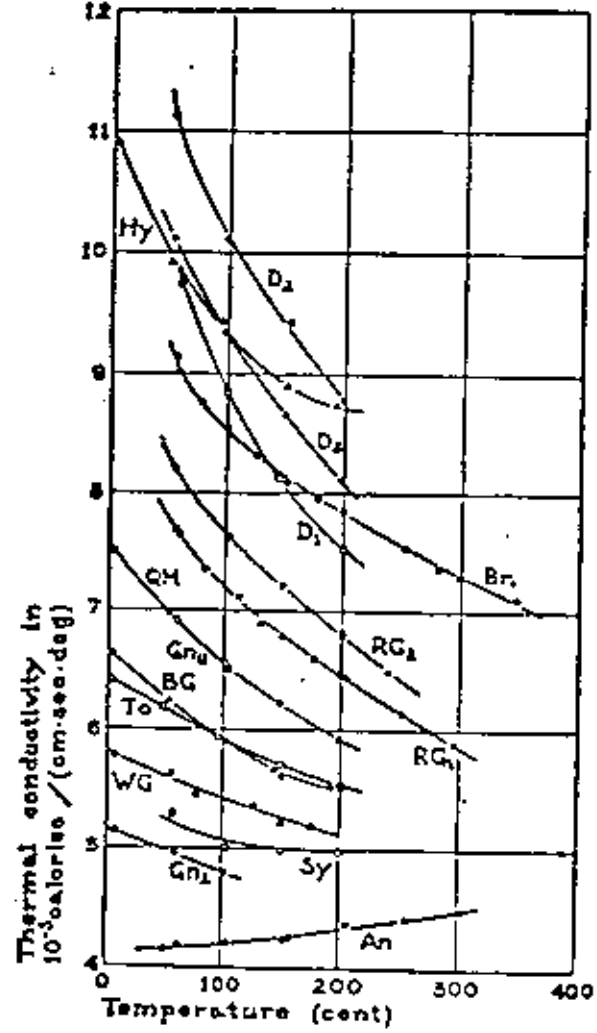

FIGURE 2 Thermal conductivity of holocrystalline rocks. (Ref. 1)

An	Anorthosite, Quebec.	RG_2	Rockport Granite 1.
$Ge_{\perp}$	Gneiss, Pelham, $\perp$ bed-plane.	RG_1	Rockport Granite 2.
$Ge_{\parallel}$	Gneiss, Pelham, $\parallel$ bed-plane.	Br	Bronzitite.
Sy	Syenite, Ontario.	Hy	Hypersthenite.
WG	Westerly Granite.	D_1	Dunite 1.
To	Tonalite, Calif.	D_3	Dunite 3.
BG	Barre Granite.	D_2	Dunite 2.
QM	Quartz monzonite, Calif.		

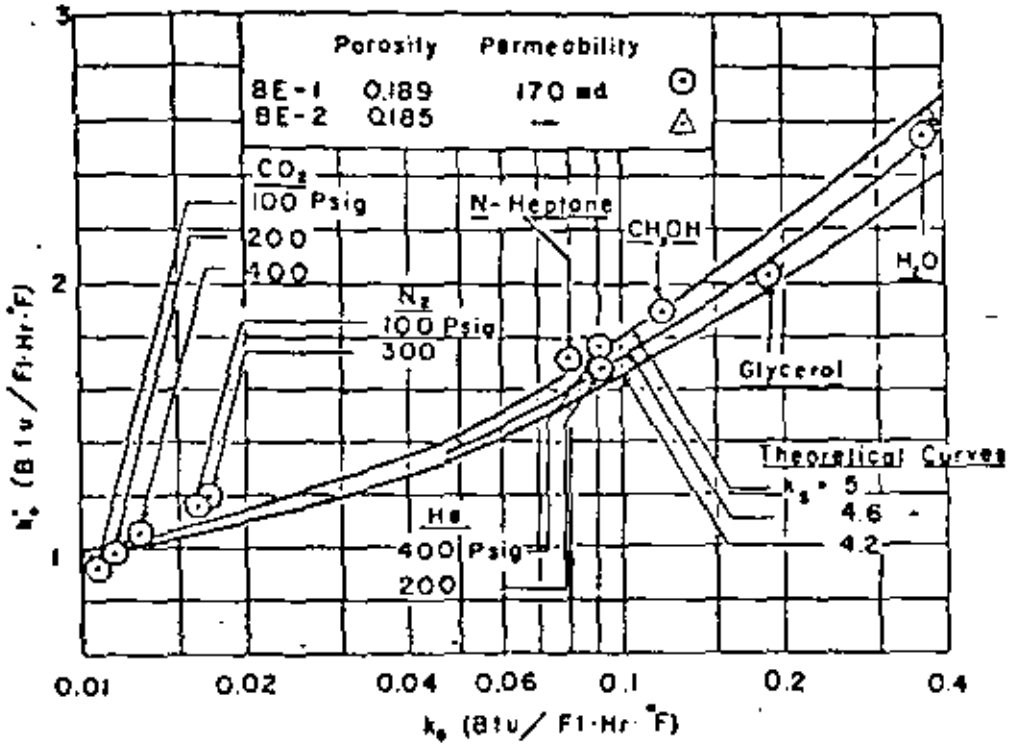

FIGURE 3 — STAGNANT CONDUCTIVITIES VS CONDUCTIVITIES OF FLUIDS, BEREA SANDSTONE.
(Ref. 4)

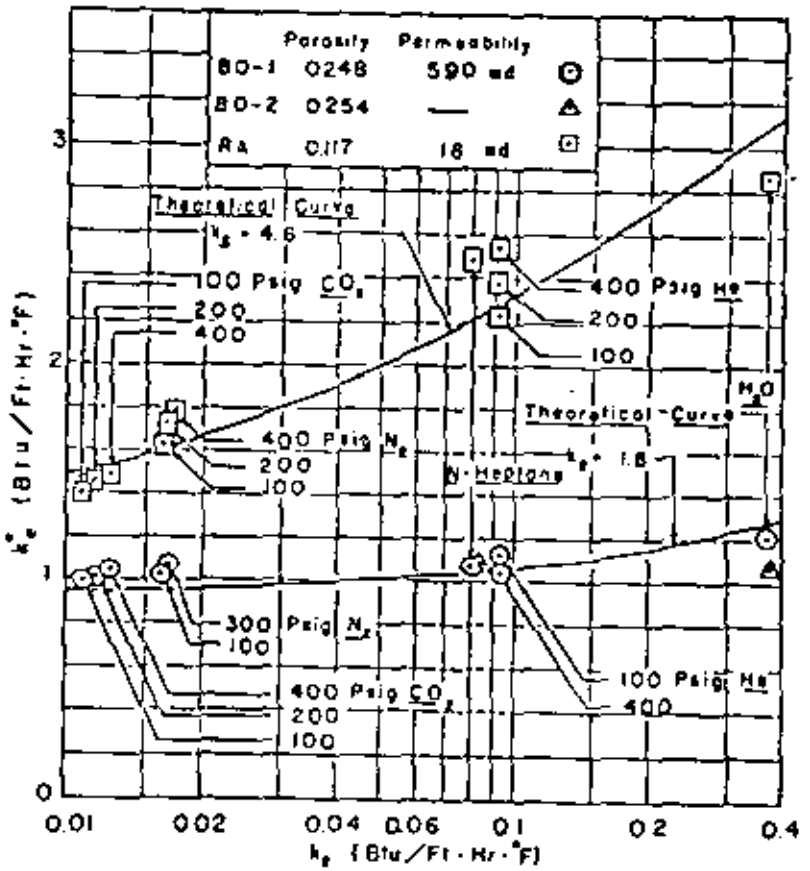

FIGURE 4 — STAGNANT CONDUCTIVITIES VS CONDUCTIVITIES OF FLUIDS, BOISE AND RANGELY SANDSTONES.
(Ref. 4)

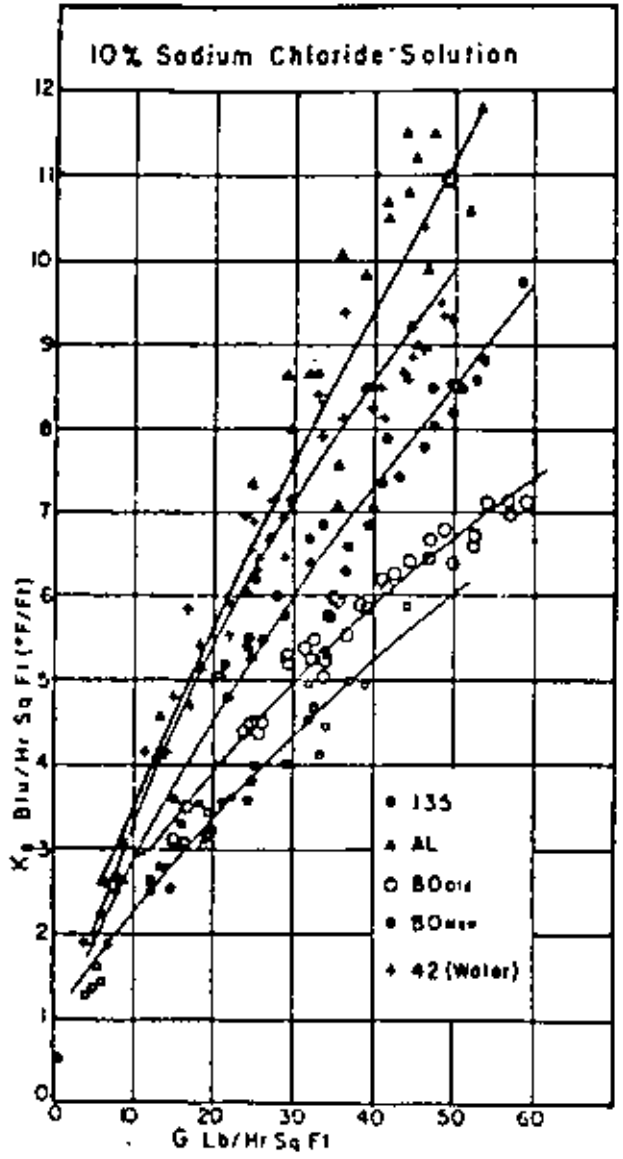

FIGURE 5 —Effective thermal conductivity (Ke) as a function of mass flow rate (G). See Ref. 5 for legend. (After Adivarahan, Kunii and Smith, Courtesy Soc. of Petrol. Engrs. of AIME.) (Ref. 5)

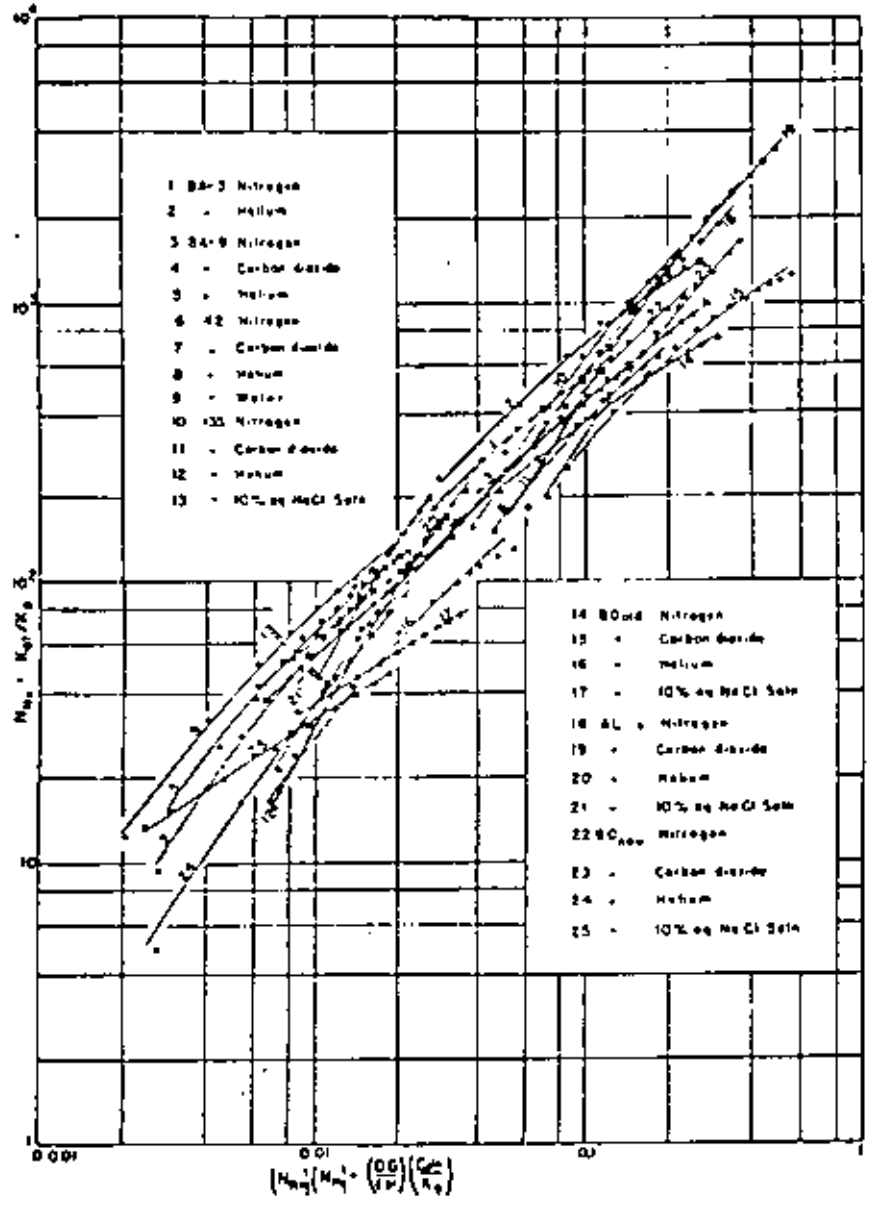

FIGURE 6 — CORRELATION OF k_{gt}/k_g WITH $(DG/\epsilon\mu)(C_p\mu/k_g)$. (Ref. 5)

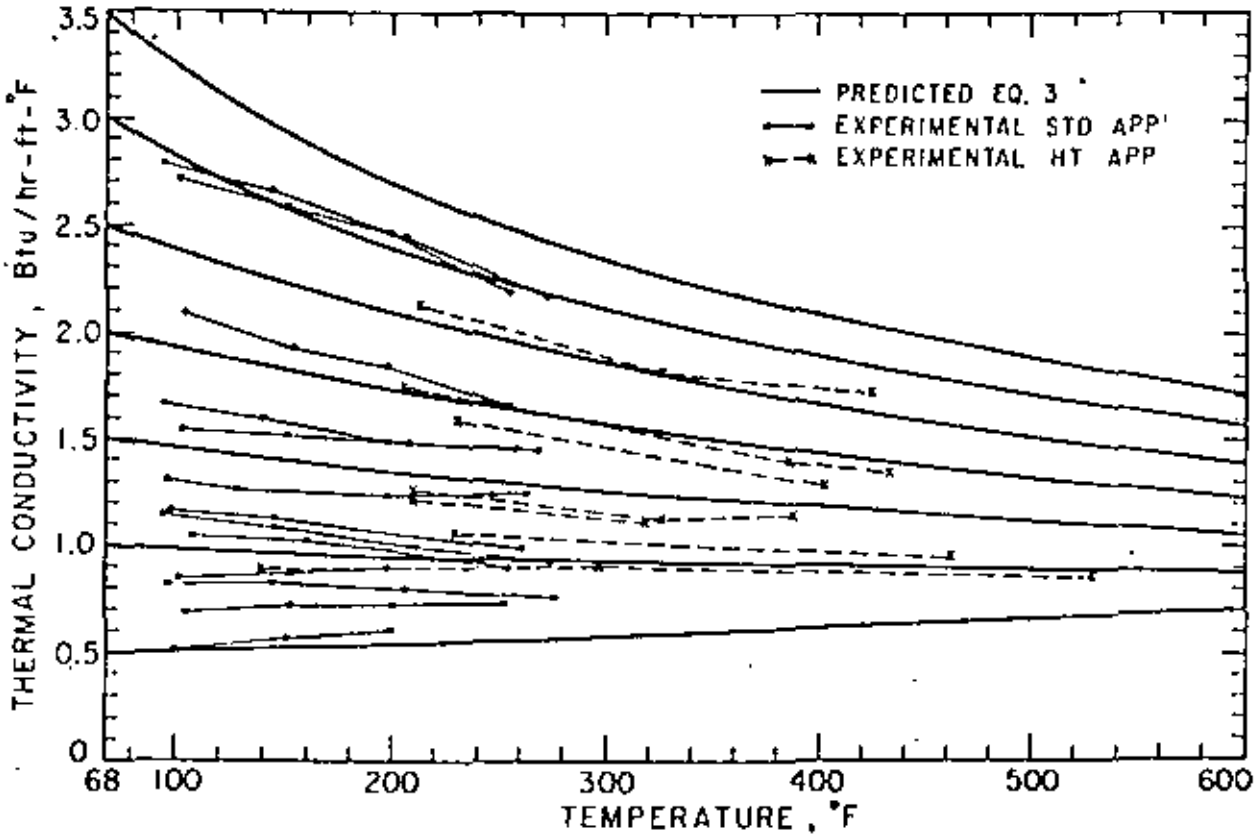

554

IGURE 7 Effect of Temperature on Thermal Conductivity of Sandstone. (Ref. 7)

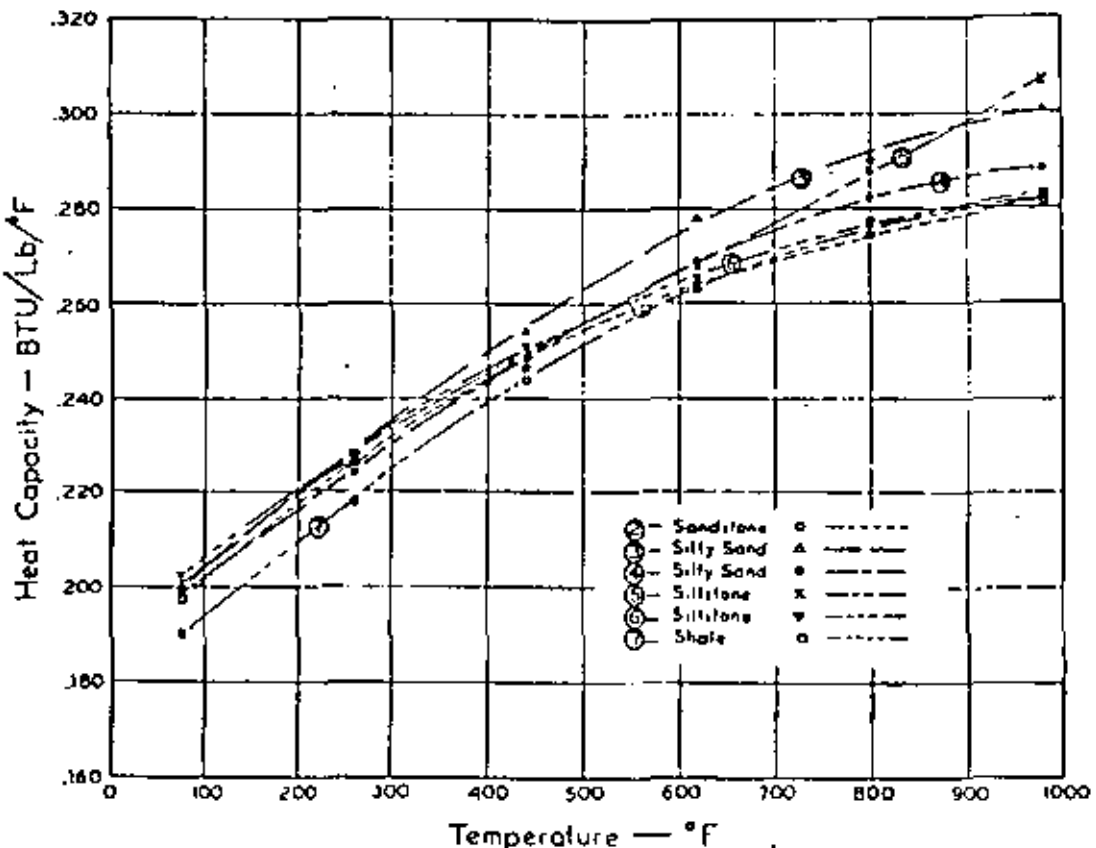

555

FIGURE 8 -Experimental Heat Capacities. (Ref. 3)

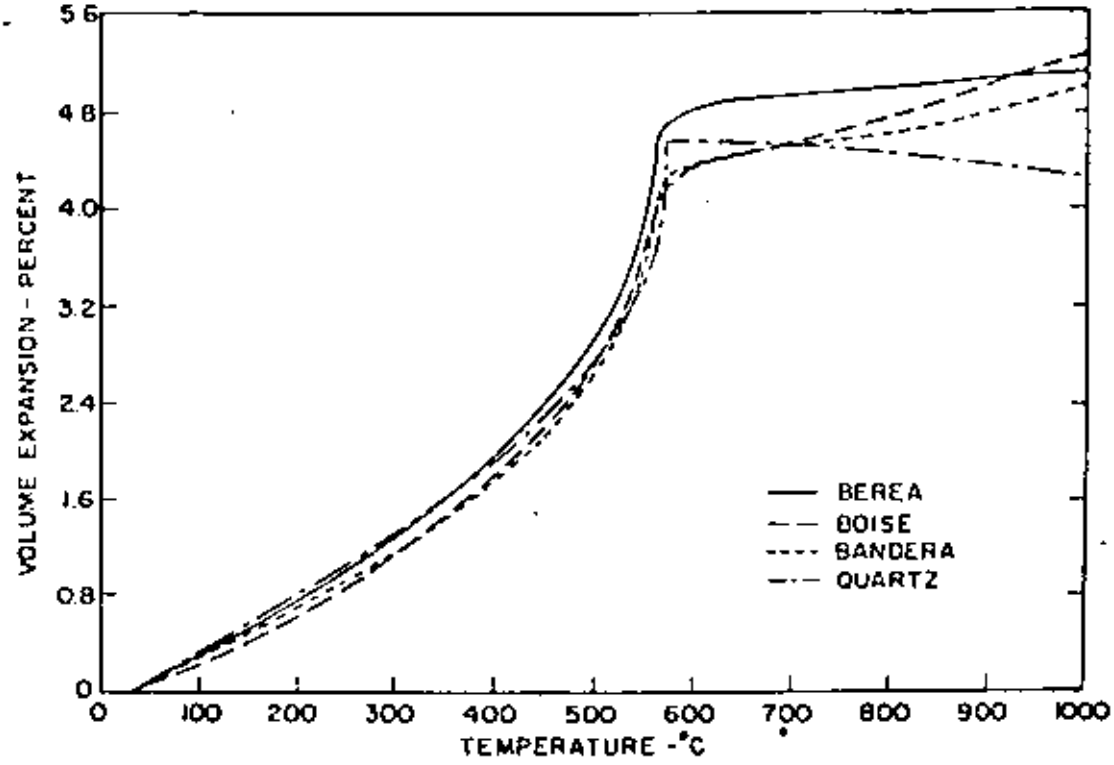

556

FIGURE 9 — VOLUME EXPANSION OF SANDSTONES.
(Ref. 12)

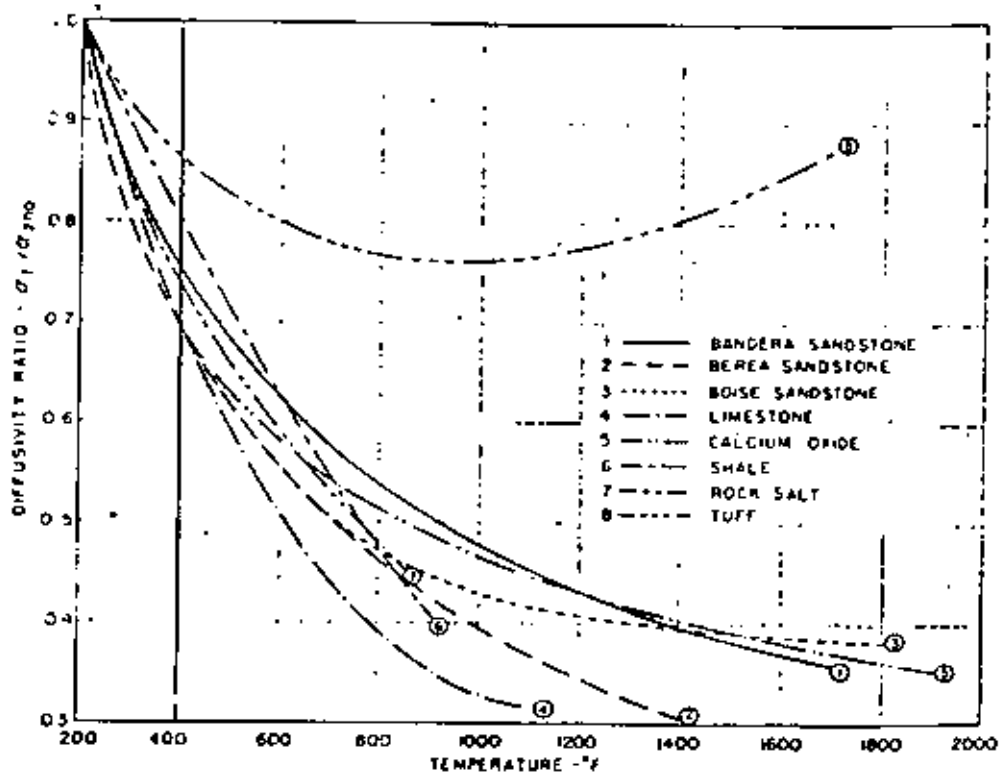

557

FIGURE 10 —THERMAL DIFFUSIVITY RATIO, INITIAL RUNS.
(Ref. 13)

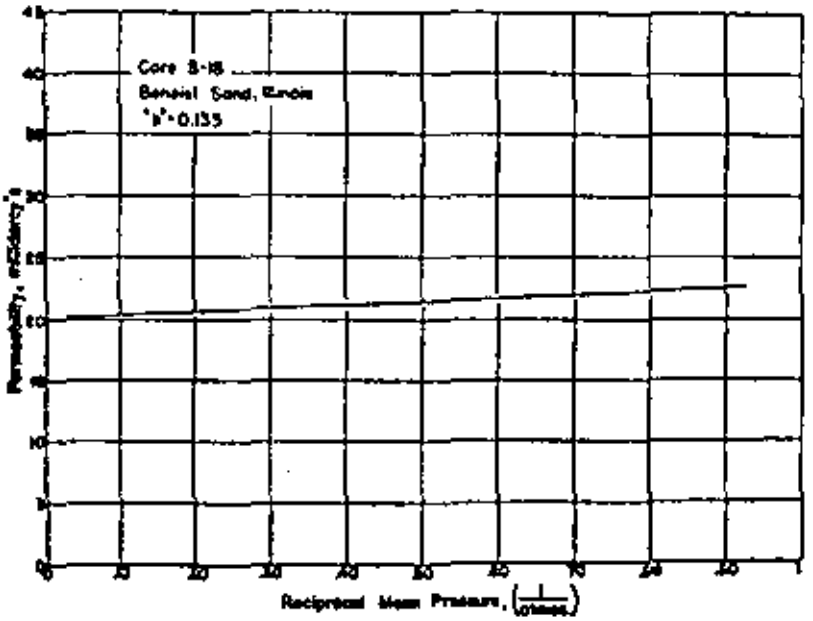

FIG. 5

558

FIGURE 11 **Relationship between the Permeability to Gas and the Mean Pressure at which Gas Flows through a Medium, a Relationship Making Possible the Determination of the Permeability of the Medium to a Non-Reacting Liquid**

(From API RP 27, Am. Petr. Inst., Aug. 1956)

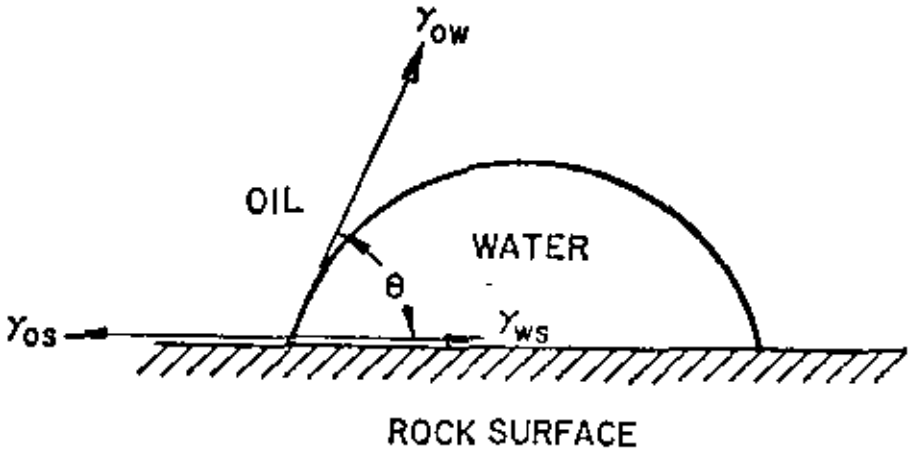

559

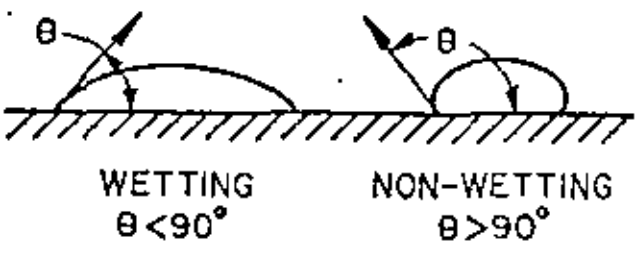

FIGURE 12 **Relationship between preferential wetting and contact angle.** (Ref. 15)

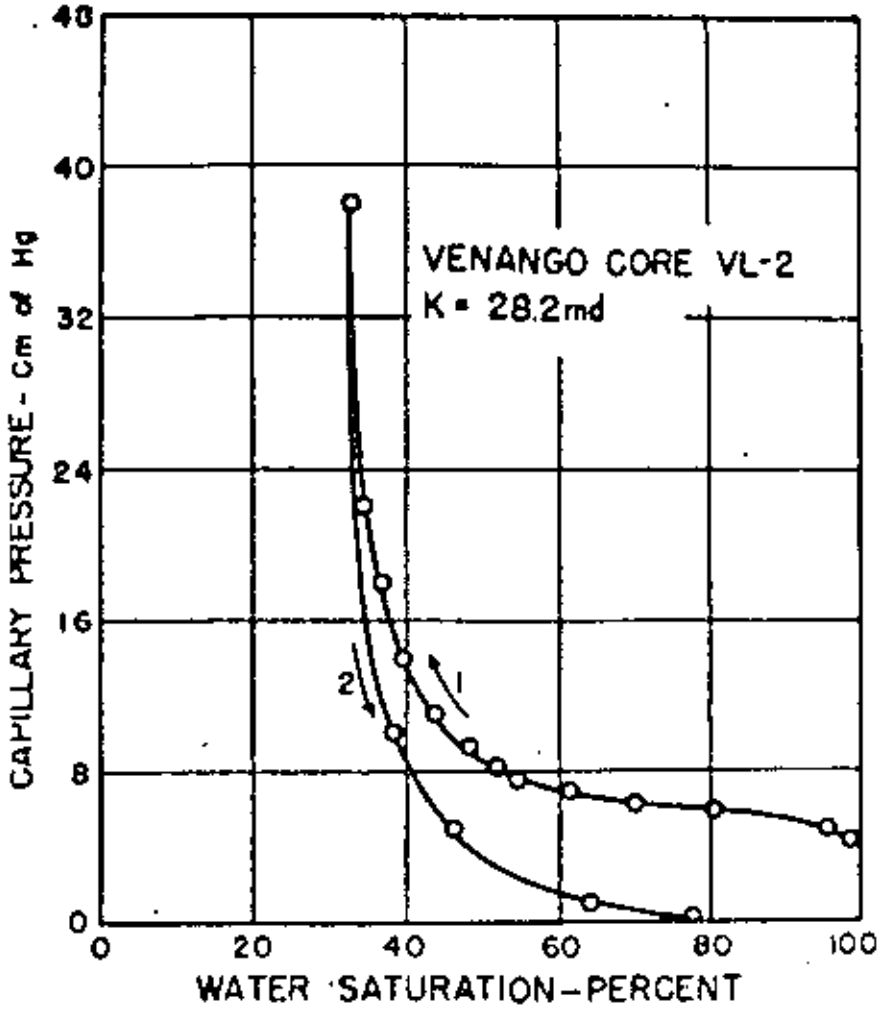

560

FIGURE 13 —Capillary pressure vs. water saturation.

Ref. 16)

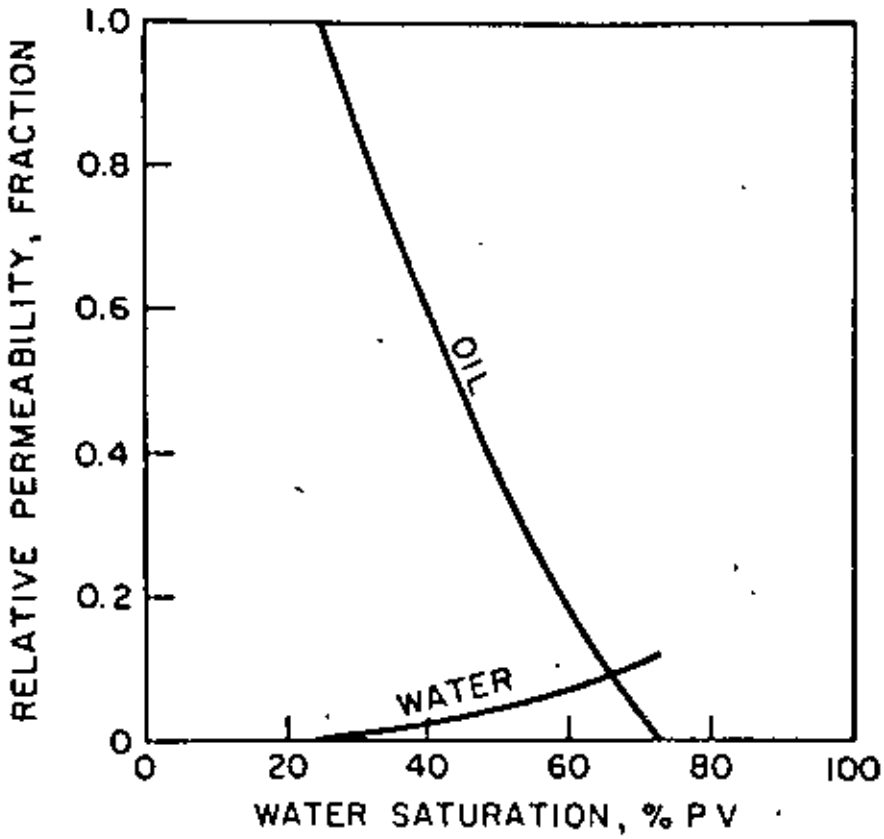

561

FIGURE 14 Typical water-oil relative permeability characteristics, strongly water-wet rock. (Ref. 17)

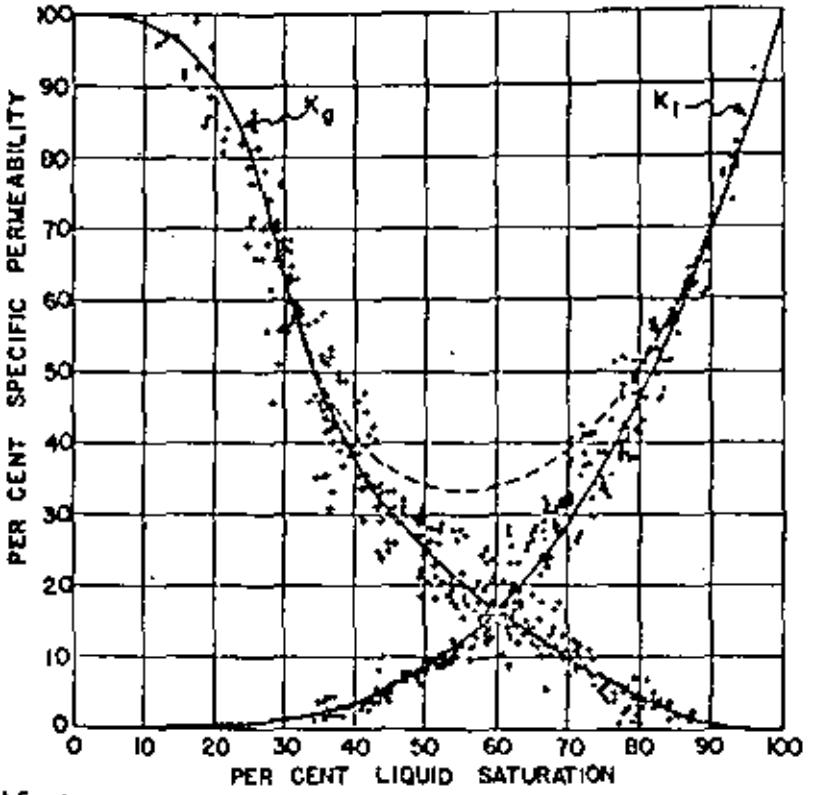

562

FIGURE 15 -PERMEABILITY-SATURATION DATA FOR FOUR DIFFERENT SANDS, INCLUDING THOSE OF FIGS. 4 AND 5.

(Ref. 18)

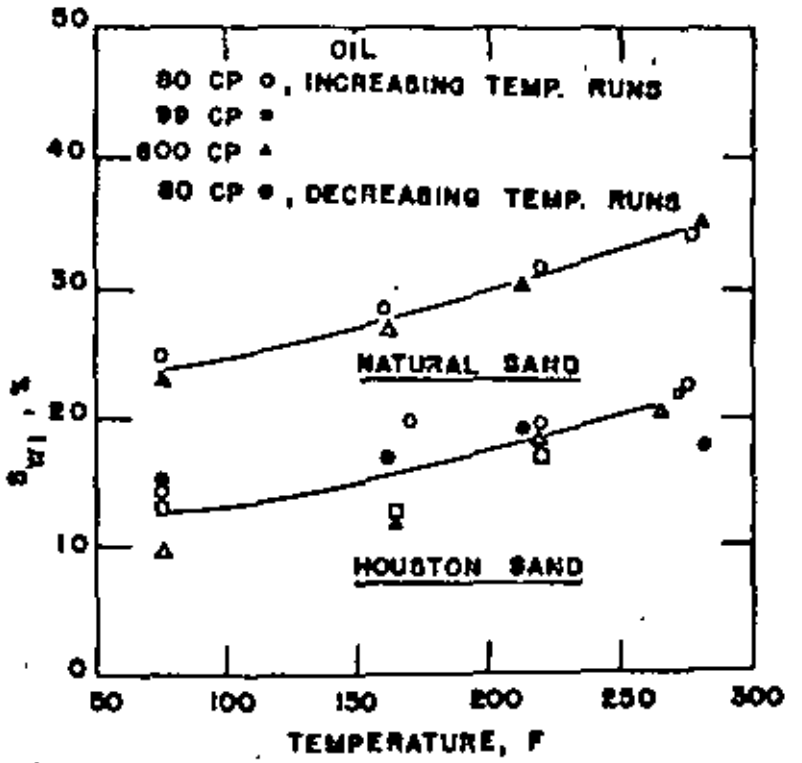

563

FIGURE 16

IRREDUCIBLE WATER SATURATION VS TEMPERATURE FOR HOUSTON SAND AND NATURAL SAND. (Ref. 19)

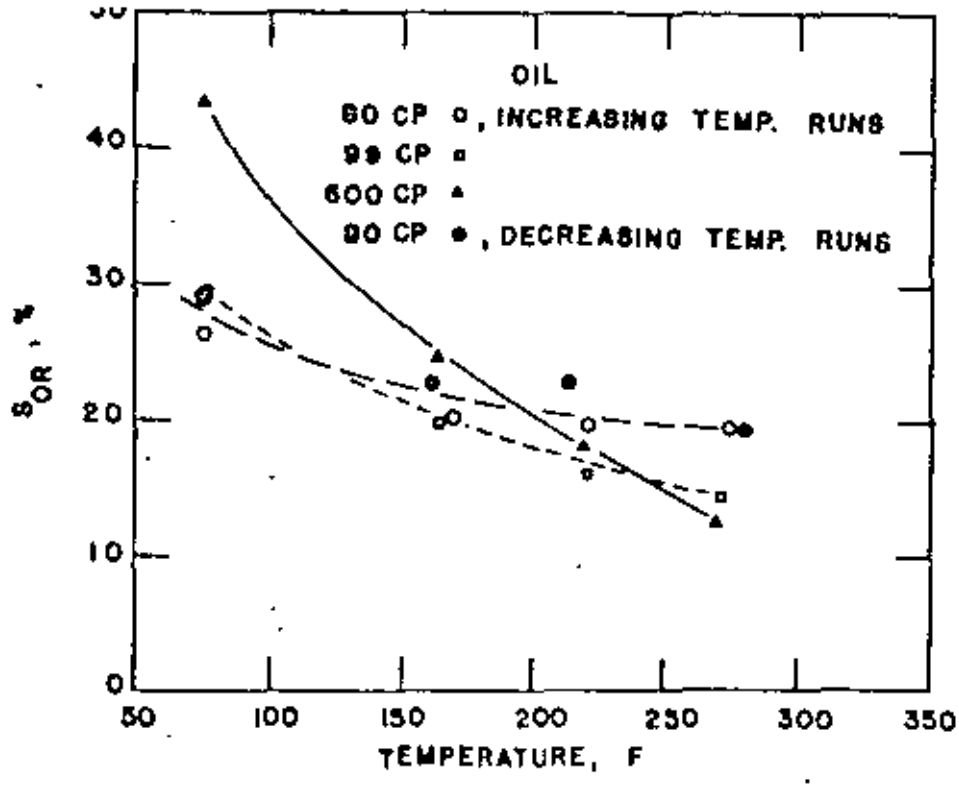

364

FIGURE 17 RESIDUAL OIL SATURATION VS TEMPERATURE FOR HOUSTON SAND. (Ref. 19)

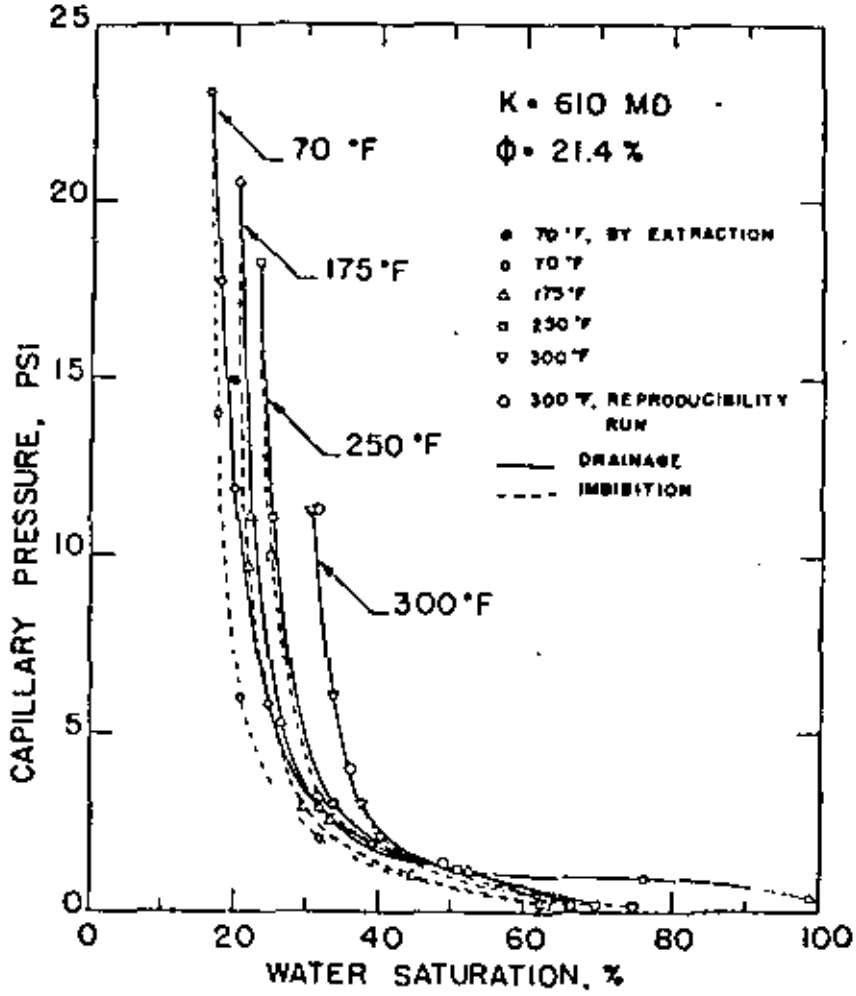

565

FIGURE 18 Capillary pressure vs water saturation for Berea sandstone core A. (Ref. 20)

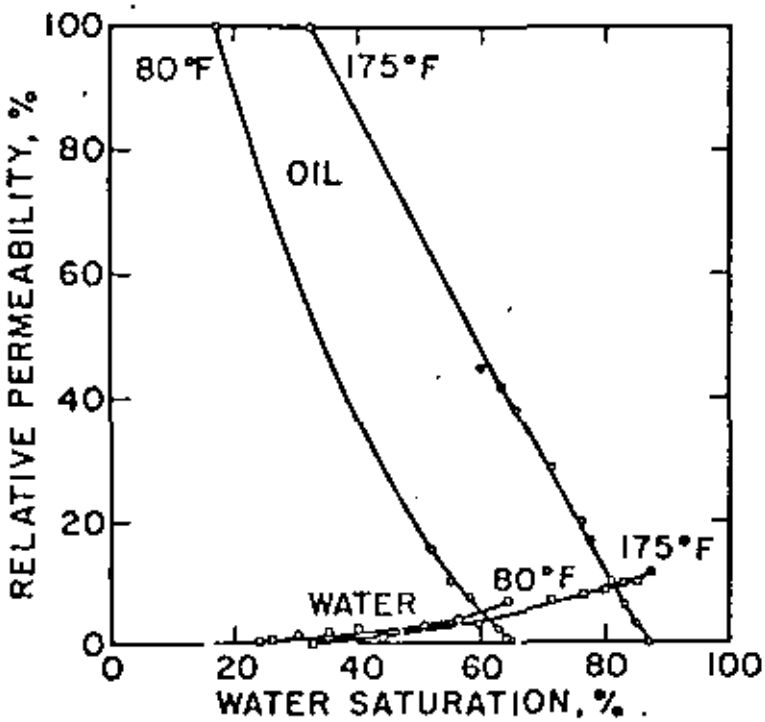

566

FIGURE 19 Individual relative permeabilities as a function of temperature; Core 4, Boise sandstone. (Ref. 21)

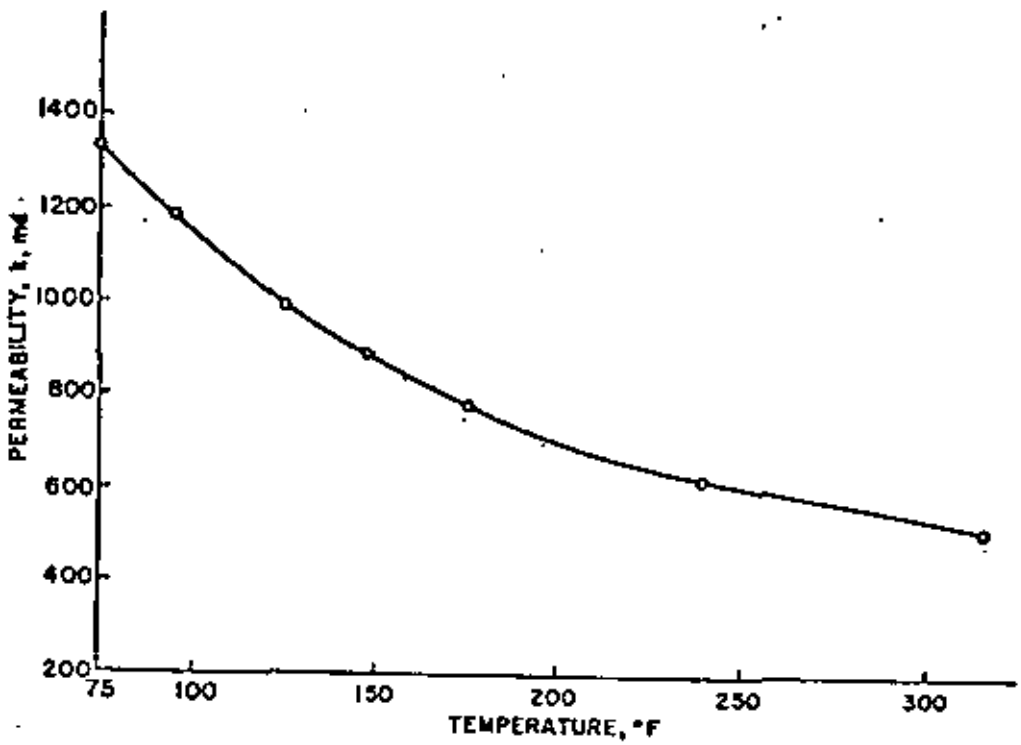

567

FIGURE 20 EFFECT OF TEMPERATURE ON ABSOLUTE PERMEABILITY OF BOISE SANDSTONE; CORE NUMBER 7 (Ref. 21)

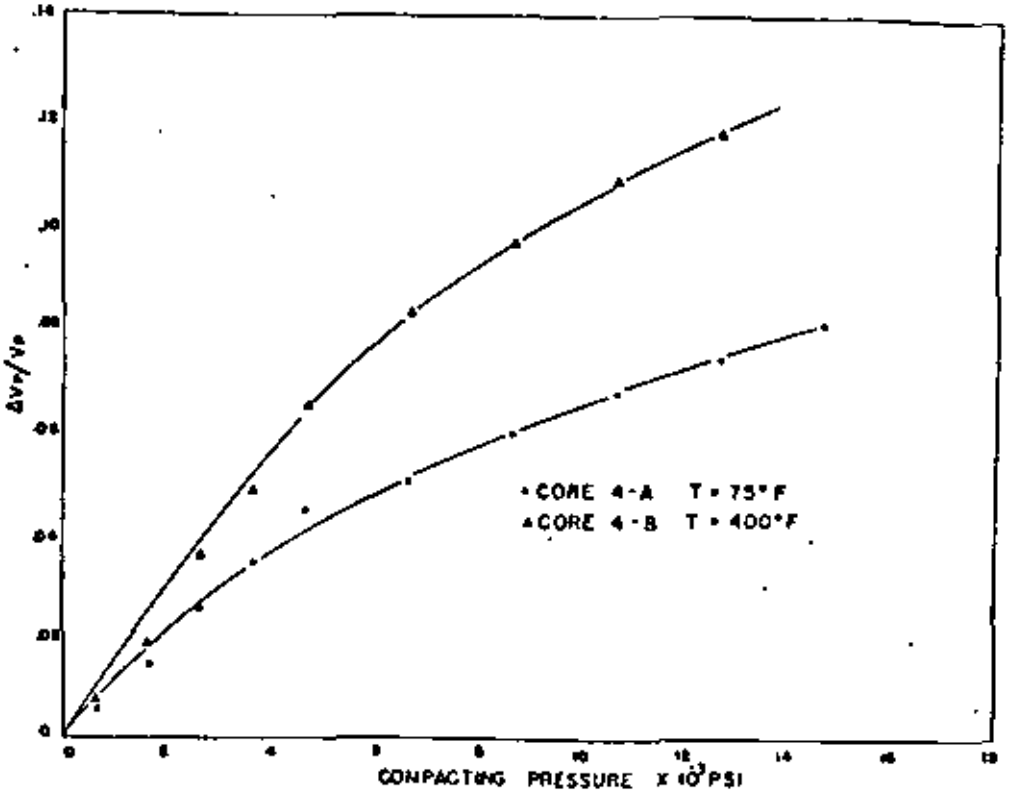

568

FIGURE 21 - Change in cumulative fractional pore volume with pressure core 4 at 75 and 400°F. (Ref. 24)

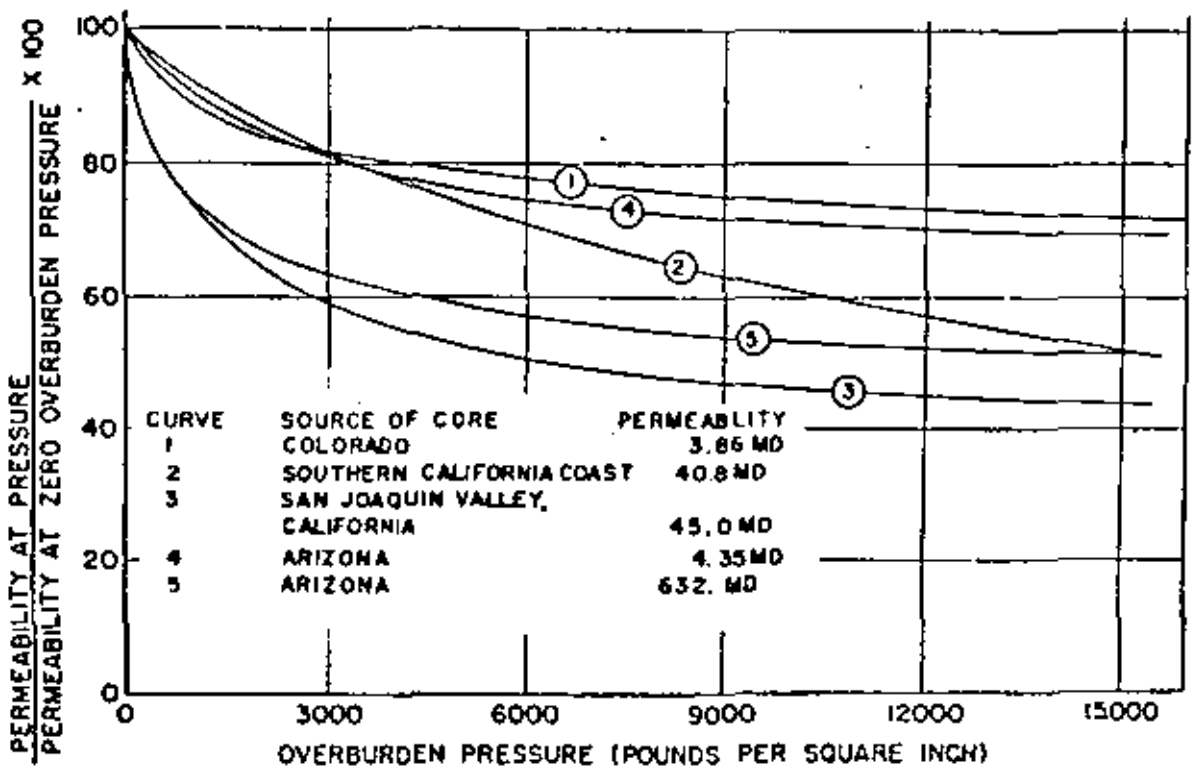

569

FIGURE 22 CHANGE IN PERMEABILITY WITH OVERBURDEN PRESSURE. (Ref. 26)

FIGURE 23

PRESSURE-TEMPERATURE DIAGRAM FOR WATER

(Ref. 38)

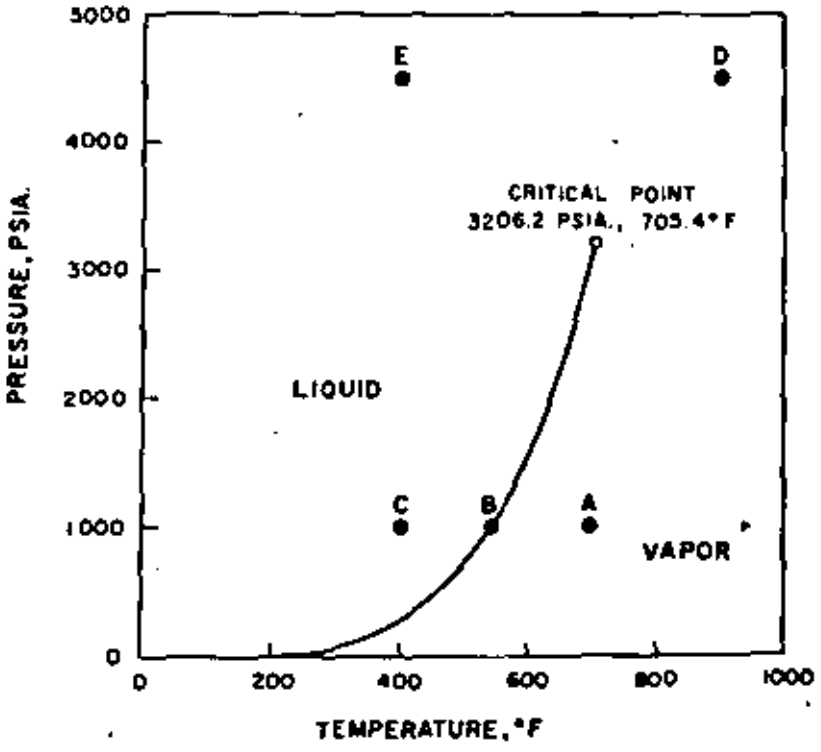

570

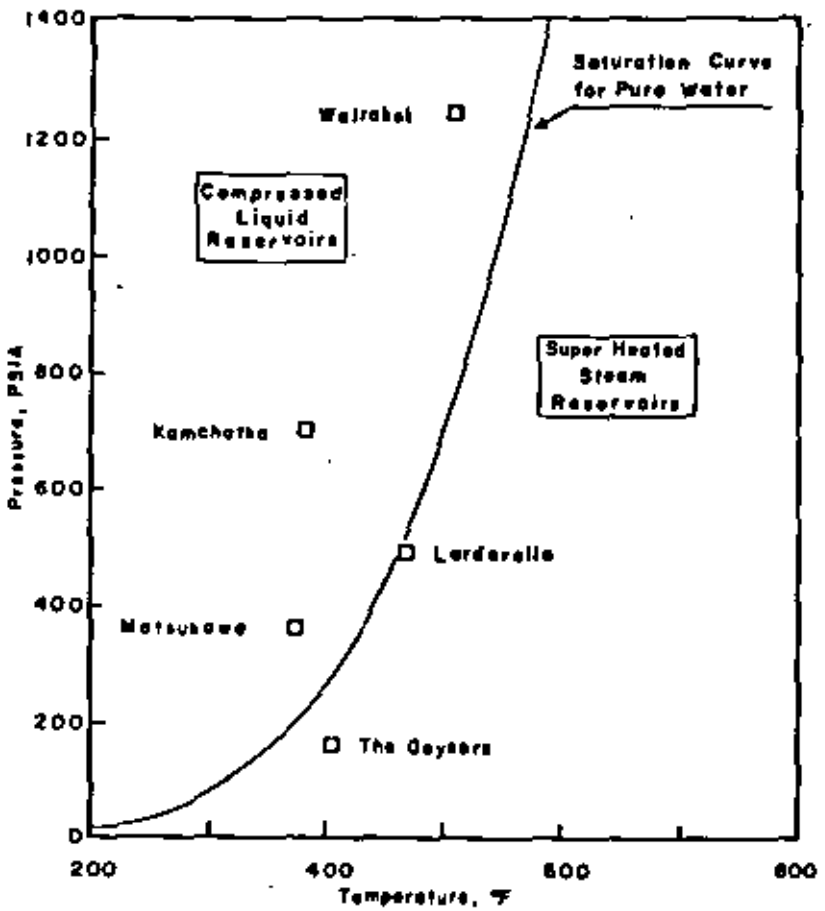

571

FIGURE 24 Reservoir temperature and pressure data for geothermal reservoirs

(Ref. 60)

FIGURE 25

PRESSURE-SPECIFIC VOLUME CHART FOR WATER

(Ref. 38)

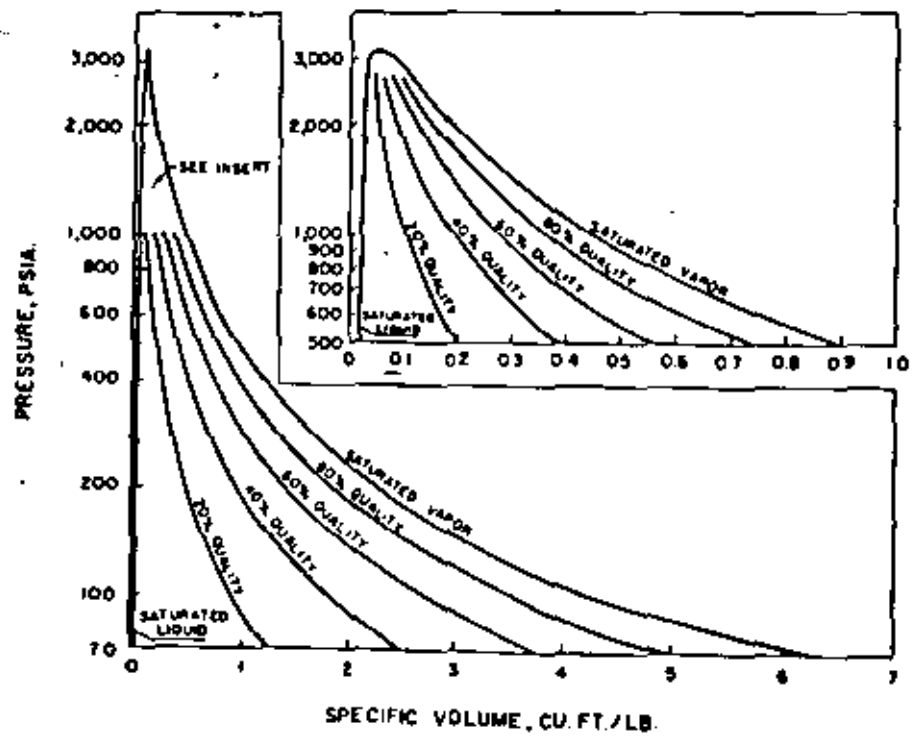

572

FIGURE 26

PRESSURE - ENTHALPY DIAGRAM FOR WATER

(Ref. 38)

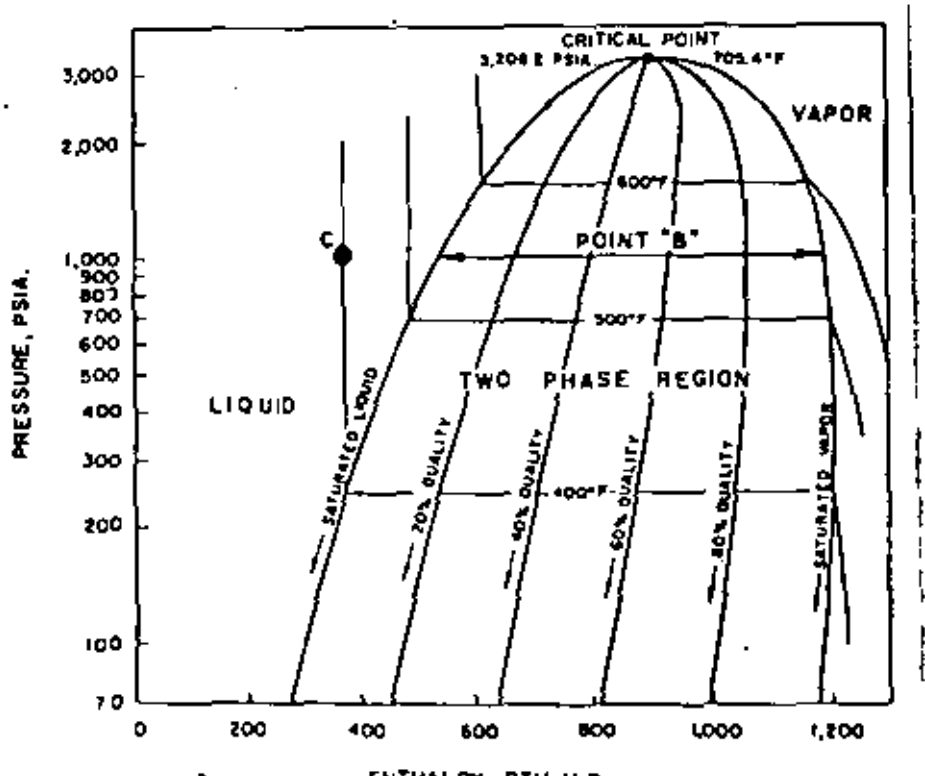

573

FIGURE 27

Viscosity of Saturated Water and Steam

(modified from Ref. 38)

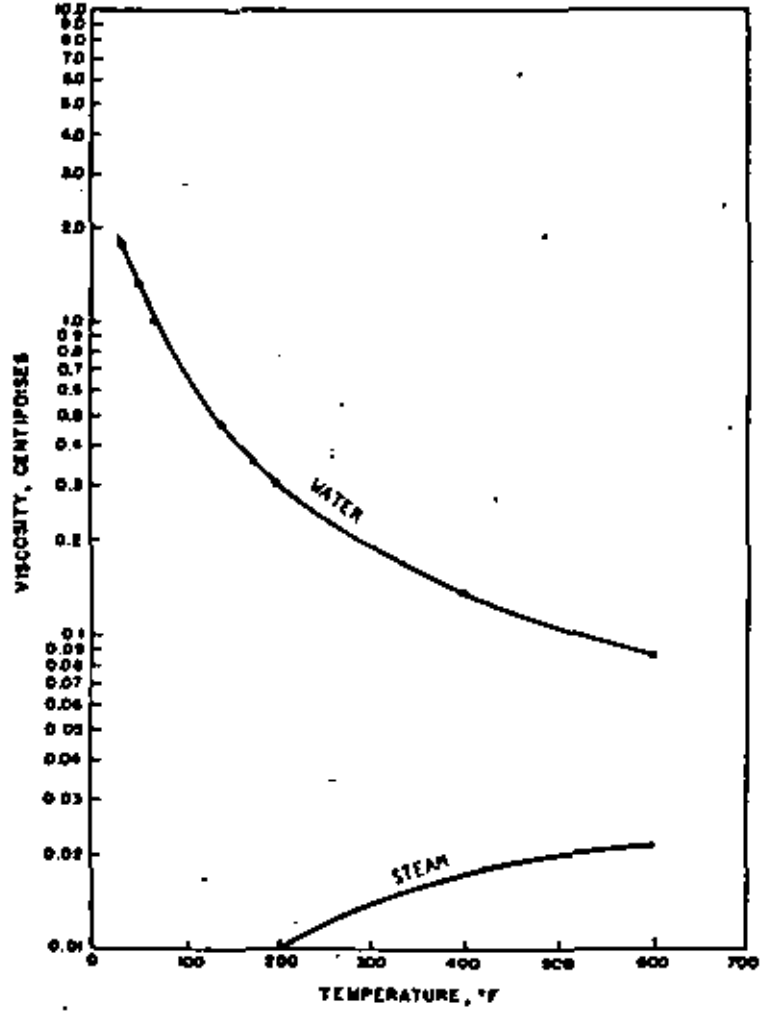

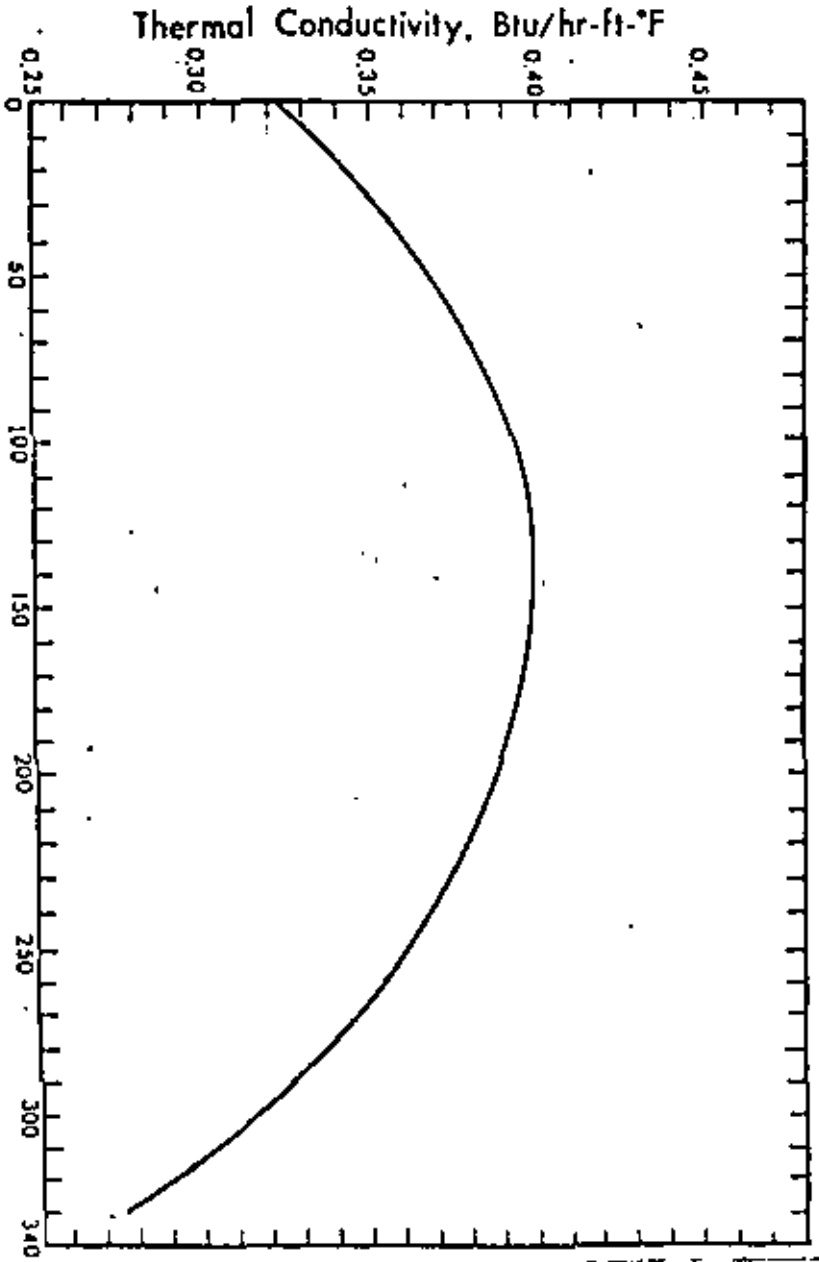

FIGURE 28. THE THERMAL CONDUCTIVITY OF SATURATED LIQUID WATER (Ref. 39)

FIGURE 29

FORMATION VOLUME FACTOR FOR PURE LIQUID WATER AS A FUNCTION OF PRESSURE AND TEMPERATURE

(Ref. 38)

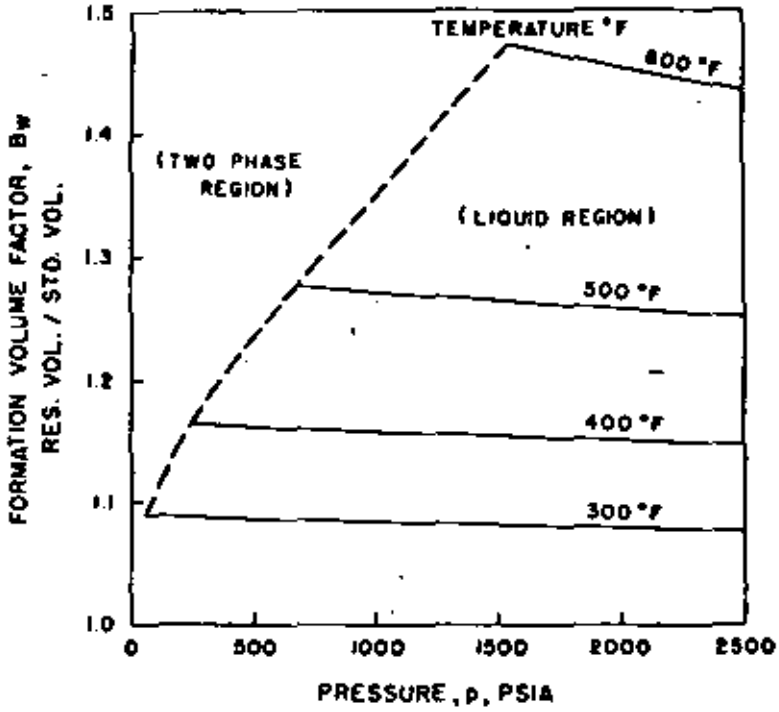

576

FIGURE 30

PRESSURE - SPECIFIC VOLUME CHART FOR SUPERHEATED STEAM

(Ref. 38)

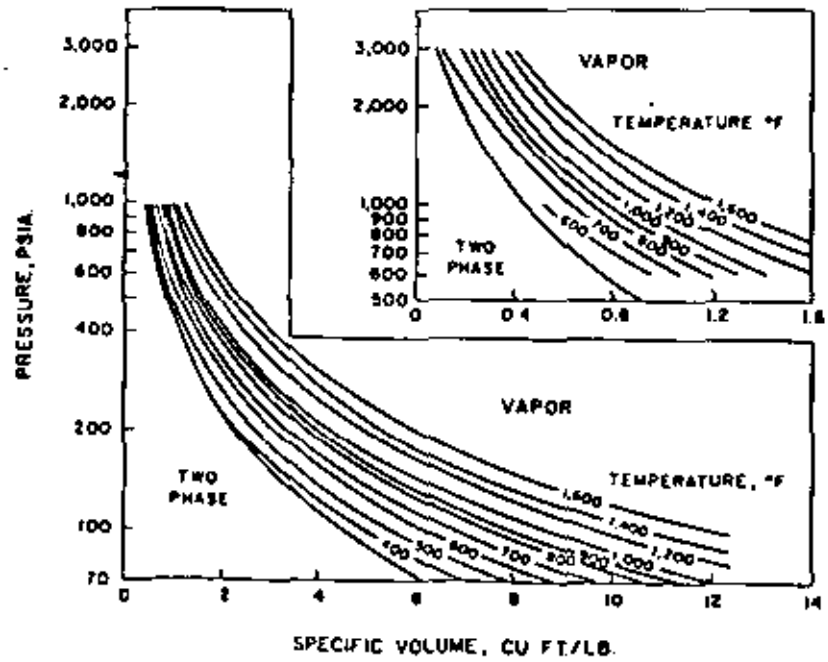

577

FIGURE 31
GAS LAW DEVIATION FACTOR FOR STEAM (Ref. 33)

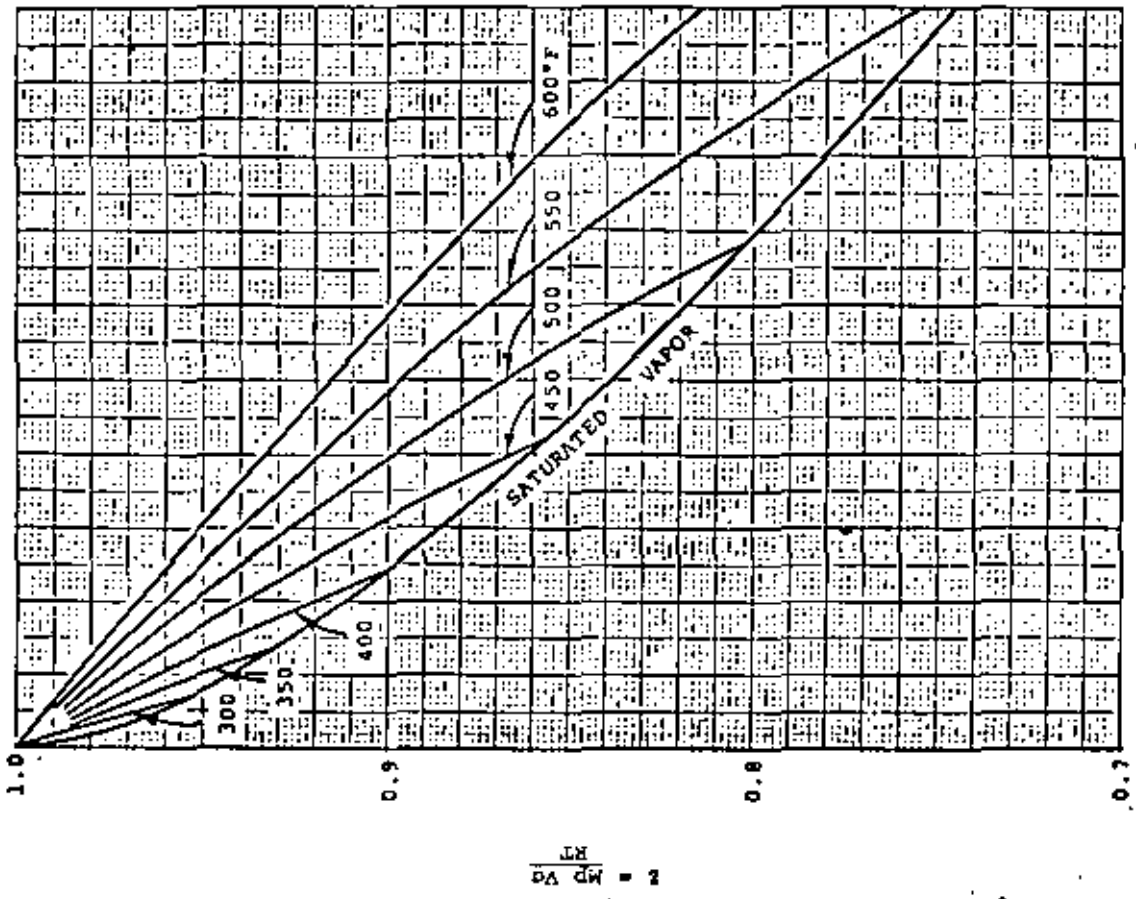

578

FIGURE 32

PRESSURE - ENTHALPY DIAGRAM FOR SUPERHEATED STEAM

(Ref. 38)

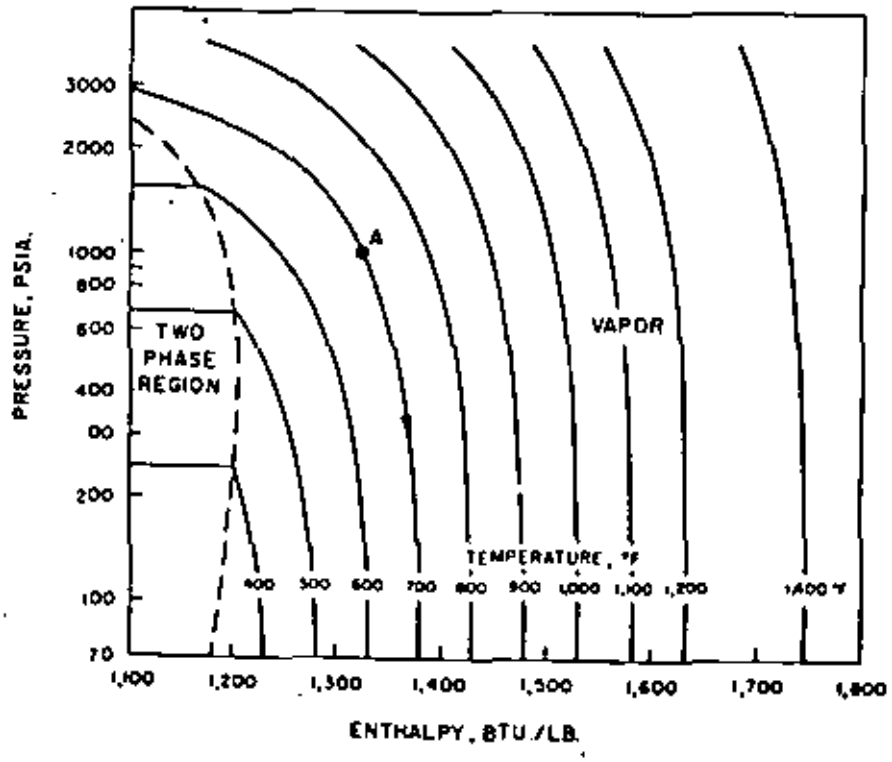

579

REFERENCES

1. Birch, Francis and Clark, Harry: "The Thermal Conductivity of Rocks and Its Dependence upon Temperature and Composition, Part I", Am. J. Science, 238, No. 8 (Aug. 1940), pp. 529-558.

2. Birch, Francis and Clark, Harry: "The Thermal Conductivity of Rocks and Its Dependence upon Temperature and Composition, Part II", Am. J. Science, 238, No. 9 (Sept. 1940), pp. 613-635.

3. Somerton, Wilbur H.: "Some Thermal Characteristics of Porous Rocks," Trans. AIME, 213 (1958), pp. 375-378.

4. Kunii, D. and Smith, J. M.: "Thermal Conductivities of Porous Rocks Filled with Stagnant Fluid," Soc. Pet. Engr. J. (Mar. 1961), pp. 37-42.

5. Adivarahou, P., Kunii, D. and Smith, J. M.: "Heat Transfer in Porous Rocks Through Which Single-Phase Fluids Are Flowing," Soc. Pet. Engr. J. (Sept. 1962), pp. 290-296.

6. Willhite, G. P., Dranoff, J. S. and Smith, J. M.: "Heat Transfer Perpendicular to Fluid Flow in Porous Rocks," Soc. Pet. Engr. J. (Sept. 1963), pp. 185-188.

7. Anand, J., Somerton, W. H. and Gomaa, E.: "Prediction of Thermal Properties of Formations from Other Known Properties," Paper No. SPE-4171, 43rd California Regional Meeting, SPE of AIME, Bakersfield, Calif., Nov. 8-10, 1972.

8. Tikhomirov, V. M.: "Conductivity of Rocks and Their Relationship with Density, Saturation and Temperature," Neftianoe Khoziaistro (in Russian), 46, No. 4 (1968), p. 36.

9. Gomaa, Ezzat E. and Somerton, W. H.: "Thermal Behavior of Multifluid-Saturated Formations, Part I: Effect of Wettability, Saturation and Grain Structure," Paper No. SPE 4896-A, 44th California Regional Meeting, SPE of AIME, San Francisco, Calif., April 4-5, 1974.

10. Gomaa, Ezzat E. and Somerton, W. H.: "Thermal Behavior of Multifluid-Saturated Formations, Part II: Effect of Vapor Saturation - Heat Pipe Concept and Apparent Thermal Conductivity," Paper No. SPE 4896-B, 44th California Regional Meeting, SPE of AIME, San Francisco, Calif., April 4-5, 1974.

11. Martin, W. L. and Dew, J. N.: "How to Calculate Air Requirements for Forward Combustion," Petroleum Engineer (Dec. 1964 and Feb. 1965).

12. Somerton, W. H. and Selim, M. A.: "Additional Thermal Data for Porous Rocks - Thermal Expansion and Heat of Reaction," Soc. Pet. Engr. J. (Dec. 1961), pp. 249-253.

13. Somerton, W. H. and Boozer, G. D.: "Thermal Characteristics of Porous Rocks at Elevated Temperatures," Trans. AIME, 219 (1960), pp. 418-422.

14. Klinkenberg, L. J.: "The Permeability of Porous Media to Liquids and Gases," Drilling and Production Practice (1941), pp. 200-213.

15. Raza, S. H., Treiber, L. E., and Archer, D. L.: "Wettability of Reservoir Rocks and Its Evaluation," Prod. Monthly (April 1968), 32, No. 4, pp. 2-7.

16. Killins, C. R., Nielsen, R. F. and Calhoun, J. C.: "Capillary Desaturation and Imbibition in Porous Rocks," Prod. Monthly (Dec. 1953) 18, No. 2, pp. 30-39.

17. Craig, F. F., Jr.: The Reservoir Engineering Aspects of Waterflooding, SPE Monograph, Vol. 3.

18. Muskat, M., Wyckoff, R. D., Botset, H. G. and Meres, M. W.: "Flow of Gas-liquid Mixtures through Sands," Trans., AIME (1937), 123, pp. 69-96.

19. Poston, S. W., Ysrael, S., Hossain, A. K. M. S., Montgomery, E. F. IV and Ramey, H. J., Jr.: "The Effect of Temperature on Irreducible Water Saturation and Relative Permeability of Unconsolidated Sands," Soc. Pet. Engr. J. (June 1970), pp. 171-180.

20. Sinnokrot, A. A., Ramey, H. J., Jr. and Marsden, S. S.: "Effect of Temperature Level upon Capillary Pressure Curves," Paper No. SPE 2517, presented at the 44th Annual SPE Fall Meeting, Denver, Colo., Sept. 28-Oct. 1, 1969.

21. Weinbrandt, R. M., Ramey, H. J., Jr. and Cassé, F.: "The Effect of Temperature on Relative Permeability of Consolidated Rocks," Paper No. SPE 4142, presented at the 47th Annual SPE Fall Meeting, San Antonio, Texas, Oct. 8-11, 1972.

22. Afinogenov, Y. A.: "How the Liquid Permeability of Rocks Is Affected by Pressure and Temperature," SNIGGIMS (1969), No. 6, pp. 34-42 (translation from Consultants Bureau, 227 W. 17 St., New York, NY 10011).

23. Lo, H. Y. and Mungan, N.: "Effect of Temperature on Water-Oil Relative Permeabilities in Oil-Wet and Water-Wet Systems," Paper No. SPE 4505, presented at the 48th Annual SPE Fall Meeting, Las Vegas, Nevada, Sept. 30-Oct. 3, 1973.

24. Von Gonten, W. D. and Choudhary, B. K.: "The Effect of Pressure and Temperature on Pore-Volume Compressibility," Paper No. SPE 2526, presented at the 44th Annual SPE Fall Meeting, Denver, Colorado, Sept. 28-Oct. 1, 1969.

25. Zoback, M. D. and Byerlee, J. D.: "Permeability, Compressibility and Effective Stress," unpublished report (Feb. 1974).

26. Fatt, I. and Davis, D. H.: "Reduction in Permeability with Overburden Pressure," Trans., AIME (1952), 195, 329.

27. Wyble, D. O.: "Effect of Applied Pressure on the Conductivity, Porosity and Permeability of Sandstones," Trans., AIME (1958), 213, pp. 430-432.

28. Dobrynin, V. M.: "Effect of Overburden Pressure on Some Properties of Sandstones," Soc. Pet. Engr. J. (Dec. 1962) 2, No. 4, pp. 360-366.

29. Gray, D. H., Fatt, I. and Bergamini, G.: "The Effect of Stress on Permeability of Sandstone Cores," Soc. Pet. Engr. J. (June 1963), pp. 95-100.

30. Wilhelmi, B. and Somerton, W. H.: "Simultaneous Measurement of Pore and Elastic Properties of Rocks under Triaxial Stress Conditions," Paper No. SPE 1706 (1967).

31. Krauskopf, K. B.: Introduction to Geochemistry, McGraw-Hill, New York, NY, 1967.

32. Butler, J. N.: Solubility and pH Calculations, Addison-Wesley, Palo Alto, CA, 1964.

33. White, E. E.: "Geochemistry Applied to the Discovery, Evaluation and Exploitation of Geothermal Energy Resources," Geothermics, Special Issue 2, Proc. of U. N. Symposium on the Development and Utilization of Geothermal Resources, Pisa, 1970, Vol. 1.

34. Fournier, R. O. and Truesdell, A. H.: "Chemical Indications of Subsurface Temperature Applied to Hot Spring Waters of Yellowstone National Park, Wyoming, U.S.A.", Geothermics, Special Issue 2, Proc. of U. N. Symposium on the Development and Utilization of Geothermal Resources, Pisa, 1970, Vol. 2, Part 1.

35. Keenan, J. H. and Keyes, F. G.: Thermodynamic Properties of Steam, John Wiley and Sons, Inc., New York, NY, 1936.

36. Meyer, C. A., McClintock, R. B., Silvestri, G. J. and Spencer, R. C., Jr.: 1967 ASME Steam Tables, Am. Soc. Mech. Engrs., 2nd ed., New York, NY, 1968.

37. Keenan, J. H.; Keyes, F. G., Hill, P. G. and Moore, J. G.: Steam Tables: Thermodynamic Properties of Water Including Vapor, Liquid and Solid Phases (English Units), John Wiley and Sons, Inc., New York, NY, 1969.

38. Whiting, R. L. and Ramey, H. J., Jr.: "Application of Material and Energy Balances to Geothermal Steam Production," J. Pet. Tech. (July 1969), pp. 893-900.

39. Farouq Ali, S. M.: Oil Recovery by Steam Injection, Producers Pub. Co., Bradford, PA, 1970.

40. Calhoun, J. C., Lewis, M., Jr. and Newman, R. C.: "Experiments on the Capillary Properties of Porous Solids," Trans. AIME, 186 (1949), pp. 189-196.

41. Edlefsen, N. E. and Anderson, A. B. C.: "Thermodynamics of Soil Moisture," Hilgardia, Calif. Agricultural Exp. Station, Univ. of Calif. at Berkeley, 15, No. 2 (Feb. 1943), p. 31.

42. Cady, G. V., Bilhartz, H. L., Jr. and Ramey, H. J., Jr.: "Model Studies of Geothermal Steam Production," Water 1972, AIChE Symposium Series (1973).

43. Amyx, J. W., Bass, D. M., Jr. and Whiting, R. L.: Petroleum Reservoir Engineering, McGraw-Hill, New York, NY, 1960.

44. Dodson, C. R. and Standing, M. B.: "Pressure-Volume-Temperature and Solubility Relations to Natural Gas-Water Mixtures," API Drilling and Production Practice, American Petroleum Institute, 1944.

45. Rowe, W. E.: "Effect of Salinity on Physical Properties of Water," Secondary Recovery of Oil in the United States, American Petroleum Institute, 1950.

46. Beal, Carlton: "The Viscosity of Air, Water, Natural Gas, Crude Oil and Its Associated Gases at Oil Field Temperatures and Pressures," Trans., AIME, 165 (1946).

47. Bridgman, D. W.: The Physics of High Pressure, McMillan Co., New York, NY, 1931.

48. Long, G. and Chierici, G. L.: "Compressibilite et Masse Specifique des Eaux de Gisement dans les Conditions des Gisements, Application a Quelque Problemes de 'Reservoir Engineering'" presented at Fifth World Petroleum Congress, 1959.

49. Van Wingen, N.: "Viscosity of Oil, Water, Natural Gas, and Crude Oil at Varying Pressures and Temperatures," Secondary Recovery of Oil in the United States, American Petroleum Institute, 1950.

50. Stanley, E. M. and Batten, R. C.: "Viscosity of Sea Water at Moderate Temperatures and Pressures," J. Geophys. Res., 74, No. 13 (June 20, 1969), pp. 3415-3420.

51. Eilerts, C. L., Carlson, H. A. and Mullens, N. B.: "Effect of Added Nitrogen on Compressibility of Natural Gas," World Oil (June-July 1948).

52. Olds, R. H., Sage, B. H. and Lacey, W. N.: "Partial Volumetric Behavior of the Methane-Carbon Dioxide System," Fundamental Research on the Occurrence and Recovery of Petroleum, American Petroleum Institute, 1943.

53. Reamer, H. H., Sage, B. H. and Lacey, W. N.: "Volumetric Behavior of Hydrogen Sulfide," Ind. Engr. Chem, 42, No. 1 (Jan. 1950), p. 140.

54. Herning, F. and Zipperer, L.: "Calculation of the Viscosity of Technical Gas Mixtures from the Viscosity of the Individual Gases," Gas-U. Wasserfach, 79 (1936).

55. Weast, R. C.: Handbook of Chemistry and Physics, The Chemical Rubber Co., Ohio, 48th ed. (1967-68).

56. Strobel, C. J.: Model Studies of Geothermal Fluids Production from Consolidated Porous Media," Engineer's thesis, Stanford Univ., July 1973.

57. Kuhn, C. S. and Koch, R. L.: "In-Situ Combustion," Oil & Gas J. (Aug. 10, 1953), 52, No. 14, p. 96.

58. Stovall, S. L.: "Recovery of Oil from Depleted Sands by Means of Dry Steam," Oil Weekly (Aug. 13, 1934), 74, p. 17.

59. Gates, C. S. and Ramey, H. J., Jr.: "Field Results of South Bebridge Thermal Recovery Experiment," Trans., AIME (1958), 213, p. 236.

60. Cady, G. V.: "Model Studies of Geothermal Fluid Production," Ph.D. dissertation, Stanford Univ., Nov. 1969.

61. Rowe, A. M., Jr.: "Thermodynamics Applied to Reservoir Engineering," Course notes for Petroleum Engineering 273, Winter 1973-74, Stanford Univ.

62. Helgeson, H. C.: "Thermodynamics of Hydrothermal Systems at Elevated Temperatures and Pressures," Am. J. Science, 267, Summer 1969, pp. 729-804.

63. Ramey, H. J., Jr.: A Reservoir Engineering Study of the Geysers Geothermal Field, 1968; submitted as evidence, Reich and Reich: Petitioners vs. Commissioner of Internal Revenue, 1969 Tax Court of the United States, 52. T.C. No. 74, 1970.

Discussion Following Ramey Paper

Rinehart

Do you think these things would hold for large, fractured mass when you have microscopic fractures with impermeable rock in between?

Ramey

In some cases we already know that they do. There are many oil and gas reservoirs that are in fact large, fractured masses. Generally speaking, the laws of nature seem to work the same there. Now some of the details on these homogeneous porous structures; the relative permeability curve details, would not be identically the same. It has amazed me to find that some of the massive, fractured reservoirs seem to follow simple mechanics.

Oki

The permeability is a function of temperature. When the temperature is increased, the permeability becomes lower; then when the temperature is reduced, the original numerical value for permeability is reached. I mean it is almost reversible.

Ramey

It is reversible. One other thing: the shapes of the curves, whether it's temperature or pressure, are almost the same. In data where permeability ratio is plotted versus effective pressure, you will note that the shape is almost identical with what you get for temperature. In our temperature work we have kept the confining pressure constant, just varying the temperature in the system, and we see this reversible result. In our data it is perhaps not totally reversible; it will move down the line and come back up slightly below its original path. But the difference is not much. Within the experimental accuracy it appears to be reversible. On the other work, on relative permeability, most of it does seem to be temperature level reversible. If you heat a core and measure relative permeability you get one value; if you cool it off and heat it up again you get the same value.

Rinehart

These are all corrected for viscosity?

Ramey

Yes.

Rinehart

Do you feel that your correction is good?

Ramey

We know it is. We've used fluids where the density of the fluid is known perfectly, we've used desensitized cores where we're not getting reaction with the core material, we've tested the fluids before and after, we've measured everything we can think of to be sure nothing has changed.

Coryell

It looks as though you are drawing attention to a large body of empirical evidence for temperature dependence of these parameters. Would you care to comment as to how you see the future, where the science is going to go, the state of the theory at the present time?

Ramey

Yes, you see a lot of interesting problems.

Coryell

You see a lot of interesting behavior, but is there the science and the basic understanding of why it's happening?

Ramey

Oh, very definitely. Everything I have shown you, I can explain I should have added that this one is almost on the forefront of knowledge and I can tell you what I think is the cause. In many cases, for example, the change in thermal conductivity with temperature will fit a very logical model of this system to the point that you can almost calculate the results you will get. Practically everything that has been done has been strongly related to underlying principles. People have been searching for ways to compute the result. Generally speaking, we have wanted this so we could patch it into some computer software and forecast what would happen under different cases. It's been necessary to generalize; it's been necessary to, at least, curve-fit to the point that is accessible to a computer. Almost everything that exists in the literature will have a very good explanation; it is not empirical. These are experimental determinations, of course; when you deal in this area, what you are talking about are experimental measurements that fit your constants. But the laws of physics still apply.

What I really deal in are reservoir models, physical models. We produce an oil reservoir, measure pressure all over it--what comes out, what goes in--and I attempt to build some mathematical picture of the thing so I can forecast what will happen under any other scheme in the future. To do this I've got to use the laws of physics. In some cases I discover that the reservoir knows some detail that I don't or I've overlooked. But generally speaking, they always make sense.

ADDENDUM TO THERMODYNAMIC AND HYDRODYNAMIC PROPERTIES OF HYDROTHERMAL SYSTEMS

By Ramey, H.J., Brigham, W.E., Chen, H.K., Atkinson, P.G., Arihara, N.

April 1974

1. The following changes should be made in the definitions related to Equation 40, at the top of page 543:

(the last three definitions):

Z_{ncg} = noncondensable gas compressibility factor

(instead of:
Y_{ncg}) = (etc.)

Y_{st} = Mole fraction steam in mixture

(instead of:
Z_{st}) = (etc.)

Y_{ncg} = mole fraction noncondensable gas in mixture

(instead of:
Y_{ncg} = mole fraction noncompressible gas in mixture)

6-9-75

DIVISION DE EDUCACION CONTINUA
FACULTAD DE INGENIERIA U.N.A.M.

CURSO: "INGENIERIA DE RESERVORIOS GEOTERMICOS"

NOTES ON RELATIVE PERMEABILITY RELATIONSHIPS

M.B. STANDING, PH.D.

TABLE OF CONTENTS

PREFACE

One of the primary functions of reservoir and production engineers is to predict, by means of valid engineering relationships, results of simultaneous flow of gases and liquids through reservoir rock. The rates of flow into or away from wells and the fraction of oil and gas that will be recovered are very important factors that the engineer is constantly concerned with. Of course, in addition to using valid engineering relationships (in contrast to looking into crystal balls) there is an implied requirement that the prediction be reasonable accurate.

Both flow and recovery of gas and oil involve relative permeability values as a function of fluid saturation. In many instances the relative permeability curve selected to represent the subsurface flow behavior has more effect on the ultimate answer than any other parameter in the equations used. Thus, it is important that the engineer have a good understanding of relative permeability behavior.

What about the sources of relative permeability data ? Basically there are four sources:

1. Guess. Take a piece of graph paper and draw curved lines simulating the shapes seen in text books, technical articles, etc. The results will be of unknown (and generally poor) accuracy and subject to argument by other engineers.

2. Analogy. Select relative permeability - saturation curves from the literature and assume your system has the same characteristics. A very favorite correlation is that of Arps and Roberts (Trans. AIME 204(1955) 120) that is reproduced on pages 386-387 of Craft and Hawkins. These results may be just as inaccurate as those mentioned above but will be more acceptable to other engineers.

3. Use measured capillary pressure-saturation data to characterize the pore structure of the reservoir rock.

Use this characteristic in empirical relationships that relate relative permeability to pore structure, saturation history, saturation and other pertinent parameters. In many instances this approach will yield fairly accurate results. Furthermore, the empirical relationships can often be used to extrapolate and average measured data in a consistant manner.

4. Laboratory measured values. These are generally believed to be the most accurate values.. Yet, in my opinion they can be fairly inaccurate if the laboratory measurements are not carefully performed. However, measured values are least apt to be questioned by other engineers.

The subject of these notes is the empirical relationships that tie to capillary pressure. I have found these to be very useful in day-to-day engineering, primarily because of the scarcity of measured relative permeability data. Furthermore, an understanding of the theory behind these relationships makes the engineer much more capable of handling and using relative permeability data.

M.B.Standing
Trondheim,Norway
August 6, 1974

NOTES ON RELATIVE PERMEABILITY RELAITONSHIPS

Introduction

Equations concerned with fluid flow in reservoir rocks make use of effective permeabilities, k_g, k_o, and k_w. Effective permeabilities are functions of:

1. pore size
2. pore size distribution
3. wettability
4. saturation
5. saturation history

Relative perms are the result of normalizing effective permeability values. Reservoir units of similar pore size, geometry, and wettability should have characteristic relative permeability relationships when plotted against saturation and saturation history.

Relative permeabilities may be expressed in terms of any specified base permeability. The three most common base values are (1) dry air permeability, k_a, measured at atmospheric pressure, (2) absolute permeability, k, and (3) effective hydrocarbon permeability at irreducible water saturation, S_{iw}. For example, consider a core sample in which the effective oil permeability at a particular saturation is 50 md. $(k_o]_{S_o,\ S_w} = 50$ md.) and the three base permeabilities are:

$k_a = 115$ md, $k = 102$ md, $k_o]_{S_{iw}} = 85$ md.

The relative permeability values could be either

$k_{ro} = 50/115 = 0.43$; $k_{ro} = 50/102 = 0.49$; $k_{ro} = 50/85 = 0.59$

Be careful to understand which base is used!

Saturation history is indicated by two terms; drainage and imbibition. Drainage relative permeability curves apply to processes in which the wetting phase is, or has been decreasing in magnitude. Imbibition relative permeability curves apply to processes in which the wetting phase is, or has been increasing in magnitude. The way of indicating drainage and imbibition values are

$k_{ro}]_{dr}$ = drainage $\qquad$ $k_{ro}]_{imb}$ = imbibition

and by use of arrows pointing the direction of wetting phase saturation change on plots.

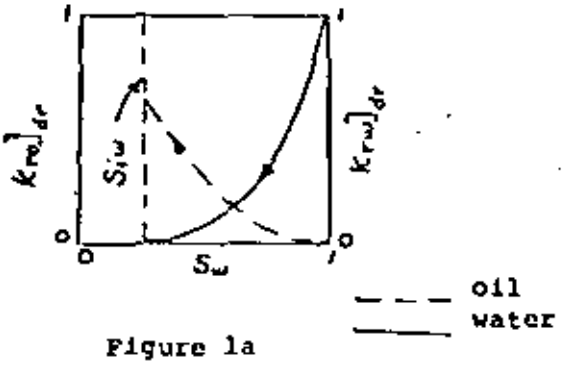

Figure 1a

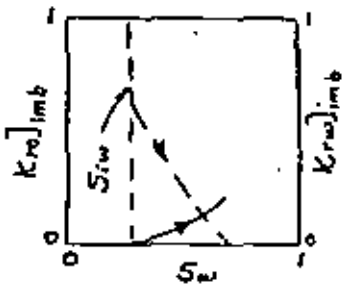

Figure 1b

Figure 1a, illustrates drainage oil and water relative permeability curves while Figure 1b illustrates imbibition curves. Water is the wetting phase in both sets of curves. Figure 2a and 2b illustrate gas and oil relative permeability curves in the presence of irreducible water, S_{iw}. Note that in this instance oil is the wetting phase and that the abcissa value is total liquid saturation, S_L. (Total liquid saturation $S_L = S_o + S_{iw}$.)

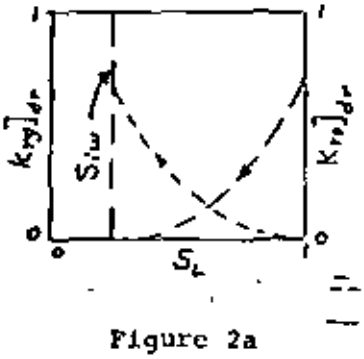

Figure 2a

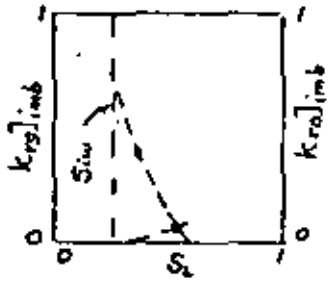

Figure 2b

Application of drainage and imbibition curves to reservoir processes are usually as follows:

Drainage Curves

1. Tarner or Muskat sol'n gas drive calculations. (gas displacing oil)
2. Gravity drainage calc's (gas replacing oil)
3. Gas drive calculations (gas displacing oil)
4. Oil or gas displacing water

Imbibition Curves

1. Waterflood calculations (water displaces oil & gas)
2. Water influx calculations (water displaces oil or gas)

Fundamental Concepts

a) Fluids in pore structure are under capillary control. For "water wet" systems water preferentially fills smallest pores, gas fills largest pores, and oil fills what is left.

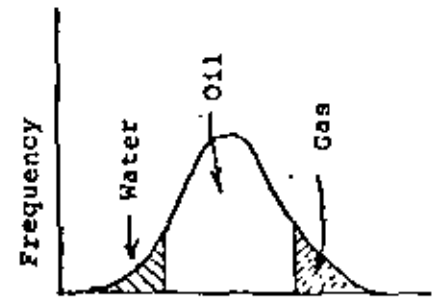

Figure 3

(1) k_{rw} depends only on amount of mobile water, $(S_w - S_{iw})$. Does not depend on whether hydrocarbon phase is oil, gas, or both.

(2) k_{rg} depends on amount (saturation) of gas present, S_g Does not depend on proportions of oil and water.

(3) k_{ro} depends on amount (saturation) of oil, s_o, and range of pore size in which it lies. k_{ro} for $s_o = 0,55$, $s_w = 0,40$, $s_g = 0.05$ will be larger than k_{ro} for $S_o = 0.55, s_w = 0.30$, $S_g = 0,15$ because oil will be distributed in smaller size pores in the second case.

b) Each fluid moves through separate groups of pores. Two or three fluids do not flow in the same pore. Saturation changes cause redistribution of pore size range occupied by the individual fluids.

c) Because of pore sizes being distributed throughout the rocks, fluids tend to "block" flow of other fluids. This requires that flow-path length change as saturation changes. (This refered to as tortuosity effect). Relative perm curves reflect average pore size of pores containing fluid and tortuosity.

Effective (Normalized) Saturations

Relative permeability relationships can be expressed most easily in terms of effective saturations, S_g^*, S_o^*, S_w^*. The effective saturation is the saturation expressed as a fraction of the pore space not occupied by irreducible (non-mobile) water. The bars below illustrate effective saturations in different reservoir systems.

Irreducible water + oil + gas

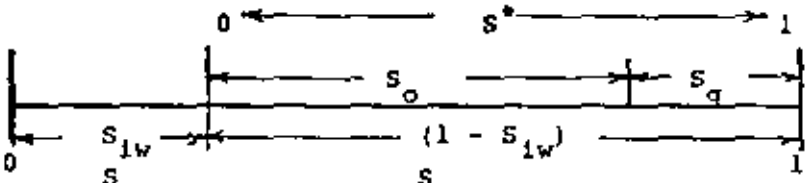

$$S_o^* = \frac{S_o}{(1 - S_{iw})} \; ; \quad S_g^* = \frac{S_g}{(1 - S_{iw})}$$

Irreducible water + mobile water + oil

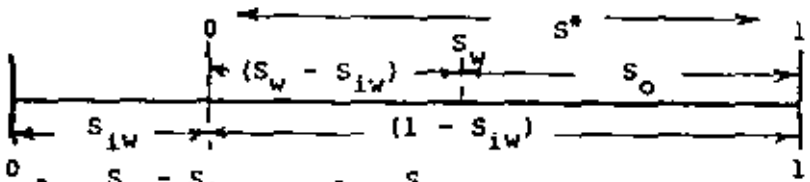

$$S_w^* = \frac{S_w - S_{iw}}{(1 - S_{iw})} \; ; \quad S_o^* = \frac{S_o}{(1 - S_{iw})}$$

Irreducible water + mobile water + oil + gas

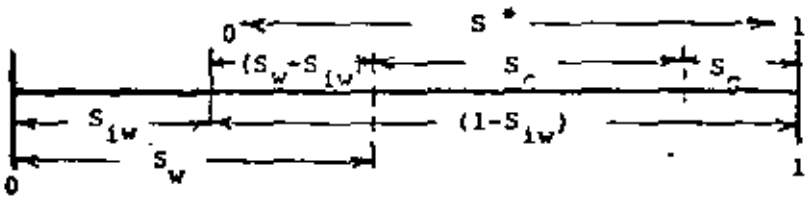

$$S_w^* = \frac{S_w - S_{iw}}{(1 - S_{iw})} \; ; \quad S_o^* = \frac{S_o}{(1 - S_{iw})} \; ; \quad S_g^* = \frac{S_g}{(1 - S_{iw})}$$

Theory of Two-Phase Drainage Relative Permeabilities

It was pointed out in the introduction that effective permeabilities are a function of pore size and pore size distribution. When the effective permeability is normalized to absolute permeability, yielding the relative permeability, the dependency on pore size is eliminated. Relative permeability, when expressed as a function of saturation, becomes strongly dependent on pore size distribution. Wettability, and saturation history are, of course, important parameters also.

The discussions that follow are aimed at developing relative permeability relationships for wetting and non-wetting fluids in rocks having some definable pore size distribution. Later the results will be applied to pore systems containing gas, oil, and water. The relative permeability and effective wetting phase saturation units that will be used are defined as follows:

$$k_{rwt} = k_{wt} \Big/ k_{wt}\Big]_{S_{wt}^* = 1} \tag{1a}$$

$$k_{rnwt} = k_{nwt} \Big/ k_{nwt}\Big]_{S_{wt}^* = 0} \tag{1b}$$

$$S_{wt}^* = \frac{S_{wt} - S_{wtr}}{1 - S_{wtr}} \tag{1c}$$

where k_{wt}, k_{nwt} = effective permeability of wetting and nonwetting phase at a given wetting phase saturation.

$k_{wt}\Big]_{S_{wt}^* = 1}$ = effective permeability of wetting phase at 100% wetting phase saturation (Point A in Figure 4)

$k_{nwt}\Big]_{S_{wt}^* = 0}$ = effective permeability of non-wetting phase at residual wetting phase saturation (Point B in Figure 4)

Figure 4 shows effective wetting and non-wetting phase permeabilities plotted against wetting phase saturation. Figure 5 shows the results of normalizing the effective permeabilities to their end point values (points A & B) and expressing the normalized, or relative permeability values as a function of effective wetting phase saturation, S_{wt}^*.

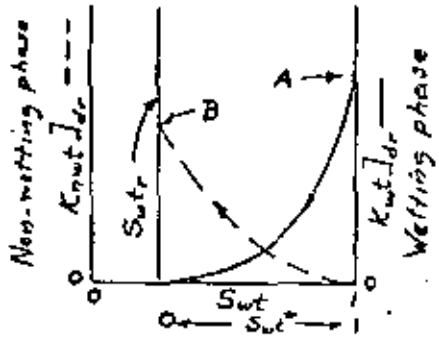

Figure 4

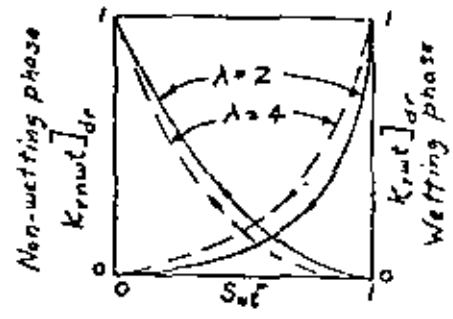

Figure 5

Figure 5 also illustrates the effect of pore size distribution on the resulting relative permeability curves. Lamda, λ, is called the pore size distribution index. The solid curves, $\lambda = 2$, are for a wide range of pore sizes, while the $\lambda = 4$ dashed curves represent a medium range of pore sizes. The larger the value of λ, the more uniform is the pore size distributions. An index of $\lambda = \infty$ represents a uniform pore size. Natural sandstones and limestones usually can be represented by pore size distribution indexes between about 0.5 and 4.

The pore size distribution index, λ, can be obtained from the shape of a capillary pressure-saturation curve, or, for a group of curves, from the shape of the Leverett J function-saturation curve. Brooks and Corey[1] [2] on the basis of a large amount of experimental data have shown that the ratio of capillary pressure to capillary entry pressure, (P_c/P_e) and effective wetting phase saturation, S_{wt}^*, can often be represented by the relationship

$$S_{wt}^* = (P_c/P_e)^{-\lambda} \qquad (2)$$

or

$$\log P_c = \log P_e - {}^1/\lambda \log S_{wt}^* \qquad (3)$$

Equation 3 is a straight line on log P_c vs log S_{wt}^* coordinates the slope of the straight line defines λ. Figure 6 is such a plot for air-water capillary pressure data on two Berea and two Boise Sandstone samples. It illustrates how pore size distribution indexes can be obtained. Water was, of course, the wetting phase in these tests.

(1) Brooks, R.H. and Corey, A.T. "Hydraulic Properties of Porous Media." Hydraulic Paper Number 3, Colorado State University, 1964.

(2) Brooks, R.H. and Corey A.T. "Properties of Porous Media Affecting Fluid Flow." Journal of the Irrigation and Drainage Division, Proc. of ASCE (1966), vol. 92, No. IR2, pages 61-88.

The early work of Burdine[3] and others associated with Gulf Research and Development Company lead to the following two relative permeability relationships in terms of the effective wetting phase saturation.

(3) Burdine, N.T. "Relative Permeability Calculations from Pore Size Distribution Data" Trans.AIME 198 (1953), 71-78.

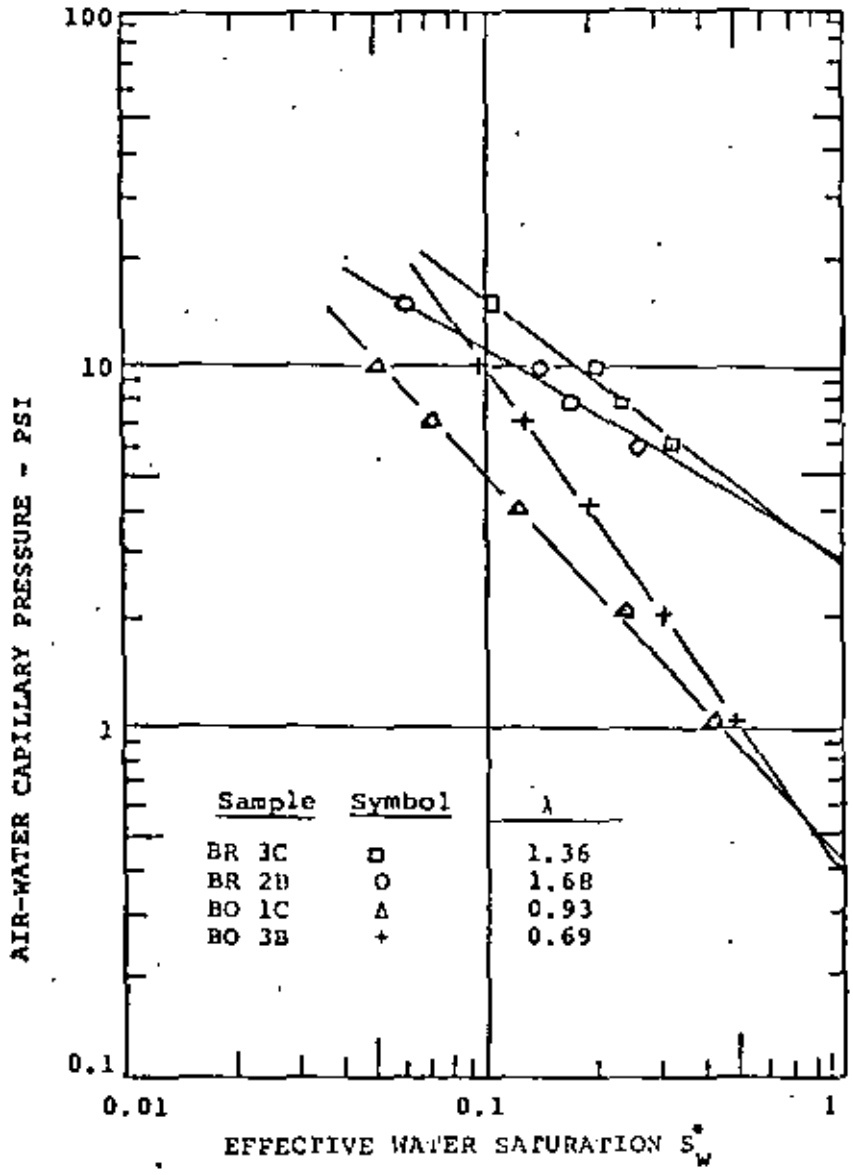

Figure 6. Log-Log Relationship of Capillary Pressure and Effective Water Saturation.
Boise and Berea Sandstone Samples.

For the wetting phase:

$$k_{rwt}\Big]_{dr} = (S_{wt}^*)^2 \frac{\int_0^{S_{wt}^*} \frac{dS_{wt}^*}{P_c^2}}{\int_0^1 \frac{dS_{wt}^*}{P_c^2}} \qquad (4)$$

For the non-wetting phase:

$$k_{rnwt}\Big]_{dr} = (1 - S_{wt}^*)^2 \frac{\int_{S_{wt}^*}^1 \frac{dS_{wt}^*}{P_c^2}}{\int_0^1 \frac{dS_{wt}^*}{P_c^2}} \qquad (5)$$

The integrals in Equations 4 and 5 can be solved in either of two ways. Where the pore size distribution index, λ, is known the solutions become:

For the wetting phase:

$$k_{rwt}\Big]_{dr} = (S_{wt}^*)^{\frac{2+3\lambda}{\lambda}} \qquad (6)$$

For the non-wetting phase:

$$k_{rnwt}\Big]_{dr} = (1 - S_{wt}^*)^2 \left[1 - (S_{wt}^*)^{\frac{2+\lambda}{\lambda}}\right] \qquad (7)$$

Where the index, λ, is not known, or where it is not constant within the saturation range of interest, one can use graphical integration methods to get a solution. This is illustrated by the following sketches.

For the wetting phase:

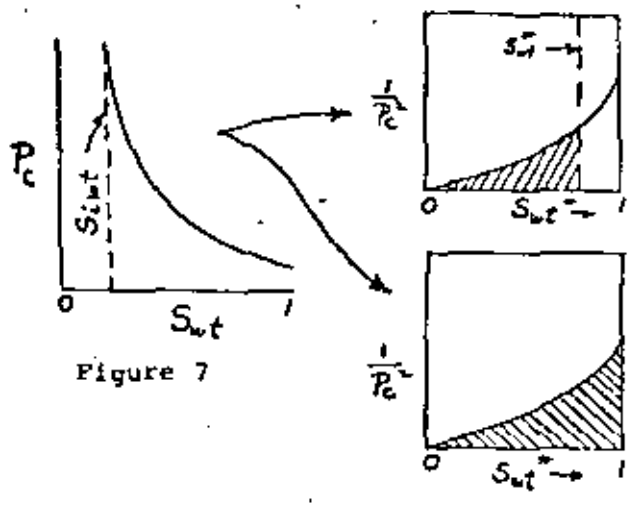

Figure 7

Shaded area under $1/P_c^2$ curve equals $\int_0^{S_{wt}^*} \frac{dS_{wt}^*}{P_c^2}$ of Equation 4

Shaded area under $1/P_c^2$ curve equals $\int_0^1 \frac{dS_{wt}^*}{P_c^2}$ of Equation 4

For the non-wetting phase :

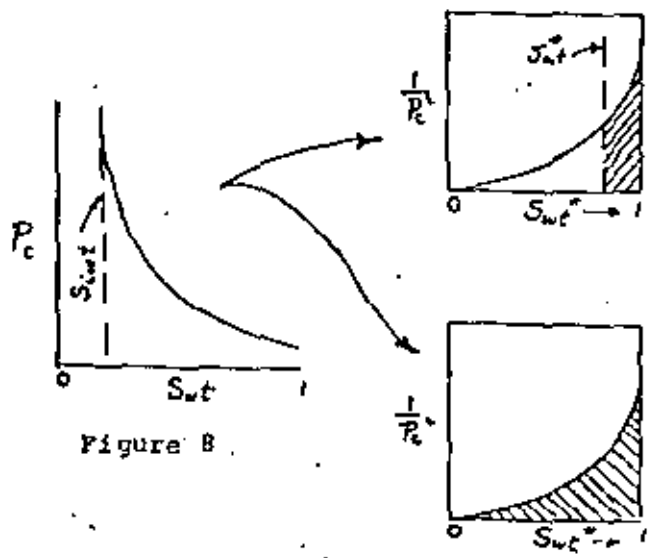

Figure 8

Shaded area under $1/P_c^2$ equals $\int_{S_{iwt}^*}^{1} \frac{dS_{wt}^*}{P_c^2}$ of Equation 5

Shaded area under $1/P_c^2$ curve equals $\int_{0}^{1} \frac{dS_{wt}^*}{P_c^2}$ of Equation 5

Note that it is not necessary to perform four graphical integrations as indicated by the sketches above. Two suffice.

The table below shows drainage relative permeability equations for several typical pore size distribution indexes.

TABLE I

Two-Phase Drainage Relative Permeability Equations

Porous Media	Dist. Index λ	k_{rwt}	k_{rnwt}
Very wide range of pore size	0.5	$(S_{wt}^*)^7$	$(1 - S_{wt}^*)^2 \left[1 - (S_{wt}^*)^5\right]$
Wide range of pore size	2	$(S_{wt}^*)^4$	$(1 - S_{wt}^*)^2 \left[1 - (S_{wt}^*)^3\right]$
Medium range of pore size	4	$(S_{wt}^*)^{3.5}$	$(1 - S_{wt}^*)^2 \left[1 - (S_{wt}^*)^{1.5}\right]$
Uniform pore size	∞	$(S_{wt}^*)^3$	$(1 - S_{wt}^*)^3$

Note: In Table I

$$k_{rwt} = k_{wt} / k_{wt}\Big]_{S_{wt}^* = 1}$$

$$k_{rwnt} = k_{nwt} / k_{nwt}\Big]_{S_{wt}^* = 0}$$

The pore size distribution indexes of 2, 4, and ∞ produce the equations proposed by Wyllie[4] to be used for cemented sandstones and oolitic and small-vugular limestones ($\lambda = 2$); poorly sorted unconsolidated sandstones ($\lambda = 4$); and well sorted unconsolidated sandstones ($\lambda = \infty$).

(4) Wyllie, M.R.J. "Relative Permeability" Petroleum Production Handbook, Chapter 25, vol. II. McGraw-Hill Publishers, 1962.

A study of many types of reservoirs has lead to the conclusion that a pore size distribution index greater than 6 should not be common for reservoirs containing hydrocarbons. This shows that most reservoir formations are likely to be in the very poorly to reasonable sorted range. The use of the pore size distribution index of 2 leads to the so-called Corey Equations, which are the best known forms of Equations 6 and 7. Corey Equations, therefore, are strictly valid only for a particular pore size distribution. They are often used however, to calculate relative permeability values when direct information on the pore structure is not known.

Referring back to Equations 1a, 1b, and to Figures 4 and 5 it will be seen that the two effective permeabilities were normalized to different base values when defining the relative permeabilities. Wetting phase permeabilities were normalized to the wetting phase permeability at 100% wetting phase saturation. If the wetting fluid is "non reactive", that is, does not react with rock components, the base permeability is, by definition, the absolute permeability of the rock, k. Thus, we can say that Equation 6 expresses a relative permeability relationship that is based on absolute permeability. On the other hand, Equation 7 is an expression in terms of effective permeability at partial wetting phase saturation, S_{wtr}, which is different than absolute permeability. Therefore, to get the non-wetting phase relative permeability expression onto an absolute permeability base it is necessary to introduce a relationship between $k_{nwt}\big]_{S_{wtr}}$ and absolute permeability, k. This is the subject of the next section.

Non-wetting Phase Permeability at Residual Wetting Phase Saturation. Consider a pore structure containing a wetting phase at residual saturation and a non-wetting phase. Figure 8 illustrates the pore size ranges that contain the two fluids. Conceptually, the absolute permeability, k, is proportional to the total area under curve. Likewise, the effective permeability to the non-wetting phase, k_{nwt}, can be said to be proportional to the area designated to contain non-wetting phase. On this basis, it is easy to see that $k_{nwt}\big]_{S_{wtr}}$ will decrease as S_{wtr} increases. This can be expressed by the relationship

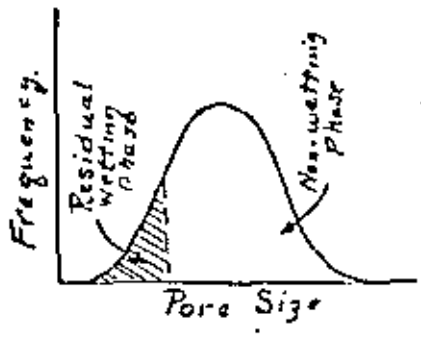

Figure 8

$$k_{nwt}\Big]_{S_{wtr}} = k \cdot f\,(S_{wtr}) \qquad (8)$$

where

$f\,(S_{wtr})$ = a function of residual wetting phase saturation

It would be expected that the saturation function in Equation 8 would depend to some degree on the pore size distribution index, λ. This has not been tested to the author's knowledge. However, results of many tests made at Chevron Oil Field Research Company lead to a general relationship that can be used until something better is available. This relationship is shown in Figure 9. An equation for the curve between saturation units of 0.2 and 0.5 is

$$k_r^o = \frac{k_{nwt}\Big]_{S_{wtr}}}{k} = 1.08 - 1.11\,S_{wtr} - 0.73\,(S_{wtr})^2 \qquad (9)$$

When the values of k_{rnwt} calculated from Equation 7 are multiplied by the value of k_r^o calculated from Equation 9, we have the relative permeability of the non-wetting phase in terms of the absolute permeability of the rock.

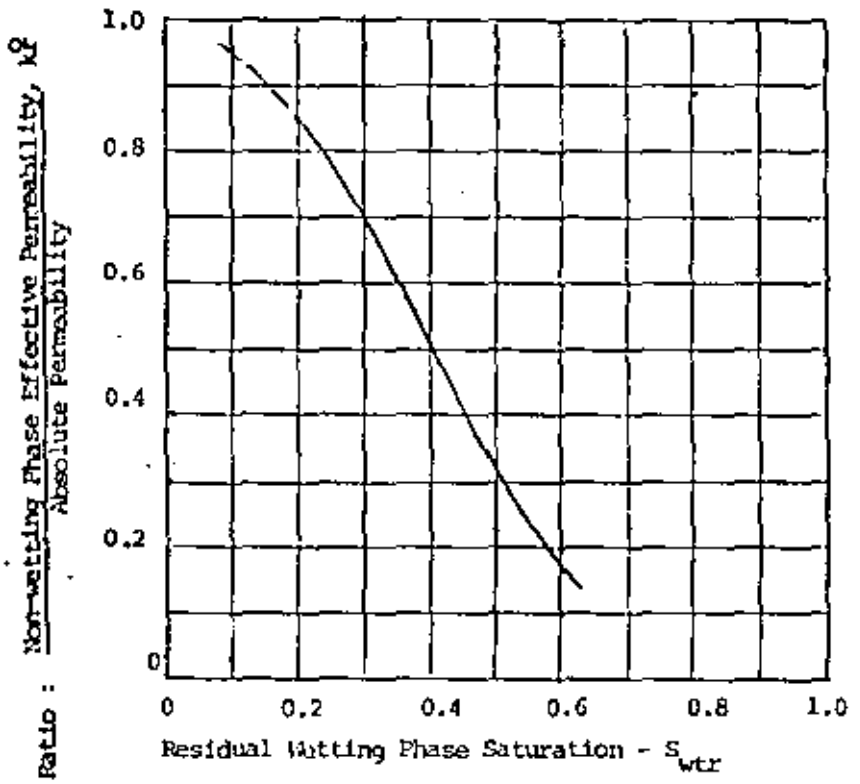

Figure 9. Average curve showing effect of residual wetting phase saturation on effective permeability of non-wetting phase.

Before considering application of the above relationships to reservoir systems is is necessary to account for so-called "critical non-wetting phase (gas) saturation" effects. This will be discussed next.

Critical Non-wetting Phase Effects. It is generally conceded that the non-wetting phase must have some finite saturation before k_{nwt} can have a non-zero value. The idea that at least one connected channel of pores must be full of non-wetting fluid before the fluid can flow. The saturation of non-wetting fluid necesary to permit flow is called "critical saturation." Most often one hears the term, "critical gas saturation", in connection with the flow of gas in a system of gas, oil, and water. However, critical saturation behavior applies to oil in an oil-water system equally well and it is best to think of the effect as being particular to the non-wetting

fluid.

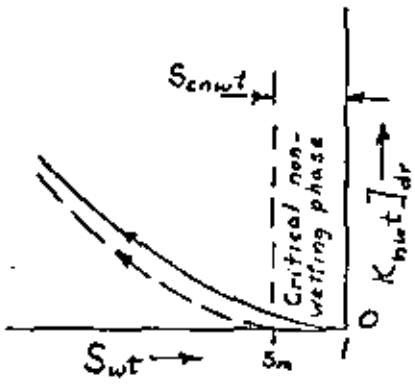

Figure 10

The requirement of a critical non-wetting phase saturation simply means that the non-wetting curve start from $S_{wt} = S_m$ in Figure 10 rather than from $S_{wt} = 1$. (Figure 10 is a blow-up of the lower right hand corner of Figure 4.) S_m is defined as the wetting phase saturation that marks the start of the non-wetting phase permeability curve. In terms of the critical non-wetting phase saturation, S_{cnwt}

$$S_m = 1 - S_{cnwt} \tag{10}$$

The method of taking critical saturation into account in Equation 7 and Table I is to change the quantity $(1 - S_{wt}^*)^2$ so that it will have zero value at the critical saturation value. The result is

$$k_{rnwt}]_{dr} = \left[1 - \frac{S_{wt} - S_{wtr}}{S_m - S_{wtr}}\right]^2 \left[1 - \left(S_{wt}^*\right)^{\frac{2+\lambda}{\lambda}}\right] \tag{11}$$

Equation 11 is, of course, still on the basis of $k_{nwt}]_{S_{wtr}}$. To place it on an absolute permeability basis only requires multiplication by k_r^o from Equation 9.

Corey and Rathjens[5] have shown that S_m values determined by back extrapolating laboratory determined relative permeability curves to $k_{rnwt} = 0$ are effected by stratification within the core. A given core sample always showed a higher value of S_m when fluid flow was parallel to bedding planes than when flow was perpendicular to bedding. Furthermore, cores that were highly stratified yielded S_m vlaues greater than unity. Within the concept that S_m is numerically equal to $(1 - S_{cnwt})$ (See Equation 10), having a value of S_m greater than tnity is impossible. On the other hand, if S_m is viewed simply as a saturation variable that is

(5) Corey, A.T. and Rathjens, C.H. "Effect of Stratification on Relative Permeability" Trans AIME 207 (1956), 353.

dependent on both stratification and critical saturation effects, and is used to limit the range of relative permeability values, then it makes sense for S_m to be greater than unity.

It should be noted that only the non-wetting phase permeabilities are affected by S_m. We do not apply the correction to the wetting phase relationships of Equation 6.

This section of the notes may appear to be complicated expressions having little use in practical engineering calculations. This is not so as will be illustrated in the section on application that follows.

Application of Two-Phase Drainage Relative Permeability Relationships

When using the relationships given so far one must keep in mind the conditions to which they apply. To reitterate, these conditions are

1. Two-phases. In petroleum reservoirs these would normally be gas-water and oil-water. Thus the relationships could apply to gas-cap conditions and to oil-zone conditions where only two phases are present.

2. Drainage. Saturation changes previous to the time of calculation and/or during the calculation time must be in the direction of decreasing wetting phase saturation. For example, it is generally believed that hydrocarbons migrate into and displace original water from petroleum bearing structures. Thus, drainage conditions would apply to calculations concerned with initial conditions found in the reservoir. A second example of drainage is injection of gas into an aquifer for gas storage purposes.

3. Wettability. One of the two phases in the pore structure must wet the rock matrix preferentially to the other. In the system gas-water, water is always the wetting phase. In oil-water systems, water is usually the wetting phase. However, some reservoir rocks appear to be preferentially oil wet, in which case Equation 6 would be used to calculate oil relative permeability values and Equation 7 would apply to water relative permeabilities. Note, however, that to use drainage relationships for oil-wet

reservoirs means that water saturation must increase—such as would occur under water flooding or aquifer influx conditions.

In preferentially water-wet reservoirs the wetting phase residual saturation, S_{wtr}, is analogous to irreducible water saturation, S_{iw}. Irreducible water saturation is approximated in most reservoir systems by the saturation corresponding to 50 psi capillary pressure in the gas-water system.

Two examples follow to illustrate the use of the relative permeability relationships presented to this point.

Example A. Calculation of Possible Water/Oil Ratio

Given: Conditions at a potential completion interval in a discovery well are believed to be as follows:

	Oil	Water
Fluid saturations, s	0.55	0.45
Irreducible saturation, S_{iw}	-	0.30
Fluid viscosities, μ	5 cp.	0.5 cp.
Form. vol. factor, B	1.5	1.05

If the producing water/oil ratio is greater than 1, it might not be profitable to complete the well in this interval. What will be the possible magnitude of the water/oil ratio?

Solution: The water/oil ratio can be obtained from radial flow equations for water and oil separately. That is,

$$q_w/q_o = \frac{k_w \mu_o B_o}{k_o \mu_w B_w}$$

Calculation of k_w and k_o yield

$$S_w^* = \frac{S_w - S_{iw}}{1 - S_{iw}} = \frac{0.45 - 0.30}{1 - 0.30} = 0.214$$

Assuming Corey equation with $\lambda = 2$

$$k_w = k \cdot k_{rw}\Big]_{dr} = k \left[S_w^*\right]^4 = 0.00021k$$

$$k_o = k \cdot k_r^o \cdot k_{ro}\Big]_{dr} = k \cdot k_r^o \cdot \left[1 - S_w^*\right]^2\left[1 - (S_w^*)^2\right]$$

From Figure 9, $k_r^o = 0.70$

$$k_o = k \cdot 0.7\left[1 - 0.214\right]^2\left[1 - (0.214)^2\right] = 0.413\ k$$

$$q_w/q_o = \frac{0.0021\ k \cdot 5 \cdot 1.5}{0.413\ k \cdot 0.5 \cdot 1.05} = \underline{\underline{0.073}}$$ Answer

Comments: Note the low effective water permeability (0.0021 k) even when mobile water saturation amounts to 15% of total pore space. This illustrates the asymtotic-to-zero shape of the water relative permeability curve when approaching the irreducible water saturation.

Example B. Calculation of Relative Gas Permeabilities

Given: A study of gas storage in an aquifer is being made. Requirement is for values of realtive gas permeabilities in the gas saturation range between 5 and 20 per cent. Capillary pressure tests indicate average pore size distribution index of 1.20 and irreducible water saturation of 0.20.

Solution: Method is to use Equations 7 and 9 in order to calculate relative gas permeabilities in terms of absolute permeability. Table 2 shows calculations. (Two sets of calculations are left for the student to do.)

TABLE 2 Calculation of Gas Relative Permeabilities--Example B

$S_{iw} = 0.20$; $S_w^* = (S_w - S_{iw})/(1 - S_{iw}) = (1.25\ S_w - 0.25)$; $S_m = 0.95$

$\lambda = 1.20$; $(2 + \lambda)/\lambda = 2.67$; $k_r^o = 1.08 - 1.11S_{iw} - 0.73(S_{iw})^2 = 0.83$

$$k_{rg} = \frac{k_g}{k} = k_r^o\left[1 - \frac{S_w - S_{iw}}{S_m - S_{iw}}\right]^2\left[1 - (S_w^*)^{\frac{2+\lambda}{\lambda}}\right]$$

① S_g	② S_w^*	③ $\frac{S_w - S_{iw}}{S_m - S_{iw}}$	④ $\left[1 - \frac{S_w - S_{iw}}{S_m - S_{iw}}\right]^2$	⑤ $(S_w^*)^{2.67}$	⑥ $\left[1 - (S_w^*)^{2.67}\right]$	⑦ k_{rg}
0.05	0.938	1.000	0	0.843	0.157	0.000
0.08						
0.11	0.862	0.920	0.0064	0.673	0.327	0.00174
0.14	0.825	0.880	0.0144	0.598	0.402	0.00480
0.17						
0.20	0.750	0.800	0.040	0.465	0.535	0.0178

Three-Phase Drainage Relative Permeability Relationships

The theory outlined for two-phase drainage relative permeability relationships in a previous section can be extended to cover three-phase behavior. The resulting three-phase relationships find application in many reservoir engineering calculations that concern simultaneous flow of gas and oil in the presence of water.

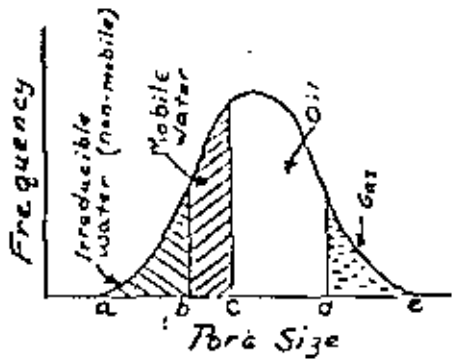

Figure 11

Figure 11 illustrates the basic concept of fluid location during flow. Irreducible water, which is considered to be the wetting phase, occupies pores of size range (a→b). Mobile water (free to move) occupies pore size range (b→c). Oil and gas occupy pore size ranges (c→d) and (d→e). As pointed out on page 3, k_{rw} depends on the amount of mobile water present, $(S_w - S_{iw})$; k_{rg} depends on the amount of gas present, S_g; but k_{ro} depends on both the amount of oil and pore range size in which it is located.

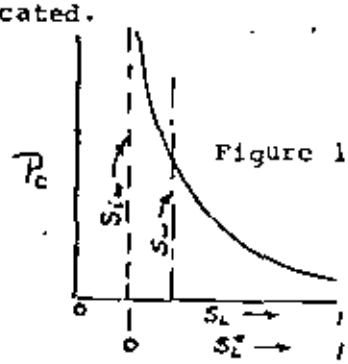

Figure 12

Figure 12 illustrates a curve of capillary pressure plotted against total liquid saturation. Total liquid is water plus oil phases. The water phase consists of irreducible (non-mobile)water and mobile water. The saturation equation can be written as

$$S_{iw} + (S_w - S_{iw}) + S_o + S_g = 1 \qquad (11)$$

The three mobile fluid saturations in Equation 11 can be converted to effective saturations as illustrated by the lowermost bar on page 4. These effective saturations are:

$$S_w^* = \frac{S_w - S_{iw}}{1 - S_{iw}} \; ; \quad S_o^* = \frac{S_o}{1 - S_{iw}} \; ; \quad S_g^* = \frac{S_g}{1 - S_{iw}} \; .$$

A fourth effective saturation for total liquid is

$$S_L^* = \frac{S_L - S_{iw}}{1 - S_{iw}} = S_w^* + S_o^* \qquad (13)$$

Extending the ideas developed by Burdine[3] (see pages 7, 8, and 9) to the three mobile phases yields equations similar to Equations 4 and 5—the major difference being that total effective saturation, S_L^*, is the independent variable. These are:

For the mobile water phase:

$$\frac{k_w}{k_w}\Big]_{S_w=1} = k_{rw} = (S_w^*)^2 \frac{\int_0^{S_w^*} \frac{1}{P_c^2}\, dS_L^*}{\int_0^1 \frac{1}{P_c^2}\, dS_L^*} \qquad (14)$$

For the oil phase:

$$\frac{k_o}{k_o}\Big]_{S_o^*=1} = k_{ro} = (S_o^*)^2 \frac{\int_{S_w^*}^{S_L^*} \frac{1}{P_c^2}\, dS_L^*}{\int_0^1 \frac{1}{P_c^2}\, dS_L^*} \qquad (15)$$

For the gas phase:

$$\frac{k_g}{k_g}\Big]_{S_g^*=1} = k_{rg} = (S_g^*)^2 \frac{\int_{S_L^*}^1 \frac{1}{P_c^2}\, dS_L^*}{\int_0^1 \frac{1}{P_c^2}\, dS_L^*} \qquad (16)$$

Note that the differences in Equations 14, 15, and 16 are the effective fluid saturations squared and the limits of integration of the upper integral expression. Note also the mobile water relative permeability is in terms of absolute permeability while the two hydrocarbon relative permeabilities are in terms of k_r^o.

To obtain solutions to the above equations requires an important assumption. It is that the capillary pressure-total liquid saturation curve obtained when gas displaces oil in the presence of water will be the same as when gas displaces water with no oil present. This means, in effect, that there will be zero residual oil phase remaining when capillary pressure is sufficient to get to irreducible water saturation. Undoubtedly this will not occur, but apparently the effect is small enough that useable relationships are obtained. At least the data presented by Corey, et al[6] on measurements on Berea sandstone samples bear this out.

(6) Corey, A.T., Rathjens, C.H., Henderson, J.H., and Wyllie, M.R.J. "Three-Phase Relative Permeability" Trans. AIME 207 (1956) page 349.

As outlined previously, when the pore size distribution index, λ, is known (See page 6-7) Equations 14, 15, and 16, can be integrated directly. The following integrated expressions are on the basis of absolute permeability, k, for all three phases. The gas relationship in Equation 19 includes S_m as a variable.

For the mobile water phase:

$$k_{rw}\Big]_{dr} = \frac{k_w}{k} = \left(\frac{S_w - S_{iw}}{1 - S_{iw}}\right)^{\frac{2+3\lambda}{\lambda}} \qquad (17)$$

For the oil phase:

$$k_{ro}\Big]_{dr} = \frac{k_o}{k} = k_r^o \left(\frac{S_o}{1 - S_{iw}}\right)^2 \left[\left(\frac{S_o + S_w - S_{iw}}{1 - S_{iw}}\right)^{\frac{2+\lambda}{\lambda}} - \left(\frac{S_w - S_{iw}}{1 - S_{iw}}\right)^{\frac{2+\lambda}{\lambda}}\right] \qquad (18)$$

For the gas phase:

$$k_{rg}\Big]_{dr} = \frac{k_g}{k} = k_r^o \left(\frac{S_g + S_m - 1}{S_m - S_{iw}}\right)^2 \left[1 - \left(\frac{S_o + S_w - S_{iw}}{1 - S_{iw}}\right)^{\frac{2+\lambda}{\lambda}}\right] \qquad (19)$$

Note that if $S_w = S_{iw}$ (no mobile water) Equation 17 reduces to zero and Equations 18 and 19 are simplified somewhat. Figure 13 illustrates the shape of the k_{ro} and k_{rg} curves for S_{iw} values of 0.2 and 0.4 calculated from Equations 18 and 19.

Note that the gas curve is not affected by the water saturation but the oil curve is affected drastically.

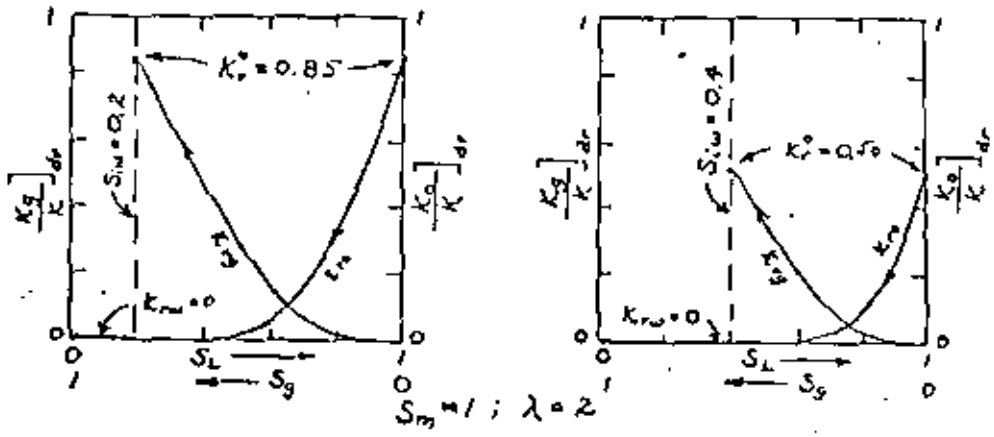

Figure 13 Three-phase drainage relative permeability curves

Example C that follows illustrates the calculation of drainage k_g/k_o vs. S_g data such as used in gas depletion type reservoirs. The basic data for the calculation is the Leverette J function curve for the Rangley Field shown on page 156 of Amyx, Bass, and Whiting.

Example C. Calculation of Drainage k_g/k_o vs S_g Relationship. Weber Sandstone, Rangely Field, Colorado

Given: Leverett J_{SW} vs S_w curve, page 156, ABW.
$S_{iw} = 0.30$; $S_w = 0.36$; $S_m = 1$; k_g/k_o required for gas saturations $0.01 < S_g < 0.11$

Solution:

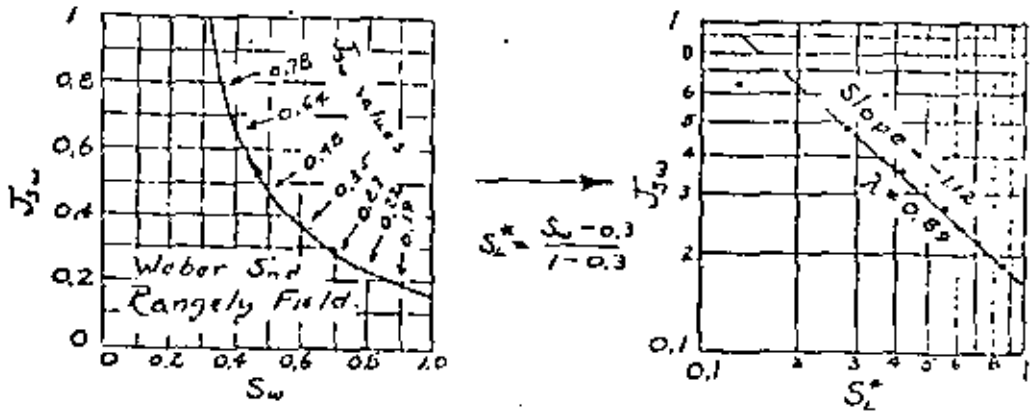

$\lambda = 0.89$: $\frac{2+\lambda}{\lambda} = 3.25$; $\frac{2+3\lambda}{\lambda} = 5.25$

$\left(\frac{S_w - S_{iw}}{1 - S_{iw}}\right) = \left(\frac{0.36 - 0.30}{1 - 0.30}\right) = 0.086$

$k_{rw}\Big]_{dr} = \frac{k_w}{k} = \left(\frac{S - S_{iw}}{1 - S_{iw}}\right)^{\frac{2+3\lambda}{\lambda}} = (0.086)^{5.25} = 2.5(10^{-6})$

$k_{ro}\Big]_{dr} = \frac{k_o}{k} = k_r^o \left(\frac{S_o}{1 - S_{iw}}\right)^2 \left[\left(\frac{S_o + S_w - S_{iw}}{1 - S_{iw}}\right)^{\frac{2+\lambda}{\lambda}} - \left(\frac{S_w - S_{iw}}{1 - S_{iw}}\right)^{\frac{2+\lambda}{\lambda}}\right]$ Eq. 18

$k_r^o = 0.70$ (Figure 9)

S_g	S_o	$\left(\frac{S_o}{1 - S_{iw}}\right)^2$	$\left(\frac{S_o + S_w - S_{iw}}{1 - S_{iw}}\right)^{3.25}$	$\left(\frac{S_w + S_w - S_{iw}}{1 - S_{iw}}\right)^{3.25}$	$\frac{k_o}{k}$
0.01	0.63	0.81	0.986	0.955	0.042
0.03	0.61	0.76	0.957	0.867	0.461
0.05	0.59	0.71	0.929	0.787	0.391
0.07	0.57	0.66	0.900	0.710	0.328
0.09	0.55	0.62	0.871	0.639	0.277
0.11	0.53	0.57	0.842	0.575	0.229

$k_{rg}\Big]_{dr} = \frac{k_g}{k} = k_r^o \left(\frac{S_g + S_m - 1}{S_m - S_{iw}}\right)^2 \left[1 - \left(\frac{S_o + S_w - S_{iw}}{1 - S_{iw}}\right)^{\frac{2+\lambda}{\lambda}}\right]$ Eq. 19

$k_r^o = 0.70$; $S_m = 1$

S_g	$\left(\frac{S_g}{1 - S_{iw}}\right)^2$	$\left[1 - \left(\frac{S_o + S_w - S_{iw}}{1 - S_{iw}}\right)^{3.25}\right]$	$\frac{k_g}{k}$
0.01	0.0002	0.045	$6.30(10^{-4})$
0.03	0.0018	0.133	$1.67(10^{-4})$
0.05	0.0051	0.213	$7.60(10^{-4})$
0.07	0.0100	0.290	$2.03(10^{-3})$
0.09	0.0165	0.361	$4.17(10^{-3})$
0.11	0.0247	0.426	$7.21(10^{-3})$

S_g	$\frac{k_g}{k_o}$
0.01	$1.16(10^{-5})$
0.03	$3.64(10^{-4})$
0.05	$1.94(10^{-3})$
0.07	$6.19(10^{-3})$
0.09	$1.51(10^{-2})$
0.11	$3.09(10^{-4})$

Answer.

Use of Corey Type Equations in Averaging and Extrapolating Laboratory Measured k_{rg}/k_{ro} Data

The petroleum engineer is often faced with the problem of adjusting results of laboratory measured k_{rg}/k_{ro} data to conditions other than those measured. For example, he may have k_{rg}/k_{ro} data taken with 20 per cent water saturation but needs to make calculations for a reservoir condition of 30 per cent water. How does he adjust the measured values to correctly account for the additional water? A second example is that he has measured k_{rg}/k_{ro} data at values from 0.1 to 100 but finds that he needs values in the region of 0.005. How does he extrapolate the measured data to lower ratios? (0.05 represents about the lowest value of k_{rg}/k_{ro} that can be determined in the laboratory.) A final example is that the engineer has k_{rg}/k_{ro} data on, say, five core samples, each of which contained a different amount of water. How can he use the data to get an average set of curves that can be used for any given water saturation?

The crux of the above is that while measured data are sometimes (not too often, however) available, the data often must be adjusted to the conditions being calculated. Methods of making such adjustments are the subject of this section.

Averaging k_{rg}/k_{ro} Data. Laboratory measured k_{rg}/k_{ro} ratio data are most often reported as a function of gas saturation, S_g. Water saturation for the conditions of measurement will be given and usually will be close to the irreducible water saturation, S_{iw}. Where a number of cores were used in the measurement program it is probable that each core contained a different amount of water. As pointed out in the previous section, k_{rg} depends primarily on the amount of gas present but k_{ro} depends primarily on the amount of oil and water.

Figure 14 illustrates three k_{rg}/k_{ro} curves, plotted on semi-logarithmic coordinates. Water saturation for each curve is different. The first step in getting an average curve is to remove the effect of the different water saturations

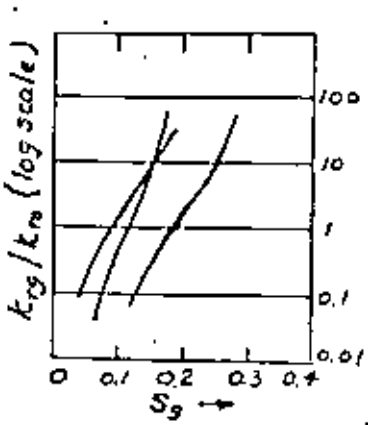

Figure 14

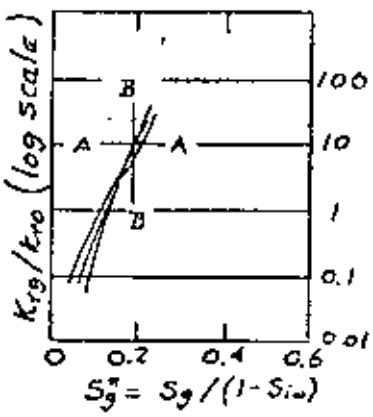

Figure 15

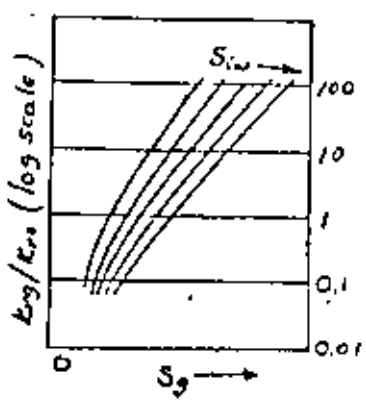

Figure 16

by normalizing gas saturation to the hydrocarbon pore volume, $(1 - S_{iw})$. This places the curves on a more common base of effective gas saturation, S_g^*

$$S_g^* = \frac{S_g}{1 - S_{iw}} \qquad (20)$$

Values of k_{rg}/k_{ro} are then plotted against S_g^* as illustrated in Figure 15. This preserves the shape of the curves but groups them closer together.

The average curve is constructed through average values k_{rg}/k_{ro} and S_g^*. The easiest way is to calculate the arithmetic average of S_g^* values at given values of k_{rg}/k_{ro} such as 0.1, 0.3, 1, 3, 10, etc. and to use these as the control points for the average curve. This is illustrated in Figure 15 as averaging along the line A-A. The other way is to select a number of S_g^* values and calculate the geometric average of the k_{rg}/k_{ro} values. This is illustrated in Figure 15 as averaging along the B-B line.

Having determined the average curve of k_{rg}/k_{ro} vs S_g^* it is a simple matter to construct a smooth curve of k_{rg}/k_{ro} vs S_g for various constant values of S_{iw}. The plot will have the appearance of Figure 16.

Gas depletion drive calculations make use of k_{rg}/k_{ro} vs S_g data. Such calculations are usually called Tarner

calculation or Muskat calculations. For most reservoir systems the Tarner and Muskat calculations will not need k_{rg}/k_{ro} data at values greater than 5. Therefore, when averaging laboratory data spend most effort on averaging the low values of k_{rg}/k_{ro} and little effort on the high values.

A second method of averaging k_{rg}/k_{ro} vs S_g data will be presented after the method of extrapolating relative permeability ratios has been presented.

Extrapolating k_{rg}/k_{ro} Data. It is difficult to measure k_{rg}/k_{ro} on core samples in the laboratory where the value is less than about 0.05. Most laboratory data fall between values of 0.1 and 100. Most reservoir calculation require values between 0.001 and 1. The problem is, how to extrapolate to lower k_{rg}/k_{ro} values in a consistent, reproducible manner that has some scientific basis.

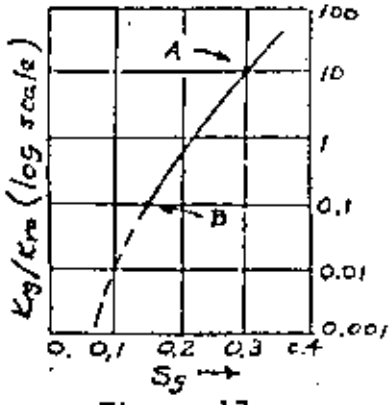

Figure 17

One method of extrapolating is graphical—use a french curve and extend the line. This method is satisfactory if the right french curve is used and the right extrapolation is made. The method is not considered to be a consistent and reproducible one.

The method outlined below is based on the work of C.E. Johnson[7] of the Chevron Oil Field Research Company, and allows one to make the extrapolation mathematically. Thus, it is consistent and reproducible, and, in addition, has some scientific basis.

(7) Johnson, C.E. "A Two-Point Graphical Determination of the Constants S_{Lr} and S_m in the Corey Equation for Gas-Oil Relative Permeability Ratio" Journal of Petroleum Technology, October 1968.

As mentioned previously, the so-called Corey Equations are general expressions for k_{rg} and k_{ro} for a pore size distribution index, λ, of 2. An equation for the ratio, k_{rg}/k_{ro} written in general terms is,

$$k_{rg}/k_{ro} = \frac{\left[1-\left(\frac{S_L-S_{Lr}}{S_m-S_{Lr}}\right)\right]^2\left[1-\left(\frac{S_L-S_{Lr}}{1-S_{Lr}}\right)^2\right]}{\left(\frac{S_L-S_{Lr}}{1-S_{Lr}}\right)^4} \quad (21)$$

The reader will recognize the similarity of this equation and Equations 18 and 19.

In using Equation 21, S_m and S_{Lr} are considered simply as two variables in the Corey ratio equation that relates the ratio k_{rg}/k_{ro} to total liquid saturation S_L. (Of course, $S_L = 1 - S_g$). For example, the point A in Figure 17 has a value of k_{rg}/k_{ro} of 10, and a corresponding value of S_L of 0.70. This combination of k_{rg}/k_{ro} and S_L could be satisfied by any number of combinations of S_m and S_{Lr} and fill the requirements of Equation 21. Similarly, point B in Figure 17 ($k_{rg}/k_{ro} = 0.1$; $S_L = 0.85$) can be fit by Equation 21 and many combinations of S_m and S_{Lr}. However, there is only one combination of S_m and S_{Lr} that will fit both points A and B. In effect, two unknowns in Equation 21 can be determined by having two solutions of the equation.

Johnson prepared three charts that are used to determine constants S_m and S_{Lr}. These are given as Figures 18, 19, and 20. In Figure 18, the gas saturation at which $k_{rg}/k_{ro} = 10$ is compared against the gas saturation at which $k_{rg}/k_{ro} = 0.1$. S_m and S_{Lr} values that fit these conditions are read from the grid. For example, values given by Points A and B on Figure 17 yield $S_m = 0.95$; $S_{Lr} = 0.5$. Similar comparisons are made for k_{rg}/k_{ro} ratios of 1 and 0.01, and 0.1 and 0.001 by Figures 19 and 20. If essentially the same values of S_m and S_{Lr} are indicated over the whole data range,

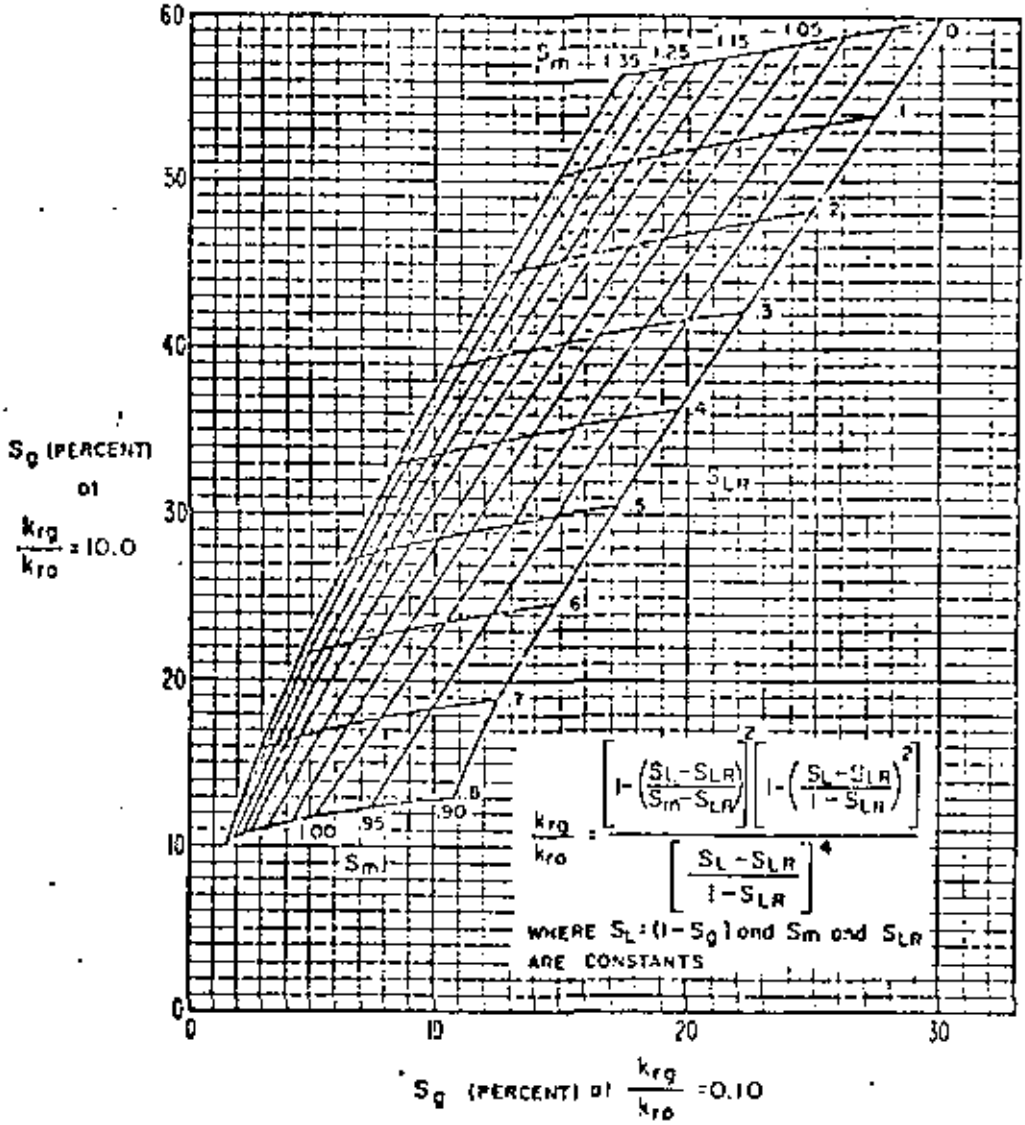

Figure 18. Chart for Calculating the Constants S_{Lr} and S_m in the Corey Relative Permeability Equation When k_{rg}/k_{ro} Have the Value of 10 and 0.1.

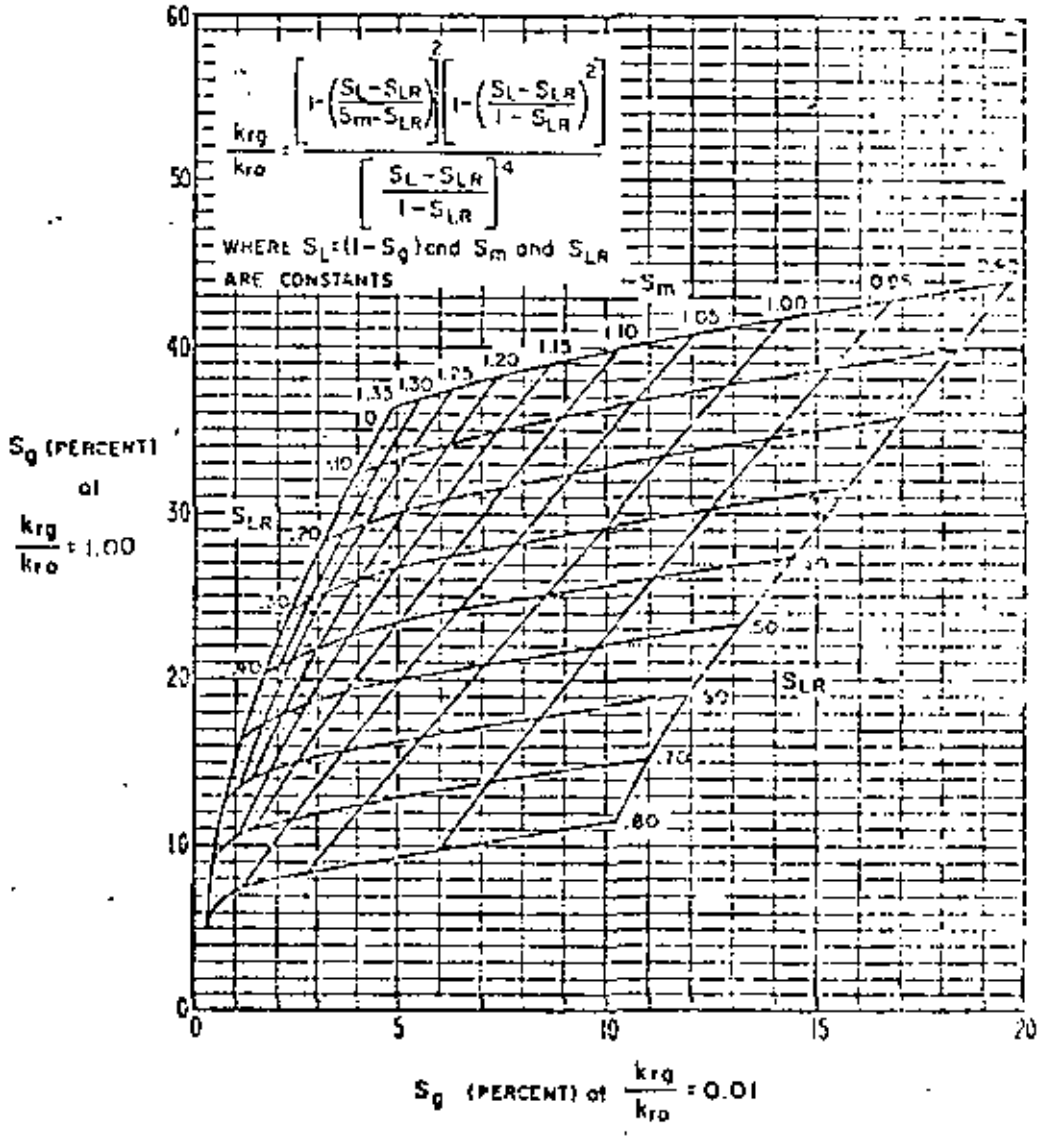

Figure 19. Chart for Calculating the Constants S_{Lr} and S_m in the Corey Relative Permeability Equation When k_{rg}/k_{ro} Have the Value of 1 and 0.01.

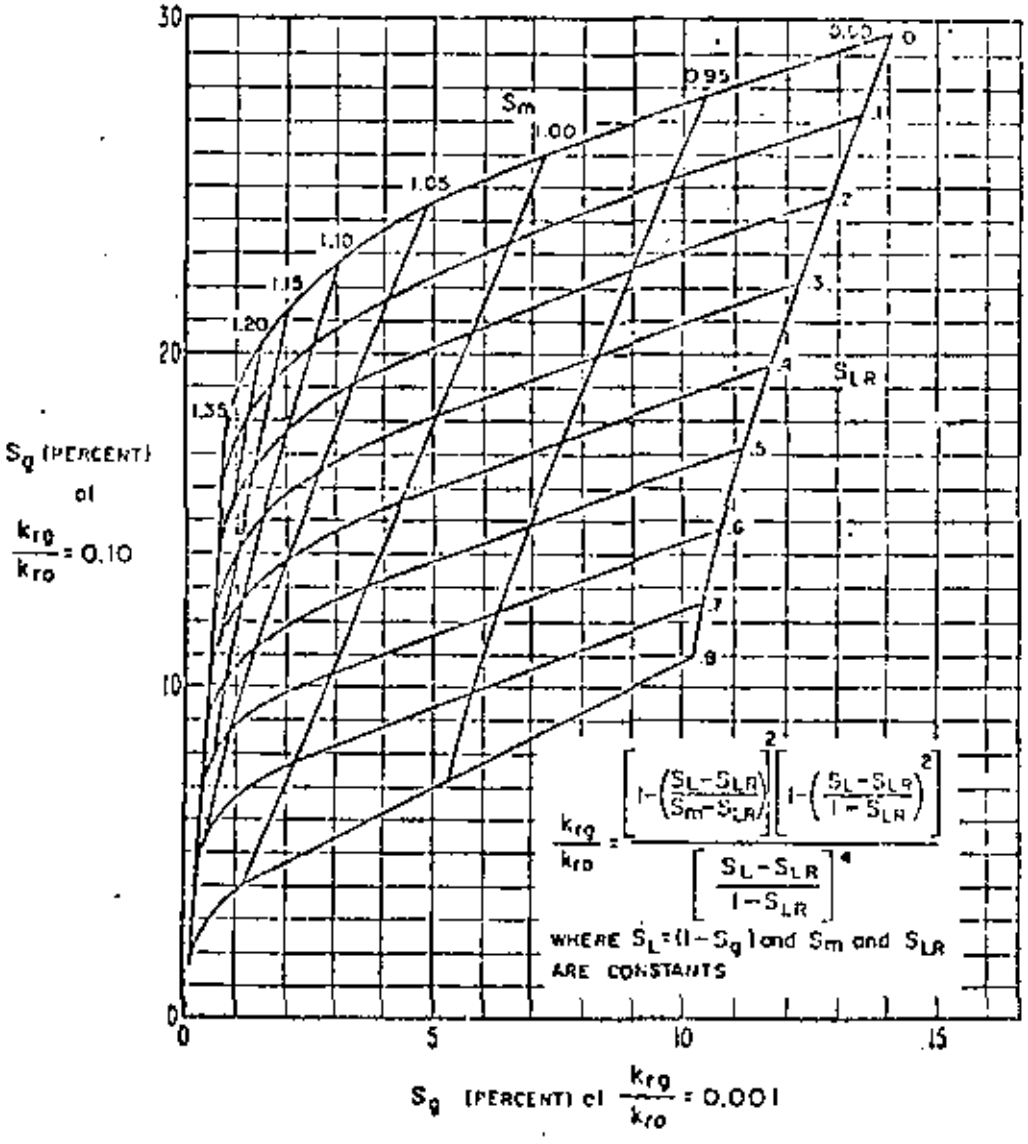

Figure 20. Chart for Calculating the Constants S_{Lr} and S_m in the Corey Relative Permeability Equation When k_{rg}/k_{ro} Have the Value of 0.1 and 0.001.

the values may be averaged and used to calculate the extrapolated part of the curve. This procedure is illustrated by the following example.

Example D. Extrapolation of k_{rg}/k_{ro} vs S_g. Data of C.R. Knopp (Trans AIME, 234 (1965)1111)

Given: k_{rg}/k_{ro} vs S_g values taken from his Figure 5A. These are, for $S_{iw} = 0.10$.

k_{rg}/k_{ro}	S_g	k_{rg}/k_{ro}	S_g
10	0.435	0.1	0.155
1	0.300	0.01	0.070

Solution:

k_{rg}/k_{ro}	S_g		S_m	S_{Lr}
10	43.5	Fig 18	1.14	0.24
1	30.0			
0.1	15.5	Fig 19	1.10	0.24
0.01	7.0	Avg.	1.12	0.24

Using $\bar{S}_m = 1.12$; $\bar{S}_{Lr} = 0.24$ and Equation 21 yield the following calculated values of k_{rg}/k_{ro}

$$k_{rg}/k_{ro} = \frac{\left[1-\left(\frac{S_L-0.24}{0.88}\right)\right]^2\left[1-\left(\frac{S_L-0.24}{0.76}\right)^2\right]}{\left(\frac{S_L-0.24}{0.76}\right)^4}$$

S_g	S_L	$\frac{S_L-0.24}{0.76}$	$\frac{S_L-0.24}{0.88}$	$\left(1-\frac{S_L-0.24}{0.88}\right)^2$	$1-\left(\frac{S_L-0.24}{0.76}\right)^2$	$\left(\frac{S_L-0.24}{0.76}\right)^4$	Calc. k_{rg}/k_{ro}	Knopp k_{rg}/k_{ro}
0.435	0.565	0.428	0.369	0.398	0.817	0.0336	9.66	10
0.300	0.700	0.605	0.523	0.224	0.634	0.134	1.06	1
0.155	0.845	0.796	0.686	0.0973	0.366	0.401	0.089	0.1
0.070	0.930	0.906	0.784	0.0467	0.176	0.680	0.0121	0.01
0.060	0.940	0.921	0.795	0.0420	0.152	0.720	0.0089	—
0.040	0.960	0.947	0.818	0.0331	0.103	0.864	0.0042	—
0.020	0.980	0.974	0.841	0.0253	0.0513	0.900	0.0014	—
0.010	0.990	0.987	0.852	0.0219	0.0256	0.949	0.0006	—

Two things are apparent from the calculations in Example D. First, the two values of S_{Lr} of 0.24 are the same for the high and low portion of the k_{rg}/k_{ro} curve. Note, however, that S_{Lr} is 2.4 times the value of S_{iw}. Do not interpret the difference of S_{Lr} and S_{iw} as being residual oil, S_{or}. In this use of the Corey ratio equation, S_{Lr} is a variable obtained when fitting a particular equation to set of data and should not be interpreted in a physical sense.

The second thing to notice is that two values of S_m were obtained. This means that a single Corey ratio equation does not fit the full range of data. Taking the average value of S_m of 1.12 yields a "best fit" curve to the data over the full range. Extrapolated values of k_{rg}/k_{ro} at gas saturations less than 0.06 were calculated using the average S_m of 1.12. An equally valid choice would have been to extrapolate the measured data by using an S_m value of, say, 1.10 to represent the lower curve. Also, one could have assigned weighting factor to the S_m values in order to get a "weighted" curve. For example, the engineer may wish to give twice the weight to the lower end of the k_{rg}/k_{ro} curve than to the upper end. The average value of S_m would then be

$$\bar{S}_m = \frac{1.14 \cdot 1 + 1.10 \cdot 2}{3} = 1.113.$$

Averaging k_{rg}/k_{ro} Data. Method 2. A method of developing an average k_{rg}/k_{ro} vs S_g^* relationship was discussed earlier. The method that follows is an alternate method that makes use of the Corey ratio equation as in the last section. This method is particularly useful where one wishes to simultaneously average, smooth, and extrapolate a group of laboratory k_{rg}/k_{ro} data.

The basis of the method is to determine S_m and S_{Lr} values for each k_{rg}/k_{ro} vs S_g curve by use of Johnson's charts (Figures 18, 19, 20). The arithmetic average of all S_m values is then determined and used to calculate the final curve. The ratio $\bar{S}_{Lr}/S_{iw}$ is determined for each curve ($\bar{S}_{Lr}$ being the average of the S_{Lr} values obtained for a given curve and S_{iw} being the water saturation in the core at the time of testing)

and plotted against S_{iw}. The trend of $\overline{S}_{Lr} / S_{iw}$ vs S_{iw} is used to obtain a value of S_{Lr} at the desired water saturation. Values of k_{rg}/k_{ro} vs S_g at the desired water saturation are then calculated using Equation 21 or Johnson's charts.

Example E illustrates the steps outlined above. In this example, k_{rg}/k_{ro} vs S_g curves were determined in the laboratory using three core samples from the formation of interest. The water saturation in each core at the time of testing corresponded to the irreducible saturation for that core. The average water saturation in the reservoir, however, is different than any of the tested values. The object is to produce a single composit k_{rg}/k_{ro} curve, adjusted to reservoir water saturation, that is usable in reservoir calculations.

Example E. Determination of Average Reservoir k_{rg}/k_{ro} Curve from Laboratory Data

Given: 1. Reservoir water saturation = 0.28

2. Following data read from laboratory measurement of k_{rg}/k_{ro} vs S_g

	Core		
	A	B	C
S_{iw} at test	0.14	0.21	0.19
S_g at k_{rg}/k_{ro} ratio of			
10	0.380	0.315	0.340
1	0.265	0.238	0.252
0.1	0.165	0.168	0.180
0.01	0.090	0.110	0.125
0.001	0.040	0.070	0.090

Solution:

	Core					
	A		B		C	
k_{rg}/k_{ro} comparisons	S_m	S_{Lr}	S_m	S_{Lr}	S_m	S_{Lr}
10 / 0.1 (Fig. 18)	1.02	0.35	0.92	0.48	0.92	0.43
1 / 0.01 (Fig. 19)	1.00	0.37	0.94	0.47	0.92	0.43
0.1 / 0.001 (Fig. 20)	1.02	0.35	0.96	0.42	0.93	0.41
Avg $\overline{S}_m$	1.01		0.94		0.92	
Avg $\overline{S}_{Lr}$		0.357		0.457		0.423
Avg $\overline{S}_{Lr}/S_{iw}$		2.55		2.18		2.23

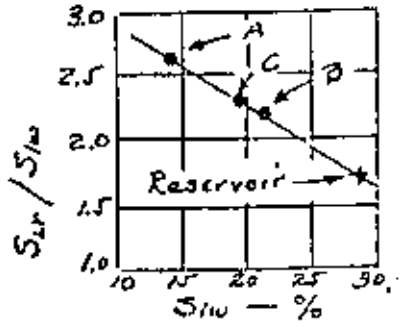

From trend plot of $\overline{S}_{Lr}/S_{iw}$ vs S_{iw}, reservoir ratio of $S_{Lr}/S_{iw} = 1.75$

For Reservoir

$$\overline{S}_m = \frac{1.01 + 0.94 + 0.93}{3} = 0.96$$

$$\overline{S}_{Lr} = 1.75 \cdot 0.28 = 0.49$$

Calculation, Average Curve:

$\overline{S}_m = 0.96$; $\overline{S}_{Lr} = 0.49$: $S_{iw} = 0.28$

From Figures 18 - 20

k_{rg}/k_{ro}	S_g
10	0.305
1	0.222
0.1	0.147
0.01	0.095
0.001	0.066

This concludes the notes on drainage relative permeability relationships. The next section will consider imbibition relative permeabilities relationships.

Theory of Two - Phase Imbibition Relative Permeabilities

Imbibition relative permeabilities apply when the wetting phase is, or has been, increasing in magnitude. The most important use of imbibition values is in waterflood calculations where water (wetting phase) is displacing oil (non-wetting phase). A similar application of imbibition values occurs in calculations concerned with influx of aquifer water into gas reservoirs.

The most important early work on imbibition relationships was that of Naar and Henderson[8]. More recently C.S. Land[9] [10] of the U.S. Bureau of Mines has extended the earlier work. The notes that follow essentially reproduce Land's work.

(8) Naar, J. , and Henderson, J.H. "An Imbibition Model-- Its Application to Flow Behavior and the Prediction of Oil Recovery" Trans AIME 222 (1961) 61.

(9) Land, C.S. "Calculation of Imbibition Relative Permeability for Two- and Three-Phase Flow from Rock Properties" Trans AIME 251 (1971) II, 149.

(10) Land, C.S., "Comparison of Calculated with Experimental Imbibition Relative Permeability" Trans AIME 251 (1971) II, 419.

The very earliest laboratory work (1950) of measuring relative permeabilities showed that direction of saturation change has an important bearing on the value of the relative permeabilities at a given saturation. This is illustrated by the two non-wetting phase curves of Figure 21.

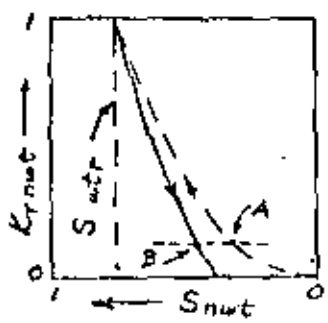

Figure 21

The reason for this behavior results from the sequence in which pores of given sizes are desaturated and resaturated during the saturation changes involved. Under drainage operations capillary forces and viscous forces both operate in the direction to promote desaturation of the largest pores first, followed by progressive desaturation of smaller and smaller pores. Under imbibition operations capillary forces and viscous forces operate, in effect,

in opposite directions. Capillary forces tend to cause resaturation of the smallest pores first while viscous forces favor resaturation of largest pores first. The net effect is that during the imbibition process a portion of the non-wetting phase becomes trapped within the pore structure and is unable to move. The result can be seen by referring to the dashed horizontal line in Figure 21. Point A represents the non-wetting phase saturation required to yield the relative permeability value indicated by the dashed line when the non-wetting phase saturation required to yield the relative permeability value indicated by the dashed line when the non-wetting phase saturation has changed from $S_{nwt} = 0$ to $S_{nwt} = A$. Continuing to desaturate to residual wetting phase saturation, S_{wtr}, and then resaturating back to the same relative permeability value (Point B) results in a greater non-wetting phase saturation because part of the non-wetting phase (saturation B minus saturation A) is trapped and does not contribute to k_{rnwt}.

The crux of Land's method of calculating two- and three-phase relative permeabilities is to correct total non-wetting phase saturation for the amount of trapped phase. The resulting "free" saturation is than used to calculate relative permeability using the same basic equations discussed previously for drainage conditions. The results seem to be quite good as indicated by the data in Reference 10.

The material that follows is presented in terms of a gas-water two-phase system in which water is the wetting phase. The reasons for doing this is that the number of subscripts are reduced (over wetting and non-wetting) and the equations are easier to compare with Land's equations. However, it should be remembered that the gas relationships apply vis-a-vis to oil in a two-phase oil-water system provided the oil-water system is strongly water wet also.

Trapped Gas Saturation. A number of technical papers have shown that initial gas saturation, S_{gi}, and residual gas saturation, S_{gr}, left after imbibition are related. The general shape of the relationship is shown in Figure 22, where

$$S^*_{gi} = S_{gi}/(1 - S_{iw}) \qquad (22)$$

$$S^*_{gr} = S_{gr}/(1 - S_{iw}) \qquad (23)$$

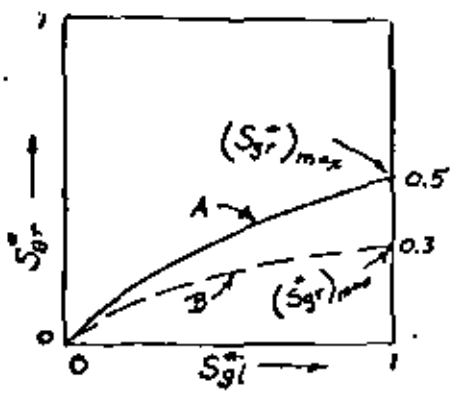

Figure 22

Land[9] found that a general equation for the relationship is

$$1/S_{gr}^* - 1/S_{gi}^* = C \qquad (24)$$

In equation 24, C is a "trapping constant" and is a function of the particular rock involved. (It probably has something to do with pore size distribution.) The value of C can be determined by simple laboratory drainage and imbibition experiments. If $(S_{gr}^*)_{max}$ represents the effective residual gas saturation in the rock after imbibing water from irreducible water saturation, S_{iw}, the value of C is, from Equation 24

$$C = 1/(S_{gr}^*)_{max} - 1 \qquad (25)$$

By way of illustration, the two curves of Figure 22 have the following trapping constants:

Curve	(S_{gr}^*)	C
A	0.5	1.0
B	0.3	2.33

Note that if no trapping occurs (This will be $S_{gr}^* = 0$) the value of C becomes infinity.

In the absence of laboratory results to determine the trapping constant it is probably best to use a value between 1 and 3. The higher values correspond to an often used rule of thumb in waterflood calculations that the residual oil left in a core after many pore volumes of water throughput will be about 20 per cent of the initial oil at the start of displacement.

The trapping constant, C, is an important parameter in the imbibition relative permeability relationships developed in the next section. When one specifies the value of C to be used he automatically fixes the relative permeability curve limits.

Imbibition Relationships, Non-Wetting Phase. Referring back to Equations 5 and 7 onpage 8, the drainage gas relative permeability, written in terms of wetting phase saturation units is (changing to gas terms)

$$k_{rg}\Big]_{dr} = (1 - S_w^*)^2 \left[1 - (S_w^*)^{\frac{2+\lambda}{\lambda}}\right] \qquad (26)$$

Recognizing that in a two-phase system $S_w^* + S_g^* = 1$, Equation 26 can be rewritten as

$$k_{rg}\Big]_{dr} = (S_g^*)^2 \left[1 - (1 - S_g^*)^{\frac{2+\lambda}{\lambda}}\right] \qquad (27)$$

The expression for the imbibition gas relative permeability is similar to Equation 27 except the gas saturation must be expressed in terms of "free" gas saturation units. This leads to

$$k_{rg}\Big]_{imb} = (S_{gF}^*)^2 \left[1 - (1 - S_{gF}^*)^{\frac{2+\lambda}{\lambda}}\right] \qquad (28)$$

To make use of Equation 28 requires that the "free" gas saturation be known as a function of total gas saturation. To do this we can say, first, that total gas saturation is equal to free gas plus trapped gas saturation. An expression for this is

$$S_g^* = S_{gF}^* + S_{gt}^* \qquad (29)$$

where S_{gt}^* is the trapped gas saturation.

A second relationship is that the trapped gas saturation, at any total gas saturation value, is equal to the residual gas saturation present when $k_{rg}\Big]_{imb} = 0$ minus the amount of free gas that gets trapped during saturation change from S_g^* to S_{gr}^*. The equation for this behavior is

$$S_{gt}^* = S_{gr}^* - \frac{S_{gF}^*}{CS_{gF}^* + 1} \qquad (30)$$

Eliminating S_{gt}^* between Equations 29 and 30 results in a quadratic in S_{gF}^*, from which

$$S_{gF}^* = \tfrac{1}{2}\left[(S_g^* - S_{gr}^*) + \sqrt{(S_g^* - S_{gr}^*)^2 + \tfrac{4}{C}(S_g^* - S_{gr}^*)}\right] \qquad (31)$$

The third and final equation that is required evaluates the amount of residual gas saturation in terms of the starting, or initial gas saturation, S^*_{gi}. It is

$$S^*_{gr} = S^*_{gi}/(C\ S^*_{gi} + 1) \qquad (32)$$

Before working an example problem to illustrate the use of Equations 28, 31, and 32 in calculating an imbibition curve for a non-wetting phase it is of interest to try and show graphically what the equations imply. Figure 23 shows three imbibition gas relative permeability curves (marked A, B, and C) and a drainage curve (dashed line) that starts at $S^*_g = 0$ and goes to $S^*_g = 1$. The starting point for any imbibition curve is a point on the drainage curve defined by the value of S^*_{gi}. At the starting point there is zero trapped gas (because the imbibition process hasn't started yet) so the value of $k_{rg}]_{imb}$ can be calculated from Equation 28 by letting $S^*_{gF} = S^*_{gi}$. Since $k_{rg}]_{imb} = k_{rg}]_{dr}$ at the starting point, the value may also be calculated from Equation 7 by noting that $S^*_{wt} = 1 - S^*_{gi}$.

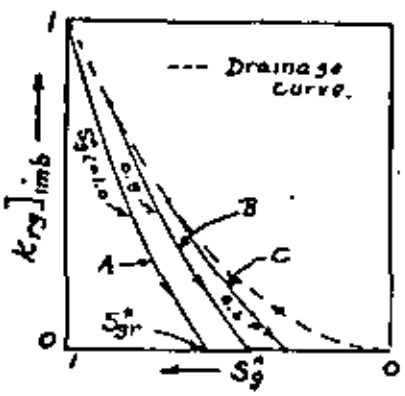

Figure 23

The bottom end of the imbibition curves is fixed by the starting gas saturation S^*_{gi} and the trapping constant, C, in accordance with Equation 32. This defines the residual gas saturation, S^*_{gr}, the saturation at which $k_{rg}]_{imb} = 0$. Note that as C in Equation 32 increases the value of S^*_{gr} decreases, or in effect moves further to the right in Figure 23. For a value of C equal to infinity, S^*_{gr} will be equal to zero, and the imbibition curve will lie exactly on the drainage curve.

The shape of the imbibition curve between the two limits is controlled by Equations 28 and 31. In general, the lower the value of C the straighter will be the $k_{rg}]_{imb}$ curve.

The notes on imbibition relative gas (non-wetting phase) permeability so far have followed Land's [9] treatment of the theory. All of Land's work considers that the drainage curve starts from $S^*_g = 0$, as illustrated in Figure 23. However, should the drainage curve start from so-called "critical" saturation, S^*_{gc}, it may be appropriate to introduce a modification into the imbibition curve equations to account for this. Otherwise, at large values of C, the computed value of $k_{rg}]_{imb}$ may become greater than $k_{rg}]_{dr}$ The imbibition relative permeability value must always be less than the drainage value.

The method of handling "critical" non-wetting phase saturation in the drainage relationship was shown by Equation 11 on page 13 of these notes. This was to introduce the parameter, S_m, defined as the wetting saturation at which the non-wetting phase relative permeability starts. A similar modification of the imbibition relative permeability relationship[11] leads to

$$k_{rg}]_{imb} = \left[\frac{(S_m - 1)}{(S_m - S_{iw})} + S^*_{gF}\frac{(1 - S_{iw})}{(S_m - S_{iw})}\right]^2 \left[1 - (1 - S^*_{gF})^{\frac{2+\lambda}{\lambda}}\right] \qquad (33)$$

(11) This is an unpublished development by M.R. Monroy of Chevron Oil Field Research Company.

The following illustration of calculating non-wetting phase imbibition relative permeability values makes use of the data on the Rangely Field, Colorado given in Example C, page 20. Pertinent information from Example C is that $\lambda = 0.89$, $S_{iw} = 0.30$, and $S_{wi} = 0.36$. The trapping constant, C, will be assumed to be 1.71.

Example F. Calculation of Imbibition k_{rg} vs S_g Relationship, Weber Sandstone, Rangely Field, Colorado.

Given: $\lambda = 0.89$, $S_{iw} = 0.30$, $S_{wi} = 0.36$, $S_m = 1$, $C = 1.71$

Solution:

$$S^*_{gi} = \frac{1 - 0.36}{1 - 0.30} = 0.914 \qquad \frac{2+\lambda}{\lambda} = 3.25$$

$$S^*_{gr} = \frac{S^*_{gi}}{C \cdot S^*_{gi} + 1} = \frac{0.914}{1.71 \cdot 0.914 + 1} = 0.357 \qquad (32)$$

$$S^*_{gF} = \frac{1}{2}\left[(S^*_g - S^*_{gr}) + \sqrt{(S^*_g - S^*_{gr})^2 + \frac{4}{C}(S^*_g - S^*_{gr})}\right] \qquad (31)$$

$$k_{rg}]_{imb} = (S^*_{gF})^2 \left[1 - (1 - S^*_{gF})^{\frac{2+\lambda}{\lambda}}\right] \qquad (28)$$

S_g	S^*_g	$(S^*_g - S^*_{gr})$	$(S^*_g - S^*_{gr})^2$	S^*_{gF}	$(S^*_{gF})^2$	$(1 - S^*_{gF})^{3.25}$	$k_{rg}]_{imb}$	$k_{rg}]_{dr}$ (1)
0.64	0.914	0.557	0.310	0.914	0.835	0.000	0.835	0.835
0.60	0.857	0.500	0.250	0.846	0.715	0.0023	0.713	0.733
0.50	0.714	0.357	0.127	0.669	0.448	0.0260	0.435	0.501
0.40	0.571	0.214	0.046	0.477	0.228	0.122	0.200	0.305
0.30	0.429	0.072	0.005	0.245	0.060	0.401	0.036	0.154
0.25	0.357	0.000	0.000	0.000	0.000	0.000	0.000	0.097

Note (1) Drainage values calculated from Equation 27 for comparison with $k_{rg}]_{imb}$

Imbibition Relationships, Wetting Phase. In two-phase systems, the entire water phase remains mobile. As water saturation increases the water invades increasingly larger size pores trapping some gas in the invaded pores. Because of the trapping of gas, at any particular water saturation value some water must occupy pores of larger size than it would occupy if gas had not been trapped. As a consequence of the increased pore size occupied by the water, $k_{rw}]_{imb}$ values are always greater than $k_{rw}]_{dr}$ values, for the same value of saturation. Figure 24 illustrates the difference in the imbibition and drainage curves. It is to be noted that the difference is small. For greater values of C and lesser values of S^*_{gi} the difference becomes even less. While equations for pore size distribution index other than 2 have not been worked out it would be expected that the differences would also be less than illustrated. For these reasons it is usual to use the same equation for imbibition and drainage. The equation can be written in simplest form as

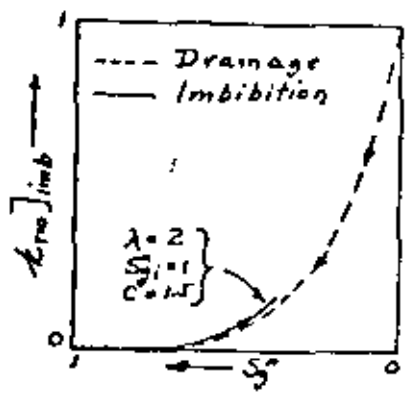

$$k_{rw}]_{imb} = k_{rw}]_{dr} = (S^*_w)^{\frac{2+3\lambda}{\lambda}} \qquad (34)$$

Equation 34 may also be written in terms of effective gas saturation units as

$$k_{rw}]_{imb} = k_{rw}]_{dr} = (1 - S^*_g)^{\frac{2+3\lambda}{\lambda}} \qquad (35)$$

Example G illustrates the calculation of a $k_{rw}/k_{ro}]_{imb}$ vs S_o curve for the Weber Sandstone in the Rangely Field, Colorado. Note that when working with ratio data that the base of both curves must be the same. For this reason,

the k_{ro} values (which were calculated as k_{rg} values in Example F) have been changed to be on an absolute permeability base by introduction of k_r^o. The values of k_{rw} are already on the absolute permeability base.

Example G. Calculation of Imbibition k_{rw}/k_{ro} vs S_o Curve. Weber Sandstone, Rangely Field, Colorado.

Given: $\lambda = 0.89$; $S_{iw} = 0.30$; $S_{wi} = 0.36$; $S_m = 1$; $C = 1.71$; $k_r^o = 0.70$

Solution:

$$k_{ro}]_{imb} = k_{rg}]_{imb} - \frac{k_g}{k}]_{S_g=1} \cdot k_r^o = \frac{k_o}{k}$$

$$k_{rw}]_{imb} = \frac{k_w}{k_w}]_{S_g=0} = \frac{k_w}{k} = (1 - S_g^*)^{\frac{a+3\lambda}{\lambda}}$$

$$\frac{2 + 3\lambda}{\lambda} = 5.25$$

S_g	S_g^*	$(1-S_g^*)$	$k_{rw}]_{imb} = (1-S_g^*)^{5.25}$	$k_{ro}]_{imb}$	$k_{rw}/k_{ro}]_{imb}$	S_w
0.64	0.914	0.086	$2.54(10^{-4})$	0.584	$4.35(10^{-4})$	0.36
0.60	0.857	0.143	$3.66(10^{-4})$	0.500	$7.36(10^{-3})$	0.40
0.50	0.714	0.286	0.00114	0.305	$4.59(10^{-3})$	0.50
0.40	0.571	0.429	0.0115	0.140	$8.21(10^{-2})$	0.60
0.30	0.429	0.571	0.0530	0.0252	2.10	0.70
0.25	0.357	0.643	0.108	0.000	∞	0.75

Values of $k_{rw}/k_{ro}]_{imb}$ in the sixth column of the above calculations are plotted against water saturation (Column 7) in Figure 25. Note that the curve becomes asymtotic to the $S_w = 0.3$ (irreducible water saturation) and the $S_w = 0.75$ (one minus residual oil saturation).

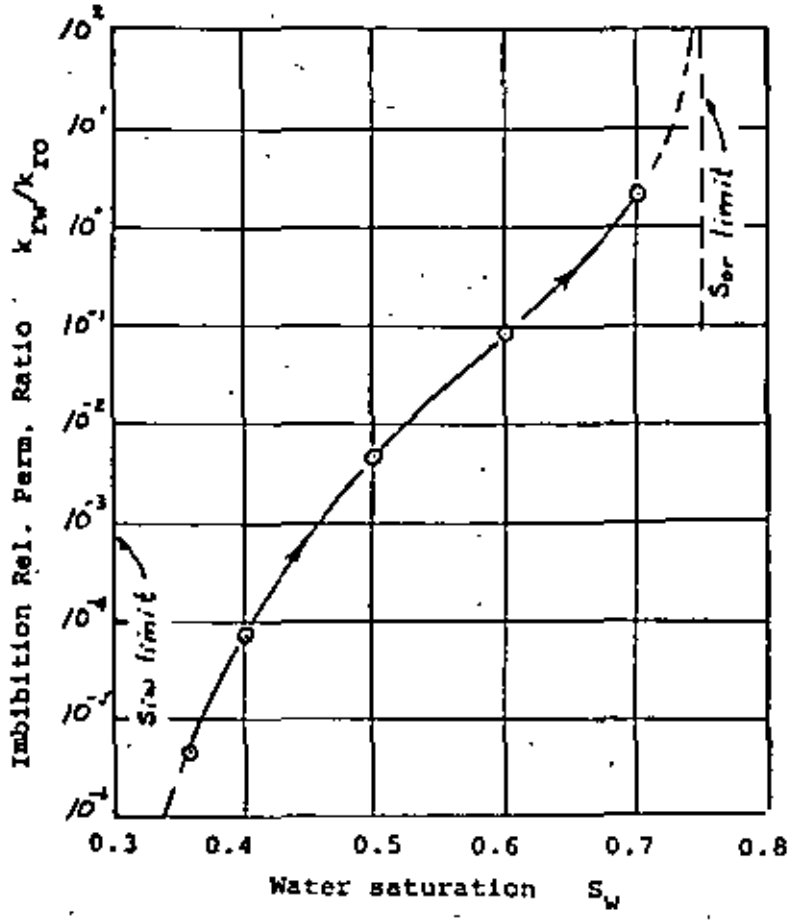

Figure 25. Plot of imbibition k_{rw}/k_{ro} values, Example G, Weber Sandstone, Rangely Field, Colo.

Averaging Imbibition k_{rw}/k_{ro} Data

Laboratory data on the imbibition relative permeability ratios are usually reported as function of water saturation. The shape of data plots will be similar to that of Figure 25. The starting water saturation will usually be near the irreducible water saturation, S_{iw}. As with drainage values, there is often need to intercorrelate the data of a number of cores and obtain an average relationship that can be used for reservoir calculations.

One procedure of averaging the data is the same as outlined on page 23 for drainage data. Convert the water

saturation parameter to effective saturation units, S_w^*, by the relationship

$$S_w^* = (S_w - S_{iw})/(1 - S_{iw}) \qquad (36)$$

This requires a value of S_{iw}. If a value is not given in the report, use the value of the lowest water saturation reported as S_{iw}. Plot the $k_{rw}/k_{ro}]_{imb}$ values on log scale against S_w^* on arithmetic scale. This will usually bunch the data so that an average curve can be easily obtained. (See page 23 for method of obtaining average values.)

A second method is as follows:

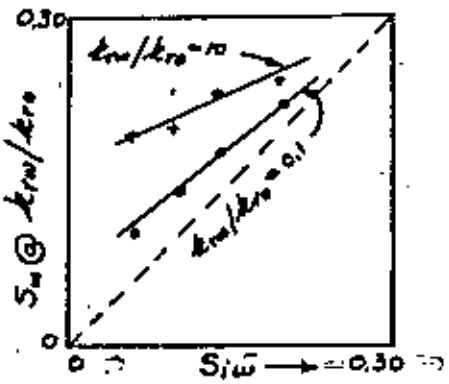

Figure 26

1. Prepare a plot of S_w on the y axis against S_{iw} on the x axis. Read values of S_w from the laboratory data at several selected values of k_{rw}/k_{ro}. Plot values of S_w vs S_{iw} as illustrated in Figure 26. Do this for all data (cores). Construct what appear to be the best average straight lines through the point. There should be one line for each $k_{rw}/k_{ro}]_{imb}$ ratio selected.
2. Plot the slope of the straight lines obtained by the above procedure against the logarithm of the selected k_{rw}/k_{ro} value and construct the best smooth curve through the points. The plot should have the appearance of Figure 27.
3. Using values from the smoothed slope vs log k_{rw}/k_{ro} curve (Figure 27) go back and adjust the slopes of the straight lines in the first plot. Do the adjusting at about mid value of S_{iw} of the original data.

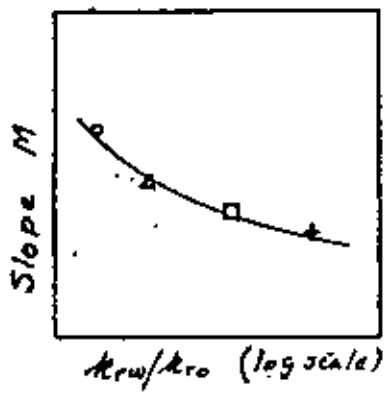

Figure 27

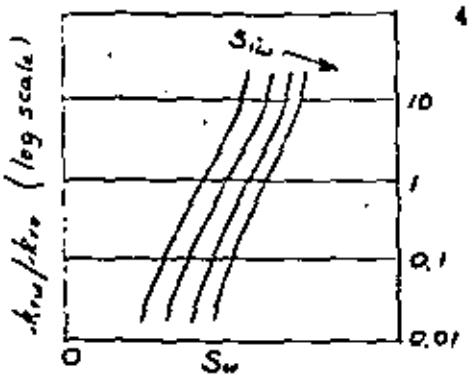

Figure 28

4. From the adjusted plot of S_w vs S_{iw} read values of S_w at selected values of S_{iw} and k_{rg}/k_{ro}. Plot these values on semilog paper of k_{rw}/k_{ro} vs S_w for lines of constant S_{iw}. The final smoothed and averaged data will have the appearance of Figure 28.

M.B. Standing
August 1974

NOMENCLATURE

C	a trapping characteristic constant of each porous media
$C = \frac{1}{(S^*_{nwr})_{max}} - 1$	
J_{sw}	Leverett function
k	absolute permeability
k_a	air permeability
k_g	effective permeability to gas
k_o	effective permeability to oil
k_w	effective permeability to water
k_{wt}	effective permeability to wetting phase
k_{nwt}	effective permeability to non-wetting phase
k_{rg}	relative permeability to gas
k_{ro}	relative permeability to oil
k_{rw}	relative permeability to water
k_{rwt}	relative permeability to wetting phase
k_{rnwt}	relative permeability to non-wetting phase
$k^o_r = k_{nwt}\big]_{S_{iw}} \Big/ k$	
λ	(lamda) pore size distribution index, exponent in equation $\frac{P_e}{P_c} = (S^*_{wt})^{\lambda}$
P_e	entry pressure
P_c	capillary pressure
ϕ	porosity
S	saturation
S_{gr}	residual gas saturation
S_{gF}	"free" (mobile) gas saturation
S_{gt}	trapped gas saturation

NOMENCLATURE (Continued)

S_o — oil saturation

S_{or} — residual oil saturation

S_w — water saturation

S_{wi} — initial water saturation (connate water saturation)

S_{iw} — irreducible water saturation

S_{Lr} — total residual liquid phase saturation

S_L — total liquid phase saturation

$S_m = 1 - S_{cnwt}$

S_{cnwt} — critical nonwetting phase saturation

S_{wt} — wetting phase saturation

S_{wtr} — residual wetting phase saturation after complete drainage

S^* — effective saturation

$S_g^* = S_g/(1 - S_{iw})$

$S_o^* = S_o/(1 - S_{iw})$

$S_w^* = (S_w - S_{iw})/(1 - S_{iw})$

$S_L^* = S_L/(1 - S_{iw})$

$S_{wt}^* = S_{wt}/(1 - S_{iw})$

$S_{gF}^* = S_{gF}/(1 - S_{iw})$ = effective "free" (mobile) gas saturation

σ — (sigma) interfacial tension

Subscripts

F — free or mobile

dr — drainage

imb — imbibition

wt — wetting phase

nwt — non-wetting phase

INGENIERIA DE RESERVORIOS GEOTERMICOS.

PROF. DR. J. RAMEY JR.

12 y 13 de Octubre de 1981.

Geothermal Systems: Principles and Case Histories
Edited by L. Rybach and L. J. P. Muffler

5. Heat Extraction from Geothermal Reservoirs

IAN G. DONALDSON

Physics & Engineering Laboratory, Department of Scientific & Industrial Research, Lower Hutt New Zealand

MALCOLM A. GRANT

Applied Mathematics Division, Department of Scientific & Industrial Research, Wellington, New Zealand

5.1. Introduction

In the practical sense the mechanisms available for the extraction of heat from geothermal reservoirs are rather limited. We may mine the fluids in the reservoir and depend on the natural replenishment of these fluids to sustain the fluid supply, or we may artificially circulate fluid through the reservoir to, in effect, mine the heat alone.

The important questions in the extraction of heat from a geothermal reservoir are how much? for how long? and of what quality? It is to the physical processes relevant to these questions that we will address the majority of our effort in this chapter. We will not consider either the economic or engineering aspects of such extraction.

Geothermal reservoirs are conveniently categorized as either 'vapor-dominated' or 'liquid-dominated'. In each case the name refers to the dominant mobile phase in the reservoir in its undisturbed state. The gradient of pressure with depth is close to that of a static column of that dominant mobile phase. The other phase may also be present and partly mobile. Thus, vapor-dominated systems contain immobile or slightly mobile water, and liquid-dominated systems may either contain liquid water only, or a steam-water mixture. It is also possible for a single reservoir to contain sections of each type. Vapor reservoirs, for example, usually have a liquid-dominated 'condensate layer' near the surface (White et al., 1971). Most reservoirs are liquid-dominated. These latter are further subdivided in this chapter into warm water, hot water and two-phase reservoirs according to how they may react under exploitation. In warm water reservoirs no boiling at all is anticipated under any expected pressure drawdowns; in hot water reservoirs any boiling is only expected to take place in the reservoir at levels above that at which almost all exploitation will take place; while in the two-phase reservoirs at least a significant proportion of the exploitation is expected to take place from within the two-phase (steam-water) zone.

The total heat contained in a geothermal reservoir may be computed if the volume of the reservoir is known and the fluid and rock properties and characteristics can be

estimated. The temperature (or enthalpy) of the fluid and the associated rock, together with the reservoir volume, are the primary factors in this heat content estimation. The temperature alone is the dominant factor in the quality estimation—the higher the temperature (or enthalpy) the higher the quality of the heat. When, however, this reservoir is mined, only a fraction of this heat energy may reach the end point of the operation. This may be due to several factors, but we may bracket these into two main categories—the efficiency of the mining operation, and the efficiency of the surface engineering procedures. This latter must depend upon the end use of the energy, as well as on many local factors. The final overall efficiency of utilisation of the geothermal reservoir requires independent study of each field and use situation. It is thus appropriate here to consider only the below ground effects, i.e. the efficiency of the mining operation.

The rate of removal of heat and fluid and the temperature of any reinjected fluid may be controlled by the end use demands. However, the below-ground processes, the actual extraction of the heat energy from the geothermal reservoir, can be studied in general terms as if they were independent of that end use. Each form, or type, of reservoir (warm water, hot water, two-phase, or vapor-dominated, generally permeable or fracture controlled, etc.) may, however, behave differently under exploitation. We therefore discuss the heat extraction from each type of reservoir in order of increasing 'dryness', starting with the 'wet' warm water systems and ending with the vapor-dominated ones. Within each category we also look at the effects of uniform permeability and/or fracture control and of naturally enhanced and artificial recharge, where these are relevant. The field examples offered are those best known to the authors, and hence, there is a strong New Zealand bias in the selection. On the other hand, these fields are all well documented so that data and experience are available for analysis and discussion. The reservoir types that do not conveniently fit our sequence—geopressured, hot-dry-rock and magma—are introduced separately at the end.

There are three themes that we emphasise throughout:

The *first* is the great difference between single-phase (water) and two-phase (water-steam) flow, as it affects pressure transmission and extraction of fluid and heat from the reservoir.

The *second* theme is that, having accepted this one division, there is a continuity in the field response, from warm-water, through liquid-dominated, to vapor-dominated systems. The continuity is provided by a scale along which a field's two-phase portion grows in importance and the two-phase region becomes drier.

The *third* theme is that the extraction of geothermal heat is a mining operation, the heat being removed from a fixed store. This store is replenished to a certain extent by the natural pre-exploitation flow, which continues after exploitation. This flow of hot water is, however, very little enhanced by any effects of the extraction. As will be seen, the pressure drop in the reservoir draws in cooler waters from around the sides, rather than additional hot waters from below.

5.1.1. *Some Background Considerations*

Before we discuss a simple basic model of a geothermal system and the behaviour of the fluid in this system under exploitation we clarify two important concepts on which some of the arguments will be based. Namely, we discuss the importance of the various flow components, and the basic well-to-reservoir link and its effect on pressures and output enthalpies. To be able to generalize our later discussion we also touch briefly on any relevant effects of likely contaminants in the fluids in geothermal systems.

(i) *Horizontal and vertical flows in geothermal systems.* Much of the international geothermal research effort naturally draws upon groundwater and petroleum engineering experience. This experience does, however, lead to a standard model of flow in confined or unconfined horizontal aquifers, and this model can be misleading in many geothermal situations. In the natural state of a geothermal system there is a strong vertical circulation. Vertical permeability must therefore exist, at least in some sections of a field. El Tatio in Chile is an atypical field in that it is apparently horizontally confined (Healy and Hochstein, 1973). It is, however, probably an outflow from a larger system with vertical circulation within the Andean mountain chain.

Although detailed well response analysis generally tends to indicate two-dimensional flows, and there are other features that suggest that some horizontal structuring predominates, these are smaller-scale features of the reservoirs. Both long-term behaviour and overall reservoir response, the indicators of the macroscopic behaviour of the system, show strong three-dimensional trends. We may thus talk of the system in the neighbourhood of individual wells in a manner that implies two-dimensional flow dominance, but in any discussion of field behaviour the three-dimensional character of the system must be taken into account.

This difference between small- and large-scale behaviour is almost certainly due to the fractured nature of most systems. Individual well tests give widely different transmissivities (permeability × aquifer thickness) reflecting the varying nature of the local fissure system from one part of the field to another. At this scale these fissures act as two-dimensional channels. On the reservoir scale, however, these channels interlink to form a full three-dimensional network. On this scale, in the two-phase zone of the reservoir, the dominant physical mechanism may be vertical motion of the two phases under gravity; in the deeper, liquid zone, the flow may be as if to a sink in a general three-dimensional medium.

(ii) *The feed point of a well.* A concept mentioned a number of times in this chapter is the feed point or feed zone of a well. Nearly all geothermal fields, excepting perhaps one such as Heber (California, U.S.A.), which taps a sandy aquifer, have significant fracture permeability. The flow to the well is not supplied by a uniform inflow over the section that penetrates some specific aquifer. Rather, the well intercepts one or a few distinct fractures. As there is usually one of these that dominates, almost all of the well's production will come from an interval of a few metres or less. This feed zone is the point in the well which will then control pressures throughout the remainder of its length. Away from this feed point pressures in the well will simply reflect the weight of the fluid column above or below this junction. This point will also often provide the one point in the well at which the well fluids are in pressure equilibrium with those in the adjacent rock. Alternatively, however, the fissure system may itself become an extension of the well, and such equilibrium may exist at only one point along its own path length.

If there is a water level in the field below which the rock is water-saturated and above which water and steam co-exist, a well will reflect the depth of its feed zone in its behaviour. 'Water-fed' wells, i.e. those feeding from below the water level, produce fluid corresponding in enthalpy to liquid water under the local reservoir conditions. The fluid entering the well is liquid water or fluid that was originally liquid at a distance but boiled on the way to the well; i.e. there may thus be a local two-phase zone surrounding the feed point of the well. Flow through this zone will, however, be isenthalpic so that the enthalpy of the fluid mixture flowing into the well will match that of the original water at a distance. In contrast, 'two-phase' wells, which feed from the established two-phase zone,

will produce a fluid of an enthalpy above that of liquid water at the feed zone temperature. Both types of well occur at Wairakei, with the two-phase wells having enthalpies ranging from only a little above that of the appropriate liquid water to that of wet, dry or even super-heated steam.

(iii) *Chemical contaminants and their effects.* Chemical contaminants occuring in geothermal reservoirs are of two types, dissolved solids and gasses. In most situations the dissolved solids are primarily of environmental concern and should have little effect on the heat extraction process. True, high concentrations of materials like calcite, as in Kizildere, Turkey, may cause such rapid clogging of wells that field production is significantly reduced. Nonetheless, if the wells and nearby rock and the associated surface plant could be kept clear, the dissolved solids would have little effect on the response of the reservoir to production. The same applies with other nuisance materials like the salt in Imperial Valley, U.S.A. Provided the fluid can be extracted and the energy utilized, the reservoir will behave much as if the geothermal fluid was of low or even nil contamination.

In contrast, any gaseous contaminants can appreciably alter the reservoir characteristics and hence, the field performance. Roughly, for higher temperature systems, the more gas present the more extensive are the naturally occuring two-phase conditions. But this is really only a shifting of the character of the reservoir along our already defined scale, towards the 'drier' conditions. Thus, provided the two-phase conditions can be defined and the gas content allowed for, the process will still fit within the range of systems considered.

5.2. Idealized Systems

5.2.1. *A Simple Basic Model*

In the introduction to this chapter we defined the primary questions relating to the utilization of energy from a geothermal reservoir as being (i) how long the resource will last under exploitation, (ii) how much heat (or energy) can we extract in that time, (iii) of what quality would this energy be? We can get some insight into the answers to these questions and into the behaviour of the reservoir under exploitation by a study of a simple general model.

The model we have chosen, and illustrated in Figure 5.1, is based on a model first produced by McNabb (1975) for the Wairakei system. The reservoir is pictured as a vertical cylinder, surrounded by cold water. In the illustration this reservoir consists of a lower hot water-saturated zone, overlain by a two-phase (steam-water) zone. Above this is a near-surface zone involving mixing with cold groundwater. This arrangement is currently in use in studies of Wairakei in New Zealand. McNabb (1975) omitted the upper cold mixing layer; removal, or expansion, of other zones might give a better match with other fields. Removal of the two-phase zone would, for example, bring the model into conformity with the warm water system; or the enthalpy or gas content might be high enough that only the two-phase zone need be pictured within the hot zone, thus giving a match with fields like Broadlands ($1\frac{1}{2}$ km to liquid) or Ngawha (>4 km to liquid) in New Zealand. At the high enthalpy limit, we have the vapor-dominated reservoir featuring a two-phase reservoir with counterflowing steam and water, and the deep water surface only a conjecture. Always present, however, is the surrounding cold water. Even the vapor-dominated systems exist in an environment of cold groundwater, although here low

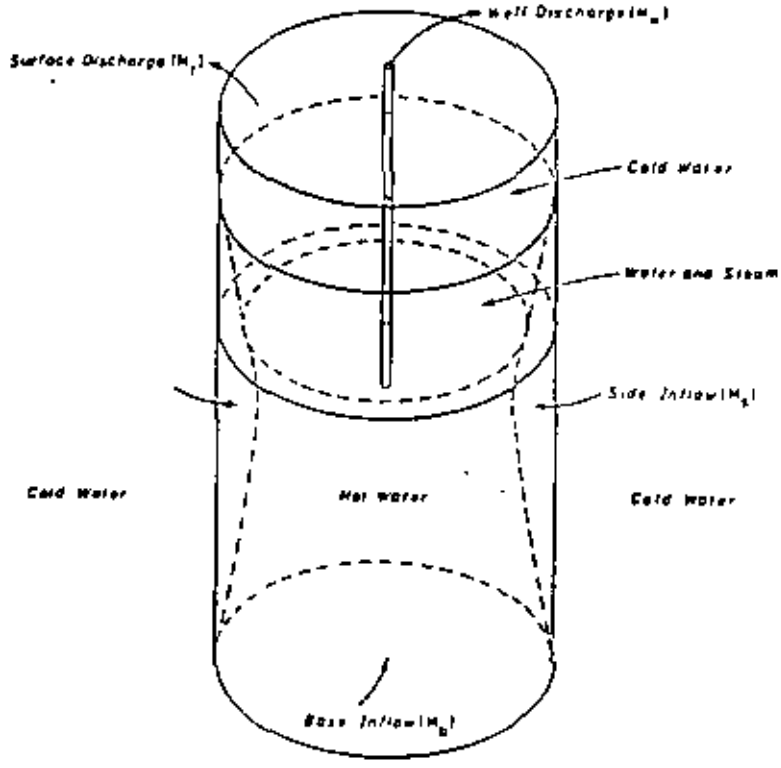

Figure 5.1. The assumed basic model (adapted from McNabb, 1975)

permeability barriers are needed around much of the field boundary to prevent flooding of the deeper, under-pressured part of the vapor system.

We idealize the zone boundaries as simple geometrical forms—planes, straight lines, or cylinders. In reality every such boundary is very diffuse and irregular. Typically at the margins of the field there are intrusions of cold water and outflows of hot water, so that the temperature pattern is quite distorted. The boundary between single-phase and two-phase conditions usually also shows considerable unevenness, with lower temperatures or gas contents giving patches of liquid flow inside the two-phase region, and patches of two-phase beneath the liquid surface. The Wairakei field is quite remarkable in this respect as its water level is very well-defined and smooth. Both the Broadlands and Kawerau fields (see Figure 5.3), in contrast, show quite irregular patterns at this boundary. The upper boundary, where cold water may enter under production, is probably the least regular of all. The main evidence at Wairakei for the entry of surface water is a single 'finger' of cold water that has quenched one well and produced some enthalpy decline in other wells. Many similar quenchings have occurred at Kawerau.

Most of these boundary irregularities are caused by the extreme variability of the permeability of the rock. However, in general, the spatial scale of these variations is usually sufficiently small that for the purposes of field-scale computations we can treat the medium as being of uniform permeability, and the boundaries as smooth and regular. Among the higher temperature fields only Kawerau in New Zealand requires to be considered as a fractured system to explain the effects of exploitation. This field is discussed specifically later. Among the warm water systems, the fractured (karstic)

limestones and dolomites at depth in the Carpathian Basin (Boldizsár, 1975) and the dike or planar systems of some Icelandic fields (Bodvarsson, 1962; 1974) also need modified treatment.

The response of the field to production is manifested by the motion of the boundaries and by decompression (boiling) within the two-phase zone. For a hot-water field, where production comes predominantly (or entirely) from the single-phase (water) zone, a good first approximation is to ignore the two-phase zone except for the fact of the fall of the water level. This gives a very simple model that has been applied to Wairakei successfully by several workers (see, for example, McNabb, 1976 or Grant, 1977a). We will therefore start with a brief discussion of the behaviour of the model in a water-only system.

5.2.2. *The Single-phase (Hot-water) Reservoir*

The model visualized is that of Figure 5.1 without the two-phase and upper zones and with all wells tapping the hot water below the (now) free surface. In the natural, undisturbed state the heat in the reservoir has been built up and maintained by a throughflow of hot water from below at the mass flow rate M_b and of enthalpy H_b. Under the assumptions that steady-state initial (pre-exploitation) conditions apply, that there is no flux of mass through the sides and that heat conduction may be neglected, the mass and heat influx at depth is equal to that discharged at the surface. The reservoir is thus isenthalpic and, neglecting the minor pressure effects, isothermal. (It should be noted that if two-phase conditions did exist above this layer the boundary pressure is still fixed at $p_f = p_{sat}(Tb)$, due to the isothermal nature of the water-saturated reservoir.)

If fluid is now withdrawn from wells in this reservoir at the rate M_w, an internal pressure drop will occur which will stimulate a flow M_s in from the sides and may alter the base inflow M_b and surface outflow M_f. For reservoir-scale calculations water may be considered incompressible, and we may write the mass balance as

$$M_b + M_s = M_w + M_f.$$

The heat balance is not so simple. The base flow still brings in the hot water and the outflows, M_w and M_f, carry out water at the reservoir enthalpy. The side flow however brings in cold water. This water does not get into the central reservoir immediately and thus does not lower the overall enthalpy. Rather it removes heat from the hot rock at the side boundaries creating a slow moving cold front that reduces the reservoir's size but not its internal enthalpy characteristics. Thus the interior remains isenthalpic and isothermal. (This means that the 'free' surface pressure, p_f, does not change even in the hot water case). Let us, however, look at these flows in turn.

(i) *The base inflow, M_b.* In most simplistic models of geothermal systems it is assumed that cold meteoric water percolates down to some considerable depth where it is heated and driven, due to the associated density decrease, back up to the surface. This flow establishes and maintains the geothermal anomaly (Wooding, 1963; Donaldson, 1970a,b). The flow path involved is a long one. It is, in fact, so long that the pressure changes occurring under exploitation do not greatly change the flow along it. Thus for Wairakei, taking a circulation depth of 10 km, the natural flux of 400 kg s^{-1} is driven by the 30 MPa difference in pressure between water columns at 20°C and 300°C. The pressure drop under exploitation, 2·6 MPa, can cause an increase of only 37 kg s^{-1}, a negligible contribution to the plant output. For other fields with smaller natural flows, the increase

would be correspondingly smaller. Thus for practical purposes, the base inflow does not change under exploitation.

(ii) *The side inflow, M_s.* The side inflow is created by the difference in pressure between the inside and outside of the hot water reservoir, a pressure difference that will be maximal at the well feed level and will tail off both above and below this level. It will, however, still exist some distance below the feed level, and hence, inflows spanning a total depth of twice or more than that of the feed zone must be considered relevant. This inflow will increase with increasing drawdown.

As has been already point out, this 'recharge' of the field with cold water will have the effect of moving in the cold side boundaries of the reservoir, the cold water pushing in the hot water already resident in the pores but being heated itself by the heat stored in the rock. If the volume flux density is v, the velocity of the thermal front is λv where λ is the volumetric heat capacity of water ($\rho_w c_w$) divided by that of the wet rock (Bodvarsson, 1972; Nathenson, 1975).

As there is no reason for the temperature within the reservoir to change until the cold front arrives, it is the inward movement of this cold front that is mining the heat from the reservoir. (The mining may, however, be limited if short circuiting occurs between the wells and the boundary).

It is important to note that this side flux will not be zero, at least until some time has elapsed, even if the mass withdrawal from the wells is quite small; i.e. we cannot just tap the throughflow of the system without some system adjustment.

(iii) *The well discharge, M_w.* The total well discharge will be controlled by several factors, some man-controlled, such as the number of wells or the valve settings, and some field-controlled, such as the field pressure. Thus additional wells may increase the total discharge while the associated additional drawdown of the field may significantly reduce it. Adding wells may produce only temporary benefits, and the field may have an 'effective' unpumped output limit that it itself sets.

As the enthalpy of the warm water reservoir has not changed, the enthalpy of the discharge will remain h_s. Any downturn in the enthalpy of the discharge must therefore suggest the entry of cooler water.

(iv) *The surface discharge, M_f.* If we increase M_w sufficiently, M_f will reverse in sign, and the water level of the system will fall. This in itself is of no great significance unless the wells are too shallow or if the hot water is overlain with cold. In this latter case a further thermal front is present, and heat mining at the upper boundary will also take place. Unfortunately, with colder water being drawn down above warmer fluid, the potential exists for gravity instability, and 'fingering' of the cold fluid down into the system must be anticipated.

The simple analysis of a hot (or warm) water system illustrates the source of energy and the effects of differing rates and depths of withdrawal. A fuller quantitative analysis could well give estimates of the available energy resource and show the advantages or disadvantages of different rates of withdrawal. This is, however, more pertinent to specific field studies than it is to a general discourse.

There are two further points that we can illustrate with this warm water system—the role of fractures, and the potential effects of reinjection.

Fractures are, in effect, preferred flow paths, and hence a well striking a fracture, or any such freer flow channel, will draw its fluid preferentially from that source. The reduced

pressure in this channel will then draw water from smaller cracks and crannies and from the rock pores. The fracture system thus acts as a distribution network for the wells while the porous intermediate beds act as a fluid and energy store. The withdrawal of water and heat from the pores and small cracks has a much longer time scale than has the transfer of fluid along the channels. If a fracture, tapped by a well, reaches a cold water boundary, the cold water will be encouraged along its path into the reservoir. This section of the cold front will move much more quickly than neighbouring areas on account of both the higher velocity and the smaller contact area with the heated rock. High withdrawal rates from wells could therefore result in the amplification of this effect with the possibility of the creation of an effectively dead field with considerable heat still stored but inaccessible to the wells and their feeding fractures. Lower flows could result in a much greater total heat output.

Reinjection of fluid into the system must result in some pressure increase in that system, at least locally. Such a pressure increase, if it affects the reservoir, will assist in maintaining the mass output of the wells. As cooler water will be injected, however, the discharge wells may also be cooled. Obviously this can occur if this fluid is injected within the reservoir and strikes a well feed-channel, as we are likely to maintain a flow path by keeping the pressure up at the reinjection well and down at the withdrawal well. In fact, reinjection at any point within the reservoir will reduce the flow path for the cooler water to the wells. In contrast, reinjection at the boundary may still maintain the field pressures but merely locally enhance the already developed cold front. Naturally the site choice must also depend on other information. Gringarten (1978) shows, for example, the very strong dependence of the reservoir lifetime and the heat recovery factor on the selected development scheme. His study suggests that these may both be increased by alternating injection and production wells; i.e., by *unitizing* geothermal aquifer production as is already done in oil and gas reservoirs, rather than using either isolated withdrawal wells or isolated withdrawal/injection well doublets.

5.2.3. *The Two-Phase System*

In the last section we discussed the behaviour of the single-phase (liquid) system. Under the assumption of incompressibility, the source of the extracted energy is shown to be at the reservoir boundary. The major distinction in geothermal fluid flow is that between the single-phase flow and the two-phase flow. In this latter we include all systems containing two phases even if one phase is immobile. For example, vapor-dominated systems are included in this latter category.

Pressure transmission. In a single-phase flow, in spite of our assumption, some fluid can be made available by decompression. In liquid-dominated geothermal systems, this is generally a negligible amount.

The speed of the diffusion front spreading through compressed liquid is high. It takes only days for a pressure pulse to cross the Wairakei field, for example. Thus the period of production by decompression, when a bore is switched on or off, lasts only this time of a few days. After this a quasi-steady state is established with a falling water level and a continuing cold recharge from the side boundaries of the field. Mass is supplied by this recharge, and energy by the cooling of the field margins. This is a very desirable mode of exploitation. It means that the wells can have a long lifetime, as their region of exploitation is the entire field.

A two-phase mixture of water and steam, on the other hand, is far more compressible

than either water or steam. It takes far longer for a pressure pulse to diffuse out to the field boundaries and induce a recharge. The greater compressibility means that more fluid is yielded from storage by a given pressure drop. Also, because two-phase conditions mean that the pressure drop is accompanied by a temperature drop, energy is mined from the rock thus cooled.

The compressibility of a two-phase steam-water mixture has been determined by a simple approximate approach by Grant and Sorey (1979). They suppose that the pressure of the fluid in a unit volume of porous rock is decreased by Δp. This causes a corresponding temperature drop (along the saturation curve $p = p_{sat}(T)$).

$$\Delta T = -\Delta p/(\mathrm{d}p_{sat}/\mathrm{d}T)$$

Heat is thus liberated from the rock, and this boils some of the water to steam. As this steam occupies more volume than the water it comes from, there is a volume increase ΔV. This may be related to the pressure drop to obtain an effective compressibility, i.e.

$$c_2 = \frac{1}{V}\frac{\Delta V}{\Delta p} = \frac{1}{\phi}\frac{1}{H_s - H_w}\frac{\rho_w - \rho_s}{\rho_s \rho_w}\frac{\overline{\rho c}}{(\mathrm{d}p_{sat}/\mathrm{d}T)}$$

Here we use the subscript 2 on the compressibility to emphasize that this is only valid under two-phase conditions. In the full expression for this compressibility, ϕ is the porosity of the medium, H_s and H_w are the enthalpies of the steam and water phases, ρ_s and ρ_w are the associated steam and water densities and $\overline{\rho c}$ is the heat capacity of the wetted rock. Full derivations of this compressibility are given by Garg (1978), Grant (1978) and Moench and Atkinson (1978). This compressibility is orders of magnitude greater than either the steam or water compressibility. From the form of derivation of c_2, it can be seen that it is not compression of each or either phase that matters, but the transfer of matter between the two. The fluid in the pores responds to a pressure drop by yielding fluid to flow and replaces the lost volume by boiling some water to steam. The mechanism is the same whether the flowing fluid is primarily water, or steam. If a cubic meter of fluid is removed from the pore space in rock at 250°C, a further 0·025 m³ boils to fill the 1·025 m³ with steam. The amount of boiling, and hence of cooling or decompression, is the same whether the fluid removed is water or steam.

The greater compressibility of the two-phase mixture means that for a given pressure drop we get a proportionately greater yield of fluid volume from each rock volume. We also take heat from the rock, by the very process of boiling. If we begin with a two-phase mixture in the rock, there is some amount of steam initially in place. When we decompress, and force boiling to take place, all the additional steam that flows is supplied from water. The heat to boil it is supplied by the rock.

The source of the extracted energy. We have already indicated that for the single-phase system, due to the rapid transmission of any pressure change, all the energy is mined from the perimeter of the reservoir after the first few days of operation or change. In the two-phase situation, however, it takes time, probably of the order of years, before this condition eventuates. It is thus of interest to see just where this energy comes from in the interim. A study of a single well penetrating and extracting its fluid from the two-phase zone is useful in this regard.

If we consider the area around the well as being initially at a uniform pressure p and a

uniform water saturation (the ratio of water volume to total pore space) S, and then allow only small perturbations from this state, a diffusion equation for pressure may be derived (Grant, 1978; Grant and Sorey, 1979).

We may thus write

$$\frac{1}{\kappa}\frac{\partial p}{\partial t}=\nabla^2 p$$

where κ is the hydraulic diffusivity ($=k/\phi\mu_t c_t$)
k is the permeability of the medium
and μ_t is the total dynamic viscosity of the fluid

$$(=F_w(S)/\mu_w+F_s(S)/\mu_s)$$

In this latter expression μ_w and μ_s are the dynamic viscosities of the independent phases (water and steam) and $F_w(S)$ and $F_s(S)$ are the water saturation dependent relative permeabilities of the water and steam phases in the mixed flow system. The relative permeability to either phase is the fraction of the actual permeability that has to be taken if Darcy's Law is to be applied to each phase independently (see, for example, Scheidegger, 1957, p. 155).

As we pointed out earlier, the analysis of single well behaviour tends to indicate a dominance of horizontal structure. We will therefore restrict this consideration to the problem of transient flow around the well in a uniform horizontal aquifer containing the two-phase mixture. The conclusions reached apply equally to other geometries, but this arrangement would appear to be most compatible with both the field behaviour and the assumptions made in the derivation of the pressure equation.

Solutions to this equation are well known (see, for example, Carslaw and Jaeger, 1959). For the case of a well opened at time $t=0$ and discharging at the constant mass rate W we have, for example,

$$p=(W\nu_t/4\pi kh)(-Ei(-r^2/\kappa t))$$

where the total kinematic viscosity ν_t is related to the kinematic viscosities of water and steam, ν_w and ν_s, by the expression

$$\frac{1}{\nu_t}=\frac{F_w(S)}{\nu_w}+\frac{F_s(S)}{\nu_s}$$

The mass of fluid stored per unit volume of rock is

$$\phi[\rho_w S+\rho_s(1-S)]$$

The rate at which fluid is lost from storage, or yielded to the flow in the reservoir, is the rate of change of this with time. This is proportional to

$$c_2\frac{dp}{dt}\propto c_2\frac{1}{t}e^{-(r^2/\kappa t)}$$

Figure 5.2 illustrates the pressure profile at time t with distance r out from the well, the rate of loss of fluid from storage with radial distance (at a particular time t), and this rate of loss with time (at a particular radius r).

After time t the pressure front has diffused out a distance of the order of $(\kappa t)^{1/2}$, the diffusion radius (Figure 5.2(a)). If we look at the pattern of fluid yield at this time, Figure 5.2(b), we see that fluid is being taken from storage (at a rate that declines as t increases) within this same diffusion radius. Little is taken beyond this circle. As Figure 5.2(b)

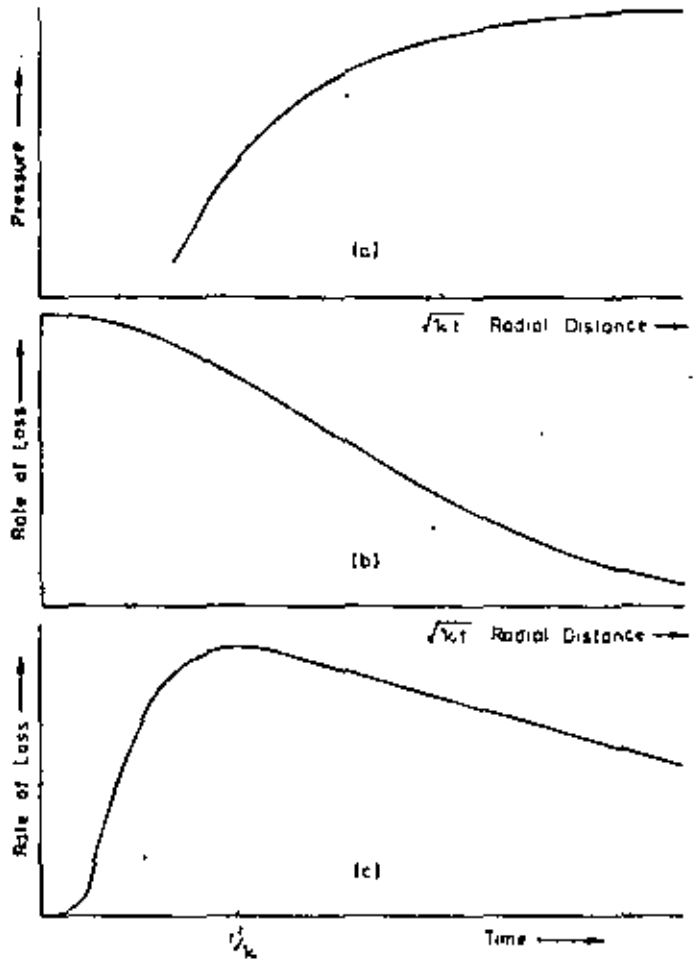

Figure 5.2. The role of the diffusion radius $(\kappa t)^{1/2}$ at any given time t after the commencement of a constant mass withdrawal from a well. (a) The profile of pressure drawdown. After this time t the pressure drop has diffused out a distance $r \approx (\kappa t)^{1/2}$. (b) The profile of rate of loss of fluid mass (kg m^{-3} s^{-1}) from the rock matrix. (c) The variation of this rate of loss of fluid mass with time at some fixed radial distance r from the well. Note the peak loss at $t \approx r^2/\kappa$

illustrates only the rate of fluid yield per unit volume, to obtain the rate of yield per unit area at the radial distance r this function must be multiplied by $2\pi r$. This product has a maximum at $r=(\kappa t)^{1/2}$ and is small for both small and large r. Thus the bulk of the fluid entering the well is supplied from a broad band around this diffusive radius.

If we look at a particular point to see the pattern of fluid yield with time, Figure 5.2(c) results. At first little fluid is yielded, as the point is outside the diffusion radius. The yield rate rises to a maximum at $t=r^2/\kappa$ as the diffusion front goes past, then slowly declines. Note that the rate of fluid yield depends on the rate at which the pressure is changing with *time*. Thus, although the pressure increases markedly with *distance* near the well, this does not mean correspondingly large amounts of fluid yield. The pattern of fluid yield from storage is very smooth, out to the diffusion radius $(\kappa t)^{1/2}$ (Figure 5.2b).

Along with the yield of mass from storage in the pore space, there is a yield of energy from the rock. The transmitted fluid is a mixture of water and steam, with an enthalpy above that of liquid water. The excess of enthalpy is supplied by the rock, and the profile of this yield of heat is proportional to that of the yield of mass. This means that the pattern of heat yield, the extraction of heat from the rock, is evenly spread out to the diffusion radius. The gradient of pressure, and hence temperature, with distance becomes very large near the well. Little heat is however transferred to the flowing fluid as the temperature of the rock is falling very little *with time*. Although there are large temperature changes near the well, the flow is nearly isenthalpic, i.e. the enthalpy of the flowing steam/water mixture stays almost static. As its pressure and temperature fall, the steam/water ratio (and hence the steam saturation) increases to maintain this condition. It is not possible under normal conditions for a quasi-steady flow to consist only of moving water at some distance, and only of moving steam at the well.

At this point it is of interest to look at two examples of two-phase systems by using variations of our simple basic model.

(i) ***The liquid-dominated two-phase system.*** If the basic model is taken, more or less in the form illustrated (Figure 5.1), with a two-phase zone overlying the single-phase water-saturated reservoir and with all exploitation wells tapping the fluid in the two-phase zone, we have a good example of the liquid-dominated two-phase system. An example of such a field is Broadlands, New Zealand, described in more detail later in this chapter.

In such a field it would take one or more years for the diffusion front to reach the edge of the field. Thus, for time less than this after turning on a well, heat and mass are withdrawn from an ever-increasing region around the well. For longer times, a quasi-steady state is established, similar to that for a liquid field in which the cold surroundings gradually encroach upon the hot zone. Again we have the situation that mass flow from the field is balanced by cold inflow, so that the ultimate mass source is outside the field. The heat flow out of the well is sustained by the heat supplied to the incoming fluid by rock cooled on the field boundary, so that again the well mines heat from the field boundary. There is also a continuing contribution of heat and mass from the two-phase zone if there is a continuing pressure decline with time.

Along with the sideways propagation of the pressure wave and of the mass and heat withdrawal front, there will also be some vertical propagation effects. In time the pressure wave will also reach the base of the steam/water zone and thence propagate relatively quickly through the water-saturated section. Water will thus boil at the interface, the interface level will drop, and energy will be extracted from the rock in the immediate vicinity. Some energy will also be mined at the sides of this hot, liquid section, even though no wells directly tap it.

(ii) ***The vapor-dominated system.*** We can use another variation of the model for a steam well in a vapor-dominated system. In this case the reservoir will contain steam and immobile water and the all-liquid zone, if it exists at all, will be assumed to be at such great depth that it does not appear in the section of the model of interest. Pressure transmission here is a particularly simple case of two-phase propagation. Only steam moves, and with the pressure drop some of the water boils to contribute more steam to that flow. In so doing, it takes heat from the rock, and this process thus mines both mass and heat from this local material.

The diffusive pressure front in these conditions can take years to travel a kilometre. Thus we can dispense with the sides of the model and think of the well as being in an

infinite medium. This ultra-simplification is compensated by a new complication—there may be a dry steam zone in the system. The water saturation changes in the two-phase zone are linearly related to the temperature changes. Hence, depending on the initial conditions, the pressure and temperature may decay enough to drop the water saturation, S, to zero. If this occurs, there will be a dry steam zone around the well. Within this dry steam zone there is a little further yield of mass by expansion of the steam, and a little further yield of energy as the steam pressure drops, creating a slight superheat of the steam. The profile of drawdown is, however, little affected by this additional zone. The steam well thus has an expanding zone of drawdown with the diffusion radius $(\kappa t)^{1/2}$. The outer parts of this are two-phase, but there may be an inner zone containing dry steam. The well draws mass and energy almost entirely from the two-phase zone—the dry zone being effectively a 'dead core' of the well's exploitation area.

If cold water is reinjected into a hot water reservoir, the idealized picture suggests establishment with time of a zone of cool water around the reinjection well. This will in turn be surrounded by a warm water zone, created by the extraction of heat from the neighbouring rock by the cooler reinjection water; beyond that will be the natural uncooled geothermal waters (Bodvarsson, 1972). A similar picture arises with reinjection into two-phase conditions: cold water by the well, then hot water, and finally the natural two-phase conditions. The hot liquid acts as a buffer between the cold liquid and the two-phase fluid.

Under most normal permeabilities and injection rates the reinjected cold water spreads radially out from the reinjection well, the pattern being distorted only to a minor extent by the bouyancy effects. The movement will naturally be enhanced along any lower permeability channels. In a vapor-dominated system, in which the vertical pressures relate much more closely to the steam conditions, the downflow of water will be much more significant.

With our limited experience with reinjection this picture can only be an idealized one. The actual performance of reinjection wells shows, however, the very strong influence of permeability variations, and the fluid motion is thus far from that of uniform radial spreading. A reinjection test has, for example, been carried out at well BR7 at Broadlands, New Zealand, for the past two years. This well has three feed zones. One of these has been accepting reinjection fluid at 90–150°C. Another, only 50 metres deeper, still contains 280°C fluid (P. F. Bixley, personal communication). Such details are difficult to allow for and, at this time, analysts can only hope that the idealized picture has some validity on the large scale.

5.3. Heat Extraction from some Typical Existing Fields

To illustrate the above idealised behaviour in some real systems we have selected some typical existing fields for discussion. As several New Zealand fields are mentioned, the locations of these are indicated in Figure 5.3. We start with the warm water reservoir and work our way through to the vapor-dominated one. The continuous nature of the change in field response may be seen as we move through the sequence of reservoir types.

5.3.1. *The Warm Water Reservoir*

For this discussion we define a warm water reservoir as one containing water at a sufficiently low temperature, under the prevailing reservoir conditions, that boiling does not occur within the reservoir environs either under natural conditions or under

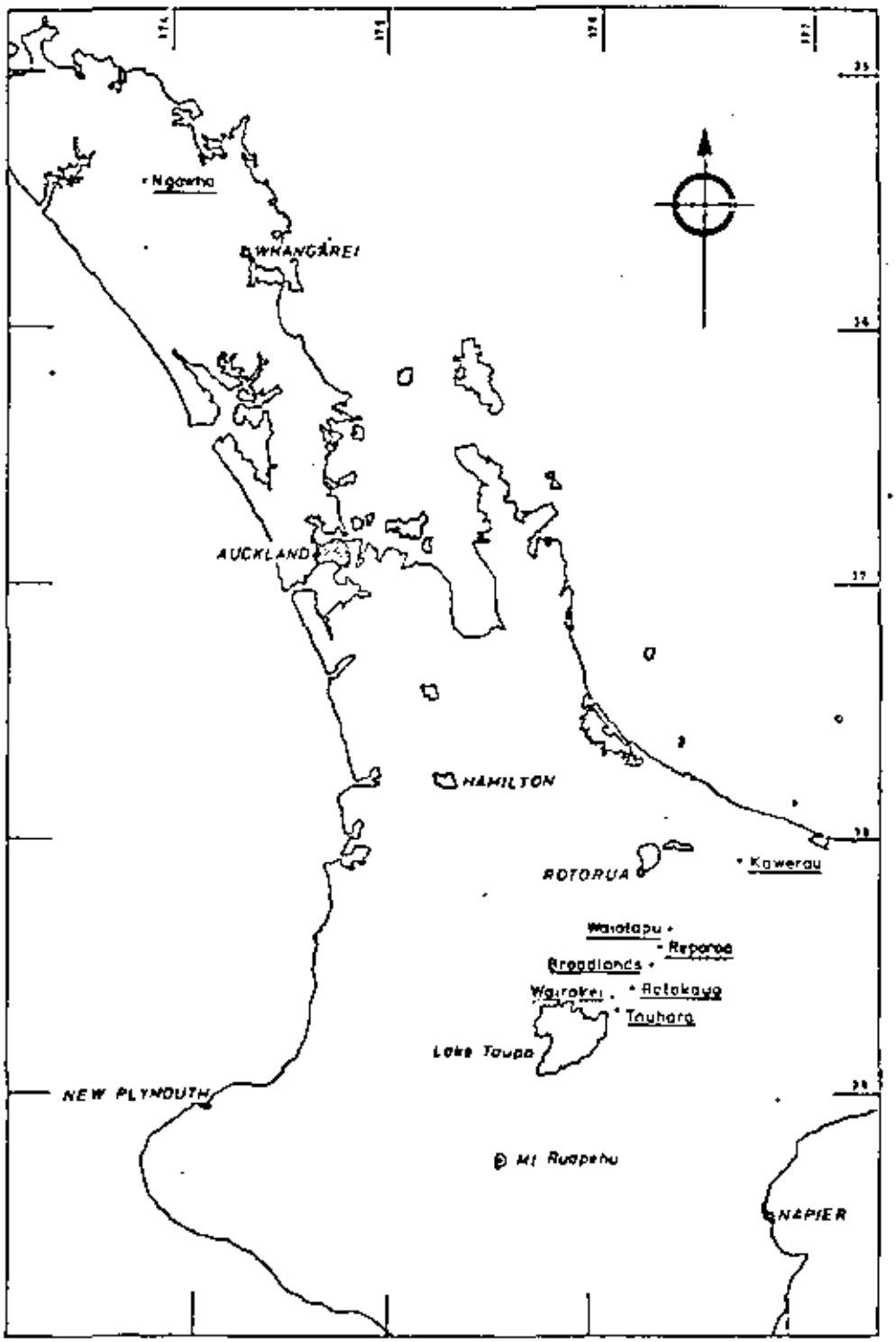

Figure 5.3. The location of the New Zealand geothermal fields discussed in this chapter

exploitation. It thus includes systems with temperatures of up to 100°C, commonly only exploited for home heating, agricultural purposes and balneological use, and the Icelandic 'low temperature systems'. It may also include some systems with recorded temperatures as high as 200°C.

A system that fits into this category, although at the high-temperature end of the scale, is that at Heber, California, U.S.A. We consider this in some detail as the geology alters the conceptual picture of the field but leaves the mechanics of heat removal much as it is in other warm water fields. The following description is based on the study of Tansev and Wasserman (1977). Figure 5.4 is Figure 1 of their paper.

The field is roughly circular, with an area of 30 km² inside a 120°C contour. The maximum temperature is 190° and a plant is planned that will use fluid at 160°. The field consists of interbedded sand and shale layers overlain by some 600 metres of shale alone. The sand is permeable, and its volume is the fluid reservoir.

Although the layering may be expected to impose a horizontal flow on the reservoir under exploitation, several features indicate the presence of vertical permeability and the absence of any boundaries. Pressure tests have, for example, investigated out to a radius of more than 6 km, i.e. beyond the boundaries of the useful reservoir.

The natural gradient of pressure with depth for this field corresponds to the static

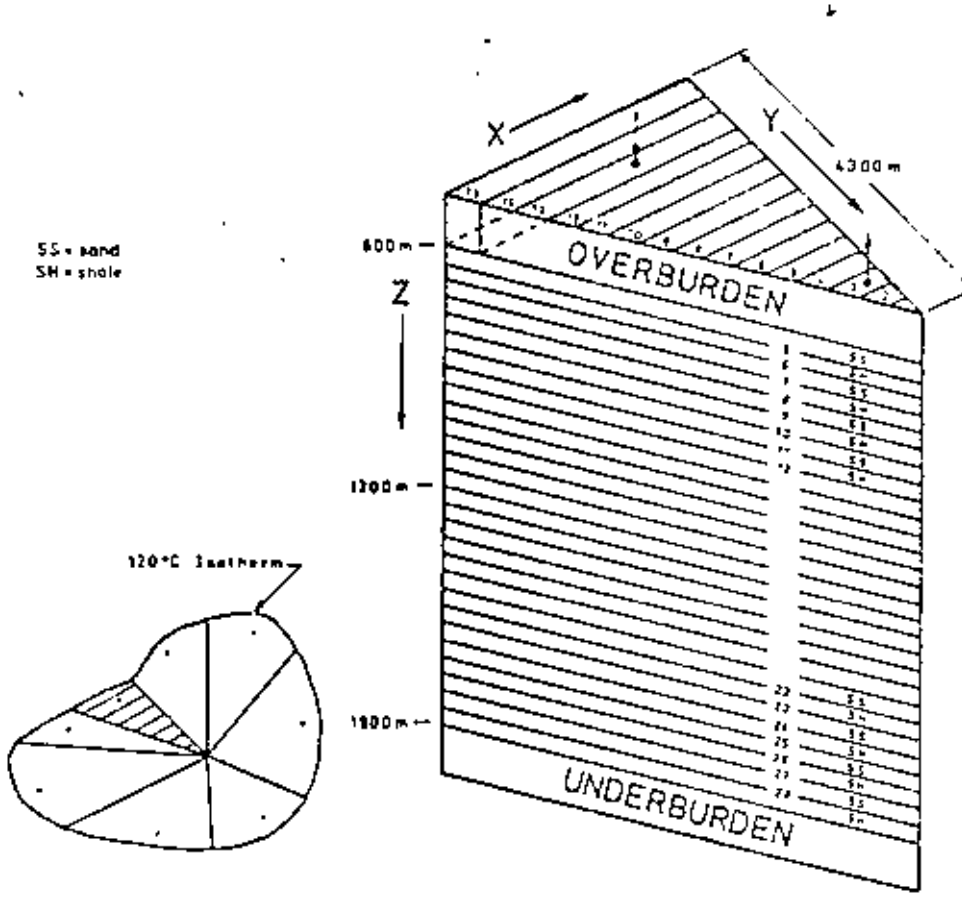

Figure 5.4. The geometry of the three-dimensional model of the Heber geothermal field (from Figure 1, Tansev and Wasserman, 1977, reproduced with permission)

pressure of water at 85°C. The temperature distribution in the reservoir is uniform vertically, but with temperatures diminishing with horizontal distance from the centre of the reservoir. This combination indicates a natural vertical circulation with the warmer central water rising while that further out, and cooler than 85°C, will be falling. This again implies permeability extending into the cooler environs of this field.

Tansev and Wasserman modelled the Heber field under exploitation assuming horizontal flow along the sand layers, with heat conduction from the interbedded shale. The flow is driven by the discharge from the producing wells and by fluid injection at the thermal boundary. Any deficit in fluid is assumed to be made up by inflow across the boundaries. Because pressure diffuses so rapidly in liquid, the liquid is assumed to be incompressible. The flow field is then determined geometrically from its sources and sinks. The main interest in the model calculations is not in the pressure field, but in the temperature, and hence the heat extraction. The pressure field does, however, vary passively as the fluid viscosity and density are allowed to vary with temperatures, and hence the fluid's resistance to flow depends on the temperature. As the fluid moves inwards, the isotherms contract. In this model, the simple sweeping out of energy along each layer is modified by conduction from the bounding shale layers. Thus at any given time the temperature profiles will be pulled in somewhat more in the sand than in the shale. It is estimated that about 30 per cent of the heat in place is recoverable.

5.3.2. *Hot Water Reservoirs*

In contrast with the warm water reservoir, boiling can occur in the hot water reservoir in both the natural and exploited states. All withdrawal will, however, take place from the water-saturated zones. Unless drilling is therefore particularly deep this implies a somewhat shallow two-phase region. Two examples are considered here.

(i) *Wairakei, New Zealand.* The classical example of such a hot water system is probably the Wairakei field in New Zealand. Although some wells do extract water and steam from the upper two-phase zone, the majority are sufficiently deep and so cased that they draw only from the deeper water section. Most of the field's behaviour may thus be explained by treating it as only a hot water system.

A typical geological section across the Wairakei field is illustrated in Figure 5.5 (from Grindley, 1965). This shows considerable horizontal structure, but again, as with the Heber field, California, the indications are that vertical connections, and hence permeability, exist at all observable levels and that vertical circulation of both fluid and heat therefore takes place.

In its natural (undisturbed) state, the Wairakei reservoir had an input temperature of 260–270°C; i.e. water at this temperature rose from depth under natural convection and heated the reservoir fluid and rocks. At a depth of about 400 m the fluid pressure and temperature were such that boiling could take place. Thus from that level to the surface, both steam and water moved upwards, the temperature and water saturation of the mixture being set by the pressure at the level concerned and by the natural heat flux. At the shallower levels, for example, the lower pressure means a lower temperature ($T = T_{sat}(p)$), and, to maintain the heat flow, a higher proportion of steam (a higher steam saturation) is required. At the surface, i.e. at 100 kPa and 100°C, under isenthalpic flow conditions, one sixth of the mass flux must be steam. This is equivalent to about 99·7 per cent of the volume flux. An estimate of the temperature, pressure and water saturation variations with depth in this natural situation is illustrated in Figure 5.6. A fuller

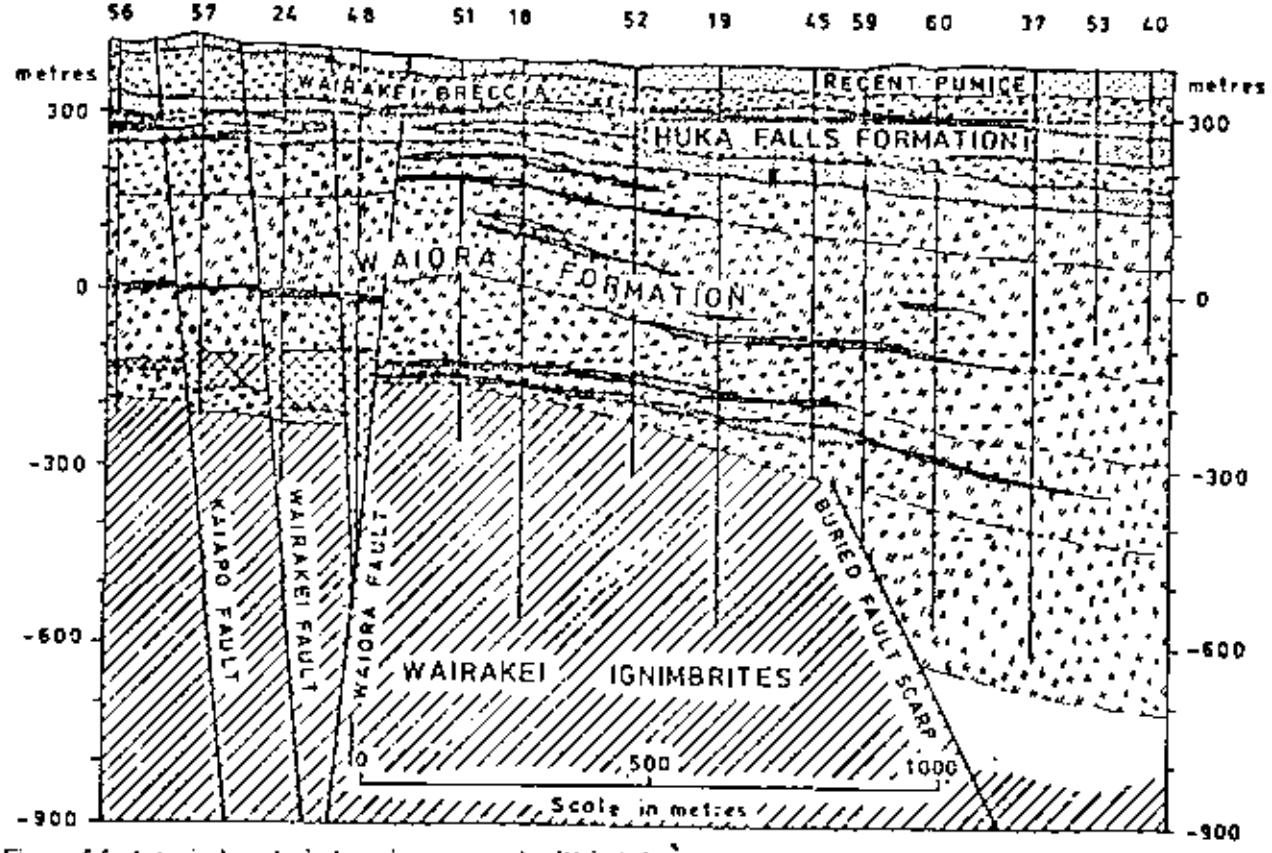

Figure 5.5. A typical geological section across the Wairakei geothermal field. This section runs approximately E W through the centre of the production area of the field (from Figure 60, Grindley, 1965 reproduced by permission of Director, N.Z. Geological Survey)

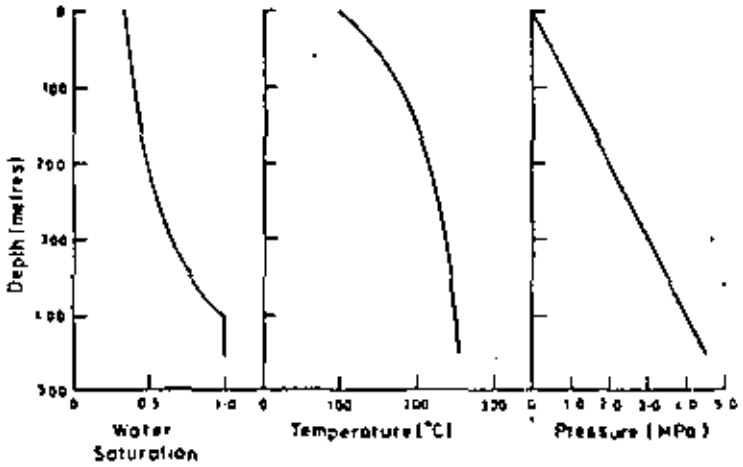

Figure 5.6. The estimated temperature, pressure and water saturation variation with depth for the Wairakei geothermal field in its natural, undisturbed state

discussion of an undisturbed system of this nature has previously been presented by one of the authors (Donaldson, 1968).

The two-phase zone is often referred to as the steam zone or steam cap. It should be remembered, however, that it contains water as well as steam, and that the pressure gradient with depth is nearly hydrostatic. It is not a static bubble of steam overlying water.

Production holes feed both from this two-phase zone and from the deeper water zone. The bulk of the wells feed deep enough to produce only liquid water (at the enthalpy of the field water). The few shallower wells feeding in the two-phase zone, in contrast, produce both liquid water and steam, and the enthalpy of their feed, essentially the proportion of steam, increases towards the surface.

Most of the production comes from beneath the water level (the water/two-phase interface). The published curves of aquifer pressures (Bolton, 1970) in fact refer to pressures averaged over the well readings taken in any given calendar month. They are adjusted to a particular level in the water-saturated section of the system.

These pressures, recently reassessed by L. J. Fradkin (personal communication) for the period 1958–68 and by one of the authors (MAG) and A. McNabb (personal communication) for earlier and later periods, are plotted for a 580 m depth in Figure 5.7. Monthly mass discharges and annual average mean discharge enthalpies (from New Zealand Ministry of Works and Development data) are also illustrated on this figure.

In the liquid zone, the outstanding feature about the Wairakei reservoir is its uniformity. The pressure drop in the field is spread nearly uniformly, with only about 100 kPa difference from the production zone to the boundaries. This is not true in the two-phase zone. There, on account of the much slower rate of pressure diffusion, there is a localized pressure defect in the production area which is apparently not present at the edge of the field.

With continuing production the pressures in this water zone have fallen steadily (Bolton, 1970), although the decline is now small (Figure 5.7). The total pressure drop is 2·6 MPa. With this pressure drop, the water level has fallen correspondingly and is now

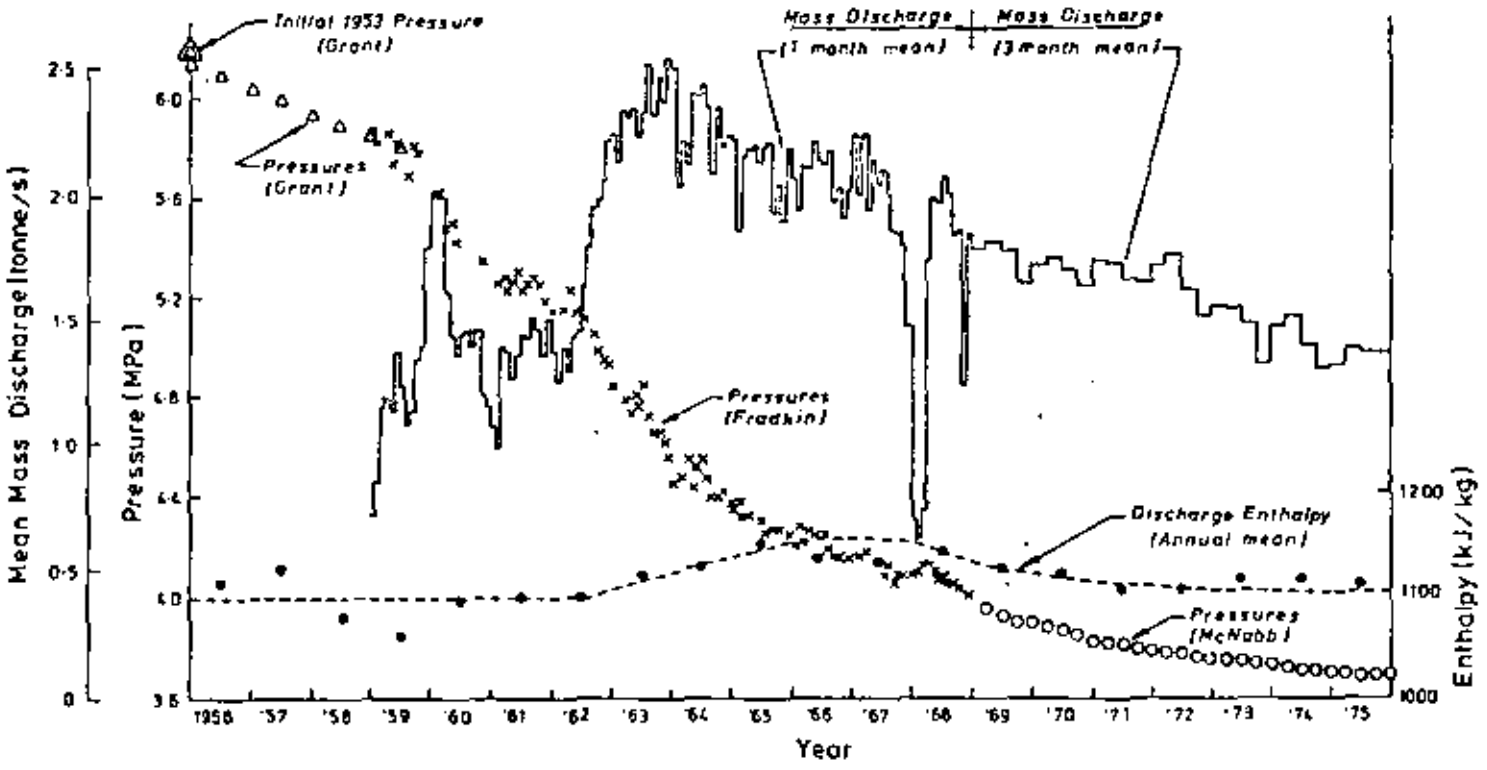

Figure 5.7. The mean mass discharges, discharge enthalpies and pressures at 580 m depth at Wairakei for the period 1955-75. The measurement data are all from New Zealand Ministry of Works and Development records. The mean monthly pressures have been estimated from these data by M. A. Grant (1953-59), L. J. Fradkin (1958-68) and A. McNabb (1969-75) (personal communications). Reproduced by permission of the International Institute for Geothermal Research, Pisa, Italy.

at a depth of 600 m. There has also been an apparent fall in the temperature of the water feeding these wells. The cause of this is not yet fully understood.

With the fall in water level, the feed zones of some wells have moved from the water zone to the two-phase section. Wells feeding from this zone are isolated. Recharge is effectively a long way off, and they thus produce their fluid by boiling in their own neighbourhood. This results in a steady and continuing local decline in pressure and temperature in the two-phase zone. With this, the performance of the two-phase wells also goes down.

In the early stages of production, most wells fed from the liquid zone, and the overall production initially had an average enthalpy of 1100 kJ/kg, i.e. near that of liquid water at 253°C. With exploitation, beginning in 1953, the two-phase zone has grown, and within it conditions have tended to become drier. Thus by 1967 the enthalpy of the two-phase wells had risen sufficiently to raise the average output enthalpy to 1160 kJ/kg. Thereafter the enthalpy fell for two reasons: the two-phase wells declined in performance more rapidly than did the water-fed wells, and there has been a slight drop off in the enthalpy of the water wells due to the temperature decrease. The enthalpy history of the discharged fluid may thus be taken as steady at around that of liquid water at 260°C with a perturbation of the order of 10 per cent over a period of a few years in the 1960's. Overall it has deviated little from that of liquid water. This, together with the pressure decay effects and the relatively minor temperature drop, suggests that the overall field response can be modelled as though all withdrawal came from below the water level, i.e. below 600 m.

There have now been several attempts to model the Wairakei field, presumably on account of the amount of data available throughout its exploitation lifespan. Whiting and Ramey (1969), for example, considered it as a compressed, sealed unit, similar in most respects to a standard oil reservoir. Marshall (1966, 1970, 1975a, 1975b), in contrast, set up a one-dimensional vertical model and allowed for the vertical throughflow and some inflow (recharge) from the sides. Detailed numerical models have now also been produced by several research groups. Mercer et al. (1975) and Mercer and Faust (1976, 1979) have developed two-dimensional horizontal models of the system, using integrated averages over the vertical dimension in the Waiora formation to give them meaningful average values of their variables for their program, while Pritchett et al. (1976a,b) have concentrated their major effort on a vertical section. To date, however, the simple drainage model (McNabb, 1975) and its more recent variations do appear to best describe and match most features of Wairakei's response to exploitation.

This model is virtually that described earlier in the section on the single-phase (hot water) reservoir. With the two-phase layer above there are only minor differences. In this case the natural state is an upflow of hot water which boils at about 400 m depth. Above this level both water and steam rise to the surface to give the natural output.

Under exploitation the water level in the model falls, and pressures in the liquid zone fall with it. The natural flow is now mainly drawn into the wells, but a surface discharge continues as a transient feature of the two-phase zone; i.e. even though the pressure gradient decreases the steam is still driven upwards. At greater depth, as was illustrated above, the natural upflow is only minimally increased by the exploitation. The pressure drop in the field thus mainly stimulates the inflow of cold water from the sides.

Associated with the fall in water level there is also drainage from the two-phase zone. The additional volume of rock exposed by the falling water level is not dry—it does in fact retain some water. This water drains downwards, and as the pressure drop slowly diffuses upwards, this drainage extends into the pre-existing two-phase zone. There may also now be some entry of cold water at the surface.

Selecting reasonable numbers for the parameters in the equations that apply for this model gives on solution the correct form for the pressure decay curve and a reasonable match of the field behaviour. With adjustment of the more doubtful parameters, good fits of the data are readily obtained. These good fits should not, however, be taken as the ultimate check on the model or the parameter values, as various factors can introduce a bias into these parameter estimates. Only the successful forecasting of field behaviour will be the indicator of real success.

It should be noted that no geological boundaries are indicated, or included even implicitly, in this model. At this level of aggregation they do not appear to exist: i.e. the fluid flows as though all strata are equivalent. There are numerous geological details in the field (see, for example, Figure 5.5 and Grindley, 1965), and these affect the performance of individual wells and can be seen in other features of the response to exploitation. The most obvious is that horizontal permeability in the field must be very high in order to produce the observed pattern of uniform drawdown right across the field. It has also been suggested that the Huka Mudstones form a cap. The initial pressure distribution and the pre-exploitation surface manifestations contradict this as these both suggest no significantly greater impediment to flow at this or any other level. These mudstones do, however, appear to affect the horizontal transmission of pressure to the adjoining Tauhara field (Wooding, 1980). For the field response, the existence of capping or otherwise is irrelevant. The field responds as an unconfined system, because of the motion of the free surface. A similar openness has been recently observed for the Momotombo reservoir in Nicaragua (Dykstra and Adams, 1977).

This simple model suggests that cold water inflow from the sides is one mechanism limiting the lifetime of a field. For ideal conditions one might therefore be able to estimate a 'recovery factor' (the fraction of the total heat in a defined reservoir that could be extracted). Such exercises have been carried out elsewhere (Nathenson, 1975; Nathenson and Muffler, 1975). Their recovery factor of 50 per cent for ideally permeable conditions corresponds with that obtained for Wairakei with this ideal model. To allow for the structural inhomogeneity, only a qualitative correction factor is possible, and Nathenson and Muffler (1975), in fact, halve their ideal figure. Current experience at Wairakei is that cooler water now enters from above in local production areas, and as this has not yet been allowed for in any analysis even this 25 per cent factor may be too high.

(ii) *Kawerau, New Zealand.* In marked contrast with Wairakei, where the geological structure appears to play only a very minor role in the control of the transfer of mass and heat within the reservoir, the Kawerau field appears to show a very strong lack of homogeneity of its structures in its behaviour. In particular, it shows the phenomenon dreaded in all discussions of reinjection but so far, fortunately, seldom seen—preferential paths for the rapid entry of cold water.

When first drilled, most Kawerau wells tap two-phase conditions, and hence Kawerau perhaps should be categorised as a two-phase field. The cooling discussed, however, quickly reduces the feed zones to the liquid state, and hence it was thought more appropriate to discuss the behaviour of this field here.

The Kawerau field is located in the New Zealand thermal belt, about 80 km north-east of Wairakei (see Figure 5.3). It has been exploited at a relatively low level for over twenty years. Drilling began in the early 1950's (Studt, 1958) to obtain steam to supply a pulp mill. Seven holes were drilled initially to a depth of about 600 m, and sufficient steam was obtained to satisfy the requirements of the time. After a few years these wells failed and some of them were deepened (Dench, 1962). This operations was successful, and the

deepened wells produced reliably for some years, the last of them only now failing. Three more holes were drilled in 1967, and a slow programme of exploration drilling recommenced in 1974 with the intent of obtaining enough steam for electric power production as well as processing in the mill. The average discharge rate over the past twenty years has thus been small, equivalent to about 20 MW (electrical).

The field was not fully defined until quite late in its development when a resistivity survey (Macdonald and Muffler, 1972) established that it covered an area of 6–8 km^2. The initial drilling had been concentrated in a very small part of this area, and even now the drilling is very uneven, with half the field having three holes and the remainder seventeen. Current drilling aims at a more even spread.

The history of development is a steady pattern of drilling deeper and deeper, and over a wider and wider area. At the same time the wells already on line were steadily declining in output. Each new sequence of drilling was to a greater depth and produced wells with higher outputs and longer life. This does not seem startling until the amount of withdrawal is considered. The withdrawal has been at an average rate of 3–6 million tonnes per year—a cumulative withdrawal to 1976 of some 80 million tonnes. By comparison, 50 million tonnes are discharged from Wairakei each year, and in an equivalent twenty years this has not produced any rundown in well performance of a similar nature.

Unfortunately, in comparison with Wairakei, the wells at Kawerau have been poorly monitored, but, from the measurements available, it is apparent that there is little, if any, drawdown in pressure in the immediate vicinity of the wells. This is consistent with the low rate of withdrawal and the good permeability indicated by well performance.

What has damaged, and eventually destroyed, well performance is a decline in temperature of the fluid tapped by the wells. Figure 5.8 illustrates this, showing temperature profiles in well KA8 at different times. KA8 was one of the original wells drilled in 1956, and at that time it was very productive from a feed at 600 m. By 1960 it had failed so it was then deepened to 900 m. A new feed was encountered at 800 m, and it is the performance of this feed that is of interest.

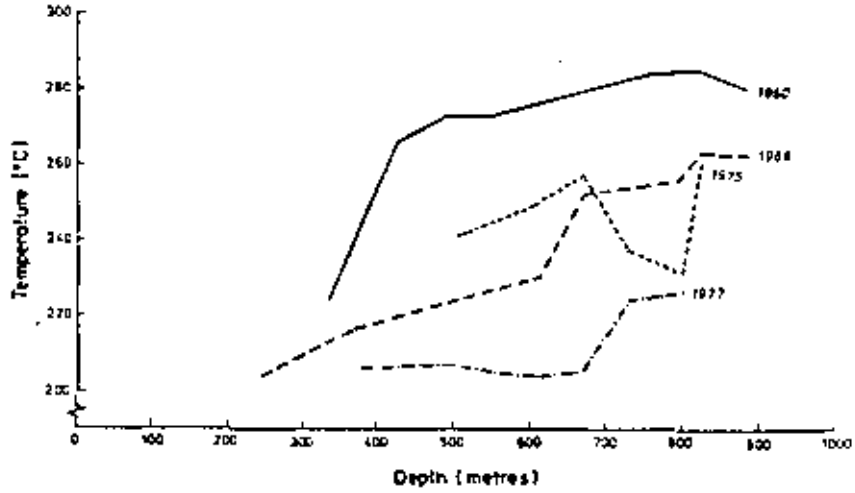

Figure 5.8. Temperature profiles down well KA8 at Kawerau, New Zealand at various times from 1960 to the present. (Data supplied by Ministry of Works and Development, New Zealand)

The first temperature profile, in 1960, indicates a maximum temperature of 285°C at the feed zone. The remaining temperatures in the well at this time are uninteresting as they simply reflect a boiling column of water above this point. The bore then produced a high enthalpy fluid—around 1400 kJ/kg. This is well above the enthalpy of liquid water at this temperature (1260 kJ/kg) indicating that the well was drawing on two-phase conditions. The bore was at this time the best in New Zealand, providing about half of the output of the entire Kawerau field. The next profile, in 1968, shows a maximum temperature of only 265°C. Pressures were also measured at that time, and these were well above saturation, indicating that the well was now drawing on liquid water at around that temperature. The enthalpy of the discharge confirmed this. Subsequent temperatures were progressively lower, with a temperature inversion eventually developing near the feed. Most recently the feed temperature was down to 205°C, and the well nearly dead.

The interpretation placed on this is that cold water is now getting right to the feed zone of the well KA8. Initially the well fed from two-phase conditions. With the withdrawal of fluid by the well, hot fluid will move in from further out, and some cooler, denser fluid may move down from above. In any system it will be the particular balance of these that will control what actually happens at the well. If the cold water inflow is sufficient it will condense some of the steam, so that the water saturation will rise. This is what in fact did happen at Kawerau, and by about 1964–65 this bore was feeding from liquid conditions; i.e. all the steam in its feed zone neighbourhood had condensed, and the well discharge enthalpy had fallen to that of liquid water. The progressive temperature decline thereafter is indicative of increasing encroachment of the cold water. Thus in this field the cold water appears to have preferential access to the permeable feed zones.

During its lifetime KA8 discharged about half of the total Kawerau field discharge, or 30 million tonnes. With a porosity of 15 per cent, this would fill a sphere of rock less than 200 metres in radius. The nearest cold water to the feed zone is the ground water some 800 m away, just below the ground surface. This water must therefore flow along permeable paths and thus only drain a very small segment of the rock of its stored heat. The well, as a means of extracting heat from the storage in the rock, failed when only the fraction of the rock containing the fissure system had cooled. The remainder of the heat not in close contact with the fissures is at present inaccessible.

Fractured reservoirs of this nature may be assessed with the simple planar model developed by Bodvarsson (1974). This model has recently been re-evaluated by Muffler and Cataldi (1978) to determine appropriate (but still theoretical) geothermal recovery factors for fractured systems. Although the fracture spacing is restricted (a 338 m spacing is assumed in the Bodvarsson and in the Muffler and Cataldi analysis), and the idealised recovery factors are too high, the study does show the significant potential increase in recoverability with lower rates of withdrawal. The estimated recoverability in fact doubles if the withdrawal is adjusted for a 100 year rather than a 25-year lifetime.

5.3.3. *Two-Phase Systems*

In their response to exploitation, and in their mode of heat removal, there is a continuous gradation between liquid- and vapor-dominated systems. The natural gradient of pressure with depth provides a clear-cut distinction between these extremal systems, but this distinction is not particularly relevant to the heat extraction. There are, for example, shallow wells at Wairakei that produce dry steam from conditions of low water saturation and behave very much like wells in a vapor system, and yet they produce from an environment that initially had a hydrostatic gradient of pressure with depth.

This continuous gradation is characterised by the increasing size of the two-phase zone.

the decreasing water saturation of this zone, and the decreasing hydraulic diffusivity. All of these go along with an increasing proportion of the heat being extracted from within the reservoir by boiling, and an equivalent decreasing proportion being mined at the margin of the field by the encroachment of cold water. This inflow of water, which appears to the reservoir as a recharge of hot fluid due to the exchange of heat between the rock and the cold fluid at the field margins, thus decreases as we move from system to system along this path from liquid- to vapor-domination.

Along this gradation we can see examples. One wet two-phase field is Broadlands, New Zealand. Another, a bit hotter and drier, is Krafla, Iceland (described by Stefánsson in this volume). Drier still, but with near hydrostatic pressure gradients, are Ngawha, New Zealand, a very gassy field, and Rotokawa, New Zealand. The shallow Wairakei wells also fit into the sequence at about this point. Finally there are the classical vapor-dominated systems, such as the The Geysers, United States, Kawah Kamojang, Indonesia, and Larderello, Italy. The geological or geophysical controls that give rise to any fields's specific location in this gradation are yet to be established. At the present time there is little forecasting of any field's characteristics. Rather, these are discovered during drilling.

In this section we will discuss two of the two-phase systems—Broadlands and Ngawha, both in New Zealand.

(i) *Broadlands, New Zealand.* This field is the wettest of the listed two-phase examples. At sufficient depth it is a conventional liquid-dominated field, i.e. similar to Wairakei, with a temperature of 310°C and a gas content of 2–3 per cent by mass. If all wells were drilled into this sector, the field would behave as a hot water system. The boiling water interface is, however, here at about 1 km depth, and most of the production takes place in the two-phase region above. These wells produce from a zone in which the temperatures are in the 250–280°C range.

A few wells, e.g. BR13, do produce from liquid conditions, but the best permeability and temperature are found in the two-phase zone. The sections of Figure 5.9 illustrate schematically a fluid state profile across the productive zone and out into the fringes of the field, and temperature and permeability profiles along this section at a depth of 600 m. The permeability profile is only indicative as actual values of the permeability and its variation are not known. It does, however, appear to decrease as we move out from the two-phase section.

Wells tapping the two-phase zone produce fluid with an average enthalpy of around 1300 kJ/kg, some 110 kJ/kg above that of liquid water at 270°C, the average production temperature. It has therefore been estimated that the liquid saturation in this zone was probably initially of the order of 80–85 per cent. It should be noted that the higher enthalpy here is a valuable asset as this heat can be converted to electrical energy at an efficiency of about 20 per cent (cf. 8–10 per cent for the liquid enthalpy).

The response to exploitation is interesting. It takes about one to two years for significant pressure disturbances to cross the two-phase zone horizontally and a longer time for them to propagate downwards to the boiling water interface. The permeability is anisotropic, being higher horizontally than vertically. Thus when a well is discharged, for the first year or so it will draw on an expanding zone in the two-phase region. Only then does it begin to feel the liquid surroundings, either at the sides or below. In this field, the behaviour at the side boundaries is complicated by the lower permeability (cf. Figure 5.9(c)), but nonetheless, just as in Wairakei, the exterior water will be pulled into the field extracting heat from the margins on the way. At the same time, the decrease in pressure in

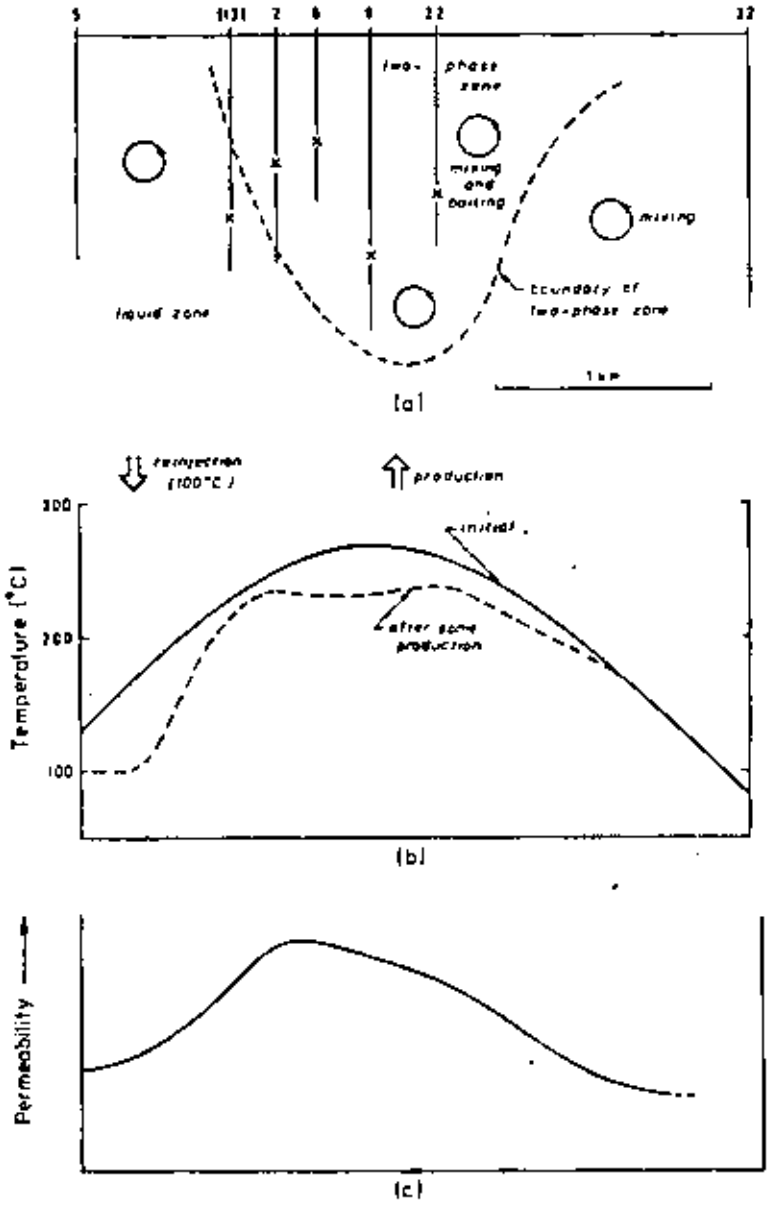

Figure 5.9. Variations across the Broadlands geothermal field, New Zealand. (a) The liquid and two-phase zones. (b) Temperature profiles at 600 m. (c) Permeability variation (qualitative only)

the centre of the field will drop the temperatures in the two-phase zone itself and lower the water level by boiling water off at the single-phase/two-phase interface. The temperature profile will thus become, after some years, that illustrated by the dashed curve in Figure 5.9(b). During this period heat will be mined from the production zone, from the neighbourhood of the dropping water/two-phase interface, and from the margins of the field. With the development of a quasi-steady field condition, after a few years' exploitation, the temperature change in the production zone and the drop in water level

will virtually cease. The bulk of the heat will then be mined from the side boundary regions.

Under exploitation, some rise in the enthalpy of the well discharge is expected. As fluid is first withdrawn and pressure falls, the saturation also falls. This increases the steam mobility and decreases water mobility, so that discharge enthalpy rises. However, the recharge fluid is principally or entirely liquid. As the field later approaches its quasi-steady exploited state, the discharge enthalpy falls again, towards the recharge enthalpy. Thus part of the response to exploitation is a transient enthalpy rise. For a suitably sized power station, the peak enthalpy is at most 50 per cent higher than the initial value (Grant 1977b). The field does not 'dry out' under exploitation—there is no way this basically liquid-dominated field will discharge dry steam.

If, as is proposed, reinjection takes place at the field boundary, an additional pressure pulse will be generated in this area, this time a positive one. This pulse will propagate through the two-phase zone at the same rate as the drawdown pulse. It will still, however, take the same order of time for the two pressure waves to interact, i.e. one to two years. In the area of recharge, pressures will also be sustained, and this will tend to reduce the drop in pressure, and hence temperature, within the field reservoir. The water level will also drop less. This will mean that less heat will be mined from within the field, either in the two-phase zone or at the water/two-phase interface. More will therefore be mined from the field margins, especially in the area of maximum reinjection. Reinjection increases the speed of advance of the cold front and hence the rate at which rock volume is being cooled.

(ii) *Ngawha, New Zealand.* Ngawha and similar fields, e.g. Matsukawa in Japan (Baba et al., 1970) and Rotokaua, in New Zealand, have one feature in common with vapor-dominated fields—the wells discharge dry or nearly dry steam—and one feature that is in contrast—pressures are hydrostatic rather than vapor-controlled. They are thus liquid-dominated fields, but with a comparatively high vapor mobility.

As this natural vapor flow is not large even though it is driven by the hydrostatic gradient, the rock permeability must be low, at least in the vertical direction. This low permeability ($\ll 10^{-13}$ m^2) has so far been confirmed by the few well tests carried out at Ngawha and Rotokaua. It is almost certainly an inherent feature of the Ngawha-type systems, and shows a second contrast with the vapor-dominated ones.

In combination with the two-phase conditions, the low permeability makes the hydraulic diffusivity extremely small. Each well will thus mine its own independent volume of rock, and the pressure wave, in effect, will never reach the side boundaries. Steam will be extracted from rock pores containing steam and immobile, or only slightly mobile, water, and this steam will be replaced by the boiling of some of that water. With continuing withdrawal, there will thus be a local decline in both temperature and pressure in both the rock pores and the well discharge. Each local 'mine' will last until the resistance to flow in the increasing volume being tapped drops the well bottom pressure and temperature to such a level that the operation can no longer be satisfactorily sustained. The volume so mined will thus depend directly on the local permeability. For maximum extraction, these local 'mines' will need to be sited quite close together, both horizontally and vertically.

As Ngawha complements its steam discharge with a high gas content (mainly CO_2), it is also essential to consider the likely chemical effects of this extraction. The chemical behaviour here is probably passive, and hence it is only the gas in or out of solution with which we will be concerned. Thus, as the pressures and temperatures decrease, gas transfer

from the liquid to the vapor will take place, and gas will continue to be discharged from the wells. This will affect the heat discharge of the system.

The initial gas content of the discharge reflects the equilibrium conditions present in the field. For well Ng1, with initial gas partial pressures of 3·0 MPa (at 230–235°C), this means 50–70 per cent gas (by mass) in the vapor phase. This gas content, however, rapidly declined, reflecting a process of boiling within the confined volume that the well exploited. This decay in gas content may thus not indicate a long term trend. This will be difficult to estimate as any recharge would also be very gassy.

In this Ngawha-type of system we also have to develop a different outlook with regard to reinjection. This will here only be a means of waste disposal. The cool liquid injected is most likely to move only slowly away from the injection well and hence will not rapidly affect the mass balance. Any pressure, and temperature, perturbation will also be restrained to the region immediately adjacent to the well input zone.

The total heat extraction potential of this system will thus be primarily restricted by the number of wells that can be drilled and discharged economically rather then by any size limitation or temperature restraint.

5.3.4. *Vapor-Dominated Systems*

The term 'vapor-dominated' was coined by White et al. (1971). The essential characteristics of the system are: (a) a discharge of steam, and (b) that this discharge comes from a region where the pressure is nearly constant with depth. The steam discharge may initially be wet, dry saturated, or superheated. There is, however, a trend for the discharge to become dry, or increasingly superheated, with exploitation. The pressure of the production zone is often around 3·3 MPa, equivalent to a saturation pressure for water and steam at 235°C. Extremal values of 2·4 MPa at Bagnore, Italy (Atkinson et al., 1978a, b), and 7·0 MPa at Travale, Italy (Atkinson et al., 1978c), have, however, been measured. In most systems there appears to be little leakage to the surface, and capping structures are generally assumed.

There are several vapor-dominated systems now known and under development or exploitation around the world. These include Larderello, Bagnore and Travale in Italy, The Geysers in the U.S.A., and Kawah Kamojang in Indonesia. These all fit in the same niche in our graded sequence and behave similarly in most respects of interest. Only a general discussion is therefore given.

In all these fields, the vapor-dominated zone occurs in a general region of water-saturated rock. There may, in fact, be geothermal liquid-dominated or cold water regions around or intermingled with the vapor region (Petracco and Squarci, 1975, Lipman et al., 1978; Cataldi et al., 1978). In the natural state there is a flow of mass and energy between the liquid and vapor zones. The exploitation behaviour is also intimately linked with that of the water within and surrounding the reservoir.

We follow White et al. (1971), and the bulk of work on vapor-dominated systems, in assuming that the vapor reservoir contains, in its natural state, immobile or only slightly mobile water. This water is the mass supply for the reservoir steam. Some authors (Brigham and Morrow, 1977; Atkinson et al., 1978a) use a 'falling water level' model in which a zone of dry steam overlies a liquid layer. In either case, a supply of liquid is needed as the amount of steam produced from these vapor fields far exceeds what could be stored in them as vapor alone (James, 1968). As it is doubtful whether these falling water level models truly model all the processes involved, we concentrate on the White model (White et al., 1971, and Truesdell and White, 1973) for this discussion.

Measurements at Kawah Kamojang in Indonesia are consistent with the White model and the presence of a dispersed water phase. The water saturation has been measured at 35 per cent (Grant, 1979). The residual saturation is not known, but it must be somewhat less than this as the steam is slightly wet, with a representative enthalpy of 2775 kJ/kg.

In the natural state of these reservoirs, we therefore anticipate an upward flow of steam and a downward flow of water. This latter is the condensate of the steam, very little of which is able to escape through the capping structures to the surface, although heat can be lost to the surface by conduction. The down flow is probably predominantly in various cracks and fractures in the system with the remaining water virtually immobile in the rock pores. (In contrast, freely available water in a relatively permeable reservoir would continue to flow to the wells.) These cracks and fractures are the fine geological structure of the reservoir, and thus the preferred paths for some flows. Water bearing strata have, for example, been encountered in The Geysers (Ramey, 1970), and wells at Kawah Kamojang frequently discharge wet steam (Grant, 1979). Corresponding with this pattern of patchiness in the flow distribution of water and steam there will also be some variation in the water saturation; i.e. some rocks will be wetter than others. There will also be some interchange of water and steam at the sides of the system, i.e. steam condensing and water boiling.

A well extracting fluid and heat from a vapor reservoir discharges either saturated or superheated steam (Truesdell and White, 1973). If the steam is superheated there is a dry zone around the well, through which the steam flows isothermally. This dry zone would have originally contained some water, but, as lowering the pressure in the vapor system reduces the water saturation, this water will have completely boiled off.

Beyond the dry zone is a zone containing immobile water. A well producing saturated steam contacts this zone directly; i.e. in this area the dry zone is not yet established. In either case, saturated or superheated, the mass and energy discharged from the well is supplied from the wetted zone. The water boils to form steam, and this flows to the well, taking the mass and the latent heat with it.

Outside the vapor-dominated section of the reservoir we may have a liquid-dominated region and rocks saturated with cooler ground water (White et al., 1971). At Larderello, for example, external cooler water supplies part of the recharge (Petracco and Squarci, 1975). As such cold water enters, it first crosses into the hot liquid region, mining heat from that boundary, and then boils, mining its latent heat from the rock, and enters the vapor reservoir. The mass supply to the well comes from the cold ground water, and the energy from the boundaries where the fluid gains enthalpy. Other recharge may come from the hyothesized deep brine layer (White et al., 1971).

In general, as the pressures in vapor-dominated geothermal reservoirs are largely well below hydrostatic, to prevent flooding by cold exterior water there must be low permeability defining boundaries on all sides. This is the case at The Geysers (Bredehoeft, J. D., Ramey H. R., Jr., personal communications) and at Kawah Kamojang. These boundaries may reduce external recharge to negligible amounts. In this event all the steam supplied to the wells comes from boiling in the vapor-dominated zone. The water in this zone supplies the mass, and the rock supplies the heat to convert this to the steam discharged by the wells.

An estimate of recoverability from a vapor-dominated reservoir, based on the model of White et al. (1971) and Truesdell and White (1973), has been made by Nathenson (1975). In their application of this approach to The Geysers, Nathenson and Muffler (1975), assuming 5 per cent for the volume percentage of water and a 240°C reservoir, estimate an ideal recovery factor of 19·4 per cent. A qualitative allowance (of 50 per cent) for structural inhomogeneity and its effects reduces this factor to 9·7 per cent. The assignment

of a recovery factor is, however, subjective, but even for a favourable vapor-dominated geothermal reservoir like Larderello–Travale with an assumed 215°C reservoir temperature the figures are low (11–19 per cent) (Muffler and Cataldi, 1978). Their intermediate estimate of 15 per cent compares with that (> 13·3 per cent) estimated from intergranular vaporization based on the model and data of Barelli et al (1975) for that area.

5.4. Other Systems

There are three other types of geothermal systems that are of interest to scientists and engineers at the present time—the geopressured system, the hot dry rock system and the magma chamber. Although these do not fit in with our sequence, the first two of these may be regarded as relatively simple variations on the basic theme. The magma chamber may perhaps be a little different.

5.4.1. *The Geopressured System*

The reservoir mechanics of a geopressured system have so far only been discussed to a very limited extent (see, for example, Pritchett et al., 1977, Garg and Pritchett, 1977, 1978, and Garg et al., 1977, 1978). These authors indicate that there are four driving mechanisms which tend to expel fluid from a geopressured stratum—water compressibility, pore collapse, evolution of methane gas, and clay dehydration or shale dewatering. The decrease in permeability accompanying pore collapse and the relative permeability effects due to the evolution of the gas tend to impede the fluid flow. This would, however, be outweighed in general by the positive driving effects.

In its simplest form a geopressured reservoir may just be regarded as a high pressure, sealed container filled with porous material saturated with compressed water and dissolved gas. Pull out the plug and the water and gas flow out, most of the boiling and separation taking place only in the wells or above ground on account of the great reservoir depths of these fields (4800 to 5000 metres in the Brazoria geothermal fairway, Texas Gulf Coast, U.S.A.; Bebout et al., 1977a,b). The majority of the water thus comes available purely from decompression in the strata. Left to run in this mode, this process would in effect give us all that water held in compression above the natural pressure. This will, however, only be a small fraction of the fluid that might be available. The fraction of the heat mined would be even smaller as the heat contained in the rock would not be touched.

Recirculation of fluid through the system is thus essential, both to maintain the pressures and to extract the heat in the rock. In this case, as we have no natural inflow (recharge) from the sides, the only cold water front will be that associated with the water from the injection wells, and if these and the extraction wells are well sited, there are good prospects of a high percentage return from this reservoir.

5.4.2. *The Hot Dry Rock System*

In various areas of the world hot but dry and impermeable rock is known to exist at relatively shallow depth. By drilling wells into this rock and fracturing the material between these wells it is possible to set up a circulation path for injected fluid to extract heat from such a system. Only one system of this nature has so far been attacked, that in the Jemez Mountains, New Mexico, U.S.A. (Laughlin, this volume). The full process and

progress with the research program to date is described in papers like Cummings et al. (1979) and Tester and Albright (1979). This discussion is therefore somewhat superficial and is aimed only at relating the process of heat extraction here to that in hydrothermal systems.

From the heat extraction point of view, the process is in fact little different from that of systems already discussed. Although there is no natural fluid, in principle we are again only mining the heat from the rock with a cold fluid, just as we are presently doing at the margins of fields like Wairakei. In this case the 'margin' is the injection well, since the cooler fluid flowing from the injection well extracts heat by conduction from the rock bounding the fissure. The success or otherwise of the venture will thus depend on the quality of the inter-well fracturing. A few dominant connectors will short-circuit the rock mass so that only a limited hot-rock volume will be accessible. This could soon be depleted of its heat. In contrast, a high-density fracture structure should access a wealth of heat.

5.4.3. *Magma Chambers*

Magma chambers are mentioned here for completeness. They appear to have considerable potential as a source of energy, but their exploitation will probably require techniques well outside the range of technologies used in exploiting the other fields and systems described in this chapter. A discussion of magma as a geothermal resource is given by Stoller and Colp (1978).

5.5. Summary

Detailed geothermal reservoir analysis is an extremely complex process. Structural complexity, three-dimensional behaviour, mixed mass and energy transport, phase changes, dissolved gasses, the likely necessity of reinjection and a welter of unknown parameters or parametric relationships all must be taken into account. For the ultimate management of geothermal resources such detailed studies may be essential, but for resource valuation the much simpler approach that has been discussed in this chapter may be all that is necessary (see, for example, Donaldson and Grant, 1978).

Heat extraction from a porous medium, and hence a geothermal reservoir, requires a generous amount of fluid to carry the heat conveniently to the exterior of the system and efficient heat transfer mechanisms to move the bulk of the stored heat from the rock to this fluid carrier. The fluid may be 'generated' within the medium, by expansion of that already compressed in the system or by expansion due to a change of phase, it may be sucked in from outside the heated area, or it may be deliberately injected by the field operators.

In this study we have shown the outward diffusion of the pressure depression from the production zone to be the stimulus both of fluid 'generation' and of the inflow of external liquid (the 'recharge'). In liquid-dominated systems, the pressure wave moves out rapidly to the field boundaries, and the recharge thus becomes the dominant mass source within only a day or so of first production. The expansion effects, except perhaps in the case of the geopressured fluid, are virtually negligible. As we move along the sequence to two-phase systems, pressure diffusion becomes slower, and boiling effects result in the replacement of some of the water discharge with steam, a definite advantage from the heat extraction point of view. For a typical system, such as Broadlands, New Zealand, however, the pressure wave still reaches the reservoir boundaries—it just takes longer, in this case the order of one to two years.

In low permeability reservoirs, such as Ngawha, New Zealand, the situation is a little different, and the wells may there tap only the local water. Again boiling will, however, sustain the discharge, at least for a time. Artificial fracturing may be of benefit in these systems.

At one extreme of our sequence, the vapor-dominated reservoir, we return to a situation akin to that of the other two-phase cases, with here the potential of boiling of all the water in the immediate vicinity of the wells.

In time the fluid thus comes from further and further away, by boiling of water, and ultimately again by an inflow at the field margins.

To all intents and purposes injection or reinjection of cooler or used fluid just replaces the cooler side inflow. The choice of location of this inflow, however, rests with the field operators.

The heat going up the well comes in part from the stored fluid. The bulk, however, comes from the rock through which it flows. It is this latter heat that we need to extract for greatest benefit. There are two main ways in which this may be done—by boiling of water in adjacent pores and cracks, or by passing cooler water through the structures. The former normally takes place right inside the reservoir, while the latter will occur at the margins of the field or around injection wells. Either is effective, although the boiling process will result in some drop in temperature at the well. The margin mining process, in contrast, is one of frontal movement with little decay in temperature on the forward side of the front except where reservoir inhomogeneities create problems.

Both vertical and horizontal flows will be important in this heat extraction process, but, for many fields, the horizontal effects appear to dominate. Pressure drops in the two-phase zone will, however, stimulate boiling at any two-phase (steam-water)/liquid interface and cause a drop in its level. Colder water layers overlying such two-phase zones may also be sucked down into the system. Since these cold layers may be closer to some wells than the water at side boundaries and they have an additional density drive, this water could ultimately be the limiting control for these wells, quenching them before they have extracted more than a fraction of the heat from the rock around them.

Fractured systems can also cause problems as fronts can move in much more quickly along such preferred paths than through the rock mass. Quenching of the well system may thus take place while the majority of the heat, stored in the rock between the various fractures, remains virtually untouched. Kawerau, New Zealand, described earlier in this chapter, is a prime example of such a fractured field.

At the start of this chapter we posed the three questions that we believe are the most crucial in geothermal reservoir development—how much energy can we extract? For how long may it be extracted? And, of what quality is the energy extracted? Answers to these questions are now available.

To answer the third question first, the quality of the extracted energy, as defined by the enthalpy of the fluid discharged, depends directly on the temperature of the reservoir and on the type of reservoir system involved. The quality increases as the reservoir temperature goes up and also as we move along the sequence of field types from the warm water to the vapor-dominated systems. In most fields the mean discharge enthalpy, and hence the energy quality, does not change greatly with exploitation until the field commences to collapse due to the cold water inflow reaching the production area. Only in the liquid-dominated two-phase systems are any significant changes anticipated, and these may only occur for a limited time. An enthalpy increase of about 50 per cent, as estimated for Broadlands, New Zealand, is as large as is to be expected anywhere.

It is the cold water inflow that defines how much heat we can extract from any reservoir. If the reservoir is homogeneous this inflow is uniform, and much of the heat

stored in the rock outside of the production zone will be swept into this zone and extracted. In this case the rate of extraction has little effect on the cumulative amount of heat extracted as exactly the same volume will be swept out with only the time-scale changed. The 'how long' thus purely depends on the rate of extraction. This rate is, however, controlled in the reservoir itself by the drawdown that can be tolerated.

If there are marked inhomogeneities in the reservoir, as have shown up at Kawerau, New Zealand, the cold front advances preferentially along the higher permeability channels, and wells are quenched while heat remains stored in the surrounding rock. Here the amount of heat extracted depends on a balance between the rate of heat transfer from the rock to the fluid in these channels and the rate of advance of the local cold fronts. The slower the advance of the cold front, the more heat is transferred, and the greater is the efficiency of the mining operation. The mining efficiency decreases significantly as the rate of extraction goes up (Bodvarsson, 1974; Muffler and Cataldi, 1978).

Provided that we can tolerate the lower rate of fluid extraction in this latter situation, the end point of both exploitations will be much the same. The mining efficiency (or recovery factor) is controlled by the geometry and nature of the reservoir. For ideal uniformly permeable liquid-dominated reservoirs this recovery factor has been estimated at about 50 per cent (Nathenson, 1975), and a similar recovery factor has been obtained with the idealised model for Wairakei. To allow for the inhomogeneous nature of the structures in these reservoirs this figure must be reduced. A subjective halving of the ideal recovery factor has been suggested by Nathenson and Muffler (1975).

For vapor-dominated reservoirs the analysis is even more complex, but even for favourable reservoirs like Larderello–Travale the recovery factors appear lower than those for their liquid-dominated counterparts. Muffler and Cataldi (1978), in their overview suggest a recovery factor of about 15 per cent for such fields, comparable with the > 13·3 per cent based on the model and data of Bardelli et al. (1975). For The Geysers, Nathenson and Muffler (1975) give an ideal 19·4 per cent and a real (subjective) 9·7 per cent.

Acknowledgements

The ideas expressed in this chapter can in no way be attributed to any one source, nor did they just come overnight. They come rather from many discussions over many years with many colleagues. The authors cannot hope to name more than a few, but we wish to thank all those colleagues, both in New Zealand and overseas, with whom we have reacted over the years.

Our specific thanks must go to our direct associates at this time, Drs Lara Fradkin and Michael L. Sorey, presently at Physics and Engineering Laboratory, Lower Hutt, New Zealand, and Drs Alex McNabb and Robin Wooding of Applied Mathematics Division, DSIR, Wellington, New Zealand, with whom we have had an almost continuous dialogue during our thinking and writing up of this work. We should also like to thank Paul Bixley, Ministry of Works and Development, Wairakei, New Zealand, and Sabodh Garg, Systems, Science and Software, La Jolla, California, U.S.A., for their comments and ready assistance.

All field data used in the studies of New Zealand fields discussed in this chapter have been made available by the New Zealand Ministry of Works and Development. The authors would like to thank the officers of that Department for making this information and data so readily available.

References

Atkinson, P., Celati, R., Corsi, R., and Kucuk, F., 1978a. 'Behaviour of two-component vapor-dominated geothermal reservoirs' presented at the 1978 California Regional Meeting of the Society of Petroleum Engineers of AIME, San Francisco, California, April 12–14, 1978. SPE Paper 7132.

Atkinson, P., Celati, R., Corsi, R., Kucuk, F., and Ramey, H. J., Jr., 1978b. 'Thermodynamic behaviour of the Bagnore Geothermal Field', presented at the Larderello Workshop on Geothermal Resource Assessment and Reservoir Engineering, Sept. 12–16, 1977. *Geothermics* 7 (2–4), 185–208.

Atkinson, P., Barelli, A., Brigham, W., Celati, R., Manetti, G., Miller, F., Meri, G., and Ramey, H. J., Jr., 1978c. 'Well testing in Travale-Radicondoli Field', presented at the Larderello Workshop on Geothermal Resource Assessment and Reservoir Engineering, Sept. 12–16, 1977. *Geothermics* 7 (2–4), 145–184.

Baba, K., Takahi, S., and Matsuo, G., 1970. 'On the reservoir at Matsukawa Geothermal Field', United Nations Symposium on the Development and Utilisation of Geothermal Resources, Pisa, Italy. *Geothermics* (Special Issue 2), 2 (2), 1440–1447.

Barelli, A., Calamai, A., and Cataldi, R., 1975, 'Stima del potenziale geotermico della fascia preappenninica centro-meridionale', *ENEL-Centro di Ricerca Geotermica, Relazione T3/949 Z*, 33 pp.

Bebout, D. G., Loucks, R. G., and Gregory, A. R., 1977a. 'Study looks at Gulf Coast Geothermal Potential', *Oil and Gas Journal*, Sept. 26, 1977.

Bebout, D. G., Loucks, R. G., and Gregory, A. R., 1977b. 'Texas geothermal prospect slated to begin operations at Martin Ranch', *Oil and Gas Journal*, Oct. 3, 1977.

Bodvarsson, G., 1962. 'An appraisal of the potentialities of the geothermal resources in Iceland', *Sixth World Power Conference, Melbourne, Australia, Paper* 206-111.

Bodvarsson, G., 1972. 'Thermal problems in the siting of reinjection wells', *Geothermics*, 1(2), 63–6.

Bodvarsson, G., 1974. 'Geothermal resource energetics', Geothermics, 3(3), 83–92.

Boldizsár, T., 1975. 'Research and development of geothermal energy production in Hungary', *Geothermics*, 4, 44–56.

Bolton, R. S., 1970. 'The behaviour of the Wairakei geothermal field during exploitation', United Nations Symposium on the Development and Utilisation of Geothermal Resources, Pisa, Italy. *Geothermics* (Special Issue 2), 1426–1439.

Brigham, W. E., and Morrow, W. P., 1977. 'P/Z behaviour of geothermal steam reservoirs', *SPE Journal* (Dec. 1977), 407–412.

Carslaw, H. S., and Jaeger, J. C., (1959), *Conduction of Heat in Solids*, Clarendon Press, Oxford (2nd Edition), 386 pp.

Cataldi, R., Lazzarotto, A., Muffler, P., Squarci, P., and Steffani, G., 1978. 'Assessment of geothermal potential of Central and Southern Tuscany', presented at the Larderello Workshop on Geothermal Resource Assessment and Reservoir Engineering, Sept. 12–16, 1977. *Geothermics* 7 (2–4), 91–132.

Cummings, R. G., Morris, G. E., Tester, J. W., and Bivins, R. L., 1979. 'Mining earth's heat: hot dry rock geothermal energy', *Technology Review*, February 1979, 59–78.

Dench, N. D., 1962. 'Reconditioning of steam bores at Kawerau', *N.Z. Engineering*, 17(10), 1–8.

Donaldson, I. G., 1968. 'The flow of steam water mixtures through permeable beds: a simple simulation of a natural undisturbed hydrothermal region', *N.Z. Journal of Science*, 11(1), 3–23.

Donaldson, I. G., 1970a. 'The simulation of geothermal systems with a simple convective model', United Nations Symposium on the Development and Utilisation of Geothermal Resources, Pisa, Italy. *Geothermics* (Special Issue 2), 649–654.

Donaldson, I. G., 1970b. 'A possible model for hydrothermal systems and methods of studying such a model', *Proceedings of the Third Australasian Conference on Hydraulics and Fluid Mechanics, Sydney, Australia*, 25–29 Nov., 1970.

Donaldson, I. G., and Grant, M. A., 1978. 'An estimate of the resource potential of New Zealand geothermal fields for power production', presented at the Larderello Workshop on Geothermal Resource Assessment and Reservoir Engineering, Sept. 12–16, 1977. *Geothermics* 7 (2–4), 243–252.

Dykstra, H., and Adams, R. H., 1977. 'Momotombo Geothermal Reservoir', *Summaries, Third Workshop Geothermal Reservoir Engineering*, Dec. 14–16, 1977, Stanford University, Stanford, California, 96–106.

Garg, S. K., 1978. 'Pressure transient analysis for two-phase (liquid water/steam) geothermal

reservoirs', *Paper SPE 7479*, presented at the 53rd Annual Fall Technical Conference SPE-AIME, October 1–3, 1978, Houston, Texas.

Garg, S. K., and Pritchett, J. W., 1977, 'Simulation of drive mechanisms in geopressured reservoirs', *Proceedings 18th U.S. Symposium on Rock Mechanics, Keystone, Colorado*, 1B5-1 to 1B5-4

Garg, S. K., and Pritchett, J. W., 1978, 'Two phase flow in geopressured geothermal wells', Third Geopressured Geothermal Energy Conference, University of Southern Louisiana, Lafayette, Louisiana, Nov. 1977. *Energy Conversion*, 18, 45–51.

Garg, S. K., Pritchett, J. W., Brownell, D. H., Jr., and Riney, T. D., 1978, 'Geopressured geothermal reservoir and wellbore simulation', *Systems, Science and Software, La Jolla, California, Report SSS-R-78-3639.*

Garg, S. K., Pritchett, J. W., Rice, M. H., and Riney, T. D., 1977, 'U.S. Gulf Coast geopressured geothermal reservoir simulation', *Systems, Science and Software, La Jolla, California, Report SSS-R-77-3147.*

Grant, M. A., 1977a, 'Approximate calculations based on a simple one-phase model of a geothermal field', *N.Z. Journal of Science*, 20, 19–25.

Grant, M. A., 1977b, 'Broadlands—a gas-dominated geothermal field', *Geothermics*, 6, 9–29.

Grant, M. A., 1978, 'Two-phase linear geothermal pressure transients—a comparison with single-phase transients', *N.Z. Journal of Science*, 21, 355–364.

Grant, M. A., 1979, 'The water content of the Kawah Kamojang geothermal reservoir', *Geothermics*, 8, 21–30.

Grant, M. A., and Sorey, M. L., 1979, 'The compressibility and hydraulic diffusivity of a water-steam flow', *Water Resources Research* 15(3), 684–686.

Grindley, G. W., 1965, 'The geology, structure, and exploitation of the Wairakei Geothermal Field, Taupo, New Zealand', *N.Z. Geological Survey Bulletin n.s. 75.*

Gringarten, A., 1978, 'Reservoir lifetime and heat recovery factor in geothermal aquifers used for urban heating', *Pure and Applied Geophysics*, 117, 297–308.

Healy, J., and Hochstein, M. P., 1973, 'Horizontal flow in hydrothermal systems', *Journal of Hydrology (N.Z.)*, 12(2), 71–82.

James, C. R., 1968, 'Wairakei and Larderello: geothermal power systems compared', *N.Z. Journal of Science*, 11, 706–719.

Lipman, S. C., Strobel, C. J., and Gulati, M. S., 1978, 'Reservoir performance of The Geysers Field', presented at the Larderello Workshop on Geothermal Resource Assessment and Reservoir Engineering, Sept. 12–16, 1977. *Geothermics* 7 (2–4), 209–220.

Macdonald, W. J. P., and Muffler, L. J. P., 1972, 'Recent geophysical exploration of the Kawerau geothermal field, North Island, New Zealand', *N.Z. Journal of Geology*, 15, 303–317.

McNabb, A., 1975, 'A model of the Wairakei geothermal field', unpublished report, Applied Mathematics Division, Department of Scientific and Industrial Research, Wellington, New Zealand.

Marshall, D. C., 1966, 'Preliminary theory of the Wairakei Geothermal Field', *N.Z. Journal of Science*, 9(3), 651–673.

Marshall, D. C., 1970, 'Development of a theory of the Wairakei Geothermal Field by the "simplest cases first" technique', United Nations Symposium of the Development and Utilisation of Geothermal Resources, Pisa, Italy. *Geothermics* (Special Issue 2), 669–676.

Marshall, D. C., 1975a, 'Theory of the Wairakei geothermal field. 1. Single-phase, drawdown model', *N.Z. Journal of Science*, 18, 453–463.

Marshall, D. C., 1975b, 'Theory of the Wairakei geothermal field. 2. Permeability and diffusivity variations', *N.Z. Journal of Science*, 18, 591–603.

Mercer, J. W., and Faust, C. R., 1976, 'Status of modelling efforts for the Wairakei Geothermal Field', *Summaries, Second Workshop Geothermal Reservoir Engineering*, Dec. 1–3, 1976, Stanford University, Stanford, California, 308–309.

Mercer, J. W., and Faust, C. R., 1979, 'Geothermal Reservoir Simulation III: Application of liquid- and vapor-dominated hydrothermal modeling techniques to Wairakei, New Zealand' *Water Resources Research*, 15(3), 653–671.

Mercer, J. W., Pinder, G. F., and Donaldson, I. G., 1975, 'A Galerkin finite-element analysis of the hydrothermal system at Wairakei, New Zealand', *Journal of Geophysical Research*, 80(17), 2608–2621.

Moench, A. P., and Atkinson, P., 1978, 'Transient-pressure analysis in geothermal steam reservoirs with an immobile vaporizing phase', *Geothermics* 7(2–4), 253–264.

Muffler, L. J. P., and Cataldi, R., 1978. 'Methods for regional assessment of geothermal resources', presented at the Larderello Workshop on Geothermal Resources Assessment and Reservoir Engineering, Sept. 12–16, 1977. *Geothermics* 7(2–4), 53–90.

Nathenson, M., 1975. 'Physical factors determining the fraction of stored energy recoverable from hydrothermal convection systems and conduction-dominated areas', *U.S. Geological Survey Open-File Report 75-525*, 35 pp.

Nathenson, M., and Muffler, L. J. P., 1975. 'Geothermal resources in hydrothermal convection systems and conduction-dominated areas'. In *Assessment of Geothermal Resources of the United States—1975*, D. E. White and D. L. Williams (Eds.), U.S. Geological Survey Circular 726, 104–121.

Petracco, C., and Squarci, P., 1975. 'Hydrological balance of Larderello Geothermal Region', *Proceedings Second United Nations Symposium on the Development and Use of Geothermal Resources, San Francisco, California*, 22–29 May, 1975, 521–530.

Pritchett, J. W., Garg, S. K., and Brownell, D. H., Jr., 1976a. 'Numerical simulation of production and subsidence at Wairakei, New Zealand', *Summaries Second Workshop Geothermal Reservoir Engineering*, Dec. 1–3, 1976, Stanford University, Stanford, California, 310–23.

Pritchett, J. W., Garg, S. K., Brownell, D. H., Jr., Rice, L. F., Rice, M. H., Riney, T. D., and Hendrickson, R. R., 1976b. 'Geohydrological environmental effects of geothermal power production phase IIA', *Systems, Science and Software, La Jolla, California, Report SSS-R-77-2998*.

Pritchett, J. W., Garg, S. K., and Riney, T. D., 1977. 'Numerical simulation of the effects of reinjection upon the performance of a geopressured geothermal reservoir', *Geothermal: State of the Art*, Transactions Annual Meeting of the Geothermal Resources Council, San Diego, California, p. 245.

Ramey, H. J., Jr., 1970. 'A reservoir engineering study of The Geysers Geothermal Field' submitted as evidence, Reich and Reich, Petitioner *v.* Commissioner of Internal Revenue, 1969 Tax Court of the United States, 52, T.C. No. 74, 1970.

Scheidegger, A. E., 1957. *The Physics of Flow through Porous Media*, University of Toronto Press, Toronto 236 pp.

Stoller, H. M., and Colp, J. L., 1978. 'Magma as a geothermal resource—a summary', *Geothermal Resources Council Transactions*, 2, 613–615.

Studt, F. E., 1958. 'Geophysical reconnaissance at Kawerau, New Zealand', *N.Z. Journal of Geology and Geophysics*, 1(2), 219–246.

Tansev, E. O., and Wasserman, M. L., 1977. 'Modeling the Heber Geothermal Reservoir', *Summaries, Third Workshop Geothermal Reservoir Engineering*, Dec. 14–16, 1977, Stanford University, Stanford, California.

Tester, J. W., and Albright, J. N., 1979. 'Hot dry rock energy extraction field test: 75 days of operation of a prototype reservoir at Fenton Hill, Segment 2 of Phase 1', *Los Alamos Scientific Laboratory, LASL-7771-MS*, 104 pp.

Truesdell, A. H., and White, D. E., 1973. 'Production of superheated steam from vapor-dominated geothermal reservoirs', *Geothermics*, 2, 154–173.

White, D. E., Muffler, L. J. P. and Truesdell, A. H., 1971. 'Vapor-dominated hydrothermal systems compared with hot water systems', *Economic Geology*, 66, 75–97.

Whiting, R. L., and Ramey, H. J., Jr., 1969. 'Application of material and energy balances to geothermal steam production', *Journal of Petroleum Technology*, 893–900 (July, 1969).

Wooding, R. A., 1963. 'Convection in a saturated porous medium at large Rayleigh number or Peclet number', *Journal of Fluid Mechanics*, 15, 527–544.

Wooding, R. A., 1980. 'Analysis of pressure drawdown measurements in the Wairakei–Tauhara geothermal area' (submitted to *Water Resources Research*).

SOCIETY OF PETROLEUM ENGINEERS
6200 North Central Expressway
Dallas, Texas 75206

PAPER NUMBER SPE 5382

Analysis of Internal Steam Drive in Geothermal Reservoirs

J. C. Martin, Chevron Oil Field Research Company, Member SPE-AIME

ABSTRACT

Reservoir analysis methods are applied to simple closed geothermal reservoirs that produce by internal steam drive. Relations are presented for the reservoir temperature, pressure, and fluid saturations, with the assumption that the fluids are produced according to their respective relative permeabilities. Calculated performances are given for various types of reservoirs. Results indicate that hot-water reservoirs can have complicated behaviors, including changing from production of hot water to dry steam.

INTRODUCTION

Testing of geothermal energy prospects has accelerated in recent years. Increased understanding is needed of the fundamental heat and fluid flow involved in geothermal reservoir production. Techniques used by petroleum production researchers are particularly well suited to the study of these fundamentals, and to geothermal reservoir engineering research in general.

References, appendix, and illustrations at end of paper.

Some geothermal reservoirs are similar to oil and gas reservoirs. The reservoir is a porous media, through which the fluids flow according to Darcy's law. Furthermore, some geothermal reservoirs have the equivalent of cap rocks.

The analogy between oil and gas reservoirs is the basis for the fundamental assumption of this paper: fluid flow in a geothermal reservoir can be treated as the flow through a porous medium, and Darcy's law and relative permeabilities are applicable.

There are many analogies between petroleum and geothermal reservoir engineering. For example, a number of the drives which supply reservoir energy are similar. The edge water drive in a petroleum reservoir is analogous to influx from cooler aquifers in geothermal reservoirs. Solution gas drive in petroleum reservoirs is analogous to two-phase internal steam drive in geothermal reservoirs. Compaction drive can occur in both. Waterflooding an oil reservoir is analogous to water cycling in a hot-water geothermal reservoir.

Methods of analysis similar to those used in petroleum reservoir engineering can be used for geothermal reservoirs as illustrated by the development of the material and heat balances in Reference 1. The present paper presents an analysis of internal steam drive, using methods analogous to those used for solution gas drive in Reference 2. The analysis presented herein is based on the following assumptions: the temperature, pressure, and fluid saturation gradients are small; the steam and hot water are produced according to their respective mobilities as determined by relative permeabilities and viscosities; and the effects of capillary pressure and gravity can be neglected. Some gravitational effects however, are treated qualitatively in the discussion. Throughout the analysis and discussion the produced steam and hot water are calculated neglecting the pressure and temperature drops near the wells and in the wellbores. The effects of these additional changes must be introduced to obtain steam and hot water production rates at the wellhead.

DISCUSSION

Temperature-Pressure Behavior

As pointed out in Reference 1, initial temperature and pressure in a geothermal reservoir determine its reservoir type. The solid line in Figure 1 presents the boiling curve for pure water. (Curves for actual geothermal brines will be modified by the dissolved salts[3].) Points to the right of the curve and below the critical temperature represent hot water reservoirs. Points to the left of the curve and also points above the critical temperature represent single-phase or steam reservoirs.

The mathematical analysis is presented in the Appendix. Ordinary differential equations are derived for the fluid saturations and reservoir pressure (for two-phase flow) and for the pressure and temperature (for single-phase flow). Equations 13 and 16 of the Appendix were solved numerically for the temperature-pressure behavior of closed geothermal reservoirs containing fresh water and having the relative-permeability curves presented in Figure 2. Other values used in the calculations are: 162 lbs/ft^3 rock grain density, 0.20 Btu/°F-lb specific heat of rock, 40 Btu/ft-day-°F thermal conductivity, and 1.0 Darcy's permeability. Results of these calculations for a porosity of .25 are presented by the dashed lines in Figure 1.

As production causes the reservoir pressure to decline, the temperature follows the dashed line that passes through initial temperature and pressure. Several such lines are presented in Figure 1. For example, from initial conditions corresponding to Point A in Figure 1, the temperature will move to the left along line 1 as the pressure declines. This case (reservoir A) corresponds to a single-phase (essentially steam) reservoir with initial temperature and pressure above the critical values. No hot water is formed during pressure depletion, since line 1 does not intersect the boiling curve. The reservoir temperature remains high after the pressure is depleted. Thus, additional energy could be extracted by water injection, beginning at any point along line 1.

The initial conditions corresponding to Point B (reservoir B) in Figure 1 represent a dry-steam reservoir in which no hot water is formed during pressure depletion and much heat would remain unproduced if the pressure were depleted. The temperature would move along line 3 as the pressure declines.

Point C (reservoir C) in Figure 1 corresponds to an initial hot water reservoir with pressure above the boiling curve. Unless a strong rock drive exists, initially the pressure declines rapidly with production, since only liquid expansion and rock compaction supply the driving energy. The reservoir performs essentially isothermally along line 4 until the boiling curve is reached. Then steam begins to be generated within the reservoir and a steam phase begins to build up within the rock pores. This supplies a gas drive similar to a solution gas drive in a petroleum reservoir. As production continues, the temperature and pressure decline along the boiling curve. The steam saturation increases with production and when it reaches its equilibrium saturation the reservoir begins to produce steam along with hot water.

The produced steam-hot water ratio continues to increase until the water saturation is reduced to its maximum immobile saturation. Then only saturated steam is produced. Water saturation continues to decline until all the water has been boiled away. The temperature then departs from the boiling curve and its decline essentially stops. The produced steam becomes increasingly superheated, as indicated by line 4 in Figure 1.

Point D (reservoir D) in Figure 1 corresponds to a relatively low-temperature hot water reservoir. Except for those cases with strong rock drives, rapid pressure decline with production should occur, since only liquid expansion and rock drive supply the driving energy above the boiling curve. Two-phase internal steam drive does not begin until the reservoir pressure has declined to a small fraction of its initial value. There is sufficient water in the pores that some water will remain even if the pressure reaches atmospheric. Most of the steam produced through pressure depletion of this type of reservoir will be at low pressures. These low pressures result in low efficiencies if used in steam turbines to produce power. For this reason power production from such reservoirs is perhaps best accomplished by cycling hot water through the reservoirs and using a binary cycle power plant (Reference 4).

Fluid and Heat Production Performance

Figures 3 and 4 present the variations of the reservoir pressure and temperature with the percent of initial fluid mass produced. Reservoirs A and B perform essentially by isothermal steam expansion; reservoirs C and D involve two-phase internal steam drive. Almost all of the initial fluid is produced from reservoirs A, B and C and much of it is produced from reservoir D. Reservoirs A and B experience little temperature drop during production and in reservoir C the temperature declines from 550 to 530°F. Thus, in these cases much heat remains in the reservoir rock at the end of pressure depletion.

Figure 5 presents the pressure versus steam saturation for reservoirs C and D. The increasing negative slope of the reservoir C curve with steam saturation reflects the increasing produced steam-hot water ratios as the steam saturation increases with pressure depletion.

Figure 6 presents the variation of pressure with the amount of heat produced which is over and above the amount of heat that would be in the reservoir if it contained only saturated steam at atmospheric pressure and 212°F. Results for reservoirs A and B indicate that relatively small amounts of the total heat are produced during pressure depletion. Figure 7 presents the pressure versus heat recovered in the form of steam and in the form of hot water for reservoirs C and D. These results indicate that more heat is produced in the form of steam than hot water. This reflects the higher heat content and the lower viscosity of the steam as compared to the hot water. Figure 8 presents the pressure versus heat produced for six hot water reservoirs with three different porosities. The increase in heat recovered with porosity for the higher initial pressure cases results from the larger volume of initial water present relative to the reservoir rock volume.

Gravity Segregation

The results presented to this point are based on the assumption that the fluids are uniformly distributed throughout the reservoir. In reality gravity segregation of the steam and hot water will begin as soon as the steam phase becomes mobile. Reservoir performance and gravity segregation studies of oil and gas in oil reservoirs indicate that in many cases segregation occurs rapidly (References 5, 6 and 7). Similar segregation of the steam and hot water should occur in geothermal reservoirs.

The results for uniformly distributed fluids are useful in visualizing the behavior of reservoirs in which rapid gravity segregation takes place and in which heat conduction, natural convection, and capillarity, can be neglected to a first approximation. Steam accumulation at the top of a reservoir resulting from gravity segregation can greatly reduce the amount of water available there to generate steam. Similarly the drainage of hot water to the lower portion of the reservoir increases the amount of water

available there for steam generation. Under gravity segregation reservoir C should perform the same as given in Figures 1 and 3 through 8 until the steam saturation reaches its equilibrium value. Then the steam phase becomes mobile and gravity segregation begins. Steam saturation will increase rapidly near the top of the reservoir. If the wells are completed high in the reservoir or significant steam coning occurs, the produced steam-hot water ratio will increase rapidly. The hot water saturation will decrease rapidly until the water in the region is exhausted. Thus this region will depart from the boiling curve at considerably higher temperatures and pressures than for reservoir C. Points low in the reservoir will have high water saturations longer than if the fluid were to remain uniformly distributed, and these points will remain on the boiling curve to lower temperatures and pressures.

If the wells are completed low in the reservoir and significant steam coning does not take place, the produced steam-hot water ratio will remain low until the steam zone has expanded sufficiently to cause production from the steam zone. Points in the steam zone will depart from the boiling curve at higher pressures and temperatures than in the uniform saturation case and the lower portion of the reservoir will remain on the boiling curve to lower pressures and temperatures.

Thus the relative amounts of steam and hot water produced will depend upon, among other things, the amount of gravity segregation, the relative permeability curves, the structural position of the completion intervals, and the amount of steam and water coning. For many conditions the amount of water initially present is so limited that much usable heat should remain in the reservoir after the water is exhausted. This heat may be distributed in a highly nonuniform manner, with generally higher temperatures in the upper portion of the reservoir. In most cases the produced steam contains much more heat than an equal mass of produced water. Thus for many conditions more total heat can be produced by completing the wells high in the reservoir, to enhance steam production and suppress water production. This should result in more of the dissolved salts being left in the reservoir. This would be an additional advantage provided problems associated with salt deposition are not too severe.

CONCLUSIONS

1. Reservoir analysis methods can be applied to those geothermal reservoirs that involve the flow of steam or hot water through porous media.

2. Hot-water reservoirs can have complicated producing characteristics including changing from hot water to steam as they are produced.

3. Under certain conditions only a relatively small amount of the heat initially contained in a geothermal reservoir will be produced during pressure depletion. Much of this heat may be contained in the produced steam even though initially the reservoir contains only hot water.

4. For many conditions where gravity segregation of the steam and hot water occur during depletion, more of the total heat can be produced by completing wells high in the reservoir to enhance steam production and suppress water production.

REFERENCES

1. Whiting, R. L. and Ramey, H. J.: "Application of Material and Energy Balances to Geothermal Steam Production", J. Pet. Tech. (July 1969) pp. 893-900.

2. Martin, J. C.: "Simplified Equations of Flow in Gas Drive Reservoirs and the Theoretical Foundation of Multiphase Pressure Buildup Analyses", Trans AIME (1959) vol. 216, pp. 309-311.

3. Hass, J. L.: "The Effect of Salinity on the Maximum Thermal Gradient of a Hydrothermal System at Hydrostatic Pressure", Econ. Geology, Vol. 66 (1971) pp. 940-946.

4. Kruger, P. and Otte, Carel: Geothermal Energy, Stanford Univ. Press, Stanford, Calif. (1973).

5. Spivak, A.: "Gravity Segregation in Two-Phase Displacement Processes", SPEJ (Dec. 1974) Vol. 14, No. 6, pp. 619-632.

6. Martin, J. C.: "Reservoir Analysis for Pressure Maintenance Operations Based on Complete Segregation of Mobile Fluids", Trans. AIME (1958) Vol. 213, pp. 220-227.

7. Martin, J. C.: "Some Mathematical Aspects of Two-Phase Flow with Applications to Flooding and Gravity Segregation Problems", Prod. Monthly (April 1958), pp. 22-35.

APPENDIX

The mathematical relations for both two-phase (boiling) and single phase flow are derived in this appendix.

Two Phase Relations

The basic equations for conditions along the boiling curve are:

Darcy's law for hot water:

$$u_w = - \frac{k\, k_{rw}}{\mu_w} \nabla p \qquad (1)$$

Darcy's law for steam:

$$u_s = - \frac{k\, k_{rs}}{\mu_s} \nabla p \qquad (2)$$

The equation of continuity for mass:

$$\nabla \cdot (\rho_w u_w + \rho_s u_s) = - \frac{\partial}{\partial t} \left[\phi(\rho_w S_w + \rho_s S_s)\right] \qquad (3)$$

The equation of continuity for heat:

$$\nabla \cdot (\rho_w h_w u_w + \rho_s h_s u_s - k_h \nabla T) = - \frac{\partial}{\partial t} \left\{\phi[\rho_w h_w S_w + \rho_s h_s S_s + (\frac{1-\phi}{\phi})\rho_r C_r T]\right\} \qquad (4)$$

saturations:

$$S_w + S_s = 1 \qquad (5)$$

Substituting equations 1 and 2 into 3 yields:

$$\nabla \cdot \lambda_f \nabla p = \frac{\partial M_f}{\partial t} \qquad (6)$$

$$\nabla \cdot \lambda_h \nabla p = \frac{\partial M_h}{\partial t} \qquad (7)$$

where

$$\lambda_f = \frac{\rho_w k\, k_{rw}}{\mu_w} + \frac{\rho_s k\, k_{rs}}{\mu_s}$$

$$\lambda_h = \frac{\rho_w h_w k\, k_{rw}}{\mu_w} + \frac{\rho_s h_s k\, k_{rs}}{\mu_s} + k_h \psi'$$

$$M_f = \phi(\rho_w S_w + \rho_s S_s)$$

$$M_h = \phi[\rho_w h_w S_w + \rho_s h_s S_s + (\frac{1-\phi}{\phi})\rho_r C_r \psi]$$

$$T = \psi(p) \qquad (8)$$

and

$$\psi' = \frac{d\psi}{dp}$$

The symbol λ_f denotes the mobility of the fluids in terms of mass: λ_h, the mobility of the heat; M_f, the mass of fluid per unit volume of reservoir rock; and M_h, the total heat per unit volume of rock.

Equations 5 and 6 can be written as

$$\frac{\partial \lambda_f}{\partial p} \nabla p \cdot \nabla p + \frac{\partial \lambda_f}{\partial T} \nabla T \cdot \nabla p + \frac{\partial \lambda_f}{\partial S_w} \nabla S_w \cdot \nabla p + \frac{\partial \lambda_f}{\partial S_s} \nabla S_s \cdot \nabla p + \lambda_f \nabla^2 p = \frac{\partial M_f}{\partial t} \qquad (9)$$

$$\frac{\partial \lambda_h}{\partial p} \nabla p \cdot \nabla p + \frac{\partial \lambda_h}{\partial T} \nabla T \cdot \nabla p + \frac{\partial \lambda_h}{\partial S_w} \nabla S_w \cdot \nabla p + \frac{\partial \lambda_h}{\partial S_s} \nabla S_s \cdot \nabla p + \lambda_h \nabla^2 p = \frac{\partial M_h}{\partial t} \qquad (10)$$

In those cases where the saturation gradient, temperature gradient, and pressure gradients are small, the vector products $\nabla p \cdot \nabla p$, $\nabla T \cdot \nabla p$, $S_w \cdot \nabla p$ and $\nabla S_s \cdot \nabla p$ are small compared to the magnitudes of $\nabla^2 p$, $\frac{\partial M_f}{\partial t}$, and $\frac{\partial M_h}{\partial t}$, and the terms containing the vector products can be neglected to a first approximation.

Equations 9 and 10 reduce to:

$$\nabla^2 p = \frac{1}{\lambda_f} \frac{\partial M_f}{\partial t} \qquad (11)$$

$$\nabla^2 p = \frac{1}{\lambda_h} \frac{\partial M_h}{\partial t} \qquad (12)$$

Equations 11 and 12 require that the variations of P, S_w, S_s, and T are small with distance. Fortunately the variations of these quantities with time need not be small.

The elimination of $\nabla^2 p$ from Equations 11 and 12 yield (replacing T by $\psi(p)$ and S_s by $1-S_w$):

$$\frac{\partial M_f}{\partial p} \frac{\partial p}{\partial t} + \frac{\partial M_f}{\partial S_w} \frac{\partial S_w}{\partial t} = \frac{\lambda_f}{\lambda_h} \left(\frac{\partial M_h}{\partial p} \frac{\partial p}{\partial t} + \frac{\partial M_h}{\partial S_w} \frac{\partial S_w}{\partial t} \right)$$

This equation reduces to the following ordinary differential equation:

$$\frac{dS_w}{dp} = \frac{\lambda_h \frac{\partial M_f}{\partial p} - \lambda_f \frac{\partial M_h}{\partial p}}{\lambda_f \frac{\partial M_h}{\partial S_w} - \lambda_h \frac{\partial M_f}{\partial S_w}} \qquad (13)$$

Equation 13 can be integrated numerically to obtain S_w as a function of P. This relation is similar to the Muskat solution gas relation which relates oil or gas saturation to reservoir pressure.

The relation between S_w and P obtained from Equation 13 can be used to eliminate S_w from λ_f, λ_h, M_f, and M_h. This allows Equations 11 and 12 be expressed in terms of pressure, ereby obtaining a partial differential equation for pressure that can be used in the ahalysis of transient well pressure data which involve two-phase flow in the reservoir.

Single Phase Flow

The temperature and pressure are not related to the boiling curve for single-phase flow. Equation 11, however, is valid and the equivalent of Equation 12 is:

$$\nabla^2 p + \frac{k_h}{\rho h \lambda} \nabla^2 T = \frac{1}{\rho h \lambda} \frac{\partial M_h}{\partial t} \qquad (14)$$

where h is the enthalpy, λ is the mobility, and M_h is the single phase equivalent of M_h.

In the case of two phase flow it was possible to obtain an ordinary differential equation for the water saturation versus pressure without neglecting the effects of heat conduction, because temperature and pressure are related by the boiling curve. Unfortulately, this is not the case for single phase flow; however, if we neglect the effects of heat conduction, Equation 14 reduces to:

$$\nabla^2 p = \frac{1}{\rho h \lambda} \frac{\partial M_h}{\partial t} \qquad (15)$$

Eliminating $\nabla^2 p$ from Equations 11 and 15 leads to the following differential equation for P and T:

$$\frac{dT}{dp} = \frac{\frac{\partial M_h}{\partial p} - h \frac{\partial M_f}{\partial p}}{h \frac{\partial M_f}{\partial T} - \frac{\partial M_h}{\partial T}} \qquad (16)$$

This equation was used to calculate T versus P for single phase flow. As expected, numerical results reveal small values of $\frac{dT}{dp}$ indicating essentially isothermal behavior.

Additional Relations

Solutions of Equations 13 and 16 yield the temperature and fluid saturations as functions of reservoir pressure. Heat and mass balances can be used to obtain the fluid and heat productions as functions of pressure. These relations are:

$$Q_f = 1 - \frac{M_f}{M_{fi}}$$

where Q_f is the fraction of the original fluid mass that has been produced and the subscipt i refers to initial conditions.

$$Q_h = \frac{M_{hi} - M_h}{M_{hi} - M_{ha}}$$

where Q_h is the fraction of the original heat that has been produced which is above the heat contained in the reservoir at atmospheric pressure and 212°F containing only saturated steam. The subscript a refers to these conditions.

Expressions for the relative amounts of heat produced in the steam and in the hot water can be obtained by integration. These relations are:

$$Q_{hw} = \left(\frac{1}{M_{hi} - M_h}\right)\int_{p_i}^{p}\left(\frac{\rho_w h_w k\, k_{rw}}{\lambda_h\, \mu_w}\right)\frac{dM_h}{dp}\,dp$$

$$Q_{hs} = \left(\frac{1}{M_{hi} - M_h}\right)\int_{p_i}^{p}\left(\frac{\rho_s h_s k\, k_{rs}}{\lambda_h\, \mu_s}\right)\frac{dM_h}{dp}\,dp$$

where Q_{hw} and Q_{hs} are the fractions of the produced heat contained in the hot water production and in the steam production respectively.

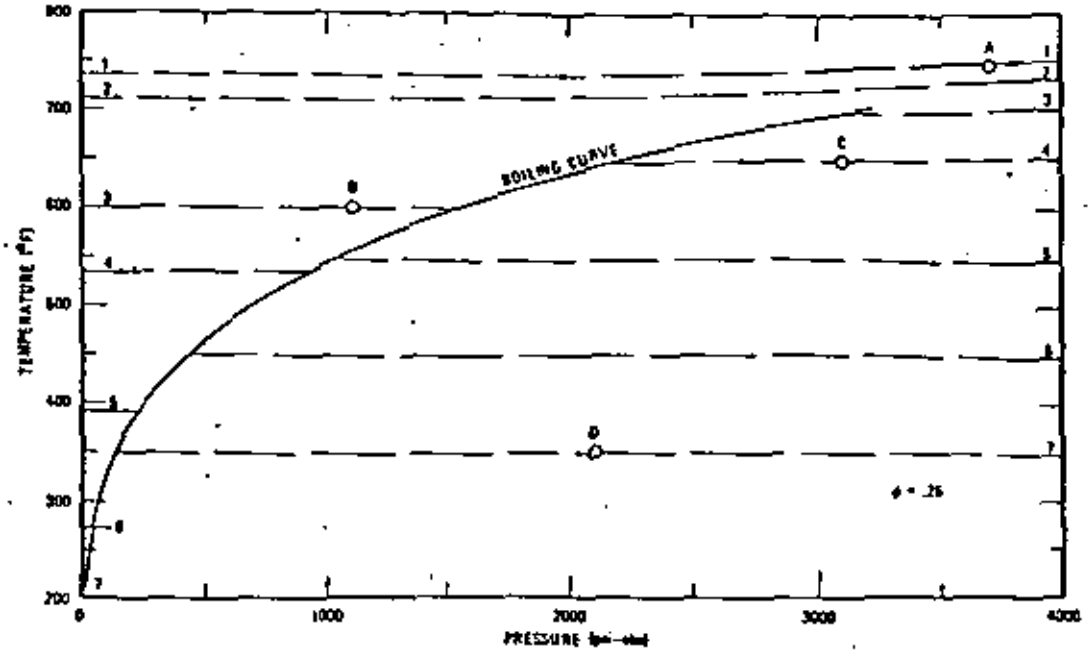

Fig. 1 - Temperature vs pressure for geothermal reservoirs containing fresh water, a porosity of .25, and with other data given in text.

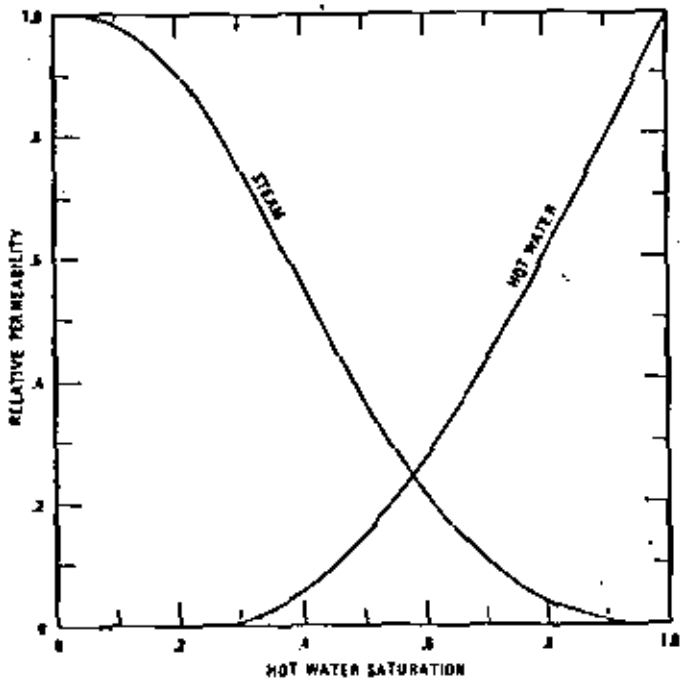

Fig. 2 - Steam and hot water relative permeability curves used in the calculations.

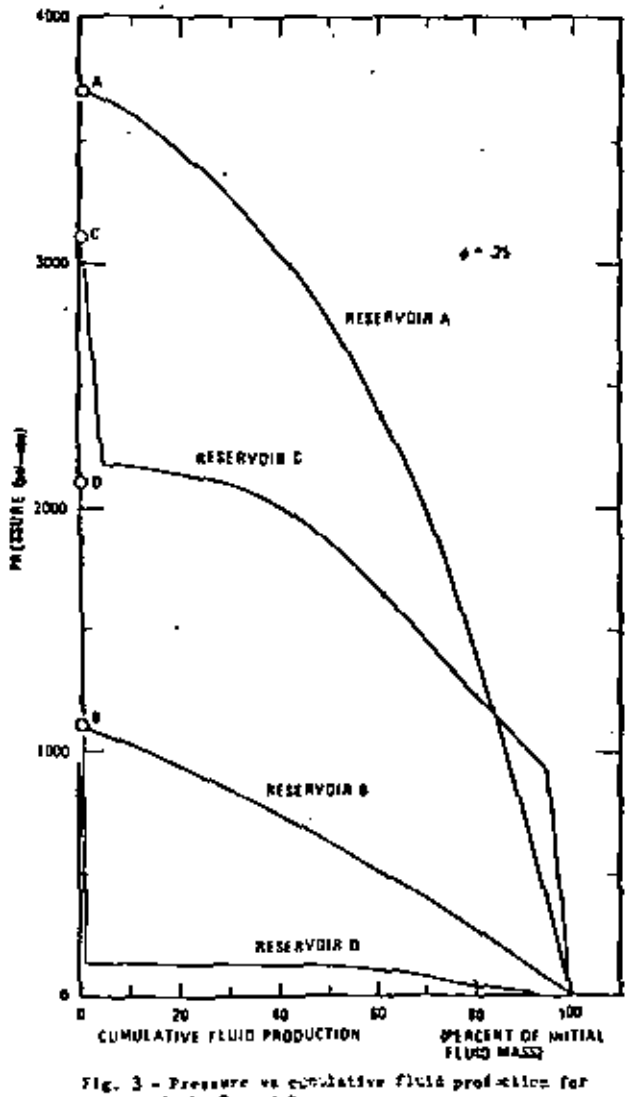

Fig. 3 - Pressure vs cumulative fluid production for reservoirs A, B, C, and D.

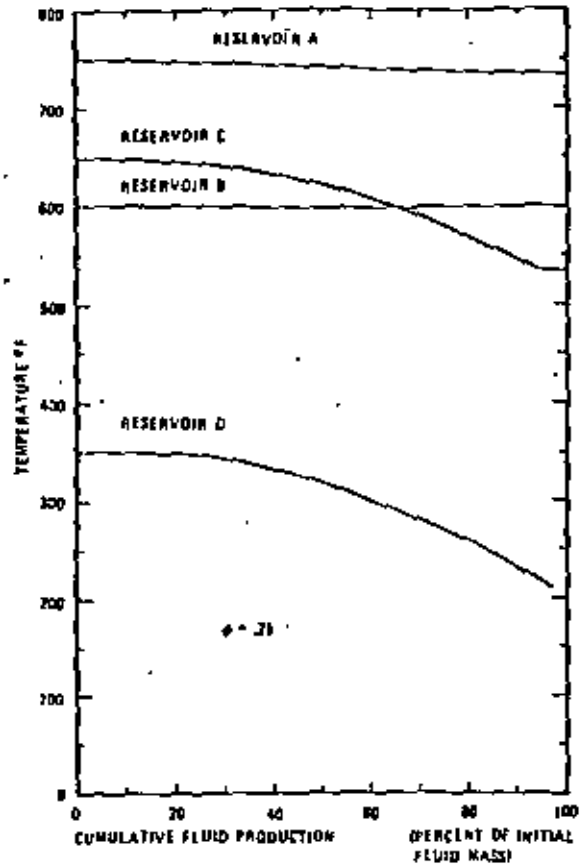

Fig. 4 - Temperature vs cumulative fluid production for reservoirs A, B, C, and D.

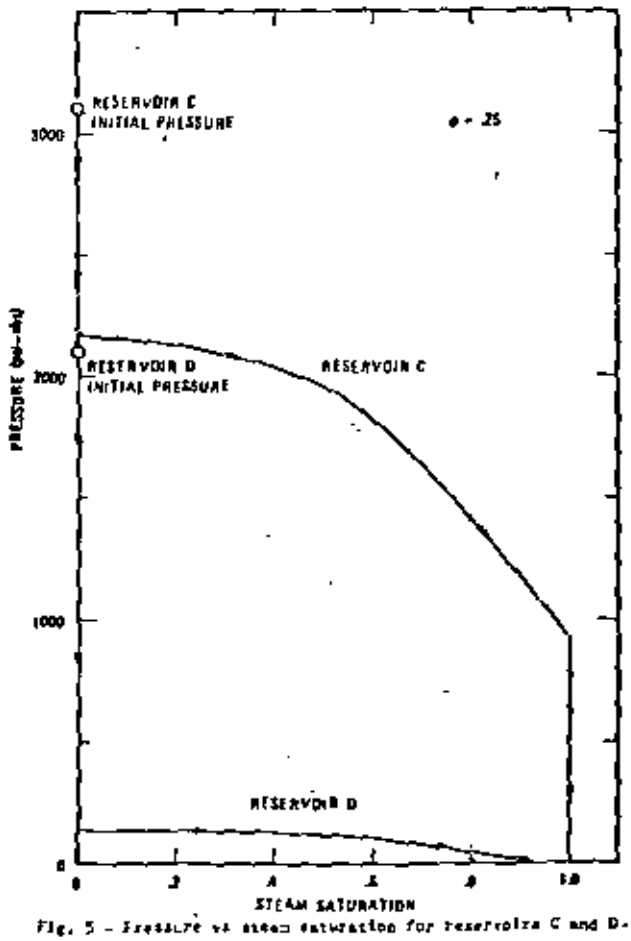

Fig. 5 - Pressure vs steam saturation for reservoirs C and D.

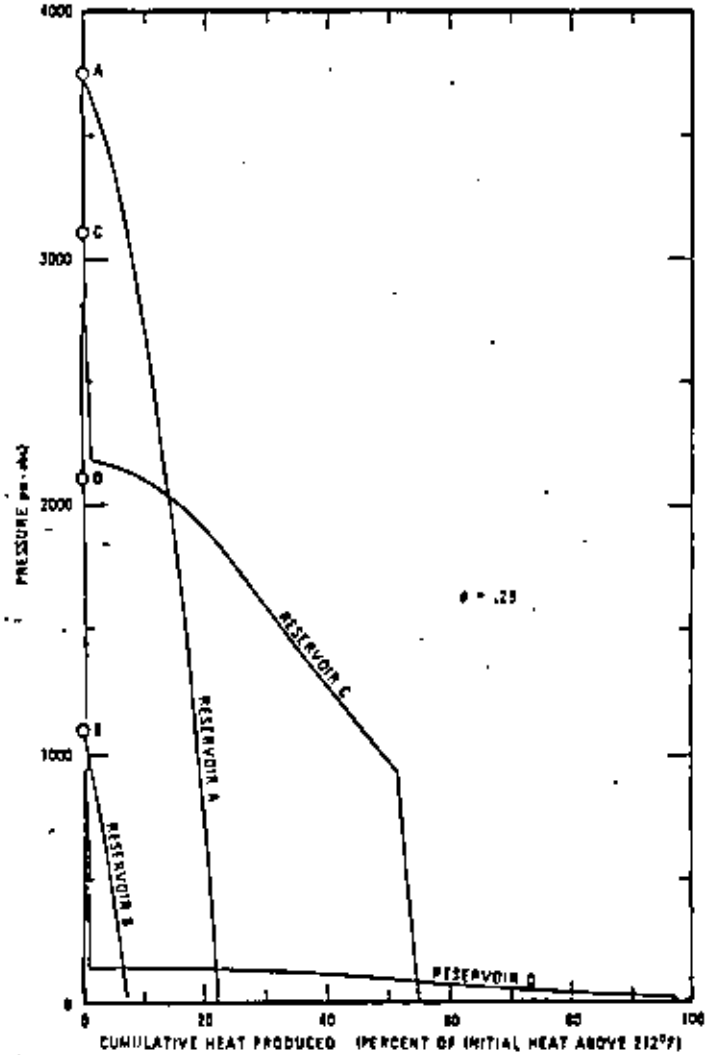

Fig. 6 - Pressure vs cumulative heat produced for reservoirs A, B, C, and D.

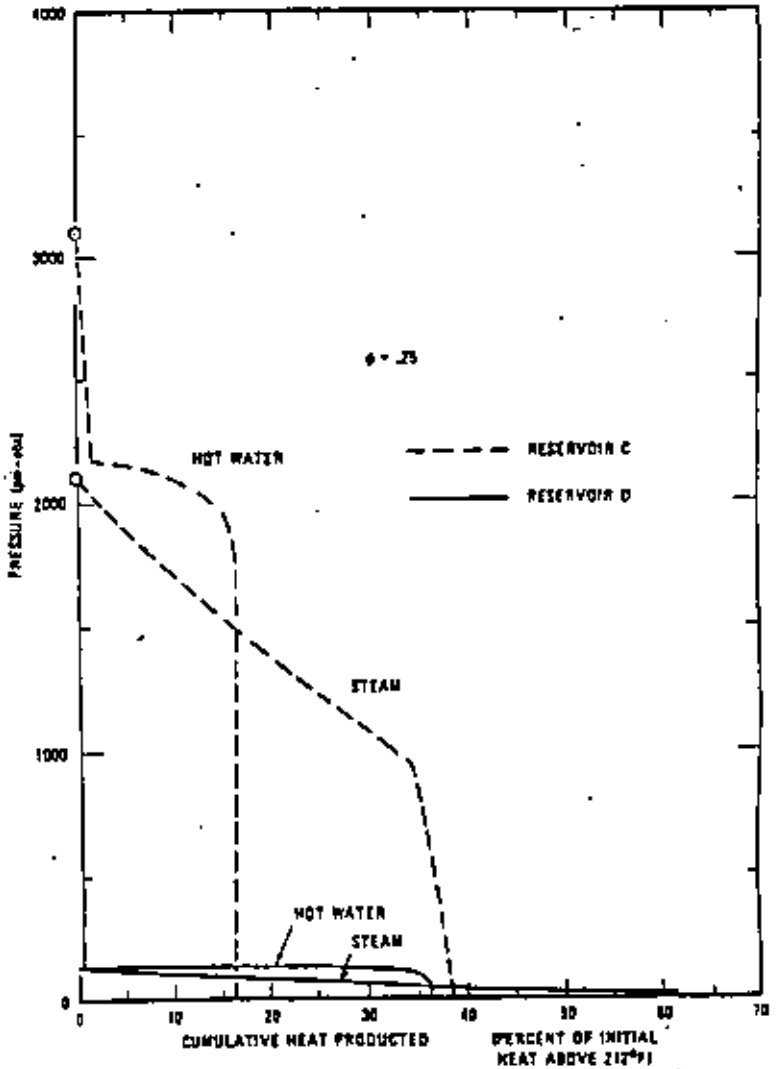

Fig. 7 - Pressure vs cumulative heat produced as steam and as hot water for reservoirs C and D.

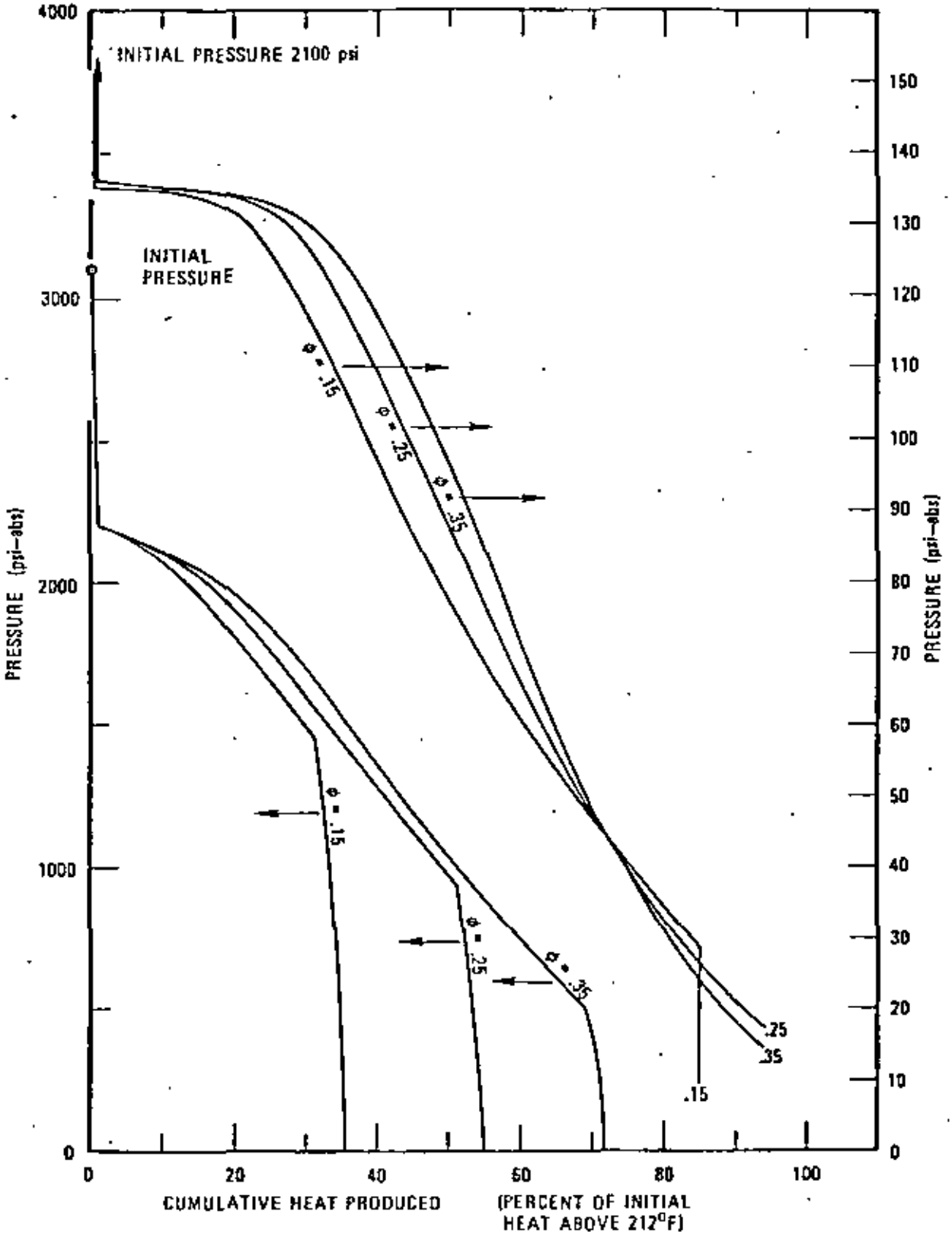

Fig. 8 - Pressure vs cumulative heat produced for three different porosities and two different initial conditions (3100 psi, 650 °F and 2100 psi, 350°F).

March 19, 1974
H. J. Ramey

Pet.E. 269

FINAL EXAMINATION

(Open book, open notes; 3 hr. maximum)

1. A geothermal reservoir contains a 10,000 ft steam cap on top of a 1,000 ft thick liquid interval. For simplification, we assume temperature is constant at 525°F throughout this reservoir.

   Given: porosity = 0.1 fraction bulk vol
   permeability = 5 md
   sandstone formation

   Find:

   (a) The mass of fluid initially in place in lbs/acre (1 acre = 43560 ft^2). State assumptions.

   (b) Assuming the system is closed and neglecting convection, what pressure, psia, would you expect to find at the shallowest point of steam entry? (That is, at the very top of the steam cap.) Explain your reasoning.

   (c) What would the pressure be at the bottom of the liquid interval, psia?

2. If an electric power plant is built which requires 22 lb of steam per kilowatt-hr, steam recovery efficiency is 60% of initial fluid in place, the power plant operates 85% of the time, and the initial fluid in place is 400 x 10^6 $\frac{lbm}{Ac}$, find:

   (a) steam reserves in megawatt-years per acre;

   (b) operating life in years of a 50-megawatt plant fed by a 1280-acre steam field.

   (c) If an average well in this field produces 65,000 lb steam/hr, how many wells would be required for the 50 MW plant?

3. The bottomhole pressure at 6200 ft is required for a static geothermal well. The wellhead pressure is measured at 435 psia, and a sonic liquid level measurement indicates liquid at 4800 ft below surface. The temperature of the fluid in the well may be assumed constant at 460°F.

4. A well is producing dry steam at 50,000 lb/hr from a 5,000 ft deep well in a vapor-dominated system. The producing enthalpy is 1200 Btu/lb. Immediately following an increase in production rate to 80,000 lb/hr, it

was found that the producing steam enthalpy increased to 1305 Btu/lb. Estimate the reservoir steam enthalpy. Assume a linear geothermal gradient to 5,000 ft. Make and list any other pertinent assumptions. Barometric pressure is 14.3 psia.

5. A well in a liquid-dominated system produces at 200,000 lb/hr initially, at pressures well above the vapor pressure at the well head. Given the data below, find the producing wellhead temperature for a 2-day flow test.

   Given: depth = 3,000 ft
   surface temperature = 85°F
   temperature at 3,000 ft = 475°F
   casing radius = 0.33 ft
   thermal cond. = 35 Btu/d-ft-°F
   thermal diff. = 1.1 ft^2/day

6. In fluid reservoir development planning, it is important to be able to produce a schedule of fluid produced vs time on a per well basis. This usually requires a combination of material balance and well deliverability for the drainage volume of a well. During the course, typical relations for a vapor-dominated system were discussed. Briefly present your ideas on a similar approach for a liquid-dominated system initially in the compressed liquid region.

3-19-74
HJR

Pet. E. 269 Final Examination

(a) We know liq & gas are in equil. at the interface. Thus the pres. at the interface and sp. vols must be (at 525°F) 848.1 psia, V_f = 0.0210 ft³/lb, and V_g = 0.5340 ft³/lb. Density of liquid will be essentially constant.

$$\frac{\text{lb liq}}{\text{ac}} = \frac{(Ah\phi)_f}{V_f} = \frac{(43560\ \text{ft}^2/\text{ac})(1000\ \text{ft})(0.1\ \text{PV})}{(0.0210\ \text{ft}^3/\text{lb})} = 207.4\times10^6\ \frac{\text{lb liq}}{\text{ac}}$$

In the gas column, the density decreases from that at the interface ($\frac{1}{0.534}\ \frac{\text{lb}}{\text{ft}^3}$) to a lower value at the surface. We know for a static column:

$$p_w/p_t = e^{\frac{.01875\,\gamma_g L}{TZ}}$$

Or

$$\frac{848}{p_t} = e^{\frac{.01875(18/29)10{,}000}{(525+460)(.84)}} = 1.151$$

$$p_t = 736.8\ \text{psia}$$

The mass of gas will be:

$$W\ \frac{\text{lb Stm}}{\text{acre}} = 43560\ \frac{\text{ft}^2}{\text{ac}}\,\phi \int_0^L \rho_{stm}\,dL' = 43560(\phi)\int_{p_t}^{p_w} \rho_{stm}\frac{dL'}{dp}\,dp$$

but $\frac{dp}{dL'} = \frac{\rho_{st}}{144}\frac{g}{g_c}$

So:

$$W\ \frac{\text{lb Stm}}{\text{acre}} = 43560\,\phi\int_{p_t}^{p_w}\rho_{stm}\frac{144}{\rho_{stm}}\,dp = 43560\,\phi(p_w - p_t)(144)$$

$$W\ \frac{\text{lb Stm}}{\text{acre}} = 43560(.1)(848-737)(144) = 69.6\times10^6\ \frac{\text{lb Stm}}{\text{ac}}$$

Total fluid = $207.4\times10^6 + 69.6\times10^6 = 277\times10^6$ lbs/ac

(b) $736.8 \text{ psia} = 722.1 \text{ psig}$

(c) pres. at bot. liq would be:

$$\text{psia} = 848 + \frac{1000 \text{ ft}}{(0.0210 \text{ ft}^3/\text{lb})(144 \text{ in}^2/\text{ft}^2)} = 848 + 330.7$$

$$= 1178.7 \text{ psia} = 1164 \text{ psig}$$

2. Problem had a typo. Shd have read $400 \times 10^6 \frac{\text{lbs}}{\text{acre}}$.

(a) $$\frac{\text{MW-yr}}{\text{ac}} = \frac{(400 \times 10^6 \text{ lb/ac})(0.6 \frac{\text{lb REE}}{\text{lb ISIP}})}{(22 \text{ lbs/kwhr})(1000 \text{ kw/MW})(365 \text{d/yr})(24 \text{hr/d})} =$$

$$= 1.245 \text{ MW-yr/ac} \text{ or } \frac{1.245}{0.85} = 1.465$$

(b) $$\frac{(50 \text{MW})(.85 \frac{\text{op yrs}}{\text{tot yrs}})(x \text{ tot yrs})}{1280 \text{ ac}} = 1.245 \frac{\text{MW yr}}{\text{ac}}$$

$$x \text{ yrs} = \frac{1.245(1280)}{50(.85)} = 37.5 \text{ yrs}$$

(c) $$\text{No. wells} = \frac{(50 \text{MW})(1000 \text{KW/MW})(22 \frac{\text{lb Stm}}{\text{KWhr}})}{65{,}000 \frac{\text{lb Stm}}{\text{hr-well}}} = 16.9 \approx 17 \text{ wells}$$

Note: efficiencies do not enter this calculation.

3. At 4800 ft liq & Atm in equil. Thus interface pres. must corr. to 460°F or 466.9 psia. The $V_f = 0.0196$. Thus the pres is:

$$P_w = 466.9 + \frac{(6200 - 4800 \text{ ft})}{(.0196 \text{ ft}^3/\text{lb})(144 \text{ in}^2/\text{ft}^2)} = 466.9 + 496 =$$

$$P_w = 962.9 \text{ psia} = 948 \text{ psig}$$

$$= \frac{2\pi k}{f(t)}\left[-\frac{aL^2}{2}\right]$$

essentially

he heat loss is independent of flow rate. Th
e heat loss must be the same before and
fter the rate change. Thus:

$$\frac{\text{heat loss, btu}}{\text{hr}} = 50{,}000(h-1280) = 80{,}000(h-1305)$$

$$h - 1280 = 1.6h - 2088$$

$$0.6h = 808$$

$$h = \underline{1346.7} \text{ btu/lb}$$

$Dt/r_2^2 = (1.1\ ft^2/d)(2d)/(.38\ ft)^2 = 15.2$, $\log t_D =$

$\log f(t) = 0.3$, $f(t) = 1.995$

$T_0 = b = 475°F$; $a = -\frac{475-85}{3000} = -0.13°F/ft$

$A = \frac{(200000\ lb/hr)(24\ hr/d)(1\ btu/lb°F)(1.995)}{2\pi(35)} = 43{,}545\ ft$

$T_{tf} = -(.13)(3000) + 475 - (-.13)(43{,}545) - (.13)(43545)e$

$T_{tf} = -390 + 475 + 5660.9(1 - 0.9334)$

$T_{tf} = -390 + 475 + 377 = \underline{462°F}$

Can use liquid flow prod. eqns until p_w
then use 2 ϕ flow in bank. first mean wel
Perhaps a modification of Fetkovich eqn; u
val. balance above VP, then 2 ϕ until ener
balance.

centro de educación continua
división de estudios superiores
facultad de ingeniería. unam

CURSO: INGENIERIA DE RESERVORIOS GEOTERMICOS.

THERMODYNAMIC AND HYDRODINAMIC PROPERTIES OF HYDROTHERMAL SYSTMS.

INSTRUCTOR: HEBER CINCO LEY.

SEPTIEMBRE, 1981.

THERMODYNAMIC AND HYDRODYNAMIC PROPERTIES OF HYDROTHERMAL SYSTEMS

by

Henry J. Ramey, Jr.
William E. Brigham
H. K. Chen
Paul G. Atkinson
Norio Arihara

Stanford University
Stanford, California, U.S.A.

April 20, 1974

From the Proceedings of an NSF conference on "The Utilization of Volcano Energy," Hilo, Hawaii, February 4-8, 1974.

THERMODYNAMIC AND HYDRODYNAMIC PROPERTIES OF HYDROTHERMAL SYSTEMS

by

Henry J. Ramey, Jr., William E. Brigham, H. K. Chen,
Paul G. Atkinson, and Norio Arihara

Stanford University
Stanford, California

INTRODUCTION

Geothermal energy has received much attention in recent years as one of the sources that can help relieve the energy crisis in the next decade. There is considerable literature on the possible methods of geothermal energy extraction, and practical usage of geothermal energy is growing worldwide.

The goal of any geothermal production system is to extract heat from the earth, and to extract it at a high enough temperature and rate that it can be used commercially to generate power or process heat. Most present geothermal systems are geared toward power generation. To evaluate these systems we must predict the amount of heat present and the rate at which it can be extracted. These are the prime factors affecting the economics of any recovery process.

These two factors--amount of heat and recovery rate--in turn depend on basic physical properties of the reservoir rocks and the fluids contained within them. The amount of heat present depends on the heat capacity and density of the rock and the fluids within it. The rate of heat extraction depends on the thermal conductivity and the fluid flow characteristics, i.e., permeability and relative permeability, of the water and steam in the rocks. All these important basic characteristics of the rock and fluids are functions of both the temperature and pressure of the reservoir system.

Fortunately there is an extensive body of literature available to help one estimate many of these fluid and rock properties. Much of this information can be found in the petroleum literature, for the petroleum industry has had an interest in the use of underground heat for oil recovery since the early 1900's. In the paper we summarize some of the data that is useful for geothermal systems. A large fraction of these data are extracted from the petroleum literature.

STORAGE AND TRANSPORT OF HEAT IN ROCKS

Neglecting heat of phase change and heat of reaction, there are three important thermal properties in any process involving heat transfer: thermal conductivity, heat capacity, and thermal diffusivity. Thermal conductivity is generally shown by the symbol, k, and units in the c-g-s system are cal/sec-cm-°C. Many of the references, however, are given in British thermal units, Btu/hr-ft-°F. The conversion factor is:

$$1 \frac{\text{Btu}}{\text{hr-ft-°F}} = \frac{4{,}134 \times 10^{-3} \text{ cal}}{\text{sec-cm-°C}} \qquad (1)$$

The specific heat generally used is the specific heat at constant pressure, or $(\partial H/\partial T)_p$, and the symbol is C_p. The c-g-s unit, cal/gm-°C, is numerically the same as the British unit, Btu/lb-°F. Thermal diffusivity is a collection of terms, $k/\rho C_p$, where ρ is the density. It is often indicated by the symbol α. This grouping is the ratio of the ability to transfer heat, k, to the ability to store heat, ρC_p. In the c-g-s system the dimensions are cm^2/sec, and in the British system ft^2/hr. Many references use British units. The conversion factor is:

$$1 \frac{ft^2}{hr} = \frac{0.258\ cm^2}{sec} \qquad (2)$$

Thermal Conductivity

An early evaluation of rock thermal conductivity was made by Birch and Clark.[1,2] They studied a broad range of rock materials including some eighteen igneous rocks, seven sedimentary and metamorphic rocks, and certain single crystals and glasses. With the exception of the anorthosites and the glasses (both man-made and natural) all the materials showed a reduction of thermal conductivity with temperature increase. This behavior is as should be expected. See Figures 1 and 2, from Birch and Clark.[1]

Probably the most important finding by Birch and Clark was that the thermal conductivity of a mixture could be estimated by assuming that the various components of the system were in series. The total thermal resistivity of the system is equal to the volumetric weighted average of resistivity of each component. The total conductivity is thus the harmonic average:

$$\frac{1}{k_{ave}} = \frac{x_1}{k_1} + \frac{x_2}{k_2} + \ldots + \frac{x_n}{k_n} \qquad (3)$$

where x = volumetric fraction of each component.

Birch and Clark's data were mostly for rocks of low porosity. Somerton[3] was an early investigator of the thermal conductivity of fluid-containing rocks. He studied unconsolidated sands, sandstones, silty sandstones, siltstone, shale and limestone. He developed an empirical equation to predict the effect of fluid saturation on the thermal conductivity of porous rocks. It was:

$$\frac{k}{k_1} = \left(\frac{k_2}{k_1}\right)^{c\phi} \qquad (4)$$

where k = thermal conductivity of fluid-saturated rock

k_1 = thermal conductivity of rock solids

k_2 = thermal conductivity of saturating fluid

ϕ = porosity - fraction

c = empirical constant approximately equal to 1.

The empirical constant, c, was actually found to range from 0.9 to 2.3 with the larger values found at lower porosities. The product, $c\phi$, ranged from 0.325 to 0.460.

In 1961 Kunii and Smith[4] measured thermal conductivities of porous rocks saturated with various fluids. They proposed an equation (their Eqn. 3) to relate the fluid saturated conductivity to the conductivity of dry rock. Some of their results are reproduced here as Figures 3 and 4 to show the correspondence of their data to their model. Water may increase conductivity more than two-fold depending on the nature of the porous medium. Their data were run on Boise, Bartlesville, Berea and Rangely sandstones.

Smith and his coworkers[5,6] also studied the effect of fluid flow on the thermal conductivity of porous systems. In general they found that thermal conductivity in the direction of flow was increased as the flow velocity increased.[5] Figure 5 shows this effect with water and brine. They made a correlation of this effect through use of the product of the Reynolds' Number and the Prandtl Number (Fig. 6). Thermal conductivity perpendicular to the direction of flow, however, remained nearly constant--unaffected by flow rate.[6]

Anand, Somerton and Gomaa[7] recently have shown empirical methods of predicting thermal conductivities of fluid saturated rocks when there is little thermal data available. These methods are based on regression analysis equations. The thermal conductivity of dry rock (containing air) was correlated as follows:

$$\lambda_d = 0.3386\ \rho^{1.034} - 3.194\ \phi + 0.5304\ k^{0.100} + 0.0131\ F - 0.0311 \qquad (5)$$

where λ_d = thermal conductivity of dry rock, Btu/hr-ft-°F

ρ = bulk density, gm/cc

ϕ = fractional porosity

k = permeability, millidarcies

F = formation electrical resistivity factor

The formation resistivity factor is a common formation evaluation term which can be extracted from electric logs. It is the ratio of the actual resistivity to that if the rock pores were totally filled with formation water. In the absence of data on this parameter, the following empirical relationship can be used:

$$F = 1/\phi^m \qquad (6)$$

where m = cementation factor, often near 2.0 for sandstones.

Where the rock is fluid saturated the thermal conductivity is higher, and Anand, et al., found the following empirical equation was useful:

$$\frac{\lambda_s}{\lambda_d} = 1 + 0.299 \left[\left(\frac{\lambda_f}{\lambda_a} \right)^{0.330} - 1 \right]$$

$$+ 4.57 \left[\frac{\phi}{(1-\phi)} \frac{\lambda_f}{\lambda_d} \right]^{0.482m} \left(\frac{\rho_s}{\rho_d} \right)^{-4.30} \quad (7)$$

where λ_s = thermal conductivity of fluid-saturated rock, Btu/hr-ft-°F

λ_f = thermal conductivity of the saturating fluid

λ_a = thermal conductivity of air

ρ_s = bulk density of saturated rock

ρ_d = bulk density of dry rock

Lastly, the effects of temperature were included. Anand, et al., used a modification of Tikhomirov's[8] correlation to show this effect. Their results were as follows:

$$\lambda_T = \lambda_{68°} - 0.709 \times 10^{-3} (T - 528) (\lambda_{68°} - 0.800) \cdot \left[\lambda_{68°} \left(T \times 10^{-3} \right)^{0.545\lambda_{68°} + 0.738} \right] \quad (8)$$

where λ_T = thermal conductivity at temperature, T, Btu/hr-ft-

$\lambda_{68°}$ = thermal conductivity at 68°F

T = temperature, °R = °F + 460

A graph of their data compared to this equation is shown in Figure 7. The match appears to be satisfactory. The equation properly predicts high conductivity materials have lower thermal conductivity at higher temperatures, while low conductivity materials exhibit increasing conductivities with temperature.

Often rocks contain two fluids rather than one. Gomaa and Somerton[16,17] discuss this effect in two recent papers. If both fluids are liquid, or if neither fluid is boiling or condensing, the thermal conductivity of the system is a simple square root relationship between the thermal conductivity and the fluid content, as follows:

$$\lambda - \lambda_1 = (\lambda_2 - \lambda_1)\ (S_2)^{1/2} \qquad (9)$$

where λ = thermal conductivity of rock containing two fluids

λ_1 = thermal conductivity of rock saturated with fluid 1

λ_2 = thermal conductivity of rock saturated with fluid 2

S_2 = the fraction of pore space filled with fluid 2

If the fluids are a liquid and vapor in equilibrium with each other, for example water and steam, the thermal conductivity may be far higher than predicted by Eqns. 8 and 9. The combination of heat transfer by boiling and mass flow by capillary pressure effects can cause the effective thermal conductivity to increase 2 to 5 fold. This is called the "heat pipe" effect. The amount of increase depends on the permeability of the rock, the latent heat of vaporization, the vapor saturation and the direction of heat flow with respect to gravity. The empirical equation they found to predict this additional term is as follows:

$$\lambda_{HP} = 0.003\ \phi^{0.357}\ k^{0.424}\ \frac{LY}{\sqrt{\nu_\ell\ \nu_v}}\ (1 + 0.107 \sin \phi)\ F(S) \qquad (10)$$

$$F(S) = \sin\left[\frac{\pi\left(1-S_{\ell}\right)}{1-S_{\ell c}}\right]\sin\left[\frac{\pi\left(1-S_{v}\right)}{1-S_{vc}}\right] \cdot \left[0.74 + 0.61S_{v} + 1.56S_{v}^{2} + 2.85S_{v}^{3}\right] \quad (11)$$

$$S_{\ell c} = 0.098\ k^{-0.236} \quad (12)$$

$$S_{vc} = 0.060\ k^{-0.236} \quad (13)$$

where S_{ℓ} and S_{v} = the fraction of pore space filled with liquid and vapor, respectively

ϕ = porosity, fraction

k = permeability, darcies

L = latent heat of vaporization, Btu/lb

γ = vapor pressure-temperature derivative, lb/in^2-

ν_{ℓ} and ν_{g} = viscosity of liquid and vapor, ft^2/day

ψ = angle of heat flow direction, positive upward

λ_{HP} = additional thermal conductivity due to heat pipe effect, Btu/hr-ft-°F

By this stage, it should be clear that there is a problem in this study with respect to symbols and units. The symbol k has been used widely to represent both the thermal conductivity and permeability. E the Greek symbol λ has been used often in various literatures to repre both heat and fluid conductivities of porous solids. Rather than tota recast equations in a single set of symbols and units, we have elected preserve the symbols of the original study, where possible, and to def symbols and units where presented. This is done because the purpose o

of studies such as this is usually to guide a reader to further information, rather than to replace it. The pertinent literature is far too voluminous for a single paper to serve a true summary purpose.

We turn now to a review of pertinent information on heat capacity and density.

Heat Capacity and Density

Somerton's[5] data on heat capacity of rocks shows that most reservoir materials behave similarly. Figure 8 shows some of the results of his work. Martin and Dew[11] point out that these data can be approximated roughly by a linear equation for heat capacity as a function of temperature:

$$c_p = \frac{T + 2000}{10{,}000} \qquad (14)$$

where c_p = heat capacity of rock, Btu/lb-°F

T = temperature, °F

Somerton also found that where rock is made up of minerals with many differing materials, the average heat capacity follows Kopp's Law, which states that the heat capacity is the mass weighted average of the constituents.

In general, rock volume changes only slightly with temperature. Further, many rocks containing large percentages of quartz behave much alike. Figure 9 shows the data of Somerton and Selim[12] for three sandstones and quartz. There is little difference in the results for the four materials.

Thermal Diffusivity

Because the thermal conductivity of many materials behaves similarly as a function of temperature, and because many materials have similar heat capacity-temperature behavior, it seems logical to expect that thermal diffusivity-temperature relationships will agree for many materials. The data of Somerton and Boozer[11] show that, indeed, many porous materials do exhibit similar trends in thermal diffusivity as a function of temperature. A notable exception was found with a tuffaceous sandstone, as seen in Figure 10; however, a fairly good approximating line could be drawn through the rest of the data in Figure 10. Thus use of this figure for quick estimation appears reasonable.

Heats of Phase Change and Reaction

In gas and oil reservoirs, very low heats of phase change and low heats of solution, plus the high heat capacity of the solid phase (rock) due to high mass of rock leads to nearly isothermal behavior for most fluid production thermodynamic paths. Exceptions are: (1) the process of oil recovery by underground combustion[57] and (2) oil recovery by steam injection.[58] The first involves release of large amounts of heat due to oxidation of a part of the oil, and the second releases heat by condensation of the injected steam. Actually several types of spontaneous oil oxidation reactions may occur leading even to ignition.[59] There appears little purpose to cite existing studies of oil oxidation reaction kinetics, other than to warn such information is available should pore space reactions become important in geothermal energy extractio We turn now to a consideration of the effects of elevated temperatures on the flow characteristics of porous rocks.

TEMPERATURE AND PRESSURE EFFECT ON PERMEABILITY OF POROUS MEDIA

It is well known that the viscous flow of fluids through porous media follows Darcy's Law, which is expressed as:

$$v = -\frac{k}{\mu}\left[\frac{dp}{ds} - \rho g \frac{dz}{ds}\right] \tag{15}$$

where v is volume rate of flow across a unit area of the porous medium, k is permeability of the medium to a fluid at constant temperature, μ is viscosity of the fluid, p is pressure, ρ is the density of the fluid, g is the acceleration due to gravity, z is the vertical coordinate, and s is the coordinate along the direction of flow.

The permeability of a porous medium to a gas phase usually exceeds the permeability of the same medium to a liquid phase. The difference in these permeabilities is due to the phenomenon known as slip[14], reactions between liquids and the solid, and relative permeabilities. Slip is related to the mean free path of the gas molecules. Consequently, the permeability of a porous medium to gas should be a function of the temperature, pressure, and the nature of the gas. Klinkenberg[14] developed the relation between the permeability of a porous medium to gas and to a non-reactive liquid, viz:

$$k_g = k_\ell \left(1 + \frac{4c\bar{\lambda}}{r}\right) \tag{16}$$

This equation was derived assuming that all the capillaries in the porous medium are of the same diameter, and are oriented at random through the

solid material. In Eqn. 16, k_g and k_l are permeabilities respectively to gas and to a single liquid phase completely filling the pores of the medium at constant temperature, $\bar{\lambda}$ is the mean free path of the gas molecules, r is the radius of capillaries, and c is a proportionality constant. Then, the mean free path can be expressed as:

$$\bar{\lambda} = \frac{1}{\sqrt{2\pi}\, d^2 n} = \frac{RT}{\sqrt{2\pi}\, p_m N d^2} \qquad (17)$$

where d is collision diameter, n is concentration of molecules per unit volume, N is Avogadro's Number, p_m is mean pressure, T is temperature, and R is universal gas constant. Therefore, by combining Eqns. 16 and 17, we obtain:

$$k_g = k_l \left(1 + \frac{4CRT}{\sqrt{2\pi}\, rNd^2 p_m}\right) = k_l \left(1 + \frac{b}{p_m}\right) \qquad (18)$$

where b is called the Klinkenberg factor, which is constant for a given gas and a given porous medium at a constant temperature. As easily seen from Eqn. 18, a graph of k_g vs. $1/p_m$ should result in a straight line with an intercept of k_l and a slope of bk_l as shown in Figure 11. Slope must become steeper as the temperature increases. Thus, the permeability to a gas is greater at low pressures, and is at a minimum at a maximum pressure of flow.

The permeability defined in Eqn. 15 requires that the porous medium is saturated completely with one homogeneous, single-phase fluid. The permeability thus defined is called the absolute permeability. When the

medium contains more than one fluid, the conductance of the medium to one fluid phase is commonly called the effective permeability. It depends on the volume fraction of each phase present in the pore space (called the saturation), the wetting characteristics of the fluids, and even the saturation history of the fluids. This will be discussed more thoroughly below. Another term, the relative permeability, is also commonly used. It is defined as the ratio of the effective permeability to some base absolute permeability value.

Wettability and Capillary Pressure

When more than one fluid exists in a porous medium, the static and flow properties of the medium depend upon the microscopic distribution of these phases within the pores. This distribution is controlled by the wettability of the porous medium. The wettability is the degree of preference of the porous medium surface for the various fluid phases. In petroleum engineering, water and oil are often considered wetting and non-wetting phase respectively. In geothermal systems that have water and steam coexisting in the same pore spaces, water will be the wetting phase and steam will be the non-wetting phase. Thus the discussion that follows concerning oil and water can in many respects be directly related to steam-water systems.

Wettability of an oil-water-solid system is schematically shown in Figure 12.[15] The terms γ_{os} and γ_{ws} are surface tension between oil and solid, and between water and solid, respectively. γ_{ow} is interfacial tension between oil and water. θ is called contact angle. Then, for the equilibrium state:

...wet conditions, whereas contact angles greater ...gh the water phase, indi-
than 90° indicate preferentially oil-wet conditions. The distribution of
either the wetting or non-wetting phase within the pore space ...
depend solely upon the saturation of that ...
the direction of the satu...
bition".

...does not
...ase, but depends also upon
...ation change. The terms "drainage" and "imbi-
...efer to flow resulting in a decrease and increase, respectively,
in the wetting phase saturation.

Since the wettability and direction of saturation change influence the fluid distribution, these factors would be expected to affect similarly both the capillary pressure and relative permeability characteristics. The capillary pressure, P_c, in porous media is defined as the pressure difference existing across the interface separating two immiscible fluids at rest, one of which wets the surfaces of the rock in preference to the other. The water-oil capillary pressure is defined as the pressure in the oil phase minus the pressure in the water phase, or:

$$P_c = P_o - P_w \tag{20}$$

For the gas-liquid case (or steam-water):

$$P_c = P_g - P_\ell \tag{21}$$

Figure 13 shows the capillary pressure characteristics of a strongly water-wet rock. It is seen in Figure 13 that the pressure in the oil phase (non-wetting) must exceed that in the water phase (wetting) before oil will enter the initially water-saturated rock. This would also be seen in a steam-water system. This entrance pressure is referred to as the threshold pressure

or displacement pressure. The minimum saturation point in Figure 13 gives the irreducible water saturation.

It has long been recognized that the vapor pressure above the curved surface of a liquid is a function of the curvature of the liquid surface. The capillary pressure is also a function of the curvature of the liquid surface. Considering that the liquid and vapor respectively are the wetting and non-wetting phases, the capillary pressure, pertaining to static equilibrium at curved surfaces of vapor-liquid phase separation, may be written as[14]:

$$P_c = P_g - P_{g'} + \frac{RT}{Mv_\ell} \ln \frac{P_{g'}}{P_g} \qquad (22)$$

where P_g is the pressure in the vapor phase, $P_{g'}$ is the equilibrium vapor pressure of the liquid above a flat surface, M is the molecular weight, and v_ℓ is the specific volume of liquid. Then, the pressure in the liquid phase is:

$$P_\ell = P_{g'} - \frac{RT}{Mv_\ell} \ln \frac{P_{g'}}{P_g} \qquad (23)$$

As the liquid is the wetting phase, $P_{g'}$ is greater than P_g. Then P_ℓ is smaller than $P_{g'}$. Therefore, if liquid pressures and temperatures are measured in the two-phase portion of the porous medium, liquid pressures must be lower than the normal (plane-surface) saturation pressures corresponding to the measured temperatures. Since capillary pressure values are a function of the liquid saturation, the vapor pressure lowering must be a function of the liquid saturation of the porous medium.

Relative Permeability

Figure 14 shows typical water-oil relative permeability characteristics for a water-wet core.[17] In this figure the permeability to oil at reservoir connate water saturation was used as the base value for relative permeabilities. These data were taken for the case where the water saturation increased while the oil saturation decreased. If the data had been taken for decreasing water saturation, there would be a marked difference. The water (wetting phase) permeability data would be unchang but the oil (non-wetting phase) permeabilities would have been higher, especially at the right hand side of the graph. Further, the end points of the curves--the irreducible water saturation and the residual oil saturation--likely would have changed.

Muskat, et al.,[18] presented relative permeability curves for gases and liquids in unconsolidated sands, as given in Figure 15, which shows that for practical purposes the curves for the relative permeabilities k_{rg} and k_{rl} are independent of the nature of the unconsolidated sand. This is in marked contrast with most consolidated media, where the relative permeabilities must nearly always be measured, for they vary widely depending on the nature of the fluids and the porous system.

Temperature Effect on Relative Permeability

The relative permeability is affected by the test environment. The important factors are temperature, pressure, fluids and core condition. Several investigators have reported experimental results of the effect of temperature on relative permeability.

Poston, et al.,[19] using unconsolidated sand, found that the irreducible water saturation increased and the residual oil saturation decrea

with increasing temperature, as shown in Figures 16 and 17. This observation can be seen another way by considering Figure 14. In effect the higher temperature caused both relative permeability curves to shift to the left on the saturation axis. Poston, et al., speculated that if the relative permeability has changed, the capillary pressure should also be temperature sensitive.

Sinnokrot, et al.,[10] studied capillary pressure behavior of three consolidated sandstones and one limestone sample over a temperature range of 75° to 325°F by the restored state method. Their work confirmed the observation of Poston, et al., that the irreducible water saturation increased and apparent residual oil saturation decreased with increase in temperature. They concluded that capillary pressure curves for sandstones were displaced toward higher wetting phase saturations with an increase in temperature level, indicating an increase in water wetness with temperature level increase. Figure 18 shows part of their work.

Weinbrandt, et al.,[21] found results similar to Poston's when increasing from room temperature to 175°F in Boise sandstone. Representative data are shown in Figure 19. They also obtained data on absolute permeability in an increasing temperature level sequence from 75 to 315°F, as shown in Figure 20. The absolute permeability decreased drastically as temperature increased. Afinogenov[22] found similar results up to temperatures of 212°F.

Lo and Mungan[23] also studied relative permeabilities as a function of temperature and found results similar to Weinbrandt, et al. and Poston. They also studied systems of differing wetness characteristics and the results were found to be similar in both oil-wet and water-wet systems.

Poston, et al., pointed out that the changes in rock-fluid charac teristics as functions of temperature level were all in a direction su gestive of an increase in water wetness with temperature increase. Contrary to this, Weinbrandt, et al., considered that temperature indu changes were too large to be explained by obvious factors such as chan in contact angle interfacial tension, etc. They speculated that most the above observations concerning temperature sensitivity may have bee a result of thermally-induced mechanical stress. Work is continuing to attempt to clarify these results and the reasons for them.

Pressure Effect on Pore Volume

Von Gonten and Choudhary[24] investigated experimentally the temper ture effect on pore volume compressibility, which is defined as:

$$c_f = -\frac{1}{V_p}\left[\frac{\partial V_p}{\partial p}\right]_T \qquad (24)$$

where V_p is pore volume and p is compacting pressure which is equal to overburden pressure minus pore pressure. Figure 21 is a plot of cumul tive fractional pore volume change versus compacting pressure for sand stone at 75°F and 400°F. The pore volume compressibility, which is th slope of these curves, becomes smaller at higher pressure.

Somerton and Selim[12] showed the effect of temperature on sandston volume, as indicated earlier in the paper in Figure 9.

Pressure Effect on Permeability

Afinogenov[22] presented data on the absolute permeability decrease as affected by external pressure. From his data he introduced an empirical formula to predict this effect:

$$\frac{k_p}{k_o} = \left(1 + \frac{127 \times 10^{-5}}{p}\right)^{-1} \qquad (25)$$

where effective pressure, p, is defined as:

$$p = p_{con} - 0.85\, p_{pore}$$

p_{con} and p_{pore} are confining pressure and pore pressure respectively in atmospheres. He deduced that this permeability decrease was due to a decrease in the cross-sectional area of the pores and to a more torturous pore space configuration under the effect of pressure.

Zoback and Byerlee[25] measured the permeability of Berea sandstone as a function of both confining pressure and pore pressure. They reported that the permeability decreased with increased confining pressure, and increased as pore pressure was increased. Qualitatively, this agrees with Afinogenov's results. They found also that pore pressure had a significantly larger effect upon permeability than did confining pressure. This does not agree with the results of Afinogenov. They speculated that the matrix through which the fluid flows has a higher compressibility than does the granular framework through which the confining pressure stresses are transmitted.

Many other investigators, such as Fatt and Davis[26], Wyble[27], Dobrynin[28], Gray, et al.[29], and Wilhelmi and Somerton[30], have reported the effect of overburden pressure on the permeability of sandstone. Figure 22 is the

rimental results provided by Fatt and Davis. The permeability of
stone decreased with increase in overburden pressure. Most of the
ease took place over the range of zero to 3000 psi overburden
sure.

PHYSICAL STATES OF WATER

The physical states of water of interest in geothermal reservoirs
compressed liquid, saturated liquid, superheated (also called dry
nsaturated) steam, saturated (or wet) steam, and the dense fluid
e.

The term "saturation" may thus have several meanings in geothermal
rvoir engineering. "Saturation" can refer to: (1) the volume frac-
of pore space occupied by a fluid phase, (2) the thermodynamic
e of the fluid phases with reference to some appropriate vapor pres-
curve, and (3) the usual sense of solids and gases being dissolved
liquid phase. Care must be used that the term "saturation" is not
nderstood.

Figure 23 is a graph of the vapor pressure curve of water, showing
position of the critical point at 221.07 bar and 374.1°C (3206.2 psia
705.4°F). Point A on this figure is in the superheated steam region,
t B is at saturation conditions where both liquid and vapor may
ist, and point C is in the compressed liquid region. Points D and E
in the dense fluid region. Figure 24 is an expanded form of Figure 23
ing the initial thermodynamic state of various geothermal fields around
world. Note that the geopressured aquifers found in the Gulf Coast
of the United States, with temperatures of 260°C (500°F) and pres-

sures in excess of 700 bar (10,000 psia), are off the scales of both Figures 23 and 24, and might be considered as dense fluids.

Gibb's Phase Rule teaches that in order to specify the thermodynamic state of a single phase of water, two independent thermodynamic properties (e.g., pressure and temperature) must be specified. But if two phases are present (e.g., saturated steam and water) specification of only one intensive property defines the system. A geothermal aquifer at saturated conditions must follow some appropriate vapor pressure curve as fluid is produced.

It can be shown from thermodynamic analysis that a geothermal system initially containing a single-phase fluid (either compressed liquid or superheated steam) will tend to deplete isothermally. But once two phases form, a system should deplete along some sort of vapor pressure curve appropriate for the fluids in the pore space.

Properties of Interest

A thermodynamic equation of state for water expresses the pressure-volume-temperature (PVT) relationships. These describe the specific volume, v, (or density, $\rho = 1/v$) as a function of pressure and temperature for the various phases. In addition we require the energy related properties, specific enthalpy, h, and specific entropy, s, and specific heats, c_p and c_v.

The transport properties that are important are viscosity and thermal conductivity. Viscosity is basically an internal resistance of the fluid to flow, due to molecular interaction. Thermal conductivity affects the rate of heat transfer of the rock-fluid system.

Data describing the forementioned properties for impure water is meager, although a fair amount is known about the solubility of numerous substances found in geothermal waters. Ionic equilibrium calculations can be used to estimate which chemicals will remain dissolved, and which ones will precipitate under changing pressure, temperature, and composition conditions. The reader is referred to textbooks on geochemistry (Krauskopf[31]) and ionic equilibrium calculations (Butler[32]) and also to work on the chemistry of geothermal systems by White[33], Fournier and Truesdell[34], and Helgeson.[62]

Equations of State

Since the early part of this century there has been an international effort to standardize the various thermodynamic and transport properties of pure water. The well-known Keenan and Keyes[35] steam tables were a result of these efforts. The ASME Steam Tables[36] are one of the more recent products of these efforts, and are used as a basis for much of the data in this report. These tables present the results of a series of accurate matching of analytic functions (the 1967 IFC Formulation for Industrial Use) to accepted and standardized experimental data (the 1963 International Skeleton Tables). The results are presented in tabular and graphical form. The analytic functions are also given, and can be programmed for use on a computer. Another recent source of water properties is the Steam Tables by Keenan, et al.[37]

The rest of this review will be devoted to describing the properties mentioned above, both for pure and impure water. Data will be presented in tabular or graphical form, and several simplified analytic forms will be discussed.

Pure Saturated Steam and Water

For conditions below the critical state (221.07 bar, 374.1°C; 3206.2 psia, 705.4°F) the liquid and vapor phases can coexist in equilibrium. When liquid and vapor are in equilibrium they are described as being saturated, and such states lie along the vapor pressure curve (see Figures 23 and 24). This curve is of great interest, and a number of simplified analytic approximations have been presented. A few will be given here. Whiting and Ramey[39] used an integrated form of the Clausius-Clapeyron equation to develop the following approximation by a least mean square curve match over the temperature range 150-315°C (300-600°F):

$$\ln p = \frac{-4667.0754}{(T + 273)} + 12.59833 \; ; \quad \text{where } p = \text{bar}, \; T = °C. \qquad (26\text{-a})$$

Or:

$$\ln p = \frac{-8400.7358}{(T + 460)} + 15.272703 \; ; \quad \text{where } p = \text{psia}, \; T = °F. \qquad (26\text{-b})$$

This match is claimed to have an average difference from the actual data of only 0.048%.

In oil and gas technology, the Cox Chart is a useful empirical technique for representing the vapor pressure curves of hydrocarbon fluids. This is a graph of ln p vs. 1/(T-77.4), T in °R, and it is useful because both hydrocarbon and water vapor pressure curves tend to graph as straight lines. Thus, by choosing two points for water at opposite ends of the vapor pressure curve we can determine that the equation of this straight line is of the form:[61]

$$\ln p = \frac{-7001.4928}{(T + 382.2)} + 14.46928 \text{ ; where } p = \text{psia, } T = {}^\circ\text{F.} \qquad (27)$$

This function is a match over the whole vapor pressure curve, whereas the Whiting and Ramey approximation is for the range 150-315°C. Finally, Farouq Ali[19] observed that a graph of pressure vs. temperature on log-log paper yields a straight line. Hence:

$$T = 115.1\ p^{0.225} \quad (T = {}^\circ\text{F},\ p = \text{psia}) \qquad (28\text{-a})$$

or

$$T = 116.7\ p^{0.225} - 17.778 \quad (T = {}^\circ\text{C},\ p = \text{bar}) \qquad (28\text{-b})$$

Equation 28 is reported to have a maximum of 1% error over the pressure range 1-200 bar (10-3,000 psia).

The specific volume of saturated steam, v_g, and water, v_f, are shown as a function of pressure on Figure 25. The overall specific volume of mixtures of steam and water can be determined at a particular pressure (or temperature) if the quality, x, of the mixture is known. Quality is defined:

$$x \triangleq \frac{\text{Mass of mixture as steam}}{\text{Total mass of mixture}} \qquad (29)$$

The effect of quality on specific volume can be seen on Figure 25, and can be calculated from tables using the relation:

$$v_{mix} = x\, v_g + (1 - x)\, v_f$$

$$= v_f + x\, v_{fg} \ , \qquad (30)$$

where v_{mix} = mixture specific volume

v_g = saturated gas specific volume

v_f = saturated liquid specific volume

$v_{fg} = v_g - v_f$

The second expression results in more accurate numerical results in hand calculations if steam quality is low.

The enthalpy of saturated steam and water is shown as a function of pressure in Figure 26. Points B and C on this diagram correspond with those on Figure 23. There is a maximum enthalpy of 2.8×10^6 Joules/kg (1204.8 Btu/lb_m) that <u>saturated</u> steam may have under any conditions. This occurs between 31.16 and 31.85 bar (452 and 462 psia).

The overall enthalpy of saturated mixtures can be calculated from the relation:

$$h_{mix} = x\, h_g + (1 - x)\, h_f$$
$$= h_f + x\, h_{fg} \qquad (31)$$

where h_{mix} = mixture specific enthalpy

h_f = saturated liquid specific enthalpy

h_g = saturated gas specific enthalpy

h_{fg} = latent heat of vaporization per unit mass

The specific enthalpy of such mixtures is shown in Figure 26.

The latent heat of vaporization per unit mass, h_{fg}, is the increase in enthalpy as a fluid vaporizes from saturated liquid to saturated steam at constant pressure or temperature. At atmospheric pressure h_{fg} is approximately 2.3×10^6 Joules/kg (1000 Btu/lb_m). Farouq Ali[19] (p. 5) has presented the approximation:

$$h_{fg} = 1318\ p^{-0.08774} \qquad (32)$$

for use in hand calculations. The maximum error is reported to be 1.9%. The units used in Eqn. 32 are p, psia; h_{fg}, Btu/lb_m.

There appears to be some uncertainty about the viscosity of saturated steam and water. Accepted values are presented in the ASME Steam Tables. Figure 27 shows the viscosity of saturated steam and water vs. temperature. The viscosities of the two phases tend to approach one another as they approach the critical temperature.

Farouq Ali[39] recommends use of the following equation for the viscosity of steam:

$$\mu/100 = 88.02 + 0.32827\ T + 0.0002135\ T^3 - \rho\ (1858 - 5.90\ T) \qquad (33)$$

where μ = viscosity of steam, centipoise

T = temperature, °C

ρ = density of steam, gm/cc

The density of steam can be determined from steam tables. For pressures up to 1000 psia, the density of steam can also be determined from the following relation developed by Farouq Ali (p. 22):

$$\rho = 0.0000440189\ p^{0.9588} \qquad (34)$$

where ρ = density of steam, gm/cc

p = pressure, psia

The thermal conductivity of water first increases as the temperature increases and reaches a maximum at about 150°C. Thereafter it decreases. This is shown in Figure 28.

Impure Saturated Water

Chemical content will tend to have the same effect on the properties of saturated water and steam as they will on the unsaturated phases. Hence, with the exception of the vapor pressure curve, discussion of the effect of impurities will be postponed until later sections.

The vapor pressure of water in a geothermal system will not necessarily be that presented in the steam tables. For a fixed pressure, the boiling temperature of water will be elevated by the presence of impurities. This is equivalent to a lowering of vapor pressure. However, the effect is usually rather small. For example, at 4.621 bar (67.013 psia) pure water would boil at 148.89°C (300°F), whereas a 100,000 ppm (parts per million) sodium chloride brine would boil at 150.62°C (303.113°F). This difference would probably not be measurable in a geothermal system. However, significant vapor pressure lowering has been observed with production of 350,000 ppm brines in the Imperial Valley, California.

The vapor pressure data presented in steam tables were measured for flat surface interfaces. If the steam-water interface is a strongly curved surface, as might occur in small pores in porous media, then there could be significant vapor pressure lowering effects (Calhoun, et al.[40]; Edlefsen and Anderson[41]). Cady, Bilhartz, and Ramey[42] have investigated this phenomenon with regard to geothermal aquifers. They did not observe vapor pressure lowering in unconsolidated sandstone cores. However, a recent study by Strobel[56] indicates a potential vapor pressure lowering at very low liquid contents in experiments with a single, consolidated core. Continued experimentation is in progress.

Pure Compressed Liquid Water

The compressed liquid region lies above the vapor pressure curves in the pressure-temperature planes of Figure 23 and Figure 24. Enthalpy and PVT behavior for compressed water is given in various tables[36,37] and in the ASME Steam Tables[36] for pressures up to 1070 bar (15,500 psia).

A technique commonly used in oil reservoir engineering for relating compressed water at some given reservoir condition to its state at surface conditions is via the formation volume factor, B_w. This is defined as the volume of liquid at reservoir conditions divided by the volume of liquid that would remain if it were brought to some standard surface conditions, commonly 20°C and 1 bar (70°F and 14.67 psia).

$$B_w \triangleq \frac{\text{initial volume of liquid at reservoir conditions}}{\text{volume of liquid remaining at standard conditions}} \qquad (35)$$

Figure 29 is a graph of the Formation Volume Factor, B_w, for pure liquid water as function of pressure and temperature. Note that for constant temperature, as pressure decreases, B_w increases slowly up to saturation conditions, below which it falls rapidly.

The specific volume-pressure behavior of a compressed liquid under an isothermal expansion or contraction process is often of interest (particularly in unsteady liquid flow through an aquifer). This P-V behavior is usually expressed in terms of the isothermal coefficient of compressibility, c_ℓ, which is defined:

$$c_\ell \triangleq -\frac{1}{v}\left(\frac{\partial v}{\partial p}\right)_T \qquad (36)$$

c_f can be viewed as the fractional decrease in specific volume caused by an isothermal unit increase in pressure. Although the isothermal compressibility of liquid water is often used in ground water hydrology and oil reservoir engineering, it appears to have been seldom reported for high values of temperature (greater than 120°C; 240°F). Table 1 summarizes high temperature results reported by Whiting and Ramey.[38] As can be seen, the isothermal compressibility for water is reasonably constant with pressure, but varies with temperature.

Table 2 presents the enthalpy of compressed pure water over a range of pressures and temperatures. It can be seen that the liquid enthalpy is only weakly dependent on pressure, but strongly dependent on temperature.

The viscosity of pure compressed water is presented in various Steam Tables.[35-37] The viscosity of high pressure liquid is almost constant with pressure, and generally only about 10-15% higher than the corresponding value for saturated liquid at the same temperature. Hence Figure 27, which shows the viscosity of saturated liquid as a function of temperature, can be used as a good estimate of compressed liquid viscosity.

The specific heat, c_p, of compressed water is also presented in the Steam Tables[35-37] for pressures up to 1035 bar (15000 psia). Values of c_p range from 4100 to 5000 Joules/Kg. °C (1.00 to 1.20 Btu/lb_m °F), except at temperatures greater than 260°C (500°F). Near the critical point values become very high.

Impure Compressed Water

The waters produced from geothermal systems often contain a dissolved chemical content high in chlorides and sulfates. Brines from some areas,

such as the Imperial Valley Salton Sea Geothermal Resource Area, have up to ten times the dissolved solids content of seawater. In addition, geothermal liquids often contain dissolved noncondensable gases.

Amyx, Bass and Whiting[41] (p. 450) state "Literature relative to the effect of composition on the properties (of water) is meager, and is limited to gas solubility data over the temperature range 32-250°F (0-121°C) at pressures ranging from 0-6000 psia (0-415 bar)." These authors summarize the work of numerous workers (Dodson and Standing[44], Rowe[45], Beal[46], Bridgman[47]) on the effect of natural gas solubility on the PVT behavior of water.

Long and Chierici[48] have presented experimental data on the PVT behavior of aqueous solutions of sodium chloride. Their results were measured for temperatures over the range 20-100°C, pressures from 2-500 kg/cm^2, and salinities from 0-300g/L. They also presented analyti curve matches giving density, ρ, as a function of salinity, pressure, an temperature over the range of experimental conditions. It is unfortunat that data for higher temperatures were not measured. But results do giv a quantitative indication of the effect of chemical composition on the PVT behavior of water.

Amyx, Bass and Whiting[43] (p. 466) present data from Van Wingen[49] o the viscosity of oil field brines at pressures to 7100 psia, and tempera tures to 300°F. This data suggests that dissolved solids have only a small effect on the viscosity of saline brines. Stanley and Batten[50] have presented data on the viscosity of sea water compared to pure water from 0-30°C. They observed that for practical purposes, the increase is not significant.

Although important information is available there is a need for PVT data for geothermal waters at conditions characteristic of geothermal reservoirs, showing the effect of chemical composition. In addition, more information is needed about the solubility and PVT characteristics of noncondensable gases dissolved in geothermal waters.

Pure Superheated Steam

Superheated steam occurs on the pressure-temperature plane at temperatures above the vapor pressure line, e.g., point A on Figure 23. This state is also called "dry" steam. The ASME Steam Tables[35] (1967, Table 3) present data for the enthalpy and PVT behavior of superheated steam for temperatures up to 815°C (1500°F). Figure 30 is a diagram showing the specific volume of dry steam as a function of pressure and temperature. One convenient means of calculating specific volumes of dry steam is via the real gas law equation of state:

$$Pv_g = \frac{zRT}{M} \qquad (37)$$

$$= z\bar{R}T$$

where P = pressure, bar

v_g = specific volume of steam, m^3/kg

z = gas law deviation (also compressibility) factor

$R = 0.08288 \ \frac{bar \cdot m^3}{kg_{mole} \cdot {}^\circ K}$

M = molecular weight of water, 18 kg/kg_{mole}

$\bar{R} = R/M = 0.004605 \ \frac{bar \ m^3}{kg \ {}^\circ K}$

T = absolute temperature, $^\circ K$

OR, for English units

p = psia

v_g = ft^3/lb$_m$

R = 10.72 $\frac{\text{ft psia}}{16 \text{ mole}^\circ\text{R}}$

M = 18 lb$_m$/lb$_{mole}$

$\bar{R}$ = 0.5956 $\frac{\text{ft psia}}{\text{lb}_m\ ^\circ\text{R}}$

T = $^\circ$R

The gas law deviation factor, z, for steam is presented in Figure 31.

Figure 32 presents a pressure-enthalpy diagram for superheated steam. Point A on this diagram corresponds to point A in Figure 23. If a dry steam reservoir were to produce at constant temperature, its state would follow the isotherms on Figure 32. As indicated by the arrow below point A, the produced steam would tend to increase in enthalpy. Whiting and Ramey[38] have suggested that this tendency is a potential means of identifying the initial state of a geothermal fluid reservoir as dry steam

Values for the viscosity of superheated steam are presented in the ASME Steam Tables[36] (1967, Table 10 and Fig. 7). Table 3 presents values of dry steam viscosity over a range of conditions. Except near the vapor pressure curve, the viscosity of dry steam is essentially independent of pressure, and is also only slightly higher than that of saturated steam at the same temperature.

The specific heat at constant pressure, c_p, of dry (and saturated) steam is presented in Table 9 of the ASME Steam Tables. Except near the vapor pressure curve and at higher pressures and temperatures, it is approximately 2100 J/kg-$^\circ$C (0.5 Btu/lb$_m$-$^\circ$F).

Mixtures of Dry Steam and Other Noncondensable Gases

Two of the recognized dry steam geothermal reservoirs in the world (the Geysers Field in California, and Larderello in Italy) are known to produce quantities of noncondensable gases along with their steam. Typically such gases contain carbon dioxide, hydrogen sulfide, ammonia, methane, and ethane. The quantity and proportions produced vary as a function of time, flow rate, and from well to well over the fields.

It is clear that the noncondensable gas content of a dry steam reservoir will effect the thermodynamic and transport properties of the produced fluid. Unfortunately, almost no experimental work seems to have been done on the properties of dry steam and noncondensable gas mixtures. However, generalized correlations have been extensively developed for natural gas mixtures of hydrocarbons. These correlations are based on reduced pressures and temperatures:

$$\text{Reduced Pressure, } p_r \triangleq \frac{\text{actual pressure}}{\text{pseudo critical pressure}} \tag{38}$$

$$\text{Reduced Temperature, } T_r \triangleq \frac{\text{actual temperature}}{\text{pseudo critical temperature}} \tag{39}$$

where the pseudo critical pressure and temperature are the molar average of the component critical values.

Amyx, Bass and Whiting[53] (pp. 260-268) have discussed and summarized correlations available for determining the PVT behavior of mixtures of natural gases with impurities such as nitrogen and carbon dioxide. On the basis of their discussion, the best method for estimating the effect of a noncondensable gas on steam compressibility appears to be through the use of an additive compressibility factor as first defined by Eilerts et al.[51]

$$Z_a = Z_{st} Y_{st} + Z_{ncg} Y_{ncg} \quad (40)$$

where Z_a = additive compressibility factor

Z_{st} = steam compressibility factor

Y_{ncg} = noncondensable gas compressibility factor

Z_{st} = Mole fraction steam in mixture

Y_{ncg} = mole fraction noncompressible gas in mixture

Amyx, Bass and Whiting[51] (pp. 260-268) present graphs of the compressibility factor, z, for nitrogen (from Eilerts et al.[51]), carbon dioxide (from Olds et al.[52]), and hydrogen sulfide (from Reamer et al.[For purposes of reservoir calculations, it is expected that the noncon- densable gas content of many geothermal steams will have a minimal eff on PVT behavior.

The effect of noncondensable gases on geothermal steam viscosity i also of interest. Again, there appears to be almost no experimental da available, and we must resort to correlations. Amyx, Bass and Whiting[(pp. 278-286) present the results of numerous correlations for natural gases. On the basis of their discussion, a rule proposed by Herning an Zipperer[54] for calculating the viscosity of mixtures of gases appears t be the most promising correlating method. In this rule the viscosity o the mixture, μ_m, is given by

$$\mu_m = \frac{\sum_{i=1}^{n} \mu_i Y_i M_i}{\sum_{i=1}^{n} Y_i M_i} \quad (41)$$

where μ_m = viscosity of mixture

μ_i = viscosity of i^{th} component

M_i = molecular weight of i^{th} component

Y_i = mole fraction of the i^{th} component in mixture

n = total number of components in the mixture

Basically this is an averaging calculation weighted by the mass of each component present. The viscosity of various gases over a range of temperatures can be found in standard physical properties reference books (e.g., see Weast[33], pp. F41-F44). For practical purposes, the non-condensable gas content will not significantly affect the viscosity of most geothermal steams.

A Note on Units

In general, equations and numerical values have been expressed in metric units (bar, °C, m, kg), with values for engineering units given in parenthesis (psia, °F, ft, lb_m). Viscosity is given in centipoise. For convenience of writing this is not true in every case. Units are always specified where equations are presented throughout the paper.

Note the following conversions:

Pressure:	1 psia	= 0.06895 bar
	1 bar	= 1.0197 kg/cm^2
	1 bar	= 0.9869 atm.
Specific Volume:	1 ft^3/lb_m	= 0.062428 m^3/kg
	1 ft^3/lb_m	= 62.43 cc/gm
Enthalpy:	1 Btu/lb_m	= 2324.4 Joules/kg
Viscosity	1 c.p.	= 6.72×10^{-4} lb_m ft sec
	1 c.p.	= 2.089×10^{-5} lb_f sec/ft^2

Acknowledgment

Preparation of this report was funded by the National Science Foundation as a portion of the study "Stimulation of Geothermal Aquifers," Grant No. GI-34925, principal investigators Drs. Paul Kruger and Henry J. Ramey, Jr., Stanford University.

TABLE 1

Isothermal Compressibility of Liquid Water, $psia^{-1}$

p,psia	300°F	400°F	500°F
700	3.793×10^{-6}	5.811×10^{-6}	7.146×10^{-6}
800	3.795×10^{-6}	5.815×10^{-6}	7.152×10^{-6}
1000	3.913×10^{-6}	5.821×10^{-6}	10.703×10^{-6}

TABLE 2

Enthalpy of Compressed Water in Btu/lb

and Joules/kg $\left[\text{(Btu/lb)}/\text{(J/kg)}\right]$ at Various Pressures and Temperatures

(Data from Ref. 36)

Temperature		Pressure, psia/bar				
°F	°C	$100/6.9$	$500/34.5$	$1000/69.0$	$2000/138.$	$5000/345$
70	21	$38.33/8.91\times10^{4}$	$39.44/9.17\times10^{4}$	$40.82/9.49\times10^{4}$	$43.58/1.013\times10^{5}$	$51.7/1.202\times10^{5}$
200	93	$168.3/3.91\times10^{5}$	$169.2/3.93\times10^{5}$	$170.3/3.96\times10^{5}$	$172.6/4.01\times10^{5}$	$179.5/4.17\times10^{5}$
400	204	X	$375.4/8.73\times10^{5}$	$376.0/8.74\times10^{5}$	$377.2/8.77\times10^{5}$	$381.2/8.86\times10^{5}$
600	316	X	X	X	$614.5/1.43\times10^{6}$	$604.6/1.40\times10^{6}$

TABLE 3

Viscosity in Centipoise of Superheated Steam at Various Conditions

(Data from Ref. 36)

Temperature		Saturation Conditions			Pressure psia bar						
°F	°C	P, psia	P, bar	c.p.	1/.06895	5/.345	10/.690	50/3.45	100/6.9	500/34.5	1000/
200	93	11.5	.79	.01	.012	.012	.012	X	X	X	X
300	149	67	4.62	.014	.014	.014	.014	.014			
400	204	247.3	17.1	.0155	.016	.016	.016	.016			
500	260	681	47.0	.0177	.0186	.0186	.0186	.0186	.0186	.0180	
600	316	1543	106.4	.02	.02	.02	.02	.02	.02	.02	.02

FIGURE 1

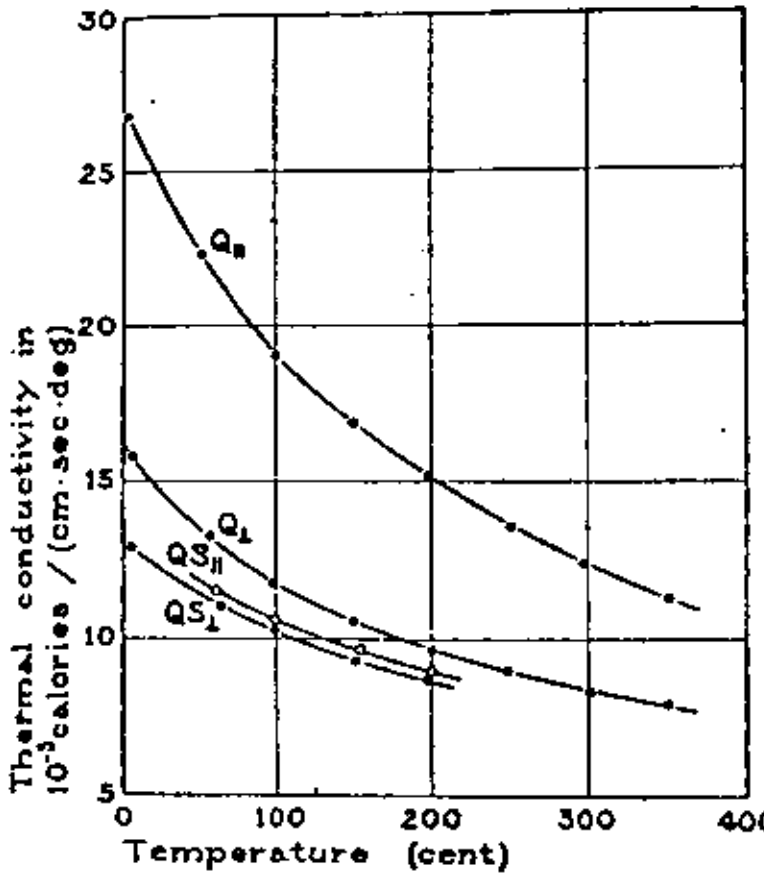

Thermal conductivity of quartz and of a quartzitic sandstone.

$QS_{\perp}$	Quartzitic sandstone, Penn., $\perp$ bed-plane.
$QS_{\parallel}$	Quartzitic sandstone, Penn., $\parallel$ bed-plane.
$Q_{\perp}$	Quartz single crystal $\perp$ optic axis.
$Q_{\parallel}$	Quartz single crystal $\parallel$ optic axis.

(Ref. 1)

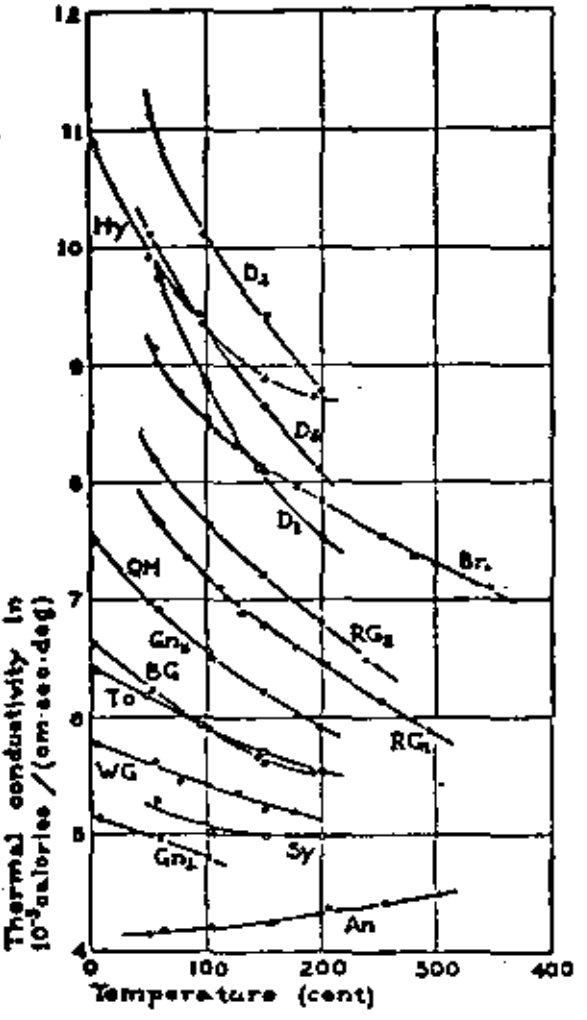

FIGURE 2 Thermal conductivity of holocrystalline rocks. (Ref. 1)

An	Anorthosite, Quebec.	RG_1	Rockport Granite 1.
Ge_1	Gneiss, Pelham, ⊥ bed-plane.	RG_2	Rockport Granite 2.
Ge_2	Gneiss, Pelham, ∥ bed-plane.	Br	Bronzitite.
Sy	Syenite, Ontario.	Hy	Hypersthenite.
WG	Westerly Granite.	D_1	Dunite 1.
To	Tonalite, Calif.	D_3	Dunite 3.
BG	Barre Granite.	D_2	Dunite 2.
QM	Quartz monzonite, Calif.		

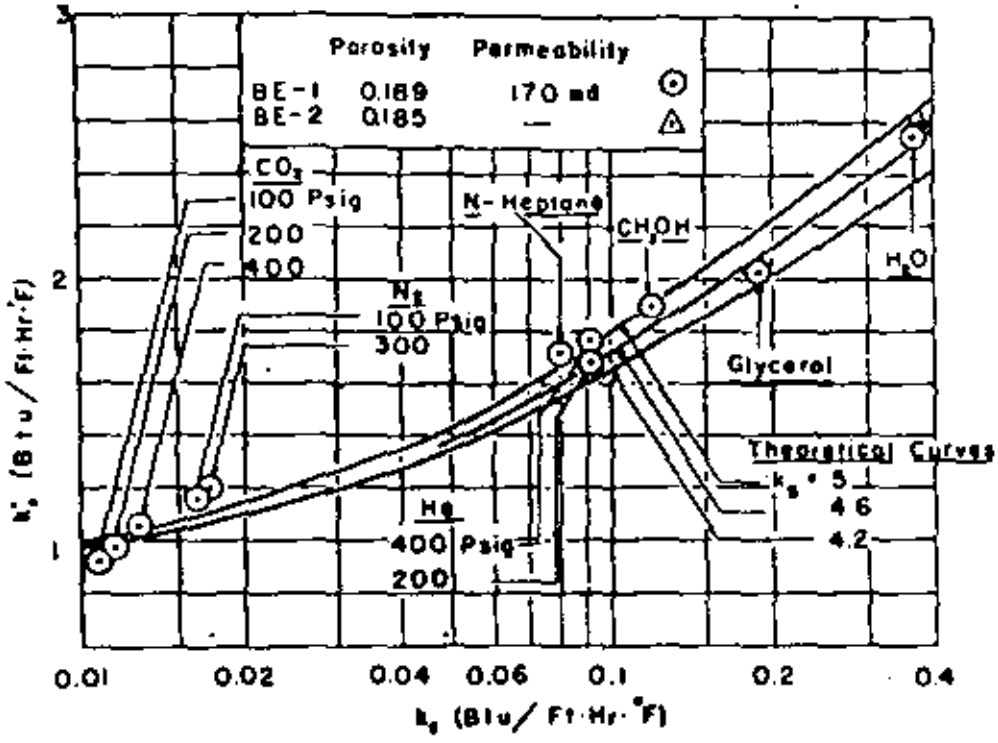

FIGURE 3 — STAGNANT CONDUCTIVITIES VS CONDUCTIVITIES OF FLUIDS, BEREA SANDSTONE. (Ref. 4)

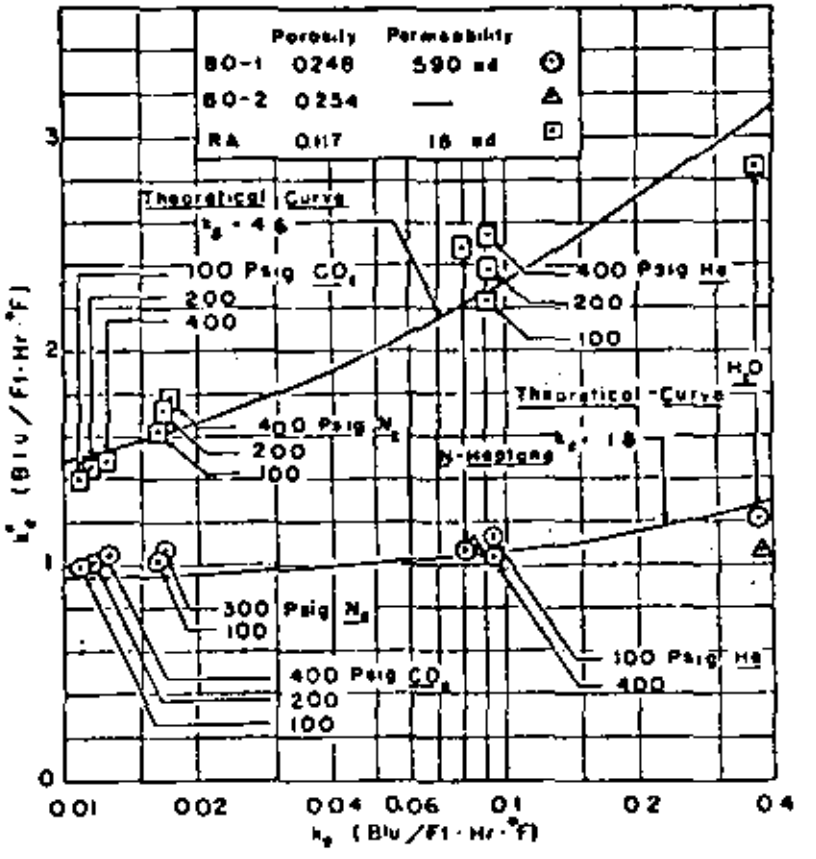

FIGURE 4 — STAGNANT CONDUCTIVITIES VS CONDUCTIVITIES OF FLUIDS, BOISE AND RANGELY SANDSTONES.

(Ref. 4)

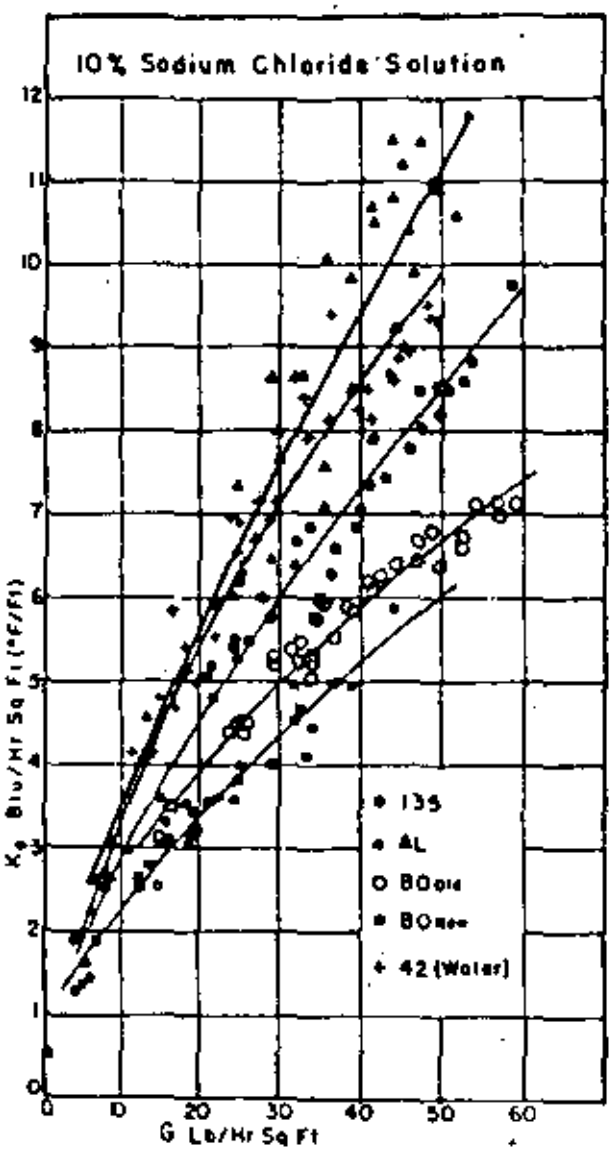

FIGURE 5 —Effective thermal conductivity (Ke) as a function of mass flow rate (G). See Ref. 5 for legend. (After Adivarahan, Kunii and Smith, Courtesy Soc. of Petrol. Engrs. of AIME.) (Ref. 5)

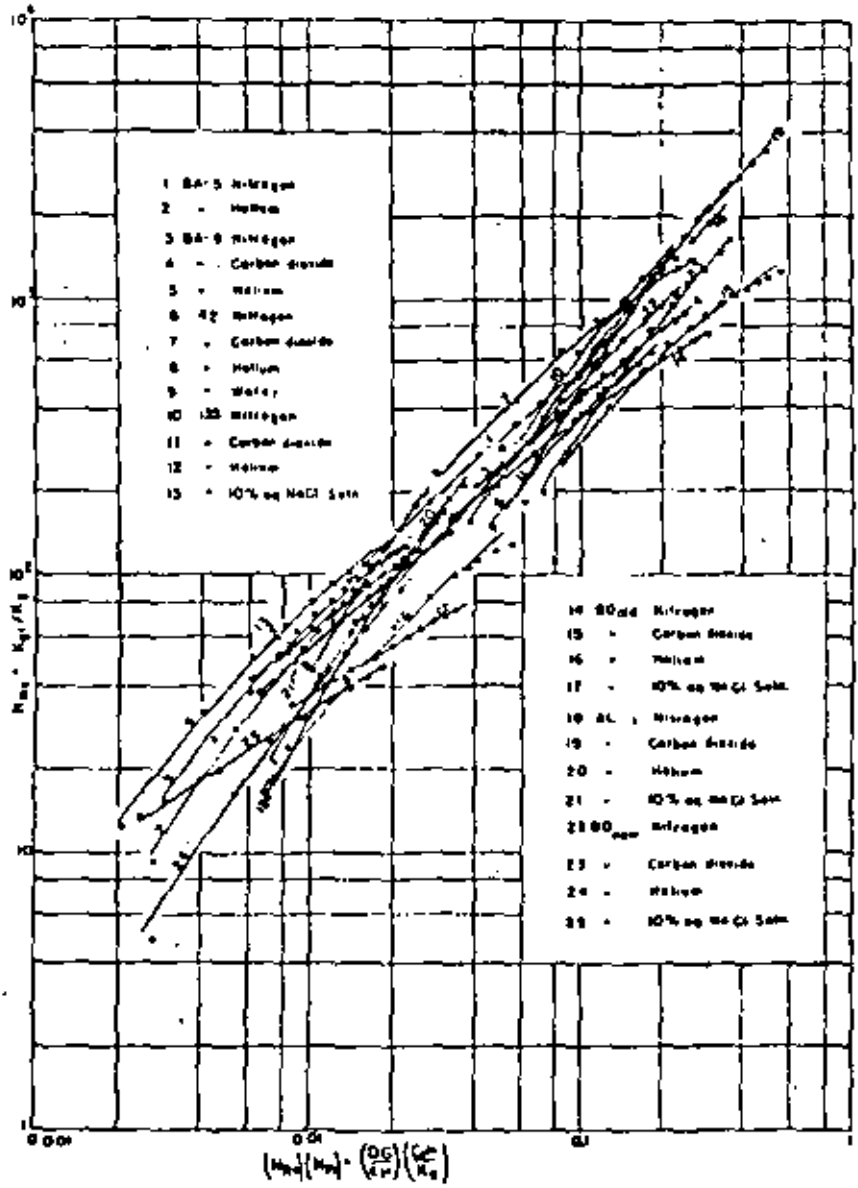

FIGURE 6 — CORRELATION OF k_{gl}/k_g WITH $(DG/\epsilon\mu)(C_p\mu/k_g)$. (Ref. 5)

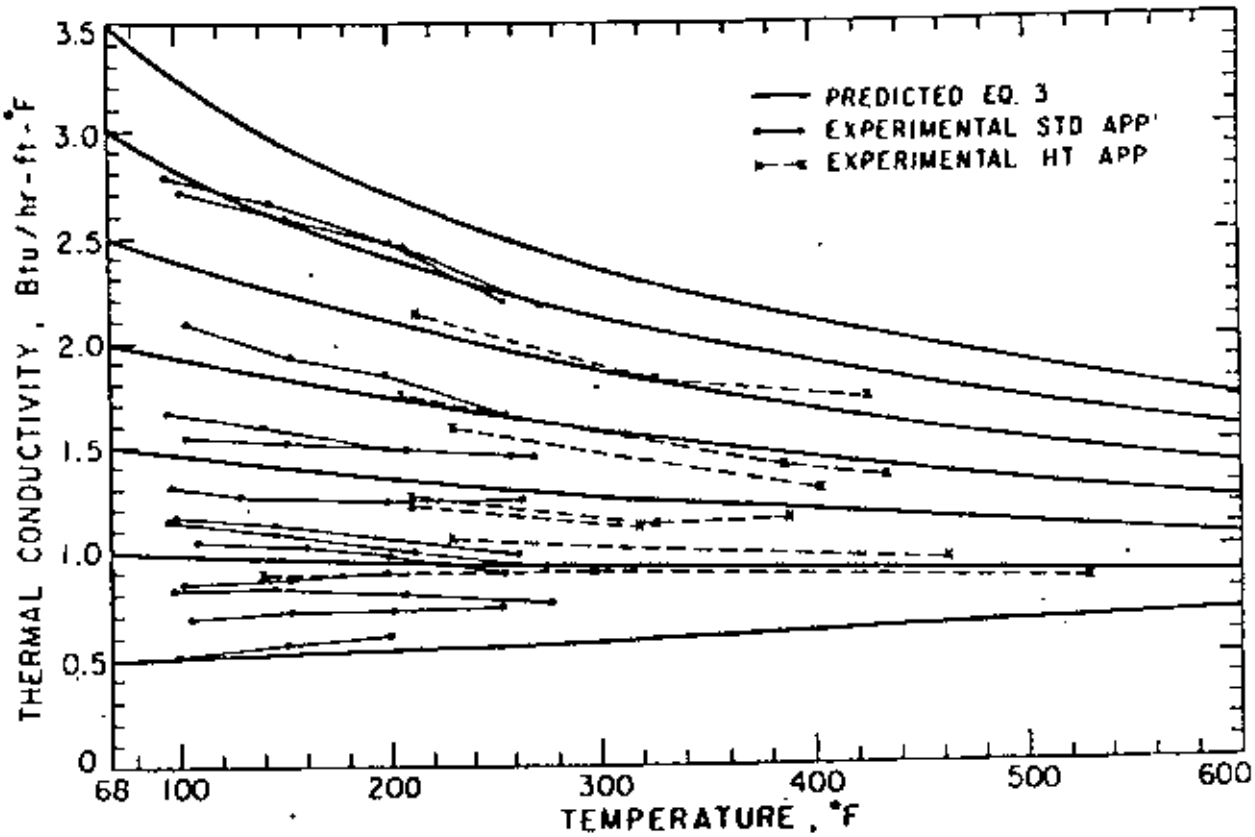

FIGURE 7 Effect of Temperature on Thermal Conductivity of Sandstone. (Ref. 7)

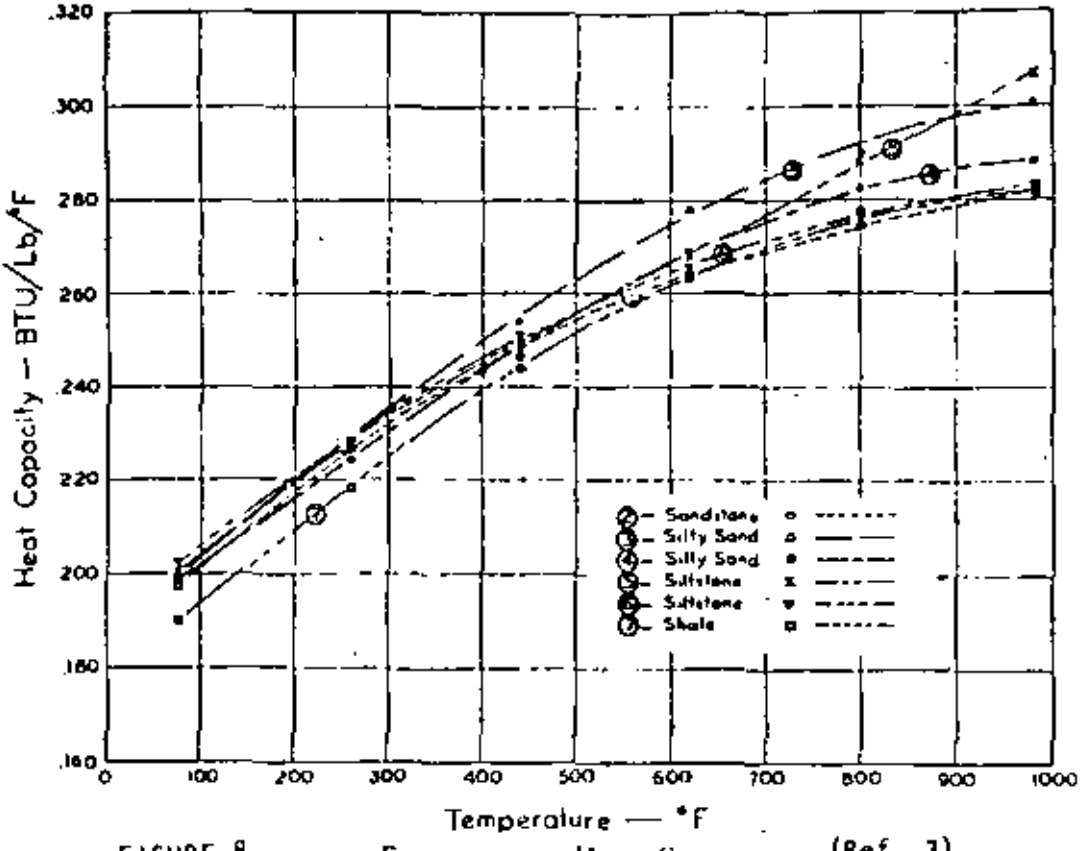

FIGURE 8 —EXPERIMENTAL HEAT CAPACITIES. (Ref. 3)

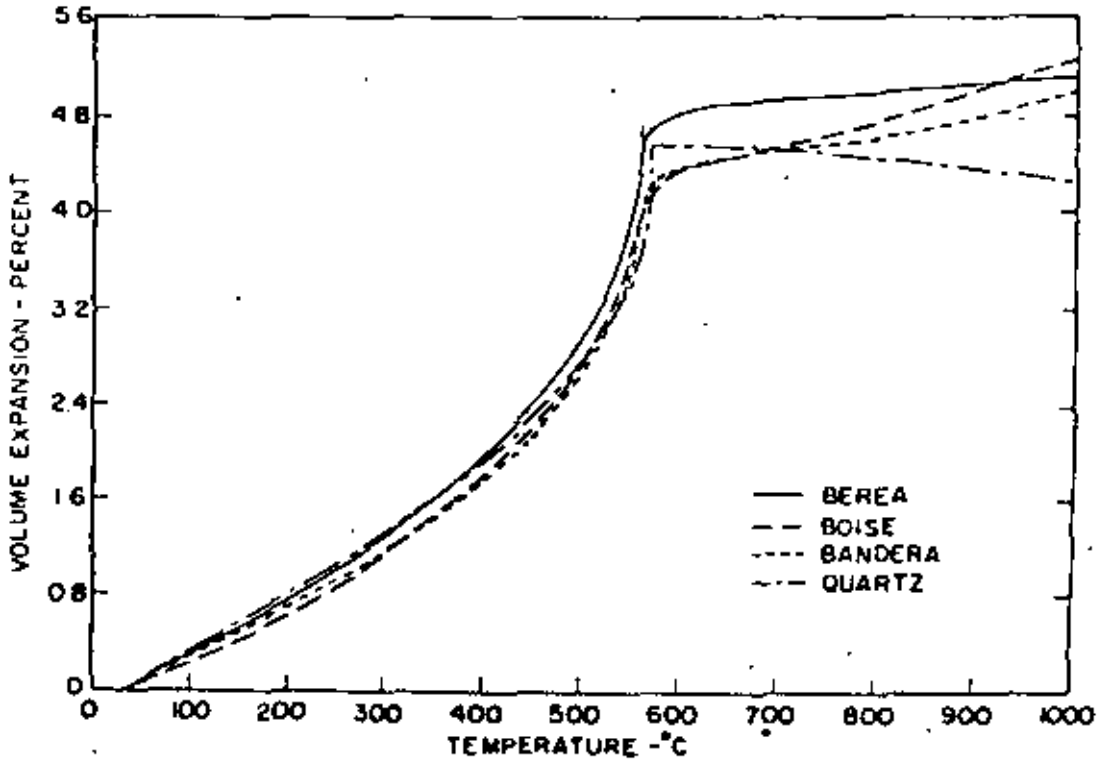

FIGURE 9 — VOLUME EXPANSION OF SANDSTONES.
(Ref. 12)

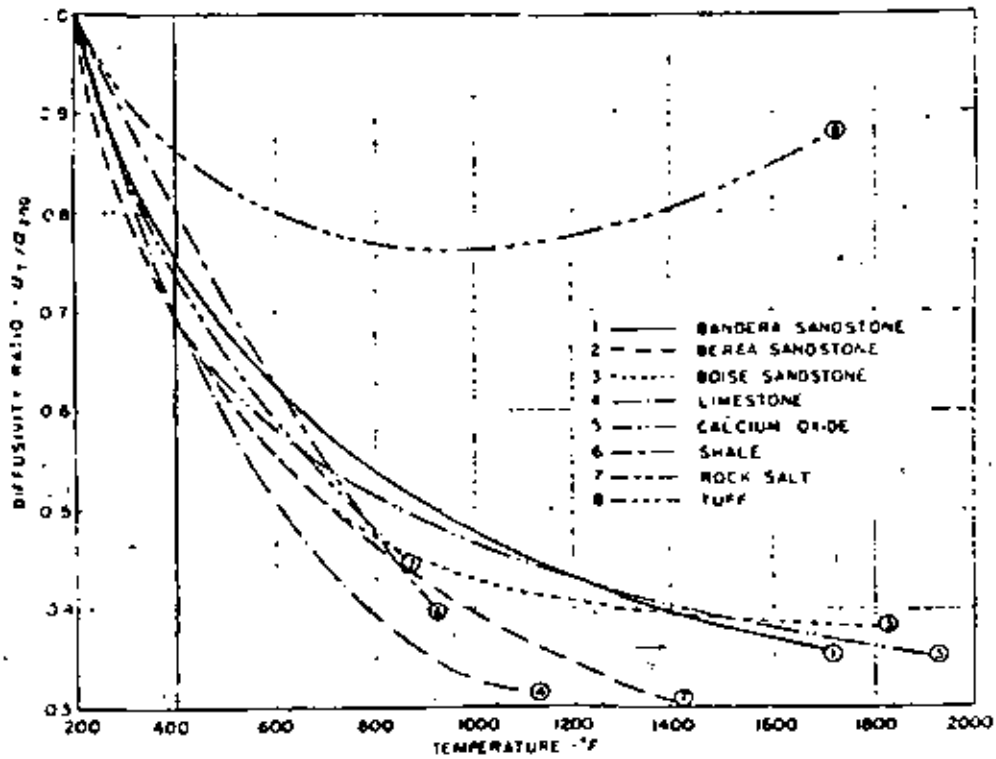

FIGURE 10 —THERMAL DIFFUSIVITY RATIO, INITIAL RUNS.
(Ref. 13)

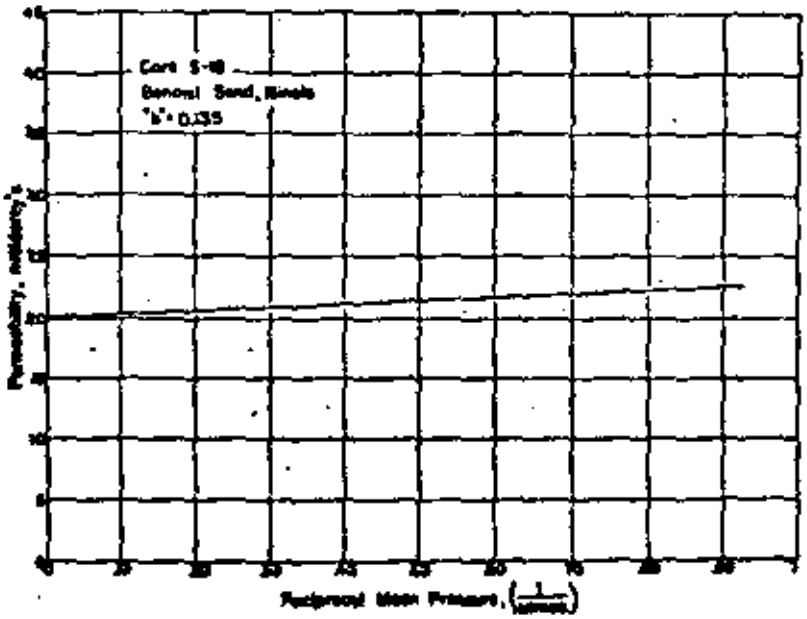

FIG. 5

FIGURE 11 **Relationship between the Permeability to Gas and the Mean Pressure at which Gas Flows through a Medium, a Relationship Making Possible the Determination of the Permeability of the Medium to a Non-Reacting Liquid**

(from API RP 27, Am. Petr. Inst., Aug. 1956)

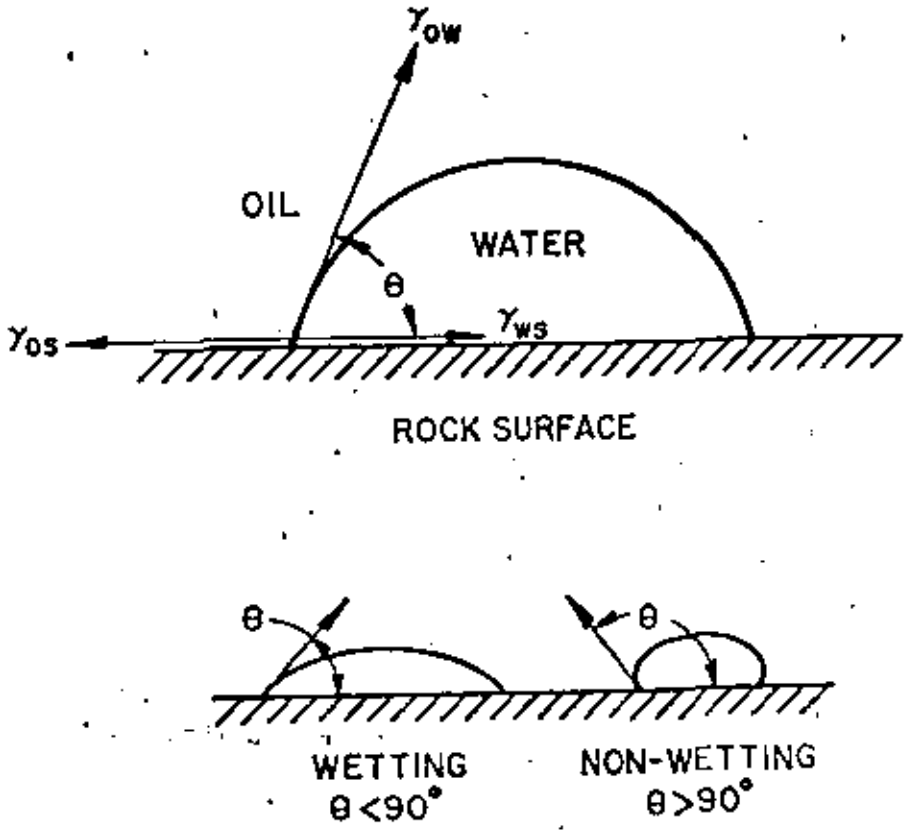

FIGURE 12 **Relationship between preferential wetting and contact angle.** (Ref. 15)

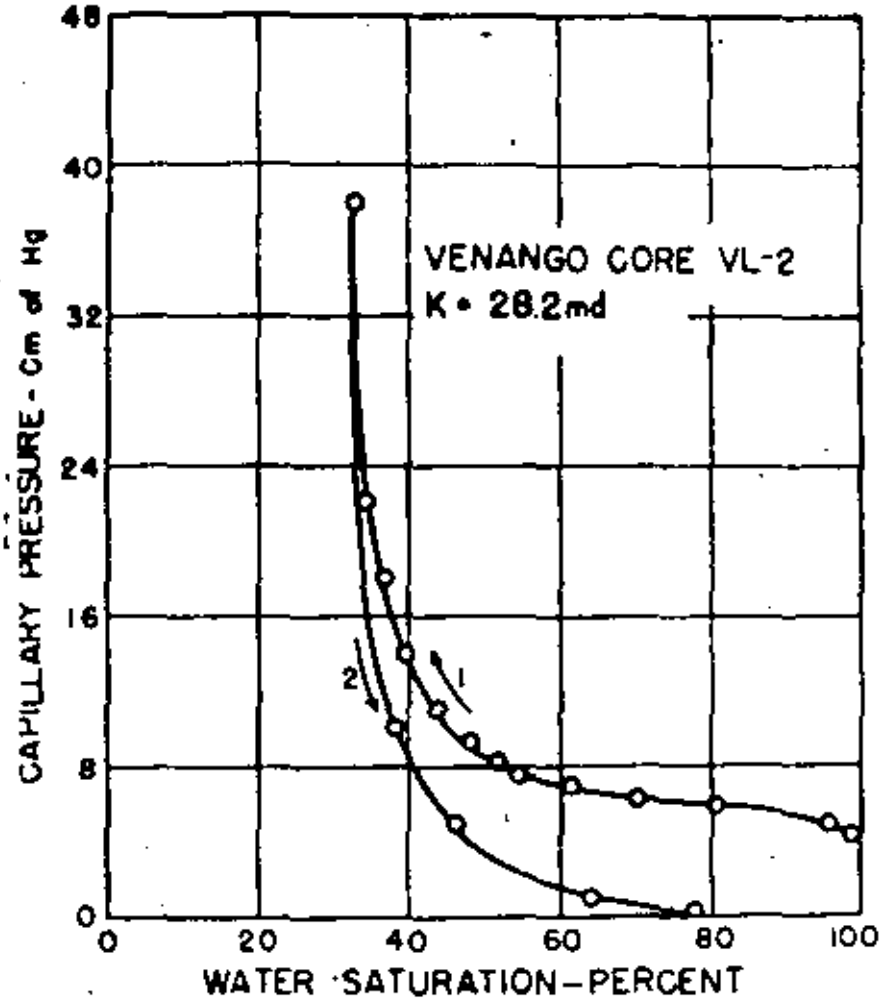

FIGURE 13 —Capillary pressure vs. water saturation.

(Ref. 16)

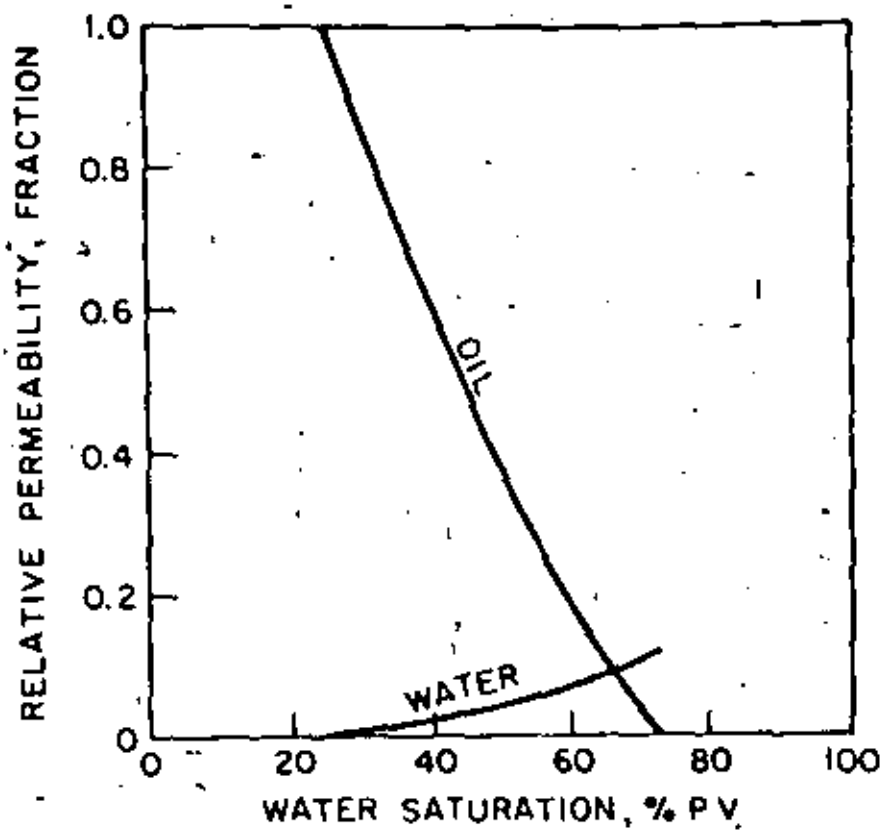

FIGURE 14 Typical water-oil relative permeability characteristics, strongly water-wet rock. (Ref. 17)

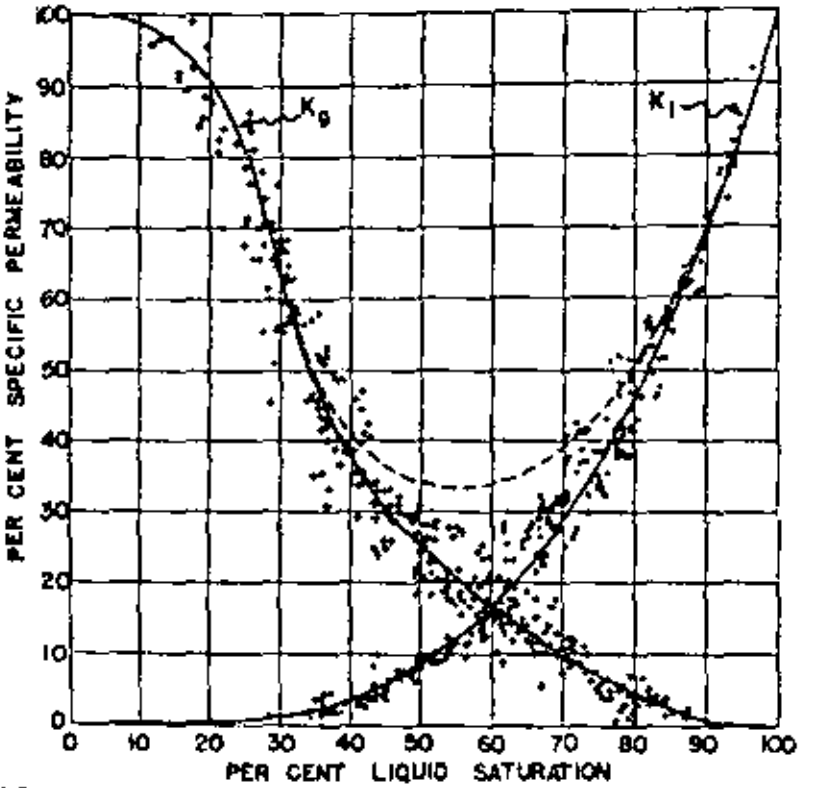

FIGURE 15 -PERMEABILITY-SATURATION DATA FOR FOUR DIFFERENT SANDS, INCLUDING THOSE OF FIGS. 4 AND 5.

(Ref. 18)

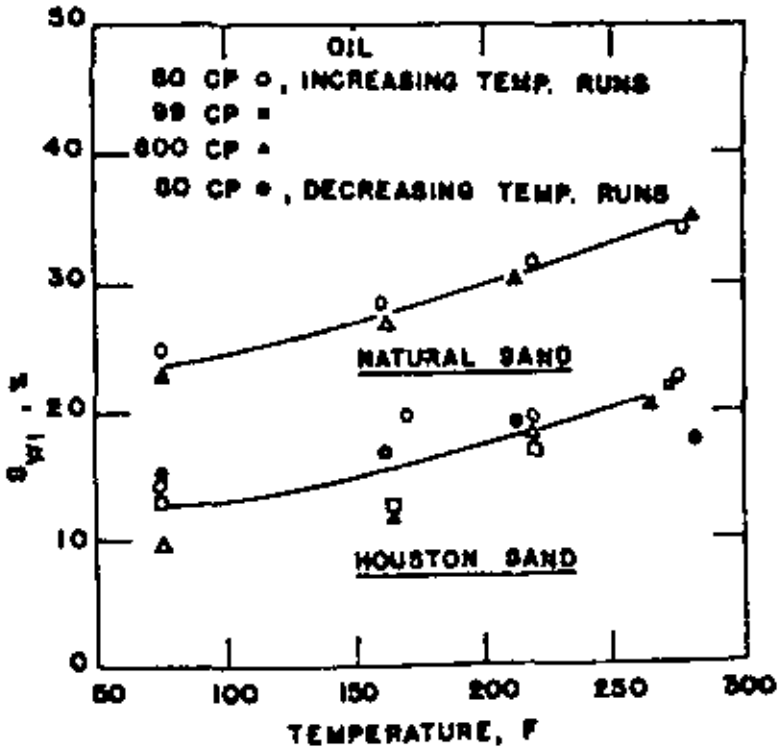

FIGURE 16

IRREDUCIBLE WATER SATURATION VS TEMPERATURE FOR HOUSTON SAND AND NATURAL SAND. (Ref. 19)

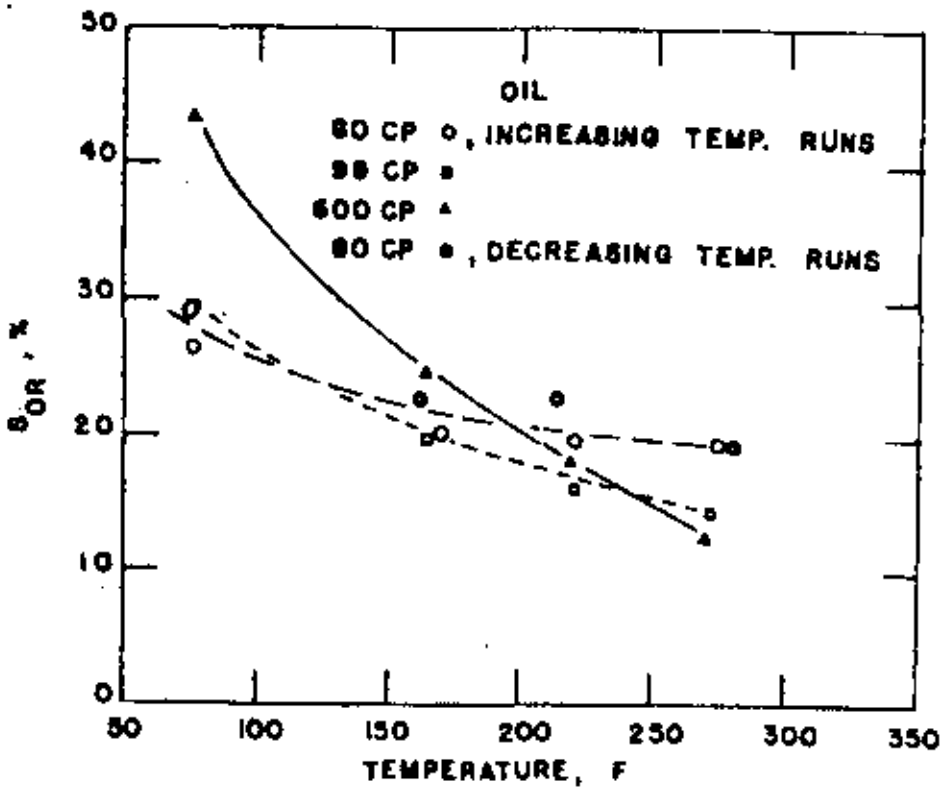

FIGURE 17 RESIDUAL OIL SATURATION VS TEMPERATURE FOR HOUSTON SAND. (Ref. 19)

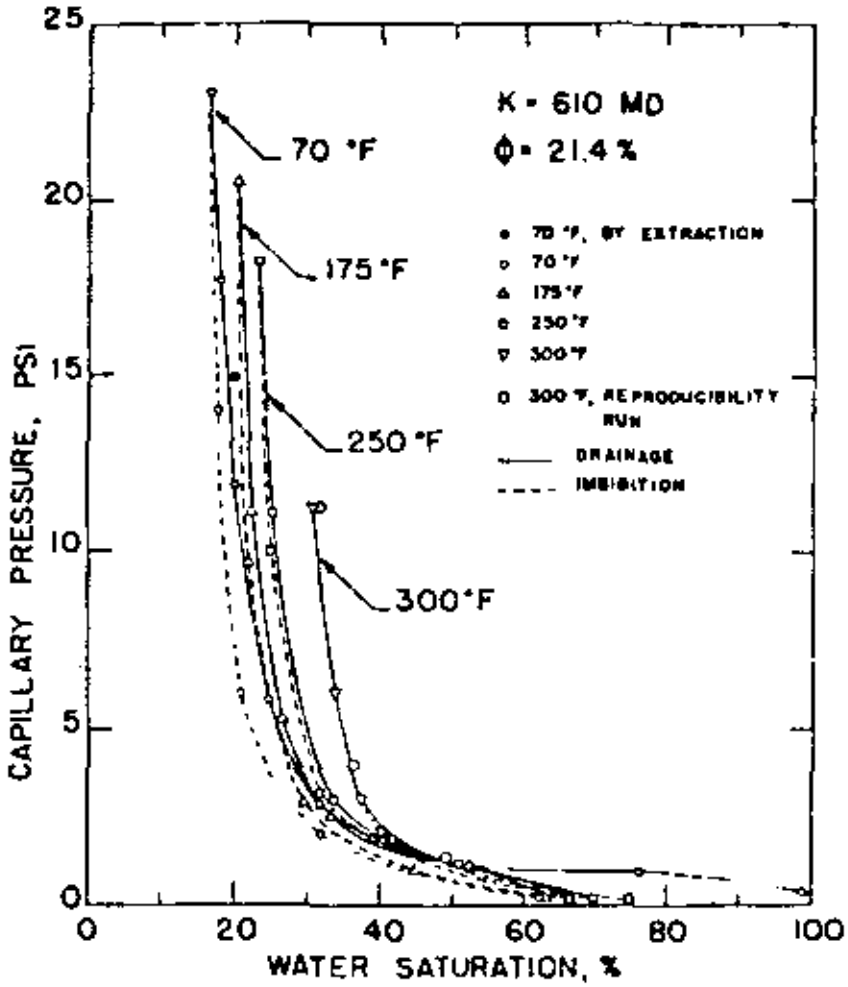

FIGURE 18 Capillary pressure vs water saturation for Berea sandstone core A. (Ref. 20)

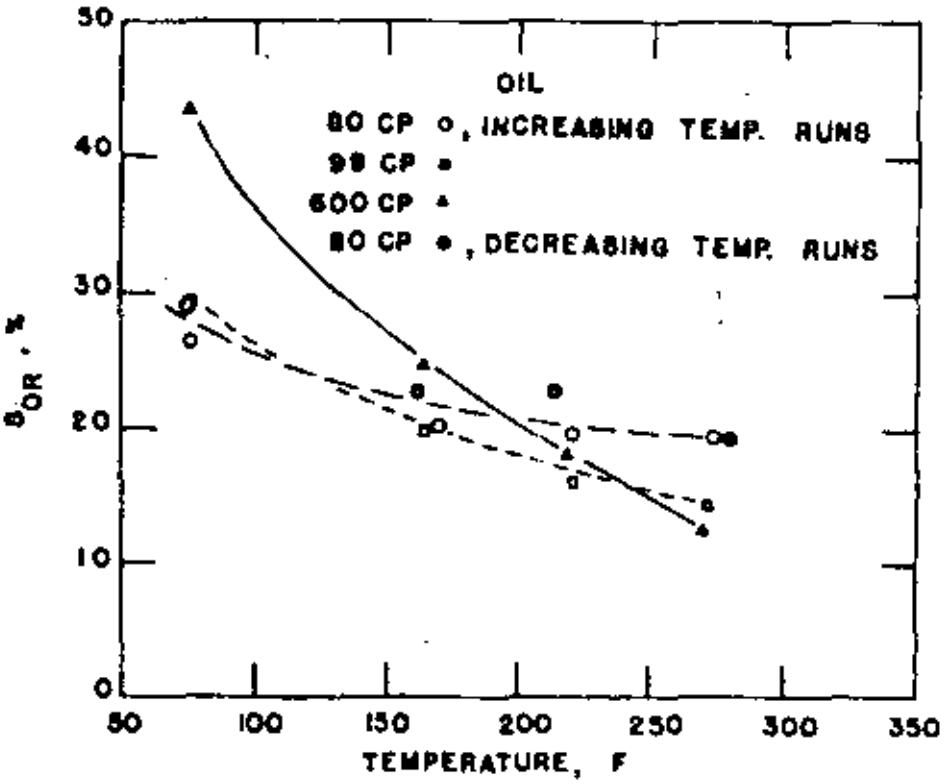

FIGURE 17 RESIDUAL OIL SATURATION VS TEMPERATURE FOR HOUSTON SAND. (Ref. 19)

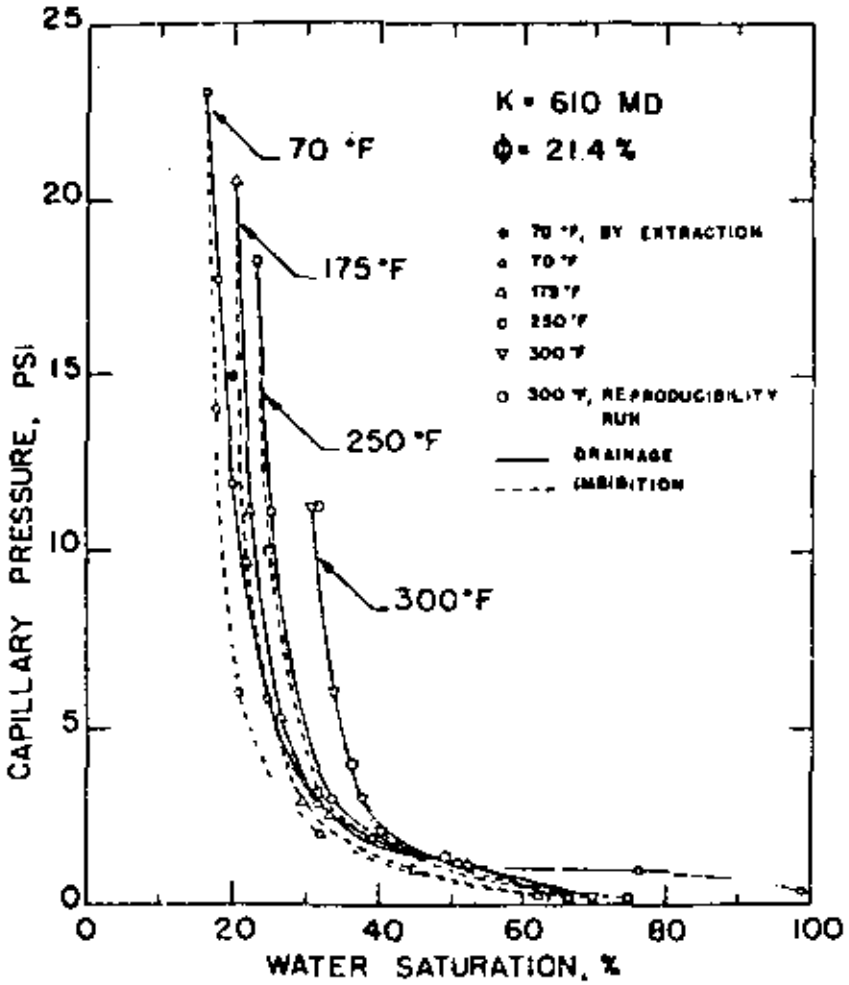

FIGURE 18 Capillary pressure vs water saturation for Berea sandstone core A. (Ref. 20)

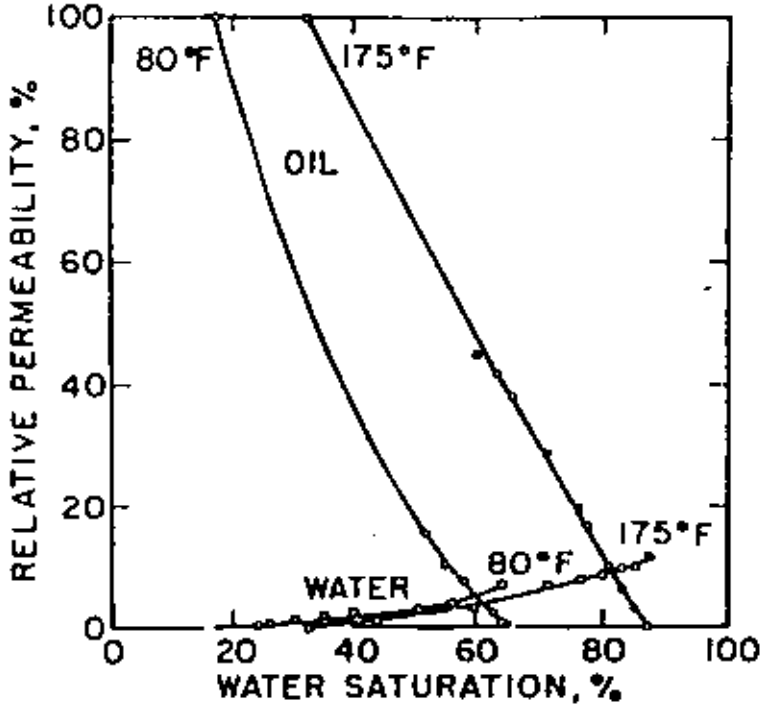

FIGURE 19

Individual relative permeabilities as a function of temperature; Core 4, Boise sandstone. (Ref. 21)

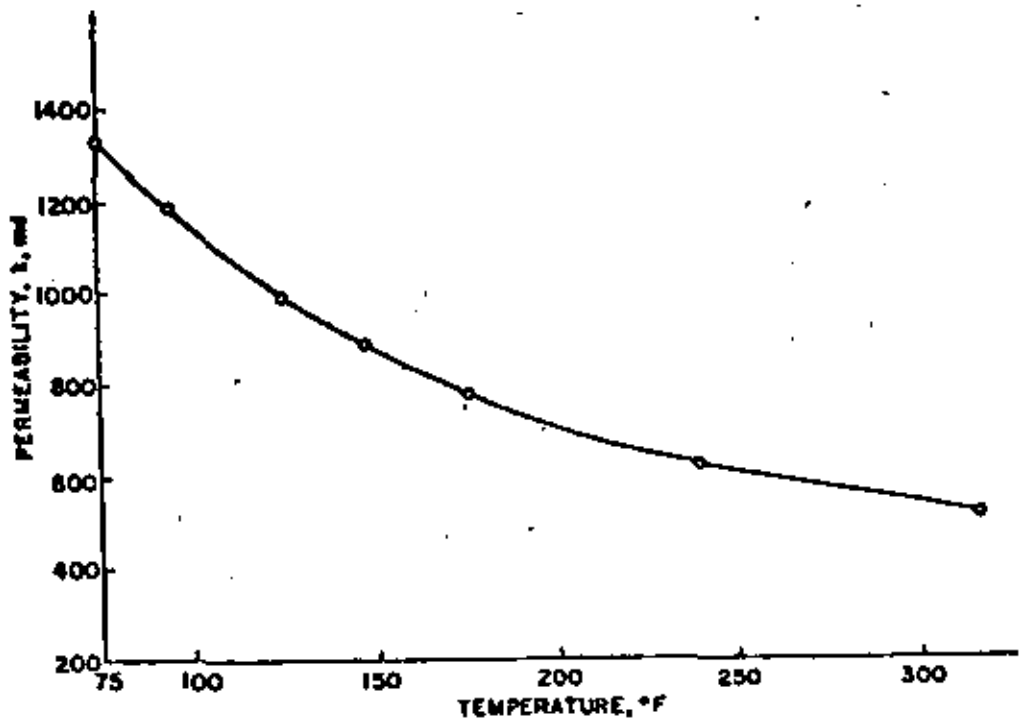

FIGURE 20 EFFECT OF TEMPERATURE ON ABSOLUTE PERMEABILITY OF BOISE SANDSTONE ; CORE NUMBER 7 (Ref. 21)

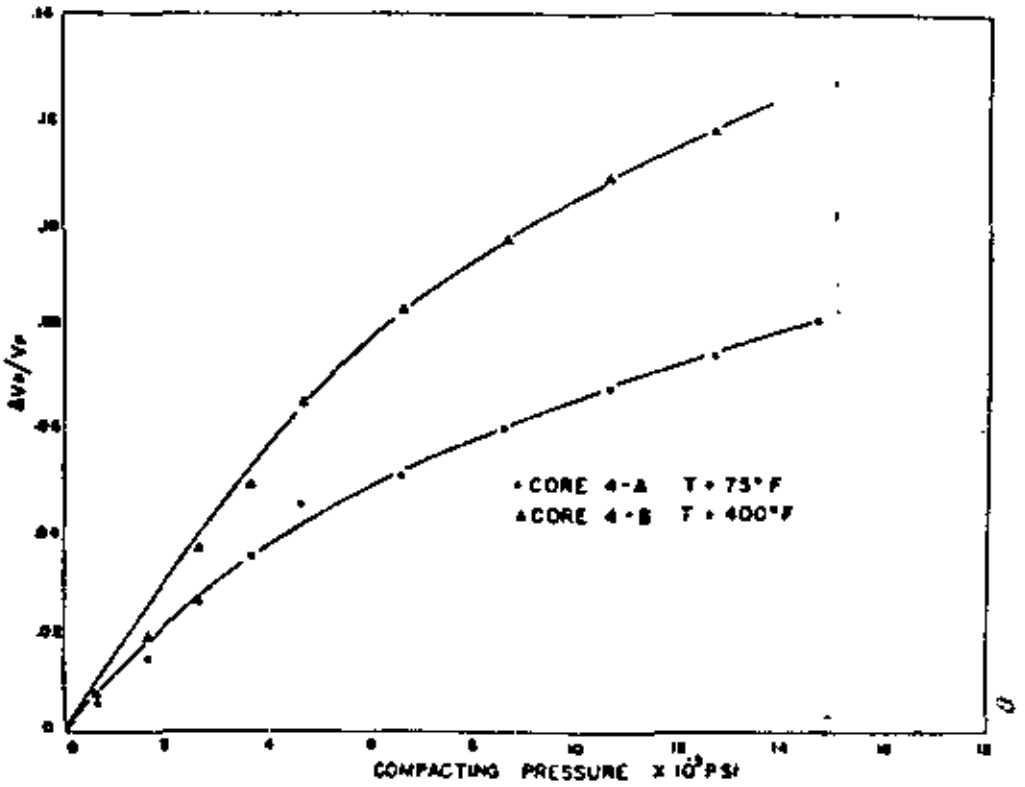

FIGURE 21 - Change in cumulative fractional pore volume with pressure core 4 at 75 and 400°F. (Ref. 24)

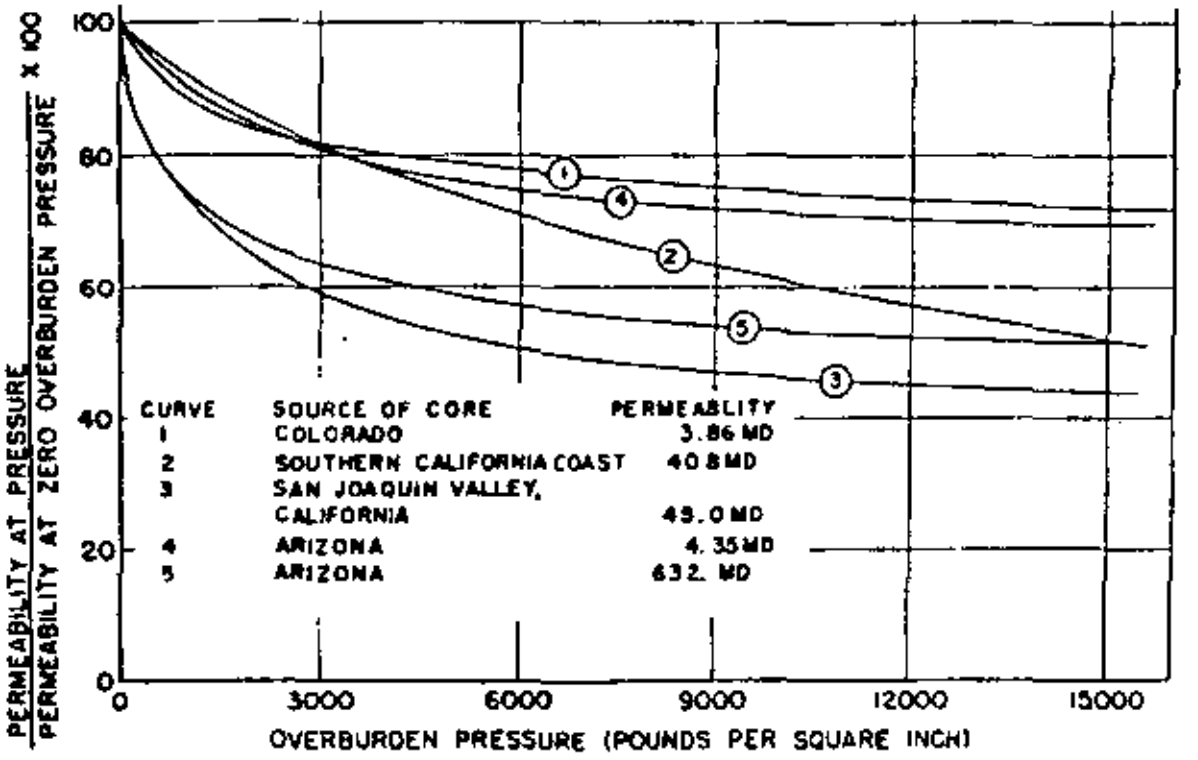

FIGURE 22 CHANGE IN PERMEABILITY WITH OVERBURDEN PRESSURE.
(Ref. 26)

FIGURE 23

PRESSURE-TEMPERATURE DIAGRAM FOR WATER

(Ref. 38)

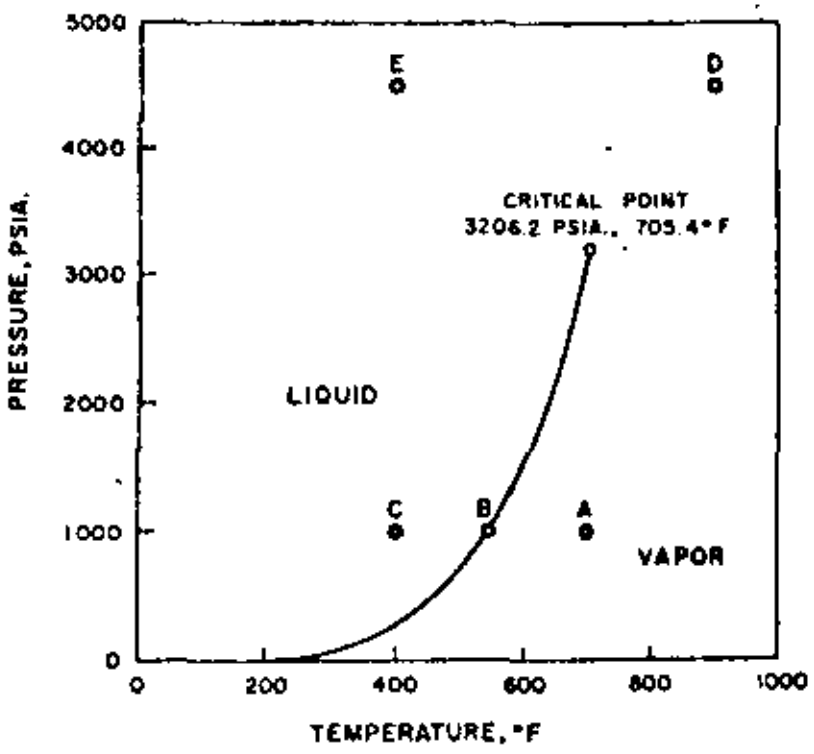

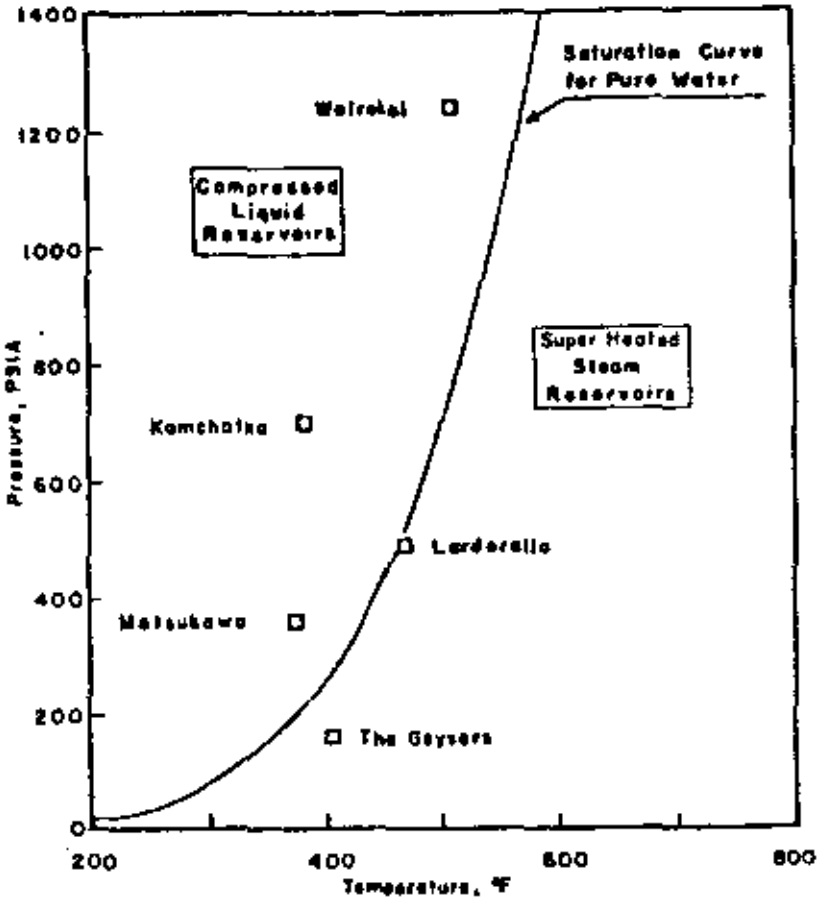

FIGURE 24 Reservoir temperature and pressure data for geothermal reservoirs

(Ref. 60)

FIGURE 25

PRESSURE-SPECIFIC VOLUME CHART FOR WATER

(Ref. 38)

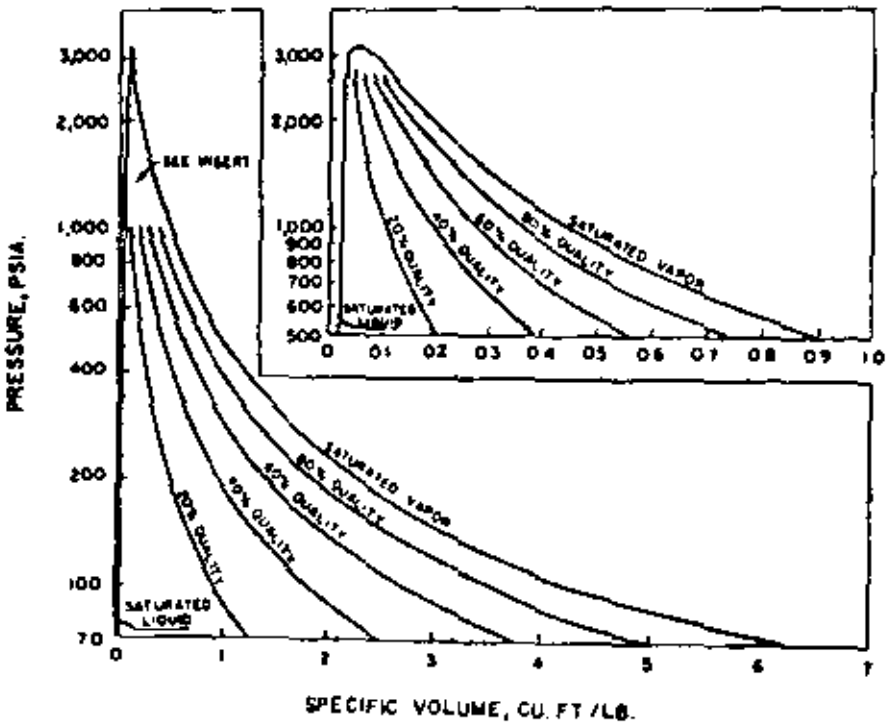

FIGURE 26

PRESSURE - ENTHALPY DIAGRAM FOR WATER

(Ref. 38)

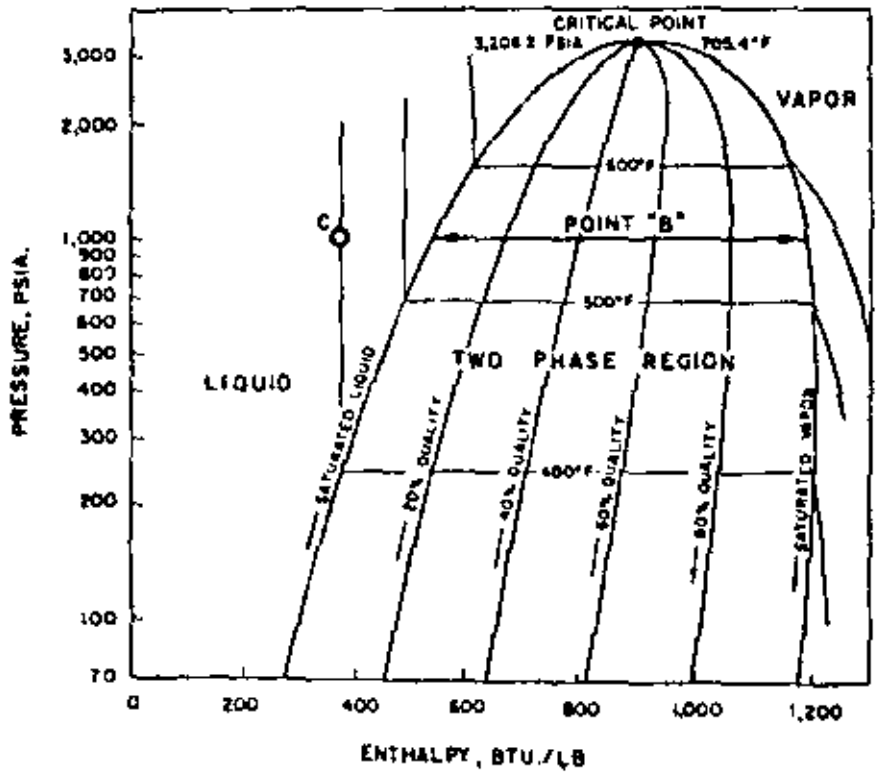

FIGURE 27

Viscosity of Saturated Water and Steam

(modified from Ref. 38)

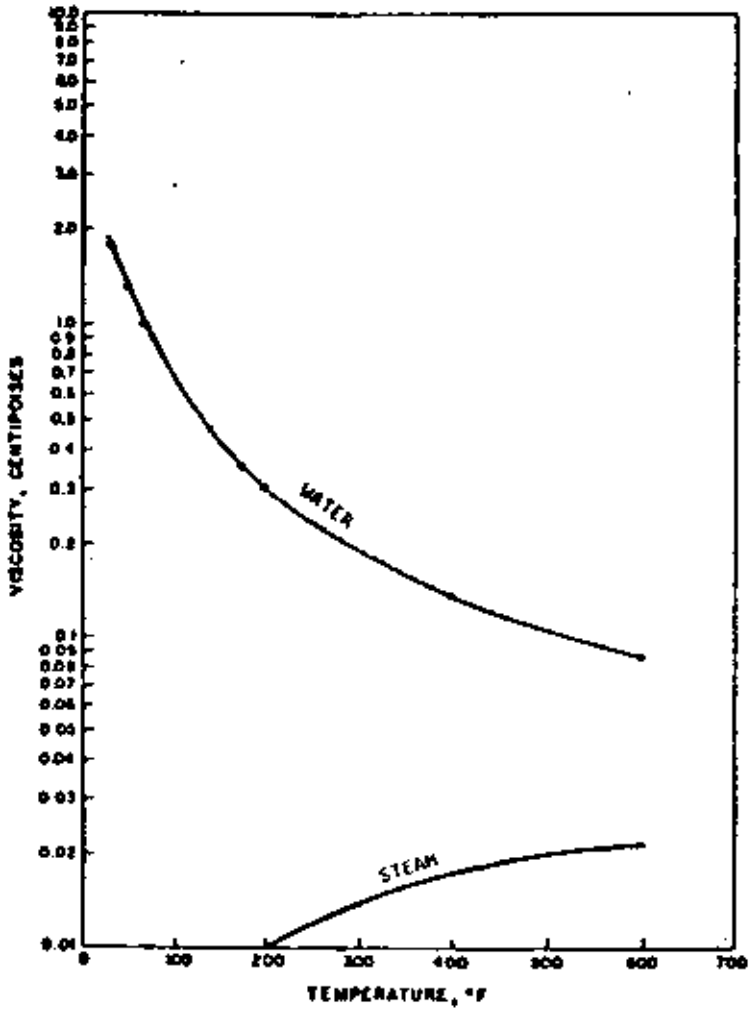

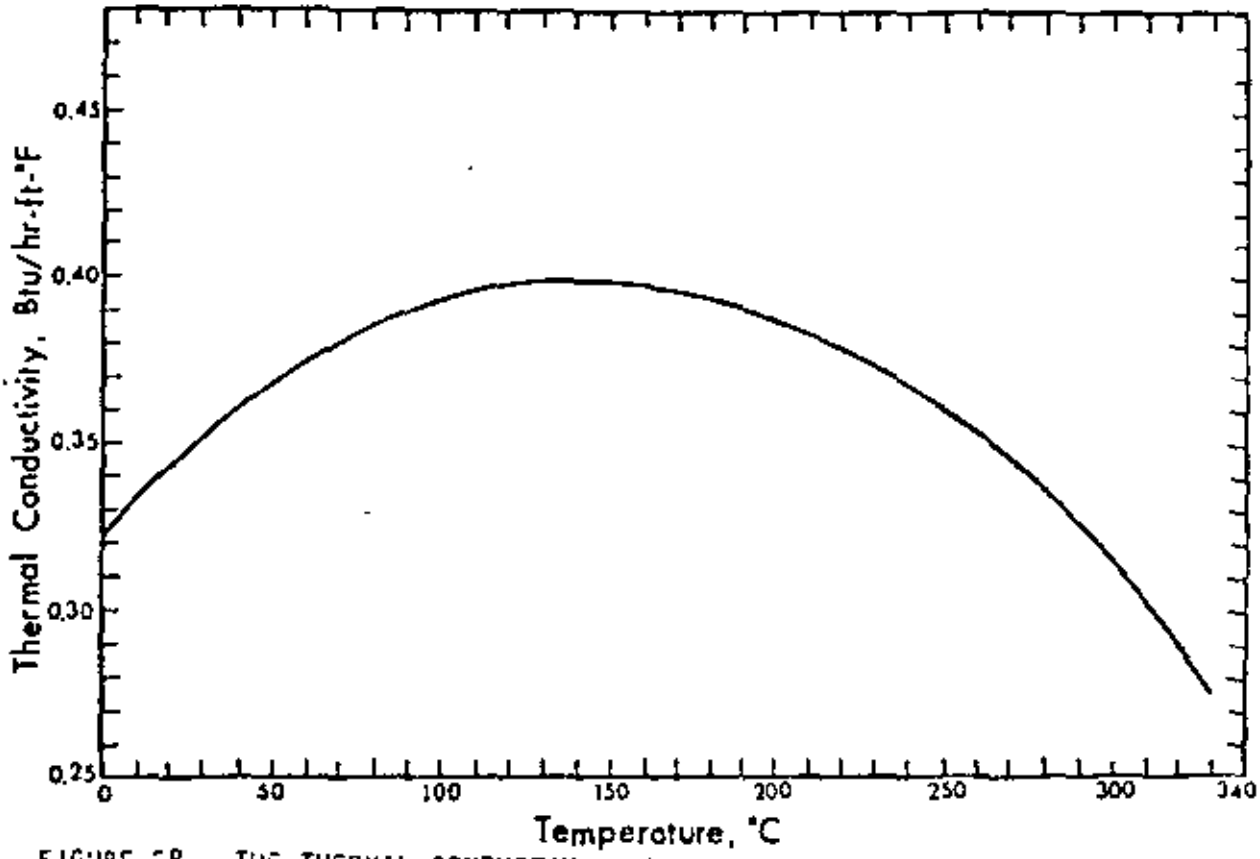

FIGURE 28. THE THERMAL CONDUCTIVITY OF SATURATED LIQUID WATER (Ref. 39)

FIGURE 29

FORMATION VOLUME FACTOR FOR PURE LIQUID WATER AS A FUNCTION OF PRESSURE AND TEMPERATURE

(Ref. 38)

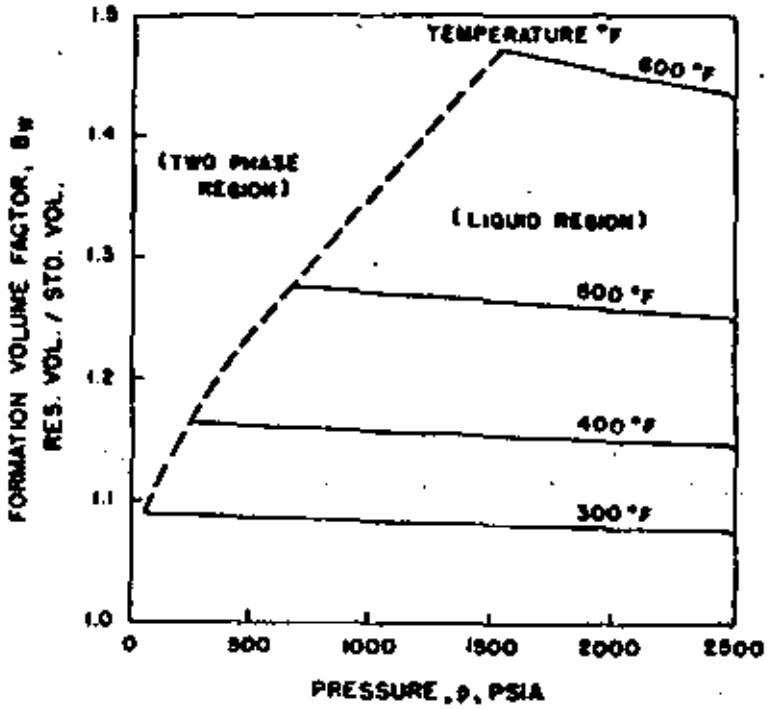

FIGURE 30

PRESSURE - SPECIFIC VOLUME CHART FOR SUPERHEATED STEAM

(Ref. 38)

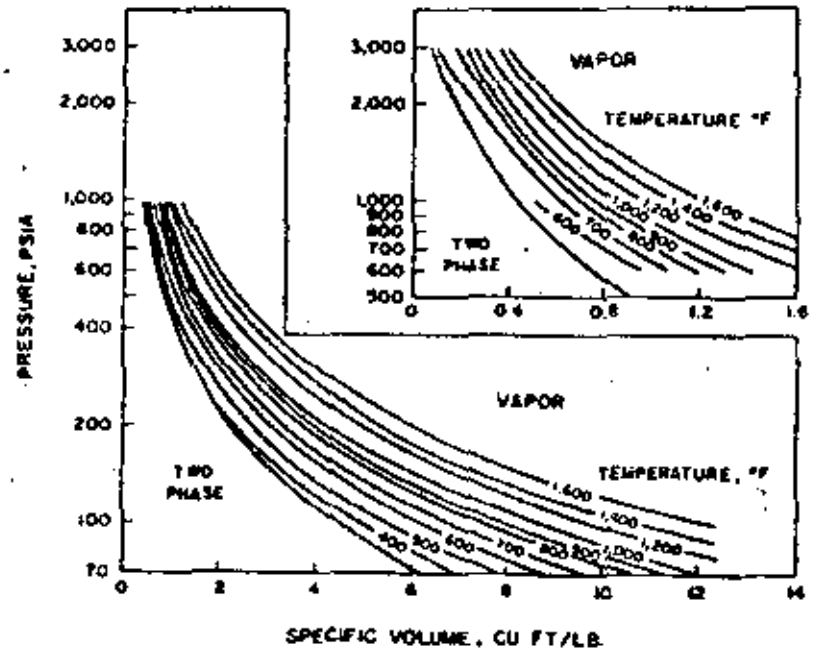

FIGURE 31
GAS LAW DEVIATION FACTOR FOR STEAM (Ref. 43)

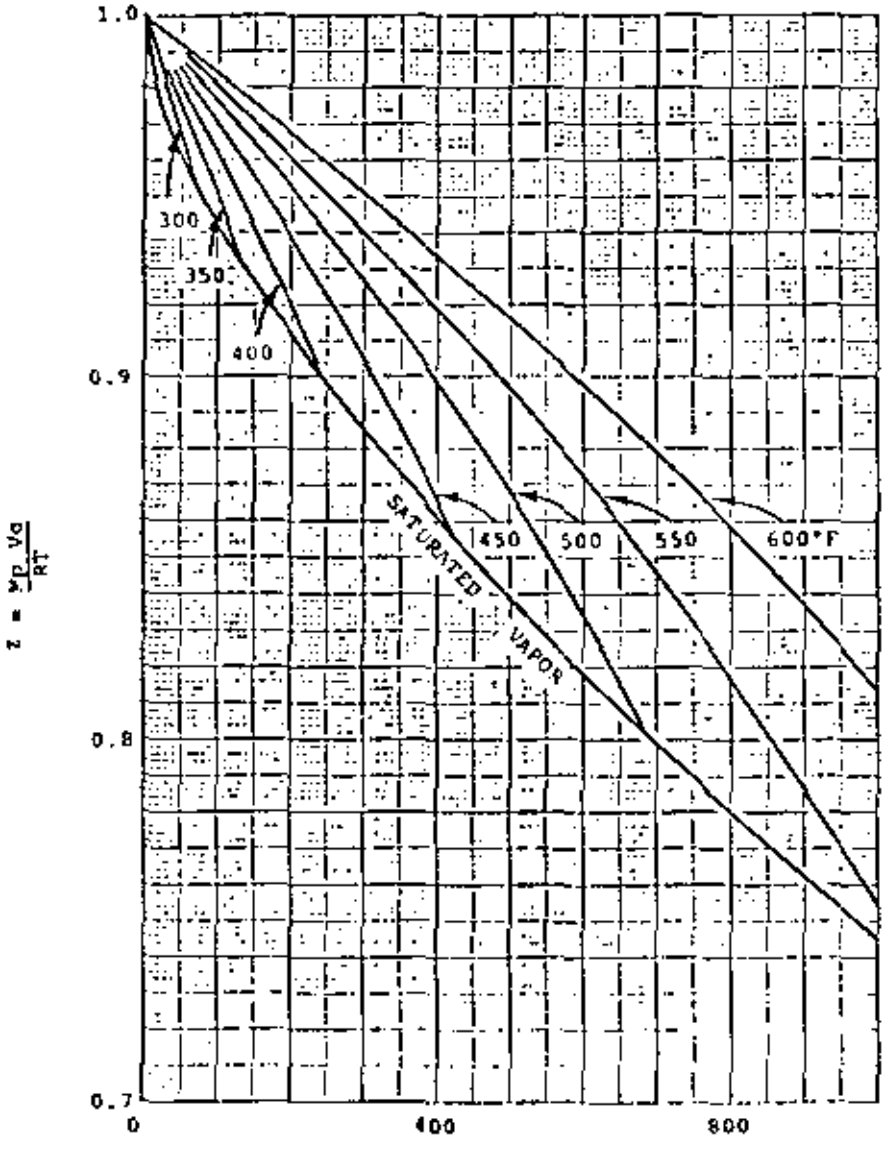

FIGURE 32

PRESSURE - ENTHALPY DIAGRAM FOR SUPERHEATED STEAM

(Ref. 38)

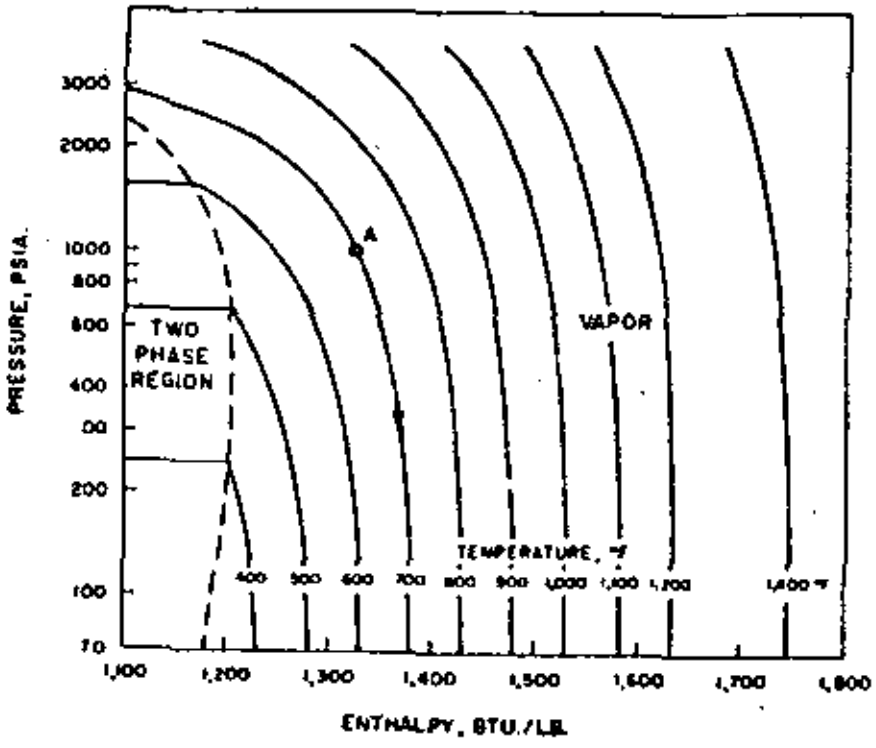

REFERENCES

1. Birch, Francis and Clark, Harry: "The Thermal Conductivity of Rocks and Its Dependence upon Temperature and Composition, Part I", Am. J. Science, 238, No. 8 (Aug. 1940), pp. 529-558.
2. Birch, Francis and Clark, Harry: "The Thermal Conductivity of Rocks and Its Dependence upon Temperature and Composition, Part II", Am. J. Science, 238, No. 9 (Sept. 1940), pp. 613-635.
3. Somerton, Wilbur H.: "Some Thermal Characteristics of Porous Rocks," Trans. AIME, 213 (1958), pp. 375-378.
4. Kunii, D. and Smith, J. M.: "Thermal Conductivities of Porous Rocks Filled with Stagnant Fluid," Soc. Pet. Engr. J. (Mar. 1961), pp. 37-42.
5. Adivarahan, P., Kunii, D. and Smith, J. M.: "Heat Transfer in Porous Rocks Through Which Single-Phase Fluids Are Flowing," Soc. Pet. Engr. J. (Sept. 1962), pp. 290-296.
6. Willhite, G. P., Dranoff, J. S. and Smith, J. M.: "Heat Transfer Perpendicular to Fluid Flow in Porous Rocks," Soc. Pet. Engr. J. (Sept. 1963), pp. 185-188.
7. Anand, J., Somerton, W. H. and Gomaa, E.: "Prediction of Thermal Properties of Formations from Other Known Properties," Paper No. SPE-4171, 43rd California Regional Meeting, SPE of AIME, Bakersfield, Calif., Nov. 8-10, 1972.
8. Tikhomirov, V. M.: "Conductivity of Rocks and Their Relationship with Density, Saturation and Temperature," Neftianoe Khoziaistro (in Russian), 46, No. 4 (1968), p. 36.
9. Gomaa, Ezzat E. and Somerton, W. H.: "Thermal Behavior of Multifluid-Saturated Formations, Part I: Effect of Wettability, Saturation and Grain Structure," Paper No. SPE 4896-A, 44th California Regional Meeting, SPE of AIME, San Francisco, Calif., April 4-5, 1974.
10. Gomaa, Ezzat E. and Somerton, W. H.: "Thermal Behavior of Multifluid-Saturated Formations, Part II: Effect of Vapor Saturation - Heat Pipe Concept and Apparent Thermal Conductivity," Paper No. SPE 4896-B, 44th California Regional Meeting, SPE of AIME, San Francisco, Calif., April 4-5, 1974.
11. Martin, W. L. and Dew, J. N.: "How to Calculate Air Requirements for Forward Combustion," Petroleum Engineer (Dec. 1964 and Feb. 1965).
12. Somerton, W. H. and Selim, M. A.: "Additional Thermal Data for Porous Rocks - Thermal Expansion and Heat of Reaction," Soc. Pet. Engr. J. (Dec. 1961), pp. 249-253.
13. Somerton, W. H. and Boozer, G. D.: "Thermal Characteristics of Porous Rocks at Elevated Temperatures," Trans. AIME, 219 (1960), pp. 418-422.
14. Klinkenberg, L. J.: "The Permeability of Porous Media to Liquids and Gases," Drilling and Production Practice (1941), pp. 200-213.

15. Raza, S. H., Treiber, L. E., and Archer, D. L.: "Wettability of Reservoir Rocks and Its Evaluation," Prod. Monthly (April 1968), 32, No. 4, pp. 2-7.

16. Killins, C. R., Nielsen, R. F. and Calhoun, J. C.: "Capillary Desaturation and Imbibition in Porous Rocks," Prod. Monthly (Dec. 1953) 18, No. 2, pp. 30-39.

17. Craig, F. F., Jr.: The Reservoir Engineering Aspects of Waterflooding, SPE Monograph, Vol. 3.

18. Muskat, M., Wyckoff, R. D., Botset, H. G. and Meres, M. W.: "Flow of Gas-liquid Mixtures through Sands," Trans., AIME (1937), 123, pp. 69-96.

19. Poston, S. W., Yerael, S., Hossain, A. K. M. S., Montgomery, E. F. IV and Ramey, H. J., Jr.: "The Effect of Temperature on Irreducible Water Saturation and Relative Permeability of Unconsolidated Sands," Soc. Pet. Engr. J. (June 1970), pp. 171-180.

20. Sinnokrot, A. A., Ramey, H. J., Jr. and Marsden, S. S.: "Effect of Temperature Level upon Capillary Pressure Curves," Paper No. SPE 2517, presented at the 44th Annual SPE Fall Meeting, Denver, Colo., Sept. 28-Oct. 1, 1969.

21. Weinbrandt, R. M., Ramey, H. J., Jr. and Cassé, F.: "The Effect of Temperature on Relative Permeability of Consolidated Rocks," Paper No. SPE 4142, presented at the 47th Annual SPE Fall Meeting, San Antonio, Texas, Oct. 8-11, 1972.

22. Afinogenov, Y. A.: "How the Liquid Permeability of Rocks Is Affected by Pressure and Temperature," SNIGGIMS (1969), No. 6, pp. 34-42 (translation from Consultants Bureau, 227 W. 17 St., New York, NY 10011).

23. Lo, H. Y. and Mungan, N.: "Effect of Temperature on Water-Oil Relative Permeabilities in Oil-Wet and Water-Wet Systems," Paper No. SPE 4505, presented at the 48th Annual SPE Fall Meeting, Las Vegas, Nevada, Sept. 30-Oct. 3, 1973.

24. Von Gonten, W. D. and Choudhary, B. K.: "The Effect of Pressure and Temperature on Pore Volume Compressibility," Paper No. SPE 2526, presented at the 44th Annual SPE Fall Meeting, Denver, Colorado, Sept. 28-Oct. 1, 1969.

25. Zoback, M. D. and Byerlee, J. D.: "Permeability, Compressibility and Effective Stress," unpublished report (Feb. 1974).

26. Fatt, I. and Davis, D. H.: "Reduction in Permeability with Overburden Pressure," Trans., AIME (1952), 195, 329.

27. Wyble, D. O.: "Effect of Applied Pressure on the Conductivity, Porosity and Permeability of Sandstones," Trans., AIME (1958), 213, pp. 430-432.

28. Dobrynin, V. M.: "Effect of Overburden Pressure on Some Properties of Sandstones," Soc. Pet. Engr. J. (Dec. 1962) 2, No. 4, pp. 360-366.

29. Gray, D. H., Fatt, I. and Bergamini, G.: "The Effect of Stress on Permeability of Sandstone Cores," Soc. Pet. Engr. J. (June 1963), pp. 95-100.

30. Wilhelmi, B. and Somerton, W. H.: "Simultaneous Measurement of Pore and Elastic Properties of Rocks under Triaxial Stress Conditions," Paper No. SPE 1706 (1967).

31. Krauskopf, K. B.: Introduction to Geochemistry, McGraw-Hill, New York, NY, 1967.

32. Butler, J. N.: Solubility and pH Calculations, Addison-Wesley, Palo Alto, CA, 1964.

33. White, E. E.: "Geochemistry Applied to the Discovery, Evaluation and Exploitation of Geothermal Energy Resources," Geothermics, Special Issue 2, Proc. of U. N. Symposium on the Development and Utilization of Geothermal Resources, Pisa, 1970, Vol. 1.

34. Fournier, R. O. and Truesdell, A. H.: "Chemical Indications of Subsurface Temperature Applied to Hot Spring Waters of Yellowstone National Park, Wyoming, U.S.A.", Geothermics, Special Issue 2, Proc. of U. N. Symposium on the Development and Utilization of Geothermal Resources, Pisa, 1970, Vol. 2, Part 1.

35. Keenan, J. H. and Keyes, F. G.: Thermodynamic Properties of Steam, John Wiley and Sons, Inc., New York, NY, 1936.

36. Meyer, C. A., McClintock, R. B., Silvestri, G. J. and Spencer, R. C., Jr.: 1967 ASME Steam Tables, Am. Soc. Mech. Engrs., 2nd ed., New York, NY, 1968.

37. Keenan, J. H., Keyes, F. G., Hill, P. G. and Moore, J. G.: Steam Tables: Thermodynamic Properties of Water Including Vapor, Liquid and Solid Phases (English Units), John Wiley and Sons, Inc., New York, NY, 1969.

38. Whiting, R. L. and Ramey, H. J., Jr.: "Application of Material and Energy Balances to Geothermal Steam Production," J. Pet. Tech. (July 1969), pp. 893-900.

39. Farouq Ali, S. M.: Oil Recovery by Steam Injection, Producers Pub. Co., Bradford, PA, 1970.

40. Calhoun, J. C., Lewis, M., Jr. and Newman, R. C.: "Experiments on the Capillary Properties of Porous Solids," Trans. AIME, 186 (1949), pp. 189-196.

41. Edlefsen, N. E. and Anderson, A. B. C.: "Thermodynamics of Soil Moisture," Hilgardia, Calif. Agricultural Exp. Station, Univ. of Calif. at Berkeley, 15, No. 2 (Feb. 1943), p. 31.

42. Cady, G. V., Bilhartz, H. L., Jr. and Ramey, H. J., Jr.: "Model Studies of Geothermal Steam Production," Water 1972, AIChE Symposium Series (1973).

43. Amyx, J. W., Bass, D. M., Jr. and Whiting, R. L.: Petroleum Reservoir Engineering, McGraw-Hill, New York, NY, 1960.

44. Dodson, C. R. and Standing, M. B.: "Pressure-Volume-Temperature and Solubility Relations to Natural Gas-Water Mixtures," API Drilling and Production Practice, American Petroleum Institute, 1944.

45. Rowe, W. E.: "Effect of Salinity on Physical Properties of Water," Secondary Recovery of Oil in the United States, American Petroleum Institute, 1950.

46. Beal, Carlton: "The Viscosity of Air, Water, Natural Gas, Crude Oil and Its Associated Gases at Oil Field Temperatures and Pressures," Trans., AIME, 165 (1946).

47. Bridgman, O. W.: The Physics of High Pressure, McMillan Co., New York, NY, 1931.

48. Long, G. and Chierici, G. L.: "Compressibilite et Masse Specifique des Eaux de Gisement dans les Conditions des Gisements, Application a Quelque Problemes de 'Reservoir Engineering'" presented at Fifth World Petroleum Congress, 1959.

49. Van Wingen, N.: "Viscosity of Oil, Water, Natural Gas, and Crude Oil at Varying Pressures and Temperatures," Secondary Recovery of Oil in the United States, American Petroleum Institute, 1950.

50. Stanley, E. M. and Batton, R. C.: "Viscosity of Sea Water at Moderate Temperatures and Pressures," J. Geophys. Res., 74, No. 13 (June 20, 1969), pp. 3415-3420.

51. Eilerts, C. L., Carlson, H. A. and Mullens, N. B.: "Effect of Added Nitrogen on Compressibility of Natural Gas," World Oil (June-July 1948).

52. Olds, R. H., Sage, B. H. and Lacey, W. N.: "Partial Volumetric Behavior of the Methane-Carbon Dioxide System," Fundamental Research on the Occurrence and Recovery of Petroleum, American Petroleum Institute, 1943.

53. Reamer, H. H., Sage, B. H. and Lacey, W. N.: "Volumetric Behavior of Hydrogen Sulfide," Ind. Engr. Chem, 42, No. 1 (Jan. 1950), p. 140.

54. Herning, F. and Zipperer, L.: "Calculation of the Viscosity of Technical Gas Mixtures from the Viscosity of the Individual Gases," Gas-U. Wasserfach, 79 (1936).

55. Weast, R. C.: Handbook of Chemistry and Physics, The Chemical Rubber Co., Ohio, 48th ed. (1967-68).

56. Strobel, C. J.: Model Studies of Geothermal Fluids Production from Consolidated Porous Media," Engineer's thesis, Stanford Univ., July 1973.

57. Kuhn, C. S. and Koch, R. L.: "In-Situ Combustion," Oil & Gas J. (Aug. 10, 1953), 52, No. 14, p. 96.

58. Stovall, S. L.: "Recovery of Oil from Depleted Sands by Means of Dry Steam," Oil Weekly (Aug. 13, 1934), 74, p. 17.

59. Gates, C. S. and Ramey, H. J., Jr.: "Field Results of South Bebridge Thermal Recovery Experiment," Trans., AIME (1958), 213, p. 236.

60. Cady, G. V.: "Model Studies of Geothermal Fluid Production," Ph.D. dissertation, Stanford Univ., Nov. 1969.

61. Rowe, A. M., Jr.: "Thermodynamics Applied to Reservoir Engineering," Course notes for Petroleum Engineering 273, Winter 1973-74, Stanford Univ.

62. Helgeson, H. C.: "Thermodynamics of Hydrothermal Systems at Elevated Temperatures and Pressures," Am. J. Science, 267, Summer 1969, pp. 729-804.

63. Ramey, H. J., Jr.: A Reservoir Engineering Study of the Geysers Geothermal Field, 1968; submitted as evidence, Reich and Reich: Petitioners vs. Commissioner of Internal Revenue, 1969 Tax Court of the United States, 52. T.C. No. 74, 1970.

Discussion Following Ramey Paper

Rinehart

Do you think these things would hold for large, fractured mass when you have microscopic fractures with impermeable rock in between?

Ramey

In some cases we already know that they do. There are many oil and gas reservoirs that are in fact large, fractured masses. Generally speaking, the laws of nature seem to work the same there. Now some of the details on these homogeneous porous structures, the relative permeability curve details, would not be identically the same. It has amazed me to find that some of the massive, fractured reservoirs seem to follow simple mechanics.

Oki

The permeability is a function of temperature. When the temperature is increased, the permeability becomes lower; then when the temperature is reduced, the original numerical value for permeability is reached. I mean it is almost reversible.

Ramey

It is reversible. One other thing: the shapes of the curves, whether it's temperature or pressure, are almost the same. In data where permeability ratio is plotted versus effective pressure, you will note that the shape is almost identical with what you get for temperature. In our temperature work we have kept the confining pressure constant, just varying the temperature in the system, and we see this reversible result. In our data it is perhaps not totally reversible; it will move down the line and come back up slightly below its original path. But the difference is not much. Within the experimental accuracy it appears to be reversible. On the other work, on relative permeability, most of it does seem to be temperature level reversible. If you heat a core and measure relative permeability you get one value; if you cool it off and heat it up again you get the same value.

Rinehart

These are all corrected for viscosity?

Ramey

Yes.

Rinehart

Do you feel that your correction is good?

Ramey

We know it is. We've used fluids where the density of the fluid is known perfectly, we've used desensitized cores where we're not getting reaction with the core material, we've tested the fluids before and after, we've measured everything we can think of to be sure nothing has changed.

Coryell

It looks as though you are drawing attention to a large body of empirical evidence for temperature dependence of these parameters. Would you care to comment as to how you see the future, where the science is going to go, the state of the theory at the present time?

Ramey

Yes, you see a lot of interesting problems.

Coryell

You see a lot of interesting behavior, but is there the science and the basic understanding of why it's happening?

Ramey

Oh, very definitely. Everything I have shown you, I can explain I should have added that this one is almost on the forefront of knowledge and I can tell you what I think is the cause. In many cases, for example, the change in thermal conductivity with temperature will fit a very logical model of this system to the point that you can almost calculate the results you will get. Practically everything that has been done has been strongly related to underlying principles. People have been searching for ways to compute the result. Generally speaking, we have wanted this so we could patch it into some computer software and forecast what would happen under different cases. It's been necessary to generalize; it's been necessary to, at least, curve-fit to the point that is accessible to a computer. Almost everything that exists in the literature will have a very good explanation; it is not empirical. These are experimental determinations, of course; when you deal in this area, what you are talking about are experimental measurements that fit your constants. But the laws of physics still apply.

What I really deal in are reservoir models, physical models. We produce an oil reservoir, measure pressure all over it--what comes out, what goes in--and I attempt to build some mathematical picture of the thing so I can forecast what will happen under any other scheme in the future. To do this I've got to use the laws of physics. In some cases I discover that the reservoir knows some detail that I don't or I've overlooked. But generally speaking, they always make sense.

ADDENDUM TO THERMODYNAMIC AND HYDRODYNAMIC PROPERTIES OF HYDROTHERMAL SYSTEMS

By Ramey, H.J., Brigham, W.E., Chen, H.K., Atkinson, P.G., Arihara, N.

April 1974

1. The following changes should be made in the definitions related to Equation 40, at the top of page 543:

(the last three definitions):

Z_{ncg} = noncondensable gas compressibility factor

(instead of:
Y_{ncg})= (etc.)

Y_{st} = Mole fraction steam in mixture

(instead of:
Z_{st})= (etc.)

Y_{ncg} = mole fraction noncondensable gas in mixture

(instead of:
Y_{ncg} = mole fraction noncompressible gas in mixture)

6-9-75

CURSO: INGENIERIA DE RESERVORIOS GEOTERMICOS.

OLADE
C.F.E.
I.I.E.
DECFI.

TEMAS: a) FUNDAMENTOS DE TERMODINAMICA.
b) CLASIFICACION DE LOS RESERVORIOS GEOTERMICOS.

INSTRUCTOR: DR. JESUS RIVERA RODRIGUEZ.

SEPTIEMBRE, 1981.

Geothermal Resources Council, TRANSACTIONS, Vol. 2 July 1978

DR. JESUS RIVERA RODRIGUEZ

APPLICATION OF TYPE CURVE PROCEDURES FOR THE ANALYSIS OF PRODUCTION DATA FROM GEOTHERMAL WELLS

DR. JESUS RIVERA-R.

COMISION FEDERAL DE ELECTRICIDAD
COORDINADORA EJECUTIVA DE CERRO PRIETO

ABSTRACT

It has been already shown[1] that the decline-curve analysis approach can be successfully applied to geothermal wells. It was shown in Reference 1 that by plotting monthly production vs. time on either semilog or log-log paper together with the rate decline models given by Arps[3], it was possible to predict the future production of wells of the Cerro Prieto Geothermal Field.

This paper shows that production forecasting can also be performed by an entirely graphical procedure. The procedure is based on the use of a basic dimensionless graph which was developed by Fetrovich[2]. He found that rate decline models developed by Arps[3] could be placed on a single log-log type curve. The aim of this paper is to show how this graph was used to handle production data from some wells of the Cerro Prieto Geothermal Field. The results obtained from the graphical procedure agreed with those obtained from that procedure reported before[1].

INTRODUCTION

In spite of the fact that decline curves are one of the most extensively used forms of production data analysis employed in the evaluation of oil reservoirs, there are quite a few published papers on their application to geothermal reservoirs. The results obtained from the application of this type of data analysis to geothermal wells of Cerro Prieto show that the method deserves more serious consideration for application to other geothermal fields around the world.

As it is well known[1,2,3] the three types of declines are exponential, hyperbolic and harmonic. The easiest one to analyze by means of conventional methods[1,3] is the exponential decline, because the hyperbolic decline is difficult to analize either mathematically or graphically. This problem has been overcome with the application of the type curve procedure[2] used in this report. As it can be seen from Figs. 1 thru 4, the basic dimensionless graph provides the type of decline, and if this decline turns out to be hyperbolic, the exponent of the equation describing this type of decline can also be determined.

FUNDAMENTAL CONSIDERATIONS

Fetrovich[2] showed that the exponential decline is actually a longtime solution of the constant-pressure case[6]. He presented a dimensionless graph in wich the exponential, hyperbolic and harmonic decline models were brought together. This graph is the basis for the analysis presented in this paper. The basic equations for the analysis are[1,2,3] as for follows:

$$W(t) = W_i \left(1 + bD_i t\right)^{\frac{1}{b}} \quad \ldots (1)$$

Eq. (1) corresponds to a hyperbolic decline. If b=0, the exponential decline is obtained

$$W(t) = W_i \exp\left(-D_i t\right) \quad \ldots (2)$$

Finally, if b=1 from eq. (1) the harmonic decline is obtained

$$W(t) = W_i \left(1+D_i t\right)^{-1} \quad \ldots (3)$$

The decline models given by eqs. (1) thru (3) were plotted as a set of log-log type curves in terms of dimensionless mass flow rate, W_D, and dimensionless time, t_D. The dimensionless variables are defined as follows[2]:

$$W_D = \frac{W(t)}{W_i} \quad \ldots (4)$$

$$t_D = D_i t \quad \ldots (5)$$

APPLICATION OF TYPE-CURVE MATCHING TO CERRO PRIETO WELLS.

The type-curve matching is not new; it has been applied for several years in analyzing constant rate pressure tran

sient data in both oil and gas wells[7, 8, 9] the procedure is as follows:

The field data are graphed on a tracing paper sheet having exactly the same size log-log coordinates as the type-curve. Next the field data curve is positioned over the type-curve, moving it so that the axes are kept parallel until field data match uniquely any one of the decline curves.

The final step of this procedure is illustrated in Figs. 1 thru 4 showing different types of match. The dashed lines in these graphs correspond to real coordinate axes; meanwhile, those variables within the dashed squares are real variables. Field data are shown as circles. Dimensionless coordinated axes are shown as continuous lines as well as the basic decline curves.

The type-curve analysis was applied to 18 producing wells of Cerro Prieto. They exhibited the three types of decline. Figs. 1 and 2 correspond to wells A and B that showed a harmonic type of declination. Fig. 3 illustrates the behavior of a well with a hyperbolic decline. From this figure it is evident that the last two points fall apart from the general trend, it is because of severe scale problem within the producing casing string which reduced drastically the productivity of the well. Well A exhibited an exponential decline as is evident from Fig. 4. Sometimes it is not possible to obtain a unique match of all of the field data points with a single curve as is illustrated in Fig. 5. The behavior of this well is believed to be due to a slowly increasing scale build-up at either the casing producing string or at the slotted linner.

The main advantage of the procedure described in this paper is that production forecasting is made by extending the line drawn through the field data points according to the dimensionless curve from the basic type-curve that uniquely matched the data points. Future production rates corresponding to any time are read directly from the real axes. The application of decline curve procedures, both the one described in this paper and that used in Reference 1, to Cerro Prieto wells on a monthly basis during 1977, produced results that agreed within 6.8 per cent for both steam and total mixture production, between the rates predicted from the theory to the production rates actually measured in the field.

NOMENCLATURE

b = decline curve exponent,

D_i = initial decline rate, t^{-1}.

t = real time, (months for t_D)

t_D = dimensionless time, (eq. 5)

W_i = initial mass flow rate, ton.

$W(t)$ = mass flows rate at time t; ton.

W_D = dimensionless mass flow rate, ton.

REFERENCES

1. Rivera, R.J.: "Decline Curve Analysis A Useful Reservoir Engineering Tool for Predicting the Performance of Geothermal Wells", Geothermal Resources Council, TRANSACTIONS, Vol. I (May, 1977), 257-259.

2. Fetrovich, M.J.: "Decline Curve Analysis Using Type Curve Analysis", Paper SPE 4629 presented at the 48th Annual Fall Meeting of the Society of Petroleum Engineers of AIME, Las Vegas, Nevada, Sept. 30-Oct. 3, 1973

3. Arps, J.J.: "Analysis of Decline Curves", Trans: AIME (1945) 160, 228 247.

4. Slider, H.C.: "A Simplified Method of Hyperbolic Decline Curve Analysis", Jour. Pet. Tech. (March, 1968) 235.

5. Gentry, R.W.: "Decline Curve Analysi Jour. Pet. Tech. (January, 1972) 38

6. van Everdingen, A.F. and Hurst, W: "The Application of the Laplace Transformation to Flow Problems in Reservoirs", Trans. AIME (1949), 186 305-324.

7. Ramey, H.J., Jr., Kumar, A. and Gulati M.S.: "Gas Well Test Analysis Under Water-Drive Conditions, Monogrpah American Gas Association (1973).

8. Agarwal, R., Al-Hussainy, R. and Ramey, H.J., Jr.: "An Investigation of Wellbore Storage and Skin Effect in Unsteady Liquid Flow: I. Analytical Treatment", Soc. Pet. Eng. Jour. (Sept., 1970) 279.

9. Earlougher, R.C., Jr.: "Advances in Well Test Analysis", SPE Monograph Series Vol. 5., Society of Petroleum Engineers, Dallas, Texas (1977).

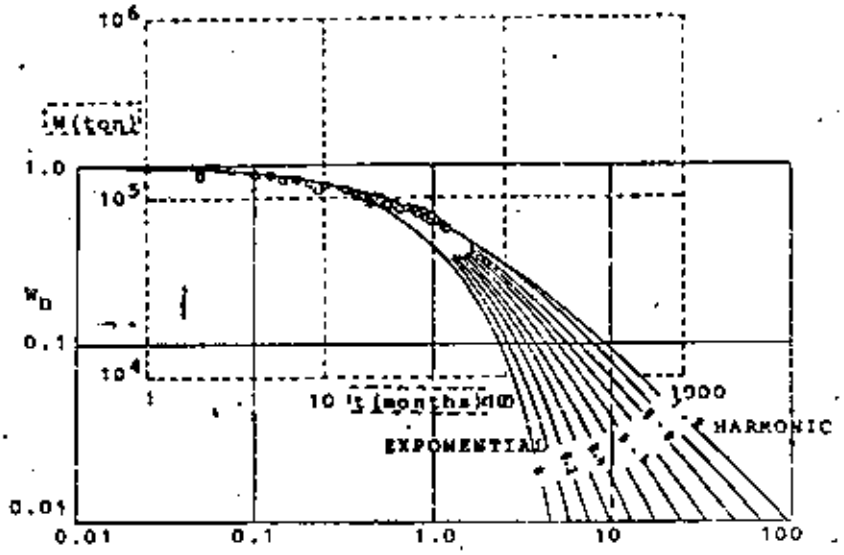

Fig. 1 Type-curve matching for well A
------ Graph on real variables, W vs. t
——— Basic graph on dimensionless variables, W_D vs. t_D
o Field data points

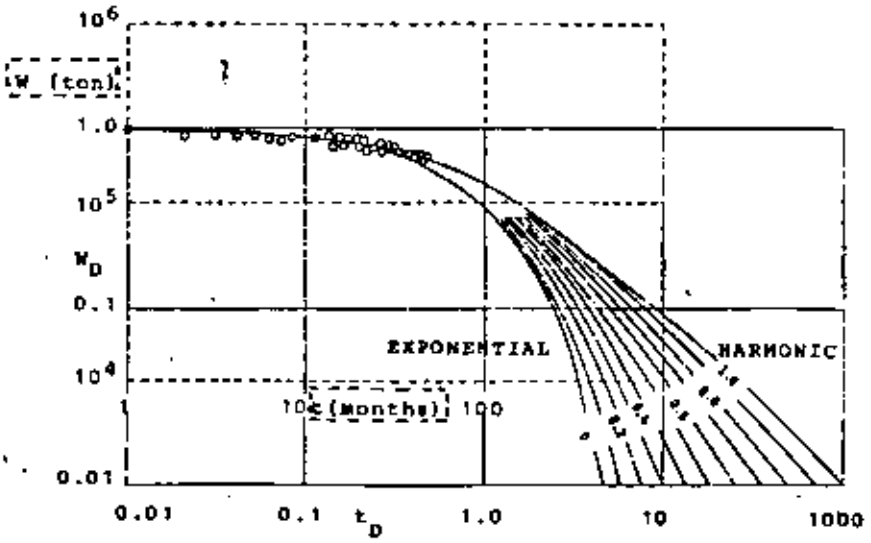

Fig.2 Type-curve matching for well B
---- Graph on real variables, W vs. t
——— Basic graph on dimensionless variables, W_D vs. t_D
o Field data points

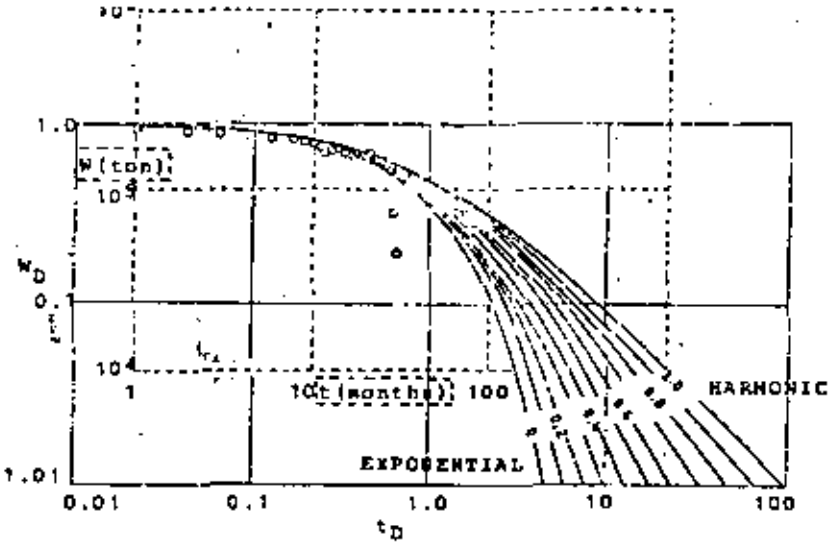

Fig. 3 Type-curve matching for well C
----- Graph on real variables, W vs. t
——— Basic graph on dimensionless variables, W_D vs. t_D
o Field data points

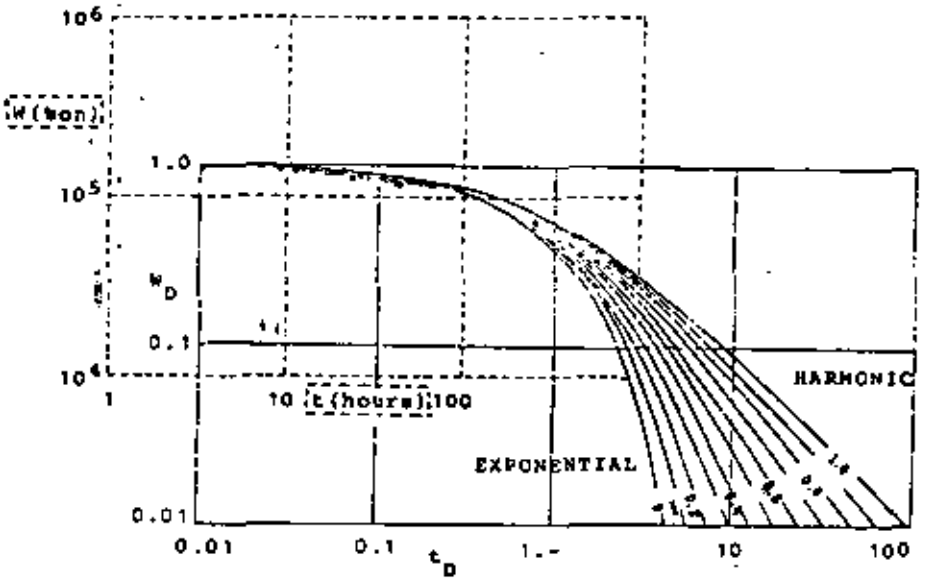

Fig. 4 Type- curve matching for well D
----- Graph on real variables, W vs. t
——— Basic graph on dimensionless variables, W_D vs. t_D
o Field data points.

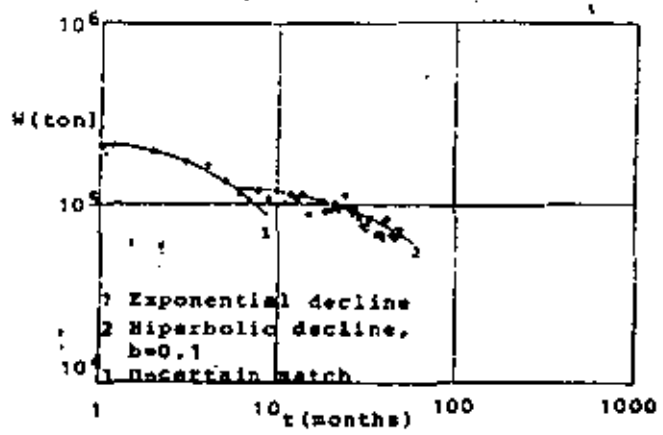

Fig. 5 Type-curve matching for well R.
o Field data points

Geothermics, Vol. 9, pp. 209–212
Pergamon Press Ltd. 1980. Printed in Great Britain.

0375–6505/80/1101–0209 $02.00/0

PRELIMINARY STUDIES OF BRINE REINJECTION AT THE CERRO PRIETO GEOTHERMAL FIELD

J. RIVERA R.,* S. MERCADO G.† and C. F. TSANG‡

Comisión Federal de Electricidad, México, D. F. Mexico, †Instituto de Investigaciones Eléctricas, Cuernavaca, Morelos, Mexico and ‡Lawrence Berkeley Laboratory, University of California, Berkeley, California, U.S.A.

Abstract—At the present time, Units 1 and 2 of the Cerro Prieto power plant generate 75 MW of power. For this purpose, about 2200 t/h of fluids are produced. Of this, 700 t/h of steam are sent to the plant and 1500 t/h of spent brine are discarded into an evaporation pond.

The thermal energy extracted is estimated to be on the order of 723×10^6 cal/h, of which about 260×10^6 cal/h is lost with the discarded water to the atmosphere. If, instead of disposing this water, it were possible to recirculate it by sending it back into the reservoir, most of the energy presently dissipated into the atmosphere could be returned underground. Reinjection would also lengthen the productive life of the reservoir because it would constitute an additional source of fluid recharge. Furthermore, reinjection of separated brines would solve the problem of surface disposal. About 1500 t/h of brine are presently sent to the evaporation pond, and the problems will become more acute when units 3 and 4, each with a 37.5-MW capacity, go on line in mid-1979. At present, a number of studies are being conducted to evaluate alternative methods of injection. The methods being considered are: cold or hot injection with open, closed or mixed systems.

For each of these systems, laboratory tests will be carried out using columns packed with different grain-sized sands. The sands used are from alluvial fans of the Cucapa range. The purpose of these tests is to establish the scale-forming tendencies of the water when injected under different conditions (Figs. 1–3. Later, similar tests will be made on models built with natural sandstones.

Because of its favorable characteristics, well M-6 (see Fig. 1) might be used in a pilot injection field test. The feasibility of reinjecting into two different levels, at 300 m, and between 527 and 741 m depth, is being evaluated. Other possible wells for reinjection could be M-3 and M-7.

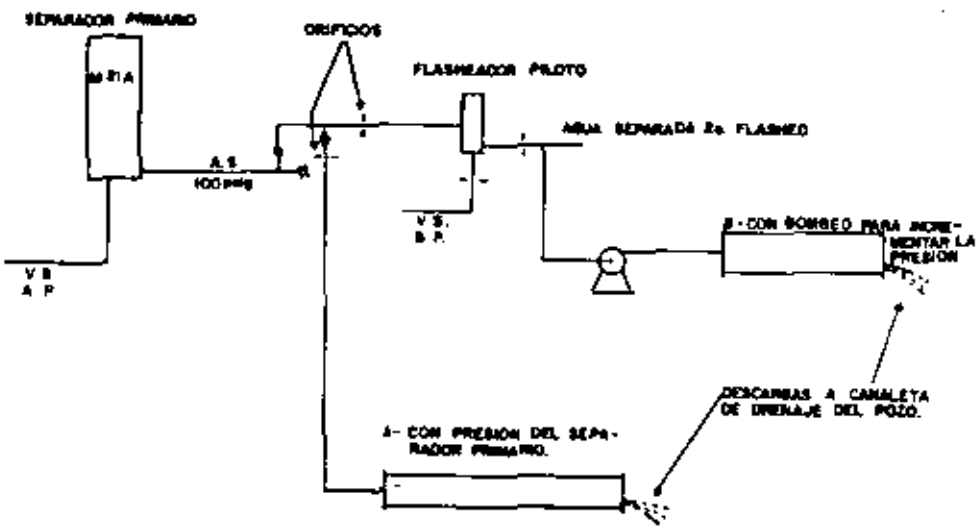

Fig. 1. Flow diagram of scaling tests in "artificial sand layers" in well M–21A, using hot water.

PROGRAM DESCRIPTION

The injection of brine into a geothermal field presents several problems that must be thoroughly evaluated before proceeding with a pilot test. This is necessary to avoid either

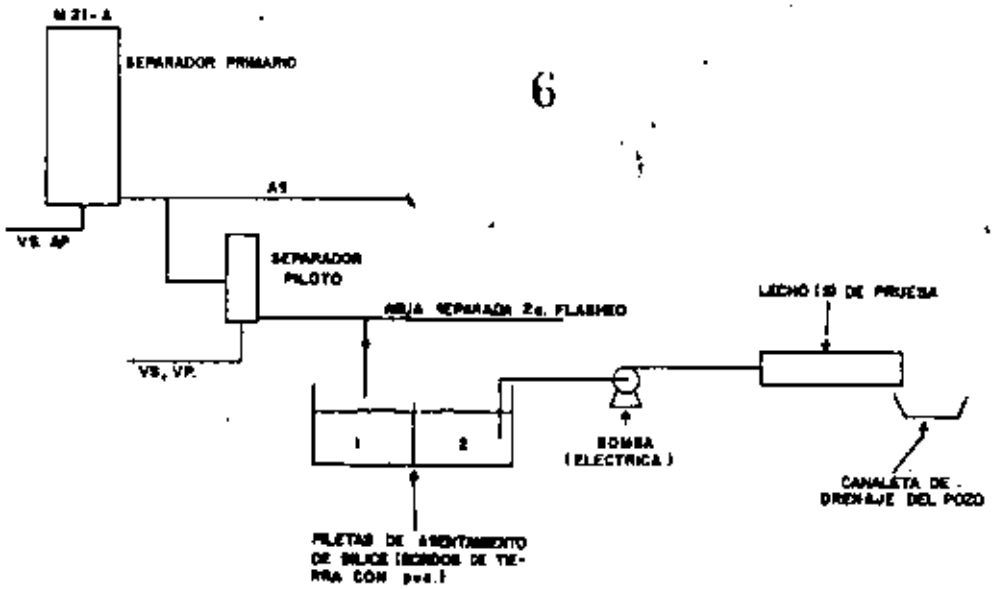

Fig. 2 Flow diagram of scaling tests in sand beds using cold separated water from which silica has been removed by settling.

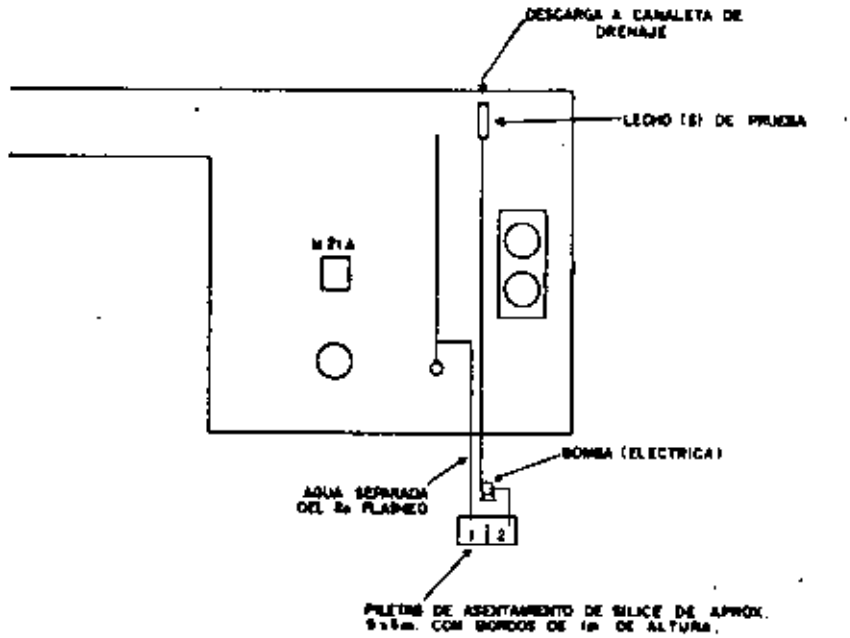

Fig. 3. General arrangement of scaling tests in sand layers in sand beds using water from which silica has been removed by settling.

lowering the production temperature of the reservoir, or plugging certain parts of it due to the chemical precipitation in the rock matrix from reactions between the injected and the reservoir water. Figures 4 – 6 show tentative sketches of the proposed apparatus for the first tests.

The process of injecting water into a reservoir is not new. For several decades the oil industry has used water injection in the secondary recovery of hydrocarbons (Rivera, 1977). It is, therefore,

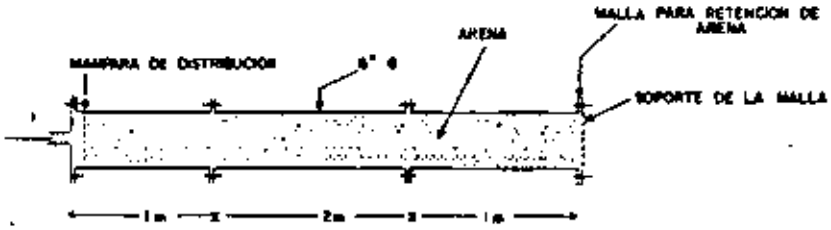

Fig. 4. Sand bed (spool type) for scaling tests and transversal examination.

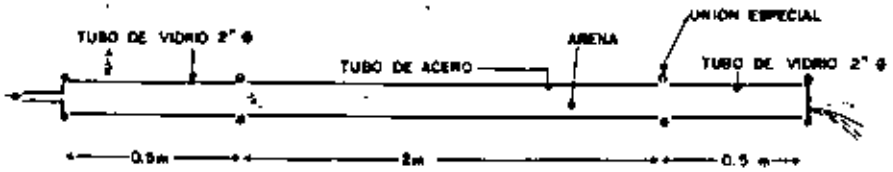

Fig. 5. Test bed for continuous observation.

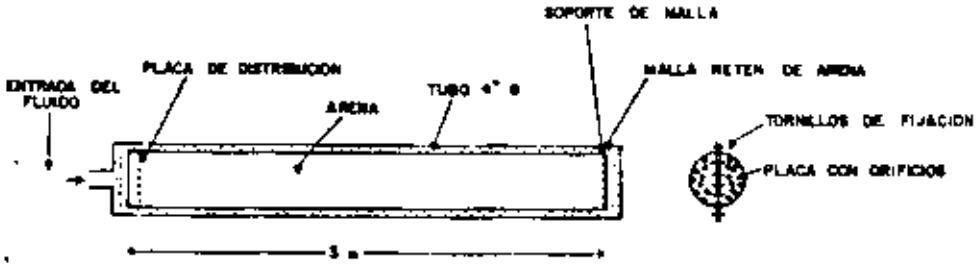

Fig. 6. Half-round type test bed for longitudinal observations.

possible to identify some common problems of water injection in both oil fields and geothermal systems. It is also important to recognize some basic differences between the two processes. Among the differences are: (a) the development of separate thermal and chemical fronts in the geothermal reservoir when brine is injected; and (b) the differences in the concentration and temperature of brines from oil fields and those produced in geothermal fields. For a system such as Cerro Prieto, which has both intragranular and fractured permeability and porosity, the basic problems are the following:

(1) corrosion of the surface installations and in the well (Uhligh, 1948);
(2) harmful effects of sulfur, iron and sludge-forming bacteria, if the injection is an open one (Armstutz and Reynolds, 1963);
(3) chemical precipitation in the surface pipes, when the effluents of several wells producing from different horizons are mixed;
(4) chemical precipitation in the porous structure of the reservoir due to incompatibility between the injected and the reservoir water;
(5) possible reduction in the permeability of the rock in the reservoir due to the swelling and/or dispersion of clays present (Jones, 1964; Hewitt, 1963).

More detailed studies are being carried out in order to be able to determine as many variables as possible before undertaking a pilot field test.

REFERENCES

Amstutz, R. W. and Reynolds, L. C. (1963) Engineering aspects of waterflood bacteriology. *J. Pet. Tech.* 1073.
Hewitt, C. H. (1963) Analytical technique for recognizing water sensitive reservoir rocks, *J. Pet. Tech.* 813.
Jones, F. O. (1964) Influence of chemical composition of water on clay blocking of permeability. *J. Pet. Tech.* 441.
Rivera, R. J. (1977) *Class Notes on Secondary Recovery of Hydrocarbons by Waterflooding*, Graduate Division, School of Engineering, University of Mexico.
Uhlig, H. H. (1948) *Corrosion Handbook*. Wiley, New York (1948).

9

DR. JESUS RIVERA RODRIGUEZ

LA INGENIERIA DE YACIMIENTOS GEOTERMICOS

por

Fernando Samaniego V. — División Fuentes de Energía Instituto de Investigaciones Eléctricas.

Jesus Rivera R. — Gerencia General de Estudios e Ingeniería Preliminar, Comisión Federal de Electricidad.

INTRODUCCION

La historia de la ingeniería de yacimientos se inicia alrededor de 1930, cuando se empezaron a realizar mediciones de los volúmenes de fluidos producidos mediante pozos perforados, además de estimaciones de las propiedades del fluido y de la roca del yacimiento por medio de mediciones de laboratorio y de registros eléctricos! Este avance acelerado en relación con la medición de propiedades de los fluidos y de la roca fue el resultado de un desarrollo rápido de la tecnología relacionada con este problema. La evaluación de yacimientos en teoría se inició con la perforación del primer pozo petrolero en 1859, pero en la práctica esto aconteció en la década de 1940 con la publicación de estudios clásicos sobre el flujo de fluidos en medios porosos[2].

El objetivo principal de la ingeniería de yacimientos es el de explotar el campo geotérmico en forma óptima. El término óptimo aplicado en este sentido, generalmente está relacionado con el punto de vista económico.

La ingeniería de yacimientos geotérmicos incluye actividades que se inician con la localización de los pozos, registros geofísicos y mediciones durante la perforación, y finalmente el cálculo de potencial del campo y predicción de su comportamiento para diversas alternativas de explotación.[3,4,5] La ingeniería de yacimientos geotérmicos puede considerarse una interfase entre los trabajos de exploración geológica y geofísica y la utilización de los fluidos producidos.

El trabajo realizado en ingeniería de yacimientos se realiza en forma contínua durante toda la vida productiva del campo geotérmico. En un principio se hace en base a modelos simplificados, dado que la información disponible acerca del yacimiento es reducida. Conforme el número de pozos y en general, la información acerca del yacimiento aumenta, se efectuan evaluaciones cada vez más exactas del potencial del campo, utilizando modelos más complejos.

CLASIFICACION DE LOS SISTEMAS GEOTERMICOS

Es posible encontrar los recursos geotérmicos en varias formas en la naturaleza, siendo las principales los yacimientos de vapor dominante, yacimientos de agua caliente, sistemas geoprezurizados y en formaciones compuestas por roca seca muy caliente.

Cada una de estas formas presenta potencial para su explotación, pero los yacimientos de vapor ofrecen las mejores características para la generación de electricidad[6]. La tecnología disponible en la actualidad para la generación de electricidad a partir de energía geotérmica se basa en el aprovechamiento únicamente de la energía contenida en el vapor. Dentro de los requerimientos necesarios con respecto al aprovechamiento del yacimiento geotérmico se tiene que presentar las siguientes características[7]: a) su temperatura debe de ser mayor o igual a 200°C, b) estar localizado a una profundidad no mayor de 3 kms, c) contener fluidos en cantidades suficientes para transmitir el calor a la superficie hasta la planta geotermoeléctrica, d) un volumen de yacimiento adecuado (mayor de 5 km^3), e) una permeabilidad tal que permita un flujo aceptable de fluidos del yacimiento hacía los pozos, y f) la presión del vapor en la superficie debe ser mayor de 7kg/cm^2, dado que es la presión mínima a la que operan la mayor parte de las turbinas actuales.

Los yacimientos de vapor son los que se buscan con mayor énfasis debido que el vapor es una fuente de energía bastante limpia desde el punto de vista de contaminación y con pocos problemas de producción. Ejemplos típicos de este tipo de yacimientos son el campo Lardarello, en Italia, y el campo Geysers, en California. Estos yacimientos se encuentran a una profundidad media de 350 m contando con una temperatura promedio de 240°C, y una presión de 35 kgs/cm^2.[7] Estos valores de presión y temperatura están relacionados con la entalpía máxima del vapor saturado (669.7 cal/gr a 236°C y 31.8 kg/cm^2).

En los yacimientos de agua caliente la fase predominante o con

tinua es el agua, y el vapor, en caso de existir, se encuentra en forma aislada en las zonas de baja presión. En la generación de electricidad por medio de la energía almacenada en este tipo de yacimientos se emplea el vapor que se separa del agua en la superficie a ciertas condiciones de presión, el cual es función de la presión de operación de las turbinas de la planta. No obstante que este tipo de yacimientos poseen un contenido bastante más alto de energía que los de vapor, los problemas inherentes para su producción y su utilización en la superficie son más complejos originando que la energía aprovechable sea menor que la correspondiente a un sistema de vapor dominante. Una dificultad con respecto al flujo en este tipo de yacimientos es cuando se alcanzan condiciones de flujo de dos fases (agua y vapor), provocando una posible depositación de sales que originalmente se encontraban disueltas en el agua caliente, lo cual produce una disminución en las condiciones originales de permeabilidad.

Los yacimientos geotérmicos pueden clasificarse de acuerdo a la localización de su temperatura y presión inicial con respecto a un diagrama presión-temperatura para el agua. La fig. 1 muestra un diagrama de este tipo, mostrando el punto crítico del agua y otros cinco puntos que representan posibles condiciones iniciales para un yacimiento geotérmico. En el caso de sistemas de agua caliente, la curva de saturación debe corresponder a una salmuera de composición igual a la del yacimiento. Con objeto de simplificar la siguiente discusión, se supondrá que no hay recarga de fluidos al yaci-

miento, es decir, la discusión se limita al caso más simple de un sistema cerrado.

El punto A corresponde a un yacimiento cuyas condiciones iniciales se localizan en la fase vapor. El proceso de producción causado por la expansión del vapor es aproximadamente isotérmico.

El punto B corresponde a un yacimiento cuyas condiciones iniciales coinciden con la curva de presión de vapor. En este caso, y dependiendo de las condiciones de Presión y Temperatura la producción del yacimiento puede variar desde agua saturada con vapor a vapor saturado, o cualquier mezcla de agua y vapor con una entalpia que va desde la del agua hasta la del vapor, a las condiciones específicas de presión y temperatura.

El punto C representa el caso en que un yacimiento geotérmico a condiciones iniciales contiene solamente agua caliente. Esta situación difiere de la discutida previamente para el punto A en que eventualmente al declinar la presión del yacimiento se alcanzarán condiciones que coinciden con la curva de presión de vapor. A partir de aquí, el mecanismo de producción será similar al discutido para el caso B. El flujo en el yacimiento para condiciones de presión superior a la presión de vapor es aproximadamente isotérmico e isoentálpico.

Los puntos D y E representan dos posibles condiciones iniciales adicionales. Los dos puntos representan condiciones de presión superiores a la presión crítica. El punto D está a una temperatura más elevada que la crítica, y representa un yacimiento geotérmico el cual al declinar la presión, alcan

zará condiciones similares a la del yacimiento de vapor cuyas condiciones iniciales están dadas por el punto A. Un yacimiento geotérmico cuyas condiciones iniciales están dadas por el punto E al declinar la presión, como consecuencia de la producción de fluido, eventualmente su mecanismo de producción será semejante al discutido para los puntos C y B. Un punto muy importante en cuanto a la producción de electricidad a partir de la energía geotérmica es el estado de los diversos sistemas geotérmicos en relación a la tecnología, problemas ecológicos y el no menos importante factor económico. La Tabla 1 presenta este tipo de datos para los diferentes sistemas geotérmicos. Una conclusión importante es que el grado de conocimiento es mayor para los recursos limitados y menor para las potencialmente grandes.

Tabla 1

ESTADO ACTUAL DE LOS SISTEMAS (YACIMIENTOS) GEOTERMICOS.

SITUACION / SISTEMA	TECNOLOGIA	PROBLEMAS ECOLOGICOS	ASPECTOS ECONOMICOS	RESERVAS
VAPOR	ESTABLECIDA	MINIMOS	ATRACTIVO	LIMITADA
AGUA CALIENTE	ESTABLECIDA PARCIALMENTE	POTENCIALMENTE GRANDES	CONDUCIDO PARCIALMENTE	LIMITADA PERO SIGNIFICANTE EN ALGUNOS PAISES
ROCA SECA	PRACTICAMENTE NO-EXISTE	DESCONOCIDO	DESCONOCIDO	POTENCIALMENTE GRANDES
GEOPRESURIZADOS	PRACTICAMENTE NO-EXISTE	DESCONOCIDO	DESCONOCIDO	DE IMPORTANCIA LOCAL

ANALISIS DE PRUEBAS TRANSITORIAS DE PRESION EN POZOS GEOTERMICOS.

El objetivo esencial en el análisis de pruebas de presión en pozos es el de determinar en forma indirecta una o más de las propiedades del yacimiento. Los datos de presión necesarios para el análisis se obtienen registrando la presión del pozo contra el tiempo después de que se produce un cambio en el gasto del pozo..

Para llevar a cabo el análisis de las presiones de fondo registradas, es importante el seleccionar u obtener una expresión matemática adecuada que pueda emplearse para propósitos de interpretación y análisis. En la obtención de esta expresión matemática se tienen que emplear las leyes físicas adecuadas para el caso, y resolverlas simultáneamente de acuerdo a las condiciones del problema en cuestión.

Para la caracterización correcta de un yacimiento geotérmico es importante que sus propiedades, permeabilidad, porosidad y compresibilidad, sean determinadas a las condiciones reales de presión, temperatura y saturación existentes en el yacimiento![10,11] Estas propiedades pueden también estimarse en el laboratorio empleando una muestra (núcleo) de la roca del yacimiento, pero los resultados obtenidos no son necesariamente confiables por varios motivos, entre ellos que la muestra representa una fracción infinitesimal con respecto al tamaño del yacimiento y a los posibles cambios que ésta pueda experimentar al pasar de condiciones del yacimiento a condiciones del laboratorio. El análisis de las presiones

registradas en los pozos permite obtener estos parámetros a las condiciones reales del yacimiento. Además de estos parámetros del yacimiento anteriormente mencionados, por medio del análisis de presiones también se puede estimar la necesidad de estimulación del pozo, y si se lleva a cabo, determinar si esta fue o no satisfactoria; el grado de comunicación (interferencia) entre los pozos; presión promedio en el área de drene del pozo o en el yacimiento; dimensión del yacimiento; etc.[12,13,14].

Los tipos más comunes de pruebas de presión para pozos de producción o de inyección son las siguientes:

a) Pozos de producción

1).- Prueba de decremento de presión

2).- Prueba de incremento de presión

3).- Pruebas de decremento a dos gastos

b) Pozos de inyección

1).- Pruebas de inyectividad

2).- Pruebas de decremento en pozos de inyección.

La Fig. 2 muestra la variación del gasto másico W y la correspondiente variación de la presión p_w para el caso de las pruebas en pozos de producción.

La Fig. 2.a presenta resultados para una prueba de decremento de presión, en la cual el pozo produce con un gasto constante W. La Fig. 2.b muestra resultados para una prueba de incre

mento de presión, en la cual el pozo produjo con un gasto W hasta cerrarse a un tiempo t_p. En la Fig. 2.c se presentan resultados para una prueba de decremento a dos gastos; el pozo produce con un gasto W, hasta un tiempo t el cual se cambia su gasto a W_2.

En las pruebas de presión discutidas previamente solamente se emplea un pozo. Hay pruebas llamadas múltiples en las cuales interviene más de un pozo, como son las de interferencia o las pulsantes. Este tipo de pruebas se emplea para cuando se desea conocer el grado de comunicación o interferencia entre los pozos del yacimiento o datos tales como la porosidad, la cual no puede obtenerse de pruebas que emplean un solo pozo.

Las técnicas de análisis de pruebas transitorias de presión han sido desarrolladas principalmente en las disciplinas de ingeniería petrolera y geohidrología. La aplicabilidad de estas técnicas a la ingeniería de yacimientos geotérmicos ha sido satisfactoriamente demostrado.[15,16, 17, 18, 19]

La información que se obtiene del análisis de pruebas de presión acerca de los parámetros del yacimiento es muy útil para los estudios de predicción del comportamiento de yacimientos geotérmicos.

SIMULACION DE YACIMIENTOS GEOTERMICOS

El propósito de la simulación es el de estimar el comportamiento del yacimiento geotérmico bajo diversas condiciones de producción.[20] El yacimiento en sí sólo puede producirse

una vez, al contrario del modelo matemático que describe el proceso de flujo en el yacimiento, el cual puede "producirse", o sea, correrse por medio de una computadora digital las veces que sea necesario. El costo involucrado en una simulación de "producción" es generalmente bajo, además de que se lleva a cabo en un tiempo relativamente corto. Por medio del comportamiento del yacimiento predicho con el modelo para diferentes condiciones de producción, se pueden seleccionar las condiciones óptimas de producción del yacimiento. Dentro del tipo de información que se puede obtener de la simulación de un yacimiento geotérmico se tiene la siguiente:

a) Efectos de la localización y espaciamiento de los pozos en la producción.
b) Efecto del gasto de los pozos en la extracción de energía.
c) Capacidad de producción del yacimiento para un cierto número de pozos localizados en puntos específicos del yacimiento.
d) Factibilidad de reinyección de fluidos, tanto cuantitativamente como la localización de los pozos inyectores más adecuada.

Los modelos matemáticos para la simulación del comportamiento de yacimientos geotérmicos pueden clasificarse en dos categorías mayores: a) modelos simplificados, y b) modelos avanzados.

En general, la regla comun en la simulación de sistemas en general, y de yacimientos en particular, es el emplear el modelo más simple que ajuste (reproduzca) su comportamiento.

Por modelos simplificados de yacimientos geotérmicos se entiende aquellos que pueden resolverse en forma sencilla, por ejemplo, haciendo uso de una calculadora de mano. Dentro de los modelos simplificados se tiene el modelo de cero dimensión. Este es un modelo de balance de materia y de energía el cual considera valores promedio para las propiedades tanto del medio poroso como del fluido. La Fig. 3.a muestra un modelo de este tipo. A estos modelos se les conoce con el nombre de cero dimensión debido a que las propiedades del medio poroso y del fluido, además de la presión, no dependen de la posición, en el yacimiento. Este modelo es el elemento básico de los modelos (simuladores) más avanzados para la predicción del comportamiento de yacimientos geotérmicos.

Otro tipo de modelo simplificado son las curvas de declinación, las cuales están basadas en modelos que describen la declinación de la producción. Su aplicación a yacimientos geotérmicos ha sido exitósamente probada.[21,22].

Dentro de los modelos avanzados se tienen los modelos numéricos para la predicción del comportamiento de yacimientos geotérmicos. Estos modelos son soluciones aproximadas a los modelos matemáticos que describen el flujo de los fluidos en el yacimiento. Este tipo de solución es necesaria debido a que el sistema de ecuaciones diferenciales en derivadas parciales que describe el flujo de fluidos en un yacimiento geotérmico, es no lineal, además de la dificultad para definir en forma matemáticamente exacta las fronteras del yacimiento.

El modelo de una dimensión Fig. 3.b sigue en cuanto a comple-

jidad al modelo de una celda (modelo de cero dimensión) en una dirección y sólo una en las dos dirección restantes. En forma similar, los modelos de dos dimensiones (Fig. 3.c) están compuestos por más de una celda en dos direcciones y solo una en la dirección restante. Finalmente, los modelos de tres dimensiones (Fig. 3.d) están compuestos de más de una celda en las tres direcciones.

Conforme al modelo empleado para una predicción es más complejo, mayor será el esfuerzo y el tiempo necesario para llevar a cabo el estudio. El costo involucrado en el estudio de predicción está directamente relacionado con el número de dimensiones del modelo empleado y el número de celdas que componen el modelo.

Una de las más importantes involucradas en la simulación del comportamiento de yacimientos geotérmicos es el grado de exactitud de los datos del yacimiento y de sus fluidos que se proporcionan al simulador. Existe una frase muy empleada en el idioma inglés la cual sintetiza la magnitud e importancia de este problema: "Garbage in, Garbage out"[23,24] O sea, si se desea llevar a cabo un estudio de predicción de aproximación aceptable, se debe de disponer de buenos datos. Con respecto a las características del yacimiento, el análisis de pruebas transitorias de presión aplicado en forma correcta y adecuada proporciona la mejor fuente de información.

NECESIDADES DE INVESTIGACION

La ingeniería de yacimientos geotérmicos comenzó a aplicarse

hace alrededor de 15 años. Uno de los primeros estudios fue el presentado por Ramey para el campo Geysers en 1968[4], y el de Whiting y Ramey[8] para el campo Wairakei en Nueva Zelandia en 1969. Después de estos estudios iniciales, la literatura relacionada con este aspecto de la geotermia ha avanzado rápidamente, debido al número importante de publicaciones que han aparecido en los últimos años.

La ingeniería de yacimientos ha sido desarrollada extensamente en otras disciplinas, como es el caso de la ingeniería petrolera. Estos conocimientos pueden aprovecharse en la ingeniería de yacimientos geotérmicos si las diferencias inherentes entre los dos tipos de sistemas se considera en forma adecuada.[4,8]

Un parámetro que complica el estudio de los yacimientos geotérmicos es la alta temperatura. Esto hace difícil el obtener datos de interés para estudios de ingeniería de yacimientos, como son temperatura y presión en el fondo del pozo. Actualmente se está llevando a cabo investigación relacionada con instrumentación que pueda resistir estas altas temperaturas existentes en el fondo del pozo, con objeto de obtener mediciones "in situ" por un período prolongado. Tambien, se está estudiando el efecto de este parámetro en las propiedades de los fluidos y de la roca, las cuales son necesarias para la correcta descripción del flujo de fluidos en el yacimiento.

Con respecto a problemas de análisis de pruebas transitorias de presión y de simulación de yacimientos, se ha considerado

que el fluido en el yacimiento es agua, en cualquiera de sus fases, líquido o vapor. Un factor muy importante el cual en este tipo de estudios no ha sido considerado es la presencia de altas concentraciones de sólidos, hasta 30 % en peso, especialmente sílice que con frecuencia se tienen en el agua caliente, los cuales influyen en el flujo de fluidos en el yacimiento. Este problema es particularmente importante cuando se alcanzan condiciones de saturación en el yacimiento, y se tienen dos fases fluyendo, agua y vapor. Esto causa depositación de sólidos en el medio poroso, disminuyendo la permeabilidad y la porosidad de la roca. El problema de depositación puede presentarse también en las operaciones de reinyección de fluidos al yacimiento, la cual se emplea para mejorar la recuperación de la energía del yacimiento, así como para resolver el problema de desecho de los fluidos producidos.

Los factores mencionados anteriormente, temperatura y contenido de sólidos, constituyen dos ejemplos de los problemas que deben de estudiarse con detenimiento si se desea tener una idea más exacta acerca del comportamiento de los yacimientos geotérmicos. Otras áreas de estudio que requieren atención son la de extracción de energía de roca seca, la cual posee un gran potencial como fuente de energía geotérmica, y la relacionada con la explotación y aprovechamiento de los sistemas geopresurizados, en los que además de la energía térmica se dispone de energía mecánica, así como de un alto porcentaje de gas asociado.

CONCLUSIONES

En este trabajo se han revisado los conceptos básicos que intervienen en la ingeniería de yacimientos geotérmicos. El empleo correcto de estas ténicas permite calcular en forma confiable el potencial de un campo geotérmico y predecir su comportamiento para diversas alternativas de explotación. Por medio de los estudios de predicción se puede seleccionar la alternativa de explotación óptima para el yacimiento geotérmico, permitiendo que la inversión realizada para su explotación redítde en el mayor provecho posible.

REFERENCIAS

1. Moore, T.V.: "Reservoir Engineering Begins Second 25 Years", The Oil and Gas Journal, Noviembre 21, 1955, pp. 148-151.

2. van Everdingen, A.F., y Hurst, W.E.: "The Application of the Laplace Transformation to Flow Problems in Reservoirs", Trans., AIME (1949) 186, p. 305-324.

3. Takahashi, P.K. y Chen, B.: "Geothermal Reservoir Engineering", Geothermal Energy Magazine (Oct., 1975) p. 7-22.

4. Ramey, H.J., Jr.: "A Reservoir Engineering Study of the Geysers Geothermal Field", presentado a Reich and Reich, Petiotioners vs. Comissioner of Internal Revenue, 1969 Tax Court of the United States, 52. T.C. No. 74, 1970.

5. Takahashi, P.K., Chen, B.H., Mashima, K.I., y Seki, A.S.: "State of the Art of Geothermal Reservoir Engineering", American Society of Civil Engineers, Journal of the Power Division (July, 1975) 101 (1), p. 111-126.

6. Ramey, H.J., Jr., Kruger, P. y Raghavan, R.: "Explosive Stimulation of Hydrothermal Reservoirs", publicado en Geothermal Energy, Stanford University Press, Stanford Ca. (1973).

7. White, D.E.: "Characteristics of Geothermal Resources", publicado en Geothermal Energy, Stanford University Press, Stanford Ca. (1973).

8. Whiting, R. L., y Ramey, H.J., Jr.: "Applications of Material and Energy Balances to Geothermal Steam Production", J. Pet. Tech. (Julio, 1969), p. 893-900.

9. Davis, W. K., y Golan, S.: "The New Energy Sources", Industrial Research (Nov. 15, 1974) p. 8-15.

10. Samaniego V., Fernando; y Pazmiño U. Jorge: "Aspectos Prácticos del Análisis Moderno de Pruebas de Presión", artículo por publicarse.

11. Samaniego V., Fernando y Cinco L., Héber: "Análisis de Presiones para Pozos Geotérmicos", presentado en el II Congreso de la Academia Nacional de Ingeniería, A. C., celebrado en Monterrey, N. L., Sept., 16-18, 1976.

12. Matthews, C. S. y Russel, D.G.: "Pressure Buildup and Flow Tests in Wells", Monografía de Society of Petroleum Engineers of AIME, Vol. I, Dallas (1967).

13. Ramey, H.J., Jr., Kumar, A., y Gulati, M. S.: "Gas Well Test Analysis Under Water Drive Conditions", American Gas Association, Arlington, Va. (1973).

14. Earlougher, R. C., Jr.: "Advances in Well Test Analysis", Monografía de Society of Petroleum of AIME, Vol. 5, Dallas (1977).

15. Ramey, H. J.,Jr.: "Pressure Transient Analysis for Geothermal Wells", Second U. N. Symposium on the Development and Use of Geothermal Resources, San Francisco (1975), Proceedings, Lawrence Berkeley Lab.,University of California.

16. Barelli, A., Manetti, G., Celati, R., y Nery, G.: "Buildup and Back Pressure Tests on Italian Geothermal Wells", Second U.N. Symposium on the Development and Use of Geothermal Resources, San Francisco (1975), Proceedings, Lawrence Berkeley Lab., University of California.

17. Ramey, H. J., Jr. y Gringarten, A. C.: "Effect of High-Volume Vertical Fractures on Geothermal Steam Well Behavior", Second U. N. Symposium on the Development and Use of Geothermal Resources, San Franciso (1975), Proceedings, Lawrence Berkeley Lab., University of California.

18. Rivera R., Jesús y Ramey, H. J., Jr.: "Application of Two-Rate Flow Tests to the Determination of Geothermal Reservoir Parameters", artículo SPE No. 6887, presentado en el "52nd. Annual Fall Technical Conference of SPE", Denver, Colo., Oct. 9-12 (1977), próximo a ser publicado en Jour. Pet. Tech.

19. Rivera R., Jesús, Samaniego V., Fernando, y Schroader, R. C.: "Pressure Transient Testing at Cerro Prieto Geothermal Field", presentado en el First Symposium on the Cerro Prieto Geothermal Field, celebrado en San Diego Ca., Sept. 20-22 (1978).

20. Cinco L., Héber, Samaniego V., Fernando, y Domínguez A., Norberto: "Métodos para Predecir el Comportamiento de un Yacimiento Geotérmico", presentado en el I Congreso de la Academia Nacional de Ingeniería, A. C., celebrado en Guanajuato, Gto., Junio 23-24, 1975.

21. Rivera, R., Jesús: "Decline Curve Analysis a Useful Reservoir Engineering Tool for Predicting the Performance of Geothermal Wells", Geothermal Resources Council, Trans., Vol. 1 (Mayo, 1977) 257-259.

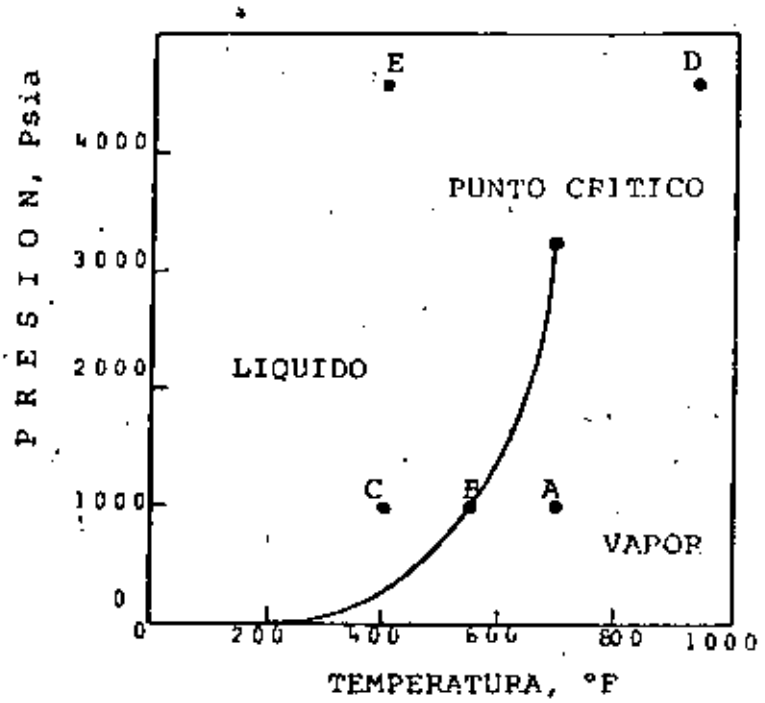

FIG. 1 DIAGRAMA PRESION - TEMPERATURA PARA EL AGUA.

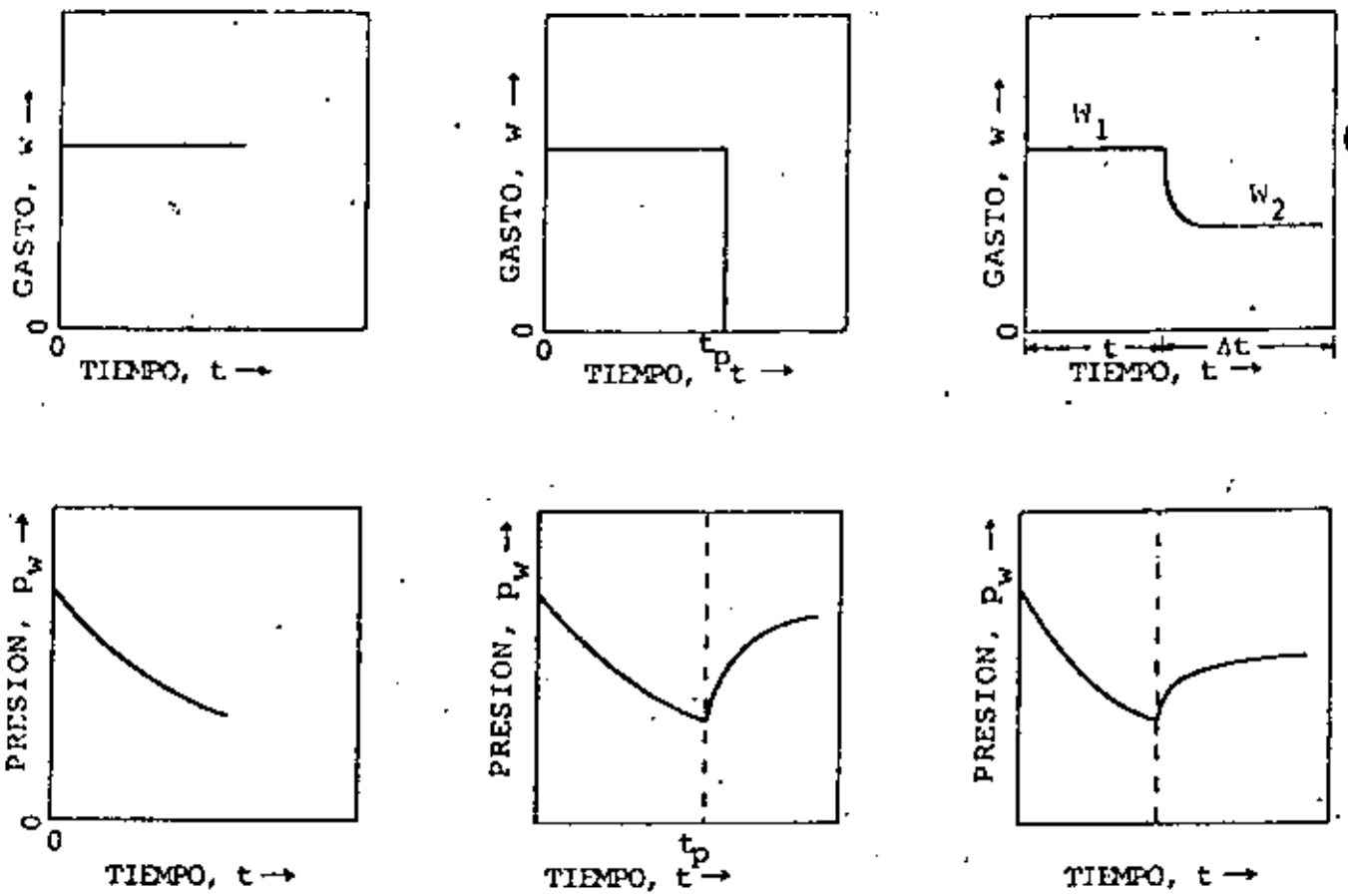

a) Prueba de decremento de presión

b) Prueba de incremento de presión

c) Prueba de decremento a dos gastos

FIG. 2 REPRESENTACION ESQUEMATICA DE LA VARIACION DEL GASTO Y DE LA PRESION DE FONDO DEL POZO.

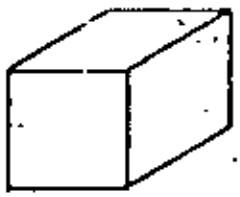

a) Modelo de cero dimensión

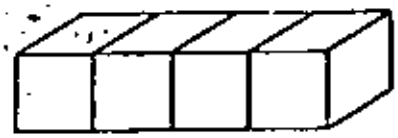

b) Modelo de una dimensión

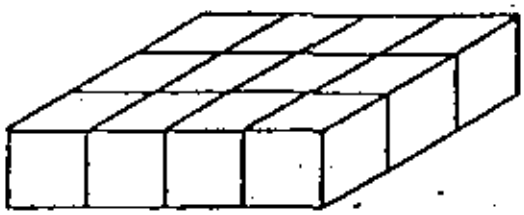

c) Modelo de dos dimensiones

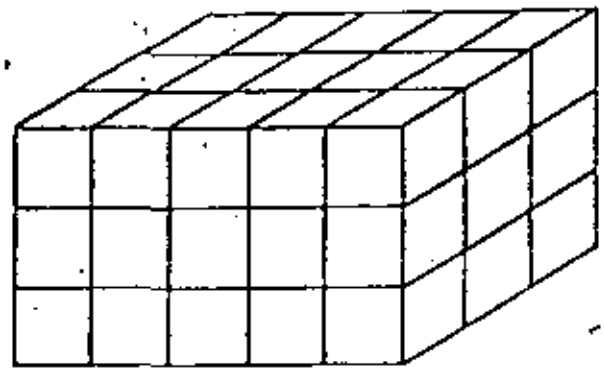

d) Modelo de tres dimensiones

FIG. 3 DIFERENTES TIPOS DE MODELOS.

GEOTHERMAL RESERVOIR ENGINEERING

Patrick K. Takahashi
University of Hawaii
Honolulu, Hawaii 96822

Bill Chen
Hilo College
Hilo, Hawaii 96720

Prepared Under
NATIONAL SCIENCE FOUNDATION
RESEARCH GRANT NO. GI-38319
And
ENERGY RESEARCH AND DEVELOPMENT
ADMINISTRATION RESEARCH GRANT
NO. E(04-3)-1093

INTRODUCTION

Activity in geothermal energy research and exploitation has recently intensified at an accelerated rate. Geothermal reservoir engineering, a once arcane and proprietary field of study, has especially begun to come of age. Why this sudden flurry of activity? No doubt the recent energy crisis provided a critical stimulus. The threat of another shortfall and higher fuel prices will serve to maintain this initial momentum.

With respect to geothermal reservoir engineering, though, one of the prime spurs has, interestingly enough, been international competition . . . or rather, cooperation. Historically, private industry in the United States has suppressed public disclosure of information on the subject. This state of affairs is no doubt an extension of traditional petro-gas practices, where "competitive edge" has been essential for the maximization of profits.

In the meantime, widespread international activity has caused an imbalance in the availability of expertise. In particular, countries such as New Zealand have gone out of their way to share their knowledge. A significant prime mover has been the United Nations, which has done a superb job of getting the world together. A ten-day United Nations Symposium on Geothermal Resources, held from May 20-29, 1975, in San Francisco, California, brought together 1300 scientific, industrial and governmental specialists to assess the current status of geothermal energy. Fifty-nine nations were represented.

This report on geothermal reservoir engineering will attempt to organize this heretofore amorphous, poorly documented area of investigation, by:

1. Crystallizing the essence of a recent survey paper (1) "State-of-the-Art of Geothermal Reservoir Engineering," which appeared in the July 1975 issue of the American Society of Civil Engineering Journal of the Power Division.

2. Summarizing the reservoir related proceedings of the United Nations Symposium, and

3. Drawing from other literature asaociated with the subject.

The report will be presented in four parts:

1. The field of geothermal reservoir engineering
2. Well testing/analysis (empirical approach)
3. Computer modelling (mathematical model approach)
4. Physical modelling

One example of a total systems study in geothermal reservoir engineering can be found in Figure 1.

GEOTHERMAL RESERVOIR ENGINEERING

Geothermal reservoir engineering can be defined to include all phases of geothermal activity beginning with the initial decision on where to place the well, to well logging during the drilling program, to well measurement, and finally, to performance prediction of the geothermal field. Simply, geothermal reservoir engineering interfaces with the initial geophysical/geological effort on one end and the actual utilization of the fluid on the other.

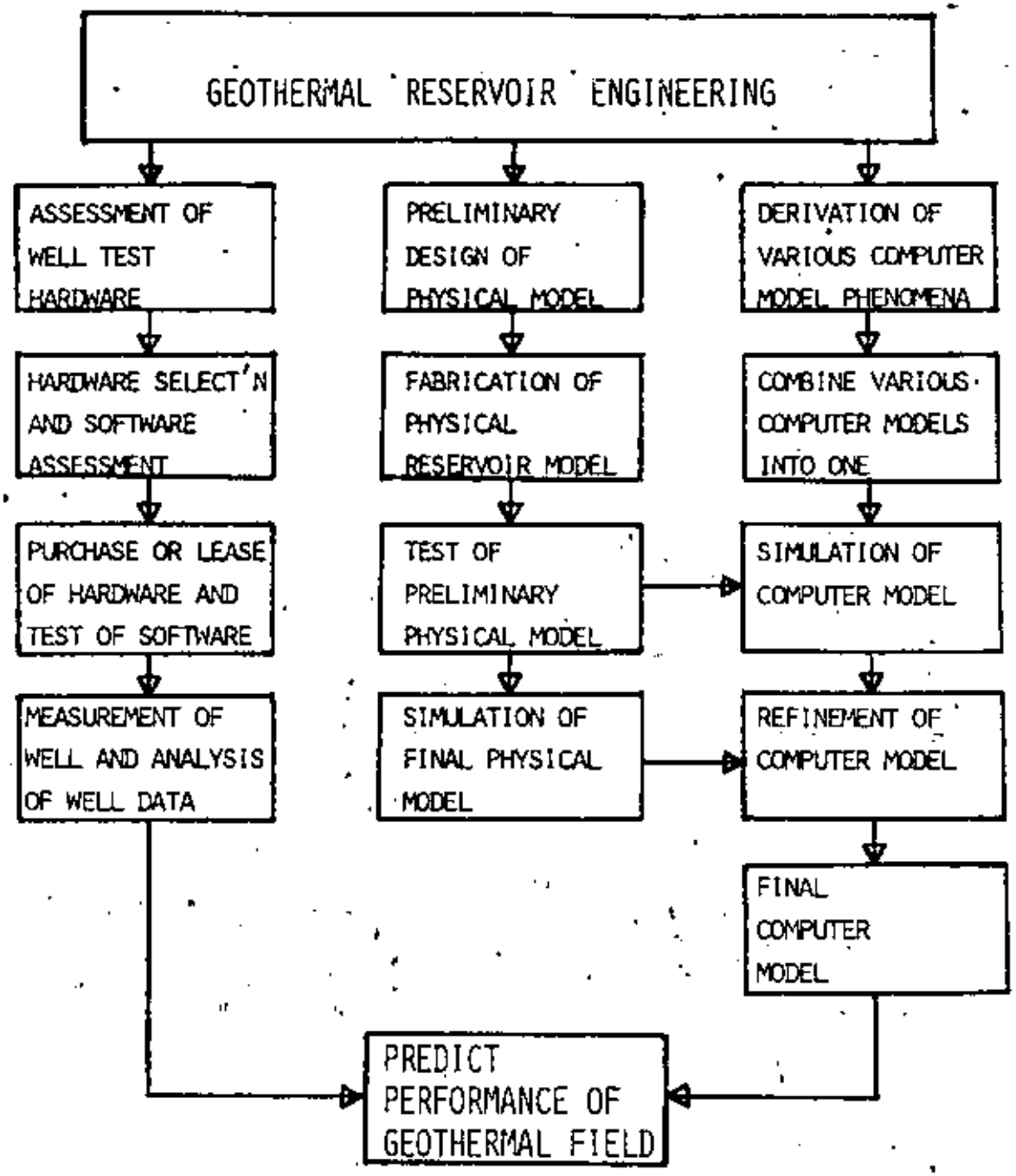

FIGURE 1. ORGANIZATIONAL PLAN FOR THE HAWAII GEOTHERMAL PROJECT TASK ON GEOTHERMAL RESERVOIR ENGINEERING

In a time perspective, the work begins quite early with mathematical and physical modelling to help predict the well sites and determine materials of construction, and continues through the entire operational life of the field, as periodic re-evaluation must be made of projected field life and optimal flow rates. Furthermore, later well stimulation efforts could be necessary.

The "state-of-the-art" in geothermal reservoir engineering is in the most part formative. Four groups in particular, though, have contributed well: New Zealand, the Bureau of Reclamation, the U.S. Geological Survey, and Stanford University. Also available are some individual investigations, as for example, Robert Whiting's reservoir engineering study of Wairakei (2).

The primary reason why the literature is relatively sparse is that private companies treat geothermal well testing, the data, and methods of analysis as proprietary. Certain legal restrictions furthermore tend to preserve this form of classification. Fortunately, there appears to be an increasing international spirit of cooperation. As mentioned earlier, the United Nations has done a remarkable job in attempting to get the world together.

Speculations on the nature of geothermal reservoirs can be found in the literature. Legally, in the United States, the U.S. Geological Survey defines a geothermal reservoir to be contained in either a known geothermal resource area (KGRA) or a potential geothermal resource area (PGRA). Geothermal reservoirs can be characterized in several other ways:

1. Depletable (self-sealed) or regenerative (recharged),
2. Physical state: vapor-steam, liquid-hot-water (normally two-phased at wellhead), solid-hot rock, liquid magma, geopressure,
3. Physical condition: temperature/pressure, size depth, production rate,
4. Degree of dissolved solid content.

There is some reason to believe that all wells are at least partially regenerative because of the meteoric (rainwater) origin of geothermal fluids (3). Furthermore, reports of measurable pressure drops in steam-dominated geothermal fields seen after rainfall lead one to suspect that perhaps fluid recharge could be significant. There seems to be no clear-cut answer to a universal definition of a geothermal reservoir.

A geothermal reservoir generally requires a heat source (magma or geopressure), needs to be confined in an aquifer, although non-permeable hot rocks can be transformed into an aquifer through hydrofracturing/thermal cracking and the addition of water, and caprock formation — to hold the hot fluid in place . . . although the latter requirement is controversial. Although vapor-dominated geothermal wells are generally contaminated with CO_2 (primarily) and H_2S, there is little dissolved solid content.

On the other hand, some of the hot water well samples in the Imperial Valley have shown as much as 30% dissolved solids by weight, and an exceptional well in the Cesana area of Italy which produced fluid containing 35% dissolved solids (8). Speculations on geothermal reservoirs have been advanced by White and Muffler (3), U.S.; Facca (4), Italy; Elder (5), New Zealand; Hayashida (6), Japan; and Yuhara (7), Japan.

George Keller, discussing results of his drilling program at Kilauea Volcano (9), concluded that evidence favored the existence of hydrothermal convection cells and, most importantly, suggested the action of self-sealing within the porous island medium.

The supposition advanced, therefore, is that Hawaiian geothermal reservoirs resemble Figure 2, with the heat source being magma at depth, which with time either: 1) induced abnormally high circulation rates resulting in flashing or thermal deposition, effectively capping the reservoir, perhaps even above sea level; or 2) intruded above the magma chamber and released energy to the surrounding aquifer, in effect forming a system composed of a cooling, vertical dike surrounded by hot fluid, which through the physical phenomenon as described in "1" has been capped into a self-sealed reservoir. In the latter case, Figure 2 needs to be modified to show a vertical low permeability formation within the convecting geothermal fluid.

Although it has been reported that hot water reservoirs are twenty times more prevalent than vapor-dominated ones (10), technical difficulties in the former have resulted in considerably more production from the latter. Table 1 shows that five vapor, eleven hot water, and two binary cycle plants are either operating or close to completion. The hot rock concept is undergoing investigation by researchers from the Los Alamos Scientific Laboratory (for New Mexico). A drill probe in Marysville, Montana recently was unsuccessful. A fourth concept, direct utilization of magma, was originally advanced by George Kennedy and David Griggs in 1960 (11).

A recent conference on volcano energy supported the reasonability of this latter scheme (12). Some preliminary work, mostly in the proposal stage, is being advanced by researchers from Sandia (New Mexico), Lawrence Livermore Laboratory, and the University of Hawaii. Finally, a fifth source could be geopressured hot brines found in the geosynclinal basin of the northern Gulf of Mexico. Water temperatures close to 200°C at 5000 meters are expected. A potential of 40,000 megawatts of power along the Texas Gulf Coast was advanced at the United Nations Symposium.

When calculating the useable energy in a geothermal reservoir, one should be aware that only 1% of the total available energy can be converted to electrical energy from a hot-water reservoir using present proven technology. The equivalent figure from a vapor-dominated reservoir is 2-5% (3). It should nevertheless be realized that on an absolute energy scale, a self-sealed liquid-dominated reservoir, per

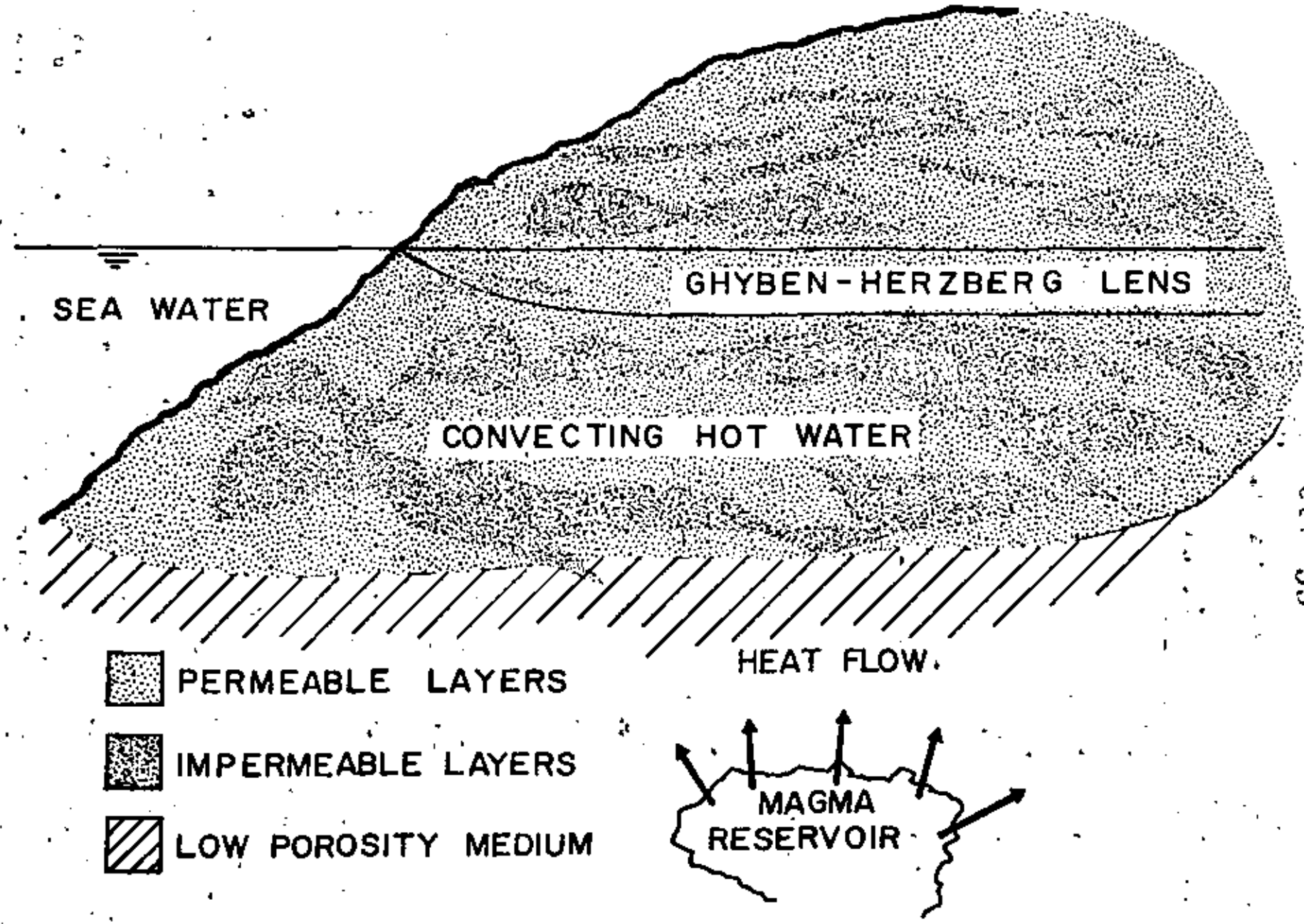

FIGURE 2. SELF SEALED;
DEPLETABLE GEOTHERMAL RESERVOIR.

TABLE 1. GEOTHERMAL PLANTS

DRY STEAM PLANTS	MW CAPACITY	INITIAL OPERATIONS
Italy		
Larderello	380	1904
Monte Amiata	28	1967
U.S.A.		
Geysers, California	502	1960
Japan		
Matsukawa	22	1966
Onikobe	25	1975
FLASHED STEAM PLANTS	**MW CAPACITY**	**INITIAL OPERATIONS**
New Zealand[1]		
Wairakei	192	1958
Kawerau	10	1969
Japan		
Otake	23	1967
Hatchobaru	50	1976
Katsukonda	50	1977
Mexico		
Pathe	3.5	1958
Cerro Prieto	70	1973
Iceland		
Krafla	70	1977
Philippines		
Tiwi	10	1969
U.S.S.R.		
Pauzhetsk	6	1967
El Salvador		
Ahuachapan	30	1975
BINARY CYCLE PLANTS	**MW CAPACITY.**	**INITIAL OPERATIONS**
U.S.S.R.		
Paratunka	1	1967
U.S.A.		
Imperial Valley, California	10-50.	Late 70's to 80's

cubic foot of reservoir, will produce more energy than a vapor-dominated one. A quick comparison of water and steam densities bears this out. Secondly, the thermal conductivity of rock precludes conduction as a mechanism for generating a geothermal well.

For example, H. Ramey has reported that the net heat recharge rate in the Big Geysers is less than 0.6% (13). However, the possibility of extraordinary fluid convection through porous medium as driven by circulating magma should not be discounted — thermal cracking of the receding, cooled magma can possibly result in high permeability. Unfortunately, unless the magma chamber is extremely large or self-sealing occurs, this energy will quickly dissipate with recharging meteoric water.

Under present economic and technical conditions a viable geothermal reservoir capable of generating electricity is generally one which: has a minimum temperature of 356°F (180°C) — to conform to current steam turbine design; is located within 10,000 feet (3,050 m) from the surface — as limited by current drilling technology; and can produce steam at a minimum rate of 40,000 lb/hr (18,120 kg/hr) with a 9-5/8 inch (24.4 cm) diameter hole.

Geothermal wells not quite satisfying the above criteria can nevertheless be used for special applications, as for example, the 158°F (70°C) binary system in the U.S.S.R., and the numerous greenhouse and other forms of direct heating uses found worldwide. Furthermore, there is every reason to believe that wells exceeding 10,000 feet (3,050 m)

will, with improved drilling technology and increasing energy fuel prices, become economically feasible.

The general nature of a geothermal reservoir is contentious. The question of its being self-sealed or regenerative has not been completely answered. The "state-of-the-art" qualitatively though, is relatively well developed compared to the quantitative, reservoir performance prediction.

WELL TESTING AND ANALYSIS

Well testing and analysis are related endeavors. This method, although appearing to be only empirical in nature, is actually well based mathematically, as the appropriate fundamental equations are first solved to facilitate graphing and quick calculations. A distinction is made between this study area and computer modelling because the latter employs advanced numerical techniques, which at this formative stage, sometimes limit real world utility. However, rapid strides are occurring.

The testing, or measurement phase, collects data or pertinent reservoir characteristics so that the nature of the reservoir can be determined by analysis. The measurements begin at the borehole with various geophysical loggings, such as electric, to determine formation resistivity and self potential, radioactivity for rock density and porosity, and acoustic for porosity. At the same time, drilling fluid and cores are analyzed for rock temperature, porosity, permeability, fluid saturation and thermal conductivity. Mud loss zones and formation changes can reveal important information. Up to and including well completion, drill-stem tests are run to obtain values of the formation pressure and temperature.

The producing well should receive both wellhead and downhole tests: initially quasi-steady state temperature and pressure surveys versus depth, followed by pressure drawdown and buildup tests. The drawdown test is a series of bottomhole pressure measurements made during a period of flow at a constant production rate. Reservoir volume, transmissivity (product of average permeability and reservoir thickness) and skin (resistance to flow at casing area) effects can be estimated. The buildup test is another series of bottomhole pressure measurements made just before and after a stepwise reduction in flowrate, or a complete shutting down of the well. Information such as the transmissivity, skin effects and flow efficiency can be estimated to aid in predicting optimal production rate and life of the reservoir.

The wellhead is continuously monitored during production to determine flowrate, energy extracted and quality and geochemistry of the fluid. If flow is two-phase, separation of liquid from steam is usually the practice. Finally, if more than one hole is drilled in the same area, well interface tests should be run to determine the reservoir connectivity, directional reservoir flow pattern, and the nature and magnitude of anisotrophic permeability.

The water pumping technique has been shown to be especially useful for hot water dominated reservoirs. New Zealand has refined this method to locate the depth of the producing zone and to obtain effective permeability.

After the well is completed and allowed to stabilize, water at a flowrate of 100 gallons per minute is pumped into the borehole. An Amerada bomb with temperature gauge is lowered into the well and the temperature is recorded versus depth. If the well temperature has a sudden increase, it means that the potential is good for utilizing the zone as a producing layer.

A second series of tests is then run at various pumping rates — 100, 200 and 300 gallons per minute — with a pressure gauge replacing the temperature gauge on the Amerada bomb. If upon a pumping rate increase from 100 to 300 gpm the pressure increase is only 20 psi, the indication is that the well formation has high permeability. A pressure increase of three figures, 100 psi or higher, means that permeability is low and the prospects for an operational well poor.

The matter of whether to use mechanical (Kuster) or electronic (Schlumberger) measurement equipment is largely an unsettled one at this time. The entire Kuster measurement package for downhole pressure, temperature and flowrate can be purchased for less than $20,000. Reliability has been good. Schlumberger electronic instrumentation is several times more expensive. In New Zealand, electronic measurement equipment has not been shown to be dependable. However, the wireline operation makes for convenient wellhead recording and presumably more accurate measurements.

In addition, there are various locally designed and specific purpose instrumentation devices available, the geothermograph being a notable example. In general, though, the high temperatures experienced in geothermal reservoirs, combined many times with high dissolved solid content, make measurement a difficult task.

An excellent overview of well-logging technology and geothermal applications was recently made available by Sandia Laboratories (14). The conclusions were:

1. Geothermal measurement requirements are not well defined due to lack of reservoir models and to log interpretation problems in unfamiliar formations.
2. Logging problems differ with geothermal well type.
3. Attempts to log geothermal wells to date often have met with marginal success.
4. Geothermal wells usually exhibit temperatures higher than normally encountered (175°C/ 350°F) in oil and gas wells.
5. Maximum claimed temperature capability of well-logging equipment is presently about 260°C (500°F). Many geothermal wells are hotter than that.
6. Special corrosion problems may be encountered in geothermal wells resulting from high

temperature and the varied natures of geothermal fluids.

7. Large-scale geothermal well-logging, such as is implied by Project Independence goals, should be done by private industry.
8. There is insufficient economic incentive at present for private industry to provide adequate geothermal logging capability.
9. Government support of geothermal well-logging technology will be required to meet the goals for geothermal resource development contained in the Project Independence report. This support can buy lead time for the process of eventual industrial development, as well as promote advances in near-term logging capability.

Using type curve and standard buildup analyses, effective permeability, porosity, effective formation thickness and average formation pressure and temperature are obtained. Using cumulative production data the energy-material balance equations can be used to estimate initial volume, pressure and temperature. Well and field performance can then be predicted. H. Ramey and R. Whiting have pioneered this technique (2, 13, 16). Of especial utility is a manuscript made available by H. Ramey, et al., comprehensively summarizing the thermodynamic and hydrodynamic properties of hydrothermal systems (15).

Papers and abstracts related to well test/analysis presented at the recent United Nations Symposium included the following:

1. E. Durucan and E. Tan (Turkey), "Geothermal Well Drilling and Well Testing in the Afyon Area."
   Three wells have been drilled. Bore hole temperature and pressure measurements, and production and gas content tests were made. Well bottom was 106°C, well bottom pressure was 1195 psig at 900 m, production rate was 20 lt/sec and gas content was about 0.35-0.375% CO_2 by weight.

2. A. Barelli, R. Celati, G. Manetti, and G. Neri (Italy), "Build-up and Back-Pressure Tests on Italian Geothermal Wells."
   Italian geothermal fields in Larderello, Travale and Mt. Amiata were analyzed using oil well test methods. Permeability thickness (hk) values ranged between 1 and 200 darcy-meters. Most commercial wells had hk values between 10 and 50 darcy-meters. Fractured flow gave negative skin effect coefficients. Back pressure curves revealed the existence of non-Darcy flow for high productivity wells.

3. R. Celati, P. Squarci, G. Stefani and L. Taffi (Italy), "Analysis of Water Levels and Reservoir Pressure Measurements in Geothermal Wells."
   The previously unknown formation pressure of Larderello field for the 1940-1955 period were determined from water level data. Initial pressures ranging from 20 to 40 ata were found.

4. G. Hitchcock and P. Bixley (New Zealand), "Observations of the Effect of a Three Year Shutdown at Broadlands Geothermal Field, New Zealand."
   Drilling and testing of 25 wells over a 5 year period resulted in a total discharge of 7.4×10^{10} pounds mass and 4.2×10^{13} Btu heat. The wells were largely closed in from August 1971 to December 1974. This shut in period, during which time many downhole pressure and temperature measurements were made, has provided a unique opportunity to examine the recharge characteristics of the reservoir.

5. R. James (New Zealand), "Optimum-Well Spacing for Geothermal Power."
   For underground systems where flow is through fissured formations, it is found that wells of fairly large discharge can be quite close together (50 m) without interactive effects. Calculations indicate that this applies to both hot water fields and to those tapping dry steam reservoirs. (The ensuing discussion brought out an opposing point of view, suggesting that realistically, for steam dominated reservoirs, well spacings an order of magnitude greater were required).

6. R. James (New Zealand), "Engineering Factors Concerning Geothermal Fluids."
   The flow of separated hot water from geothermal well-head separators is usually measured by orifice meters. Improper separation can cause significant errors in estimation of water flow rate. Other wellhead plumbing devices were mentioned to reduce steam loss.

7. R. James (New Zealand), "Rapid Estimation of Electric Power Potential of Discharging Geothermal Wells."
   By means of a lip pressure tapping at the end of the pipe discharging geothermal fluid to the atmosphere under the usual conditions of critical flow (mixture at sonic velocity), it is shown that a fairly accurate estimate can be made of the amount of electric power of which the well is capable. This applies both to wells deriving their flows from a dry steam reservoir and to those based on a pressurized hot water system.

8. R. James (New Zealand), "Draw-down Test Results Differentiate Between Crack Flow and Porous Bed Permeability."
   Down-hole tests on geothermal wells under flowing conditions show that when discharge is plotted against pressure draw-down, the type of curve obtained indicates how fluid enters the well — whether from a crack or from

porous strata. It is also possible to estimate the width of crack and how much flow would be increased by under-reaming.

9. K. Kalagiri (Japan), "The Production Techniques in the Vapor Dominated System (Matsukawa Geothermal Field)."
In the Matsukawa geothermal field, 240 tons per hour of steam has been produced since 1974 from seven wells. The power generated is 22 mw. The geothermal steam supplied to the turbine is at a pressure of 3.6 kg/cm² and temperature of 180°C (36°C superheat).

10. Sirri Kavlakoglu (Turkey), "A Method to Determine Reservoir Temperature and Porosity in Geothermal Fields."
A new method for determining reservoir temperature based on surfacial geophysical measurements is suggested. An equation is presented with temperature (T) as a function of reservoir porosity (ϕ) and resistivity (ρr), and the surface hot water (at temperature t) resistivity (ρt):

$$T = \frac{0.81\rho_t[t + 21.54]}{\phi^2\rho_r} - 21.54$$

11. R. Lengquist and A. Hansen (U.S.A.), "Geothermal Steam Piping Systems at Big Geysers, California, U.S.A."
Steam conditions are 120 psi and 360°F (8.44 kg/cm² /185°C). Non condensibles total 0.2 to 0.5%, 90 to 95% CO_2. For protection against overpressure, modulating type relief valves backed up by rupture discs at 170 psi are used. The pipes, A53 — Grade B carbon steel, show almost no corrosion, but have experienced water and dust erosion at turns and restrictions. In-line separators are used to minimize wear. Pipe insulating material of 3" fiberglass blanket with asbestos aluminum vinyl cover results in a total heat loss of 0.15 Btu/ft²/°F. Noise abatement attenuates steam to atmosphere noise to 80 dBa at 100 feet.

12. L. Lorenson, C. Walkup, E. Mones (U.S.A.), "Polymeric and Composite Materials for Use in Systems Utilizing Hot, Flowing Geothermal Brine."
Laboratory flow tests with 300°C brine have shown that polymers containing either substantial aromaticity, fluorine, carbonized structure or aliphatic unsaturation which has been crosslinked, show considerable stability, while the presence of water sensitive groups such as imide, amide or ester is detrimental. In actual well flow tests, a fluorocarbon polymer has exhibited the most resistance to both erosion and scale deposition.

13. K. Mathias (U.S.A.), "The Mesa Geothermal Field — A Preliminary Evaluation of Five Geothermal Wells."

Well Mesa	Depth (Meters)	Bottom Hole Temperature (°C)	Shut-in Pressure (Bars)	Max. Flow (kg/min)
6-1	2448	202	4.5	1600
6-2	1830	184	7.4	890
5-1	1830	157	4.6	1000
8-1	1829	180	4.8	—
31-1	1882	158	4.6	—

All wells utilize either slotted production casing or a slotted liner opposite producing zones. Wells 6-1 and 6-2 are supplying fluids for test desalting operations.

14. M. Nathenson (U.S.A.), "Some Reservoir Engineering Calculations for the Vapor-Dominated System at Larderello, Italy."
Bottom-hole flowing properties were calculated from wellhead data can
- be constant — Prala 2, 236°C
- increase — Prala 4, 194 to 214°C in 6 years
- decrease — Larderello 85, 270 to 254°C in 10 years

The initial mass of fluid in place for the northeast zone of Larderello (56 km²) was estimated to require 19 km of thickness assuming 5% porosity (steam), and 832 m, assuming 20% porosity and 10% of pore volume as water.

15. H. Ramey (U.S.A.), "Pressure Transient Analysis for Geothermal Wells."
The study presented the fundamentals of modern pressure transient analysis as applied to geothermal wells to determine:
a) the quantitative importance of precipitation within the pore space
b) plugging of pore space adjacent to wellbore, in the reservoir proper or at the perimeter
c) a decline in driving force (reservoir pressure)

Both vapor and liquid dominated reservoirs can be analyzed.

16. H. Ramey, P. Kruger, A. London and W. Brigham (U.S.A.), "Geothermal Reservoir Engineering Research at Stanford University."
The overall thrust of the program is the development of basic information on the flow of fluids, heat, and important trace chemicals in geothermal systems, and to develop mathematical and computer models of these flows.

17. H. Ramey (U.S.A.) and A. Gringarten (France), "Effects of High Volume Vertical Fractures on Geothermal Steam Well Behavior."
Pressure-time performance data in combination with log-log type curve matching and semi-log graphing were used to compute transmissivity and fracture volume/length.

18. R. Robinson and R. Morse (U.S.A.), "A Study of the Effects of Various Reservoir Parameters on the Performance of Geothermal Reservoirs."
The effect of production rate on the ultimate heat produced for open and closed reservoir systems was studied. The results indicate that the total amount of heat which may be produced is limited and that heat recharge by rock conduction and fluid influx resulted in little additional heat recovery. That is, fluid reinjection apparently will not prolong the life of the reservoir. For maximum production, the reservoir pressure should be reduced to a point where the superpressured water will flash to steam within the pores of the rock.

19. J. Tomasson and T. Thorsteinsson (Iceland), "Use of Injection Packer for Hydrothermal Well Stimulation in Iceland."
Three to four fold increases in production have been obtained through the use of the inflatable packer. Water injection at 30 to 100 liters per second serve to reopen producing horizons clogged by drill cuttings and circulating mud. Zeolite and calcite vein deposits are also removed to increase permeability.

20. K. Ushijima, K. Matsumoto, T. Noguchi and K. Nishikawa (Japan), "A Thermometer for Geothermal Thermometry in a Geothermal Well."
An accurate and inexpensive thermometer using a platinum wire resistor as a sensing probe was developed to log temperatures in a borehole at conditions up to 300°C and 150 bar. The thermometer was checked at the Otake geothermal field up to 176°C and 340 meters down.

21. E. Bolgarina (U.S.S.R.), "Methods of Evaluation of Thermal Water Reservoirs of the Porous and Porous-Formational Type."
Conventional downhole apparatus was used to study a reservoir. Correlation of flow intensity diagrams with well logging data helped to estimate the filtrating properties of rocks and trace their lateral and vertical irregularities, as well as to specify the conditions of interlayer drainage.

22. B. Dominguez Aguirre, F. Javier and B. de la Mora (Mexico), "Current Method for the Opening and Beginning of Well Exploitation in the Cerro Prieto Geothermal Field, Mexico."
A gradual increase of wellhead pressure was found to be the optimal means of starting a well. The sudden-start method was found to damage the well.

COMPUTER MODELLING

In a sense, there is very little difference in subject content between this section and the previous one. A more accurate separation could possibly be made splitting well measurement from analysis, combining well analysis and computer modelling, as the latter two are both computer based studies. However, it is appropriate to create a distinct category, as this relatively new science has largely derived from the aerospace industry, as opposed to the petroleum based techniques of the previous section. In short, advanced numerical methods are used to solve a set of partial differential equations. The state of this art is rapidly advancing.

However, computer models have yet to be developed to compete with the "petroleum" techniques. Variable physical system configurations (as would be expected for geothermal reservoirs), high reservoir flow rates (Rayleigh numbers considerably in excess of 1000), dynamic two phase flow, precipitation of material from solution, the lack of high temperature/pressure brine properties data and, in many instances, the limitations imposed by the computer itself, generally constrain solutions to interesting mathematical exercises. Real world utility has not yet been shown.

On the other hand, the petroleum techniques have their limits too. Can a reservoir be presumed approximately isothermal? System configurations and other assumptions manytimes oversimplify the actual conditions. Thus, there is reason to believe that significant breakthroughs should be forthcoming in computer simulation studies for predicting reservoir performance.

The state-of-the-art was presented at a special (unofficial) session at the U.N. Symposium. The following is a thumbnail sketch of what is occurring today in this field:

1. I. Aladiev, V. Trusov, A. Peredery, E. Strigin, E. Saperov and V. Farzinov (U.S.S.R.), "Heat-Mass Transfer Processes at Aquiferous Systems with Artificially Increased Permeability."
A mathematical model composed of differential equations is used to describe heat and mass transfer processes in the zone of artificially increased permeability. The model was checked by investigating thermal disturbance propagation created by a chemical explosion.

2. P. Cheng and K. Lau (U.S.A.), "The Effect of Steady Withdrawal of Fluid in Confined Geothermal Reservoirs."
The governing equations in terms of temperature and pressure are of elliptic type involving a delta function which represents the withdrawal of fluid. The set of nonlinear partial differential

equations with singular functions are approximated by a set of nonlinear algebraic equations by the finite difference method. Numerical solutions for a selected set of parameters are obtained for both cylindrical and rectangular reservoirs.
It is found that velocity distribution in the reservoirs is significantly affected even if the withdrawal rate is low. As the withdrawal rate is increased, the mushroom shape of isotherms associated with free convection (i.e., at zero withdrawal rate) in reservoirs with high permeability begins to contract, and eventually collapses at a sufficiently high withdrawal rate. The location of the withdrawal site also has a significant effect on heat transfer and fluid flow characteristics in a geothermal reservoir.

3. C. Faust and J. Mercer (U.S.A.), "Mathematical Modeling of Geothermal Systems."
The continuity equations for mass, momentum and energy in porous media were reduced to two non-linear partial differential equations in which the dependent variables were fluid pressure and enthalpy. The equations were solved by a numerical method that combined a Galerkin-finite element approximation in space and a finite difference approximation in time. Results compared favorably with an analytical solution for the one-dimensional, steady, vertical flow of hot water in a porous medium.

4. S. Garg, J. Pritchett, D. Brownell and D. Kassoy (U.S.A.), "Simulation of Geothermal Reservoirs."
A numerical procedure has been devised for solving the fluid and heat flow in the absence of geologic motion for multiphase water; methods have also been developed and tested to describe the response of the geologic matrix as the pore-pressure distribution evolves in space and time. Sample numerical calculations illustrating the effects of (1) local geology and (2) withdrawal and reinjection of fluid on large scale convection patterns in hydrothermal reservoirs are presented.

5. T. Lasseter (France), P. Witherspoon and M. Lippman (U.S.A.), "Multiphase Multidimensional Simulation of Geothermal Reservoirs."
A mathematical method of modeling geothermal reservoirs has been developed using a computer program called SHAFT (Simultaneous Heat and Fluid Transport). This program solves numerically the coupled equations describing the simultaneous transport of mass and energy by a two-phase fluid in porous media. Solutions can be obtained for transient or steady-state conditions in one, two, or three dimensions. For systems where the flow field is independent of the temperature distribution, the flow result is only computed once at the beginning and subsequently only energy calculations are made, which can save significant computer time.

In addition to the above, several papers are available covering flow in wellbore, as for example:
M. Nathenson, "Flashing Flow in Hot Water Geothermal Wells,"
U.S.G.S. preliminary report.
and the entire reservoir:
P. Witherspoon, S. Neuman, M. Sorey and M. Lippmann, "Modelling Geothermal Systems," May 1975.

The above is merely a sampling of the type of investigation presently proceeding. It would be foolhardy to say that the above *is* the state-of-the-art. There is no doubt that significant work has already been accomplished superceding the sampling.

PHYSICAL MODELLING

Physical modelling is taking two paths: the area of the reservoir in the immediate vicinity of the borehole, called chimney for stimulation studies, and the entire reservoir. Very little physical modelling work has been accomplished thus far. Reference #1 can be consulted for both historical and theoretical information.

Of the recent work, A. Hunsbedt and P. Kruger have reported the following (Second U.N. Symposium Abstracts, San Francisco, California, 20-29 May, 1975):

> "A laboratory model of stimulated geothermal reservoirs has been constructed and used to study the behavior of stimulated geothermal reservoirs created by artificial fracturing techniques. The model operates by pressure reduction with or without geofluid recharge with initial pressure and temperature up to 800 psia and 500°F, respectively. Data have been obtained on the transient behavior of the reservoir resulting from steam production for model rock loads (granite) with two different porosities. Calibration of the model was made using only liquid in the model. The results show that thermal energy stored in the fractured rock media can be effectively extracted by reducing system pressure and letting boiling take place in the rock formation. For the conditions of these experiments, an average of 90 percent of the thermal energy stored in the rock between the process temperature limits was extracted. Highest rock energy extraction was achieved with boiling controlled by recharge to take place near the top of the rock mass. The fraction of initial reservoir liquids that can be produced upon pressure reduction appears to depend on the reservoir porosity, with the highest fraction observed for the lowest porosity. A mathematical model for the fluid production process has been developed and early results indicate that the observed model reservoir behavior can be predicted."

Work is continuing.

There has not been any reported laboratory study of the entire geothermal reservoir. H. Henry and F. Kahout studied underground properties for liquid waste disposal, but only up to 43°C (17). R. Wooding, in the late 60's, conducted small scale (13 3 cm radius cylinder) experiments up to 67°C. At the unofficial session of the U.N. Symposium, W. Sadeh and H. Shen of Colorado State reported on their intention to initiate laboratory modelling of a geothermal fluid convection with very large viscosity variations. The discussion following their presentation revealed widespread interest in physical modelling. Various possible experiments were suggested by the audience. S. Bories and M. Combarnous (France) have briefly looked at experimental results on thermal convection in a homogeneous and isotropic porous layer and postulated two possible ways of describing the heat transfer process (18).

The geothermal reservoir engineering group at the University of Hawaii has been developing a physical modelling program for the past year and a half. It is premature to disclose any significant findings at this time. A report will be forthcoming late in the year (1975).

In summary, a Rayleigh number range between 40 and 1000 (see Reference #1 for details) will be studied. Two models have been fabricated, one unpressurized, the second pressurized. A larger, more comprehensive model is being designed. Table 2 lists he physical characteristics and status of the models.

Figure 3 is a photo of the unpressurized model (#1) and Figure 4 is a photo of the pressurized model (#2) tank without the peripherals, while Figure 5 is a schematic diagram of the model with accouterments. Figure 6 is of the 24 point recorder and heater. The key components in addition to the tank are:

1. Esterline Angus 24 point recorder using resistance temperature detectors.
2. Stan-trol heaters and controller sensor systems (two 2 kw and two 1 kw), capable of varying heater surface temperature between ambient and 1800°F. The heaters are convertible to any shape desired — from a two dimensional theoretical point source to a three dimensional source. Three possible system configurations are drawn in Figure 7.
3. Haskell air driven by hydraulic pump to simulate compressed water conditions.
4. Sanborn dual channel recorder for supplementary continuous temperature/pressure measurements and spot checks.

The vessel itself, representing the geothermal reservoir, has been provided with the following options:

1. Medium: glass beads, three mesh sizes available; sand and consolidated sand.
2. Fluid: freshwater; dissolved solids content (chlorides, sulfates, carbonates and silicates) to 35% by weight.
3. Thickness: up to two feet on unpressurized model (#1), one foot on model #2 and four feet on model #3.

The models will be used to conduct the following types of experiments:

1. Test fundamental information, as for example . . . Does convection initiate at a Rayleigh number of 40? . . . Is a geothermal reservoir an open or closed system? . . . What happens during reinjection? . . . How is the Ghyben-Herzberg lens influenced by geothermal exploitation?
2. Check the concept of geothermal reservoir self-sealing.
3. Determination of data to enable computer models to refine predictive capability.

SUMMARY

The field of geothermal reservoir engineering will show significant advancement during the next few years. The progress will be an accelerated one because of improved international communications, the availability of larger and faster computers and the threat of energy shortfalls, which will result in continuing high level funding of research and development for alternate energy sources.

TABLE 2. PHYSICAL MODELS OF GEOTHERMAL RESERVOIRS

Model	Size(ft^3)	Pressure (atm)	Temperature Maximum (°F)	Probes	Status
#1	3	1	212	10	completing tests
#2	3-1/3	14	382	23	ready for tests
#3	30+	20+	500+	23	initial design

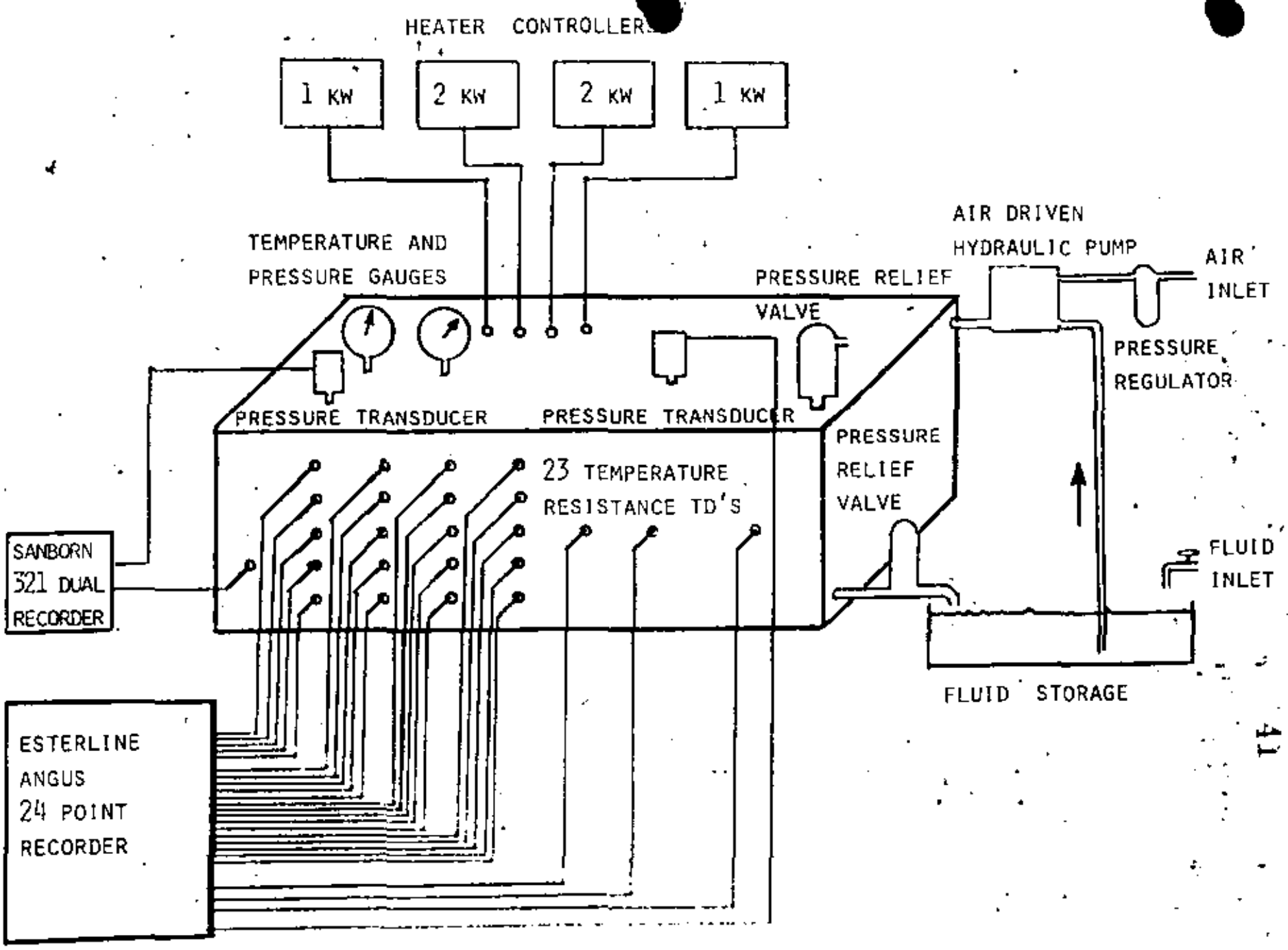

FIGURE 5. SCHEMATIC DIAGRAM OF PRESSURIZED GEOTHERMAL RESERVOIR PHYSICAL MODEL

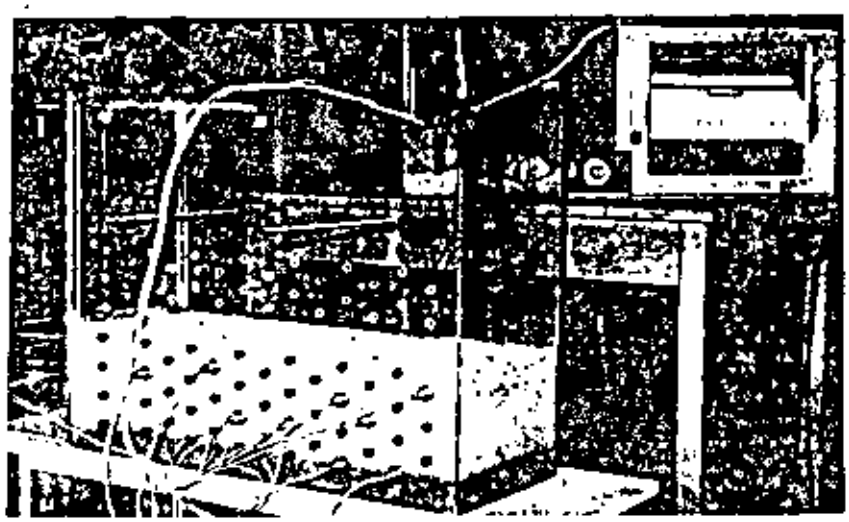

FIGURE 3. Photograph of Unpressurized Model and Peripherals

FIGURE 4. Photograph of Pressurized Vessel

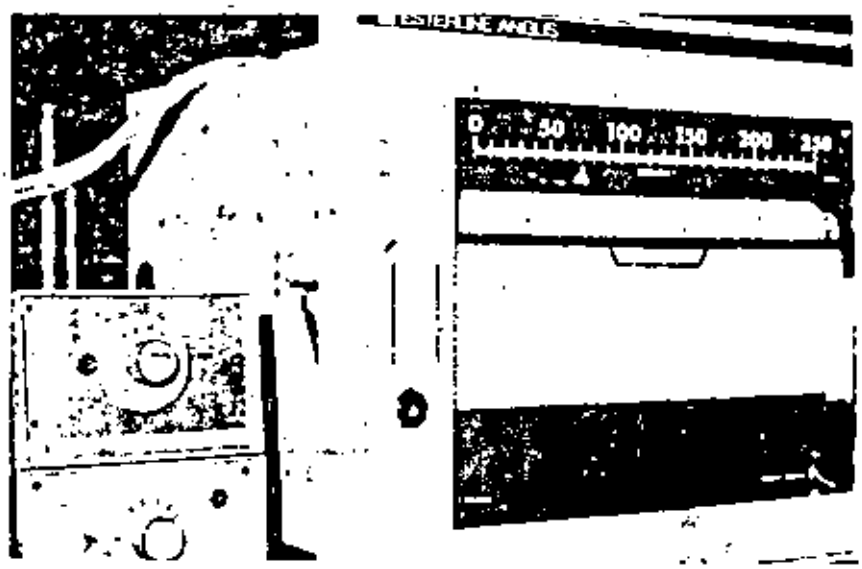

FIGURE 6. Photograph of 24 Point Recorder and Heater Controllers

POINT SOURCE IN 2-D MODEL CENTERED AT BOTTOM OF RESERVOIR

APPROXIMATE EXPONENTIAL SOURCE CENTERED AT BOTTOM OF RESERVOIR

VERTICAL DIKE HEAT SOURCE

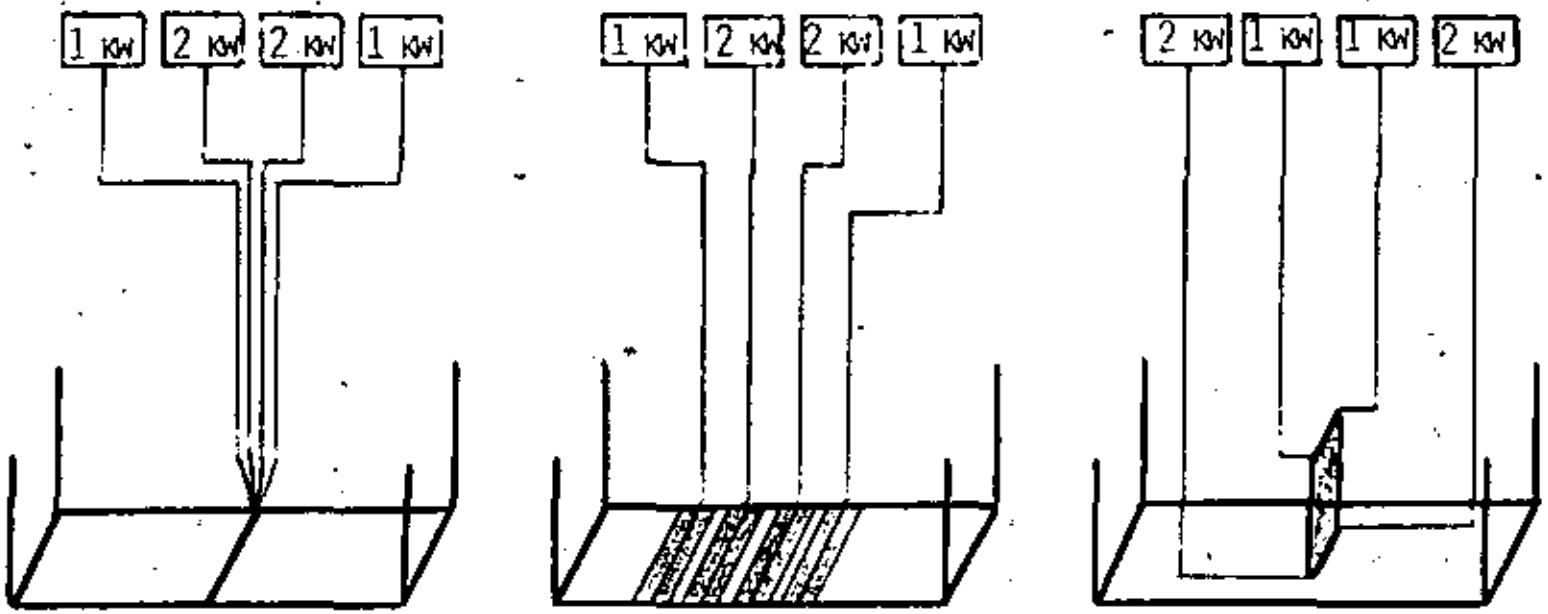

FIGURE 7. HEATING ELEMENT CONFIGURATIONS

REFERENCES

1. Takahashi, P., Chen, B., Mashima, K. and Seki, A., "State-of-the-Art of Geothermal Reservoir Engineering," *American Society of Civil Engineering Journal of the Power Division*, 101 (1), 111, July 1975.

2. Whiting, Robert L., "A Reservoir Engineering Study of the Wairakei Geothermal Steam Field," Private Communication.

3. Muffler, L.J.P. and White, D.E., "Geothermal Energy," *The Science Teacher*, Vol. 39, No. 3, March 1972.

4. Facca, Giancarlo, "Structure and Behavior of Geothermal Fields," *Geothermal Energy*, UNESCO, 1973, pp. 61-69.

5. Elder, John W., "Physical Processes in Geothermal Areas," *Terrestial Heat Flow*, W.H.K. Lee, Editor, No. 8, 1965, pp. 211-239.

6. Hayasnida, T. and Ezima, Y., "Development of Otake Geothermal Field," *U.N. Symposium on the Development and Utilization of Geothermal Resources*, Pisa, 1970.

7. Yuhara, K., "Morphological, Hydrological and Thermal Characteristics of Active Volcanoes Having no Geothermal Areas, and Artificial Hydrothermal Systems for Utilizing their Latent Internal Heat Energy," *Proceedings of the Utilization of Volcano Energy Conference, Hilo, Hawaii*, February 4-8, 1974, pp. 391-413.

8. Krieger, J., "Geothermal Energy Stirs Worldwide Action," *Chemical and Engineering News*, June 9, 1975, pp. 21-26.

9. Keller, George V., "Drilling at the Summit of Kilauea Volcano," prepared for the National Science Foundation, March 15, 1974, p. 42.

10. White, D.E., "Geochemistry Applied to the Discovery Evaluation and Exploitation of Geothermal Energy Resource," Raporteur's Report, *United Nations Symposium on the Development and Utilization of Geothermal Resources*, Pisa, 1970.

11. Kennedy, George C. and Griggs, David T., *Power Recovery from the Kilauea Iki Lava Pool*, RM-2696-AEC, December 12, 1960.

12. Colp, John L. and Furumoto, A.S., *The Utilization of Volcano Energy*, proceedings of a conference held at Hilo, Hawaii, February 4-8, 1974.

13. Ramey, Henry, "A Reservoir Engineering Study of the Geysers Geothermal Field," Private Correspondence, 1973.

14. Baker, L., Campbell, A. and Hughen, R., "Well-Logging Technology and Geothermal Applications: A Survey and Assessment with Recommendations," SAND 75-0275, Sandia Laboratories, Albuquerque, New Mexico, May 1975.

15. Ramey, H., Jr., Brigham, W., Chen, H., Atkinson, P. and Arihara, N., "Thermodynamic and Hydrodynamic Properties of Hydrothermal Systems," (see Hilo Conference, reference #7).

16. Whiting, R. and Ramey, H., "Application of Material and Energy Balance to Geothermal Steam Production," *Journal of Petroleum Technology*, July 1969, pp. 893-900.

17. Henry, H. and Kahout, F., "Circulation Patterns of Saline Groundwater Affected by Geothermal Heating as Related to Waste Disposal," *Underground Wastewater Management and Environmental Implications*, Vol. 18, 1973, pp. 202-221.

18. Borles, S. and Combarnous, M., "Free Convection in Geothermal Fields: Physical Understanding and Mathematical Modeling," International Seminar on Future Energy Production—Heat and Mass Transfer Problems, Dubrovnik, Yugoslavia, August 25-30, 1975.

Acknowledgment

The work upon which this publication is based was submitted in part by funds provided by the National Science Foundation of the United States under Grant GI-38319 and the Energy Research and Development Administration of the United States under Grant E(04-3)-1093.

ABOUT THE AUTHOR:

Dr. Patrick K. Takahashi is an associate Professor of Civil Engineering at the University of Hawaii. He holds a B.S. in Chemical Engineering from Louisiana State University.

Geothermal Resources Council, TRANSACTIONS, Vol. 1 May 1977

DECLINE CURVE ANALYSIS - A USEFUL RESERVOIR ENGINEERING TOOL FOR PREDICTING THE PERFORMANCE OF GEOTHERMAL WELLS.

By
Dr. Jesús Rivera R.
Coordinadora General del Proyecto
Geotérmico de Cerro Prieto.
Comisión Federal de Electricidad.
Melchor Ocampo No. 455 4° piso.
México 5, D.F.

45

This paper was prepared for the 1977 Annual Meeting of the Geothermal Resources Council to be held in San Diego, California, May 9-11, 1977.

ABSTRACT

This paper shows that the theory of decline curve analysis, which has been widely used in the petroleum industry for quite a long time, [1,2,3] can be applied for predicting and studying the behavior of both geothermal wells and geothermal reservoirs as a whole. A study was made of several wells of the geothermal field of Cerro Prieto, México [4]; this work includes the results obtained for three of them, which were judged to be the more representative cases.

In addition to the application of the decline curve theory, an analysis of the history of flowing well conditions was made by means of the data of pressure vs depth and temperature vs depth taken during the wells productive life. All these data were analyzed together in order to know what the conditions of the wells were after been flowing for some time. Predictions of future production from the wells were made based upon the assumptions of both hyperbolic and exponential declination type.

INTRODUCTION

The two basic problems that a reservoir engineer has to face when handling the fluid production from a field are the determination of the future production of the wells and an estimation of their future productive life. In the petroleum industry, analysis of production curves for answering these problems had been tried as early as 1915[1], reaching a great popularity before world war II. During this war because of severe production curtailments, production decline curves lost most of their usefulness; however, this type of analysis had a strong comeback after the conflict was over.

There are several factors that could affect the performance of either a particular well or a reservoir. Among them, the geothermal literature has expressed major concern about the potential effect of precipitation of solids either at the wellbore face[11] or within the reservoir porous structure. In addition to this possibility there are other factors which could be responsible in accounting for the reduction in flow rates, they are a decrease in the average formation pressure and/or a variation in the physical characteristics of the wells due to either scaling or collapse of the casing production string.

references and illustrations at end of paper.

GENERAL BACKGROUND

The obvious way of analyzing well production data is by plotting it versus time, and so it was the first method used[2]. It was found that after some time and depending upon the rates imposed on the well, the production rate began to drop off or decline fairly regularly. After treating the production data in this way for some time, it was recognized that by plotting it in a convenient coordinated system, a mathematical form could be given to the declining curve, which will make it possible to extrapolate the data into the future in order to predict productions in a reasonably manner.

Arps[1,2] presents a complete analysis on the shapes of decline curves and develops the mathematical expressions that could be fitted to a set of data showing a particular behavior. The basic equations are as follows*:

Exponential or Constant Rate Decline:

$$q = q_0 \exp(-at) \quad - - - \quad (1)$$

where,

$$a = -\ln(1-D) \quad - - - \quad (2)$$

$$D = \frac{q_t - q_{t+\Delta t}}{q_t \Delta t} \quad - - - \quad (3)$$

Hyperbolic Decline:

$$q = q_0 (1 + a_0 t)^{-\frac{1}{h}} \quad - - \quad (4)$$

* Nomenclature is given at end of paper.

where, $a_o = h\left(\frac{1}{1-D}\right)^{\frac{1}{h}} - 1$ - - - (5)

Harmonic Decline:

$$q = \frac{q_o}{1+a_o t} \quad - - - \quad (6)$$

APPLICATION TO GEOTHERMAL WELLS AT CERRO PRIETO.

The decline curve theory was applied to several wells of the Cerro Prieto Geothermal Field. Figs. 1 thru 3 show the production data from three of the wells plotted vs time on a semilogarithmic scale. Several other ways of plotting the data were tried, such as production rate vs time in months on loglog scales and fluid production vs cumulative fluid production on semilog scale.

Well A shown in Fig. 1 exhibits two well-defined features in its production curve. It is apparent that presents a characteristic hyperbolic decline during a period of aproximately 25 months of its productive life, starting a sharp declination after that. This abrupt change in the production curve has been attributed to a drastic change in the physical characteristics of the well, which could be due to either growth of scaling above a critical value, or collapse of the production string due to thermally induced stresses.

Well B shown in Fig. 2 presents a declination of the harmonic type, which can be mathematically described by eq. 6. there are shown two approaches for extrapolation into the future, the first one given by curve (1) follows the general trend of the curve; meanwhile, curve (2) shows an exponential extrapolation based upon the data from the last year. The last type of extrapolation can be considered on the conservative side.

The behavior of well C is shown in Fig. 3. It shows a sharp exponential decline during the first stage of production. This behavior has been attributed to physical damage of the well and/or ill-completion techniques. A workover was performed on the well at the end of 1974; however, the damage on the well still remained after the job was completed, as it is apparent from the production curve registered after the well was brought back into production.

CONCLUSIONS

Bases upon the results of the study described in this work, the following conclusions can be drawn.

1. It is possible to describe the behavior of a geothermal reservoir and/or geothermal wells through the application of decline curve analysis.

2. Extrapolation to future of decline production curves is a sound reservoir engineering tool, providing that physical characteristics of the well and properties of the reservoir remain fairly the same.

3. Analysis of production declination curves when properly coupled with profiles of pressure and temperature under flowing conditions, provide an auxiliary tool in diagnosis of some well problems.

NOMENCLATURE

Letters.

a	=	exponential decline factor
a_o	=	constant defined by eq. (5)
D	=	decline rate as a decimal
h	=	hyperbolic decline exponent
q	=	production rate at any time t.
q_o	=	initial production rate.
t	=	time

GREEK SYMBOLS.

Δt = magnitude of time step.

SPECIAL SYMBOLS.

ln = natural logarithm.
exp = e, base of natural logarithms.

REFERENCES.

1. Arps, J.J.: "Analysis of Decline Curves", Trans. AIME (1945) 160, 228-247.
2. Mind, T.E.W.: Principles of Oil Well production, Mc Graw-Hill Book Co., (1964).
3. Campbell, J.M.: Oil Property Evaluation, Prentice-Hall Inc., (1959).
4. Arps, J.J.: "Estimation of Primary Oil Reserves," Trans. AIME (1956) 207, 182-191.
5. Ramsay, H.J. and Guerrero, E.T.: " The Ability of Rate-Time Decline Curves to predict Production Rates," Jour. Pet. Tech. (January 1969) 139-141.
6. Bronz, F.: "On the Use and Misuse of Production Decline Curves", Producers Monthly (Sep., 1963), 22-25.
7. Fethovich, M.J.: "Decline Curve Analysis Using Type Curves", Paper SPE 4629 presented on the 48th Annual Fall Meeting of the Society of Petroleum Engineers of AIME, Las Vegas, Nevada, Sept. 30-Oct. 3, 1973.
8. Rivera, R.J., and Acero, A.M. "Estudio sobre la situación que guardan los pozos - M-8, M-9, M-15A, M-20, M-25, M-39 y M-46, y sus necesidades de Reparación", CFE Internal Report (January 1977).
9. Slider, H.C.: "A Simplified Method of - Hyperbolic Decline Curve Analysis", Jour. Pet. Tech. (March, 1968), 235.
10. Gentry, R.W.: "Decline Curve Analysis," Jour. Pet. Tech. (January, 1972), 38.
11. Ramey H.J., Jr.: "Pressure Transient Analysis for Geothermal wells," Second - United Nations Symposium on the use and Development of Geothermal Energy, San Francisco, Calif. (May 20-29, 1975).

Fig. 1

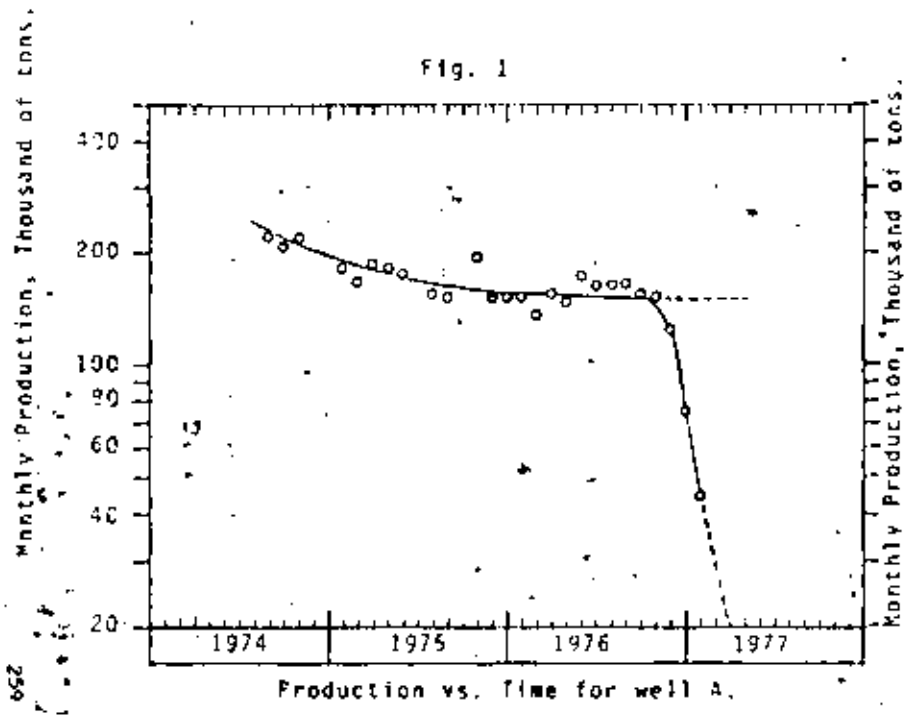

Production vs. Time for well A.

Fig. 2

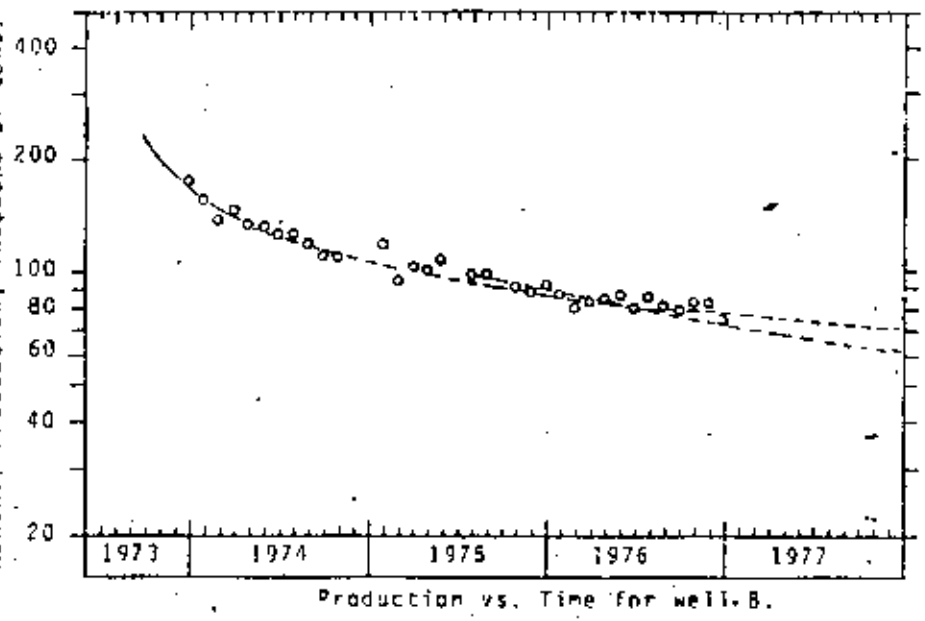

Production vs. Time for well B.

Fig. 3

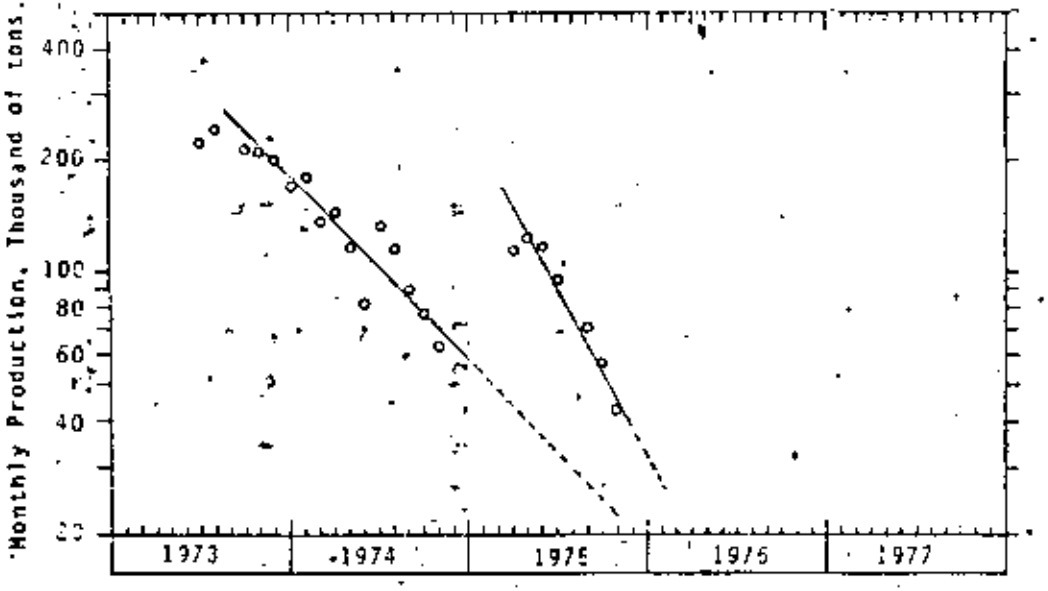

Production vs. Time for well C.

VARIATIONS ON A THEME BY MOLLIER

(A study of the properties of steam and hot water)

H. CHRISTOPHER ARMSTEAD

1. INTRODUCTION

The 'state' of steam, hot water and steam/water mixtures can be expressed in terms of the following five inter-dependent variables:

Pressure ..... 'P'
Temperature ..... 'T'
Dryness ..... 'd'
Enthalpy ..... 'I'
Entropy ..... 'O'

If any two of these variables be selected as rectangular coordinates of a chart, the other three variables may be represented on that chart by a series of curves, or 'contours'. There are, of course, ten possible pairs of coordinates, as can be seen from the following table, and thus there are ten possible forms of chart which can represent the thermodynamical properties of steam and hot water.

	I	O	d	P	T
I	—	I/O	I/d	I/P	I/T
O		—	O/d	O/P	O/T
d			—	d/P	d/T
P				—	P/T
T					—

Each of the five variables features in four charts. One of these charts—I/O—is of course the well known **Mollier Diagram** that is so convenient for steam expansion and compression studies and so widely used by the designer of heat engines. It is of interest to examine the characteristics of the other nine charts in order to see whether any of them could serve a useful purpose.

2. DERIVATION OF CHARTS

Any of the ten possible charts can be derived from Callendar's steam tables.

If ... I_s = the enthalpy of saturated steam at pressure 'P'
I_w = the enthalpy of saturated water at pressure 'P'
If ... L = the latent heat of evaporation at pressure 'P'
If ... I_m = the enthalpy of a wet mixture at pressure 'P' and of dryness 'd'
O_s = the entropy of saturated steam at pressure 'P'
O_w = the entropy of saturated water at Pressure 'P'
O_m = the entropy of a wet mixture at pressure 'P' and of dryness 'd'

Then .... $I_m = d.I_s + (I - d)I_w = d(I_s - I_w) + I_w = d.L + I_w$

or ... $\underline{I_m = d.L + I_w}$

Also ... $O_m = d.O_s + (I - d)\,^{\circ}_{w} = d(O_s - \,^{\circ}_{w}) + O_w$

or ... $\underline{O_m = d(O_s - \,^{\circ}_{w}) + O_w}$

It is from these two formulae and their derivatives that the wet zones can be charted: elsewhere, in the superheat and water zones, Callendar's steam tables may be used directly, where applicable. The detailed construction of the charts is a laborious process; and for the purpose of this study only roughly approximate curves have been drawn without much detail of interpolation, in order to determine their general characteristics.

Each of the ten possible charts will now be examined in turn. They are illustrated in Fig. 1 to 10 (inclusive).

3. ENTHALPY/ENTROPY CHART — (I/O) — Figs. 1-A and 1-b.

As already stated, this is the well known Mollier Diagram. Every student of thermodynamics is familiar with that part of the diagram which deals with super-heated, dry saturated and moderately wet steam (Fig. 1-A). There is, however, another end of the chart that is less widely known and which deals with boiling water and very wet steam (Fig. 1-B). It is difficult to represent both these diagrams in a single chart without undue sacrifice of space or scale.

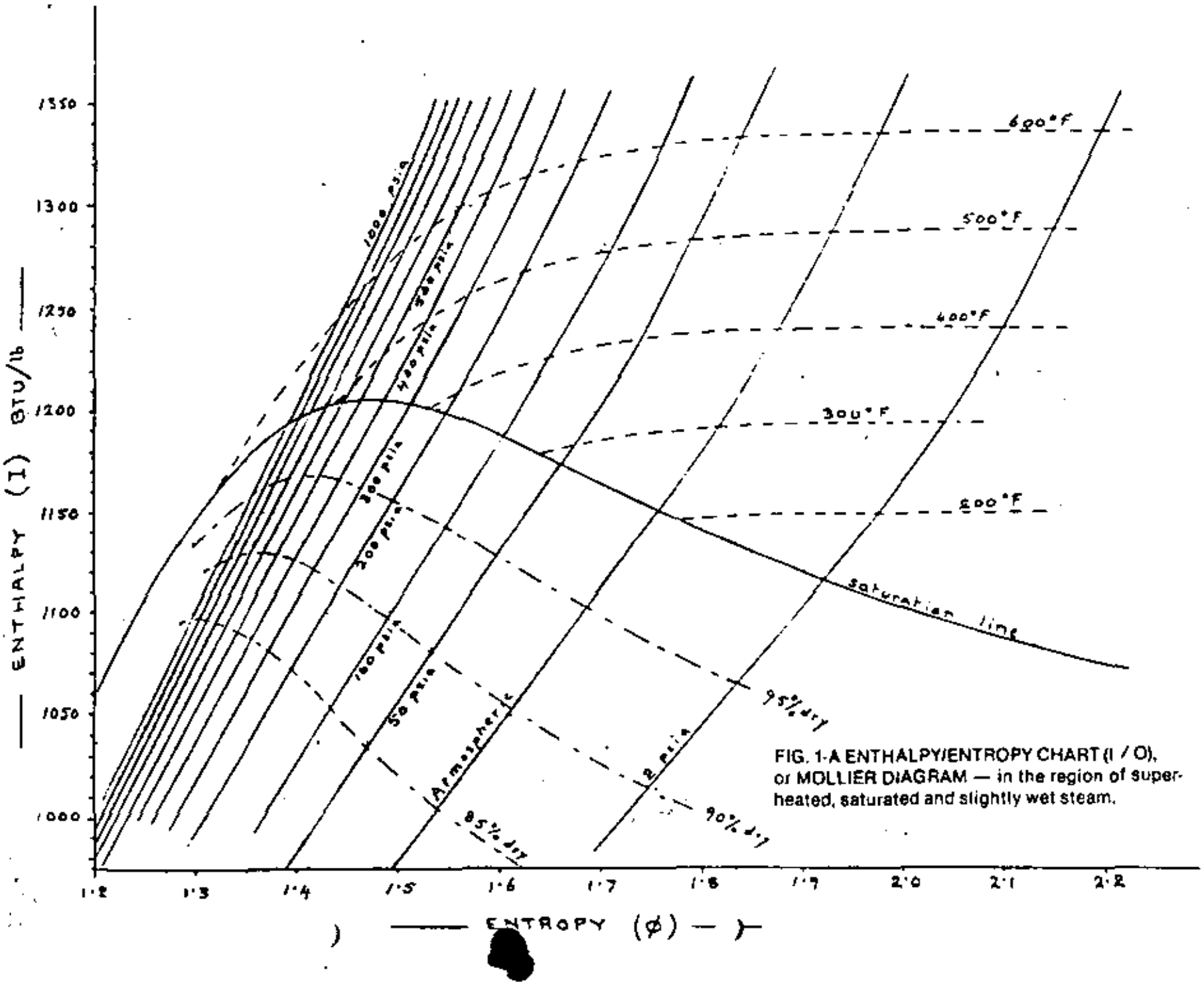

FIG. 1-A ENTHALPY/ENTROPY CHART (I / O), or MOLLIER DIAGRAM — in the region of superheated, saturated and slightly wet steam.

The great merit of the Mollier Diagram is that two of the most important theoretical forms of expansion or compression — the **isenthalpic** and the **isentropic** — can be represented on the diagram by straight horizontal and vertical lines, respectively. Another advantage of Fig. 1-A is that the lines of constant pressure, constant temperature and constant dryness are relatively splayed out from one another so that points can be 'fixed' with fair precision. This advantage, however, does not apply to Fig. 1-B, in which these three classes of line are bunched close together, making the chart very confusing.

In fact, the constant pressure lines have been deliberately omitted from Fig. 1-B for the sake of clarity; but they are of course, 'parallel' to the isotherms. It is also true that the isotherms have been omitted from the wet steam zone of Fig. 1-A, but in that case the interpolation of temperatures is clearly defined along the dry saturated steam line and can be carried through into the wet zone at constant pressure. In Fig. 1-B, the narrow angle of approach of the constant temperature lines to the saturated water line makes accurate interpolation more difficult.

4. ENTHALPY/DRYNESS CHART — (I/d) — Fig. 2

This chart has been only partly drawn: if plotted in greater detail it would become very confusing. This is because the enthalpy of dry saturated steam, after reaching a maximum value of 1205.6 BTU/lb in the vicinity of 450° F., starts to fall again with rising pressure and temperature. As a result, the lines of constant temperature and pressure cross one another at higher dryness factors. For clarity, the constant pressure lines have therefore been omitted; but they would, of course, be 'parallel' to the isotherms. The decreasing slope of the lines with rising temperature is due to the falling latent heat as the critical temperature (about 706° F.) is approached, at which point the latent heat becomes zero and the I/d line horizontal.

The constant entropy lines are of a curious shape: they approach approximate verticality at a value of about 1.05 at a dryness factor of about 0.5.

An advantage of this chart is that **isothermal** lines, representing a third important theoretical form of expansion or compression, are straight; so that changes of condition can be quickly noted for isothermal expansion or compression at different temperatures within the wet zone.

5. ENTHALPY/PRESSURE CHART — (I/P) — Fig. 3

A logarithmic pressure scale has been adopted for this chart so as to flare out the upper part of the saturation boundary loop and thus make interpolations more legible at high pressures. Although the vertical scale has here been shown in gauge pressures it could equally well have been drawn in terms of absolute pressures; the only effect, apart from extending the chart downwards into the vacuum zone, would have been to show a splaying out of the saturation and dryness lines towards the left at very low pressures.

Although the isotherms and dryness lines are fairly well spaced out, the value of this chart is impaired by the fact that the isentropic lines are too nearly vertical at lower pressures, so that isentropic and isenthalpic operations cannot be clearly differentiated from one another.

6. ENTHALPY/TEMPERATURE CHART — (I/T — Fig. 4)

This chart is somewhat similar in form to Fig. 3, but both coordinates have been drawn to linear scales; neither being logarithmic. The similarity is due to the interdependence of temperature and pressure in the wet zone. The chief merit of the chart is that **isothermal** changes are represented by horizontal straight lines which can be carried through into the superheat zone. **Isenthalpic** expansion or compression is, of course, represented by vertical straight lines, which cut the dryness and isentropic lines at less acute angles than in Fig. 3, thus enabling rather better 'fixes' to be given to points.

7. ENTROPY/DRYNESS CHART — (O/d) — Fig. 5

This is a curious chart. As a result of the crossing of the isotherms (and of the lines of equal pressure, which have been omitted for clarity) isentropic expansions are from left to right at the lower end of the chart and from right to left at the upper end. The middle zone is extremely confusing.

8. ENTROPY/PRESSURE CHART — (O/P) — Fig. 6

This chart has some of the same characteristics as Fig. 3, including a logarithmic vertical scale (this time in terms of absolute pressures) which has the effect of splaying out the width of the upper part of the saturation loop. It also has some of the unfavourable characteristics of Fig.

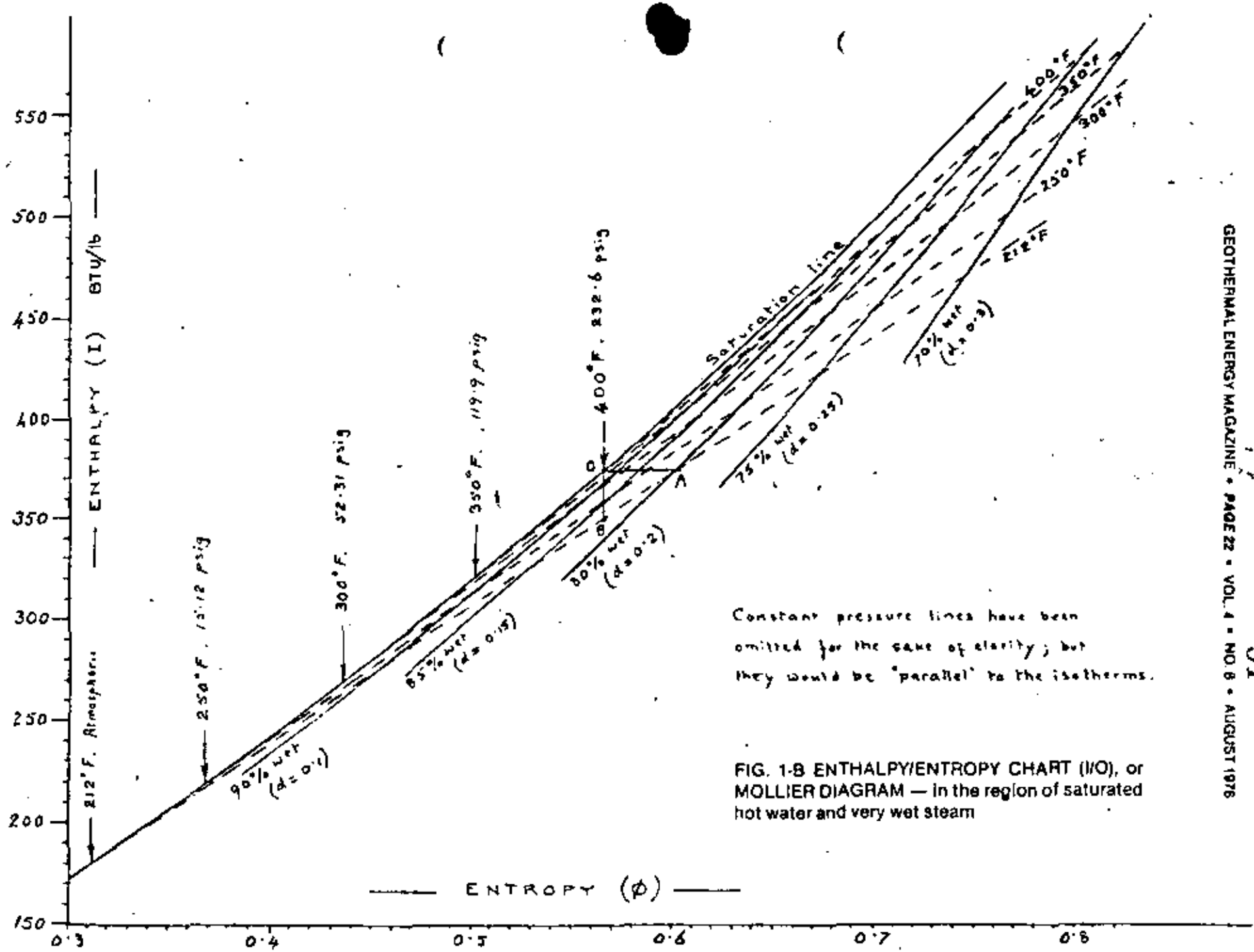

Constant pressure lines have been omitted for the sake of clarity; but they would be 'parallel' to the isotherms.

FIG. 1-8 ENTHALPY/ENTROPY CHART (I/O), or MOLLIER DIAGRAM — in the region of saturated hot water and very wet steam

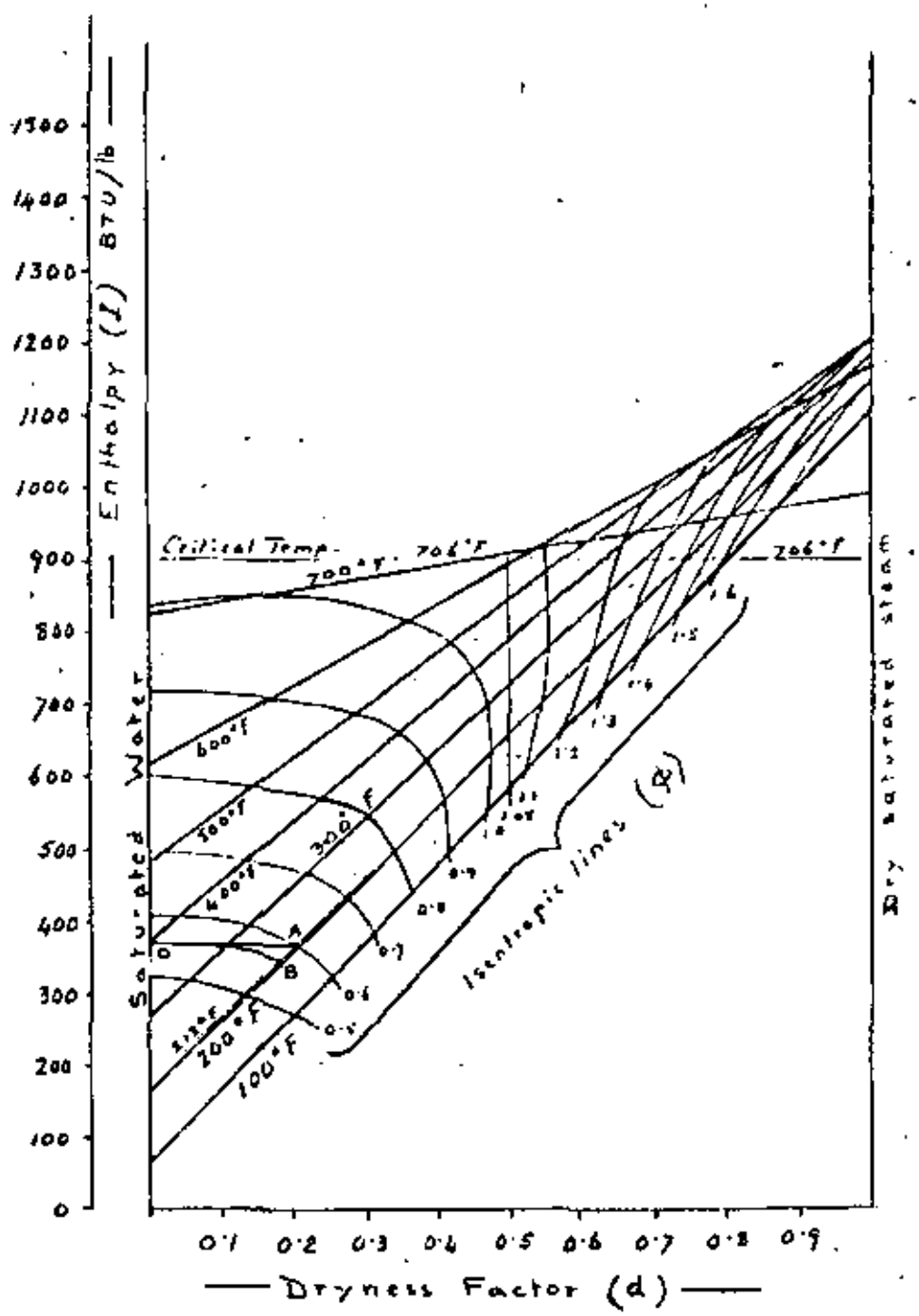

FIG. 2 ENTHALPY/DRYNESS CHART (I/d)
Constant pressure lines not shown, to avoid confusion; but they are 'parallel' to the isotherms.

GEOTHERMAL ENERGY MAGAZINE • PAGE 24 • VOL. 4 • NO. 6 • AUGUST 1976

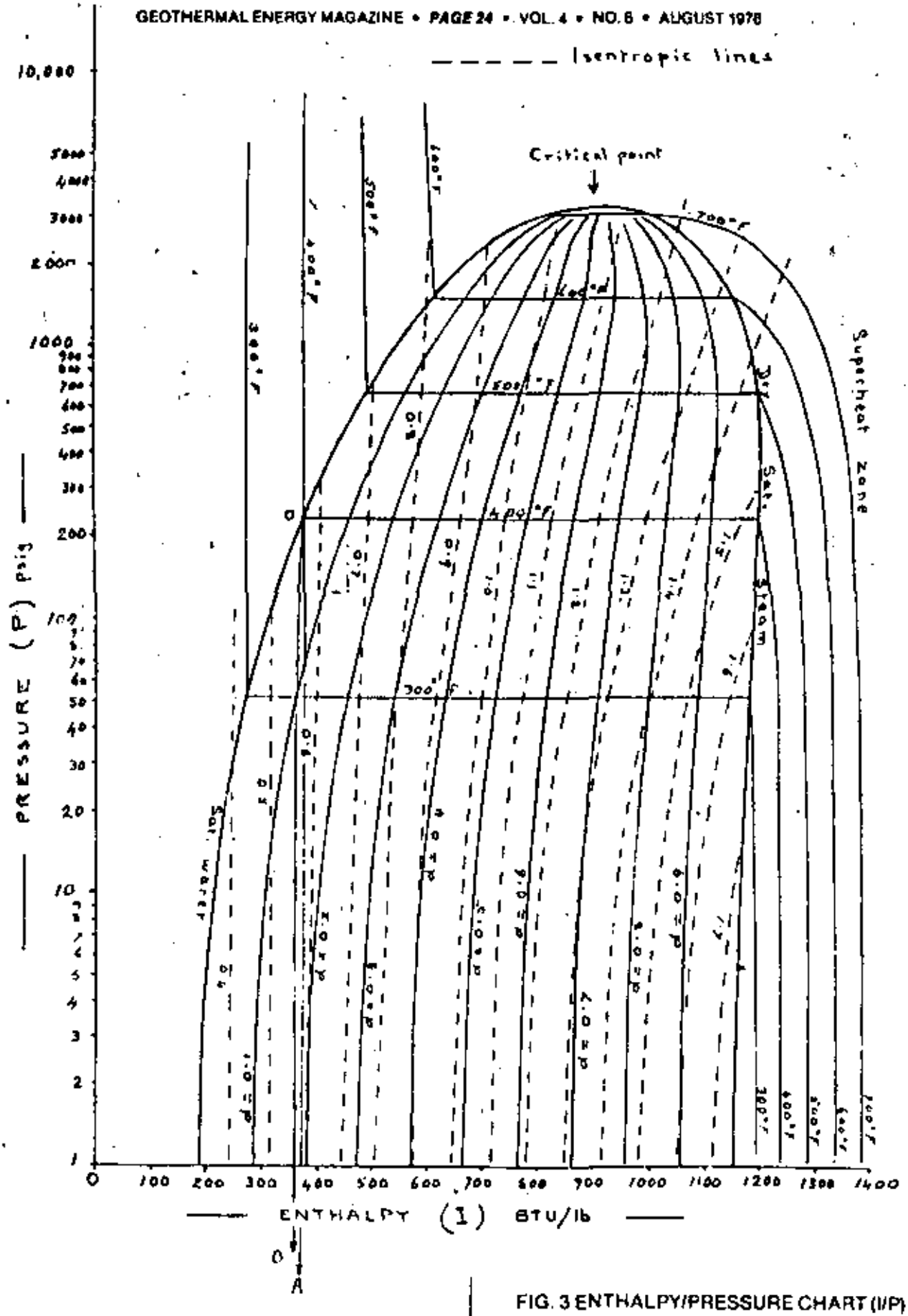

FIG. 3 ENTHALPY/PRESSURE CHART (I/P)

GEOTHERMAL ENERGY MAGAZINE • PAGE 25 • VOL. 4 • NO. 8 • AUGUST 1976

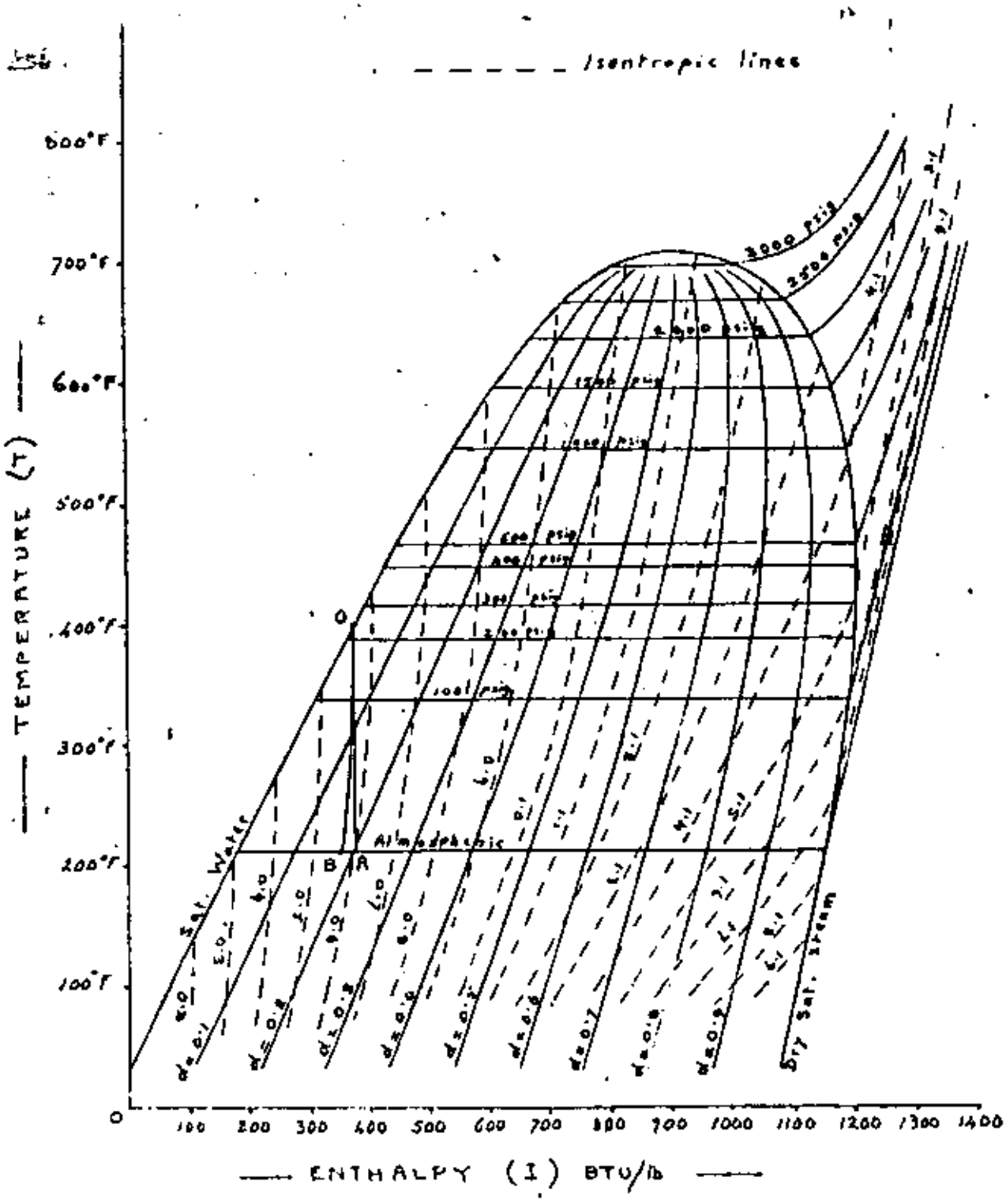

FIG. 4 ENTHALPY/TEMPERATURE CHART (I/T)

GEOTHERMAL ENERGY MAGAZINE • PAGE 26 • VOL. 4 • NO. 8 • AUGUST 1976

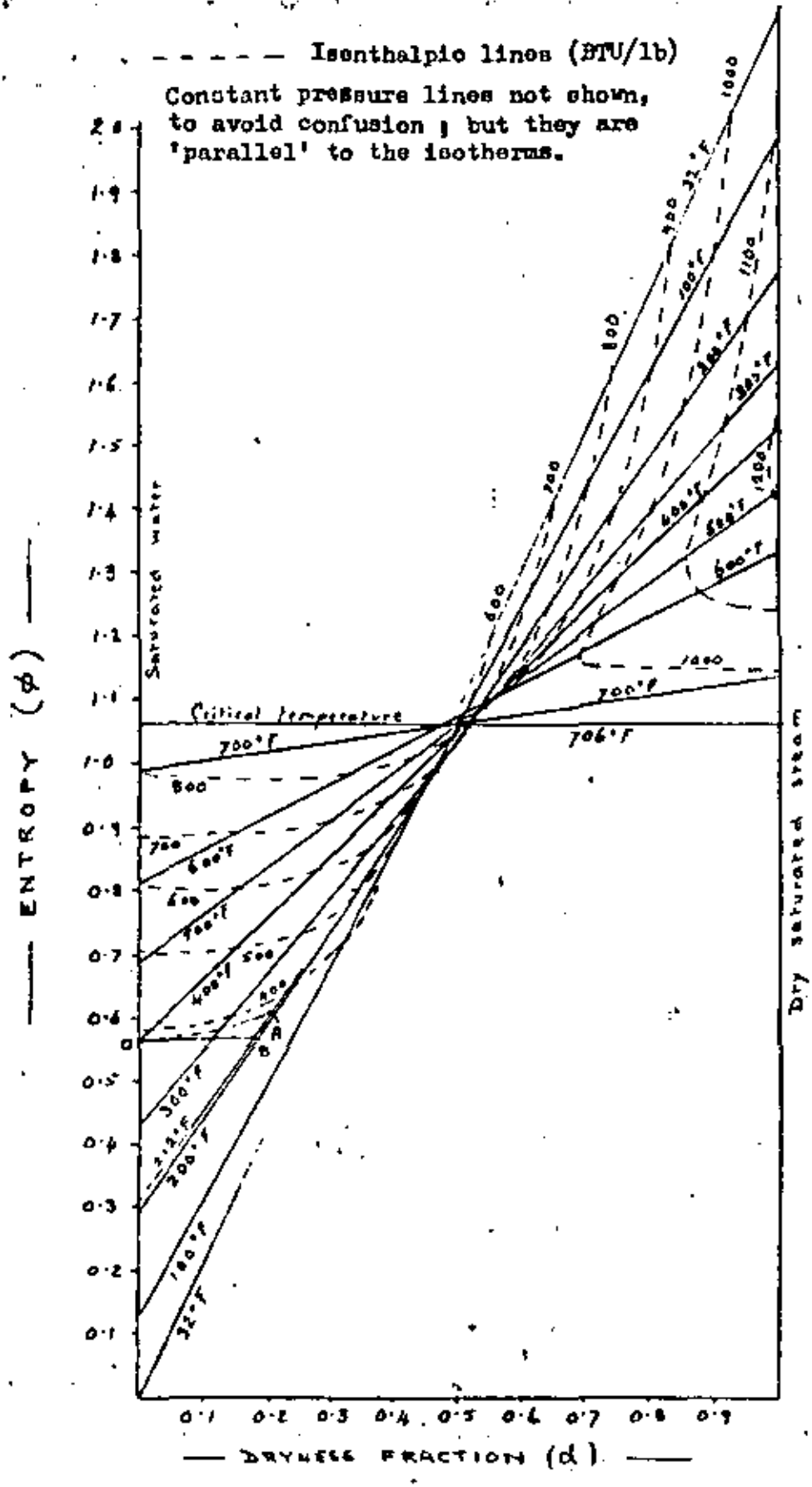

FIG. 5 ENTROPY/DRYNESS CHART (O/d)

3, but possesses rather better clarity of detail, especially in the superheat zone.

9. ENTROPY/TEMPERATURE CHART — (O/T) — Fig. 7

The relationship between this chart and Fig. 6 is similar to that between Figs. 4 and 3. It is clearer than Fig. 6 for purposes of interpolation, especially at lower temperatures and pressures. Isothermal changes are, of course, represented by horizontal straight lines which can be carried through into the superheat zone.

10. DRYNESS/PRESSURE CHART — (d/P) — Fig. 8

The disadvantages of Fig. 3—that the lines of constant dryness, constant entropy and constant enthalpy are insufficiently splayed out from one another—apply also to this chart. It will be noted that the isentropic lines for values of 1.0 and less bend over to the left with rising pressure, while for values of 1.1 and more they bend over to the right. At a dryness of about 0.5 and an entropy value of about 1.05 the isentropic line would be approximately vertical, as with Fig. 2.

11. DRYNESS/TEMPERATURE CHART — (d/T) — Fig. 9

Better angles of intersection between the lines of constant dryness and the isenthalpic and isentropic lines are here apparent, by comparison with Fig. 8; but the scale of the isentropic lines is rather compressed towards the right side of the chart. The same directional tendencies of the isentropic lines may here by observed as in Fig. 8. Isothermal changes within the wet zone may be clearly studied in this chart, as they are represented by horizontal straight lines.

12. PRESSURE/TEMPERATURE CHART — (P/T) — Fig. 10

Unlike all the preceding charts, Fig. 10 features no dryness lines. The entire wet zone is compressed within a single curve. This, of course, is because the same temperature/pressure relationship is valid for wet steam of all qualities and for dry saturated steam. It is only in the superheated zone that temperature and pressure are not directly inter-related and that entropy and enthalpy will have individual 'contours'. This chart can give clear information about superheated steam, but none concerning wet steam other than the pressure/temperature relationship. Isentropic and isenthalpic lines in the water zone are too closely bunched together to be informative.

13. PROPERTIES OF STEAM AND HOT WATER: GENERAL.

The ten charts described above can serve to illustrate very graphically some of the properties of steam and hot water, as will now be shown:

A.) **Flashing hot water.**

As an illustration of the flashing that results from the throttling of boiling water—an isenthalpic process—all the charts with the exception of Figs. 1-A and 10 have been marked up to show the expansion of boiling water at 400° F. (247.3 psia) to atmospheric pressure and temperature. In every case such an expansion is represented by a line (not always straight)—'OA. The final condition of the fluid after this isenthalpic expansion is 79.9% wet, or 20.1% dry.

In other words, 20.1% of the fluid at 400° F. would flash into steam if its pressure were throttled to atmospheric conditions. It will be noted that the line 'OA' is straight in Figs. 1-B, 2, 3 and 4 and that it is curved in Figs. 5, 6, 7, 8 and 9. It will also be noted that in Fig. 3 it is not possible to show the full expansion range because the vertical scale has been shown in terms of gauge, and not absolute, pressures. Thus atmospheric pressure is at an infinite distance below the base line; but from the approaching verticality of the dryness lines at lower pressures it is clear that point 'A' will lie fairly close to the 20% dryness line 'at infinity'.

If, on the other hand, the water at 400° F. (saturated) were expanded isentropically, doing work in the process at 100% efficiency, this would be represented in every case by the line 'OB' on the same charts. This line 'OB' shows that the available heat drop would be 24.3 BTU/lb (375.2—350.9) and that the final wetness would be 82.4%—i.e. that 17.6% of the water would be flashed into steam.

These figures (20.1% flash for isenthalpic and 17.6% for isentropic) clearly illustrate the different results from the two forms of expansion. The small scale of the accompanying charts is such that the figures cannot be determined with close accuracy, but if the charts were produced on a sufficiently large and precise scale, with interpolated contours (as with the printed Mollier Diagrams that can be purchased), the true

GEOTHERMAL ENERGY MAGAZINE • PAGE 28 • VOL 4 • NO 8 • AUGUST 1976

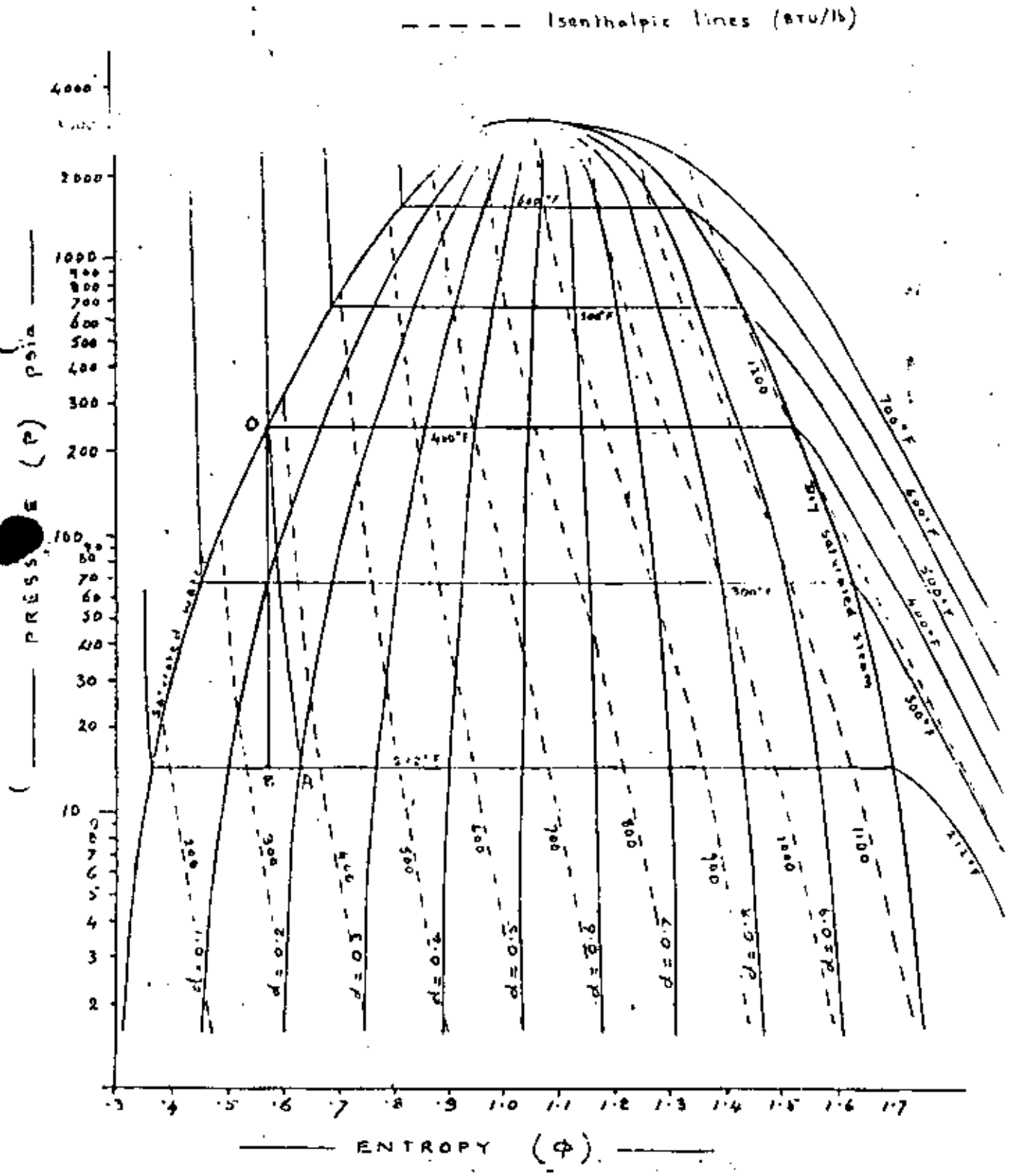

FIG. 6 ENTROPY/PRESSURE CHART (O/P)

GEOTHERMAL ENERGY MAGAZINE • PAGE 30 • VOL. 4 • NO. 8 • AUGUST 1978

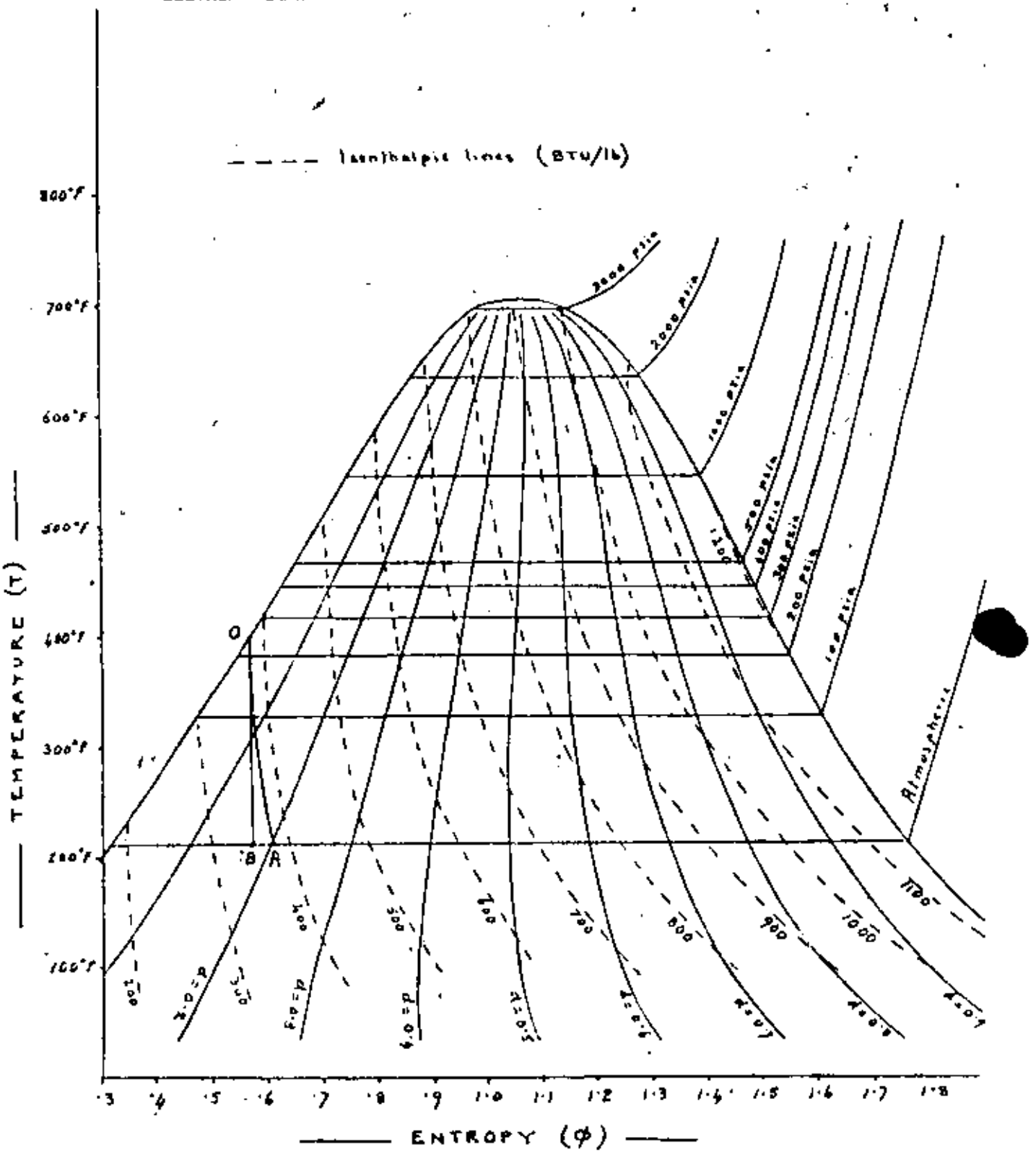

FIG. 7 ENTROPY/TEMPERATURE CHART (O/T)

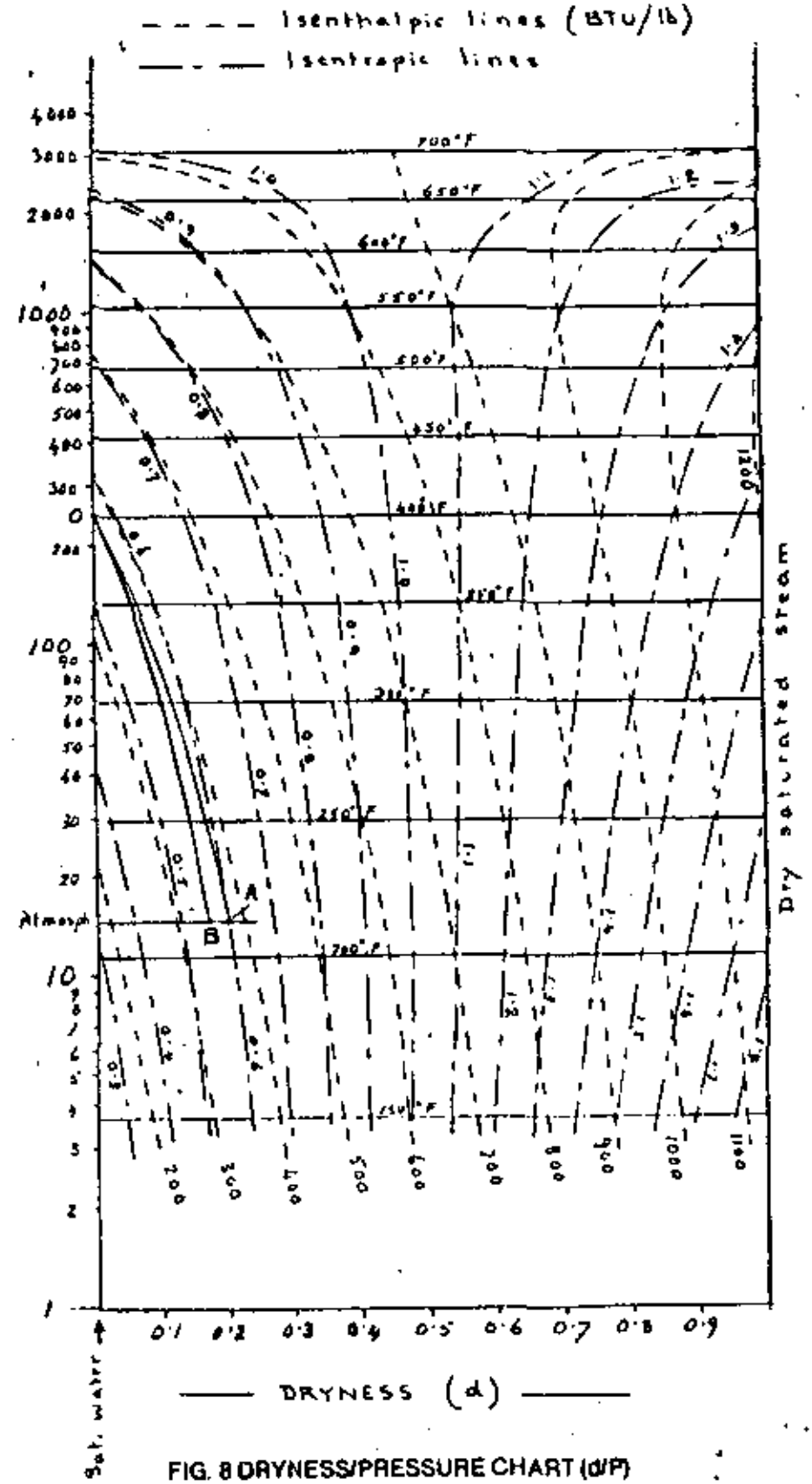

FIG. 8 DRYNESS/PRESSURE CHART (d/P)

figures could be gauged very closely.

It will be noted that the isenthalpic expansion yields a higher quantity of flash steam than the isentropic, to the extent of 2½% of the weight of the hot water in the example chosen (20.1 — 17.6%), owing to the reconversion into heat of the kinetic energy of expansion in the first case. More detailed discussion of these two methods of expansion can be found from 'The extraction of power from hot water', Paper 174, Section C4, World Power Conference, Moscow, 1968, by the present author.

Isothermal expansion of boiling water requires substantial intake of heat (i.e. increased enthalpy), as may be seen from all the charts except Figs. 1-A and 10.

B.) **Enthalpy 'hump'.**

The phenomenon referred to in Section 4 above, that the enthalpy of dry saturated steam attains a maximum value of 1205.6 BTU/lb at about 450° F., is clearly brought out in Figs. 1-A, 3, 4 and 6, and by implication in Figs. 5, 6, 7, 8, 9 and 10.

C.) **Isenthalpic expansion of dry saturated steam.**

At temperatures below about 450° F. this form of expansion will always have the effect of superheating dry saturated steam, though the effect is accompanied by some loss of temperature (Joule-Thomson effect). This loss of temperature follows from the angular diversion between the isotherms and the isenthalpic lines, as can be seen from Figs. 1-A and 3. But for very high temperatures and pressures, exceeding about 450 psia and 457° F., isenthalpic expansion of dry saturated steam at first causes slight wetness (owing to the 'enthalpy hump'), but after a certain degree of expansion (to less than about 447° F.) the steam becomes superheated. This can clearly be seen from Fig. 1-A where isenthalpic expansion of dry saturated steam from a point to the left of the 'enthalpy hump' must pass through a wet zone before recrossing the saturation line and entering the superheat zone. The same effect can be seen, though less obviously, from Figs. 3 and 4.

D.) **Isentropic expansion of dry saturated steam.**

In every case this will always result in increased wetness, as can be seen from Figs. 1-A, 3, 4, the upper part of Fig. 5, Figs. 6, 7, 8 and 9. It is, of course, well known that steam, in passing through a turbine tends to become wet in the lower pressure stages of expansion. This is because its expansion, when doing useful mechanical work, approaches (without quite achieving) the isentropic condition. The expansion of superheated steam isentropically, reduces the degree of superheat; and if extended sufficiently it will first become dry saturated and then wet.

E.) **Wetting and drying effects of isentropic expansions in the wet zone.**

Owing to the change of direction of slope of the isentropic lines in Fig. 2, it will be seen that isentropic expansion of moderately dry condition fluid (exceeding 0.5 dryness) has a wetting effect, whereas the isentropic expansion of boiling water or of steam of more than 0.5 wetness has a drying effect. This can also be seen from Figs. 3, 4, 5, 6, 7, 8 and 9, while the drying effect of isentropically expanding hot water is clear from Fig. 1-B.

F.) **Cerlical conditions.**

Although the critical conditions of water / steam cannot be clearly discerned from Fig. 1-A, they are graphically demonstrated by the 'humps' of Figs. 3, 4, 6 and 7; also by the horizontal lines of Figs. 2 and 5. With all charts having dryness as a coordinate (Figs. 2, 5, 8 and 9) the critical point cannot be shown since saturated water and dry saturated steam are represented by vertical parallel lines which cannot meet at a 'hump' except at infinity.

14. CHART DISCONTINUITIES

Owing to the fact that temperature and pressure are fixedly inter-related in the wet steam zone, but not in the superheat zone, some sudden directional changes are inevitable where smooth lines cross the saturation boundary. For example, in Fig. 1-A isotherms run parallel to the lines of constant presure in the wet steam zone but suddenly diverge on crossing the saturation line.

In that figure, lines of constant pressure, enthalpy and entropy run smoothly and uninterruptedly across the saturation line; but not the isotherms. Other charts show similar discontinuities. For example, temperatures change direction in Figs. 3 and 6 while pressures do so in Figs. 4 and 7 at the saturation boundary.

GEOTHERMAL ENERGY MAGAZINE • PAGE 34 • VOL. 4 • NO. 8 • AUGUST 1976

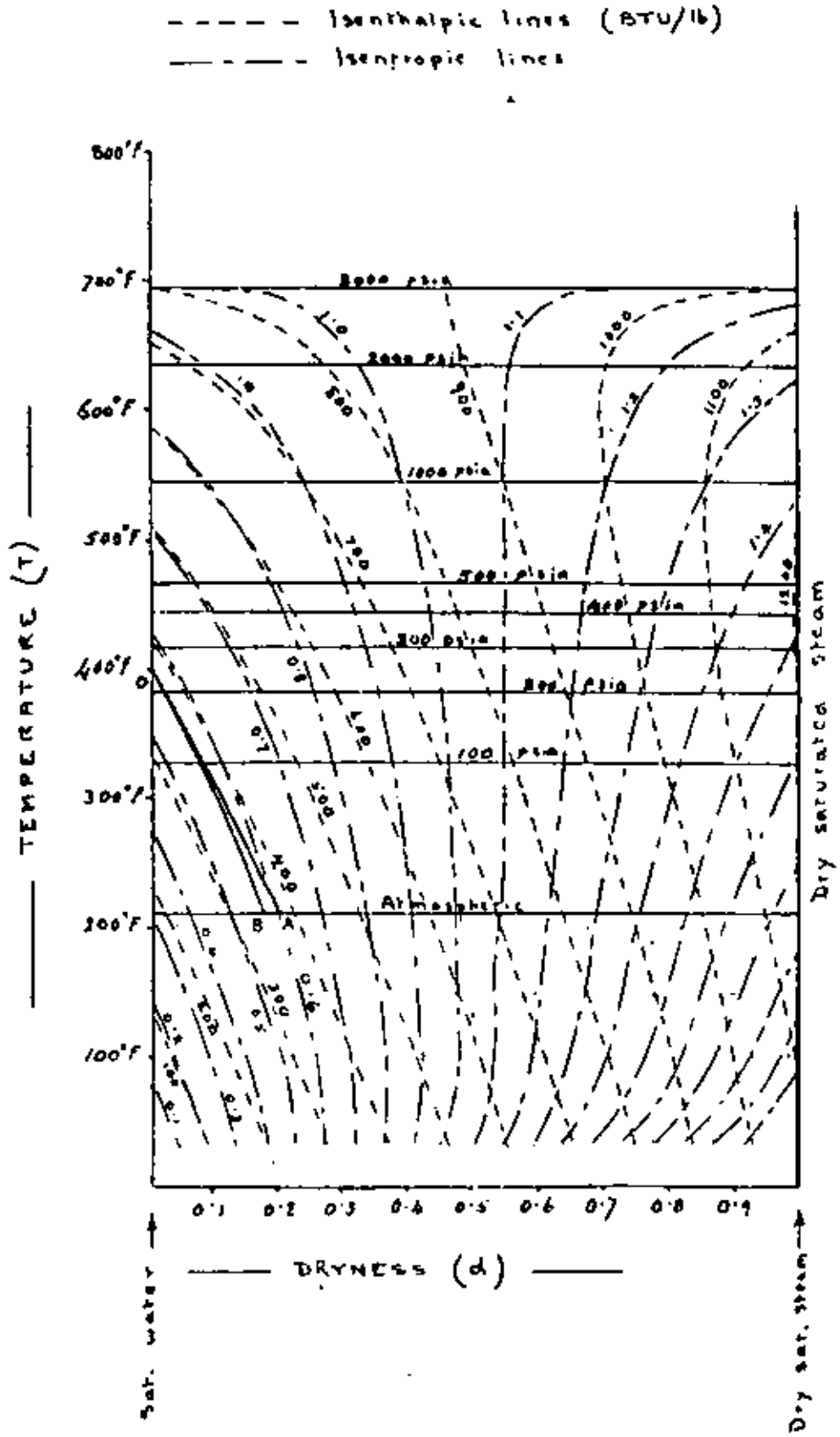

FIG. 9 DRYNESS/TEMPERATURE CHART (d/T)

GEOTHERMAL ENERGY MAGAZINE • PAGE 33 • VOL. 4 • NO. 8 • AUGUST 1976

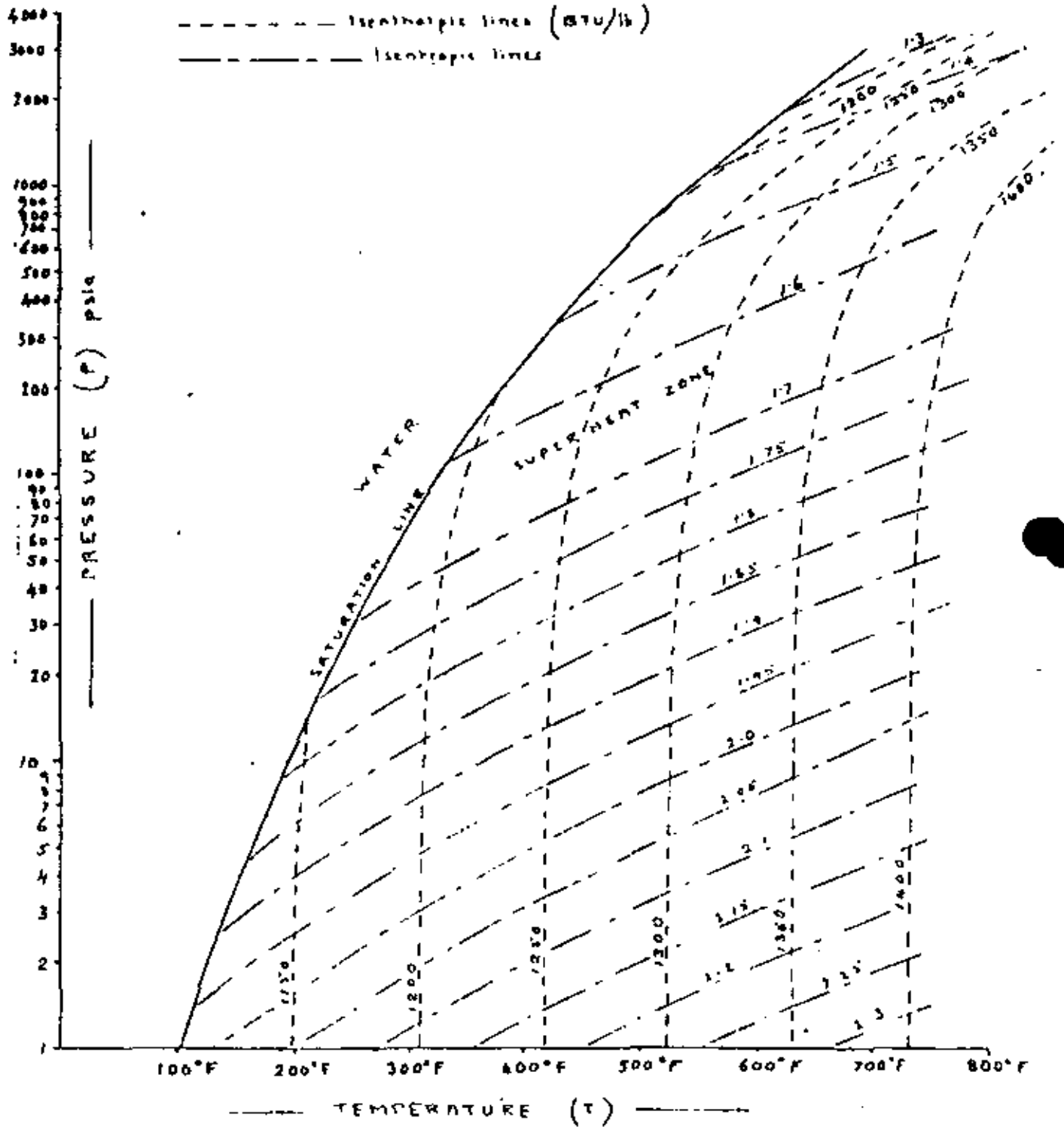

FIG. 10 PRESSURE/TEMPERATURE CHART (P/T)

GEOTHERMAL ENERGY MAGAZINE • PAGE 36 • VOL. 4 • NO. 8 • AUGUST 1976

15. CONCEPT OF NEGATIVE WETNESS OR SUPER-DRYNESS

From the formulae quoted in Section 2 it will be seen that dryness can be expressed either as

$$\frac{I_m - I_w}{L} \ldots \text{or as} \ldots \frac{O_m - O_w}{O_s - O_w}$$

It is tempting to suggest that by substituting higher values of 'I' and 'O' in place of 'I_m' and 'O_m' these formulae could enable Figs. 2, 5, 8 and 9, all of which have dryness as the horizontal axis, to be extended into a superheat zone to the right of the dry saturated steam boundary.

Certainly if 'I' and 'O' were to take on values representative of superheated steam, the expressions shown above would attain values exceeding 1.0, which would imply super-dryness or negative wetness. Moreover, an examination of the four figures drawn to a dryness base suggest that the lines and curves within the wetness zone might be extensible to the right of the dry saturated steam line.

However, on closer examination it will be found that little could be gained by so doing. It is true that the terminal directions of the isentropic and isenthalpic lines can be defined by choosing fictitiously high values for 'I_m' and 'O_m' which enable phantom points to be plotted on vertical lines of dryness having values exceeding 1.0 or less than 0, and on the extensions of the isotherms. But apart from that it is not possible to extend pressures and temperatures into the superheat zone on those charts without confusion.

For example, it would be tempting to suggest that the isotherms in Fig. 2 could be extended as straight lines beyond the saturation boundary. But these isotherms in the wet zone are also lines of constant pressure. The extended straight lines could not possibly represent both pressures and temperatures, since the two are no longer directly inter-related in the superheat zone. An example will illustrate the difficulty of achieving anything useful by extending either the constant pressure or constant temperature lines beyond the saturation boundary, even at deflected angles:

Consider wet steam at 300° F. and 67.01 psia. At these conditions we have : . . .

$O_s = 1.6359$
$O_w = 0.4371$
$I_w = 269.7$
$L = 910.5$

Now if a 'super-dryness' of 1.1 had any real meaning, then . . .

$$1.1 = \frac{I - 269.7}{910.5}, \quad \text{or} \quad I = 1271.2$$

$$\text{also } 1.1 = \frac{O - 0.4371}{1.6359 - 0.4371}, \quad \text{or} \quad O = 1.7558$$

Now superheated steam that satisfies these conditions of 'I' and 'O' would be at about 60 psia and 475° F., neither of which values lie on an extension of the 300° F./67.01 psia line crossing the wet zone. Thus isotherms *and* lines of constant pressure, if extended into the superheat zone, would *both* divert from the direction of the straight lines crossing the wet zone. Any attempt to draw isotherms and lines of constant pressure to the right of the saturation boundary would result in a confused and closely bunched maze of crossing lines.

16. VALUE OF CHARTS (Figs. 1 to 10 inclusive).

One conclusion of this analysis is that no chart can really rival the Mollier Diagram in general usefulness and clarity in the zone of superheated, dry saturated and moderately wet steam. Very possibly Mollier considered some or all of the charts here presented and made his choice accordingly.

For studying the phenomena of boiling water and very wet steam, however, the Mollier Chart shown in Fig. 1-A is really less satisfactory than Fig. 2 (I/d), Fig. 5 (P/d) or Fig. 7 (O/T).

Fig. 7 is generally quite a satisfactory chart in all zones, while Figs. 2, 3, 4, 5, 6, 7, 8 and 9 are useful for studying *isothermal* changes.

In Fig. 1-A the efficiency of an expansion in a turbine can be represented by a direct proportion of the vertical isentropic heat drop between two pressures; whereas with Figs. 5 and 7 the spacing of the isenthalpic lines is not uniform, so that interpolation becomes more difficult.

17. FLASH CHART

There is one more chart worth mentioning, though it does not form one of the series of ten described above. This is the 'Isenthalpic Flash Chart' (Fig. 11), which gives a very useful means of approximately estimating the proportion of flash steam formed when the pressure of boiling water is dropped through a prescribed range. (The word 'approximately' applies only to a flash

GEOTHERMAL ENERGY MAGAZINE • PAGE 37 • VOL. 4 • NO. 8 • AUGUST 1976

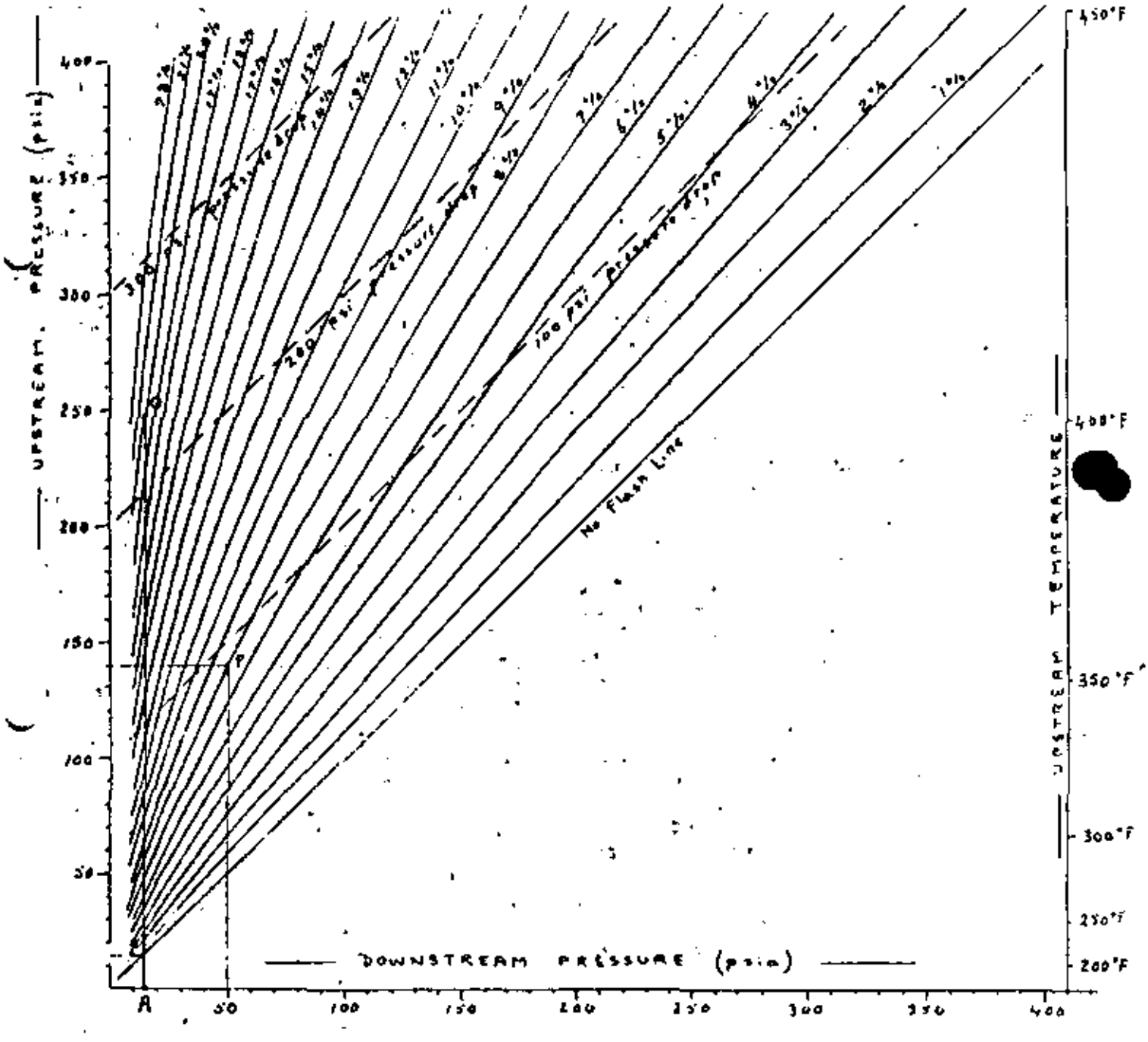

FIG. 11 ISENTHALPIC FLASH CHART

chart drawn to the small scale of the figure here presented: if drawn to a large scale it could be very accurate). The proportion of flash steam formed by the throttling of boiling water is given by the formula . . .

$$\frac{H_w - h_w}{L}$$

where . . . H_w is the enthalpy of the boiling water before throttling
H_w is the enthalpy of the residual water after flashing
L is the latent heat of evaporation at the downstream pressure.

For example, the case taken in Section 13(l) above (expansion from 232.6 psig, or 247.3 psia, to atmospheric pressure) is represented by the vertical line 'OA' in Fig. 11, which shows that about 20% flash would result.

Another example, represented by the point 'P' on the same chart shows that boiling water at 140 psia, in dropping its pressure isenthalpically to 50 psia would yield about 8% flash (more precisely 8.079% by calculation).

A similar chart could be prepared to show the flash percentages resulting from *isentropic* expansion of boiling water, but it would be of less use than Fig. 11 as isentropic expansion is a perfect ideal that is never realized in practice.

18. CONCLUSION

The analysis of Figs. 1 to 10 here presented may be regarded largely as an interesting mental exercise in thermodynamical virtuosity of rather limited practical value. It does, however, suggest that for the study of boiling water and very wet steam, Figs. 2, 5 and 7 are preferable to the Mollier Diagram, and that several of the charts are preferable to the Mollier Diagram for studying *isothermal* changes. For straightforward isenthalpic flashing calculations, Fig. 11 can be very useful (for example in geothermal work, where large quantities of boiling water often have to be handled).

Geothermics (1970) - SPECIAL IS

U.N. Symposium on the Development and Utilization of Geothermal Resources, Pisa 1970, Vol. 2,

The Behaviour of the Wairakei Geothermal Field During Exploitation

R. S. Bolton *

ABSTRACT

Since the first bore discharged at Wairakei in 1951, the total mass drawn from the field up to the middle of 1969 was 660,000,000 tons. Over this period, the rate of discharge has varied considerably from the gradual build up in the early years, to relatively sudden and substantial increases and decreases which have been imposed on the system from time to time.

This paper describes the changes which have taken place in the underground pressures and temperatures and in the nature of the discharge from the field during exploitation. The relationship between these factors is discussed, and the conclusion presented that the Wairakei system consists basically of a highly permeable hot water aquifer contained within almost impermeable boundaries. Under exploitation, the dominant influence on the system is the saturation temperature pressure relationship for water, but the withdrawal of steam from the upper levels, and the existence of a hot inflow at the lower levels have also played an important part.

A satisfactory mathematical model having a predictive ability has not yet been formulated, but from a consideration of the past behaviour, in general terms, the power output of the Wairakei station can be sustained at or near its present level for a number of years to come.

Introduction

General

Since the first bore was discharged at Wairakei in 1951 the total mass withdrawn from the field to the middle of 1969 was approximately 660,000,000 tons. The removal of this mass has, as could be expected, been accompanied by changes in the aquifer conditions. Both pressures and temperatures at depth have fallen, the former substantially. The other change of importance is that both the field discharge, and the discharge from individual bores has declined. This paper describes the changes that have taken place, the relationships between them, and an interpretation of the aquifer based on them.

It should be noted that this paper is concerned only with changes in pressure, temperature and discharge. Other changes which have taken place are covered in the papers presented to this conference by Grover (1970) who discusses the gas compositions of the fluids discharged, Hatton (1970) who discusses ground level movements, and Hunt (1970) who discusses gravitational changes.

* Ministry of Works, P.O. Box 12041, Wellington, New Zealand

Definition of the Wairakei field

In this paper, the Wairakei field is defined approximately as the area bounded by the Wairakei stream in the north and north-east, the Waikato river to Huka Falls in the south-east, the Waipouwerawera stream in the south and Poihipi road in the west. These features may be seen on Figure 1. This area has been defined on the basis of observed changes in pressures.

Definition of groupings of bores

When discussing the various changes, different groupings of bores are referred to. These groupings are essentially geographical, and are defined as:

a) *Production area bores* - these are in the area served by the steam mains, although not necessarily connected to them.

b) *Outer area bores* - these are bores outside the area served by the steam mains, but within the area affected by exploitation.

c) *Peripheral bores* - this group comprises five bores (bores 33, 36, 223, 224 and 111-21) which are on or outside the boundaries of the Wairakei field as defined above, and which stand shut with no wellhead pressure.

Geology

The geology of the field is an important factor in the exploitation. Full details have been published elsewhere (Grindley 1965) but the main features in the production area may be summarised as:

a) *Surface formations* - pumice and loosely consolidated breccias to about 400 feet.

b) *Huka falls formation* - mudstone-siltstone layers, interbedded in some areas with breccias. This formation ranges from about 400 to 600 feet in thickness. It is generally impermeable and acts as a cap rock although the natural activity indicates that fissure permeability is present.

c) *Waiora formation* - reasonably well consolidated breccia with mudstone-siltstone stringers and silicified lenses. In the western part of the production area, the lower contact of this formation is about 2000 feet

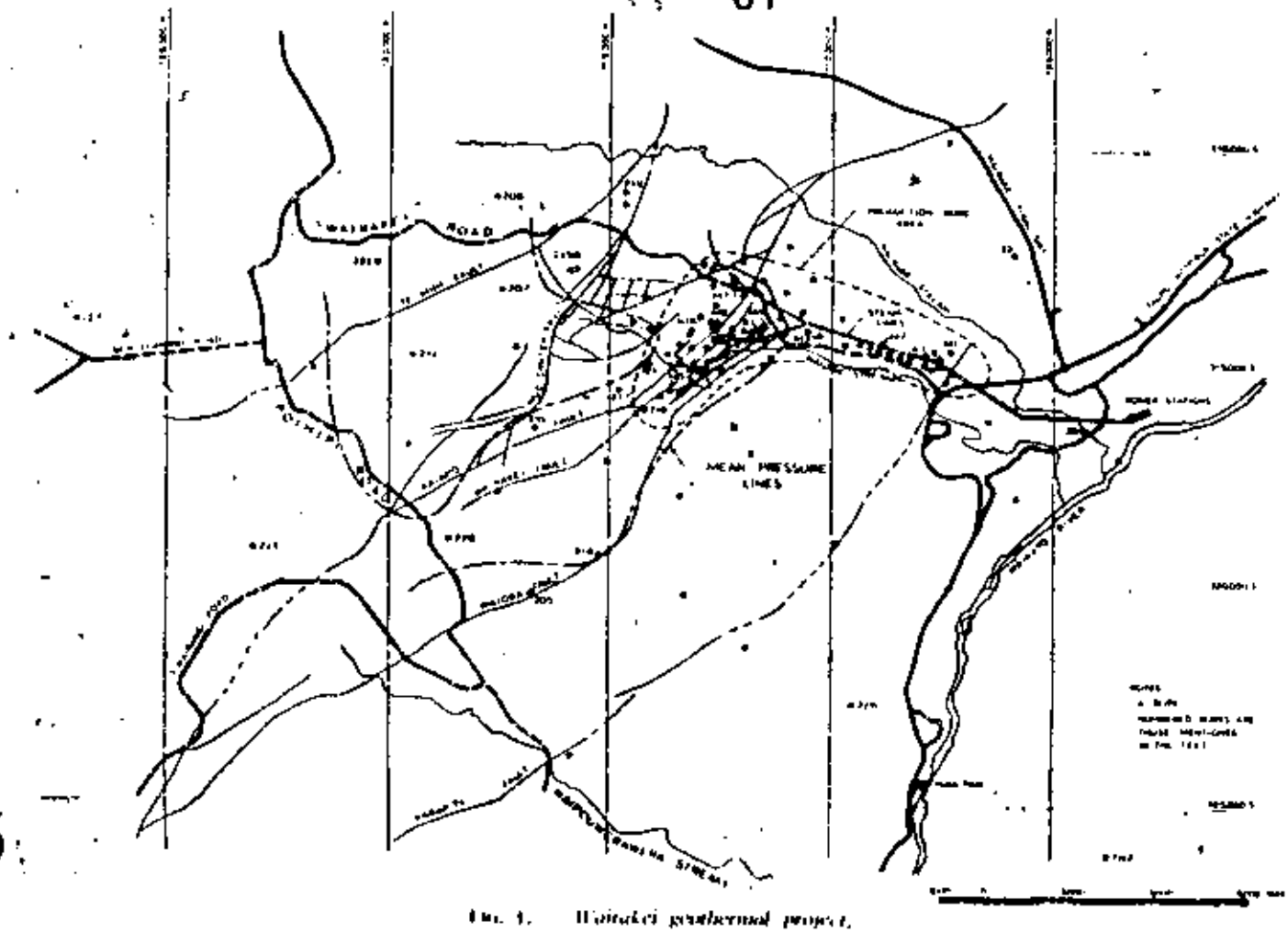

FIG. 1. *Wairakei geothermal project.*

deep, but to the east, the lower contact dips very sharply and the formation has not been drilled to its full depth. Generally speaking, the formation is permeable and provides a significant proportion of the fluid production.

d) *Wairakei ignimbrites* - the contact between the Wairakei ignimbrites and the Waiora formation is very broken, and provides the main production zone. The ignimbrite itself has a very low production capability.

In the outer area, there are substantial rhyolite intrusions in the Waiora formations. In the upper levels, the Huka Falls and Waiora formations thin out and in the lower levels, the contact between the Waiora formation and the Wairakei ignimbrite is displaced downwards by some 1500 feet.

The other important geological feature is, of course the extensive faulting in the area. As may be seen from Figure 1 the main faulting system runs in a south-west-north-east direction, with transverse faulting in the regions of most intensive natural activity. From drilling, it is evident that the faults can be open at depth, and there is little doubt they exert a strong influence on the underground flow conditions.

Trends in downhole pressures

General

Pressures discussed in this paper are those at a level 900 feet below sea level (Reduced Level or R.L. -900). This level is not considered to be critical, the pressure at all levels below water level showing the same pattern as those at R.L. -900.

From pressure measurements and other observations, it is clear that, before exploitation began, the Waiora formation was filled with hot water to the underside of the Huka formation. The pressures below the mudstone were essentially hydrostatic, with a small superimposed pressure which did not exceed 30 psi. Temperatures are discussed later, but to define the term hot water used above, the temperature increased with depth below the mudstone, following the pressure temperature saturation curve for water, to a maximum which varied with the bore, but which did not exceed 260°C.

Pressure trends within the field

While in general the drop in pressure has amounted to about 300 psi, in the eastern part of the production

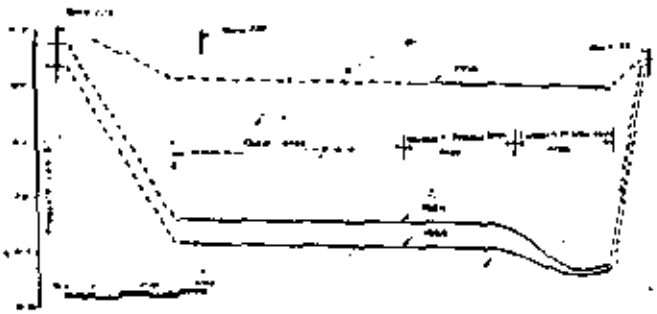

FIG. 2. *Pressure profiles in 1956, 1964, and 1968 (pressures at R.L.-900).*

area, the fall has been greater, and is about 350 psi. On the other hand, the fall in the outer area has been almost the same as that in the western, or main part of the production area. In detail, to the north and south of the outer area, pressures are slightly higher than those in the production area. Between these two zones however, and reaching from the production area to the western boundary of the field, the pressures are the same as those in the production area.

These features of the behaviour of the pressures are shown in Figure 1 and 2. The latter shows the pressure profiles in 1956 before there was any substantial exploitation, and in 1964 and 1968. Figure 1 shows among other things, mean pressure contours for the outer and western production area bores for the first three months of 1968. The close correspondence between the mean pressure contours and the major faulting pattern in the field is noticeable.

Figure 3 shows the decline in pressures with time, together with the average monthly production expressed in terms of kilopounds per hour. As can be there is a close correlation between the rate of pressure and the output. One aspect, which is particularly noticeable in recent years, is that in any period where the rate of discharge has been sensibly constant, pressures decline at a decreasing rate.

In the first three months of 1968, the addition of new generating capacity to the New Zealand electrical system gave the opportunity for a brief, partial shutdown of the Wairakei field. In this period, the output from the field was reduced to approximately one third of the normal discharge. During the shutdown, pressure rose throughout the field by approximately 11 psi. As soon as the field was reopened, the pressures began falling. While the rise which occurred was small relative to the total drop in pressure it was nevertheless significant.

PERIPHERAL BORES

Bore 33: Bore 33, situated about 6500 feet to the east of the production area is 1600 feet deep. It was drilled in 1963 and the maximum temperature measured in the bore was 88°C. The water level (Figure 4) has fallen more or less uniformly since the bore was drilled, at a rate of fall which appears to be independent of the mass discharge from the field. That is to say, the fall in the early years is the same as at present, even though the mass discharge is now 7 times larger.

Bore 224: Bore 224 is situated about 5 miles west of the production area, and 6500 feet from the nearest bore in the field. It was drilled at the end of 1963 to

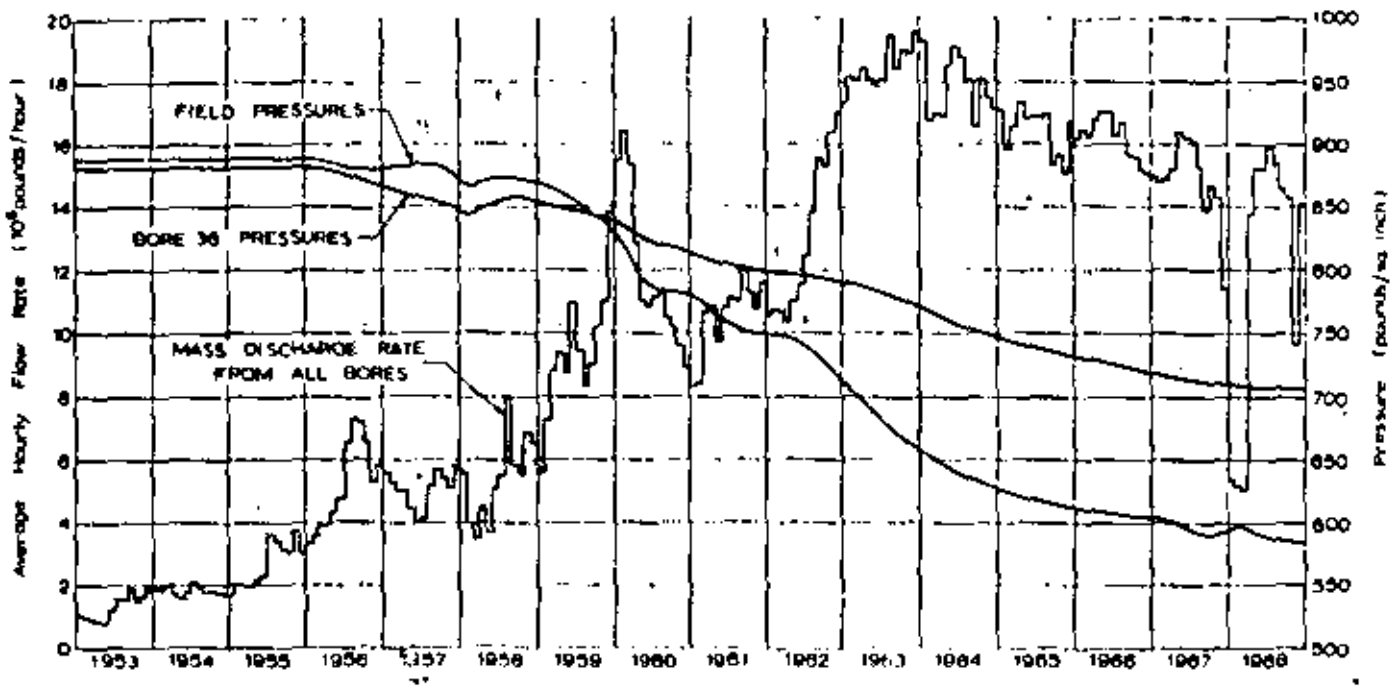

FIG. 3. *Field discharge rate and pressures: bore 36 pressures (pressures shown are at R.L. 900).*

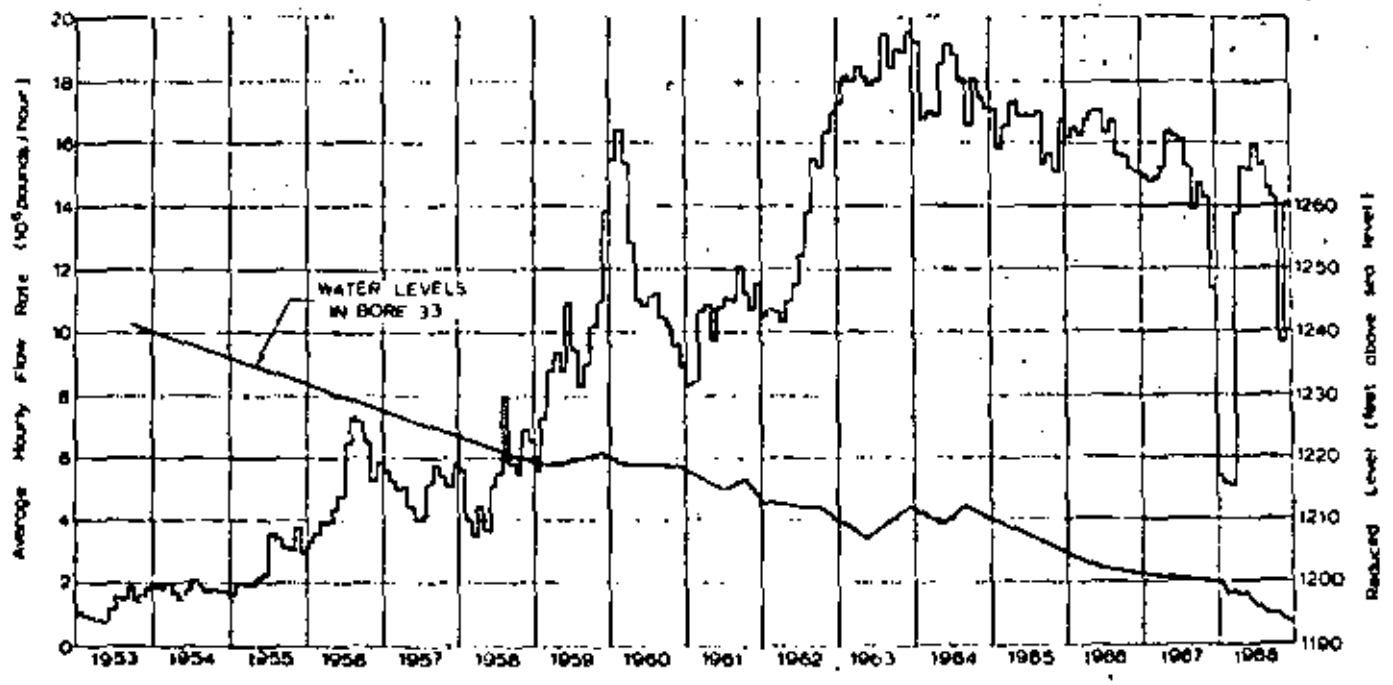

Fig. 4. — Water levels in bore 33.

a depth of 4100 feet. The maximum temperature measured in this bore was 82°C.

Figure 5 shows the water levels in this bore from May 1964, some 5 months after completion, to the end of 1968. There has been a fall of nearly 300 feet in this period, with the fall in the earlier years steeper. This fall is equivalent to a pressure decline at R.L. -900 of approximately 43 psi. In the same period, pressures in the field fell by about 100 psi.

Bore 223: Bore 223 is probably one of the most significant, and certainly one of the most interesting of the peripheral bores. It is situated some 2½ miles south-west of the centre of the production area, and is drilled to 4481 feet. It was completed in August 1963, and the maximum temperature was 123°C at hole bottom, measured 16 days after completion. This temperature had fallen to less than 100°C three months after completion, and has never exceeded this subsequently. Since completion, pressures in this bore at R.L. -900 have been lower than, and have followed the trends in the pressures in the field. During the shutdown in early 1968, the water levels in bore 223 responded immediately to the changes in field discharges. This is shown in Figure 6.

Bore 36: Bore 36 is 9500 feet east-south-east of the production area. It was completed in September 1954 at a depth of 2006 feet. The maximum temperature in this bore was 146°C at 1300 feet depth.

The pressures at R.L. -900 are shown on Figure 3, which also shows the field pressures. The pressures in bore 36 were initially lower than those in the field, and followed them fairly closely. However, in 1959,

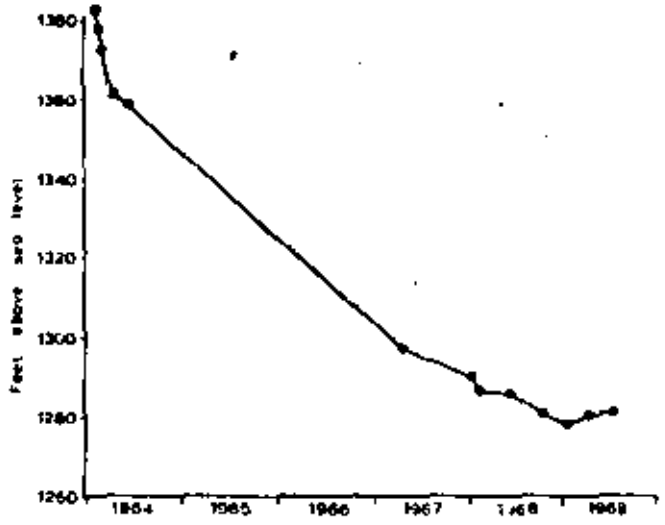

Fig. 5. — Water levels in bore 224.

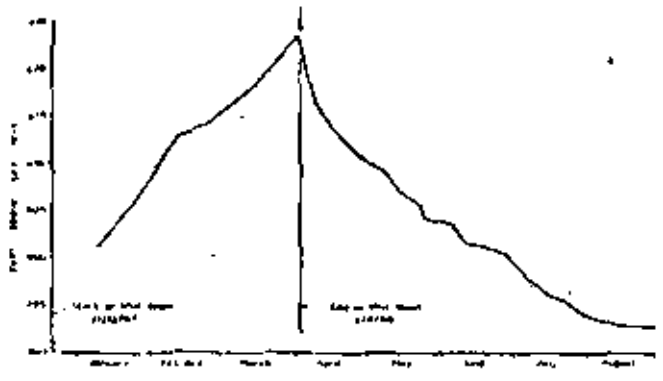

Fig. 6. — Effect of partial shutdown on bore 223 water levels.

when the field pressures began to decline more rapidly, the rate of fall in pressure in bore 36 became less. This difference in the rates of decline has persisted until at the present time, pressures in bore 36 are about 120 psi higher than those in the field.

Water levels were also measured in this bore during the 1968 partial shutdown. The water levels were not influenced by the shutdown, but were declining at a rate equivalent to 20 feet per year, and stood at R.L. -870 in January 1968.

Bore TH 2: This bore is 3 miles to the southeast of the Wairakei production area, and is situated in what is considered to be a separate geothermal area, called Tauhara. It was completed in May 1966 at a depth of 3988 feet, the maximum temperature being 255°C. In spite of this high temperature, the bore stands with no wellhead pressure, and with water level about 500 feet below the surface.

Downhole pressures in this bore are somewhat erratic but from the middle of 1967, water level measurements have provided a reliable indication of pressure changes in the bore. They have shown that the water level is declining at a rate equivalent to 20 feet a year. It will be noted that this is the same rate of fall as in bore 36. It is also of interest that the water level in bore 36 is some 30 feet higher than that in bore TH 2.

Trends in downhole temperatures

General

There have been several thousands of temperature runs taken in the Wairakei bores over the years. From these runs, it is clear that downhole temperatures have fallen, but there are a number of factors which must be taken into account when interpreting this fall. While a discussion on the interpretation of downhole runs is outside the scope of this paper, the extent to which the distribution of temperatures measured in a bore represents the distribution in the surrounding formation is of importance. In many cases, the borehole temperatures can be taken as formation temperatures, but not in all. On the other hand, the maximum temperature measured in a stable temperature run can reasonably be assumed to correspond to formation temperature at that level. In this context, stability is somewhat loosely defined as not changing rapidly over a few days. The temperatures discussed in this paper are therefore the maximum temperatures measured in temperature runs, which as far as can be ascertained are stable.

Temperatures vary both with bore location and with depth. These factors have been taken into account by dividing the bores into three groups geographically, and the depth into intervals of 400 feet. The groups selected are the eastern production area bores, the western production area bores and the outer area bores. The latter group includes bores 205, 206, 207, 210, 212, 215, 218, 219, 220 and 222. Bores 216 and 217 are considered with the western production area bor[illegible] and the cold outer area bores have been excluded.

Trends with depth and time

Figures 7, 8, and 9 show the average maximum temperature with depth for each of the three groups respectively. The average is the average of all maxima occurring in the period of time and the depth interval concerned, and is plotted at the centre point of the depth interval. To give an indication of the reliability of the averages, the standard deviation and number of observations are shown for each.

The production area bores were divided into three periods, and the outer area bores into two. The time intervals are different for each group, the difference being dictated in part by the number of observations available, and in part by the apparent variation with time.

The dependence of temperature on depth is shown clearly by Figure 7 for the eastern production area bores. The significant features of Figure 7 are, however, that there has been no change in the average for the lowest depth interval, and that above this level, temperatures have fallen with time, the rate of fall increasing with decreasing depth.

For the western production area bores, the dependence of temperature on depth is not so well de[illegible] This is in part because the depths considered are gre[illegible] than those for the eastern production area bores. The

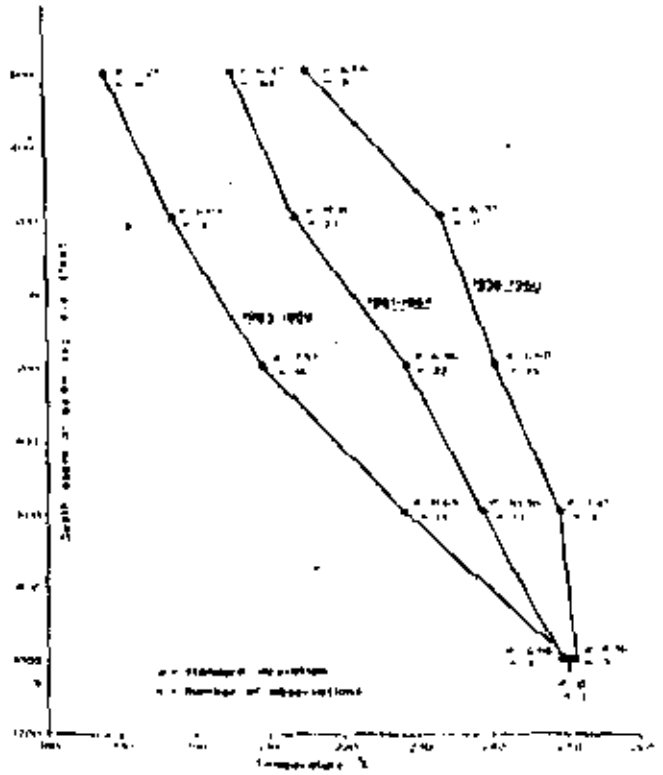

FIG. 7. *Eastern production area bores: average maximum temperature against depth.*

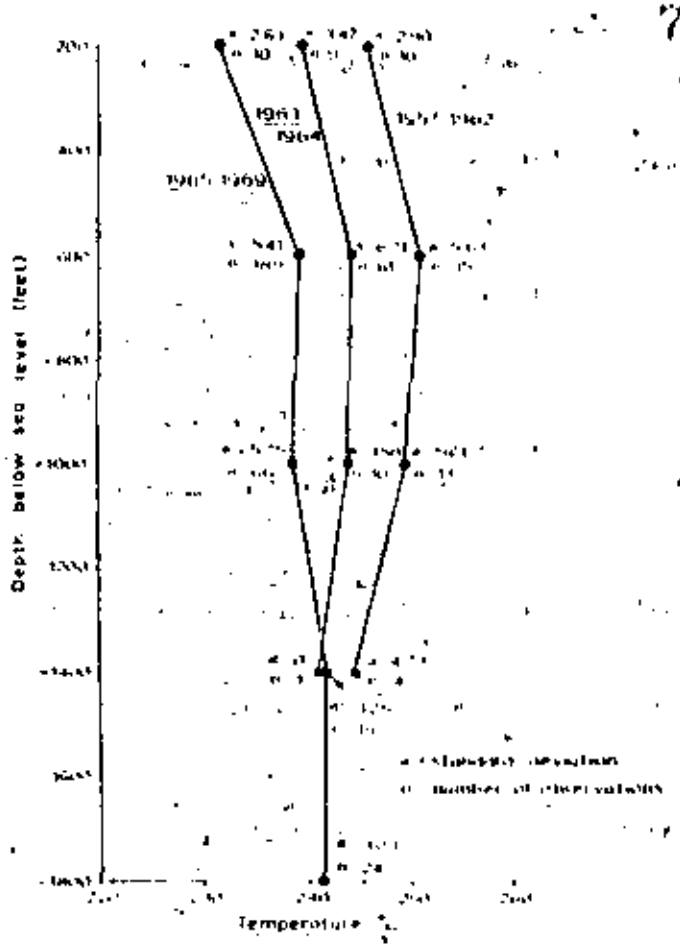

FIG. 8. — *Western production area bores: average maximum temperature against depth.*

temperatures at the upper levels have fallen, but for these bores, the rate of fall with depth is more uniform.

For the outer area bores, the main feature is that there appears to have been no change with time. The bores in this group are considerably deeper than those in the other two groups and the dependence of temperature on depth is only very slightly evident.

The curves on Figures 7, 8, and 9 cannot be taken to represent the true distribution of temperature with depth in the formation nor do they show in detail how the temperatures have varied with time. Nevertheless, they show clearly the manner of the temperature fall. That is to say, at the greatest depths there has been no detectable change in temperature, but at the upper levels, the temperatures have fallen, the fall increasing with decreasing depth.

Trends with time: western production area bores

To examine in more detail the temperature variation with time, the mean temperature for each six monthly period from July 1957 to December 1968 was determined for the western production area bores. All observations used in deriving the curves on Figure 8 were included, and some depth effect is therefore present. This however, is relatively small.

The mean temperatures are shown on Figure 10. The smooth curve for the trend in temperature has been drawn on the assumption that the changes have occurred smoothly within the range encompassed by the 95% confidence limits for the means. The wide confidence interval in the early years results mainly from the small number of observations available for analysis in those years.

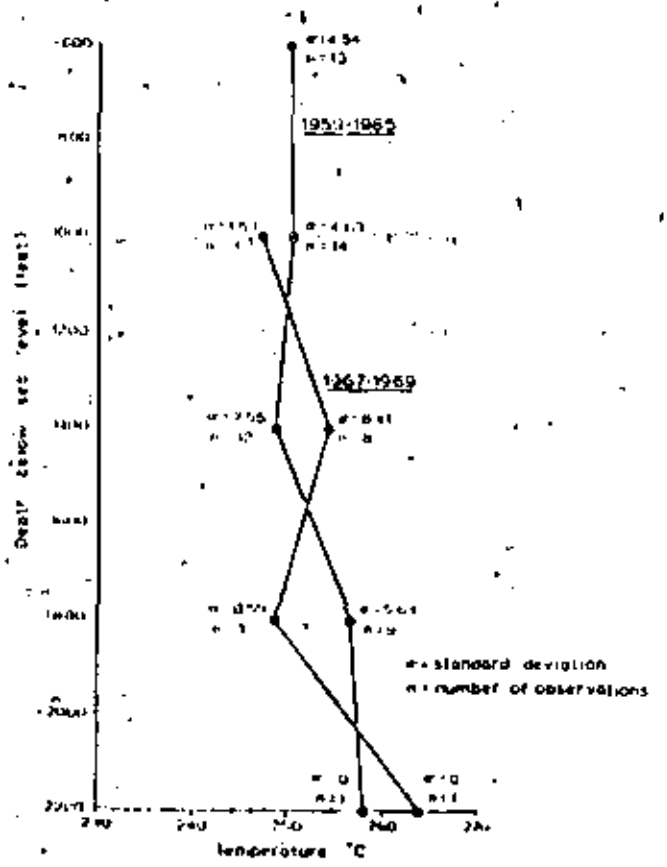

FIG. 9. — *Outer area bores: average maximum temperature against depth.*

Figure 10 shows that the average fall in the maximum temperatures for the western production area bores has been approximately 12°C, and that the main fall has occurred over the period 1963-1964.

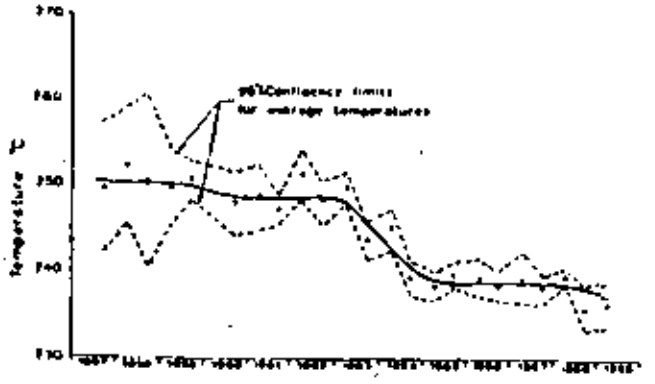

FIG. 10. — *Western production area bores: average temperatures*

Temperatures in bore 121

In December 1968, bore 121 at Wairakei was completed at 7400 feet (R.L. -5900) with slotted liner in the bottom 2160 feet. This bore, situated in the western production area, penetrated the ignimbrite which underlies the Waiora formation, and in which the temperature reversal (decline with depth) below R.L. -1000 on Figure 8 occurs. From the discharge characteristics of the bore, the formation permeability in the bottom length is low, compared with that at the production levels.

Figure 11a shows the temperature rise at hole bottom since the bore was completed. At the time of writing, some 230 days after completion, the bottom hole temperature was still rising. The long heating up period is abnormal, compared with other holes drilled at Wairakei, but is probably related to long periods of cooling while drilling the bore, together with the impermeable nature of the formation. The latest temperature shown, approximately 270°C, is higher than any measured previously at Wairakei, although not as high as had been measured in other fields. The temperature distribution over the bottom 1300 feet of the bore is shown in Figure 11b. This curve is the mean of the two temperature runs on the bore measured on the 18th and 25th of July 1969, and shows that the temperature is increasing with depth.

Trends in bore and total field discharges

General

The withdrawal of a large mass has resulted in the changes in underground pressures and temperatures described in the previous sections. These changes have, in turn, influenced the rate at which both the field as a whole, and the individual bores can discharge. It is possible that changes in the rates of discharge of individual bores are also influenced by chemical deposition, but there is insufficient evidence available at present to make even a qualitative assessment of any effects due to this cause.

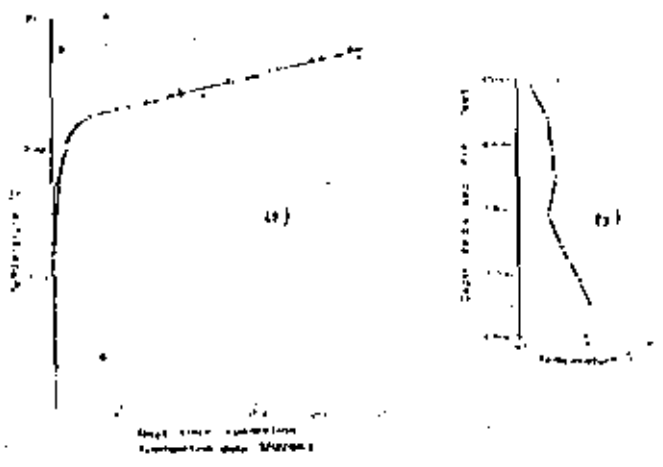

FIG. 11. *a) Bore 121, rate of temperature increase at hole bottom. b) Bore 121, temperature distribution over the bottom 1400 ft.*

Total field discharge

The changes in the discharge rate of the field as a whole, are very strongly influenced by the manner in which the field is operated. It is therefore difficult to make a reliable quantitative estimate of the effect of underground changes on the discharge rate. The main operational functions which affect the field discharge rate are changes in the number of bores discharging and changes in the wellhead operating pressure of the bores. Moreover, the very big differences in the characteristics of individual bores mean that the particular bores discharging can influence the total rate of discharge on the field.

In general terms, the effect of downhole changes on the total field discharge may be seen in the mass discharge curve on Figure 3. From a peak in the latter half of 1963, the average rate had declined to about 80% of this maximum by the end of 1968. In this period, the number of bores discharging remained substantially constant, the various irregularities in the curve being the result of station operation.

If the total field discharge is examined in terms of average bore outputs, the relationship between downhole changes and changes in field discharge rates become clearer. Figure 12 shows the enthalpy of th

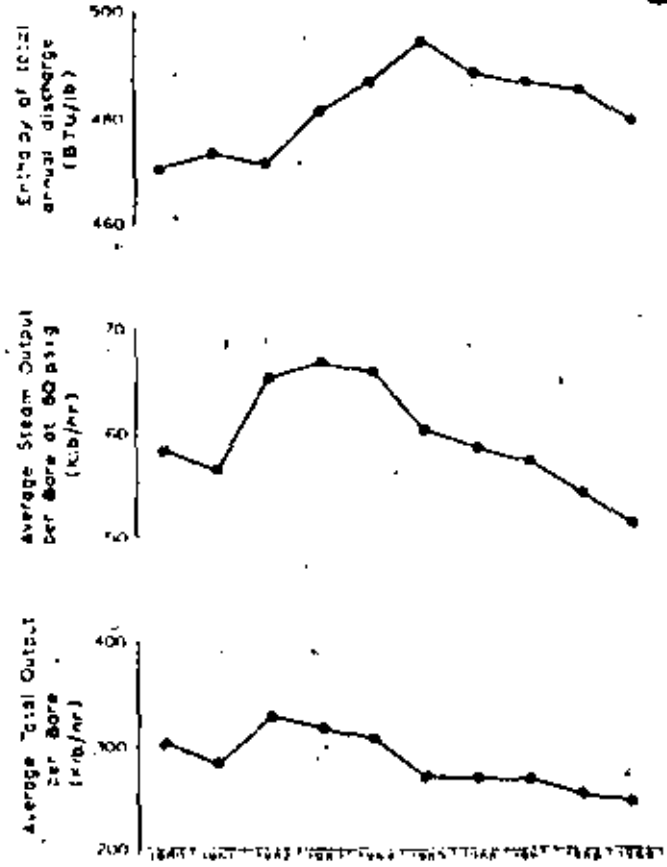

FIG. 12. *Average field discharge characteristics.*

tal annual output, and the average mass and steam discharges per bore, determined for the average number of bores discharging. The latter was determined for each year by summing the number of months individual bores were discharging and dividing by 12. For 1968, the averages are based on the latter 9 months of the year because the effects of the field operation during the partial shutdown over the first 3 months were sufficient to mask the influence of changes in underground conditions. Also, the averages for 1969 are based on the first 6 months operation only.

Referring to Figure 12 the average total discharge was at its peak in 1962. The lower figures in 1960 and 1961 were due mainly to the fact that predominantly low output bores were discharging in this period. After 1962, the average discharge fell relatively steeply from 1964 to 1965, the fall being more gradual from 1962 to 1964, and from 1965 to the present. The enthalpy of the average field discharge was substantially constant over the years 1960-1962 at approximately 470 BTU/lb. This figure is only slightly higher than the enthalpy corresponding to the average temperature in the western production area bores over the same period (Figure 10). From 1962, the enthalpy rose to a peak in 1965, and has since fallen gradually.

The average steam, based on an assumed pressure of 80 psig, follows in general the total discharge. However, the influence of changes in enthalpy can be seen from the peak steam output which occurred in 1963. The steam output in 1969 is just over 75% of the peak output in 1963.

The changes which have taken place in the rate of discharge from the field as a whole have been illustrated using the total field output and enthalpy as measured, together with the average number of bores discharging. In this manner, the influence of variations in the number of bores and the characteristics of individual bores discharging is minimised, but the trends shown still include the effect of reducing wellhead operating pressures. However, this does not invalidate the conclusions reached regarding trends, because the reduction in pressure has been relatively small and its effect is to maintain outputs. In other words, the downward trend would have been greater had the wellhead pressures not been reduced.

Individual Bore Discharge

The effects of downhole changes on the output of individual bores is illustrated by Figure 13 which shows the changes which have occurred in bore 43, situated in the eastern production area, and bore 81, a western production area bore. The curves show for each bore the total output, steam output and enthalpy against wellhead pressure measured by output tests before and after the main draw down had occurred. The maximum pressure at which the bores would discharge is also shown. Bore 43 was originally a high pressure

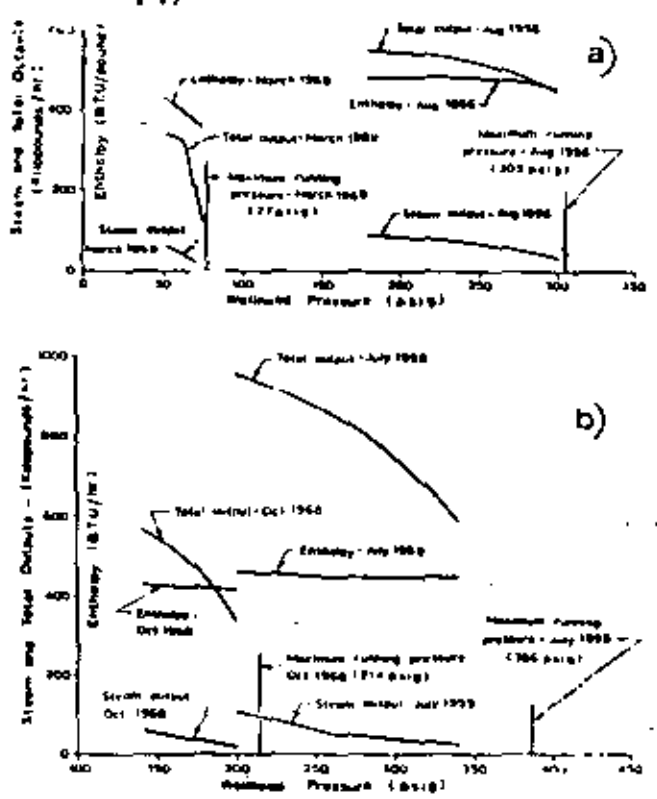

Fig. 13. — *a) Bore 43 output characteristics. b) bore 81, output characteristics.*

bore, but, for obvious reasons, is now operating at intermediate pressure. Bore 81 is still operating as a high pressure bore, but at a considerably reduced output.

Power Generation

The total generation from Wairakei reached a peak of 1290 million kWh in 1965, and has been maintained at over 1200 million since. This is shown in the lower graph on Figure 14. The figures for 1968 are based on the station operating over the whole year at the same average figure as for the latter 9 months (i.e. the effects of the shutdown have been removed) and

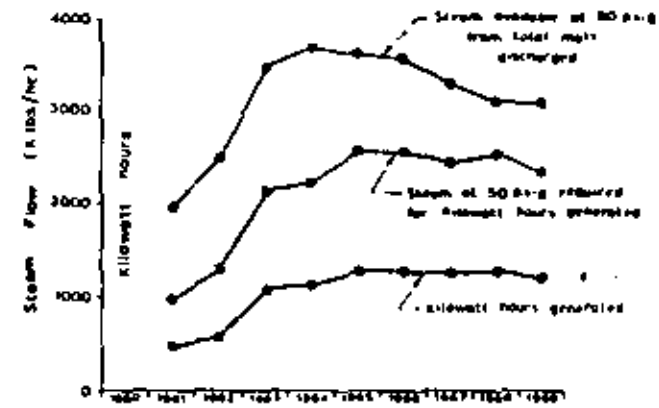

Fig. 14. *Kilowatt hours generated, steam required and steam available.*

similarly, for 1969 the generation for the whole year is based on that for the first 6 months. The reason why it has been possible to maintain the generation rate in spite of the marked decline in output as described above is shown on the other two graphs in Figure 14.

The first shows the steam flow required using the assumptions that all generation was from steam at a turbine stop valve pressure of 50 psig, and that 17 pounds of steam are required per kWh at this pressure. The other curve shows the total steam available at a wellhead pressure of 80 psig from the total mass discharged. Clearly, on the basis of these assumptions, there has always been a surplus of steam.

The bores have not, of course, all been operated at 80 psig wellhead pressure, but at either a pressure which was initially 200 psig and which has subsequently been reduced, or at 80 psig. It should be noted that these are average pressures, the pressures for individual bores depending on the distance from the powerhouse and the length of branchline. The use of the two operating pressures has resulted in the large apparent surplus of steam in the earlier years, because the separated water from the high pressure wells was wasted. This meant, of course, that the steam obtainable by flashing the separated water at 200 psig to 80 psig was not in fact available. A discussion on the design of the scheme is outside the scope of this paper, but it is obvious that the same electrical power could have been generated with substantially smaller drawoff from the field had the scheme been designed originally as a single pressure system. This would in turn have been reflected in the behaviour of the field. At an early stage a pilot scheme to use the high pressure hot water was installed and tested, but was not extended because the water output from the particular wells selected decreased substantially.

It has been possible to maintain the electric power output using methods which in fact tend towards the concept of a single pressure system. The first is to reduce the turbine stop valve pressure of the high pressure machines, which in turn reduces the wellhead pressure of the high pressure wells and leads to an increase in output. Further, as the output of a high pressure well declines, at the appropriate time the production is transferred to the intermediate pressure steam transmission system. The third method is to gather the separated water from a group of high pressure wells, and flash this to give steam at intermediate pressure. For details of the earlier pilot hot water scheme, and present use of separated high pressure water, see the paper by Wilcox (1970) presented to this conference.

To conclude this section, the following table shows the changes which have occurred in the relative numbers of the bores on production to the powerhouse between 1962 and 1969.

	Intermediate Pressure Bores	High Pressure Bores
Number of bores in 1962	26	[redacted]
Number of bores *downgraded*	9 (1) (2)	14 (3)
Number of bores drilled since 1962	2	10 (3)
Number of bores in 1969	32	29

Relationship between temperatures, pressures and discharge

Theoretical considerations

When exploitation began, the aquifer was filled with hot water which in the upper levels was at, or near the boiling point temperatures for the aquifer pressure. With increasing depth, temperatures increased to a maximum while pressures continued rising indefinitely with depth. In these circumstances, the changes in aquifer conditions will be influenced predominantly by the saturation pressure/temperature relationship for water. That is to say, if the pressure at any level falls below the saturation pressure, boiling must occur, and the temperature must fall.

Starting with the initial conditions described above, Figure 15a illustrates diagramatically the effects of exploitation. It is assumed that after a given mass has been withdrawn, the system is allowed to stabilise. In Figure 15a the mass withdrawn is represented by a fall in water level x, which, in the absence of any other factor, is equivalent to a fall in pressure at the water level from *a* to *b*. This fall in pressure would be accompanied by the fall in temperature *A* to *B* in Figure 15b. However, the formation rock temperature cannot fall in this fashion nor can it remain higher than water temperature. Therefore, by transfer of heat from the rock to the water, an equilibrium temperature will

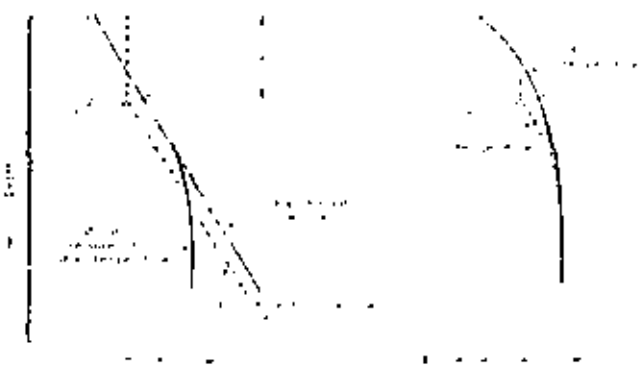

Fig. 15. *Diagrammatic representation of aquifer behaviour.*

(1) This includes one bore abandoned because of broken casing.

(2) Downgraded intermediate pressure bores cannot charge to the steam mains, although they may still be capable of discharging.

(3) This includes one intermediate pressure bore which was upgraded to high pressure after reconditioning.

be reached between *A* and *B*. This is shown as *C* in Figure 15b. Since saturation conditions exist at the water level, the pressure will fall correspondingly to *c* (Figure 15a).

Below water level, pressures at all depths will fall by the amount *a-c*, the temperature will fall with depth down to the depth where the pressure exceeds the saturation pressure and heat will be made available from the depth over which the temperature fall occurs. Above water level, the pressure will remain substantially constant at *c*, the water level pressure. That is to say, the formation will be steam filled. For this to occur, the top level of the formation will have to be heated up and the heat for this comes from the heat made available by the cooling which occurs lower down. In the absence of any other loss of heat, the final pressure distribution will be determined by balancing the heat required to heat the upper levels with the heat made available by cooling lower in the aquifer, after making allowance for the heat extracted with the mass drawn off.

With continued drawoff, and neglecting any effects of inflow, stability will not be reached. Nevertheless, the system will always be trying to reach stability and in doing so will demonstrate the effects of stability. That is to say, pressures and temperatures at the top of the aquifer will increase, water level will drop, the pressure from somewhere above water level and at all depths below will decrease and the temperature will decrease to the level where the pressure reaches saturation pressure.

Returning to the assumption of stability, the stable pressure and temperature distribution throughout the aquifer is dependent on the heat balance between heating and cooling the levels above and below water level, assuming no other loss of heat. A loss of heat, for instance, by drawing steam from the upper levels, will have a marked influence on the aquifer conditions. In effect, a greater amount of heat is required than that necessary to heat the top levels of the formation, and since this heat must come from cooling in the vicinity of the water level, the amount of cooling will be greater. That is to say, the temperature and pressure drops will be greater than indicated on Figure 15.

If an inflow is assumed, and also that there is a loss of heat from the upper levels, the system will behave differently again. The assumption of an inflow implies that pressures at depth are influenced not only by conditions within the aquifer, but also by conditions outside. As long as the inflow is less than the drawoff, pressures at depth in the aquifer will continue to fall and the inflow increase. At the same time, the loss of heat from the upper levels will depress pressures and temperatures in the upper levels, which, with the drop in water level due to the imbalance between inflow and drawoff, will provide the pressure drop necessary to increase the inflow. As the inflow increases, pressures at depth will tend to stabilise. The loss of heat from the upper levels will, however, continue to reduce the temperature and pressure at the water level. The net result will be that when inflow equals drawoff, water levels will start to rise.

The output from an individual bore will depend among other things, on the heat and pressure energy content of the fluid feeding into the bore. As long as the feed zone is below the level of temperature change, any change in output will be that due to pressure change. The change in heat energy due to a small change in temperature is relatively large, so that as temperatures in the feed zone fall, the effect on output should also be large. However, because the changes which occur are relatively gradual, a sudden change in the output characteristics is unlikely. The other aspect of the discharge characteristics is that as the water level falls, more of the open hole is exposed to steam, so that the proportion of steam in the discharge increases. That is to say, the discharge enthalpy will increase. This process will, of course, reverse if the water level rises.

The above discussion assumes a water level in the aquifer, but because conditions are not stable, the presence of a discrete water level is unlikely. The more likely fluid distribution with depth is steam at the upper levels, water at the lower levels, with mixtures of steam and water of varying density between. Because the physical nature of the bores is different to that of the formation, measurements in the bores over this zone do not necessarily represent formation conditions. Therefore, while pressure runs in Wairakei bores generally show a definite water level, the fact that a similar water level exists in the formation cannot be taken as proven.

In any system dominated by the saturation pressure/temperature relationship, the temperature at any level must fall when the pressure falls below the saturation pressure for the temperature at that level. It follows that for a given change in pressure, the change in temperature will be greatest in the upper levels, and will decrease with increasing depth until at and below the level where the pressure equals the saturation pressure, there will be no change. Also, with a continuing change in conditions, the depth over which the saturation pressure/temperature relationship obtains will increase.

Comparison of Theoretical and Actual Behaviour

There is no doubt that the behaviour of the Wairakei field under exploitation matches that of an aquifer dominated by the saturation temperature/pressure relationship in which heat is lost from the upper levels, and into which there is an inflow.

The first point of similarity is that the temperature fall has been greatest in the upper levels and has decreased with increasing depth to the stage where there

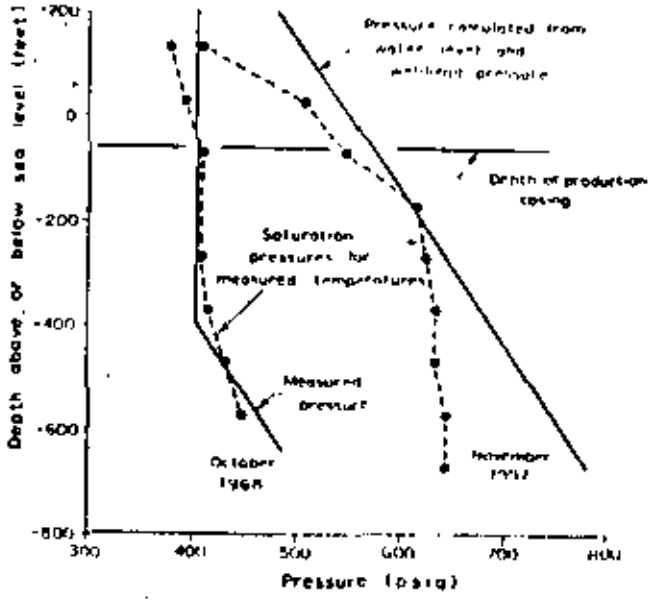

FIG. 16. *Pressure relationships - bore 27.*

has been no change in temperatures. Also, as may be seen from Figures 16 and 17 which show the relationship between measured and saturation pressures in bores 27 and 60 at different times, saturation conditions apply over a much greater range of depth now than was previously the case.

From Figure 10, the main fall in temperature in the western production area bores occurred in 1963 and 1964. This is about a year later than the fall in pressure which began in 1962, following the increase in production in that year. However, reference to Figure 12 shows that from 1963 to 1965, the enthalpy of the total discharge rose, after a number of years in which it had been close to that of water at the mean temperature over the production levels. Taken in conjunction with the marked drop in temperature which occurred over the same period, there seems little reason to doubt that this increase in enthalpy resulted from steam being drawn from the upper levels in the formation. The probable sequence of events following the increase in discharge in 1962 is that the pressure commenced dropping immediately, to the extent that, while a discrete water level would be unlikely, a greater proportion of open hole was exposed to steam or a steam water mixture, and the proportion of steam in the discharge thereby increased. This, in effect, represents a loss of heat from the upper levels which accelerated the drop in rock and water temperatures.

From Figure 3 it can be seen that the pressures have responded rapidly to changes in the rate of discharge. Moreover, with prolonged discharge at a relatively constant rate, the pressures have tended towards stability. The fall in pressures at depths below the level at which aquifer pressure equals saturation is influenced not only by the mass drawoff, but also by adjustments in the distribution of heat in the upper levels and by loss of heat from these levels. The mass withdrawal acts to reduce pressures, as does the loss of heat from the upper levels, while the redistribution of heat in the upper levels tends to maintain pressure. As long as the total drawoff comes from within the confines of the aquifer, pressures must continue to decline at a rate which bears a fixed relationship to the rate of drawoff. Therefore, if pressures are to approach stability, as is happening at Wairakei, mass must be drawn at a decreasing rate from within the aquifer. In other words there must be an increasing inflow to the aquifer. The pressure rise which occurred during the partial shutdown in the first quarter of 1968 is confirmation that there is an inflow to the Wairakei field. The only reasonable alternative explanation for this pressure rise is that it was due to drainage from the upper levels, but this explanation has to be discarded because it requires porosity and permeability characteristics of the formation which the drilling shows do not exist. At the time of the shutdown, the inflow was estimated to be approximately two thirds of the normal field discharge. The gravitational changes in the Wairakei field described by HOSE (1970) also suggest the existence of an inflow to the field.

The temperature of the inflow and the temperature fall which has occurred are the two most important factors in the continued exploitation of the field. While the fall in temperature is clearly the result of the system following the saturation pressure/temperature relationship, the alternative, that it is due to a cold inflow, must be examined.

A cold inflow to the upper levels is in its effect, the same as a loss of heat from the upper levels, because heat would have to be supplied by cooling in the vicinity of the water level, not only to heat up the upper levels of the formation but also to heat up the cold inflow. Temperatures and pressures would then be depressed below the equilibrium condition which would exist in the absence of the requirement for additional heat.

Figure 18 shows the temperatures since 1963 in seven holes drilled into the top of the Waiora formation. Three of these bores are in the eastern production area, and four in the western production area. If there was a cold inflow to the upper levels of sufficient magnitude to have a significant influence on temperatures and pressures, it would be reasonable to expect the temperatures in these holes to show a well defined, and continuing decline, particularly in recent years. As can be seen, no such decline is apparent.

For this reason, together with the fact that the temperature falls can be reasonably accounted for otherwise, it is unlikely that there is any substantial cold inflow to the upper levels. A substantial cold inflow at depth is unlikely, as is simply demonstrated by the fact that there has been no change in temperatures at the deepest levels. Therefore, while the possibility of

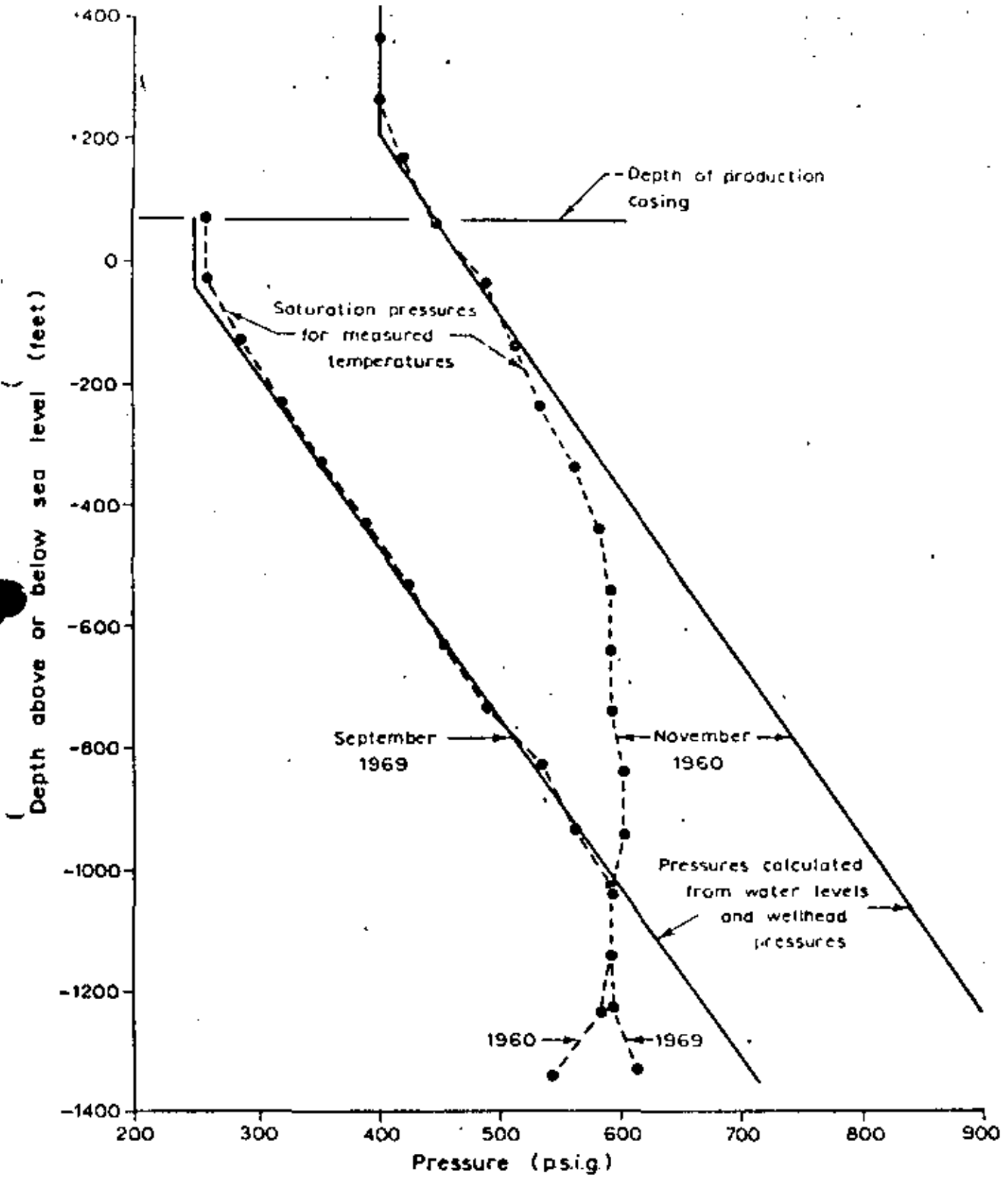

FIG. 17. — *Pressure relationship - bore 60.*

small, localised intrusions of cold water cannot be excluded, if present, they are not yet of sufficient magnitude to affect temperatures generally and, on the basis of evidence available, the inflow must be hot. In this context, hot means that the temperature is equal to or greater than the maximum measured in the field.

Physical nature of the Wairakei field and surrounding region

The response of pressures in the outer area bores to changes in the field discharge has been extremely rapid, with the consequence that at any time, the fall in pressure over the whole field has been almost uniform. Since some of the outer area bores are over a mile from the production area from which the main drawoff has taken place, it follows that there is a high lateral permeability over the field. The very high permeability is probably due to the broken contact zone at the top of the ignimbrite. In the eastern production area, the contact between the ignimbrite and breccia dips very steeply, and the bores in this region produce from the breccia. The breccia, while sufficiently permeable to allow useful production, is considerably less permeable than the contact zone, with the result that a somewhat higher drawdown has occurred in the eastern area.

As a result of exploitation, very steep pressure gradients have been established, separating the hot, pressure responsive field from the surrounding cold region, and suggesting the presence of an almost impermeable boundary. There is no geological feature to account for this boundary, the only difference being that within the field, thermal alteration and chemical deposition have taken place. The probable explanation for the boundary is that it is the result of chemical deposi

Steep pressure gradients also exist outside the fi between bores 224 and 225, where the gradient is 58 psi/1000 feet, and between bores 33 and 36, where the gradient is 54 psi/1000 feet. These are minimum gradients. They suggest a low permeability barrier running in an east-west direction outside the field, but again, there is no geological evidence to suggest what the nature of the barrier might be.

Outside the field, it is evident that in the vicinity of bore 33 the water level has declined at an approximately constant rate since exploration began, and gives no indication of being influenced by the drawoff from the field. In the bore 224 area, on the other hand, the rate of fall in the water level has varied, and does show a correlation with the pressure drop in the field.

Bore 223 has a number of well defined characteristics. It is cold, although showing slight indications of heat at the bottom. Pressures are, by extrapolation, lower than those within the field down to a depth of at least 1600 feet below sea level. The bore is some 2 miles from the centre of production, and yet responds immediately to changes in the field discharge. Also, the major faulting system in the field extends beyond the vicinity of bore 223.

The rapid response to changes in field disch[illegible] implies a highly permeable path between bore 223 a[illegible]

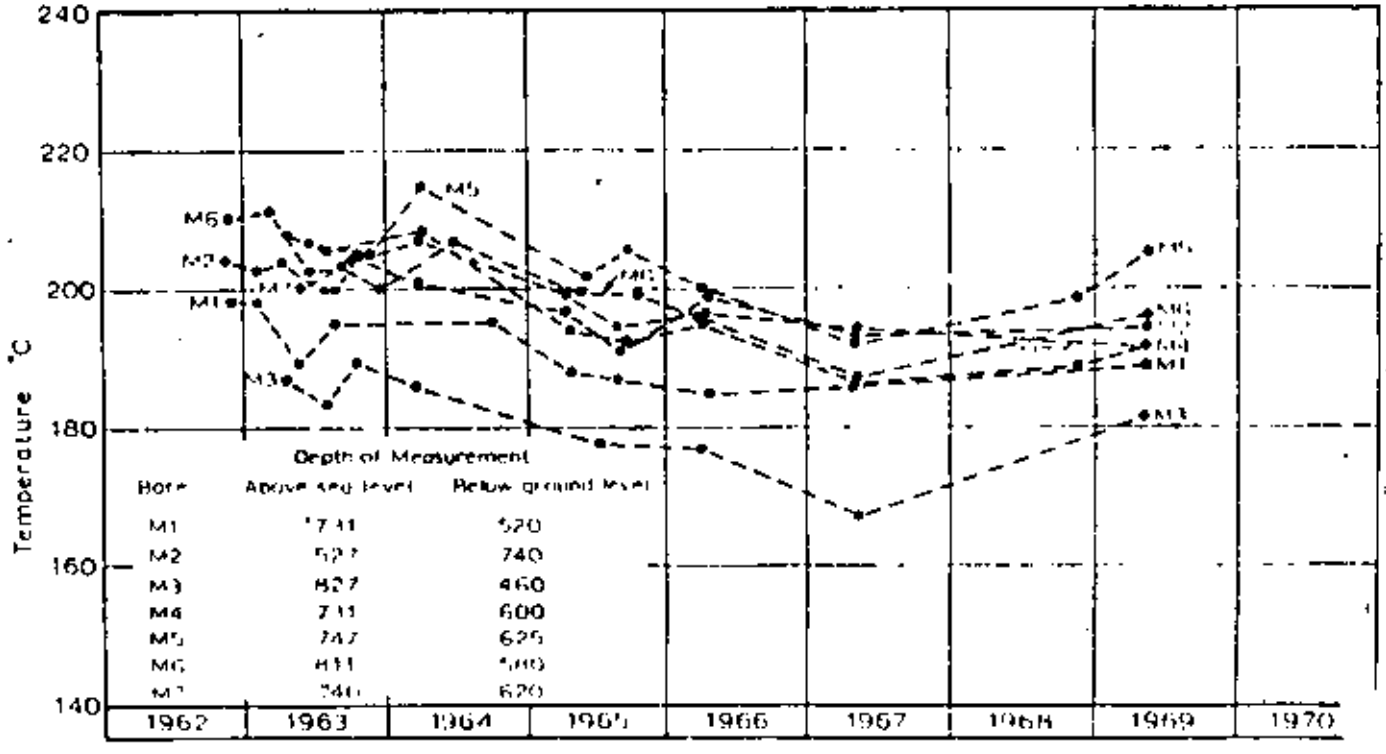

Fig. 18 *Shallow monitor bore temperatures*

the production area which can obviously be provided by the fault system. The pressure differential, together with the high permeability, implies a flow between 223 and the field. This flow cannot be above R.L. -1600, cause the direction of the pressure differential would quire the flow to be outwards, in which case, the temperatures in the 223 should be much higher than they are. The flow is therefore from 223 into the field, and at depths below R.L. -1900 feet. The indications of heat at hole bottom when drilled suggest that at greater depths, the temperatures will be higher. A reasonable explanation for this temperature distribution with depth is that a cold down flow in the vicinity of 223 mixes with a hot flow which is either upwards or lateral.

The resultant mixture then flows into the field along the fault system. By this means, not only are the low temperatures measured in bore 223 accounted for, but the direction of the hot water inflow to the field indicated. Also, the drop in water level in bore 224 would be a reflection of the downward flow in the vicinity of 223.

The interesting feature of the bore 36 pressure decline is that whereas in the early years the pressures were lower than and followed the field pressures closely, they are now considerably higher. The pressures referred to are, of course, those at R.L. -900, and the inference to be drawn from the comparison of the pressures is that the level of communication between bore [redacted] and the field is above R.L. -900. If the level of communication was below R.L. -900, pressures in bore 36 would still be following those in the field. The pressures in the field being higher than in 36 in the early years, it is probable that there was some out flow at that time. Because the pressure differential at R.L. -900 is now reversed, it does not necessarily follow that there is now an inflow, as this is determined by the pressure differential at the level of communication. It is in fact possible that the flow, if still present, is outwards. While the water level in bores 36 and TH 2 to the south are both falling at the same rate, the water level in 36 is about 30 feet higher than in bore TH 2. This suggests that the flow in the vicinity of bore 36 has a component in the southerly direction, which would not be expected if the flow were into the field.

It will be noted that the peripheral bores discussed lie to the east and the west of the field. Pressures in the most northerly bores drilled, bores 219 and 222, have fallen to the same extent as the other bores in the field, and both have temperatures of 250°C or higher. In the south, bores 208 and 226 pressures have followed the field pressures although temperatures in these bores, at 180°C and 200°C, are somewhat lower than encountered in the field. Thus the northern and southern boundaries have not been defined by drilling. is, however, a reasonable inference that similar boundaries exist in these regions as do to the east and west.

Conclusion

From the changes which have occurred in the underground pressures and temperatures, and in the discharge characteristics of both the field as a whole and individual bores, a reasonable idea of the nature of the Wairakei geothermal system can be obtained. Briefly, it can be described as a hot aquifer having a high permeability, contained within almost impermeable boundaries separating it from the surrounding cold regions. The behaviour of the hot aquifer under exploitation is dominated by the saturation temperature/pressure relationship, modified by the withdrawal of steam from the upper levels, and by an increasing inflow of hot water at depth.

At this stage, a satisfactory mathematical model of the system enabling future performance to be predicted reliably has not been formulated. Nevertheless, it is possible to make general predictions concerning the future of the field.

If it were desired to increase the output from the station by increasing the field discharge from depth, it is certain that there would be a further fall in both pressures and temperatures. This in turn would be accompanied by a decrease in the output from existing bores, so that the loss from these would have to be offset against the increase from the new bores.

Increasing production by withdrawing steam from the upper levels will have the same effect, but these will be spread over a longer period. This is because removing heat from the upper levels rather than removing mass will be the main factor causing the pressure and temperature drop.

If no attempt is made to increase the field discharge by drilling new bores, the output from the station could be maintained at, or close to, its present level for some years to come. This, of course, is due to the stabilising influence of the hot inflow.

Acknowledgements

The author would like to thank Mr F. R. Askin, Commissioner of Works, for his permission to publish this paper.

REFERENCES

Grange R. B. 1970 — Interpretation of gas composition from the Wairakei field over 10 years. *U.N. Symp. Development Utilization Geothermal Resources, Pisa.*

Herron I. W. 1970 — Ground subsidence of a geothermal field during exploitation. *U.N. Symp. Development Utilization Geothermal Resources. Pisa.*

Hunt T. M. 1970 — Net mass loss from the Wairakei geothermal field, New Zealand. *U.N. Symp. Development Utilization Geothermal Resources. Pisa.*

Wright D. M. 1970 — Recovery of flash steam from hot bore water. *U.N. Symp. Development Utilization Geothermal Resources. Pisa.*

Grindley G. W. 1965 — The geology, structure and exploitation of the Wairakei geothermal field, Taupo, New Zealand. *Bull. N.Z. geol. Surv.*, 75.

Analysis of Internal Steam Drive in Geothermal Reservoirs

J. C. Martin, SPE-AIME, Chevron Oil Field Research Co.

Introduction

Testing of geothermal energy prospects has accelerated in recent years. Increased understanding is needed of the fundamental heat and fluid flow involved in geothermal reservoir production. Techniques used by petroleum production researchers are particularly well suited to the study of these fundamentals and to geothermal reservoir engineering research in general.

Some geothermal reservoirs are similar to oil and gas reservoirs. These reservoirs are porous media through which the fluids flow according to Darcy's law. Furthermore, some geothermal reservoirs have the equivalent of cap rocks.

The analogy of geothermal reservoirs with oil and gas reservoirs is the basis for the fundamental assumption of this paper; fluid flow in a geothermal reservoir can be treated as flow through a porous medium, and Darcy's law and relative permeabilities are applicable.

There are many analogies between petroleum and geothermal reservoir engineering. For example, a number of the drives that supply reservoir energy are similar. The edge water drive in a petroleum reservoir is analogous to influx from cooler aquifers in geothermal reservoirs. Solution gas drive in petroleum reservoirs is analogous to two-phase, internal steam drive in geothermal reservoirs. Compaction drive can occur in both types of reservoir. Waterflooding an oil reservoir is analogous to water cycling in a hot-water geothermal reservoir.

Methods of analysis similar to those used in petroleum reservoir engineering can be used for geothermal reservoirs, as illustrated by the development of the material and heat balances in Ref. 1. The present paper presents an analysis of internal steam drive using methods similar to those used for solution gas drive in Ref. 2. The analysis is based on the following assumptions. The temperature, pressure, and fluid saturation gradients are small; the steam and hot water are produced according to their respective mobilities as determined by relative permeabilities and viscosities; and the effects of capillary pressure and gravity can be neglected. Some gravitational effects, however, are treated qualitatively in the discussion. Throughout the analysis and discussion, the produced steam and hot water are calculated neglecting the pressure and temperature drops near the wells and in the wellbores. The effects of these additional changes must be introduced to obtain steam and hot-water production rates at the wellhead.

Discussion

Temperature-Pressure Behavior

As pointed out in Ref. 1, initial temperature and pressure in a geothermal reservoir determine its reservoir type. The solid line in Fig. 1 presents the boiling curve for pure water. (Curves for actual geothermal brines will be modified by the dissolved salts.[3]) Points to the right of the curve and below the critical temperature represent hot-water reservoirs. Points to the left of the curve and above the critical temperature represent single-phase or steam reservoirs.

The mathematical analysis is presented in the Appen-

Petroleum reservoir analysis methods are applied to simple closed geothermal reservoirs that produce by internal steam drive. The fundamental assumption is that fluid flow in a geothermal reservoir can be treated as flow through a porous medium, and Darcy's law and relative permeabilities are applicable. Calculated performances are given for various types of reservoirs. Results indicate that hot-water reservoirs can have complicated behaviors.

dix. Ordinary differential equations are derived for the fluid saturations and reservoir pressure for two-phase flow and for the pressure and temperature for single-phase flow. Eqs. A-13 and A-16 were solved numerically for the temperature-pressure behavior of closed geothermal reservoirs containing fresh water and having the relative permeability curves presented in Fig. 2. Variations of single-phase and relative permeabilities with temperature were neglected in these calculations. Other values used in the calculations are 162-lb/cu ft rock grain density, 0.20-Btu/°F-lb specific heat of rock, 40-Btu/ft-D-°F thermal conductivity, and 1.0 darcies permeability. Results of these calculations for a porosity of 25 percent are represented by the dashed lines in Fig. 1.

As production causes the reservoir pressure to decline, the temperature follows the dashed line that passes through the initial temperature and pressure. Several such lines are presented in Fig. 1. For example, from initial conditions corresponding to Point A, the temperature will move to the left along Line 1 as the pressure declines. This case (Reservoir A) corresponds to a single-phase (essentially steam) reservoir with initial temperature and pressure above the critical values.

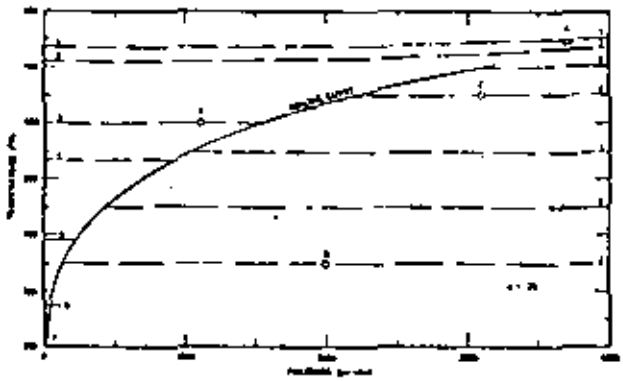

Fig. 1 — Temperature vs pressure for geothermal reservoirs containing fresh water, a porosity of 25 percent, and with other data given in text.

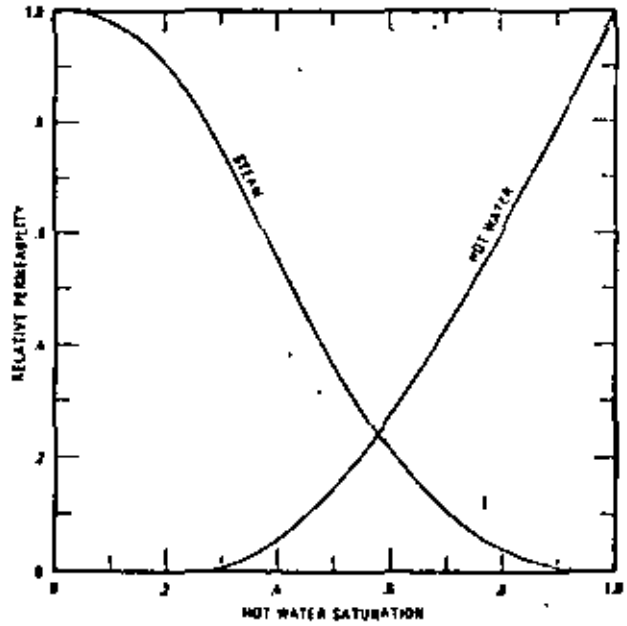

Fig. 2 — Steam and hot-water relative permeability curves used in the calculations.

No hot water is formed during pressure depletion, since Line 1 does not intersect the boiling curve. The reservoir temperature remains high after the pressure is depleted. Thus, additional energy could be extracted by water injection, beginning at any point along Line 1.

The initial conditions corresponding to Point B' (Reservoir B) in Fig. 1 represent a dry-steam reservoir in which no hot water is formed during pressure depletion, and much heat would remain unproduced if the pressure were depleted. The temperature would move along Line 3 as the pressure declines.

Point C (Reservoir C) in Fig. 1 corresponds to an initial hot-water reservoir with pressure above the boiling curve. Unless a strong rock drive or a water drive exists, the pressure initially declines rapidly with production, since only liquid expansion and rock compaction supply the driving energy. The reservoir performs essentially isothermally along Line 4 until the boiling curve is reached. Then steam begins to be generated within the reservoir and a steam phase begins to build up within the rock pores. This supplies a gas drive similar to a solution gas drive in a petroleum reservoir. As production continues, the temperature and pressure decline along the boiling curve. The steam saturation increases with production, and when it reaches its equilibrium saturation the reservoir begins to produce steam along with hot water.

The produced-steam/hot-water ratio continues to increase until the water saturation is reduced to its maximum immobile saturation. Then, only saturated steam is produced. Water saturation continues to decline until all water has been boiled away. The temperature then departs from the boiling curve and its decline essentially stops. The produced steam becomes increasingly superheated, as indicated by Line 4 in Fig. 1.

Point D (Reservoir D) in Fig. 1 corresponds to a relatively low-temperature hot-water reservoir. Except for those cases with a strong rock drive or a water drive, rapid pressure decline with production should occur since only liquid expansion and rock drive supply the driving energy above the boiling curve. Two-phase internal steam drive does not begin until the reservoir pressure has declined to a small fraction of its initial value. There is sufficient water in the pores that some water will remain even if the pressure reaches atmospheric level. Most of the steam produced through pressure depletion of this type of reservoir will be at low pressures. These low pressures result in low efficiencies if used in steam turbines to produce power. For this reason, power production from such reservoirs is perhaps best accomplished by cycling hot water through the reservoirs and using a binary-cycle power plant.[4]

Fluid and Heat Production Performance

Figs. 3 and 4 present the variations of the reservoir pressure and temperature with the percent of initial fluid mass produced. Reservoirs A and B perform essentially by isothermal steam expansion; Reservoirs C and D involve two-phase, internal steam drive. Almost all the initial fluid is produced from Reservoirs A, B, and C, and much of it is produced from Reservoir D. Reservoirs A and B experience little temperature drop during production, and in Reservoir C the temperature declines from 650° to 530°F. Thus, in these cases, much heat

remains in the reservoir rock at the end of pressure depletion.

Fig. 5 presents the pressure vs steam saturation for Reservoirs C and D. The increasing negative slope of the Reservoir C curve with steam saturation reflects the increasing produced-steam/hot-water ratios as the steam saturation increases with pressure depletion.

Fig. 6 presents the variation of pressure with the amount of heat produced, which is more than the amount of heat that would be in the reservoir if it contained only saturated steam at atmospheric pressure and 212°F. Results for Reservoirs A and B indicate that relatively small amounts of the total heat are produced during pressure depletion. Fig. 7 presents the pressure vs heat recovered in the form of steam and hot water for Reservoirs C and D. These results indicate that more heat is produced in the form of steam than of hot water. This reflects the higher heat content and the lower viscosity of the steam as compared with the hot water. Fig. 8 presents the pressure vs heat produced for six hot-water reservoirs with three different porosities. The increase in heat recovered with increased porosity for the higher initial pressure cases results from the larger volume of initial water present relative to the reservoir rock volume.

Gravity Segregation

The results presented thus far are based on the assumption that the fluids are distributed uniformly throughout the reservoir. In reality, gravity segregation of the steam and hot water will begin as soon as the steam phase becomes mobile. Reservoir performance and

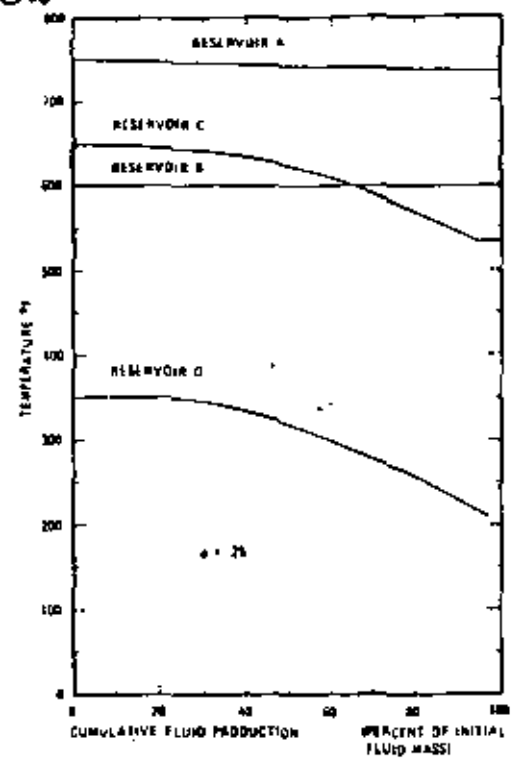

Fig. 4 — Temperature vs cumulative fluid production for Reservoirs A, B, C, and D.

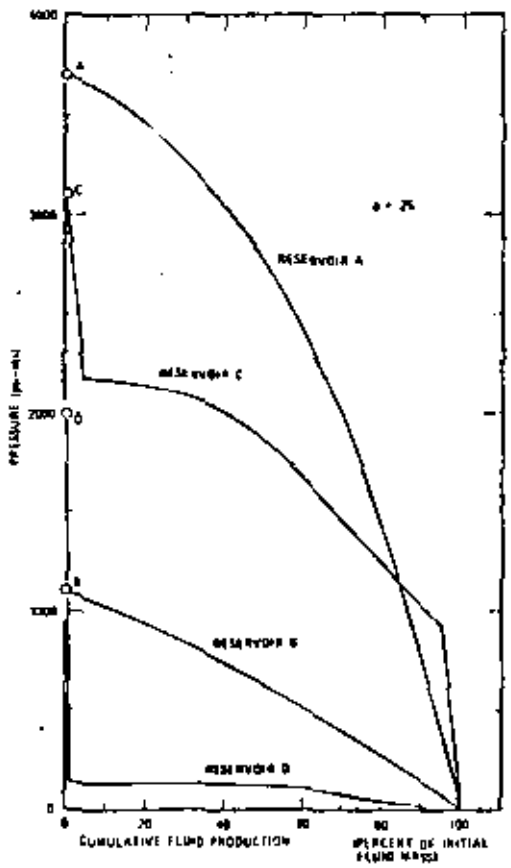

Fig. 3 — Pressure vs cumulative fluid production for Reservoirs A, B, C, and D.

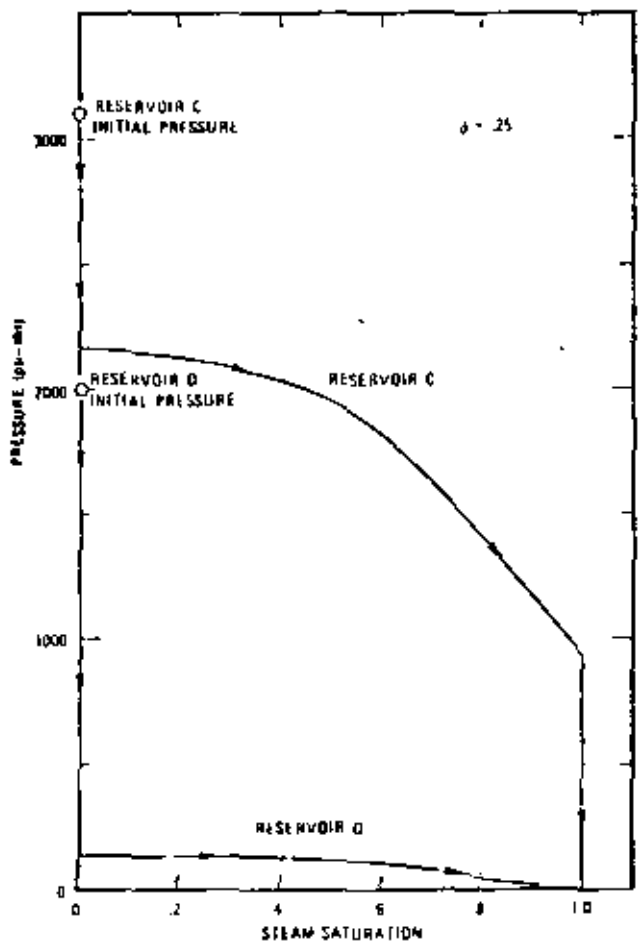

Fig. 5 — Pressure vs steam saturation for Reservoirs C and D.

gravity segregation studies of oil and gas in oil reservoirs indicate that, in many cases, segregation occurs rapidly.[5-7] Similar segregation of the steam and hot water should occur in geothermal reservoirs.

The results for uniformly distributed fluids are useful in visualizing the behavior of reservoirs in which rapid gravity segregation takes place and in which heat conduction, natural convection, and capillarity can be neglected to a first approximation. Steam accumulation at the top of a reservoir resulting from gravity segregation can greatly reduce the amount of water available for steam generation. Similarly, the drainage of hot water to the lower portion of the reservoir increases the amount of water available there for steam generation. Under gravity segregation, Reservoir C should perform as shown in Fig. 1 and Figs. 3 through 8 until the steam saturation reaches its equilibrium value. Then the steam phase becomes mobile and gravity segregation begins. Steam saturation will increase rapidly near the top of the reservoir. If the wells are completed high in the reservoir or if significant steam coning occurs, the produced steam/hot-water ratio will increase rapidly. The hot-water saturation will decrease rapidly until the water in the region is exhausted. Thus, this region will depart from the boiling curve at considerably higher temperatures and pressures than for Reservoir C. Points low in the reservoir will have high water saturations longer than if the fluid were to remain uniformly distributed, and these points will remain on the boiling curve to lower temperatures and pressures.

If the wells are completed low in the reservoir and significant steam coning does not take place, the produced-steam/hot-water ratio will remain low until the steam zone has expanded sufficiently to cause production from the steam zone. Points in the steam zone will depart from the boiling curve at higher pressures and temperatures than in the uniform-saturation case, and the lower portion of the reservoir will remain on the boiling curve to lower pressures and temperatures.

Thus, the relative amounts of steam and hot water produced will depend on, among other things, the amount of gravity segregation, the relative permeability curves, the structural position of the completion intervals, and the amount of steam and water coning. For many conditions, the amount of water initially present is so limited that much usable heat should remain in the reservoir after the water is exhausted. This heat may be distributed in a highly nonuniform manner, with generally higher temperatures in the upper portion of the reservoir. In most cases, the produced steam contains much more heat than does an equal mass of produced water. Thus, for many conditions, more total heat can be produced by completing the wells high in the reservoir to enhance steam production and suppress water production. This should result in more of the dissolved salts being left in the reservoir. This would be an additional advantage, provided problems associated with salt deposition are not too severe.

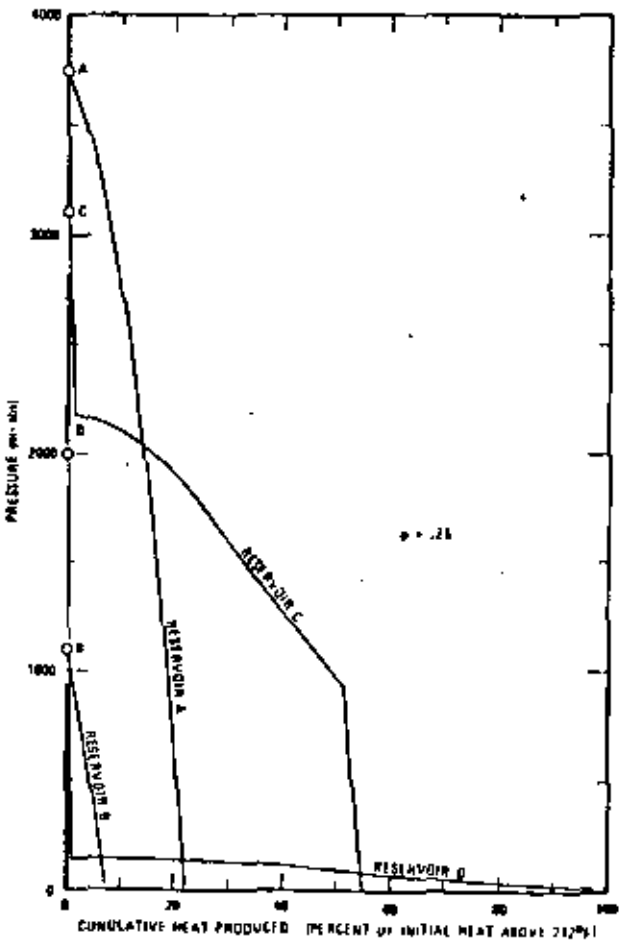

Fig. 6 — Pressure vs cumulative heat produced for Reservoirs A, B, C, and D.

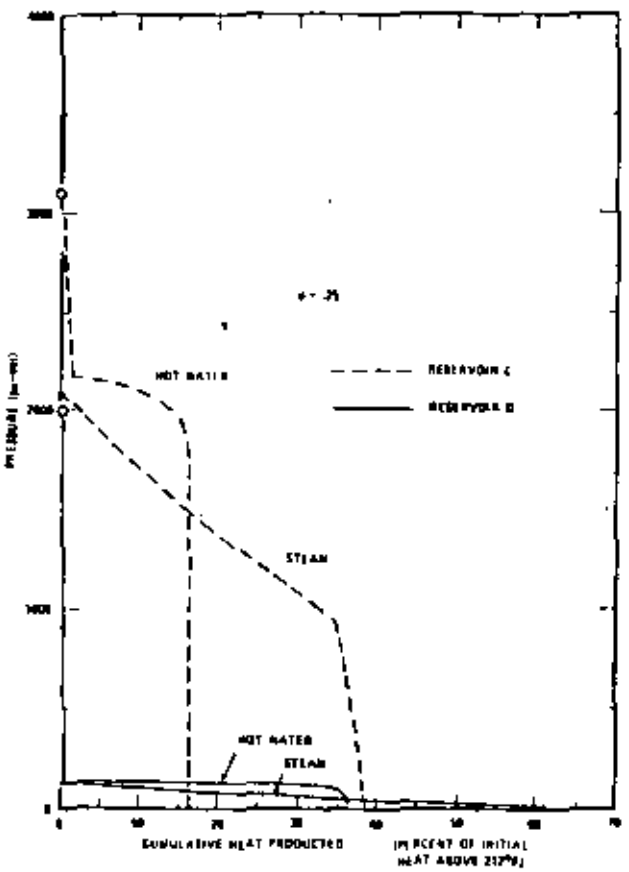

Fig. 7 — Pressure vs cumulative heat produced as steam and as hot water for Reservoirs C and D

Conclusions

1. Reservoir analysis methods can be applied to those geothermal reservoirs that involve the flow of steam or hot water through porous media.

2. Hot-water reservoirs can have complicated producing characteristics, including changing from hot water to steam as they are produced.

3. Under certain conditions, only a relatively small amount of the heat initially contained in a geothermal reservoir will be produced during pressure depletion. Much of this heat may be contained in the produced steam even though the reservoir initially contains only hot water.

4. For many conditions where gravity segregation of the steam and hot water occur during depletion, more of the total heat can be produced by completing wells high in the reservoir to enhance steam production and suppress water production.

Nomenclature

C_r = specific heat of formation solids
f_f = fraction of the original fluid mass that has been produced (Eq. A-7)
f_h = fraction of the original heat that has been produced (Eq. A-18)
f_{hs} = fraction of the produced heat that is contained in the steam (Eq. A-19)
f_{hw} = fraction of the produced heat that is contained in the hot water (Eq. A-20)
H = total heat per unit volume of reservoir rock (see fourth equation following Eq. A-7)
h = enthalpy
k = single-phase permeability
k_h = thermal conductivity
k_r = relative permeability
m_f = mass of fluid per unit volume of reservoir rock (see third equation following Eq. A-7)
p = pressure
S = saturation
T = temperature
t = time
u = velocity as given by Darcy's law
Λ_f = mobility of fluid mass (see first equation following Eq. A-7)
Λ_h = mobility of heat (see second equation following Eq. A-7)
$\lambda = \frac{(k)(k_{rs})}{\mu_s} + \frac{(k)(k)_{rw}}{\mu_w}$ = fluid mobility
μ = viscosity
ρ = density
ϕ = porosity
ψ = temperature on boiling curve expressed as function of fluid pressure (Eq. A-8)

Subscripts

a = atmospheric
f = fluid
h = heat
i = initial
s = steam
w = water
σ = solid portion of reservoir rock
$1p$ = single phase

References

1. Whiting, R. L. and Ramey, H. J., Jr.: "Application of Material and Energy Balances to Geothermal Steam Production," *J. Pet. Tech.* (July 1969) 893-900; *Trans.*, AIME, 246.
2. Martin, J. C.: "Simplified Equations of Flow in Gas Drive Reservoirs and the Theoretical Foundation of Multiphase Pressure Buildup Analyses," *J. Pet. Tech.* (Oct. 1959) 309-311; *Trans.*, AIME, 216.
3. Bass, J. L.: "The Effect of Salinity on the Maximum Thermal Gradient of a Hydrothermal System at Hydrostatic Pressure," *Econ. Geology* (1971) 66, 940-946.
4. Kruger, P. and Otte, C.: *Geothermal Energy*, Stanford U. Press, Stanford, Calif. (1973).
5. Spivak, A.: "Gravity Segregation in Two-Phase Displacement Processes," *Soc. Pet. Eng. J.* (Dec. 1974) 619-632; *Trans.*, AIME, 257.
6. Martin, J. C.: "Reservoir Analysis for Pressure Maintenance Operations Based on Complete Segregation of Mobile Fluids," *Trans.*, AIME (1958) 213, 220-227.
7. Martin, J. C.: "Some Mathematical Aspects of Two-Phase Flow With Applications to Flooding and Gravity Segregation Problems," *Prod. Monthly* (April 1958) 22-35.

APPENDIX

The mathematical relations for both two-phase (boiling) and single-phase flow are derived with all equations written for consistent sets of units. Conversion constants must be introduced if oilfield units are used.

Two-Phase Relations

The basic equations for conditions along the boiling curve are the following.

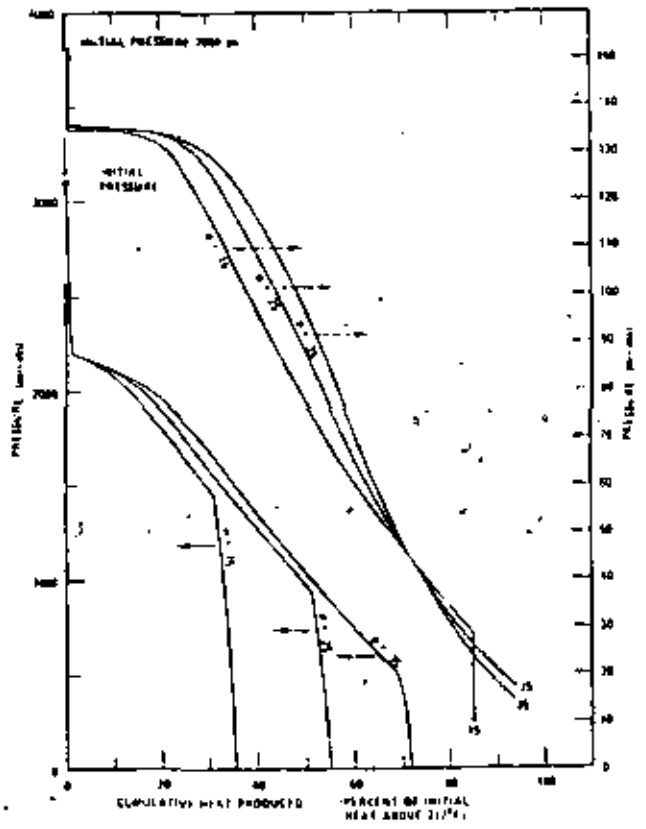

Fig. 8 — Pressure vs cumulative heat produced for three different porosities and two different initial conditions (3,100 psi, 650°F and 2,000 psi, 350°F).

Darcy's law for hot water:

$$u_w = -\frac{(k)(k_{rw})}{\mu_w}\nabla p. \quad \text{(A-1)}$$

Darcy's law for steam:

$$u_s = -\frac{(k)(k_{rs})}{\mu_s}\nabla p. \quad \text{(A-2)}$$

The equation of continuity for mass:

$$\nabla(\rho_w u_w + \rho_s u_s) = -\frac{\partial}{\partial t}\left[\phi(\rho_w S_w + \rho_s S_s)\right] \quad \text{(A-3)}$$

The equation of continuity for heat:

$$\nabla(\rho_w h_w u_w + \rho_s h_s u_s - k_h \nabla T)$$
$$= -\frac{\partial}{\partial t}\left\{\phi\left[\rho_w h_w S_w + \rho_s h_s S_s + \left(\frac{1-\phi}{\phi}\right)\rho_\sigma C_\sigma T\right]\right\} \quad \text{(A-4)}$$

Saturations:

$$S_w + S_s = 1. \quad \text{(A-5)}$$

Substituting Eqs. A-1 and A-2 into Eqs. A-3 and A-4 yields

$$\nabla(\Lambda_f \nabla p) = \frac{\partial m_f}{\partial t} \quad \text{(A-6)}$$

$$\nabla \Lambda_h \nabla p = \frac{\partial H}{\partial t} \quad \text{(A-7)}$$

where

$$\Lambda_f = \frac{(\rho_w k)(k_{rw})}{\mu_w} + \frac{(\rho_s k)(k_{rs})}{\mu_s}$$

$$\Lambda_h = \frac{(\rho_w k)(k_{rw})}{\mu_w} + \frac{(\rho_s h_s k)(k_{rs})}{\mu_s} + k_h \psi'$$

$$m_f = \phi(\rho_w S_w + \rho_s S_s)$$

$$H = \phi\left[\rho_w h_w S_w + \rho_s h_s S_s + \left(\frac{1-\phi}{\phi}\right)\rho_\sigma C_\sigma \psi\right]$$

$$T = \psi(p)$$

and

$$\psi' = \frac{d\psi}{dp} \quad \text{(A-8)}$$

Λ_f is the mobility of the fluids in terms of mass; Λ_h is the mobility of the heat; m_f is the mass of fluid per unit volume of reservoir rock; and H is the total heat per unit volume of rock.

Eqs. A-6 and A-7 can be written as

$$\frac{\partial \Lambda_f}{\partial p}\nabla p \cdot \nabla p + \frac{\partial \Lambda_f}{\partial T}\nabla T \cdot \nabla p + \frac{\partial \Lambda_f}{\partial S_w}\nabla S_w \cdot \nabla p + \frac{\partial \Lambda_f}{\partial S_s}\nabla S_s \cdot \nabla p + \Lambda_f \nabla^2 p = \frac{\partial m_f}{\partial t} \quad \text{(A-9)}$$

$$\frac{\partial \Lambda_h}{\partial p}\nabla p \cdot \nabla p + \frac{\partial \Lambda_h}{\partial T}\nabla T \cdot \nabla p + \frac{\partial \Lambda_h}{\partial S_w}\nabla S_w \cdot \nabla p + \frac{\partial \Lambda_h}{\partial S_s}\nabla S_s \cdot \nabla p + \Lambda_h \nabla^2 p = \frac{\partial H}{\partial t} \quad \text{(A-10)}$$

In those cases where the saturation gradient, temperature gradient, and pressure gradients are small, the vector products $\nabla p \cdot \nabla p$, $\nabla T \cdot \nabla p$, $\nabla S_w \cdot \nabla p$, and $\nabla S_s \cdot \nabla p$ are small compared with the magnitudes of $\nabla^2 p$, $\partial m_f/\partial t$, and $\partial H/\partial t$, and the terms containing the vector products can be neglected to a first approximation.

Eqs. A-9 and A-10 reduce to

$$\nabla^2 p = \frac{1}{\Lambda_f}\frac{\partial m_f}{\partial t} \quad \text{(A-11)}$$

$$\nabla^2 p = \frac{1}{\Lambda_h}\frac{\partial H}{\partial t} \quad \text{(A-12)}$$

Eqs. A-11 and A-12 require that the variations of p, S_w, S_s, and T are small with distance. Fortunately, the variations of these quantities with time need not be small.

Equating the left sides of Eqs. A-11 and A-12 yields (replacing T with $\psi(p)$ and S_s with $1-S_w$)

$$\frac{\partial m_f}{\partial p}\frac{\partial p}{\partial t} + \frac{\partial m_f}{\partial S_w}\frac{\partial S_w}{\partial t} = \frac{\Lambda_f}{\Lambda_h}\left(\frac{\partial H}{\partial p}\frac{\partial p}{\partial t} + \frac{\partial H}{\partial S_w}\frac{\partial S_w}{\partial t}\right).$$

This equation reduces to the following ordinary differential equation.

$$\frac{dS_w}{dp} = \frac{\Lambda_h(\partial m_f/\partial p) - \Lambda_f(\partial H/\partial p)}{\Lambda_f(\partial H/\partial S_w) - \Lambda_h(\partial m_f/\partial S_w)} \quad \text{(A-13)}$$

Eq. A-13 can be integrated numerically to obtain S_w as a function of p. This relation is similar to the Muskat-solution gas relation which relates oil or gas saturation to reservoir pressure.

The relation between S_w and p obtained from Eq. A-13 can be used to eliminate S_w from Λ_f, Λ_h, m_f, and H. This allows Eqs. A-11 and A-12 to be expressed in terms of pressure, thereby obtaining a partial differential equation for pressure that can be used in the analysis of transient well pressure data that involve two-phase flow in the reservoir.

Single-Phase Flow

The temperature and pressure are not related to the boiling curve for single-phase flow. For single-phase flow, Eq. A-11 reduces to

$$\nabla^2 p = \frac{1}{\rho\lambda}\frac{\partial m_f}{\partial t} \quad \text{(A-14a)}$$

and Eq. A-12 reduces to

$$\nabla^2 p + \frac{k_h}{\rho h\lambda}\nabla^2 T = \frac{1}{\rho h\lambda}\frac{\partial H_{1p}}{\partial t} \quad \text{(A-14b)}$$

where h is the enthalpy; λ is the mobility; and H_{1p} is the single-phase equivalent of H.

In the case of two-phase flow it was possible to obtain an ordinary differential equation for the water saturation vs pressure without neglecting the effects of heat conduction because temperature and pressure are related by the boiling curve. Unfortunately, this is not the case for single-phase flow; however, if we neglect the effects of heat conduction, Eq. A-14b reduces to

$$\nabla^2 p = \frac{1}{\rho h \lambda} \frac{\partial H_{1p}}{\partial t} \quad \text{.....(A-15)}$$

Eliminating $\nabla^2 p$ from Eqs. A-14a and A-15 leads to the following differential equation for p and T.

$$\frac{dT}{dp} = \frac{(\partial H_{1p}/\partial p) - h(\partial m_f/\partial p)}{h(\partial m_f/\partial T) - (\partial H_{1p}/\partial T)} \quad \text{.....(A-16)}$$

This equation was used to calculate T vs p for single-phase flow. As expected, numerical results reveal small values of dT/dp, indicating essentially isothermal behavior.

Additional Relations

Solutions of Eqs. A-13 and A-16 yield the temperature and fluid saturations as functions of reservoir pressure. Heat and mass balances can be used to obtain the fluid and heat productions as functions of pressure. These relations are

$$f_f = 1 - \frac{m_f}{m_{fi}} \quad \text{.....(A-17)}$$

Original manuscript received in Society of Petroleum Engineers office Feb. 14, 1975. Revised manuscript received Oct. 15, 1975. Paper (SPE 5382) was first presented at the SPE-AIME 45th Annual California Regional Meeting, held in Ventura, April 2-4, 1975.

This paper will be included in the 1975 Transactions volume.

where f_f is the fraction of the original fluid mass that has been produced and the subscript i refers to initial conditions.

$$f_h = \frac{H_i - H}{H_i - H_a} \quad \text{.....(A-18)}$$

where f_h is the fraction of the original heat produced that is above the heat contained in the reservoir at atmospheric pressure and 212°F containing only saturated steam. The subscript a refers to these conditions.

Expressions for the relative amounts of heat produced in the steam and in the hot water can be obtained by integration. These relations are

$$f_{hw} = \left(\frac{1}{H_i - H}\right) \int_{p_i}^{p} \left(\frac{\rho_w h_w k\, k_{rw}}{\lambda_h\ \mu_w}\right) \frac{dH}{dp}\, dp, \quad \text{..(A-19)}$$

$$f_{hs} = \left(\frac{1}{H_i - H}\right) \int_{p_i}^{p} \left(\frac{\rho_s h_s k\, k_{rs}}{\lambda_h\ \mu_s}\right) \frac{dH}{dp}\, dp. \quad \text{...(A-20)}$$

where f_{hw} and f_{hs} are the fractions of the produced heat contained in the hot-water production and in the steam production, respectively. **JPT**

CURSO: INGENIERIA DE RESERVORIOS GEOTERMICOS.

OLADE
C.F.E.
I.I.E.
DECFI.

FLUJO DE FLUIDOS Y CALOR EN MEDIO POROSO.

INSTRUCTOR: DR. HEBER CINCO LEY

SEPTIEMBRE, 1981.

THERMODYNAMIC BEHAVIOUR OF THE BAGNORE GEOTHERMAL FIELD

P.Atkinson, R.Celati, R.Corsi, H.Ramey

Introduction

The Bagnore geothermal field lies on the south-western edge of Mt.Amiata volcano. This region is approximately 80 km south-east of Larderello and 120 km north-west of Rome (Fig.1).

A major feature of this field is the presence and behaviour of carbon dioxide (CO_2). The history, geology and hydrology of Bagnore are first presented in this paper.

The various thermodynamic and chemical equilibrium concepts are used to attempt to describe and justify the CO_2 behaviour in the field.

Two models of the Bagnore field are presented. They attempt to describe different features of the Bagnore production history. The first model addresses the question of the source of initial high CO_2 content by using chemical equilibrium concepts. The second model attempts to describe the history of the field by using the thermodynamics of vapour-liquid equilibria.

The philosophy of the modelling work can be described by summarizing three features of the models. The first feature is that we wish to develop models

which account for a small number of physical processes. This allows for a more direct study of the interaction of the processes under consideration. The second feature of the models is that they do not require a detailed description of the spatial variations throughout the reservoir. Finally, the models need to include sufficient processes so as to bear some resemblance to real systems.

At the end of the paper some new insights into the nature of the Bagnore field are discussed. These are based on geohydrological evidence, and are supported by mathematical modelling.

History

Drilling exploration began at Bagnore in August 1958 in an area without surface manifestations, and was completed in November 1962. Twenty-one wells were drilled , at depths ranging from 346 to 1475 m, and an average depth of 765 m; average spacing of the wells is 1.4/km^2 (Fig.2).

The zone explored covers an area of 15 km^2, but the producing wells covered about 4-5 km^2. Initially eight wells were productive , supplying two exhausting-to-atmosphere 3.5 MW power units. Six wells were not commercial and 7 were dry (Cataldi, 1967).

After a few years production some wells were no longer utilizable, mainly because an increasing

amount of liquid water appeared in their fluid; only five wells are currently supplying the power plant.

Fluid production was 180 t/h in 1962 and after 15 years production this decreased to 95 t/h.

Table 1 shows the production characteristics of the wells not long after their blow-out and again in 1976.

By the time exploration began in the Bagnore field a geothermal technology had been developed so that our record of production characteristics is fairly complete.

The commercial wells produced a fluid of relatively uniform composition and state and measurements in shut-in wells show a uniform pressure distribution across the field.

The initial composition of the fluid revealed a very high uncondensable gas content (81% by weight, mainly CO_2), which fell fairly rapidly over a period of approximately two years.

This field was chosen for a zero-dimensional study because of the uniformity in producing and reservoir conditions and because data are available from the beginning of exploitation.

Geology and hydrogeology of Bagnore

The stratigraphic sequence in Bagnore area is characteristic of Central-Southern Tuscany, including

Larderello and Travale geothermal fields.

Starting with the deepest terrains known in this area , we have:

-1) a basal terrigenous complex, consisting mainly of phyllites and quartzites of the Paleozoic-Triassic ("basement" and lower part of the Tuscan series);

-2) a mainly carbonate complex (Tuscan series) with, at the base, dolomites and anhydrites (Upper Triassic), massive limestones and cherty stratified limestones (Lower Jurassic), marls and radiolarites (Middle-Upper Jurassic);

-3) an upper terrigenous complex (Tuscan series),with at its base, a shaly formation (Scaglia),overlain by Nummulite-bearing calcarenites and, in some places, sandstones (Macigno)(Eocene-Oligocene);

-4) a mainly shaly flysch facies complex,containing marly and arenaceous formation ("Alberese-Pietraforte" group (Cretaceous-Eocene);

-5) a mainly clay complex of the Lower-Middle Pliocene, lying unconformably over all the lower complexes;

-6) a volcanic complex, formed by lava and lava domes of a mainly quartz-latitic composition. This complex forms the Mt.Amiata massif (1738 m)(absolute age 0.45 m.y.)

The presence of this volcanic body distinguishes Mt.Amiata geothermal area from the other Tuscan geothermal areas.

The sequence of the main tectonic events affecting this area can be summarized as follows:

-1) a compressional-type tectonics (Miocene) caused most of the carbonate complex and upper terrigenous complex of the Tuscan series to be thrust from west to east as a nappe (Tuscan nappe).

The flysch complex ("Alberese-Pietraforte group") was also thrust eastward into the study area, over the Tuscan nappe.

As this nappe is discontinuous, the flysch complex can also rest on the underlying Paleozoic-Triassic terrigenous complex.

-2) tensional tectonics (Upper Miocene-Early Quaternary) resulted in step faults and horst and graben;

-3) a regional-type uplift (Quaternary) reached its maximum intensity (about 1000 m) in this area.

Mt.Amiata volcanism is tied to one of the last tensional tectonic phases (late Quaternary) and probably the formation of the geothermal anomalies still existing in this area are also tied to the same phases.

The hydrogeological situation in the study area is characterized by:

-a) an upper permeable complex, consisting of Mt. Amiata volcanites. Permeability is due to porosity and fracturation;

-b) an impermeable complex, comprising the mainly

clay formations of the Lower-Middle Pliocene, the flysch facies Cretaceous-Eocenic terrains and the upper terrigenous complex of the Tuscan series;

c) a lower permeable complex made up of the mainly carbonate formations of the Tuscan series and the basal terrigenous complex. Permeability through fracturation is generally high in the carbonate formations, especially at the contact with the allochthonous terrains of the flysch facies complex and, above all, at the top of the structural uplifts.

Extrapolating our knowledge of Larderello-Travale geothermal areas to this area, it could be said that the permeability of the basal terrigenous complex formations is generally low, except in the structural highs.

Complex c) forms the main reservoir of the geothermal fluids; the zones in which it outcrops are recognized absorption areas of the meteoric waters and recharge areas of the reservoir.

Mt.Amiata volcanic complex, with its volcanic chimneys and volcano-tectonic faults, also forms an important local recharge area (Fig.3).

Bagnore field lies on the south-west margin of Mt.Amiata volcanic massif, in correspondence to a positive structure of the terrains forming the reservoir (Figs.4,5 and 6).

Figure 7 shows the trend of the top of the reservoir,as defined from drilling data (elevation of the first fracture met with below the cover terrains, with respect to sea-level). From this figure a positive anticlinal-type structure appears, that extends NE-SW and is separated from another, smaller positive structure situated in correspondence to B7 well.

Figure 6 shows the connection between Mt.Amiata volcanic complex (upper permeable complex) and the geothermal reservoir underlying the cover.

Intitial conditions of Bagnore

The first well drilled in Bagnore field, B1, was shut-in a few days after its completion. The amount of fluid produced was negligible and pressure build-up reached 22 kg/cm^2 abs., from which it is possible to calculate a pressure of 23.5 kg/cm^2 abs. at the top of the reservoir.

No reliable reservoir temperature measurement was made in the central part of the field, where the wells blew out spontaneously during drilling, but estimates of initial reservoir temperature were obtained from the analysis of different data, i.e.:

1) extrapolation to the top of the reservoir of the surface temperature gradient, measured in shallow thermometric wells (average depth 35 m), gives reservoir temperatures of 220 °C in the centre of the field and 160-215 °C on its boundaries.

These values are not considered as being precise due to the lithological heterogeneities and the possibility of water circulation through some permeable layers (calcarenites, sandstones, etc.) in the cover formation.

2) Downhole temperature measurements were made in peripheral unproductive wells some years after their completion, so that temperature equilibrium was reached in the borehole. The maximum value, measured in the wells close to the productive area, is 165 °C.

3) Assuming phase equilibrium exists between carbon dioxide and water in initial conditions, we can write(assuming ideal solution):

$$y_{H_2O}\, p = x_{H_2O} p^{o}\ (T) \simeq p^{o}(T)$$

where $p^{o}(T)$ is the saturation pressure of pure water at temperature T, and y and x the mole fractions in gas and liquid. From the calculated initial partial pressure of steam we obtain T = 174 °C.

4) Bottomhole temperatures in flowing wells were calculated from well-head data considering the fluid to be a mixture of ideal gases.

The highest values were obtained in the early period of exploitation, in wells producing at wellhead pressures close to the static reservoir pressure: the maximum value was 173 °C.

In conclusion, 175 °C seems to be a g od estimate for initial reservoir temperature.

When the first well, B1 ,reached the top of the reservoir and blew out,the fluid composition was nearly 100% non-condensable gas and production was negligible. Drilling

continued until, after some tens of metres, there was a strong increase in production and the non-condensable gas content dropped to 81%.

The value of 99 - 100% non-condensable gas clearly cannot be representative of the average fluid composition in a reservoir where temperature measurements show that the partial pressure of steam must be greater than 5 - 6 kg/cm^2

Furthermore, assuming this initial composition, the decline curve of the gas/steam ratio presents an unjustified discontinuity, while an assumed initial value of 81% gives a regular curve (Fig.8). Therefore, the value of 81% was accepted as the initial non-condensable gas content.

The gas initially produced probably came from some relatively cold pockets at the top of the structure.

We obtained an indication of fluid homogeneity in the gas cap by comparing the simultaneous production of wells crossing isolated fractures at different depths (Fig.9). The result was a fairly homogeneous fluid composition that is in agreement with the choice of a zero-dimensional model for the field.

The substantial homogeneity of the fluid in the gas cap is also confirmed by the fact that the gas/steam ratio was practically independent of delivery pressure in the wells producing dry fluid, as shown in Fig.10. The data shown in this Figure were gathered during back-pressure tests.

The non-condensable gas was almost always mostly CO_2. At the beginning of production the CO_2 content in the non-condensable gas was 94 ÷ 96% by weight. CH_4 was 3 ÷ 5% and the concentrations of all the other components (H_2,

H_2S, N_2) were generally less than 1%.

During production there was a fast decrease in the CH_4 content and an increase in CO_2 to the present values (98 ÷ 99% CO_2). The well B18 maintains a gas composition different from the other wells (96% CO_2, 4% CH_4).

Production characteristics at Bagnore

Figure 11 shows the evolution of reservoir pressures in Bagnore field during its production life. The data were obtained from periodic shut-in of producing wells and from wells that were shut-in for long periods. The graph represents bottomhole pressures, as calculated from wellhead data.

The producing wells tend to exhibit rapid pressure build-ups to values that are areally uniform. Moreover, most of the shut-in wells measured tend to show uniform pressure throughout the field.

Two wells (B3 and B7) on the north-west boundary of the field have anomalous wellhead pressures: these pressures have been increasing over a period of 15 years. These data have not been considered as they were shown to be non -representative of reservoir behaviour on the base of hydrogeological considerations. The graph shows a fairly rapid pressure drawdown over a period of approximately two years, after which decline was very slow.

The history of the non-condensable gas content for the producing wells (Fig.12) shows a fast decrease in this variable during the first few years of production after which it levelled off to an essentially constant value.

The rapid fall in non-condensable gas content and reservoir pressure appear simultaneous. A fairly good areal uniformity of the gas phase composition is apparent from these data, but not so good as it is in the case of pressure.

The wells not considered in the pressure data also exhibited an anomalous behaviour as regards their non-condensable gas content.

The average values of the non-condensable gas content are given in Fig.13; the areal average is representative of the fluid in the reservoir, while the weighted average is representative of the fluid produced. These two values are similar.

In order to explain the simultaneous rapid decrease in pressure and non-condensable gas content, the p/z ratio was plotted versus cumulative production, as shown in Fig. 14.

z values for the H_2O-CO_2 mixture were calculated according to corresponding states law, Amagat's law and Dalton's law. In the pressure and temperature range of our system the three methods gave z values in agreement within 1%.

Two distinct nearly straight-line sections appear in the curve: the first corresponds to the early production period, during which the fast depletion in pressure and non-condensable gas fraction occurred. The second corresponds to the subsequent period, and is characterized by a slow pressure decline and a nearly constant fluid composition.

The first straight line can be explained by assuming

that initially there was an accumulation of non-condensable gas in the positive structure of the reservoir, and that this gas was exhausted during the first years of production.

Subsequently, fluid production came primarily from boiling liquid. This is reflected in the second straight line. These observations have been verified in the thermodynamic modelling described below.

The graph refers to the pressure decline of a multicomponent fluid of variable composition. As a first approximation we can consider two components, steam and non-condensable gas.

The mechanisms of generation, the conditions that determine the initial state and the processes taking place during the production period are, in general, different for the different components. Therefore, we tried to examine the steam and non-condensable gas separately. The relative p/z versus cumulative production graphs are shown in Figs. 15 and 16.

The compressibility factor z used in these graphs is the same as was calculated for the gas mixture. In fact, we have for the mixture:

$$pV = zn\,RT$$

and multiplying both sides of this equation by the mole fraction of the i^{th} component

$$y_i pV = zy_i nRT = zn_i RT$$

or

$$\frac{(y_i p)}{z} = n_i \frac{RT}{V}$$

Therefore, the ratio $(y_i p)/z$ is the quantity to be used for the mass balance considerations.

The curve for steam exhibits a regularly decreasing slope, thus indicating that the extraction of non-condensable gas from the reservoir has not affected in any significant way the decline of steam partial pressure.

A detailed analysis of this curve can be performed with coupled mass and energy balances.

The curve for non-condensable gas confirms that practically all the gas initially present in the cap was produced during the first two years.

During this period the partial pressure of the non-condensable gas decreased by ~ 15 kg/cm^2 and then remained nearly constant, thus suggesting the existence of some non-condensable gas recharge.

The first part of the curve, representing the fast pressure decline, is a straight line; this may indicate that, as far as non-condensable gas is concerned, Bagnore reservoir behaves as a constant volume isothermal closed gas reservoir.

Assuming this is true for Bagnore, the mass of gas initially in place results $\sim 2 \times 10^9$ kg, which, at the initial conditions of the reservoir, occupies a volume of $\sim 10^8$ m^3. From these values and the initial fluid composition, we obtain a mass of steam initially in place of $\sim 0.5 \times 10^9$ kg, which is only about 3% of the steam produced up to now. This result suggests that the steam currently produced originates primarily from boiling liquid.

A possible value for the rock volume containing the gas, estimated from geological data, is $\sim 2 \times 10^9 m^3$. The major uncertainty in this estimation is in the reservoir thickness.

Using this value we obtain the pore volume occupied by the gas as $\sim 5\%$ of the rock volume.

These values may be used as a first guess in our producing-state thermodynamic model of the field.

However, we cannot be so sure of our hypothesis of a closed gas reservoir, as simultaneous phenomena such as CO_2 generation and water influx must be taken into account when modelling the actual system.

Furthermore, a possible slight curvature can be hidden be systematic errors when calculating average quantities. In fact, the p/z average values are calculated on an areal basis which does not account for existing but unknown changes in reservoir thickness and porosity.

The amount of gas that can be released by the solution in the period of rapid decrease of pressure cannot be neglected. In fact, the volume of CO_2-satured liquid required to release all the CO_2 produced during this period, with a partial pressure drop of ~ 15 kg/cm^2, comes to $\sim 35 \times 10^7 m^3$ water. This corresponds approximately to a total rock volume of 7 km^3 (using 5% porosity) which is a reasonable order of magnitude.

Another interesting observation is that some of the wells that were initially good producers have since "watered-out". This fact may indicate that during the first period of production the volume of the gas cap did

not remain constant, due to a rising of the gas-water interface.

In the time-depth graph of Fig.17 the schematic stratigraphic profiles of the "watered-out" wells are placed in the proper position with respect to the depth axis, while their positions on the time axis corresponds to the date when liquid water first appeared in the fluid produced.

The curve in the figure represents the elevation of the gas-water interface in the reservoir, according to the simple hypothesis that this interface rises in direct proportion to the drop in reservoir pressure, so as to maintain at all times the hydrostatic equilibrium conditions (Fig.18):

$p + \rho_w g h_i = \rho_w g h_e$, where ρ_w = water density and g= gravitational acceleration.

The piezometric level around the field, except for a limited boundary zone in the north-east where there is a high piezometric gradient, is uniformly 230-235 m a.s.l. (Fig.2).

We assumed that this hydrostatic head controls the reservoir pressure, and calculated the hypothetical position of the interface with constant h_e = 235 m a.s.l.

The drilling histories of the wells in this field provide much information on the depth of productive fractures and the thickness of the producing intervals of the boreholes.

For several wells drilling began with mud, and continued with air after a productive fracture was crossed and well production started.

In these cases records were kept of the depth at which

increased production occurred.

The fractures and fractured reservoir intervals crossed by the wells are also shown in Fig.17, from which we can see that two-phase production began in the wells when the hypothetical interface reached the deepest productive fractures.

The data generally do not permit a reconstruction of the progressive watering out of these wells, as they were shut-in after being excluded from the pipeline network. Significant production data after two-phase-production began are reported for B4 well only (Fig.19).

The production from this well came almost entirely from the (+ 48, + 125) m depth interval. This figure shows that there was a gradual decrease in steam production and a simultaneous increase in liquid water during the time the interface was supposed to be rising through this depth interval.

Figure 20 refers to wells B6, B8 and B12, that never produced , and to B16 which produced liquid water and steam soon after its completion.

The position of the stratigraphic profiles on the time axis here represent completion date.

These data can be interpreted by considering that when the dry wells were completed the water-gas interface was already far above the fractures, and that when B16 was completed, the interface had already reached the lower part of the productive interval.

From these considerations we can conclude that the dry wells might have been productive if they had been drilled at an earlier date.

Due to the limited depth of the wells in the central area no information exists on whether such phenomena also occurred in this zone.

Wells that have always produced dry steam and gas have crossed fractures above the present hypothetical position of the interface.

The anomalous behaviour of well B7 may also be explained by the rise of the interface.

As can be seen in Figs.5 and 7, this well passed through a small local positive structure of the reservoir, located beside the much larger main structure of Bagnore field.

This small dome, from which B7 took its fluid, probably remained isolated from the rest of the field before the well began two-phase production.

Well B3, which also showed an anomalous wellhead pressure, is located in a zone of high piezometric levels on the northern boundary of the field. After having produced gas and steam with large amounts of liquid, and for very short periods, it was unable to produce spontaneously.

Whenever the well was shut-in there was always liquid water in the borehole above the producing fractures. Thus, the wellhead pressure represents only the pressure of the gas evolved from the underlying liquid.

All these data indicate a water influx into the reservoir. However, it is possible that during the first production period the water entering the system had flooded only a fraction of the reservoir volume, with no significant change in the total gas cap volume.

The different behaviour shown by the last part of the

p/z curve for non-condensable gas suggests that a source of gas exists.

This source cannot be represented by the release of CO_2 from the liquid solution as a consequence of the small, recent decrease in CO_2 partial pressure, since the mass of liquid necessary to explain the non-condensable gas production would be too large, involving a rock volume of $\sim$900 km^3. This behaviour and its implications are discussed below.

An initial-state model of Bagnore

The initial partial pressure of CO_2 in the Bagnore system was in the range 10 to 15 atm. The purpose of the initial-state model described below was to see if this relatively high partial pressure could be explained on the basis of simple chemical equilibria considerations.

The model describes a three-phase (gas-liquid-rock) system in chemical and thermodynamic equilibrium. The gas phase contains CO_2 and H_2O vapour. The liquid phase consists primarily of liquid water, but in addition contains dissolved CO_2 in the form of H_2CO_3, as well as the ions Ca^{++}, H^+, HCO_3^- and CO_3^{--}. The rock phase is a calcium carbonate species.

Five chemical equilibrium relations between the various components were written. Values of the equilibrium coefficients as a function of temperature were taken from Helgeson (1969). An expression for the charge balance in the liquid was also written.

In the first variation of this model, it was hypothesized

that all carbonate species in the vapour and liquid phases are derived only from local carbonate rock.

When expressed mathematically, this model resulted in a system of seven non-linear equations in seven unknowns. This set of equations was solved using standard numerical techniques. The ratio of vapour volume to liquid volume appeared as a parameter in the solution. Solutions for the values of this parameter of 0.1, 1.0, and 10.0 were essentially the same. Figures 21 and 22 present results for a value of this ratio equal to 1.0 only.

Figure 21 presents $\log_{10}$ of calculated and measured concentrations of CO_2, H^+ and Ca^{++}, vs. temperature. Partial pressures in atm describes the concentration of CO_2 in the vapour, while ionic concentrations are in terms of moles per 1000 g water. Calculated values are connected by curves, while measured values are assigned a location. The temperature of the two wellhead water samples was 98°C while the estimated initial reservoir temperature was 175°C. It can be seen from this figure that the intial partial pressure of CO_2 in the field is at least two orders of magnitude larger than that calculated using this model. Measured pH and Ca^{++} concentration are also larger than those calculated, although by only an order of magnitude or less.

Figure 22 presents $\log_{10}$ of calculated and measured H_2CO_3, HCO_3^-, and CO_3^{--} concentrations vs. temperature. Concentrations are in terms of moles per 1000 g water. Calculated concentrations are substantially smaller than those measured in the field.

In the second variation of the chemical equilibrium model,

an external source of carbonate species is allowed. In this case it is necessary to fix one unknown in order to have a mathematically determinate system. This was done for a Ca^{++} concentration of 48 ppm, which corresponds to measurements in the field. Preliminary results were obtained by assuming (according to Ellis 1963) that HCO_3^- is the dominant carbonate ion in the liquid (this will be verified at a later date). The calculated partial pressure of CO_2 at 175°C was found to be 11.5 atm, while that at 180°C was 15.7 atm. This range is in close agreement with values measured in the field.

Consequences of these results are discussed below.

A producing-state model of Bagnore

Uniform levels of pressure and producing non-condensable gas content have been observed across the productive portions of the Bagnore field. This observation gave a basis for thinking that a lumped-parameter mathematical model of the field would exhibit the production characteristics observed at Bagnore. A formulation similar to the "falling liquid level" model of Brigham and Morrow (1974) was chosen as being most appropriate for Bagnore.

The reservoir is considered to consist of two regions. The upper region is a continuum of rock and vapour at uniform thermodynamic conditions. The lower region is a continuum of liquid and rock, also at uniform thermodynamic conditions. The regions may be at different temperatures, but are in pressure equilibrium. As vapour production occurs from the vapour region, evaporation may occur from

the liquid into the vapour region. This may cause the water level to fall, decreasing the size of the liquid region. Finally, water influx into the liquid region may occur as the pressure in this region falls.

The two-lump system is considered to contain two fluid components : water and CO_2. These co-exist as a homogeneous vapour phase in the upper region. In the lower region the liquid water contains dissolved CO_2. A schematic of this model is presented in Fig.23.

The model under discussion has features which are similar to the "falling liquid level" model of Brigham and Morrow (1974). However, their model described only a single-component system (H_2O) and did not account for liquid influx. The model being described also has features in common with that described by Grant (1977). Grant's model is a single-lump, two-component (H_2O,CO_2) formulation, wherein rock, liquid and vapour are considered as a uniform continuum. His model also allowed for liquid influx and was successfully used to describe production characteristics from the Broadlands field in New Zealand.

The general formulation of this model is not limited to carbon dioxide as the non-condensable gas. The model is equally applicable to any non-condensable gas so long as the appropriate equation of state is used. In this work polynomial approximations to the equations of state for water and carbon dioxide as individual components were used. Then ideal solution laws were used to describe mixtures of the two components (e.g., Dalton's, Raoult's and Henry's laws). Such an assumption is reasonable for the

pressures and temperatures at Ragnore.

Mass, energy and component balances were written on a rate basis for each of the two regions. This resulted in a non-linear algebraic system of six equations in six unknowns. This system was solved using standard numerical techniques to obtain a calculated field history.

Results

The measured total instantaneous production rate from the field was used as input for the calculations. The calculated reservoir pressure and producing non-condensable gas content histories were then compared with values measured in the field. Most runs used values of initial reservoir pressure and temperature (23.4 atm., 175°C), as discussed above.

It was found necessary to include liquid influx in order for calculated long-time non-condensable contents to level off at a value greater than zero, as has occurred in the field (see Fig.24). All of the results presented below include the effects of a steady-state recharge function of the form:

$$\text{Recharge rate} = A(p_{\text{external}} - p_{\text{reservoir}})$$

If no recharge is included, calculated producing non-condensable gas content drops rapidly to zero. Similar calculated behaviour also occurs if there is a relatively small gas cap, and the influx water has a dissolved CO_2 content equal to that initially found in the reservoir (Case II-1, Fig.24). On the other hand, a relatively large initial gas cap (twenty times that for Case II-1) with

liquid influx of relatively high CO_2 content (fifty times the initial reservoir liquid value) displays quite different behaviour (Case III-7, Fig.24).

The duration of the blowdown curve of non-condensable producing gas content can be changed by adjusting the initial size of the gas cap. Cases II-2 and II-3 (see Fig.25) correspond to an initial gas cap size part way between Cases II-1 and III-7, and present the best comparison to date between calculated and field non-condensable producing gas histories. Case II-2 corresponds to water influx with a dissolved CO_2 content equal to that initially found in the reservoir. In case II-3 this value is 25 times as large.

Figure 26 presents calculated reservoir pressure histories for all four cases previously presented. The shapes of these curves can be adjusted by changing parameters such as the relative gas cap/liquid region sizes, reservoir porosity and initial reservoir temperature. Cases II-2 and II-3 also represent the best comparison to date between calculated and measured reservoir pressure histories.

Figures 24,25 and 26 present only a sampling of results from the twenty cases which have been studied to date. These cases demonstrate that calculated histories of pressure and producing non-condensable gas content are sensitive to values of the input parameters. Efforts to date have not resulted in a set of parameters which produce an accurate match between calculated and field histories. Further work along this line remains to be done. However, calculations made to date suggest that values of most of

the parameters required for a reasonable match are geohydrologically plausible. One exception to this is the very high dissolved CO_2 content of the recharge liquid required to obtain reasonable long-time calculated non-condensable producing gas contents.

The set of parameters which produces a good match between field and calculated histories will be very useful. First, the magnitudes of the parameters can be examined within the known geohydrological framework in order to gain an increased understanding of the production mechanisms active in the reservoir. Second, these parameters can be used to calculate future field behaviour under alternate field development plans.

Conclusions

This paper has presented a description of the Bagnore geothermal field. Thermodynamic and chemical equilibrium conditions were used to investigate the field behaviour quantitatively.

Chemical equilibrium calculations indicate that the CO_2, liquid carbonate ionic species, and carbonate rocks, are in equilibrium with one another. These calculations also indicate, however, that the liquid and vapour carbonate species are not derived from local rock only.

Thermodynamic considerations were used to evaluate the evolution of the field as fluid was produced. These calculations support the hypothesis that the initial decline in field pressure and producing CO_2 content was caused by a "blowdown" of the gas cap. They furthermore indicate that subsequent production from the field has come from

boiling liquid below the gas cap.

A mathematical lumped-parameter model of the Bagnore field was successfully developed. This model shows promise in being able to accurately reproduce the observed field history. If a successful match between calculated and field results can be obtained, then valuable quantitative inferences regarding the magnitude of various field parameters may be made.

In order for calculated long-time producing CO_2 contents to equal those measured in the field, it has been found necessary to assume a liquid influx of very high CO_2 content. Early calculations suggest that the CO_2 content of influx liquid needs to be ten to fifty times that initially found in the field. This finding is consistent with the earlier findings that the external carbonate source must be found to justify the high initial CO_2 content of the reservoir.

It has been suggested (Truesdell, 1977) that the necessary factor of ten to fifty may correspond to the initial ratio of total carbonates to total H_2O at Bagnore. The implication of such a correspondence is that the source of initial and current CO_2 is the same.

A suggestion concerning the mechanism of external CO_2 has been given by White (1977).

This is that there may be a steady upward seepage of CO_2 from a deeper metamorphic or magmatic source.

The fact that there were initially no surface hydrothermal manifestations does not strongly support this hypothesis.

However, very slow seepage through the cap rock and surface soils cannot be ruled out.

References

Brigham,W.E. and Morrow,W.B.(1974)P/Z behaviour for geothermal steam reservoirs. SPE Paper 4899, presented at the Annual California Regional Meeting of the Society of Petroleum Engineers of AIME, San Francisco,California.

Cataldi R. (1967) Remarks on the geothermal research in the region of Monte Amiata (Tuscany,Italy). Bulletin Volcanologique,XXX,pp.243-270.

Ellis,A.J.(1963) The solubility of calcite in sodium chloride solution at high temperatures. Amer.J.Sc.,v.261,pp. 259-267.

Grant,M.A.(1977) Broadlands -A gas-dominated geothermal field. Geothermics,v.6,1/2 (in press).

Helgeson,H.C.(1969)Thermodynamics of hydrothermal systems at elevated temperatures and pressures. Amer.J.Sc.,v.267, pp.729-804.

Truesdell,A.H.(1977) Oral communication

White,D.E.(1977) Oral communication

TABLE 1

Well	Date	Well head Temperature °C	Well head Pressure Kg/cm^2 abs	flow rate ton/h	noncondensable gas% (weight)
B1	4-29-59	148	4.2	173.6	81
B2	10- 7-59	143	3.7	215	75
B4	1-15-60	153	11.1	38	75
B5	4-27-60	123	4.9	86	69
B7	8-13-60	127	3.2	158.5	83
B9	12- 1-60	123	3	84.5	56
B2bis	6-10-61	156	5.6	46	10
B18	11-17-62	153	5.5	11.5	18
B19	7-10-62	155	5.3	56.7	10.4
B1	8-11-76	139	2.86	18.3	8.3
B2bis	8-11-76	140	3.27	18.7	6.6
B5	8-11-76	133	2.95	15.4	7.3
B18	8-11-76	132	2.97	10.3	14.3
B19	8-11-76	151	3.45	31.2	7.1

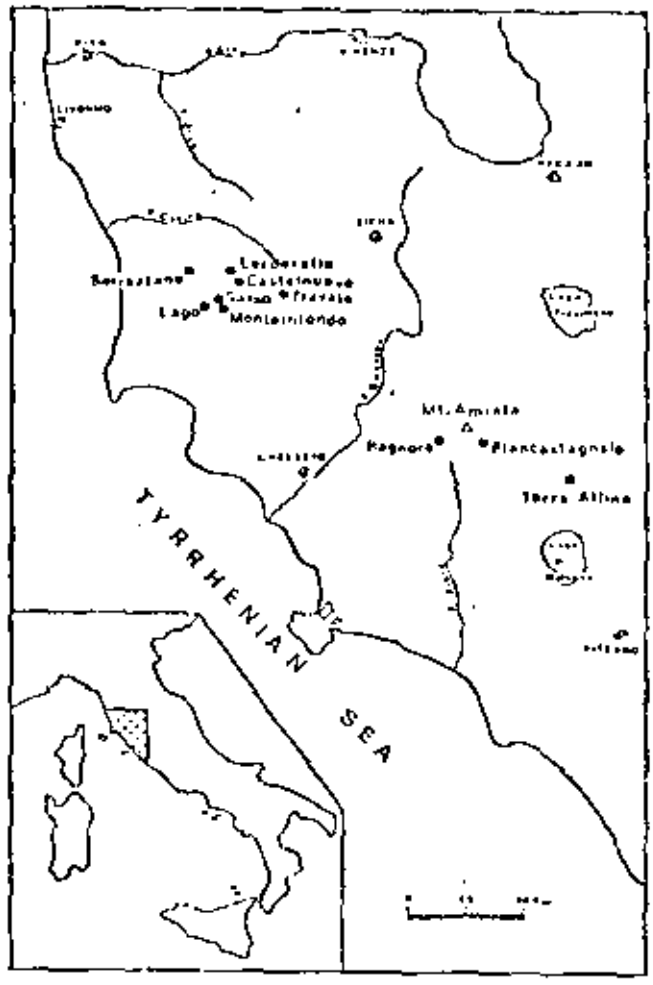

Fig. 1.- Location of Bagnore geothermal field.

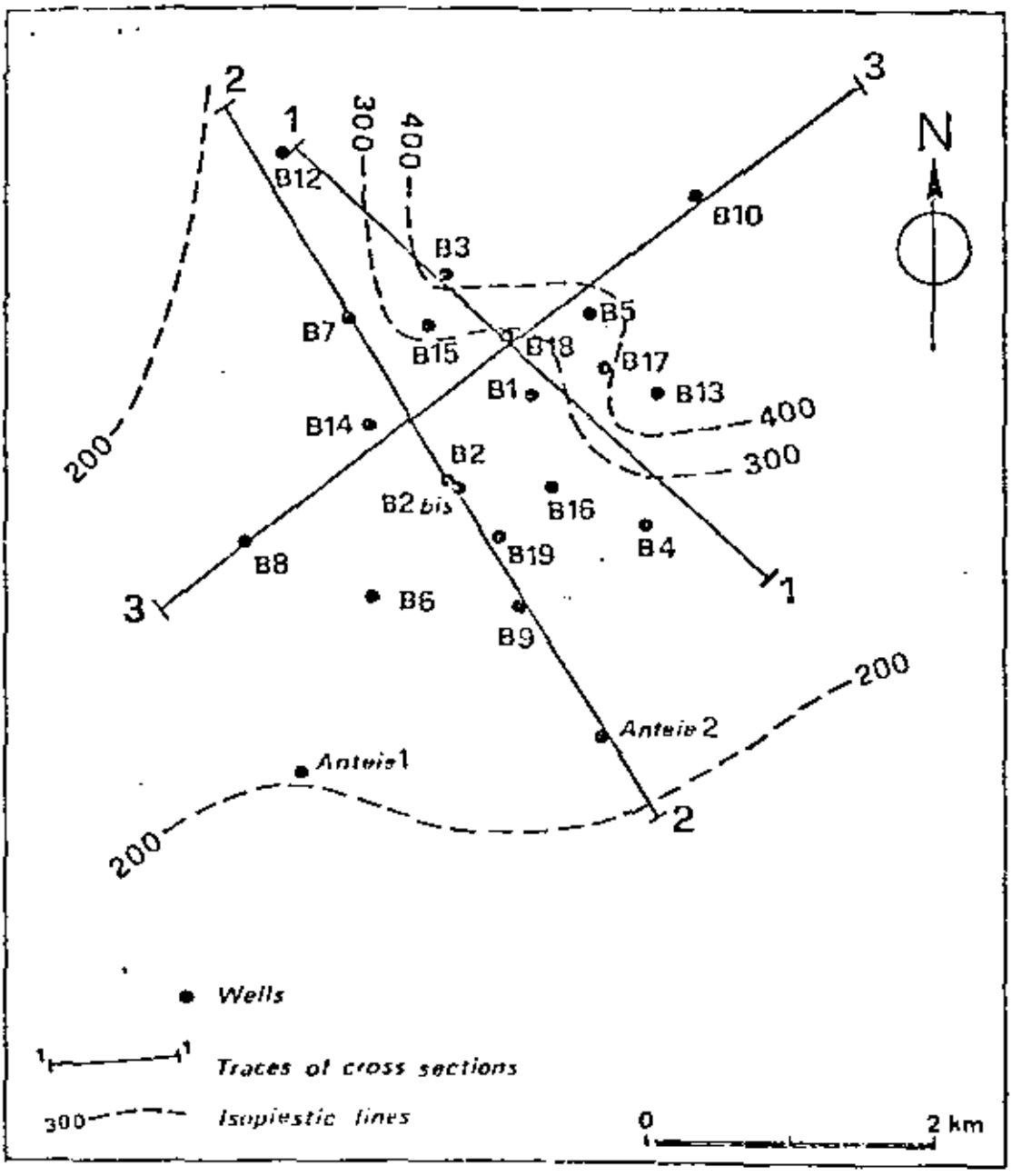

Fig.2 - Location of wells in Bagnore field; isopiestic lines at the field boundaries; traces of cross-sections.

(elevations in meters a.s.l.)

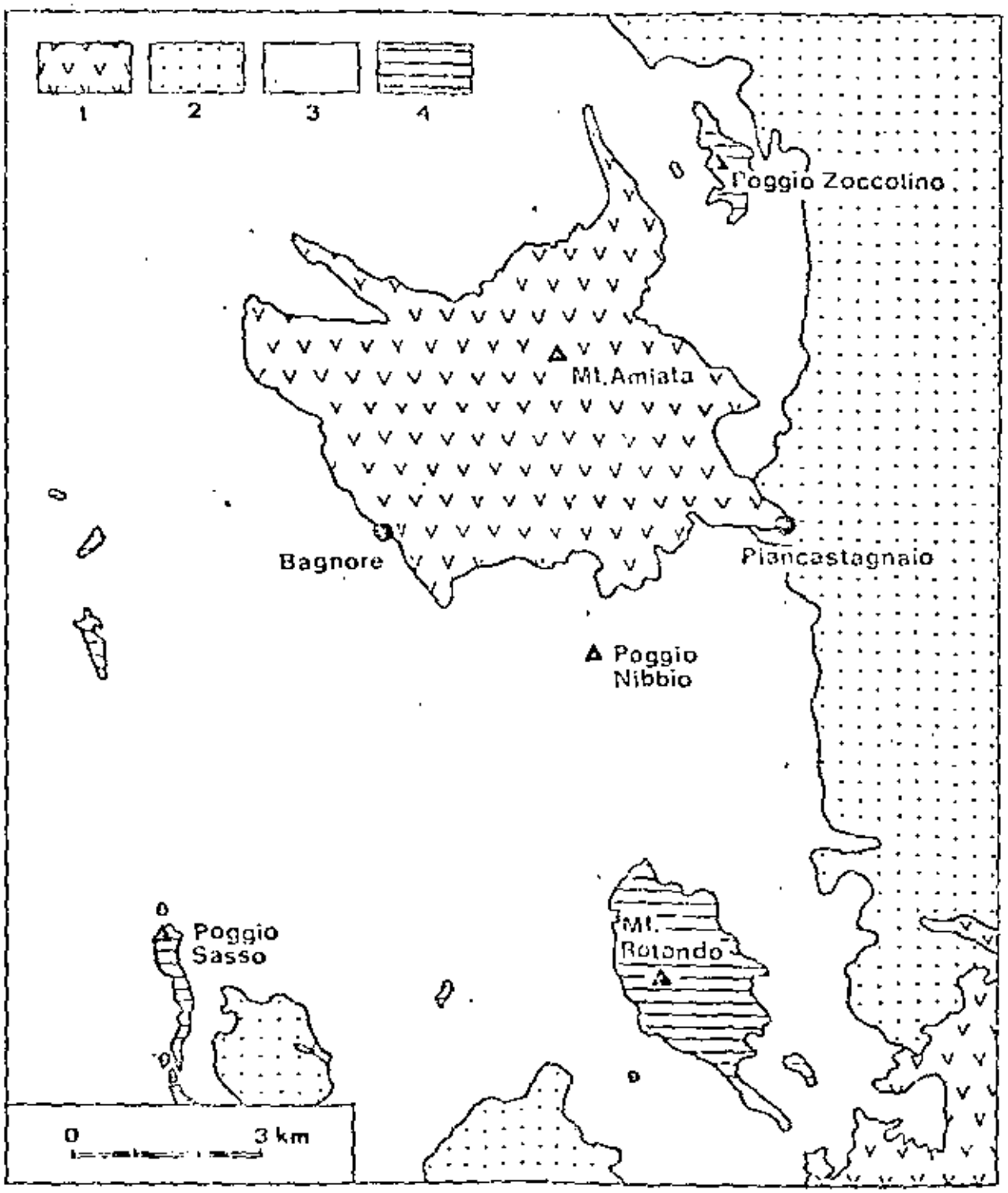

Fig. 3 - Main hydrogeological complexes in Mt.Amiata geothermal region. 1- volcanic complex (Quaternary); 2- mainly clay complex (Lower-Middle Pliocene); 3- mainly silty "flysch facies complex (Cretaceous-Eocene); 4-mainly [illegible] (Upper Jurassic).

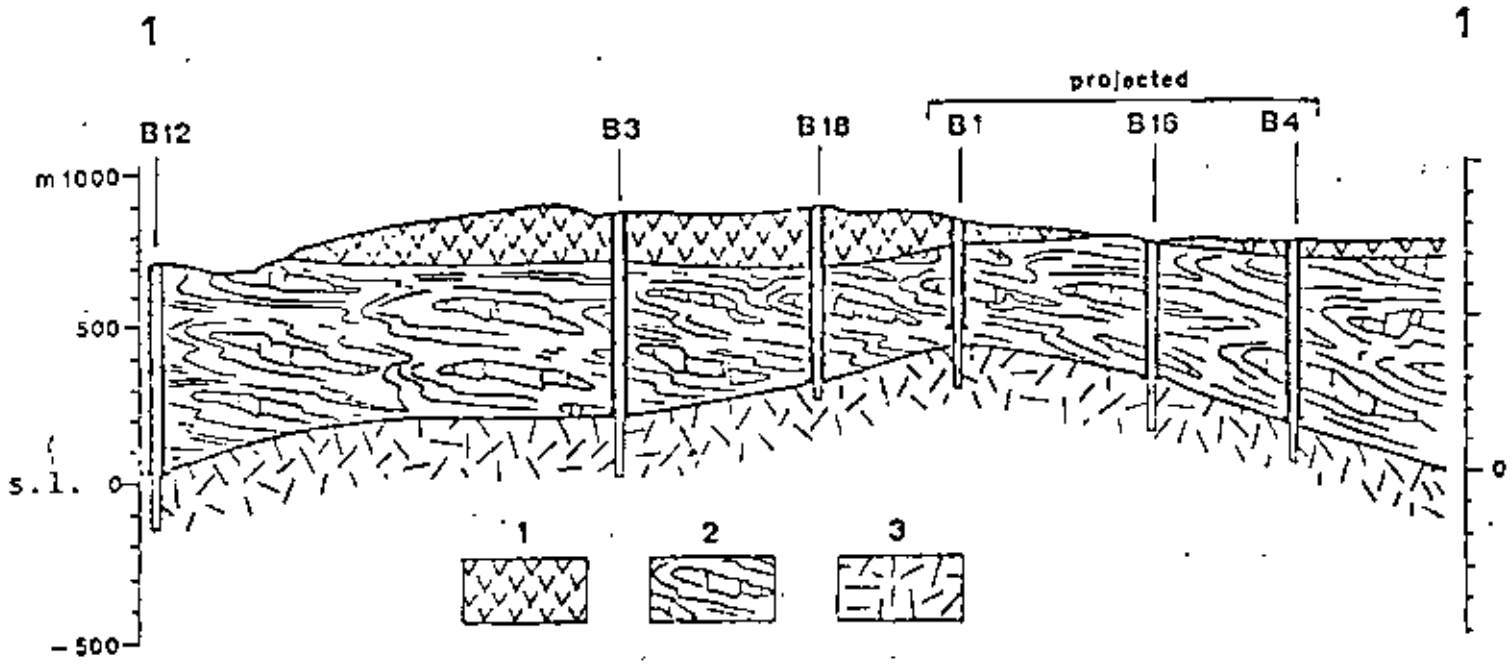

Fig.4 - Cross-section through Bagnore field (see Fig.2).
1 -volcanites; 2 -cap-rock; 3 -reservoir.

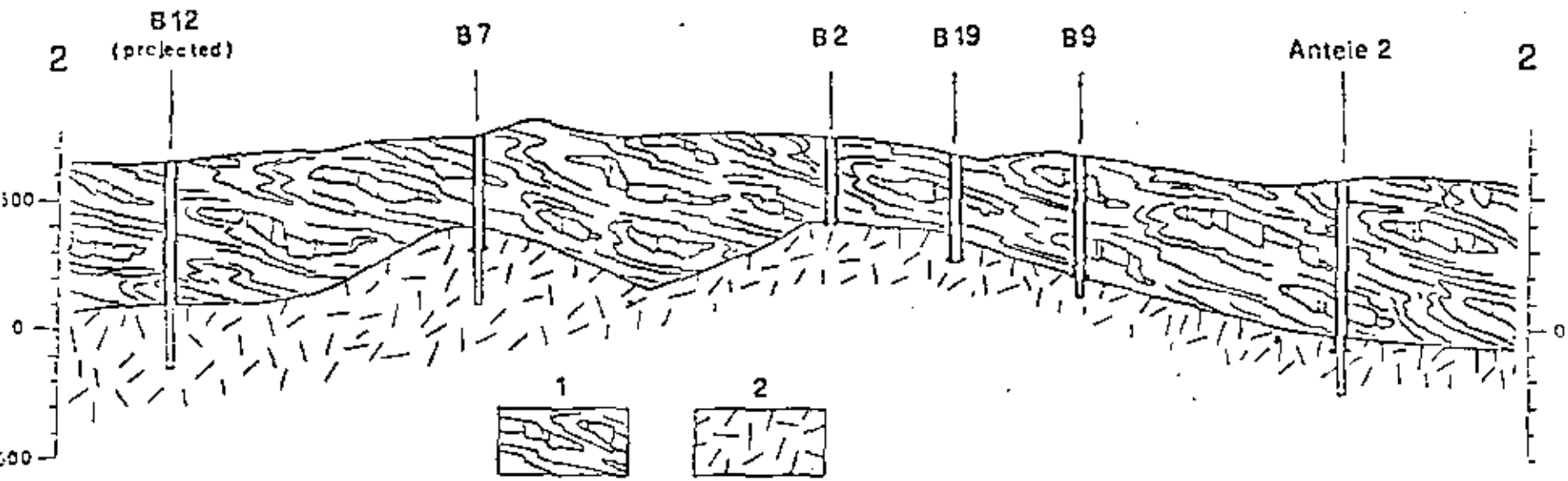

Fig.5 - Cross-section through Bagnore field (see Fig.2).
1 -cap-rock; 2 -reservoir.

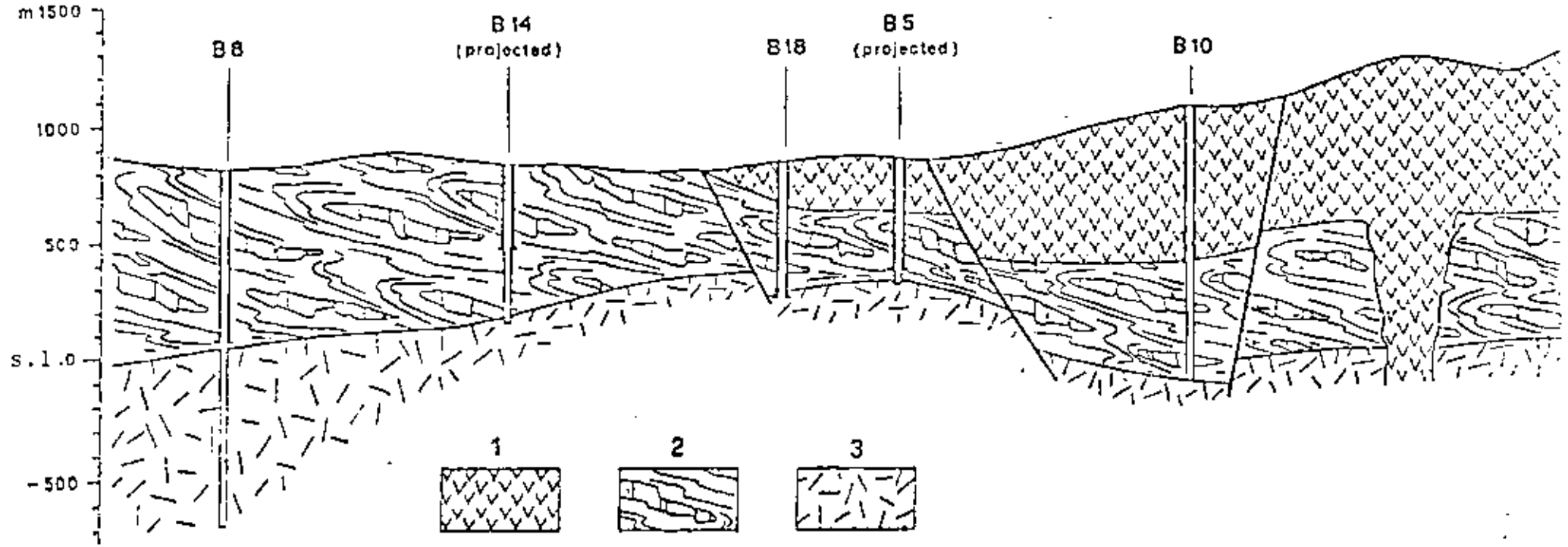

Fig.6 - Cross-section through Bagnore field(see Fig.2).
1 -volcanites; 2 -cap-rock; 3 -reservoir.

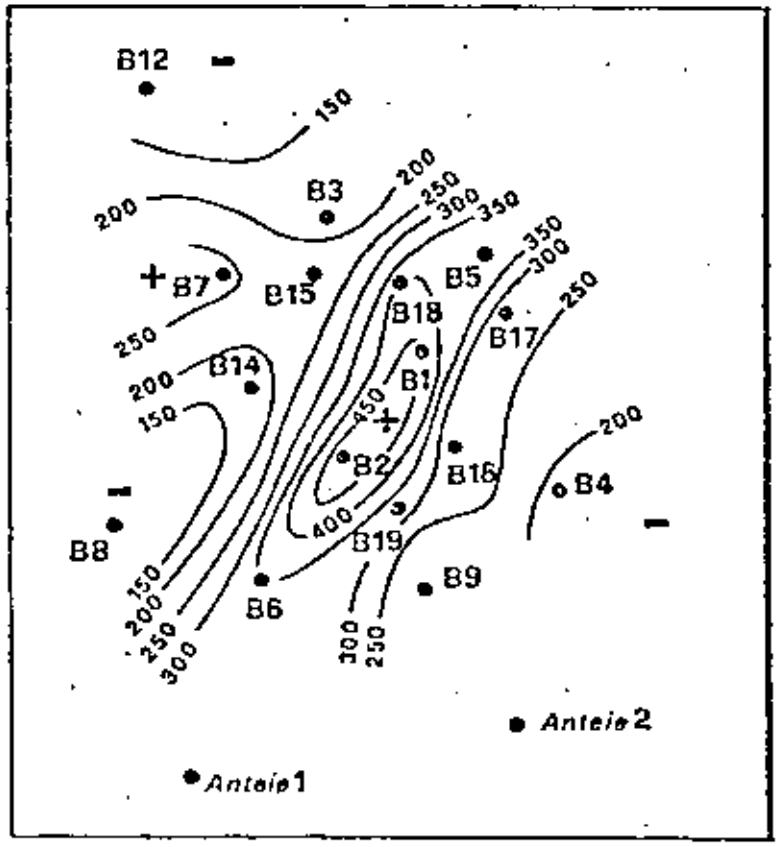

Fig.7 - Elevation of the first fractures met by the wells below the cover terrains.(m a.s.l.)

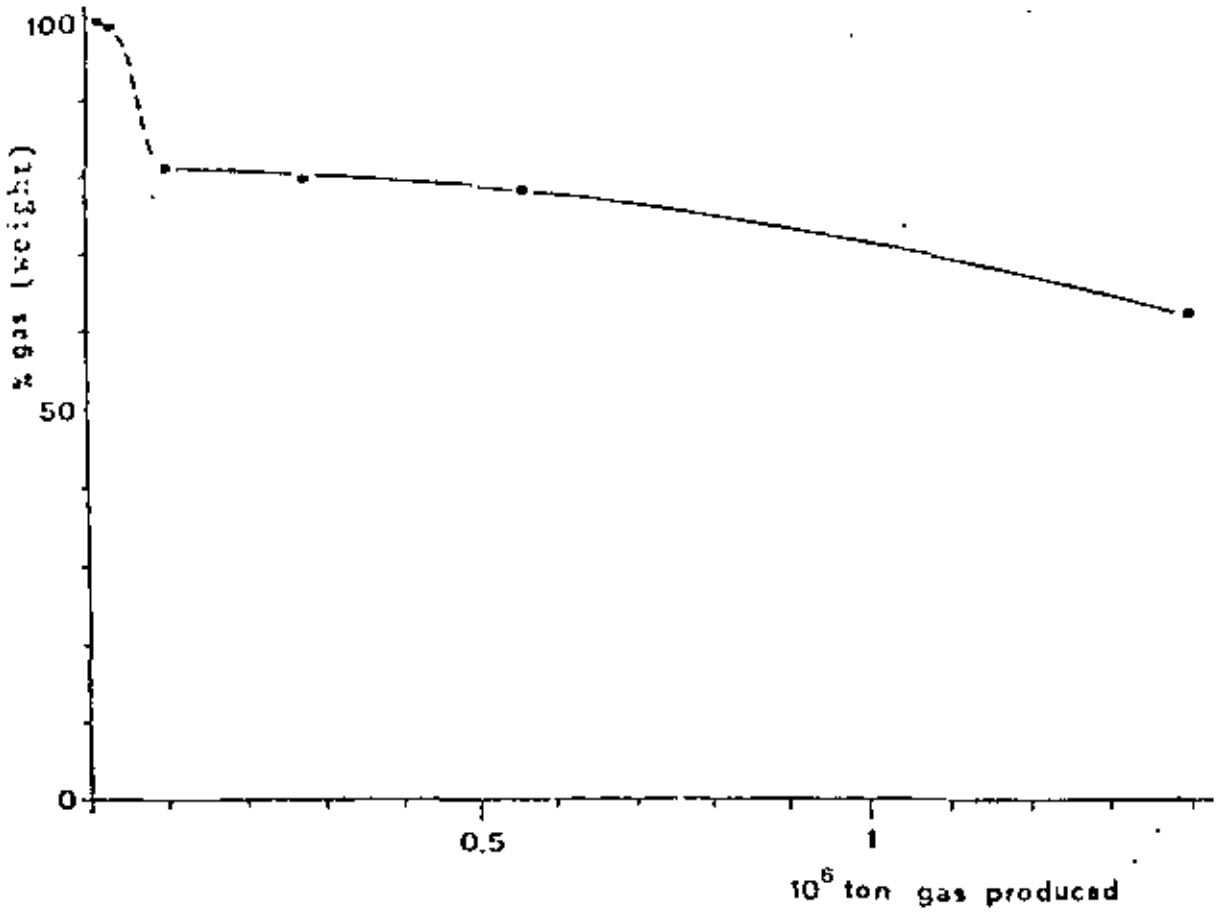

Fig.8- Noncondensable gas content in the fluid during the first production period of Bagnore field.

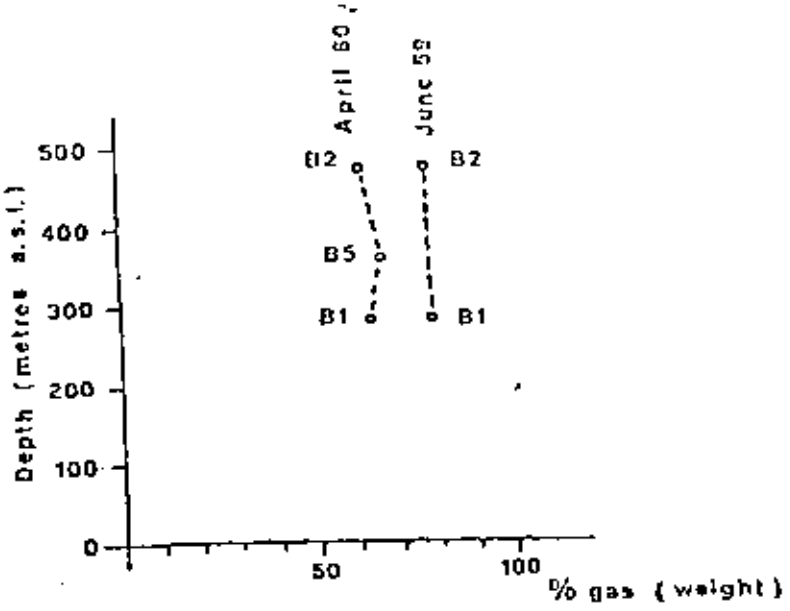

Fig.9- Noncondensable gas content in the fluid produced from fractures at different depths in the reservoir.

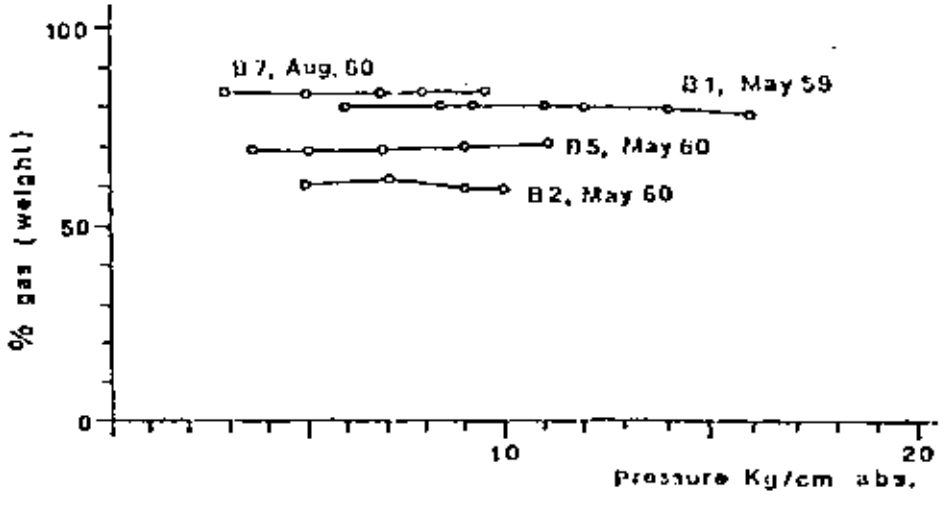

Fig.10- Noncondensable gas content versus delivery pressure for some productive wells.

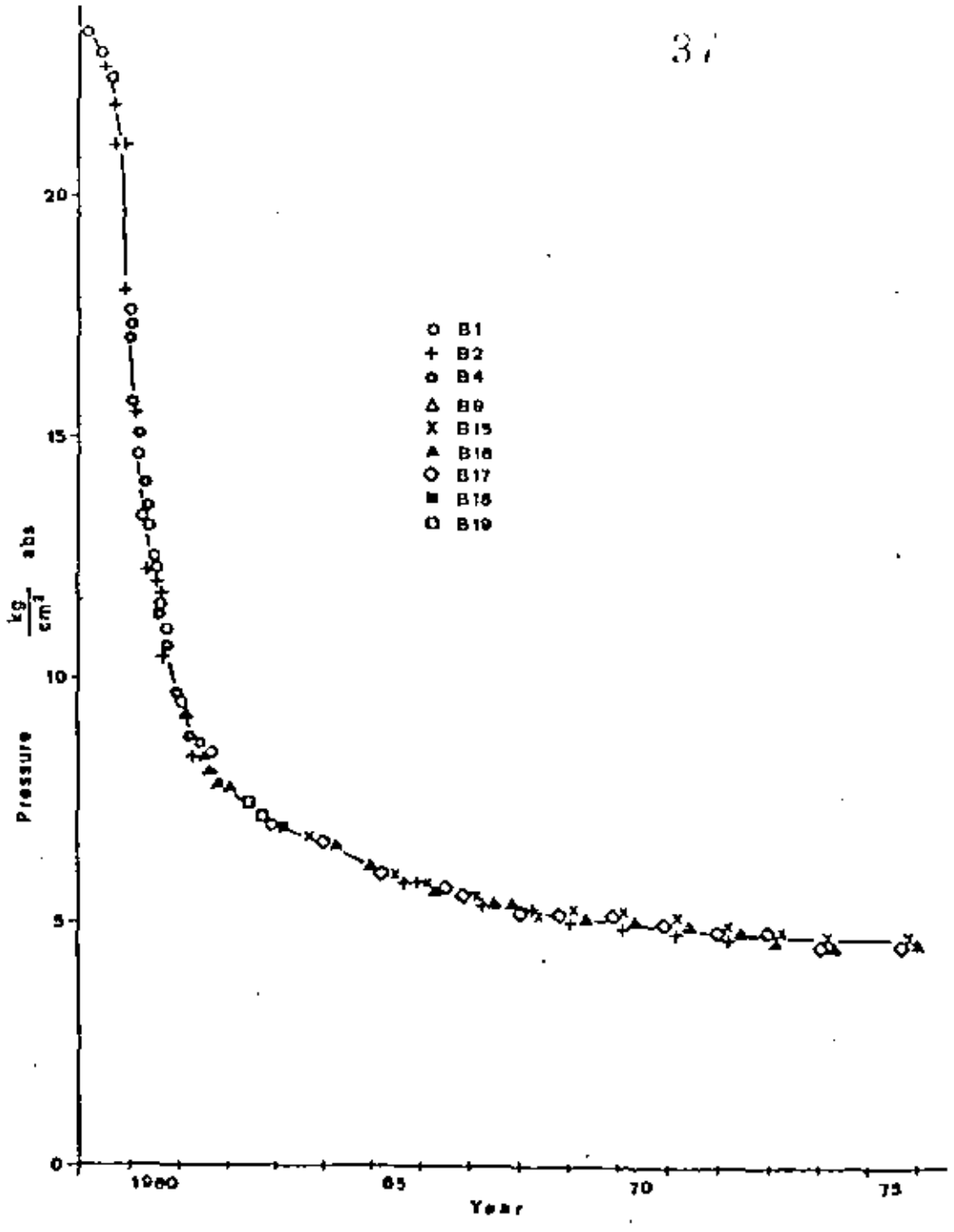

Fig.11 - Reservoir pressure in Bagnore field.

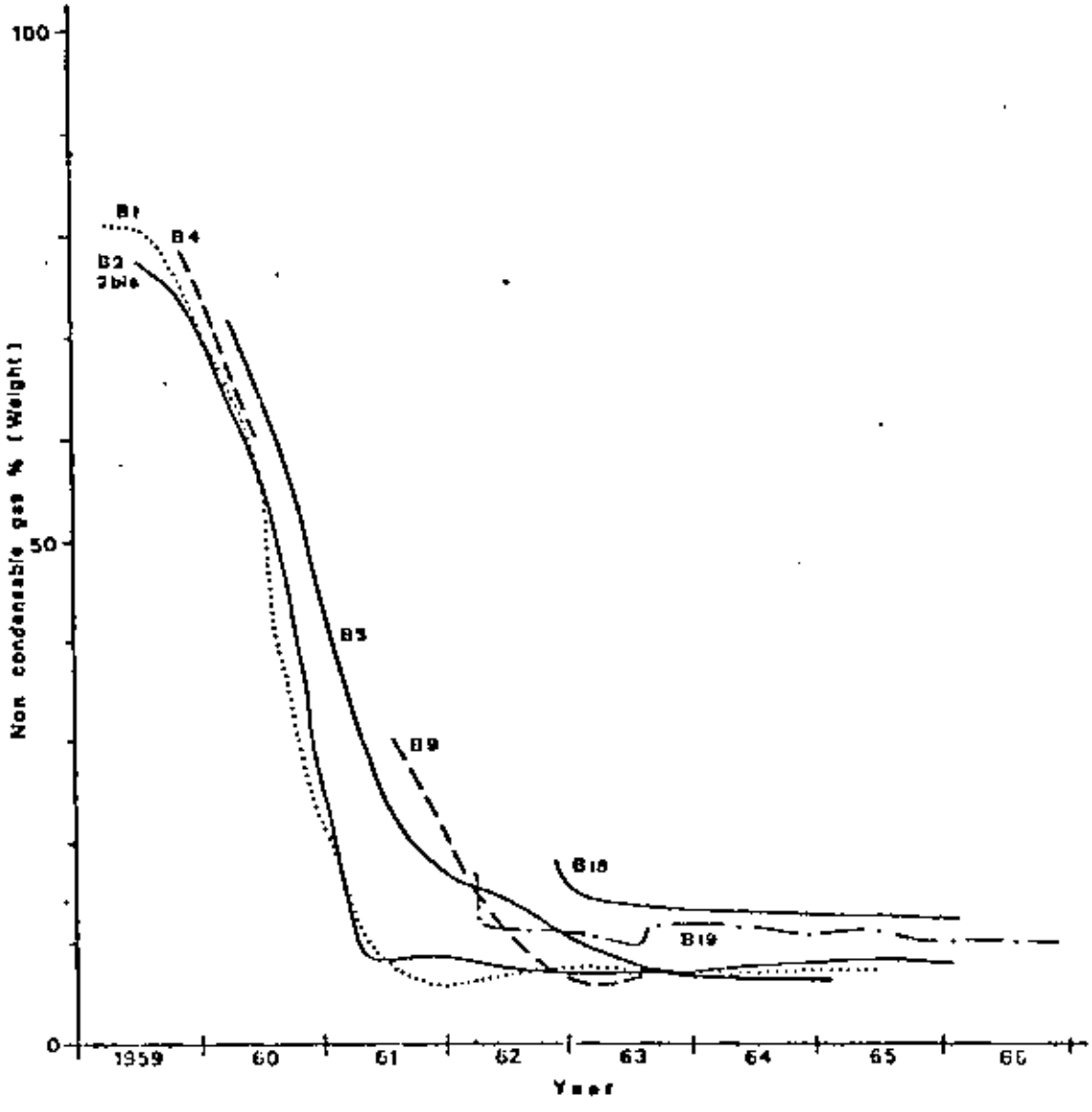

Fig.12 - Noncondensable gas content in the fluid produced by Bagnore wells.

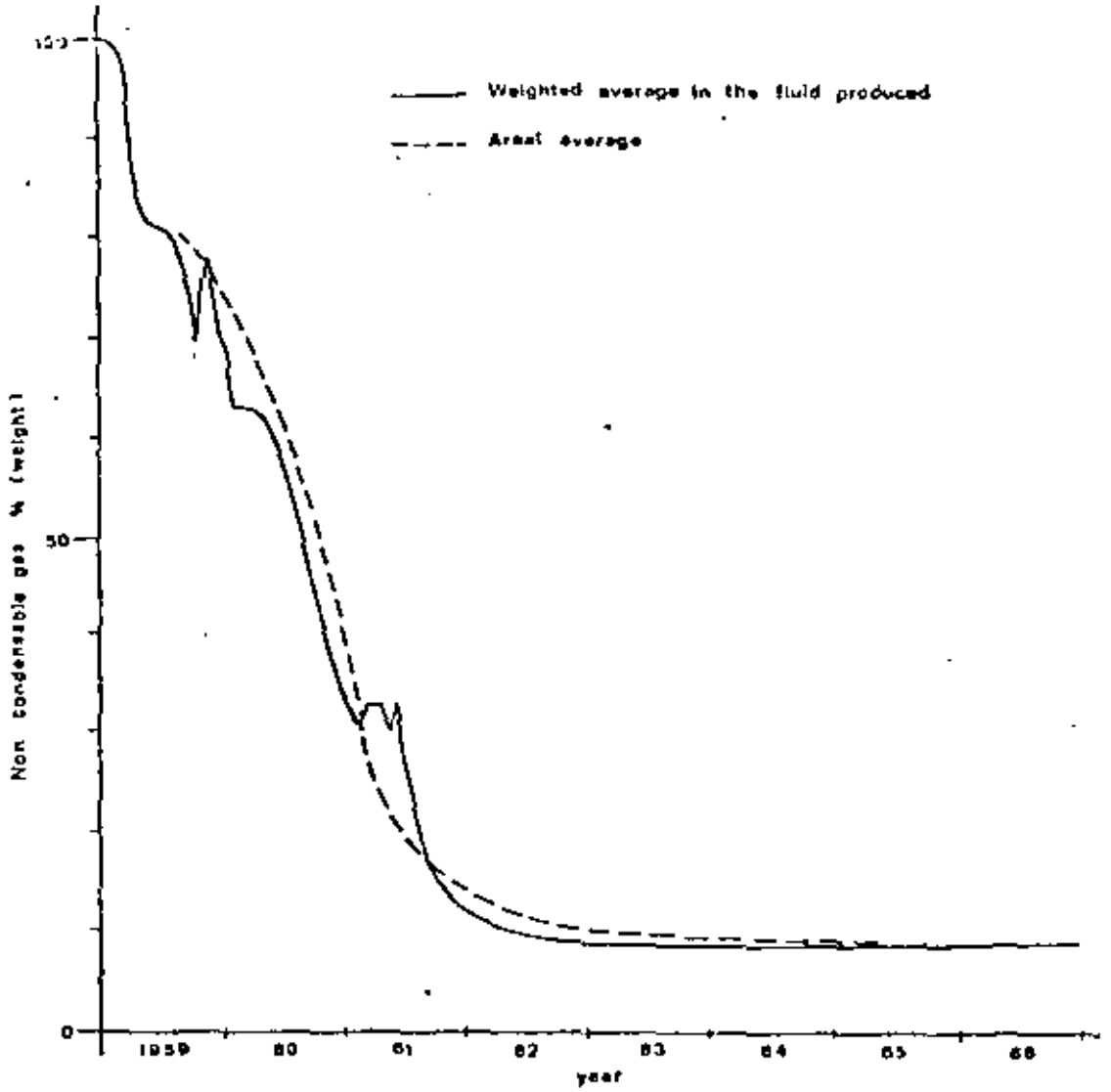

Fig. 13- Average noncondensable gas content

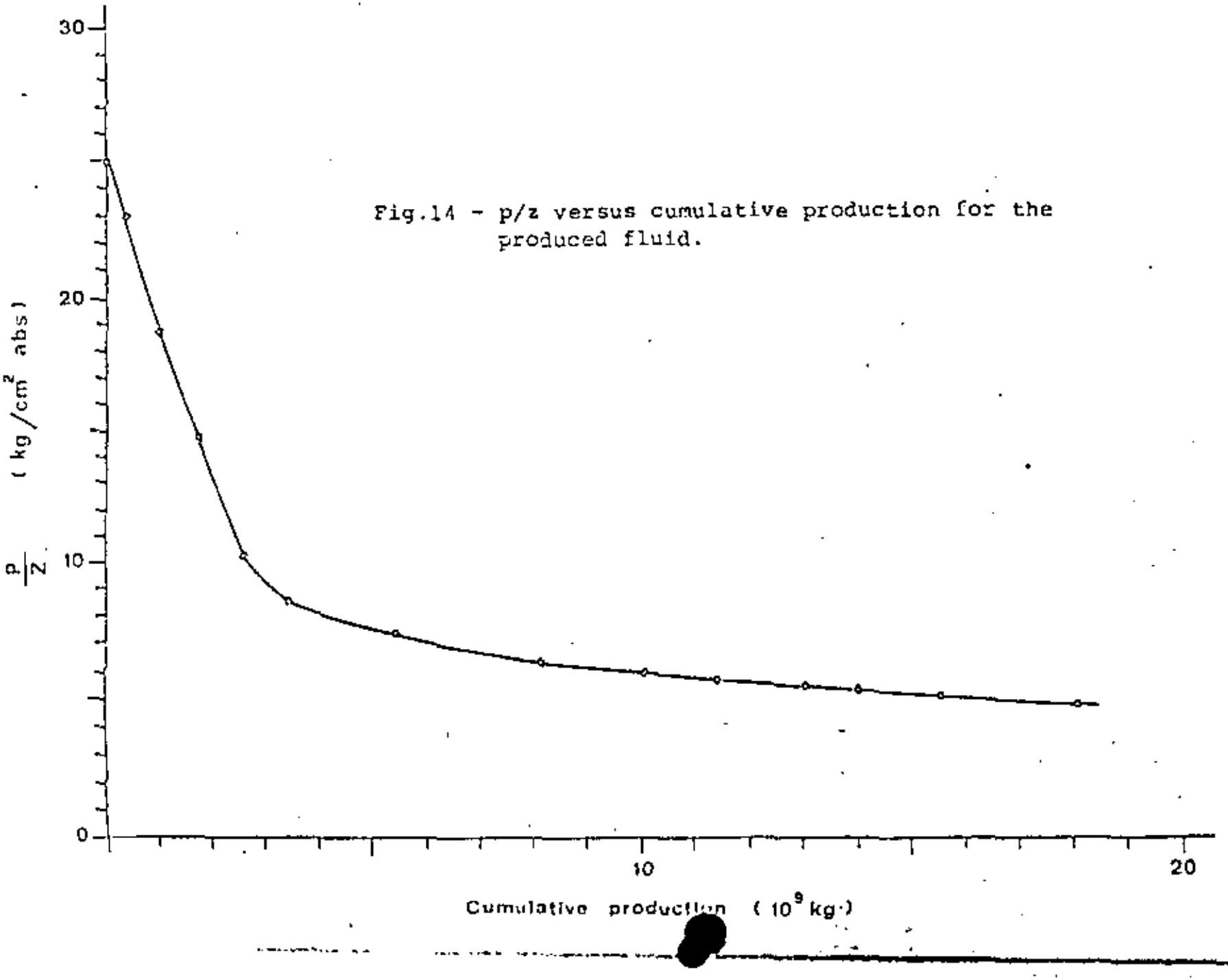

Fig.14 - p/z versus cumulative production for the produced fluid.

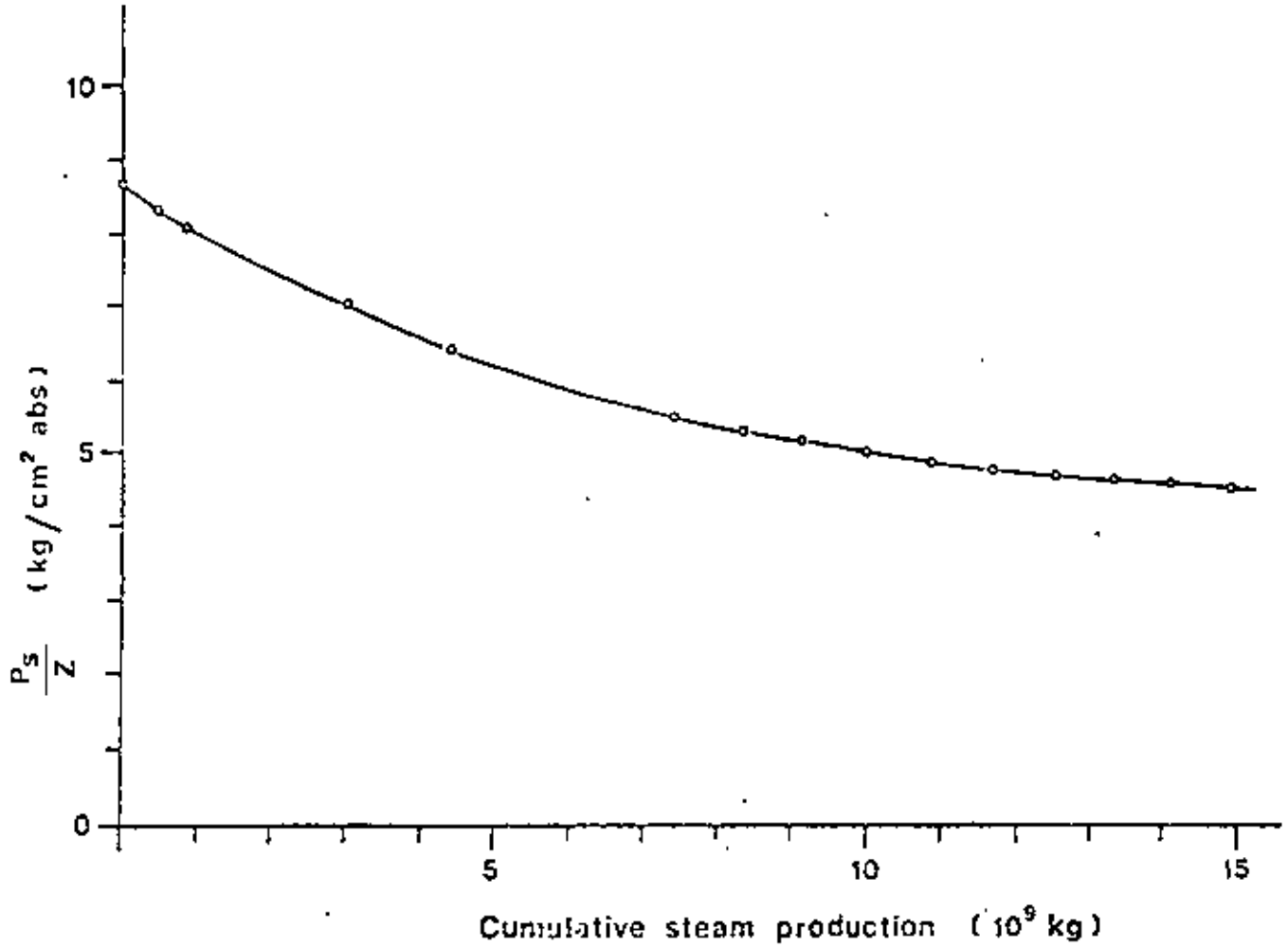

Fig.15 - p/z versus cumulative production for steam

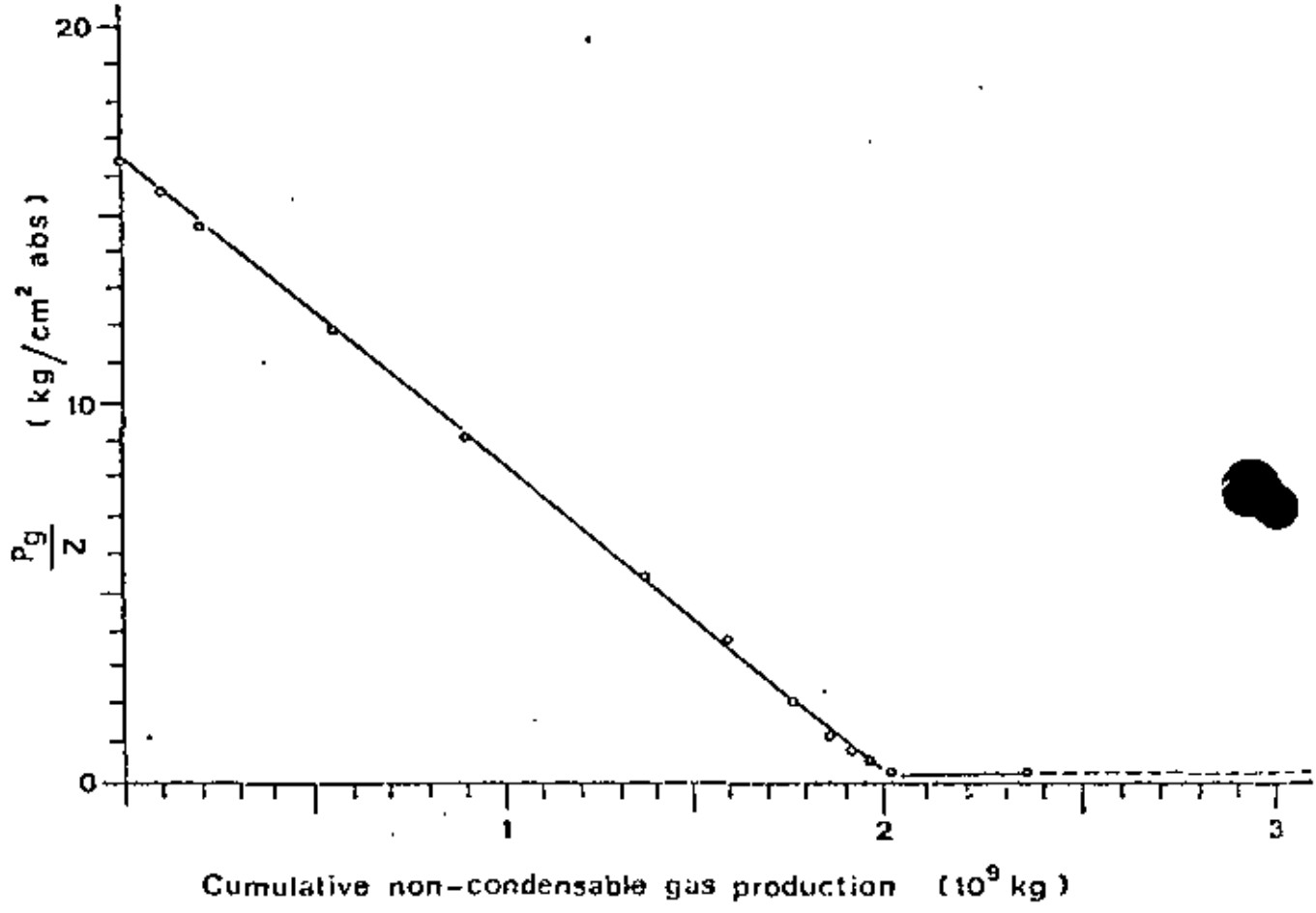

Fig.16 - p/z versus cumulative production for non-condensable gas

1) fractures
2) fractured intervals
3) reservoir
4) cap-rock
5) casing

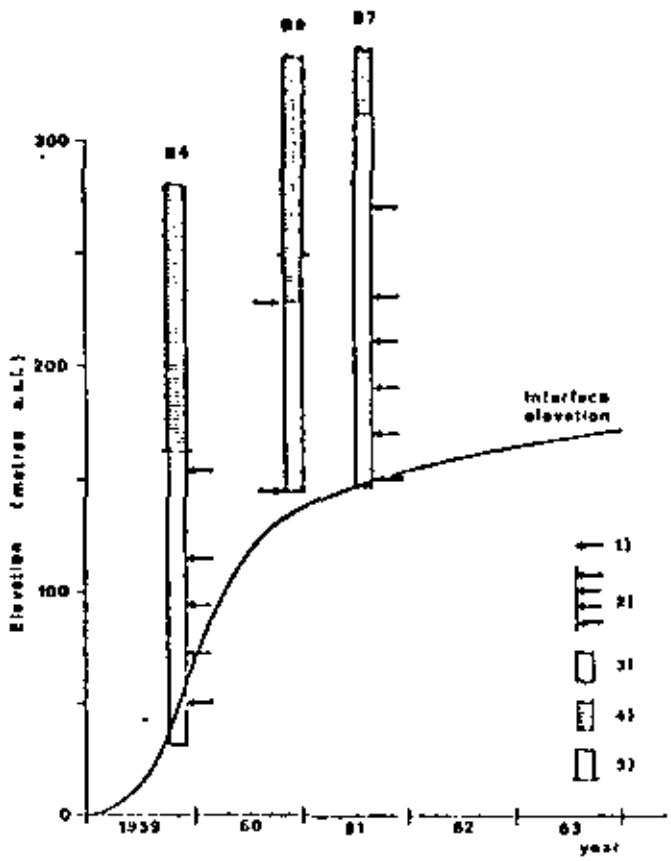

Fig.17 - Correlation between the depth of the fractures and the hypothetical position of the gas-water interface. Productive wells.

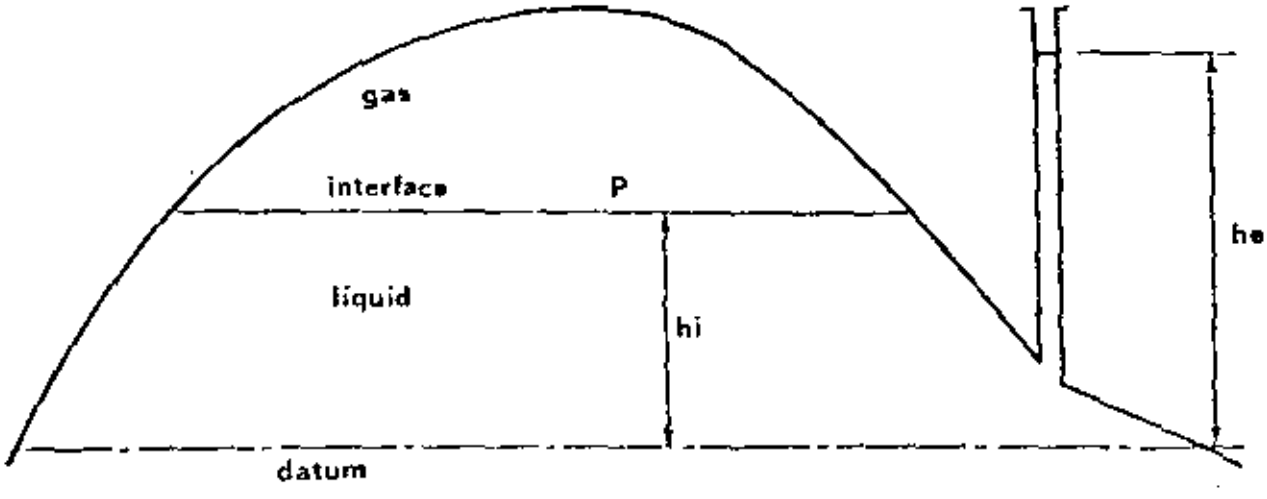

Fig.18 - Explanation of the quantities in the hydrostatic equilibrium equation.

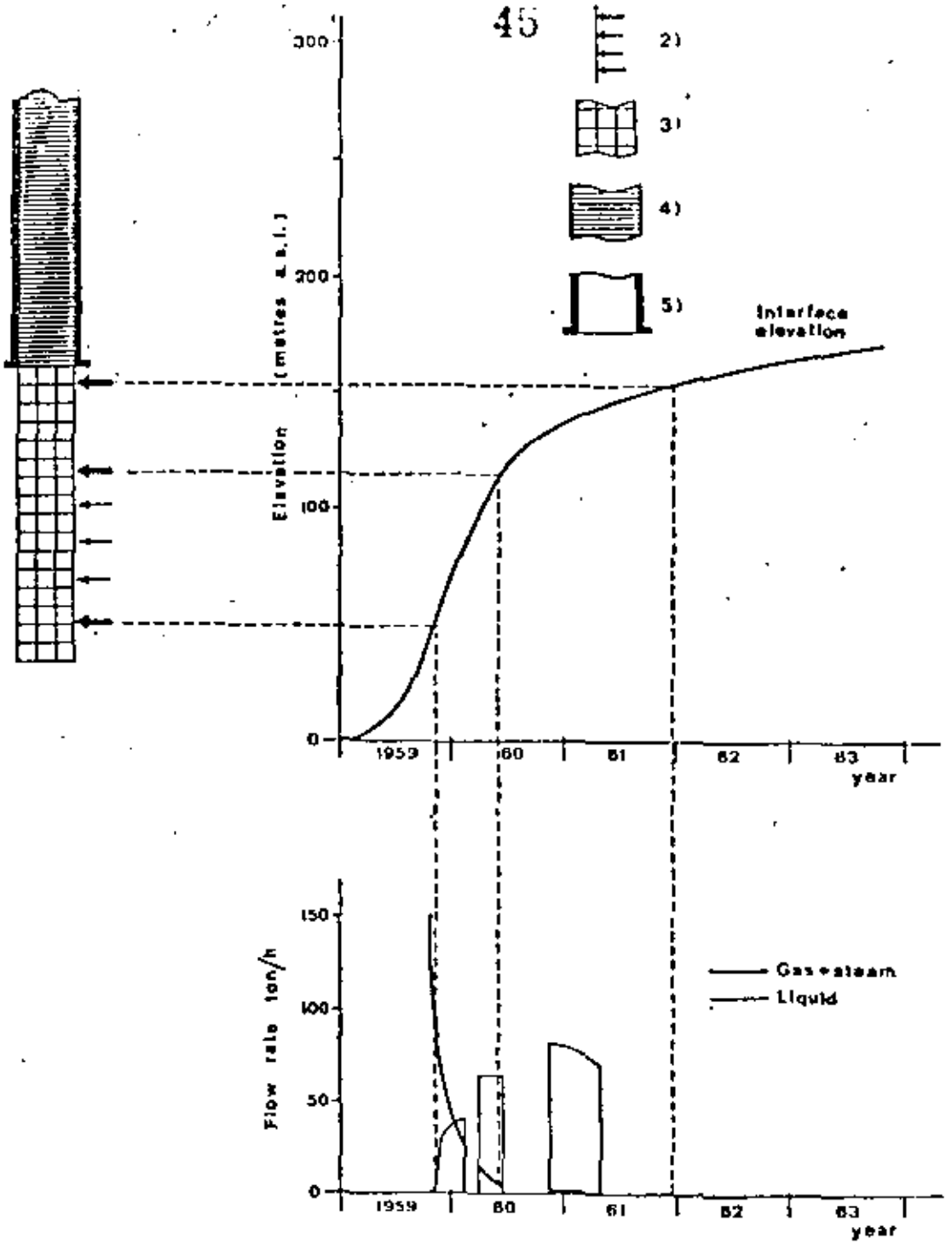

Fig.19 - Correlation between production and the hypothetical position of the gas-water interface for B4 well.
1) fractures; 2) fractured intervals; 3) reservoir; 4) cap-rock; 5) casing.

46

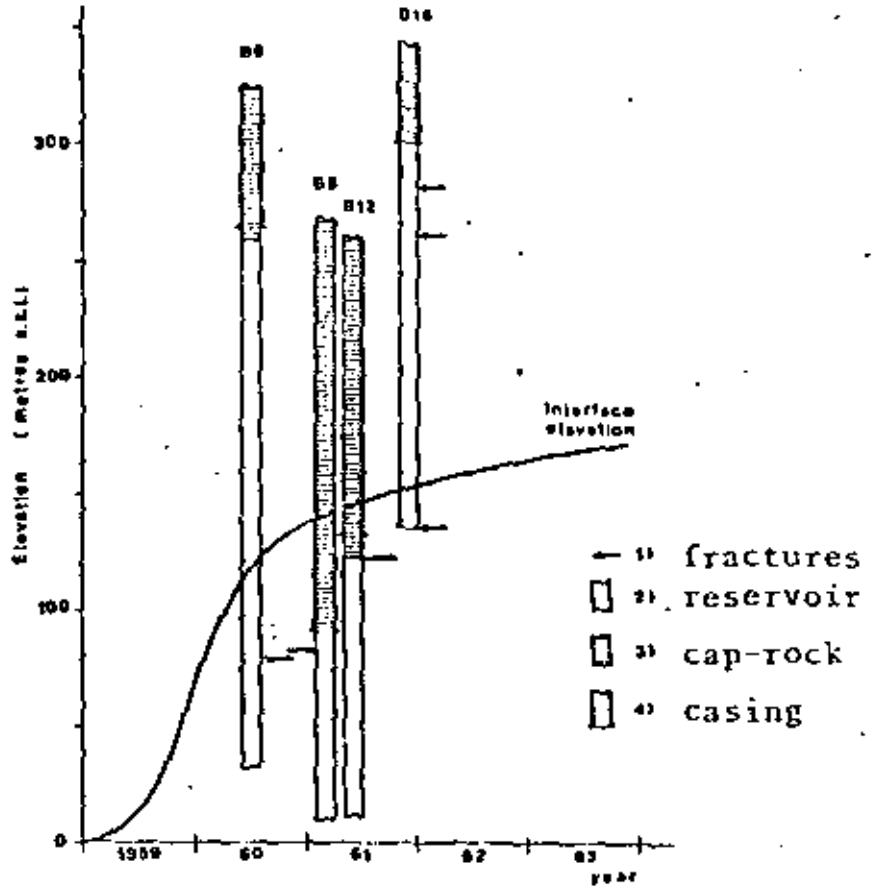

Fig.20 - Correlation between the depth of the fractures and the hypothetical position of the gas-water interface. Dry and non-commercial wells.

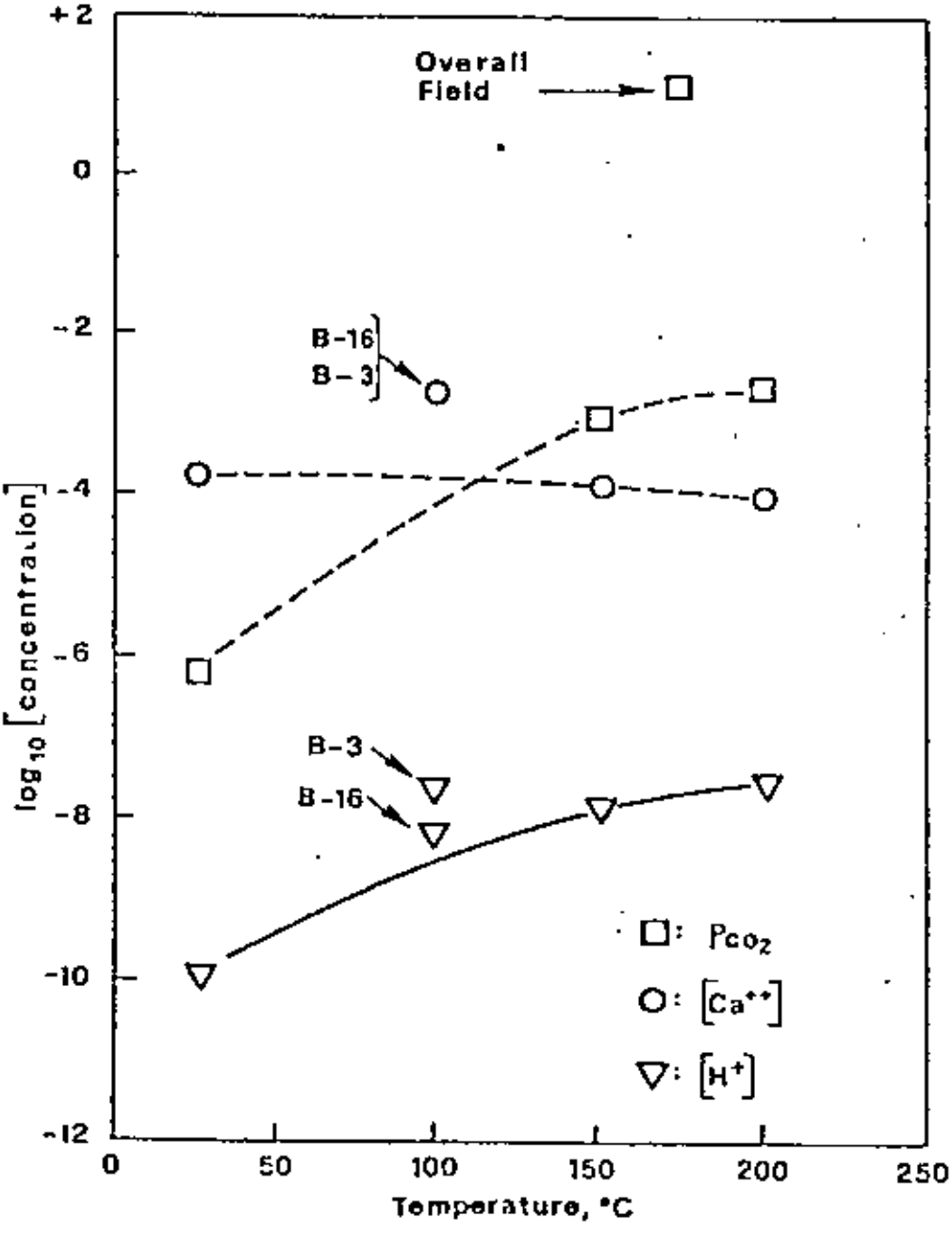

Fig.21- Calculated and measured concentrations of CO_2 partial pressure, pH, and (Ca^{++}).

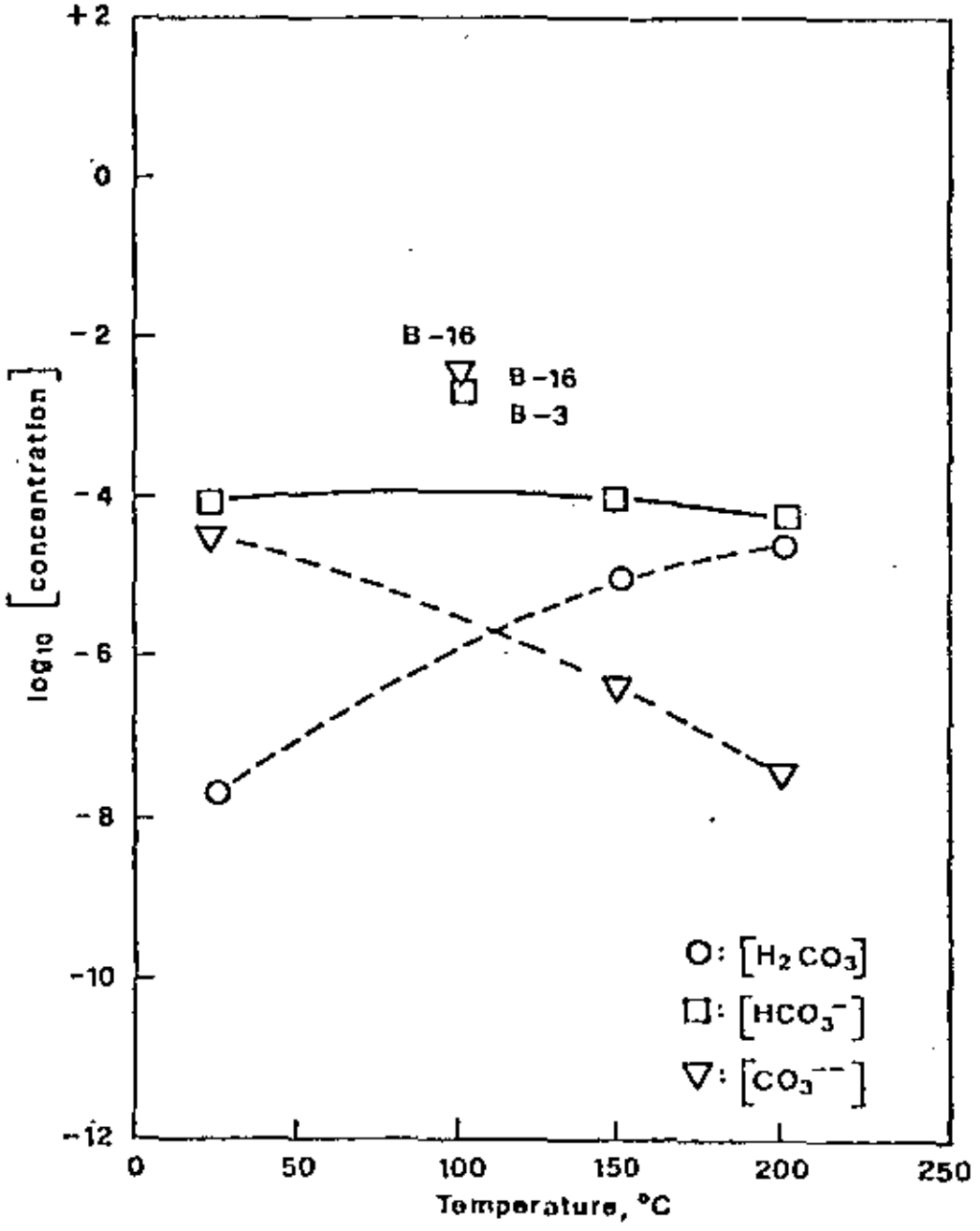

Fig.22- Calculated and measured concentrations of H_2CO_3, HCO_3^-, and CO_3^{--}.

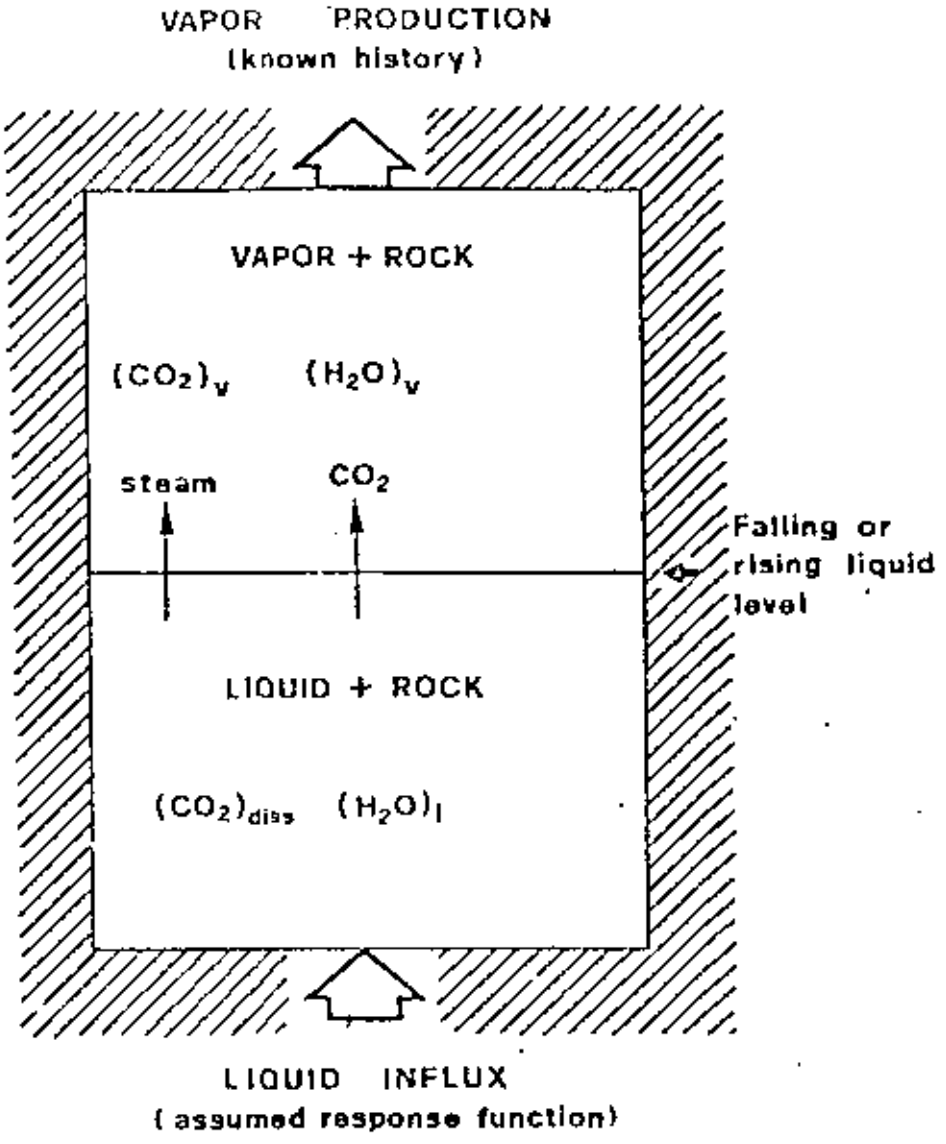

Fig.23- Schematic of producing state model.

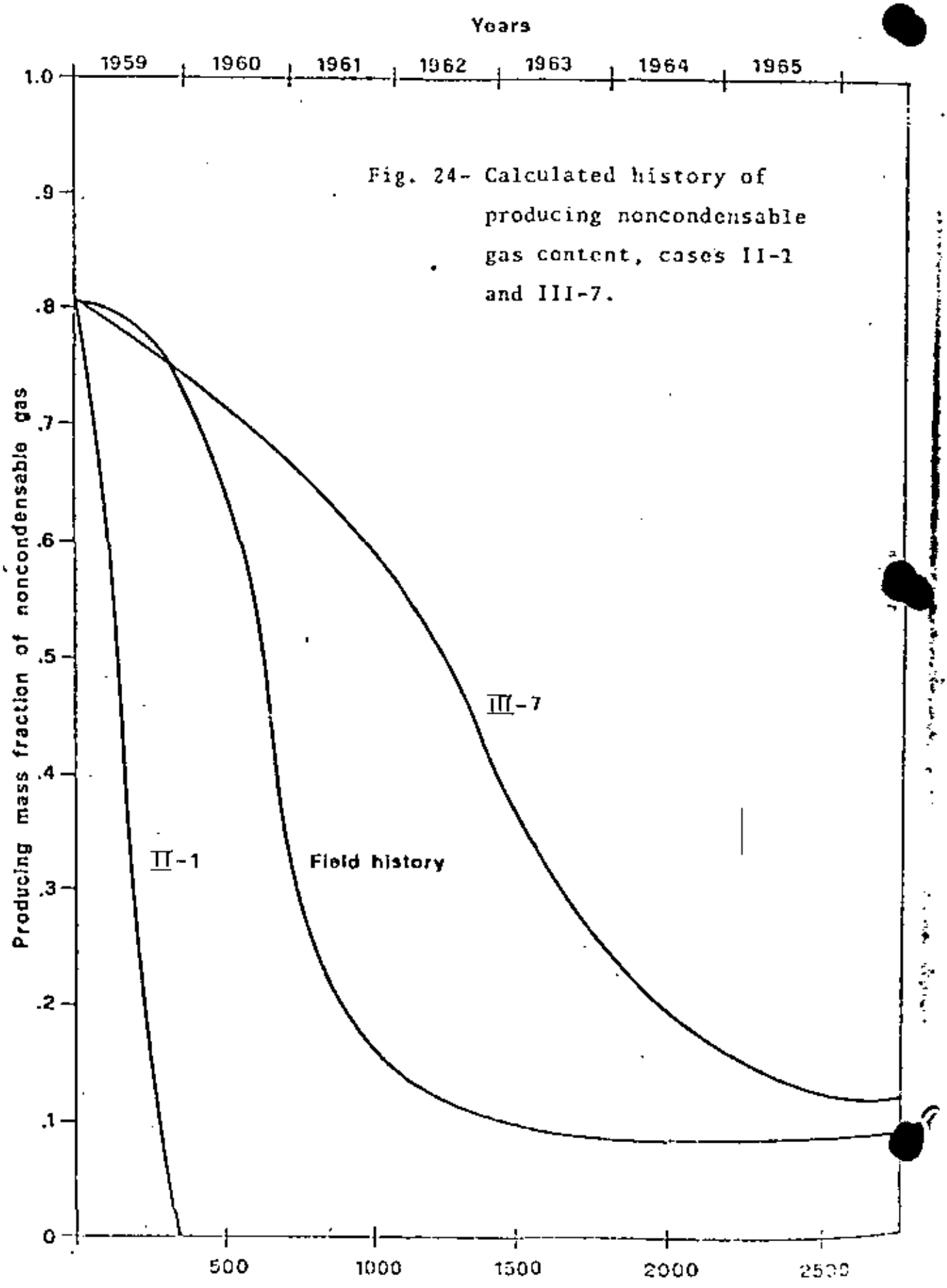

Fig. 24- Calculated history of producing noncondensable gas content, cases II-1 and III-7.

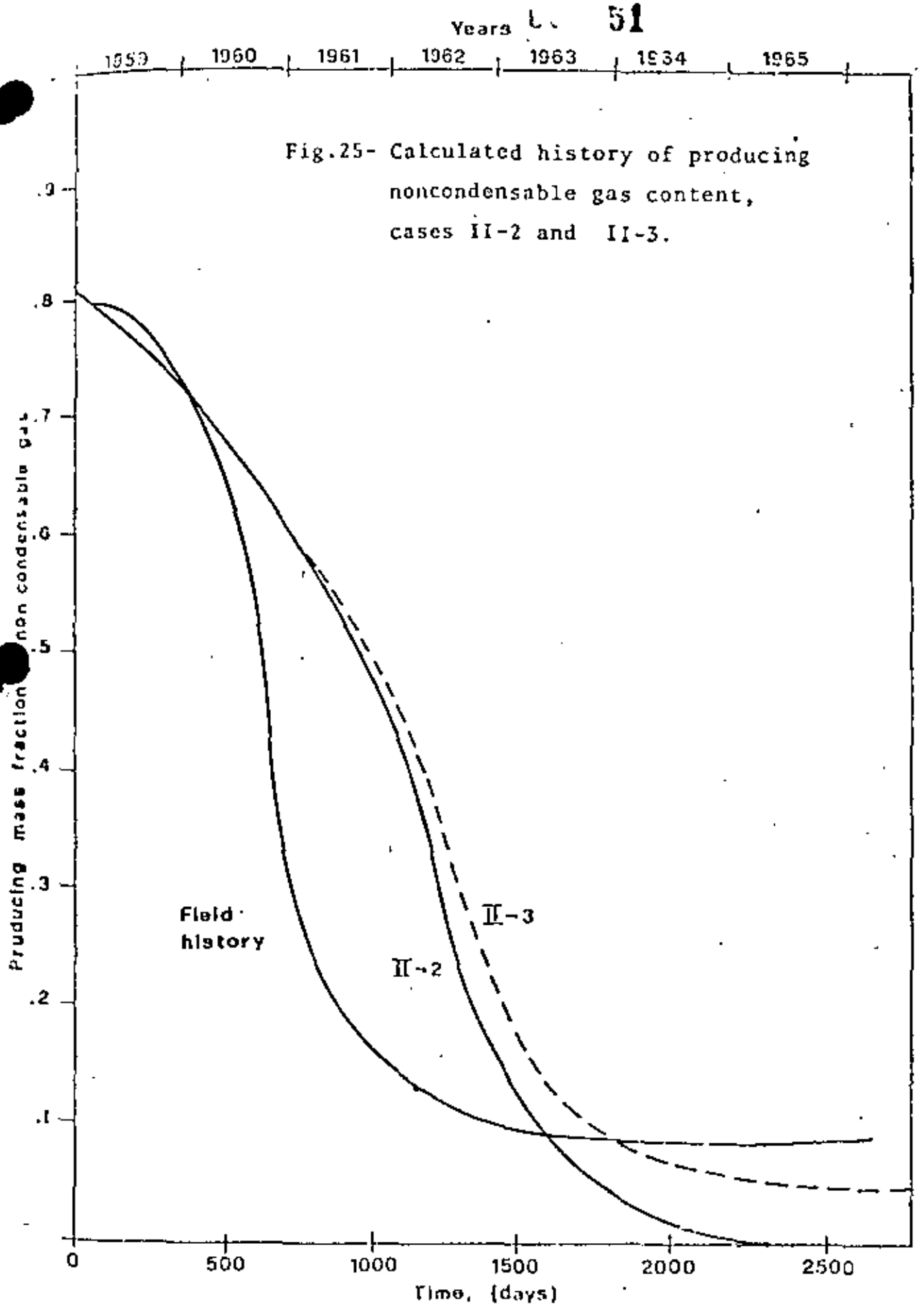

Fig.25- Calculated history of producing noncondensable gas content, cases II-2 and II-3.

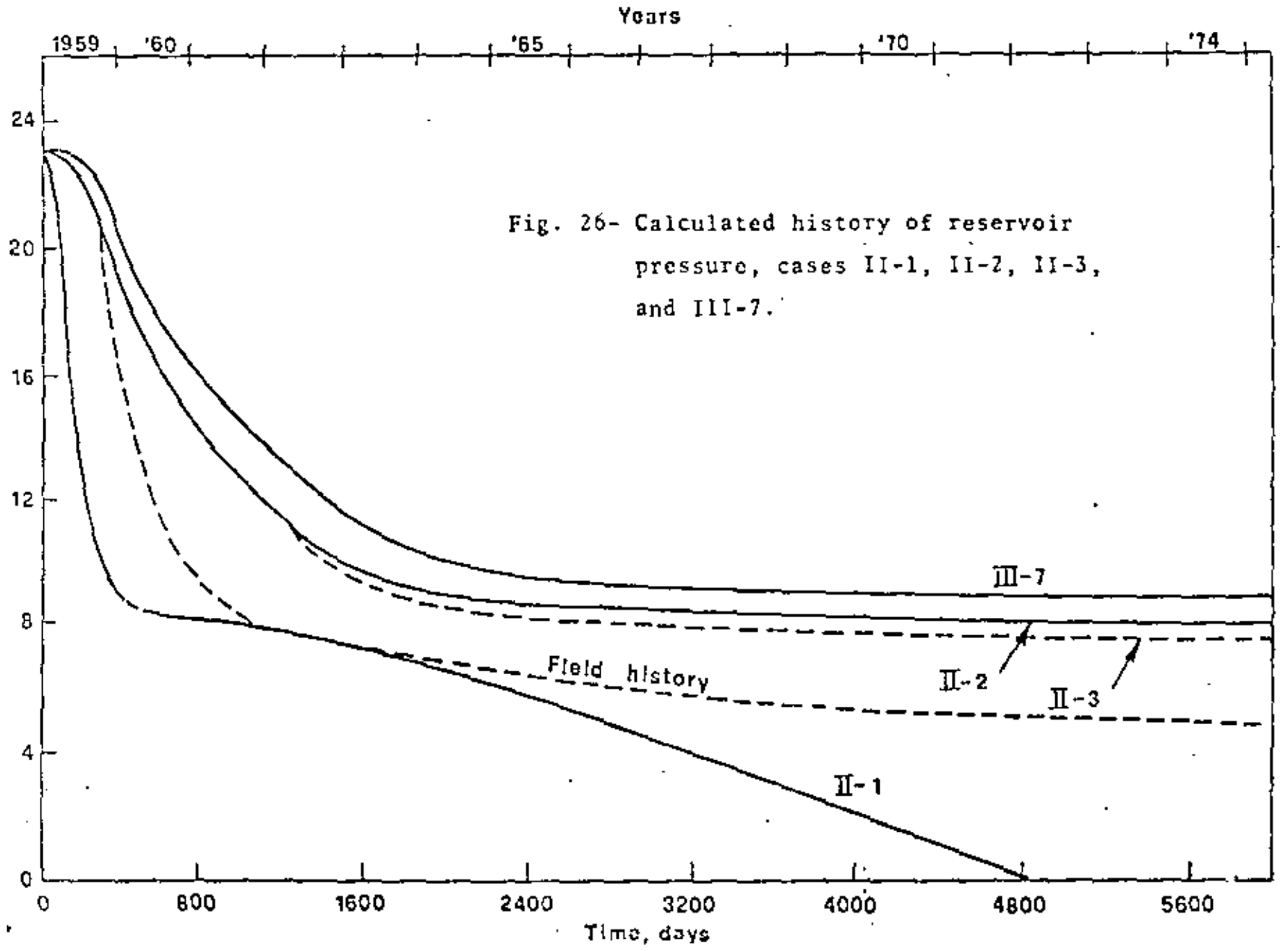

Fig. 26- Calculated history of reservoir pressure, cases II-1, II-2, II-3, and III-7.

CURSO: INGENIERIA DE RESERVORIOS GEOTERMICOS.

OLADE.
C.F.E.
I.I.E.
DECFI.

PRUEBAS DE PRESION.

INSTRUCTOR: DR. FERNANDO SAMANIEGO V.

SEPTIEMBRE, 1981.

SPE

SPE 7480

WELL TESTING IN TWO-PHASE GEOTHERMAL WELLS

by Alain C. Gringarten, Member SPE-AIME, B.R.G.M.

This paper was presented at the 53rd Annual Fall Technical Conference and Exhibition of the Society of Petroleum Engineers of AIME, held in Houston, Texas, Oct. 1-3, 1978. The material is subject to correction by the author. Permission to copy is restricted to an abstract of not more than 300 words. Write: 6200 N. Central Expy., Dallas, Texas 75206.

ABSTRACT

This paper deals with the possibility of using usual oil well transient pressure testing methods in hot water wells when flashing occurs in the wellbore. Multiple rate analysis techniques have been successfully applied to available data on a well drilled by B.R.G.M. in the former French Territory of Afars and Issas. Practical recommendations concerning such tests are also included.

INTRODUCTION

Well established pressure transient analysis techniques are routinely used in oil and gas wells for the determination of reservoir parameters[1,2]. In recent years, improvements in these techniques have allowed a better understanding of complex reservoir and well behavior, as in the presence of skin, wellbore storage[3], or fractures[4].

Only recently have these methods been applied to geothermal systems. For a number of years, geothermal well testing was based on empirical methods[5], that, although useful for estimating geothermal field production potential, gave limited knowledge on the reservoir itself.

Pressure transient techniques have been applied successfully in vapor dominated geothermal reservoirs[6,7]. It was found that gas well analysis methods apply to steam wells and that wellhead measurements were generally adequate for analysis, thus eliminating the need for downhole instrumentation.

In water dominated systems, on the contrary, transient well testing can be far more complex, depending upon whether two-phase flow develops with flashing in the wellbore or in the formation. Usual oil well methods have already been shown to apply when no flashing develops[8]. On the other hand, they apparently cannot be used when flashing occurs in the formation[9]. Very little information was available until recently on the case of hot water wells in which flashing occurs at some depth in the wellbore. This is mainly due to the difficulty of bottom hole data gathering, that often results in mechanical damage of the measuring devices because of the high temperatures involved, and of the high production rates of boiling geothermal fluids.

A two rate flow test, conducted on one well in the Cerro Prieto field was recently presented by Rivera and Ramey[10]. The data were satisfactorily interpreted by means of models suggested by Russel[11], Selim[12], and Odeh and Jones[13,14].

To the author's knowledge, no other example of transient test in a two-phase well has been published in the literature. Unpublished data, however, were available from a well drilled in 1975 by B.R.G.M. in the French Territory of Afars and Issas (now Republic of Djibouti).

Analysis of these data, which include pressure build-up as well as two rate flow tests is presented hereafter.

ASAL WELL

The Asal rift, located 80 km west of Djibouti, is one of the active "rifts-in rift" structures of the Afar depression, a transition between the Gulf of Aden and the Red Sea ridges.

Attention was drawn to this zone because of the presence of a graben structure, and of geochemical particularities of various hot springs. Two wells were drilled on the S-W margin of the rift, at locations chosen mainly from geological considerations. The first hole (Asal 1) reached a hot water geothermal reservoir, the second, one kilometer away, was dry.

Both wells found, from top to bottom, a recent basaltic series, then a thick rhyolitic volcanic series, and finally an old tectonic, tilted, basaltic series, where the reservoir is located. The first well was drilled to a depth of 1330 m, where heavy mud losses occured, while the second well reached 1550 m. An important normal fault appears to separate the two wells.

A schematic of Asal 1 wellhead is presented in figure 1. The well could be produced either vertically through a 6" tube, or horizontally

References and illustrations at end of paper.

through a calibrated pipe. Four sizes were available (namely, 6", 4", 2" and 1") which were used to control the well flow rate. In addition, a 2" stainless steel tubing was lowered into the wellbore to a depth of 650 m, for wireline temperature and pressure measurements with bourdon-tube type gauges. As the well could not initially start by itself, the same tubing was used for inducing it into production by air lift. The initial water level in the well was at an approximate depth of 200 m below the well head.

The flow rate history of ASAL 1 well is presented on figure 2. After completion, the well was produced through a 6" outlet for 6 days in preparation for a build-up test for obtaining reservoir parameters (flow period # 1). Mechanical problems, however, were encountered with the stuffing box on the lubricator attached to the 2" stainless steel tubing, and these required the closing of the well for about 9 hours in order to retrieve the measuring devices (flow period # 2). During this unplanned pressure build-up, temperature and pressure could only be measured at the wellhead and are shown on figure 3.

It can be noticed on figure 3 that the wellhead temperature drops suddenly after 400 minutes. This apparently corresponds to steam condensation in the wellbore and defines the time limit after which the well has to be induced into production.

The well was again started by air-lift and flown through the 6" outlet for approximately 4 days (flow period # 3) before being shut-in for 20 hrs (flow period # 4). In order to obtain the well characteristic curve relating wellhead pressure and mass-flow rate, the well was again started by air-lift, flown for 43 hours with a 4" outlet (flow period # 5), shut-in for 3 hours (flow period # 6), and open again with the 6" outlet. Because of the short 4" pressure build-up duration, the well was able to start by itself. After about 3 hours of 6" production (flow period # 7), the 6" outlet was changed into a 2" outlet; the well was then produced for 3 days (flow period # 8), shut-in for 7 hours (flow period # 9), open again with the 6" outlet (flow period # 10) which was changed into a 1" outlet after 3 hours (flow period # 11). During this final test, there was evidence that the flow could not be sustained, and no build-up was attempted.

Although the primary objective of these last tests was to obtain the well characteristic curve, bottomhole measurements were taken throughout the duration of most individual flow period, in order to check the results of the second 6" build-up test. Temperature and pressure measurements were also performed at various depths in the wellbore, and are shown on figures 4 and 5, respectively. They indicate a reservoir temperature of 253°C, and show the presence of a flashing front at approximately 870 m with the 6" outlet, 850 m with the 4" outlet and 700 m with the 2" outlet.

TYPE - CURVE ANALYSIS

Asal 1 bottomhole pressure data that were available for flow periods 4, 6, 7, 8, 9, 10 and 11 are shown on the log-log plot of figure 6. For each individual flow period, the difference between the bottomhole pressure during the test and that at the beginning of the test is plotted versus the time since the beginning of that test.

Although no unique quantitative estimate of the reservoir parameters can be deduced from figure 6, important quantitative information can be obtained.

By comparing the log-log plot of figure 6 with the skin and storage type curves published in ref. 3, it becomes apparent that none of the flowing tests had been run long enough for the radial flow logarithmic approximation to apply. On the other hand, that approximation does apply to the 2" flowing test, which had a much longer duration, and to the various build-up tests.

The comparison also suggests that the early time behavior of the well is of the changing wellbore storage type, going from liquid level controlled storage to compressibility controlled storage, when flashing or condensation occurs.

Figure 6 further indicates that the radial flow logarithmic approximation applies sooner for build-up than for drawdown tests. This is somewhat opposite to what is generally observed in single phase wells, and may be due to the two-phase nature of the flow.

Another comment regarding figure 6 is that, although a dry well had been drilled one kilometer away from ASAL 1, no impermeable boundary is apparent on the log-log plot.

Figure 6 was also used to estimate the mass flow rates under reservoir conditions during the various flow periods.

As no separator was available, these were first deduced from James' lip pressure method[2] : James observed that, as a fairly large flow of steam or steam-water mixture was expanded along a pipe to the atmosphere, the pressure at the extreme end (lip) of the pipe was greater than the atmospheric pressure, and proportional to the mass flowing, and the enthalpy, as in the following formula :

$$\frac{G\,E^{1.102}}{P_L^{0.96}} = 11\,400. \qquad (1)$$

where G is the mass velocity (in lb/sq ft.sec), E is the stagnation enthalpy (in Btu/lb, at reservoir conditions), and P_L the critical lip pressure (in psi absolute).

James's formula was transformed for the present study into a more convenient system of units to yield :

$$w = 692.35\, P_L^{0.96}\, E^{-1.102}\, d^2 \qquad (2)$$

where w is expressed in tons/hr*, P_L in bars*, and d in inches.

Data for mass flow rate calculations are summarized in Table 1. The enthalpy value used in Eq. 1 was that for pure water, although the geothermal fluid salinity was of the order of 200,000 ppm. Enthalpy values for highly saline brines are not readily available in the literature.

As indicated in Table 1, the lip pressure was uniquely defined only with the 6" outlet, corresponding to a rate of approximately 83 t/hr. With the 4" and 2" outlets, on the contrary, the

* Metric units are used throughout this paper : 1 ton = 10^3 kg; 1 bar = 10^5 Pa

lip pressure was oscillating between two extreme values, because of the slug nature of the flow, and only a range of rate values could be obtained by applying Jones' formula (71 - 83 t/hr and 40 - 54 t/hr, respectively). According to Jones[16], such pulsations could have been eliminated by using a glycerine-damped pressure gauge with a needle valve. By throttling the valve, the lip pressure stabilizes at the correct value, between the two extreme ones.

However, by comparing the relative position of the different curves on figure 6, it appears that the rates with the 4" and 2" outlets were more likely 71 and 23 t/hr, respectively. In the same way, the rate with the 1" outlet seems to be equal to 11 t/hr.

MULTIPLE RATE ANALYSIS

Quantitative analysis of Asal I bottomhole pressure data was performed with a variable drawdown model, similar to that proposed by Odeh and Jones[13]. The well was considered as having been produced at different flow rates, $q_1, q_2, \ldots q_n$. Assuming the radial flow logarithmic approximation valid for each one of the flow periods, the bottomhole well pressure during the n^{th} test is equal to :

$$P_{wf_n} = P_i - \frac{q_n \nu}{4\pi kh} \left\{ \sum_{j=1}^{n} \frac{q_j - q_{j-1}}{q_n} \ln (t_n - t_{j-1}) \right.$$

$$\left. + \ln \frac{k}{\phi \mu c r_w^2} + 0.80907 + 2S \right\} \qquad (3)$$

in Darcy units.

With geothermal metric units, Eq. (3) becomes :

$$P_{wf_n} =$$

$$- 0.228 \frac{w\nu}{kh} \sum_{j=1}^{n} (w_j - w_{j-1}) \ln 60 (t_n - t_{j-1})$$

$$+ P_i - 0.228 \frac{w_n \nu}{kh} (\ln \frac{k}{\phi \mu c r_w^2} - 8.434 + 2S) \qquad (4)$$

In Eq.(4), k is expressed in darcy, t in minutes, and r_w in meters.

Therefore, by graphing P_{wf} versus $\sum (w_j - w_{j-1}) \ln 60 (t_n - t_{j-1})$ in cartesian coordinates, one should obtain a straight line, the slope of which is equal to :

$$m = - 0.228 \frac{w\nu}{kh} \qquad (5)$$

This slope is independant of the flow rate. The intercept of the straight line can be used to calculate the skin, if p_i and ϕ are known. In the case of a build-up test ($w_n = 0$), the intercept is equal to the initial pressure p_i.

Build-up test analysis

A plot of P_{wf} during the second 6" build-up test (flow period # 4), versus the multiple rate function, (expressed in tons/hr), is shown on figure 7.

A straight line of slope $m = 3.6\ 10^{-3}$ is clearly evident on figure 7. Substituting $m = 3.6\ 10^{-3}$ into Eq. (5) and taking $w = 1.25\ 10^{-3}$ m /s/g and $\mu = 0,2$ cp yields :

$$kh = 15,9 \text{ Dm.}$$

($\mu = 0,2$ cp was obtained by extrapolating published viscosity curves[1] to a temperature of 253°C and a salinity of 200,000 ppm).

The calculated initial pressure is 76,6 bars, which compares reasonably well with the value of 77,4 bars measured before the test.

It can be observed in figure 7 that data points for build-up times greater than 6 hours deviate from the straight line. This is a consequence of the condensation effect already noticed on figure 3 during the first 6" build-up (flow period # 2).

The early time deviation (for build-up times less than 20 minutes) is caused by wellbore storage effects.

In the same way, analysis of the 4" build-up test (flow period # 6) yields a kh value of 15,0 Dm and a p_i value of 76,4 bars (figure 8).

kh and p_i from the 2" build-up (flow period # 9) are equal to 16,8 Dm and 77,2 bars, respectively (figure 9).

Flowing test analysis

A plot of p_{wf} versus the multiple rate function for the two 6" flowing tests (flow periods # 7 and 10) is shown on figure 10. The slope for the first one (# 7) is equal to $7,2\ 10^{-3}$, which yields kh = 8 Dm, while that for the second one (# 10) is equal to $10,2\ 10^{-3}$ (kh = 5,6 Dm). As expected from figure 6, these kh values are much lower than those obtained before, and are not correct. On the other hand, the analysis shown on figure 11 of the 2" flowing test (flow period # 0) yields a slope equal to $3,5\ 10^{-3}$, corresponding to kh = 16,3 Dm, which is consistent with the results of the build-up test analyses.

The sudden increase in bottom hole pressure indicated on figure 11 is likely to be caused by a decrease in the flow rate. The same phenomena appears on figure 12, in the analysis of the 1" flowing test (flow period # 11), during which the well was not able to sustain the flow : the last recorded pressure is roughly equal to the initial pressure. All the other pressure points fall on a straight line, whose slope is equal to $3,2\ 10^{-3}$. The corresponding kh is equal to 17,8 Dm, which agrees well with the build-up tests results.

SKIN EVALUATION

It is not possible to obtain the skin factor directly from the multiple rate analysis plot, because of insufficient reservoir information. The skin factor, however, can be evaluated from a type curve match, with a dimensionless pressure given by :

$$P_D = \frac{kh}{0.228} \frac{\Delta P}{w_{n-1} \nu} - \frac{\Delta P}{2 w_{n-1} m} \qquad (6)$$

for a build-up test, or

$$P_D = \frac{kh}{0.228} \frac{\Delta P}{(w_n - w_{n-1}) \nu} - \frac{\Delta P}{2(w_n - w_{n-1}) m} \qquad (7)$$

for a flowing test.

The type curve match is shown on figure 13, and indicates a skin approximately equal to 25. This high skin value is probably due to rocks plugging the bottom of the hole : although the well was drilled to 1190 m, the pressure gauge could only be lowered to a depth of approximately 1050 m. This would also explain why, although the formation is known to be fractured, no fracture controlled flow period is apparent on the log-log plot of figure 6.

CONCLUSIONS

The following conclusions can be reached from the present study:

A) Two phase geothermal well testing can be carried out with standard bourdon-tube type instruments for extended periods of time at temperatures as high as 253°C and salt content of the order of 200,000 ppm.

B) Usual multiple rate techniques can be used in two phase geothermal wells for obtaining reservoir characteristics from bottom hole transient pressure data. Type curve matching also provides useful qualitative and quantitative reservoir information.

C) Early time bottom hole pressure appear to be wellbore storage controlled. There are indications that wellbore storage changes from liquid level type to compressibility type, as a consequence of water flashing or steam condensing in the wellbore. These wellbore storage effects appear to last longer in drawdown and double-rate tests than in build-up tests (200 mn compared to 20 mn for the well Asal 1 studied in this paper). This has to be taken into account when planning such tests.

D) When the well is not artesian, there is no practical avantage of running long build-up tests, because of the effects of steam condensation in the wellbore (6 hours was the practical limit in the case of well Asal 1).

NOMENCLATURE

c	=	total fluid compressibility, bar^{-1}
E	=	enthalpy, kcal/kg
h	=	formation net thickness, m
k	=	permeability , darcy
m	=	slope of straight line
n	=	constant rate intervals
p	=	pressure, bar
q	=	volumetric flow rate, m^3/hr
r_w	=	wellbore radius, m
S	=	skin factor
t	=	producing time, min
w	=	mass flow rate, t/hr
u	=	viscosity, cp
v	=	specific volume, m^3/kg
ϕ	=	porosity, fraction

Subscripts

i	=	initial condition
j	=	constant rate interval
w	=	wellbore or water
wf	=	flowing conditions at well bottom

ACKNOWLEDGEMENT

The work reported in this study was supported in part by the Commission of the European Communities (Contract 081-76 EGF, Geothermal Energy Program). The author is grateful to the Commission of the European Communities and to the management of the Bureau de Recherches Géologiques et Minières for permission to publish this paper.

REFERENCES

1. Matthews, C.S., and Russell, D.G. : "Pressure build-up and flow tests in wells" Monograph series, Society of Petroleum Engineers of AIME, Dallas,(1967), Volume 1.

2. Earlougher, R.C. : "Advances in well test analysis" Monograph series, Society of Petroleum Engineers of AIME, Dallas, (1977), Volume 5.

3. Agarwal, R.G., Al-Hussainy, R. and Ramey, H.J., Jr: "An investigation of wellbore storage and skin in transient liquid flow - I: analytic treatment", Soc. of Pet. Eng. J, Sept. 1970, 279.

4. Gringarten, A.C., Ramey, H.J., Jr and Rag avan: "Applied pressure analysis for fractured wells" Pet. Tech., July 1975, 887.

5. James, R. : "Factors controlling borehole performance"U.N. Symposium on the Development and Utilization of Geothermal Resources, Pisa Proceedings (Geothermics, Spec.Iss.2) V.2 pt.2 p 1502.

6. Ramey, H.J., Jr and Gringarten A.C. : "Effect of high volume vertical fractures on geothermal steam well behavior", Proceedings, 2nd U.N. Symposium on the Development and use of geothermal resources, San Francisco , California (USA), May 20-29, 1975, V.3, p. 1759.

7. Barelli, A., Manetti, G., Celati, R. and Neri, G. : "Build-up and back-pressure tests on italian geothermal wells", Proceedings, 2nd U.N. Symposium on the Development and use of geothermal resources, San Francisco, California (USA), May 20-29, 1977, V.3, p.1537.

8. Witherspoon, P.A., Narasimhan, T.N. and Mc Edwards, D.G. : "Results of interference tests from two grothermal reservoirs", SPE paper 6052 51st Annual Fall Meeting, New Orleans, Oct.3-6, 1976.

9. Gulati, M.S. : "Pressure and temperature build-up in geothermal wells" Proceedings, Stanford geothermal workshop, Stanford University, Dec. 15-17, 1975.

10. Rivera, J.R. and Ramey, H.J., Jr : "Application of two-rate flow tests to the determination of geothermal reservoir parameters", SPE paper 6867, 52nd Annual Fall Meeting of SPE, Denver, Oct. 9-12, 1977.

11. Russell, D.G. : "Determination of formation characteristics by two-rate flow tests", J. Pet. Tech., Dec. 1962, 1349.

12. Odeh, A.S. and Jones, L.G. : "Two-rate flow test, variable rate case", J. Pet. Tech., Janv. 1974, 93.

13. Selim, M.A. : "A modification of the two-rate flow method for determination of reservoir parameters", J. Institute of Petroleum, V. 53, N° 527, Nov. 1967, 343.

14. Odeh, A.S. and Jones, L.G. : "Pressure drawdown analysis, variable rate case", J. Pet. Tech., Aug. 1965, 960.

15. James, R. : "Alternative methods of determining enthalpy and mass flow" Proceedings, U.N. Conference on new sources of energy, Rome, 1961.

16. James, R. : "Private communication" Orléans (France), Nov. 1977.

TABLE I

MASS FLOW RATE MEASUREMENTS

OUTLET DIAMETER (inch)	LIP PRESSURE (bar)	ABSOLUTE LIP PRESSURE (bar)	CALCULATED MASS FLOW RATE t/hr (from JAMES' formula)	ESTIMATED MASS FLOW RATE t/hr
6"	0.5	1.5	83	83
4"	2-2.5	3-3.5	71 - 83	71
2"	6-8.5	7.9.5	40 - 54	23
1"	not available			11

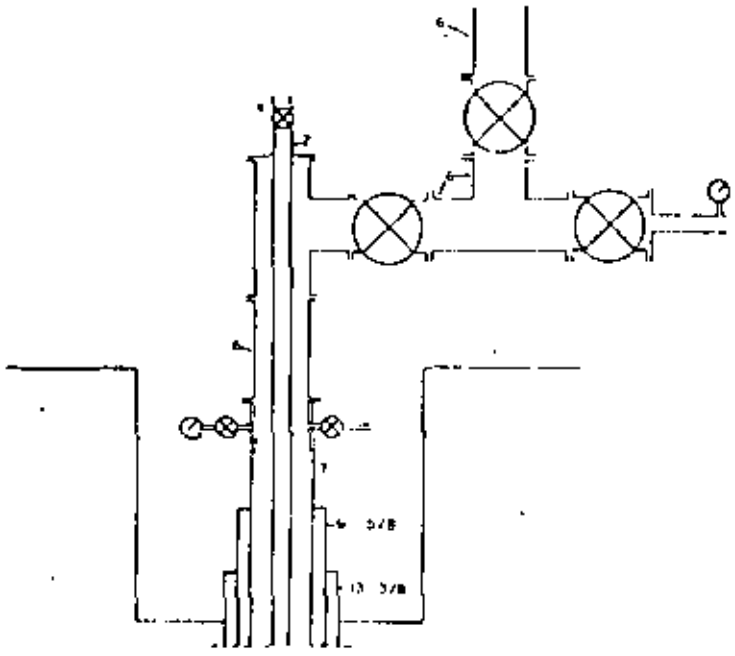

Fig. 1 - Schematic of ASAL 1 well.

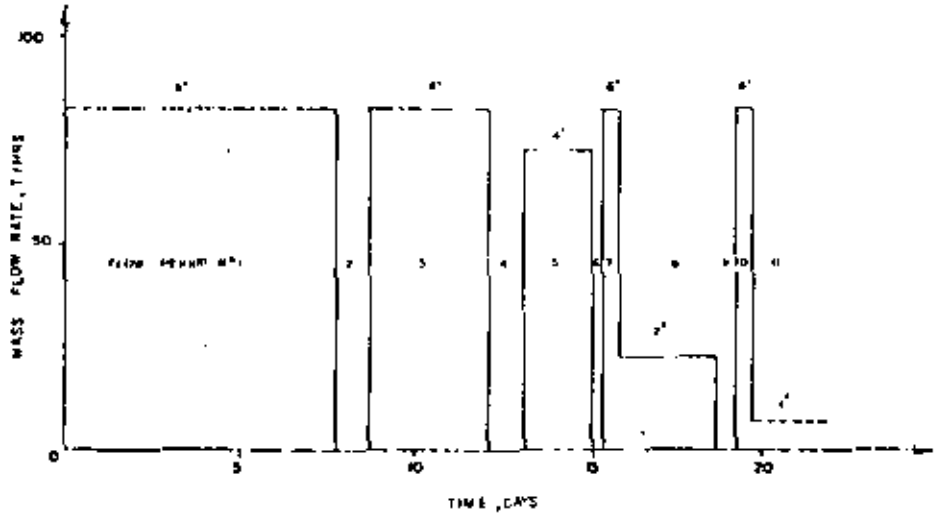

Fig. 2 - Mass flow rate changes during ASAL 1 tests.

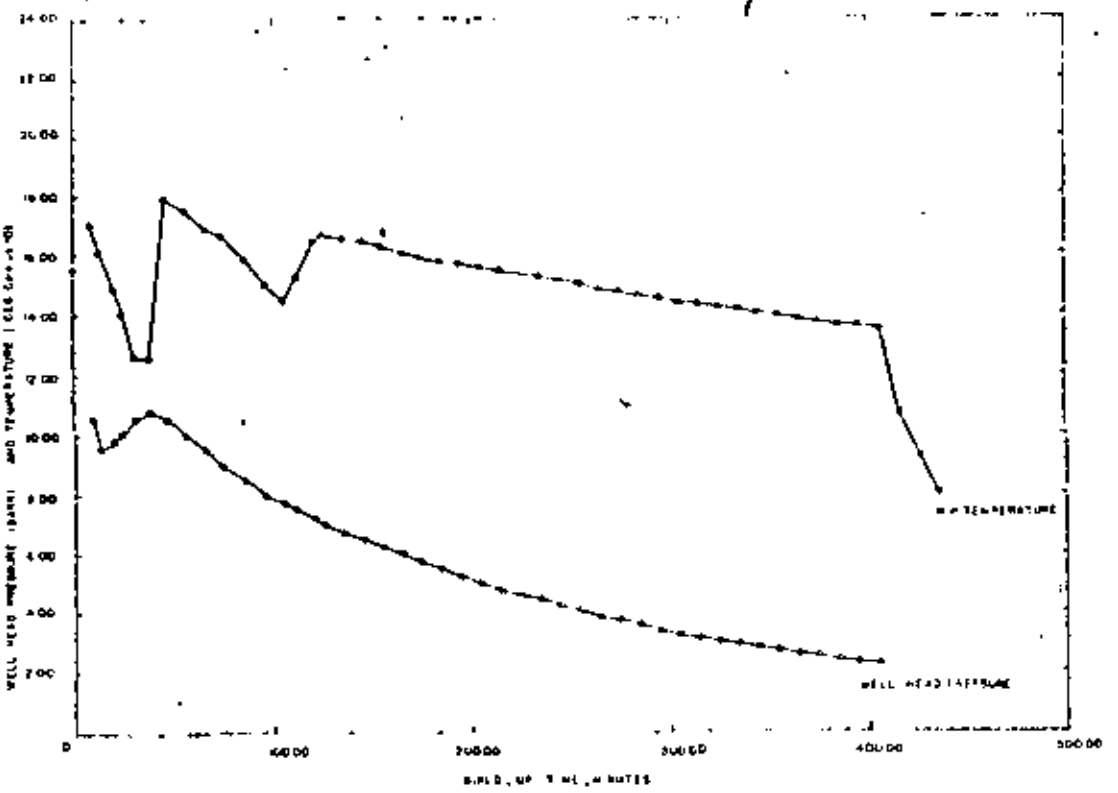

Fig. 3 - ASAL 1 pressure build-up test (6" outlet, flow period #2).

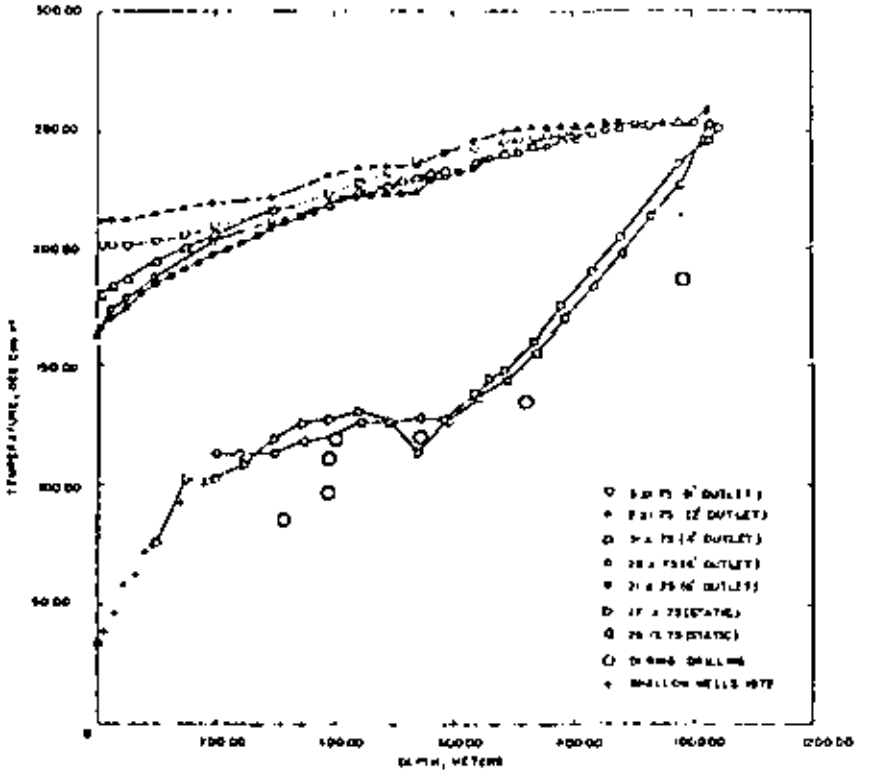

Fig. 4 - Temperature profiles in well ASAL 1.

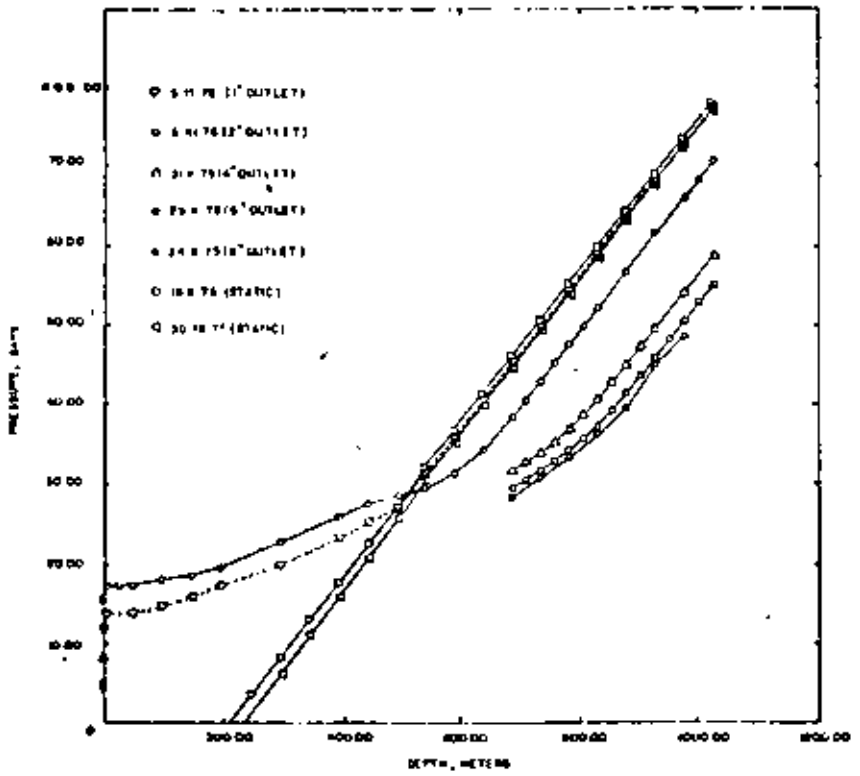

Fig. 5 - Pressure profiles in well ASAL 1.

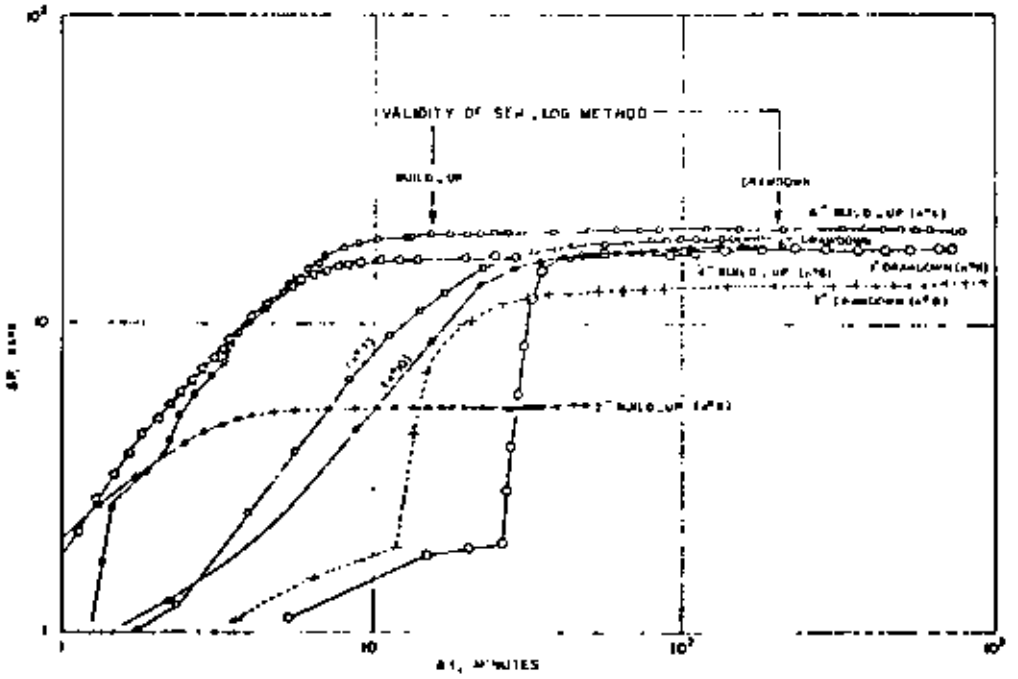

Fig. 6 - ASAL 1 pressure tests.

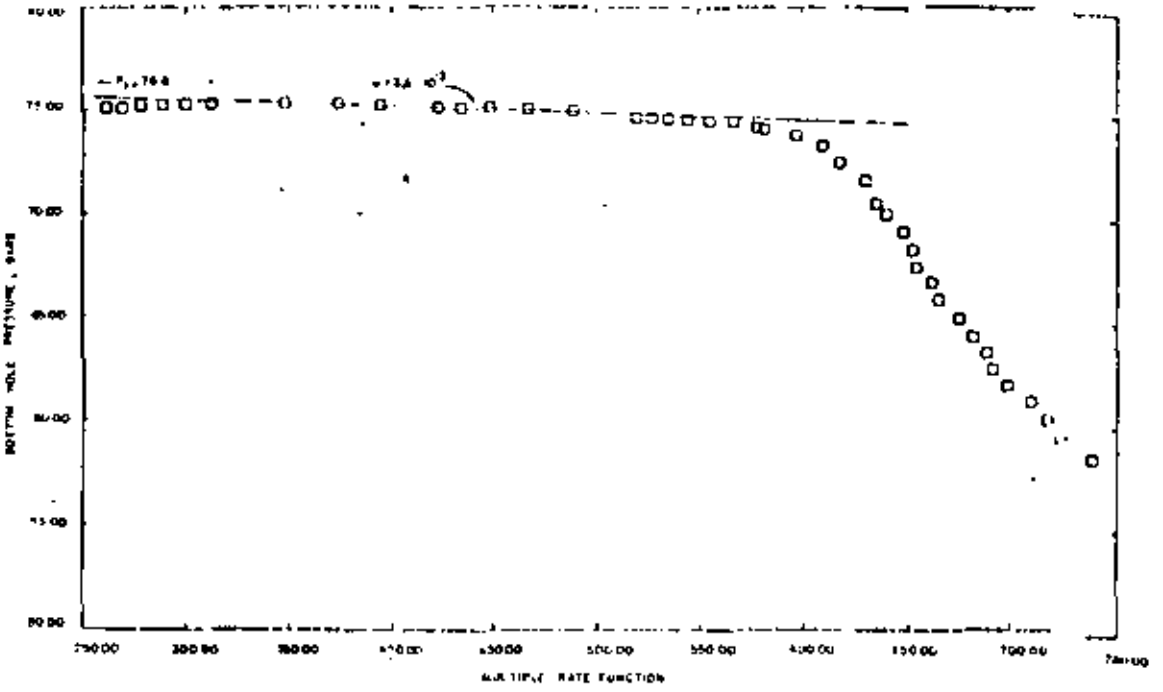

Fig. 7 - ASAL 1 pressure build-up test (6" outlet, flow period #4).

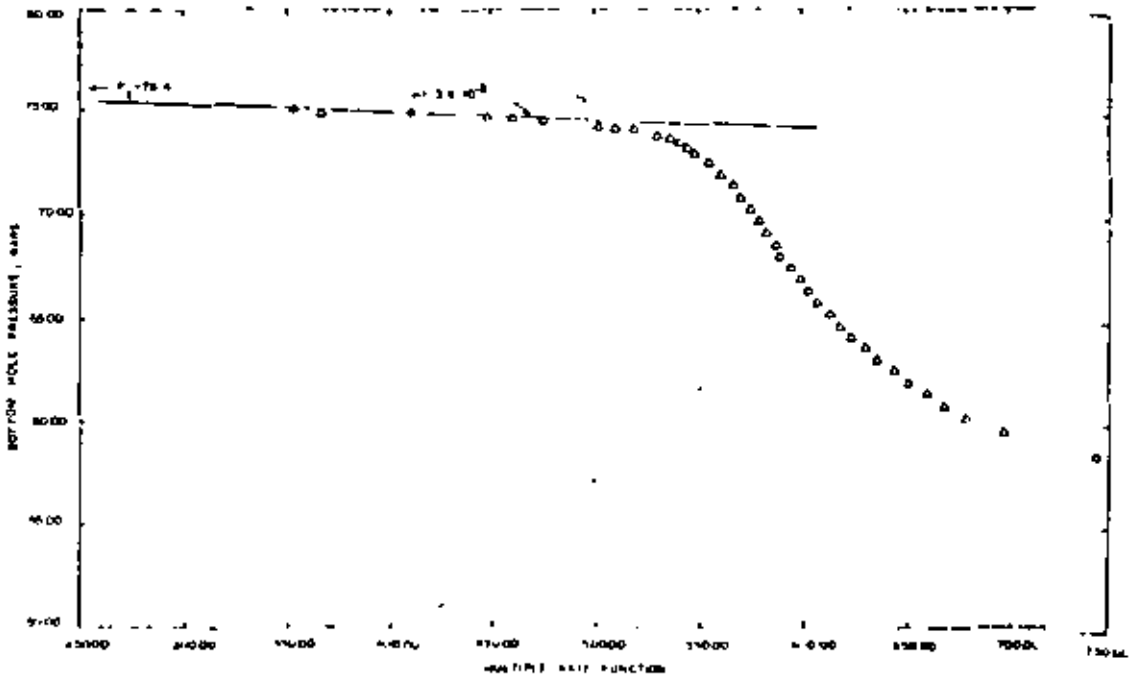

Fig. 8 - ASAL 1 pressure build-up test (4" outlet, flow period #6).

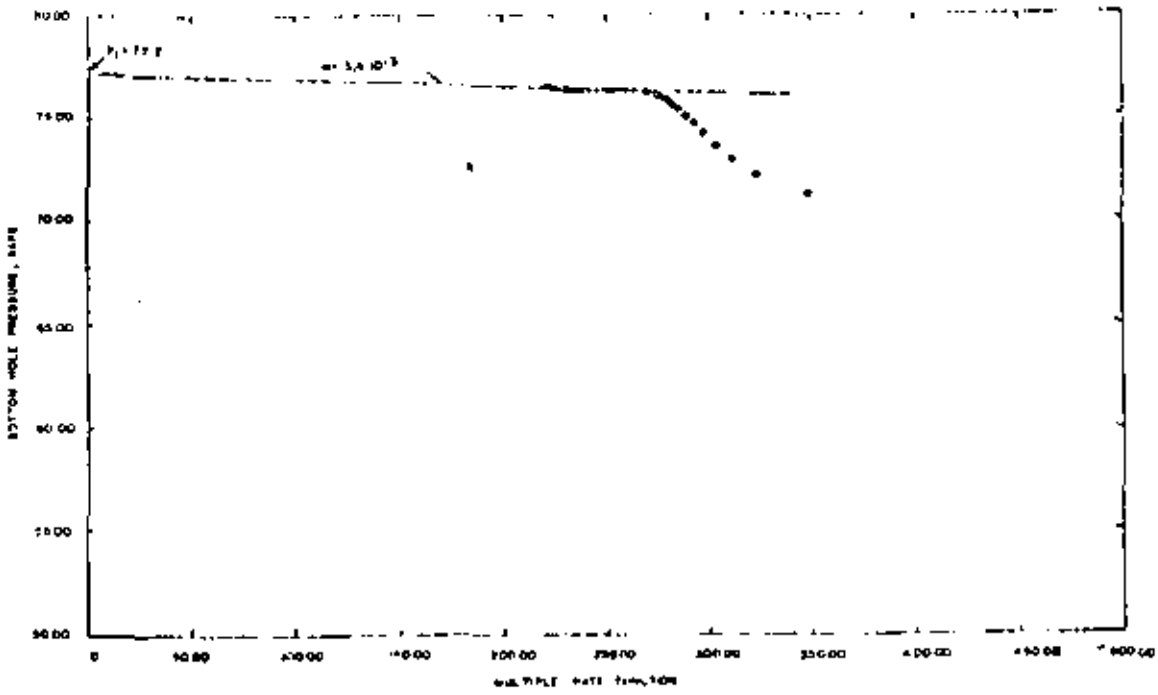

Fig. 9 - ASAL 1 pressure build-up test (2" outlet, flow period #9).

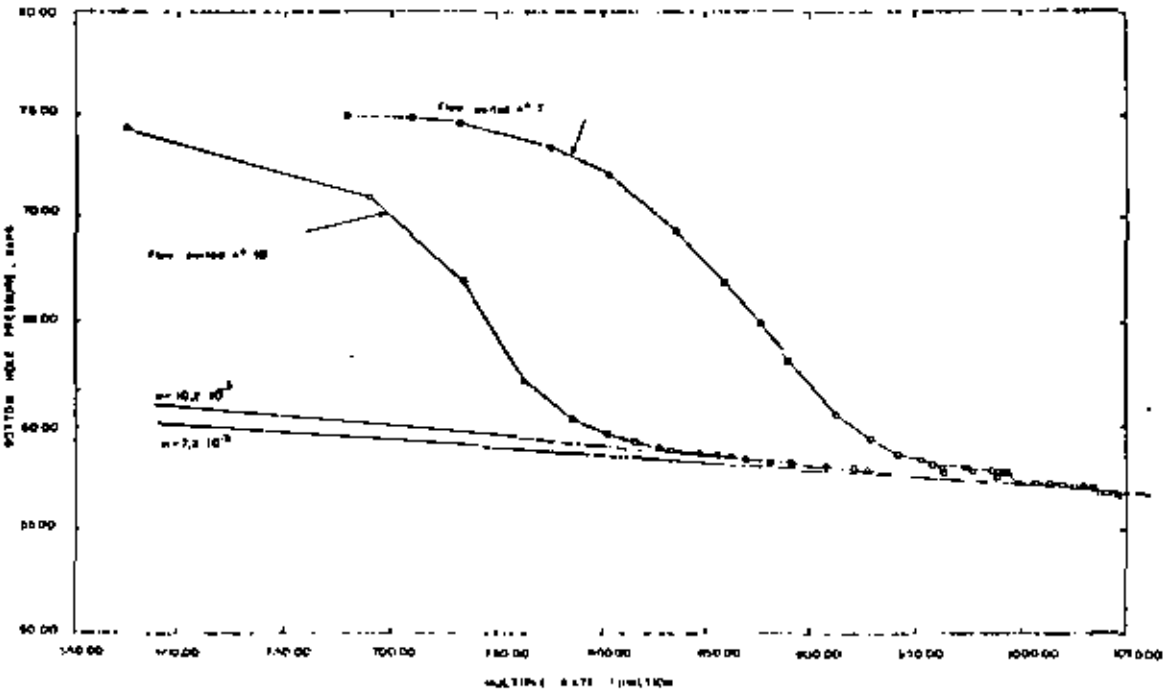

Fig. 10 - ASAL 1 pressure flowing tests (6" outlet, flow perids #7 and 10).

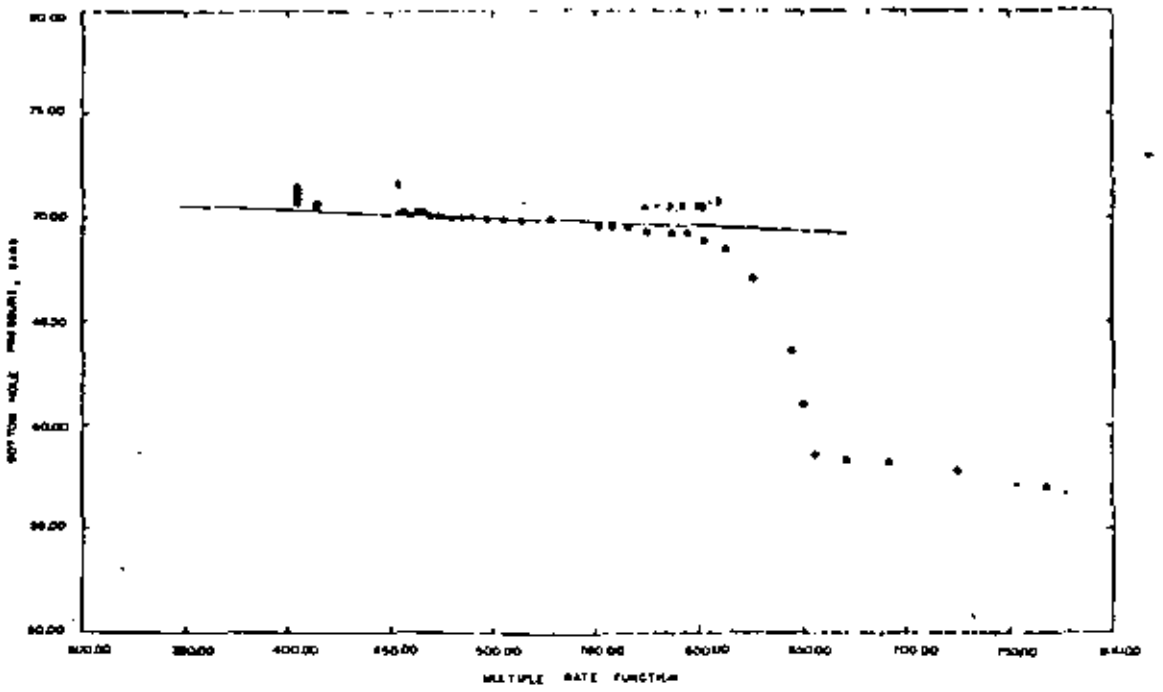

Fig. 11 - ASAL 1 pressure flowing test (2" outlet, flow period #8).

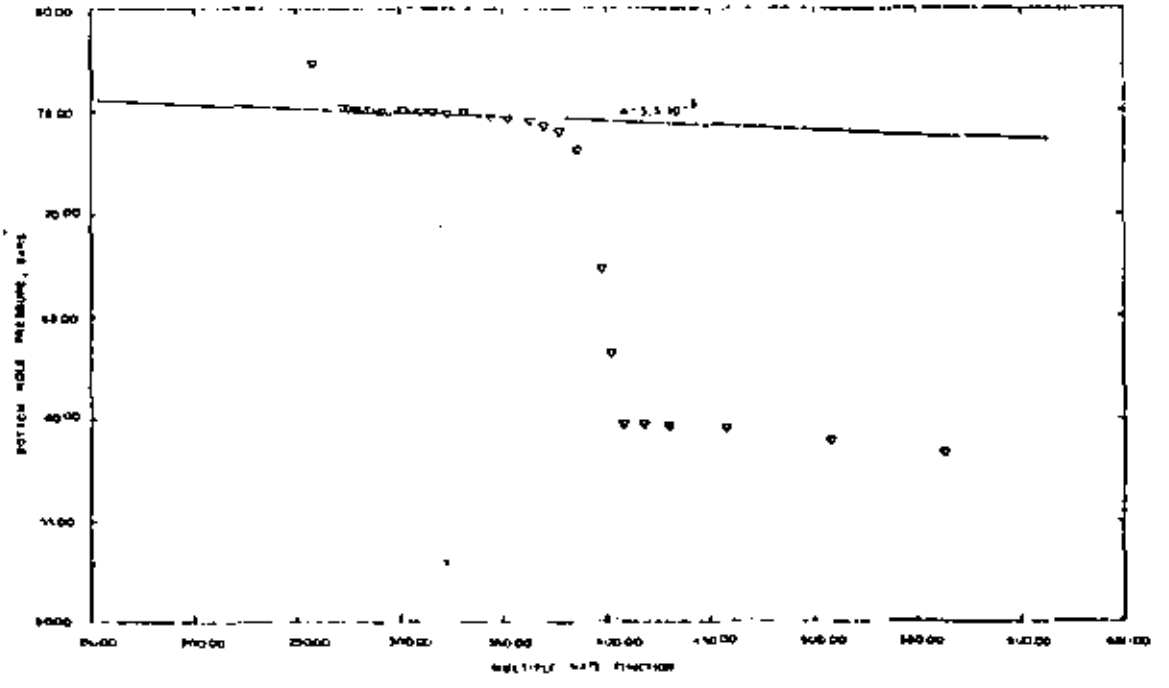

Fig. 12 - ASAL 1 pressure flowing test (1" outlet, flow period #11).

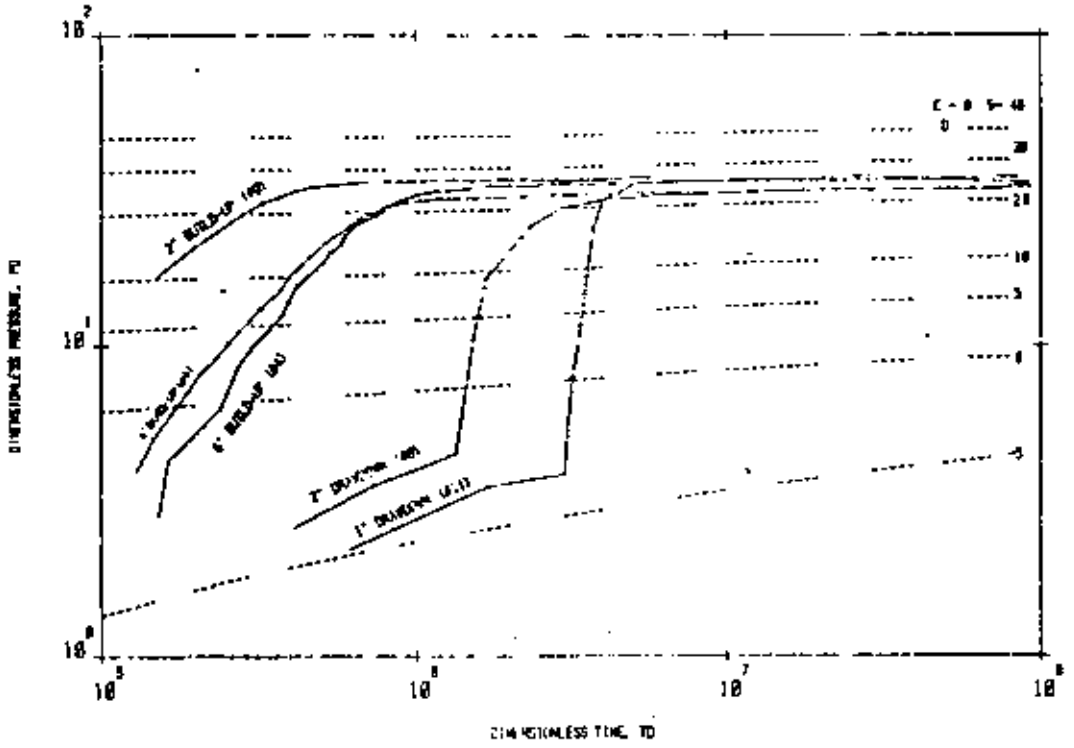

Fig. 13 - Type curve matching with skin and storage type curves (ref.3).

Wellbore Storage Effects in Geothermal Wells

Constance W. Miller, Lawrence Berkeley Laboratory

Abstract

The early-time response in the well testing of a homogeneous reservoir customarily is expected to give a unit slope when the logarithm of pressure is plotted vs. the logarithm of time. It is shown that this response is a special case and that another nondimensional parameter must be defined to describe the set of curves that could take place for each value of the wellbore storage coefficient C_D. In addition, the effect of temperature changes along the bore is shown to increase the time when wellbore storage is important.

Introduction

The petroleum industry's technique of assessing oil and gas reservoirs by well testing has been extended to the geothermal field by a number of workers.[1-3] However, at least two important differences between a geothermal field and an oil or gas field must be considered in analyzing geothermal well test data. First, the kh/μ value of a geothermal field is usually much larger than that of an oil or gas field because the reservoir thickness h is greater in a geothermal field and the viscosity μ is smaller (k is the permeability). Second, heat loss in the wellbore, which can be ignored in oil and gas fields, is significant in geothermal bores.

The concept of wellbore storage – which has been considered quite extensively[4,5] and refined in such detailed studies as those of Agarwal *et al.*,[6] Wattenberger and Ramey,[7] and Ramey[8] – usually is treated as a boundary condition on the reservoir flow. The boundary condition used is

$$q_{sf} = q_s + C\frac{dp_w}{dt}, \quad \ldots\ldots\ldots\ldots\ldots\ldots\ldots\ldots (1)$$

where dp_w/dt is the flowing pressure change with time in the wellbore. However, dp_w/dt is not necessarily independent of position in the well. When dp_w/dt is dependent on the measurement point, a plot of $\log(p_{sf})$ vs. $\log(t)$ will not result in a unit slope at early times. This study will consider wellbore storage by looking at the flow in the well itself while treating the reservoir as simple homogeneous radial flow into the well.

Heat loss from the well and temperature changes along the bore also have been ignored because oil and gas fields can be treated as isothermal. Heat transfer from the well and heating of the fluid in the well is usually a very slow process. When very long times are considered, these temperature effects can become important. Once the early transient behavior is over and a semilog straight line of p_{sf} vs. $\log(t)$ is expected in the pseudosteady region, temperature changes in the well can alter the slope of that line so that the slope would no longer be $q\mu/4\pi kh$. The duration and importance of any temperature changes will be considered.

A numerical model of transient two-phase flow in the wellbore with heat and mass transfer has been developed. It is used to investigate (1) the early-time interaction of the well flow with that of the reservoir and (2) the longer-time effect of temperature changes on the well test data.

Concept of Wellbore Storage

Wellbore storage is the capacity of the well to absorb or supply any part of a mass flow rate change out of a well/reservoir system. For a change in flow rate at the surface of the well, the sandface mass flow rate usually is expressed as

$$w_{sf} = w_s + \rho c V\frac{dp_w}{dt}. \quad \ldots\ldots\ldots\ldots\ldots\ldots\ldots\ldots (2)$$

At time $t = 0^+$, when the surface mass flow rate is

0197-7520/80/0012-8203$00.25

increased, the change in the sandface rate is zero and the well is supplying all of the increase in flow rate. As the pressure in the well drops, the reservoir begins to supply part of the increased flow. The sandface rate steadily increases and approaches the surface flow rate as the well supplies less and less of the additional flow. The rate of increase in the sandface flow depends on the reservoir properties.

Because the change in w_{sf} is initially zero, it is assumed that the initial slope of the dp_w/dt curve gives the storativity of the well and that when p_w and t are plotted on a log-log scale, a unit slope will result. Such a plot is measured only, though, if p_w is some average pressure in the well, because $\rho cV(dp_w/dt)$ actually should be written as

$$\frac{1}{L}\int_0^L \rho cV\frac{dp_w}{dt}dx.$$

However, it would be difficult to determine an appropriate average pressure, and it is the downhole pressure that is used in the analysis of well test data. If the downhole pressure is measured, dp_{sf}/dt must be zero at $t=0^+$ because there is a finite time for changes made at wellhead to arrive downhole. If one plots the downhole pressure vs. time on a log-log scale, a unit slope is not necessarily seen. It is of interest to determine what should be measured downhole and if this early transient effect can be correlated with a nondimensional factor.

Eq. 2 can be nondimensionalized:

$$\frac{w_{sf}}{w_s}=1-C_D\frac{dp_D}{dt_D}, \quad \ldots\ldots\ldots\ldots\ldots\ldots\ldots\ldots (3)$$

where

$$p_D=2\pi(kh/\mu)(p_{sf}/w_s)r_w,$$

$$t_D=kt/\phi\mu c_R r_w^2,$$

and

$$C_D=\rho cV/\rho_{sf}2\pi\phi c_R hr_w^2.$$

The determination of ρcV for a two-phase or flashed system will be discussed. Also, the nondimensionalization was done using the sandface density explicitly instead of using a formation volume factor. Generally, p_D is plotted vs. t_D on a log-log scale for different wellbore storage factors C_D. However, as stated above, these plots are generated by assuming that the fluid in the well is mixed thoroughly, meaning that dp_w/dt is not a function of position in the well, even an isothermal well. Before one can assume that this uniformly mixed condition is valid, the wave nature of the original disturbance at wellhead must be damped out. When dp_w/dt is a function of position in the well, Eq. 2 and, therefore, Eq. 3 are not valid because of the question of what pressure should be used for p_w. Nevertheless, once the initial transient effects in the well have died out and dp_w/dt is no longer a function of position, Eqs. 2 and 3 should be valid for the isothermal case, provided one uses $\int_0^L \rho c(V/L)dx$ in the expression for C_D. The approach of the true behavior to that given by Eq. 3, however, can occur during or after the period when the unit slope is expected. Although Eq. 3 will not be valid as written at the very early times, it will be shown that the downhole pressure vs. time data can be correlated using another nondimensional parameter for the cases considered here—i.e., a single-phase reservoir, with the fluid single phase, two phase, or flashing in the bore. The expected drawdown curve will be described by the C_D factor as well as this additional parameter. The derivation of this parameter is made by neglecting the change in fluid head which occurs when the fluid is not isothermal. The calculation will show that the effect of the fluid head change is a longer-term effect, and neglecting it will not alter significantly the initial plot of p_{sf} vs. t.

To achieve a given surface mass flow rate, the pressure at wellhead must be decreased by Δp. This pressure drop, then, propagates down the well and interacts with the reservoir. If the reservoir can supply only a small percentage of the surface flow for that pressure drop Δp, the well will continue to supply most of the fluid until the well pressure has dropped further. Because the sandface flow rate is given by $2\pi r(kh/\mu)\rho\partial p/\partial r$ for a single-phase reservoir, the ability of the reservoir to deliver its fluid depends on the value of kh/μ. When kh/μ is relatively low, the nonuniformity of dp_w/dt in the well is damped out before the reservoir can supply any significant portion of the surface flow. Because w_{sf} is still negligible when dp_w/dt is no longer a function of position, a unit slope will be measured if p_{sf} is plotted vs. t on a log-log scale. This condition is true when an oil reservoir is tested. A typical kh value is 600 md-ft (1.8×10^{-13} m^3), and for a viscosity of 1 cp (1×10^{-3} Pa·s), kh/μ is about 600 md-ft/cp (1.8×10^{-10} m^3/Pa·s). However, there are cases when the reservoir can supply a significant portion of the surface flow rate before dp_w/dt is uniform in the well. In geothermal reservoirs, kh can be large [e.g., 30,000 to 90,000 md-ft (9×10^{-12} to 2.7×10^{-11} m^3)] and μ is low [0.1 cp at 572°F (1×10^{-4} Pa·s at 300°C)]. Because of the large value of kh/μ, the reservoir is capable of supplying a much greater quantity of fluid for the original pressure drop Δp. The initial sandface flow from the reservoir when the pressure pulse arrives downhole can even be equal to or greater than the desired sandface flow rate. The nondimensional parameter used to correlate the data is the ratio of the surface mass flow rate that results from the initial pressure drop made at wellhead to the reservoir flow rate that can be achieved for the same Δp. This parameter is written as

$$w_D=\frac{w_s}{(w_{sf})_i},$$

where $(w_{sf})_i$ is defined as the initial flow from the reservoir for the sudden drop in pressure Δp at the sandface. However, $(w_{sf})_i$ will be estimated, and it is this estimate that will be used in determining w_D. The initial flow from the well is just the surface flow rate because all the fluid is initially from the well.

One calculates the pressure drop Δp given this latter condition.

To derive w_D in terms of the fluid properties and reservoir conditions, several assumptions were made.

1. The velocity of the fluid from the reservoir is described by $(k/\mu)\partial p/\partial r$, so the reservoir is single phase. The ability of w_D to correlate the early-time data of a two-phase reservoir has not been done because of the difficulty of obtaining similarity solutions for two-phase flow in the reservoir itself.

2. The compressibility of the fluid in the well is not a strong function of position. A nonflashing two-phase flow is not necessarily ruled out here. However, the assumption does seem to preclude a flashing well. The extension of the derivation to include the flashing system is considered later.

3. The flow in the well is isentropic. The effect of change in the fluid head in the well, therefore, will be ignored in this initial derivation. This effect depends on a much longer time and is considered in the next section. It will be shown in the calculations that the change in fluid head will have a small effect on these initial pressure curves.

4. The pressure pulse at wellhead travels as a step change. Friction effects will smear the front out, but the pulse interaction takes place over the entire height of the reservoir, and it is assumed that the smearing effect takes place over a smaller distance than this height.

5. No skin effect is considered.

For a step change in surface mass flow rate, all of the mass is taken initially from the bore. As it is usually the surface flow rate that is assumed to be kept constant during a well test, the surface flow rate will be prescribed, and the initial pressure pulse needed to achieve this flow rate is calculated. Given this pressure change, the initial flow from the reservoir is determined.

When all the mass is taken from the well, the decrease in mass in the well must equal the total mass out or

$$(\Delta\rho)\,\pi r_w^2 \Delta x = \rho q \Delta t, \quad \ldots\ldots\ldots\ldots\ldots\ldots\ldots\ldots (4)$$

where Δx is the distance down the well from which the mass is taken. This distance is just the distance the signal has propagated. Assuming the flow is isentropic (an approximation), Eq. 4 can be rewritten as

$$(\Delta\rho)\,\frac{\Delta x}{\Delta t} = \left(\frac{\partial \rho}{\partial p}\right)_s \Delta p \,\frac{\Delta x}{\Delta t} = \frac{\rho q}{\pi r_w^2},$$

or

$$\Delta p = \left(\frac{\partial \rho}{\partial p}\right)_s^{-1} \frac{\rho q}{\pi r_w^2}\,\frac{\Delta t}{\Delta x}.$$

The disturbance travels at the local speed of sound, a, so

$$(\Delta x/\Delta t) = a = (\partial p/\partial \rho)_s^{1/2}, \quad \ldots\ldots\ldots\ldots\ldots\ldots (5a)$$

and

$$\Delta p = \left(\frac{\partial \rho}{\partial p}\right)_s^{-1/2} \frac{\rho q}{\pi r_w^2}. \quad \ldots\ldots\ldots\ldots\ldots\ldots (5b)$$

The sandface flow at any time is

$$w_{sf} = 2\pi r_w \frac{kh}{\mu} \rho_{sf} \frac{\partial p}{\partial r}. \quad \ldots\ldots\ldots\ldots\ldots\ldots (6)$$

Now the initial sandface flow is estimated by describing $\partial p/\partial r$ as $\Delta p/r_w$ (the initial pressure drop in the well divided by the radius of the well), so $(w_{sf})_i$ is obtained from Eq. 6:

$$(w_{sf})_i = 2\pi \frac{kh}{\mu} \rho_{sf} \left(\frac{\partial \rho}{\partial p}\right)_s^{-1/2} \frac{\rho q}{\pi r_w^2}. \quad \ldots\ldots\ldots\ldots\ldots\ldots (7)$$

Since $\rho q = w_s$, one can obtain the nondimensional parameter w_D using the estimate for $(w_{sf})_i$:

$$w_D = \frac{w_s}{(w_{sf})_i} = \frac{\mu}{kh}\,\frac{r_w^2}{2}\,\frac{1}{\rho_{sf}} \left(\frac{\partial \rho}{\partial p}\right)_s^{1/2}. \quad \ldots\ldots\ldots\ldots\ldots\ldots (8)$$

The storage coefficient C_D represents the ratio of the ability of the well to store fluid to that of the reservoir, while the nondimensional parameter w_D represents the ratio of the ability of the well to give up its fluid to that of the reservoir. We see that this latter quantity depends on the value of kh/μ of the reservoir and on the rate of signal propagation in the well. The reservoir may have a large storage capacity but, because of a low permeability-thickness factor and high viscosity, it may not be able to deliver the fluid very rapidly. Transient changes in the well would die out before the reservoir could deliver any significant portion of the flow rate. However, for the same storage coefficient, the value of kh/μ could be large enough that the reservoir could deliver large quantities of fluid while the transient changes in the well were still important. The very early-time data will be different in these two cases, although C_D would be the same. To describe this early-time data completely, one needs to use both the storage coefficient and the nondimensional parameter w_D.

We now extend this discussion to include a two-phase or flashing system. First, it is necessary to define C_D in these cases and then to consider whether w_D still can be used to correlate the early-time data. The storage coefficient is defined in the petroleum literature by assuming dp_w/dt is not a function of position. The same approach will be used here. Therefore, although the plot of p_D vs. t_D will deviate at early times from those developed in the literature, these plots must approach the expected curves at later times when dp_w/dt is not a function of position. Eq. 2 actually should be written as

$$w_{sf} = w_s - \int_0^L A \left(\frac{\partial \rho}{\partial p}\right)_s \frac{\partial p}{\partial t}\, dx. \quad \ldots\ldots\ldots\ldots\ldots\ldots (9)$$

If the equation is nondimensionalized and if one looks at the case where $\partial p_w/\partial t$ is not a function of x,

$$\frac{w_{sf}}{w_s} = 1 - \frac{A}{2\pi r_w^2 \phi c_R h}\,\frac{dp_D}{dt_D}\,\frac{1}{\rho_{sf}} \int_0^L \left(\frac{\partial \rho}{\partial p}\right)_s dx, \quad \ldots\ldots\ldots\ldots\ldots\ldots (10)$$

so

$$C_D = \frac{AL}{2\pi r_w^2 \phi c_R h}\,\frac{1}{\rho_{sf}} \left(\frac{\overline{\partial \rho}}{\partial p}\right)_s,$$

and

$$\frac{\overline{\partial\rho}}{dp_s} = \frac{1}{L}\int_0^L (1-\alpha)\left(\frac{\partial\rho}{\partial p}\right)_1 + \alpha\left(\frac{\partial\rho}{\partial p}\right)_2 dx, \quad \ldots\ldots(11)$$

where α is a function of x. For a single-phase system, $\alpha=0$.

It is now necessary to determine if w_D still can be used to correlate the early-time data for the two-phase or flashing case. In the preceding derivation, it was assumed that $(\partial\rho/\partial p)_s$ was not a function of x. If the flow is two-phase, but not flashing, α usually is not a strong function of position. Therefore, as long as the flow can be described by $v=-(k/\mu)\partial p/\partial r$, none of the assumptions made are violated and w_D is appropriate. When the fluid is flashing, however, α is a strong function of position, especially where the fluid starts to flash.

The value of $(\partial\rho/\partial p)_s$ in the flashed region is on the order of 4.2×10^{-2} lbm/cu ft-psi (10^{-4} kg/m^3·Pa) and in the single-phase region it is about 4.2×10^{-4} lbm/cu ft-psi (10^{-6} kg/m^3·Pa). Such a change cannot be ignored. The derivation of w_D depends on the storage capacity of the well and the speed of signal propagation. The time for the signal to propagate in the single-phase region is about an order of magnitude smaller than in the two-phase region. Also, the storativity of the well in the single-phase region is two orders of magnitude less than in the flashed region. The changes in the well are controlled entirely by the two-phase region. When the signal arrives at the two-phase boundary in the well, it essentially can be assumed to be at the reservoir boundary, meaning that the single-phase region acts merely as a connection between the two-phase region and the reservoir. The signal is propagated instantaneously over that region. Then in the derivation of w_D, the single-phase region can be neglected and the average value of $(\partial\rho/\partial p)_s$ will be that of the flashed region. In this region, $(\partial\rho/\partial p)_s$ will be a weak function of position again, so the derivation for w_D is still appropriate.

Using w_D and C_D, it will be shown that the downhole pressure can be correlated even when the well transients are important. A numerical program is used to derive the nondimensional plots. It will be seen that in all cases, the p_D vs. t_D plot (where p_D is the nondimensionalized downhole pressure) will approach the nondimensional plots derived in petroleum literature.

Transient Flow in Wellbore

Several papers in the literature have dealt with flow in a geothermal well.[9-12] However, all these papers assume steady-state flow – i.e., $\partial p_w/\partial t=0$ and the mass into the well equals the mass out of it. Obviously these models cannot consider the effect of the interaction of a pressure wave propagating down the well into the reservoir, and they cannot be used to describe the flow when wellbore storage is important. Steady-state models can be used to obtain wellhead conditions when the downhole pressure is approximately constant and when wellbore storage is over. The intent of this work, though, is to consider the very early-time data, so a transient model of the flow is necessary.

To investigate the nonuniform changes in the well in detail, a numerical model to simulate compressible transient flow in a wellbore has been developed. The model is capable of handling single-phase as well as two-phase flow with mass transfer (e.g., steam/water flow) and includes the heat transfer between the ground and the well. The one-dimensional equations of mass, momentum, and energy in the well are solved, as well as a radial Darcy flow equation for a homogeneous single-phase reservoir. The equations are

$$\frac{\partial\rho}{\partial t}+\frac{\partial}{\partial x}(\rho v)=0, \quad \ldots\ldots(12)$$

$$\frac{\partial}{\partial t}(\rho v)+\frac{\partial}{\partial x}(\rho v^2)+\frac{\partial p}{\partial x}+\rho g+\frac{f\rho v^2}{4r_w}=0, \quad \ldots(13)$$

and

$$\frac{\partial}{\partial t}(\rho E)+\frac{\partial}{\partial x}(\rho E v)-\frac{2U}{r_w}(T_f-T_w)+p\frac{\partial v}{\partial x}=0 \quad \ldots\ldots(14)$$

in the well and

$$\frac{\partial p}{\partial t}=\frac{k}{\phi c_R\mu}\left(\frac{\partial^2 p}{\partial r^2}+\frac{1}{r}\frac{\partial p}{\partial r}\right) \quad \ldots\ldots(15)$$

in the reservoir.

An equation of state is used to relate density to pressure and energy. A more complete description of the numerical model is given in the Appendix. For the initial calculations presented here, a constant friction factor was used and no slip was assumed. Many interesting and meaningful transient results are possible without going into a more elaborate description of the friction and slip. The program is used to investigate the initial transient nature of the wellbore and to determine the duration of temperature changes. The inclusion of slip will not alter significantly the effects being considered here. Initially the behavior of dp_{sf}/dt will be investigated, with no heat loss assumed, to show how consideration of the transient changes in the well will alter the curves developed in the petroleum literature. The effect of temperature changes will be considered in the following section.

Adiabatic Flow

Using the developed numerical model, calculations were performed to generate the deviation of the drawdown (or buildup) curve from the unit slope for different values of w_D and C_D. The calculations were done for $C'_D=25$ and 100 [the C'_D factor is calculated using $(\partial\rho/\partial p)_E$ instead of $(\partial\rho/\partial p)_s$] with $w_D=0.1$, 1.0, and 10.0. For all calculations, the length of the well was 6,561.7 ft (2000 m) and the radius was 0.0323 in. (0.082 cm). The mass flow rate per unit area out was kept constant at 102.4 lbm/sq ft-s (500 kg/m^2-s). No heat loss was assumed. The downhole pressure was adjusted to obtain flashing or

TABLE 1 – DIMENSIONAL VALUES USED FOR GENERATING NONDIMENSIONAL WELLBORE STORAGE PLOTS

W_D	C_D	kh (m^3)	μ (Pa·s)	ϕch (m/Pa)	Downhole Pressure (Pa)	Downhole Temperature (°C)
10.0	25	6.4×10^{-14}	0.2×10^{-3}	0.32×10^{-7}	2.9×10^{7}	200
1.0	25	6.4×10^{-13}	0.2×10^{-3}	0.32×10^{-7}	2.9×10^{7}	200
0.1	25	6.4×10^{-12}	0.2×10^{-3}	0.32×10^{-7}	2.9×10^{7}	200
10.0	100	4×10^{-13}	0.9×10^{-4}	0.53×10^{-8}	2×10^{7}	320
1.0	100	4×10^{-12}	0.9×10^{-4}	0.53×10^{-8}	2×10^{7}	320
0.1	100	4×10^{-11}	0.9×10^{-4}	0.53×10^{-8}	2×10^{7}	320

no flashing. The reservoir parameters used for the calculations are given in Table 1. The results are shown in Figs. 1A and 1B. Each plot included the analytical solution for both a wellbore storage curve derived by assuming (dp_D/dt_D) is not a function of position in the well and the $C_D=0$ curve. The particular analytical solution chosen for comparison is for a value close to that of the numerical calculations. The small difference between the C_D used for the numerical calculations and the C_D of the analytical curve is discussed later. The $C_D=0$ curve is just the Theis curve. The general behavior of the transient flow in the well can be described using these figures.

In Fig. 1A, liquid water was assumed to flow under a positive head to generate the curves for the different values of w_D. The average value of $(\partial\rho/\partial p)_\xi$ in the well was 3.0×10^{-4} lbm/cu ft-psi (7×10^{-7} kg/m^3·Pa), and the C_D factor for this plot is 25. Included in the figure are points calculated for a flashed system where the average value of $(\partial\rho/\partial p)_\xi$ is 1.7×10^{-2} lbm/cu ft-psi (4×10^{-5} kg/m^3·Pa). Fig. 1B and some points in Fig. 1A are for calculations that assume that the water is flashing about 1,640 ft (500 m) down the well but still flowing under a positive head. A friction factor of 0.04 was used for all calculations except for one case in Fig. 1B. To generate the different curves, kh, μ, and ϕch were varied. The arrival time of the initial pulse downhole is the same if the average compressibility is not changed. However, the time has been nondimensionalized by $(k/\mu c\phi r_w^2)t$, so the nondimensionalized arrival time will be different when the reservoir parameters are varied.

The first case to consider is $w_D>1$, illustrated in the figures by $w_D=10$. The fluid in the well may not be very compressible, but because the reservoir is even less responsive, the well must continue to supply the surface flow rate long after the initial pressure arrives downhole. For Δp_i, the flow from the reservoir is significantly less than the surface flow rate. Actually, this case serves as a check on the numerical calculations. There always will be some initial delay, but this delay is a very small portion of the initial curve. Once the pressure disturbance arrives downhole, the pressure change with time there increases abruptly. After the downhole pressure drops to what it would be at this time, if the well had responded uniformly, the $\log p_D$ vs. $\log t_D$ curve follows a unit slope. In both figures the unit slope is calculated for the $w_D=10$ case, as expected. As

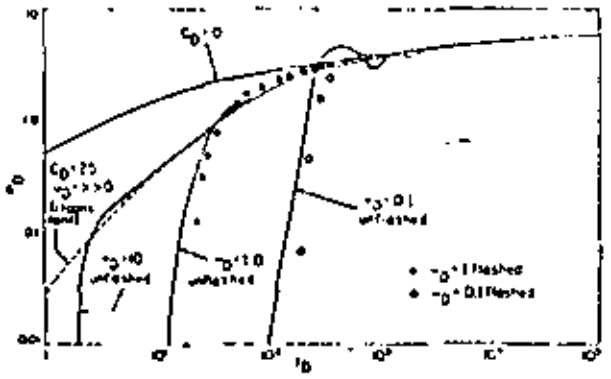

Fig. 1A – Nondimensional plot of sandface pressure vs. time for $C_D=25$ and $w_D=0.1$ to 10.

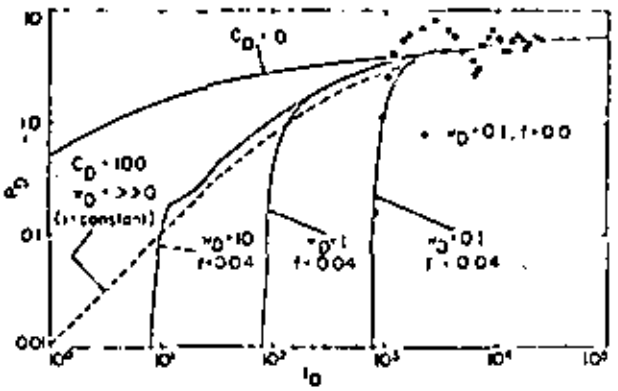

Fig. 1B – Nondimensional plot of sandface pressure vs. time for $C_D=100$ and $w_D=0.1$ to 10.

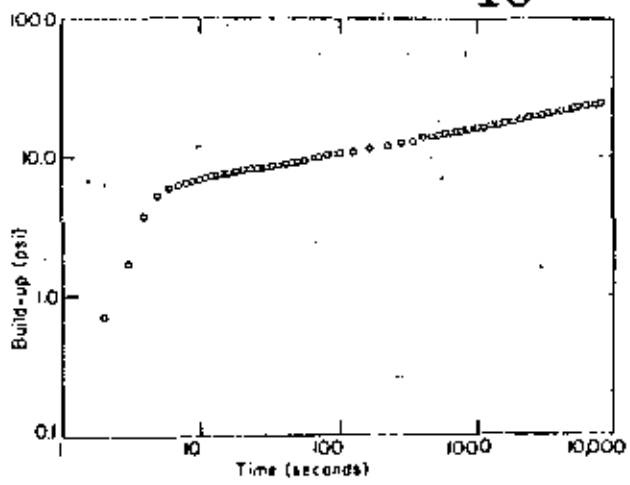

Fig. 2—Buildup data from the geothermal well RRGE2 at Raft River.[13]

noted, included on each plot is the analytic solution for the wellbore storage curve when $dp_w/dt \neq fn(x)$. In Fig. 1A the C_D should be calculated with $(\partial p/\partial p)_s$, while the estimation of C_D for the calculations was done here using $(\partial p/\partial p)_E$. Only $(\partial p/\partial p)_E$ could be calculated in the numerical solution because the steam tables were fit with polynomials and $p = fn(P,s)$ was not included. The error in the estimation for C_D is less in the single-phase case because the difference between these two derivatives is negligible. As the fluid flashes more, $(\partial p/\partial p)_s$ and $(\partial p/\partial p)_E$ start to differ. For the single-phase case plotted in Fig. 1A, the calculations fall on the analytical solution for the $w_D = 10$ case. In Fig. 1B (the two-phase case), the calculations fall on a unit slope corresponding to a C_D that is slightly less than the plotted analytical curve for $C_D = 100$, as expected.

When $w_D = 1$, the pressure drop needed to achieve a step change in flow rate at the surface is close to the pressure drop needed to obtain this same flow rate from the reservoir. The pressure change with time is initially zero, but once the disturbance reaches downhole, it rises abruptly until it reaches the expected drawdown curve. Since $w_{sf})_i \approx w_s$, this occurs after the expected wellbore storage curve is almost over. The plot is shown in the figures by $w_D = 1$. The actual value of $(w_{sf})_i$ when $w_D = 1$ is less than w_s. In the derivation, $(\partial p/\partial r)_i$ was estimated as $\Delta p_i/r_w$. The actual value of $(\partial p/\partial r)_i$ at the reservoir is always less than this, so that $(w_{sf})_i < w_s$ when $w_D = 1$. The error in estimating $(\partial p/\partial r)_i$ as $\Delta p_i/r_w$ is just the same percent for all cases, so w_D still can be used to correlate the early-time behavior.

The third interesting case is when $w_D < 1$. When the given pressure drop arrives downhole, the reservoir will be so responsive that it can supply more fluid than the well could for the same pressure drop. This situation produces an oscillation illustrated in Fig. 1A by $w_D = 0.1$. The pressure drop is so large that the reservoir supplies more fluid than is being taken out at the surface. The pressure in the well will be increased, and this increase will propagate back up the well. The interaction between the reservoir and the well produces the oscillation which slowly dies out. For the liquid-filled well in Fig. 1A, the time of the oscillations is a couple of seconds. However, the large oscillations seen in Fig. 1A for $w_D = 0.1$ are not observed in Fig. 1B, where a flashed system was used for the calculations. The oscillations have been damped out by friction effects. The friction term is dependent on the flow velocity squared. Thus, for the same mass flow rate, there will be more dampening in the flashed system than in the unflashed, because the velocity is greater. One can see the influence of the friction factor in Fig. 1B, where one calculation was done with $f = 0$ in the case $w_D = 0.1$. The effect of the friction factor decreases as w_D increases.

A lack of one-to-one slope at early times has been observed in the field. Fig. 2 plots data obtained from a field test of a liquid-filled well at the Raft River geothermal project.[13] The data were taken with a Hewlett-Packard pressure gauge, capable of providing readings every second with a resolution of 0.01 psi (0.07 kPa). The well was flowing and then was shut in. Any error in the initial buildup because of temperature effects on the instrument should not be important as the instrument already had been heated. (The fluid was flowing under a positive head before it was shut in.) When the data were analyzed, the lack of the unit slope was observed but no explanation was given. The signal that the well was shut in takes about 1 to 2 seconds to arrive downhole. The pressure then builds up very quickly and approaches the curve that would exist if the well behaved uniformly. Using the measured properties of the reservoir [$\phi ch = 8.9 \times 10^{-2}$ ft/psi (4×10^{-6} m/Pa), $kh = 49{,}940$ md-ft (1.5×10^{-11} m^3), $\mu = 0.2$ cp (2×10^{-4} Pa·s)], the wellbore storage coefficient is 0.35 and $w_D = 0.2$. For this low value of w_D one should see oscillations in the p_D vs. t_D curve. However, these oscillations are damped out if the flow rate change is less than a step function. For the case plotted in Fig. 2, it probably would be hard to achieve a step-rate change because the typical time needed to close a valve is longer than the required time for a pressure signal to propagate to the bottom of the well. Even without a step-rate change in flow rate, the plot is still not a unit slope, emphasizing even more that the unit slope is only a special case when the reservoir is less responsive than the well.

A plot of the pressure pulse as it propagates into the well and interacts with the reservoir gives more insight into the well/reservoir interaction. Figs. 3A, 3B, and 3C plot the pressure distribution in the well as a function of time for a drawdown test and for different values of w_D. The first two calculations are done with water throughout the well, and the third case is for water that has flashed about 1,640 ft (500 m) down the well.

For the cases in Figs. 3A and 3B, the propagation of the signal is the same until the pulse arrives at the formation/well boundary. Then the pressure distributions in the well will start to differ. The value of kh/μ is greater in Fig. 3A than in 3B, so w_D will be

... in Fig. 3A, the changes of pressure with time ... have been plotted in a nondimensional ... Fig. 3A has been split into three successive ... to illustrate the oscillations in the well as a ... of time. Fig. 3B is only one graph because ... change with time quickly becomes ... To illustrate that there is no difference in ... propagation of the pressure pulse, the first ... of Fig. 3A and the graph of Fig. 3B have been ... that the dimensional units coincide. Once ... arrives at the reservoir, the two cases start ... In Fig. 3A, the reservoir supplies more fluid ... being taken out at the surface, and an increase ... travels up the bore, canceling out part of ... pressure decrease. This pulse produces an ... in pressure that is too large in the well. When ... decrease in pressure arrives at the surface, the ... must decrease again to sustain the flow rate. ... a pressure oscillation in the well that slowly ... out. In Fig. 3B, the reservoir has a relatively low ... of kh/μ. Even when the initial pressure drop ... downhole, the reservoir cannot supply very ... fluid. The pressure must continue to drop in ... well, and dp_w/dt will be a very weak function of ... in the well.

In Fig. 3C, the signal propagation is different ... there is a boundary between the two-phase ... and the liquid. The boundary tends to distort ... pressure pulse because most of the pulse ... from the boundary while a small portion ... This is how the single-phase region ... as just a connection between the two-... region and the reservoir. The pressure pulse ... with the liquid interface is essentially the ... with the reservoir boundary except for ... damping. The pulse then oscillates in the two-... region. The propagation of the signal is ... slow in the two-phase region – about 230 to ... ft/s (70 to 150 m/s).

... sound speed is low in a two-phase region ... of the lower density and high com-... However, once the pulse reaches the ..., the signal is propagated about 10 times faster ... the compressibility is lower. Because of this ... in propagation speed, the changes in the ... are relatively uniform. For larger values of ... pressure will drop faster in the liquid region ... pressure change in the well will become more ... more quickly. For $w_D > 1$ the pressure drop ... closer to Fig. 3B, even though there is a two-... region.

... question still is whether w_D can be used as a ... dimensional parameter to describe this in-... when different fluids are used in the well – ... C_D and w_D are kept the same while the fluid ... in the well and the reservoir properties are ..., will the same curve be generated? It might ... that changes in the two-phase region ... be correlated by a term w_D that was ... by assuming no abrupt changes in the initial ... pulse. However, when the fluid flashes, the ... region dominates the effects in the well and ... can ignore the single-phase region. ... phase region then acts almost as a single-

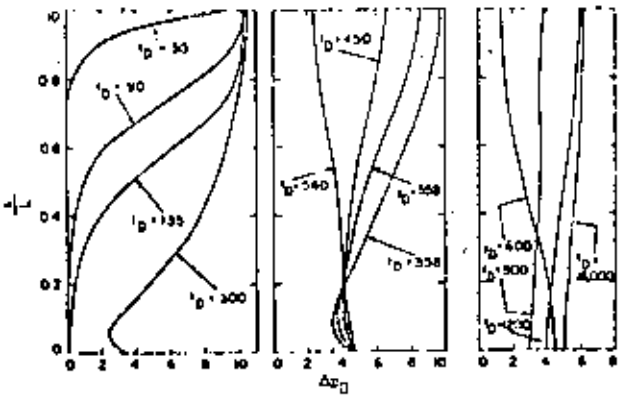

Fig. 3A – Pressure profile in a well as a function of time ($w_D = 0.1$, $C_D = 25$, and fluid is not flashing).

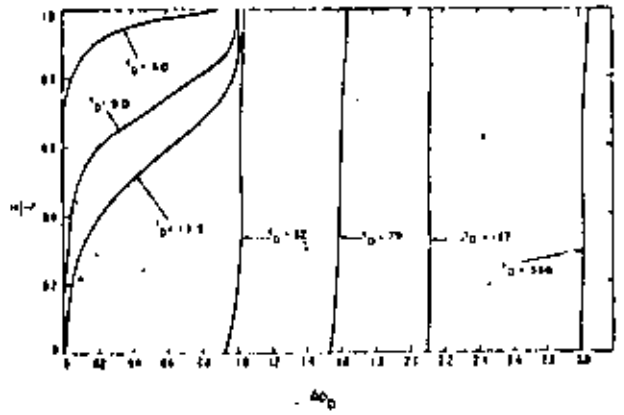

Fig. 3B – Pressure profile in a well as a function of time ($w_D = 1.0$, $C_D = 25$, and fluid is not flashing).

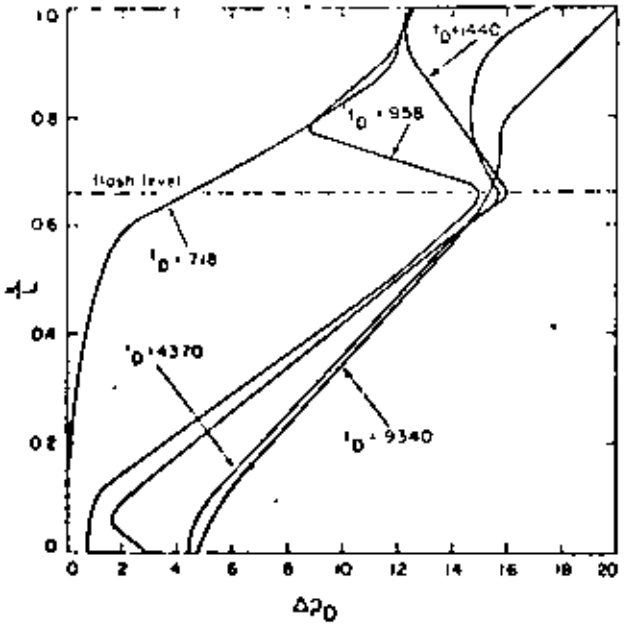

Fig. 3C – Pressure profile in a well as a function of time ($w_D = 0.1$, $C_D = 100$, and fluid is flashing in the bore).

TABLE 2 – DIMENSIONAL VALUES USED FOR CALCULATING DRAWDOWN IN WELLBORE FOR DIFFERENT AVERAGE COMPRESSIBILITIES IN THE BORE

Conditions	kh (m^3)	ϕch (m/Pa)	μ (Pa·s)	$(\partial\rho/\partial p)_T$ (kg/m^3·Pa)
Unflashed	6.4×10^{-13}	8.0×10^{-8}	2×10^{-4}	7.0×10^{-1}
Unflashed	4.5×10^{-13}	2.3×10^{-8}	9×10^{-5}	1.4×10^{-4}
Flashed	4.0×10^{-12}	5.0×10^{-7}	9×10^{-5}	4.0×10^{-3}

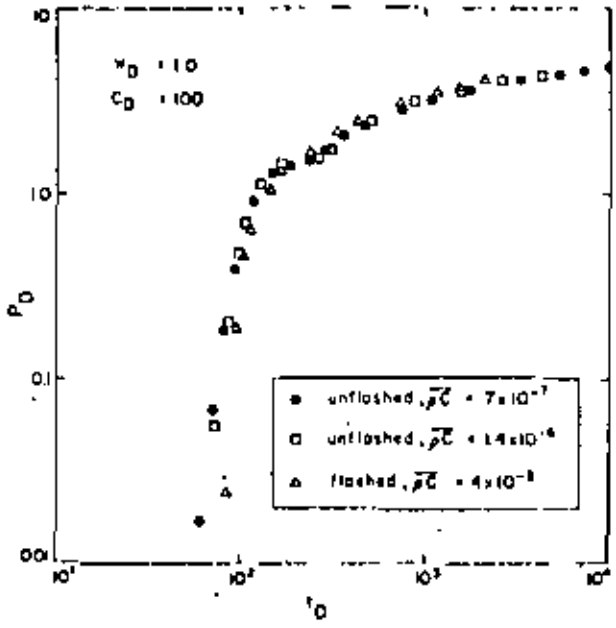

Fig. 4 – Nondimensional plot of sandface pressure vs. time for different average compressibilities in the well but for the same values of C_D and w_D.

phase case with a large compressibility, and the parameter w_D then can be used to correlate the initial behavior.

If the fluid in the well is not varied, but μ, k, and h are changed such that kh/μ remains constant, the generated curve is the same. The calculation depends on kh/μ, and if this is not varied, the interaction of the well and reservoir will not change. (There is a very slight difference in the calculations as h is varied, but the size of the change is too small to be of any use.) A more interesting case is if the fluid properties in the well are varied but the reservoir properties are adjusted to give the same w_D and C_D. Under these circumstances, will the same curve be generated? Fig. 4 shows this comparison when $C_D = 100$ and $w_D = 1.0$. Two calculations are for a liquid-filled well and the third is for a flashed system. The reservoir values used are given in Table 2.

It is a little hard to contrive a case where w_D and C_D will be the same when the average compressibility in the well varies as much as it does between these two cases. Some of the reservoir properties used may be a little extreme. However, one can see that there is excellent agreement between the three different cases. Again, the constant friction factor of 0.04 was used. The other properties of the well are the same as those used for the calculations done for Fig. 3. The agreement is especially good when $w_D > 1$. As w_D decreases, pressure changes in the well become more nonuniform and the assumptions used in deriving w_D become less valid. Oscillations can occur in some cases, and the size of the oscillations depend on the friction factor. Because friction losses are more significant in a flashing system, the p_D vs. the t_D curve for this latter case will start to deviate at early times from the single-phase case that has the same values of w_D and C_D. Oscillations would occur in a single-phase case but would be damped out for the two-phase case. This situation exists when $w_D << 1$. However, from the very rough analysis used to estimate it, w_D can describe the flow for both two- and single-phase flow over a wide range of cases.

Heat Loss Effects

The change in energy of the reservoir fluid while flowing through the wellbore is due both to the heating of the fluid in the bore and to heat loss out of the bore. The effect of this energy loss is to change the fluid head in the well and to increase the time when wellbore storage is important. The heating of the fluid in the bore is important when a well has not been flowing. A geothermal temperature gradient will exist down the bore. When the well starts to flow, the temperature of the fluid in the bore increases and the fluid head in the bore decreases. Because of this decrease, the wellhead pressure increases, although the downhole pressure is decreasing. The downhole pressure itself is not affected significantly by this fluid head because it is the properties of the reservoir that control the flow from the reservoir and not the properties of the fluid in the well. The effect of any energy change is to alter the rate at which the sandface flow rate approaches the surface flow rate – i.e., wellbore storage is increased. The density of the fluid is affected significantly by changes in energy, and the duration of transient energy effects is much longer than transient pressure changes. However, the time when wellbore storage should be over when the flow is not isothermal is not obvious from the plots. The rate of the energy change can be slow enough so that one can obtain a straight line on a plot of p_D vs. $\log(t_D)$ but with just a slightly increased slope resulting in a smaller estimate for kh.

Fig. 5 illustrates the effect of fluid heating in the bore on the transient downhole pressure. Plotted in the figure is the nondimensional downhole pressure vs. the nondimensional time for both an initially

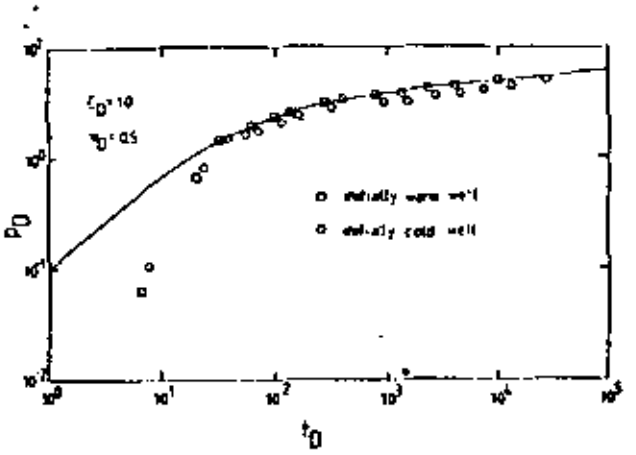

Fig. 5 – Transient sandface pressure for an isothermal well and for a well that initially has a temperature gradient along the bore.

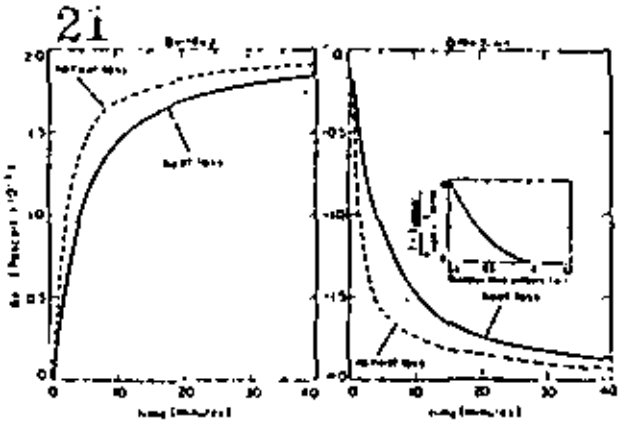

Fig. 6 – Effect of heat loss on a buildup and a drawdown test.

warm well (the flow is isothermal) and an initially cold well [the temperature in the well before flowing is linear from 68°F (20°C) at the wellhead to 392°F (200°C) downhole]. One can see that there is little difference in the initial drawdown for the two cases (w_D still could be used to correlate this early drawdown data), but that at later times the plots start to differ. At much later times, when the flow in the initially cold well becomes isothermal, the plots must coincide again. For the isothermal case, wellbore storage depends only on the changes in density because of pressure changes. When the downhole pressure is not changing significantly with time, the sandface flow rate will be approximately equal to the surface flow rate and wellbore storage will be over. Changes in the energy have a much longer time effect. Wellbore storage will be important until $\partial E/\partial t = 0$ throughout the well. For a well that is initially at the geothermal gradient, a minimum time for $\partial E/\partial t \approx 0$ is the transit time for a fluid particle in the well. For a flow of 800 gal/min (5.05×10^{-2} m^3/s) in a liquid-filled well of 5,905 ft (1800 m) with a radius of 0.295 ft (0.09 m), this transit time is approximately 15 minutes. Any heat loss to the surrounding rock will increase the time until $\partial E/\partial t \approx 0$. The duration of wellbore storage based on pressure changes alone would be only 38 seconds for the cases plotted in Fig. 5.

In most cases when testing a well, the well will be flowed until the change at wellhead steadies out; then flow tests will be started. However, even in this situation the heat loss of the fluid in the bore will change because of the increase or decrease in the fluid transit time in the well. As stated previously, the effect of the heat loss is a slight alteration of the p_D vs. t_D plot. If one ignored it completely and analyzed the downhole data with methods developed in the petroleum literature, the value of kh calculated would be too small. The numerical model of the transient behavior of the fluid in the well has been used to model the flow with heat transfer. The temperature change in the rock surrounding the wellbore was assumed to be radial only and was calculated using

$$\frac{\partial T}{\partial t} = \alpha\left(\frac{\partial^2 T}{\partial r^2} + \frac{1}{r}\frac{\partial T}{\partial r}\right). \quad \ldots\ldots\ldots\ldots\ldots\ldots (16)$$

Heat transfer is especially important in two-phase geothermal wells because of the large temperature changes that occur along the bore. Fig. 6 is a plot of p_{wf} vs. t for a buildup and a subsequent drawdown test. To simulate the heat loss from the well, a temperature gradient from ambient to the reservoir temperature was assumed far from the well and a small temperature buildup was used near the bore. A nondimensional representative temperature profile is given by the insert in Fig. 6. It is assumed that the well has been flowing so that the initial heating of the well has been completed. In the figure, the plots on the left (labeled buildup) show Δp vs. time during buildup with and without heat loss. The calculations had the well flowing 12 hours before the buildup test calculation was begun. The plots on the right (labeled drawdown) show the same for the subsequent drawdown test. The fluid flowed into the well from a simple, homogeneous reservoir with a kh value of 22,272 md-ft (6.7×10^{-12} m^3). The heat transfer coefficient used between the fluid and the wellbore was specified as a function of flow rate and density. For turbulent flow in a pipe, $N_{Nu} = 0.023 N_{Re}^{0.8}$ ($N_{Pr} = 1$), and $U = 0.023 \times (\rho v)^{0.8}/\mu^{0.8} D^{0.2}$ (Ref. 14). In the two-phase region, the heat transfer coefficient was averaged between the steam and liquid. However, the heat transfer is controlled by the properties of the rock and any error in the heat transfer coefficient U will be negligible. The rock properties used for the heat loss calculations were a thermal conductivity of 1.04 BTU/hr-ft-°F (1.8 W/m·°C) and a thermal diffusivity of 1.08×10^{-5} sq ft/s (1×10^{-6} m^2/s).

It can be seen from the figure that the heat transfer causes the pressure to change initially at a slower rate

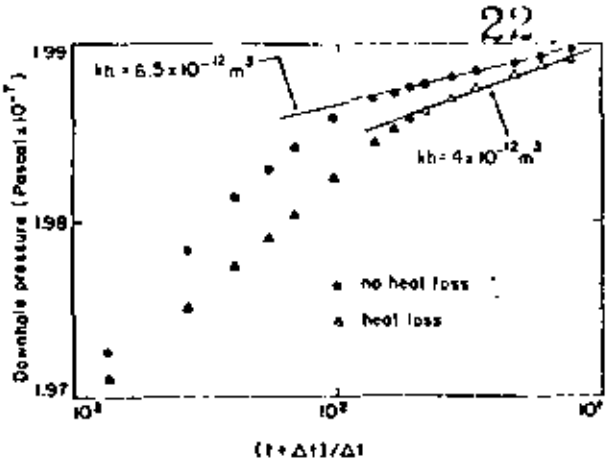

Fig. 7 – Effect of heat loss on a buildup curve shown on a semilog plot of p vs. t.

for both the buildup and the drawdown tests. The deviation between the two cases is smaller initially. It increases and then will decrease when $\partial E/\partial t = 0$. During a buildup test, the enthalpy of the exiting fluid decreases because of the increased time that the fluid is in the well. As the enthalpy decreases, the fluid can condense or compress more for the same pressure, so more fluid flows into the well with a smaller pressure rise. In a drawdown, the enthalpy of the fluid increases in time and the density will decrease. For the same pressure, more fluid will exit the well, so the initial drawdown pressure is less. As the enthalpy change steadies out, the drawdown (or buildup) curve with heat loss must approach the curve without heat loss. Enthalpy changes from acceleration or deceleration are not important in the pseudosteady region because these changes already have taken place. It is only the changes from heat loss that affect the slope of the p_D vs. t_D curve in this region.

Fig. 7 shows the error in the kh value if the test is analyzed assuming heat loss is not important. The figure is a plot of p vs. $\log[(t+\Delta t)/\Delta t]$ for the buildup test where $t = 12$ hours. Assuming that $kh = q\mu/4\pi m$, where m is the slope of the straight-line portion, then the kh obtained is about 21,608 md-ft (6.5×10^{-12} m^3) in the buildup. Although not plotted, the analysis gives 22,938 md-ft (6.9×10^{-12} m^3) in the drawdown for no heat loss. The actual value used was 22,272 md-ft (6.7×10^{-12} m^3). However, if the same analysis is used when heat loss is important, different values for kh are obtained – i.e., 13,297 md-ft (4×10^{-12} m^3) in the buildup and 17,619 md-ft (5.3×10^{-12} m^3) in the drawdown. The longer the test is run, the less significant the heat loss is, as shown by the approach of the two slopes toward one another at later times. The straight-line semilog plot shown in Fig. 7 is seen after about 10 minutes when heat loss is zero and after 20 minutes when heat loss is present.

Conclusions

The early-time response of a unit slope when $\log(p_{sf})$ is plotted vs. $\log(t)$ is a special case; actually there are a whole series of curves for each value of C_D, a series that can be defined by the nondimensional time w_D. An expression for w_D was determined that is applicable when the compressibility in the well is relatively constant. Even in two-phase wells, where the compressibility changes by orders of magnitudes, w_D still can be used to correlate the flow because the two-phase region dominates and the compressibility is approximated as constant in the two-phase region. In addition, it has been shown that the temperature changes will increase the time when wellbore storage is important, and if this increase is ignored, one still can obtain a straight line on a plot of p_{sf} vs. $\log(t)$ but the slope of that line will be larger than $q\mu/4\pi kh$.

Nomenclature

A = area of wellbore
c = isentropic compressibility, $(1/\rho)(\partial\rho/\partial p)_s$
c_f = compressibility of reservoir
C = wellbore storage, $\rho cV/\rho_{sf}$
C_D = wellbore storage coefficient, $(\partial\rho/\partial p)_s V/\rho_{sf} 2\pi\phi c_R h r_w^2$
C_D^* = $(\partial\rho/\partial p)_E V/\rho_{sf} 2\pi\phi c_R h r_w^2$
D = diameter of well
E = specific energy
f = friction factor
g = gravity
h = reservoir thickness
i = specific enthalpy
k = permeability
L = depth of wellbore
N_{Nu} = Nusselt number
N_{Pr} = Prandtl number
N_{Re} = Reynolds number
p = pressure
p_D = nondimensional downhole pressure, $2\pi(kh/\mu)(\rho_{sf}/w_s)p_w$
Δp_i = initial pressure drop in well
q = volume flow rate
r_w = radius of wellbore
s = specific entropy
t = time
t_D = nondimensional time $(k/\mu\phi c_R r_w^2)t$
T_f = temperature in rock surrounding the wellbore
T_w = temperature of fluid in wellbore
U = heat transfer coefficient
v = velocity
V = volume
w = mass flow rate
w_D = nondimensional parameter $w_s/(w_{sf})_i$
$(w_{sf})_i$ = initial change in sandface mass flow rate
α = thermal diffusivity
ϕ = porosity
ρ = density
μ = absolute viscosity

Subscripts
i = initial
s = surface
sf = sandface
w = well

Acknowledgment

This work was supported by the Div. of Geothermal Energy, U.S. DOE, under Contract No. W-7405-ENG-48.

References

1. Rivera-R., J. and Ramey, H.J. Jr.: "Application of Two Rate Flow Tests to the Determination of Geothermal Reservoir Parameters," paper SPE 6887 presented at the SPE 52nd Annual Technical Conference and Exhibition, Denver, Oct. 9-12, 1977.
2. Gringarten, A.C.: "Well Testing in Two-Phase Geothermal Wells," paper SPE 7480 presented at the SPE 53rd Annual Technical Conference and Exhibition, Houston, Oct. 1-3, 1978.
3. Kihara, D., Chen, B., Yuen, P., and Takahashi, P.: "Summary of Results of HGP-A Well Testing," *Proc.*, Third Workshop, Geothermal Reservoir Engineering, Stanford U., Stanford, CA (1977).
4. van Everdingen, A.F. and Hurst, W.: "The Application of the Laplace Transformation to Flow Problems," *Trans.*, AIME (1949) 186, 305-324.
5. Earlougher, R.C. Jr.: *Advances in Well Test Analysis*, Monograph Series, Society of Petroleum Engineers, Dallas (1977) 5.
6. Agarwal, R.G., Al-Hussainy, R., and Ramey, H.J. Jr.: "An Investigation of Wellbore Storage and Skin Effect in Unsteady Liquid Flow: I. Analytical Treatment," *Soc. Pet. Eng. J.* (Sept. 1970) 279-290; *Trans.*, AIME, 249.
7. Wattenbarger, R.A. and Ramey, H.J. Jr.: "An Investigation of Wellbore Storage and Skin Effect in Unsteady Liquid Flow: II. Finite Difference Treatment," *Soc. Pet. Eng. J.* (Sept. 1970) 291-297; *Trans.*, AIME, 249.
8. Ramey, H.J. Jr.: "Short-Time Well Test Data Interpretation in the Presence of Skin Effect and Wellbore Storage," *J. Pet. Tech.* (Jan. 1970) 97-104; *Trans.*, AIME, 249.
9. Nathenson, M.: "Flashing Flow in Hot-Water Geothermal Wells," *J. Research*, USGS (1974) 2, No. 6, 743-751.
10. Gould, T.L.: "Vertical Two-Phase Steam Water Flow in Geothermal Wells," *J. Pet. Tech.* (Aug. 1974) 26, 833-842.
11. Sugiura, T. and Farouq Ali, S.M.: "A Comprehensive Wellbore Steam-Water Flow Model for Steam Injection and Geothermal Applications," paper SPE 7966 presented at the SPE California Regional Meeting, Ventura, April 18-20, 1979.
12. Garg, S.K. and Pritchett, J.W.: "Two Phase Flow in Geopressured Geothermal Wells," *Energy Conversion* (1976) 18, 45-51.
13. Narasimhan, T.N. and Witherspoon, P.A.: "Reservoir Evaluation Tests on RRGE 1 and RRGE 2, Raft River Geothermal Project, Idaho," Report No. LBL-5958, Lawrence Berkeley Laboratory, Berkeley, CA (1977).
14. Holman, J.P.: *Heat Transfer*, McGraw-Hill Book Co. Inc., New York City (1977) 203-207.
15. Harlow, F.H. and Welch, J.E.: "Numerical Calculation of Time-Dependent Viscous Incompressible Flow," *Phys. Fluids* (1965) 8, 2182.

APPENDIX

A numerical model of transient two-phase flow was used to study wellbore flow. A brief outline of the model and its limiting assumptions is given here.

Flow in the well is described by equations for continuity, momentum, and energy (Eqs. 12 through 14). An equation of state also is needed to relate the state variables p, e, and ρ:

$$d\rho = \frac{1}{\rho}\left(\frac{\partial \rho}{\partial E}\right)_p (\rho dE) + \left(\frac{\partial \rho}{\partial p}\right)_E dp. \quad \ldots\ldots\ldots (A\text{-}1)$$

Equilibrium was assumed, so the equation of state was based on the thermodynamic steam/water tables. The friction losses have been written as a friction factor f times $\frac{1}{2}(\rho v^2/r_w)$. For these calculations, the slip between the phases was assumed to be zero and the friction factor was kept constant. Although both slip and friction effects can be important and should be included accurately, they will not alter the physical phenomena being discussed in this paper.

The method of the numerical model is to combine all four equations (Eqs. 12 through 14 and A-1) to obtain an expression for the new pressure. The pressure is solved implicitly. Once the new pressure is known, the value of ρdE is obtained from Eq. 14, and the density can be evaluated using Eq. A-1. Given the new density, the velocity is evaluated using the continuity equation, and the energy is obtained from knowing ρ and ρdE. The state variables are defined at node points, while the velocity is calculated at half-node points. The method used is similar to the pressure method developed for incompressible fluids by Harlow and Welch,[15] except that compressibility has been included.

The finite difference of the continuity equation is

$$\frac{\rho_j^{t+1} - \rho_j^t}{\Delta t} = -\frac{(\rho v)_{j+\frac{1}{2}}^{t+\frac{1}{2}} - (\rho v)_{j-\frac{1}{2}}^{t+\frac{1}{2}}}{\Delta x}, \quad \ldots\ldots (A\text{-}2)$$

where j denotes the node points and t denotes the time level. The equation is written in an implicit fashion to eliminate time-step restrictions. The expression for $(\rho v)^{t+1}$ can be obtained from the momentum equation. The finite difference form of the momentum equation is

$$\frac{(\rho v)_{j+\frac{1}{2}}^{t+\frac{1}{2}} - (\rho v)_{j+\frac{1}{2}}^{t}}{\Delta t} = -\frac{(\rho v^2)_{j+\frac{1}{2}}^{t} - (\rho v^2)_{j-\frac{1}{2}}^{t}}{\Delta x}$$

$$-\rho_{j+\frac{1}{2}} g - f\left(\frac{\rho v_j^2}{4 r_w}\right)^t. \quad \ldots\ldots\ldots\ldots (A\text{-}3)$$

The pressure term is evaluated implicitly to reduce the time restriction imposed by the small compressibility of the fluid, while the advection effects are treated explicitly. If the pressure term were evaluated explicitly, the time restriction would be limited by the propagation of the pressure signal over the finite space difference, approximately $\Delta t < \Delta x/(\partial p/\partial \rho)_s^{\frac{1}{2}}$ or $\Delta t < \Delta x + 3{,}937$ ft/s (1200 m/s) for a liquid. However, the restrictions on the advection are only the order of $\Delta x/v$ where v is the fluid velocity.

The energy equation is finite-differenced as

$$\rho_j\left(\frac{E_j^{t+1} - E_j^t}{\Delta t}\right) = -\rho_j^{t+1} v_{j+\frac{1}{2}}^t \frac{v_{j+\frac{1}{2}}^t - v_{j-\frac{1}{2}}^t}{\Delta x}$$

$$+ 2U\frac{T_r - T_w}{r_w} - \frac{(\rho v E)_j^t - (\rho v E)_{j-1}^t}{\Delta x}. \quad (A\text{-}4)$$

Upwind differencing is used for the advection form.

The expression for flow advection must be altered when the flow is not in the positive direction. The method of solution is to rewrite the density in terms of E and p:

$$\Delta\rho = \frac{1}{\rho}\left(\frac{\partial\rho}{\partial E}\right)(\rho\Delta E) + \left(\frac{\partial\rho}{\partial p}\right)\Delta p. \quad \ldots\ldots\ldots (A\text{-}5)$$

to obtain $(\rho\Delta E)$ from Eq. A-4 and to use Eq. A-5 in the continuity of Eq. A-1. Eqs. A-1 and A-2 then are combined and an expression for the unknown pressure p is determined. The resultant equation is

$$\begin{aligned}
&-(2+r)p_j^{t+1} + p_{j+1}^{t+1} + p_{j-1}^{t+1} \\
&= -rp_j^t + \frac{\Delta x}{\Delta t}\left(\rho v_{j+\frac{1}{2}} - \rho v_{j-\frac{1}{2}}\right)^t \\
&\quad -\left(\rho_{j+\frac{1}{2}} - \rho_{j-\frac{1}{2}}\right)^t g\Delta x - \left(\rho_{j+\frac{1}{2}} v^2_{j+\frac{1}{2}}\right. \\
&\quad \left. -2\rho_{j-\frac{1}{2}} v^2_{j-\frac{1}{2}} + \rho_{j-3/2} v^2_{j-3/2}\right)^t \\
&\quad -f\left(\rho_{j+\frac{1}{2}} v^2_{j+\frac{1}{2}} - \rho_{j-\frac{1}{2}} v^2_{j-\frac{1}{2}}\right)^t \frac{\Delta x}{4r_w} \\
&\quad -\left(\frac{\Delta x}{\Delta t}\right)^2\left(\frac{1}{\rho}\frac{\partial\rho}{\partial E}\right)\rho_j\left(E_j^{t+1} - E_j^t\right),
\end{aligned}$$

where

$$r = \left(\frac{\Delta x}{\Delta t}\right)^2\left(\frac{\Delta\rho}{\partial p}\right)_E.$$

The expression for $E_j^{t+1} - E_j^t$ is obtained from Eq. A-4.

The pressure in the reservoir and the temperature change around the bore are solved using a finite difference of the radial diffusion equation. A grid was generated by using a logarithmic transformation. The pressure was kept constant 4,921 ft (1500 m) from the well while the temperature was maintained at the initial geothermal gradient 19.6 ft (6 m) from the well. The finite difference of the radial diffusion equation used was

$$\frac{p_j^{t+1} - p_j^t}{\Delta t} = \frac{k}{\mu\phi c}\,\frac{2}{(r_{j+1} - r_{j-1})}\left[r_{j+\frac{1}{2}}\left(\frac{p_{j+1} - p_j}{r_{j+1} - r_j}\right) - r_{j-\frac{1}{2}}\left(\frac{p_j - p_{j-1}}{r_j - r_{j-1}}\right)\right].$$

SI Metric Conversion Factors

cp	×	1.0*	E−03	= Pa·s
cu ft	×	2.831 685	E−02	= m^3
°F		(F−32)/1.8		= C
ft	×	3.048*	E−01	= m
lbm	×	4.535 924	E−01	= kg
psi	×	6.894 757	E+00	= kPa

*Conversion factor is exact.

SPEJ

Original manuscript received in Society of Petroleum Engineers office July 2, 1979. Paper accepted for publication April 4, 1980. Revised manuscript received Sept. 14, 1980. Paper (SPE 8203) first presented at the SPE 54th Annual Technical Conference and Exhibition, held in Las Vegas, Sept. 23-26, 1979.

SPE

Society of Petroleum Engineers of AIME

SPE 8231

A PARALLELEPIPED MODEL TO ANALIZE THE PRESSURE BEHAVIOR OF GEOTHERMAL STEAM WELLS PENETRATING VERTICAL FRACTURES

by Heber Cinco-Ley, Member SPE-AIME, W.E. Brigham, M. Economides, F.G. Miller, and H.J. Ramey Jr., Stanford Univ.; A. Lorelli and G. Manetti, ENEL

ABSTRACT

Reservoir geometry is often the basis for development of models used to analyze field transient pressure data. The presence of a deep horizontal steam-water interface or boiling front first gave rise to the idea of a constant pressure boundary. Faults suggest vertical no-flow boundaries, and impermeable rocks overlying the steam zone indicate a no-flow cap.

In the past, parallelepiped models have been used to analyze the results of predesigned buildup and well interference tests. The model described herein is of more general use, and can be used to analyze long-term pressure-production well data. In this study, it is applied to analyze pressure data of a drawdown test for a geothermal reservoir.

As in earlier models, the boiling front is assumed to be a constant fluid-pressure boundary, and the sides --as well as the top--are assumed to be impermeable boundaries. Equations of reservoir pressure behavior are derived using Green's functions and source functions. Graphs describing dimensionless pressure as a function of time and various reservoir parameters are provided. Partially penetrating fractures common to many geothermal well systems are considered in the development of the model.

INTRODUCTION

Many geothermal areas are characterized by reservoirs whose dimensions are controlled by sealing faults or low permeability boundaries. Some of these reservoirs produce steam diluted with small quantities of noncondensable gases. There is often evidence of boiling water at a considerable distance from the producing horizon (presumably lying below the steam cap). In addition, the transient pressure behavior of these wells sometimes indicates they intersect large, high conductivity fractures. These are natural fractures; no hydraulic fracturing has been done in any of these wells.

This general description leads naturally to a model in the shape of a parallelepiped with closed boundaries on five sides and a constant pressure boundary on the bottom. The fracture intersecting the well can be simulated as a rectangular-shaped source or sink. Such a system was described by Atkinson et al.[1] for a limited set of geometric conditions which approximated the producing system in the Travale area, in Italy. Because of the success of this approach, personnel at Stanford University and at ENEL, in Pisa, have developed general programs for generating long-term pressure-production forecasts for a variety of parallelepiped conditions and well-fracture geometries. This approach appears to be generally useful, for many geothermal systems worldwide will have fault-controlled geometry of the type described here.

The purpose of this work is to determine which unique characteristics of such systems can be identified. This, in turn, will lead to greater confidence in predictions of the long-range producing characteristics of these systems.

DESCRIPTION OF THE MODEL

Let us consider a well intersected by a vertical fracture in a parallelepiped reservoir, as shown in Fig. 1. The system is bounded laterally by vertical impermeable planes; the top of the reservoir is a horizontal no-flow boundary, and underlying the reservoir there is a constant pressure plane.

The general assumptions for this model are as follows:

1) The well produces at a constant flowrate in an anisotropic, homogeneous reservoir of constant properties (k and ϕ are independent of pressure and temperature).

2) The reservoir contains a slightly compressible fluid of constant viscosity, μ, and compressibility, c. Although this assumption is not valid, there is considerable evidence that it is a good approximation for gaseous systems when the m(p) function is used.

3) There are small pressure gradients and negligible gravity effects in the reservoir.

References and illustrations at end of paper

4) Well fluid production is via a vertical fracture which partially penetrates the reservoir. The top of the fracture can be located at any elevation and the fracture can extend to any depth.

5) The initial pressure, p_i, is the same throughout the reservoir.

Although the fracture can be located anywhere in the reservoir and the reservoir dimensions can be chosen arbitrarily (the Barelli and Manetti model), the only cases studied in this paper are those in which the fracture is located in the center of a parallelepiped reservoir of square horizontal cross-section, with the fracture oriented parallel to two of the vertical boundaries (Fig. 2).

As shown by Gringarten and Ramey, the pressure drop in a reservoir with any boundary conditions can be expressed as:

$$\Delta p = \frac{1}{\phi c_t} \int_0^t S(x,y,z,\tau)\, d\tau \qquad (1)$$

where $S(x,y,z,\ )$ represents the source function for the particular reservoir-well system. The term S depends on both the geometry and the boundary conditions of the system. The appendix shows the derivation of the source function for the parallelepiped model considered in this study.

The dimensionless pressure drop at any point in the reservoir can be given by either of the two following equations:

$$p_D(x_D,y_D,z_D,x_{De},y_{De},h_D,h_{fD},z_{fD},t_{Dxf}) = \frac{\pi}{8}\frac{h_D}{h_{fD}} \int_0^{t_{Dxf}} \frac{1}{\sqrt{\tau}} \left\{ \sum_{n=-\infty}^{\infty} e^{-\frac{(y_D-2ny_{De})^2}{4\tau}} \right\} \left\{ \sum_{n=-\infty}^{\infty} \left[\operatorname{erf} \frac{x_D-2nx_{De}+1}{2\sqrt{\tau}} + \operatorname{erf} \frac{x_{fD}-2nx_{De}-1}{2\sqrt{\tau}} \right] \right\}$$

$$\left\{ \sum_{n=-\infty}^{\infty} \left[- \operatorname{erf} \frac{z_D + \frac{h_{fD}}{2} + z_{fD} + 4nh_D}{2\sqrt{\tau}} - \operatorname{erf} \frac{-z_D + \frac{h_{fD}}{2} - z_{fD} - 4nh_D}{2\sqrt{\tau}} + \operatorname{erf} \frac{z_D - \frac{h_{fD}}{2} - z_{fD} + 4nh_D}{2\sqrt{\tau}} + \operatorname{erf} \frac{\frac{h_{fD}}{2} - z_D + z_{fD} - 4nh_D}{2\sqrt{\tau}} + \operatorname{erf} \frac{z_D + \frac{h_{fD}}{2} + z_{fD} + 4nh_D - 2h_D}{2\sqrt{\tau}} + \operatorname{erf} \frac{-z_D + \frac{hf_D}{2} - z_{fD} - 4nh_D + 2h_D}{2\sqrt{\tau}} - \operatorname{erf} \frac{z_D + \frac{hf_D}{2} - 2h_D - z_{fD} + 4nh_D}{2\sqrt{\tau}} - \operatorname{erf} \frac{\frac{hf_D}{2} - z_D + 2h_D + z_{fD} - 4nh_D}{2\sqrt{\tau}} \right] \right\} d\tau \qquad (2)$$

Or, alternatively:

$$p_D(x_D,y_D,z_D,x_{De},y_{De},h_D,h_{fD},z_{fD},t_D) = \frac{4h_D}{h_{fD}y_{De}x_{De}} \int_0^{t_{Dxf}} \left[1 + 2\sum_{n=1}^{\infty} e^{-\frac{n^2\pi^2\tau}{y_{De}^2}} \cos\frac{n\pi y_D}{y_{De}} \right] \left[1 + \frac{2x_{De}}{\pi}\sum_{n=1}^{\infty} e^{-\frac{n^2\pi^2\tau}{x_{De}^2}} \cos\frac{n\pi x_D}{x_{De}} \sin\frac{n\pi}{x_{De}} \right] \left[\sum_{n=1}^{\infty} \frac{e^{-\frac{(2n-1)^2\pi^2\tau}{4h_D^2}}}{(2n-1)} \sin\frac{(2n-1)\pi h_{fD}}{4h_D} \sin\frac{(2n-1)\pi z_{fD}}{2h_D} \sin\frac{(2n-1)\pi z_D}{2h_D} \right] d\tau \qquad (3)$$

where the dimensionless terms in the equations are defined as follows:

$$p_D = 1.291\times10^{-2}\ \frac{h\sqrt{k_x k_y}\,h\,(p_i^2-p_{wf}^2)}{zTqu}$$

$$t_{Dxf} = 0.3604\ \frac{k_x t}{\phi\mu c_t x_f^2}$$

$$x_D = \frac{x}{x_f}\ ;\ y_D = \frac{y}{x_f}\sqrt{\frac{k_x}{k_y}}\ ,\ x_D = \frac{z}{x_f}\sqrt{\frac{k_x}{k_y}}$$

$$x_{De} = \frac{x_e}{x_f}\ ;\ y_{De} = \frac{y_e}{x_f}\sqrt{\frac{k_x}{k_y}}\ ;\ h_D = \frac{h}{x_f}\sqrt{\frac{k_x}{k_z}}$$

$$h_{fD} = \frac{h_f}{x_f}\sqrt{\frac{k_x}{k_z}}\ \text{and}\ z_{fD} = \frac{z_f}{x_f}\sqrt{\frac{k_x}{k_z}} \qquad (4)$$

Although Eqs. 2 and 3 are equivalent, Eq. 2 is the better for calculations of dimensionless pressure drop at small values of time, and Eq. 3 better for large values of time. These solutions obtained are valid for both anisotropic and isotropic reservoirs according to Eq. 4.

Wellbore Pressure Behavior

A computer program was written to calculate the pressure drop at any point in the system, at any dimensionless time, $t_{D_{xf}}$. Several runs were made by considering different values of dimensionless formation thickness, h_D, fracture penetration ratio, x_e/x_f, and dimensionless fracture height, h_f/x_f. The dimensionless formation thickness varies from 2 to 20, the fracture penetration goes from 2 to 10, and the fracture height is assumed to be unity.

Figures 3 through 6 show a log-log graph of p_D/h_D versus $t_{D_{xf}}$ for the cases mentioned above. The wellbore pressure was calculated at the locations recommended by Cinco et al.[4] for the case of a partially penetrating well (i.e., $y_D = 0$, $x_D = 0.732$, and $z_D = z_{f_D} = 0.232$).

All cases exhibit a unique one-half straight line for small values of time. This behavior is caused by the linear flow behavior in the vicinity of the fracture. The equation for wellbore pressure during this early time period can be derived from Eq. 2 by using the short-time approximation of the error functions.

$$p_D(t_{D_{xf}}) = \sqrt{\pi t_{D_{xf}}}\ h_D$$

for $t_{D_{xf}} \leq 0.016$*

*According to Gringarten et al.[4]

At large values of time, the wellbore pressure drop stabilizes indicating steady-state flow in the system. Figure 7 presents the stabilized value of pressure drop as a function of both fracture penetration x_e/x_f and dimensionless formation thickness.

Figures 3 through 5 show that over a large region of the graph the curves for pressure response at a fractured well in a parallelepiped reservoir are similar in slope to the infinite conductivity vertical fracture solution for an infinite reservoir.

Figure 8 is a graph of dimensionless wellbore pressure versus the logarithm of dimensionless time. This graph clearly indicates that these systems do not exhibit the characteristic semilog straight line portion of the pressure versus log time relationship arising from conventional methods of analysis for radial flow.

The fracture penetration ratio has a strong effect on the transient pressure behavior in a parallelepiped reservoir, as shown by Fig. 9. A higher penetration produces a higher pressure drop, because of a smaller porous volume in the system.

Figure 3 shows that when the fracture penetration ratio is high, type-curve analysis methods can be applied to determine the dimensionless formation thickness and the characteristics of the formation and fracture. However, in a case for a low-fracture penetration ratio (Fig. 6), type-curve analysis may not give a unique answer for dimensionless formation thickness because the curves for different cases are too close together to give a good match.

The effect of dimensionless formation thickness on pressure behavior is shown in Figs. 3 through 6. Pressure response for a thick formation is high because the effect of the constant pressure boundary occurs late in dimensionless time.

As mentioned, a large portion of the curves for different cases are similar in shape during early and intermediate time, to the infinite conductivity vertical fracture solution. However, these solutions will provide completely different results from type-curve analysis. When analyzing pressure data for a fractured well in a parallelepiped reservoir, the infinite conductivity solution gives large estimates of permeability as well as low estimates for fracture length.

Although in this work only drawdown solutions are presented, they can be extended to produce both buildup and multiflow rate solutions by using the principle of superposition.

EXAMPLE OF APPLICATION

Flowing wellhead pressure was measured in a dry steam well during a period of two years. The flowing bottomhole pressure and additional well and reservoir information are given in Table 1.

Figure shows a log-log graph of pressure squared difference versus flow time. The pressure data on this figure show the characteristic features of the behavior of a fractured well in a parallelepiped reservoir: early data approach a one-half slope straight line, and the late portion of the

pressure data seems to reach a stabilized value. Figure 11 also shows the application of the type-curve matching technique for this case. The following match points are obtained:

$$(p_i^2-p_{wf}^2) = 10^2 \quad [K_g/cm^2]^2 \; ; \; p_D/h_D = 0.3$$

$$t = 1 \text{ day} \; ; \; t_{Dx_f} = 0.26$$

and

$$h_D = 10$$

From Table 1 and the definition of dimensionless pressure drop:

$$p_D = \left(\frac{p_D}{h_D}\right) \cdot h_D = 0.3 \times 10 = 3$$

$$3 = \frac{1.291\times10^{-2}(18)(k_x k_y)^{1/2} \; x_f\sqrt{\frac{k_z}{k_x}} \; (10^2)}{(0.85)(553)(205)(0.019)}$$

$$\therefore (k_z k_y)^{1/2} x_f = 23.63 \text{ darcy-meters}$$

From the definition of dimensionless time:

$$0.26 = \frac{0.3604(k_x)(1)\times24}{(0.16)(0.019)(0.0)x_f^2}$$

$$\therefore \frac{k_x}{x_f^2} = 9.138\times10^{-7} \text{ darcy/m}^2$$

Evidently,

$$k_x k_y k_z = [(k_z k_y)^{1/2} x_f]^2 \left(\frac{k_x}{x_f^2}\right) = (23.63)^2 (9.138\times10^{-7})$$

$$= 5.1\times10^{-4} \text{ darcy}^3$$

$$\sqrt{k_x k_y k_z} = 0.0799 \text{ darcy}$$

If $k_x = k_y = k_z = k$,

$$k = 0.0799 \text{ darcy}$$

$$x_f = 295 \text{ meters}$$

and

$$h = 2950 \text{ meters}$$

CONCLUSIONS

From the analysis of the results obtained in this work, the following conclusions may be drawn:

1) The pressure behavior of a fractured well in a parallelepiped reservoir exhibits several flow periods.

2) Initially, a linear flow dominates the behavior of the system.

3) At later times, side boundary effects are felt through an increasing rate of pressure decline.

4) At large values of time, steady-state flow is established; as a consequency, the wellbore pressure remains constant.

5) Type-curve analysis can be applied to determine the constant pressure boundary depth whenever the fracture penetration is high.

6) Although the early and intermediate time behavior of infinite conductivity vertical fracture solutions is similar to the behavior of a fractured well in a parallelepiped reservoir, results from type-curve analysis for both cases are different.

7) The parallelepiped model seems to be adequate for dry steam reservoirs with a water steam surface.

NOMENCLATURE

c = isothermal compressibility, cm^2/Kg

h = formation thickness, m

h_f = fracture height, m

k = permeability, darcies

M = molecular weight, gr/gr mole

p = pressure, Kg/cm^2

p_i = initial pressure, Kg/cm^2

p_{wf} = flowing bottomhole pressure, Kg/cm^2

q = mass flowrate, ton/hr

S = source function

t = time, hrs

T = reservoir temperature, °K

x = distance in x-direction, m

x_f = half-fracture length, m

x_e = boundary location in x-direction, m

y = distance in y-direction, m

y_e = boundary location in y-direction, m

z = distance in z-direction, m

z_f = elevation of midpoint of fracture, m

Z_i = gas deviation factor, dimensionless

μ = viscosity, cp

ϕ = porosity, fraction

Subscripts

D = dimensionless

e = external

f = fracture

i = initial

w = wellbore

t = total

Special Functions

$$\mathrm{erf}(x) = \frac{2}{\sqrt{\pi}} \int_0^x e^{-\eta^2} d\eta$$

ACKNOWLEDGEMENT

This work was developed under Contract ENEL 1673600 through the Department of Energy.

REFERENCES

1. Atkinson, P., Barelli, A., Brigham, W.E., Celati, R., Manetti, G., Miller, F.G., Neri, G., and Ramey, H.J., Jr.: "Well Testing in Travale-Radicondoli Field," Proc., ENEL-ERDA Workshop, Larderello, Italy, Sept. 12-16, 1977, 1-75.

2. Al-Hussainy, R., Ramey, H.J., Jr., and Crawford, P.B.: "The Flow of Real Gases Through Porous Media," J. Pet. Tech. (May 1966), 624-636; Trans., AIME ( )___, 232.

3. Gringarten, A.C., and Ramey, H.J., Jr.: "The Use of Source and Green's Functions in Solving Unsteady Flow Problems in Reservoirs," Soc. Pet. Eng. J. (Oct. 1973), 285-296; Trans., AIME (255,

4. Cinco-Ley, H., Ramey, H.J., Jr., and Miller, F.G.: "Unsteady-State Pressure Distribution Created by a Well with an Inclined Fracture," Paper SPE 5591, presented at the 50th Annual Fall Meeting, SPE of AIME, Dallas, Texas, Sept. 28-Oct. 1, 1975.

5. Gringarten, A.C., Ramey, H.J., Jr., and Raghavan, R.: "Pressure Analysis for Fractured Wells," Paper SPE 4051, presented at the 47th Annual Fall Meeting, SPE of AIME, San Antonio, Texas, Oct. 8-11, 1972.

TABLE 1

DRAWDOWN TEST DATA

Flowrate, q, Ton/hr	205	Porosity, ϕ, fraction	0.16
Viscosity, μ, cp	0.019	Reservoir temperature, T, °K	553
Gas deviation factor, Z	0.85	Molecular weight, M, lb/lb-mole	18
Compressibility, c_t, $(Kg/cm^2)^{-1}$	0.01	Initial pressure, p_i, Kg/cm^2	55

t (days)	$(p_i^2-p_{wf}^2)(Kg/cm^2)^2$	t (days)	$(p_i^2-p_{wf}^2)(Kg/cm^2)^2$
1	188	90	788
2	228	100	828
3	253	120	871
4	271	140	927
5	287	160	982
6	305	180	1032
7	318	200	1066
8	330	240	1134
9	343	280	1174
10	352	320	1205
15	401	360	1233
20	441	400	1254
25	478	440	1263
30	503	480	1279
35	534	520	1288
40	562	560	1297
45	587	600	1304
50	618	640	1307
60	664	680	1310
80	747	720	1310

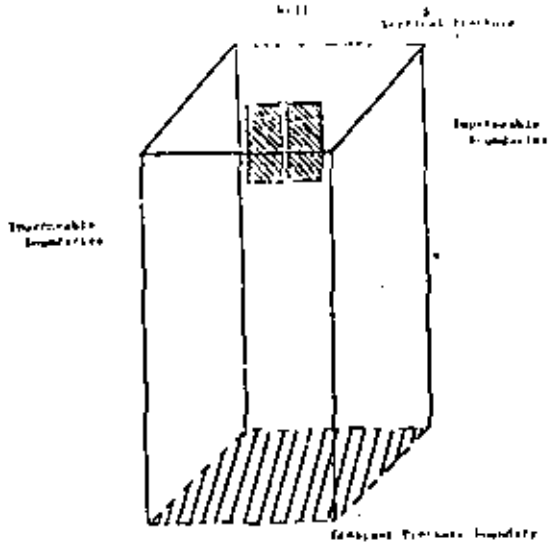

Fig. 1 - Fractured well in a parallelepiped reservoir.

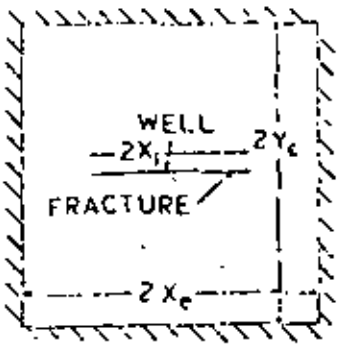

Fig. 2 - Fractured well in the center of a square parallelelpiped reservoir.

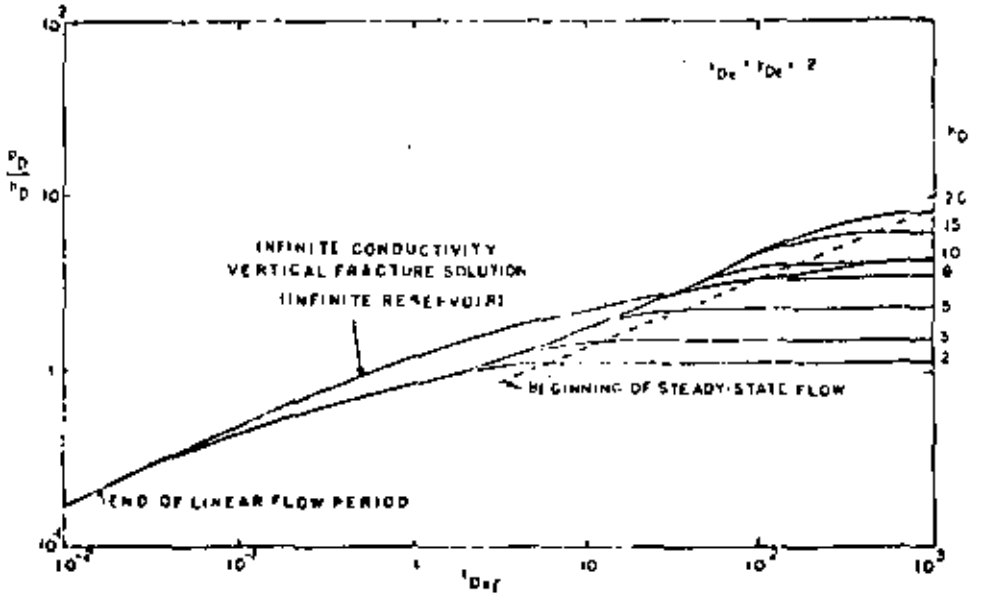

Fig. 3 - Log p_D/h_D vs log t_{Dx_f} for a fractured well in a parallelepipec reservoir ($x_e/x_f = 2$).

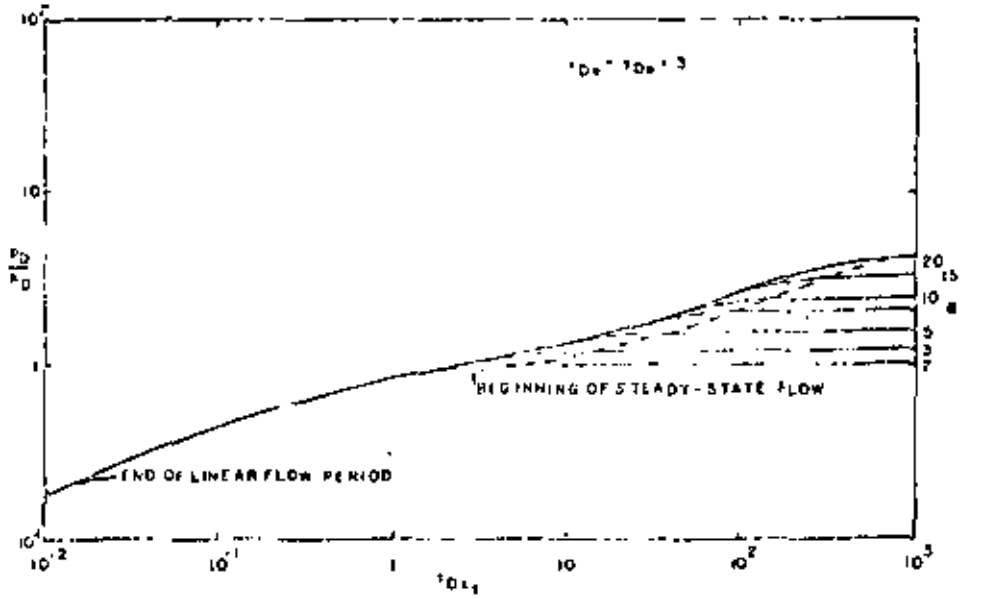

Fig. 4 - Log p_D/h_D vs log t_{Dx_f} for a fractured well in a parallelepiped reservoir ($x_e/x_f = 3$).

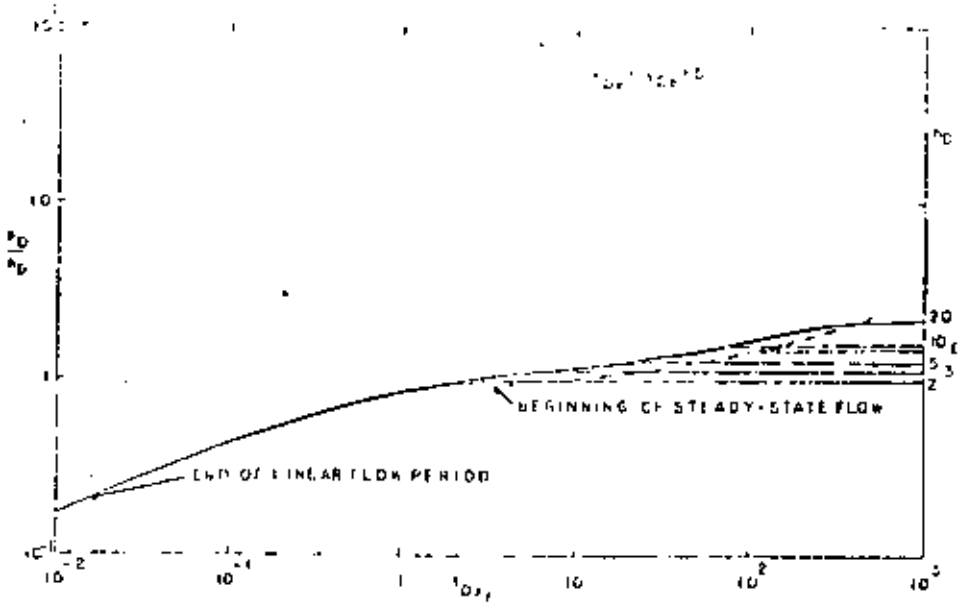

Fig. 5 - Log p_D/q_D vs log t_{Dx_f} for a fractured well in a parallelepiped reservoir ($x_e/x_f = 5$).

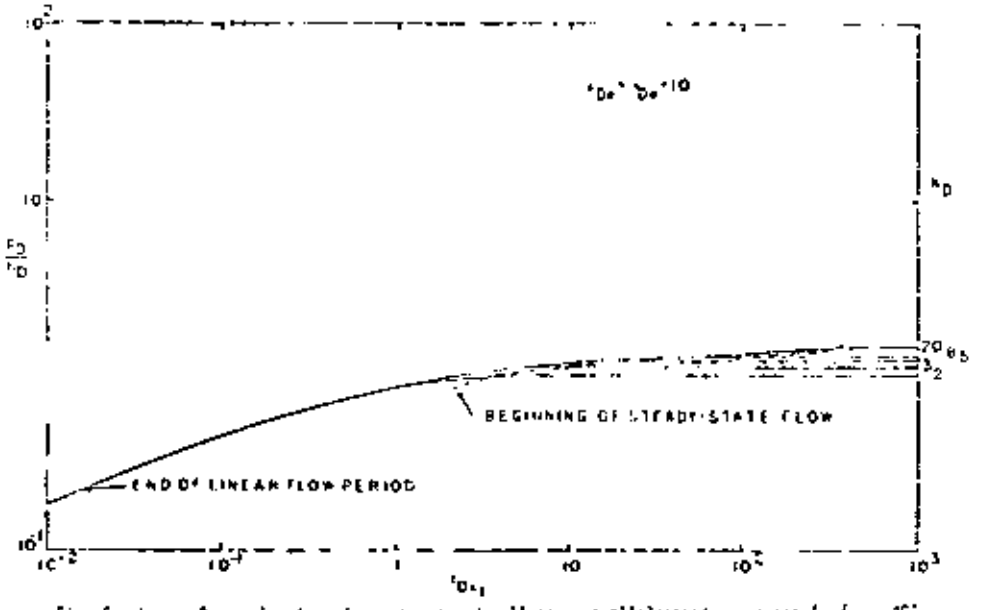

Fig. 6 - Log p_D/h_D vs log t_{Dx_f} for a fractured well in a parallelepiped reservoir ($x_e/x_f = 10$).

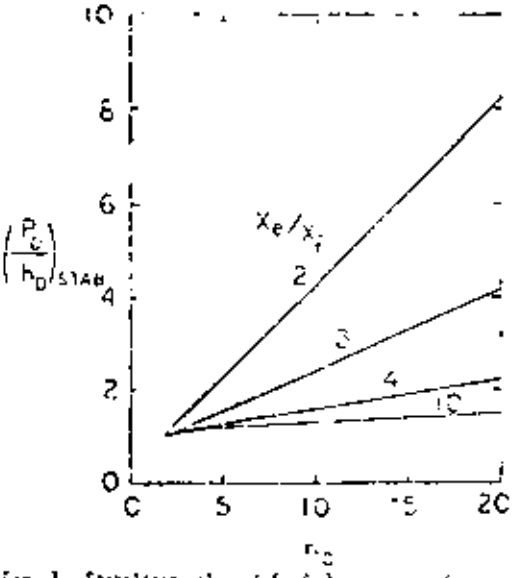

Fig. 7 - Stabilized value of (p_D/q_D) vs r_D as a function of x_e/x_f.

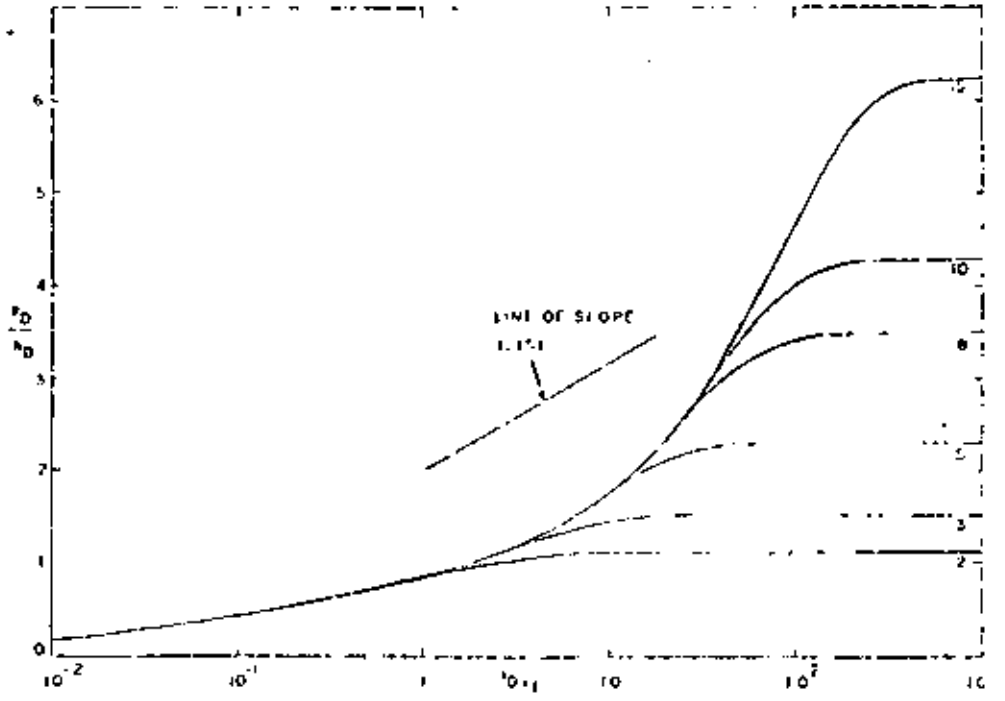

Fig. 8 - p_D/q_D vs log t_{Dx_f} for a fractured well in a parallelepiped reservoir ($x_e/x_f = 2$).

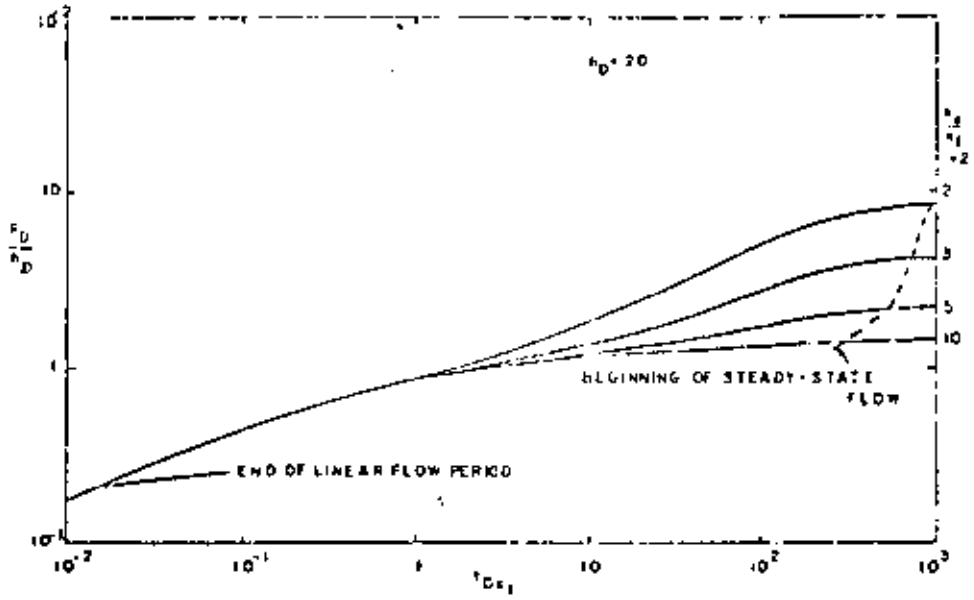

Fig. 9 – Log p_D/p_D' vs t_{Dx_f} for a fractured well in a parallelepiped reservoir (h_D = 20).

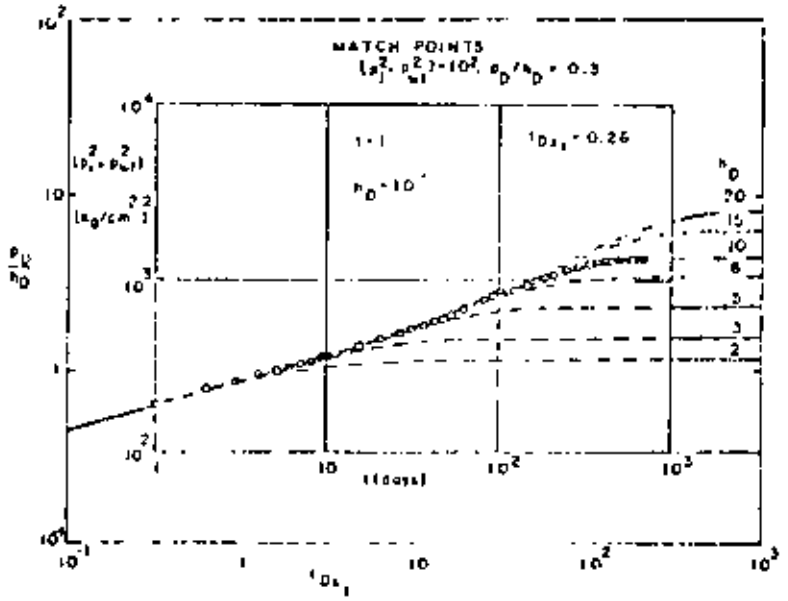

Fig. 10 – Type curve matching for example 1

Pressure Transient Analysis for Geothermal Wells

HENRY J. RAMEY, JR.
Stanford University, Stanford, California 94305, USA

ABSTRACT

Throughout the geothermal literature, concern has been expressed many times about the potential effect of precipitation of solids at the wellbore face, throughout the drainage region of a geothermal well, and about the periphery of a geothermal reservoir as cold recharge fluid contacts the warmer geothermal fluids. Many field observations indicate such concern. For example, it is well known that steam wells in Larderello, Italy, decline in rate during production, and have an active life of about 12 years. Similar declines in production rate are often observed in the production histories of gas and oil wells. For this reason, the specialty of pressure transient analysis has been developed to aid determination of the reason for such rate decline. In addition to precipitation or plugging of the porous media near the well face, other reasons for decline in producing rates include a decrease in the formation pressure and low initial formation permeability. A review of the history of pressure transient analysis and applications to geothermal wells are presented in this paper.

INTRODUCTION

Throughout the geothermal literature, much concern has been expressed regarding potential precipitation of solids at the wellbore face, throughout the drainage volume of a geothermal well, or at the periphery of the drainage volume where recharging cold fluid meets the hot geothermal reservoir. The potential damage to the productivity of a geothermal well, not to mention the reservoir proper, is the main reason for such concern. Similar concern for decline in productivity or for low producing rates of gas and oil wells, has been evident in the petroleum literature of the United States almost from the time of the drilling of the Drake well in Pennsylvania in 1859. Within ten years of that time patents aimed at improving the producing characteristics of oil wells began to appear.

[redacted]. The purposes of pressure-transient analysis include the following: (1) determination of the condition of the well, that is, whether the sand face at the wellbore is damaged or has been stimulated; (2) the quantitative value of the permeability in the drainage volume of the well; (3) the mean formation pressure; and (4) quantitative information concerning the shape and size of the drainage volume and its porosity. Quantitative information on the preceding four items obviously would furnish answers to questions such as: is the low productivity of a given well due to plugging of the well, low formation permeability, or a low driving force and/or formation capacity available for moving fluid into the well? This information would provide a sound basis for decisions involving costly stimulation of a well, or perhaps other operating procedures.

Quantitative tools have been available for performing such tasks since the early 1950's. In view of the potential importance of this information, it is worth considering why it has not been used to much extent to date. There are several reasons, one being a mistaken impression in geothermal circles that oil reservoir engineering can be applied only to closed systems not subject to water recharge. Another reason pertinent to pressure-transient analysis is a widespread belief common in both geothermal and petroleum scientific communities: that the simplifying assumptions common to most analytical solutions are not applicable to real, nonideal reservoirs—particularly fractured reservoirs. This belief is logical, but largely not correct. [redacted] Many fractured systems have been found to behave like ideal homogeneous systems with, at most, simple anisotropy.

We now turn to a brief review of the history of the development of pressure-transient analysis to provide a bridge to the current state of this technology.

HISTORY

In the petroleum literature alone more than 300 technical papers have been published on the subject of pressure-transient analysis in the past 45 years. A similar number of publications exists on pump test analysis in the field of ground-water hydrology. This literature has developed because the pressure behavior of a well is easily measured, and is a highly useful quantity. Instruments for measuring maximum pressures in oil wells were developed and used in the United States during the early 1920's (Carter, 1961). These devices included bourdon tube gauges which would record via a stylus mark on a blackened metal sheet, and the measurement of liquid levels in wells utilizing floats or sonic echoes. By 1931 continuously recording instruments, such as the Amerada and Humble and MacDonald gauges, were available (Millikan and Sidwell, 1931).

One of the early applications for bottom-hole pressures in wells was a measurement of the "static" formation pressure. After a well had been closed in for a period of time such as 24 to 72 hours, a bottom-hole pressure measurement was made as an indication of the static formation

pressure. These static measurements indicated the formation pressure in permeable, high-productivity reservoirs. Engineers soon recognized that static pressure measurements depended greatly upon the closed-in time. The lower the permeability, the longer the time required for the pressure in the well to stabilize. This led to the important realization that when a well was closed in, the duration of the pressure build-up was a reflection of the permeability of the reservoir rock around that well. It appears that one of the first determinations of formation permeability for pressure-transient data was published by Moor, Schilthuis, and Hurst in 1933. Many papers concerning pressure transients caused by water influx into oil reservoirs began to appear in the following years.

A classic study of pressure-transient analysis involved in the pump testing of water wells was published by Theis in 1935. Among other things, Theis discussed analysis of pressure recovery data. Pressure recovery data are referred to as pressure build-up data in petroleum engineering, and consist of information obtained after a well had produced at a constant rate for a period of time, and was then shut in and its pressures allowed to equalize. Theis suggested a form of graphing and analysis which remains one of the basic techniques employed in petroleum engineering to this day. The method was discovered independently some fifteen years later by Horner. The Theis pressure recovery graph of ground-water hydrology is known as the Horner pressure build-up graph in petroleum engineering. Horner did introduce the important concept of estimating the mean formation pressure which would be obtained in an enclosed reservoir system at an infinite shut-in time.

In 1937, Muskat introduced a graphical method for determining the ultimate static formation pressure from bottom-hole pressure-transient data. [illegible] engineering that had [illegible] digital computers [illegible].

During the 1940's there were many classic studies. Many important papers appeared as Geological Survey water supply papers. Notable are publications by Wenzel in 1942, and Cooper and Jacob in 1946. Jacob also prepared a classic chapter in the book edited by Rouse, on engineering hydraulics, in 1950. Because the readership of this paper is apt to be familiar with publications in ground-water hydrology in the geophysical, geological, and civil engineering literatures, the main emphasis in this paper will be on publications in the specific area of petroleum engineering. Also notable in the 1940's was a publication by Elkins in 1946, which presented graphs for interference analysis similar to those used today, and publications by Arps and Smith in 1949 dealing with pressure build-up, and a classic study by Van Everdingen and Hurst in 1949. The Van Everdingen and Hurst study presented applications of the Laplace transformation for solving transient flow problems in reservoirs. The main application stressed was estimation of transient water influx (water recharge) into oil reservoirs. However, the authors did discuss applications to pressure-transient analysis for individual wells during presentation of the material in the late 1940's. It is clear that many researchers were investigating quantitative analysis of pressure transient data in the late 1940's.

WELL TESTING FROM 1950 TO 1966

In 1950, two separate publications appeared which are generally recognized as providing the fundamental basis for modern well test analysis. These included the paper by Horner, and the paper by Miller, Dyes, and Hutchinson. The Miller, Dyes, Hutchinson study indicated that static pressures during pressure build-up should be graphed vs the logarithm of the shut-in time. On the other hand, Horner study indicated that static build-up pressure should be graphed versus the logarithm of a time ratio involving the sum of the producing time plus the shut-in time, divided by the shut-in time. Both graphs were reported to produce straight lines, the slope of which was inversely proportional to the formation permeability by precisely the same relation. Confusion between the validity of the results of these two methods remains to this date, despite the fact that Ramey and Cobb (1971) showed that the Horner (or Theis) graph was generally the most reliable.

Figure 1 presents a Miller-Dyes-Hutchinson graph for a well in the center of a square whose outer boundary is subject to a full recharge, that is, constant pressure (Ramey, Kumar, and Gulati, 1973). Dimensionless build-up pressures are graphed vs dimensionless shut-in time. The dimensionless producing time prior to shut-in is shown as a parameter. The dimensionless groups are defined as follows:

$$p_{D_s} = \frac{kh(p_i - p_{ws})}{0.4568 r_w q B \mu}, \text{ for liquid flow} \quad (1)$$

$$p_{D_s} = \frac{Mkh(p_i^2 - p_{ws}^2)}{0.2789\, q \mu\, ZT}, \text{ for flow of steam or gas} \quad (2)$$

$$t_D = \frac{0.3604\, kt}{\phi \mu c_t r_w^2} \quad (3)$$

$$t_{DA} = \frac{0.3604\, kt}{\phi \mu c_t A} = t_D (r_w^2/A) \quad (4)$$

Identification of symbols and units is presented in Table 1. A delta symbol before the symbol t for time indicates a period of time Δt after the producing period of time t.

Graphs similar to Figure 1 may be found for many different well drainage shapes, for wells located at almost any position within the shape, and with any combination of closed or recharge boundaries on the shape. See Ramey, Kumar, and

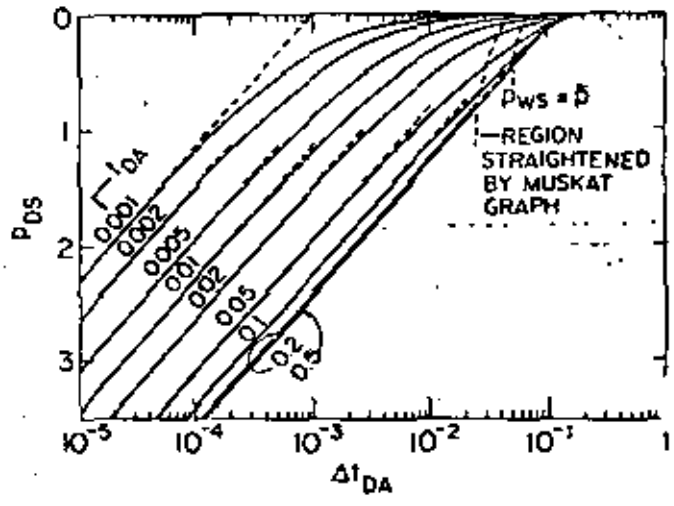

Figure 1. Miller-Dyes-Hutchinson graph for a well in the center of a constant-pressure square.

Table 1. Nomenclature.

Symbol	Meaning
k	= effective permeability to flowing phase, darcies
h	= net formation thickness, m
p	= pressure, kg/cm²
v_s	= specific volume at standard conditions, cc/gm
q	= production rate, tons/hr (1000 kg/hr)
B	= formation volume factor, reservoir volumes/std volume
μ	= viscosity of flowing fluid, centipoise
M	= molecular weight, gm/gm-mole
Z	= real gas law deviation factor ($pv = ZnRT$)
n	= gm moles
R	= 84.78 (cu cm-kg/cm²)/(moles-°K)
T	= absolute formation temperature, °K
p_D	= dimensionless pressure
t_D	= dimensionless time
ϕ	= porosity, fraction of bulk volume
c_t	= total system effective isothermal compressibility, $(kg/cm^2)^{-1}$
r	= radial distance from a constant rate well, m
r_w	= well radius, m
A	= drainage area, m²
t	= time, hr
m	= slope of semi-log graph, (kg/cm²)/log cycle for liquid; $(kg/cm^2)^2$/log cycle for gases
s	= skin effect, dimensionless
Δp_{skin}	= see Eq. 10
FE	= flow efficiency, see Eq. 11
p^*	= Horner's false pressure at $(t + \Delta t)/\Delta t = 1$
C_D	= dimensionless storage constant, see Eqs. 13 and 14
C	= wellbore storage, tons/(kg/cm²) See Eq. 13
C'	= wellbore storage, tons/$(kg/cm^2)^2$ See Eq. 14
x_e	= half length of side of square enclosing a vertically fractured well, see Fig. 11, m
x_f	= vertical fracture length from center of well to tip of fracture, m
r_f	= horizontal fracture radius, m
$\bar{p}$	= volumetric average pressure within drainage region resulting from constant-rate production for a time t
r_D	= dimensionless radius, r/r_w
c_g	= isothermal compressibility of gas, $(kg/cm^2)^{-1}$
Subscripts	
w	= bottom hole, well
t	= surface
s	= static (zero surface production rate)
f	= flowing
r	= radial dimension
z	= vertical dimension
D	= dimensionless
f	= fracture
A	= based on drainage area A
i	= initial
1 hr	= at one hour on semi-log straight line or its extension

Gulati, 1973. The parallel straight lines in the lower left-hand portion of Figure 1 possess a slope inversely proportional to the effective permeability to the flowing phase, or to the total mobility (k/μ) for all phases flowing in the case of multiphase flow (Matthews and Russell, 1967). The relationship between the slope and the permeability is:

$$k = 0.5258 \frac{v_w q B \mu}{mh}, \text{ for liquids} \qquad (5)$$

$$k = (0.3210) \frac{q\mu ZT}{mh M}, \text{ for steam or gases} \qquad (6)$$

The slope m has units of pressure per log cycle for liquids, and pressure squared per log cycle for steam. Figure 1 may also be used to find both the mean pressure $\bar{p}$ and the recharge pressure p_r.

Figure 2 is a general Horner graph for a well in the center of a constant pressure square (full recharge). An infinitely long shut-in would cause a time ratio of unity, and a dimensionless buildup pressure p_{DS} of zero because the well would return to the initial pressure p_r on the recharge boundary. The parallel lines on the lower right-hand portion of Figure 2 bear the same relationship between slope and permeability as given previously by Eqs. (5) and (6). The build-up lines appear to move to the right as producing time prior to shut-in increases. The static pressure within the drainage region at the shut-in time can also be found from the dashed line.

Figure 3 presents a Horner-type graph for a well in a closed square—a depletion case. One distinct difference from the previous figure is that the lines appear to move downwards, rather than to the right. This behavior is a characteristic difference between closed and water-drive shapes which can be identified from series of pressure measurements with longer producing time

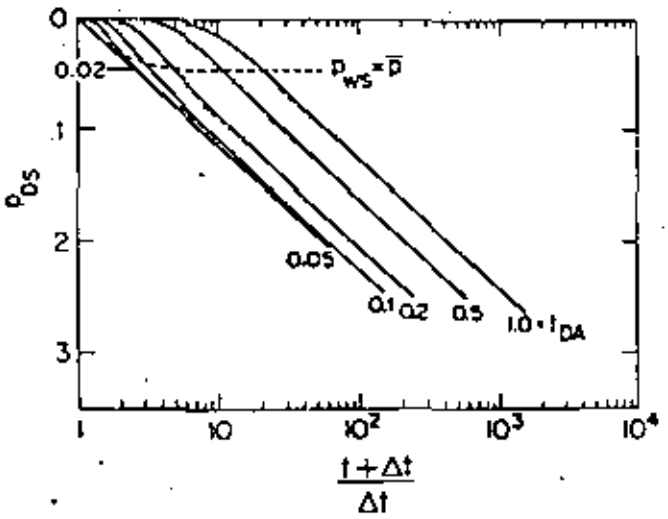

Figure 2. Horner graph for a well in the center of a constant-pressure square.

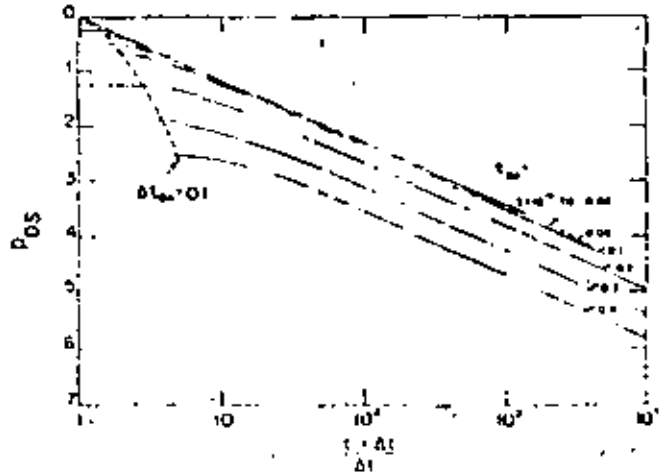

Figure 3. Horner graph for a well in the center of a closed square.

Another important use of Figures 2 and 3 is estimation of the porosity. If the initial pressure p_i is known, field values of p_{DS} can be calculated from:

$$p_{DS} = \frac{p_i - p_{ws}}{0.87m} \quad (7)$$

Because the time ratio for the field data and the dimensionless time ratios are the same, field data can be graphed on either Figures 2 or 3 (or other appropriate figures for other shapes) and the value of the dimensionless producing time, t_{DA}, read as a parameter. From Eq. (4), $\phi c_t/A$ can be calculated because k should be known from the slope of the normal build-up graph. In the event that the thickness, h, is not known, then $\phi c_t hA$ may be calculated—the reservoir pore volume-compressibility product.

Figure 4 presents a Muskat graph for the case of a well in the center of a constant-pressure square. The slopes of the parallel straight lines are related to the porosity of the system, while the pressure intercepts may be related to the effective permeability of the flowing phase. This interesting build-up graph can often be prepared with very little knowledge of reservoir conditions. However it should be used with care with full knowledge of the pitfalls involved in the graph. The same can be said of all of the common build-up graphs. Recent studies show it is possible to investigate each type of graph thoroughly by empirical methods and to clearly define the regions of usefulness of each graph (Ramey and Cobb, 1971; Kumar and Ramey, 1974).

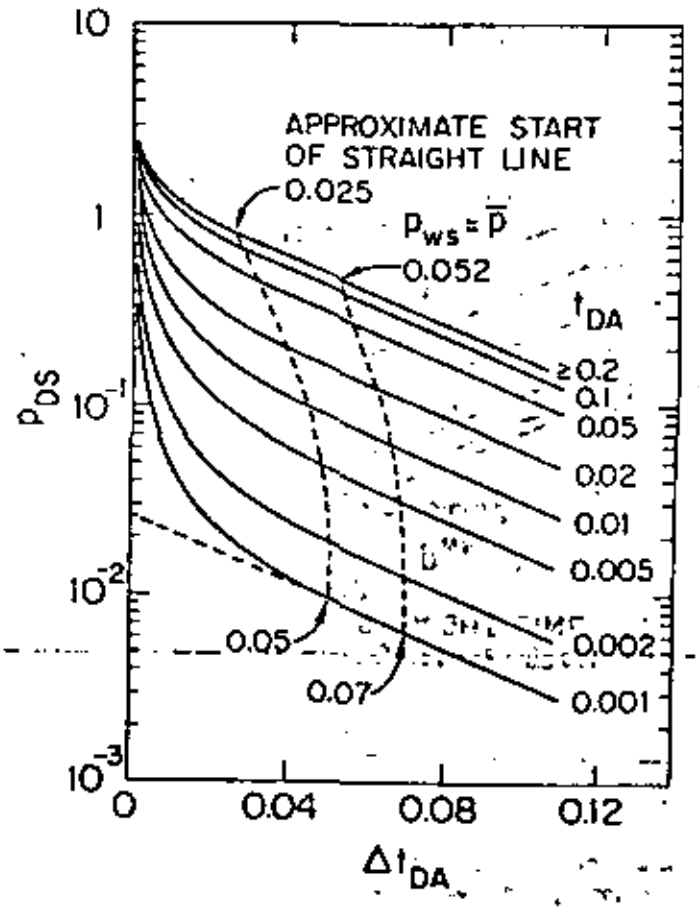

Figure 4. Muskat graph for a well in the center of a constant-pressure square.

The preceding methods have been applied to geothermal well data with success (Ramey, 1970; Ramey and Gringarten, 1975; and Barelli et al., 1975). Figure 5 presents a Horner build-up graph for a geothermal steam well at The Geysers. The proper semi-log straight line is shown by the solid li... Table 2 presents other pertinent data for this transient tes... Unfortunately, all well tests do not look like Figure 5... straight lines... at The Geysers. Table 3 presents other information for this well test. Fortunately, new methods are now available to aid selection of the proper straight line, as will be discussed in a later section.

In the 15-year period from 1950 through 1965, many important basic papers in pressure-transient analysis appeared in the petroleum engineering literature. Notable are publications by Van Everdingen (1953) and Hurst (1953), concerning the concept of the skin effect and the quantitative effect of wellbore damage on the performance of a well; the classic study by Matthews, Brons, and Hazebroek in 1954, concerning determination of mean pressure for closed reservoir systems; Perrine's review of pressure build-up analysis in 1956, which presented the first sound analysis of multiphase-flow pressure-transient analysis; and in 1959, Martin presented the theoretical foundation for Perrine's method for multiphase flow.

Let us consider just a few of these findings in more detail. The Van Everdingen... effect of skin... on pressure-transient analysis in geothermal...

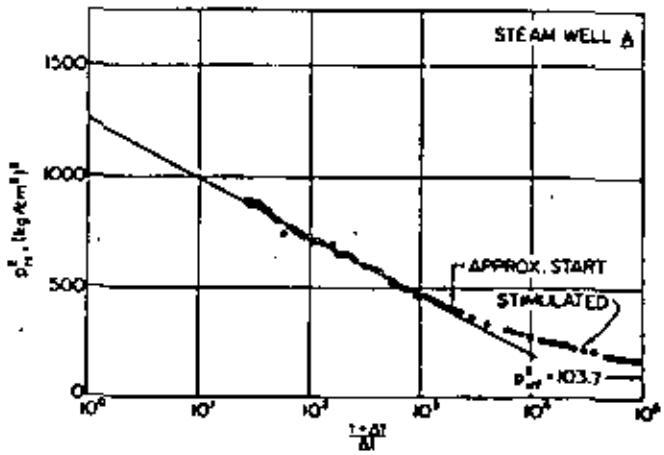

Figure 5. Horner buildup graph for Geysers Steam Well A.

Table 2. Pressure buildup data for Steam Well A.

Symbol	Value
q	= 26 tons/hr
t	= 12 240 hr
r_w	= 0.122 m
μ	= 0.0226 centipoise
c_g	= 0.032 (kg/cm²)⁻¹
Z	= 0.84
T	= 515°K
M	= 18 gm/gm mole
m	= 262 (kg/cm²)²/log cycle
p^{*2}_{1hr}	= 260
p^{*2}_{ws}	= 103.7
$\bar{p}^{*2}$	= 1245

Total depth is 663 m; open hole below 110 m.

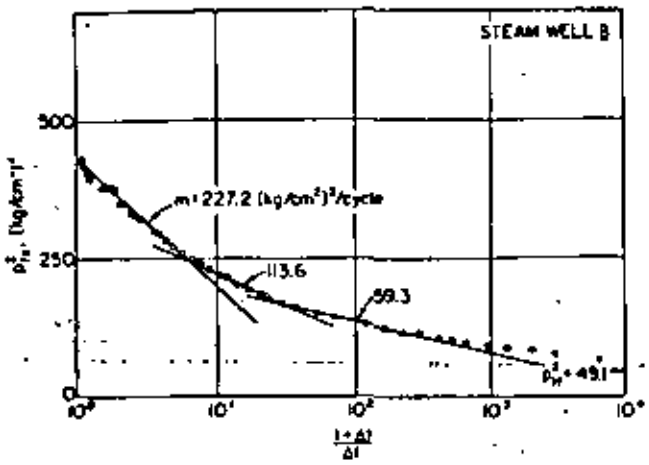

Figure 6. Horner buildup graph for Geysers Steam Well B.

testing. These investigators said that they had found that producing pressures generally did exhibit semi-log straight lines, but they appeared to be displaced. They reasoned that some resistance to flow existed at the sand face, and that it could be handled by adding a dimensionless pressure drop across a skin at the well face:

$$\frac{kh(p_i - p_{wf})}{0.4568 v_{sc} q B \mu} = p_D + s \qquad (8)$$

Eq. (8) applies for liquid flow, and a similar expression may be written for steam flow by using the form of Eq. (2). The skin effect, s, can be found by combining the flowing pressure p_{wf} at the instant of shut-in and a pressure obtained from the semi-log straight line during build-up at one hour of shut-in time, p_{1hr}. This pressure must be read on the straight line or its extension. The proper relationship [illegible]:

$$s = 1.151\left[\frac{p_{1hr}^2 - p_{wf}^2}{m} - \log_{10}\frac{k}{\phi \mu c_t r_w^2} + 0.0387\right] \qquad (9)$$

The pressure drop [illegible] caused by the skin effect is

$$\Delta p_{skin} = 0.87\, m s \qquad (10)$$

The pressure drop across the skin is usually used to compute the flow efficiency of the well. [illegible]

Table 3. Pressure buildup data for Steam Well B.

Symbol	Value
q	= 26.7 tons/hr
t	= 540 hr
r_w	= 0.122 m
μ	= 0.02 centipoise
c_g	= compressibility of steam, 0.054 (kg/cm²)⁻¹
Z	= 0.884
T	= 489 K
M	= 18 gm/gm mole
m	= 59.3 (kg/cm²)²/log cycle
p_{1hr}^2	= 93 (kg/cm²)²
p_{wf}	= 49.1
p^{*2}	= 434.7
p_i	= 21.4 kg/cm²

Total depth = 761.5 m, open hole below [illegible] m

$$FE = \frac{p^* - p_{wf} - \Delta p_{skin}}{p^* - p_{wf}} \qquad (11)$$

For liquid flow, Eq. (9) is slightly modified: the pressures are not squared.

The dimensionless skin effect has the following interpretation. The value of s will be positive if the well is damaged, zero if neither damaged nor stimulated, and negative if the well is stimulated. The flow efficiency is the ratio of the actual flow rate per unit pressure drop (productivity index) to an ideal flow rate per unit pressure drop neglecting the pressure loss across the skin.

The effect of the skin can be seen in the early portion of a pressure build-up test. If a well is stimulated and has a negative skin effect, the early portion of the build-up will appear as shown for the Steam Well A case on Figure 5. The build-up pressures will approach the semi-log straight line from above. If a well is damaged, build-up pressures will approach the semi-log straight line from below as indicated in the right-hand portion of Figure 7 for Steam Well C case. Another important phenomenon can cause a build-up to have the same early shape as the damaged curve for Figure 7. This effect is known variously as wellbore storage, annulus unloading, and afterflow. The cause of the effect is that the sand-face fluid flow rate does not respond instantaneously to changes caused at the wellhead. If a well is suddenly opened at a constant rate, the first production results from expansion or depletion of wellbore fluids (annulus unloading). If a well is suddenly shut in at the surface, fluid continues to pass through the sand face at the bottom hole as if nothing had happened (afterflow). Both effects are a result of the wellbore storage volume. Because the wellbore storage effect causes the same appearance as a damaged wellbore in the early build-up data, it is possible to mistake a storage effect for wellbore damage. An example of such an effect for a steam well was presented by Ramey (1970) and reanalyzed by Ramey and Gringarten (1975) at this same symposium.

[illegible] Examples are partial penetration of the formation, cementing casing in place and gun perforating, bore inclination from the vertical, hydraulic fracturing, acidization, boiling or gas evolution from produced liquids, condensation of liquids from produced gases, and inertial (non-Darcy) flow effects at high velocities, to name a few. [illegible]

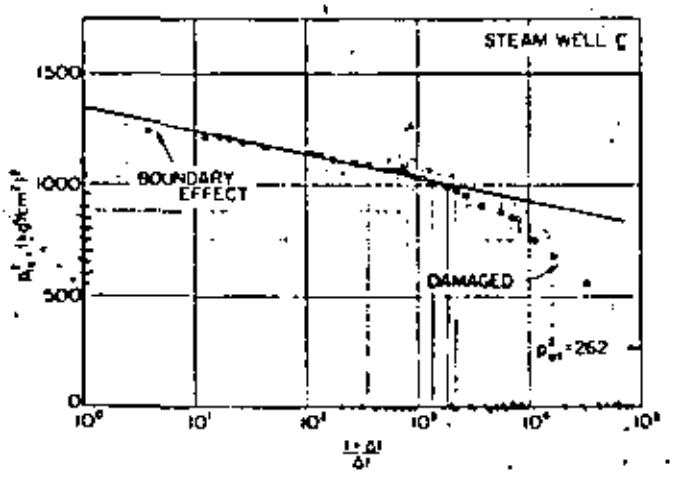

Figure 7. Horner buildup graph for Geysers Steam Well C.

[illegible] Many published studies are available which can be used to estimate the order of magnitude of such pseudo-skin effects (Brons and Marting, 1961; Harris, 1966; Ramey, 1965; Gringarten, Ramey, and Raghavan, 1975).

Let us now consider the classic study by Matthews, Brons, and Hazebroek in 1954. One important contribution was a generalization of Horner's method for determination of the ultimate static formation pressure from a buildup to include many rectangular shapes with wells in various positions within the shape. They presented figures similar to that of Figure 8. Figure 8 applies to the case of a well in the center of a constant pressure square. Horner suggested extending the semi-log straight line to a time ratio of unity, and calling this extrapolated pressure a "false" pressure p^*. Figure 8 presents a method for correcting the false pressure p^* to either p_i or $\bar{p}$ for the constant pressure square case. Another important contribution of the Matthews, Brons, and Hazebroek study was a method for dividing closed reservoirs into per-well drainage shapes. Ramey, Kumar, and Gulati (1973) presented a monograph dealing with the recharged reservoir shapes. Matthews, Brons, and Hazebroek provided the basis for this study by pointing out the usefulness of superposition of infinite arrays of wells. Figure 9 shows one such array. It contains the answer to two important problems: fluid reinjection, and generation of constant-pressure outer boundaries.

We now turn to consideration of other important studies in the 1950's. A number of important papers began to appear in the early 1950's in the area of transient flow of ideal gases through a porous medium. In regard to practical applications, the papers by Aronofsky and Jenkins (1953), Bruce (1953), and Tracy (1956), are important. Both the Aronofsky and Jenkins, and Bruce et al. studies were aimed at the same problems, that is, the transient flow of ideal gases through porous media. Each study produced a classic result. The Aronofsky and Jenkins study is notable because of the introduction of the concept of the transient drainage radius for flow of gases. The Bruce, et al. study is notable for introduction of the concept of alternating direction implicit finite difference calculations. It is clear that one study or the other would have been stopped had both groups been functioning within the same research laboratory.

The Aronofsky and Jenkins work inspired a number of studies of the effect of pressure variation of fluid and rock properties. See Al-Hussainy, Ramey, and Crawford (1966). A "real gas potential" was introduced which coupled fluid viscosity and density variation with pressure with stress-sensitive permeability. [illegible] for liquid flow [illegible]. It appears that dependence of fluid and rock properties on pressure can usually be handled practically.

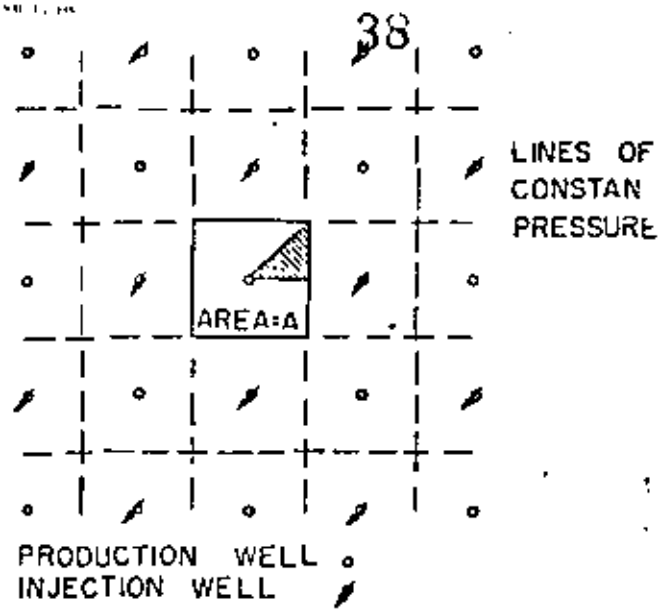

Figure 9. Infinite array to generate a well in the center of a constant pressure square, or a developed five-spot injection production pattern.

By the mid-1960's, the details of well test analysi apparently were thoroughly investigated. This led the Society of Petroleum Engineers of the AIME to commission the preparation of a monograph on the subject, "Pressure Build-Up and Flow Tests in Wells," by Matthews and Russell. The result was published in 1966. To underscore the importance of this subject, the Society of Petroleum Engineers also commissioned the production of a Reprint Series Manual No. 9 titled, "Pressure Analysis Methods." The Matthews and Russell monograph was the first in a series of monographs intended to aid a program of self-education by members of the Society of Petroleum Engineers.

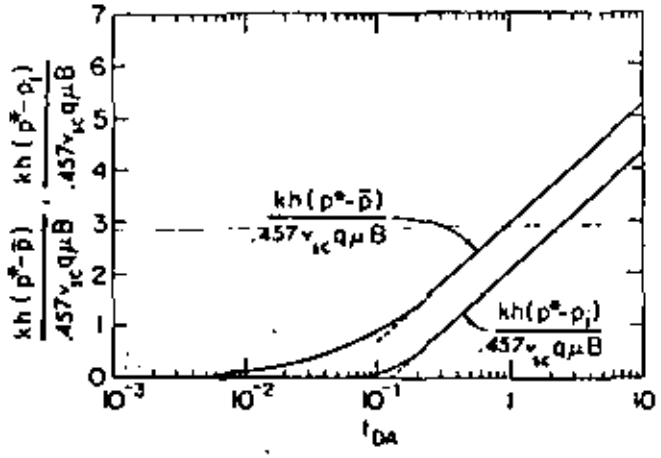

Figure 8. Matthews-Brons-Hazebroek graph for a well in the center of a constant-pressure square.

MODERN PRESSURE ANALYSIS

A study of wellbore storage (Ramey, 1965) and the skin effect began to bear interesting fruit by the end of the decade (Ramey, 1970; Agarwal, Al-Hussainy, and Ramey, 1970). A renewed interest in using log-log type curves to study the early pressure data prior to the onset of the usual semi-log straight line led to a number of important findings. Figure 10 is a log-log type curve for pressures measured in a well produced at constant rate with a skin effect. The unit slope straight lines emanating from the lower left portion of the graph represent pressures controlled altogether by wellbore storage. In effect, there is no flow through the sand face during times when the unit slope is evident. Then there is a transition to the flat, zero wellbore storage lines passing across the graph. When the transition lines reach the flat portion, the correct semi-log straight line starts for these cases, because the flat lines are semi-log straight for

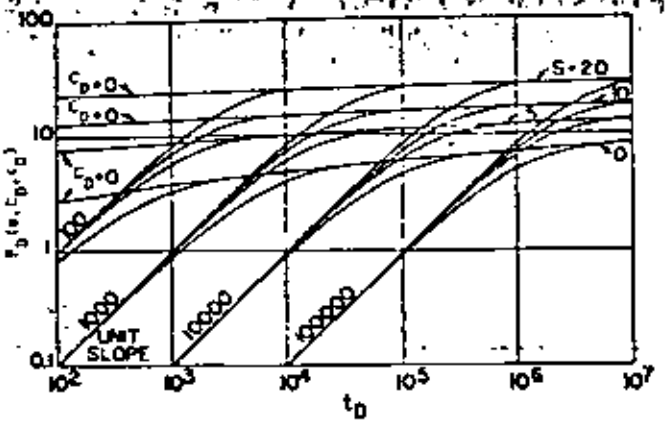

Figure 10. p_D vs t_D for a well with storage and a skin effect.

times of about 5. The time of start of the semi-log straight line can be expressed (Ramey, Kumar, and Gulati, 1973):

$$t_D = C_D(60 + 3.5\,s) \qquad (12)$$

where:

$$C_D = \frac{C\,B\,\gamma_w}{2\pi\phi h c_t r_w^2}, \text{ for liquids} \qquad (13)$$

$$C_D = \frac{27\,C'ZT}{M\phi h c_t r_w^2}, \text{ for gases.} \qquad (14)$$

In the 1970 study, it was recommended that type-curve matching be used to obtain permeability and skin effect by means of Figure 10. [illegible] This procedure plus general diagnostic uses make Figure 10 a very useful type curve.

One result of this study was that it became apparent that it would be necessary to specify the physical nature of the skin effect for pressures prior to the onset of the semi-log straight line. An acidized well with an annular zone of high permeability near the well could have the same negative skin effect as a fractured well with a large, vertical

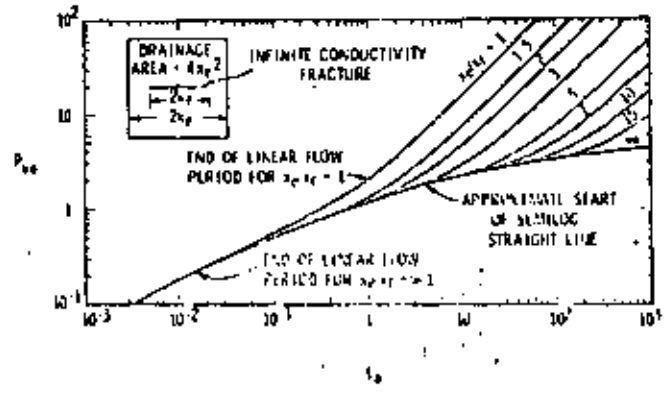

Figure 11. p_{wD} vs t_D for an infinite-conductivity vertical fracture in the center of a closed square or in an infinitely large reservoir.

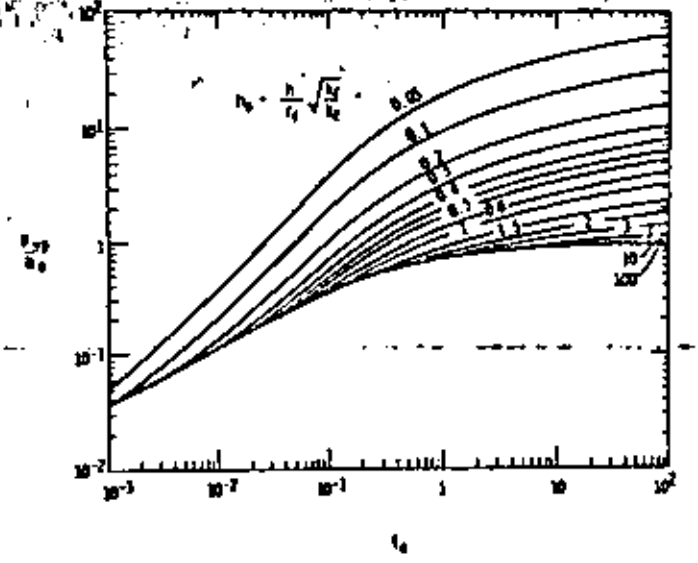

Figure 12. p_{wD}/h_D vs t_D for a constant-flux, circular horizontal fracture in the center of the interval.

fracture. But it was likely that these two cases would not have the same early time behavior. Likewise, it was not likely that wells with the same skin effect, but vertical or horizontal fractures, would exhibit the same early time behavior. To answer these speculations, studies of annular skin regions (Wattenbarger and Ramey, 1970), and fractured wells (Gringarten, Ramey, and Raghavan, 1974) were made. Figures 11 and 12 present log-log type curves for vertical and horizontal fractures.

Figure 11 presents the producing pressures for a well with a vertical fracture in the center of a closed square, or in an infinitely large reservoir. It is a simple matter to place the fractured well in almost any position within any sort of drainage shape. The left-hand side of this curve is a straight line of slope 1/2. This period represents linear flow normal to the surface of the fracture. Later, the fracture behaves like a circular well with a radius half the distance from the center to the top of the fracture, $x_f/2$. This sort of log-log type curve reveals the presence of fractures and can be used in matching whether a semi-log straight line can be found or not. Permeability may be found from the pressure match (Ramey and Gringarten, 1975), the fracture length x_f from the time match, and the drainage area, or a minimum estimate of the drainage area may be found from the parameter x_e/x_f.

Figure 12 presents a log-log type curve for a single horizontal fracture located at the center of the interval. The left-hand portion of the lowest line on the graph is also linear and of slope 1/2. This represents vertical flow normal to the fracture surface. Because there is a vertical flow component, it is necessary to specify both the radial and vertical permeabilities. [illegible]. The dimensionless time for the horizontal fracture is based upon the radius of the fracture, r_f.

Figure 13 presents a log-log type curve for the build-up data of Steam Well A (see Fig. 5). Almost two log cycles of half-slope line are evident. One important use of such a graph is to locate the start of the correct semi-log straight line. Wattenbarger and Ramey (1970) noticed that the start of the semi-log straight line corresponded roughly to a

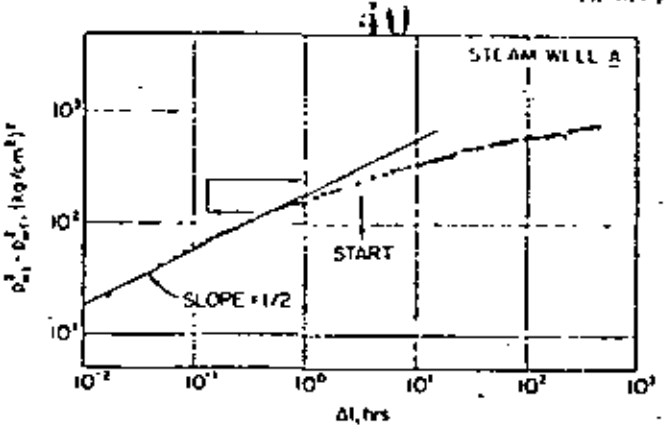

Figure 13. Log-log type curve for pressure buildup for Geysers Steam Well A.

Table 4. Pressure buildup data for Steam Well C.

Symbol	Value
q	= 302 Mlbs/hr
t	= 552 hr
r_w	= 0.122 m
μ	= 0.0225 cps
c_g	= 0.037 (kg/cm²)⁻¹
Z	= 0.84
T	= 515°K
M	= 18 gm/gm mole
m	= 210 kg/cm²/F/log cycle
p_{wf}^2	= 1042 (kg/cm²)²
p_{wa}^2	= 262
p^{*2}	= 1333
$\bar{p}^2$	= 1240 (after 15 months shut in)

Total depth 1120 m, open hole below 155 m.

pressure difference about twice that at the top of the half-slope log-log line. This rule, the double-delta-p rule, is shown by the arrows on Figure 13. This can be used to select the proper straight line when several are indicated as shown on Figure 6.

The wellbore storage [redacted] has been in use for 10 years, the fracture type curves for 4 years. Extensive field experience has been gained in gas and oil reservoirs and in several geothermal reservoirs. [redacted] One natural gas reservoir was found to have fracture porosity only. Hydraulic fracturing produced only propped, high-conductivity storage volume, not a single planar fracture. In other fractured systems, widely spaced trending fractures were evident in pressures measured in a producing well, but apparently caused only simple anisotropy in interference testing. [redacted]. By interference testing is meant the sort of test wherein one well is producing and the resulting pressure drop is measured in a distant well. [redacted] Figure 14 (also known as Lord Kelvin's point source, the Theis solution, and so on).

CONCLUDING REMARKS

In the preceding, I have focused on the positive aspects of pressure-transient analysis. The result may be misleading.

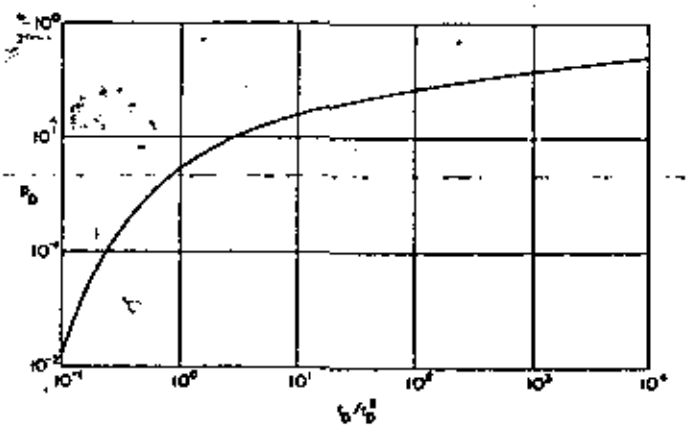

Figure 14. p_D vs t_D/r_D^2 for the continuous line source solution (Theis solution).

Pressure-transient analysis may not always be practical. One common problem in both oil and geothermal reservoirs may be called the thick sand problem. For thick sands, the product of permeability-thickness may be so great that the semi-log straight line has a negligible or undetectable value at practical producing rates. This likelihood is evident from Eqs. (5) or (6). Even in this case, important results may be obtained by an experienced, sophisticated analyst under fortunate circumstances.

[redacted] The presence of a boiling liquid interface in a vapor-dominated system would be evident as a constant-pressure interface. This interface would be horizontal, rather than vertical as is assumed in most of the available solutions. Generally, production of new solutions is not difficult, and usually does not require large amounts of computer time. Analytical solutions are usually much better than finite-difference solutions for short-time results.

[redacted]. It can be said that results appear reasonable. It is certain that continued work in this area will lead to development of valid models which can be used to analyze pressure-time data from geothermal reservoirs and produce information not available from any other source. One important weapon in this study will be the development of new pressure- and temperature-sensing tools. Several new pressure-measuring devices are currently being used in oil wells to measure pressures to almost 7×10^{-3} kg/cm². It is certain that similar instruments will become available for geothermal applications in the near future. What is impossible today will be easy tomorrow.

REFERENCES CITED

Agarwal, R. G., Al-Hussainy, R., and Ramey, H. J., Jr., 1970, An investigation of wellbore storage and skin effect in unsteady liquid flow—1, Analytical treatment: Soc. Petroleum Engineers Jour. (September), p. 279.

Al-Hussainy, R., Ramey, H. J., Jr., and Crawford, P., 1966, The flow of real gases through porous media: Jour. Petroleum Technology, v. 18, no. 5, p. 645.

Aronofsky, J., and Jenkins, R., 1953, Unsteady radial f of gas through porous media: Jour. Applied Mechan. v. 20, p. 210.

Arps, J. J., and Smith, A. E., 1949, Practical use of bottom hole pressure buildup curves: Reprint paper no. 851-23-I, Tulsa, Oklahoma meeting, API.

Bartill, A., Celati, R., Manetti, G., and Neri, G., Buildup and back-pressure tests on Italian geothermal wells: Second UN Symposium on the Development and Use of Geothermal Resources, San Francisco, Proceedings, Lawrence Berkeley Lab., Univ. of California.

Brons, F., and Marting, V. E., 1961, The effect of restricted fluid entry on well productivity: Jour. Petroleum Technology (February), p. 172.

Bruce, G. H., Peaceman, D. W., Rachford, H. H., and Rice, J. D., 1953, Calculations of unsteady state gas flow through porous media: AIME, Trans., v. 198, p. 79.

Carter, D. V., 1961, History of petroleum engineering: API.

Cooper, H. H., Jr., and Jacob, C. E., 1946, A generalized graphical method for evaluating formation constants and summarizing well field history: Am. Geophys. Union Trans., v. 27, p. 526.

Earlougher, R. C., Jr., Ramey, H. J., Jr., Miller, F. G., and Mueller, T. D., 1968, Pressure distributions in rectangular reservoirs: Jour. Petroleum Technology, v. 20, no. 2, p. 199.

Elkins, L. F., 1946, Reservoir performance and well spacing—silica arbuckle pool, Kansas: Drill. and Prod. Prac., API, p. 109.

Gringarten, A. C., and Ramey, H. J., Jr., 1974, Unsteady state pressure distributions created by a well with a single horizontal fracture, partial penetration, or restricted entry: Soc. Petroleum Engineers Jour. (August), SPE 3819, p. 413.

Gringarten, A. C., Ramey, H. J., Jr., and Raghavan, R., 1974, Unsteady state pressure distributions created by a well with a single infinite conductivity vertical fracture: Soc. Petroleum Engineers Jour. (August), p. 347.

——, 1975, Pressure analysis for fractured wells: Jour. Petroleum Technology (July).

Harris, M. H., 1966, The effect of perforating on well productivity: Jour. Petroleum Technology (April), p. 518.

Horner, D. R., 1950, Pressure buildup in wells: Third World Petroleum Congress, Proc., Leiden, E. J. Brill, v. 2, p. 503.

Houpeurt, A., 1953, Etude analogique de l'ecoulement radial circulaire transitoire des gas dans les milieux poreux: Revue IFP, v. 8, p. 129.

Hurst, W., 1953, Establishment of the skin effect and its impediment to fluid flow into a wellbore: Petroleum Engineering (October), v. 25, p. B-6.

Jacob, C. E., 1940, Flow of water in elastic artesian aquifers: AGU Trans., v. 2, p. 574.

——, 1950, chapter, *in* Rouse, H., ed., Engineering hydraulics, Proceedings of the Fourth Hydraulics Conference, Iowa Institute of Hydraulics Research, June, 1949: New York, John Wiley & Sons.

Kumar, A., and Ramey, H. J., 1974, Well test analysis for a well in a constant pressure square: Soc. Petroleum Engineers Jour. (April), p. 107.

Martin, J. C., 1959, Simplified equations of flow in gas drive reservoirs and the theoretical foundation of multiphase pressure buildup analyses: AIME Trans., v. 216, p. 309.

Matthews, C. S., and Russell, D. G., 1967, Pressure buildup and flow in wells, Henry L. Doherty Series Monographs, Vol. 1: Dallas, Henry L. Doherty Memorial Fund of AIME.

Miller, C. C., Dyes, A. B., and Hutchinson, C. A., Jr., 1950, The estimation of permeability and reservoir pressure from bottom hole pressure buildup characteristics: AIME Trans., v. 189, p. 91.

Millikan, C. V., and Sidwell, C. V., 1931, Bottom hole pressures in oil wells: AIME Trans., v. 92, p. 194.

Moore, T. V., Schilthius, R. J., and Hurst, W., 1933, The determination of permeability from field data: Proc., API Bulletin 211, p. 4.

Muskat, M., 1937, The use of data on the buildup of bottom hole pressures: AIME Trans., v. 123, p. 44.

Perrine, R. L., 1956, Analysis of pressure buildup curves: Drill. and Prod. Prac., API, p. 482.

Ramey, H. J., Jr., 1965, Non-darcy flow and wellbore storage effects in pressure build-up and drawdown of gas wells: Jour. Petroleum Technology (February), p. 223.

——, 1970, Short-time well test data interpretation in the presence of skin effect and wellbore storage: Jour. Petroleum Technology (January), p. 97.

Ramey, H. J., Jr., and Cobb, W. M., 1971, A general pressure buildup theory for a well in a closed drainage area: Jour. Petroleum Technology (December), p. 1493.

Ramey, H. J., Jr., and Gringarten, A. C., May, 1975, Effect of high-volume vertical fractures on geothermal steam well behavior: Second Symposium on the Development and Use of Geothermal Resources, San Francisco, Proceedings, Lawrence Berkeley Lab., Univ. of California.

Ramey, H. J., Jr., Kumar, A., and Gulati, M., 1973, Gas well test analysis under water drive conditions: AGA, Arlington, Virginia.

SPE Reprint Series No. 9, 1967, Pressure analysis methods: Dallas, SPE of AIME.

Theis, C. V., 1935, The relationship between the lowering of piezometric surface and rate and duration of discharge of wells using ground water storage: AGU Trans., v. 2, p. 519.

Tracy, G. W., 1956, Why gas wells have low productivity: Oil and Gas Jour. (August), p. 84.

Van Everdingen, A. F., 1953, The skin effect and its influence on the productive capacity of a well: AIME Trans., v. 198, p. 171.

Van Everdingen, A. F., and Hurst, W., 1949, The application of the Laplace transformation to flow problems in reservoirs: AIME Trans., v. 186, p. 305.

Wattenbarger, R. A., and Ramey, H. J., Jr., 1970, An investigation of wellbore storage and skin effect in unsteady liquid flow—2: Soc. Petroleum Engineers Jour. (September), p. 291.

Wenzel, L. K., 1942, Methods of determining permeability of water bearing materials with special reference to discharging well methods: U.S. Geological Survey, W.S.P., p. 887.

SPE 7963

WELL TEST ANALYSIS OF HGP-A

by B.H. Chen, D.H. Kihara, A. Seki,
and P.C. Yuen, U. of Hawaii

ABSTRACT

Since the successful initial flashing on July 2, 1976, HGP-A has undergone five flash discharge tests with the longest one lasting 42 days. Production records including wellhead pressure and temperature, production rate and steam quality were kept for drawdown analysis. After two of the discharge tests, Kuster pressure bombs were lowered to the bottom repeatedly to record pressure data for buildup analysis.

Initial analyses of the drawdown and buildup tests indicate that the Kapoho Geothermal Reservoir, where HGP-A is located, seems to be in a tight formation with possible severe mud damage in the well. The reservoir also appears to be a liquid-dominated system but with two-phase flow during the discharge of HGP-A. Evidence of this claim will be presented in this paper.

The pressure drawdown and buildup analyses were performed with the traditional single-phase petroleum reservoir engineering techniques modified when necessary.

INTRODUCTION

The experimental well, HGP-A, drilled under the auspices of the Hawaii Geothermal Project, is located on the island of Hawaii near the eastern rift of Kilauea volcano. Drilling was completed to a depth of 6450 feet (1966 m) in April 1976. The well is cased to 2230 feet (680 m) below the wellhead, which is approximately 600 feet (183 m) above sea level. A slotted liner is placed from the end of the casing to bottomhole. Cuttings and core samples obtained during drilling indicate that the region is composed of volcanic basalt with a profile that contains open fracture zones separated by relatively impermeable layers.[1]

References and illustrations at end of paper.

The well has undergone five flash discharge tests since an initial flashing on July 2, 1976. Figure 1 is a sketch of the equipment and instrumentation for the discharge tests. As shown, the method involves basically the James technique[2] for measuring total mass flow with twin cyclone separators for separation of steam and water. A 90° V-notch weir is used to measure the liquid flow rate, permitting steam quality and specific enthalpy to be calculated. A recovery tube is mounted on the wellhead to permit temperature and pressure profiles to be obtained and water samples to be gathered during quiescent and discharge periods.

Since the temperature of the reservoir in general exceeds 300°C (572°F) with a maximum recorded temperature of 358°C (676°F), no electronic equipment can survive the extreme conditions downhole. Therefore, Kuster Amerada RPG-3 Type subsurface recording temperature and pressure gauges were selected to provide all temperature and pressure measurements downhole.

DOWNHOLE FLOW CHARACTERISTICS

During January and March 1977, the flow tests consisted of a series of discharges in which the flow was throttled by placing orifice plates of various sizes in the discharge line. The results are summarized in Table 1. Pressure and temperature profiles taken during the throttled flow tests are shown in Figures 2 and 3. These profiles indicate that the fluid in the wellbore is at saturation conditions with a mixture of liquid and vapor flowing up to the wellhead. Since the steam quality at the wellhead is high and no steam/water interface is found in the wellbore, the conclusion is that flashing occurs in the formation rather than in the wellbore.

Examination of Figure 2 shows that the pressure profiles are essentially three constant slope lines meeting at the junction of the casing and the slotted liner and at approximately 4300 feet (1311 m). These constant pressure gradient

lines indicate that the major production zones may be near the bottomhole and in the vicinity of 4300 feet (1311 m).

SSURE TRANSIENT TESTS

While data sufficient to assess a producible geothermal field can be obtained only from a number of properly-spaced wells, some limited reservoir information can be obtained from a single geothermal well by utilizing the theory developed for oil and gas fields.[3] These standard petroleum engineering techniques, however, assume single phase flow, while the flow in HGP-A is definitely two-phase, so that caution is required in interpreting the results of these analyses.

PRESSURE DRAWDOWN ANALYSIS

Wellhead pressure vs. time plotted on log-log scales for type-curve matching and on semi-log scales for a pressure drawdown analysis are shown in Figures 4 and 5, respectively. The initial pressure was obtained from Figure 6. These data can be used in a pressure drawdown analysis to obtain information about the geothermal reservoir and the following observations can be made:

1. The analysis is based on a constant production rate during the discharge, and this condition was impossible to achieve. In order to apply the theory, a normalized pressure was obtained by dividing the measured pressure by the concomitant production rate.

2. There was some overpressure at the wellhead prior to the start of the test. Consequently, opening the valve took some effort and about 2 to 3 minutes were needed to open the valve completely. Thus there is an uncertainty of that amount in the determination of zero time.

3. The theory is for bottomhole pressure whereas the data in Figures 4 and 5 are for wellhead pressure. Thus the assumption must be made that wellhead pressure is proportional to downhole pressure and the proportionality factor remains constant throughout the test.

Within these restrictions and assumptions, some information can be obtained. To normalize the pressure with respect to production the pressure relation can be written as:

$$\frac{P_i - P_{wf}}{q} = \frac{162.6\mu B}{kh}\left(\log_{10} t + \log_{10}\frac{k}{\phi\mu C_t r_w^2} - 3.23 + 0.87s\right) \qquad (1)$$

The left side of equation (1) is a linear function of $\log_{10}t$ so that a plot of $\frac{P_i - P_{wf}}{q}$ vs. $\log_{10}t$ will yield a straight line with a slope, m, psi/STB/day/cycle, where

$$|m| = \frac{162.6\mu B}{kh} \qquad (2)$$

and this equation can be used to calculate the permeability-thickness, kh.

Equation (1) can also be used to calculate the skin effect factor, s. Letting p_{1hr} be the value of p_{wf} for t=1 hour on the correct semi-log straight line, equation (1) can be rearranged to yield

$$s = 1.15\left(\frac{\frac{P_i - P_{1hr}}{q}}{|m|} - \log_{10}\frac{k}{\phi\mu C_t r_w^2} + 3.23\right) \qquad (3)$$

By using (3), the pressure drop due to the skin effect can be calculated from

$$\frac{\Delta P_s}{q} = 0.87\,|m|s \qquad (4)$$

and the flow efficiency

$$FE = \frac{\frac{P_i - P_{wf} - \Delta P_s}{q}}{\frac{P_i - P_{wf}}{q}} \qquad (5)$$

With the assumptions made previously, a log-log type-curve plot of $\frac{P_i - P_{wf}}{q}$ vs. t for the drawdown test is shown in Figure 4. The two unit-slope lines shown verify the existence of wellbore storage effects. From the end of the second straight line, it appears that the semi-log straight line or the radial flow period started at about 10 hours after the test was begun.

Figure 5 is a semi-log graph of $\frac{P_i - P_{wf}}{q}$ vs. $\log_{10}t$. An analysis of the plotted data shows that the permeability thickness

$$kh = \frac{162.6(24\text{ hr/day})(0.09\text{ cp})(1.5\text{ res bbl/std bbl})}{(350\text{ lb/bbl})(1.11\times10^{-3}\text{ psi/lb/hr/cycle})}$$

$$kh = 1356\text{ md-ft}\ \left(0.408\mu m^2 - m\right)$$

and if the thickness of the producing layer is assumed to be h = 1000 ft (305 m) then the permeability

$$k = 1.4\text{ md}\ \left(1.38\times10^{-3}\mu m^2\right)$$

The skin effect factor

$$s = 1.15\left[\frac{5.23\times10^{-3}}{1.11\times10^{-3}} - \log_{10}\frac{1.4}{(0.03)(0.09)\left(8\times10^{-6}\right)\left(\frac{8.755}{24}\right)^2} + 3.23\right]$$

$$= -0.86$$

The small negative skin effect factor suggests that skin damage is not present. Therefore, the flow efficiency of the well is approximately 1, or the well is discharging as much as it is able to produce.

Figure 7 shows the total mass flow rate vs. time in the drawdown test. Note that the flow rate did not change significantly after the initial five or six hours of flow. However if we neglect the fact that the flow is not constant and plot the wellhead pressure vs. time as in Figure 8 we would have obtained a slope

$$|m| = 11 \text{ psi/cycle } (76 \text{ kPa/cycle})$$

Assuming q = 86.00 Klb/hr (10.8 kg/s), one would have obtained

$$kh = \frac{162.6(86{,}000 \text{ lb/hr})(24 \text{ hr/day})}{(350 \text{ lb/bbl})} \cdot \frac{(0.09 \text{ cp})(1.5 \text{ res bbl/std bbl})}{(11 \text{ psi/cycle})}$$

$$= 11{,}200 \text{ md-ft } (3.37\mu m^2 - m)$$

which is one order of magnitude greater than the normalized value.

PRESSURE BUILDUP ANALYSIS

Following the December discharge, a pressure buildup test was conducted, with bottomhole pressure being measured using two Kuster KPG pressure elements and recorders in tandem to ensure that pressure data were acquired in spite of equipment malfunction because of the high temperature. Figure 9 is a log-log type curve of the difference between bottomhole pressures during static (no flow) and flow conditions. It shows two distinct wellbore storage effects; the top of the second wellbore storage interval is indicated by the arrow A. Arrow B indicates the onset of the radial flow period, roughly 70 hours after the well is shut in. From these curves, the product of permeability and production zone thickness (kh) is calculated to be approximately 880 millidarcy-feet ($0.265\mu m^2$ - m), with the pressure drop across the mud-damaged skin of the well being 560 psi (3861 kPa).

Bottomhole pressure measurements made after HGP-A was shut in following the January test produced data and plots similar to those for the December test. However, close examination of the data shows that two consecutive straight-line approximations may be made to the Horner plot (Figure 10). Interpretation of this occurrence is that there are at least two different production layers in the wellbore with different kh values. The same effect is also present in the December data, but until it was reproduced in the January test, little credence was given to it. The results of these analyses are summarized in Table 2.

DISCUSSION

From the above analyses, it appears that the Kapoho Geothermal Reservoir, where HGP-A is located, has a fairly tight formation with a permeability thickness of approximately 1000 millidarcy-feet ($0.301\mu m^2$ - m). During production, the HGP-A wellbore contains steam and water at saturation and flashing appears to occur in the formation. There are possibly two production layers, one at bottomhole and another at approximately 4300 ft (1311 m) from the wellhead. The buildup analyses show that HGP-A may have severe skin damage.

As stated before, one cannot obtain the characteristics of the Kapoho Geothermal Reservoir with only one producing well. Thus the above conclusions are preliminary and present the best estimates at this time. It is also evident that pressure buildup analyses are more reliable than the pressure drawdown analyses.

ACKNOWLEDGMENTS

The results reported were obtained with support from the U.S. Energy Research and Development Administration, the U.S. Department of Energy, the State of Hawaii, and the County of Hawaii.

Special thanks are due to Dr. Henry J. Ramey, Jr., who has encouraged us in conducting the tests and analyses.

NOMENCLATURE

P_i = initial pressure, psi (kPa)
P_{wf} = flowing pressure, psi (kPa)
P_{wh} = wellhead pressure, psi (kPa)
P_{ws} = shut in pressure, psi (kPa)
q = production rate, std bbl/day (m^3/day)
μ = viscosity, cp (Pa·s)
B = formation volume factor, res vol/std vol
k = permeability, md (μm^2)
h = formation thickness, ft (m)
t = time, hr (hr)
ϕ = fractional porosity
C_t = total system effective isothermal compressibility, psi^{-1} (kPa^{-1})
r_w = well radius, ft (m)
s = skin effect factor

REFERENCES

1. Kingston, Reynolds, Thom and Allardice, Ltd.: "Hawaii Geothermal Project Well Completion Report, HGP-A", (September 1976).

2. James, R.: "Measurement of Steam-Water Mixtures Discharging at the Speed of Sound to the Atmosphere", New Zealand Engineering, October 1966, pp. 437-441.

3. Ramey, H.J., Jr.: "Practical Use of Modern Well Test Analysis", presented at the 46th Annual California Regional Meeting of the Society of Petroleum Engineering of AIME (April 1976).

TABLE 1

PRELIMINARY THROTTLED FLOW DATA

Orifice Size (Inches)	(mm)	Total Mass Flow Rate (Klb/hr)	(kg/s)	Steam Flow Rate (Klb/hr)	(kg/s)	Steam Quality (%)	Wellhead Pressure (psig)	(kPa)	Wellhead Temp. (°F)	(°C)
8	(203)	101	(12.7)	64	(8.1)	64	53	(352)	295	(164)
6	(152)	99	(12.5)	65	(8.2)	66	54	(372)	300	(167)
4	(102)	93	(11.7)	57	(7.2)	64	100	(689)	338	(188)
3	(76)	89	(11.2)	54	(6.8)	60	165	(1138)	372	(207)
2-1/2	(64)	84	(10.6)	48	(6.1)	57	237	(1634)	401	(223)
2	(51)	81	(10.2)	43	(5.4)	53	293	(2020)	419	(233)
1-3/4	(45)	76	(9.6)	39	(4.9)	52	375	(2585)	439	(244)

TABLE 2

COMPARISON OF PRESSURE DRAWDOWN AND BUILDUP TESTS

	Constant Production Drawdown	December Buildup One Layer	December Buildup Two Layer	January Buildup Two Layer
Permeability thickness, kh, md-ft (μm^2 - m)	1356 (0.408)	880 (0.265)	1553 (0.467)	1089 (0.328)
Apparent skin factor, s	-0.86	4.3	14.8	4.3
Pressure drop across skin, psi (kPa)	---	561 (3868)	1098 (7570)	575 (3964)
Flow efficiency	1	0.65	0.38	0.60

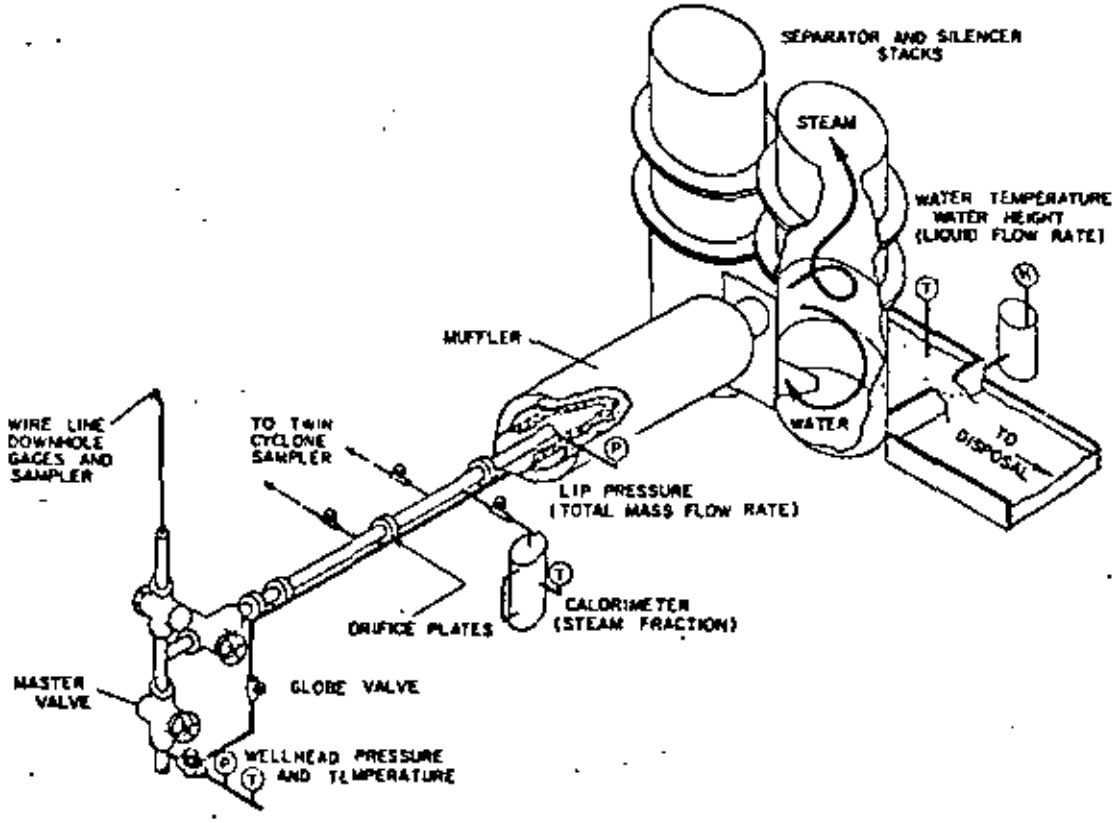

Fig. 1 - Flow test equipment and instrumentation.

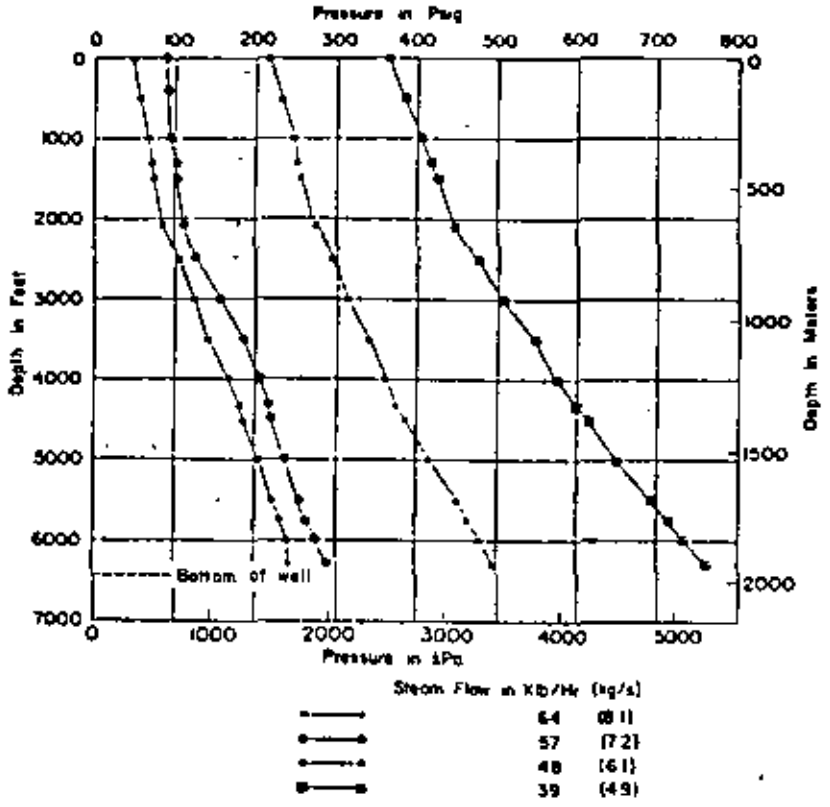

Fig. 2 - Pressure profiles for HGP-A.

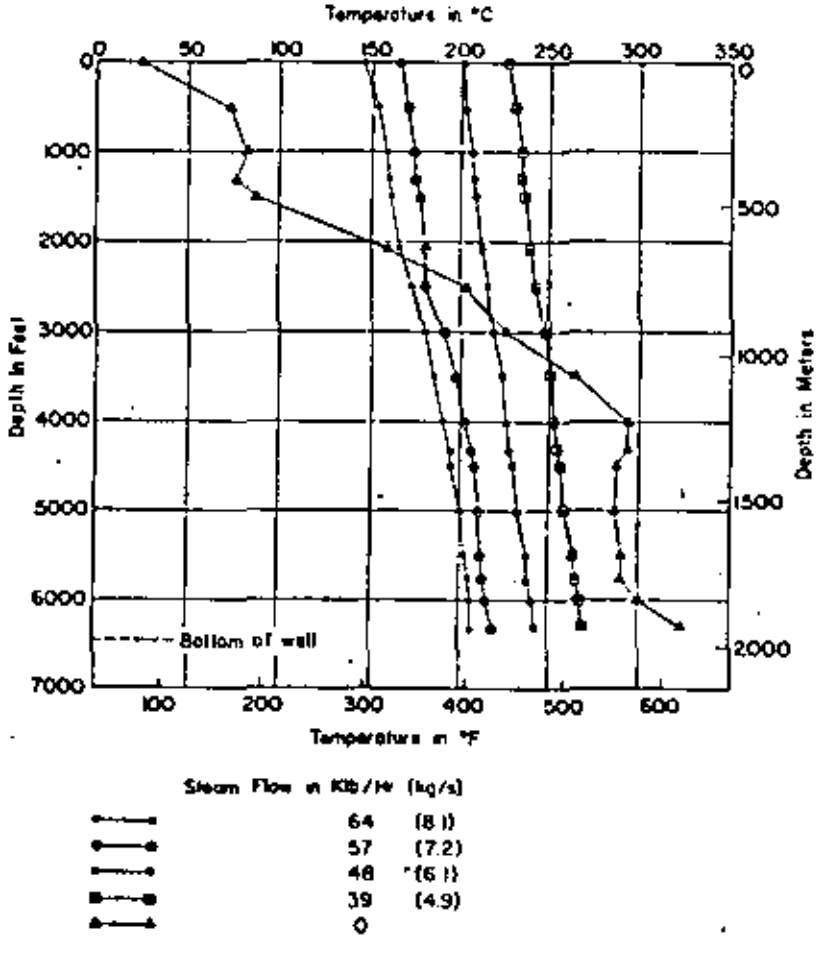

Fig. 3 - Temperature profiles for HGP-A.

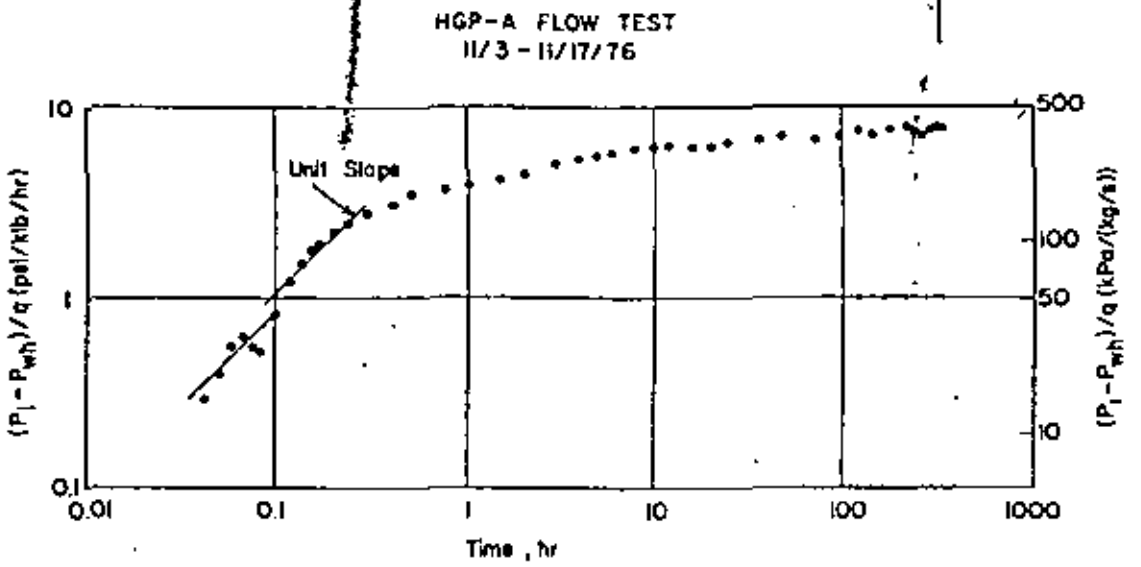

Fig. 4 - Log-log plot of November 1976 discharge test data.

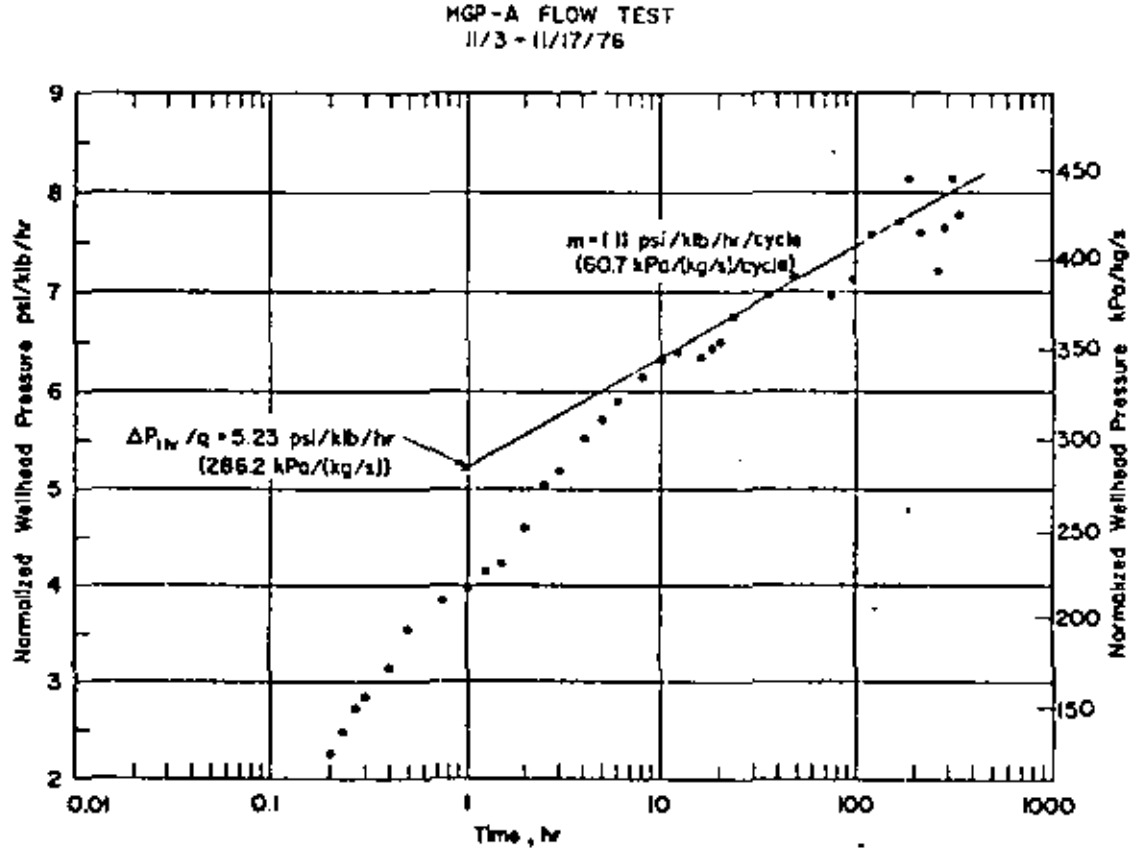

Fig. 5 - Semi-log plot of November 1976 discharge test data.

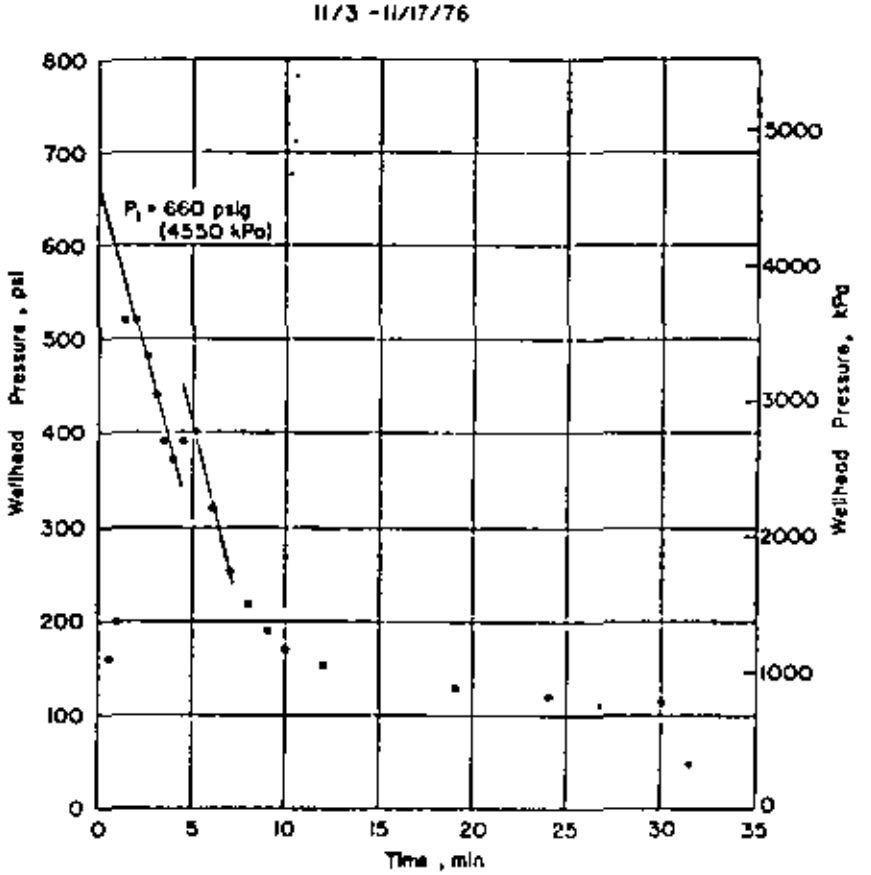

Fig. 6 - Linear plot of initial data for November 1976 discharge test.

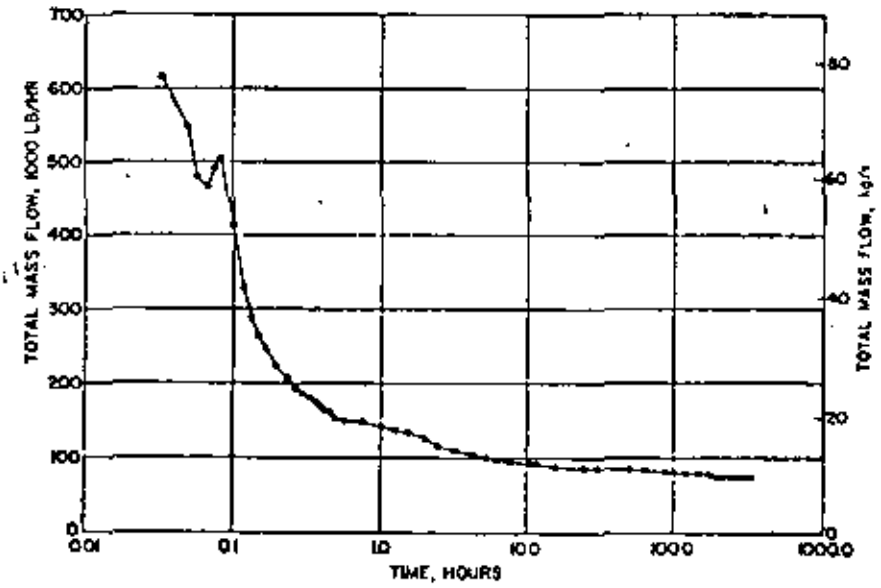

Fig. 7 - Total mass flow as a function of time.

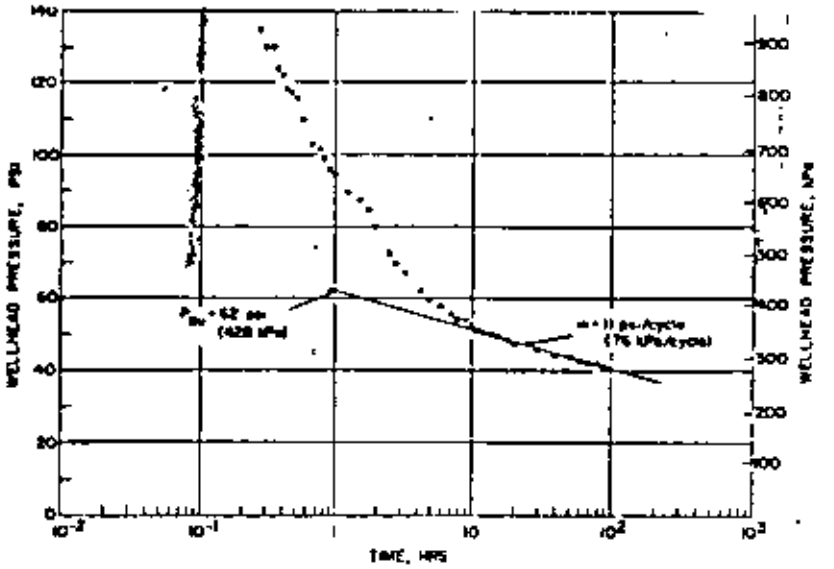

Fig. 8 - Wellhead pressure as a function of time.

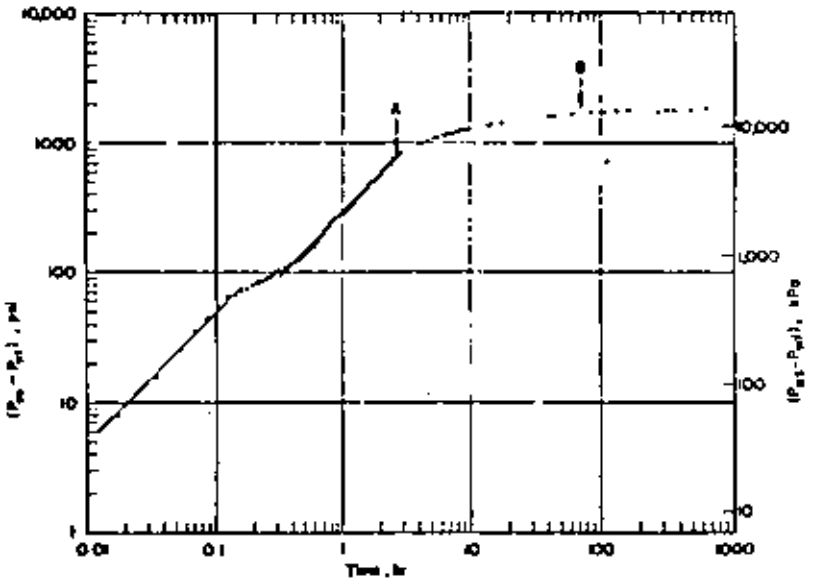

Fig. 9 - Log-log plot of December 1976 buildup test data.

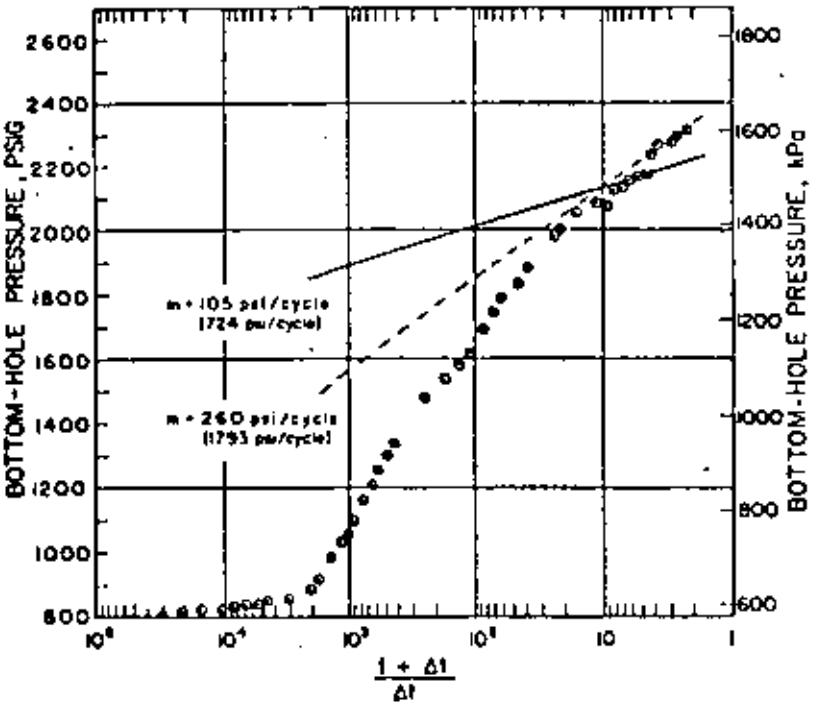

Fig. 10 - Semi-log plot of January/February 1977 buildup test data.

SPE

Society of Petroleum Engineers of AIME

SPE 7479

PRESSURE TRANSIENT ANALYSIS FOR TWO-PHASE (LIQUID WATER/STEAM) GEOTHERMAL RESERVOIRS

by S. K. Garg, Systems, Science and Software

This paper was presented at the 53rd Annual Fall Technical Conference and Exhibition of the Society of Petroleum Engineers of AIME, held in Houston, Texas, Oct. 1-3, 1978. The material is subject to correction by the author. Permission to copy is restricted to an abstract of not more than 300 words. Write 6200 N. Central Expy., Dallas, Texas 75206.

ABSTRACT

A new diffusivity equation for two-phase (liquid water/steam) flow in geothermal reservoirs is derived. The geothermal reservoir may either be initially two-phase or may evolve into a two-phase system during production. Solutions of the diffusivity equation for a continuous line source are presented; the solutions imply that the plot of bottomhole pressure versus $\log_{10}$(t = time) should be a straight line. The slope of the straight line is inversely proportional to the total kinematic mobility (defined in the text). Comparison of the theory with a limited number of computer simulated drawdown histories shows excellent agreement.

INTRODUCTION

In petroleum engineering and groundwater hydrology, well tests are routinely conducted to diagnose the well's condition and to estimate formation properties. Analysis of well test data may be made to yield quantitative information regarding (1) formation permeability, storativity and porosity, (2) the presence of barriers and leaky boundaries, (3) the condition of the well (i.e., damaged or stimulated), (4) the presence of major fractures close to the well, and (5) the mean formation pressure. Well testing procedures (and the quality of information obtained) depend on the age of the well. During temporary completion, testing involves producing the reservoir using a temporary plumbing system (e.g., Drill Stem Testing); and the estimates obtained for the formation parameters are not very accurate. After completion, testing is usually performed in the hydraulic mode. In hydraulic testing, one or more wells are produced at controlled rates and changes in pressure within the producing well itself or nearby observation wells (interference tests) are monitored.

A major concern of well testing is the interpretation of pressure transient data. Much of the existing literature (see Matthews and Russell[1] and Ramey[2] for reviews) deals with isothermal single-phase (water/oil) and isothermal two-phase (oil with gas in solution, free gas) systems. There is, in general, a lack of a methodology for the analysis of nonisothermal reservoir systems, either single or two-phase (liquid water/steam). Geothermal reservoirs commonly involve nonisothermal two-phase (water/steam) flow during well testing. In this paper, we present a theoretical framework for analyzing multiphase pressure transient data in geothermal systems.

References and illustrations at end of paper.

TWO-PHASE (LIQUID WATER/STEAM) FLOW IN GEOTHERMAL SYSTEMS

We consider a fully penetrating well located in infinite reservoir of thickness H. We will neglect any variations in either formation or fluid properties in the vertical direction (this is a common assumption in pressure transient analysis). The geothermal system may either be two-phase prior to production, or may evolve into a two-phase system as a result of fluid production. In the latter case, a boiling front will propagate outwards from the wellbore. The boiling front may be treated as a constant pressure boundary (p=saturation pressure corresponding to the local reservoir temperature).

For the sake of simplicity, let us consider a reservoir which is initially two-phase everywhere. Furthermore, it is convenient to assume that the pressure (and hence temperature) is uniform throughout the system. In radial geometry, the pressure response is governed by the following diffusivity equation (see Appendix for a derivation of equation (1)):

$$\frac{\partial p}{\partial t} - \frac{(k/\nu)_T}{\phi \rho C_T}\left[\frac{1}{r}\frac{\partial p}{\partial r} + \frac{\partial^2 p}{\partial r^2}\right] = 0 \quad \ldots\ldots \quad (1)$$

We are interested in solutions of equation (1) for the case of flow into a centrally located well at a constant mass rate of production M. Mathematically, we have at $r = r_w$

$$r \left.\frac{\partial p}{\partial r}\right|_{r=r_w} = - \frac{M}{2\pi H (k/\nu)_T} \quad \ldots\ldots \quad (2)$$

For the sake of mathematical convenience, the boundary condition at $r=r_w$ is replaced by the "line source"

approximation, i.e.,

$$\lim_{r\to 0} r \frac{\partial p}{\partial r} = -\frac{M}{2\pi H}(k/\nu)_T \quad \ldots\ldots\ldots\ldots \quad (3)$$

The "line source" boundary condition yields identical results (from a practical viewpoint) with those obtained with the original condition.[1,3] We also require that initially (t=0) the reservoir is at a uniform pressure p_i, and that at $r=\infty$ (for all t) we have

$$\lim_{r\to\infty} p(r,t) = p_i \quad \ldots\ldots\ldots\ldots\ldots \quad (4)$$

The solution for equation (1) subject to the boundary conditions (3) and (4) can be written as follows[4]

$$p(r,t) = p_i + \frac{M}{4\pi H (k/\nu)_T} Ei\left\{-\frac{r^2}{4t}\frac{\phi\rho C_T}{(k/\nu)_T}\right\} . \quad (5)$$

Equation (5) implies that the pressure at the wellbottom $p_w(t)$ is

$$p_w(t) = p_i + \frac{M}{4\pi H (k/\nu)_T} Ei\left[-\frac{r_w^2}{4t}\frac{\phi\rho C_T}{(k/\nu)_T}\right] = \quad (6)$$

For $[4t (k/\nu)_T/\phi r_w^2 \rho C_T] > 100$, equation (6) yields the approximate solution:[1]

$$p_w(t) = p_i - \frac{1.15 M}{2\pi H (k/\nu)_T}\left\{\log_{10}\left[\frac{t (k/\nu)_T}{\phi r_w^2 \rho C_T}\right] + 0.351\right\} \quad \ldots\ldots\ldots\ldots \quad (7)$$

Equation (7) implies that a plot of p_w versus $\log_{10}t$ should be a straight line. Let m be the slope of this straight line; then we have

$$(k/\nu)_T = \frac{1.15 M}{2\pi H m} \quad \ldots\ldots\ldots\ldots \quad (8)$$

Substituting from equation (8) into equation (7), we obtain for compressibility C_T

$$\frac{1}{C_T} = \frac{\phi r_w^2 \rho}{t(k/\nu)_T}\ \text{Antilog}_{10}\left[\frac{p_i - p_w(t)}{m} - 0.351\right] . \quad (9)$$

PROPAGATING FLASH-FRONT

Theoretical considerations for the case when a flash front propagates into an initially single-phase reservoir are much more complex than those outlined above for the purely two-phase case. In this instance, the reservoir is two-phase for $r < R$ ($R = R(t)$ denotes the location of the flash-front) and is single phase for $r > R$. The flow behavior in these two regimes is governed by

$$\frac{\partial p_j}{\partial t} - \left[\frac{(k/\nu)_T}{\phi\rho C_T}\right]_j \frac{1}{r}\frac{\partial}{\partial r}\left[r\frac{\partial p_j}{\partial r}\right] = 0 \quad \ldots\ldots \quad (10)$$

where j=1 and 2 denote the two-phase and single-phase regions, respectively. The definitions for the various quantities in equation (10) for the two-phase region (j=1) have already been given. In the single-phase region (j=2), we have:

$$[(k/\nu)_T]_2 = k\rho_\ell/\mu_\ell$$

$$\rho_2 = \rho_\ell$$

$$(C_T)_2 = ((1-\phi)/\phi)\, C_m + C_f$$

Note that with the above definitions, equation (10) (in the single-phase region) reduces to the usual diffusivity equation for the isothermal flow of a liquid of small and constant compressibility.

We will assume that the reservoir is initially at a uniform pressure p_i and temperature T_i. We will, furthermore, require the fluid flow to be isothermal in the single-phase region ($r > R$); in practice, this implies no severe restriction as temperature changes in single-phase flow are usually very small. The boundary conditions at the wellbore and at infinity are:

$$\lim_{r\to 0} r\frac{\partial p_1}{\partial r} = -\frac{M}{2\pi H [(k/\nu)_T]_1} \quad \ldots\ldots\ldots \quad (11a)$$

$$\lim_{r\to\infty} p_2(r,t) = p_i \quad \ldots\ldots\ldots \quad (11b)$$

In addition to the boundary conditions (11), we need to satisfy continuity conditions on mass flow and pressure at the flash-front (r=R). Mathematically, we have at r=R:

$$\left[(k/\nu)_T \frac{\partial p}{\partial r}\right]_1 = \left[(k/\nu)_T \frac{\partial p}{\partial r}\right]_2 \quad \ldots\ldots\ldots \quad (12a)$$

$$p_1 = p_2 = p_s(T_i) \quad \ldots\ldots\ldots \quad (12b)$$

To develop a solution for equations (10) subject to the boundary conditions (11) and (12), we note that these equations are similar to the equations for melting and freezing with cylindrical symmetry presented by Carslaw and Jaeger.[4] The solution for the present case can, therefore, be obtained by following the general approach of Carslaw and Jaeger. We have thus:

$$0 < r < R: \quad p = p_s + \frac{M}{4\pi H [(k/\nu)_T]_1}\left[Ei\left(-\frac{r^2}{4t}\left[\frac{\phi\rho C_T}{(k/\nu)_T}\right]_1\right) - Ei(-\lambda^2)\right] \quad \ldots\ldots \quad (13a)$$

$$r > R: \quad p = p_i + \frac{p_s - p_i}{Ei\left(-\lambda^2\left[(k/\nu)_T/\phi\rho C_T\right]_1/\left[(k/\nu)_T/\phi\rho C_T\right]_2\right)} \times Ei\left(-\frac{r^2}{4t}\left[\frac{\phi\rho C_T}{(k/\nu)_T}\right]_2\right) \quad \ldots\ldots\ldots \quad (13b)$$

where

$$R = 2\lambda \left[\left\{ \frac{(k/\nu)_T}{\phi\rho\, C_T} \right\}_1 t \right]^{1/2} \quad \ldots\ldots\ldots \quad (13c)$$

and λ is the root of

$$[(k/\nu)_T]_2 \frac{P_s - P_i}{Ei\left(-\lambda^2 \left\{(k/\nu)_T/\phi\rho C_T\right\}_1 / \left\{(k/\nu)_T/\phi\rho C_T\right\}_2\right)} \times \exp\left(-\lambda^2 \left\{(k/\nu)_T/\phi\rho C_T\right\}_1 / \left\{(k/\nu)_T/\phi\rho C_T\right\}_2\right) = \frac{M}{4\pi H} \exp(-\lambda^2) \quad \ldots\ldots\ldots \quad (13d)$$

Equation (13a) yields the following expression for well-bottom pressure $p_w(t)$

$$p_w(t) = p_s + \frac{M}{4\pi H [(k/\nu)_T]_1} \left[Ei\left(- \frac{r_w^2}{4t} \left[\frac{\phi\rho\, C_T}{(k/\nu)_T} \right]_1 \right) - Ei(-\lambda^2) \right] \quad \ldots\ldots\ldots\ldots \quad (14)$$

For $4t\,[(k/\nu)_T]_1/r_w^2[\phi\rho C_T]_1 > 100$, equation (14) can be approximated as follows:

$$p_w(t) = p_s - \frac{M\, Ei(-\lambda^2)}{4\pi H\,[(k/\nu)_T]_1} - \frac{1.15\, M}{2\pi H[(k/\nu)_T]_1} \left\{ \log_{10}\left[t\, \frac{[(k/\nu)_T]_1}{r_w^2 (\phi\rho C_T)_1} \right] + 0.351 \right\} \quad \ldots\ldots\ldots\ldots\ldots\ldots \quad (15)$$

Equation (15), like equation (7), implies that a plot of p_w versus $\log_{10} t$ should be a straight line and that $[(k/\nu)_T]_1$ is given by equation (8).

NUMERICAL RESULTS

In order to test the validity of the preceding theory, the Systems, Science and Software (S^3) reservoir simulator MUSHRM[5] was exercised in one-dimensional radial configuration to generate a series of drawdown histories. All of the cases described below were simulated using a 50 zone ($\Delta r_1 = \Delta r_2 = \ldots = \Delta r_{11} = 1$m (3.281 feet); $\Delta r_{12} = 1.2\,\Delta r_{11}$, $\Delta r_{13} = 1.2\,\Delta r_{12}$, ..., $\Delta r_{50} = 1.2\,\Delta r_{49}$) radial grid.

The reservoir rock is assumed to be a sandstone with the following properties (unless otherwise indicated):

$\rho_R = 2.65\ 10^3$ kg/m^3 (165.4 lbm/ft^3)

$\phi = 0.2$

$C_m = 0$ MPa^{-1} (0 psi^{-1})

$K_R = 5.25$ W/m.K (3.03 Btu/h.ft^2.°F/ft)

$C_R = 1$ kJ/kg.K (0.239 Btu/lbm °F)

$k = 0.1\ \mu m^2$ ($\sim$ 0.1 darcy)

$S_{\ell r} = 0.3$

$S_{gr} = 0.05$.

Relative permeabilities R_ℓ and R_g are represented by the Corey equations and the mixture (rock-liquid-vapor) thermal conductivity is approximated by Budiansky's formula.[5] The mass withdrawal rate is assumed to be 0.14 kg/s.m (0.094 lbm/s.ft.).

In the numerical examples discussed here, the effect of mass withdrawal is represented by a volumetric sink term in the well-block (radial extent $r = 0$ to $r = \Delta r_1$). For purposes of comparison with the analytical results presented earlier, it is necessary to define an equivalent radius r_w at which the calculated well-block pressure is equal to the actual flowing pressure due to a continuous line source/sink.

In the numerical simulation of reservoir behavior, it is often necessary to employ well-blocks (i.e., a grid block containing a well) with dimensions much larger than the wellbore radius. Naturally, the pressure calculated for the well-block will be, in general, different from the actual flowing bottomhole pressure. Van Poolen, et al.[6] stated that the calculated press for a well-block should be the average pressure in t portion of the reservoir represented by the block. A. suming steady-state single-phase flow in the well-block (but not in the reservoir as a whole), this implies that the calculated well-block pressure should be equal to the actual flowing pressure at a radius r_w,

$$\ln \frac{r_w}{r_0} = \frac{R^2 \ln (R/r_0)}{R^2 - r_0^2} - \frac{1}{2} \quad \ldots\ldots\ldots\ldots \quad (16a)$$

where r_0 is the actual well radius and R is the radius of the grid block. For $R \gg r_0$, equation (16a) simplifies to

$$r_w = R \exp(-1/2) \quad \ldots\ldots\ldots\ldots \quad (16b)$$

$$\sim 0.6065\ R$$

Equations (16a) and (16b), strictly speaking, hold only for a well located in the center of a radial grid block. For rectangular grid blocks (with dimensions Δx, Δy), equation (16b) is usually replaced by the following expression

$$\frac{r_w}{\sqrt{\Delta x\ \Delta y}} = \frac{0.6065}{\sqrt{\pi}} \quad \ldots\ldots\ldots\ldots \quad (17)$$

Assuming $\Delta x = \Delta y$, equation (17) yields

$$\frac{r_w}{\Delta x} = 0.342.$$

Peaceman[7] examined the grid pressures obtained in the numerical solution of steady incompressible single-phase flow into a single well located in the center of a square grid block ($\Delta x = \Delta y$) and concluded that the well-block pressure should be equal to the actual flowing pressure at a radius of 0.2 Δx (and not at the radius given by equation (17)).

In an attempt to evaluate the significance of Peaceman's results for numerical simulation, Garg, et al.[8] analyzed the numerical solution of steady incompressible single-phase flow into a single well located in both radial and rectangular grid blocks. It is found that the equivalent radius depends, among other things, on the shape of the grid block (radial or rectangular) and the type of mesh (uniform or stretch) employed. Thus, for example, use of uniform radial mesh yields $r_w/R \simeq 0.5615$ in the limit $N \to \infty$, where N denotes the number of grid blocks.

Garg, et al.[8] also compared the numerical solution for transient, slightly compressible (water) single-phase flow into a single well with the line-source solution for the diffusivity equation (see, e.g., Matthews and Russell[1]). It was concluded that the equivalent radius (i.e., the radius at which the actual flowing pressure is equal to the calculated well-block pressure) is approximated by 0.56 R. In this work, we will, therefore, assume that r_w in transient single-phase flow (and also approximately in transient two-phase flow) is given by 0.56 R.

Figure 5 shows five examples of [illegible] was produced at a constant rate. As can be seen, the drawdown data closely fit a straight line; furthermore, the values of $(k/\nu)_T$ computed from the slope of the straight line are in excellent agreement with the actual values in the well-blocks (see Tables 1-5 for the actual values). Note that the actual values (Tables 1-5) vary over a range; this variation is the result of slow changes (except at very early times not considered in drawing the straight line) in steam saturation in the computational well-block as a result of continued production. Figure 3 (drawdown history c) and Table 3 present an especially interesting case; in this case the liquid, initially immobile, becomes mobile for $t > \sim 2\ 10^5$s due to condensation in the well-block. The condensation is caused by a drop in pressure (and hence temperature); in drawing the straight line the pressure data for $t > \sim 2\ 10^5$s was ignored. If the computation had been carried for times sufficiently greater than $t > 2\ 10^5$s, one would see another straight line segment (with a different slope).

Table 6 compares the compressibility C_T values inferred from the slope of the straight line and equation (9) with the actual values. The agreement is quite good for Cases b, c and d. In Cases a and e, the inferred values are quite a bit larger than the actual values; this disagreement is not really surprising in view of the extremely large changes in $(k/\nu)_T$ very early times (see Tables 1 and 5). Large values of $(k/\nu)_T$ at very early times lead to relatively small pressure drops compared to those implied by the straight line. Stated somewhat differently, at early times, equation (7) with constant $(k/\nu)_T$ cannot be used to calculate the well-block pressure in Cases a and e.

Figures 6 and 7 show two additional drawdown histories generated by NUSMP. In these examples, the reservoir was initially single-phase liquid everywhere. In the case shown in Figure 6, a flash-front starts propagating outward from the wellbore at $t \sim 0$; it takes, however a finite time for conditions to stabilize in the two-phase region. For $t > 5\ 10^5$s the data lie on a straight line; and the kinematic mobility calculated from the slope of this straight line agrees quite well with the actual range of values. Figure 7 presents a more interesting case; in this instance the liquid water does not start flashing at the instant the production starts. Thus, we have a short time of single-phase flow followed by a propagating flash-front. The two-phase part of the drawdown curve has a relatively long flat part; this part of the curve is associated with boiling only in the computational well-block. Since the flow behavior in the two-phase region is primarily governed by the location of the flash-front, it follows that a failure to adequately resolve the location of the flash-front in numerical simulations (as it happens when the two-phase flow is restricted to one or two computational zones) would lead to physically meaningless results. In other words, the flat part of the curve in Figure 7 is a purely numerical phenomenon and has no physical significance. A straight line is again seen to fit the late-time data; once again the computed value of $(k/\nu)_T$ is in good agreement with the actual range of values. We have also examined the numerical solutions (Figures 6 and 7) for flash-front velocities; the flash-front position, as a function of time is given by (within numerical precision) $R(t) = A\ t^{1/2}$ where A is constant. The latter observation is in agreement with equation (13c).

CONCLUDING REMARKS

The analytical solutions for two-phase flow discussed in the preceding sections provide a potentially powerful tool for the analysis of pressure transient data from multiphase geothermal systems. Determination of the total kinematic mobility only requires the measurement of mass flow rate M and the bottomhole pressures p_w. The mass flow rate M can be measured at the well-head provided there is no loss of the produced fluid to the non-producing formations as the fluid travels through the wellbore to the well-head. Practical techniques exist for measuring the needed variables. It should be noted that the present analysis does not require separate measurements for liquid and vapor phase mass flow rates. Such data, if available, may be combined with the analysis of the preceding sections to yield additional information regarding relative permeabilities, etc.

NOMENCLATURE

C_f = isothermal liquid compressibility

C_m = formation compressibility

C_R = heat capacity of the rock matrix

C_T = total compressibility, equation (A.12b)

h = enthalpy of liquid/vapor mixture

$= (1-Q)\ h_\ell + Q\ h_g$

$h_\ell (h_g)$ = liquid (vapor) enthalpy

$h_{g\ell}$ = heat of vaporization $= h_g - h_\ell$

h_R = enthalpy of rock matrix

H = formation thickness

k = absolute permeability

K_R = thermal conductivity of the rock grain

m = slope of p_w versus $\log_{10} t$ straight line

M = mass production rate

p = pressure

p_i = initial reservoir pressure

$p_s(T_i)$ = saturation pressure at $T = T_i$

p_w = well-bottom pressure

Q = steam quality = $S\,\rho_g/\rho$

r = radius

r_w = wellbore radius

$R(t)$ = instantaneous position of the flash-front

$R_\ell(R_g)$ = relative liquid (vapor) permeability

S = vapor volume fraction

$S_{\ell r}(S_{gr})$ = residual liquid (vapor) saturation

t = time

$(k/\nu)_g$ = kinematic mobility for the vapor = $k\,R_g\rho_g/\mu_g$

$(k/\nu)_\ell$ = kinematic mobility for the liquid = $k\,R_\ell\rho_\ell/\mu_\ell$

$(k/\nu)_T$ = total kinematic mobility = $(k/\nu)_\ell + (k/\nu)_g$

$\mu_\ell(\mu_g)$ = liquid (vapor) dynamic viscosity

ρ = mixture (liquid and vapor) density = $(1-S)\,\rho_\ell + S\rho_g$

$\rho_\ell(\rho_g)$ = liquid (vapor) density

ρ_R = rock grain density

ϕ = porosity

ACKNOWLEDGMENTS

This work was performed under Systems, Science and Software IR&D research project No. 93102-06. I would like to thank my colleagues Dr. T. R. Blake, Mr. J. W. Pritchett, Dr. M. H. Rice and Dr. T. D. Riney for many helpful discussions.

REFERENCES

1. Matthews, C. S. and Russell, D. G.: Pressure Buildup and Flow Tests in Wells, Society of Petroleum Engineers of AIME, Monograph No. 1, Dallas, Texas (1967).

2. Ramey, H. J., Jr.: "Pressure Transient Analysis for Geothermal Wells", Proceedings Second United Nations Symposium on the Development and Use of Geothermal Resources, San Francisco, California, Volume 3 (May 1975), 1749-1757.

3. Mueller, T. D. and Witherspoon, P. A.: "Pressure Interference Effects within Reservoirs and Aquifers", Journal of Petroleum Technology (April 1965), 471-474.

4. Carslaw, H. S. and Jaeger, J. C.: Conduction of Heat in Solids, Oxford University Press, London, 2nd Edition (1959), 294-296.

5. Garg, S. K., Pritchett, J. W., Rice, M. H. and Riney, T. D.: "U.S. Gulf Coast Geopressured Geothermal Reservoir Simulation", Systems, Science and Software, La Jolla, California, Report SSS-R-77-3147 (1977).

6. Van Poolen, H. K., Breitenbach, E. A. and Thurnau, D. H.: "Treatment of Individual Wells and Grids in Reservoir Modeling", Journal of Petroleum Technology (December 1968), 341-346.

7. Peaceman, D. W.: "Interpretation of Well-Block Pressures in Numerical Reservoir Simulation", paper SPE 6893 presented at Society of Petroleum Engineers 52nd Annual Fall Meeting, Denver, Colorado, October 9-12, 1977.

8. Garg, S. K., Pritchett, J. W., Brownell, D. H., Jr. and Riney, T. D.: "U.S. Gulf Coast Geopressured Geothermal Reservoir Simulation - Year 2", Systems, Science and Software, La Jolla, California, Report SSS-R-78-3639 (1978).

9. Donaldson, I. G.: "The Flow of Steam Water Mixtures through Permeable Beds: A Simple Simulation of a Natural Undisturbed Hydrothermal Region", New Zealand Journal of Science, Volume 11 (1968), 3-23.

10. Mercer, J. W., Jr., Faust, C. and Pinder, G. F.: "Geothermal Reservoir Simulation", Proceedings NSF/RANN Conference on Research for the Development of Geothermal Energy Resources, Jet Propulsion Laboratory/California Institute of Technology, Pasadena, California (1974), 256-267.

11. Brownell, D. H., Jr., Garg, S. K. and Pritchett, J. W.: "Governing Equations for Geothermal Reservoirs", Water Resources Research, Volume 13 (1977), 929-934.

12. Garg, S. K. and Pritchett, J. W.: "On Pressure-Work, Viscous Dissipation and the Energy Balance Relation for Geothermal Reservoirs", Advances in Water Resources, Volume 1 (1977), 41-47.

13. Moench, A. F. and Atkinson, P. G.: "Transient Pressure Analysis in Geothermal Steam Reservoirs with an Immobile Vaporizing Liquid Phase - Summary Report", Proceedings Third Stanford Workshop on Geothermal Reservoir Engineering, Stanford, California (1977), 64-69.

APPENDIX: DERIVATION OF DIFFUSIVITY EQUATION FOR TWO-PHASE (LIQUID WATER/STEAM) FLOW IN POROUS MEDIA

The balance equations for two-phase flow in porous media have previously been discussed by Donaldson,[9] Mercer, et al.,[10] Brownell, et al.[11] and Garg and Pritchett.[12] For the present application, the most general form of the balance laws will not be required. In particular, we will assume that (1) the rock porosity depends only upon the fluid pressure, (2) the rock matrix, the liquid and the vapor are in local thermal equilibrium and that heat conduction is negligible, (3) the liquid and the vapor are in local pressure equilibrium such that the capillary pressure is negligible, and (4) the fluid flow is governed by Darcy's law. The second assumption implies that we need consider only the mixture (rock, liquid, vapor) energy balance.

With these assumptions, the balance equations for mass and energy in radial geometry can be written as follows[12]

Mass (Liquid and Vapor)

$$\frac{\partial}{\partial t}(\phi\rho) - \frac{1}{r}\frac{\partial}{\partial r}\, r\left[(k/\nu)_T \frac{\partial p}{\partial r}\right] = 0 \quad \ldots \quad (A.1)$$

Energy (Rock, Liquid and Vapor)

$$\frac{\partial}{\partial t}[(1-\phi)\rho_R h_R + \phi\rho h - \phi p] - \frac{1}{r}\frac{\partial}{\partial r}\left\{r[(k/\nu)_\ell h_\ell + (k/\nu)_g h_g]\frac{\partial p}{\partial r}\right\} = 0 \quad \ldots \quad (A.2)$$

The first term in equation (A.1) can be expanded and rewritten in the following form:

$$\frac{\partial}{\partial t}(\phi\rho) = \rho\frac{\partial\phi}{\partial t} + \phi\left[\left(\frac{\partial\rho}{\partial p}\right)_h \frac{\partial p}{\partial t} + \left(\frac{\partial\rho}{\partial h}\right)_p \frac{\partial h}{\partial t}\right]$$

On noting that[5]

$$\frac{\partial\phi}{\partial t} = (1-\phi)\, C_m \frac{\partial p}{\partial t} \quad \ldots \quad (A.3)$$

we obtain

$$\frac{\partial(\phi\rho)}{\partial t} = \phi\rho\left\{\left(\frac{1-\phi}{\phi}\right) C_m \frac{\partial p}{\partial t} + \frac{1}{\rho}\left(\frac{\partial\rho}{\partial p}\right)_h \frac{\partial p}{\partial t} + \frac{1}{\rho}\left(\frac{\partial\rho}{\partial h}\right)_p \frac{\partial h}{\partial t}\right\} \quad \ldots \quad (A.4)$$

We will now proceed to express $\partial h/\partial t$ in terms of $\partial h/\partial r$, $\partial p/\partial t$ and $\partial p/\partial r$.

For geothermal applications, it will suffice to assume that

$$h_R = c_R T \quad \ldots \quad (A.5a)$$

where T is the common local temperature of the rock matrix and the pore fluids. Under the steam dome (i.e., two-phase regime), temperature T is a unique function of fluid pressure p.

$$T = T(p) \quad \ldots \quad (A.5b)$$

Combining equations (A.5a) and (A.5b) and differentiating w.r.t. t, we have

$$\frac{\partial h_R}{\partial t} = c_R \frac{dT}{dp}\frac{\partial p}{\partial t} \quad \ldots \quad (A.6)$$

Substituting for $\partial/\partial t\,(\phi\rho)$ from equation (A.1), for $\partial\phi/\partial t$ from equation (A.3), and for $\partial h_R/\partial t$ from equation (A.6) into equation (A.2), we obtain:

$$\left\{-(1-\phi)\, C_m\rho_R h_R + (1-\phi)\,\rho_R c_R \frac{dT}{dp} - \phi - (1-\phi)\, C_m p\right\} \times \frac{\partial p}{\partial t} + \phi\rho\frac{\partial h}{\partial t} = \left\{(k/\nu)_\ell h_\ell + (k/\nu)_g h_g - (k/\nu)_T h\right\}\frac{1}{r}\frac{\partial}{\partial r}\left(r\frac{\partial p}{\partial r}\right) + \frac{\partial p}{\partial r}\left\{\frac{\partial}{\partial r}[(k/\nu)_\ell h_\ell + (k/\nu)_g h_g - (k/\nu)_T h] + (k/\nu)_T\frac{\partial h}{\partial r}\right\} \quad \ldots \quad (A.7)$$

We next note that in practical geothermal applications, the last two terms in the brackets on the left hand side of equation (A.7) (ϕ and $(1-\phi)\, C_m p$) are liable to be negligible compared to the first two terms. Also, we have

$$h_\ell - h = -Q h_{g\ell}$$
$$h_g - h = (1-Q) h_{g\ell} \quad \ldots \quad (A.8)$$

Substitution of equation (A.8) in equation (A.7) yields:

$$\phi\rho\frac{\partial h}{\partial t} = (1-\phi)\rho_R h_R\left[C_m - \frac{1}{T}\frac{dT}{dp}\right]\frac{\partial p}{\partial t} + h_{g\ell}\,(k/\nu)_T\left[\frac{(k/\nu)_g}{(k/\nu)_T} - Q\right]\frac{1}{r}\frac{\partial}{\partial r}\left(r\frac{\partial p}{\partial r}\right) + \frac{\partial p}{\partial r}\left\{\frac{\partial}{\partial r}\left[h_{g\ell}\,(k/\nu)_T\left(\frac{(k/\nu)_g}{(k/\nu)_T} - Q\right)\right] + (k/\nu)_T\frac{\partial h}{\partial r}\right\} \quad \ldots \quad (A.9)$$

Combining equations (A.1), (A.4) and (A.9) we obtain:

$$\phi\rho\left\{\left(\frac{1-\phi}{\phi}\right) C_m + \frac{1}{\rho}\left(\frac{\partial\rho}{\partial p}\right)_h + \frac{1}{\rho^2}\left(\frac{\partial\rho}{\partial h}\right)_p \left(\frac{1-\phi}{\phi}\right)\rho_R h_R \left[C_m - \frac{1}{T}\frac{dT}{dp}\right]\right\}\frac{\partial p}{\partial t} - (k/\nu)_T \left[1 - \frac{1}{\rho}\left(\frac{\partial\rho}{\partial h}\right)_p h_{g\ell}\left\{\frac{(k/\nu)_g}{(k/\nu)_T} - Q\right\}\right]\frac{1}{r}\frac{\partial}{\partial r}\left(r\frac{\partial p}{\partial r}\right) + \frac{\partial p}{\partial r}\left\{-\frac{\partial}{\partial r}(k/\nu)_T + \frac{1}{\rho}\left(\frac{\partial\rho}{\partial h}\right)_p (k/\nu)_T \frac{\partial h}{\partial r} + \frac{1}{\rho}\left(\frac{\partial\rho}{\partial h}\right)_p \frac{\partial}{\partial r}\left[h_{g\ell}(k/\nu)_T\left(\frac{(k/\nu)_g}{(k/\nu)_T} - Q\right)\right]\right\} = 0 \quad \ldots\ldots\ldots \quad (A.10)$$

An examination of the numerical solution for equations (A.1) and (A.2) with a constant rate of mass production (e.g., Cases 1-5 discussed elsewhere in this paper) reveals the following important points:

1. The total kinematic mobility $(k/\nu)_T$ increases with increasing distance r from the wellbore.

2. In the vicinity of the wellbore, we have

$$\left|(k/\nu)_T\left[1 - \frac{1}{\rho}\left(\frac{\partial\rho}{\partial h}\right)_p h_{g\ell}\left\{\frac{(k/\nu)_g}{(k/\nu)_T} - Q\right\}\right]\frac{1}{r}\frac{\partial}{\partial r}\left(r\frac{\partial p}{\partial r}\right)\right| >> \left|\frac{\partial p}{\partial r}\left\{-\frac{\partial}{\partial r}(k/\nu)_T + \frac{1}{\rho}\left(\frac{\partial\rho}{\partial h}\right)_p (k/\nu)_T\frac{\partial h}{\partial r} + \frac{1}{\rho}\left(\frac{\partial\rho}{\partial h}\right)_p \frac{\partial}{\partial r}\left[h_{g\ell}(k/\nu)_T\left(\frac{(k/\nu)_g}{(k/\nu)_T} - Q\right)\right]\right\}\right| \quad \ldots\ldots\ldots \quad (A.11)$$

This strong inequality does not, however, hold for radial distances greater than a few borehole radii.

3. Both the radial terms in equations (A.10) are maximum (in an absolute sense) near the wellbore, and fall off rapidly with increasing radial distance r.

4. The radial terms in equation (A.10) are of opposite signs.

We now replace equation (A.10) by the following diffusivity equation:

$$\phi\rho\, C_T \frac{\partial p}{\partial t} - (k/\nu)_T \frac{1}{r}\frac{\partial}{\partial r}\left(r\frac{\partial p}{\partial r}\right) = 0 \quad \ldots \quad (A.12a)$$

where

$$C_T = \left\{\left(\frac{1-\phi}{\phi}\right) C_m + \frac{1}{\rho}\left(\frac{\partial\rho}{\partial p}\right)_h + \frac{(1-\phi)}{\phi}\frac{1}{\rho^2}\left(\frac{\partial\rho}{\partial h}\right)_p \rho_R h_R \left[C_m - \frac{1}{T}\frac{dT}{dp}\right]\right\} \Big/ \left\{1 - \frac{1}{\rho}\left(\frac{\partial\rho}{\partial h}\right)_p h_{g\ell}\left[(k/\nu)_g/(k/\nu)_T - Q\right]\right\} \quad (A.12b)$$

Note that $(k/\nu)_T$ in equation (A.12a) represents the value of the total kinematic mobility in the vicinity of the borehole. The approximations involved in deriving equation (A.12a) (i.e., (1) neglecting the second radial term in equation (A.10) and (2) replacing $(k/\nu)_T$ by its value near the wellbore) are strictly speaking valid only in the immediate neighborhood of the borehole. Even though equation (A.12a) is not expected to apply at large radii, its use should not cause large errors in the computed response since pressures change only very slowly at large radial distances from the borehole.

The diffusivity equation (A.12a) forms the basis for our analysis of two-phase flow in geothermal systems. Unlike in single-phase isothermal flow, the total compressibility C_T in two-phase flow (c.f., equation (A.12b)) has no simple interpretation; consequently its determination from well-tests, in the absence of data regarding rock thermomechanical properties and detailed knowledge regarding the thermodynamic state of the produced fluid, may have only limited practical utility.

We shall now briefly consider a geothermal steam reservoir with an immobile vaporizing liquid phase in the pores. In this case, we have

$$(k/\nu)_\ell = 0, \quad (k/\nu)_T = (k/\nu)_g = k_g\rho_g/\mu_g \quad . \quad (A.13)$$

where $k_g = kR_g$. Substituting from equation (A.13) into equation (A.12) and rearranging terms, we obtain:

$$\frac{\partial p}{\partial t} - \frac{k_g}{\phi\,\mu_g\, C_T'}\frac{1}{r}\frac{\partial}{\partial r}\left(r\frac{\partial p}{\partial r}\right) = 0 \quad \ldots\ldots \quad (A.14)$$

where

$$C_T' = \frac{\rho\, C_T}{\rho_g} \quad \ldots\ldots\ldots \quad (A.15a)$$

$$C_T = \left\{\left(\frac{1-\phi}{\phi}\right) C_m + \frac{1}{\rho}\left(\frac{\partial\rho}{\partial p}\right)_h + \frac{(1-\phi)}{\phi}\frac{1}{\rho^2}\left(\frac{\partial\rho}{\partial h}\right)_p \rho_R h_R \left[C_m - \frac{1}{T}\frac{dT}{dp}\right]\right\} \Big/ \left\{1 - \frac{1}{\rho}\left(\frac{\partial\rho}{\partial h}\right)_p h_{g\ell}\,(1-Q)\right\} \quad (A.15b)$$

We note that equation (A.14) is identical (albeit with a different definition for the total compressibility) to the diffusivity equation for isothermal single-phase reservoir systems; this fact provides the fundamental justification for the application of classical single-

phase procedures to determine the steam-phase permeability of a geothermal steam reservoir with an immobile vaporizing liquid phase (see, e.g., Moench and Atkinson[13]).

57

TABLE 1

ACTUAL $(k/\nu)_i$ (i = ℓ, g, T) AND VAPOR SATURATION (S) VALUES IN THE WELL-BLOCK FOR SIMULATED DRAWDOWN HISTORY (a)

Time s		Vapor Saturation (S)	$10^8\ (k/\nu)_\ell$ s	$10^8\ (k/\nu)_g$ s	$10^8\ (k/\nu)_T$ s
0		0.050	79.85	0	79.85
0.576	10^4	0.163	37.26	0.22	37.48
0.1296	10^5	0.169	35.43	0.26	35.69
0.3456	10^5	0.175	34.00	0.29	34.29
0.7056	10^5	0.178	33.12	0.31	33.43
0.14256	10^6	0.181	32.36	0.33	32.69
0.35856	10^6	0.185	31.52	0.36	31.88
0.71856	10^6	0.187	30.96	0.37	31.33
0.100656	10^7	0.188	30.69	0.38	31.07

TABLE 2

ACTUAL $(k/\nu)_i$ (i = ℓ, g, T) AND VAPOR SATURATION (S) VALUES IN THE WELL-BLOCK FOR SIMULATED DRAWDOWN HISTORY (b)

Time s		Vapor Saturation (S)	$10^8\ (k/\nu)_\ell$ s	$10^8\ (k/\nu)_g$ s	$10^8\ (k/\nu)_T$ s
0		0.350	6.71	3.48	10.19
0.504	10^4	0.400	3.59	4.90	8.49
0.1224	10^5	0.402	3.49	4.90	8.39
0.3384	10^5	0.404	3.41	4.88	8.29
0.6984	10^5	0.404	3.39	4.84	8.23
0.14184	10^6	0.405	3.37	4.79	8.16
0.35784	10^6	0.405	3.34	4.74	8.08
0.71784	10^6	0.406	3.30	4.71	8.01
0.100584	10^7	0.406	3.29	4.69	7.98

TABLE 3

ACTUAL $(k/\nu)_i$ (i = ℓ, g, T) AND VAPOR SATURATION (S) VALUES

IN THE WELL-BLOCK FOR SIMULATED DRAWDOWN HISTORY (c)

Time s		Vapor Saturation (S)	$10^8\ (k/\nu)_\ell$ s	$10^8\ (k/\nu)_g$ s	$10^8\ (k/\nu)_T$ s
0		0.702	0	23.02	23.02
0.432	10^4	0.731	0	22.26	22.26
0.1152	10^5	0.734	0	22.13	22.13
0.3312	10^5	0.734	0	21.99	21.99
0.6912	10^5	0.729	0	21.89	21.89
0.14112	10^6	0.714	0	21.80	21.80
0.35712	10^6	0.662*	0*	19.12*	19.12*
0.71712	10^6	0.624	0.02	16.58	16.60
0.100512	10^7	0.623	0.02	16.53	16.55

*Liquid slightly mobile

TABLE 4

ACTUAL $(k/\nu)_i$ (i = ℓ, g, T) AND VAPOR SATURATION (S) VALUES

IN THE WELL-BLOCK FOR SIMULATED DRAWDOWN HISTORY (d)

Time s		Vapor Saturation (S)	$10^8\ (k/\nu)_\ell$ s	$10^8\ (k/\nu)_g$ s	$10^8\ (k/\nu)_T$ s
0		0.160	35.38	0.10	35.48
0.720	10^4	0.298	10.84	0.96	11.80
0.144	10^5	0.301	10.47	0.97	11.44
0.360	10^5	0.305	10.02	0.99	11.01
0.720	10^5	0.308	9.68	1.01	10.69
0.144	10^6	0.309	9.58	1.00	10.58
0.360	10^6	0.312	9.27	1.00	10.27
0.720	10^6	0.314	9.00	1.01	10.01
0.1008	10^7	0.315	8.87	1.01	9.88

TABLE 5

ACTUAL $(k/v)_i$ (i = x, g, T) AND VAPOR SATURATION (S) VALUES IN THE WELL-BLOCK FOR SIMULATED DRAWDOWN HISTORY (a)

Time, s		Vapor Saturation (S)	$10^8\ (k/v)_x$, s	$10^8\ (k/v)_g$, s	$10^8\ (k/v)_T$, s
0		0.050	24.49	0	24.49
0.720	10^4	0.236	19.21	0.45	19.66
0.144	10^5	0.241	18.50	0.47	18.97
0.360	10^5	0.246	17.62	0.50	18.12
0.720	10^5	0.250	16.94	0.53	17.47
0.144	10^6	0.254	16.42	0.54	16.96
0.360	10^6	0.256	16.01	0.56	16.57
0.720	10^6	0.259	15.56	0.57	16.13
0.1008	10^7	0.261	15.35	0.58	15.93

TABLE 6

COMPARISON OF ACTUAL (C_{tact}) AND INFERRED (C_{tinf}) COMPRESSIBILITIES

Drawdown Case	Time, s		C_{tact}, MPa^{-1} (10^{-2} psi^{-1})	C_{tinf}, MPa^{-1} (10^{-2} psi^{-1})	C_{tinf}/C_{tact}
a	0.14256	10^6	1.80 (1.24)	6.83 (4.70)	3.79
b	0.14184	10^6	0.286 (0.197)	0.305 (0.211)	1.07
c	0.6912	10^5	0.309 (0.213)	0.399 (0.275)	1.29
d	0.144	10^6	1.99 (1.37)	2.91 (2.00)	1.46
e	0.144	10^6	3.75 (2.59)	8.79 (6.06)	2.34

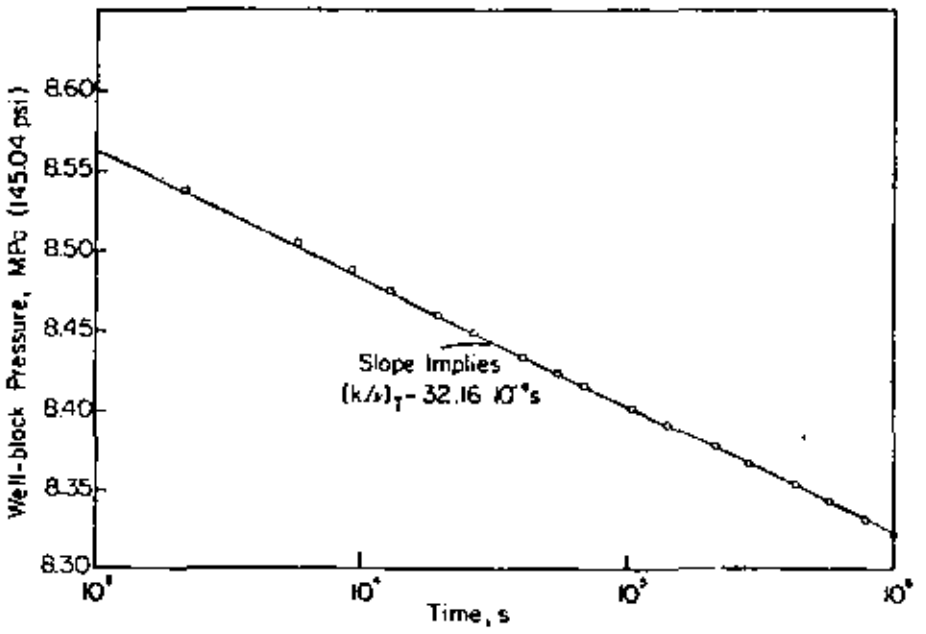

FIG. 1 - SIMULATED DRAWDOWN HISTORY (a). RESERVOIR IS INITIALLY TWO-PHASE EVERYWHERE (p=8.599 MPa ~ 1247.2 psi, S=0.05). SEE TABLE 1 FOR ACTUAL $(k/v)_T$ VALUES.

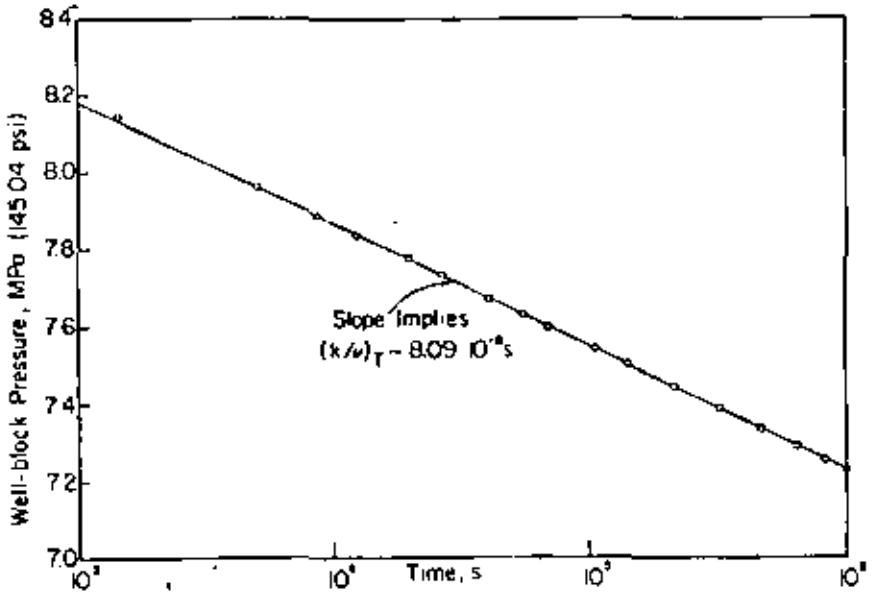

FIG. 2 - SIMULATED DRAWDOWN HISTORY (B). RESERVOIR IS INITIALLY TWO-PHASE EVERYWHERE (p=8.5991 MPa = 1247.2 psi, S=0.35). SEE TABLE 2 FOR ACTUAL $(k/\nu)_T$ VALUES.

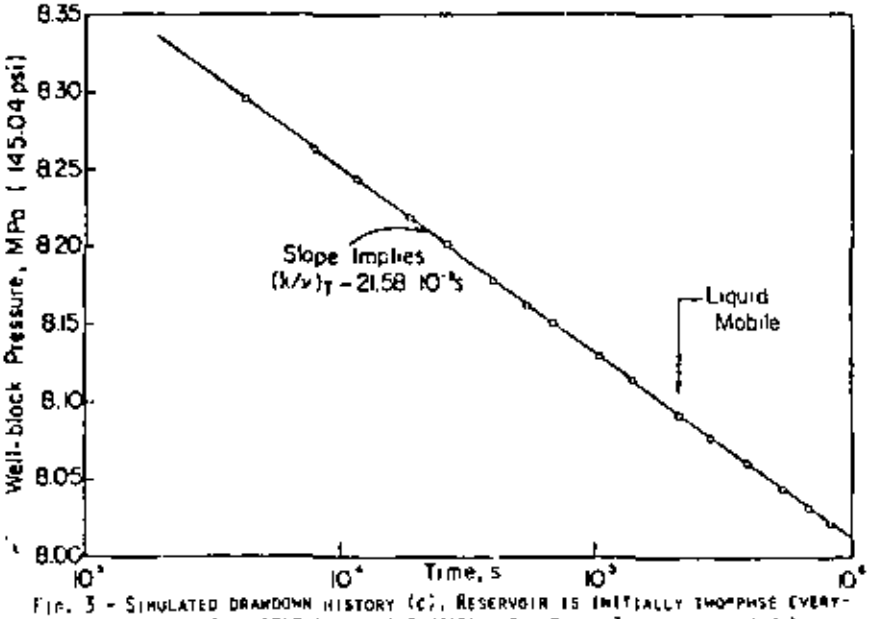

FIG. 3 - SIMULATED DRAWDOWN HISTORY (C). RESERVOIR IS INITIALLY TWO-PHASE EVERYWHERE (p=8.5991 MPa = 1247.2 psi, S=0.7015). SEE TABLE 3 FOR ACTUAL $(k/\nu)_T$ VALUES

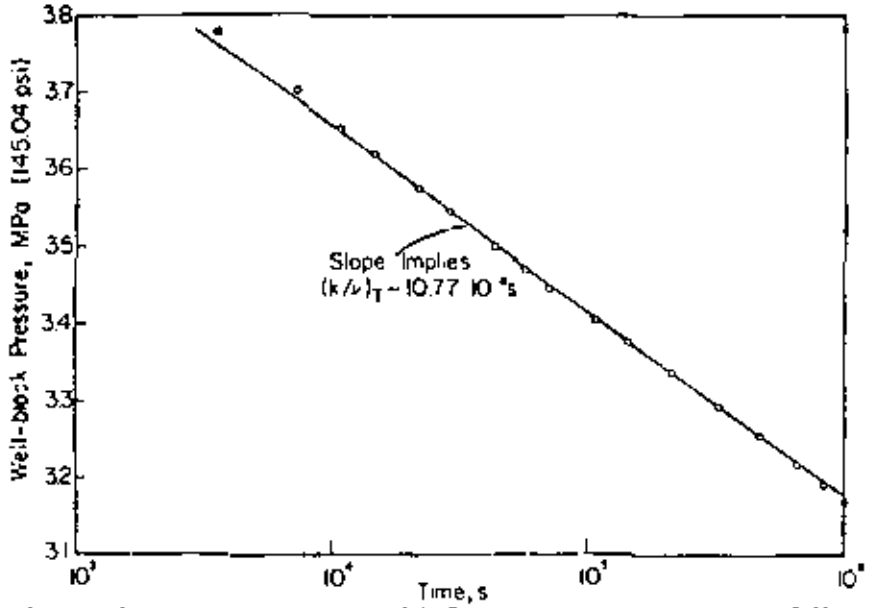

FIG. 4 - SIMULATED DRAWDOWN HISTORY (D). RESERVOIR IS INITIALLY TWO-PHASE EVERYWHERE (p=3.9808 MPa = 577.4 psi, S=0.1604). SEE TABLE 4 FOR ACTUAL $(k/\nu)_T$ VALUES.

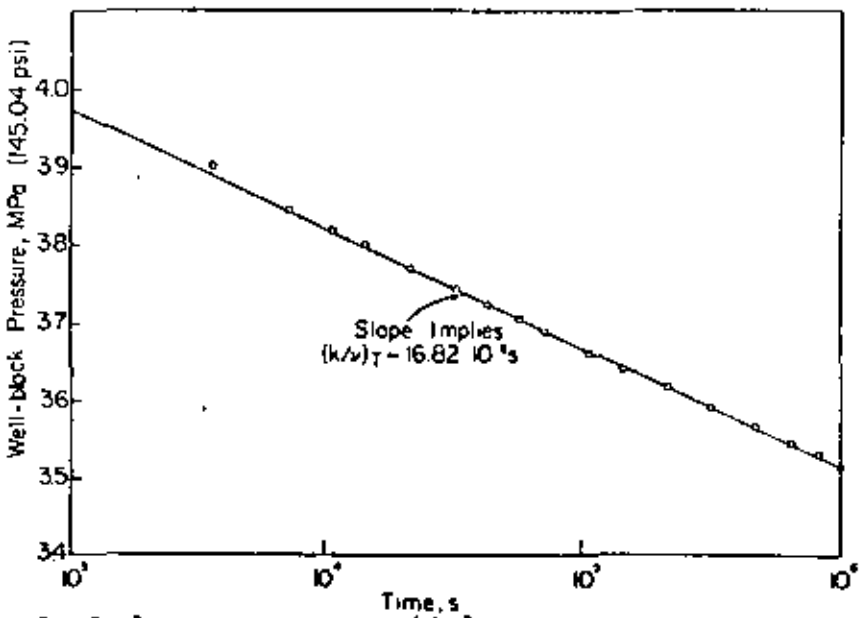

FIG. 5 - SIMULATED DRAWDOWN HISTORY (E). RESERVOIR IS INITIALLY TWO-PHASE EVERYWHERE (P=3.9808 MPa ~ 577.4 PSI, S=0.0.05). SEE TABLE 5 FOR ACTUAL $(k/\nu)_T$ VALUES.

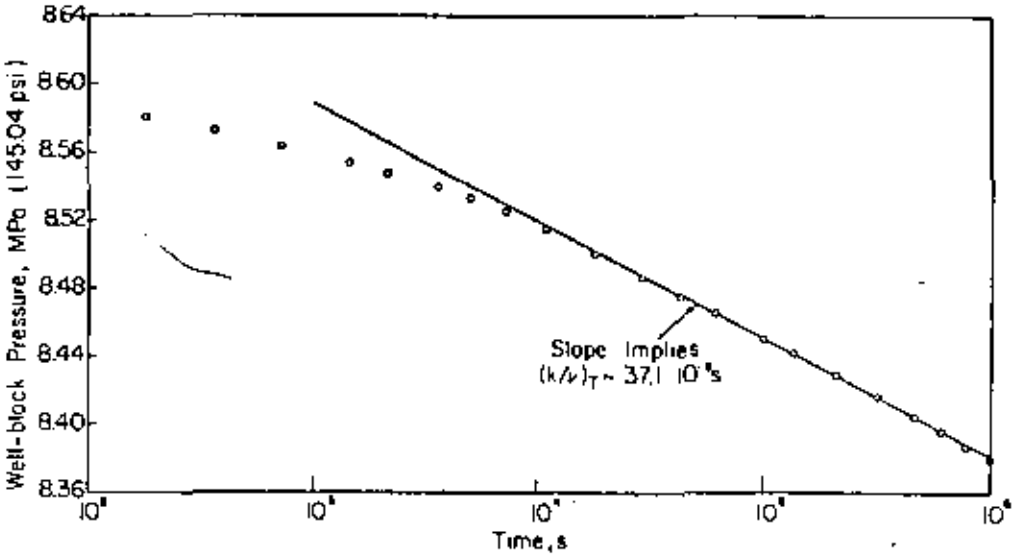

FIG. 6 - SIMULATED DRAWDOWN HISTORY (F). RESERVOIR IS INITIALLY SINGLE-PHASE (LIQUID) EVERYWHERE (P=8.62 MPa ~ 1250.2 PSI, T=573.15K=572°F). ACTUAL RANGE OF $(k/\nu)_T$ VALUES FOR POINTS LYING ON THE STRAIGHT LINE IS (36.1-42.3) 10^{-8}s.

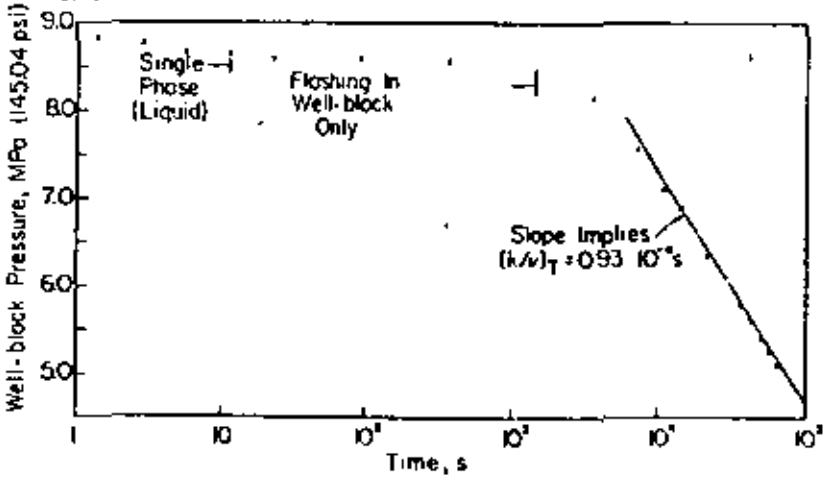

FIG. 7 - SIMULATED DRAWDOWN HISTORY (G). RESERVOIR IS INITIALLY SINGLE-PHASE EVERYWHERE (P=9.000 MPa ~ 1305.3 PSI, T = 573.15K=572°F). ABSOLUTE PERMEABILITY k FOR THIS CASE IS 0.01 μm^2 (~ 0.01 DARCY) AND THE ACTUAL RANGE OF $(k/\nu)_T$ VALUES FOR POINTS LYING ON THE STRAIGHT LINE IS (0.93-1.15) 10^{-8}s.

SPE

Society of Petroleum Engineers of AIME

SPE 6887

APPLICATION OF TWO-RATE FLOW TESTS TO THE DETERMINATION OF GEOTHERMAL RESERVOIR PARAMETERS

by Jesus Rivera-R., Member SPE-AIME, Comisión Federal de Electricidad, and Henry J. Ramey, Jr., Member SPE-AIME, Stanford U.

This paper was presented at the 52nd Annual Fall Technical Conference and Exhibition of the Society of Petroleum Engineers of AIME, held in Denver, Colorado, Oct. 9-12, 1977. The material is subject to correction by the author. Permission to copy is restricted to an abstract of not more than 300 words. Write: 6200 N. Central Expy., Dallas, Texas 75206.

ABSTRACT

This paper deals with the application of well-established pressure transient analysis techniques to the determination of geothermal reservoir parameters. Among the pressure transient techniques available, those concerned with two-rate flow testing were chosen. A two-rate test may permit obtaining data while reducing interruption of power generation. Two-rate techniques have been applied successfully to both oil and gas reservoirs; however, no data have been published to date--to the authors' knowledge--on the application of this method to liquid-dominated geothermal reservoirs. Data from one test run on a well in the Cerro Prieto Geothermal Field are shown. The field data were interpreted by means of four different models. Three of the models produced results that agreed with each other, the fourth one produced data scatter.

INTRODUCTION

The Cerro Prieto Geothermal Field is located about 30 kilometers south of Mexicali, Baja California. As shown in Figure 1, this field is situated at the southern end of the Salton-Mexicali trough, which includes other thermal anomalies of great interest, such as Heber and East Mesa. The reservoir is a liquid-dominated system having a cap rock made of impervious plastic clays. This cap acts as a seal, keeping the hot water trapped and preventing the dissipation of heat to the surface. Figure 2 shows a schematic geological cross section of the reservoir drawn in an East-West direction.[1] The permeable layers consist of alternating shale and sandstone layers resting on a highly fractured granitic basement. Basement rocks were encountered in one of the wells at a depth of approximately 2500 meters. The thickness of the cap rock varies, according to the location of the wells, from 700 up to almost 1000 meters in the portion of the field already drilled.

The first exploratory well in the area was drilled in 1961, and in 1964, four more exploratory wells were drilled. After an extensive field-test program, the Comisión Federal de Electricidad started the construction of a 75-MW geothermal power plant in 1968. The plant was located in the Mexicali valley and named for the Cerro Prieto volcano. This plant started commercial operation in April 1973, and has been in operation since that date. The turbines operate on steam from 14 wells. The geothermal fluid is obtained as a water-vapor mixture, because flashing takes place at some depth inside the wellbore. The separated hot brine is disposed of in an evaporation pond; however, plans are being made to evaluate the feasibility of reinjecting at least part of the spent liquid.

Although well testing and pressure transient analysis techniques have been widely applied by petroleum engineers to gas and oil reservoirs (to find mean formation pressure, skin factor, and average permeability and porosity), the application of the same techniques to geothermal reservoirs encounters problems that are not commonly found in petroleum applications. In hot-water wells,[3] two-phase flow and heat transfer influence the pressure response when the wells are shut-in. In addition to this, gathering of the data is difficult because of the high temperatures involved. Bottom-hole temperatures in the range of 300 to 320 °C are common in the Cerro Prieto Field. Until recently, there were no bottom-hole pressure measuring devices that could withstand such temperatures for more than three hours. Another problem is mechanical damage due to extreme buffeting by the high production rates of boiling geothermal fluids. Rates in excess of 24,000 B/D are common.

Considering these facts, it was decided that the best choice for obtaining pressure-time data by means of standard bourdon-tube type pressure bombs would be short-time duration drawdown tests. These tests could be run by changing the flow rate to some predetermined value after the well was stabilized at a given constant rate for some time. This type of test is known in petroleum technology as a "two-rate" flow test. It was first proposed by Russell[4] in 1962. Further improvements in this technique were introduced by Selim[5] and Odeh and Jones.[6] Two-rate flow tests had been applied extensively in both gas

References and illustrations at end of paper.

and oil reservoirs; however, no data have been published to date on an application of this technique to liquid-dominated geothermal reservoirs to the authors' knowledge. The three techniques mentioned above were used for interpretation of the data; additionally, the data were analyzed as a variable-rate drawdown case according to the Odeh and Jones[7] method.

TWO-RATE FLOW TEST

In preparation for the test, the well was stabilized for a period of approximately 48 hours at a constant rate of 111 tons/hour. The flow rate was measured several times during this stabilization period. A pressure bomb was lowered into the well, measuring the bottom-hole pressure for approximately 20 minutes prior to the rate change, in order to have a dependable value for the flowing pressure prior to the change in rate.

The producing rate was changed to a value of 66.1 tons/hour. A record as continuous as possible was kept of water and steam production, and changes in wellhead pressure.

Figure 3 shows the mass-flow rate and bottom-hole pressure during the test. After stabilized conditions were evident from wellhead measurements, the flow rate was increased to a value as close to the initial flow rate as possible, following the procedure suggested by Selim.[5]

INTERPRETATION OF THE DATA

The data obtained from this test were interpreted by means of the models suggested by Russell,[4] Selim[5] and Odeh and Jones (two-rate tests[6] and drawdown variable rate[7]). The results obtained from the application of these models are as follows.

Russell's[4] Model

The interpretation equation as presented by Russell[4] is as follows:

$$p_{wf} = p_i - \frac{162.6 q_2 B\mu}{kh}\left(\log \frac{k}{\phi\mu c r_w^2} - 3.23 + 0.87\, s\right) - \frac{162.6 q_1 B\mu}{kh}\left(\log \frac{t+\Delta t'}{\Delta t'} + \frac{q_2}{q_1}\log \Delta t'\right) \quad (1)$$

Equation 1 is in standard oil field units. The nomenclature is presented at the end of the paper. Changing these units into metric geothermal units and expressing the flow rates in terms of mass rates, Eq. 1 can be written as:

$$p_{wf} = p_i - 527.4\,\frac{w_2 v_{sc} B\mu}{kh}\left(\log \frac{k}{\phi\mu c r_w^2} + 0.891 + 0.87\, s\right) - 527.4\,\frac{w_1 v_{sc} B\mu}{kh}\left(\log \frac{t+\Delta t'}{\Delta t'} + \frac{w_2}{w_1}\log \Delta t'\right) \quad (2)$$

From Eq. 2 it is evident that by graphing p_{wf} vs. $\left(\log \frac{t+\Delta t'}{\Delta t'} + \frac{w_2}{w_1}\log \Delta t'\right)$ a straight line should be obtained whose slope is given by:

$$m_R = 527.4\,\frac{w_1 v_{sc} B\mu}{kh} \quad (3)$$

Figure 4 shows the result of graphing the data according to Eq. 2. The kh is obtained as 1,946 md-m, and the skin factor as -5.28. The details of the calculations are shown in the appendix.

The equation for the skin factor in geothermal units is given by the following expression:

$$s = 1.151\left(\frac{w_1}{w_1 - w_2}\,\frac{p_{1hr} - p_{wf}}{m_R} - \log \frac{k}{\phi\mu c r_w^2} - 0.891\right) \quad (4)$$

The average reservoir pressure in the volume drained by the well was obtained by means of the Matthews, et al.,[8] method.

SELIM MODIFICATION[5] OF RUSSELL'S MODEL

Selim observed that the results obtained from a two-rate test were sensitive to the slope of the straight line drawn according to the method proposed by Russell. He suggested modification of the method by returning the well to the producing rate it had prior to the test once the well had reached stable conditions. The pressures and flow rates should be measured until new stabilized conditions are reached.

The equation originally proposed by Selim is:[5]

$$p_{wf} = p_i - \frac{162.6 q_3 B\mu}{kh}\left(\log \frac{k}{\phi\mu c r_w^2} - 3.23 + 0.87\, s\right) - \frac{162.6 q_2 B\mu}{kh}\left(\log\left[\frac{(\frac{q_1}{q_2})t+\Delta t'+\Delta t''}{\Delta t''}\right] + \frac{q_3}{q_2}\log \Delta t''\right) \quad (5)$$

Equation 5 is expressed in standard oilfield units. Changing these units into metric geothermal units and expressing the flow rates in terms of mass, this equation can be expressed as:

$$p_{wf} = p_i - 527.4\,\frac{w_2 v_{sc} B\mu}{kh}\left(\log \frac{k}{\phi\mu c r_w^2} + 0.891 + 0.87\, s\right) - 527.4\,\frac{w_2 v_{sc} B\mu}{kh}\left(\log \frac{(\frac{w_1}{w_2})t+\Delta t'+\Delta t''}{\Delta t''} + \frac{w_3}{w_2}\log \Delta t''\right) \quad (5)$$

From Eq. 6 it is evident that graphing P_{wf} vs. $\left(\log\left[\frac{(\frac{w_1}{w_2})t+\Delta t'+\Delta t''}{\Delta t''}\right]+\frac{w_3}{w_2}\log\Delta t''\right)$ a straight line is obtained whose slope is

$$m_S = \frac{527.4\, w_2 v_{sc} B\mu}{kh} \qquad (7)$$

Figure 5 shows the graph obtained by plotting the data according to Eq. 6.

Selim[5] showed that the slope calculated by means of Russell's method and that calculated using the modification he suggested should hold the following relationship:

$$\frac{m_R}{m_S} = \frac{w_1}{w_2} \qquad (8)$$

Equation 8 represents an additional constraint that the straight line portions of Eqs. 2 and 6 must satisfy. It can be used to select the appropriate straight line portion in the event that several straight sections are present due to scatter of the field data. Three straight line segments are evident in Fig. 5. The one labelled number 2 satisfies Eq. 8 and was considered to be the correct one. Results were kh was 1,905 md-m. Details of the calculations are included in the appendix.

ODEH AND JONES[7] VARIABLE DRAWDOWN MODEL

The field data obtained during the transient conditions after the change in rate were analyzed as a variable drawdown case having w_1 and w_2 as the initial and final flow rates. The result of this analysis is shown in Fig. 6 and the calculations are included in the appendix. The kh product obtained from this method was 1,990 md-m and agreed well with those determined by the methods mentioned before. The interpretation equation in oilfield units given in the original paper is as follows:

$$\frac{P_i-P_{wf}}{q_n} = \frac{162.6B\mu}{kh}\left(\sum_{i=0}^{n-1}\frac{\Delta q_i}{q_n}\log(t_n-t_i) - 3.228 + 0.87\,s + \log\frac{k}{\phi\mu c r_w^2}\right) \qquad (9)$$

Writing this equation in metric geothermal units and expressing the flow rate in terms of mass, this equation can be written as follows:

$$\frac{P_i-P_{wf}}{w_n} = 527.4\,\frac{v_{sc}B\mu}{kh}\left(\sum_{i=0}^{n-1}\frac{\Delta w_i}{w_n}\log(t_n-t_i) + 0.8926 + 0.87s + \log\frac{k}{\phi\mu c r_w^2}\right) \qquad (10)$$

Therefore, by graphing

$$(P_i-P_{wf}) \text{ vs. } \sum_{i=0}^{n-1}\frac{\Delta w_i}{w_n}\log(t_n-t_i)\ ,$$

a straight line is obtained whose slope is given by the following equation:

$$m_{ODV} = 527.4\,\frac{v_{sc}B\mu}{kh} \qquad (11)$$

ODEH AND JONES[6] TWO-RATE MODEL

This method is similar to the one described before, except that it includes second differences of the flow rates as shown by Eq. 13 below. The field data were analyzed according to Eq. 12 below. Figure 7 shows the graph obtained by plotting the data according to Eq. 14. Scatter of the data points is observed, making it very difficult to find a proper straight line. Fitting a straight line to the data points by means of linear regression produced a kh product of 2,860 md-m, much higher than that obtained with the models described before. The calculations are included in the appendix.

The original equation[7] in oilfield units is as follows:

$$\frac{P_{wf}|_{t=\Delta t}-P_{wf}|_{t=0}}{\Delta q_n} = \frac{162.6B\mu}{kh}\left(\frac{1}{\Delta q_n}\sum_{i=0}^{n-1}\Delta\Delta q_i\log(t_n-t_i) + \log\frac{k}{\phi\mu c r_w^2} - 3.23 + 0.87\,s\right) \qquad (12)$$

where:

$$\left.\begin{aligned}\Delta q_i &= q_o - q_i\\ \Delta\Delta q_i &= \Delta q_{i+1} - \Delta q_i\\ \Delta q_o &= 0\\ \Delta q_n &= q_o - q_n\end{aligned}\right\} \qquad (13)$$

Expressing Eq. 12 in metric geothermal units and using mass-flow rate instead of volumetric-flow rate, this equation can be written as follows:

$$\frac{P_{wf}|_{t=\Delta t}-P_{wf}|_{t=0}}{w_n} = 527.4\,\frac{v_{sc}B\mu}{kh}\left(\frac{1}{\Delta w_n}\sum_{i=0}^{n-1}\Delta\Delta w_i\log(t_n-t_i) + \log\frac{k}{\phi\mu c r_w^2} + 0.87s + 0.891\right) \qquad (14)$$

where

$$\left.\begin{aligned} \Delta w_i &= w_o - w_i \\ \Delta\Delta w_i &= \Delta w_{i+1} - \Delta w_i \\ \Delta w_o &= 0 \\ \Delta w_n &= w_o - w_i \end{aligned}\right| \qquad (15)$$

Graphing:

$$\frac{p_{wf}|_t - p_{wf}|_{t=0}}{\Delta w_n} \text{ vs. } \frac{1}{\Delta w_n}\sum_{i=0}^{n-1} \Delta\Delta w_i \log (t_n - t_i) ,$$

a straight line is obtained whose slope is given by:

$$m_{OJT} = 527.4\,\frac{v_{sc} B \mu}{kh} \qquad (16)$$

CONCLUSIONS

The equations reported to describe two-rate flow tests have been converted to metric geothermal form and used to analyze a test for a geothermal well which produces a boiling brine. The interpretive equations are presented and an example calculation made for each of four methods. Good agreement was obtained from the application of the models of Russell,[4] Selim,[5] and Odeh and Jones drawdown variable-rate case.[7] However, scatter of the data was observed when the two-rate Odeh and Jones[6] technique was used. Other conclusions reached include the following.

1. Two-rate flow tests can be used for calculating basic geothermal reservoir parameters.

2. Russell's[4] model and the modification by Selim[5] seem to produce better results than the technique proposed by Odeh and Jones.[6] However, the Odeh and Jones variable-rate method[7] gave results comparable to those of Russell and Selim.

3. Two-rate flow tests for geothermal wells can be carried out with standard bourdon-tube type pressure instruments at temperatures as high as 315°C. One reason for this result is that it appears possible to conduct a test in a period of time as short as 3 hours. It is not known whether this is a general observation, and the main criterion of success used herein was reasonableness of the results. However, the interpretive equations and example calculations should be useful for two-rate tests of any duration.

NOMENCLATURE

B = brine formation volume factor, (volume, reservoir conditions/volume, standard conditions)
c_t = total fluid compressibility, $(Kg/cm^2)^{-1}$
h = formation net thickness, m
k = permeability, md
m = slope of a straight line
n = constant rate intervals in Odeh and Jones model
p = pressure, Kg/cm^2
p_i = initial pressure, Kg/cm^2
p_{wf} = flowing bottom-hole pressure, Kg/cm^2
p_{1hr} = flowing bottom-hole pressure 1 hr after the rate change, Kg/cm^2
q = volumetric flow rate, bbl/day
r_w = wellbore radius, cm
s = skin factor, dimensionless
t = producing time to instant of rate change, hrs
t' = producing time measured from first rate change, hrs
t'' = producing time measured from second rate change, hrs
v = specific volume, cm^3/gr
w = mass flow rate, ton/hr
y = correlation parameter in Odeh and Jones method

GREEK SYMBOLS

μ = viscosity, cp
ν = specific volume, cm^3/gr
ϕ = porosity, fraction

SUBSCRIPTS

1 = conditions prior to rate change
2 = conditions after first rate change
3 = conditions after second change
f = initial condition
OJT = refers to Odeh and Jones two-rate model
OJV = refers to Odeh and Jones variable drawdown model
R = refers to Russell's model
S = refers to Selim's model
sc = standard conditions
w = wellbore
wf = flowing conditions

ACKNOWLEDGEMENT

The authors wish to thank the Comisión Federal de Electricidad for permission to publish the field data presented in this paper. The assistance received from Ing. Hector Alonso E. and Ing. Jorge Guiza L. is also acknowledged.

REFERENCES

1. "Cerro Prieto - Underground Power," Comisión Federal de Electricidad Pamphlet (1971).

2. Ramey, H.J., Jr.: "Pressure Transient Analysis for Geothermal Wells," Second United Nations Symposium on the Use and Development of Geothermal Energy, San Francisco, Ca., May 20-29, 1975.

3. Gulati, M.S.: "Pressure and Temperature Build-Up in Geothermal Wells," Stanford Geothermal Workshop, Stanford University, Dec. 15-17, 1975.

4. Russell, D.G.: "Determination of Formation Characteristics by Two-Rate Flow Tests," J. Pet. Tech., December 1962, pp. 1347-1355.

5. Selim, M.A.: "A Modification of the Two-Rate Flow Method for Determination of Reservoir

Parameters," J. Institute of Petroleum, v. 53, no. 527, November 1967, pp. 343-352.

6. Odeh, A.S., and Jones, L.G.: "Two-Rate Flow Test, Variable Rate Case," J. Pet. Tech., January 1974, pp. 93-99.

7. Odeh, A.S., and Jones, L.G.: "Pressure Drawdown Analysis, Variable Rate-Case," J. Pet. Tech., August 1965, pp. 960-964.

8. Matthews, C.S., Brons, F., and Hazebroek, P.: "A Method for Determination of Average Pressure in a Bounded Reservoir," Trans. AIME, v. 201, 1952, pp. 182-191.

APPENDIX - TWO-RATE FLOW CALCULATIONS

The test data are shown on Fig. 1 and a listing is given in Table 1. The data were interpreted by four methods. A brief description of the interpretation follows.

Russell's[4] Model

From Fig. 4, a straight line of slope = 3.719 is obtained. According to Eq. 3 in the text:

$$3.719 = 527.4 \frac{w_1 v_{sc} B\mu}{kh}$$

$$kh = \frac{527.4\, w_1 v_{sc} B\mu}{3.719}$$

$$kh = \frac{527.4\ (111)\ (1.043)\ (1.185)\ (0.1017)}{3.719}$$

$$= 1,946 \text{ md-m}$$

The skin factor is obtained from Eq. 4:

$$s = 1.151 \left[\frac{111}{111-66.1} \frac{60.5-54.9}{3.719} - \log\left(\frac{36}{(0.20)(0.1017)(119\times10^{-6})(0.27)} \right) - 0.891 \right]$$

$$s = 5.28$$

Selim's[5] Model

From Fig. 5, three straight lines are obtained whose slopes are as follows:

$$m_{S1} = -5.5$$
$$m_{S2} = -2.3$$
$$m_{S3} = -2.0$$

According to the restriction imposed by Eq. 8 in the text, the ratios for the straight line portions are:

$$\frac{m_R}{m_{S1}} = \frac{3.719}{5.5} = 0.68$$

$$\frac{m_R}{m_{S2}} = \frac{3.719}{2.3} = 1.62$$

$$\frac{m_R}{m_{S3}} = \frac{3.719}{2.0} = 2.0$$

The ratio of the flow rates is:

$$\frac{w_1}{w_2} = \frac{111}{66.1} = 1.68$$

Therefore, the second straight line portion (the one having a slope of 2.3) is the correct one.

From Eq. 7 in the text:

$$2.3 = 527.4 \frac{w_2 v_{sc} B\mu}{kh}$$

$$kh = \frac{527.4\ (66.1)\ (1.043)\ (1.185)\ (0.1017)}{2.3}$$

$$kh = 1,905 \text{ md-m}$$

Odeh and Jones[7] Variable Drawdown Model

From Fig. 6, the slope of the straight line is 0.0333.

From Eq. 11 in the text:

$$0.0333 = \frac{527.4\, v_{sc} B\mu}{kh}$$

$$kh = \frac{527.4\ (1.043)\ (1.185)\ (0.1017)}{0.0333}$$

$$kh = 1,990 \text{ md-m}$$

Odeh and Jones[6] Two-Rate Model

From Fig. 8, the slope of the straight line is 0.0228.

From Eq. 16 in the text:

$$0.0228 = \frac{527.4\, v_{sc} B\mu}{kh}$$

$$kh = \frac{527.4\ (1.043)(1.185)(0.1017)}{0.0228} = 2,860 \text{ md-m}$$

TABLE 1

TWO-RATE FLOW TEST DATA

Total Time (min)	Time Ellapsed since Rate Change (min)	Wellhead Pressure psi	Wellhead Pressure kg/cm^2	Bottom-Hole Pressure psi	Bottom-Hole Pressure kg/cm^2	Mass Flow Rate ($\frac{ton}{hr}$)
0		432	30.4	779.9	54.9	111.0
15		432		779.9	54.9	111.0
16	1	432	30.4	779.9	54.9	101.4
18	3	510	35.9	822.2	57.9	86.0
19	4	520	36.6	828.0	58.3	70.2
20	5	528	37.2	830.9	58.5	67.4
21	6	526	37.0	832.4	58.6	67.4
22	7	522	36.8	833.8	58.7	66.1
23	8	520	36.6	835.3	58.8	66.1
24	9	518	36.5	835.3	58.8	66.1
25	10	518	36.5	836.7	58.9	- -
26	11	518	36.5	838.2	59.0	66.1
27	12	518	36.5	838.2	59.0	- -
28	13	518	36.5	838.2	59.0	66.1
29	14	518	36.5	839.7	59.1	- -
30	15	518	56.5	839.7	59.1	- -
31	16	518	36.5	841.1	59.2	- -
32	17	518	56.5	842.6	59.3	66.1
33	18	518	36.5	842.6	59.3	- -
34	19	518	36.5	842.6	59.3	- -
35	20	518	36.5	842.6	59.3	- -
36	21	518	36.5	842.6	59.3	- -
37	22	518		842.6	59.3	67.4
38	23	498	35.1	828.0	58.3	- -
39	24	430	30.3	817.8	57.6	68.6
40	25	428	30.1	810.5	57.1	108.0
41	26	432	30.4	806.1	56.8	113.2
42	27	432	30.4	801.7	56.5	114.7
43	28	432	30.4	800.3	56.4	115.7
44	29	439	30.9	798.8	56.3	114.7
45	30	444	31.3	797.4	56.2	- -
46	31	443	31.2	793.0	55.8	115.3
47	32	442	31.1	787.2	55.4	- -
48	33	442	31.1	785.7	55.3	- -
50	35	- -	- -	784.3	55.2	- -
51	36	- -	- -	784.3	55.2	- -
52	37	- -	- -	784.3	55.2	- -
53	38	- -	- -	784.3	55.2	- -
54	39	- -	- -	784.3	55.2	- -
55	40	436	30.7	784.3	55.2	109.7
59	44	- -	- -	784.3	55.2	111.0
60	45	- -	- -	785.7	55.3	- -

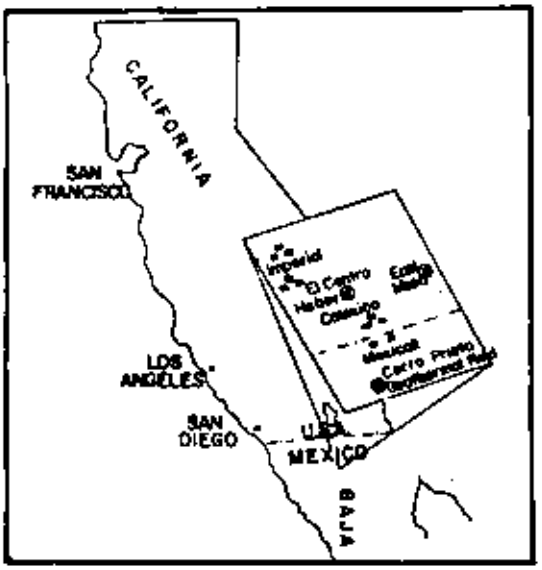

Fig. 1 - Schematic representation of the location of the Cerro Prieto Geothermal Field.

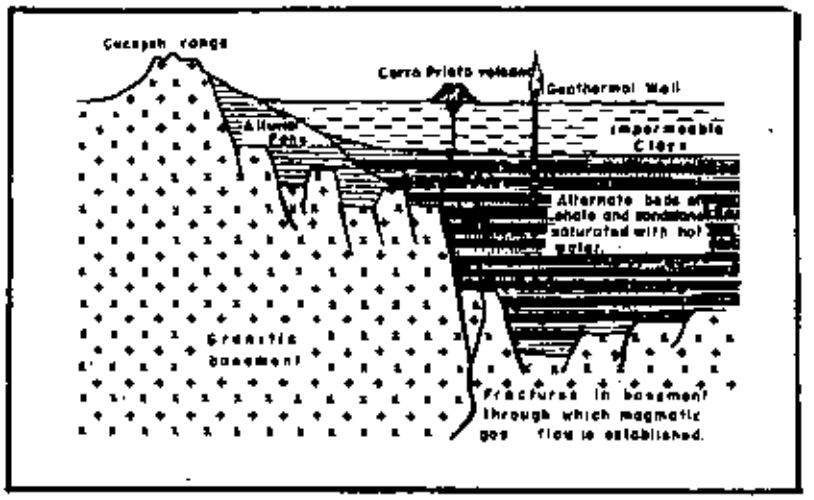

Fig. 2 - Ideal geological cross-section of the Cerro Prieto Reservoir. (After Ref. 1).

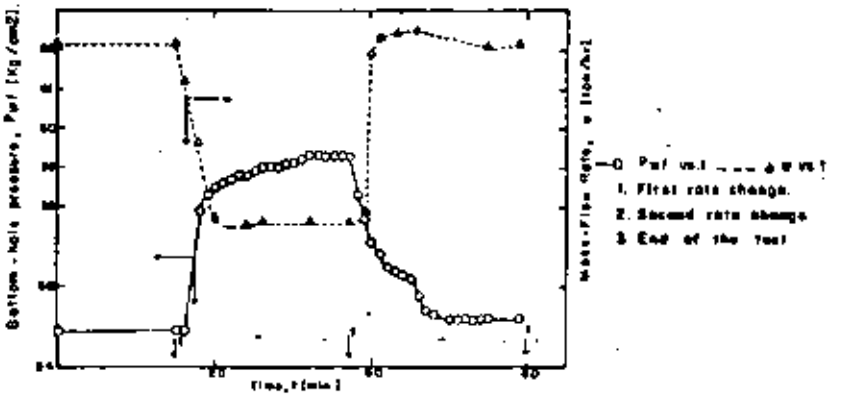

Fig. 3 - The bottom-hole pressure and mass flow rate during the two-rate flow test.

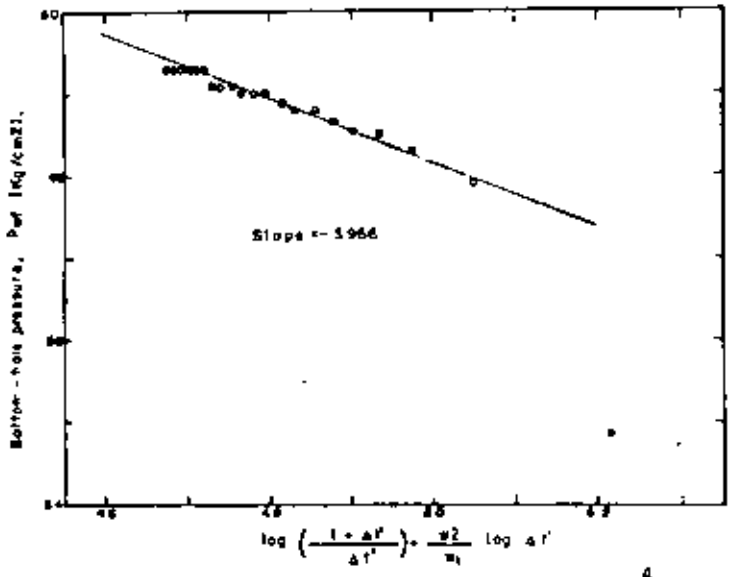

Fig. 4 - Two-rate graph for Russell's Method.[4]

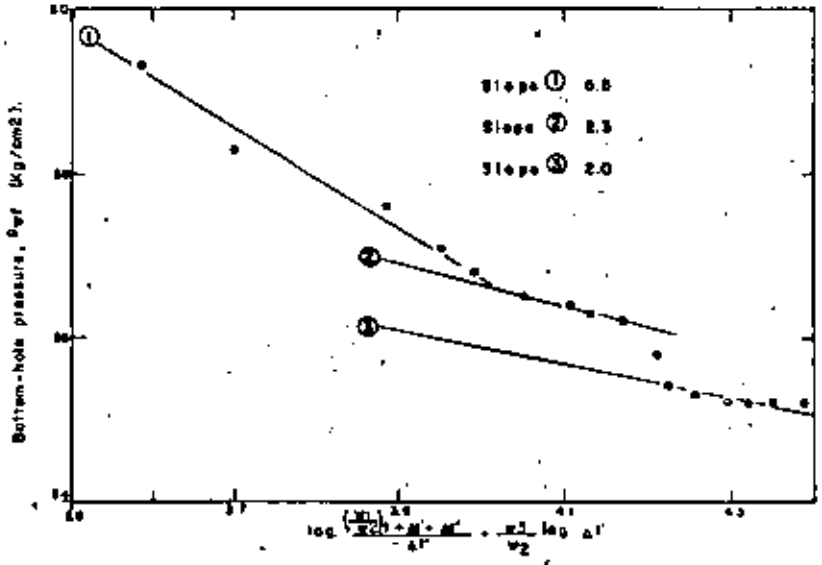

Fig. 5 - Two-rate graph for Selim's[5] Method.

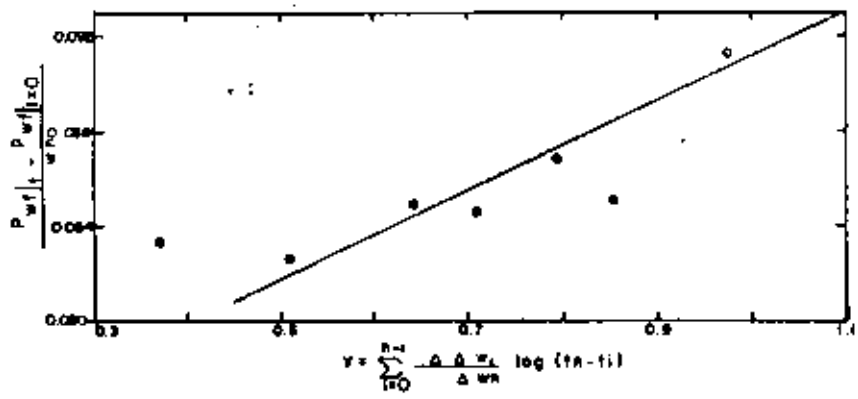

Fig. 6 - Odeh and Jones[7] Variable Drawdown Model.

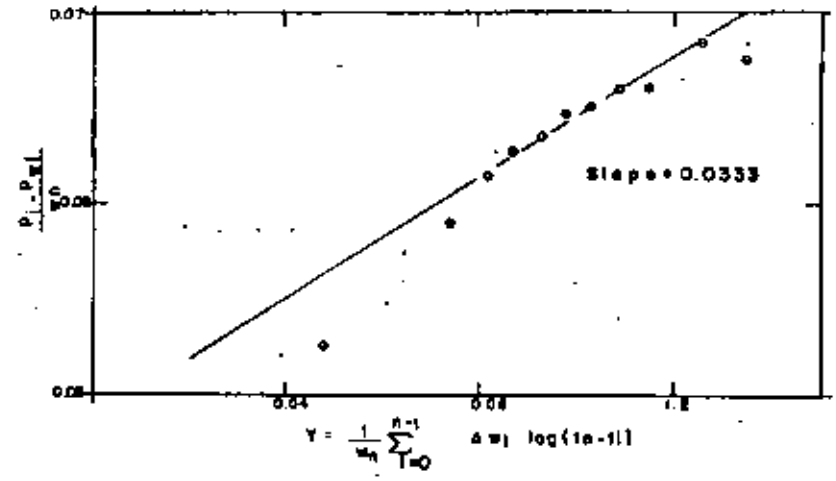

Fig. 7 - Odeh and Jones[6] Two-Rate Model.

Geothermics, Vol. 9, pp. 189–196
Pergamon Press Ltd. 1980. Printed in Great Britain.

70

0375–6505/80/1101–0189$02.00/0

PRESSURE TRANSIENT TESTING AT CERRO PRIETO GEOTHERMAL FIELD.

J. RIVERA R*., F. SAMANIEGO V†., and R. C. SCHROEDER‡

Comision Federal de Electricidad, Mexicali, Baja California, México, †Instituto de Investigaciones Electricas, México, D.F., México and ‡Lawrence Berkeley Laboratory, Berkeley, CA, U.S.A.

Abstract—The Cerro Prieto geothermal reservoir may be classified as a liquid-dominated system whose initial temperature and pressure conditions place it in the liquid-saturated region. In this field commercial power production began in 1973 and has continued since that date.

Because of the inherent problems in applying pressure build-up tests to wells producing two-phase fluids, it was decided to use variable flow tests of short duration known as two-rate tests. In these tests a variation in the well flow rates can be used to interpret the transient pressure response in order to determine reservoir parameters such as permeability, well-bore damage and mean reservoir pressure in the well drainage area. Some examples will illustrate the application of this technique.

Pressure drawdown tests have been planned in some of the wells in the field. On the other hand, a well interference test has been made in the southern part of the field using M-90, M-91, M-50 and M-51 as production wells and M-101 as an observation well. The interpretation of this test using curve-matching procedures is illustrated.

In the future, several of these tests are planned which will take advantage of the wells being drilled in new areas of the field.

NOMENCLATURE

B	brine formation volume factor, (volume, reservoir conditions/volume, standard conditions).
C_t	total fluid compressibility $(kg/cm^2)^{-1}$
h	formation net thickness, m
k	permeability, md
m	slope of a straight line
p	pressure, kg/cm^2
p_i	initial pressure, kg/cm^2
p_{wf}	flowing bottom-hole pressure, kg/cm^2
p_{1hr}	flowing bottom-hole pressure 1 hr after the rate change, kg/cm^2
q	volumetric flow rate, bbl/day
r	radial distance, m
r_w	wellbore radius, cm
s	skin factor, dimensionless
t	producing time to instant of rate change, h
$\Delta t'$	producing time measured from first rate change, h
V	specific volume, cm^3/g
W	mass flow rate, t/h
μ	viscosity, cp
ϕ	porosity, fraction

Subscripts

D	dimensionless
i	initial condition
M	matching
R	refers to Russell's model
sc	standard conditions
w	wellbore
wf	flowing conditions.

INTRODUCTION

Interference testing is preferred in some instances over single well tests depending on the type of information required (Earlougher 1977). Interference tests provide information about

*Present address: División de Estudios de Post-grade de la Facultad de Ingenieria, UNAM, México 20, D.F., México.

reservoir connectivity, which is important because the number of wells in a reservoir usually increases, causing mutual interference of wells. Another important datum obtained from this test is reservoir porosity, which cannot be obtained from a single-well test (Matthews and Russell, 1967; Ramey *et al.*, 1973).

Modern transient pressure analysis techniques have been basically developed in the fields of petroleum engineering and hydrogeology. Its use on geothermal reservoirs has been shown to be possible (Ramey, 1975; Barelli *et al.*, 1975; Ramey and Gringarten, 1975; Rivera and Ramey, 1977; Witherspoon *et al.*, 1978; Garg, 1978a). Ramey (1975) has presented a summary of transient pressure analysis techniques for geothermal wells. Field examples of pressure buildup tests have been discussed by Barelli *et al.* (1975), and by Ramey and Gringarten (1975); Rivera and Ramey (1977) have presented field results of two-rate flow tests; and Witherspoon *et al.*, (1978) have shown results of interference tests. All of these studies fall in the single phase category. Recently, the two phase flow problem (liquid water and steam) has been addressed by Garg (1978a, 1978b). He discusses a theory for well test analysis of multiphase fluid-flow pressure data.

The purpose of this paper is to present the analysis of an interference test performed in the Cerro Prieto Geothermal Field. Four active production wells (M-50, 51, 90 and 91) and one monitoring well M-101 were involved in this test. In addition, a brief description of the two-rate flow testing efforts carried out at Cerro Prieto is discussed.

GENERAL BACKGROUND

The Cerro Prieto Geothermal Field is located about 30 km south of Mexicali, Baja California. This field is located at the southern end of the Salton-Mexicali trough, which includes other geothermal anomalies such as Heber and East Mesa. It is a liquid-dominated system having a cap rock made of impervious plastic clays. The permeable layers consist of alternating shale and sandstone layers resting on a highly fractured granitic basement.

Comisión Federal de Electricidad started the construction of a 75 MW geothermal power plant in 1968. This plant started commercial operation in April 1973, and has been in operation since that date. The geothermal fluid is obtained as a water – steam mixture, with flashing of the brine taking place at some depth inside the wellbore. The separated hot brine is disposed of in an evaporation pond; however, a project is in progress in order to reinject at least part of the spent liquid (Rivera *et al.*, 1978).

TWO-RATE FLOW TESTS

Among the transient pressure analysis techniques available for obtaining reservoir basic parameters (Earlougher, 1977; Matthews and Russell, 1967; Ramey, 1975) the technique known as 'two-rate flow test' was selected (Rivera and Ramey, 1977). Basically, these tests are performed by changing the flow rate to some predetermined value after the well was stabilized at a given constant rate for some time.

The interpretation equations (Rivera and Ramey, 1977) are as follows:

$$P_{wf} = P_i - 527{\cdot}4\frac{W_2 V_w B\mu}{kh}\left(\log\frac{k}{\phi\mu c_t r_w^2} + 0{\cdot}891 + 0{\cdot}87\,s\right)$$
$$- 527{\cdot}4\frac{W_1 V_w B\mu}{kh}\left(\log\frac{t+\Delta t'}{\Delta t'} + \frac{W_2}{W_1}\log\Delta t'\right) \qquad (1)$$

From Equation (1) it is evident that by plotting

$$P_{wf} \text{ vs } \log\frac{t+\Delta t'}{\Delta t'} + \frac{W_2}{W_1}\log\Delta t'$$

a straight line should be obtained whose slope is given by:

$$m_R = 527{\cdot}4 - \frac{W_1}{} \frac{V_w B \mu}{kh} m \qquad (2)$$

The equation for the skin factor is given by the following expression:

$$s = 1{\cdot}151 \left[\frac{W_1}{W_1 - W_2} \frac{P_{1hr} - P_{wf}}{m_R} - \log \frac{k}{\phi \mu c_t r_w^2} \right] - 0{\cdot}891 \qquad (3)$$

Figures 1 and 2 show the results obtained from the application of the two-rate flow technique to wells M-21A and M-25 at Cerro Prieto. In well M-21A a good straight line section was developed; however, in well M-25 no straight line is evident. Most of the tests conducted so far have shown the development of good straight line sections.

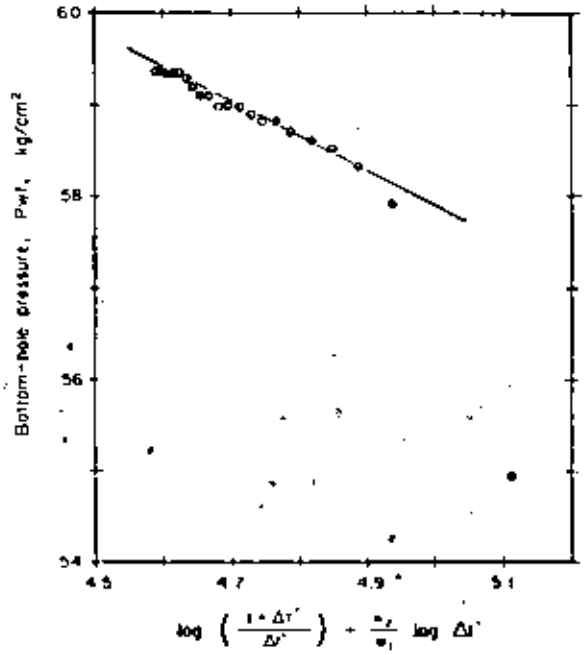

Fig. 1. Two-rate flow test for well M-21A.

INTERFERENCE TEST

An interference test is a multiple-well technique which has the advantage of investigating more reservoir than a single-well test. Because of this fact, it was decided to run an interference test in the southern portion of the Cerro Prieto Geothermal Field. This portion of the field has not as yet been exploited and several wells were already available to carry out this test. Figure 3 shows the location of the wells, and Fig. 4 illustrates both the production history of the active wells (M-50, 51, 90 and 91) and the transient pressure behavior at the observation well (M-101).

The test was performed taking advantage of the fact that the new wells drilled in that portion of the field should be brought into production one at a time. However, this also imposed an extra difficulty in analyzing the data, because of strong variations of flow rates, as can be seen in Fig. 4. This study presents the results of a first attempt to analyze the data obtained from the early part of the test when only well M-91 was flowing. The procedure used was type curve

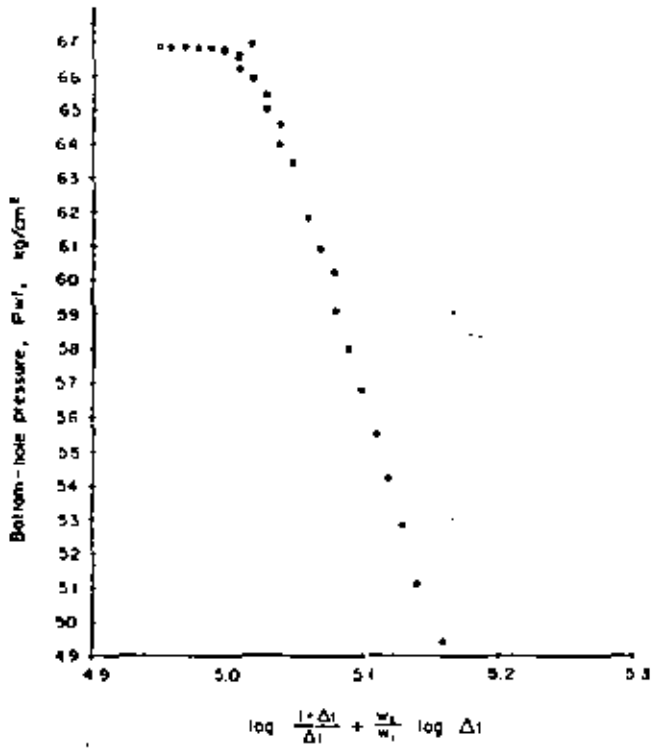

Fig. 2. Two-rate flow test for well M-25.

matching by means of the line source solution. A more rigorous analysis that considers the rate variation is underway. Fig. 5 shows the results obtained from this analysis. The match-point obtained is as follows:

For

$$(\Delta P)_M = 1 \text{ psi}, \quad (P_D)_M = 1{\cdot}8 \times 10^{-2},$$
$$(t)_M = 100 \text{ days}, \quad \left(\frac{t_D}{r_D^2}\right)_M = 0{\cdot}63,$$

where the dimensionless variables are defined as follows:

$$P_D = 1{\cdot}5388 \times 10^{-4} \frac{k\,h\,\Delta P}{W\,V_w\,B\,\mu} \tag{4}$$

$$\frac{t_D}{r_D^2} = 0{\cdot}0008366 \frac{kt}{\phi \mu\, c_t\, r^2} \tag{5}$$

Table 1 shows the pressure interference data. Table 2 below shows the values of the variables in equations (4) and (5).

Actually, it is possible to obtain two good matches of the data points with the type curve. The match shown in Fig. 5 was obtained by taking into account the set of drawdown data. On the other hand, it is also possible to obtain a good match by using only those points concerned with the drawdown produced by well M-91 alone. Table 3 below illustrates the results obtained in those cases mentioned before.

74

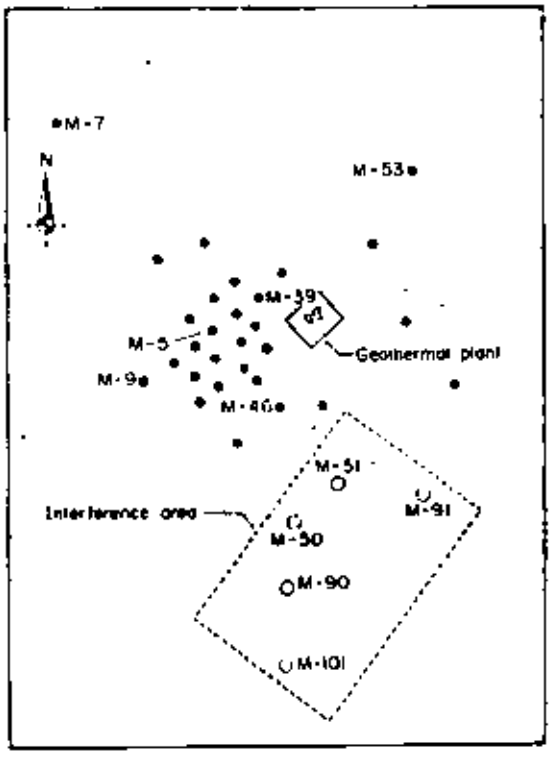

Fig.3. Location of the wells.

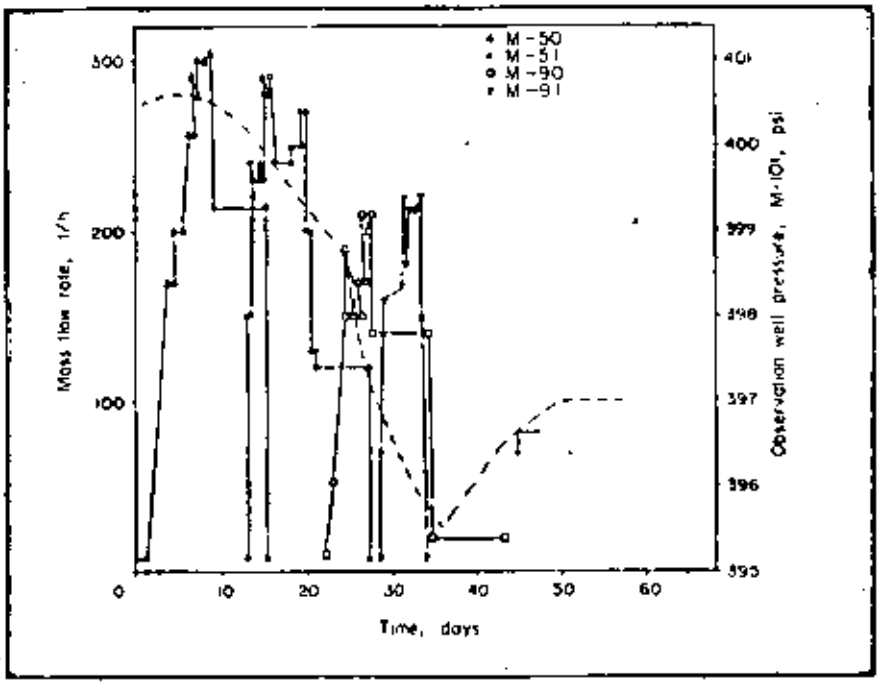

Fig. 4. Active wells production schedule and observation well pressure.

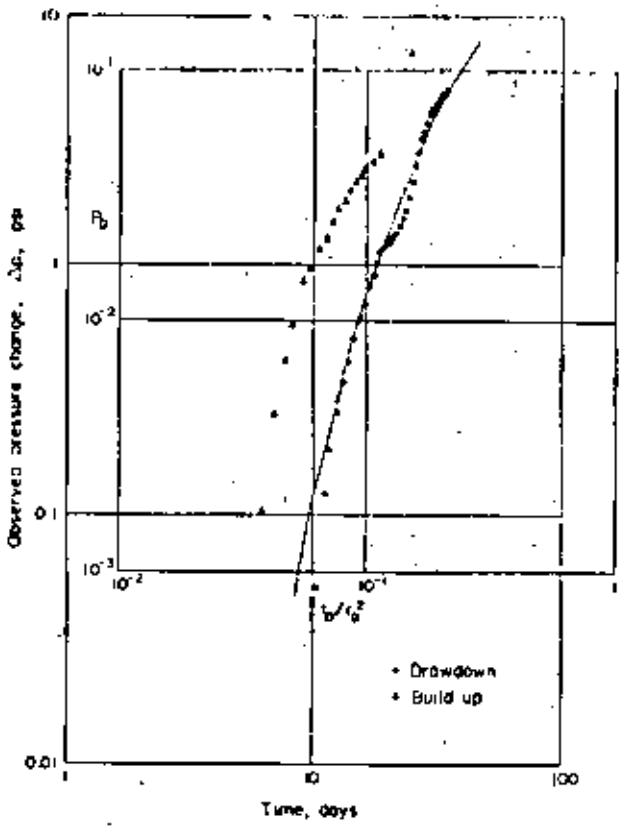

Fig. 5. Type curve match of an interference test, active wells M-90, M-91, M-50, and M-51. Observation well M-101, Cerro Prieto geothermal field.

Table 1. Pressure interference data

Total time (days)	Well pressure at 1000 ft (psi)	Pressure drop (psi)	Total time (days)	Well pressure at 1000 ft (psi)	Pressure drop (psi)
9·72*	400·50	0	23·08	397·40	3·10
10·42	400·45	0·065	27·78	397·15	3·35
11·11	400·38	0·12	28·479	396·90	3·60
11·81	400·32	0·18	29·17	396·90	3·90
12·50	400·25	0·25	29·86	396·40	4·10
13·194†	400·17	0·33	30·56	396·25	4·4
13·89	400·10	0·40	31·25	396·10	4·5
14·58	400·00	0·50	31·94	395·95	4·55
15·28	399·90	0·60	32·64	395·85	4·65
15·97‡	399·82	0·68	33·33	395·75	4·75
16·67	399·70	0·80	34·01	395·65	4·85
17·36	399·62	0·88	34·72	395·55	4·95
18·06	399·52	0·98	35·42	395·50	5·00
18·75	399·40	1·10	36·11	395·55	4·95
19·44	399·35	1·15	36·81	395·70	4·80
20·14	399·32	1·18	37·50	395·80	4·70
20·83	399·25	1·25	38·19	395·90	4·60
21·53§	399·20	1·30	38·89	396·00	4·50
22·22	399·10	1·40	39·58	396·10	4·40
22·92	399·00	1·50	40·28	396·20	4·30
23·61	398·90	1·60	40·97	396·25	4·25
24·31	398·70	1·80	41·67	396·35	4·15
25·00	398·60	2·10	42·36	396·45	4·05
25·69	398·10	2·40	43·06	396·55	3·95
26·39	397·75	2·75	43·75	396·60	3·90

* Well M-91 producing. All others shut-in.
† Well M-51 starts production.
‡ Well M-91 shut-in.
§ Well M-90 starts production.
¶ Well M-50 starts production.

Table 2. Values used in calculations of capacity (kh) and storativity ($\phi c_t h$).

q = Average flow rate = 185.1 [t/h]	76
B_w = 1.041 [cm³/g]	
μ = 1.185 [cp] (at 240°C, sat.)	
μ = 0.1017 cp	
ℓ = 1500 m	

Table 3. Summary of results obtained from match points.

Data points matched	kh (md · m)	$\phi c_t h$ (kg/cm²)⁻¹	k* (md)	ϕc_t†
All drawdown	38664	0.0210	38	38
Only well 5491	55738	0.01946	54	16
Average	46206	0.0203	46	27

* In calculating k and ϕ a net pay thickness of 1000 m was assumed; well log data should be considered in order to determine a more realistic value of h.
† A value of 119×10^{-6} (kg/cm²)⁻¹ was considered for c_t.

A more rigorous mathematical analysis of the data which takes into account superposition in time of the influence of the four active wells, as well as the closest row of producing wells from that part of the field on exploitation is in progress.

CONCLUSIONS AND RECOMMENDATIONS

The main purpose of this study has been to present the results of the analysis of two-rate flow tests and a preliminary analysis of an interference test performed in the Cerro Prieto Geothermal Field. From the results of this study the following points can be drawn.

1. Two-rate flow tests seem to be an adequate and quick technique for obtaining reservoir parameters in the drainage area of a well. It is necessary to take into account the total fluid mobility when two-phase flow is taking place.
2. It is convenient to plan in advance a more adequate schedule of production for the active wells involved in an interference test, in order to provide a convenient way to analyze the results obtained from the pressure response at the observation well.
3. From the results obtained, it is evident that the portion of the reservoir studied in the interference test is a very complex, probably highly fractured, structure.
4. Since presence of fractures could be inferred from both well electrical logs correlation and interference response, it seems convenient to take this fact into account in the interpretation of the pressure response data.
5. The results of the interference test presented in this work are only preliminary; a more comprehensive and rigorous analysis is underway.

REFERENCES

Barelli, A., Manetti, G., Celati, R., and Neri, G. (1975). Buildup and back pressure tests on Italian geothermal wells. *Proc. 2nd U.N. Symposium Development and Use of Geothermal Resources, San Francisco*, 3, 1537–1546.

Earlougher, R. C., Jr. (1977) *Advances in Well Test Analysis*. Monograph Series, Society of Petroleum Engineers of AIME, Dallas, 5.

Garg, S. K. (1978a). Pressure transient analysis for two-phase geothermal reservoirs. *Geothermal Resources Council, Trans.* 2, 203–206.

Garg, S. K. (1978b). Pressure transient analysis for two-phase (liquid water/steam) geothermal reservoirs. Paper SPE 7479, to be presented at the *53rd. Annual Fall Technical Conference*, Houston, TX., 1–4 Oct.

Matthews, C. S. and Russell, D. G. (1967). *Pressure Buildup and Flow Test in Wells*, Monograph Series, Society of Petroleum Engineers of AIME, Dallas, 1.

Ramey, H. J., Jr. (1975). Pressure transient analysis for geothermal wells. *Proc. 2nd U.N. Symposium Development and Use of Geothermal Resources, San Francisco*, 3, 1749–1757.

Ramey, H. J., Jr. and Gringarten, A. C. (1975). Effect of high-volume vertical fractures on geothermal steam well behavior. *Proc. 2nd U.N. Symposium Development and Use of Geothermal Resources, San Francisco*, 3, 1759–1762.

Ramey, H. J., Jr., Kumar, A. and Gulati, M. S. (1973). *Gas Well Test Analysis Under Water-Drive Conditions*, AGA, Arlington, Va.

Rivera, R. J., Mercado, G. S., and Tsang, C. F. (1978). Preliminary studies of reinjection of the produced brine at Cerro Prieto Geothermal Field. *Joint CFE/DOE Cooperative Program Symposium San Diego, CA*.

Rivera, R. J., and Ramey, H. J., Jr. (1977). Application of two-rate flow tests to the determination of geothermal reservoir parameters. Paper SPE 6887. Presented at the *52nd Annual Fall Technical Conference and Exhibition of SPE*, Denver, CO., 9 – 12 October.

Witherspoon, P. A., Narasimham, T. N. and McEdwards, D. G. (1978). Results of interferences tests from two geothermal reservoirs. *J. Pet. Tech.* **30**, 10 – 16.

SPE

SPE 8348

WELL TESTING AT LOS AZUFRES GEOTHERMAL FIELD

by Jesus Rivera-R., Comision Federal de Electricidad; and
Mehmet Saltuklaroglu, ELC, Electroconsult, Members SPE-AIME

This paper was presented at the 54th Annual Fall Technical Conference and Exhibition of the Society of Petroleum Engineers of AIME, held in Las Vegas, Nevada, September 23-26, 1979. The material is subject to correction by the author. Permission to copy is restricted to an abstract of not more than 300 words. Write SPE, 6200 N. Central Expy., Dallas, Texas 75206.

ABSTRACT

It is important to determine reservoir characteristics as early in the life of the reservoir as possible. This paper presents a summary of the efforts made by Comision Federal de Electricidad to evaluate Los Azufres field by means of the implementation of standard pressure transient analysis techniques to geothermal reservoirs. Among these techniques, constant injection, falloff, multiple-rate injection, build-up, drawdown, two-rate and variable rate tests have been applied. Discussion is presented on constant injection, falloff, two-rate and variable rate testing. Interference testing is now being conducted on a small portion of the field.

INTRODUCTION

After the discovery of a geothermal field has been confirmed by successfully drilling one or more wells, the reservoir engineer has to obtain as much information out of them as possible. This information is needed in order to perform a proper evaluation of the field, before the utility company can proceed with the construction of an electric power generating facility.

Among those geothermal fields undergoing exploration in Mexico, Los Azufres is the one in the most advanced stage of exploration. This geothermal field is located some 300 kilometers southwest of Mexico City, in the state of Michoacan in Central Mexico. As shown in Figure 1, this field is situated on the E-W oriented neo-volcanic axis. It is a highly fractured system, located on neo-quaternary volcanic deposits overlying a basement which is believed to be made of limestone. The lower part of the igneous deposits is constituted by microgranular andesites which are overlaid at places by ryolites and pyroclastics.

References and illustrations at end of paper.

There are many thermal manifestations and alteration zones around the field which are related to tectonic activity and are located near faults and fracture zones. To date, 8 wells have been drilled in the field, 6 of them are for production and 2 injectors. Three more wells are on the drilling stage and 6 additional wells are schedulled to be drilled during 1979. Figure 2 illustrates the main faults and the location of the wells.

The wells so far drilled in this area are sited near the known major faults. The reason behind this may of selecting locations is that because of the tightness of igneous rocks, the main production is thought to come through fractures. The deepest well is 2450 m and the shallowest is 960 m deep.

Los Azufres field is under the last stage of the feasibility study, which has been carried out in order to determine the optimum size of turbines to be installed for electricity generation. This field has been divided into several possible producing areas called "modules" around the main fracture zones. This areas will be developed independently from each other. Thus, reference will be made in the text to Laguna Verde Module, Agua Fria Module and Tejamaniles Module, among them the latter is under intensive drilling development (See Fig. 2).

Figure 3 shows a typical temperature survey and well completion of this field. Wells are drilled using low density bentonitic mud from surface up to the top of the reservoir and with water from that depth downwards.

Los Azufres reservoir is a liquid-dominated system having a steam cap located on the Tejamaniles Module, in the zone of well A-6, whose productivity test showed a 99 percent steam. Figure 4 illustrates a

cross-section going from well A-10 up to well A-11 drawn on a SE-NW direction through the field. This section shows a correlation of the production zone based upon calculated static bottom-hole temperatures whose range is from 270 to about 298°C.

WELL TESTING PROGRAM

As it was stated before, standard pressure transient analysis techniques, adapted to geothermal systems have proven to be of great help to evaluate wells at Los Azufres field. Among those techniques published in the literature, pressure build-up, drawdown, two-rate and variable rate flow, injection and interference testing have been applied in this field.

INJECTION TESTING

The possibility of obtaining commercial production from igneous rocks is to encounter secondary permeability, which in Los Azufres is represented by highly fractured volcanic rock. An index of these permeable zones observed in drilling the well is to have lost of drilling fluid circulation. If this lost is big enough and the static bottom-hole temperature is within commercial ranges (greater than 230°C), a short-term injection test is performed.

Injection tests[1,2,3] are carried out as a part of completion procedures in this field by using standard bottom-hole pressure bombs. The main purpose of these tests is to obtain early information about the well and reservoir parameters, which could be helpful in selecting the most appropriate zone for completion of the well; in addition they can be used in order to predict future well performance. These type of tests have been found easier and quicker to perform than drawdown and build-up tests and the results obtained from them are judged to be reasonably good.

Within the several types of tests available in the literature, those known as injection, multiple-rate injection and falloff tests have been employed in this field. Results obtained from typical injection and falloff tests are described below. For more detailed description of these tests the reader should refer to Reference 3.

Several temperature surveys are carried out in order to determine temperature distribution before any injection test is performed. Injection rates commonly used in this field are 4528, 10870 and 13580 bbl/day. The usual procedure is to run an injection test at any of the rates mentioned above for a period of 3 to 4 hours, recording changes in bottom-hole pressure by means of a standard bourdon-tube type pressure bomb. Immediately after injection stops, the falloff period is recorded in order to obtain enough data to check the results obtained from the analysis of injection data.

When results obtained from analysis of constant rate injection and falloff data are not conclusive, two-rate injection tests have been conducted. However, it has been observed that in those wells applied, dispersion of the data is present, making the interpretion difficult.

Interpretation of injection and falloff data is made by applying well-known pressure transient analysis techniques already reported in the literature[1,2,3]. Results of a test conducted in well A-2 are shown in Figs. 5 thru 8.

First, a log-log plot of bottom-hole pressure difference versus either injection or shut-in time is tried in order to determine the duration of wellbore storage effects. Then by using the type-curve procedure, a match is obtained between field data and published type curves[2,4]. Dimensionless pressure and time are according to the usual definition[1]:

$$p_D = \frac{kh}{141.2qu\beta}\,\Delta p \qquad (1)$$

$$t_D = \frac{0.0002637kt}{\phi u\, c_t r_w^2} \qquad (2)$$

Figs. 5 and 6 show the match obtained by fitting the data obtained in an injection and falloff test to the type-curves published by Agarval et al[2]. Data of these test are shown in Table 1. Calculations of reservoir parameters are included in the Appendix. It has been observed that sometimes it is difficult to obtain a unique match. In these cases, an estimation of C_D has been made in order to reduce uncertainty in the match.

From experience of application of injection tests in this field[3], it has been observed that in a log-log plot the transition period between the section of slope 1 and the start of the semilog straight line is very short in undamaged wells as that shown in Figs. 5 and 6; meanwhile, in damaged wells it can be very long (it usually takes about 2 1/2 to 3 hours).

After the correct start of the semilog straight line has been determined, analysis of the data by these methods is performed. Figs. 7 and 8 show data from injection and falloff tests respectively. Techniques for this type of analysis are well known and the basic equations are as follows[1]:

For a constant rate injection test, the bottom-hole injection pressure is given by the following equation:

$$p_{wf} = p_{1hr} + m \log t \qquad (3)$$

and the skin factor is as follows:

$$s = 1.1513\left[\frac{p_{1hr}-p_i}{m} - \log\left(\frac{k}{\phi\mu c_t r_w^2}\right) + 3.2275\right] \quad (4)$$

where:

$$p_{1hr} = p_i + m\left[\log\left(\frac{k}{\phi\mu c_t r_w^2}\right) - 3.2275 + 0.86859s\right] \quad (5)$$

$$m = \frac{-162.6qB\mu}{kh} \quad (6)$$

For a falloff test following a constant injection period, the bottom-hole pressure is given by the following equation:

$$p_{ws} = p^* - m\log\left(\frac{t_p + \Delta t}{\Delta t}\right) \quad (7)$$

A plot of p_{ws} vs $\log\left(\frac{t_p + \Delta t}{\Delta t}\right)$ should show a straight line whose slope m is given by the following expression:

$$m = \frac{162.6qB\mu}{kh} \quad (8)$$

and the skin factor is given by the following equation:

$$s = 1.1513\left[\frac{p_{1hr}-p_{wf}(\Delta t=0)}{m} - \log\left(\frac{k}{\phi\mu c_t r_w^2}\right) + 3.2275\right] \quad (9)$$

Calculation of these tests are illustrated in the Appendix, Table 2 shows a comparison of the results obtained by using both type-curve and standard semilog techniques. As it can be observed from this table, results from both methods are in good agreement. Generally speaking, results obtained from semilog methods should be prefered to those obtained from graphical procedures.

MULTIPLE RATE TESTS.

After the wells have produced some time, multiple-rate production tests [5,6] have been applied to check values of (kh/μ) obtained by means of injection and falloff tests. Thus far, the application of these techniques have proven to be successfull. For well A-2, the value of (kh/μ) obtained from a multiple-rate test is 86910 md-ft, which is in the range of those reported in table 2.

Application of two-rate flow tests[6] to wells with low (kh/μ) values, producing fluid in a two-phase flow regime from the bottom of the hole up to the surface, have shown scatter of the data, making the interpretation very uncertain.

INTERFERENCE TESTING

Interference testing is underway in a portion of the field known as Tejamaniles Module (See Fig. 2). Wells A-2, A-6, A-7 and A-8 are involved in this test. Basic information is expected to be obtained which will help in selecting well spacing and the most convenient well grid orientation in the zone.

CONCLUSIONS

From results of tests described in this paper, the following conclusions can be reached:

1.- Constant rate, injection tests falloff tests have proven to be successful in obtaining geothermal reservoir parameters in Los Azufres Field.

2.- Short term injection tests seem to be adecuate in providing a quick and reasonable good estimate of basic parameters in geothermal reservoirs located on igneous rocks, whose main production takes place through fractures.

3.- Standard pressure transient analysis techniques seem to find application in liquid-dominated geothermal systems similar to Los Azufres Field.

NOMENCLATURE

- B = brine formation volume factor, (volume, reservoir conditions/volume, standard conditions).
- C_D = dimensionless wellbore storage coefficient.
- c_t = Total compressibility, $(psi)^{-1}$
- h = formation net thickness, ft.
- k = permeability, md.
- m = slope of a straight line.
- p = pressure, psi.
- p_i = initial pressure, psi.
- p_{wf} = flowing bottom-hole pressure, psi.
- p_{1hr} = flowing bottom-hole pressure at 1hr, psi.
- p_{ws} = static bottom-hole pressure, psi.
- p_D = dimensionless pressure.
- q = volumetric flow rate, bbl/day.
- r_w = wellbore radius, ft.
- s = skin factor, dimensionless.
- t = time, hrs.
- t_p = injection time, hrs.
- Δt = shut-in time, hrs.

GREEK SYMBOLS

- μ = viscosity, cp.
- ϕ = porosity, fraction.

ACKNOWLEDGEMENTS

The authors wish to thank the Comisio Federal de Electricidad for permission to publish the field data presented in this paper. The assistance received from Ing. Alfonso Aragon-Aguilar in processing the data and helpful discussions with Dr. Fernando Samaniego-Verduzco are also acknowledged.

REFERENCES

1. Earlougher, R.C., Jr.: Advances in Well Test Analysis, Society of Petroleum Engineers of AIME Monograph Volume 5. The Society, New York (1977).

2. Agarval, R.G., Al-Hussainy, R., and Ramey, H.J.,Jr.: "An Investigation of Wellbore Storage and Skin Effect in Unsteady-Liquid Flow": I Analytical Treatment, Soc. Pet. Eng. Jour. (Sept., 1970) 279-290.

3. Saltuklaroglu, M., and Rivera-R.,J.: "Injection Testing in Geothermal Wells", Proceedings, Fourth Workshop on geothermal Reservoir Engineering, Stanford, C.A. (Dec. 13-15, 1978) 176-187.

4. Earlougher, R.C.,Jr. and Kersch, K.M.: "Analysis of Short Time Transient Test Data by Type-Curve Matching", J. Pet. Tech. (July 1974) 793-800.

5. Odeh, A.S. and Jones, L.G.: "Pressure Drawdown Analysis, Variable-Rate Case", J. Pet. Tech. (Aug. 1965) 960-964.

6. Rivera-R, J., and Ramey, H.J.,Jr.: "Application of two-Rate Flow Tests to the Determination of Geothermal Reservoir Parameters", paper SPE 6887 presented at SPE-AIME. 52nd Annual Technical Conference, Denver, Colorado, Oct 9-12, 1977.

APPENDIX - RESERVOIR PARAMETERS CALCULATIONS

INJECTIVITY TESTS.

A. Injection test.

a). Type-curve procedure.
From Fig. 5, the match point is as follows:
For $(t)_M$=100 min, $(t_D)_M$=8.4x10^4, s= -2
For $(\Delta p)_M$=10 psi, $(p_D)_M$=1.28
From eq.(1) in the text:

$$\frac{kh}{\mu} = 141.2\, qB\, \frac{(p_D)_M}{(\Delta p)_M} = 141.2(4528)(1)\frac{1.28}{10}$$

$$= 81837\left(\frac{md-ft}{cp}\right)$$

From eq.(2) in the text:

$$\phi c_t h = \frac{0.0002637}{r_w^2}\,\frac{kh}{\mu}\,\frac{(\Delta t)_M}{(t_D)_M} =$$

$$= \frac{0.0002637}{(0.463)^2}\,(81837)\,\frac{1.667}{8.4\times10^4}$$

$$= 1.99\times10^{-3}\ (ft/psi)$$

b). Semilog analysis.
From Fig. 7 : m = 6.96 psi/cycle.
From eq.(6) in the text:

$$\frac{kh}{\mu} = \frac{162.6qB}{m} = \frac{162.6(4528)(1)}{6.96}$$

$$\frac{kh}{\mu} = 105814\left(\frac{md-ft}{cp}\right)$$

From eq.(4) in the text:

$$s = 1.1513\left\{\frac{838.1-818.5}{6.96} - \log\left[\left(\frac{105814}{1.99\times10^{-3}}\right)\left(\frac{1}{0.463^2}\right)\right] + 3.2275\right\} = -2.7$$

From Fig.7 it is evident from the change in slope, that a barrier is located close to the wellbore which is corroborated by geologic evidence (see Figs. 2 and 4). Distance to this barrier is as follows:

$$L = 0.01217\sqrt{\left(\frac{kh}{\mu}\right)\left(\frac{1}{\phi\mu c_t}\right)t_x} = 0.01217$$

$$\sqrt{105814\left(\frac{1}{1.99\times10^{-3}}\right)\left(\frac{1}{0.463^2}\right)} = 192\ ft.$$

B. Falloff test.

a). Type - curve procedure.
From Fig. 6, the match point is given by:
For $(t)_M$=100 min; $(t_D)_M$=6.4x10^5, s= -1
For $(\Delta p)_M$=10psi, $(p_D)_M$=1.4
From eq.(1) in the text:

$$\frac{kh}{\mu} = 141.2(4528)(1)\frac{1.4}{10} = 89509\left(\frac{md-ft}{cp}\right)$$

From eq(2) in the text:

$$\phi c_t h = \frac{0.0002637}{(0.463)^2}(89509)\frac{1.667}{6.4\times10^5} = 2.87\times10^{-4}\ \left(\frac{ft}{psi}\right)$$

b). Semilog analysis.
From Fig. 8 : m = 7.1 psi/cycle
From eq.(8) in the text:

$$\frac{kh}{\mu} = \frac{162.6(4528)(1)}{7.1} = 103705\left(\frac{md-ft}{cp}\right)$$

From eq.(9) in the text:

$$s = 1.1513\left\{\frac{811-849}{7.1} - \log\left[(103705)\left(\frac{1}{2.87\times10^{-2}}\right)\left(\frac{1}{0.463^2}\right)\right] + 3.2275\right\} = -1.3$$

Table 1

Data from injection and falloff tests in well A-2. q_{inj}=4528 bbl/day.

INJECTION		FALLOFF	
Time (min)	Pwf (psi)	Time (min)	Pws (psi)
0	818.5	1	848.2
1	825.7	3	847.3
2	827.9	4	832.3
4	830.0	5	827.2
6	831.5	6	821.3
8	832.3	7	819.2
10	833.0	8	819.2
12	833.0	9	819.2
14	833.7	10	817.6
16	833.7	12	817.6
18	835.1	22	815.5
28	837.9	32	813.4
38	840.2	42	812.0
48	840.9	52	811.2
58	841.6	62	809.7
68	843.1	72	809.7
78	845.3	80	809.7
88	846.7		
98	848.2		
108	848.2		
118	848.9		
128	848.9		
138	848.9		
148	847.9		
210	847.9		

Table 2

Summary of results obtained applying Type-curve and semilog techniques. Injection rate =4528 bbl/day.

	$\frac{kh/\mu}{(md\text{-}ft)/cp}$	$\frac{c_t h}{ft/psi}$	s
INJECTION			
Type-curve	81837	1.99×10^{-3}	-2
Semilog	105814		-2.7
FALLOFF			
Type-curve	89509	2.87×10^{-3}	-1
Semilog	103705		-1.3

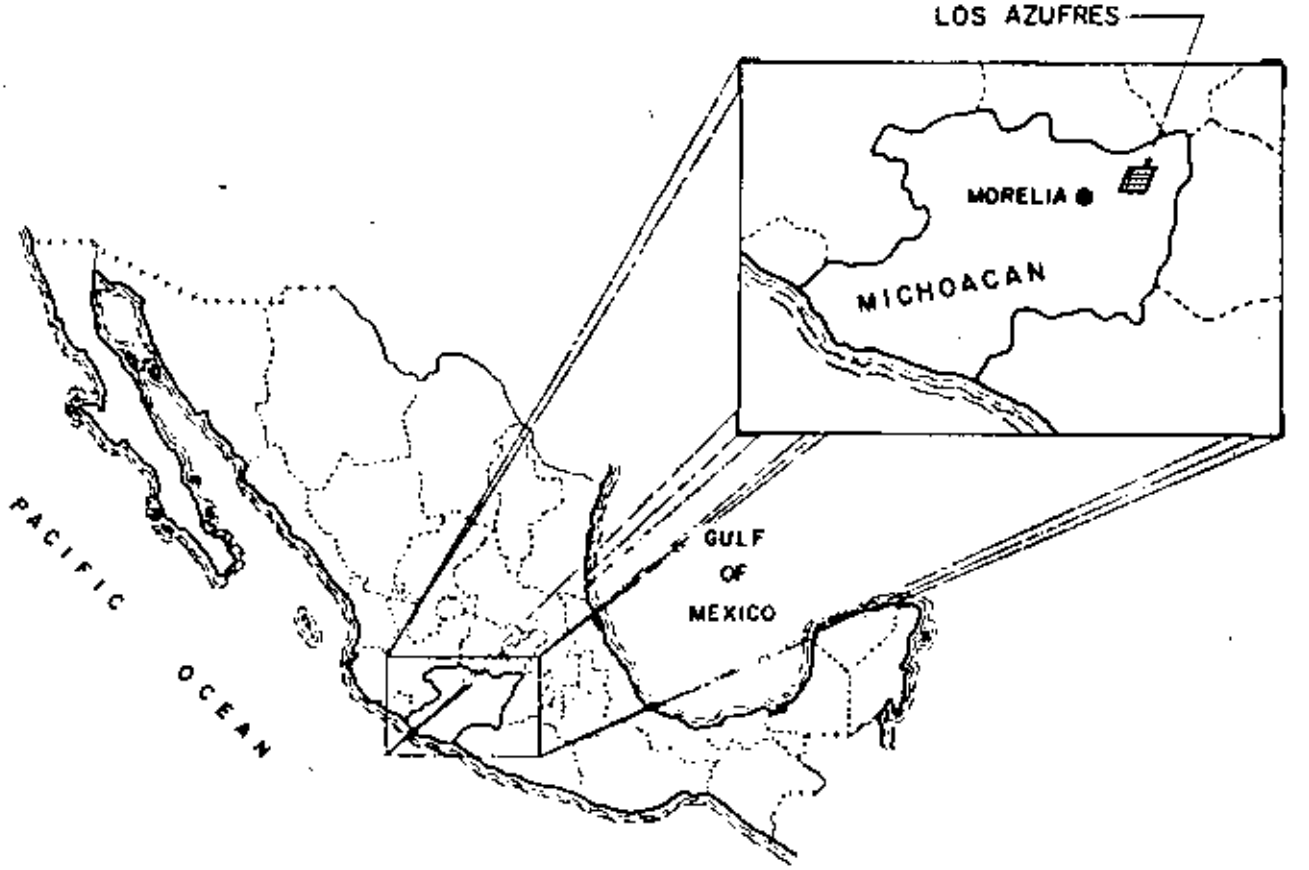

Fig. 1 - Location on Los Azufres geothermal field.

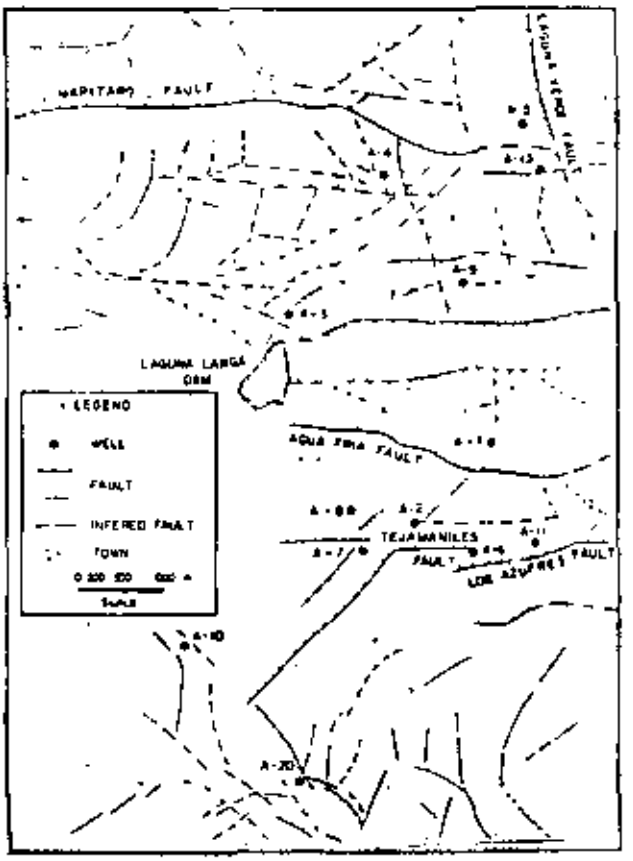

Fig. 2 - Location of wells and main faults.

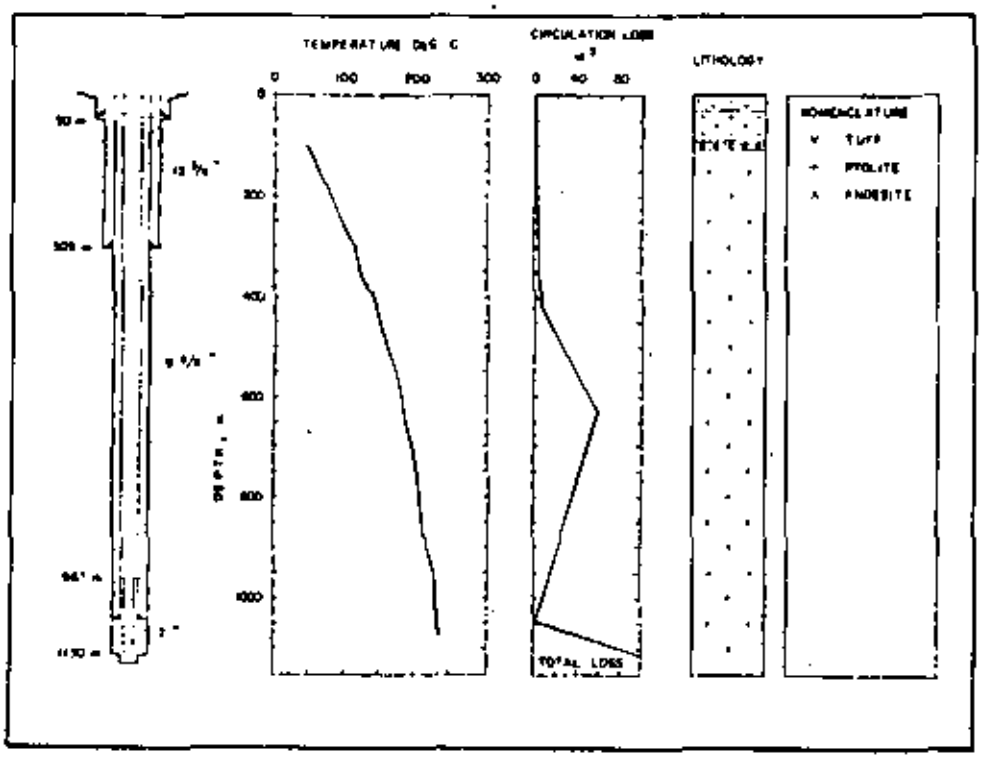

Fig. 3 - Completion, temperature, loss of circulation and lithology of well A-2.

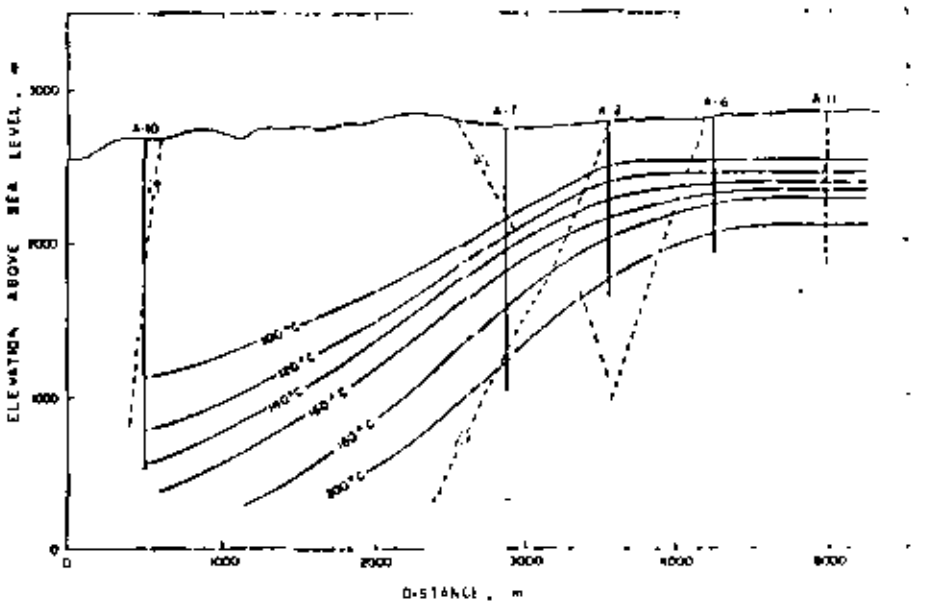

Fig. 4 - Cross-section through the field on a NE-SW direction.

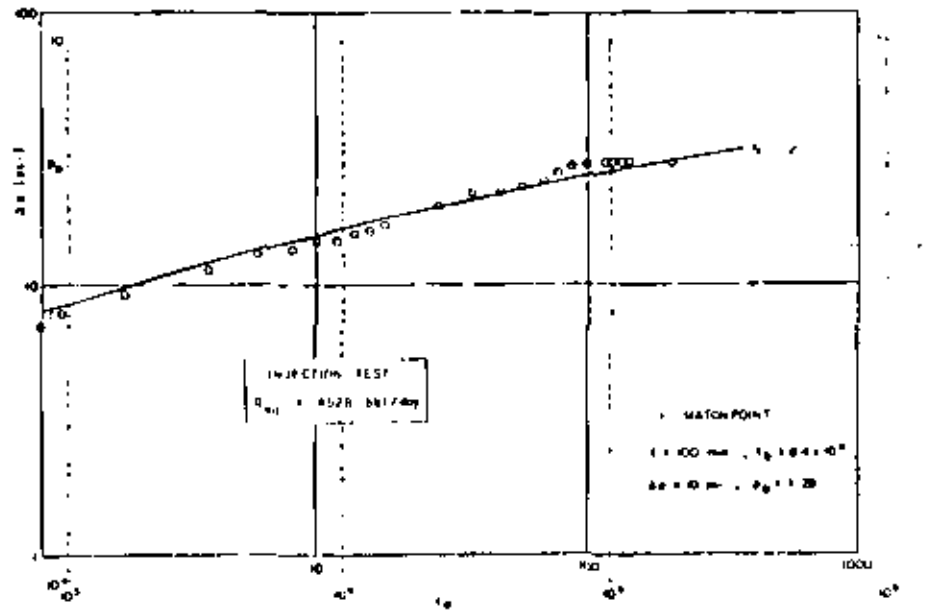

Fig. 5 - Type-curve match of data from an injection test in well A-2. Q_{inj}=4528 bbl/day.

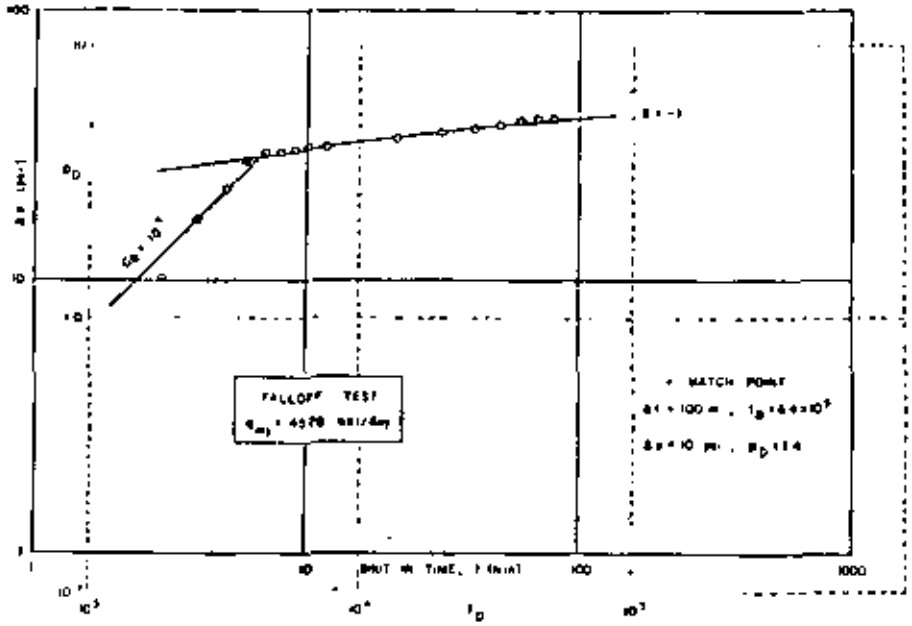

Fig. 6 - Type-curve match of data from a falloff test in well A-2 after a constant rate injection.

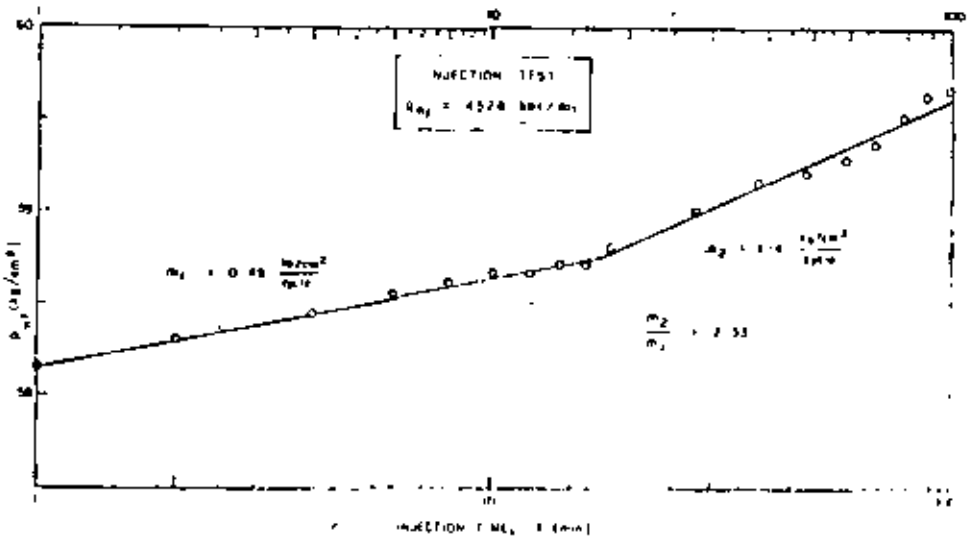

Fig. 7 - Injection test in well A-2. $q_{inj.}$=4528 bbl/day.

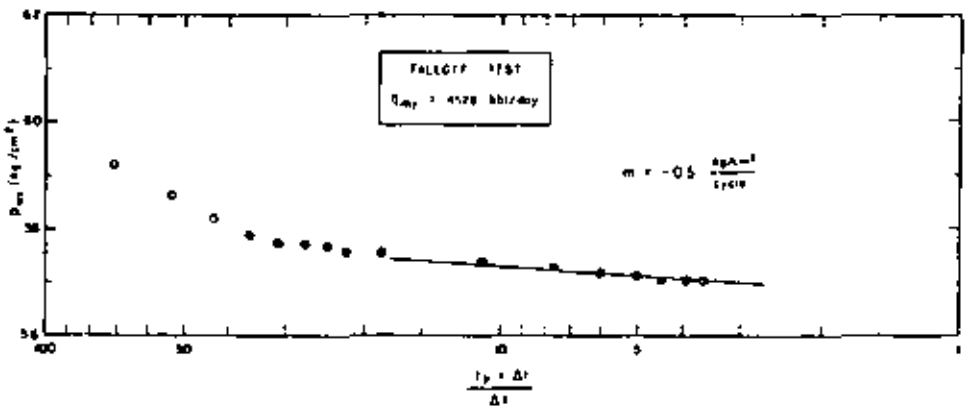

Fig. 8 - Falloff test in well A-2. q_{inj}=4528 bbl/day.

CURSO: "INGENIERIA DE RESERVORIOS GEOTERMICOS"

ESTADO ACTUAL DEL DESARROLLO GEOTERMICO EN EL SALVADOR.

PROF. ING. RODOLFO CACERES RODRIGUEZ

OCTUBRE 16, 1981.

ESTADO ACTUAL DEL DESARROLLO GEOTERMICO DE EL SALVADOR.

I. INTRODUCCION

Desde finales de la década de los 60, El Salvador se empeñó en un desarrollo de los recursos geotérmicos del país como una fuente de energía que era factible de ser utilizada en la generación eléctrica.

Fué en la década de los 70 donde se culminó dicho programa, al concluir la construcción de la 3a. Unidad Geotérmica en la Central de Ahuachapán, lo cual completa el grupo 3 turbinas de vapor de media presión con una capacidad instalada de 95000 KW.

II. ESTADO DE EXPLOTACION DEL RECURSO GEOTERMICO

El desarrollo en la explotación del Campo Geotérmico de Ahuachapán, se basó inicialmente en el aprovechamiento del vapor de media presión (6.0 kg/cm^2g), que proviene de la separación de la mezcla agua vapor que asciende en forma expontánea del reservorio.

Bajo dicho concepto de diseño, es necesario extraer aproximadamente 1800 T/H de mezcla agua-vapor para producir 30,000 KW con una turbina de media presión que estubiese diseñada para trabajar a una presión de admisión entre 4 kg/cm^2a y 5 kg/cm^2a para un valor de entalpía de mezcla de 230 Kcal/kgm.

Del total de la masa extraída, el vapor de media presión representaba del 16% al 18%, siendo el porcentaje restante: agua a presión que debe ser rechazada al ambiente sin ser utilizada.

...../2

...../2

Inicialmente se construyeron e instalaron 2 grupos generadores de 30,000 KW cada una, las cuales utilizaban vapor de media presión y cuyas características técnicas principales se describen en la tabla No.1.

El agua residual se descargaba en parte a través de una canaleta de concreto hacia el mar y en parte se reinyectaba en las zonas profundas del reservorio como una política de explotación para mantener la presión en el acuífero productor y un medio para eliminar el agua residual.

Después de análisis cuidadosos en la producción de pozos y mediciones para conocer la respuesta del reservorio a una explotación comercial a gran escala se decidió ampliar la capacidad instalada mediante la instalación en grupo generador de 35,000 KW pero con la modalidad de ser accionado por una turbina de doble presión la cual utilizaría el vapor de baja presión que se obtienen por vaporización súbita (flashing) del agua que es separada a boca de pozo.

Las características Técnicas de el turbo-generador de 35,000 KW se detallan en la tabla-2.

El grupo turbo-generador que constituye la 3a. Unidad Geotérmica de Ahuachapán es una unidad más eficiente con relación al aprovechamiento del recurso geotérmico ya que genera mayor potencia eléctrica para una cantidad de mezcla agua-vapor extraída del reservorio.

El incremento en la eficiencia del aprovechamiento se basa en que es accionado por vapor de baja presión que no puede ser

...../3

aprovechado por las dos primeras unidades que fueron instaladas, además de una entrada principal de vapor de media presión.

III. POZOS EN EXPLOTACION EN EL CAMPO GEOTERMICO DE AHUACHAPAN.

Para una capacidad instalada de 95,000 KW se habían perforado hasta fines de 1978 un total de 30 pozos en un área de -- 1.5 KM^2.

Los pozos perforados se distribuyen actualmente de la siguiente forma:

- Pozos en explotación para la 1a. Unidad: 5 pozos
- Pozos en explotación para la 2a. Unidad: 5 pozos
- Pozos en explotación para la 3a. Unidad: 5 pozos
- Pozos para reinyección al reservorio: 4 pozos
- Pozos de reserva para futura explotación: 4 pozos
- Pozos de observación y control de reservorio 2 pozos
- Pozos exploratorios: 7 pozos.

Los pozos de reserva para futura explotación son pozos que inicialmente no reunieron las características de presión o flujo para su inmediata explotación; pero que por evolución en las características termodinámicas del reservorio será posible utilizarlo en un futuro.

Adicionalmente al grupo de 30 pozos, actualmente se encuentra en proceso de perforación los pozos Ah-31 y Ah-32 en la zona sur del Campo Geotérmico para ampliar e incorporar dicha zona (aproximadamente 1 Km^2) a la explotación geotérmica.

Dicha decisión se ha tomado en base a que se ha comprobado que la zona sur del Campo es la zona de recarga y la de ma--

yor temperatura, lo cual es conveniente desde el punto de vista del aprovechamiento energético.

Las características de producción de los pozos geotérmicos en explotación se detallan en las tablas 3 y 4; y a pesar que se obtendrá un exceso en potencia disponible con relación a la capacidad instalada, es una práctica en el manejo de campo ya que se necesita dar mantenimiento rotativo a los equipos de separación e instalaciones superficiales; y además requiere mantener una relación extracción/reinyección para no sobre-explotar zonas de producción muy localizadas.

IV. DESARROLLO GEOTERMICO EN OTRAS ZONAS

Adicionalmente al desarrollo de la zona sur del Campo Geotérmico de Ahuachapán, la Comisión Ejecutiva Hidroeléctrica del Río Lempa está desarrollando los recursos geotérmicos en otras zonas del país.

IV-I CAMPO GEOTERMICO DE BERLIN, DEPARTAMENTO DE USULUTAN

Se ha finalizado la etapa de factibilidad para la instalación de un grupo turbo-generador de 55,000 KW.

Se tienen a la fecha preparados 6 pozos, dos de ellos de alta producción (más de 8 MW) y los demás de media producción contándose con energía disponible para generación de 20,000 KW a partir de fluídos geotérmicos -- con una temperatura entre 300°C y 310°C en el reservorio.

Para 1982 se iniciará el desarrollo del Campo Geotérmico mediante la perforación de la Batería de pozos para la Central, la cual deberá estar en línea para 1986; y los

...../5.

estudios de ampliación de la zona de explotación con la estimación del potencial adicional de la zona para considerar la construcción de una 2a. Central.

IV.II. CAMPO GEOTERMICO DE CHIPILAPA-DEPARTAMENTO DE AHUACHAPAN

Se ha iniciado durante el presente mes los estudios de factibilidad que culminará con la perforación de 3 pozos exploratorios profundos, que en forma adicional al pozo Chipilapa No.1 perforado en 1968 confirmafa el potencial geotérmico de la zona.

IV.III. CAMPO GEOTERMICO DE SAN VICENTE-DEPARTAMENTO DE SAN VICENTE.

Los estudios de factibilidad principian en 1984 a continuación de los estudios en Chipilapa.

En dicho Campo Geotérmico ya se encuentra perforado un pozo Exploratorio perforado con una temperatura superior a 220°C.

V. PERSPECTIVAS EN ENERGIA GEOTERMICA.

En forma definitiva la energía geotérmica en El Salvador constituye una parte importante del plan de expansión energética del país hasta el año 2000 y esto se basa en los resultados exitosos de las exploraciones, su costo comercialmente competitivo y alto grado de asimilación de la tecnología geotérmica con el gradual desarrollo de una tecnología nacional. Todo esto se refleja en el hecho que actualmente la generación eléctrica de la Central Geotérmica de Ahuachapán constituye del 35% al 45% de la generación bruta nacional.

...../6

COMISION EJECUTIVA HIDROELECTRICA DEL RIO LEMPA SAN SALVADOR

6. REFERENCIAS.

- Nitsubishi Heavy Industries. " Instruction Book for Turbine Plant" Vol. M-1. Ahuachapán Geothermal Power Plant, Agosto/1975.

- Fuji Electric Co. "Instruction Book for Turbine "3rd. -- Unit. Ahuachapán Geothermal Power Plant, Enero 1981.

- Cáceres J.R. "Tercera Unidad - Planta Geotérmica de Ahuachapán" Reporte Técnico SRG-SI-IMP-0102, Abril, 1980.

JRCR/Bda
Agosto, 1981.

TABLA No.1

CARACTERISTICAS TECNICAS PRINCIPALES DEL GRUPO TURBOGENERADOR GEOTERMICO.

1a. Y 2a. UNIDAD. CENTRAL GEOTERMICA DE AHUACHAPAN

1. Tipo de Turbina.	De impulso y doble flujo.
2. Potencia Nominal	30,000 KW
3 Potencia Máxima (F.P.93.5%)	35,000 KW
4. Velocidad.	3,600 RPM.
5. Presión Nominal de vapor en el colector.	0.59 Mpa. a (6.0 Kg/cm^2 a)
6. Presión nominal del vapor en la válvula de admisión.	0.56 Mpa. a (5.7 Kg/cm^2 a)
7. Temperatura del vapor en la válvula de admisión.	156.1°C
8. Humedad del vapor de admisión.	0.1%
9. Presión en el Condensador.	8.33 Kpa.a (0.085 Kg/cm^2 a)
10. Número de etapas en la turbina.	Doble flujo de 5 etapas.
11. Longitud del último alabe.	520 mm.
12. Peso del rotor.	11,800 Kg.
13. Consumo de vapor a potencia nominal.	230,000 Kg/hr.
14. Consumo de vapor a potencia máxima.	265,700 Kg/hr.
15. Tipo de Condensador.	Tipo Barometrico de contacto directo.
16. Temperatura de entrada del agua de enfriamiento al condensador.	27°C
17. Temperatura de salida del agua en el pozo de bombas.	40.3°C
18. Caudal de Agua de enfriamiento.	8,650 m^3/hr.
19. Tipo de eyectores para el vacio del condensador.	Eyectores de vapor de 2 etapas.
20. Presión de succión del eyector.	7.84 Kpa.(0.80 Kg/cm^2 a)
21. Capacidad de extracción del eyector.	460 Kg/h de gas no condensable 165 Kg/hr. de aire 260 Kg/h de vapor.
22. Consumo de vapor del eyector (2 etapas)	4,100 Kg/hr.
23. Capacidad de las bombas de agua de circulación (2 Bombas)	4,600 m^3/hr.
24. Tipo de torre de enfriamiento.	Flujo cruzado, tiro inducido
25. Flujo de agua circulando en la torre de enfriamiento.	9,025 m^3/hr.
26. Temperatura de diseño de la torre de enfriamiento.	22.0°C (bulbo humedo)
27. Superficie húmeda de la torre.	44,370 m^2
28. Pérdidas por evaporación.	215 m^3/hr.
29. Flujo de aire inducido en la torre.	162,945 m^3/minuto.
30. Constructor y Suministrante.	Mitsubishi Heavy Industries.

JRCR/Bda
Agosto, 1981.

TABLA No.2

CARACTERISTICAS TECNICAS PRINCIPALES DE GRUPO TURBOGENERADO GEOTERMICO. 3a. UNIDAD - CENTRAL GEOTERMICA DE AHUACHAPAN.

1. Tipo de Turbina.	De impulso, doble flujo, doble presión y de condensación.
2. Potencia nominal.	35,000 KW
3. Potencia Máxima	40,000 KW
4. Velocidad.	3,600 RPM
5. Presión nominal del vapor de media presión en la admisión.	0.54 Mpa. (5.59 Kg/cm^2 a)
6. Presión Nominal del vapor de baja presión en la admisión.	0.15 Mpa. (1.53 Kg/cm^2 a)
7. Humedad del vapor de admisión.	Menor del 0.1%
8. Presión en el Condensador.	8.33 Kpa. (0.085 Kg/cm^2 a)
9. Número de etapas en la turbina.	Doble flujo de 7 etapas.
10. Longitud del último alabe.	565 mm.
11. Peso del rotor	33,500 kg.
12. Consumo de vapor de media presión a potencia nominal.	176,770 Kg/hora.
13. Consumo de vapor de baja presión a potencia nominal.	145,000 Kg/hora.
14. Tipo de condensador.	Tipo barometrico de contacto directo.
15. Temperatura del agua de circulación en el condesador.	27°C
16. Flujo de vapor circulando en el condensador.	315.59 T/h
17. Caudal de agua de circulación.	12,260 m^3/hora
18. Tipo de eyectores para el vacio del condensador.	Eyectores de vapor de 2 etapas.
19. Consumo de vapor en el eyector.	5.96 T/h.
20. Capacidad de extracción de gases.	605.6 Kg/hora
21. Capacidad de las bombas de agua para circulación. (2 bombas).	6,700 m^3/hora
22. Tipo de torre de enfriamiento.	Flujo cruzado, tiro inducido.
23. Flujo de agua circulando en la torre de enfriamiento.	12,800 m^3/hora.
24. Temperatura de diseño de la torre.	22°C (bulbo húmedo)
25. Superficie húmeda de la torre	32,640 mts. x 5 celdas
26. Pérdidas de evaporación en la torre.	294 m^3/hora.
27. Flujo de aire inducido en la torre.	122,000 m^3/minuto
28. Cosntructor y suministrante.	Fuji electric Co. Ltd.

JRCR/Bda
Agosto/81

TABLA No.3

CARACTERISTICAS DE PRODUCCION DE POZOS GEOTERMICOS EN EXPLOTACION. CAMPO GEOTERMICO DE AHUACHAPAN.

Pozos	Presión de Separación (Mpa. g)	Masa de vapor (Kg/seg.)	Masa de Agua (Kg/seg.)
1a. Unidad			
AH-1	0.50	10.77	64.4
AH-6	0.54	20.16	5.0
AH-7	0.51	8.64	37.4
AH-17	0.65	28.89	0.0
AH-24	0.53	8.64	52.78
2a. Unidad			
AH-20	0.56	18,19	31.67
AH-21	0.60	18.94	79.17
AH-22	0.56	9.24	45.33
AH-23	0.56	14.79	47.22
AH-26	0.56	11.71	5.00
3a. Unidad			
AH-4	0.54	23.74	30.00
AH-27	0.56	11.11	63.33
AH-28	0.55	12.58	73.89

JRCR/Bda
AGOSTO/81

TABLA No.4

POTENCIA TERMODINAMICA ESTIMADA DE POZOS GEOTERMICOS EN EXPLOTACION, A PRESIÓN DE SEPARACION. CAMPO GEOTERMICO DE AHUACHAPAN.

Pozo	1a. Unidad. MP	2a. Unidad. MP	3a. Unidad MP	3a. Unidad BP	TOTAL
AH-1	4,400 KW			1800 KW	6200 KW
AH-6	7,800 KW				7800 KW
AH-7	4,000 KW				4000 KW
AH-17	13,300 KW				13,300 KW
AH-24	3,500 KW			1500 KW	5,000 KW
	33,000 KW				
AH-20		8,200 KW		1100 KW	9,300 KW
AH-21		7,400 KW		2400 KW	9,800 KW
AH-22		4,500 KW		1400 KW	5,900 KW
AH-23		5,100 KW		1300 KW	6,400 KW
AH-26		5,100 KW			5,100 KW
		30,300 KW			
AH-4			10,700 KW		10,700 KW
AH-27			7,000 KW	1900 KW	8,900 KW
AH-28			6,600 KW	2100 KW	8,700 KW
			24,300 KW	13500 KW	
			37,800 KW		
					101,100 KW

Notas:
- Potencia Termodinámica a presión de separación.
- Eficiencia térmica de 1a. y 2a. Unidad: 72 %.
- Eficiencia térmica de 3a. Unidad:79%.
- No se han considerado pérdidas de transmisión (energía a presión de Separación).
- No se ha considerado consumo de vapor en eyectores, sellos de vapor y otras pérdidas.
- No se ha considerado el consumo interno de la Central por servicios Auxiliares.

JRCR/Bda
Agosto/81.

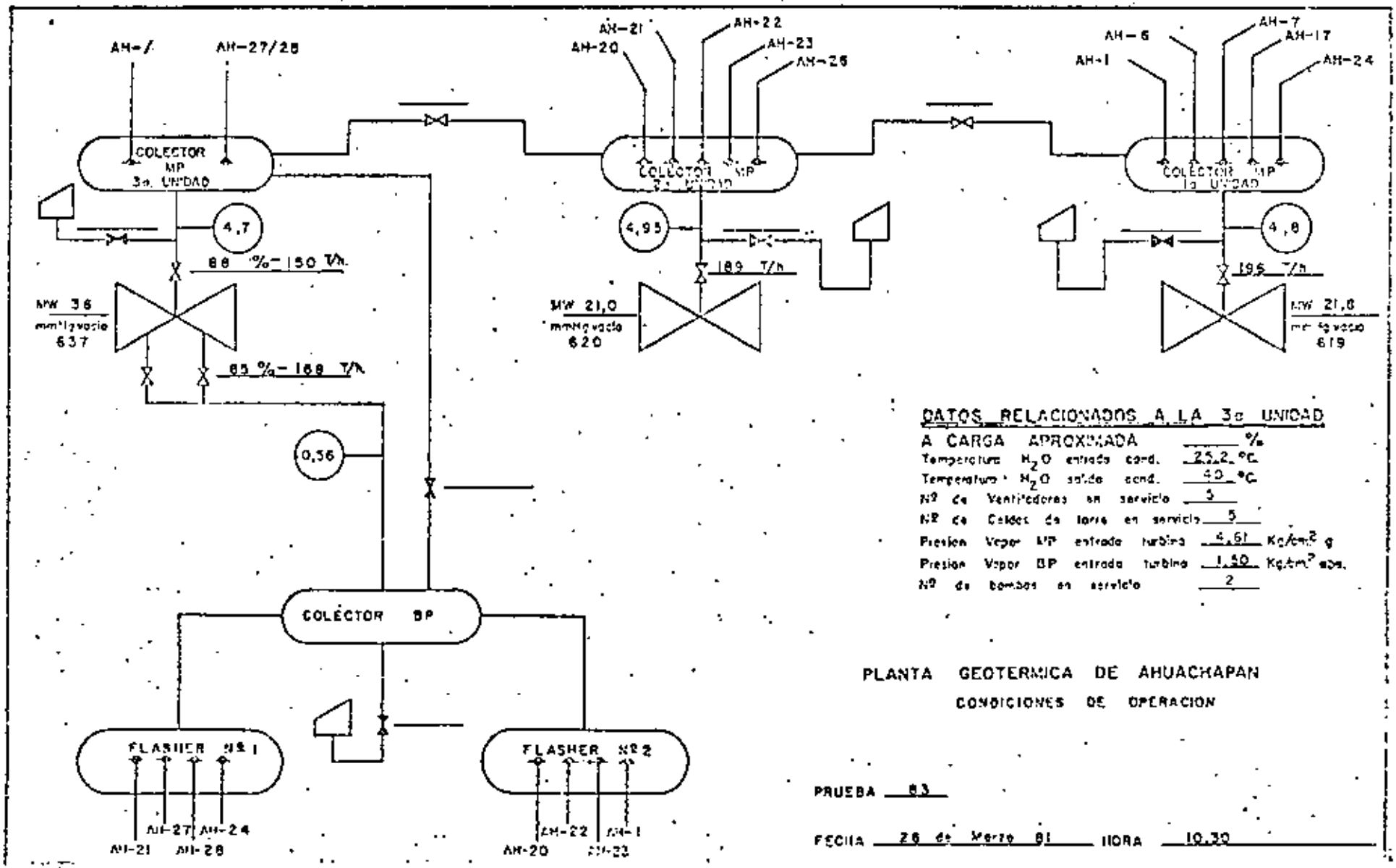

DATOS RELACIONADOS A LA 3a UNIDAD

A CARGA APROXIMADA ____ %

Temperatura H_2O entrada cond. 25,2 °C

Temperatura H_2O salida cond. 40 °C

Nº de Ventiladores en servicio 5

Nº de Celdas de torre en servicio 5

Presion Vapor MP entrada turbina 4,61 Kg/cm² g

Presion Vapor BP entrada turbina 1,50 Kg/cm² abs.

Nº de bombas en servicio 2

PLANTA GEOTERMICA DE AHUACHAPAN

CONDICIONES DE OPERACION

PRUEBA 83

FECHA 26 de Marzo 81 HORA 10.30

C H A P T E R 9

RESERVOIR ENGINEERING CONCEPTS

by

INSTRUCTORES: DR. FERNANDO SAMANIEGO V.
DR. HEBER CINCO LEY.

ABSTRACT

A review of the basic principles of geothermal reservoir engineering is presented. It is concluded that predictions of reasonable accuracy can be made with actually available methods for the majority of geothermal systems saturated with fluids. Discussion of this chapter includes the practical aspects of reservoir engineering, such as well test analysis, and mathematical reservoir simulation.

INTRODUCTION

Geothermal reservoir engineering is related in many aspects to oil and gas reservoir engineering. These latter branches of petroleum engineering started its development about the 1930's (Richardson, 1973). On the contrary, it seems that geothermal reservoir engineering started at the end of the sixties with classic studies on the Wairakei field (Whiting and Ramey, 1969) and the Geysers Field. (Ramey, 1970). Geothermal reservoir engineering can be defined as to include activities which begin with locating the wells including among other things work like well logging while drilling and flow measurements, identification of the production mechanism, and finally performance prediction of reservoir behavior to find the optimum production conditions that would lead to maximum economic heat recovery.

The basic tasks of the reservoir engineer are the prediction of the long term behavior of the well and the reservoir (Ramey , 1977). There are a few important questions that he must answer: (a) what is the optimum development plan for the reservoir?; (b) how many wells and what kind of pattern will be required for optimum development of the reservoir?; (c) what will be the rate of production for the wells?; (d) how much heat will be recovered?; (e) what will be the variation of temperature versus time; (f) would it be feasible to implement an enhanced recovery process to recover additional heat?; To answer all these, and other possible questions, the engineer needs to undertake a continuous very careful work since the beginning of the life of the reservoir. As production from the reservoir increases, more data becomes available, and the reservoir engineer has more data for history matching purposes, allowing him to update previous studies, and consequently to make better predictions

of the reservoir behavior. It is unfortunate that we only know everything about the reservoir when it is fully depleted.

It is important that the reservoir engineer quantitatively appreciate the physical processes that occur within the geothermal system. This would allow him to choose the optimum exploitation conditions for the reservoir. This process can be divided in three main steps: (a) in this first step the physical processes associated with the particular geothermal system under study must be identified and used to develop a conceptual model of the reservoir; (b) a careful assesment of the physical and thermal properties of the rock and fluids needs to be carriedout: These data will be extremely useful for simulation studies purposes; and (c) a mathematical or physical model of the reservoir is developed, using the previously determined information about the reservoir. This model should include the properly identified initial and boundary conditions for the system. Once the model is at hand, it can be updated and refined as new production data becomes available. The reservoir response under production should be carefully matched with the model. This technique of matching the observed production history data by means of a suitable model, and using the model to predict future performance is one which is fundamental to the subject of reservoir engineering.

About the middle of the 1960's geothermal reservoir engineering relied heavily on the theory developed for oil and gas reservoir engineering. In cases where the characteristics of the geothermal and petroleum systems are alike, the oil and gas reservoir engineering techniques can be properly employed, if inherent differences in the

systems are considered. Examples of successful applications of these techniques to geothermal reservoirs have been published in the literature (Whiting and Ramey, 1969; Ramey, 1970; Atkinson et al., 1978). There are several factors that make geothermal reservoir engineering a unique subject in itself. To name a few, it can be mentioned the problem of high temperature in the reservoir; the type of formation which contain the fluid, being in many cases highly fractured and of volcanic type; chemical depositation of solids during flow of fluids in the reservoir; and steam flashing. Due to the interest in geothermal energy, geothermal reservoir engineering has shown great advancements in the last 15 years. (Takahashi et al.,1978

This chapter, presents a review of the basic principles of geothermal reservoir engineering. The presentation includes a discussion of some of the practical aspects of reservoir engineering, such as well test analysis, and also a discussion on mathematical reservoir simulation.

TYPES OF GEOTHERMAL SYSTEMS

Geothermal systems can be classified in four main types: (a) vapor-dominated (dry steam); (b) liquid dominated (hot-water); (c) geopressured (hot) accumulations; and (d) dry (hot-rock) formations. Each one of these systems has potential for exploitation but the vapor-dominated offers the optimum conditions for electricity production. According to White (1973), technology currently available for geothermal electricity generation makes use of steam. Based on present day state of knowledge from geothermal steam there are some requirements that have to be met for

electricity generation: (a) temperature of reservoir should be high (at least 180°C, but preferably above 200°C); (b) reservoir depth less than 3 Km; (c) adequate reservoir volume; (d) the reservoir should contain natural fluids to tranferring the heat to surface and power plants; (e) permeability of the formation should be adequate to ensure sustained delivery of fluids to wells at high enough rates to meet power production needs; (f) no major unsolved technology problems. Unfortunately, these characteristics are not easily found in earth's crust.

Vapor-Dominated Systems.

The vapor-dominated system is the rarest found in nature and the most sought after (Burnham, 1973), because it is a clean enviromentally safe energy source with minor production problems. There are few vapor-dominated systems, among them two of the most important are the Lardarello fields of Italy and The Geysers of California, which produce dry or superheated steam with no associated liquid (White, 1973). This is the reason why they are commonly known as "dry-steam" systems but White et al. (1971) have concluded that liquid water and vapor usually coexist in the reservoir, being vapor the continuous, pressure controlling phase.

These vapor systems contain far less heat than the hot-water systems (Ramey et al., 1973), but as mentioned earlier, problems related with its utilization are minor. The production mechanism of steam reservoirs is similar to that of natural-gas reservoirs, because pressure is reduced by the expansion of the gas in-place. The fractional mass production of original mass in place is usually high, somewhere close to 85-90 percent. However, the situation for

energy recovery is quite different, being quite low. Ramey et al., (1973) show a table where they compare the recovery for a hot-water and a steam reservoir, showing for the latter a fractional energy recovery of 5.6 percent. This is so, because most of the heat is stored in the rock, and since the steam flow process in the reservoir is essentially isothermal, almost none of the heat contained in the rock is recovered. To recover heat stored in the rock, the production process should reduce the rock temperature. For these systems, additional energy can be recovered by means of an enhanced recovery process, using liquid reinjection to the reservoir.

Hot-Water Systems.

In hot water systems, water is the continuous, pressure-controlling fluid phase. These systems may contain some vapor, found as discrete bubbles in the shallow, low-pressure zones. Among geothermal systems discovered to date, hot liquid dominated systems are far more common than vapor-dominated systems (White, 1973). Water in these reservoirs is a dilute aqueous solution containing sodium, pottasium, lithium, calcium, chloride, bicarbonate, sulfate, borate, and high percent of silica. Some of the most important liquid-dominated systems are those located in the Imperial Valley in California, Wairakei in New Zealand, and Cerro Prieto, in Mexico.

As mentioned previously, the energy content of these systems is higher than that for the vapor-dominated systems. Ramey et al. (1973) have shown that the fractional energy recovery for this kind of systems is higher than for the vapor-dominated systems. This is caused by flashing of the water in the reservoir, or by reinjection of water.

These are key factors in the recovery of geothermal energy from these systems. The problems encountered in the utilization of these systems are more difficult than those found for the vapor-dominated systems, but strong research programs under way may overcome these difficulties in the future.

Geopressured (hot) accumulations.

The geopressured systems are composed by sediments that contain fluids at pressures far greater than normal (hidro static). Knapp et al. (1977) present an explanation for the existance of these high pressure zones. Briefly, these zones have a highly impermeable overlying formation, preventing the migration of fluids out of the zone, causing that the fluids saturating this zone partially bear the overburden load. This results in an increase in sediment and fluid pressure. Pressure gradients in a geopressured zone ussually approach lithostatic pressure, or 1 psi/ft. The geopressured sediments have a low thermal conductivity and high heat capacity, causing the system's temperature to be high. The most important geopressured zone known to date is the Gulf coast region of the United States which extends in land and offshore from Texas to the Mississipi estuaries.

Fluids contained in geopressured systems are commonly saturated with methane. At the pressure and temperatures encountered, the quantity of methane associated with water saturating the system can be important. This is an additional benefit that can be obtained from the exploitation of these accumulations. Another factor that propitiates the solution of methane in the water of these reservoirs is water salinity, which is lower under the geopressured

conditions than for normal conditions (Burst, 1969). Low salinity waters can hold more methane in solution than high salinity waters.

Dry (hot-rock) Formations.

Hot dry formations are systems which do not contain water to act as heat transport medium. The incidence of this type of geothermal resources is far greater than that of the fluid saturated geothermal sites (Burnham and Stewart, 1973). These resources can be an important energy supply, provided that means can be found to extract and use such heat economically. The most simple practical, and economical way to recover heat from these systems is introducing water into the formation, permitting it to circulate until it has been heated to a useful high temperature, and then recovering the fluid as steam or hot-water (Smith et al., 1973 and 1975). These authors present a discussion of the research regarding dry formations carried out by Los Alamos Scientific Laboratory of the University of California.

Frequently, dry formations have very low permeability, and the problems of containing and recovering the injected water can be overcome by means of creating flow passages of big enough surface area, through which it can flow a useful flow of water, for economically long periods of time. This would allow heat recovery through contact of the water with the area of the flow passages. The basic heat extraction system tested consists of an injector and a producer well, the passage (communication) being a hydraulic fracture.

Geothermal systems saturated with fluids (convective systems) can be classified with respect to the location of its initial conditions on a pressure-temperature diagram.

Such a classification has been presented by Whiting and Ramey (1969) and by Martin (1975). Fig. 9.1 presents a pressure-temperature diagram for pure water. The solid line is the boiling curve. Similar diagrams for geothermal brines should be accordingly modified as to include dissolved salts. It is helpful to follow events subsequent to producing a reservoir at different assumed initial conditions.

There are several points in Fig. 9.1 that have to be considered. Point A represents the initial conditions for a single-phase (steam) reservoir that initially existed entirely within the vapor region. There is no formation of hot-water, since for the conditions of this reservoir basically the flow is isothermal and the boiling curve is not crossed. At the end of production the temperature of the reservoir would be high. Thus, additional energy can be recovered by water injection. Point B represents the initial conditions for a reservoir; these conditions fall on the vapor pressure curve, and consequently, there are two phases (hot-water and steam) originally present in the reservoir. The analog of this reservoir in petroleum reservoir engineering is the gas-cap reservoir. Whiting and Ramey (1969) discuss that for this system, production is a mixture of hot-water and steam that could range from saturated liquid to saturated steam. Point C corresponds to a reservoir that originally had only hot-water. The production mechanism is such that eventually, as reservoir pressure declines, the conditions of the vapor-pressure curve will be reached. From then on, production is similar to that of reservoir B previously discussed. While the reservoir fluid is hot-water, the flow in the reservoir is essentially isothermal and isoenthalpic; when the vapor-

pressure curve is reached, the pressure and temperature decline along this curve.

Also shown in Fig. 9.1 are two more points: D and E.Point D corresponds to a reservoir which originally existed at conditions of pressure and temperature above the critical values. As pressure declines due to production, a reservoir of this type would eventually become similar to reservoir A. These reservoirs usually do not show pressure temperature conditions such as to cross the vapor-pressure re curve. Point E represents a reservoir whose initial condition of pressure is higher than the critical pressure re. Due to production from the reservoir, pressure will decline, and the reservoir eventually becomes similar to reservoir C and B.

From the previous discussion, and from that of Whiting and Ramey (1969), it can be inferred, that for performance prediction purposes, it is necessary to know mass production and enthalpy of the produced fluids. It has also been pointed out that the reservoir rock is an important potential source for energy recovery.

It is of interest to know in a general sense what is the state of technology development, enviromental impact, economics, and availability of the different geothermal systems. Table 9.I shows such type of information, for present time conditions. This table is a modified version of that presented by Davis and Colan(1974). A striking fact drawn from this table is that our knowledge is more complete for those resources that are limited in extent. If geothermal energy is to be an important worldwide source of energy, the technology for energy recovery from dry

(hot-rock) formations has to be fully developed. This will need an extensive research program to evaluate all aspects related to these systems, like, enviromental impact, and economics, besides the necessary technology development. Such efforts are presently under way (Smith, et al., 1973; Murphy, 1975).

TABLE 9.I

Assesment of geothermal systems.

SITUATION / SYSTEM	TECHNOLOGY	ENVIRONMENTAL IMPACT	ECONOMICS	RESOURCE AVAILABILITY
Vapor-Dominated	Established	Small	Attractive	Limited
Liquid-Dominated	Partially established	Potentially large	Known but uncertain	Limited but significant in some areas.
Dry (hot-rock) formations	Only partially developed	Unknown	Partially known	Potentially large
Geopressured (hot) accumulations	Only partially developed	Unknown	Partially known	Limited but significant in some areas.

PRESSURE TRANSIENT ANALYSIS FOR GEOTHERMAL WELLS

Transient Pressure testing consists of recording the pressure variation versus time in the well or neighboring wells after the flow rate of the well(s) is changed, and, subsequently, estimating the reservoir and well properties. This technique estimates these data at the in-situ conditions of pressure, temperature, and fluid saturation prevailing in the reservoir. From the analysis of pressure transient tests, among other data, the following information can be obtained:

- Permeability thickness product (kh) in the drainage volume of the well, and permeability (k).
- Condition of the well, represented by the skin factor (s).
- Average pressure within the drainage volume ($\bar{p}$).
- Porosity of the drainage volume (ϕ)
- Pore volume of the reservoir (V_p), and its shape.
- Reservoir and fluid discontinuites (faults, etc.).

The above information would be extremely useful to help analyze, improve, and forecast reservoir performance. Ramey (1975) presents an example of practical use of this data. He states that quantitative information on the previously listed items would answer questions that are usually raised such as: is the low productivity of a well caused by

plugging of the well, low formation permeability, or a low driving force and/or formation capacity for moving fluid into the well?.

Thus, transient pressure testing is an extremely useful tool for reservoir diagnosis. Transient pressure testing is sometimes referred as a practical application of reservoir engineering (Duke, 1978). In specific situations (Earlougher, 1977) it is indispensable for correct well or reservoir analysis; for example, in definition of near-wellbore and interwell conditions as opposed to composite properties that would be obtained from steady-state tests.

To carry out a transient pressure analysis of field data, it is important to choose or obtain an adequate mathematical expression that can be used for interpretation and design of the test. This expression can be derived by properly combining the physical laws that describe the specific fluid flow problem in the reservoir, and considering the production condition of the well.

Transient pressure tests can be classified in two main types: (a) single well tests, and (b) multiple well tests. Single well tests, as its name indicates, are those that involve only one well, producer or injector. These tests require measuring of the well's pressure response after a rate change has taken place. On the order hand, multiple well tests directly involves more than one well. In tests like this, a rate change in a well called active, creates a pressure response in a neighbor well called observation well. Both pressure responses for single and multiple wells can be analyzed for reservoir properties. The most important single and multiple well tests are as follows:

a) Single Well Tests

1) Drawdown tests
2) Buildup tests
3) Injectivity tests
4) Falloff tests
5) Multiple-rate tests

b) Multiple Well Tests

1) Interference tests
2) Pulse tests

Fig. 9.2 shows an squematic representation of the variation of the mass rate w and pressure versus time during three different types of transient pressure tests: Fig.9.2.a. a drawdown test; Fig.9.2.b. a buildup test; and Fig.9.2.c. a two-rate test. The most simple type of pressure drawdown test , shown in this figure, consists of a series of bottom-hole pressure measurements made over a period of time with the flow rate constant. Before the test, pressure throughout the reservoir should be uniform, i.e., static. If the constant rate production and the static pressure condition are not met, methods are available which can be used (Matthews and Russell, 1967; Earlougher, 1977). According to the purpose they are performed for, there are two types of drawdown tests: (a) short term drawdown are used to estimate the formation permeability, and wellbore condition; (b) long term or reservoir limit tests, are used to estimate the reservoir volume.

A pressure buildup test consists of a series of shut-in bottom-hole pressure, p_{ws} , measurements made at immediately before and at times Δt after shut-in. Again, the most simple buildup test is such that the well produced with a constant

rate, w, for a period of time before shut-in. (Fig. 9.2.b) These tests are conducted in wells for similar purposes as drawdown tests: (a) to estimate the flow capacity of the formation, Kh, in the drainage volume; (b) to estimate the well condition, s; and (c) to determine the average (static) pressure in the reservoir.

A two-rate test is a particular case of a multiple-rate test. It consists of a series of flowing bottom-hole pressure measurements made at times Δt after a rate change of the well (Fig. 9.2.c). The two-rate tests provide information about: (a) formation permeability, and (b) wellbore condition; and (c) average drainage volume pressure at the start of the test.

While drawdown and buildup tests are conducted in production wells, their counterpart in injection wells are the injectivity and the falloff tests. An injectivity test consists of a series of bottom-hole pressure, p_{wf}, measurements made over a period of time with the injection flow rate constant. The type of information that can be obtained from the analysis of these tests is the same as from drawdown tests. A falloff test consists of a series of bottom-hole pressure measurements made immediately before and at times Δt after stopping injection. Once more, the most simple falloff test is that where injection is at constant rate, w, until the well is shut-in at time t. The possible information to be obtained from these tests is the same as from pressure build-up tests.

Multiple-well transient tests consist of a series of pressure measurements of the pressure response in one or more observation wells, after a rate change on an active neigh-

bor well. The most simple multiple-well transient test involves only one active and one observation well. Analysis could also be made of pressure response when there are more than one active and observation wells, but it will be more complicated. Fig. 9.3 squematically illustrates the use of two wells in an interference or pulse test. The observation well is shut-in for pressure measuring purposes. As discussed by Matthews and Russell (1967), the name pressure interference comes from the fact that the pressure drop caused by the active (producers or injectors) wells at the shut-in observation well "interferes with" the pressure at the observation well.

In an interference test the duration of the rate change is long, opposite to what happens in a pulse test where duration of rate change is shorter, but the analysis technique for reservoir properties is more elaborated. Multiple-well tests can give information about reservoir properties that cannot be obtained from ordinary single well tests. For instance, it is possible to estimate reservoir connectivity. A test like this may answer questions such as: is the area of the reservoir closed to a well being drained by other wells, and if so, how fast? This test would also help to determine the preferential reservoir flow patterns. This could be accomplished by selectively opening wells that surround the shut-in well.

It has been previously discussed that flow in a geothermal reservoir can be steam, hot-water, or a mixture of steam and hot-water. Thus, it is of interest to present analysis techniques for these three different cases, for some of the most used pressure transient tests.

Transient Pressure Analysis for Steam Wells.

Due to the fact that single-phase (steam or hot-water) flow in geothermal reservoirs is essentially isothermal (Whiting and Ramey, 1969), transient pressure analysis techniques are usually derived based on a strict analogy with the single-phase isothermal flow techniques developed by petroleum engineers and hydrogeologists. The laminar flow of a slightly compressible fluid, in a radial, horizontal, isotropic reservoir, under the condition of small pressure gradients in the reservoir, and aplicability of Darcy's law, and that the rock and fluid properties are independent of pressure, is expressed by the diffusivity equation (Muskat, 1938; Matthews and Russell, 1967; Earlougher, 1977). For convinience, the solution to this reservoir fluid flow problem is usually expressed in dimensionless form. The following groups have been defined by Ramey (1975), and Ramey and Gringarten (1975).

Dimensionless Pressure for Flow of Steam.

$$p_D(r_D, t_D) = \frac{M \times h(p_i^2 - p^2)}{\alpha \, w \, Z \, T} \qquad (9.1)$$

Dimensionless Time

$$t_D = \frac{\beta \, Kt}{\phi \, \mu \, c_t \, r_w^2} \qquad (9.2)$$

Dimensionless Radial Distance

$$r_D = \frac{r}{r_w} \qquad (9.3)$$

where α and β are unit constants. Table 9.II shows some of the most used unit systems, and the corresponding values for α and β.

TABLE 9.II
Absolute and Hybrid System of Units Used in Geothermal Reservoir Engineering.

Variable	S I System*	Hybrid System
k	$metre^2$	md
h	m	m
p	$newton/metre^2$ = pascal	Kg_f/cm^2
w	Kg/sec	Ton/hr
v_{sc}	$metre^3/Kg$	cm^3/gm
B	$metre^3_{rc}/metre^3_{sc}$**	$metre^3_{rc}/metre^3_{sc}$
μ	Kg/metre. sec	cp
t	sec	hours
ϕ	fraction	fraction
c_t	$(Newton/metre^2)^{-1}$	$(Kg_f/cm^2)^{-1}$
r	metre	metre
α	26.1201	77.459×10^3
β	1	0.000348
δ	$1/2\pi$	456.7869
ε	$1/2\pi$	$1/2\pi$
η	2.6465	27

* SI is the abbreviation for International System of Units.

** rc stands for reservoir conditions and sc for standard conditions.

The pressure in the reservoir at any point in space and time can be estimated from Eq. 9.1 if the particular p_D for the system under consideration is known. The dimensionless pressure p_D is a function of the type of system, infinite or finite, and of the boundary conditions, rate or pressure specified. For a well producing at a constant rate w , assuming the conditions for the flow of a fluid of constant and small compressibility apply , and for infinite acting conditions, the p_D can be expressed by the line source solution (Earlougher, 1977):

$$p_D\ (r_D,\ t_D) = -\frac{1}{2} E_i\left(-\frac{r_D^2}{4 t_D}\right) \qquad (9.4)$$

For transient pressure analysis purposes, the pressure of interest is the wellbore pressure. For this condition, $r = r_w$, and combining Eqs. 9.1, 9.2, 9.3 and 9.4, and using the logarithmic approximation to the exponential integral, an expression for the wellbore pressure can be obtained as follows:

$$p_{wf}^2 = p_i^2 - 1.1513\alpha \frac{w\ \mu\ Z\ T}{MKh}\left[\log \frac{Kt}{\phi\ \mu c_t\ r_w^2} + \log \frac{4\beta}{\gamma} + 0.86859\ s\right] \qquad (9.5)$$

where $\gamma = 1.7810724$, and log means base 10 logarithm.

This equation can be used for interpretation of a steam drawdown test. It can be observed, that it describes a straight line relationship between p_{wf}^2 and log t. Theoretically, a plot of flowing bottom-hole pressure data vs the logarithm of time (usually called a "semilog plot")

should be a straight line with slope m, given by the following expression:

$$m = \frac{1.1513\alpha\, w_g Z T}{M k h} \qquad (9.6)$$

From this equation, the capacity of the formation can be obtained:

$$kh = \frac{1.1513\alpha\, w_g Z T}{m M} \qquad (9.7)$$

By rearring Eq. 9.5, an expression for the skin factor, s, can be obtained:

$$s = 1.1513 \left[\frac{p_i^2 - p_{1hr}^2}{m} - \log \frac{k}{\phi \mu\, c_t\, r_w^2} - \log \frac{4\beta}{\gamma} \right] \qquad (9.8)$$

For pressure buildup testing, the bottom-hole shut-in pressure of the well may be expressed by means of the principle of superposition for a well producing at rate w until time t (Fig.9.2.b), and at zero rate thereafter. Thus, at any time after shut-in, the wellbore pressure may be expressed,

$$p_{ws}^2 = p_i^2 - \alpha \frac{w_g Z T}{M k h} \left(p_D([t+\Delta t]_D) - p_D(\Delta t_D) \right) \qquad (9.9)$$

Substituting Eq. 9.5 into Eq. 9.9:

$$p_{ws}^2 = p_i^2 - m \log \left(\frac{t+\Delta t}{\Delta t} \right) \qquad (9.10)$$

This equation can be used for interpretation of a buildup

test. It describes a straight line relationship between p_{ws}^2 and log $(t+\Delta t)/\Delta t$. Theoretically, a plot of shut-in bottom-hole pressure data vs the log $(t+\Delta t)/\Delta t$ should be a straight line with slope m given by Eq. 9.6. Fig. 9.4 shows a squematic Horner plot of pressure buildup data. The straight line portion of the Horner plot can be extrapolated to $(t+\Delta t)/\Delta t=1$, the equivalent to infinite shut-in time, to obtain an estimate of p_i. This is only valid for infinite acting systems during the flow period. For times after the exterior boundary affects production, the extrapolated pressure is p*. This value can be used to estimate the average drainage volume pressure (Matthews, Bronz, and Hazebroeck, 1954). As pointed out by Matthews and Russell (1967) an equation describing the pressure behavior for an infinite acting reservoir may be immediately rewritten for the finite reservoir case by substituting p* by p_i.

The skin factor, s, may also be estimated from pressure buildup analysis. An expression for this factor can be obtained by combining the expressions for flowing and shut-in pressures, given by Eqs. 9.5 and 9.10:

$$s = 1.1513\left[\frac{p_{1hr}^2 - p_{wf}^2\ (\Delta t=0)}{m} - \log\frac{k}{\phi\mu c_t r_w^2} - \log\frac{4e}{\gamma}\right] \qquad (9.11)$$

In this equation, $p_{wf}\ (\Delta t=0)$ is the measured flowing bottom-hole pressure immediately before shut-in. The p_{1hr}^2 pressure must be obtained from the straight line portion of the pressure buildup test 1 hour after shut-in, or from its extrapolation if the straight line portion of the test has not been reached at this time. This also holds true for other

types of tests, as the drawdown test previously discussed.

The early deviation of a transient pressure test from a straight line may be caused, between other factors by wellbore storage (van Everdingen and Hurst, 1949; Ramey, 1965; Agarwal, Al-Hussainy and Ramey 1970). This can be caused by expansion or compression of fluids in the wellbore, and by liquid level movements in the wellbore. This effect has to be properly considered for accurate test design and interpretation.

Example 9.1 Pressure Buildup Test Analysis - Horner Method

This is a pressure buildup test for Geysers steam well C, presented by Ramey (1975). Table 9.III shows the reservoir data regarding this test. Fig. 9.5 shows a semilogarithmic plot of test data. As previously mentioned, wellbore storage affects transient pressure behavior and, therefore, should be considered in all transient pressure analysis. This will be considered later in this chapter. A straight line appears to start at a ratio approximately equal to 1000. This corresponds to a shut-in time of 0.55 hrs. From the slope of the straight line portion of the test pressure plot, and from Eq. 9.7, the product kh may be estimated

$$kh = \frac{1.1513(77.459\times10^{3})(102.3)\,(0.0225)\;\;(0.84)\,(515)}{(210)\,(18)} = 23\,491 \quad \text{md-m}$$

The skin factor can be estimated by Eq. 9.11. However, since no data about the average drainage volume pressure at the start of the test, p_i , and porosity ϕ are given, it cannot be computed for this particular example.

TABLE 9.III

Pressure Buildup Data for Steam Well C

w = 102.3 Ton/hr	T = 515°K
t = 552 hr	M = 18 gm/gm mole
r_w = 0.122 m	m = 210 $(Kg/cm^2)^2$/log cycle
μ = 0.0225 cp	p^2_{1hr} = 1 047 $(Kg/cm^2)^2$
c = 0.037 $(Kg/cm^2)^{-1}$	p_{wf}^2 = 262 $(Kg/cm^2)^2$
z = 0.84	p^{*2} = 1333$(Kg/cm^2)^2$

Total depth 1120 m; open hole below 155 m.

Transient Pressure Analysis for Hot-Water Wells.

As previously mentioned, the reservoir fluid flow of hot-water can be described based on a strict analogy with the single-phase isothermal flow techniques. Once again, it is assumed that flow in the reservoir is approximately described by the diffusivity equation. For hot-water reservoir flow problems, the dimensionless pressure group has been defined by Ramey (1975):

$$p_D\ (r_D\ ,\ t_D\ ) = \frac{kh\ (p_j - p)}{\delta\ w_{sc} B\ \mu} \qquad (9.12)$$

where δ is a conversion unit constant (Table 9.II)

For a well producing at a constant rate w, and considering that all the assumptions mentioned for the reservoir steam-flow problem hold, Eq. 9.12 can be combined with Eq. 9.4, for conditions at the wellbore, $r=r_w$, to obtain an expression for the wellbore pressure:

$$p_{wf} = p_i - 1.15136 \frac{v_{sc}\, w\, B\, \mu}{\kappa h} \left[\log \frac{\kappa t}{\phi \mu c_t r_w^2} + \log \frac{4\phi}{\gamma} + 0.80859\, s \right] \qquad (9.13)$$

This equation can be used for interpretation of a hot-water drawdown test. Theoretically, according to Eq. 9.13, a plot of flowing bottom-hole pressure data vs. the logarithm of time should be a straight line, with slope m given by the following expression:

$$m = \frac{1.15136\, v_{sc}\, w\, B\, \mu}{\kappa h} \qquad (9.14)$$

From this expression, the flow capacity of the formation can be obtained:

$$\kappa h = \frac{1.15136\, v_{sc}\, w B \mu}{m} \qquad (9.15)$$

An expression for the skin factor, s , can be obtained by a rearrangement of Eq. 9.13:

$$s = 1.1513 \left[\frac{p_i - p_{1hr}}{m} - \log \frac{\kappa}{\phi \mu c_t r_w^2} - \text{Log} \frac{4\phi}{\gamma} \right] \qquad (9.16)$$

The basis for pressure buildup analysis is the principle of superposition. Following a similar procedure as for the steam reservoir flow problem, an expression for the shut-in bottom-hole pressure, p_{ws}, can be written as follows:

$$p_{ws} = p_i - m \log \left(\frac{t + \Delta t}{\Delta t}\right) \qquad (9.17)$$

This equation can be used for interpretation of a hot-water buildup test. Theoretically, according to this Eq. 9.17, a plot of shut-in bottom-hole pressure data vs the log $(t + \Delta t)/\Delta t$ should be a straight line with slope given by Eq. 9.14. An squematic Horner plot of pressure builup data would look like that shown in Fig. 9.4 for a steam well, with p_{ws}^2 being replaced by p_{ws}. With regard to the extrapolation of the straight line portion of the buildup curve, for infinite shut-in time, $(t + \Delta t)/\Delta t=1$, the pressure obtained is p^*. This can be used to estimate the average drainage volume pressure.

The skin factor, s, may also be estimated from pressure buildup analysis. An expression for this factor can be obtained by combining the expressions for flowing and shut-in pressures, given by Eqs. 9.13 and 9.17:

$$s = 1.1513 \left[\frac{p_{1hr} - p_{wf}(\Delta t=0)}{m} - \log \frac{k}{\phi \mu c_t r_w^2} - \log \frac{4\beta}{\gamma} \right] \qquad (9.18)$$

Everything that was discussed regarding p_{wf} $(\Delta t=0)$ and p_{1hr}, for the steam flow problem, applies for this hot-water flow problem. With respect to the wellbore storage effect, it can affect a transient pressure test in much the same way as for a steam well (Gringarten, 1978).

The transient pressure analysis theory just presented for hot-water wells can be far more complex, if two-phase flow develops, either in the wellbore or in the formation. The petroleum engineering and hydrogeologist methods of analysis have been shown to apply correctly to geothermal wells

when no flashing occurs (Whitherspoon, 1978), but when flashing develops in the formation, they apparently cannot be used (Gulati, 1975; Garg, 1978). It was only recently (Rivera and Ramey, 1977; Gringarten, 1978) that information became available in which flashing occurs in the wellbore. This is chiefly due to mechanical problems caused by the hostile, hot geothermal enviroment, and high flow rates of boiling fluids, making difficult the data gathering of bottom-hole pressure, because the recording instrument could easily damage under these conditions.

Another type of test that has been successfully used in hot-water wells is multiple-rate testing. It is often inconvenient to shut-in a well for a pressure buildup survey because it involves loss of production and sometimes it is difficult, for a variety of reasons, to start production after the survey. Also, the previously described drawdown testing techniques of analysis require a constant flow rate There are many cases where it is impractical or imposible, to maintain a constant rate long enough, and this type of simplified pressure drawdown test cannot be carried out. Therefore, multiple-rate testing appears frequently as an alternative for the determination of reservoir parameters. Multiple-rate tests may range (Earlougher, 1977) from one with uncontrolled, variable rate, to one with a series of constant rates, to producing a well at constant bottom-hole pressure conditions with a continuously changing flow rate. This type of tests have been tested with high success for hot-water wells. (Rivera and Ramey, 1977; Gringarten, 1978; Saltuklaroglu and Rivera, 1978). One particular case of a multiple rate is when there are only two different flow rates. This simplifies both, testing and analysis. This type of tests are called two-rate

(Russell, 1963). Multiple-rate tests provide information about: (a) formation flow capacity, and (b) well condition, represented by the skin factor. The average drainage volume pressure prevailing at the beginning of the test can also be estimated.

To develop a general equation, the pressure test is divided into intervals, during each of which production rate can be considered constant. The flow rate-time schedule is as follows:

$$w = w_1 \quad , \quad 0 \leq t \leq t_1$$

$$w = w_2 \quad , \quad t_1 \leq t \leq t_2$$

$$w = w_3 \quad , \quad t_2 \leq t \leq t_3$$

$$\vdots$$

$$w = w_N \quad , \quad t_{N-1} \leq t$$

This discretization of a possible continuously changing flow rate may be improved as the time intervals become smaller. The pressure drop during the time period n can be expressed by means of the principle of superposition and Eq. 9.13:

$$p_{wf} = -1.15136 \frac{\nu_{sc}}{Kh} \frac{B\,\mu}{} \sum_{j=1}^{n} (w_j - w_{j-1}) \log (t-t_{j-1}) + p_i$$

$$- 1.15136 \frac{\nu_{sc}}{Kh} \frac{w_N B\mu}{} \left[\log \frac{K}{\phi \mu c_t r_w^2} + \log \frac{4\beta}{\gamma} + 0.86859\, s \right]$$

(9.19)

This expression can be rearranged in the following form:

$$\frac{p_i - p_{wf}}{w_N} = 1.15136 \frac{v_{sc} B\mu}{Kh} \sum_{j=1}^{N} \left[\frac{(w_j - w_{j-1})}{w_N} \log (t - t_{j-1}) \right]$$

$$+ 1.15136 \frac{v_{sc} B\mu}{Kh} \left[\log \frac{K}{\phi \mu c_t r_w^2} + \log \frac{4\beta}{\gamma} + 0.86859 s \right] \qquad (9.20)$$

Eq. 9.20 is the interpretation equation used for a general hot-water multiple-rate test. It describes a straight line relationship of slope

$$m' = \frac{1.1513 \delta v_{sc} B\mu}{Kh} \qquad (9.21)$$

and intercept

$$b' = m' \left[\log \frac{K}{\phi \mu c_t r_w^2} + \log \frac{4\beta}{\gamma} + 0.86859 s \right] \qquad (9.22)$$

Multiple-rate pressure transient data follow a straight line when plotted in cartesian coordinates as (Fig. 9.6):

$$\frac{p_i - p_{wf}}{w_N} \text{ vs } \sum_{j=1}^{N} \frac{(w_j - w_{j-1})}{w_N} \log (t - t_{j-1})$$

Earlougher (1977) clearly states, that to make this plot correctly, it is important that the rate corresponding to each plotted pressure point is w_N-the last rate that can

affect that pressure. As time goes on, the number of rates may increase and the last rate may change; but each pressure is identified with the rate occurring when that pressure was measured. It should be clear that there may be more than one pressure reading associated with one specific rate. It is important to keep in mind that this multiple-rate theory assumes transient flow conditions throughout the whole test. This is due to the fact that the interpretation equation has been derived based on the line source solution, only valid for infinite acting systems(transient flow conditions). Thus, the separate flow periods should be of short duration so that transient flow will prevail at each rate through the whole test.

From the slope of the multiple-rate pressure curve, given by Eq. 9.21, the formation permeability may be estimated:

$$K = \frac{1.15136 v_{sc} B\mu}{m'h} \qquad (9.23)$$

Also, from the intercept of the pressure curve, given by Eq. 9.22, the skin factor can be estimated:

$$s = 1.1513 \left[\frac{b'}{m'} - \log \frac{K}{\phi \mu c_t r_w^2} - \log \frac{4\beta}{\gamma} \right] \qquad (9.24)$$

Example 9.2 Multiple - Rate Test Analysis

This is a test for a hot-water well, ASAL 1, located in the French Territory of Afars and Issas (now Republic of Djibouti), presented by Gringarten (1978). Flashing of the hot-water occurred at some depth in the wellbore. The mass rate variation is shown in Fig. 9.7. The pressure

data measured during the second C" buildup test(Flow period # 4),was graphed (Fig. 9.8) in a slightly different manner to that just described Gringarten plots p_{ws} , instead of the group $(p_i - p_{ws})/w_N$, and the time units used are minutes instead of hours. The pressure coordinate was changed because of uncertainty of the average drainage volume pressure for this well, p_i. Other than that, the method of analysis is the same. Fig. 9.8 shows a straight line portion of slope $m'=3.6\times10^{-3}$. Other data needed to analyze the test is μ= 0.2 cp and $v = 1.25\times10^{-3}$ m/Kg (this is equivalent to $v_{sc}B$ in Eq. 9.21). Substituting these values into Eq. 9.21, considering the change of units (Gringarten's Eq. 5, p.3) yields:

$$Kh = \frac{0.228\ v\ \mu}{m'} = \frac{0.228\ (1.25\times10^{-3})(0.2)}{3.6\ \times\ 10^{-3}} = 15.9 \text{ Darcy-meter}$$

The calculated average drainage volume pressure from the test is 76.6 bars (1 bar =14.503 psi), which agrees reasonably with a measured value before the test of 77.4 bars.

It can be observed from Fig. 9.3 that deviations from the straight line occurs at short-times (portion a-b, Fig.9.4) and at late times(portion c-d, Fig. 9.4) It will be discussed that the short-time deviation (for buildup times less than 20 minutes) is caused by wellbore storage effects. For long times (buildup times greater than 6 hours) the data points deviates from the straight line portion of the pressure curve, due to steam condensation in the wellbore.

Interference Testing for Geothermal Reservoirs.

Interference testing is preferred in some instances over single well tests depending on the type of information required (Rivera, et al., 1978) It has been previously mentioned that

important data like reservoir connectivity, and porosity can be estimated from analysis of these tests. Reservoir connectivity is an important data, because the number of wells in a reservoir usually increases, causing mutual interference of wells. The application of these tests to hot-water geothermal reservoirs has been successfully reported in the literature (Witherspoon, et al., 1978; Rivera et al., 1978; and Narasimhan et al., 1978).

Interference tests are usually analyzed by a type curve matching technique. The type curve used is the line source solution, for an infinite acting system, plotted in a log-log paper in terms of p_D vs t_D/r_D^2 (Ramey et al., 1973; Earlougher, 1977). Fig. 9.9 presents this type curve for a well located in an infinite acting system. The type curve matching technique consists of plotting the observation well pressure drop, $\Delta p = p_i - p$, on the ordinate vs flowing time, t, on the abscissa of a log-log paper of the same size as Fig. 9.9. Normally, a tracing paper is placed over the type curve, and the major grid lines are traced for reference. The grid of Fig. 9.9 (not shown) is used to plot actual data on the tracing paper. Next, the data plot is moved vertically and horizontally over Fig. 9.9, keeping the grids of the type-curve and those of the data plot parallel to each other until the best match is obtained with the type-curve. A convinient match point is picked and the values of $(\Delta p)_M$ and $(t)_M$ are read from the data plot. The corresponding points lying directly under this point on Fig. 9.9 are $(p_D)_M$ and $(t_D)_M$. The formation permeability is estimated from the pressure match-point data and the definition of p_D given by Eq. 9.12:

$$K = \frac{\phi \nu_{BC} \, w B_0}{h} \frac{(p_D)_M}{(\Delta p)_M} \qquad (9.25)$$

In a similar way, the porosity - compresibility product is estimated form the time match point data and the definition of t_D and r_D by Eqs. 9.2 and 9.3:

$$\phi c_t = \frac{\beta}{r^2} \frac{\kappa}{\mu} \frac{(t)_M}{(t_D/r_D^2)_M} \qquad (9.26)$$

This type curve analysis method is simple, fast, and of good accuracy, provided the conditions for applicability of the line source p_D solution are met; that is, when $r_D = r/r_w > 20$ and $t_D/r_D^2 > 0.5$ (Earlougher, 1977).

Example 9.3 Type Curve Matching Analysis of a Pressure Interference Test.

This is a pressure interference test carried out in the liquid dominated Cerro Prieto Geothermal Field, located in México. These results are taken from a paper by Rivera et al. (1978). The observation well was M-101, and there were four active wells, M-50, M-51, M-90, and M-91. They analyzed the early pressure drop response at the observation well M-101, while the only active well was M-91, and the other three wells were shut-in. Fig. 9.10 shows the type-curve match presented by these authors. Table 9.IV show other related data for the test. From the results of the match point data, and from Eq. 9.25 and 9.26 the following estimates for the reservoir parameters are obtained:

$$Kh = 456.7869(1.043)(185.3)(1.185)(0.1017)\frac{(1.8\times10^{-2})}{(1)(1/14.22)} = 2723 \text{ md-m}$$

and

$$\phi c_t h = \frac{0.000348}{(1550)^2}\frac{(2723)}{(0.1017)}\frac{(100)(24)}{(0.63)} = 0.0148 \text{ m/(Kg/cm}^2\text{)}$$

TABLE 9.III
Reservoir Related Data for Interference Test (After Rivera et al., 1978)

w = 185.3 (ton/hr)

v_{sc} = 1.043 cm^3/gm

B = 1.185 $metre_{rc}^3/metre_{sc}^3$

μ = 0.1017 cp

r = 1550 m

Pressure Transient Analysis for Two-Phase Flow.

Up to now, most of the discussion has been based on single-phase isothermal reservoir flow. However, sometimes flow conditions in the reservoir are such that two-phase flow would occur, causing the flow to be non-isothermal. Garg (1978 a, 1978 b) has recently presented a theory for analysis of two-phase pressure transient data in geothermal wells. He considers two different situations: (a) a reservoir which is originally two-phase everywhere, and (b) a reservoir which originally contained hot-water, but after production, the pressure drop resulted in a flashing front propagating away from the wellbore. He derives a diffusivity-type equation which resembles quite closely the diffusivity equation. This type of analogy has been found for other reservoir fluid flow problems (Martin, 1959). Based on this similarity of the equations that describe the flow problem, Garg derives an expression for the flowing bottom-hole pressure for the two above mentioned reservoir situations:

(a) Two-phase flow everywhere in the reservoir at initial conditions.

$$p_{wf} = p_i - 1.15136 \frac{w}{(K/v)_t\, h} \left[\log \frac{(K/v)_t\, t}{\phi\, \rho\, c_t\, r_w^2} + \log \frac{4\,\beta}{\gamma} \right] \qquad (9.27)$$

and

(b) Hot-water everywhere in the reservoir at initial conditions, with a flashing-front propagating after two-phase pressure conditions are reached.

$$p_{wf} = p_i - \frac{\delta}{2}\frac{w}{[(K/v)_t]_1 h} E_i\,(-\lambda^2) - 1.15136 \frac{w}{[(K/v)_t]_1 h} \left[\log \frac{(K/v)_t\, t}{(\phi\rho c_t)_1\, r_w^2} + \log \frac{4\,\beta}{\gamma} \right] \qquad (9.28)$$

where

$(K/v)_t$ = Total kinematic mobility = $(K/v)_w + (K/v)_s$

$(K/v)_w$ = Kinematic mobility for the water = $KK_{rw}\, \rho_w / u_w$

$(K/v)_s$ = Kinematic mobility for the steam = $KK_{rs}\, \rho_s / u_s$

λ = Roots of Eq. 13d. of Garg' paper (1978b), p. 3

1 = Subscriptdenoting the two-phase region

Eqs. 9.27 and 9.28 can be used for interpretation of a two-phase flow drawdown test. Theoretically, according to these equations, a plot of flowing bottom-hole pressure data vs

the logarithm of time should be a straight line with slope m given by the following expression:

$$m = \frac{1.1513\ \phi \quad w}{(\kappa/\nu)_t h} \qquad (9.29)$$

From this expression, the total kinematic mobility can be estimated:

$$(\kappa/\nu)_t = \frac{1.1513\ \phi \quad w}{m h} \qquad (9.30)$$

Recently, a sound theoretical basis for the estimation of the kinematic mobility from pressure interference testing has been suggested (Pruess, et al., 1978). This is an extension of Garg's theory of analysis for two-phase flow.

Example 9.4 Two-Phase Flow Pressure Transient Test with a Propagating Flashing-Front.

This is a simulated test presented by Garg (1978b). Single phase (hot-water) conditions prevail for some time after the start of production, until eventually, the pressure level has declined enough to reach the two-phase flow conditions, and a flashing front propagates away from the well. Fig. 9.11 shows a semilog plot of the results of this test. At early times, up to about = 12 seconds, hot-water flow conditions prevail in the vicinity of the well. From this time on, two-phase flow conditions start to be operating, and for a period of time related to numerical approximations, the curve is relatively flat; after the numerical problem is overcome, for late times, the pressure data follow approximately a straight line. The computed value of $(\kappa/\nu)_t$,

obtained form the slope of the straight line portion of the pressure curve of Fig. 9.11, and Eq. 9.30, agrees well with the actual range of values for this parameter.

Modern Well Test Analysis

According to Ramey (1970) modern well test analysis specifies that the well be tested for a period of time long enough to reach and define a proper "straight line", when pressure transient data are plotted in semilogarithmic manners. It was not until the end of the 60's that pressure data recorded before the straight line is reached, started to be analyzed. It has been since then realized that this early time data could be extremely helpful for test interpretation purposes. The early time data, also called "short-time data", are influenced by the effects of several factors, like wellbore storage, flow through perforations, partial penetration, and well stimulation such as fracturing or acidizing.

"Short-time data" can usually be analyzed by a log-log type curve matching technique similar to that previously described for interference testing. The type-curve is a log-log graph of the solution of a specific reservoir fluid flow problem, plotted in terms of p_D vs t_D. The type curve should be chosen as to closely represent the field situation. Perhaps, the most used type-curve to date has been that presented by Agarwal et al. (1970), and Watts nberger and Ramey (1970) for the pressure transient behavior of a well, including wellbore storage and skin damage (Fig. 9.12). This type curve can be used to approximately determine the start of the correct semilog straight line. The curves of Fig. 9.12 show an early unit slope straight line

portion, representing wellbore storage deminated flow conditions, followed by a transition to the relatively flat curves for cero wellbore storage. The point where the curves including wellbore storage reach the cero wellbore storage curves, represents the start of the correct semilog straigh line. This time can be expressed (Ramey et al 1973):

$$t_D = C_D\,(60 + 3.5\,s) \qquad (9.31)$$

where

$$C_D = \frac{\epsilon C B\, v_{sc}}{\phi h c_t r_w^2}\,, \quad \text{for hot-water} \qquad (9.32)$$

$$C_D = \frac{n C' 2T}{M \phi h c_t r_w^2}\,, \quad \text{for steam} \qquad (9.33)$$

For a good semilog analysis of the pressure transient data, the duration of the test should be at least ten times the time given by Eq. 9.31. This would provide a minimum of a log cycle of pressure field data, allowing a proper trace ment of the straight line portion of the pressure curve.

There are many type-curves presently available for pressure analysis of short-time data. The difference between them is the well condition that they consider, like a well with a horizontal fracture (Gringarten et al., 1974), a well with a vertical fracture(Gringarten et al., 1975; Cinco et al., 1978), etc.

Type curve matching techniques can be used, in combination

with other data, to identify the near wellbore conditions, and as mentioned, to determine the correct start of the semilog straight line. With a properly estimated start of the semilog straight line, the results obtained from the semilog analysis are more accurate than those coming from log-log type-curve matching. As pointed out by Cringarten et al. (1975) a combination of type-curve matching techniques with conventional semilog analytical methods permits a highly confident analysis of field data.

Example 9.5 Modern Well Test Analysis of a Pressure Transient Test in a Steam Well.

Example 9.1 showed the analysis of a pressure buildup test presented by Ramey(1975). The purpose of this example is to illustrate how type-curve matching techniques can be used to identify the correct start of the semilog straight line. Fig. 9.13 shows a type-curve match of the buildup data to the type curve of Fig. 9.12. It is seen that field data fairly matches the curve for $c_D = 10^2$ and $s = 5$, but more important than this, the data reaches the type-curve for $c_D = 0$ at Δt equal to 0.3 hours. This corresponds to a $(t+\Delta t)/\Delta t$ value of 1841. Examination of Fig. 9.5 shows that, according to type-curve analysis, the start of the straight line has been correctly identified. As previously pointed out, any other information in addition to the start of the straight line, should only be taken in a qualitative sense.

SIMULATION OF GEOTHERMAL RESERVOIRS

The word "simulate" has been defined by Webster as "to assume the appearance of without the reality". To the reservoir

engineer, the term reservoir simulation means the process of deducing the physical behavior of a real reservoir from the performance of a model. There are two basic types of models: (a) physical (for example a laboratory sandpack), and (b) mathematical. A mathematical model of a physical system consists of a set of partial differential equations subject to certain simplifying assumptions, together with an appropiate set of boundary conditions, which describes the physical processes active in the reservoir (Peaceman, 1978; Coats, 1969; C richlow, 1977).

Reservoir simulation applies the concepts and techniques of mathematical modeling to the analysis of the behavior of geothermal reservoir systems. Most often the term reservoir simulation is used with regards to the hydrodynamics of flow within the reservoir, but in a more general sense, it refers to the total geothermal system , which includes mainly the reservoir itself, the tubing, and the surface facilities. A simulator can be defined as a group of computer programs that implement the mathematical model in a digital computer.

The main purpose of simulation is to estimate the behavior of a geothermal reservoir under a variety of exploitation schemes. This is extremely advantageous because the reservoir can be produced only once, and the model can be produced or "run" as many times as needed, with low cost, and over a short period of time. From observation of model performance, under a variety of producing conditions, the optimum exploitation conditions for the reservoir can be selected. Some of the information that can be obtained from reservoir simulation studies is as follows:

1. The capability of a reservoir of producing significant quantities of energy over meaningful periods of time.

2. The number of wells and spacing required for optimum development of the reservoir.

3. The effect of the rate of production of the wells on total energy recovery.

4. Variation of fluid temperature vs time.

5. Feasibility of implementation of an enhanced recovery process to recover additional heat.

Reservoir models range in complexity from simple ones for fairly homogeneous systems, where average values for reservoir properties, such as permeability and porosity, are adequate to describe its behavior, to those used for highly heterogeneous systems, where fragmentation into blocks (cells) is necessary. To choose a model that would represent a particular reservoir requires a good understanding of the reservoir and a detailed examination of the data available (Odeh, 1969). A model that fits a particular reservoir may not be appropriate for another reservoir, despite the apparent existance of similarities between them. As pointed out by Odeh (1969), a reservoir model is useful only when it reasonably matches the field situation. A general rule (Coats, 1969) that should be followed in reservoir simulation is to "select the least complicated model and grossest reservoir description which will allow the desired estimation of reservoir performance".

In other words, the model to be used should be the simplest

that duplicates reservoir behavior.

The discussion presented in this section includes a brief review of some of the simple reservoir models (zero dimension), and also of the more complex (multi-dimensional) models, suited for numerical simulation.

Whiting and Ramey's Model (1969)

The model developed by Whiting and Ramey is zero dimensional because rock, fluid properties, and pressures values are not a function of location in the reservoir. These parameters are calculated as average values for the whole reservoir. This type of models has also been called lumped-parameter models.

The model presented by Whiting and Ramey can be used for performance forecasting of reservoir behavior (Ramey, et al., 1973). Where some field development already exists and production is in progress, a mathematical model for fluid flow in the reservoir can be postulated. The reservoir size and its productivity can be determined by matching measured production data (mass produced, enthalpy produced, reservoir pressure and temperature, etc.) with the corresponding parameters of the mathematical model. Once all model parameters, and their relationships, have been identified, the model can be used for performance production forecasting under different assumed exploitation schemes.

The model of the reservoir system developed by Whiting and Ramey is shown in Fig. 9.14. The system contains rock, water, and steam. The reservoir system has a bulk volume V_r and a porosity ϕ. The cumulative fluid production at any given time is W_p; the cumulative heat production associated

with this fluid production is Q_p. The model also considers heat loss, Q_L, and mass fluid loss, W_L, due to convection in, for example, hot springs, fumaroles, etc. The authors have discussed that heat loss, Q, at the reservoir boundary is negligible and should not importantly affect reservoir behavior. Water recharge, W_e, and its associated energy (cumulative enthalpy, H_e) are also considered.

The model of Whiting and Ramey considers the following basic assumptions (Ramey, et al., 1973):

1. Thermodynamic equilibrium (temperature of rock, water, and steam are equal).

2. Pressure and saturation are uniform throughout the reservoir.

3. Uniform fluid production, which implies that fluid production comes from all parts of the reservoir.

A combined mass, energy, and volumetric balance gives the following expression:

$$W_p (H_p - E_c) + W_L (H_L - E_c) + Q =$$

$$W \{ E_i - E_c + [(1-\phi)/\phi][s_i v_{wi} + (1-s_i) v_{wi}] \rho_r C_{vr} (T_i - T_c) \}$$

$$+ (H_e - E_c)(B/v_{we}) \int Q_D (t_D) \, dp_D \qquad (9.34)$$

where

H_p = enthalpy of produced fluids

W = initial mass of hot-water and steam in reservoir bulk volume, V

E = Internal energy

Q = Conductive heat loss

ϕ = Porosity of rock matrix

x = Steam quality

v = Specific volume

ρ_r = Density of rock and contained fluids

C_{vr} = Specific heat at constant volume of reservoir rock and contained fluids

T = Temperature

B = Water recharge constant

$Q_D(t_D)$ = Dimensionless cumulative recharge, corresponding to dimensionless time, t_D.

Δp_n = Pressure drop at any time n

The subscripts p, L, c, i, r, s, w, and e indicate produced, loss, current, initial, reservoir, steam, liquid water, and recharge values, respectively. The model given by Eq. 9.34 can be simplified, according to the situation of a specific reservoir. For instance, for a reservoir containing only hot-water, this equation reduces to

$$(W_p + W_L)v_w = W(v_w - v_{wi}) + BX\, Q_D(t_D)\Delta p_n \qquad (9.35)$$

It is common to find that reservoirs are associated with adjacent aquifers. Due to production, reservoir pressure declines, causing that the aquifer reacts by yielding up water. If water recharge is influencing reservoir behavior, it has to be properly considered for accurate reservoir performance predictions. One of the most useful methods for calculating water recharge is that of van Everdingen and Hurst (1949). Miller et al. (1978) present an excellent review of water recharge into geothermal reservoirs (see also Whiting and Ramey (1969), p.897).

Whiting and Ramey applied the model for liquid hot-water, Eq. 9.35, to the Wairakei geothermal reservoir in New Zealand. A least-mean-squares fit to the production history from 1956 to 1961 was used to obtain estimates for the initial water in place and the initial pressure. Once the optimum model parameters were determined, a prediction of reservoir performance through 1965 was made, indicating excellent agreement between measured and calculated values (Fig. 9.15).

Brigham and Morrow's Model (1977)

Brigham and Morrow have presented a zero dimensional model for vapor-dominated systems. They considered three cases regarding the distribution of hot-water and steam, and assumed the system to be closed, and that energy is derived from the rock mass itself.

The first system is completely filled with steam with no water present. Flow in this system is esentially isothermal because the heat capacity of the rock is large compared with that of steam. Then, to study the system's behavior only a mass balance needs to be taken. Under these reservoir flow conditions, a steam reservoir can be treated as an ordinary petroleum gas reservoir (Craft and Hawkins, 1959), where average reservoir pressure divided by the gas deviation factor, p/z, is plotted vs cumulative production, resulting in a straight line. The intercept on the abscissa is equal to the original mass of fluid in place, m_{gi}. The equation is

$$p_f/z_f = (p_i/z_i)\left(\frac{m_{gi} - (m_p)_s}{m_{gi}}\right) = (p_i/z_i)\left(\frac{m_{gi}}{m_{gi}}\right) \qquad (9.36)$$

where:

p = reservoir pressure
m_g = mass of steam
Δm_g = mass of steam produced during a depletion step
i = subscript for the initial conditions of a depletion step
f = subscript for the end conditions of a depletion step

The reserve forecasting procedure, using Eq. 9.36, will be used to compare predictions for the other two cases.

The second model considers that the steam zone is separated from an underlying liquid zone by a horizontal interface at which boiling takes places. As steam is produced, water boiling will take place, resulting in a liquid level drop. This model is called the falling liquid level model. Flow in the steam zone is assumed to be isothermal, but on the water zone, non-isothermal flow conditions would prevail. A mass and energy balance is made for the water zone.

The third model also considers that the steam zone has an underlying liquid zone, but assumes that liquid boiling takes place throughout the whole liquid zone, and that liquid level does not drop. This model is called the constant liquid level model. Consequently, in this system a steam saturation will continuously build up within the liquid zone. The energy equation for this system resembles that of Whiting and Ramey (1969), with the exception that only steam flows out of the system. The authors have solved the falling liquid level and the constant liquid level models for three hypothetical reservoirs, of porosity equal to 0.05, 0.10, and 0.20. It was assumed that the volume of the steam zone was the same as the volume of the

liquid zone (calculations were also made, not reported, for systems of a ratio of steam to liquid zone equal to nine, showing results very close to the results for a unity ratio). Fig. 9.16 shows the results of these authors for a steam falling liquid level system (their Fig. 1). From the results of this figure, and from other results shown by Brigham and Morrow, the following conclusions have been made. For low porosity reservoirs, an extrapolation of the p/Z vs cumulative production plot will be too optimistic, while for high porosity reservoirs will be pessimistic. A porosity of about 0.10 will give approximately correct predictions. The constant liquid level model predicts higher recovery for a given reservoir pressure than the falling liquid level model. The presence of even a small water zone in the lower portion of the system, is an important fraction of total system's mass, and can significantly affect the p/Z prediction procedure. Finally, they conclude that the steam zone of the reservoir remains isothermal whether or not there is a water boiling zone below the steam. This causes characterization problems, because pressure, temperature, and enthalpy measurements are not sufficient to determine the original state of the reservoir fluid system. An application of the p/z vs cumulative production to actual field data has been presented by Ramey (1970a).

Other Zero-Dimensional Models.

Another zero-dimensional model for the simulation of geothermal reservoirs has been presented by Martin (1975). His model is valid for single and two-phase flow; it was derived following the logic behind solution gas drive petroleum reservoirs. To the authors' knowledge, this model has not received field application.

One more zero dimensional model is that presented by Atkinson et al. (1978). In their model they considered a steam and a water zone. They included in the steam zone the presence of carbon dioxide and other noncondensable gases, and also that water could recharge the reservoir. This model was successfully evaluated matching the production history of the Bagnore steam field in Italy.

Numerical Geothermal Reservoir Simulation

When important heterogeneities exist in the reservoir, rock and/or fluid properties (permeability, saturation, pressure, viscosity, etc.) vary in space, and simple zero-dimensional models can no longer be used for prediction of reservoir performance . A model which considers the variation of rock and fluid properties is called a distributed parameter model. A reservoir where properties vary in space, is usually divided in blocks (cells), assigning to each one of them average values for rock and fluid properties. For a multicell model like this, the basic building block is the previously described, zero dimensional model.

A mathematical model for describing fluid flow in a geothermal reservoir includes equations for the conservation of mass, momentum, and energy for water and steam, and an equation specifying the state of the system (Faust and Mercer , 1975; Thomas and Pierson, 1978). A review of the literature shows that several such models have been presented (Faust and Mercer, 1975; Thomas and Pierson, 1978; Coats, 1977; Brownell et al., 1975; Lasseter, et al, 1975). These models differ from each other according to the assumptions applied. A model for the flow of hot-water and steam, written for a general coordinate system, consists of the

following equations:

$$\nabla\cdot\left[\frac{K\,K_{rw}\,\rho_w}{\mu_w}(\nabla p-\rho_w g\nabla z)+\frac{K\,K_{rs}\,\rho_s}{\mu_s}(\nabla p-\rho_s g\nabla z)\right]-q$$

$$=\frac{\partial}{\partial t}(\phi\rho_w S_w+\phi\rho_s S_s) \qquad (9.37)$$

Energy balance for the water-steam-rock system.

$$\nabla\cdot\left[\frac{K\,K_{rw}\,\rho_w\,H_w}{\mu_w}(\nabla p-\rho_w g\nabla z)+\frac{K\,K_{rs}\,\rho_s\,H_s}{\mu_s}(\nabla p-\rho_s g\nabla z)\right]+\nabla\cdot(\bar{K}\nabla T)$$

$$-q_{HL}-q_H=\frac{\partial}{\partial t}\left[(\phi\rho_w S_w U_w+\phi\rho_s S_s U_s)+(1-\phi)(\rho c_p)_r T\right]$$

(9.38)

where

K	=	absolute permeability
K_{rs} (K_{rw})	=	relative permeability for steam (water)
ρ_s (ρ_w)	=	steam (water) density
μ_s (μ_w)	=	steam (water) viscosity
p	=	pressure
g	=	acceleration of gravity
q	=	mass (source) production rate
ϕ	=	porosity
S_s (S_w)	=	steam (water) saturation
H_s (H_w)	=	enthalpy of saturated steam (water)
$\bar{K}$	=	thermal conductivity
T	=	temperature
z	=	vertical coordinate measured positively downward

q_{HL} = heat loss rate
q_H = enthalpy production rate
ρ_r = average rock-grain density
H_r = rock enthalpy

The pressure-enthalpy-internal energy approach followed in the previous mathematical model is one of the different possible to be taken. Another approach followed by other authors uses density and internal energy as the unknown variables (Brownell, et al., 1975; Lassater, et al., 1975). The use of fluid pressure and enthalpy (internal energy is related to enthalpy by the thermodynamic expression H=U+ p/ρ) seems a logic thing to do, because they define the thermodynamic state of the system, and are usually obtained in field operations.

In the derivation of Eqs. 9.37 and 9.38 the following assumptions have been made (Mercer et al., 1974; Faust and Mercer, 1975):

1) The reservoir is treated as a porous medium

2) Capillary pressure effects are negligible. This means that the pressure in the water and steam phases are equal.

3) Thermal equilibrium exists among all phases-hot-water, steam, and rock.

4) Validity of Darcy law for two-phase flow

5) Thermal conductivity is a property of the medium.

6) The geothermal fluid is pure water.

Releasing of one or more of the previous assumptions will no doubt increase the accuracy of predictions in specific situations, but will also change the complexity and economics of the study. At present time, there are geothermal mathematical models more complete than that given by Eqs. 9.37 and 9.38. An example is Coat's model (1977) where he considers capillary effects, and the thermal dependance of relative permeability. Other recent models include the effect of inert gases (Zyvolski and Sullivan, 1978), and the effect of precipitation of dissolved salts in porosity and permeability (Todd et al., 1978).

In order to solve the two nonlinear partial differential equations given by Eqs. 9.37 and 9.38, it is necessary to assume some additional functional and algebraic relations between the variables involved. For a complete discussion of this subject, the paper by Coats (1977) should be referred to. As an example of the relations needed, the steam and water saturation must add to unity

$$S_s + S_w = 1 \qquad (9.39)$$

To solve the mathematical model given by Eqs. 9.37 and 9.38, and its additional relations, the proper reservoir boundary conditions should be considered. Analytical solutions can be obtained by the classical methods of mathematical physics only for simple reservoir situations, such as homogeneous

systems with regular boundaries (i.e., a single well in the center of a radial reservoir). Thus, the nonlinear partial differential equations 9.37 and 9.38 describing the flow of fluids in geothermal reservoirs have to be solved by an approximate method. If it is desired that approximate values of the solution to the mathematical model be obtained, then some numerical process is formulated which will produce these values after a finite number of calculations. With the advent of high-speed computers, it became increasingly desirable to produce algorithms which are applicable to a wide class of problems and which, at the same time, lead to increasingly more accurate approximations with an additional expenditure of computer time alone. Numerical methods have been extensively used because they meet these two criteria. These methods have proved to be highly successful for obtaining solutions to very complex reservoir situations. A numerical model (simulator), as previously defined, is a group of computer programs that use numerical methods to obtain an approximate solution to the mathematical model. Further discussion of the numerical solution to the mathematical model is beyond the scope of this chapter. They include finite difference techniques, finite element methods, or a combination of the two.

CONCLUSIONS

The main purpose of this chapter was to provide a brief review of presently available techniques for prediction of geothermal reservoir behavior. It seems that predictions of reasonable accuracy can be made with actually available methods for the majority of geothermal systems saturated with fluids (convective systems), but, there is a lack of knowledge for other types of systems, as the hot-dry for-

mations. It is expected that geothermal reservoir engineering will continue to show advancement due to the strong research program currently under way.

Discussion of this chapter has included the practical aspects of reservoir engineering, such as well test analysis, and a brief presentation of mathematical reservoir simulation. The reservoir data obtained from pressure transient analysis best represents actual reservoir conditions, and it is extremely useful as input for reservoir simulation studies. Reservoir simulation studies are initially carried out with simple models, which are continuously updated and refined as new production data becomes available. As a simple matter, the model used should be the simplest that duplicates reservoir behavior. A properly conducted reservoir engineering study would lead to the determination of the optimum exploitation conditions for the particular reservoir.

NOMENCLATURE*

B = water-recharge constant, Reservoir Simulation Section

B = formation volume factor, $metre^3_{rc}/metre^3_{sc}$

b' = intercept on semilog plot of transient-test pressure data normalized by rate, $Kg/cm^2/(ton/hr)$, Eq. 9.22

c = compressibility, $(Kg/cm^2)^{-1}$

C = wellbore storage constant for hot-water, $ton/(Kg/cm^2)$ Eq. 9.32

C' = wellbore storage constant for steam, $ton/(Kg/cm^2)$, Eq. 9.33

C_D = dimensionless wellbore storage constant, Eqs. 9.32 and 9.33

C_{vr} = specific heat at constant volume of reservoir rock and contained fluids

E = internal energy

g = acceleration of gravity

h = formation thickness, m

H = enthalpy

K = absolute permeability

K_r = relative permeability, fraction

m = slope of linear portion of semilog plot of pressure transient data, $Kg/cm^2/cycle$

m' = slope of the data plot for a multiple-rate test, $Kg/cm^2/(cycle\ Ton/hr)$, Eq. 9.21

M = molecular weight, gm/mole

p = pressure, Kg/cm^2

q = mass (source) production rate

q_H = enthalpy production rate

q_{HL} = heat loss rate

Q = conductive heat loss

r = radius, m

s = van Everdingen-Hurst skin factor

t = time, hours

Δt = running testing time, hours

T = temperature, °K

W = production rate, tons/hr

* Unless otherwise stated, the units are those of the SI

W = initial mass (hot-water and steam in the reservoir), Eq. 9.34

x = steam quality, fraction

Z = real gas deviation factor

α = conversion factor, Eq. 9.1

β = conversion factor, Eq. 9.2

γ = constant equal to 1.7810724, Eq. 9.5

δ = conversion factor, Eq. 9.12

ε = conversion factor, Eq. 9.32

η = conversion factor, Eq. 9.33

μ = viscosity, cp

v = specific volume, cm^3/gm

v_w = specific volume of saturated liquid water

v_s = specific volume of saturated steam

v_{wi} = initial specific volume of saturated liquid water

v_{si} = initial specific volume of saturated steam

ρ = density

$\bar{K}$ = thermal conductivity

ϕ = porosity, fraction

Subscripts

c = current

D = dimensionless

e = recharge

f = flowing, force

i = initial

j = index

L = loss

M = match point in type-curve matching

N = last-rate interval in a multiple-rate flow test

p = produced

r = reservoir, rock

rc = reservoir conditions

s = shut-in, steam
t = surface
sc = standard conditions
t = total
w = wellbore, water
1hr = data from straight-line portion of semilog-plot at 1 hour of test time, extrapolated if necessary.

Special Functions

$$\text{exponential integral} = E_i(-x) = -\int_x^{\infty} \frac{e^{-u}}{u}\, du$$

REFERENCES

Agarwal, R. G., Al-Hussainy, R., and Ramey, H. J., Jr., 1970. An Investigation of Wellbore Storage and Skin Effect in Unsteady Liquid Flow: I. Analytical Treatment. Soc. Pet. Eng. J. (Sept.), pp. 279-290.

Atkinson, P. G., Celati, R., Corsi, R., and Kucuk, F., 1978. Behavior of two Component Vapor-Dominated Geothermal Reservoirs. Ann. California Regional Meeting, Soc. Pet. Eng., San Francisco, Ca., paper SPE No. 7132.

Brownell, D. H., Garg, S. K., and Pritchett, J. W. 1975. Computer Simulation of Geothermal Reservoirs. Ann. California Regional Meeting, Soc. Pet. Eng., Ventura Ca., paper No. 5381.

Burnham, J. B., and Stewart, D. H., 1973. Recovery of Geothermal Energy from Hot, Dry Rock with Nuclear Explosives. In P. Kruger and K. Otte (Eds.) Geothermal Energy Resources, Production and Stimulation. Stanford University Press, Stanford, Ca., pp. 223-230.

Burst, J. F., 1969. Diagenesis of Gulf Coast Clayey Sediments and its Possible Relation to Petroleum Migration. Bull. Am. Assoc. Pet. Geologists, 53 (1): 73-93.

Crichlow, H. B., 1977. Modern Reservoir Engineering - A Simulation Approach. Prentice-Hall, Englewood Cliffs. N. J.

Cinco-Ley, H., Samaniego V. F., and Domínguez, A. N., 1978. Transient Pressure Behavior for a Well with a Finite-Conductivity Vertical Fracture. Soc. Pet. Eng. J. (Aug.), pp. 253-264.

Coats, K. H., 1969. Use and Misuse of Reservoir Simulation Models. J. Pet. Tech. (Nov.), pp. 1391-1398.

————————, 1977. Geothermal Reservoir Modelling. Ann. Fall Technical Conference, 52nd., Soc. Pet. Eng., Denver Colo., paper No. 6892.

Craft, B. C., and Hawkins, M. F., 1959. Applied Petroleum Reservoir Engineering. Prentice-Hall, Englewood Cliff, N. J.

Dake, L. P., 1978. Fundamentals of Reservoir Engineering. Developments in Petroleum Science, 8, Elsevier, Amsterdam: 433 pp.

Davis, W. K., and Golan, S., 1974. The New Energy Sources. Ind. Research. (Nov. 15), pp. 8-15.

Earlougher, R. C., Jr., 1977. Advances in Well Test Analysis. Monograph Series, Society of Petroleum Engineers of AIME, Dallas, Tex.: 264 pp.

Faust, C. R., and Mercer, J. W., 1975. Mathematical Modelling of Geothermal Systems. Second U. N. Symposium on the Development and Use of Geothermal Resources, San Francisco, Ca., Proc. Lawrence Berkeley Lab., University of California, Berkeley Ca., pp. 1635-1641.

Mercer, J. W., Faust, C., and Pinder, G. F., 1974. Geothermal Reservoir Simulation. Proc. of N.S.F., Conference on Research for the Development of Geothermal Energy Resources, Pasadena, Ca., pp. 256-267.

Miller, F. G., Cinco, H., Ramey, H. J., Jr., and Kucuk, F., 1978. Reservoir Engineering Aspects of Fluid Recharge and Heat Transfer in Geothermal Reservoirs. Trans Geothermal Resources Council, 2: pp. 449-452.

Murphy, H. D., 1975. Hydraulic-Fracture Geothermal Reservoir Engineering. Stanford Geothermal Reservoir Eng., Workshop, SGP-TR-12, pp. 174-177.

Muskat, M., 1938. The Flow of Homogeneous Fluids Through Porous Media. Mc Graw-Hill Book, Co., New York, N. Y.

Narasimhan, T. N., Schroader, R. C., Goranson, C. B., and Benson, S. M., 1978. Results of Reservoir Engineering Tests, 1977, East Mesa, California. Ann. Fall Technical Conference, 53rd, Soc. Pet. Eng., Houston, Tex., paper No. 7482.

Odeh, A. S., 1969. Reservoir Simulation... What is it? J. Pet. Tech. (Nov.), pp. 1383-1388.

Peaceman, D. W., 1977. Fundamentals of Numerical Reservoir Simulation. Elsevier, Amsterdam.

Pruess, K., Schroader, R. C., and Zerzan, J., 1978. Studies of Flow Problems with the Simulator Shaft 78. Stanford Geothermal Reservoir Engineering Workshop, Stanford, Ca., Proc.: Stanford University (in print).

Ramey, H. J., Jr., 1965. Non-Darcy Flow and Wellbore Storage Effects in Pressure Buildup and Drawdown of Gas Wells. J. Pet. Tech. (Feb.), pp. 223-233.

————————, 1970a. A Reservoir Engineering Study of the Geysers Geothermal Field. Testimony for the Trial of Reich and Reich vs Commissioner of the Internal Revenue, Tax Court of the U.S., 52 T. C. No. 74.

————————, 1970b. Short-Time Well Test Data Interpretation in the Presence of Skin Effect and Wellbore Storage. J. Pet. Tech. (Jan.), pp. 97-104.

————————, 1975. Pressure Transient Analysis for Geothermal Wells. Second U. N. Symposium on the Development and Use of Geothermal Resources, San Francisco, Ca., Proc. Lawrence Berkeley Lab., University of California, Berkeley, Ca., pp. 1749-1757.

————————, 1976. Practical Use of Modern Well Test Analysis. Ann. Fall Technical Conference, 51st, Soc. Pet. Eng., New Orleans, La., paper No. 5878.

----------, 1977. Petroleum Engineering Well Test Analysis- -State of the Art. Proceeding: Invitational Well Testing Symposium, Oct. 19-21, Lawrence Berkeley, Lab., Berkeley, Ca., pp. 5-9.

Ramey, H. J., Jr., Kruger, P., and Raghavan, R., 1973a. Explosive Stimulation of Geothermal Reservoirs. In P. Kruger and K. Otte (Eds.), Geothermal Energy Resources, Production and Stimulation. Stanford University Press, Stanford, Ca., pp. 231-249.

Garg, S. K., 1978a. Pressure Transient Analysis for Two-Phase Geothermal Reservoirs. Trans. Geothermal Resources Council, 2: pp. 203-206.

————————, 1978b. Pressure Transient Analysis for Two-Phase (Liquid Water/Steam) Geothermal Reservoirs. Ann. Fall Technical Conference, 53rd., Soc. Pet. Eng., Houston Tex., paper No. 7479.

Gringarten, A. C., 1978. Well Testing in Two-Phase Geothermal Wells. Ann. Fall Technical Conference, 53rd, Soc. Pet. Eng., Houston, Tex., paper No. 7480.

Gringarten, A. C., and Ramey, H. J., Jr., 1974a. Unsteady-State Pressure Distributions Created by a Well with a Single Horizontal Fracture, Partial Penetration or Restricted Entry. Soc. Pet. Eng. J. (Aug.), pp. 413-426.

Gringarten, A. C., Ramey H.J., Jr., and Raghavan, R., 1974b. Unsteady-State Pressure Distributions Created by a Well with a Single Infinite Conductivity Vertical Fracture. Soc. Pet. Eng. J. (Aug.), pp. 347-360.

Gringarten, A. C., Ramey, H. J., Jr., and Raghavan, R., 1975. Applied Pressure Analysis for Fractured Wells. J. Pet. Tech. (July), pp. 887-892.

Gulati, M. S., 1975. Pressure and Temperature Buildup in Geothermal Wells. Stanford Geothermal Reservoir Engineering Workshop, Stanford Ca., Proc.: Stanford University, SGP-TR-12, pp. 69-73.

Knapp, R. M., Isokkari, O. F., Garg, S. K., and Pritchett, J. W., 1977. An Analysis of Production from Geopressured Geothermal Aquifers. Ann. Fall Technical Conference, 52nd, Soc. Pet. Eng., Denver, Colo., paper No. 6825.

Lasseter, T. J., Witherspoon, P. A., and Lippmann, M. J. 1975. Multiphase Multidimensional Simulation of Geothermal Reservoirs. Second U. N. Symposium on the Development and Use of Geothermal Resources, San Francisco, Ca., Proc. Lawrence Berkeley Lab., University of California, Berkeley, Ca., pp. 1715-1723.

Martin, J. C., 1959. Simplified Equations of Flow in Gas Drive Reservoirs and the Theoretical Foundation of Multi-phase Pressure Buildup Analysis. Trans. Am. Inst. Min. Metall. Eng., 216: pp. 309-311.

————————, 1975. Analysis of Internal Steam Drive in Geothermal Reservoirs. J. Pet. Tech. (Dec.), pp. 1493-1499.

Matthews, C. S., Brons, F., and Hazebroock, P., 1954. A Method for Determination of Average Pressure in a Bounded Reservoir. Trans. Am. Inst. Min. Metall. Eng., 201: pp. 182-191.

Matthews, C. S., and Russell, D. G., 1967. Pressure Buildup and Flow Tests in Wells. Monograph Series, Society of Petroleum Engineers of AIME, Dallas, Tex.: 167 pp.

Ramey, J. H., Jr., Kumar, A., and Gulati, M. S., 1973b. Gas Well Test Analysis Under Water-Drive Conditions Amer. Gas Assoc., Arlington, Va.

Ramey, H. J., Jr., and Gringarten, A. C., 1975. Effect of High-Volume Vertical Fractures on Geothermal Steam Well Behavior. Second U. N. Symposium on the Development and Use of Geothermal Resources, San Francisco, Ca., Proc. Lawrence Berkeley Lab., University of California, Berkeley, Ca., pp. 1759-1762.

Richardson, J. G., and Stone, H. L., 1973. A Quarter Century of Progress in the Application of Reservoir Engineering. J. Pet. Tech. (Dec.), pp. 1371-1379.

Rivera, R. J., and Ramey, H. J., Jr., 1977. Application of Two-Rate Flow Tests to the Determination of Geothermal Reservoir Parameters. Ann. Fall Technical Conference, 52nd, Soc. Pet. Eng., Denver, Colo., paper No. 6887.

Rivera, R. J., Samaniego V. F., and Schroader, R. C., 1978. Pressure Transient Testing at Cerro Prieto Geothermal Field. First Symposium on the Cerro Prieto Geothermal Field, San Diego, Ca., Proc.: Lawrence Berkeley Lab., University of California, Berkeley, Ca. (in print).

Russell, D. G., 1963. Determination of Formation Characteristics from Two-Rate Flow Tests. J. Pet. Tech. (Dec.), pp. 1347-1355.

Saltuklaroglu, M., and Rivera R. J., 1978. Injection Testing in Geothermal Wells. Stanford Geothermal Reservoir Engineering Workshop, Stanford, Ca., Proc.: Stanford University (in print).

Smith, M., Potter, R., Brown, D., and Aamodt, R. L., 1973. Induction and Growth of Fractures in Hot-Rock. In P. Kruger and K. Otte (Eds.), Geothermal Energy Resources, Production and Stimulation. Stanford University Press. Stanford, Ca., pp. 251-268.

Smith, M., Aamodt, R. L., Potter, R. M., and Brown, D. W. 1975. Man-Made Geothermal Reservoirs. Second U. N. Symposium on the Development and Use of Geothermal Resources, San Francisco, Ca., Proc. Lawrence Berkeley Lab., University of California, Berkeley, Ca., pp. 1781-1787.

Takahashi, P. K., Chen, B. H., Mashima, K. I., and Seki, A. S., 1975. State-of-the-Art of Geothermal Reservoir Engineering. J. of the Power Div., A.S.C.E., 101 (July), pp. 111-126.

Thomas, L. K., and Pierson, R. G., 1978. Three Dimensional Geothermal Reservoir Simulation, Soc. Pet. Eng. J. (April), pp. 151-161.

Todd, L., Mercer, J. W., and Faust, C. R., 1978. Simulation of Geothermal Reservoirs Including Changes in Porosity and Permeability due to Silica-Water Reactions. Stanford Geothermal Reservoir Engineering Workshop, Stanford Ca., Proc.: Stanford University (in print).

van Everdingen, A. F., and Hurst, W., 1949. The Application of the Laplace Transformation to Flow Problems in Reservoirs. Trans. Am. Inst. Min. Metall. Eng., 186, pp. 305-324.

Wattenbarger, R. A., and Ramey, H. J., Jr., 1970. An Investigation of Wellbore Storage and Skin Effect in Unsteady Liquid Flow: II. Finite Difference Treatment. Soc. Pet. Eng. J. (Sept. 1970), pp. 291-297.

White, D. E., 1973. Characteristics of Geothermal Resources ... . In P. Kruger and K. Otte (Eds.), Geothermal Energy Resources, Production, and Stimulation. Stanford University Press, Stanford, Ca., pp. 69-94.

White, D. E., Muffler, L. J. P., and Truesdell, A. H., 1971. Vapor Dominated Hydrothermal Systems Compared with Hot-Water Systems. Econ. Geol., V. 66 , pp. 75-97

Whitherspoon, P. A., Narasimhan, T. N., and McEdwards, D. G. 1978. Results of Interference Tests from Two Geothermal Reservoirs. J. Pet. Tech. (Jan.), pp. 10-16.

Whiting, R. L., and Ramey, H. J., Jr., 1969. Applications of Material and Energy Balances to Geothermal Steam Production. J. Pet. Tech. (July), pp. 893-900.

Zyvolski, G. A., and O'Sullivan, M. J., 1978. Simulation of the Broadlands Geothermal Field, New Zealand. Stanford Geothermal Reservoir Engineering Workshop, Stanford, Ca. Proc.: Stanford University (in print).

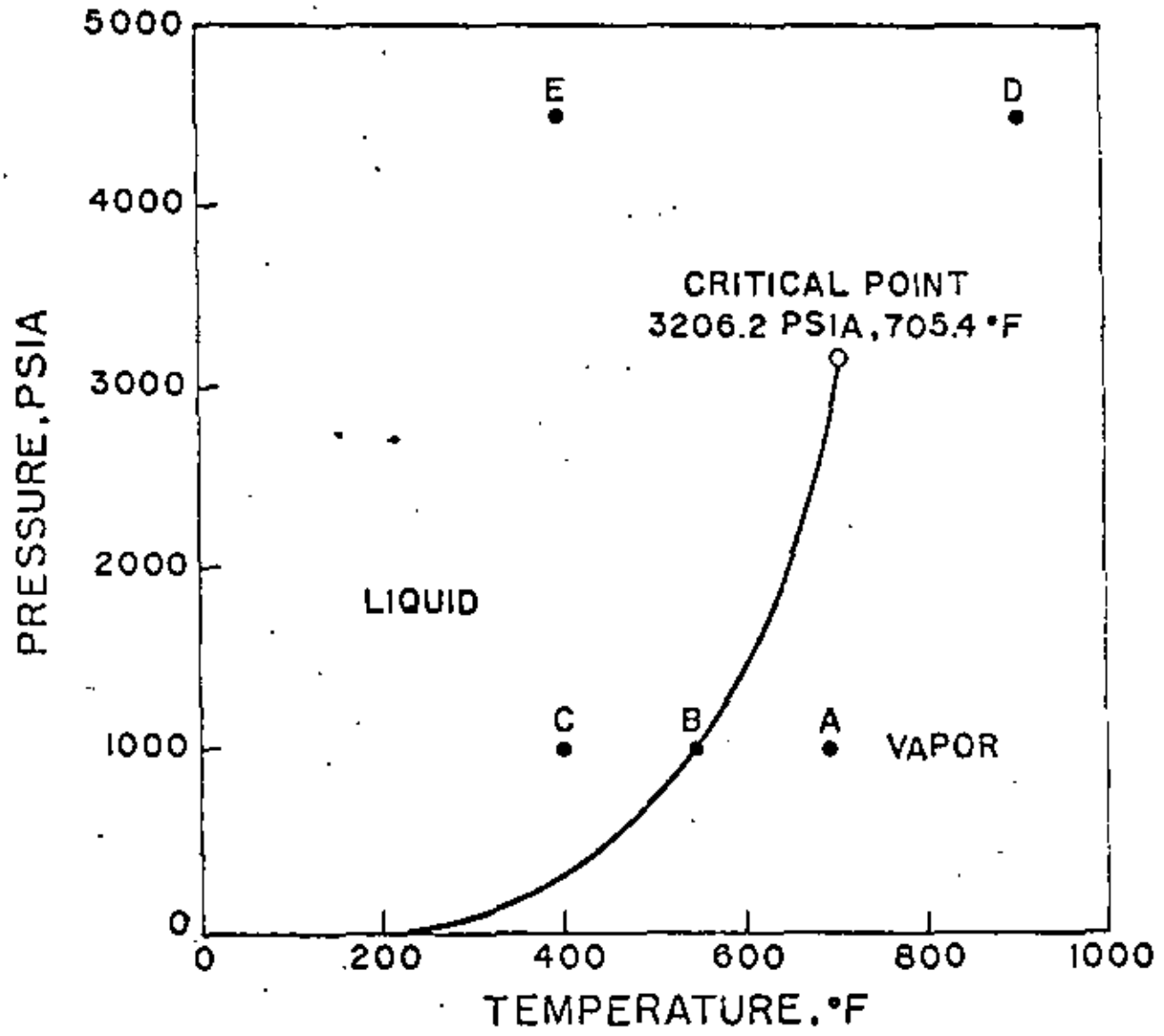

Fig. 9.1 — Pressure-temperature diagram for water (After Whiting and Ramey, 1969, Fig.1, p.894. Courtesy of the S.P.E. of A.I.M.E.)

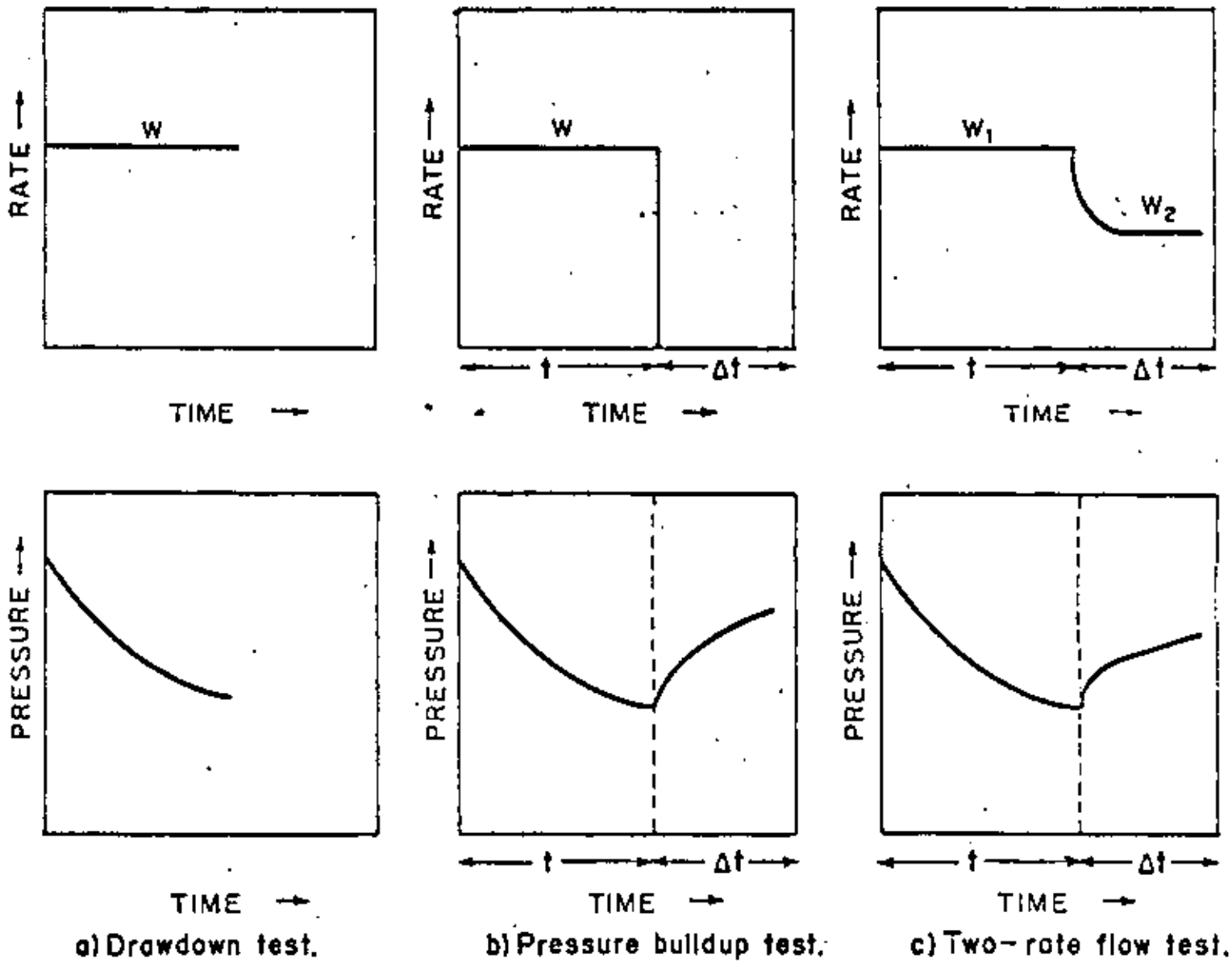

a) Drawdown test. b) Pressure buildup test. c) Two-rate flow test.

Fig. 9.2 – Variation of mass-flow rate and bottom-hole pressure versus time for various pressure transient tests.

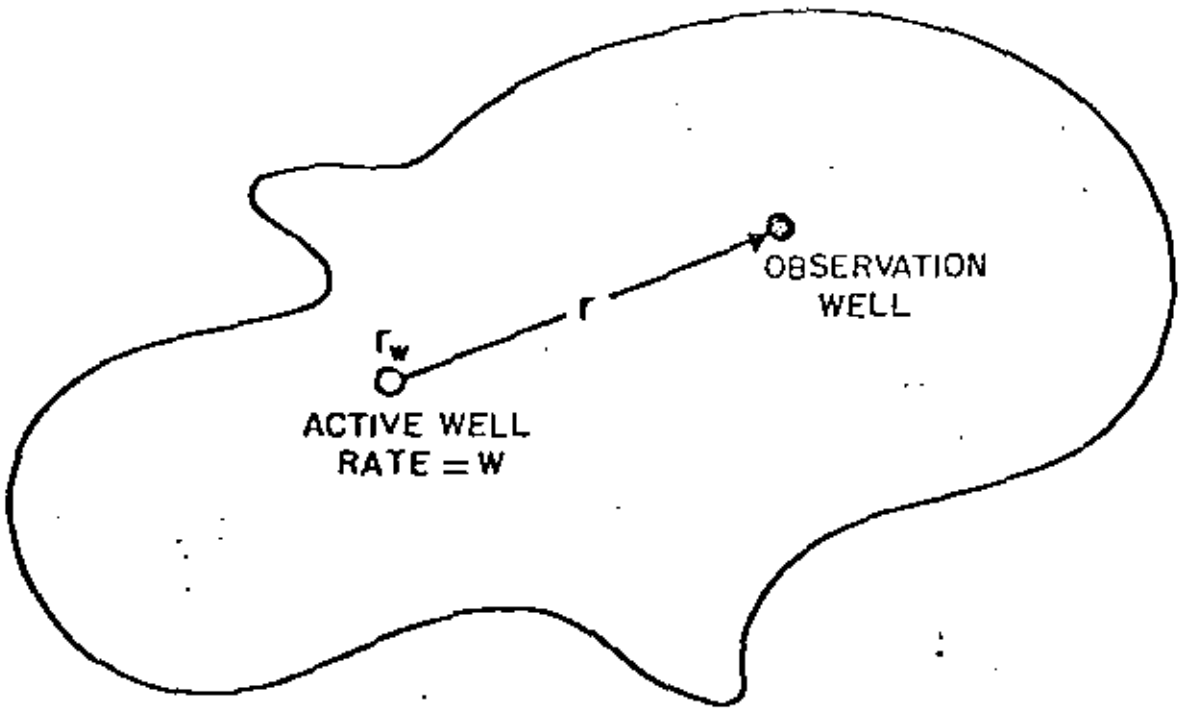

Fig. 9.3 – Squematic of an active and observation wells in an interference test.

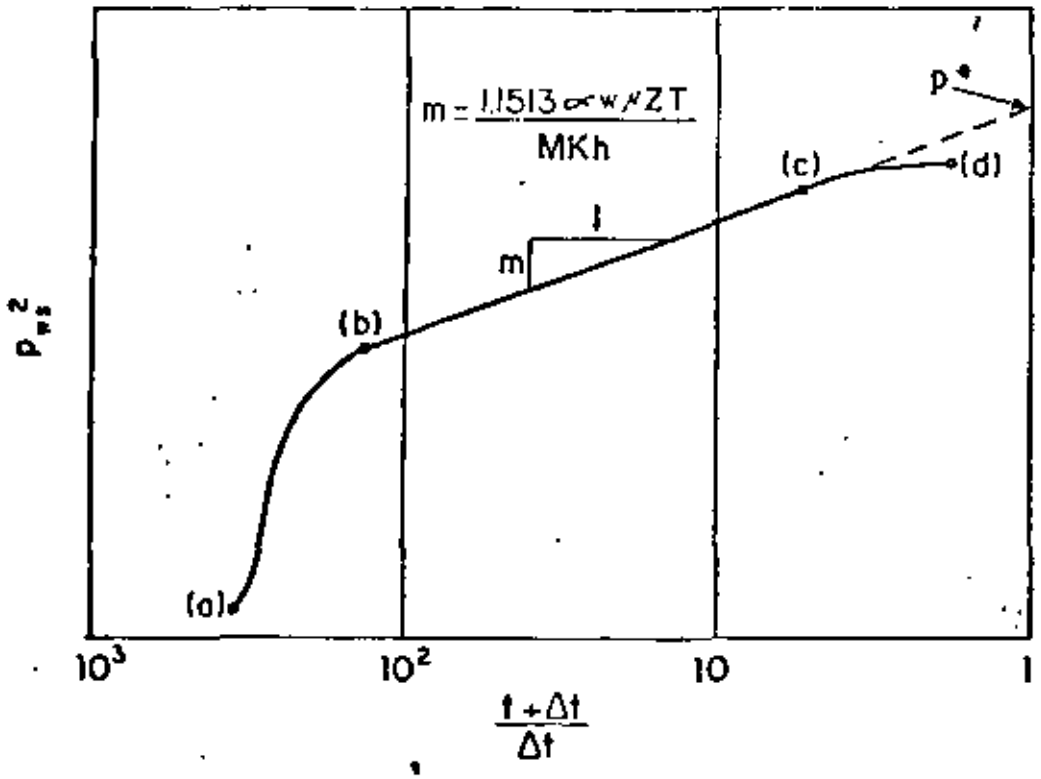

(a)–(b) Short-time data.

(b)–(c) Semilog straight line portion.

(c)–(d) Boundary effects.

Fig. 9.4 – Schematic representation of a Horner plot for pressure buildup data.

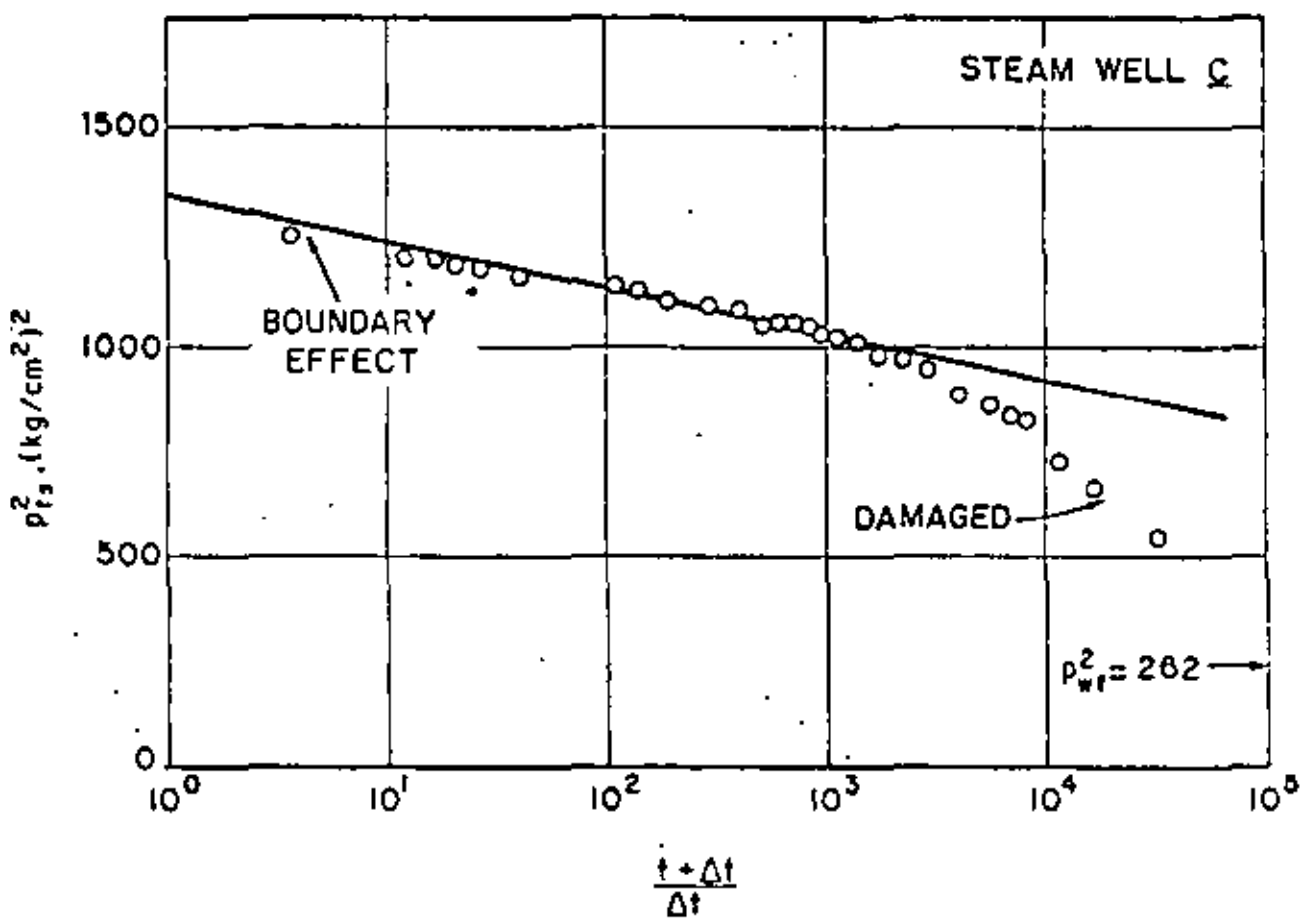

Fig. 9.5—Horner buildup graph for Geysers Steam Well C. (After Ramey, 1975, Fig. 7, p. 1753)

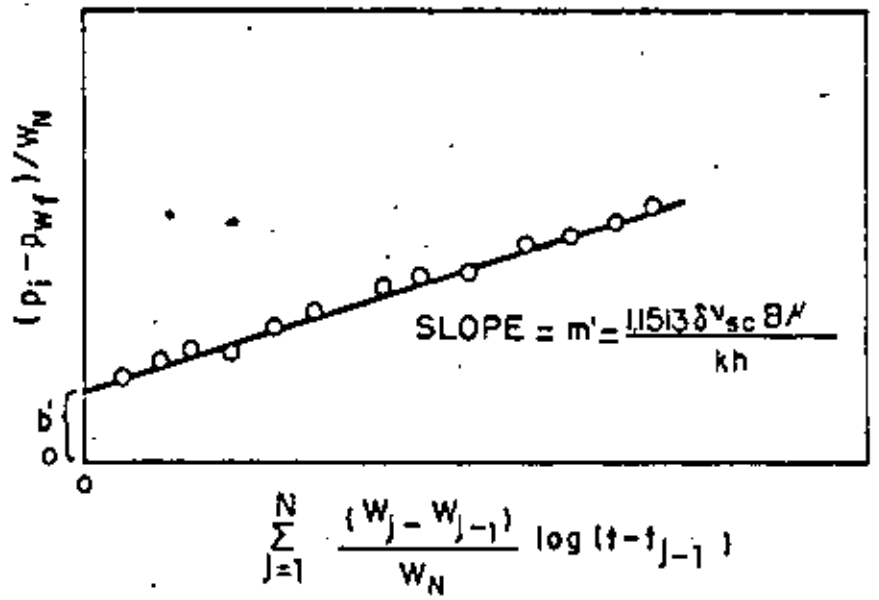

Fig. 9.6 – Schematic representation of a multiple-rate test.

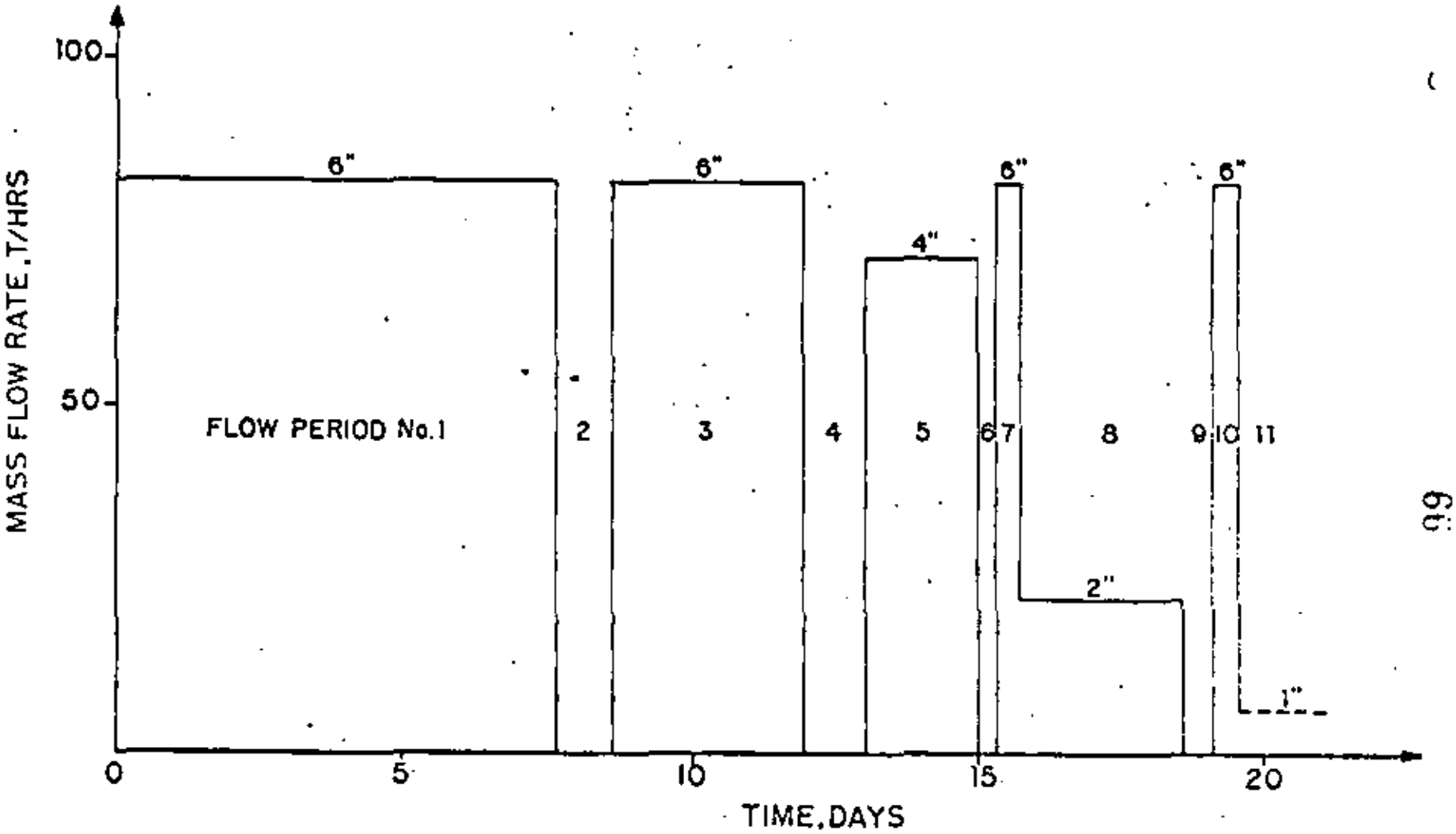

Fig. 9.7—Mass flow rate changes during ASAL 1 tests. (After Gringarten, 1978, Fig. 2, p. 6. Courtesy of the S.P.E. of A.I.M.E.)

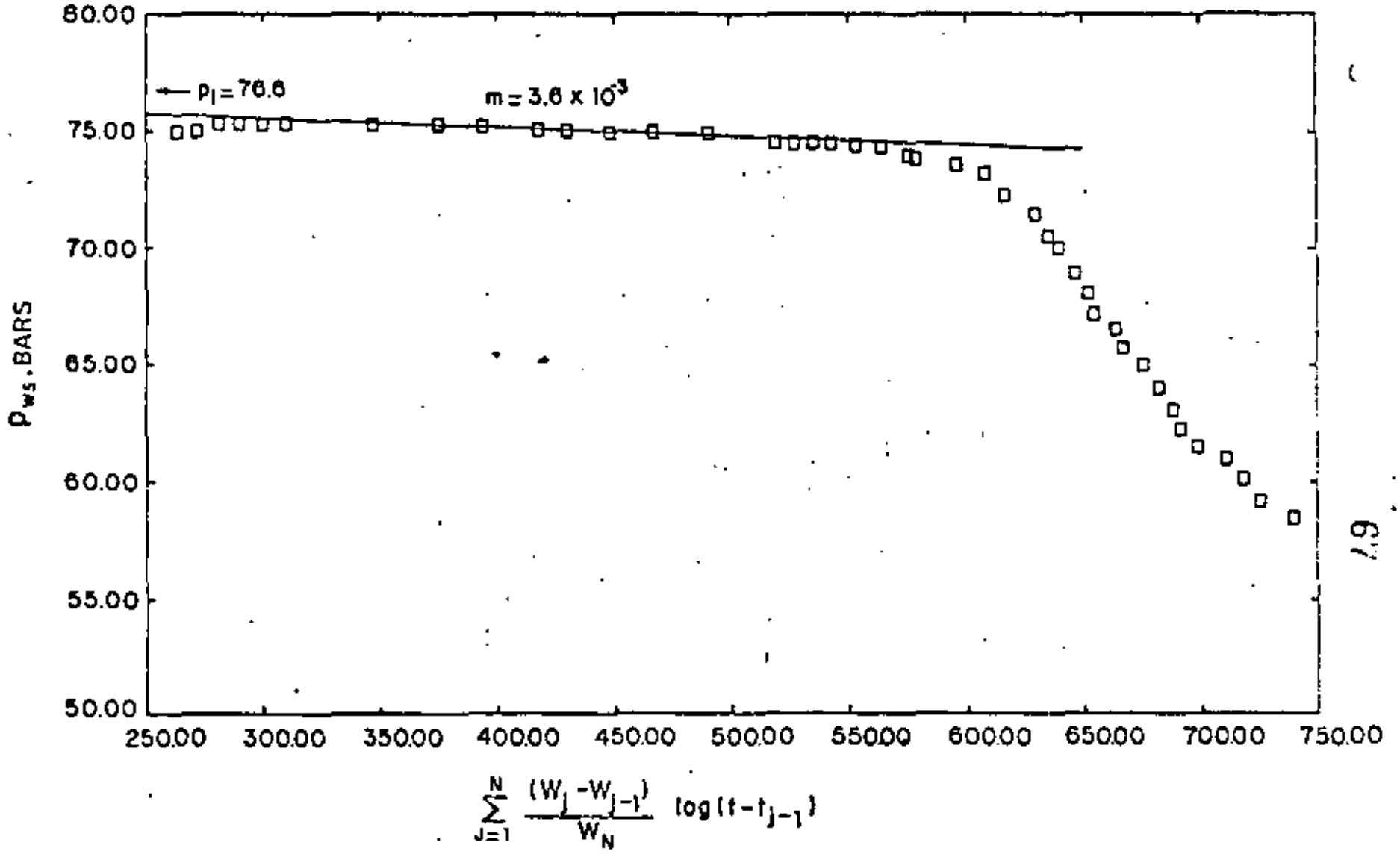

Fig. 9.8 – ASAL 1 pressure build-up test (6" outlet, flow period #4) (After Gringarten, 1978, Fig. 7, p. 9. Courtesy of the S.P.E. of A.I.M.E.)

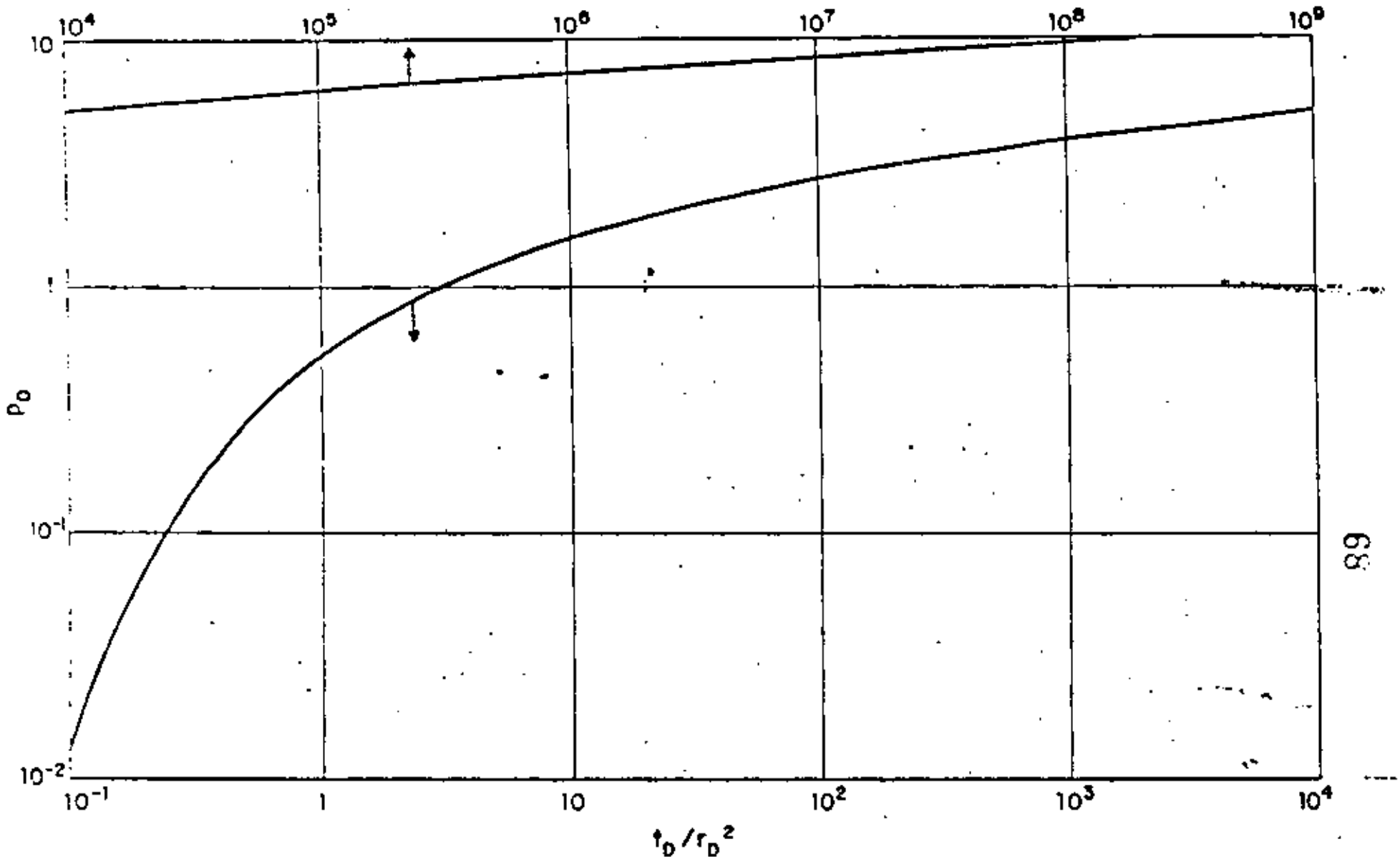

Fig. 9.9 – Dimensionless pressure for a single well in an infinite system, no wellbore storage, no skin. Exponential-integral solution. (After Earlougher, 1977, Fig. C.2, p. 194. Courtesy of S.P.E. of A.I.M.E.)

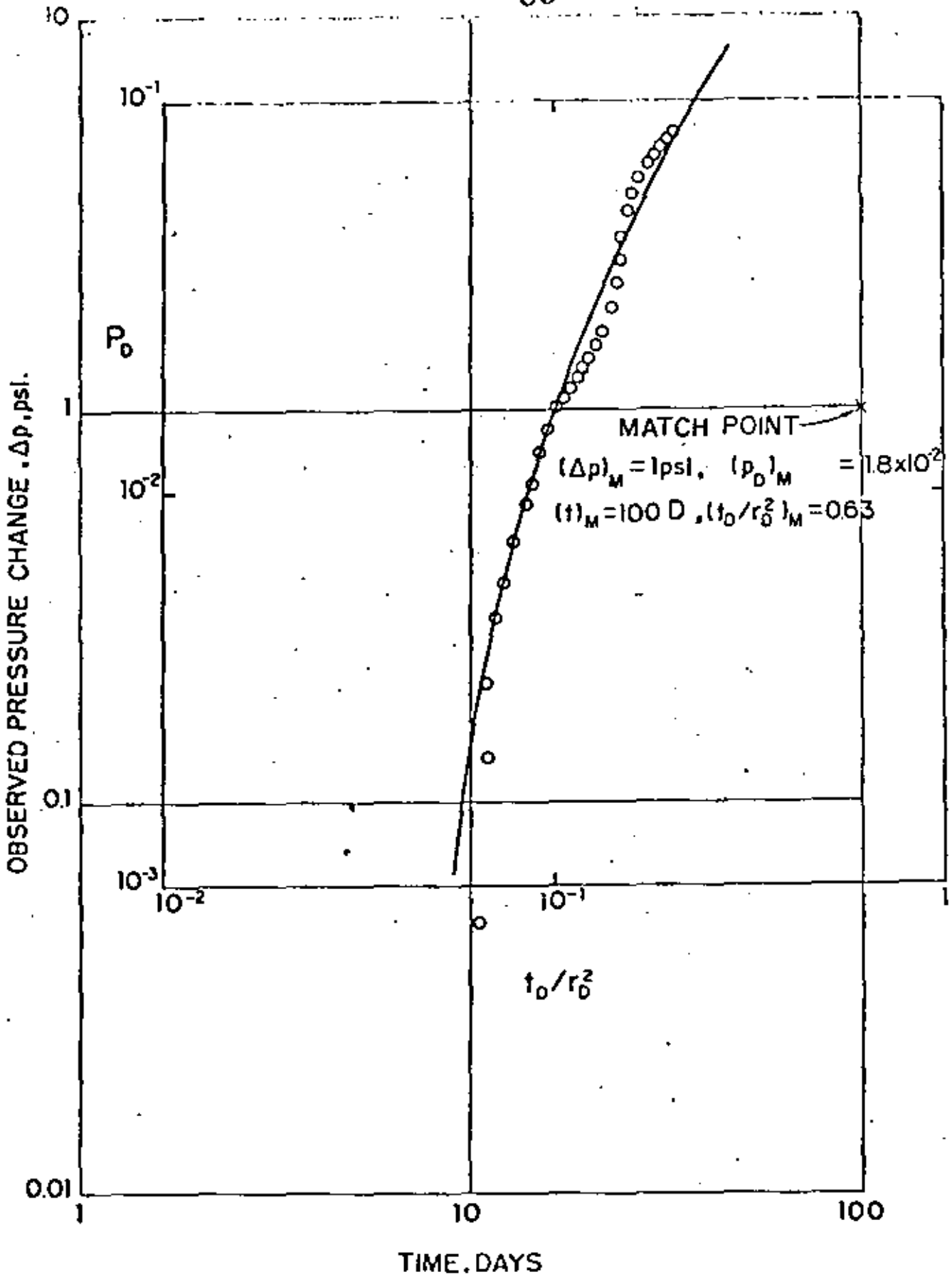

Fig. 9.10 – Type curve match of an interference test, active wells M-91, M-90, M-51, M-50. Observation well M-101. Cerro Prieto Geothermal Field (After Rivera et al, 1978 Fig 5)

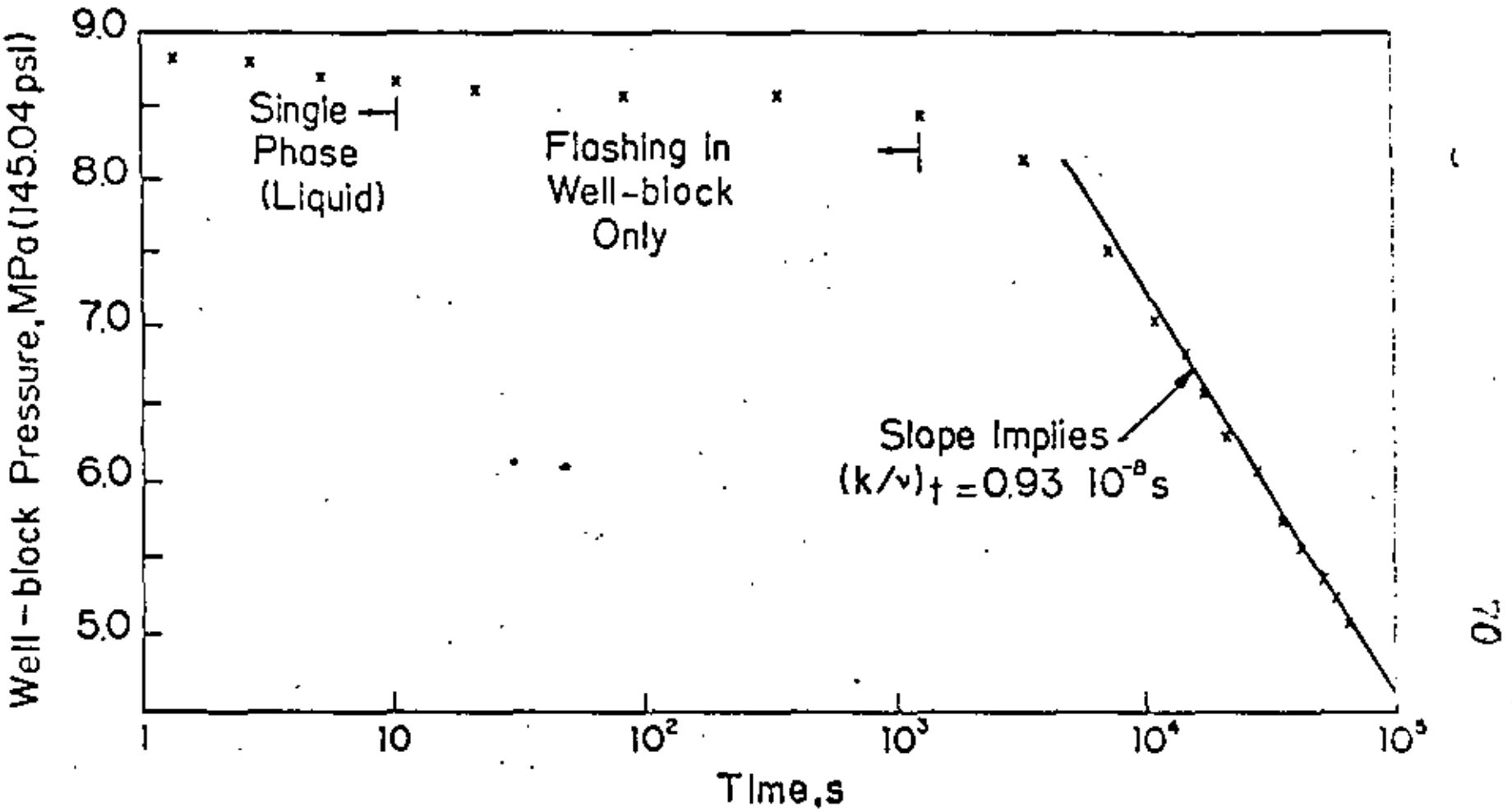

Fig. 9.11 – Simulated drawdown history (g). Reservoir is intially single-phase everywhere ($p = 9.000$ MPa ~ 1305.3 psi, $T = 573.15$K = 572°F). Absolute permeability k for this case is 0.01 μm^2 (~0.01 darcy) and the actual range of $(k/\nu)_t$ values for points lying on the straight line is $(0.93\text{-}1.15)10^{-8}$s. (After Garg, 1978 b, Fig. 7, p.12. Courtesy of the S.P.E. of A.I.M.E.)

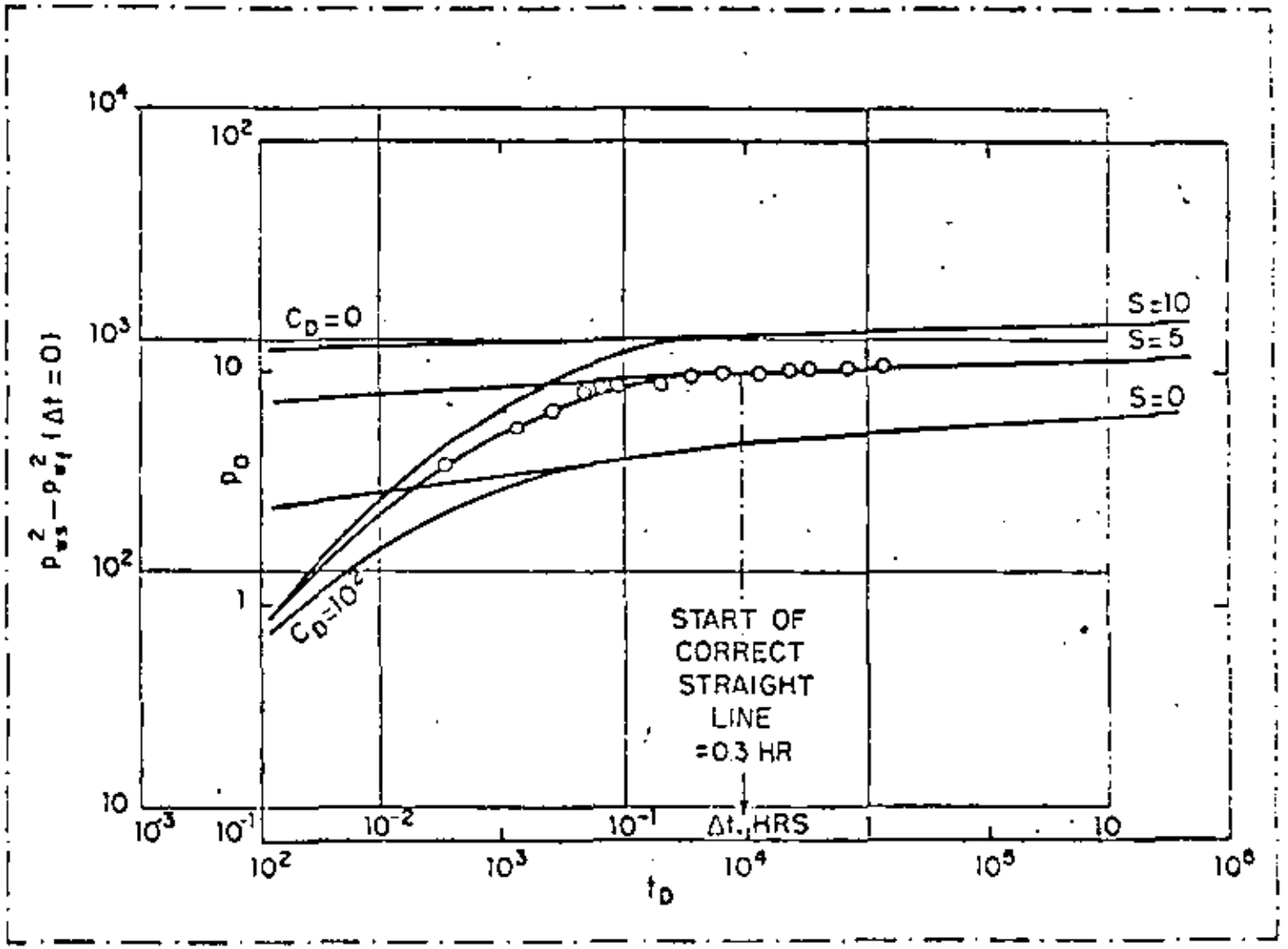

Fig. 9.13 – Type curve match of buildup data for steam well C to the type-curve of Fig. 9.12

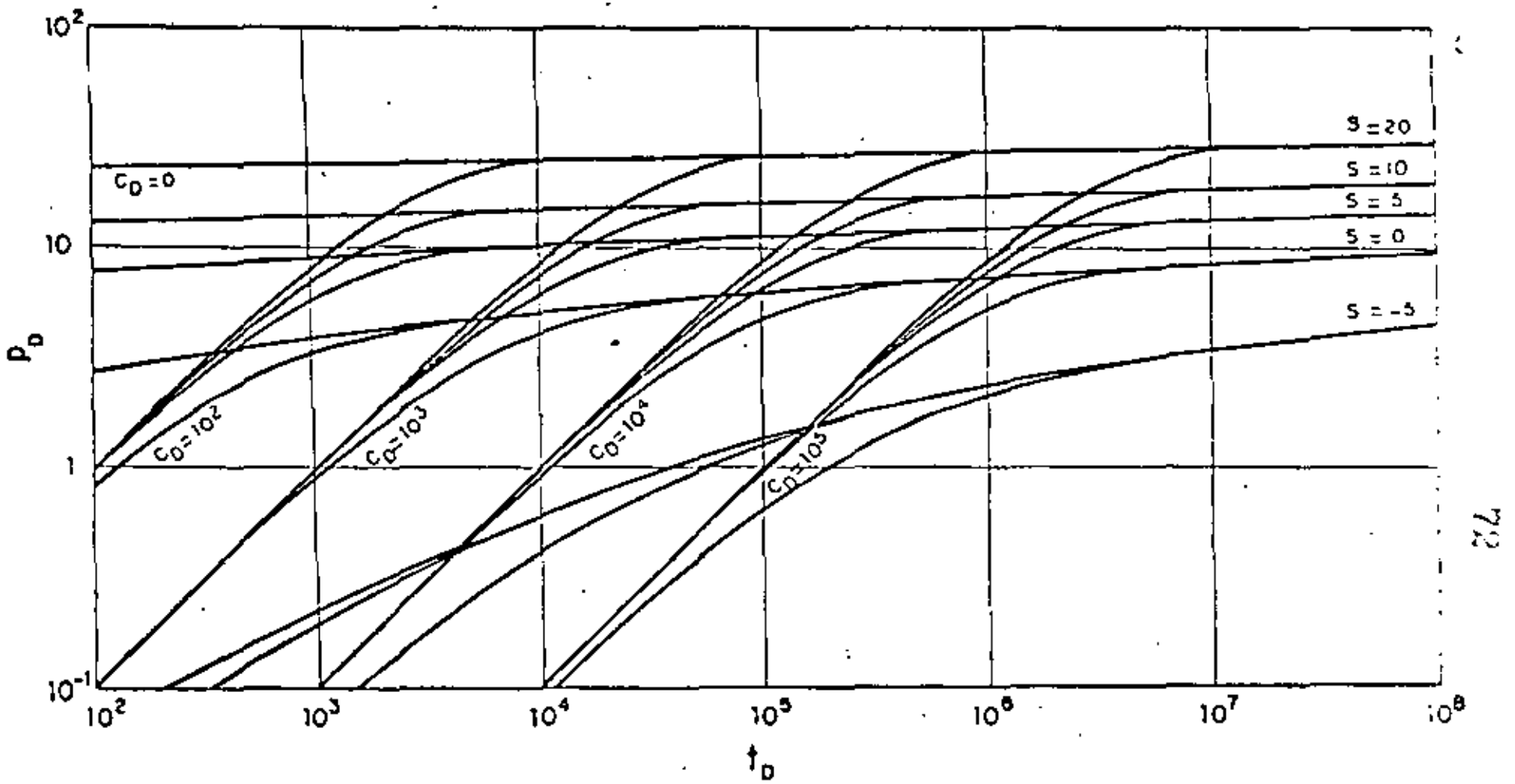

Fig. 9.12 – Dimensionless pressure for a single well in an infinite system, wellbore storage and skin included (After Agarwal, Al-Hussainy, and Ramey: 1970. Graph courtesy H.J. Ramey, Jr.)

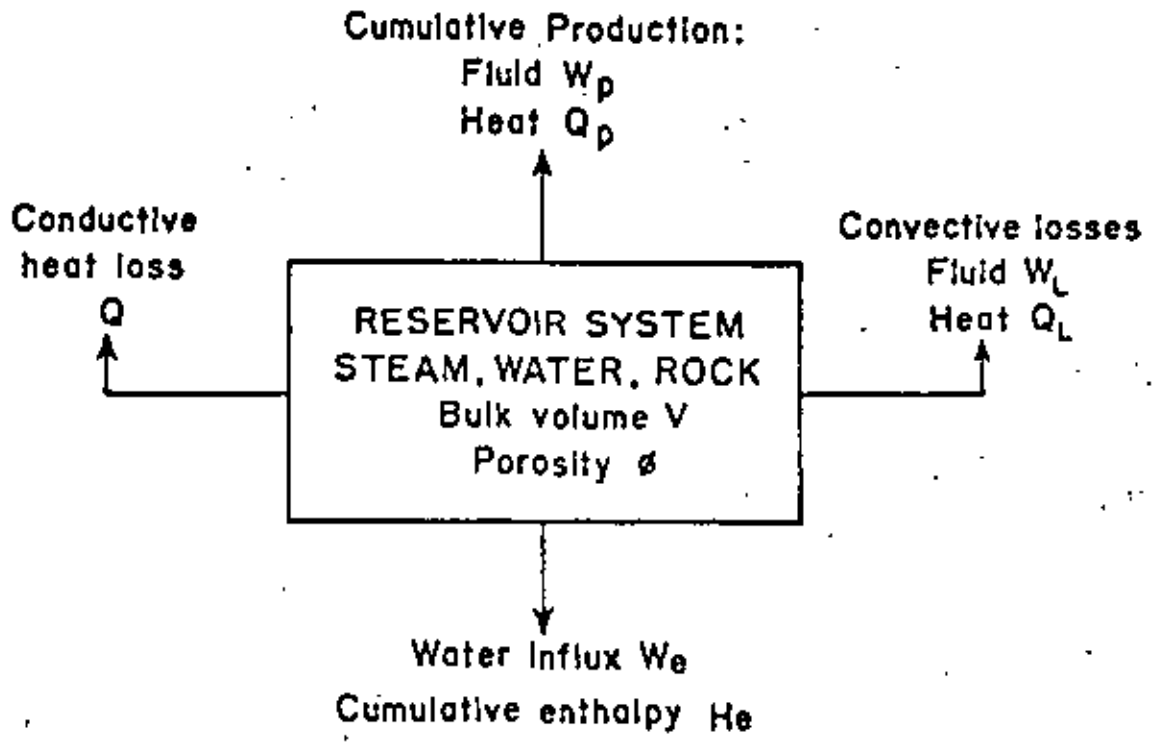

Fig. 9.14 – Schematic diagram of reservoir model (After Whiting and Ramey, 1969, Fig.4, p.895. Courtesy of the SPE. of A.I.M.E.)

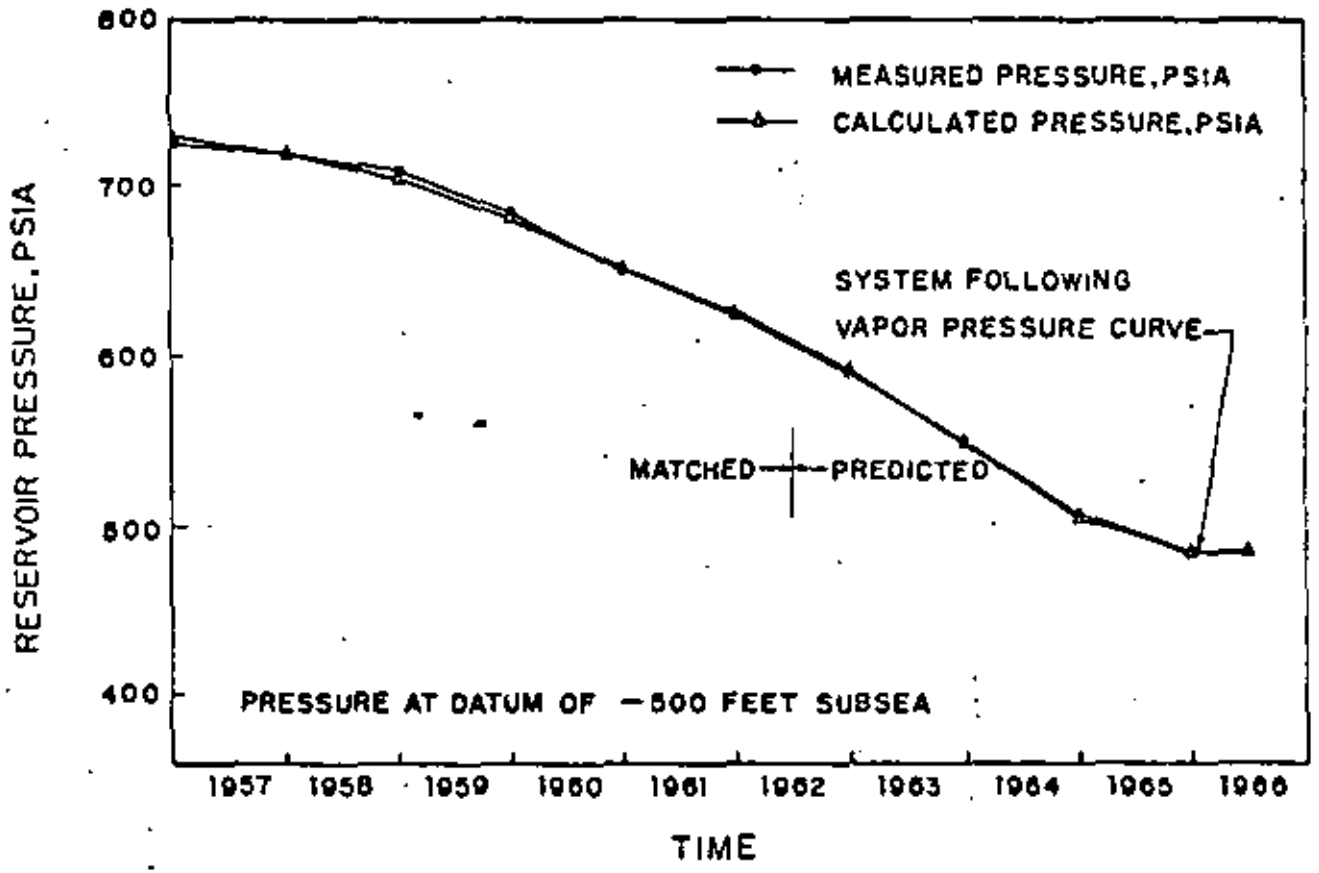

Fig. 9.15 — Prediction of geothermal reservoir performance. (After Whiting and Ramey, 1969, Fig. 5, p. 898. Courtesy of the S.P.E. of A.I.M.E.)

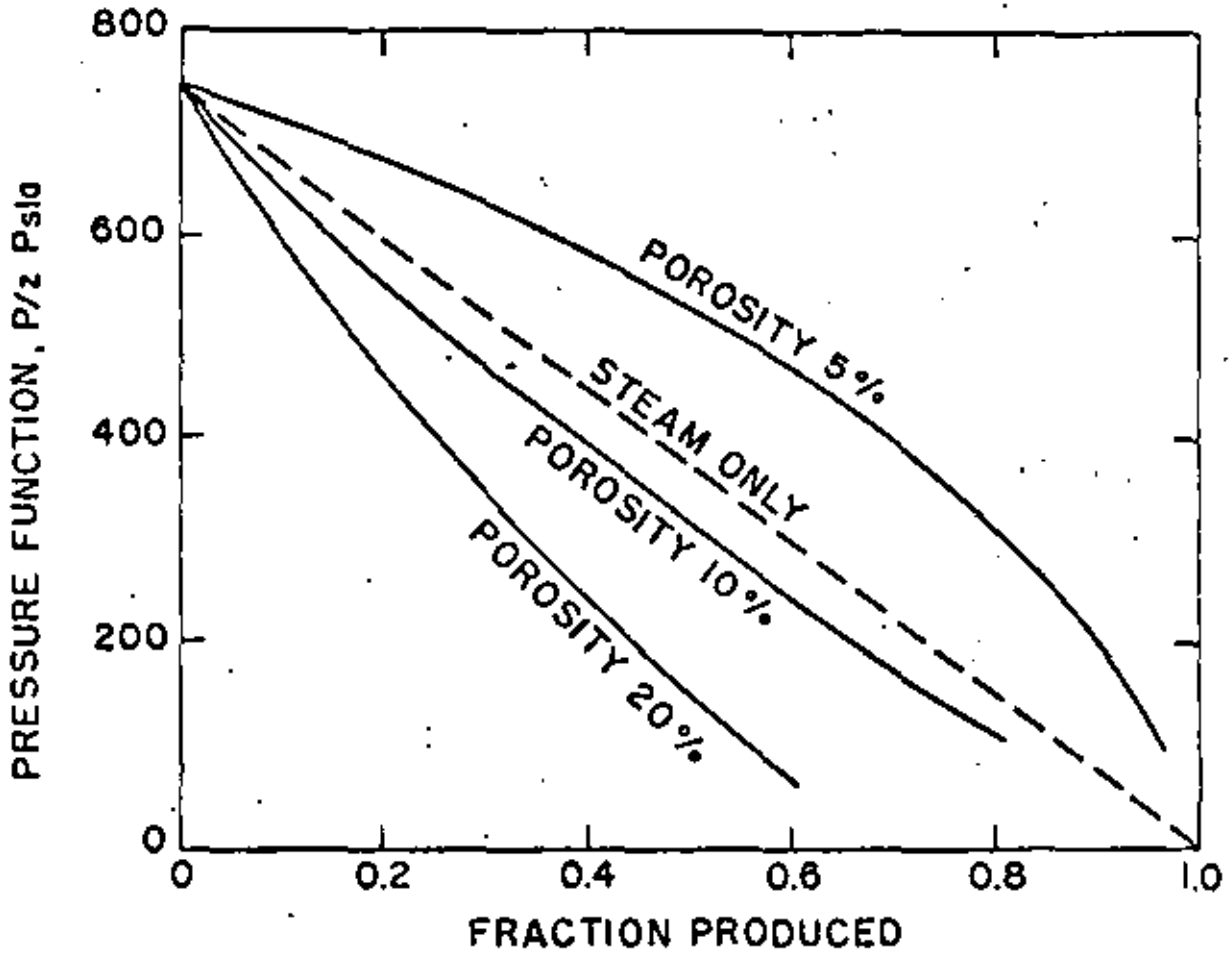

Fig. 9.16 – Pressure depletion vs. recovery, falling liquid level. (After Brigham and Morrow, 1977, Fig. 1. Courtesy of the S.P.E. of A.I.M.E.)

DIVISION DE EDUCACION CONTINUA
FACULTAD DE INGENIERIA U.N.A.M.

CURSO: INGENIERIA DE RESERVORIOS GEOTERMICOS

NOTAS COMPLEMENTARIAS

SEPTIEMBRE, 1981.

Palacio de Minería Calle de Tacuba 5 primer piso México 1, D. F. Tel: 521-40-20 Apdo. Postal M-2285

SUMMARY OF RESERVOIR ENGINEERING DATA: WAIRAKEI GEOTHERMAL FIELD, NEW ZEALAND

J. W. Pritchett, L. F. Rice and S. K. Garg
Systems, Science and Software
La Jolla, California 92038

ABSTRACT

This is an abbreviated summary of the final project report[1] on an extensive collection of fundamental field information concerning the history of the Wairakei geothermal field in New Zealand. The purpose of the effort was to accumulate any and all pertinent data so that various theoretical reservoir simulation studies may be carried out in the future in a meaningful way. Categories of data considered include electrical resistivity measurements, magnetic force surveys, surface heat flow data and a catalog of surface manifestations of geothermal activity, geological and stratigraphic information, residual gravity anomaly surveys, laboratory measurements of formation properties, seismic velocity data, measurements of fluid chemical composition, monthly well-by-well mass and heat production histories for 1953 through 1976, reservoir pressure and temperature data, and measurements of subsidence and horizontal ground deformation. The information is presented in three forms. A review of all the data is contained in the final project report.[1] The present report summarizes that information. In addition, a magnetic tape suitable for use on a computer has been prepared. The magnetic tape contains a bank of information for each well in the field, on a well-by-well basis. For each well, the tape contains the completion date, the surface elevation, the bottomhole depth, the geographic location, the slotted and perforated interval locations, the bottomhole diameter, locations of known casing breaks, the geologic drilling log, fault intersections, shut-in pressure measurements, and month-by-month production totals of both mass and heat for each month from January 1953 through December 1976.

INTRODUCTION

This summary report presents a brief discussion of the results of a six-month effort to acquire and summarize data pertaining to the character, performance and response to production of the Wairakei geothermal field in New Zealand. The complete report[1] consists of two volumes containing approximately 850 pages. The purpose of the work was to assemble a data base which would be of use in reservoir engineering studies, particularly large-scale numerical simulations of the mass and heat flow and associated phenomena over the lifetime of the field. The Wairakei geothermal system is of particular interest since it was the first (and until 1973 the only) liquid-dominated geothermal reservoir to be exploited for electrical power. Drilling began at Wairakei in 1950 and ceased in 1968; mass production rates reached a peak in the mid-1960's and have been slowly declining since. Thus, a substantial production history for a liquid-dominated geothermal system has been accumulated which is unique in the world.

The data collection process was accomplished in four phases. First, a search was made for all relevant data available concerning Wairakei in the United States. This information generally fell into two categories: published journal papers and reports, and a substantial collection of raw data accumulated by James Mercer of the U. S. Geological Survey in 1972, which he kindly contributed to the present effort. Once this data was gathered and assessed, one of the present authors (Pritchett) made a two-week visit to New Zealand in November 1977. It was during this visit that the bulk of the information was gathered. Pritchett was given free access to the Wairakei files and was provided ample help by the New Zealanders, both at the Ministry of Works (MOW) and the Department of Scientific and Industrial Research (DSIR) headquarters in Wellington and at Wairakei itself. The data was then organized in final form for the comprehensive final report.[1] Finally, the present summary report was prepared.

In line with the basic purpose of the work, only data relevant to the reservoir mechanics were considered. Thus, for example, little discussion of such matters as the power plant design, the economics of the system, plant management and the like is included. Emphasis was placed upon information which is not generally available in the U. S. For example, the geology of the Wairakei area is very intricate and forms a fascinating subject in itself. Grindley[2] has already written a 130 page book on the subject, and hence the section on geologic structure in the report is largely a précis of his work and that of Healy.[3] Similarly, the pressure-drawdown data for the field have been discussed by Bolton;[4] therefore, the discussion of pressures follows Bolton very closely, but includes data for the interval 1969-1976 which Bolton, obviously did not treat.

From the standpoint of the reservoir engineer, the data bank available concerning Wairakei is somewhat frustrating. On the one hand, enormous amounts of information are available concerning geological structure, production rates, discharge enthalpy, pressure trends, and many other subjects. On the other, certain measurements which are of great importance in reservoir engineering either were not made at all, or were made in such a way that the results are ambiguous or misleading. The two most important parameters which fall into this category are the permeabilities of the various formations and the early temperature distribution in the field.

As regards permeabilities, the classical procedure in the petroleum industry for determining effective formation permeability is the wellhead test. For several reasons (not the least of which is the fact that a rapid-response pressure gauge capable of withstanding the geothermal

environment was not then available), such tests were never performed in the early days at Wairakei. Now that the technology for making pressure-transient tests is available, the long history of production has resulted in the creation of a two-phase (water/steam) system in the area of principal production which renders the interpretation of such a test very difficult and uncertain. Lacking well-test information, core samples from Wairakei have been tested in the laboratory. These laboratory results indicate, however, matrix permeabilities for the principal producing aquifer which are several orders of magnitude smaller than the minimum required to sustain reservoir production at the observed rate. The Wairakei field is located in an intensely faulted and seismically active region; clearly, most of the effective reservoir permeability consists of "fracture permeability" as opposed to "matrix permeability".

The situation is somewhat different concerning the early temperature distribution in the field. The procedure was to shut a well in for a period of time and then to make temperature measurements at various levels within the well, thereby constructing a temperature/depth profile for the well. A substantial amount of information of this sort is available. There are, however, at least two serious difficulties with this approach. First, it often turns out that the shut-in time was insufficient to permit thermal equilibration between the rock outside the well and the fluid inside. An even more serious difficulty is that the Wairakei temperature/depth measurements were made inside cased wells. Due to the formation of convective cells in the fluid within the well, under such circumstances the vertical temperature distribution within the well may never equilibrate with that of the rock outside, irrespective of the duration of the shut-in interval. Therefore, although a maximum temperature found within a well at a particular time may indeed reflect the rock temperature at that particular depth, the remainder of the temperature-depth profile should be regarded with considerable suspicion. A preferable procedure for determining the temperature-depth profile would have been to make measurements during drilling, allowing for temperature equilibration at different depths during the drilling of the well prior to making the temperature measurement. It should be assumed that the pre-production temperature distribution in the field is simply not well known.

Lest the reader become discouraged, it should be reiterated that in other respects the data available from Wairakei are excellent and quite complete. Wairakei is almost certainly the best-documented geothermal field in the world (with the possible exception of Lardarello), at least in the public domain. As can be seen from the main report, the available information on geological structure, reservoir pressure, well-by-well production histories and other quantities is complete enough that the principal unknowns (permeability and initial temperature) can likely be estimated or at least bracketed by good engineering judgement with the help of numerical simulation studies.

At this point, it is worthwhile to discuss the way in which the data are presented. Generally speaking, measured quantities are given in the same system of units as that in which they are obtained. Thus, for example, pressures are usually expressed in pounds per square inch. Mass of fluid produced is given in pounds, and enthalpies are provided in BTU/pound relative to liquid-saturated conditions at 0°C. Temperatures, however, are given in degrees Celcius. Depths are measured in feet, usually with respect to sea level; for example, the notation "RL-900" refers to a depth of 900 feet below mean sea level (and roughly 2,500 feet below the surface at Wairakei's altitude). Geographic locations (i.e., locations of wells and the like) were provided in as many as three different coordinate systems, but by far the bulk of the data was in feet, with respect to the 1949 Maketu datum; this system was adopted throughout for this report.

The report[1] actually consists of three parts. The first of these is the lengthy written document, Volume I. In addition, substantial amounts of data are contained on a magnetic computer tape, and computer programs have been written which permit interrogation of this tape. For the benefit of those who lack ready access to a large computer, all the data on the tape are also reproduced (in a form more amenable to human consumption) in Appendix D, which forms the rather bulky Volume II of the report. It is hoped, however, that the presentation of the data in computer readable format will facilitate the use and manipulation of these data for input to numerical reservoir simulation computer programs.

Not all the data acquired during the course of this project are to be found on the magnetic tape. Generally speaking, the data on the tape have been restricted to information which (a) readily lends itself to digital representation, and (b) is too cumbersome for efficient presentation in a written report. The data on the tape are organized on a well-by-well basis. That is, for a particular well, all relevant data are presented in a particular data block on the tape. The tape thus consists of a linear series of such data blocks, one for each well in the field. For each well, the data on the tape consists of the following:

1. The coordinates of the wellhead in feet with respect to the 1949 Maketu datum, and the altitude of the wellhead (in feet) above sea level.

2. The depth of the bottom of the well (in feet, with respect to sea level); also, if the well was deviation drilled, the depth at which deviation began and the 1949 Maketu coordinates of the well bottom.

3. The month and year during which the well was completed.

4. The depth (in feet with respect to sea level) at which major geologic formation interfaces were encountered during drilling.

5. The depth (feet, RL) of the top and bottom of the major slotted interval in the well.

6. Numbers, diameters and top and bottom altitudes of gun-perforation intervals.

7. The diameter of the well bottomhole (inches).

8. Depths (in feet, with respect to sea level) where fissures or faults were encountered during drilling.

9. Depths (feet, RL) where casing breaks were detected.

10. For each month from January 1953 to December 1976 (inclusive), the total mass of fluid (in pounds) and the total heat (BTU) produced during the month. The mean discharge enthalpy may be computed by dividing the heat production by the mass production.

11. Pressure measurements, as applicable.

12. Occasional general comments concerning unusual events or characteristics of the well.

In the written portion of the report, the sources and general implications of the data on the magnetic tape are discussed at some length. Also discussed are data of other kinds which did not readily lend themselves to digital representation. The complete report consists of fourteen chapters plus four appendices. Chapter II contains a general description of the history of the development and exploitation of the Wairakei field. In Chapter III, the results of electrical resistivity and magnetic surveys are presented. The former indicates, in an approximate manner, the thermal boundary of the field; the latter suggests, among other things, that the source of hot fluid lies to the west of the present production area, and that natural groundwater flow is generally from west to east. Chapter IV discusses the natural geothermal surface manifestations in the Wairakei area and the changes in these phenomena that have occurred over the years. In Chapter V the geological structure of the Wairakei field is described, based principally on borehole evidence. This chapter amounts to a summary of the previous work of Healy[3] and Grindley,[2] supplemented by more recent data relevant to the nearby Tauhara field and certain later boreholes. Chapter VI consists basically of data concerning laboratory measurements of rock density, porosity and permeability, and also contains comments relevant to the bulk effective permeability of the reservoir. In Chapter VII, seismic data are presented. Briefly, seismic surveys intended to map geologic layering have been relatively unsuccessful due to absorption in the unconsolidated surface layer, but seismic velocity measurements in the various strata, when compared to laboratory measurements, strongly suggest an extensive fracture structure. Chapter VII presents data relevant to the chemical composition of the fluids discharged from the Wairakei bores. These data indicate that, for practical reservoir engineering purposes, the fluid may be regarded as pure H_2O. In Chapter IX, temperature distributions within the field and trends in temperature with time are described. As discussed above, however, serious uncertainties exist concerning the temperature data. Chapter X describes trends in the drilling program, the spatial and temporal distribution of the production of mass and heat, and changes with time of such quantities as mean discharge enthalpy. Also discussed are uncontrollable-discharge "accidents" that have occurred, and the various sources of mass and heat production data which are contained on the magnetic tape. Chapter XI summarizes the numerous pressure measurements made at Wairakei. It is shown that the pressure trends within the field are consistent with two-phase behavior, and that the rate of pressure drop has been declining in recent years in spite of sustained production rates. Pressure evidence to define the hydrodynamic boundaries of the field is described and correlated with temperature data. It is also demonstrated that the Wairakei field communicates strongly with the Tauhara field to the southeast. In Chapter XII, gravity survey data are discussed. It is shown that changes in gravity anomaly measurements indicate an increasing rate of natural recharge over the years. In Chapter XIII, the ground motion that has accompanied fluid production at Wairakei is described. Both vertical motions (subsidence) and horizontal deformations have been measured. In Chapter XIV, the data on the magnetic tape are discussed in detail; Appendices A, B and C show various examples of output available from the magnetic tape, examples of computer programs suitable for interrogating the tape, and user-instructions for the tape. Finally, Appendix D (presented as Volume II of the report) contains, in condensed form, the detailed data available on the tape.

The sections which follow in this document before you are only summaries of the information contained in the chapters discussed above.

DEVELOPMENT OF THE WAIRAKEI GEOTHERMAL FIELD

Between Mt. Ruapehu (an active volcano) in the center of New Zealand's North Island and White Island in the Bay of Plenty some 150 miles to the northeast, lies a 20 mile wide belt in which numerous surface manifestations of geothermal activity are to be found. Within this region (see Fig. 1) which is believed to be associated with the Tonga-Samoa submarine volcanic ridge,[2] geysers, hot springs, steam vents, large regions of steaming ground, and evidence of hydrothermally-altered rocks are common.

Most of the electrical generating capacity of the North Island consists of a series of hydroelectric power stations along the Waikato River, which has its origins at Lake Taupo near the south end of the thermal belt and discharges to the sea near Auckland to the north. In 1950, a joint effort was made by the Ministry of Works (MOW) and the Department of Scientific and Industrial Research (DSIR) to assess the geothermal potential of the thermal belt generally, and in particular, the vicinity of Wairakei just to the north of Lake Taupo. The principal surface manifestations of thermal activity at Wairakei are the Karapiti area

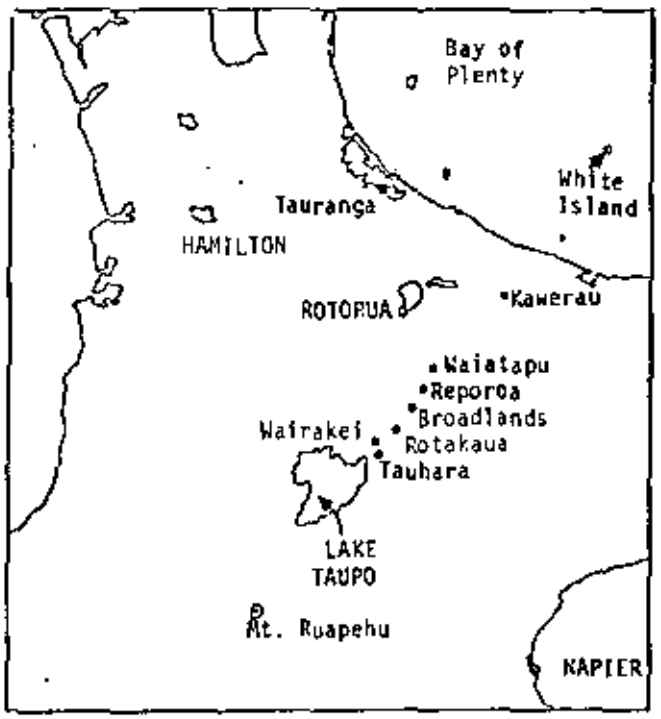

Figure 1. Thermal areas, hot springs and volcanoes of the thermal belt, North Island, New Zealand.

in the south, Geyser Valley to the north, and the Waiora Valley to the west. The conclusions of the study,[6] generally speaking, were that some potential definitely existed for power production using shallow drilling alone, and that much more might exist if deep wells were drilled.

In 1955, a decision was made to construct a power plant capable of producing 69 megawatts of electrical power and, as a by-product, to provide heavy water for the British Atomic Energy Authority. The heavy water scheme was soon abandoned, but by 1957 the first stage (59 MW) of the power plant was under construction. In 1953, a program of deep drilling was begun that soon demonstrated the existence of a much larger resource than had been estimated based upon the earlier relatively shallow bores.

Drilling activity at Wairakei ceased in 1968; since then, mass production rates have been declining at about 4 percent per year. Bore field pressures have dropped over 350 psi over the years, and temperatures have likewise dropped. Various modifications have, however, improved the thermal efficiency of the system such that the electrical generating capacity has been maintained.

Wairakei has been producing electrical power since the mid-1960's at an average of about 140 MW. It is now regarded in New Zealand as an operating facility which is slowly being depleted but which will doubtless continue to produce power for many years to come, and no fundamental changes are contemplated.

ELECTRICAL AND MAGNETIC MEASUREMENTS

The results of surface resistivity surveys are generally interpreted as being indicative of the presence or absence of hot water at depth. That is, as temperature increases, the electrical conductivity of electolytes also increases. Low resistivities tend to occur in regions surrounding a geothermal anomaly. As a general practice, the "boundary" of a geothermal reservoir is considered to correspond to resistivities in the range of 10-20 ohm-meters. The reservoir itself, in its central region, may have resistivities less than 5 ohm-meters, while the surrounding relatively cold rock is often characterized by resistivities as high as 100 ohm-meters or more.

A resistivity survey was carried out in the Wairakei area in 1963-1964; Fig. 2 shows the resistivity contours resulting from that survey. These contours definitely indicate two large low resistivity regions, at Wairakei and at Tauhara, with a relatively narrow neck connecting them. Even more compelling evidence for such a connection is provided by the pressure data discussed elsewhere in the report.[1]

A vertical magnetic force survey was reported by Cullington.[7] Modriniak and Studt[8] drew attention to the contrast between the low intensities in the vicinity of the Waiora Valley at the western end of the bore field and the high intensities in the vicinity of Geyser Valley. They believe that this general increase in magnetic intensity from west to east across the bore field indicates that the source of hot fluid is to the west, and that the general flow is from west to east. They drew this conclusion by noting that hydrothermally altered ignimbrite is much less polarized than relatively unaltered ignimbrite.

NATURAL HEAT FLOW AT THE SURFACE

Prior to its development as a geothermal power system, Wairakei and its immediate neighborhood were popular tourist attractions, in large measure due to the various geysers, hot pools and similar phenomena in the vicinity.[9] The most prominent of these features were the geysers in Geyser Valley (just north of the main bore field), the thermal pools of the Waiora Valley (just to the west), the Karapiti area to the south of the bore field, including the Karapiti Blowhole fomarole, and the geysers at Spa Sights in the Tauhara area.

During the years of production at Wairakei, much of this natural activity has subsided. Activity in Geyser Valley began to decrease preceptibly as early as 1954, and the attraction was closed in 1972. The Waiora Valley, on the other hand, has retained most of its activity. The Karapiti Blowhole has ceased to discharge, as have the geysers at Spa Sights. As a general rule, throughout the area, surface manifestations such as geysers and hot springs have declined, whereas "steaming ground" has become more extensive.

Numerous natural heat flow assessments of Wairakei have been carried out.[5,10-16] Estimates for the total heat flow vary, but Grindley[17] indicates that the total natural flow has increased

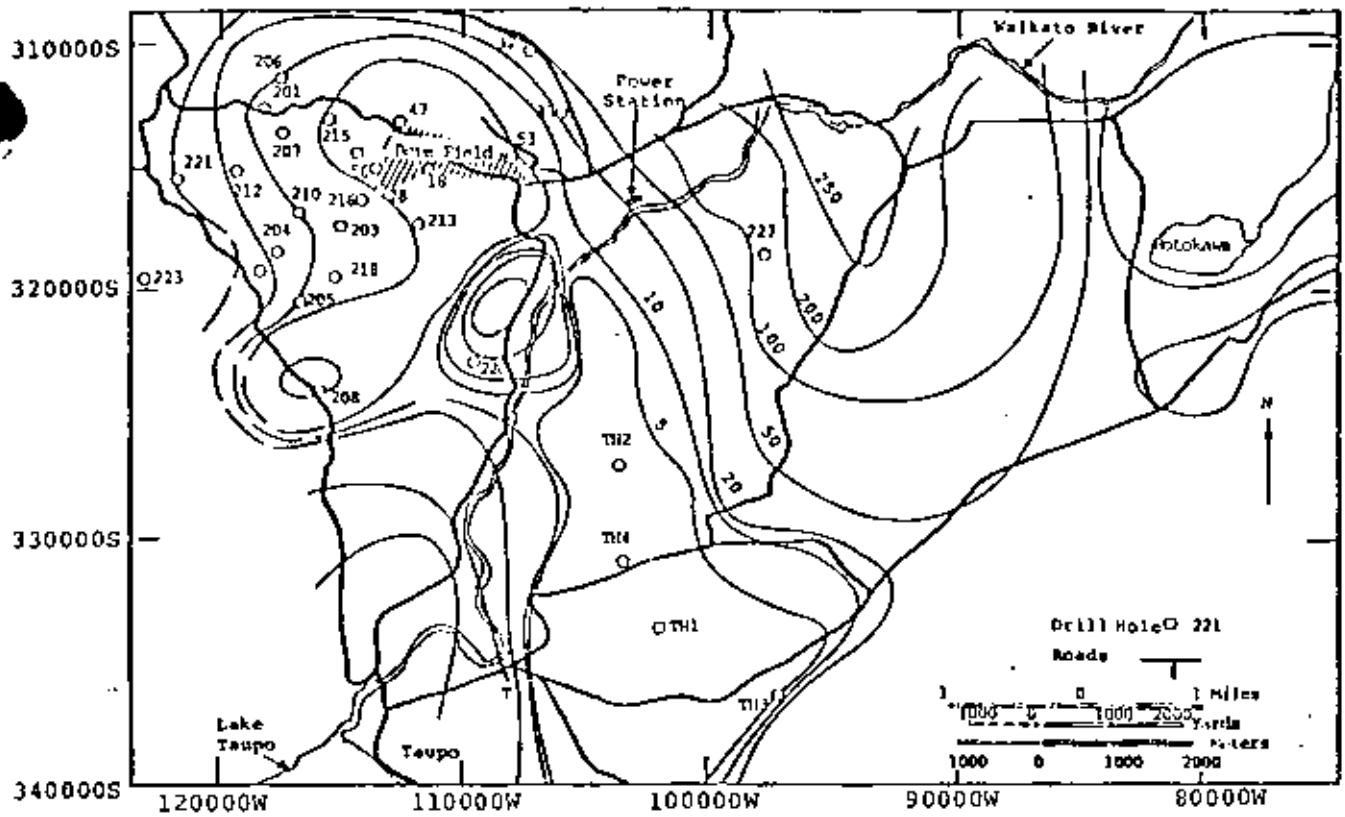

Figure 2. Resistivity contours values in ohm-meters.

from about 450 to about 750 megawatts over the life of the field. Substantial amounts of shallow temperature data have been collected. Figure 3 shows temperature contours at a depth of 1 meter over the Wairakei field in 1966. Dawson and Fisher[18] showed that, at this depth, diurnal variations in air temperature do not penetrate. The regions of high heat flow are seen to be at Geyser Valley, Waiora Valley and Karapiti, as well as at other isolated locations. The overall heat flow pattern changed only slightly between 1958 and 1966.

GEOLOGICAL STRUCTURE

The Wairakei geothermal field includes the area of Geyser Valley, the Waiora hot springs, and the Karapiti fumarole area. The field lies to the west of the Waikato River and to the north of Lake Taupo. The Tauhara geothermal region lies to the south-southeast of the Wairakei geothermal area and is associated with low lying acid volcanoes. In the Tauhara field, the stratigraphic sequence forms a shallow basin, which is thickest near bore TH1 and thins to the north, west and south. The eastern edge of the basin extends beneath Mt. Tauhara. Pressure evidence clearly shows that Tauhara is part of the same aquifer system as the Wairakei field. Therefore, any analysis of Wairakei necessitates examination of the Tauhara region as well. Hence, the stratigraphy of the combined area is discussed here.

The geology of the Wairakei geothermal area has been described in general by Grange[19] and in greater detail by Grindley[2] and Healy.[3] The geology of Tauhara has also been discussed by Grindley, et al.[20] It is not the intent of the present authors to reiterate the extensive geologic analyses already concluded. Rather, a discussion of the geologic structure necessary for reservoir engineering studies of the hydrothermal area has been undertaken.

With the continuing development of the Wairakei field since the early 1950's and with the commencement of subsurface exploration at Tauhara in 1964, a stratigraphic picture of the entire hydrothermal region has been evolving, primarily through examination of the outcrops in the region and, more importantly, through the data obtained from drilling logs. The well summaries presented in Volume II of the report[1] give the geologic formations penetrated by each bore. This information was obtained through examination of the drilling logs presented by Grindley.[2] His information was supplemented by the examination of well logs for recent bores not included in his report. Indeed, those addtional bores have provided important information about the subsurface structure.

Figure 4 shows a general topographic map of the entire Wairakei/Tauhara region. The portion of the map within the small rectangle has been enlarged in Fig. 5 to give a more detailed picture of the main production area. These two maps identify the locations of all bores and major surface features in the region. In the next several paragraphs, the characteristics and general distributions of the principal members of the stratigraphic sequence will be discussed in detail. Figure 6 shows a cross-section running approximately E-W across the main bore field. The full report contains many such cross-sections to give a better geologic picture of the entire region. In the following subsections, each major

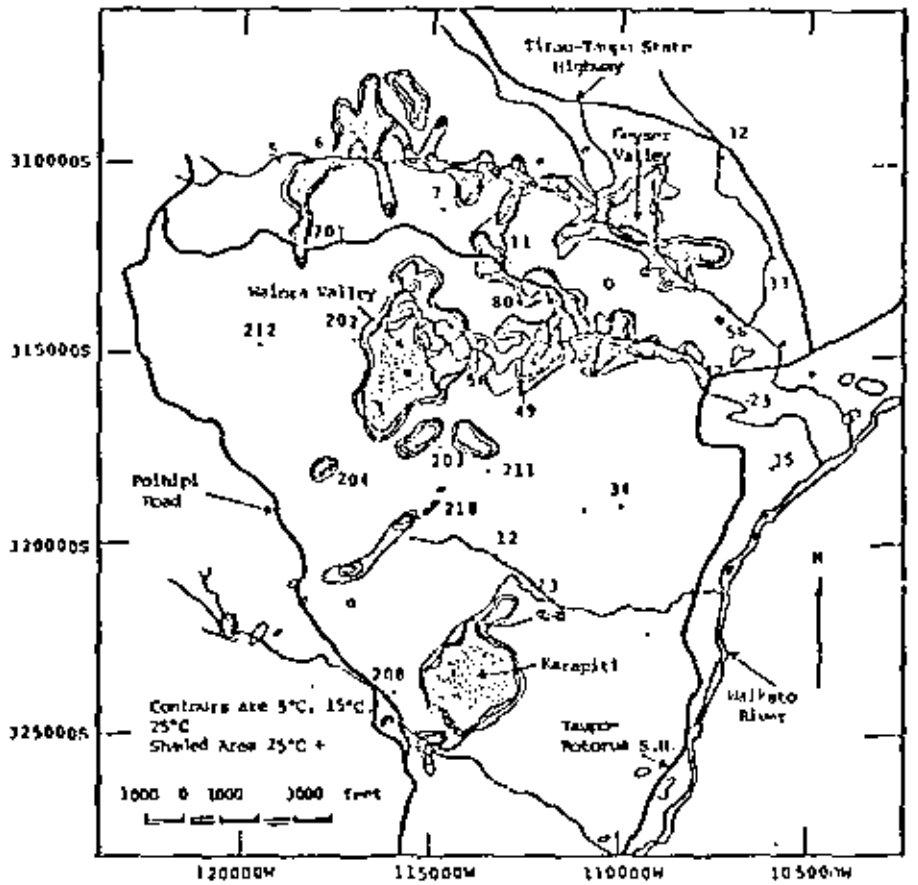

Figure 3. Temperature elevation above mean air temperature at 1 meter depth - 1966.

formation is briefly described, proceeding from deep to shallow. For more details, see the full report.[1]

Ohakuri Group

This group is composed of pumice breccias and pumiceous sediments. In the Wairakei area, the name is applied to the pumiceous pyroclastics and sediments underlying the Wairakei Ignimbrites in the region of bores 219 and 121. In bore 219, the Ohakuri Group was encountered from RL-1633 to the bottom of the hole at RL-2304. In bore 121, which was drilled in 1968, the formation was encountered at RL-3885. From that point to the bottom of the hole at RL-5940, it alternates with layers of andesite. Evidence from bore 121 suggests that the Ohakuri Group is virtually impermeable.[22]

Wairakei Ignimbrites

The Wairakei Ignimbrites have been encountered in 54 wells at Wairakei and Tauhara. The Wairakei Ignimbrite is a dense quartz-bearing formation with, according to Healy,[3] also abundant plagioclase with minor hypersthene and biotite. The ignimbrite layer lies approximately 2000 feet below the surface in the main production area and is at least 1700 feet thick in bore 48. To the northwest, in bore 219, the formation has thinned to about 800 feet and to the west in bore 121 the formation is approximately 3400 feet thick.

Waiora Formation

The Waiora Formation lies above the Wairakei Ignimbrites. It consists of pyroclastic rocks, tuffaceous sandstones, silty sandstones, grey siltstone, ignimbrites and interbedded sediments. In the main production region, the Waiora lies about 600-700 feet below the present land surface and is approximately 1500 feet thick. In the southeast and eastern regions where the ignimbrites dip steeply, the Waiora is up to 3000 feet thick. The formation has been encountered in all but a few holes at Wairakei and Tauhara. This formation is the primary aquifer which supports the production from the region. It is, in general, sandwiched between the ignimbrites below and the Huka Falls formation above. These serve essentially as aquitards. From drill logs, the formation is known to be thicker to the west in the Te Mihi Basin, where bore 207 was drilled into at least 2000 feet of the formation without encountering the underlying ignimbrites. Similarly, to the east in the Taupo-Reporoa Basin holes 60 and 37 encountered about 2500 feet of Waiora without finding the ignimbrites.

Waiora Valley Andesite

Lying interbedded with the Waiora, a little above the ignimbrite, is the Andesite Formation. It is dense and has been hydrothermally altered. The formation has been encountered in 31 wells in the region. It appears closely associated with the Waiora, Wairakei and Upper Waiora Faults, and according to Grindley[2] appears to have been

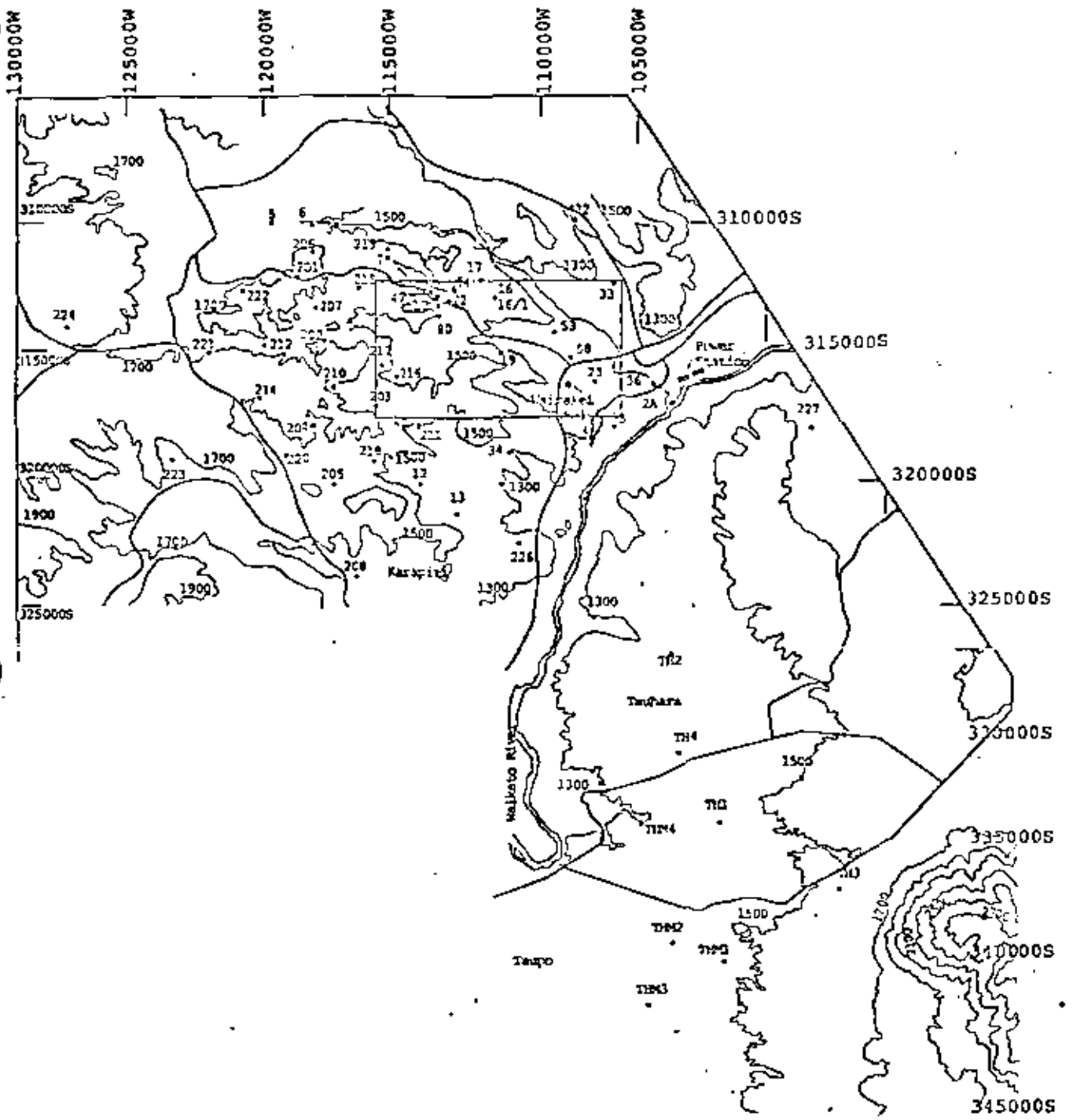

Figure 4.. Topography of Wairakei/Tauhara region showing peripheral bores (rectangular) outline denotes region shown in Fig. 5).

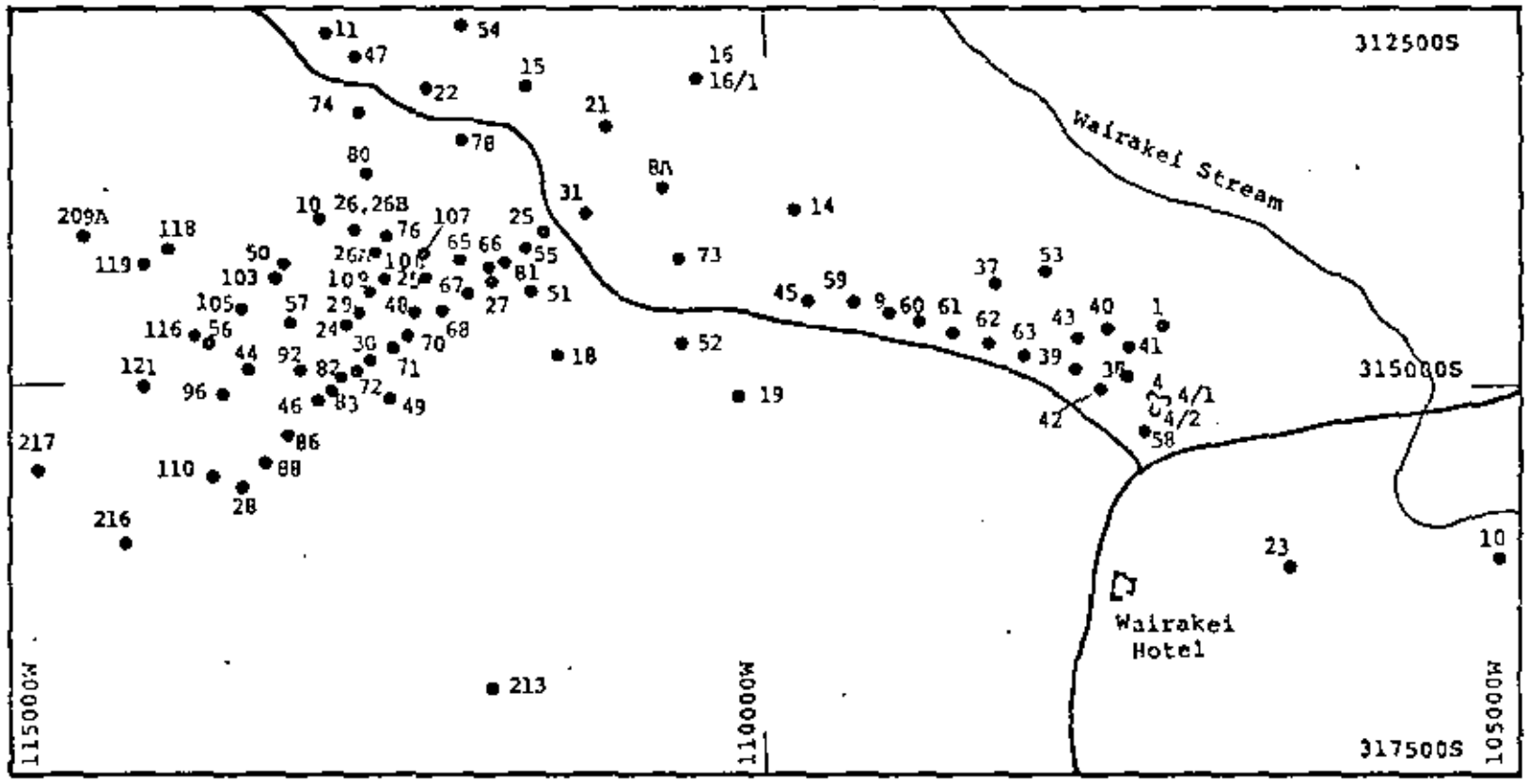

Figure 5. Bore locations in main bore field.

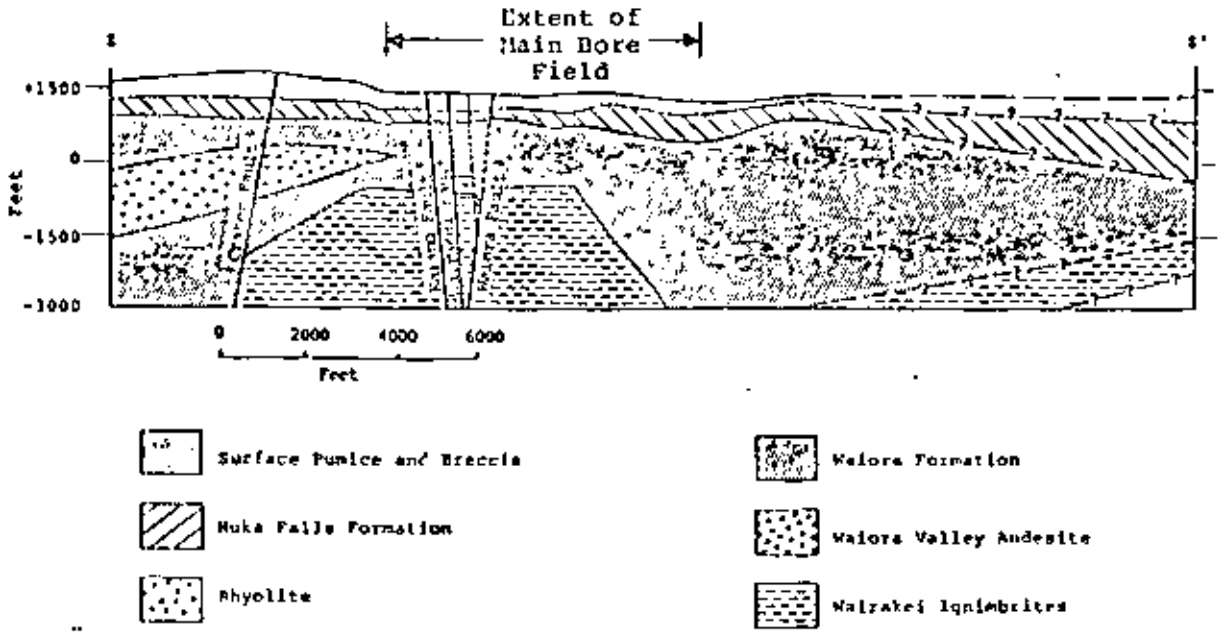

Figure 6. Section 22'.[21]

extruded along fissures at fault intersections. ... from these intersections, it appears to thin rapidly.

Haparangi Rhyolite

This name denotes the subsurface rhyolites which are encountered in drillholes in the southwestern region of the production area and also in bore 219 in the north. The formation has been encountered in 27 bores. The rhyolite encountered at Wairakei includes pumiceous, perlitic, spherulitic and banded lithoidal rhyolites, and varies from about 1600 feet thick at bore 208, to 1520 feet in 205, to 1460 feet in 210, to 230 feet in 213 and to 200 feet in bore 28. The thinning of the formation from south to north is consistent with the postulate that the flow occurred from the south.

Huka Falls Formation

This name applies to the grey siltstones, mudstones, and sandstones between the top of the Waiora formation and the base of the Wairakei breccia. This formation has been encountered in all boreholes at Wairakei with the exception of 208 and 223. It is believed to have originated as an ancient lake-bed. In general, it ranges from less than 200 feet in the southwest and northwest to between 200 and 300 feet in the western part of the production area.

Wairakei Breccia

This formation was apparently laid down as ash-flow deposits and conformably overlies the Huka Falls formation. It has been drilled in nearly all of the bores in the area, however, it is absent east of bore 4. The maximum thickness encountered in the drilling was about 550 feet in holes 5 and 6.

Recent Pumice Cover

This name applies to the pumice alluvium, wind-blown ash and lapilli and ash showers which have been deposited over the Wairakei breccia. They are found in all bores at Wairakei and are in general fairly thin layers (less than 100 feet). The pumice cover is of no real significance to this report or the stratigraphy of the region.

There are three major structures which are identifiable in the area; the Wairakei Block, the Taupo-Reporoa Basin and the Te Mihi Basin. According to Grindley,[2] the Wairakei Block is an elliptic structure extending in the north-northeasterly direction. He believes that the high gravity and magnetic values recorded at the southern end of the region may be due to the thick intrusions of rhyolite which lie in that region. The northern end of the block are characterized by lower magnetic values. Grindley believes that the ignimbrites bounded by faults may indicate there has been an uplift in the basement rock. This area of presumed uplift actually corresponds to the large concentration of deep hydrothermal activity. Indeed, over the main production region, the surface of the ignimbrites lies at about RL-700 whereas away from

the main bore field the surface of the ignimbrites is deeper; as much as 1300 feet deeper to the east.

To the east of the Wairakei Block is the Taupo-Reporoa Basin which trends again in a north-northeasterly direction between the Kaingaroa Plateau and the Paeroa and Wairakei Blocks. The greywacke basement in this region is postulated by Modriniak and Studt[8] to be about RL-8500, approximately 4000 feet lower than in the Wairakei Block. Drillholes in the eastern part of the field have provided evidence of sloping into the basin. As Grindley[2] comments, the total displacement of the ignimbrites is at least 750 feet along the fault.

The Kaiapo Graben and the Te Mihi Basin lie to the west of the Wairakei Block. The Graben is bounded by faults. The block tilts slightly eastward by about 10° and is bounded on the east by the Kaiapo Fault. The Te Mihi Basin lies as a northeasterly extension of the Graben. According to Grindley[2] it does not appear to have been fault produced.

Faults are dominant features throughout the entire Wairakei region. However, the Tauhara region is less strongly fault-dominated. Essentially all faults have a northeasterly orientation. It should be noted that the production from the region is believed to be strongly influenced by faults - indeed, as evidenced by laboratory work, the rock formations tend to have low matrix permeability. Hence, the flow through the system is believed to be primarily through the faults and associated fractures. As Grindley[2] comments, drilling of successful wells at Wairakei depends upon the intersection of the borehole with a fault -- thereby providing the necessary increased permeability. Many wells were in fact drilled in an attempt to intersect major faults. The full report[1] gives a more complete discussion of the faulting of the region.

ROCK PROPERTIES

The rock properties of principal interest for reservoir engineering studies are the porosity, permeability, density, thermal conductivity and heat capacity of the various layers. If bulk deformation effects (i.e., subsidence) are of interest, the thermoelastic properties of the rock are also required. The available laboratory data concerning these properties makes it clear, however, that the behavior of the reservoir cannot be explained in terms of the properties of the rock samples alone. That is, measured porosities are higher and permeabilities are much lower than one would expect based upon the performance of the reservoir.

Clearly, much of the effective permeability of the reservoir as a whole arises from the fracture network known to be present within the system. Since these fractures do not penetrate the entire body of the reservoir and consequently do not intersect all pores, the effective porosity (or fluid volume) for the reservoir as a whole is doubtless smaller than the actual pore volume fraction measured in individual rock samples. Likewise, the presence of such a fracture network would tend to explain the discrepancy between laboratory and in situ values for seismic velocities. Thus, for example, theoretical analyses of the reservoir response at Wairakei have used effective permeabilities of the order of 100 millidarcies and porosities of about 20 percent for the Waiora aquifer and have obtained fairly good history matches.[21,23] Grindley[2] has pointed out that the effective permeability for a well penetrating the Waiora formation appears to be dependent upon the number and size of fissures it intersects as much as upon any other parameter. This observation certainly suggests that the bulk of the Waiora permeability is "fracture permeability" as opposed to "matrix permeability". Thus, the data to be presented in this section should be used with caution.

Banwell[21] reports mean saturated and dry densities of 16 core samples taken from some of the early bores as 1.86 and 1.55 grams/cm^3, respectively. These cores were taken from holes drilled to depths of between 1500 and 2000 feet, but the locations of the cores themselves were not reported. Presumably, they represent the Huka Falls mudstones and/or the Waiora aquifer, most probably the latter. These measurements imply a porosity of 31 percent and a grain density of 2.25 grams/cm^3 for the region.

More recently, Hendrickson[21] presented the results of an exhaustive suite of thermomechanical tests upon five core samples taken from various layers in the Wairakei field; one from the surface layer, one from the Huka formation, two from the Waiora, and one from the deep Ignimbrites. Hendrickson noted that the effective porosity of a rock sample may be determined if the dry and saturated densities are known, but that the true porosity may be higher if some of the pore-space is unconnected. He, therefore, pulverized some of the sample material to obtain a direct measure of grain density and hence total porosity. For the surface pumice, Huka Falls and Waiora formations, the porosities were in range 38 percent - 49 percent. For the ignimbrite sample, porosity was about 18 percent. Permeability measurements were also conducted on the Huka Falls and Waiora samples, which yielded matrix permeabilities less than 0.1 millidarcy. In addition, Hendrickson reports measurements of thermal and elastic properties for the rock samples.[1,21]

SEISMIC MEASUREMENTS

Seismic velocity data at Wairakei are rather sparse. Penetration is handicapped by poor shooting conditions in the shallower loosely compacted pumice beds. The ignimbrites show a substantial variation in seismic velocity[8] reflecting the variation in degree of welding. Poorly welded ignimbrites cannot be distinguished seismically from alluvium or non-welded tuffs. Available velocity data,[8] when compared with laboratory measurements of seismic velocities performed by Hendrickson[21] show the laboratory values for P wave velocities to be higher than the in situ values; this difference is indicative of the presence of extensively fractured formations at Wairakei.

COMPOSITION OF THE GEOTHERMAL FLUIDS

Compared to many other geothermal fields elsewhere in the world, the water withdrawn from Wairakei is remarkably pure. Most of the information presented by Pritchett, et al.[1] is derived from the work of Wilson,[25] Ellis,[26] and Glover.[27] The total dissolved solids loading is about 4×10^{-3} by mass, consisting of primarily sodium and potassium chlorides with a smaller amount of silica and a few trace minerals. This mass loading is about one-eighth that of seawater. The incondensible gas molar fraction in the steam component of the discharge (separated at one atmosphere) is about 6.4×10^{-4}. About 90 percent of this gas is CO_2 with the bulk of the remainder being H_2S. For reservoir engineering purposes, therefore, the Wairakei fluids may be adequately treated as pure H_2O.

TEMPERATURE MEASUREMENTS

Grange[19] presented a description of the thermal activity in New Zealand as part of a general geological survey. However, it was not until the 1950's when the development of Wairakei commenced that a somewhat regular observation of temperature in boreholes was undertaken. As Banwell[24] comments, the temperature measured in boreholes cannot always be considered as an accurate reflection of the true ground temperature. This is because of convective currents which may be occurring in the borehole and because of the lack of equilibration time between drilling operations which cool the formation and some of the temperature runs which were made. However, once drilling operations have ceased, a longer standing or equilibration time is possible so that the temperature run made in the hole may yield a somewhat reliable maximum temperature in the hole.

Banwell[24] believes that bore 9, near the center of the field, could be regarded as typical of a bore in the main production region. Temperature runs made prior to 1955 appear to show that the ground temperature was above the boiling point for hydrostatic pressure at depth. Grange believes that there was initially a supply of super-heated steam in the reservoir, however, he comments that it appeared to be limited.

In 1958, temperatures measured in 25 boreholes from 1500 feet to 4000 feet deep were used to map a series of horizontal temperature profiles extending from sea level to 1640 feet below sea level. These maps are presented in the report.[1] According to Banwell these isotherms show a complex convective pattern in the western area of the field. There are cold recharge channels at several different levels with hot recharge occurring primarily at the surface of the ignimbrite formation with movement from a hot water source in the west.

As Grindley[2] comments, many fluctuations occur in the data due to geothermograph errors, the authors wish to reiterate that all reported temperature information should be used with great caution. Inasmuch as the data were recorded in cased holes, it is difficult to accurately determine the relation between the measured values and the true ground temperatures. However, the authors would feel remiss if they did not record the data available to them.

Bolton[28] points out that, over the years, temperature in the upper layers of the Waiora formation have declined, whereas at sufficiently great depth temperatures have remained essentially unchanged over the production history. In Fig. 7, average maximum temperatures in the shallow regime for wells in the production area at the beginning of 1963, 1964, 1965, 1966, 1967 and 1969 are plotted as functions of the mean bore field pressure referred to a horizon 900 feet below sea level at the same times. These data were taken from Bolton.[28] As can be seen, the data can be fitted with a straight line with slope approximately equal to 11 psi/°C. Figure 8 shows the slope of the phase line as a function of temperature. That is, if P_s is the vapor pressure of water at a temperature T_s, then the quantity plotted in Fig. 8 is dP_s/dT_s in pounds per square inch per degree Centigrade. Note that dP_s/dT_s is equal to 11 psi/°C, which turns out to be about the maximum temperature in the reservoir. In other words, the temperature decline in the upper layer noted by Bolton may be explained as a consequence of water flashing to steam in the upper part of the reservoir, and the fact that deep temperatures have not changed is because at greater depth the fluid has not flashed, but is still all-liquid. Thus, it is not necessary to hypothesize cold-water recharge to explain the temperature drop.

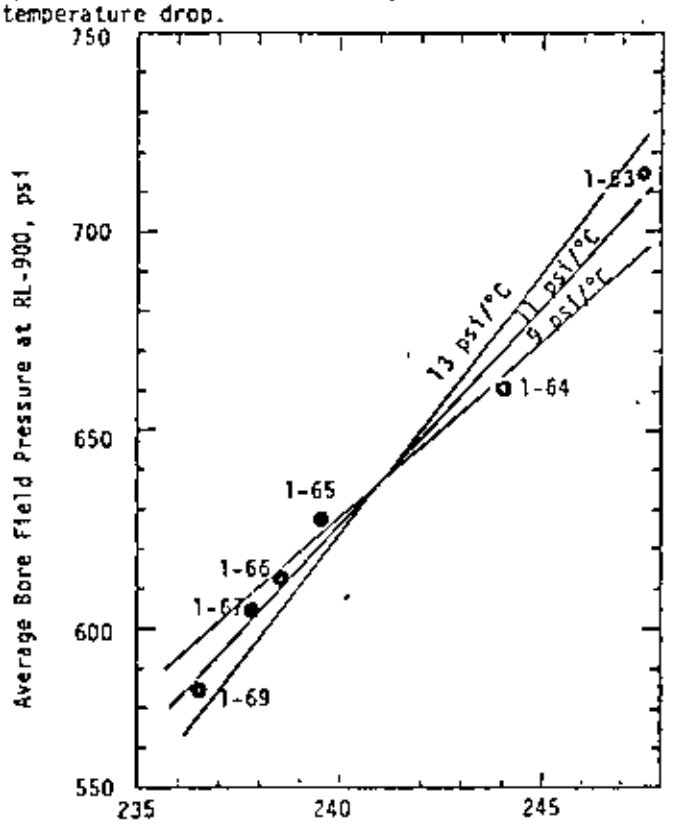

Figure 7. Average bore field pressure at RL-900 versus average maximum bore temperatures; temporal trend.

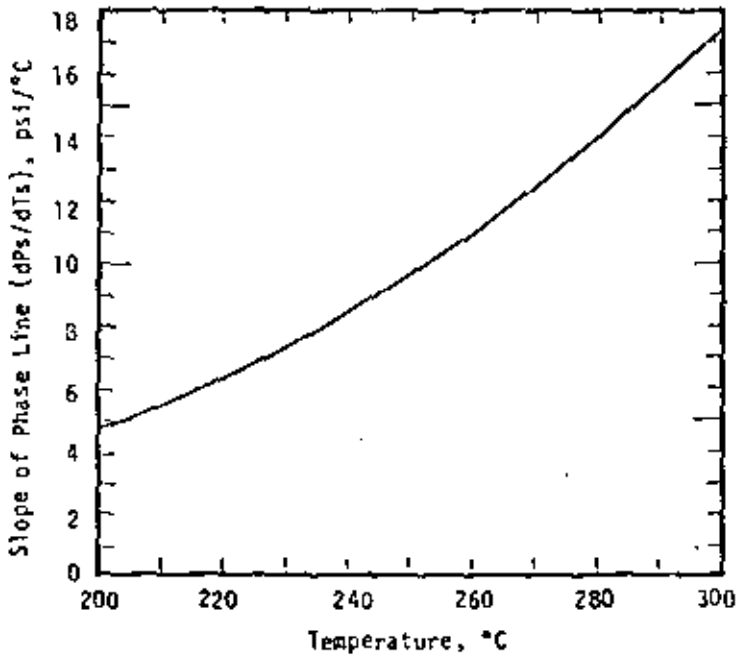

Figure 8. Slope of phase line versus temperature.

General trends in temperatures such as discussed above are probably meaningful. As Bolton[4,29] has pointed out, temperature maxima observed in wells after a long shut-in interval are probably representative of formation temperatures at the depth of the observed maxima. The detailed structure of the temperature profiles are much more questionable owing to the convective heat transfer within the shut-in wells as discussed previously. Data of this sort should be used with great caution.

MASS AND HEAT PRODUCTION

A total of 141 bores exist in the Wairakei/Tauhara field. Of these, 12 are shallow pressure-temperature monitor holes (26P and M1-M7 at Wairakei; THM1-THM4 at Tauhara) from which no fluid production takes place. Four deep bores are located in the Tauhara field (TH1-TH4) and little production has taken place there for reasons discussed in the section on pressure measurements. Of the remaining 125 bores, 26 consist of the "200 series" (bores 201-208, 209A, 210-224, 226-227). The 200 series bores are generally located to the north, south and west of the main bore field and were considered investigative bores when drilled, even though many of them are potentially good producers of high enthalpy fluid. Owing to their large relative distance from the power station, only bore 216 has been used for power production.

Sixty-five of the remaining 99 bores have produced, over their lifetime (herein defined as 1 January 1953 - 31 December 1976) a mass of fluid in excess of 5×10^9 pounds per well. These 65 bores account for about 95 percent of the total fluid produced from the entire system (Wairakei plus Tauhara plus 200 series bores). Thirty-four bores have produced over 30×10^9 pounds each, accounting for 73 percent of the total production, and seventeen bores have produced over 50×10^9 pounds each. These seventeen bores account for 45 percent of the fluid production for the system as a whole. To date, the most productive bore at Wairakei (in a mass sense) has been bore 30 (total production 81.213×10^9 pounds) followed closely by bore 27 (80.650×10^9 pounds).

Total mass production for the Wairakei/Tauhara system as of 31 December 1976 was 2329×10^9 pounds; the mean enthalpy of the discharged fluid was 481.04 BTU/pound. The total mass and energy production for each well are summarized in tabular form in Table 10.1 of Pritchett, et al.[1]

Drilling activity ceased at Wairakei in December 1960, with the completion of non-productive bore 121, which is also by far the deepest well in the area (7400 feet). The early bores were all fairly shallow and relatively unproductive. The most productive wells tend to be drilled to depths between 500 and 1000 feet below sea level. Under the main bore field, this level corresponds to the base of the Waiora formation, the andesite extrusion, and the top of the ignimbrite layer. Occasionally, a well drilled deeper into the ignimbrites will strike a fissure and prove productive, but generally speaking the vicinity of the Waiora/Ignimbrite contact has proven to be the best level for production. Accordingly, a large fraction of the bores were completed at this level. Based on the performance of the first six deep bores, three of which intercepted fissures, most production wells were deliberately sited in such a way as to intercept faults at the most productive horizon.[2]

Although the entire Wairakei/Tauhara field has now been extensively drilled, over 96 percent of the fluid production has come from the "main bore field"; a relatively small area of about one half square miles centered about one and one-half miles WNW of the power station and extending approximately from 107,000W to 114,000W and from

312,500S to 316,500S with respect to the 1949 Maketu datum.

The production rate from the field as a whole changed substantially over the years. Figure 9 shows that the rate of discharge increased to a peak in early 1964. Thereafter, with the decline and termination of drilling activity, the field pressure drop has resulted in a decline in total production of about four percent per year. The "partial shut-down" of early 1968 discussed elsewhere in the report can be clearly seen in the plot.

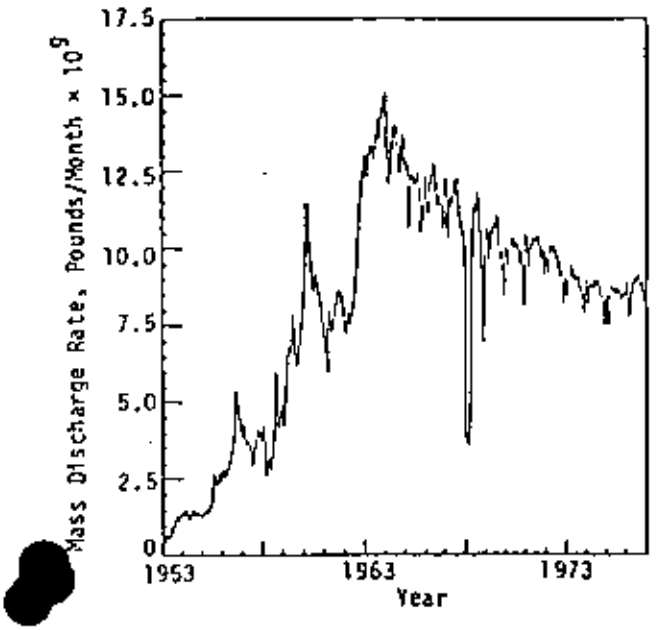

Figure 9. Mass discharge rate (all bores) as a function of time.

In Fig. 10, the trend of the average output enthalpy for all wells is displayed as a function of time. The raw data has considerable scatter, particularly during the early years when mass production rates were low. Note, however, the peak in early 1968 corresponding to the partial shut-down. This peak occurs because high enthalpy wells were preferentially maintained on production during this interval. The smoothed curve indicates a gradual increase in mean discharge enthalpy up to about 1965 followed by an equally gradual decrease. One interpretation of this trend is as follows. At early times, the steam (as opposed to liquid water) mass fraction entering the bores increased with time owing to the gradual increase in reservoir volume occupied by steam and the envelopment of the bores by a steam/water mixture. Later, however, steam and water continued to enter the bores but the drop in general reservoir pressure and temperature was accompanied by a drop in the specific enthalpy of both steam and water, resulting in a decline in mean enthalpy with time.

The overall variation of total enthalpy with time is not great; the same cannot be said, however, for the variation from bore to bore in lifetime average enthalpy. As mentioned earlier, the average discharge enthalpy for all fluid withdrawal from the system is 481.64 BTU per pound. The 200 series bores appear to be preferentially located in regions of relatively high steam quality; for those bores alone, located to the northwest, west and southwest of the main bore field, the mean lifetime discharge enthalpy is 629.20 BTU per pound. It is unfortunate that the distance to the power plant precluded more production from this area.

During the course of the drilling program at Wairakei, three mishaps occurred resulting in uncontrolled discharges from wells. Bore 201, located about a mile west-northwest of the main bore field, struck a fissure at RL+501 feet resulting in a loss of circulation and hence a loss of pressure during drilling in May 1958. The resulting flow was able to penetrate into permeable surface breccias and erupt from the surface along the line of the fault a short distance from the drilling rig. The flow shut itself off in short order and little discharge occurred.

In April 1960, an eruption of water and steam on a hillside began near bore 50 within the main bore field. For some time, it was believed that bore 50 was responsible for the discharge, but in fact the eruption was caused by a casing break at about 600 foot depth in bore 26 which had been producing fluid normally since 1954. The casing break permitted fluid to escape upward due to flaws in the cementing around the hole into the permeable layers above, and then to the surface. This activity persisted for several months, generating a mudslide which buried the bore 26 wellhead. Bore 26A was successfully deviation-drilled into the hole below the break, relieving pressure and bringing the discharge to a stop in November 1960. Bore 26 was then cemented up. The total mass and heat discharge rates were estimated as 1.7×10^8 pounds per month and 1.6×10^{11} BTU per month, respectively, for April 1960 through November 1960, yielding an average discharge enthalpy of 941 BTU/pound and a total uncontrolled discharge of 1.36×10^9 pounds.

By far the most spectacular and significant eruption to take place at Wairakei was that of bore 204, often called the "Rogue Bore". Thompson[30] has summarized the history of bore 204 which is sited approximately one mile southwest of the main bore field near the Wairakei fault. Drilling began in February 1969. After considerable trouble with circulation losses which probably resulted in a poorly cemented upper casing, in early May the drill-bit penetrated a cavity at a depth of 1224 feet and dropped five feet. The hole came under pressure and a violent eruption of dry steam, mud and rocks commenced. Within a few days, a crater 50 feet in diameter and 100 feet deep had been created, with the discharge emerging from the stub of the casing at the bottom. The eruption of steam continued for several months.

In October, the discharge abruptly became substantially wetter, and in a few days filled the cavity with water. Within a short time, the phenomenology had changed completely to periodic geysering within the water-filled crater, pronounced ground vibrations and occasional overflow

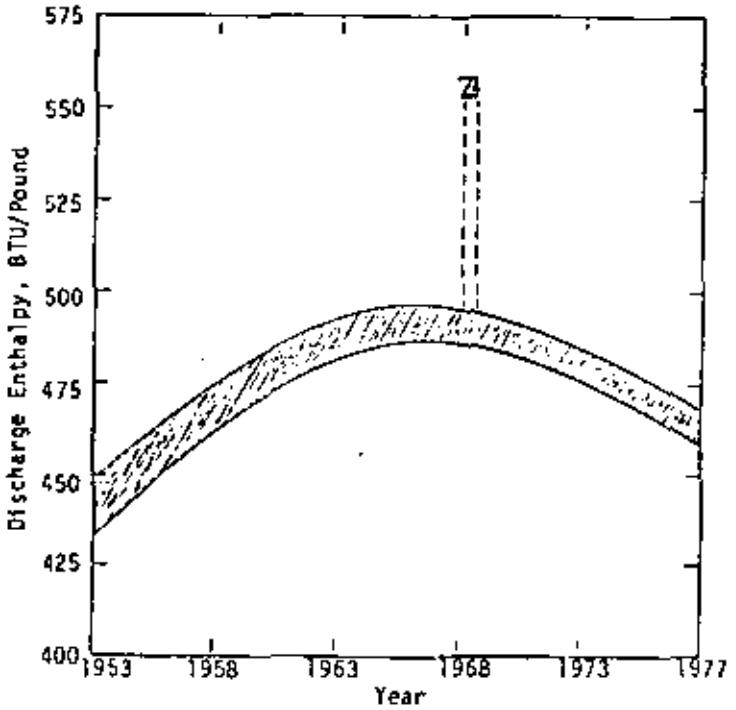

Figure 10. Trend in total field discharge enthalpy (all bores).

of the water in the crater. This general state of affairs persisted for many years with varying intensity until 1973 when between August and November activity slowly declined, water levels dropped in the crater and the whole system cooled down. By early 1974, the crater was entirely dry and activity had utterly ceased. From 1968 until late 1973, the "Rogue Bore" became a popular tourist attraction owing to the ground vibration and visual spectacle produced by the discharge.

Once again, no direct measures of enthalpy or discharge rates are available for bore 204. Estimates of the discharge enthalpy and flow rates for the period of uncontrolled discharge have been based on values discussed by Thompson[30] and Banwell[31] and on the discharge enthalpy of other wells in the area. The total discharge is estimated at 8.1×10^9 pounds with a mean discharge enthalpy of 500 BTU/pound.

Aside from the estimates for uncontrolled discharge listed above, the well-by-well monthly mass and heat production data stored on the magnetic tape were taken directly from data banks maintained by the Ministry of Works in New Zealand. This data was obtained in three different forms. Monthly mass and heat production totals for each well were at one time kept on a data file manipulated by programs written for an IBM model 650 computer. The punched card decks containing this data have long since been lost and the IBM 650 itself now resides as an inert exhibit at the Museum of Transport and Technology in Auckland. Microfilm copies of output listings of the monthly totals from January 1953 through December 1962 were, however, retained and were the source of data for the present compilation up to that date. Production prior to 1953 was very slight: total field production for 1952 was approximately one-third that for 1953 (which was itself very small) and in earlier years even less.

From January 1963 through December 1966, hand written logs were maintained, once again, of monthly total mass and heat production for each well. Finally, starting in January 1967, a new computerized system was implemented which recorded, among other things, weekly mass and heat production figures for each well. A magnetic tape containing this information was kindly supplied by R. S. Bolton of the Ministry of Works for this study. Thus, a complete record of monthly mass and heat production figures for each well from January 1953 through December 1976 was compiled.

PRESSURE MEASUREMENTS

Extensive measurements of pressures have been carried out in the main Wairakei bore field as well as in surrounding holes over the years. Bolton[4,28] provides an excellent summary of the bore field pressure data and that for some of the peripheral bores, particularly as they relate to the discharge history, for the interval 1953 through 1968. Bolton[28] also presents substantial detail concerning the pressure response to the partial shut-down of early 1968. Grant[33,34] discusses pressure response in the Tauhara field and performed an analysis suggesting substantial hydraulic connection between Wairakei and Tauhara. In this section, this work is summarized and extended as necessary to include the most recent available pressure data. Substantial amounts of

pressure data are also included in the bore-by-bore data summaries contained on the magnetic tape. For a more detailed treatment, see Pritchett, et al.[1]

Borehole pressures at Wairakei were generally determined in one of two ways. In the early days, no direct measurements of pressure were made. Frequently, however, temperature profiles were measured in shut-in wells. The applicability of this data as concerns true formation temperatures is somewhat questionable (as discussed elsewhere) but, if the water level in the well is known, it is possible to calculate a density profile from the temperature profile in the well. Then, by assuming hydrostatic equilibrium, the pressure-depth curve within the bore may be determined.

Beginning about 1959, an Amerada Bourdon-tube type pressure gauge was acquired and by 1962 most pressure profiles in the bores were obtained by direct measurement. Bolton[29] estimates the accuracy of the earlier indirect determinations as ± 20 psi and of the direct measurements as ± 10 psi.

A summary of the pressure-depth profiles determined by either method for the entire history of the Wairakei field would be exceedingly cumbersome. The raw data and charts upon which such a summary need necessarily be based are contained in files occupying approximately fifteen linear feet of book shelf space at the Ministry of Works laboratory facility near the Wairakei site. Instead, Bolton and others have found it expedient to consider pressure data from each hole, at a particular time, referred to certain discrete imaginary horizontal planes within the reservoir. The two most popular choices are the RL-500 and RL-900 levels (500 feet and 900 feet below sea level, respectively). Since within the shut-in bores the pressure distribution is essentially hydrostatic, a single datum such as at one or another of these levels can then approximate the entire pressure profile at a particular point in time.

On the magnetic tape which is an essential part of the report, numerous such values of pressure at both RL-500 and RL-900 have been recorded as a function of time. Many wells have data at both levels. The RL-500 data extends from 1955 to 1976; RL-900 data is available only for the interval 1959 to 1967, plus some data for 1968.

As Bolton[4] and others have pointed out, the pressure response of the main bore field to fluid withdrawal has been remarkably uniform across the entire area, suggesting a high degree of horizontal communication and thus a high permeability for the Waiora aquifer. The pressure data for RL-500 for all data on the tape is given in Fig. 11 and for RL-900 in Fig. 12 as a function of time. Note the similarity in the two sets of data. This same information is presented somewhat differently in Fig. 13, which illustrates the pressure drop as a function of total cumulative discharge. It can be seen that there is little difference between the RL-500 and RL-900 data, except for a shift in scale due to the greater hydrostatic head at RL-900. Actually, there is a slight areal dependence of pressure. Bolton[4] indicates that pressures are somewhat lower in the eastern portion of the bore field than elsewhere, but that the difference between the two areas is not large in comparison with the overall drawdown. A general pressure increase exists from east to west across the field. This tends to confirm the conclusions drawn from magnetic evidence that the general flow in the system prior to production was from west to east.

Three distinct regions in the pressure history of the bore field can be discerned (see Figs. 11 and 12). Pritchett, et al.,[21] using a numerical two-phase two-dimensional vertical section reservoir simulation has attempted to explain the behavior as follows. During the early years (prior to 1958 or so), boiling begins below the Huka mudstones and a steam cap forms near the top of the Waiora aquifer - this process maintains nearly-constant pressures at early times at the deeper production horizons. Later (1959-1963), the two-phase region begins to invade the production horizon, and pressures drop rapidly due to fluid mobility inhibition owing to the relative permeability effect. Still later (post 1965) the entire Waiora aquifer below the main production area begins to boil; the drawdown curve begins to flatten since vaporization around the wells provides pressure support for the system as a whole. Also, as discussed elsewhere, gravity measurements suggest a substantial increase in recharge rate in this latter period, which would provide additional pressure support. At present, pressures in the aquifer are declining only very slowly even though fluid withdrawal rates remain quite high. Figure 13 also supports this general overall hypothesis. As time goes on, the slope of the drawdown-discharge curve decreases, due both to increasing recharge and to a gradual increase in overall fluid compressibility as more and more liquid water in the formation flashes to steam.

The relevance of Fig. 13 to the character of the reservoir response (i.e., single-phase versus two-phase flow) may be shown in the following way. Let us tentatively assume that the pore space in the reservoir is filled entirely with compressed liquid water at an average temperature of 250°C. We will take the average thickness of the Waiora aquifer as 1300 feet, and assume that the effective "area" of the reservoir is 15 km^2, as estimated by Grindley.[2] We further assume that the porosity is 35 percent, and that (according to gravity change evidence) the recharge rate was about one-half the production rate in the early years (pre-1964). It may be shown that the average drawdown versus withdrawal curve will be given approximately by:

$$\frac{dP}{dM_p} = -B\left(\frac{\dot{M}_p - \dot{M}_R}{\dot{M}_p}\right) / (\phi HA)$$

where

P = pressure

M_p = cumulative mass produced

$\dot{M}_p$ = production rate

$\dot{M}_R$ = recharge rate

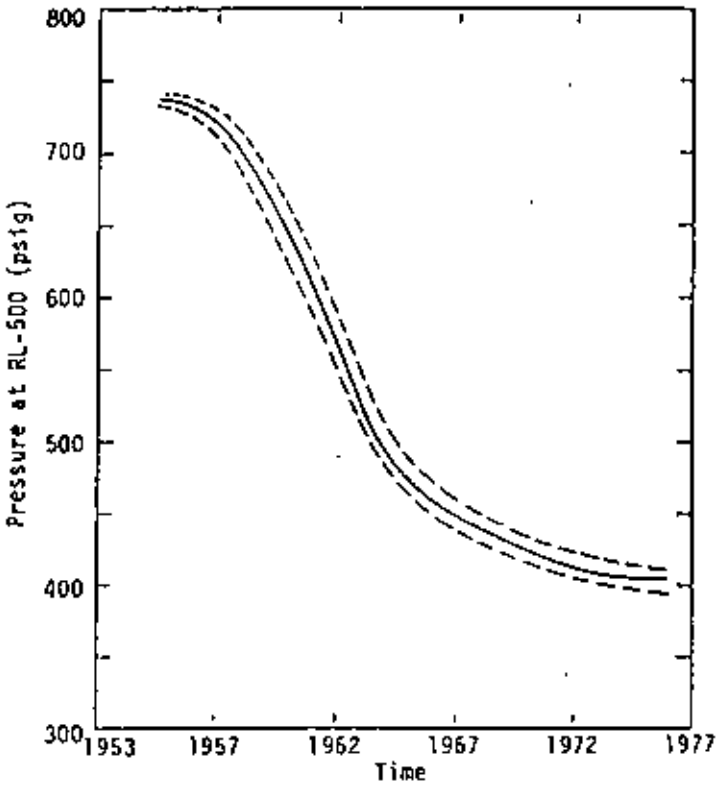

Figure 11. Pressure measurements at RL-500 as a function of time for bores following the trend of the main bore field.

ϕ = porosity

H = aquifer thickness

A = reservoir area

B = $(\partial P/\partial \rho)_{T=const}$; available from steam tables.

Using the values listed above and assuming that, for compressed liquid water at 250°C, B = 8.93 × 10^5 m^2/sec^2, we obtain

$$\frac{dP}{dM}_p \approx -14{,}000 \text{ psi}/10^{12} \text{ pound.}$$

Figure 13 indicates a much smaller value; about -300 psi/10^{12} pound at early times, and even smaller later. That is, the actual response of the reservoir is much more compressible than it would be were it single phase, by a factor of order 50. This appears to be conclusive evidence for two-phase (water/steam) flow throughout the Wairakei history.

In early 1968, a temporary surplus occurred in the New Zealand electrical power grid due to the commissioning of new equipment at the Marsden hydroelectric station. Advantage was taken of this circumstance to perform a "partial shut-down" of the Wairakei geothermal plant which began on December 21, 1967 and lasted 104 days; that is, to perform a "shut-in test" on a grand scale.[32] Although electrical output was reduced by about half, the total mass production rate was cut by a factor of three by retaining on-line only bores of unusually high enthalpy production. The response of the bore field to this perturbation was dramatic. Within a few weeks, pressures throughout the field began noticeably to increase - although the data is somewhat scattered, the pressure rise averaged about 11 psi by the end of the shut-down. Once the shut-down was over, pressures quickly dropped again to their pre-shut-down values. Bolton[29] and others (the authors included) feel that any adequate theoretical model of the transient behavior of the Wairakei field should be capable of reproducing the pressure-transient effects of the partial shut-down.

Bolton[4] presents a summary of the pressure data for other bores surrounding the main bore field in an attempt to establish the locations of hydrological boundaries for the field. For the subsequent discussion, reference should be made to Fig. 14, which shows (among other things) the spatial relationships among the various peripheral wells, the main bore field, and the "resistivity boundary" of the Wairakei/Tauhara field. For the purpose of this figure, the resistivity boundary

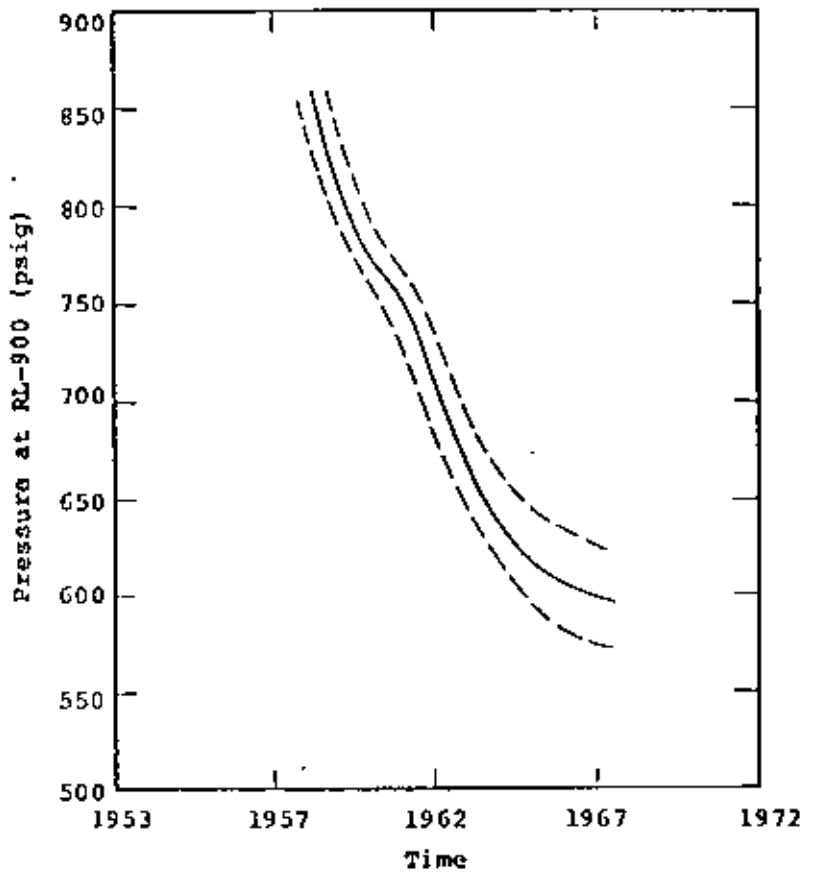

Figure 12. Pressure measurements at RL-900 as a function of time for bores following the trend of the main bore field.

is taken as the region between the 10 and 20 ohm-meter contours.

Bore 36 is located to the southeast of the main bore field near the power station between the 10 and 20 ohm-meter resistivity contours. It produces fluid of only moderate temperature and has consequently never been used for power generation. Prior to 1959, pressures in bore 36 followed those in the main bore field. Thereafter, however, when the main bore field pressure began to drop rapidly, the rate of pressure decline in bore 36 remained much the same as before. The disparity in pressures between the bore field and bore 36 has been increasing ever since.

Bore 33, located to the northeast of the main bore field just outside the resistivity boundary appears to have little if any connection to the field.

Bores 219, 206 and 222 represent the northern limit of drilling and lie to the northwest of the bore field. All are high-temperature bores with maximum temperatures exceeding 250°C. Pressure histories for all three bores follow the trends of the main bore field. Thus, the northwest boundary of the field has not been established by drilling.

Bore 224 is the westernmost hole drilled at Wairakei, and is cold (T_{max} = 82°C). It is well beyond the 20 ohm-meter contour as well. Pressures in bore 224 are, however, influenced to some extent by fluid production from the bore field.

Bore 223 is located west-southwest of the bore field, well beyond the resistivity boundary. It is also a cold well but, somewhat surprisingly, the pressures in bore 223 follow the main bore field very closely. Bolton[4] speculates that the bore is fault-connected to the main bore field, and that the low temperatures are due to a local down-flow of cold water which meets an up-flow of hot water from below at a depth below the bottom of the hole; the mixed fluid then flows toward the bore field through the fault system at a deep level.

Bores 221, 212, 214, 210, 220 and 205 are located somewhat closer to the bore field along the resistivity boundary, between bore 223 and the main bore field. Temperatures in bores 214 and 220 are somewhat lower than the main field; the other four wells are quite hot ($\geq$ 250°C). None of the six have been produced extensively; pressures in all six follow the main bore field very closely.

Bore 208 (to the south-southwest of the bore field) and bore 226 (due south) are both

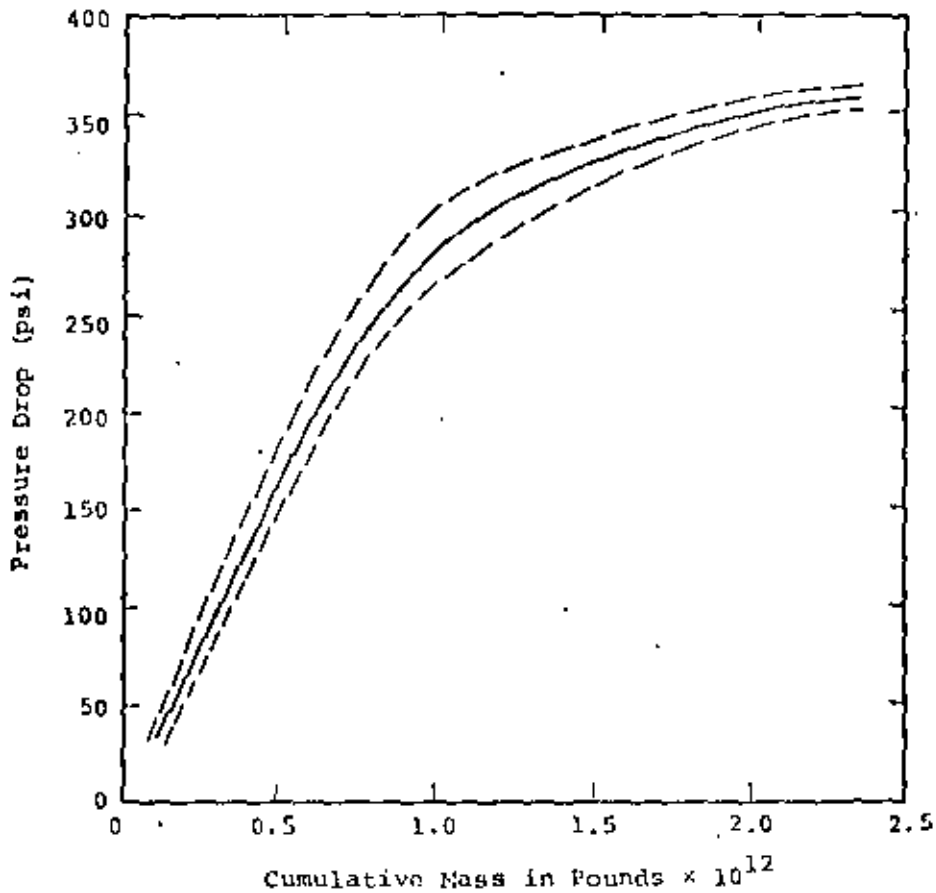

Figure 13. Main bore field pressure drop as a function of cumulative produced fluid mass. Plot includes RL-900 and RL-900 data.

somewhat cooler than the major production bores, and neither has been produced for power. Both lie within "islands" of higher resistivity within the general resistivity low. Pressures in both holes follow main bore field trends. Thus, as in the case to the north, the southern boundary of the field has not been established by drillhole pressure evidence.

The bores in the Tauhara field were drilled late in the history of the Wairakei development program - the first (TH1 - originally designated bore 225) was completed in June 1964. It had originally been thought that the Tauhara field was a separate resource, but it soon became apparent that the drawdown from Wairakei was influencing Tauhara. It was, therefore, feared that power production from Tauhara would cause premature depletion of Wairakei. Consequently, only eight holes were drilled at Tauhara of which four were shallow monitor bores. Total fluid production from Tauhara has been about 5.9×10^9 pounds, of which 95 percent was from bore TH1; Tauhara production as a whole amounts to about 0.25 percent of the total for the system.

Since production had been taking place at Wairakei for more than a decade before the completion of bore TH1, no direct measures of early pressures are available for the Tauhara bores. Grant[33] has estimated the initial gauge pressures in the four deep Tauhara bores at various levels as if the bores were located at the center of the main Wairakei bore field with the same wellhead heights. He concluded that substantial pressure reductions had taken place at Tauhara prior to th time the bores were drilled. The greatest pressure reduction is believed to have taken place in bore TH2; approximately 240 psi at the time of completion in May 1966. At this same time, the pressure drop in the main bore field was about 270-280 psi. Drawdowns in the other three bores are less, owing to their greater distance from tl main production area. There can be little doubt that the two reservoirs are connected, probably ' a thin neck between bores 226 and TH2. Indeed, the pressure drop at Tauhara has caused some con cern in the nearby town of Taupo, where surface manifestations such as increases in regions of steaming ground have been noted in recent years. It seems clear that, in modeling the behavior of the Wairakei field, it is essential to consider Wairakei and Tauhara as two parts of a single, larger geothermal field.

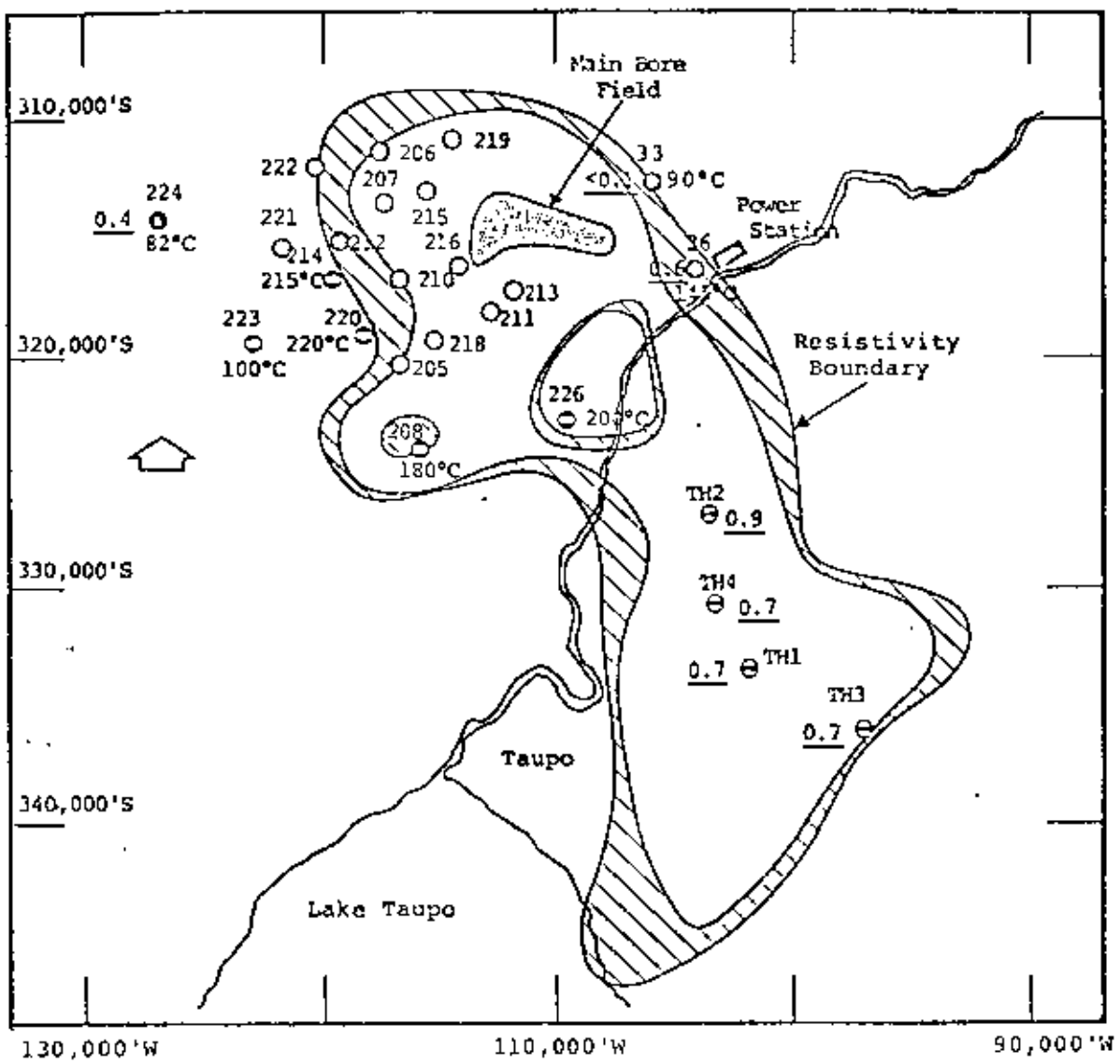

25 ○ Location and numbers of bores with maximum temperature > 225°C and with pressure histories matching main bore field.

36
0.6 ○ Bore with maximum temperature < 225°C
145°C (i.e., 145°C) and with total pressure drop only a fraction (i.e., 0.6) of that of the main bore field as of mid-1968.

223
○ Bore with low maximum temperature whose
100°C pressure history follows main bore field.

TH2
0.9 ○ Bore with maximum temperature > 225°C with less pressure drop than main bore field.

Figure 14. Pressure and temperature distribution surrounding the main bore field.

GRAVITY MEASUREMENTS

Gravity surveys of the Wairakei/Tauhara vicinity were carried out in 1950[35] and in 1961, 1967, 1968, 1971 and 1974.[36,37] Hunt[38] indicates that the changes between successive gravity surveys must be due principally to vertical motion of the ground surface (subsidence) and to net mass changes in the field.

Hunt[37] noted that even though comparable quantities of water were withdrawn from the field in the intervals 1961-1967 and 1967-1974, the gravity changes in the earlier interval (corrected for subsidence effects) were substantially greater than the later changes. He, therefore, concluded that the rate of recharge increased between the earlier and later intervals. Using data from Benchmark A97, located near the eastern edge of the bore field and adjacent to the region of maximum subsidence, Hunt then qualitatively estimated the cumulative mass balance as a function of time for Wairakei, as shown in Fig. 15.

SUBSIDENCE AND SURFACE DEFORMATION

Ground subsidence at Wairakei was first measured in 1956 when benchmark levels were compared with those established in 1950.[39] A subsidence network was then established, first on the steam main supports and then outward in the field. Periodic measurements have indicated that the area affected by subsidence exceeds 11.5 square miles.[40] It is noteworthy that the area of maximum subsidence lies outside the main production region. Maximum subsidence at Wairakei is of the order of 15 feet; this has been accompanied by horizontal movements of the order of 1.5 feet.[41]

A benchmark (A93) situated about 3 miles northeast of Wairakei has been arbitrarily chosen as datum for precise leveling. Indications are that any subsidence that may be occurring at this point is likely to be small. Local subsidence in the bore field is measured relative to benchmark TH7 located in the power house. The power house is not completely outside the zone of subsidence; it is, however, believed to be sufficiently so for local subsidence checks.

A horizontal control network was set up in 1966 and repeated in 1968, 1969, 1972 and 1975. The last horizontal survey was done in 1977.[42]

Periodic surveys of benchmarks have indicated that the area affected by subsidence (> 10 mm/year) exceeds 11.5 square miles (Fig. 16). Within this area are two zones each of about 0.4 square miles which have subsided comparatively rapidly. The zone at Karapiti - an area of natural thermal activity about 2 miles south of the production field - was the most rapidly subsiding part of the survey network until about 1963, when the subsidence rate decreased to the same rate as for the surrounding ground surface.[40]

Around 1960 the subsidence rate of benchmark A97 began to increase and over the next several years the zone of rapid subsidence immediately north of the eastern production field (Fig. 16) was delineated. Subsidence at BM A97 is shown in Fig. 17. This region of subsidence is of substantial economic interest as both the steam mains and waste water canals from the production field cross this area. Benchmarks in this region, as noted elsewhere, are surveyed annually.

The last comprehensive survey of benchmarks was conducted in 1971. The subsidence history at several selected benchmarks is presented in the report.[1] Figure 18 shows the average subsidence rate in the Wairakei production field (relative to benchmark TH7 in the power house) for the period 1964-1974.

The horizontal movement vectors at Wairakei for the period 1966-1974 show that vector movement is towards the center of subsidence. Annual horizontal movement between 1960 and 1977 was between 4.3 inches/year at a radius of 800 feet from the center of subsidence decreasing to about 0.6 inches/year at 2500 feet radius.

DATA COMPILED ONTO MAGNETIC TAPE

A primary product of the project is a magnetic tape which contains a summary of well-by-well information for the bores at Wairakei and Tauhara. This compilation of data includes information such as locations, completion dates, geologic horizons

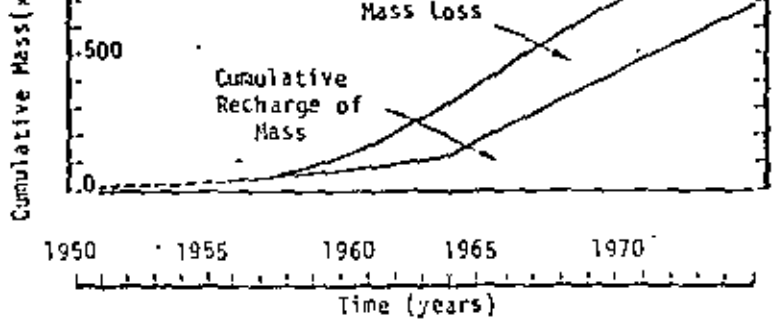

Figure 15. Cumulative recharge and cumulative net mass loss, estimated from corrected gravity differences at benchmark A97, Wairakei Geothermal Field.[37]

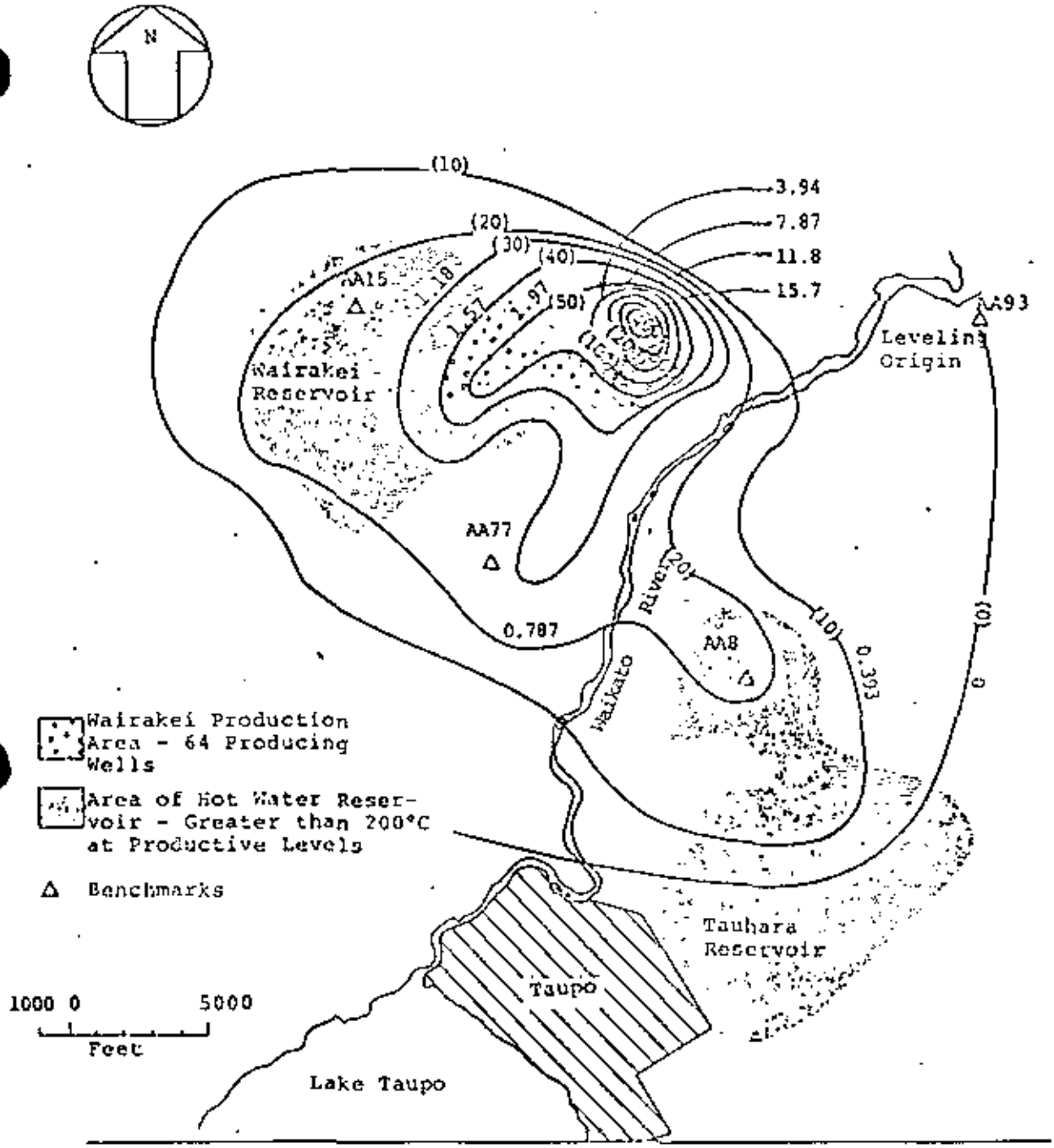

Figure 16. Average land subsidence rates, 1956-1971. Contours of equal subsidence in inches per year. Values in parenthesis are millimeters per year.

CURSO: "INGENIERIA DE RESERVORIOS GEOTERMICOS"

OCTUBRE, 1981.

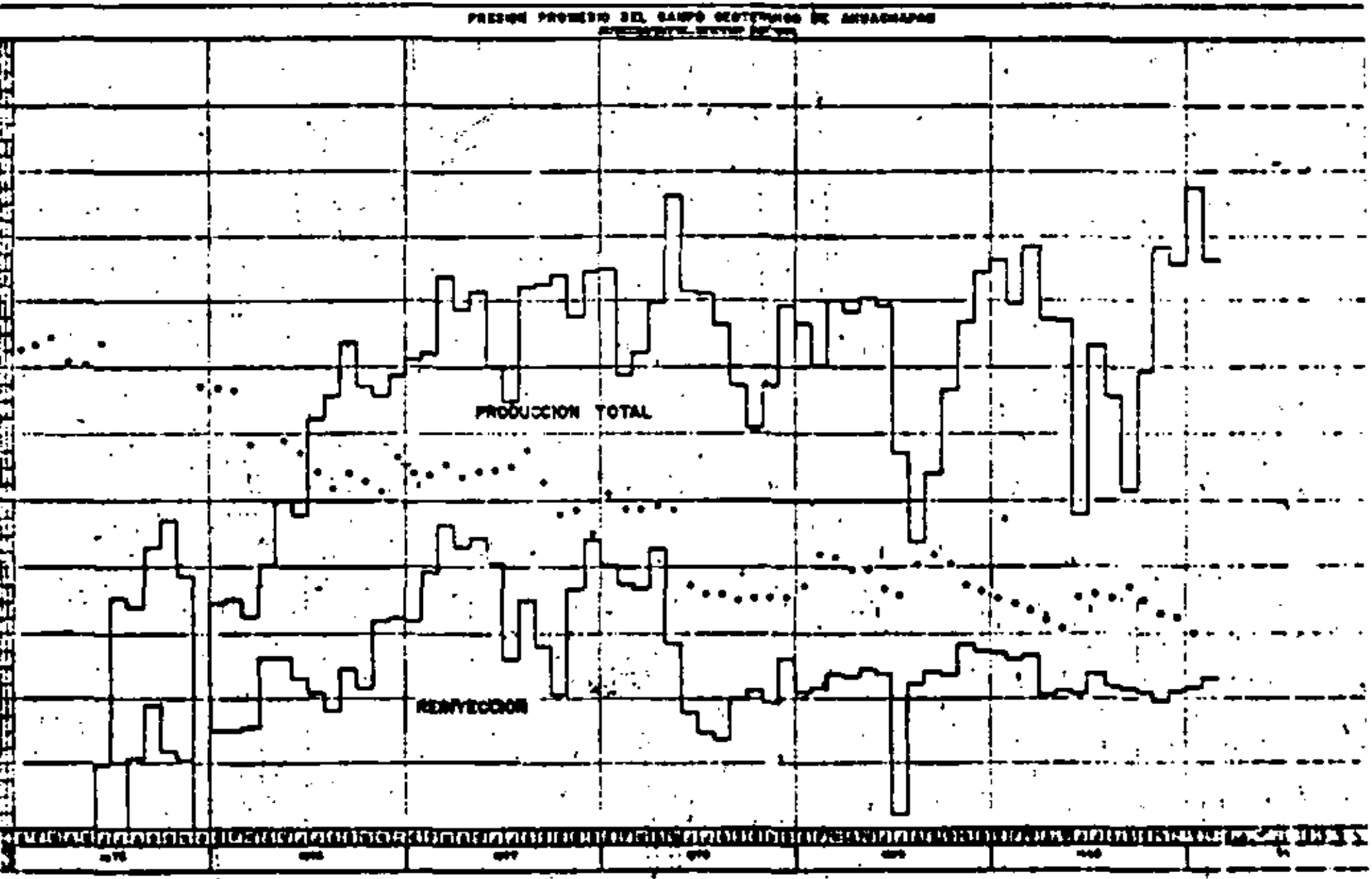

FIG. ___, Comparación ___ al de la presión promedio del campo con la extracción de ___.

AÑO / MES	1968	1969	1970	1971	1972	1973	1974	1975	1976	1977	1978	1979	1980	
ENERO		20.7	217.7	220.0	696.3	692.7	00.0	29. .8	567.1	781.4	861.7	1113.4	1251.3	
FEBRERO		96.5	182.7	183.9	693.3	21.3	00.0	112 .8	408.4	680.0	658.1	970.	1127.5	
MARZO		84.3	407.5	81.6	768.7	70.6	00.0	111 .3	338.9	781.6	708.6	1173.0	1302.0	
ABRIL		00.0	90.0	185.6	691.9	230.3	00.0	. .8	278.7	711.8	737.1	1148.8	1138.0	
MAY		27.8	116.8	16.0	708.6	421.4	884.0	330.3	473.2	748.9	1388.3	1176.8	1128.6	
JUN		30.9	223.6	15.6	961.8	218.5	846.3	160.2	492.1	890.0	1278.1	1164.7	848.1	
JULIO		20.7	304.8	178.2	628.0	203.9	976.0	680.4	821.2	776.8	1330.4	1106.2	988.2	
AGO	31.0	38.5	276.3	242.5	877.6	191.3	484.9	365.9	950.5	934.0	1283.9	487.4	880.3	
SEPTIEMBRE	178.9	21.6	378.9	400.0	814.3	231.0	000.0	683.8	978.1	1090.7	841.3	678.1	606.4	
OCTUBRE	1205	000	532.9	0000	439.3	56.4	291.8	799.9	804.0	1268.5	791.5	820.0	977.9	
NOVIEMBRE	250.6	20.3	489.7	1152	867.4	000.0	406.0	849.0	875.0	815.8	988.9	1094.4	1376.7	
DICIEMBRE	244.9	22.0	493.6	988	841.6	127.9	432.0	000.0	728.9	894.3	1080.4	1208.3	1295.1	
Σ	889.9	251.3	3825.0	1964.7	7896.3	2465.1	3710.7	4596.7	7435.1	9828.2	11928.1	12236.6	12612.3	
ACUMULADO	8258	1077.1	5002.1	6966.8	14863.1	16650.4	20361.1	24957.8	32370.8	42200.1	54228.2	66464.8	79077.1	

COMISION EJECUTIVA HIDROELECTRICA DEL RIO LEMPA C E L

RECURSOS GEOTERMICOS

CONTROL DE MASA META EXTRAIDA KILOTONS
ANUACHAPAN

DIAGRO M. CHOUSY R.	APROBO S. CUELLAR
DIBUJO F. ZAMORA R.	REVISO M. CHOUSY

TABLA 2, Control anual de masa extraída. (1968-1980).

POZO / MES	AH—2	AH—8	AH—29	AH—19			TOTAL	ACUMULADO
ENERO	823760	119381	203453	—			546602	[illegible] 20410840
FEBRERO	218198	111079	100167	—			519042	20929882
MARZO	214656	119381	195991	—			530028	21459910
ABRIL	147328	93079	181938	—			422336	21882246
MAYO	182487	99850	181462	—			417798	22300044
JUNIO	147810	93060	170190	—			411360	22711404
JULIO	185327	98410	151901	31956			475194	23186598
AGOSTO	189052	62748	131048	73127			456078	23642676
SEPTIEMBRE	164782	—	181372	110670			456824	24099500
OCTUBRE	121699	53027	171806	96449			441981	24541481
NOVIEMBRE	149089	107076	191309	—			391474	24932955
DICIEMBRE	190575	95739	152900	17978			423092	25356047
TOTAL	2030851	1012923	1894287	361177			5403888	

TABLA 6. Control mensual de agua reinyectada por pozo (1988).

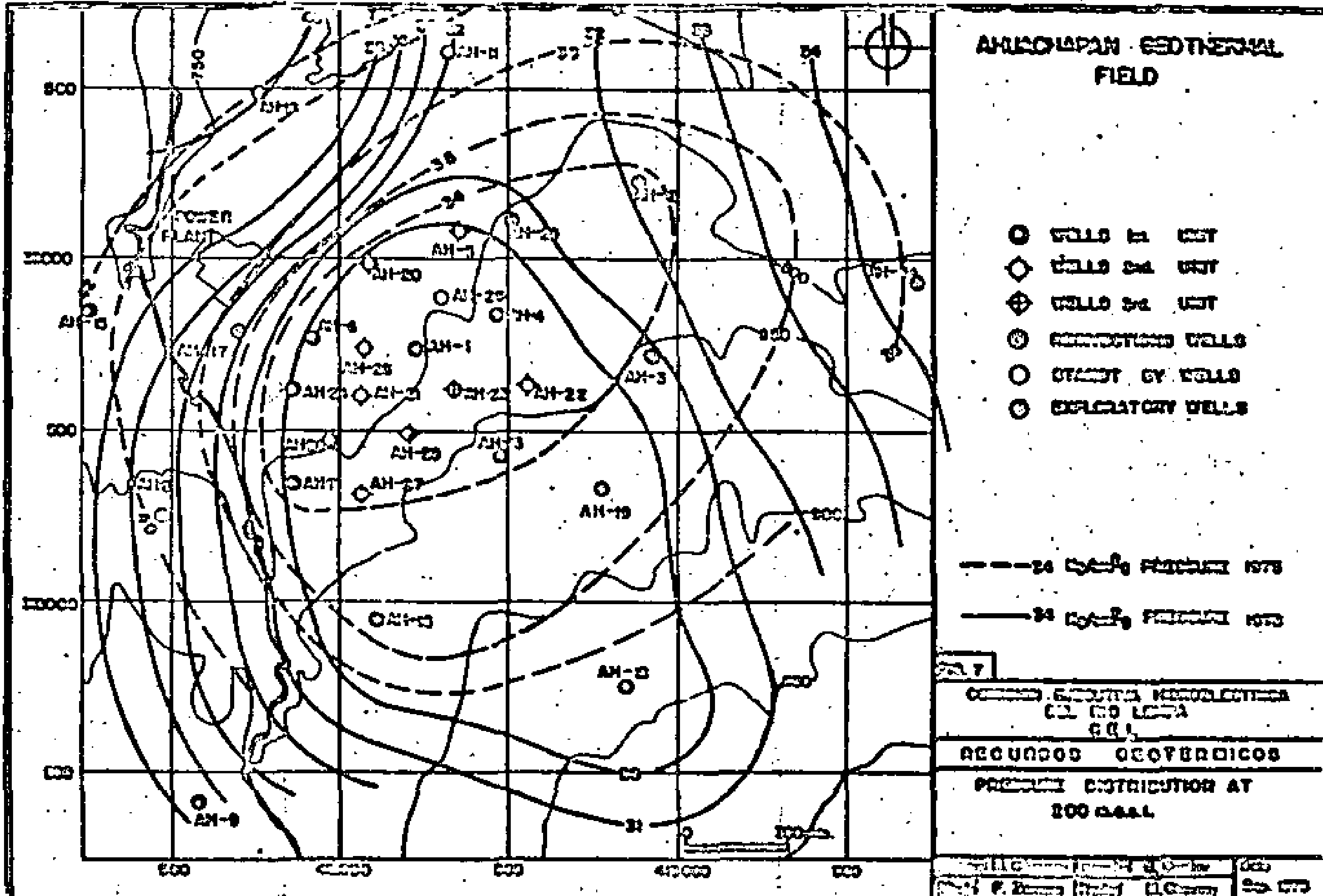
AHUACHAPAN GEOTHERMAL
FIELD
POWER
PLANT
RECURSOS GEOTERMICOS
PRESSURE DISTRIBUTION AT
200 m.s.l.

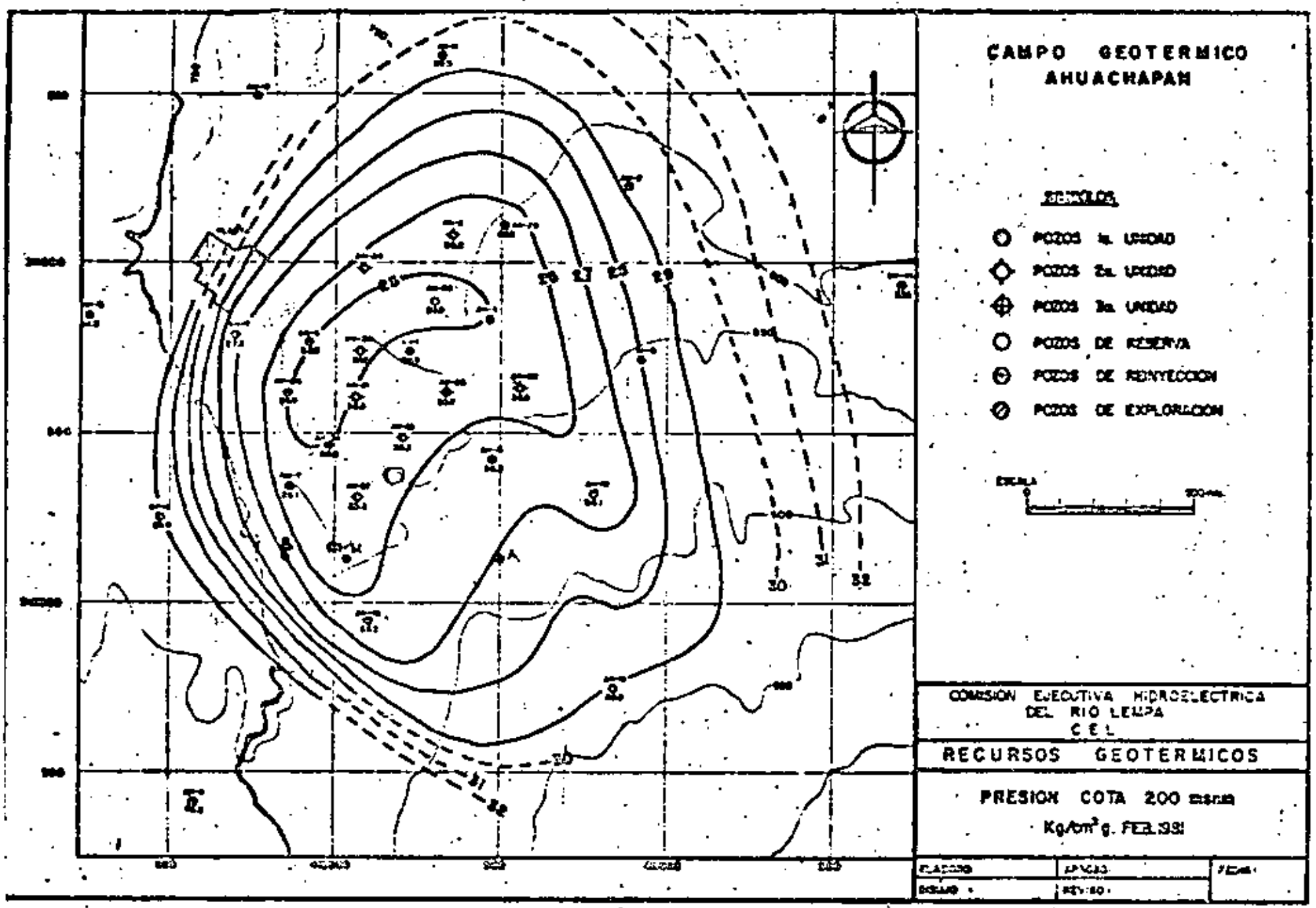

FIG. Distribución de presiones a Febrero 1

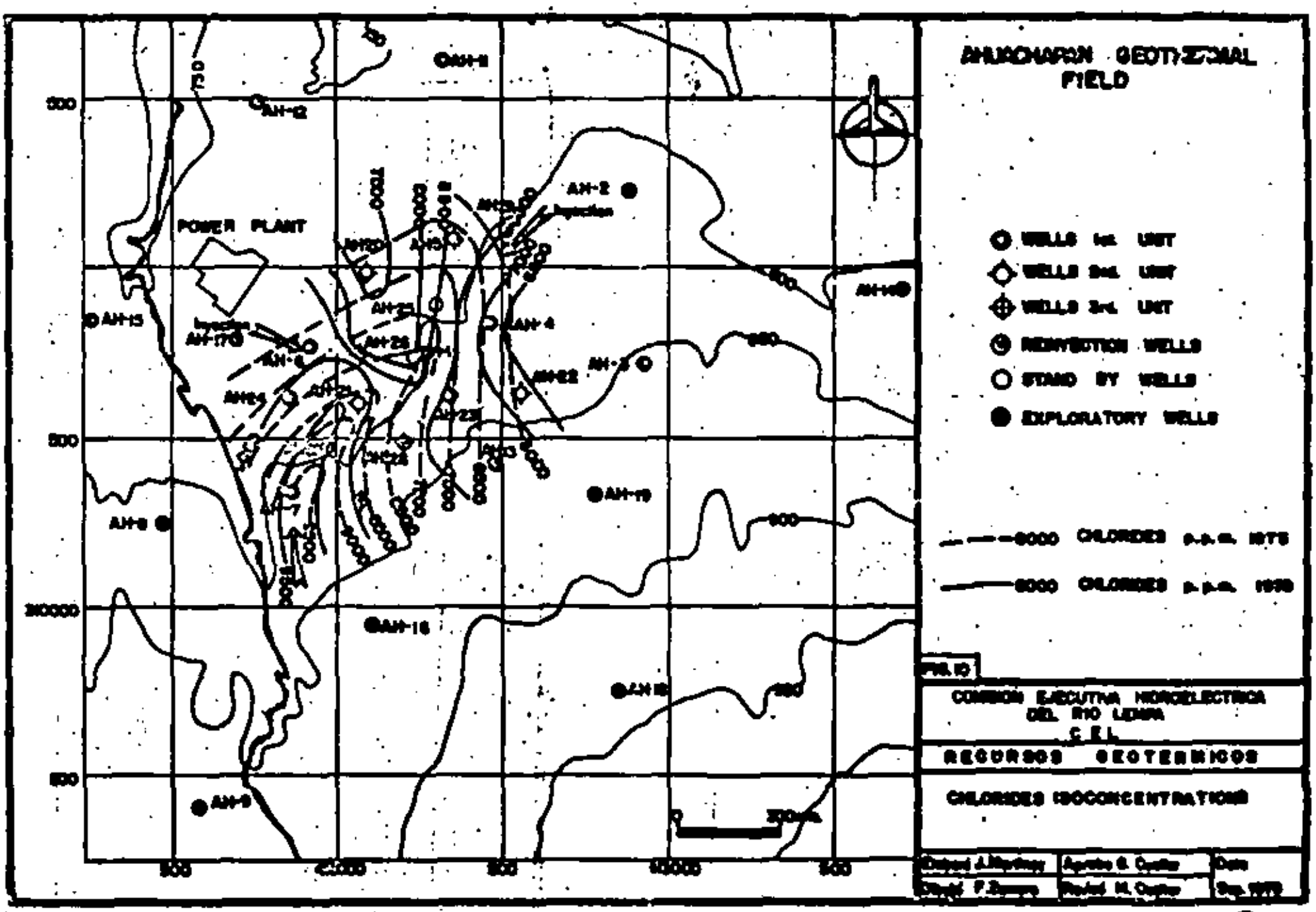
AHUACHAPAN GEOTHERMAL FIELD
POWER PLANT
AH-1
AH-2
AH-3
AH-4
AH-5
AH-6
AH-7
AH-8
AH-9
AH-10
AH-11
AH-12
AH-13
AH-14
AH-15
AH-16
AH-17
AH-18
AH-19
AH-20
AH-21
AH-22
AH-23
AH-24
AH-25
AH-26
AH-27
AH-28
Injection
WELLS 1st. UNIT
WELLS 2nd. UNIT
WELLS 3rd. UNIT
REINYECTION WELLS
STAND BY WELLS
EXPLORATORY WELLS
6000 CHLORIDES p.p.m. 1975
6000 CHLORIDES p.p.m. 1978
FIG. 10
COMISION EJECUTIVA HIDROELECTRICA DEL RIO LEMPA
C. E. L.
RECURSOS GEOTERMICOS
CHLORIDES ISOCONCENTRATIONS
Sept. 1978

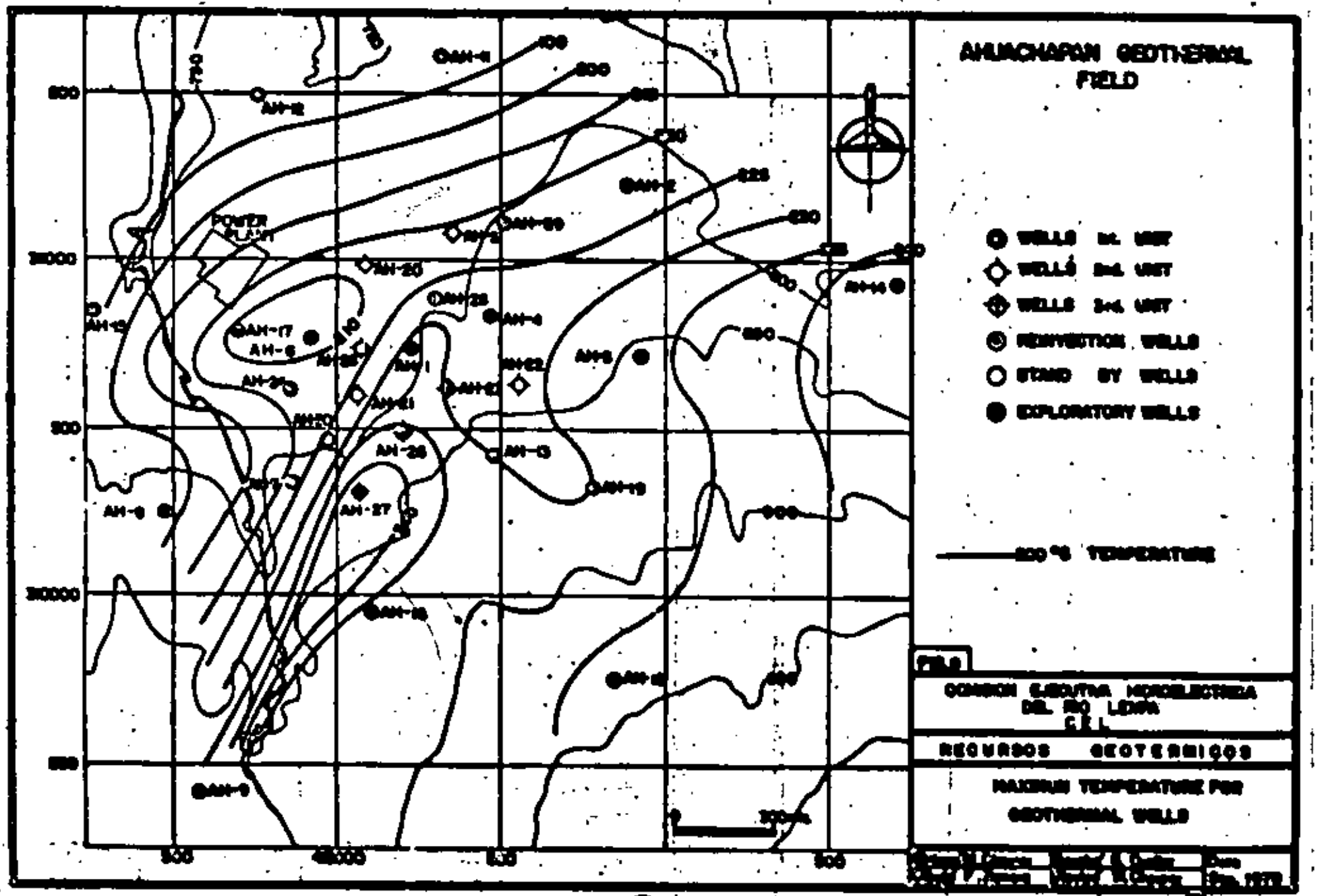
AHUACHAPAN GEOTHERMAL FIELD
WELLS 1st. UNIT
WELLS 2nd. UNIT
WELLS 3rd. UNIT
REINYECTION WELLS
STAND BY WELLS
EXPLORATORY WELLS
°C TEMPERATURE
COMISION EJECUTIVA HIDROELECTRICA DEL RIO LEMPA
C.E.L.
RECURSOS GEOTERMICOS
MAXIMUM TEMPERATURE FOR GEOTHERMAL WELLS

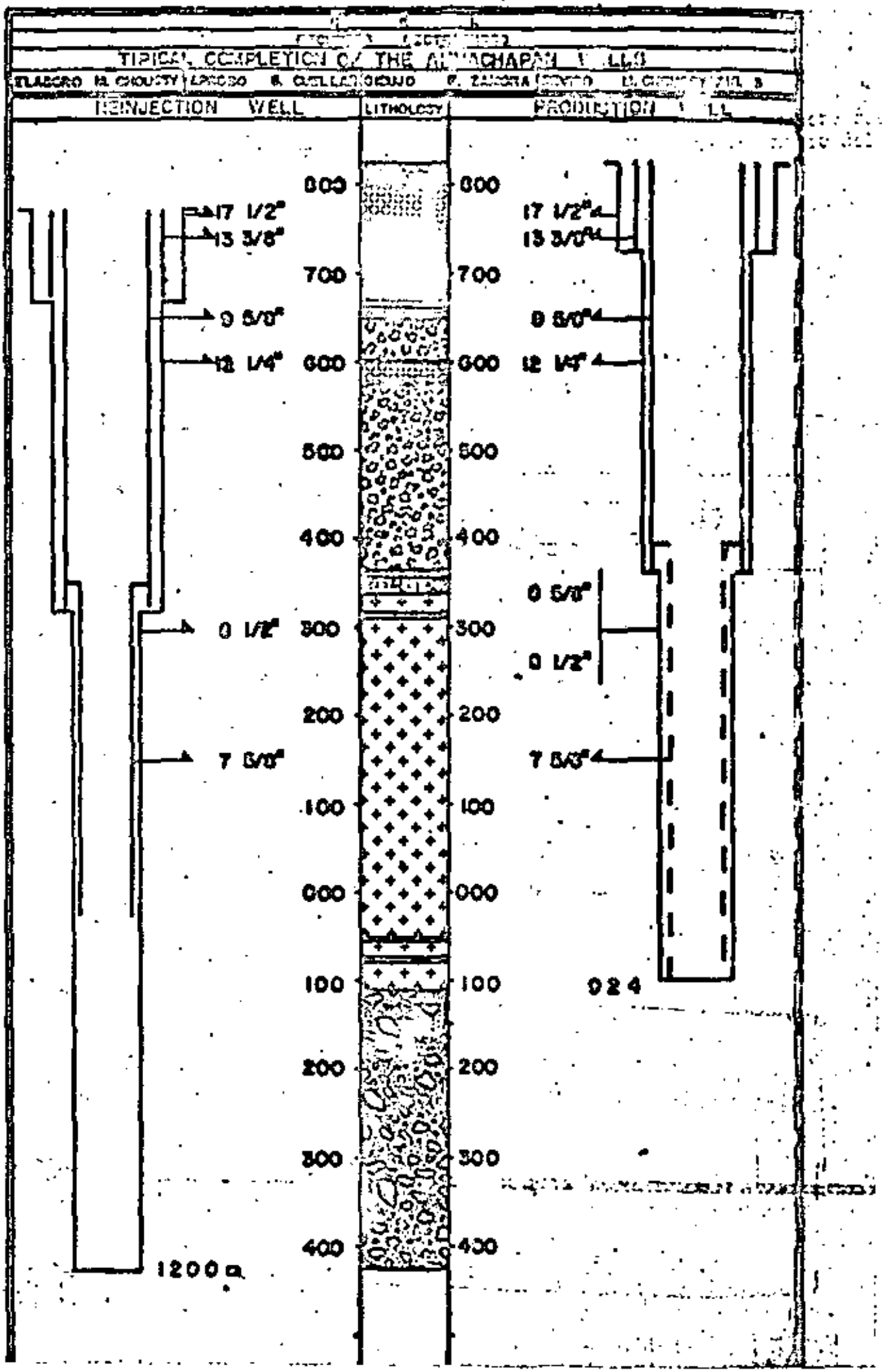
TIPICAL COMPLETION OF THE ATLACHAPAN 1 WELL
REINJECTION WELL
LITHOLOGY
PRODUCTION WELL
17 1/2"
13 3/8"
9 5/8"
12 1/4"
8 1/2"
7 5/8"
1200 m
800
700
600
500
400
300
200
100
000
100
200
300
400

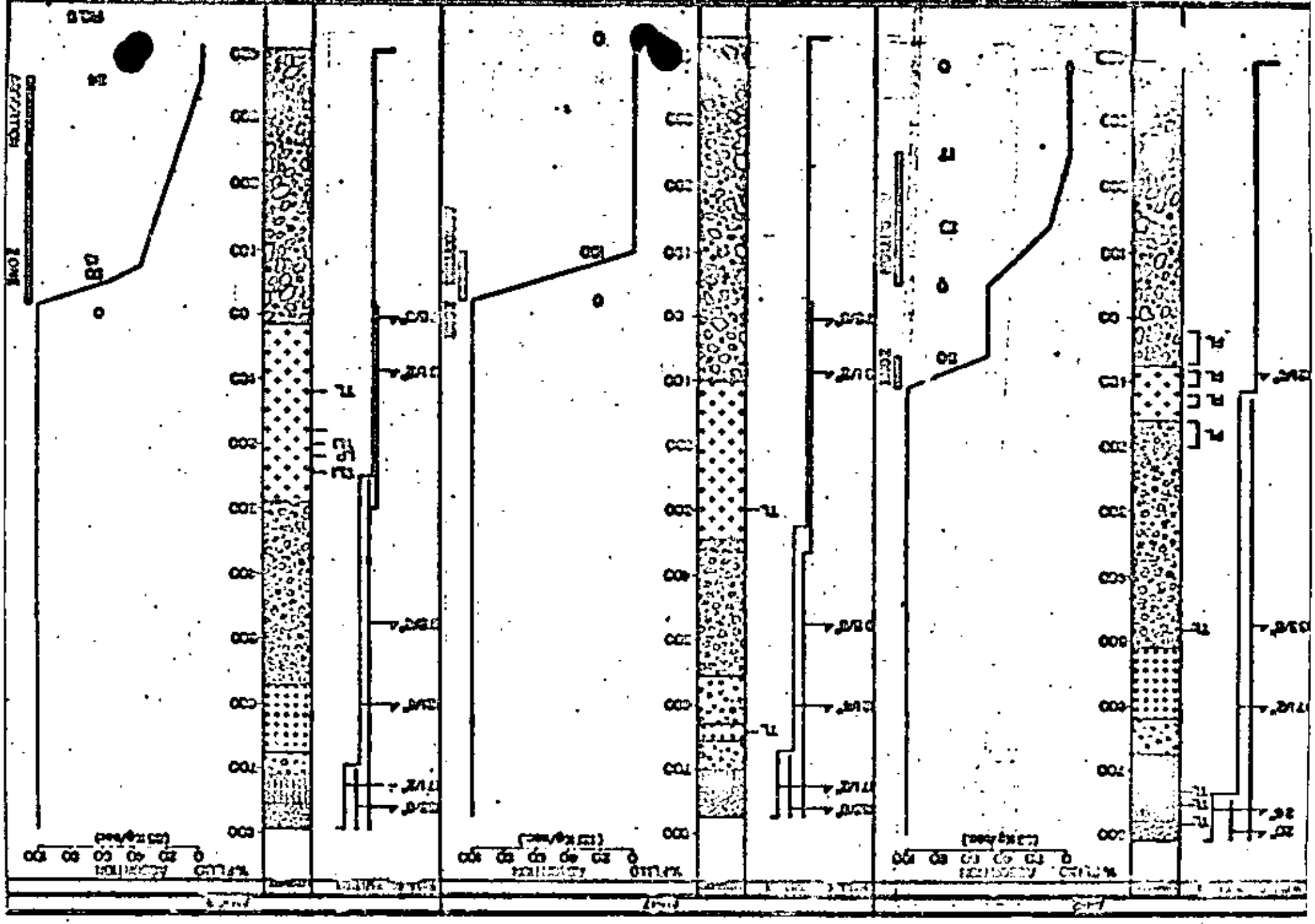

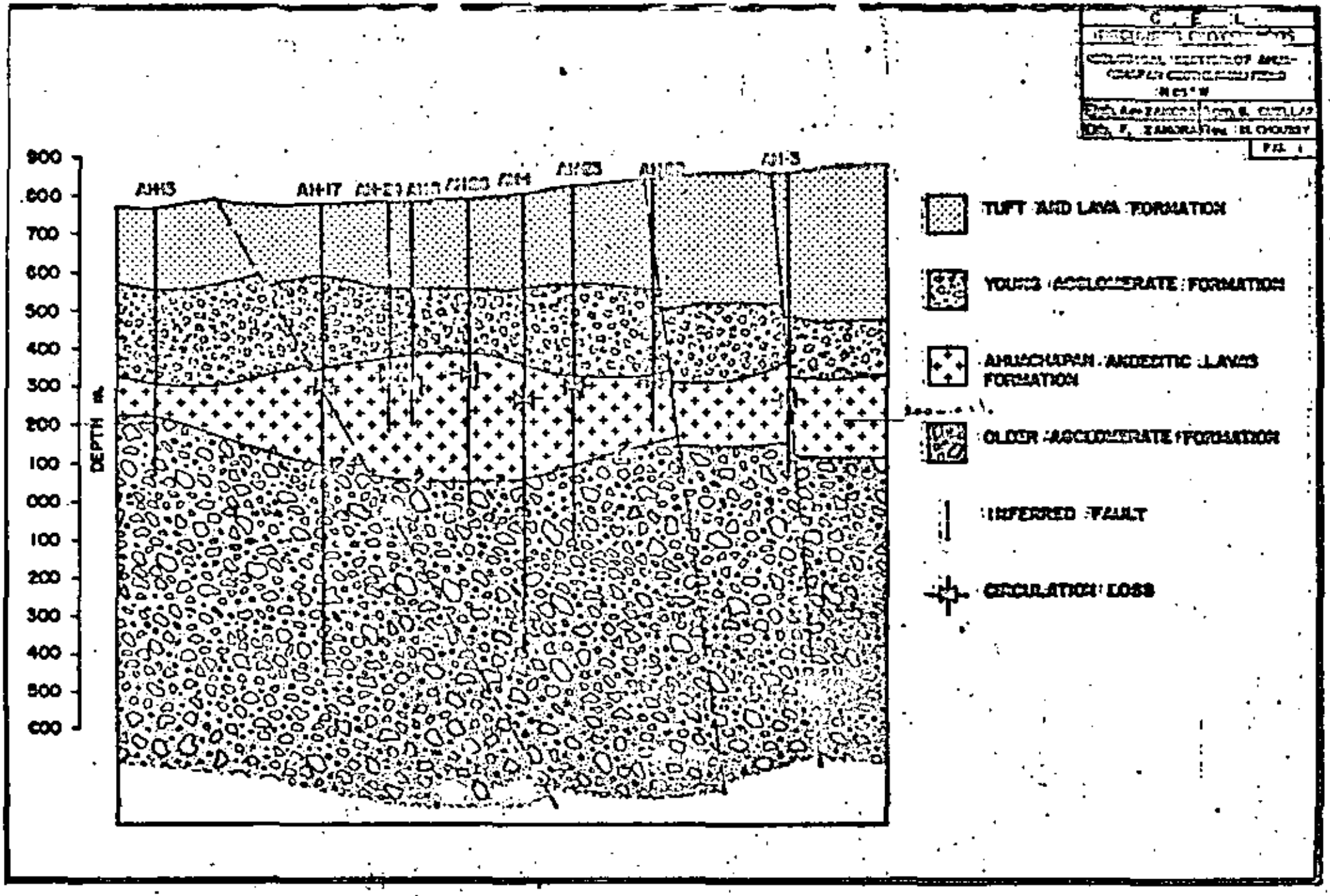
DEPTH in
900
800
700
600
500
400
300
200
100
000
100
200
300
400
500
600
TUFF AND LAVA FORMATION
YOUNG AGGLOMERATE FORMATION
ANUCHAPUN ANDESITIC LAVAS FORMATION
OLDER AGGLOMERATE FORMATION
INFERRED FAULT
CIRCULATION LOSS

AH-17

PERFILES DINAMICOS DE PRESION - TEMPERATURA Y FLUJO. 2-10-80

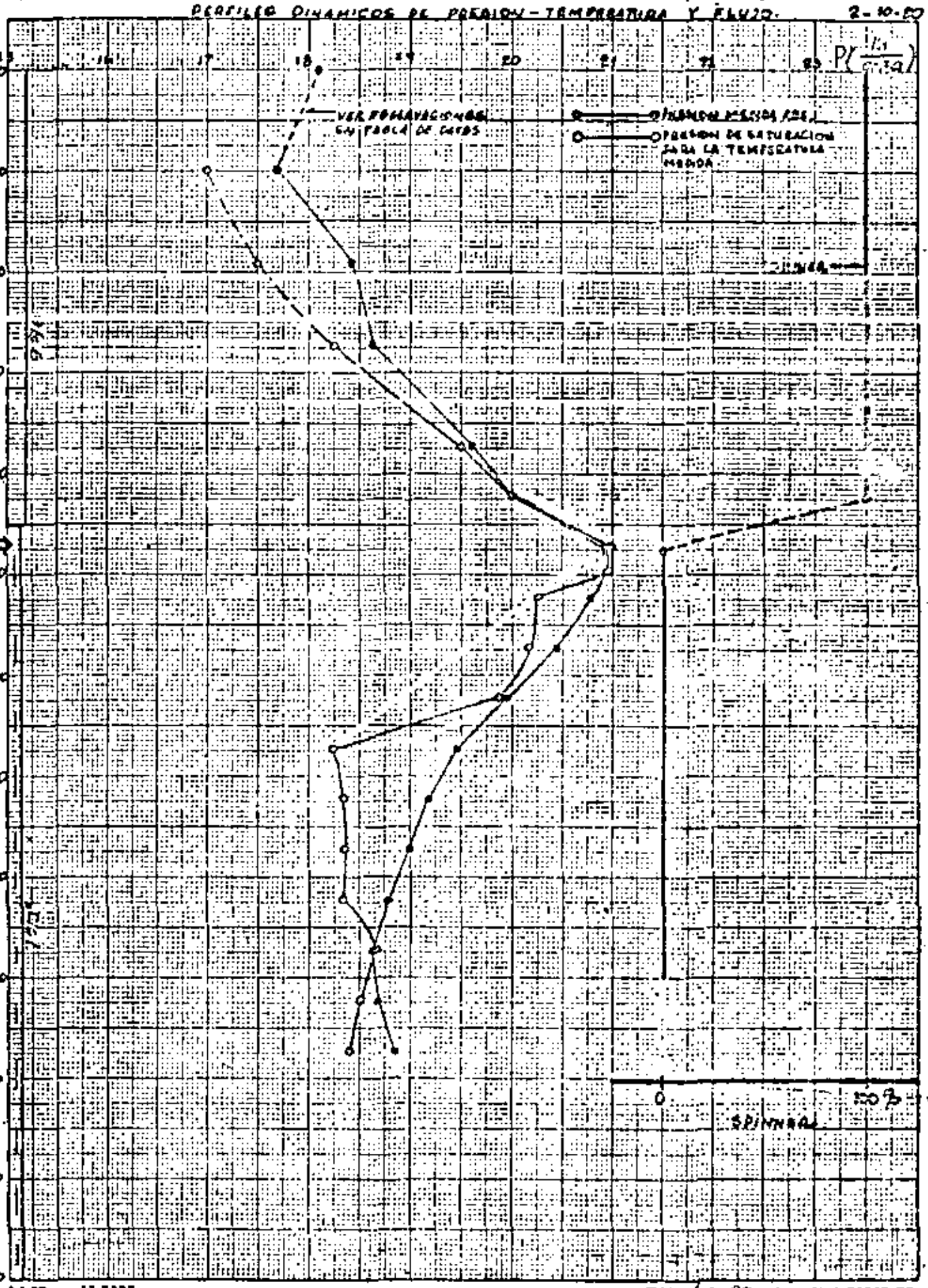

PERFILES ESTATICOS DE P Y T. (11-4-80).

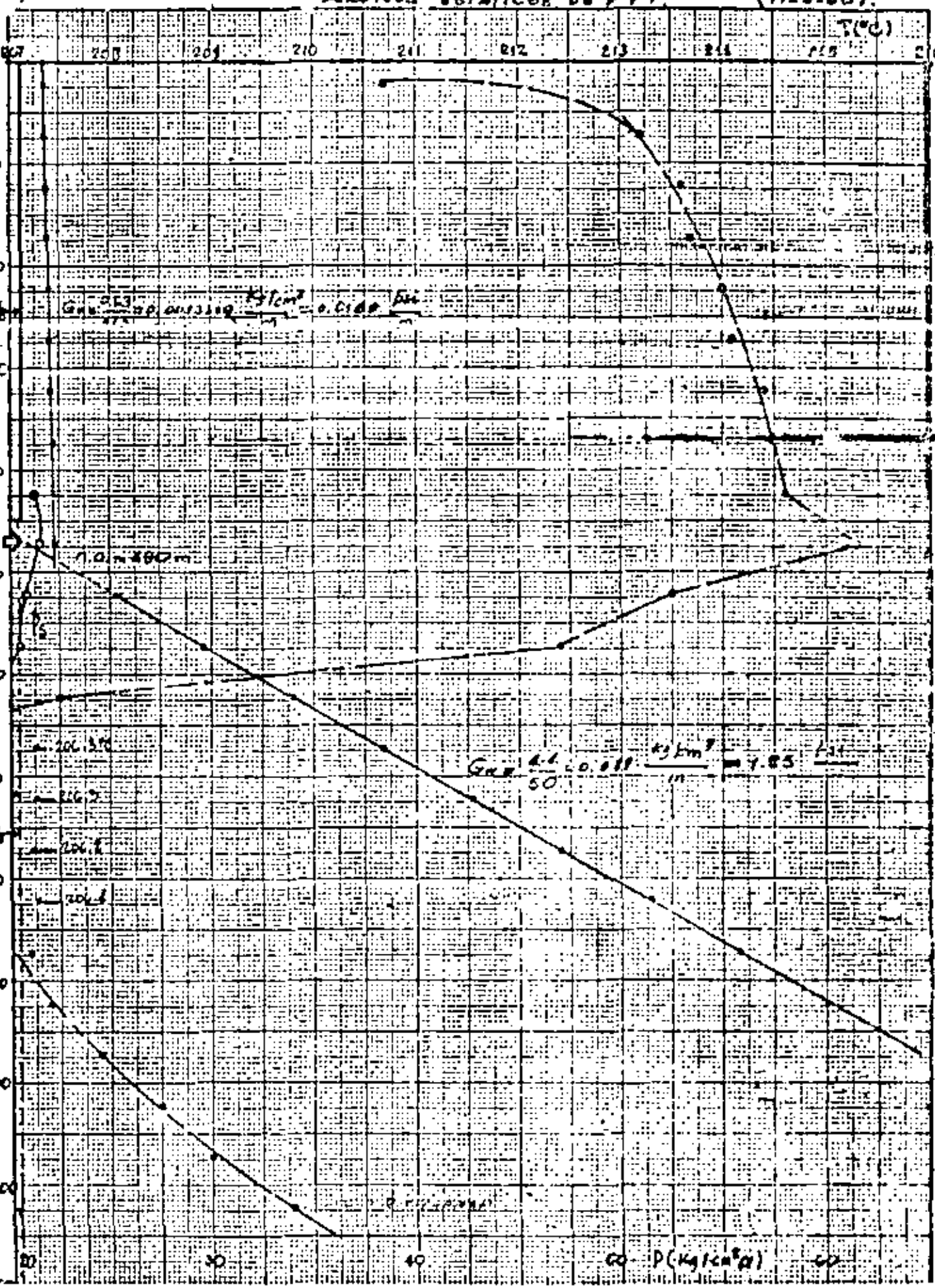

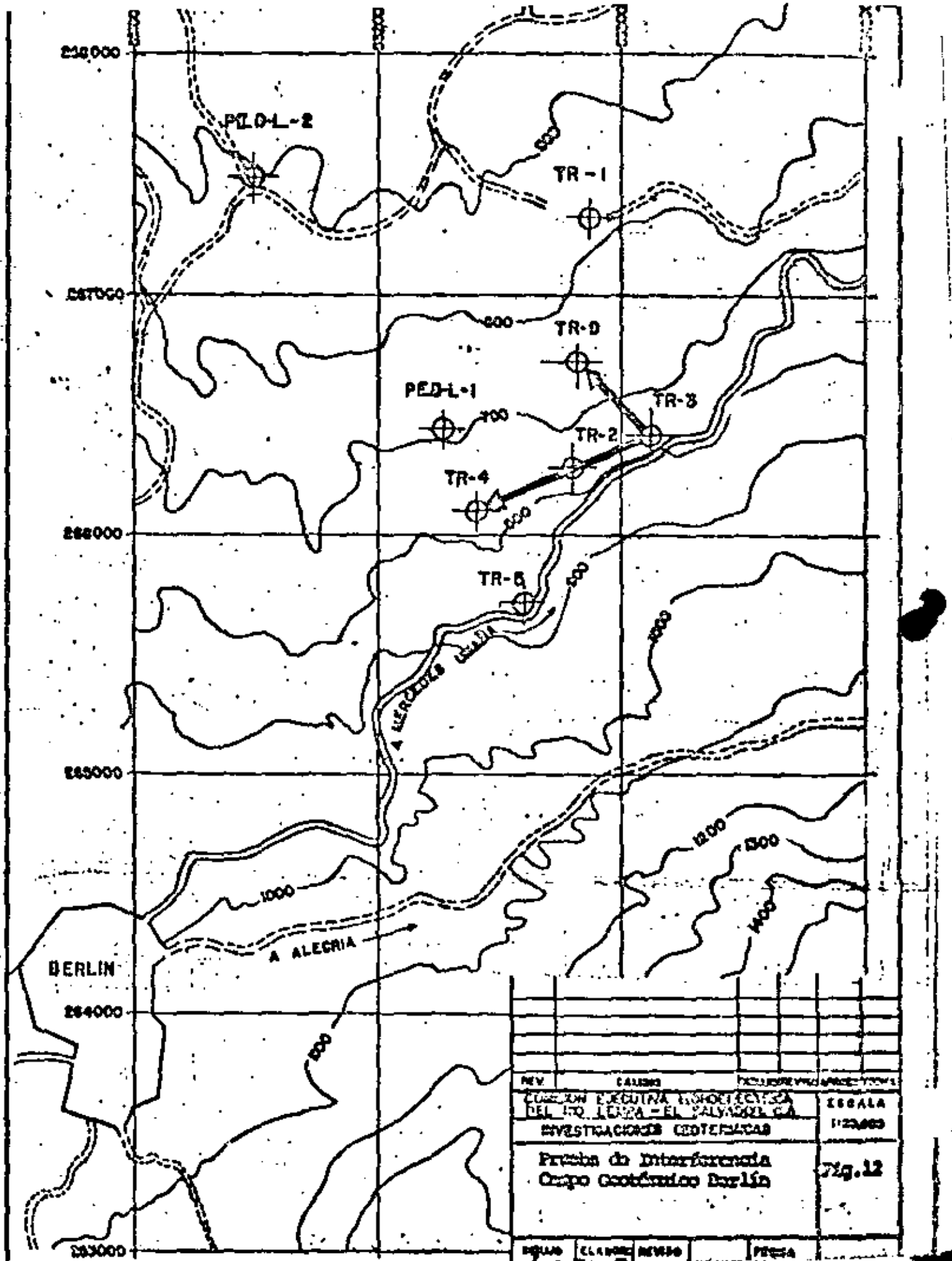

REV	CAUSO		
COMISION EJECUTIVA HIDROELECTRICA DEL RIO LERMA - EL SALVADOR, GTO.			ESCALA 1:25,000
INVESTIGACIONES GEOTECNICAS			
Prueba de Interferencia Campo Geotécnico Berlín			Fig. 12
DIBUJO	CALCULO	REVISO	FECHA

CURSO: INGENIERIA DE RESERVORIOS GEOTERMICOS"

OCTUBRE, 1981.

COMISION FEDERAL DE ELECTRICIDAD

PROGRAMA DEL ESTUDIO GEOHIDROLOGICO EN LA ZONA GEOTERMICA "LOS AZUFRES -CUITZEO"

I. Localización y superficie del área de estudio.

La zona geotérmica "Los Azufres-Cuitzeo", se localiza en la porción Nororiental del Estado de Michoacán y parte Sureste del Estado de Guanajuato, entre los paralelos 19°30' y 20°10' de latitud Norte, y entre los meridianos 100°20' y 101°25' de longitud Oeste de Greenwich; cubre una superficie de 4500 Km2 (Figura No. 1).

Desde el punto de vista hidrológico la región de estudio forma parte de la cuenca cerrada del Lago de Cuitzeo, cuenca del Río Lerma y cuenca del Medio Balsas.

Fisiográficamente la zona geotérmica está ubicada en el eje neovolcánico.

II. OBJETIVO DEL ESTUDIO

El estudio geohidrológico tiene por finalidad alcanzar los siguientes objetivos:

1. Determinar la recarga al acuífero/s de la región, a través de un estudio directo de agua subterránea.
2. Calcular el volumen aprovechable de agua subterránea, sin inducir efectos nocivos al acuífero/s.
3. Definir las condiciones actuales de explotación en que se encuentra el acuífero.
4. Delimitar las formaciones volcánicas acuíferas que puedan permitir el almacenamiento y circulación de agua, asimismo, conocer su funcionamiento a partir del ámbito geológico de la región y definir las características hidrogeológicas de las formaciones volcánicas, para que a partir de estos conocimientos se pueda precisar las posibilidades de recarga de los campos geotérmicos de Los Azufres, Araró y San Agustín del Maíz, Mich., y recomendar los sitios y zonas más favorables para la perforación de pozos de reinyección del fluido geotérmico.
5. Definir la intercomunicación entre aguas superficiales y las aguas subterráneas, determinar si es agua fósil o reciente, estos aspectos se estudiarán mediante la interpretación de análisis químicos e isotópicos del agua.

6. Conocimiento de la Geometría del Sistema Acuífero.

Los objetivos anteriores se pueden alcanzar, desarrollando las siguientes etapas:

1. Conocimiento del ámbito geológico clasificado con criterio hidrogeológico.
2. Funcionamiento de recarga y descarga del acuífero.
3. Censo o inventario de los aprovechamientos de agua subterránea y volumen de extracción.
4. Distribución de la calidad del agua subterránea y su relación con las formaciones geológicas y con el funcionamiento del acuífero.
5. Dotación del agua subterránea.
6. Relación entre agua subterránea y agua superficial.
7. Determinación de los parámetros hidrodinámicos del acuífero.
8. Medición de los niveles estáticos de los pozos en forma sistemática y nivelación con altímetro.

III. DESARROLLO DEL ESTUDIO

III.1 Información existente

Geología.- Existen estudios geológicos regionales y locales del área a estudiar, éstos requerirán verificación con el fin de darle un criterio hidrogeológico.

Geofísica.- Actualmente se están llevando a cabo estudios a nivel local y regional de resistividad, sísmicos y magnetométricos del área de estudio. En base al análisis de estos estudios, se propondrán otras áreas, con el fin de obtener la dimensión y distribución en el espacio de los materiales acuíferos.

Geoquímica.-La sección de geoquímica ha realizado la interpretación de los análisis físico-químicos de las aguas termales y gases, los cuales serán reinterpretados para establecer cualitativamente las posibles direcciones dominantes del flujo subterráneo, asimismo, se efectuará un muestreo sistemático y estratégico tanto de las aguas superficial y subterránea, con el fin de saber si hay relación entre ellas, de agua superficial con el agua subterránea.

Hidrología Subterránea.- A la fecha se han realizado, dentro del área geotérmica, 17 perforaciones con profundidad promedio de 1800 m. Estos sondeos de exploración y explotación definen espesores y profundidades de las unidades litotermales e hidroestratigráficas, así como niveles piezométricos.

También se tiene noticia por medio de publicaciones, que, en los valles de Morelia-Queréndaro y valle de Maravatío, existen perforaciones y probablemente existan algunas diseminadas en otros poblados.

Hidrología Superficial.

a) Climatología.- En la actualidad hay información de 40 estaciones climatológicas dentro y fuera del área de estudio, estos registros se analizarán y depurarán para calcular la media anual de precipitación pluvial, evaporación y temperatura dentro de un periodo mínimo de 15 años.

Con el trazo de las isoyetas y un índice de infiltración para cada formación volcánica se podrá dar un valor de percolación a los acuíferos.

b) Hidrometría.- En la región de estudio existen datos hidrométricos de 20 estaciones controladas por la SARH y CFE.

Con los gastos medios diarios en M3/s de las corrientes principales, se construirán los hidrogramas correspondientes los cuales se analizarán por el método de las curvas de recesión o decaimiento para determinar los volumenes almacenados por el acuífero y el volumen de recarga a los acuíferos en las subcuencas tributarias de la estación hidrométrica.

c) Aprovechamientos de agua superficial.- En la cuenca del Lago de Cuitzeo, se localiza la Presa Cointzio sobre el río Grande de Morelia, cuyos objetivos son suministrar agua potable a la ciudad de Morelia, riego/agrícola, generación de energía eléctrica y regulación de avenidas; además las presas derivadoras La Huerta, Xoconole y Zacapendo sobre el mismo río, que funcionan para regar el Distrito de Riego No. 20.

La Presa Malpaís se localiza sobre el Río Queréndaro, lo que funciona para riego en la Tercera Unidad del Distrito de Riego No. 20.

Por lo que se refiere a la cuenca del Alto Lerma, el área de estudio abarca la margen izquierda del Río Lerma desde la confluencia del río Cachiví hasta la Presa Solís. En esta subcuenca se localizan los siguientes almacenamientos superficiales: Presa la Cortina, Presa Torre Blanca y Presa derivadora San Ramón, sobre el río San Ramón que es afluente izquierdo del arroyo Cachiví. Sobre el arroyo el Fresno que es afluente del río Cahivi, se localiza una depresión conocida con el nombre de Laguna del Fresno. Tanto el volumen de la laguna como los almacenamientos de las presas, se utilizan para riego del valle de Maravatío.

Con respecto a la cuenca del Medio Balsas, el área de estudio, abarca parte de la subcuenca del Río Cutzumala, que es afluente del Río Balsas. El Río Cutzumala, a lo largo de recorrido, recibe los siguientes nombres: Taximaroa, Turundeo, Río Grande, Tuxpan, Zitácuaro y Cutzumala. En esta subcuenca existen 3 presas de almacenamiento, denominadas Agostitlán, Pucuato y Sabaneta, que fueron construidas para aprovechar en riego las aguas del río Agostitlán, Pucuato y Apuro en beneficio de 4,800 Has.

Topografía.- La región de estudio, es cubierta por 12 hojas topográficas escala 1:50,000 editadas por Detenal:

1. Puruándiro
2. Moroleón
3. Acámbaro
4. Presa Solís
6. Cuitzeo
7. Zinapécuaro
8. Maravatío
9. Pátzcuaro
10. Morelia
11. Tzizio
12. Ciudad Hidalgo

III.2 TRABAJOS DE CAMPO

III.2.1 Censo de Aprovechamientos Hidráulicos

Se efectuaran recorridos de campo para localizar los aprovechamientos de agua subterránea (pozos, manantiales, norias, galerías) ubicándolos en fotografías aéreas verticales escala 1:25,000, para luego transferirles a los planos topográficos escalas 1:50,000. Todos los aprovechamientos censados deberán identificarse en el campo con el número que les corresponda. Asimismo, se recabarán sus características constructivas y régimen de operación.

III.2.2 Observaciones Piezométricas

En el transcurso del censo, se seleccionarán los pozos o norias y manantiales que por su ubicación y características constructivas, sean representativos de los niveles piezométricos de los acuíferos. Se efectuarán 12 recorridos mensuales de observaciones de niveles piezométricos en los pozos seleccionados.

III.2.3 Nivelación

Los pozos seleccionados serán nivelados para referir sus brocales al nivel del mar. La nivelación será por medio de un altímetro y estará apoyada en los bancos de nivel instalados en la región de estudio.

III.2.4 Cálculo del volumen de extracción de agua subterránea

Cuando se trate de pozos de uso agrícola, la estimación de la extracción se basará en caudales y tiempo de bombeo y/o en flujos,superficies y láminas de riego.

En el caso de pozos destinados a generar electricidad, la estimación se basará en las descargas de agua y tiempo de operaciones.

El volumen de extracción de todos los aprovechamientos, cuya extracción individual sea poco significativa (pozos no equipados o equipados con bombas de diámetro menor de 2") se estimará globalmente.

III.2.5 Pruebas de Bombeo.

Las pruebas de bombeo se llevarán a cabo en los pozos que presenten condiciones favorables para la ejecución, en especial se buscarán pozos en los que puedan realizarse pruebas con pozo de observación.

Mediante las configuraciones piezométricas se seleccionarán los pozos para llevar a cabo las pruebas, dando preferencia a pozos situa-

dos en secciones en las que interese cuantificar el caudal del flujo subterráneo.

Estas mismas pruebas se van a llevar a cabo en los pozos productores de vapor, con el fin de obtener los coeficientes de transmisibilidad y almacenamiento.

III.2.6 Muestreo de Agua

Con el objeto de tener información de apoyo, se obtendrán muestras para análisis químicos convencionales y análisis isotópicos de Deuterio y Tritio.

III.2.6.1 Muestreo de agua para análisis químicos e isotópicos

Con apoyo en el plano base, en donde están consignados los pozos y con el común acuerdo del asesor en análisis isotópicos, se seleccionarán los sitios para el muestreo de agua subterránea para análisis químicos e isotópicos.

Para análisis químicos las muestras se tomarán en recipientes lavados y enjuagados con agua de la misma fuente por muestrear, el volumen mínimo de muestra requerida es de un litro. La muestra deberá tomarse después de una hora de operación , (cuando sea de pozo) tiempo necesario para que la muestra sea representativa del agua almacenada y transmitida por el acuífero. En el momento de tomarla se medirá temperatura, p.h., resistividad, datos que serán anotados en el recipiente junto con la información necesaria para su identificación. Las muestras serán analizadas por la CFE. como mínimo deberán obtenerse las concentraciones siguientes: sólidos totales disueltos, calcio, magnesio, sodio o potasio, cloruros, sulfatos, bicarbonatos, nitratos, boro, litio y silicio.

III.2.6.2 Muestreo de agua para Análisis Isotópicos (deuterio y tritio).

Para análisis de deuterio, con botellas de 20ml. de capacidad es suficiente, debiéndose llenar éstos totalmente y lavarse completamente para evitar intercambio isotópico con el aire.

El tamaño de botella para análisis de tritio deberá ser de 1 litro, con objeto de poder determinar pequeñas cantidades de este isótopo. Una condición importante del muestreo es la de tener precaución a fin de que la muestra sea representativa ya sea de la corriente superficial elegida o bien del acuífero subterráneo seleccionado.

Los análisis isotópicos serán realizados por laboratorios especializados que hayan participado en la verificación de calidad de resultados, hecha a través del Organismo Internacional de Energía Atómica con sede en Viena.

La condición anterior tiene por objeto, el alcanzar la confianza necesaria de que los resultados de los análisis isotópicos sean correctos y permitan llegar a conclusiones adecuadas con relación al objeto de estudio.

III.2.6.3. Muestreo de Gases.

El muestreo debe realizarse con precauciones para no perder gases, ya que entonces se falsearían los resultados; las actividades que se midan deben referirse al instante del muestreo. Los gases a determinar son: H_2S, SO_2, CO_2, CO, H_2 y principalmente Rn222, Ar, Kr. y Xe.

Un elevado contenido de Rn^{222} en ciertos puntos de un acuífero puede indicar aportes más profundos a través de fracturas, además el contenido en gases nobles, principalmente As, Kr y Xe indica claramente el origen atmosférico de gran parte del agua subterránea.

III.2.7 Geología

La sección de geohidrología llevará a cabo un levantamiento hidrogeológico, apoyado en los estudios geológicos que cubren el área Los Azufres Cuitzeo.

PROCESAMIENTO E INTERPRETACION DE LA INFORMACION

IV.1 Plano Base

Con apoyo en 12 cartas topográficas escala 1:50,000 editadas por Detenal, se formará un plano base escala 1:100,000, en el que deberán señalarse vías de comunicación, ciudades y poblados importantes, ríos y arroyos principales, serranías y cerros, así como todas aquellas referencias de utilidad.

IV. 2 Información Climatológica

Con base en los registros de datos climatológicos se hará una descripción del clima, precipitación pluvial, evaporación potencial y temperatura del área estudiada.

En este capítulo se indicarán los datos climatológicos disponibles número y nombre de las estaciones climatológicas existentes dentro y fuera del área de estudio, consignando su ubicación en el plano así como el tiempo de operación y tipo de datos registrados en cada una de ellas.

Dentro del concepto de precipitación pluvial se tratarán los aspectos siguientes: variación de la precipitación anual, en un período mínimo de 15 años; precipitación media anual del área estudiada en el mismo intervalo; distribución de la lluvia en el área y precipitaciones medias mensuales del intervalo estudiado.

Referente a la evaporación potencial y temperatura, se indicará su valor medio anual y su distribución en el año.

IV.3 Recursos Hidráulicos Superficiales.

Se describirá la red hidrográfica del área estudiada, se hará mención de la información hidrométrica disponible, indicando estaciones hidrométricas existentes con sus respectivos tiempos de operación. Cuando se trata de ríos perennes, se analizará el flujo base para determinar los volumenes descargados por el acuífero al río y la recarga al acuífero en el área tributaria de la estación, señalando las hipótesis hechas en el análisis.

Lo que toca a los aprovechamientos de agua superficial, se hará una descripción de las obras de almacenamiento, conducción y distribución, mencionando los volumenes de agua utilizados y su distribución por usos.

En el caso de zonas irrigadas con agua superficial, se presentará especial atención a la información que permita inferir los volumenes infiltrados a lo largo de cauces y canales, y a los volumenes descargados por drenes.

En un plano se ilustrará la red hidrográfica, las principales obras de aprovechamiento de agua superficial y las áreas beneficiadas.

IV.4 Censo de Aprovechamientos de Agua Subterránea.

Se formará un plano de localización de aprovechamiento de agua subterránea, el número definitivo de cada pozo estará formado por el número progresivo que le haya correspondido en el censo.

Respecto a los volumenes de extracción de agua subterránea, se mencionarán los datos básicos utilizados en su estimación, como son: superficie y láminas de riego, caudales y tiempo de operación.

V. Geología

Con base en los planos geológicos que cubren el área de estudio, se elaborará un plano hidrogeológico, en el que mostrarán las principales unidades hidrogeológicas. En el mismo plano se hará una breve descripción de la litología de cada formación (porosidad, granulometría, grado de cementación, fracturamiento, disolución, etc. Mediante símbolos se ilustrarán fallas, rumbos, echados, pliegues, etc., asimismo se destacará la red hidrográfica. Se elaborarán secciones geológicas, apoyadas en cortes geológicos de pozos y en sondeos geofísicos.

Lo anterior tendrá por objeto definir el ámbito geológico en que se mueve el agua subterránea y del modelo conceptual del acuífero.

VI. Hidrogeoquímica.

Los resultados de los análisis químicos serán debidamente ordenados y procesados para llevar a cabo el estudio hidrogeoquímico. El ordenamiento incluirá la elaboración de una tabla resumen de resultados. El procesamiento consistirá en la elaboración de configuraciones de curvas de isovalores (contenidos iónicos, relaciones iónicas, STD, RN,etc.), de gráficas y diagramas (Shoeller, Piper..). El análisis e interpretación tendrá por objeto inferir: influencia de las formaciones geológicas en la calidad del agua, zonas probables de recarga, direcciones predominantes del flujo subterráneo, variación de la calidad del agua con la profundidad.

Referente a los resultados de análisis isotópicos, serán analizados y procesados para determinar la influencia de las aguas superficiales hacia el acuífero y/o la magnitud de las aportaciones laterales de agua subterránea de las sierras circunvecinas hacia el acuífero.

La interpretación se basará en la tabla de concentraciones de

$$\delta D = \frac{(^{D}/_{H}\text{ muestra} - (^{D}/_{H})\text{ SMOW}}{C\ ^{D}/_{H}\text{ SMOW}} \times 1000$$

la propiedad del isótopo estable D es aplicado e interpretado para diferencias aguas con diferentes orígenes.

Por lo que respecta al isótopo radiactivo tritio, en base a su detección se puede conocer el tiempo transcurrido desde que el agua se precipitó sobre la superficie.

VIII. Piezometría.

Para el procesamiento e interpretación de los datos piezométricos se utilizarán planos adecuados, en los que se indiquen los límites del acuífero estudiado.

Los números de pozos nivelados y sus respectivas elevaciones del brocal, se presentarán en una relación. En un plano se mostrará la ubicación de estos pozos, además se graficarán los hidrografes de los pozos de observación. También se mencionará la información piezométrica disponible, tiempo cubierto por las observaciones, número y frecuencias de las mismas.

VII. 1 Red de Flujo Subterráneo

Se presentarán configuraciones de los niveles estáticos correspondiente a un tiempo determinado, en base a ellas se hará una descripción de la red de flujo subterráneo, haciendo mención de las zonas de recarga y descarga, dirección de flujo, gradiente hidráulico, influencia de ríos, lagunas, etc.

VII.2 Evolución Piezométrica.

Según el tiempo cubierto por las observaciones piezométricas, se seleccionarán intervalos de tiempo con el objeto de formar planos con curvas de igual evolución de nivel estático. Para el trazo de estas curvas se tomaron en cuenta todos los factores que pueden influir en la evolución, tales como características hidráulicas del acuífero, zonas de recarga y descarga, distribución y magnitud del bombeo.

VII.3 Profundidad a los niveles estáticos

La profundidad a los niveles estáticos del acuífero se ilustrarán mediante un plano de curvas de igual profundidad. Se indicará rango de profundidades, distribución en el área, influencia de la topografía, zonas probables de descarga por evapotranspiración.

VII.4 Pruebas de Bombeo.

Se señalará el método utilizado para interpretar las pruebas, los resultados de la interpretación de las pruebas se resumirán en una tabla que contenga el número del pozo utilizado, duración de la prueba, caudal, caudal específico, transmisibilidad, coeficiente de almacenamien-

to, las gráficas con los datos observados serán anexadas.

. En un plano se mostrará la localización de los pozos utilizados para realizar las pruebas, anotando los valores respectivos de la transmisibilidad. Cuando la distribución de los valores muestra alguna tendencia, se trazarán curvas de iso-transmisibilidad, tomando en cuenta para ello la geología del área estudiada.

. Un caso especial va a ser para efectuar pruebas de bombeo en los pozos productores de vapor y en los pozos de inyección.

VIII BALANCE AGUA SUBTERRANEA

Si la información disponible lo permite se efectuará un balance de agua subterránea, se mencionarán las consideraciones hechas para plantear el balance, así como los términos que se pretenden deducir.

. Con base en los resultados del balance, se inferirá la recarga total del acuífero, se discutirá si esta recarga se considera representativa de una condición media anual, según haya sido la precipitación pluvial ocurrida en el período de tiempo considerado en el balance.

Tomando en cuenta la relación recarga-explotación y las características de la zona estudiada como son, mecanismo de recarga y descarga, litología y geometría del acuífero, profundidad a los niveles estáticos, distribución de la calidad del agua, distribución de la explotación existente, etc.; se mencionarán recomendaciones generales para la explotación futura del acuífero, señalando en forma cualitativa o cuantitativa (siempre y cuando los datos lo permitan), los efectos probables que se inducirán con las recomendaciones propuestas.

IX PROGRAMA DE OBSERVACIONES Y EXPLORACIONES

Se propondrá un programa para continuar recolectando la información que permita afinar los resultados obtenidos y actualizar permanentemente el estudio. El programa incluirá, selección de pozos de observación; proponiendo frecuencia de observación; selección de pozos para muestreo de agua, señalando también frecuencia del muestreo. Si es necesario se propondrán exploraciones geofísicas y sondeos mecánicos.

Atentamente.

SECCION DE GEOHIDROLOGIA

Ing. Fidel Cedillo Rodríguez . Ing. Román Silva Pérez

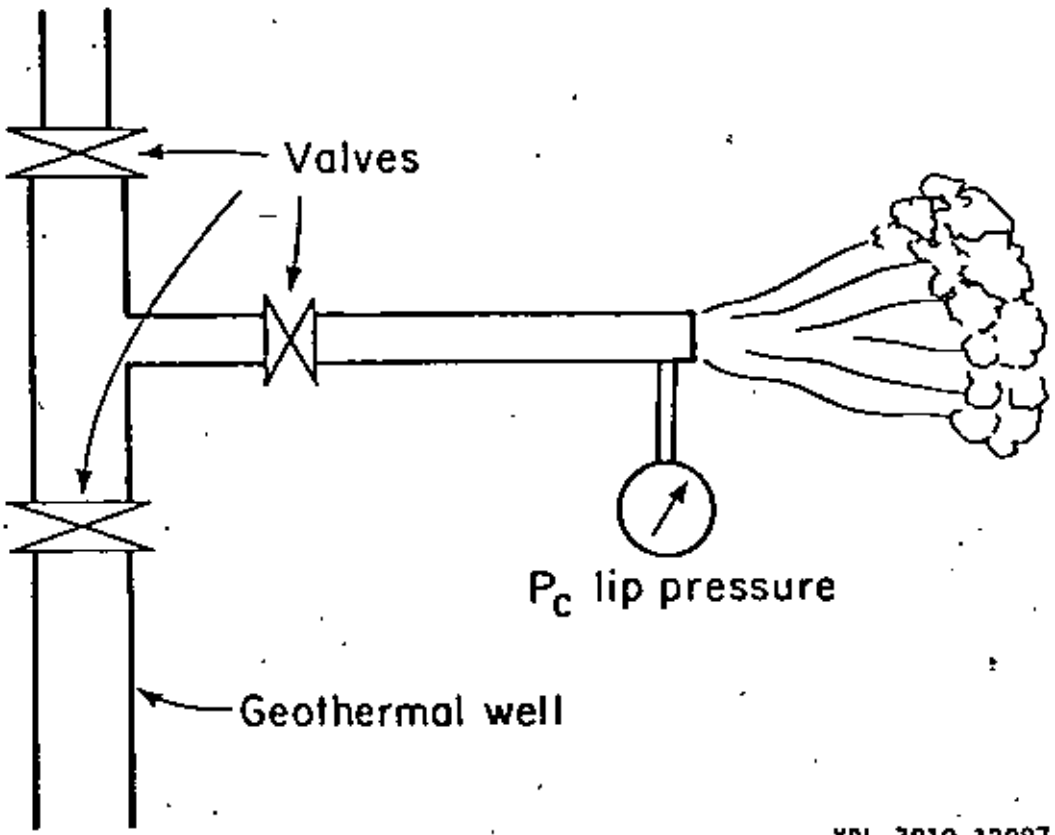

Figure 2. Schematic set-up for measuring mass flow rates by the James Method.

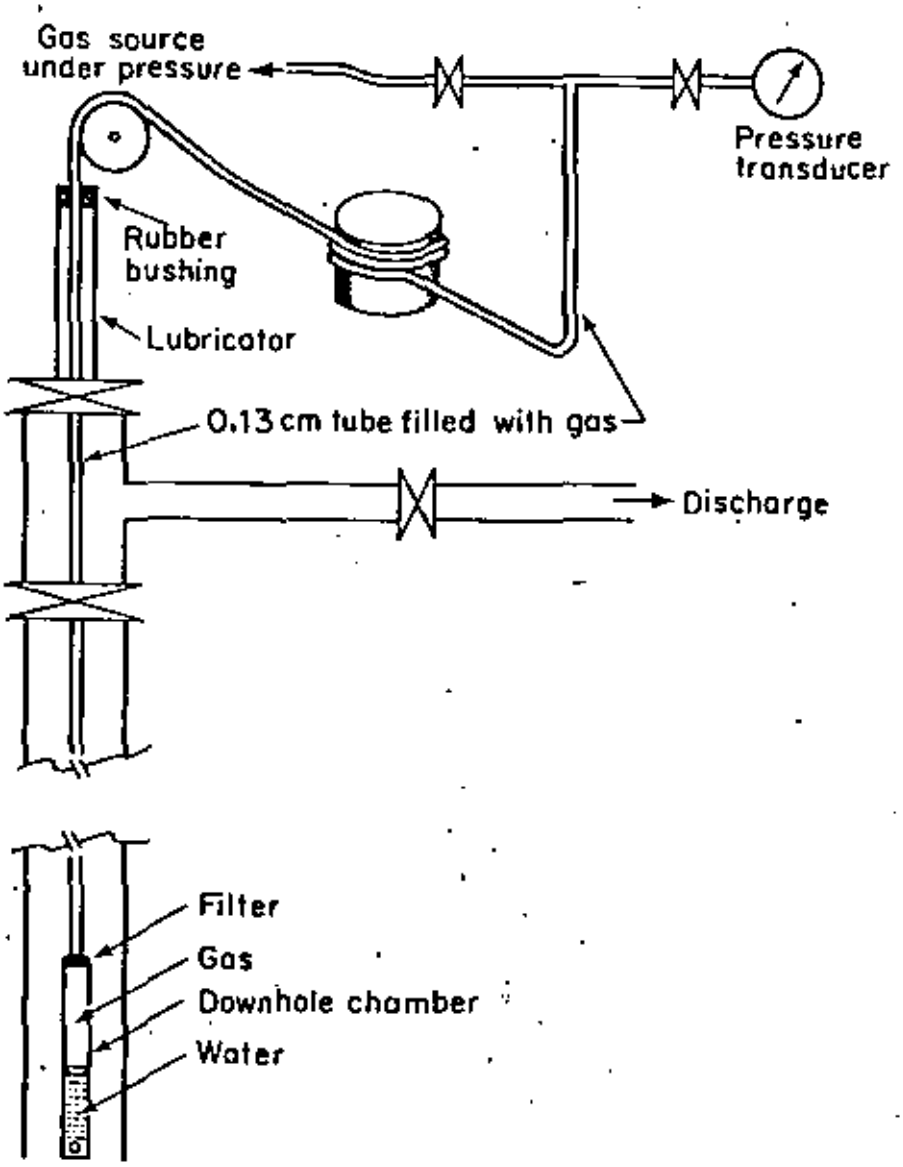

XBL 7810-12086

Figure 3. Schematic of downhole pressure monitoring set-up using the gas-transmitter system.

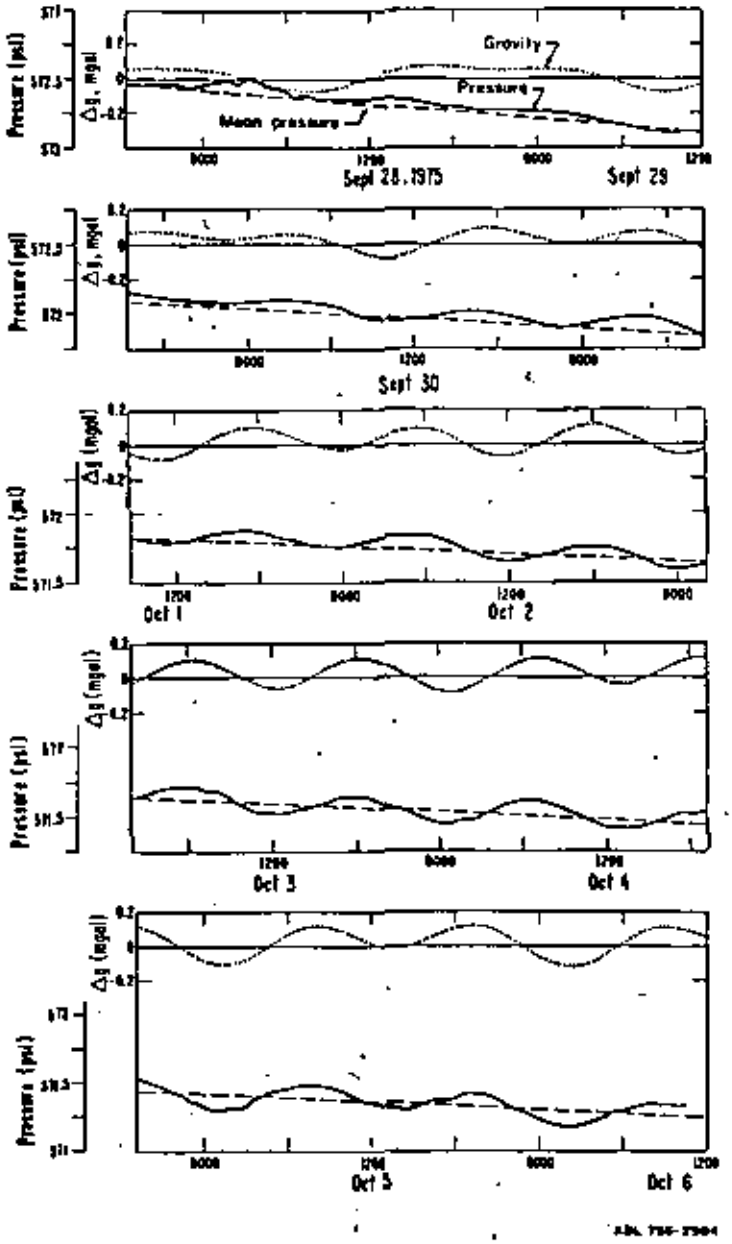

Figure 4. Correlation between reservoir pressure and computed changes in Earth's gravity in a geothermal well in the Raft River Valley of Idaho.

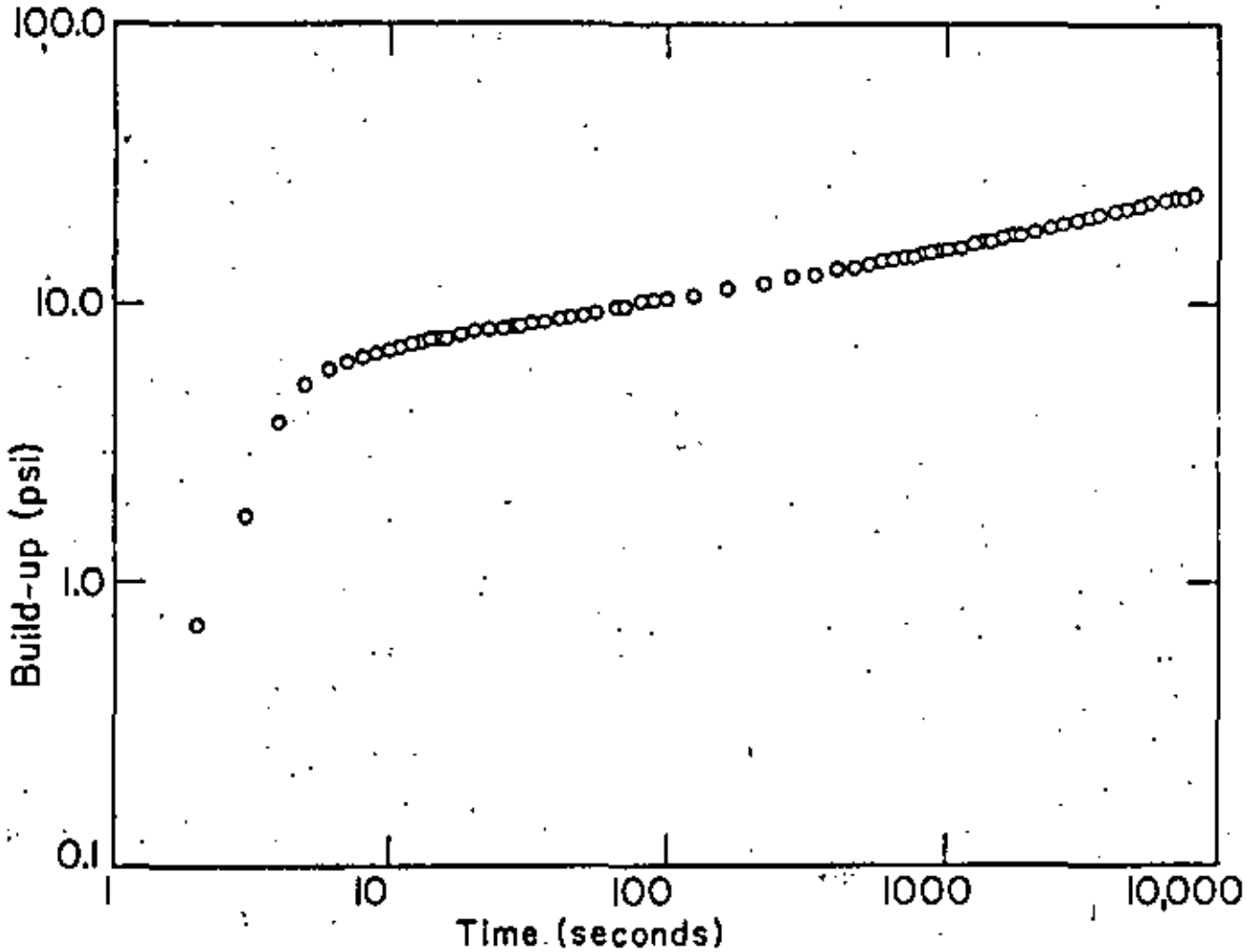

Figure 5. Buildup data from a geothermal well in Raft River Valley, Idaho, showing resolution of early time data.

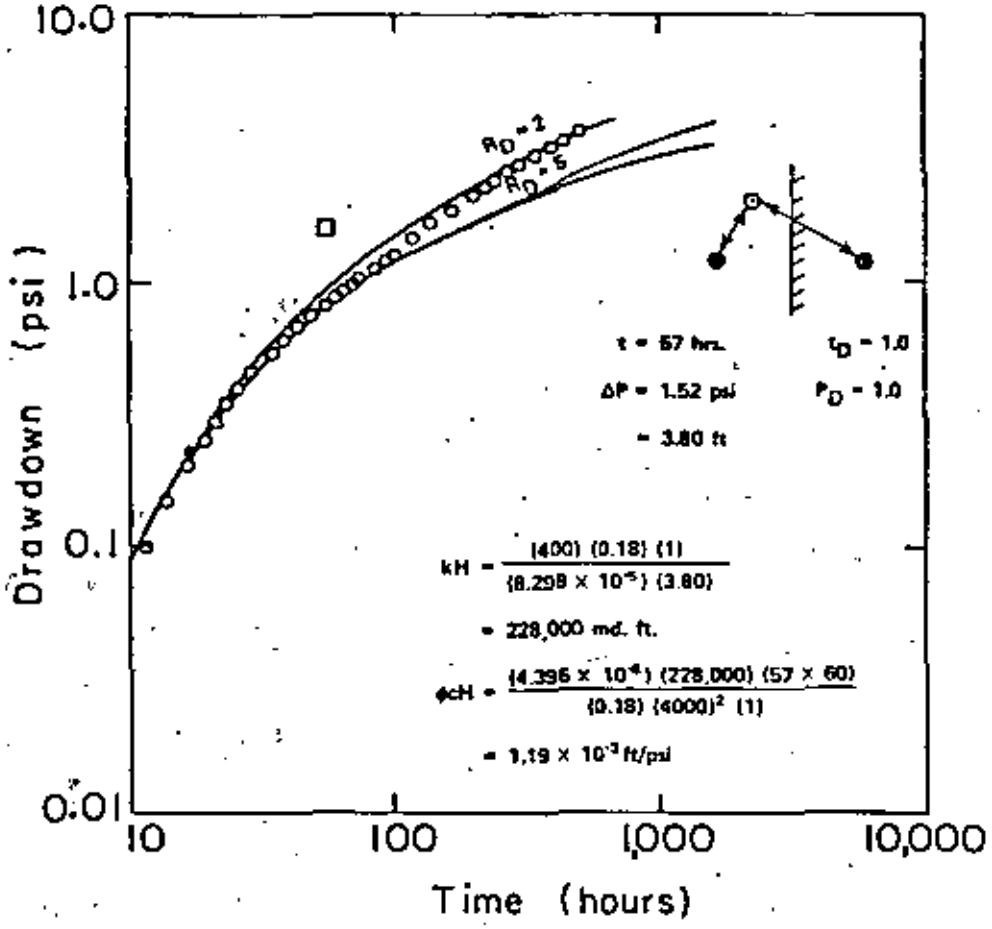

Figure 6. Interpretation of Interference Test between two geothermal wells in Raft River Valley, Idaho.

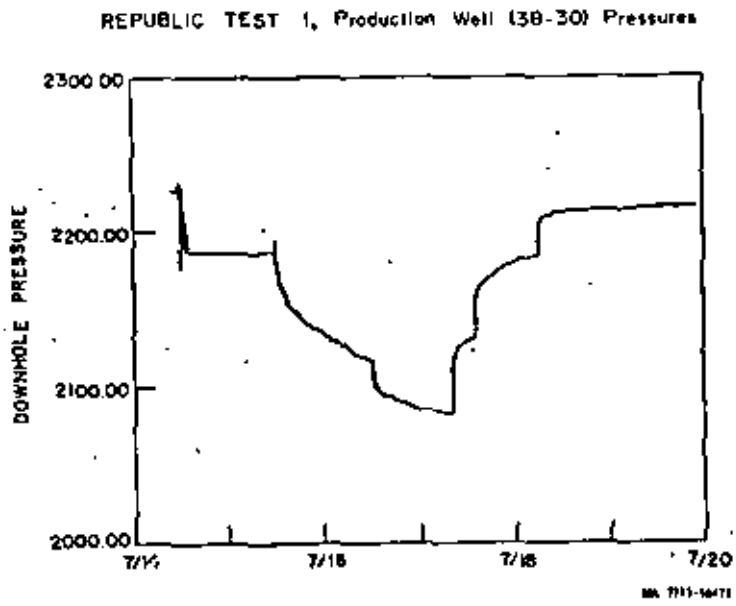

Figure 7. Step-drawdown data from a geothermal well at East Mesa in California.

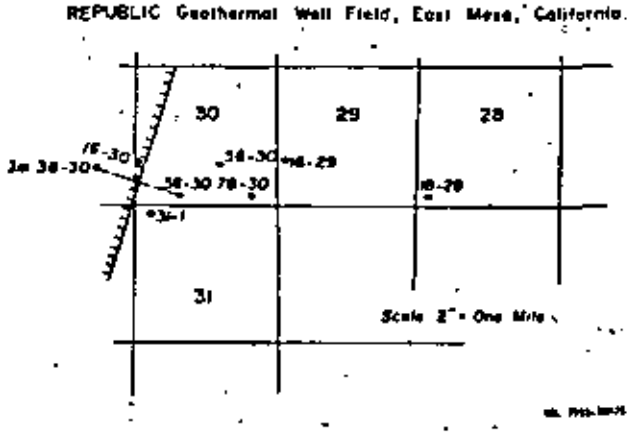

Figure 8. Well test analysis leading to inference of barrier boundary: East Mesa geothermal reservoir, California.

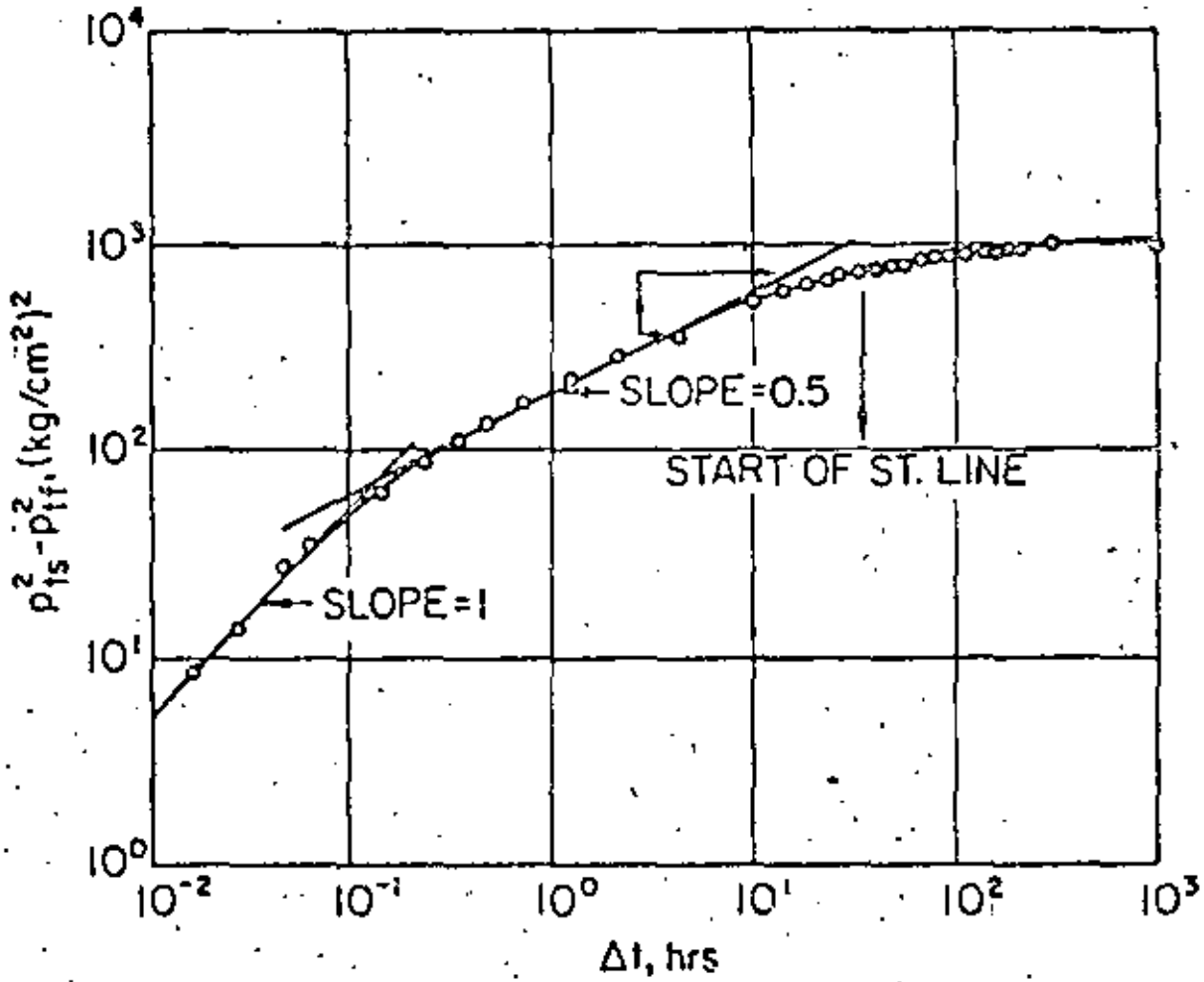

XBL 7810-11971

Figure 10. Well Test Interpretation of a Steam Well at the Geysers (after Ramey and Gringarten, 1975).

DIRECTORIO DE ASISTENTES AL CURSO DE "INGENIERIA DE RESERVORIOS GEOTERMICOS". C.F.E., OLADE, I.I.E., -- DECFI. DEL 7 DE SEPTIEMBRE AL 5 DE NOVIEMBRE, 1981.

NOMBRE Y DIRECCION:	EMPRESA Y DIRECCION:
1.- ABREGO NAVA HUGO MONTE ALBAN # 3913 COL. NARVARTE MEXICO 12, D.F. TEL: 519 02 85	
2.- ALFONSO AGUAYO ANASTACIO MANZANA 54, LOTE 43 1a. SECCION COL. SAN AGUSTIN ECATEPEC, EDO. DE MEXICO	C.F.E. LOS AZUFRES, CD. HIDALGO, MICH.
3.- FERNANDO ASCENCIO CENDEJAS OBREGON # 302, CD. SALAMANCA, GTO. TEL: 807 16	C.F.E. CD. MORELIA TEL: 304 53
4.- JESUS RODOLFO RODRIGUEZ CACERES CALLE 31 PTE. # 1039 COL. LAYCO CD. SAN SALVADOR. EL SALVADOR TEL: 25 57 48	COMISION EJECUTIVA - HIDROELECTRICA DEL - RIO LERMA. (CEL). 9a. CALLE PONIENTE # 950 CENTRO DE GOBIERNO CD. SAN SALVADOR EL SALVADOR TEL: 22 08 55
5.- ESTEBAN CARREÑO BRACAMONTES AV. PADRE KINO # 1399 CORREO APDO. POSTAL E-8 COL. FRACC. VISTA HERMOSA CD. MEXICALI, B.C.	COORD. EJECUTIVA CERRO PRIETO. C.F.E. APDO. POSTAL 3-636 MEXICALI, B.C. TEL: 28501 al 09 ext. 158
6.- FIDEL CEDILLO RODRIGUEZ NORTE 70-A # 3631 COL. LA JOYA MEXICO 14, D.F. TEL: 551 10 14	C.F.E. OKLAHOMA # 85 COL. NAPOLES MEXICO 18, D.F. TEL 536 93 15
7.- ENRIQUE ALFONSO CONTRERAS LOPEZ CALLE LA LUZ No. 3 COL. CHAPULTEPEC CD. CUERNAVACA, MORELOS TEL: 4 38 11 x 320 2	I.I.E. INT. INTERNADO PALMIRA s/n COL. PALMIRA CD. CUERNAVACA, MOR. TEL: 4 38 11
8.- VICTOR GARCIA FLORES CARACAS-VENEZUELA TEL: 0248 3333 6	MINISTERIO DE ENERGIA Y MINAS. TORRE NORTE-CENTRO SIMON - BOLIVAR PISO 19 DIRECCION DE GEOLOGIA

Cont

	NOMBRE Y DIRECCION:	EMPRESA Y DIRECCION:
9.-	JUAN GONZALEZ GOMEZ CAMPAMENTO "AGUA FRIA" MICH. CD. HIDALGO Z.P. 1	C.F.E. MELCHOR OCAMPO # 35 CD. HIDALGO TEL: 409 44
10.-	HECTOR GUTIERREZ PUENTE SALVADOR GONZALEZ HERREJON # 52 COL. CUAUHTEMOC CD. MORELIA, MICH.	C.F.E. SALVADOR GONZALEA H. # 52 COL. CUAUHTEMOC CD. MORELIA, MICH. TEL: 304 53
11.-	JORGE HERNANDEZ NAVA AV. 3 No. 88 COL. SAN PEDRO DE LOS PINOS MEXICO 18, D.F. TEL: 516 39 83	C.F.E. MELCHOR OCAMPO # 35 CD. HIDALGO, MICHOACAN TEL: 409 44
12.-	JESUS GUILLERMO JAIMES MALDONADO SALVADOR GONZALEZ HERREJON # 52 COL. CUAUHTEMOC CD. MORELIA, MICH.	C.F.E. SALVADOR GLZ. HERREJON # 5 COL. CUAUHTEMOC CD. MORELIA, MICH. TEL: 304 53
13.-	RAFAEL ARMANDO MENDEZ LOZANO BOGOTA-COLOMBIA; CALLE 3 # 52-A24	CONSULTORIA TECNICA COLOMBIANA-CONTECOL, S.A.- CARRERA 21 # 86-A-28 BOGOTA, COLOMBIA TEL: 2578 578
14.-	JOSE LUIS MORA PEREZ AV. JUAREZ # 431 CD. CELAYA, GTO. TEL: 265 11	OFNA. DE ESTUDIOS Y EVALUA CION, GEOTERMIA, LOS AZUFR DR. SALVADOR GLZ. HERREJON No. 52, COL. CUAUHTEMOC CD. MORELIA, MICH. TEL: 304 53
15.-	LUIS FELIPE PINEDA MILLA EDIFICIO LAZARUS TEGUCIGALPA AC. HONDURAS TEL: 22 04 09	EMPRESA NACIONAL DE ENERGI ELECTRICA. (E.N.E.E.) TEGUCIGALPA, D.C. HONDURAS TEL: 22 84 71 y 22 85 10 ext. 25
16.-	CARLOS RODRIGUEZ FLORES GUILLERMO PRIETO # 13-INT. 10 CD. HIDALGO, MICH.	CAMPO GEOTERMICO LOS AZUFRES, MICH. AGUA FRIA, MICH.
17.-	RAMON RIVERA CORRADO CARROCEROS 1640 CD. MEXICALI, B.C.	C.F.E. APDO. POSTAL 3-636 COL. CERRO PRIETO CD. MEXICALI, B.C. TEL: 285 09

Cont.

	NOMBRE Y DIRECCION:	EMPRESA Y DIRECCION:
18.-	HERNAN JORGE ROSALES BUSTILLOS 1310, POTOSI, BOLIVIA TEL: 236 37	CORPORACION REGIONAL DE DESARROLLO DE POTOSI, CALLES LA PAZ-OMISTE, POTOSI, CASILLA No. 230 TEL: 247 49
19.-	DIOGENES RIOS ARGUELLO GL. MAXIMO JEREZ-# 421	INSTITUTO NICARAGUENSE DE ENERGIA SOBRE BY PASS
20.-	ROMAN SILVA PEREZ 5 DE FEBRERO No. 63-301 COL. CENTRO MEXICO 1, D.F.	C.F.E. OKLAHOMA # 85, 7° PISO COL. NAPOLES, MEXICO 18, D.F. TEL: 536 93 15
21.-	ANDRES TEJERO ANDRADE AV. MORELOS # 230-5 ACAPANTZINGO, CUERNAVACA	I.I.E. INTERNADO PALMIRA, CUERNAVACA, MORELOS TEL: 438 11